

**MINERALOGY, MINERAL CHEMISTRY, AND GENESIS OF PRECIOUS  
METAL-BEARING VOLCANOGENIC MASSIVE SULFIDE DEPOSITS IN THE  
NEWFOUNDLAND APPALACHIANS, CANADA: THE MING DEPOSIT AS  
EXAMPLE**

by

© Stefanie M. Brueckner

A doctoral thesis submitted to the

School of Graduate Studies

in partial fulfillment of the requirements for the degree of

Doctor of Philosophy

Department of Earth Sciences

Memorial University of Newfoundland

May 2016

St. John's, Newfoundland and Labrador

An understanding of the natural world  
and what's in it is a source of not only  
a great curiosity but great fulfillment.

David Attenborough

There are three principal means of acquiring knowledge...  
observation of nature, reflection, and experimentation.  
Observation collects facts; reflection combines them;  
experimentation verifies the result of that combination.

Denis Diderot



## COMMENTS ON CORRECTIONS

At the time of the oral defense, results from this thesis were published in 3 peer-reviewed journals (chapters 2, 4, and 5) and in a reviewed conference proceeding (chapter 2). In order to avoid any discrepancies between the published papers and the content of this thesis documented in chapters 2 to 5, changes regarding content were not incorporated in the text of this thesis. Therefore, only suggestions regarding spelling and grammar were incorporated into this thesis; the thesis is consistently written in American English.

The thesis was passed with distinction and all three examiners complimented on the thorough and outstanding work of this thesis and had only minor comments. However, a general definition of terms used throughout this thesis and a further explanation of some comments are made here, since the author of this thesis found many comments of the examiners helpful and supportive regarding the major arguments made in this thesis.

### Definitions

Certain terms were not clearly explained in the thesis and are defined here:

- (i) ***Bimodal-mafic volcanogenic massive sulfide deposit:*** Barrie and Hannington (1999) classified volcanogenic massive sulfide deposits based on their host rock sequences. One classification is bimodal-mafic. “The bimodal-mafic type is defined as having >50%

mafic rocks and >3% felsic rocks in the host stratigraphic succession, with subordinate siliclastic rocks. Most have a ratio of mafic/felsic volcanic rocks of 3:1 or greater, but felsic rocks are commonly the immediate host rocks. They predominate in late Archean and early Proterozoic rocks. In broad terms, the composition of the host rocks reflects primitive volcanic arc, or primitive rifted volcanic arc settings. The mafic volcanic rocks are generally basaltic and tholeiitic, although they may be transitional to calc-alkaline; felsic volcanic rocks are commonly high silica rhyolites or transitional with calc-alkaline rhyolites.” (Barrie and Hannington, 1999, p. 4)

(ii) **Green mica:** Green mica is common trace alteration mineral in the footwall rocks of the Ming deposit. Although, a fuchsite composition (Cr-bearing mica) is assumed, no chemical analyses have been done on this mineral phase yet. Therefore, the general term green mica is used here instead. Moreover, the green color can also be caused by enriched V and/or Ba compositions in mica as reported by Lee and Lee (2003).

(iii) **Myrmekitic intergrowth/myrmekite:** Myrmekitic intergrowth or myrmekite is defined as the “[V]ermicular (worm-like, symplectitic) intergrowth of quartz and sodic plagioclase (generally oligoclase), formed by replacement of K-feldspar, typically in deformed granitic

rocks.” (Vernon, 2004, p.486). The term was used in this thesis to give the reader a mental image of the described worm-like intergrowth between two or more ore minerals, because textural descriptions involving ore mineral phases are rare. It was not intended to equalize the genesis of quartz-feldspar myrmekites with intergrowth textures between two or more ore minerals, because the latter were significantly differently formed than the former. In order to avoid genetic misinterpretations regarding the intergrowth of two or more ore minerals, the more general term symplectite (i.e., “[W]orm-like (vermicular) intergrowth of minerals”; Vernon, 2004, p.493) is also used in the thesis.

(iv) **Plunge:** Plunge is the vertical angle between the inclined linear feature (here: orebodies of the Ming deposit) and an imaginary horizontal plane (here: surface). Up plunge and down plunge refer to the upper part and the lower part of the inclined orebody, respectively.

(v) **Precious metal-bearing volcanogenic massive sulfide deposit:**

The term precious metal-bearing volcanogenic massive sulfide deposits is used here to describe volcanogenic massive sulfide deposits with Au grades between 1-3.46g/t and <31t Au. Mercier-Langevin et al. (2011) defined volcanogenic massive sulfide deposits with >3.46g/t Au as auriferous, with >31t Au as anomalous,

and with >3.46g/t Au and >31t Au as Au-rich. However, they did not provide a terminology for volcanogenic massive sulfide deposits with 1g/t > Au > 3.46 g/t and <31t Au, although many volcanogenic massive sulfide deposits have such Au grades and Au tonnages and are therefore more enriched in Au than base metal volcanogenic massive sulfide deposits.

(vi) **Rambler rhyolite:** Rambler rhyolite is used as a synonym for Rambler Rhyolite formation. The Rambler Rhyolite formation is a “2.5km wide sequence of quartz-phyric, rhyodacitic, felsic tuff and tuff breccia [...]. The upper parts of the Rambler Rhyolite formation host the volcanogenic massive sulfide deposits of the Rambler and Ming mines. [...] A sample of rhyolite immediately below the mineralization yielded a U-Pb zircon age of ca. 487 Ma (V. McNicoll, unpublished data, 2008).” (Skulski et al, 2010, p.323) In this thesis, stratigraphic observations were predominantly acquired from drill holes. Due to the limited length of (underground) drill holes, the Rambler rhyolite is only observed for several tens to hundreds of meters.

(vii) **Spatially proximal orebodies:** The term spatially proximal orebodies refers to the distance between the different orebodies of the Ming deposit, which are separated from each other by Rambler

rhyolite and mafic dikes. The orebodies occur close to each other; usually the distance between each orebody is <100m.

### **General remarks**

Many questions of the examiners were answered during the oral defense; however, there are some questions and comments, which in the opinion of the author of this thesis need further explanation:

- (a) *Circumstantial evidence for syngenetic precious metal emplacement (chapter 3) and magmatic input to hydrothermal fluid (chapters 3 to 5):*** The genesis of metamorphosed volcanogenic massive sulfide deposits is complex due to the metamorphic overprint. Deciphering original (syngenetic) features from secondary (orogenic) features is a time-consuming and complicated task with sometimes mixed results. The arguments provided in this thesis, especially in chapter 3 are circumstantial and based on detailed stratigraphical, mineralogical, and chemical observations, because this multi-purpose approach is the best possible line of work to distinguish between primary and secondary features. Moreover, a detailed description how metamorphism changes the stratigraphy, ore mineralogy, ore textures and/or ore chemistry of volcanogenic sulfide deposits is not available in literature. Therefore, circumstantial evidence and comparison to

other ancient and modern volcanogenic deposits is at the moment the only approach to determine the relative timing of precious metal emplacement; and that was done in this thesis. A similar line of circumstantial arguments is provided especially in chapter 5 to argue for a magmatic input to the hydrothermal fluid. Detailed textural, mineralogical, and chemical observations are linked to each other and comparisons to other studies are made to argue for a magmatic input to the hydrothermal fluid. It also should be mentioned, that detailed textural, mineralogical, and mineral chemical studies on precious metal-bearing volcanogenic massive sulfide deposits have been very rare in literature and more studies such as this thesis are needed to provide further data regarding the relative timing of precious metal emplacement and a possible magmatic input.

**(b) *Role of metamorphism on  $\delta^{34}\text{S}$  composition (chapter 4):*** The role of metamorphism on the isotope composition in metamorphosed deposits is an on-going debate (e.g., Crowe, 1994; Ohmoto and Goldhaber, 1997; Seal, 2006). However, studies have shown that moderate metamorphism (greenschist to amphibolite facies conditions) and deformation have an insignificant or only local influence on the sulfur isotope composition (Bachinski, 1977, 1978; Cook and Hoefs, 1997; Bailie, 2010). Possible approaches to test

the influence of metamorphism on the sulfur isotope composition of sulfides in metamorphosed deposits are limited especially if only one isotope system, like in this study, was applied. Nevertheless, the methods of Gregory and Criss (1986) and Gregory et al. (1989) when comparing  $\delta^{34}\text{S}$  compositions of neighboring mineral pairs have shown to be efficient in determining if isotopic re-equilibration took place or not. Therefore, this same approach was applied in this thesis, because other isotope analyses (e.g., O isotopes, Cu isotopes, Se isotopes) were not applied due to time constraints. Moreover, no other method has been proposed to test the influence of metamorphism on  $\delta^{34}\text{S}$  compositions of sulfide phases in metamorphosed volcanogenic massive sulfide deposits.

(c) ***Sample strategy for whole rock samples (chapter 5):*** In total, 36 samples were analyzed for whole rock sulfide geochemistry with the most samples from the 1806 and 1807 zones. The bias in sampling between the different orebodies is due to sample availability. Samples from the 1806 and 1807 zones were taken from underground mapping. In contrast, drill core sections from the other orebodies were analyzed, because underground access to these orebodies was not available at the time of this study. In order to avoid taking fully mineralized samples from drill core sections that would be of value for Rambler Metals & Mining Canada Ltd in the

future, only a limited number of drill core halves were taken for whole rock sulfide geochemistry from the Ming South orebodies and the Lower Footwall Zone.

**(d) *Discrepancies in architecture in genetic models proposed in chapters 3 (Fig. 3-14) and 5 (Fig. 5-14):*** The model described in chapter 3 (Fig. 3-14) is based on results of the 1806 Zone alone and at that time of the study a simplified model was proposed in which the different orebodies formed a consistent ore lens. However, with ongoing research also involving the other orebodies a more evolved model was proposed in chapter 5 (Fig. 5-14) that takes into account the spatial separation of the orebodies and the relative location of the orebodies to each other. It should be mentioned, however, that the model proposed in Fig. 5-14 is not to scale.

## References

- Bachinski DJ (1977) Sulfur isotopic composition of ophiolitic cupriferous sulfide deposits, Notre Dame Bay, Newfoundland. *Economic Geology* 72:243-257
- Bachinski DJ (1978) Sulfur isotopic composition of thermally metamorphosed cupriferous iron sulfide ores associated with cordierite-antophyllite rocks, Gull Pond, Newfoundland. *Economic Geology* 73:64-72
- Bailie R, Gutzmer J, Strauss H, Stüeken E, McClung C (2010) Sulfur isotope characteristics of metamorphosed Zn–Cu volcanogenic massive sulfides in the Areachap Group, Northern Cape Province, South Africa. *Mineralium Deposita* 45:481-496. doi: 10.1007/s00126-010-0285-8
- Barrie CT, Hannington MD (1999) Classification of volcanic-associated massive sulfide deposits based on host-rock composition In: Barrie CT, Hannington, M.D. (ed) *Volcanic-associated massive sulfide deposits:*



- Processes and examples in modern and ancient settings. Society of Economic Geologists, Boulder, CO, pp 1-11
- Cook NJ, Hoefs J (1997) Sulfur isotope characteristics of metamorphosed Cu-(Zn) volcanogenic massive sulfide deposits in the Norwegian Caledonides. *Chemical Geology* 135:307-324
- Crowe DE (1994) Preservation of original hydrothermal  $\delta^{34}\text{S}$  values in greenschist to upper amphibolite volcanogenic massive sulfide deposits. *Geology* 22
- Gregory RT, Criss RE (1986) Isotopic Exchange in open and closed systems. *Reviews in Mineralogy and Geochemistry* 16:91-127
- Gregory RT, Criss RE, Taylor Jr. HP (1989) Oxygen isotope exchange kinetics of mineral pairs in closed and open systems: Applications to problems of hydrothermal alteration of igneous rocks and Precambrian iron formations. *Chemical Geology* 75:1-42. doi: Doi 10.1016/0009-2541(89)90019-3
- Lee CH, Lee HK (2003) Vanadium and barium-bearing green mica with coaly metapelite from the Ogcheon Supergroup, Republic of Korea. *Journal of Asian Earth Science* 21:343-351. doi: 10.1016/S1367-9120(02)00016-0
- Mercier-Langevin P, Hannington MD, Dubé B, Bécu V (2011) The gold content of volcanogenic massive sulfide deposits. *Mineralium Deposita* 46:509-539. doi: 10.1007/s00126-010-0300-0
- Ohmoto H, Goldhaber MB (1997) Sulfur and carbon isotopes In: Barnes HL (ed) *Geochemistry of hydrothermal ore deposits*, 3rd edition. 3rd edition edn. John Wiley & Sons, New York, pp 517-611
- Seal II RR (2006) Sulfur isotope geochemistry of sulfide minerals In: Vaughan DJ (ed) *Sulfide mineralogy and geochemistry*. pp 633-677
- Skulski T, Castonguay S, McNicoll V, van Staal C, Kidd W, Rogers N, Morris W, Ugalde H, Slavinski H, Spicer W, Moussallam Y, Kerr I (2010) Tectonostratigraphy of the Baie Verte oceanic tract and its ophiolite cover sequence on the Baie Verte Peninsula. Current Research Newfoundland and Labrador Department of Natural Resources, Geological Survey Report 10-1:315-335
- Vernon, RH (2004) A practical guide to rock microstructure. University Press, Cambridge

## ABSTRACT

The Ming deposit, Newfoundland Appalachians, is a metamorphosed (upper greenschist to lower amphibolite facies), Cambro-Ordovician, bimodal-mafic volcanogenic massive sulfide (VMS) deposit that consists of several, spatially-associated, elongated orebodies composed of stratabound semi-massive to massive sulfides and/or discordant sulfide stringers in a rhyodacitic footwall. Copper is the main commodity; however, the deposit contains precious metal-bearing zones with elevated Au grades.

In this study, field observations, microscopy, and micro-analytical tools including electron microprobe, laser ablation inductively coupled plasma mass spectrometry, and secondary ion mass spectrometry were used to constrain the relative timing of precious metal emplacement, the physico-chemical conditions of hydrothermal fluid precipitation, and the sources of sulfur, precious metals, semi-metals and metals.

The ore mineral assemblage is complex and indicates an intermediate sulfidation state. Pyrite and chalcopyrite are the dominant ore minerals with minor sphalerite and pyrrhotite, and trace galena, arsenopyrite and cubanite. Additional trace phases include tellurides, NiSb phases, sulfosalts, electrum, AgHg±Au alloys, and oxides. Silver phases and precious metals occur predominantly in semi-massive and massive sulfides as free grains, and as grains spatially associated with arsenopyrite and/or sulfosalts. Precious metal phases occurring between recrystallized pyrite and within cataclastic pyrite are rare. Hence, the

complex ore assemblage and textures strongly suggest syngenetic precious metal emplacement, whereas metamorphism and deformation only internally and locally remobilized precious metal phases.

The ore assemblage formed from reduced, acidic hydrothermal fluids over a range of temperatures ( $\approx 350$  to below  $260^{\circ}\text{C}$ ). The abundance of telluride and Ag-bearing tetrahedrite, however, varies strongly between the different orebodies indicating variable  $f\text{Te}_2$ ,  $f\text{Se}_2$ ,  $m_{\text{Bi}}$ , and  $m_{\text{Sb}}$  within the hydrothermal fluids. The variations in the concentrations of semi-metals and metals (As, Bi, Hg, Sb, Se, Te), as well as Au and Ag, were due to variations in temperature but also to a likely contribution of magmatic fluids into the VMS hydrothermal system from presumably different geothermal reservoirs.

Sulfur isotope studies indicate at least two sulfur sources: sulfur from thermochemically-reduced seawater sulfate and igneous sulfur. The source of igneous sulfur is the igneous footwall, direct magmatic fluid/volatiles, or both. Upper greenschist to lower amphibolite metamorphic conditions and deformation had no significant effect on the sulfur isotope composition of the sulfides at the Ming deposit.

## **ACKNOWLEDGEMENTS**

A PhD thesis is a journey, academically and personally. Many people accompanied me on this journey and helped building and shaping the ideas presented in this thesis.

My foremost thanks goes to my supervisor Stephen Piercey, who gave me the opportunity, a challenging topic and the freedom to develop my own ideas. Steve also accepted my way of working – detailed, meticulous, and on the fringe of perfection. I learned from him through the years and I am very thankful for the scientifically challenging discussions I had with him throughout my PhD. A huge thanks also goes to my co-supervisor Paul Sylvester, who brought me to Newfoundland. Paul was a great mentor especially for the analytical side of the thesis and I enjoyed many fruitful discussions with him. I benefitted also from the knowledge and kindness of many faculty members of the Department of Earth Sciences at Memorial University; special thanks go to Graham Layne, Toby Rivers, Tom Calon, Derek Wilton, Henry Longerich, and Roger Mason. The thesis would not be where it is now without the technical support of David Grant, Michael Shaffer, Glenn Piercey, Yanan Liu (University of Toronto), and Joe Petrus (Laurentian University). I learned a lot from these people and it was a pleasure to work with and learn from them; Dave, Michael, and Glenn in particular gave me helpful technical and analytical advice for the scanning electron microscope and secondary ion mass spectrometer.

I also want to thank the ladies at the department office – Danyelle Drodge, Jillian Kean, Michelle Miskell, Dianne Guzzwell, and Jane O'Neill – and the ladies from the Geological Association of Canada. The logistic support of Keir Hiscock and Darren Smith throughout the years is also acknowledged. Thanks also to Derek Parsons and Ron Tobin.

This thesis would have not been possible without the staff at Rambler Metals & Mining, Canada Limited. These great people provided the core field logistics and made me feel at home in Newfoundland. There are too many people to name personally; however, special thanks go to Larry Pilgrim, Stephanie Maloney, Tim Sanford, Peter Mercer, Norman Williams, George Ogilvie, Hubert Jenkins, Bert, Kirk, Wayne, and Ewan.

I also thank Baerbel Sarbas, Ute Busch, Uwe Nohl, Bernd Kalbskopf, Brigitte Stoll, Klaus Peter Jochum, and Ulrike Weiss from the GEOROC and GeoReM databases. They all encouraged me to follow my dreams and to pursue a PhD. They have been amazing friends and great mentors throughout the years.

During my thesis, I formed also great friendships and those friends gave me strong mental support. Words cannot describe my gratitude, but nevertheless the simple word thanks goes in particular to two amazing men and friends – Dean Courage and Praise Nyade – for their constant support. I also thank Jean-Luc Pilote, Connor McKinley, Matt Minnett, Mary Leaman, Kate Souders, and Michelle Kelvin for their friendship.

Also I want to thank my parents and brother for their amazing support - personally and financially. Without their trust I could not have done it.

Finally, special thanks to Dianne, Dillon, and Gabrielle Peterson – you are truly special and you guided me through the really tough times.

## TABLE OF CONTENTS

<b>Comments on Corrections</b>	<b>i</b>
Definitions	i
General remarks	v
References	viii
<b>Abstract</b>	<b>x</b>
<b>Acknowledgements</b>	<b>xii</b>
<b>List of Tables</b>	<b>xxiii</b>
<b>List of Figures</b>	<b>xxvi</b>
<b>List of Abbreviations</b>	<b>xxxi</b>
Tectonic setting and geology	xxxii
Methodology	xxxiii
Mineralogy	xxxiv
Units	xxxvi
Results	xxxvii
Miscellaneous	xxxviii
<b>List of Appendices</b>	<b>xl</b>
<b>List of Electronic Appendices</b>	<b>xli</b>
<b>Co-authorship Statement</b>	<b>xlii</b>
<b>Chapter 1 Introduction</b>	<b>1</b>
1-1 Introduction and overview	2

1-2	Relative timing of precious metal enrichment in metamorphosed volcanogenic massive sulfide deposits	5
1-3	Sulfur isotope composition of sulfides as possible indicator for the source of sulfur	7
1-4	Metal transport, possible metal sources, and deposition mechanisms in precious metal-bearing volcanogenic massive sulfide deposits	10
1-5	Objectives of this study	15
1-6	Thesis structure	16
	References	17
<b>Chapter 2</b>	<b>Stratigraphy, mineralogy, geochemistry, and genesis of an Au-rich volcanogenic massive sulfide (VMS) system from the Baie Verte Peninsula, NW Newfoundland, Canada: The 1806 Zone as an example from the Ming Mine, Rambler Camp</b>	<b>28</b>
	Abstract	29
	Keywords	30
2-1	Introduction	30
2-2	Tectonic setting	31
2-3	Methods	33
2-4	Stratigraphy, petrography, and mineralogy	35
2-4-1	Stratigraphy	35
2-4-2	Petrography	36
2-4-2-1	Rambler rhyolite with sulfide stringer and semi-massive to massive sulfide horizon	36
2-4-2-2	Turbidite sequence	38
2-4-2-3	Mafic dikes	38



	2-4-2-4	Felsic dikes	39
2-5		Mineralogy	41
	2-5-1	Sulfide and oxide mineralogy	41
	2-5-2	Alteration mineralogy	49
2-6		Geochemistry	49
2-7		Discussion	51
2-8		Conclusions	52
		Acknowledgements	54
		References	54
<b>Chapter 3</b>		<b>Evidence for syngenetic precious metal enrichment in an Appalachian volcanogenic massive sulfide system: The 1806 Zone, Ming mine, Newfoundland</b>	<b>57</b>
		Abstract	58
3-1		Introduction	60
3-2		Lithotectonic setting	64
	2-2-1	Baie Verte Peninsula	64
	2-2-2	Consolidated Rambler VMS camp	70
3-3		Geology of the 1806 Zone	72
	3-3-1	Rambler rhyolite	72
	3-3-2	Mineralized zones	78
		3-3-2-1 Semi-massive to massive sulfides	78
		3-3-2-2 Silicified horizon	79
	3-3-3	Hanging wall mafic, felsic, and mixed volcanoclastic rocks	80

3-3-4	Mafic and felsic dikes	80
3-3-4-1	Mafic dikes	80
3-3-4-2	Felsic dikes	81
3-3-5	Hydrothermal alteration	81
3-4	Sulfide and oxide mineralogy	83
3-5	Mineral chemistry	91
3-5-1	Analytical methods	91
3-5-1-1	Bulk metal analysis	91
3-5-1-2	Semi-quantitative energy-dispersive X-ray (EDX) imaging/spectroscopy	91
3-5-1-3	Electron probe microanalysis (EPMA)	92
3-5-2	Results	95
3-5-2-1	Assay data (Activation Laboratories)	95
3-5-2-2	Semi-quantitative energy-dispersive X-ray	95
3-5-2-3	Electron probe microanalysis	97
3-6	Discussion	122
3-6-1	Syn-genetic vs. syn-orogenic precious metal emplacement	122
3-6-1-1	Architecture	123
3-6-1-2	Alteration	124
3-6-1-3	Metal zoning	125
3-6-1-4	Ore assemblages and paragenesis	126

	3-6-1-5	Influence of deformation and metamorphism	129
	3-6-2	Deposition model for the 1806 Zone and hydrothermal ore fluid conditions	130
	3-7	Conclusions	135
		Acknowledgements	137
		References	138
		Appendix A3-1	146
		Appendix A3-2	148
		Appendix A3-3	148
<b>Chapter 4</b>		<b>Variations of sulfur isotope signatures in sulfides from the metamorphosed Ming Cu(-Au) volcanogenic massive sulfide deposit, Newfoundland Appalachians, Canada</b>	<b>149</b>
		Abstract	152
		Keywords	152
	4-1	Introduction	152
	4-2	Geologic Background	155
	4-2-1	Baie Verte Peninsula	155
	4-2-2	Consolidated Rambler VMS camp	157
	4-2-3	Ming mine	158
	4-3	Sulfide mineralogy	168
	4-4	Sulfur isotope geochemistry	170
	4-4-1	Methodology	170
	4-4-2	Results	175

	4-4-2-1	Silicified horizon of the 1806 Zone	175
	4-4-2-2	Semi-massive to massive sulfides	176
	4-4-2-3	Footwall mineralization	177
4-5		Discussion	181
	4-5-1	Isotopic equilibrium	181
	4-5-2	Sulfur sources	184
	4-5-3	Changes in sulfur isotope composition with stratigraphic position	195
	4-5-4	Influence of metamorphism on sulfur isotope composition and comparison to other deposits	199
4-6		Conclusions	202
		Acknowledgements	203
		References	204
		Appendix A4-1	212
		Appendix A4-2	215
		Appendix A4-3	216
		Appendix A4-4	221
		Appendix A4-5	235
		Appendix A4-6	238
<b>Chapter 5</b>		<b>Mineralogy and mineral chemistry of the metamorphosed and precious metal-bearing Ming deposit, Canada</b>	<b>243</b>
		Abstract	244
		Keywords	246

5-1	Introduction	246
5-2	Tectonic setting	248
5-3	Stratigraphy, alteration, and mineralization styles	256
5-3-1	Stratigraphy and alteration of the Rambler rhyolite	256
5-3-2	Mineralization styles	258
5-4	Sulfide and precious metal mineralogy	261
5-4-1	Mineral abundances	261
5-4-2	Mineral textures	265
5-4-2-1	Replacement textures	265
5-4-2-2	Decomposition textures	273
5-4-2-3	Textures of unknown origin	273
5-4-2-4	Deformation textures	274
5-4-2-5	Precious metal textures	274
5-4-3	Paragenesis	276
5-5	Whole rock geochemistry and ore mineral chemistry	278
5-5-1	Whole rock sulfide geochemistry	279
5-4-2	EPMA and LA-ICP-MS	286
5-6	Discussion	297
5-6-1	Hydrothermal fluid conditions	297
5-6-1-1	Common metal sulfides	298
5-6-1-2	Role of elements of the epithermal suite and precious metals	302
5-6-1-2-1	Te, Bi, and Se	302

	5-6-1-2-2	Ag and Au	309
	5-6-1-2-3	As, Sb, and Hg	311
	5-6-2	Genesis of the orebodies at the Ming deposit	312
	5-6-2-1	Source of metals	312
	5-6-2-2	Genetic model	315
5-7		Conclusions	321
		Acknowledgements	322
		References	323
		Appendix A5-1	333
		Appendix A5-2	345
		Appendix A5-3	366
<b>Chapter 6</b>		<b>Conclusions and suggestions for further research</b>	<b>371</b>
	6-1	Conclusions	372
	6-2	Suggestions for further research	375
		References	379

## **Electronic Appendix**

## LIST OF TABLES

<b>Table 2-1</b>	Sulfide and oxide mineralogy representative of the 1806 Zone on the example of two samples from drill core RMUG08-140, Section 22	41
<b>Table 3-1</b>	Deformation events developed in the Pacquet Harbour Group, Baie Verte oceanic tract (BVOT)	68
<b>Table 3-2</b>	Assay data for Cu, Zn, Pb, Ag, and Au of the semi-massive to massive sulfide lens from three representative drill holes	98
<b>Table 3-3</b>	Microprobe data for selected samples from the up plunge (UP) and down plunge (DP) of the 1806 Zone	108
<b>Table 3-4</b>	Summary of microprobe analyses – mineral phases, their calculated mineral formula, and detected minor elements	120
<b>Table A3-1</b>	Analyzed samples for EPMA data, their occurrence within the 1806 zone, their mineralogy, and their analyzed phases	146
<b>Table A3-2</b>	Detection limits for all 17 elements analyzed in sulfides, precious metals and oxides in April 2011 and January 2012 on the microprobe at UT	148
<b>Table A3-3</b>	Electron microprobe data on sulfides, sulfosalts, precious metals and oxides; See electronic Appendix accompanying this thesis	148
<b>Table 4-1</b>	Characteristics of the different mineralization styles at the Ming deposit	165
<b>Table 4-2</b>	Summary of abundance and textures for pyrite, chalcopyrite, pyrrhotite, arsenopyrite, and galena in the different mineralization styles of the Ming deposit	173
<b>Table A4-1</b>	Results of measured $^{34}\text{S}/^{32}\text{S}$ ratio, calculated instrumental mass fractionation (IMF), and $\delta^{34}\text{S}$ analysis corrected for IMF of the used in-house standards analyzed via SIMS	216
<b>Table A4-2</b>	Analyzed samples from the Ming deposit, their brief	

	description, sulfide mineralogy, and results of S isotope analysis	221
<b>Table A4-3</b>	Isotopic fractionation between plotted mineral pairs for temperatures of 250-500°C	237
<b>Table 5-1</b>	Combined, measured, and indicated resource data for orebodies of the Ming	255
<b>Table 5-2</b>	Different mineralization styles within the orebodies at the Ming deposit	259
<b>Table 5-3</b>	Mineral abundance of metal sulfides, sulfosalts, precious metals and oxides in the orebodies of the Ming deposit	262
<b>Table 5-4</b>	Results of whole rock metal analysis for the different orebodies at the Ming deposit	283
<b>Table 5-5</b>	Pearson's correlation coefficients of selected elements for massive sulfides and stringer sulfides from all orebodies of the Ming deposit	285
<b>Table 5-6</b>	Microprobe results of major and minor elements for mineral phases from the Ming deposit and their calculated mineral formulae	288
<b>Table 5-7</b>	Summary of occurrence, preferred host minerals, mineral associations, and favored transport and precipitation conditions for elements of the epithermal suite and precious metal-bearing elements at the Ming deposit	307
<b>Table A5-1</b>	Summary of precision and accuracy for RMs and duplicates used in this study	347
<b>Table A5-2</b>	Precision data for major element components of analyzed minerals; n - number of analysis	355
<b>Table A5-3</b>	Limit of detection (LOD) for major and minor elements analyzed by EPMA	356



<b>Table A5-4</b>	Precision and accuracy for reference materials NIST 610, MASS-1, and Po725 calibrated against NIST 610, themselves and with various internal standards	360
<b>Table A5-5</b>	Detailed results of whole rock geochemistry for 36 mineralized samples from the Ming deposit	366
<b>Table A5-6</b>	Results of EPMA (major and minor elements in wt.%) and LA-ICP-MS (trace elements in ppm) analysis for analyzed mineral phases	370

## LIST OF FIGURES

<b>Figure 2-1</b>	Geologic map of the studied area	34
<b>Figure 2-2</b>	Stratigraphic section of drill core RMUG08-140, 1806 Zone	40
<b>Figure 2-3</b>	BSE images and line scan from samples of the 1806 Zone	44
<b>Figure 3-1</b>	Simplified geologic map from the Baie Verte Peninsula	67
<b>Figure 3-2</b>	Detailed geologic map of the Pacquet Harbour Group (PHG) hosting the Ming (Main) Mine and previously mined volcanogenic massive sulfide deposits	69
<b>Figure 3-3</b>	Resource data for the newly explored zones at the Ming deposit	73
<b>Figure 3-4</b>	Stratigraphic drill core sections from the up plunge and down plunge portions of the 1806 Zone	74
<b>Figure 3-5</b>	Underground map from the 720 level (up plunge portion) of the 1806 Zone	76
<b>Figure 3-6</b>	Rambler rhyolite and sulfide mineralization at the 1806 Zone	82
<b>Figure 3-7</b>	Sulfide mineral abundance within the 1806 Zone from the down plunge portion to the up plunge portion for base metal sulfides including arsenopyrite, the most abundant sulfosalts, precious metals, and oxides	85
<b>Figure 3-8</b>	Reflected light images of sulfide assemblages and textures from semi-massive to massive sulfides, sulfide stringer and silicified horizon	88
<b>Figure 3-9</b>	Metal zoning in the semi-massive to massive sulfide lens of the 1806 Zone	96
<b>Figure 3-10</b>	Back-scattered electron (BSE) images and Energy dispersive x-ray spectrometry (EDX) scans done by SEM	

	on two precious metal samples from the up plunge portion for selected elements	103
<b>Figure 3-11</b>	Compositional plots for various sulfide and sulfosalt phases based on electron probe micro-analyses (EPMA)	106
<b>Figure 3-12</b>	Compositional plots for electrum based on EPMA data	107
<b>Figure 3-13</b>	Paragenetic chart for the syn-genetic deposition of sulfides, sulfosalts, precious metals, and cassiterite at the 1806 Zone	127
<b>Figure 3-14</b>	Depositional model for the genesis of the 1806 Zone	131
<b>Figure 4-1</b>	Location of the study area within Newfoundland, Canada (left) and the Baie Verte Peninsula, Newfoundland (right)	156
<b>Figure 4-2</b>	Detailed geologic map of the Pacquet Harbour Group (PHG) hosting the Ming (Main) mine and previously mined volcanogenic massive sulfide deposits	159
<b>Figure 4-3</b>	Simplified 3-D view of the different orebodies of the Ming deposit	161
<b>Figure 4-4</b>	Simplified stratigraphy of the Ming deposit with photographs of the different mineralization styles	163
<b>Figure 4-5</b>	Typical sulfide mineral assemblages and textures from the different mineralization styles of the Ming deposit	166
<b>Figure 4-6</b>	Histogram of $\delta^{34}\text{S}$ values of sulfides from the different mineralization styles, a sample of Fe oxide schlieren in Rambler rhyolite on top of massive sulfide, and a sample of mineralized quartz vein within a mafic dyke of the Lower Footwall Zone of the Ming deposit	179
<b>Figure 4-7</b>	Box-Whisker plot showing the variations in $\delta^{34}\text{S}$ values of sulfides from the different mineralization styles of the Ming deposit	180
<b>Figure 4-8</b>	$\delta$ - $\delta$ plot for neighbouring pyrite-chalcopyrite mineral pairs	183

<b>Figure 4-9</b>	Measured and calculated $\delta^{34}\text{S}$ values of pyrrhotite in the silicified horizon of the 1806 orebody	190
<b>Figure 4-10</b>	Measured and calculated $\delta^{34}\text{S}$ values of chalcopyrite from the semi-massive to massive sulfides	191
<b>Figure 4-11</b>	Measured and calculated $\delta^{34}\text{S}$ values for chalcopyrite in semi-massive to massive sulfides and in the footwall	194
<b>Figure 4-12</b>	Sulfur isotope data for different sulfur sources, metamorphosed VMS deposits including this study, and orogenic Au deposits of the Pacquet Harbour Group (PHG)	201
<b>Figure A4-1</b>	Box-Whisker plot of the results for sulfide reference materials used for IMF calibration and quality control of SIMS microanalyses	215
<b>Figure A4-2</b>	$\delta$ - $\delta$ plots for neighbouring mineral pairs	236
<b>Figure 5-1</b>	Geology of Newfoundland and simplified geology of the Baie Verte Peninsula	251
<b>Figure 5-2</b>	Detailed geological map of the Pacquet Harbour Group (PHG) with VMS deposits of the Rambler camp	252
<b>Figure 5-3</b>	Textural relationships between various sulfide minerals in the 1807, 1806, MSUP, and MSDP orebodies	267
<b>Figure 5-4</b>	Textures of metal sulfides, tellurides, and electrum in the LFWZ	269
<b>Figure 5-5</b>	Textural variations of precious metals in 1807, 1806, MSUP and MSDP orebodies	271
<b>Figure 5-6</b>	Paragenetic chart of the most abundant metal sulfides, sulfosalts and precious metals occurring at the Ming deposit	278
<b>Figure 5-7</b>	Compositional plots of selected major and trace elements from mineralized samples of the Ming deposit	281

<b>Figure 5-8</b>	Box-Whisker plots showing variations in elements of the epithermal suite and precious metals in the orebodies of the Ming deposit	282
<b>Figure 5-9</b>	Major compositions of sulfides and sulfosalts analyzed by EPMA	287
<b>Figure 5-10</b>	Histograms of LA-ICP-MS data for selected trace elements for pyrite, chalcopyrite, and pyrrhotite	294
<b>Figure 5-11</b>	Histograms of LA-ICP-MS data of selected trace elements for sphalerite, arsenopyrite, galena, cubanite, and tetrahedrite-tennantite	296
<b>Figure 5-12</b>	Comparison of average metal concentrations between the different orebodies from the Ming deposit	298
<b>Figure 5-13</b>	Temperature vs log $fS_2$ diagram showing varying Fe contents in sphalerite co-existing with pyrite (py) – pyrrhotite (po)	301
<b>Figure 5-14</b>	Genetic model for the syngenetic formation of the Ming VMS deposit	317
<b>Figure A5-1</b>	Location of orebodies (white ovals) relative to surface geology (modified after Skulski et al., 2010) with selected surface and underground drill holes (white and black circles) and mapped underground levels (stars)	333
<b>Figure A5-2</b>	Underground maps of the 375 level (top) and 469 level (bottom) of the 1807 Zone	334
<b>Figure A5-3</b>	Stratigraphy and simplified alteration for selected surface drill hole sections from the 1807 Zone orebody	337
<b>Figure A5-4</b>	Stratigraphy and simplified alteration for selected underground drill holes from the 1806 Zone orebody	339
<b>Figure A5-5</b>	Stratigraphy and simplified alteration for selected underground drill holes from the Ming South Up Plunge (MSUP) orebody	341

**Figure A5-6** Stratigraphy and simplified alteration for selected surface drill holes (RM06-04e, -04m) and drill hole sections (RM06-04d, -04l) from the Ming South Down Plunge (MSDP) and the Lower Footwall Zone (LFWZ) orebodies

343

## LIST OF SYMBOLS, NOMENCLATURE OR ABBREVIATIONS

### Tectonic Setting and Geology

BVBL	– Baie Verte Brompton Line
BVOT	– Baie Verte oceanic tract
D/DP	– Ming South Down Plunge
DP <sub>1806</sub>	– Down Plunge of the 1806 Zone
LFWZ	– Lower Footwall Zone
md(?)	– (Assumed) mafic dike
MSDP	– Ming South Down Plunge
MSUP	– Ming South Up Plunge
PHG	– Pacquet Harbour Group
q±c	– Quartz ± carbonate veins
RM04	– Rambler Metals & Mining Canada Limited surface drill hole from 2004
RMUG08	– Rambler Metals & Mining Canada Limited underground drill hole from 2008
R <sub>rhy</sub>	– Rambler rhyolite
R <sub>q-eye rhy</sub>	– Quartz eye-bearing Rambler rhyolite
sul	– (Semi-)Massive sulfide(s)
U/UP	– Ming South Up Plunge
UP <sub>1806</sub>	– Up Plunge of the 1806 Zone
VMS	– Volcanogenic massive sulfide

## Methodology

AAS	– Atomic absorption spectrometry
ActLabs	– Activation Laboratories
BSE	– Back-scattered electron
CV-FIMS	– Cold vapor flow injection mercury system
CV <sub>av</sub>	– Average coefficient of variation
EPMA	– Electron probe micro-analysis
EDX	– Energy dispersive x-ray spectrometry
EDS detector	– Energy dispersive detector
FA-Gra	– Fire assay with gravimetric finish
ICP	– Inductively coupled plasma
ICP-OES	– Inductively coupled plasma optical emission spectrometry
IMF	– Instrumental mass fractionation
INAA	– Instrumental neutron activation analysis
IR	– Infrared digestion
IRMS	– Isotope mass ratio spectrometry
LA-ICP-MS	– Laser ablation inductively coupled plasma mass spectrometry
LIF crystal	– Lithium fluoride crystal
LOD	– Limit of detection
LOQ	– Limit of quantification
MRP	– Mass-resolving power
PET crystal	– Pentaerythritol crystal
RD	– Relative difference



RL	– Reflected light
RM	– Reference material
RSD	– Relative standard deviation
SEM	– Scanning electron microscopy
SIMS	– Secondary ion mass spectrometry
TIMS	– Thermal ionization mass spectrometry
TD-ICP-MS	– Total digestion inductively coupled plasma mass spectrometry
TD-ICP-OES	– Total digestion inductively coupled plasma optical emission spectrometry

### **Mineralogy**

Ag-Ccp	– Ag-bearing/argento chalcopyrite
AgCuFeS	– Unnamed AgCuFeS phase
Ag-Hg±Au/ AgHg±Au	– Silver-mercury±gold alloy
Ag-Tet-Ten	– Ag-bearing tennantite-tetrahedrite
Ag-Tet/Ag-Trt	– Ag-bearing tetrahedrite
Allo	– Alloclastite
Alt	– Altaite
Amp	– Amphibole
Asp/Apy	– Arsenopyrite
Bio/Bt	– Biotite
BiTe	– Unidentified bismuth telluride
Bn	– Bornite

Boul	– Boulangerite
Breit	– Breithauptite
Carb	– Carbonate
Cass/Cst	– Cassiterite
Cbn	– Cubanite
Ccp	– Chalcopyrite
Chl	– Chlorite
Chr	– Chromite
Claus	– Clausthalite
Col	– Coloradoite
El	– Electrum
Ep	– Epidote
FeTi ox	– Fe ± Ti ± Cr oxides
Gn	– Galena
Gn*	– Galena with (Bi-)telluride exsolution lamellae
Gud	– Gudmundite
Hess	– Hessite
Hg-Stp	– Mercurian stephanite
Loel	– Löllingite
Mag	– Magnetite
Mia	– Miargyrite
med-Fe Sp	– Medium/intermediate Fe sphalerite
Men	– Meneghinite

Mol	– Molybdenite
Nis	– Nisbite
NiSb	– Unidentified NiSb phase
Ni-Sb-S	– Unknown Ni-Sb sulfide
Po	– Pyrrhotite
Py	– Pyrite
Pyr	– Pyrargyrite
Qtz/Qz	– Quartz
Serc/Ser	– Sericite
Sp	– Sphalerite
Stn	– Stannite
Sul	– Sulfide(s)
Tet-Ten	– Tetrahedrite-tennantite
Tnt	– Tennantite
Tnt-Trt	– Tennantite-tetrahedrite
Trt	– Tetrahedrite
Tsu	– Tsumoite
Ull	– Ullmanite
unnamed BiTe	– Unnamed bismuth telluride
Will	– Willyamite

## Units

a.p.f.u./apfu	– Atom(s) per formula unit
cm	– Centimeter
cps	– Counts per second
Da	– Dalton
eV	– Electronvolt
g/t	– Gram(s) per ton
Hz	– Hertz
K	– Kelvin
keV	– Kilo electronvolt
J/cm <sup>2</sup>	– Joule per square centimeter
kV	– Kilo volt
L/min	– Liter per minute
m	– Meter
Ma	– Million years
min	– Minute(s)
mm	– Millimeter
ms	– Milliseconds
ns	– Nanoseconds
oz	– (Troy) ounce
pA	– Pico Ampere
ppb	– Parts per billion
ppm	– Parts per million

s	– Seconds
t	– (Metric) ton(nes)
vol. %	– Volume percentage
W	– Watt
wt. %	– Weight percentage
°	– Degree(s)
°C	– Degrees in Celsius
%	– Percentage
‰ / ‰ VCDT	– Per mille / per mille relative to Vienna Cañon Diablo Troilite
µm	– Micro-meter(s)

## Results

1σ	– 1 sigma (68% confidence level)
Av	– Average
Max	– Maximum value
Min	– Minimum value
n	– Number of analyses
NA	– No analysis
nd	– Not detected
no.	– Number
Sb/(Sb+As) <sup>o</sup>	– Molecular Sb/(molecular Sb + molecular As)
SEM	– Standard error mean
Std/Stddev	– Standard deviation

$\text{Zn}/(\text{Zn}+\text{Fe})^\circ$  – Molecular Zn/(molecular Zn + molecular Fe)

### Miscellaneous

A, B, and C – Equilibrium isotopic fractionation constants between two minerals or relative to  $\text{H}_2\text{S}$

$a_{\text{S}_2}$  – Activity of sulfur

b – Proportion of sulfur derived from thermochemical (seawater) sulfate reduction

BSR – Bacterial sulfate reduction

*cont.* – Continued

CREAIT – Core Research Equipment and Instrument Training Network

$f/f$  – Atomic fraction of parent sulfate reduced to sulfuric acid relative to the original amount of sulfate present or fractionation of early Ordovician seawater sulfate

$f_{\text{TSR}}$  – Fractionation of early Ordovician seawater sulfate by thermochemical sulfate reduction

$f_{\text{O}_2}$  – Oxygen fugacity

$f_{\text{S}_2}$  – Sulfur fugacity

$f_{\text{Se}_2}$  – Selenium fugacity

$f_{\text{Te}_2}$  – Tellurium fugacity

Ltd – Limited

$m_{\text{Bi}}$  – Molality of bismuth

$m_{\text{H}_2\text{S}}$  – Molality of sulfuric acid

$m_{\text{Sb}}$  – Molality of antimony

$m_{\Sigma\text{metals}}$  – Molality of total metals

MAF-IIC	– Micro-analysis facility
MUN	– Memorial University
NSERC	– Natural Science and Research Council of Canada
pH	– Power of the concentration of the hydrogen ion
T	– Temperature
T <sub>min</sub>	– Minimum temperature
T <sub>max</sub>	– Maximum temperature
TSR	– Thermochemical (seawater) sulfate reduction
VCDT	– Vienna Cañon Diablo Troilite
UT	– University of Toronto
UTM NAD83, Zone 21N	– Universal transverse Mercator coordinate system North American Datum 1983, Zone 21 North
v.	– Version
vs./vs	– Versus
WGS 84	– World Geodetic System 1984
$\alpha_{\text{H}_2\text{S-SO}_4}$	– Equilibrium sulfur isotopic fractionation factor between sulfide and sulfate (the ratio of $^{34}\text{S}/^{32}\text{S}$ of sulfide to sulfate) during thermochemical (seawater) sulfate reduction
$\delta^{34}\text{S}$	– Isotopic ratio of $^{34}\text{S}/^{32}\text{S}$ ratio of a compound/mineral relative to $^{34}\text{S}/^{32}\text{S}$ ratio of Cañon Diablo Troilite
$\delta_1, \delta_2$	– Measured $\delta^{34}\text{S}$ value of mineral phases 1 and 2
$\Delta_{1-2}$	– Difference in isotopic sulfur composition between mineral phases 1 and 2/Isotopic fractionation between mineral phases 1 and 2
@	– At

## LIST OF APPENDICES

<b>Appendix A3-1</b>	Sample description	146
<b>Appendix A3-2</b>	Detection limits	148
<b>Appendix A3-3</b>	Results EPMA analysis	148
<b>Appendix A4-1</b>	Methodology	212
<b>Appendix A4-2</b>	Accuracy and precision of analyzed reference materials	215
<b>Appendix A4-3</b>	Results of reference material analyses	216
<b>Appendix A4-4</b>	Results of sulfur isotope analyses on sulfides from the Ming deposit	221
<b>Appendix A4-5</b>	Isotopic equilibrium	235
<b>Appendix A4-6</b>	Calculations used for modelling S sources at the Ming deposit	238
<b>Appendix A5-1</b>	Stratigraphy	333
<b>Appendix A5-2</b>	Analytical methods	345
<b>Appendix A5-3</b>	Results of whole rock geochemistry, EPMA, and LA-ICP-MS	366



## LIST OF ELECTRONIC APPENDICES

<b>Table A3-3</b>	Electron microprobe data on sulfides, sulfosalts, precious metals and oxides
<b>Table A5-6</b>	Results of EPMA (major and minor elements in wt.%) and LA-ICP-MS (trace elements in ppm) analysis for analyzed mineral phases
<b>Electronic Appendix eA1</b>	Detailed coordinates of logged drill hole sections from the Ming deposit
<b>Electronic Appendix eA2</b>	Stratigraphic sections of logged drill holes from the Ming deposit
<b>Electronic Appendix eA3</b>	Detailed mineralogy of sulfide samples from the Ming deposit based on RL and partly SEM observations
<b>Electronic Appendix eA4</b>	Compilation of methods applied to sulfide samples from all orebodies of the Ming deposit
<b>Electronic Appendix eA5</b>	Detailed results of EPMA (major and minor elements in wt.%) and LA-ICP-MS (trace elements in ppm) analysis for analyzed mineral phases of sulfides from the Ming deposit.

## **CO-AUTHORSHIP STATEMENT**

The manuscript presented in chapter 2 entitled “Stratigraphy, mineralogy, geochemistry, and genesis of the Au-rich volcanogenic massive sulfide (VMS) system from the Baie Verte Peninsula, NW Newfoundland, Canada: The 1806 Zone as an example from the Ming mine, Rambler camp” was published on pages 899-911 in World Gold 2011 - Proceedings of the 50<sup>th</sup> Annual Conference of Metallurgists of CIM, Montreal, QC, Canada, edited by Guy Deschênes, Roussos Dimitrakopoulos, and Jocelyn Bouchard. The paper is co-authored by Stephen J. Piercey and Paul J. Sylvester (Memorial University of Newfoundland), Larry Pilgrim, Stephanie Maloney, Darrell Hyde, and George Ogilvie (Rambler Metals & Mining Canada Ltd). As first author, I formulated the majority of research questions and conclusions, and undertook literature review, sample collection, data analysis and interpretation. The co-authors helped to formulate and shape ideas in the paper, provided guidance for data collection and interpretation, and played an important role editorially. The manuscript was written and submitted by me.

The manuscript presented as Chapter 3 entitled “Evidence for syngenetic precious metal enrichment in an Appalachian Volcanogenic Massive Sulfide (VMS) System: The 1806 Zone, Ming Mine, Newfoundland, Canada” has been published in the journal Economic Geology (2014), volume 109, pages 1611-1642. The paper is co-authored by Stephen J. Piercey and Paul J. Sylvester (Memorial University of Newfoundland), Stephanie Maloney (former Rambler

Metals & Mining Canada Ltd, now Vale, Voisey's Bay Mine Site), and Larry Pilgrim (Rambler Metals & Mining Canada Ltd). As first author, I formulated the majority of research questions and conclusions, and undertook literature review, sample collection, data analysis and interpretation. The co-authors helped to formulate and shape ideas in the paper, provided guidance for data collection and interpretation, and played an important role editorially. The manuscript was written and submitted by me.

The manuscript presented as Chapter 4 entitled "Variations of sulfur isotope signatures in sulfides from the metamorphosed Ming Cu(-Au) volcanogenic massive sulfide deposit, Newfoundland Appalachians, Canada" has been published in the journal *Mineralium Deposita* (2015), volume 50, pages 619-640. The paper is co-authored by Stephen J. Piercey, Graham D. Layne (Memorial University of Newfoundland), Paul J. Sylvester (former Memorial University of Newfoundland, now Texas Tech University), and Glenn Piercey (Memorial University of Newfoundland). As first author, I formulated the majority of research questions and conclusions, and undertook literature review, sample collection, data analysis and interpretation. The co-authors helped to formulate and shape ideas in the paper, provided guidance for data collection and interpretation, and played an important role editorially. The manuscript was written and submitted by me.

The manuscript presented as Chapter 5 entitled "Mineralogy and mineral chemistry of the metamorphosed and precious metal-bearing Ming deposit,

Canada” has been published in the journal *Ore Geology Reviews* (2016), volume 72, pages 914-939. The paper is co-authored by Stephen J. Piercey, Jean-Luc Pilote, Graham D. Layne (Memorial University of Newfoundland), and Paul J. Sylvester (Texas Tech University). As first author, I formulated the majority of research questions and conclusions, and undertook literature review, sample collection, data analysis and interpretation. The co-authors helped to formulate and shape ideas in the paper, provided guidance for data collection and interpretation, and played an important role editorially. The manuscript was written and submitted by me.

## CHAPTER 1

## 1-1 INTRODUCTION AND OVERVIEW

Volcanogenic massive sulfide (VMS) deposits form on or below the seafloor by acidic to near neutral, reduced to weakly oxidized hydrothermal fluids of varying temperatures ( $T \approx 200\text{--}400^\circ\text{C}$ ; Franklin et al., 1981; Large, 1992; Ohmoto, 1996). These fluids can transport semi-metals and metals resulting in the deposition of common commodities Cu, Zn, and/or Pb and sometimes additional metals, such as Au, Ag, Bi, Se, and others, at economic concentrations (Franklin et al., 1981; Franklin, 1993, 1996; Galley et al., 2007). Volcanogenic massive sulfide deposits are formed in various tectonic settings (arcs, rifts, seamounts) and have formed from Archean to present (Franklin et al., 1981; Franklin, 1993, 1996; Hannington et al., 1995; Herzig and Hannington, 1995; Huston et al., 2010). Their modern analogues are black, grey, and white smokers on the modern seafloor (Hannington et al., 1995, 2005; Galley et al., 2007).

Auriferous or Au-rich VMS deposits are one subclass of VMS deposits. Mercier-Langevin et al. (2011) classified VMS deposits with more than 3.46g/t Au as auriferous, whereas VMS deposits with more than 3.46g/t Au and 31t Au are Au-rich. However, many VMS deposits worldwide have Au grades between 1.00-3.46g/t and Au has been mined as important byproduct from these precious metal-bearing VMS deposits (Franklin et al., 2005; Mosier et al., 2009). Therefore, the enrichment of Au in VMS deposits is economically important, although Au grade and tonnage may not classify them as either auriferous or Au-rich.

The genesis of precious metal-bearing VMS deposits has been highly debated especially when the deposit has been metamorphosed and/or is enriched in elements of the epithermal suite (As, Bi, Hg, Sb, Se, Sn, Tl; Tourigny et al., 1989, 1993; Larocque et al., 1993; Bergman-Weihed et al., 1996; Sillitoe et al., 1996; Mercier-Langevin et al., 2007, 2013, 2015). Of particular interest has been the relative timing of precious metal enrichment, specifically when it occurred in association with base metal deposition (syngenetic), with an epigenetic metal input due to the overprint of younger (epithermal or intrusion-related) systems or with later metamorphic fluids (synorogenic). Moreover, the physico-chemical conditions ( $T$ ,  $pH$ ,  $fO_2$ ,  $fS_2$ ) of the hydrothermal fluid during metal transport and deposition, and possible magmatic contributions to the hydrothermal fluid, have been of particular interest to researchers (Lydon, 1988; Hannington and Scott, 1989; Large, 1992; Ohmoto, 1996; Sillitoe et al., 1996).

In recent years, field observations, standard reflected light microscopy, and whole rock geochemistry on mineralized samples have been complemented by scanning electron microscopy (SEM) and/or high-precision micro-analytical techniques including secondary ion mass spectrometry (SIMS), electron microprobe analysis (EPMA), and/or laser ablation inductively coupled plasma mass spectrometry (LA-ICP-MS) to determine: (1) detailed ore mineral assemblages; (2) syngenetic and synorogenic textures; (3) origin of sulfur, and semi- and other metals including Au, Ag, and elements of the epithermal suite; and (4) the detailed mineral chemistry of ore minerals in order to reveal the

formation history of precious metal-bearing VMS deposits (e.g., Huston et al., 1995; Butler and Nesbitt, 1999; Törmänen and Koski, 2005; Wagner et al., 2007; Maslennikov et al., 2009; McClenaghan et al., 2009). However, these micro-analytical techniques have been applied commonly only to pyrite, chalcopyrite, and/or sphalerite, whereas other ore minerals including sulfosalts and precious metals have not been measured, although sulfosalts and precious metals can provide a more detailed picture of the hydrothermal fluid conditions during deposition due to their elevated concentration in elements of the epithermal suite and precious metals. These elements are often much more sensitive to changes in hydrothermal fluid conditions than Cu, Zn, and/or Pb and indicate that other chemical parameters ( $f\text{Te}_2/f\text{S}_2$ ,  $f\text{Se}_2/f\text{S}_2$ ,  $m_{\text{Bi}}$ ,  $m_{\text{Sb}}$ ) of the hydrothermal ore fluid that are also of importance (Afifi et al., 1988a, b; Huston et al., 1995, 1996; Simon and Essene, 1996; Seward and Barnes, 1997; Simon et al., 1997).

A critical review of the different formational aspects of metamorphosed and deformed, precious metal-bearing VMS deposits is briefly given below. Each of these aspects was further investigated in this thesis and the results are presented in the manuscripts in the following chapters.



## **1-2 RELATIVE TIMING OF PRECIOUS METAL ENRICHMENT IN METAMORPHOSED AND DEFORMED VOLCANOGENIC MASSIVE SULFIDE DEPOSITS**

Ancient precious metal-bearing VMS deposits are often metamorphosed and deformed, which usually obscures primary depositional features and relationships that illustrate the timing of precious metal enrichment. Moreover, metamorphosed precious metal-bearing VMS deposits have often Au±Cu veins (Marquis et al., 1990; Tourigny et al., 1989; 1993; Mercier-Langevin et al., 2007), show remobilization of Au±Ag (Laroque et al., 1993), and/or are in close vicinity to orogenic Au deposits (Evans and Wells, 1998; Evans, 2004; Skulski et al., 2009). All these features make it difficult to establish the relative timing of precious metal emplacement (i.e., syngenetic, epigenetic or synorogenic). Tourigny et al. (1993) and Laroque et al. (1993) showed that Au is likely to be deposited syngenetically in metamorphosed VMS deposits despite showing metamorphic features such as Au-Cu veins (Tourigny et al., 1993) or precious metal remobilization (Laroque et al., 1993). These studies showed that precious metals could be remobilized internally by metamorphic fluids but originated from within the semi-massive to massive sulfides of the VMS deposit. Hence, metamorphism and deformation refined VMS deposits internally. Nevertheless, post-genetic metamorphism and deformation hinder constraining the timing of precious metal emplacement and detailed textural, mineralogical, and micro-analytical investigations are required to distinguish between syngenetic and

synorogenic precious metal emplacement in metamorphosed, precious metal-bearing VMS deposits.

Despite metamorphism and deformation, distinct features typical of auriferous and Au-rich VMS deposits are often lacking in precious metal-bearing VMS deposits and make determination of the correct timing of precious metal emplacement difficult. For instance, auriferous and Au-rich VMS deposits are usually close to felsic intrusive or felsic volcanic rocks, show advanced argillic style alteration, are associated with a complex sulfide mineralogy, and are enriched in elements of the epithermal suite (Sillitoe et al., 1996; Dubé et al., 2007; Galley et al., 2007; Hannington et al., 1999a). In contrast, precious metal-bearing VMS deposits usually have features of both base metal and auriferous/Au-rich VMS deposits. For instance, felsic volcanic rocks and a complex ore mineralogy enriched in elements of the epithermal suite are common for precious metal-bearing VMS deposits, whereas advanced argillic style alteration is often not developed and rather propylitic or sericitic and chloritic alteration of the felsic footwall is observed (Large, 1992; Larocque et al., 1993). Therefore, relative timing of precious metal emplacement in metamorphosed, precious metal-bearing VMS deposits can only be constrained by careful examination of field relationships, mineral assemblages, mineral textures, and mineral chemistry of ore and/or alteration minerals. Moreover, each metamorphosed, precious metal-bearing VMS deposit has to be investigated separately to determine the relative timing of precious metal emplacement,

because features vary between deposits and even within one mineral district (Large, 1992; Hannington et al., 1999a; Galley et al., 2007).

### **1-3 SULFUR ISOTOPE COMPOSITION OF SULFIDES AS POSSIBLE INDICATOR FOR THE SOURCE OF SULFUR**

Among stable isotope systems, sulfur isotopes are the predominant system applied to hydrothermal ore deposits (Huston, 1999), because sulfur is a major component of most ore minerals and sulfur isotopes allow constraining possible sources of sulfur (Ohmoto and Rye, 1979; Ohmoto and Goldhaber, 1997; Seal, 2006). Determining possible sources of sulfur in VMS deposits gives indications regarding the formation of semi-massive to massive sulfides and sulfide stringers in VMS deposits.

In general, four different sulfur sources can be distinguished: (1) seawater; (2) sulfur leached from igneous wall rocks and/or from magmatic fluids originated from subvolcanic magma chambers; (3) metamorphic fluids, and (4) sulfur reduced by bacterial activity in reduced sediments (Claypool et al., 1980; Shanks et al., 1995; Goodfellow and Peter, 1996; Ohmoto and Goldhaber 1997; Gemmell and Sharpe 1998; Canfield 2001; Shanks 2001; Kampschulte and Strauss, 2004; Seal 2006; Hoefs, 2009). Constraining sulfur to one or more of these sources has genetic implications for the origin of the hydrothermal fluids responsible for the transport and deposition of semi-metals and metals in VMS deposits. Moreover, constraints on the source(s) of sulfur also give implications for possible sources

of semi-metals and metals and fluids in precious metal-bearing deposits and provide an important tool for understanding the genesis of VMS deposits.

Most studies have shown that reduced seawater sulfate is the dominant source for sulfur in Phanerozoic VMS deposits (Gemmell and Sharpe, 1998; Huston, 1999). However, contributions from wall rock, magmatic fluids and/or metamorphic fluids and/or reduced sediments are often additional sulfur sources in some ore deposits, including VMS deposits (Goodfellow and Peter, 1996; Alt and Shanks, 2011). Distinguishing between these additional sources is difficult, because sulfur isotopic compositions of igneous wall rock, magmatic fluid and metamorphic fluid often are very similar (Hoefs, 2009).

Metamorphism can complicate the identification of sulfur sources in metamorphosed VMS deposits. However, the influence of metamorphic fluids can be constrained by determining whether isotopic equilibrium was attained during metamorphism or not. Isotopic equilibrium between neighboring phases is discussed in literature (Crowe, 1994; Bailie et al., 2010). Kinetic investigations suggest that isotopic equilibrium is rarely reached during both deposition and greenschist to amphibolite facies metamorphism (Ohmoto and Goldhaber, 1997; Wagner et al., 2004; Seal, 2006). Geothermometry often is applied to neighboring phases in order to constrain formation and/or metamorphism temperature; however, results show that isotope equilibrium is often insufficient, especially in moderately metamorphosed deposits, which give ambiguous temperatures for both deposition and metamorphism (Bailie et al., 2010). Hence, isotopic

equilibration in metamorphosed VMS deposits must be carefully examined before geothermometry is attempted for neighboring mineral pairs.

Despite the fact that reduced seawater sulfate is the predominant source of sulfur in VMS deposits, Huston (1999) showed that low positive  $\delta^{34}\text{S}$  values in sulfides also indicate possible sulfur contributions from igneous wall rock and/or magmatic fluids; however, distinguishing between both without further tools is extremely difficult. Nevertheless, isotopic sulfur compositions of various sulfides in (metamorphosed) VMS deposits provide an important insight into the genesis of VMS formation. Moreover, a detailed, *in situ* investigation of isotopic sulfur composition in various sulfides is a preferable approach to constrain sulfur sources and to determine if isotopic re-equilibration took place during greenschist/amphibolite facies metamorphism. Determining the sulfur isotopic composition of individual sulfides gives much more detailed information regarding the sulfur source(s) and possible metamorphic effects on sulfide minerals than  $\delta^{34}\text{S}$  values of mineral separates, because the latter are often heterogeneous giving a range of  $\delta^{34}\text{S}$  values that represent multiple phases rather than solely the phases of interest.

Another important aspect regarding the sulfur isotopic composition especially in minerals refers to the used analysis technique. Conventional and *in situ* techniques are both common (Bradshaw et al., 2008; Bailie et al., 2010); however, conventional techniques including gas chromatography and mass spectrometry demand mineral separation prior to analysis that is often time

consuming and/or involves hazardous materials (Seal, 2006). Moreover, spatial relations to neighboring minerals and grains are destroyed by these techniques. Therefore, *in situ* analyses are preferred especially if a high amount of samples and various mineral phases are analyzed. Laser  $\text{SF}_6$  and SIMS are both accepted methods for *in situ* sulfur isotope analysis (Seal, 2006). Advantages of *in situ* SIMS analyses are a relatively small crater size in the analyzed mineral phases that allows analyzing relatively small grains ( $<40\text{ }\mu\text{m}$ ) and avoids possible cracks and inclusions within the analyzed mineral. Additionally, *in situ* SIMS analyses have a high accuracy and precision and hence are a potentially powerful technique for *in situ* micro-analysis (Kozdon et al., 2010).

#### **1-4 METAL TRANSPORT, POSSIBLE METAL SOURCES, AND DEPOSITION MECHANISMS IN PRECIOUS METAL-BEARING VOLCANOGENIC MASSIVE SULFIDE DEPOSITS**

Copper, Zn and/or Pb are the main commodities in VMS deposits. Additionally, Ag, As, Au, Bi, Hg, In, Mo, Sb, Se, and Te and other semi-metals and metals can be important mineable commodities as well. Deposits enriched in precious metals (i.e., auriferous and Au-rich VMS deposits) typically have a diverse metal suite and complex ore mineralogy that often includes sulfosalts, antimonides, arsenides, selenides, and/or precious metals (Tourigny et al., 1989; Bergman Weihed et al., 1996 and references therein; Hannington et al., 1999a; Grammatikopoulos et al., 2005; Novoselov et al., 2006; Maslennikov et al., 2009). The transport and deposition of metals and semi-metals in VMS deposits is

predominantly controlled by: (1) physico-chemical hydrothermal fluid conditions (e.g., temperature, pH, redox state, and sulfidation state); (2) the interaction of the fluid with wall rock and/or ambient seawater; and (3) water depth (Lydon, 1988; Large, 1992; Franklin, 1993, 1996; Ohmoto, 1996; Seward and Barnes, 1997; Hannington et al., 1999a; Galley et al., 2007; Monecke et al., 2014). Hence, an understanding of metal solubility, metal transport in hydrothermal fluids and metal deposition mechanisms is essential for understanding the formation of VMS deposits.

Volcanogenic massive sulfide deposits are regulated by a magmatic heat source (i.e., magma chamber, subvolcanic intrusion) within oceanic or continental crust and work as a (magmatic-)hydrothermal plumbing system on and just below the seafloor (Franklin et al., 1981; Franklin, 1993, 1996). Hydrothermal fluids are generated predominantly from cold seawater entering the crust via fractures and faults, which are steadily heated as they circulate through the crust. During this heating and circulation the hydrothermal fluids react with the wall rock altering both the composition of the wall rock and the hydrothermal fluids, with attendant changes in intensive variables of the hydrothermal fluid ( $T$ ,  $pH$ ,  $fO_2$ ,  $fS_2$ ; Mottl and Holland, 1978; Mottl et al., 1979; Bischoff and Rosenbauer, 1983; Seyfried et al., 1999). During fluid-rock interaction, semi-metals and metals are leached from the wall rock and subsequently transported in the hydrothermal fluid. Metal deposition eventually occurs when the hydrothermal fluids discharge on the

seafloor via vents and mix with cool ambient seawater (Lydon 1988; Large 1992; Ohmoto, 1996; Hannington et al., 1999a; Galley et al., 2007).

Although the general formation of VMS deposits is well understood (Hannington et al., 1986; Auclair et al., 1987; Fouquet et al., 1993, 1996; Herzig et al., 1993; Herzig and Hannington, 1995; Humphris and Tivey, 2000), many questions remain unanswered; particularly regarding how semi-metals and other metals are transported and which parameters control both their transport and deposition in VMS deposits. Studies have been focused especially on the main commodities Cu, Zn, and Pb, and precious metals Ag and Au, and the parameters controlling transport and deposition of these metals are well constrained (Seward, 1973, 1976; Lydon, 1988; Large, 1992; Gammons and Williams-Jones, 1995; Ohmoto 1996; Seward and Barnes, 1997; Stefánsson and Williams-Jones, 2003, 2004; Williams-Jones et al., 2009). However, ambiguities exist regarding how (aqueous state vs gaseous state) and as what complexes (chloro-, thio- and/or hydro-complex) semi-metals and other metals such as Sb, Bi, Te, Se, or Hg are transported (Varekamp and Buseck, 1984; Wood et al., 1987; Afifi et al., 1988a; Zhang and Spry, 1994; McPhail, 1995; Simon and Essene, 1996; Wood and Samson, 1998). Furthermore, intensive parameters controlling solubility, transport and deposition are often more complex and less understood compared to Cu, Zn, Pb, Ag, and Au. This is exacerbated by a lack of experimental studies for elements of the epithermal suite, results that are vague, and thermodynamic properties that vary between studies (Afifi et al., 1988a;



Barnes, 1979; Zhang and Spry, 1994; McPhail, 1995; Wood and Samson, 1998; Simon and Essene, 1996). Moreover, elements of the epithermal suite can form a wide range of ore minerals present in hydrothermal deposits and are often elevated trace components in base metal sulfides, which make constraining thermodynamic properties even more difficult. Therefore, constraining the physico-chemical conditions of hydrothermal fluids responsible for transport and deposition of semi-metals and metals found in precious metal-bearing and auriferous/Au-rich VMS deposits from thermodynamic calculations alone is very challenging and may result in inaccurate results.

In recent years, the application of high-resolution microscopy (SEM) and micro-analytical techniques such as LA-ICP-MS on ore minerals has provided insights into the formation of mineral assemblages in VMS deposits and the distribution of trace elements in mineral phases (Butler and Nesbitt, 1999; Törmänen and Koski, 2005; Wagner et al., 2007; Bradshaw et al., 2008; Maslennikov et al., 2009). These studies demonstrated that physico-chemical conditions for transport and deposition of semi-metals and metals in VMS deposits are complex. Although detailed mineralogical and micro-analytical studies on ore minerals provide a valid tool constraining metal transport and deposition conditions, such studies are restricted in number and only common sulfides (pyrite, chalcopyrite, sphalerite, pyrrhotite, arsenopyrite) have been analyzed. Hence, further investigations including sulfosalts and precious metals

are needed to further define physico-chemical conditions of hydrothermal fluids responsible for transport and deposition of semi-metals and other metals.

Another critical issue in precious metal-bearing VMS formation is the mechanism of deposition. In general, metal deposition occurs due to changes in the physio-chemical conditions of the hydrothermal fluid (Lydon, 1988; Large 1992; Ohmoto, 1996; Galley et al., 2007) caused by: (1) boiling; (2) mixing with ambient seawater; and/or (3) conductive cooling (Hannington et al., 1999a; Huston 2000; Galley et al., 2007). In the case of boiling, phase separation between the liquid and vapor phase occurs due to pressure release, whereas the hydrothermal fluids are ascending within the crust leading to deposition of precious metals (Bischoff and Rosenbauer, 1984; Butterfield et al., 1990). Boiling is controlled by water depth, temperature of the hydrothermal fluids, the salinity content, and volatile abundance of the fluids (Monecke et al., 2014). Despite the importance of boiling, evidence for this in ancient metamorphosed VMS deposits is often difficult to establish. Mixing of hydrothermal fluids with ambient seawater on the seafloor also has pronounced effect on metal deposition due to rapid and drastic changes in T, pH, redox and sulfidation state of the hydrothermal fluid (Lydon, 1988; Large, 1992; Ohmoto, 1996; Galley et al., 2007). In contrast, conductive cooling of hydrothermal fluids due to water-rock interaction is less effective on metal precipitation and locally restricted to the direct interface between cooler wall rock and hotter hydrothermal fluid (Haymon and Kastner, 1983).

Distinguishing in particular between boiling and mixing with ambient seawater as dominant deposition mechanism is a challenging task in metamorphosed and deformed, and precious metal-bearing VMS deposits.

## **1-5 OBJECTIVES OF THIS STUDY**

This thesis addresses three important aspects of the genesis of metamorphosed, precious metal-bearing VMS deposits, including: (1) the relative timing of precious metal emplacement; (2) the origin of sulfur in different sulfides; and (3) the physico-chemical conditions of hydrothermal fluids that were responsible for metal transport and precipitation. The latter aspect also addressed changes in the physico-chemical conditions of the circulating and ascending hydrothermal fluids due to interaction with wall rock, seawater and possible magmatic volatiles/fluids.

The Cambro-Ordovician, bimodal mafic, precious metal-bearing Cu VMS Ming deposit, Newfoundland Appalachians, Canada, was chosen as study site because: (1) the Ming deposit is metamorphosed to upper greenschist/lower amphibolite facies and located in close vicinity to Silurian-Devonian orogenic Au deposits; (2) the Ming deposit has a complex mineral assemblage consisting of a variety of metal sulfides, sulfosalts, and precious metals and shares characteristics observed in epithermal Au deposits such as the occurrence of tellurides and selenides; and (3) the different, but spatially associated orebodies of the Ming deposit show mineralogical and compositional variations.

In order to constrain the genesis of the Ming deposit, field observations of the distribution of ore types and their host rocks from drill core logging and underground mapping were combined with reflected light microscopy, geochemistry on mineralized samples and with micro-analytical techniques including SEM, SIMS, EPMA, and LA-ICP-MS on different ore minerals. Combining classic techniques with cutting edge analytical methods were used to: (1) distinguish between syn-genetic and epi-genetic textures particularly for precious metals; (2) constrain sources of sulfur, semi-metals and other metals; and (3) constrain the physico-chemical conditions of the hydrothermal fluids that formed the Ming deposit. Answering these questions has implications for other ancient, metamorphosed, precious metal-bearing VMS deposits worldwide.

## **1-6 THESIS STRUCTURE**

This thesis is divided into six chapters. The first chapter provides the theoretical background to the thesis and outlines the main problems to be solved.

The second and third chapters focus on the 1806 Zone, which is enriched in Au. The second chapter gives a general geologic overview regarding stratigraphy, petrography of the footwall, and alteration of the 1806 Zone. It provides observations that are not discussed in detail in chapter three, but which are nevertheless important regarding the geology of the 1806 Zone. The third chapter is much more detailed in its mineralogical and chemical observations. In the third chapter, the Au-enriched 1806 Zone of the Ming deposit is used to understand the relative timing and mechanisms of precious metal emplacement

at the Ming deposit and addresses the question of whether gold enrichment in the deposit had a syngenetic or synorogenic origin (Tourigny et al., 1989, 1993; Marquis et al., 1990; Larocque et al., 1993; Evans and Wells, 1998; Evans, 2004). Stratigraphic, mineralogical, and micro-analytical results are obtained and the effects of both syngenetic and subsequent metamorphism on the occurrence of precious metals in the 1806 Zone are addressed. The results provide further constraints on processes that are responsible for precious metal emplacement in metamorphosed VMS deposits worldwide.

In the fourth chapter, the results of detailed sulfur isotope analyses of various sulfides from the Ming deposit are presented. Sulfur isotopes from sulfides are widely used to determine possible sulfur sources in hydrothermal deposits (Ohmoto and Rye, 1979; Ohmoto and Goldhaber, 1997; Huston, 1999; Seal, 2006). In this chapter, *in situ* SIMS analyses on pyrite, chalcopyrite, pyrrhotite, galena, and arsenopyrite provide a detailed picture about isotopic variations within the Ming deposit. The results of these *in situ* SIMS analyses are critically discussed with regard to possible sulfur sources of the Ming deposit and limitations to the application of sulfide mineral geothermometry in hydrothermal systems that were also metamorphosed and deformed.

The fifth chapter combines detailed mineralogical and geochemical data for the mineralized samples, including EPMA and LA-ICP-MS analysis of ore minerals from all orebodies of the Ming deposit to constrain the genesis of the deposit. Particular focus is on the hydrothermal fluid conditions and sources of

semi-metals and other metals (wall rock, seawater, subvolcanic intrusion) in the Ming deposit. The results are critically discussed in the context of implications for other metamorphosed and precious metal-bearing VMS deposits worldwide.

Conclusions are summarized in chapter 6. The last chapter also addresses suggestions for further research. An electronic Appendix containing additional data including detailed micro-analytical data, coordinates and stratigraphy of logged drill cores, and detailed mineralogical observations accompany the thesis.

## References

- Afifi AM, Kelly WC, Essene EJ (1988a) Phase relations among tellurides, sulfides, and oxides: I. Thermochemical data and calculated equilibria *Economic Geology* 83:377-394 doi:10.2113/gsecongeo.83.2.377
- Afifi AM, Kelly WC, Essene EJ (1988b) Phase relations among tellurides, sulfides, and oxides: Part II. Applications to telluride-bearing ore deposits *Economic Geology* 83:395-404 doi:10.2113/gsecongeo.83.2.395
- Alt JC, Shanks WC (2011) Microbial sulfate reduction and the sulfur budget for a complete section of altered oceanic basalts, IODP Hole 1256D (eastern Pacific). *Earth and Planetary Science Letters* 310:73-83. doi: 10.1016/j.epsl.2011.07.027.
- Auclair G, Fouquet Y (1987) Distribution of selenium in high-temperature hydrothermal sulfide deposits at 13° North, East Pacific Rise *Canadian Mineralogist* 25:577-587
- Bailie R, Gutzmer J, Strauss H, Stüeken E, McClung C (2010) Sulfur isotope characteristics of metamorphosed Zn–Cu volcanogenic massive sulfides in the Areachap Group, Northern Cape Province, South Africa *Mineralium Deposita* 45:481-496 doi:10.1007/s00126-010-0285-8
- Barnes HL (1979) Solubilities of ore minerals. In: Barnes HL (ed) *Geochemistry of hydrothermal ore deposits*, 2<sup>nd</sup> edn. John Wiley & Sons, pp 404-460
- Bergman-Weiher J, Bergström U, Billström K, Weiher P (1996) Geology, tectonic setting, and origin of the Paleoproterozoic Boliden Au-Cu-As

- deposit, Skellefte district, northern Sweden *Economic Geology* 91:1073-1097
- Bischoff JL, Rosenbauer RJ (1983) A note on the chemistry of seawater in the range 350°–500°C *Geochimica et Cosmochimica Acta* 47:139-144
- Bischoff JL, Rosenbauer RJ (1984) The critical point and two-phase boundary of seawater, 200–500°C *Earth and Planetary Science Letters* 68:172-180
- Bradshaw GD, Rowins SM, Peter JM, Taylor BE (2008) Genesis of the Wolverine volcanic sediment-hosted massive sulfide deposit, Finlayson Lake District, Yukon, Canada: Mineralogical, mineral chemical, fluid inclusion, and sulfur isotope evidence *Economic Geology* 103:35-60
- Butler IB, Nesbitt RW (1999) Trace element distributions in the chalcopyrite wall of a black smoker chimney: Insights from laser ablation inductively coupled plasma mass spectrometry (LA-ICP-MS) *Earth and Planetary Science Letters* 167:335-345 doi:Doi 10.1016/S0012-821x(99)00038-2
- Butterfield DA, Massoth GJ, McDuff RE, Lupton JE, Lilley MD (1990) Geochemistry of hydrothermal fluids from axial seamount hydrothermal emissions study vent field, Juan de Fuca ridge: Subseafloor boiling and subsequent fluid-rock interaction *Journal of Geophysical Research* 95:12895-12921
- Canfield DE (2001) Biogeochemistry of sulfur isotopes. In: Valley JW, Cole, D.R. (ed) *Stable isotope geochemistry*, vol 43. *Reviews in Mineralogy and Geochemistry*. pp 607-636
- Claypool GE, Holser WT, Kaplan IR, Sakai H, Zak I (1980) The age curves of sulfur and oxygen isotopes in marine sulfate and their mutual interpretation *Chemical Geology* 28:199-260
- Crowe DE (1994) Preservation of original hydrothermal  $\delta^{34}\text{S}$  values in greenschist to upper amphibolite volcanogenic massive sulfide deposits *Geology* 22
- Dubé B, Gosselin P, Mercier-Langevin P, Hannington M, Galley A (2007) Gold-rich volcanogenic massive sulphide deposits. In: Goodfellow WD (ed) *Mineral deposits of Canada: A synthesis of major deposit-types, district metallogeny, the evolution of geological provinces, and exploration methods*, vol Special Publication No. 5. Geological Association of Canada, Mineral Deposits Division, pp 75-94

- Eldridge CS, Barton Jr. PB, Ohmoto H (1983) Mineral textures and their bearing on formation of the Kuroko orebodies. In: Ohmoto H (ed) The Kuroko and related massive sulfide deposits, vol 5. vol Economic Geology Monograph. Society of Economic Geologists, Boulder, CO, pp 241-281
- Evans DTW (2004) Epigenetic gold occurrences, Baie Verte Peninsula, (NTS 12H/09, 16 and 12I/01), Newfoundland vol Mineral Resource Report 11. Government of Newfoundland and Labrador, Department of Natural Resources, Geological Survey, St. John's, NL
- Evans DTW, Wells C (1998) Epigenetic gold mineralization, Baie Verte Peninsula, Newfoundland Current Research Newfoundland Department of Mines and Energy, Geological Survey Report 98-1:39-51
- Fouquet Y, von Stackelberg U, Charlou JL, Erzinger J, Herzig PM, Muehe R, Wiedicke M (1993) Metallogenesis in back-arc environments: The Lau Basin example Economic Geology 88:2154-2181 doi:10.2113/gsecongeo.88.8.2154
- Fouquet Y, Knott R, Cambon P, Fallick A, Rickard D, Desbruyeres D (1996) Formation of large sulfide mineral deposits along fast spreading ridges. Example from off-axial deposits at 12°43' N on the East Pacific Rise Earth and Planetary Science Letters 144:147-162
- Franklin JM (1993) Volcanic-associated massive sulphide deposits. In: Kirkham RV, Sinclair WD, Thorpe RI, Duke JM (eds) Mineral Deposit Modeling. Geological Association of Canada, Special Paper 40, pp 315-334
- Franklin JM (1996) Volcanic-associated massive sulphide base metals. In: Eckstrand OR, Sinclair WD, Thorpe RI (eds) Geology of Canadian Mineral Deposit Types. Geological Survey of Canada, Geology of Canada Series no. 8, Ottawa, ON, pp 158-183
- Franklin JM, Lydon JW, Sangster DF (1981) Volcanic-associated sulfide deposits. In: Skinner BJ (ed) Economic Geology Seventy-Fifth Anniversary Volume. Society of Economic Geologists, pp 485-627
- Franklin JM, Gibson HL, Jonasson IR, Galley AG (2005) Volcanogenic massive sulfide deposits. In: Hedenquist JW, Thompson JFH, Goldfarb RJ, Richards JP (eds) Economic Geology 100th Anniversary Volume, 1905-2005. Society of Economic Geologists, pp 523-560
- Galley AG, Syme R, Bailes AH (2007) Metallogeny of the Paleoproterozoic Flin Flon Belt, Manitoba and Saskatchewan. In: Goodfellow WD (ed) Mineral deposits of Canada: A synthesis of major deposit-types, district



metallogeology, the evolution of geological provinces, and exploration methods, vol Special Publication No. 5. Geological Association of Canada, Mineral Deposits Division, pp 509-531

Gammons CH, Williams-Jones AE (1995) Hydrothermal geochemistry of electrum: Thermodynamic constraints *Economic Geology* 90:420-432

Gemmell JB, Sharpe R (1998) Detailed sulfur isotope investigation of the TAG hydrothermal mound and stockwork zone, 26° N, Mid-Atlantic Ridge. In: Herzig PM, Humphris SE, Miller DJ, Zierenberg RA (eds) *Proceedings of the Ocean Drilling Program, Scientific Results*, vol 158. College Station, TX, pp 71-84

Goodfellow WD, Peter JM (1996) Sulfur isotope composition of the Brunswick No. 12 massive sulphide deposit, Bathurst Mining Camp, New Brunswick: Implications for ambient environment, sulfur source, and ore genesis *Canadian Journal of Earth Sciences* 33:231-251

Grammatikopoulos TA, Roth T, Valeyev O (2005) Compositional variation in Hg-Ag-rich tetrahedrite from the polymetallic Eskay Creek deposit, British Columbia, Canada *Neues Jahrbuch Mineralogische Abhandlungen* 181:281-292 doi:10.1127/0077-7757/2005/0025

Hannington MD, Peter JM, Scott SD (1986) Gold in sea-floor polymetallic sulfide deposits *Economic Geology* 81:1867-1883

Hannington MD, Scott SD (1989) Sulfidation equilibria as guides to gold mineralization in volcanogenic massive sulfides: Evidence from sulfide mineralogy and the composition of sphalerite *Economic Geology* 84:1978-1995

Hannington MD, Jonasson IR, Herzig PM, Petersen S (1995) Physical and chemical processes of seafloor mineralization at mid-ocean ridges. In: Humphris SE, Zierenberg RA, Mullineaux LS, Thomson RE (eds) *Seafloor hydrothermal systems: Physical, chemical, biological, and geological interactions*, vol Geophysical Monograph 91. American Geophysical Union, Washington, DC, pp 115-157

Hannington MD, Poulsen KH, Thompson JFH, Sillitoe RH (1999a) Volcanogenic gold in the massive sulfide environment. In: Barrie CT, Hannington, M.D. (ed) *Volcanic-associated massive sulfide deposits: Processes and examples in modern and ancient settings*, vol 8. *Reviews in Economic Geology*. Society of Economic Geologists, Boulder, CO, pp 325-351

- Hannington MD, Bleeker W, Kjarsgaard I (1999b) Sulfide mineralogy, geochemistry, and ore genesis of the Kidd Creek deposit: Part II. The bornite zone. In: Hannington MD, Barrie, C.T. (ed) The Giant Kidd Creek volcanogenic massive sulfide deposit, western Abitibi Subprovince, Canada, vol 10. Economic Geology Monograph. Society of Economic Geologists, Boulder, CO, pp 225-266
- Hannington MD, De Ronde CEJ, Petersen S (2005) Sea-floor tectonics and submarine hydrothermal systems. In: Hedenquist JW, Thompson, J.F.H., Goldfarb, R.J., Richards, J.P. (ed) Economic Geology 100th Anniversary Volume, 1905-2005. Society of Economic Geologists, pp 111-141
- Haymon RM (1983) Growth history of hydrothermal black smoker chimneys Nature 301:695-698 doi:Doi 10.1038/301695a0
- Haymon RM, Kastner M (1981) Hot spring deposits on the East Pacific Rise at 21°N: Preliminary description of mineralogy and genesis Earth and Planetary Science Letters 53:363-381
- Herzig PM, Hannington MD, Fouquet Y, von Stackelberg U, Petersen S (1993) Gold-rich polymetallic sulfides from the Lau back arc and implications for the geochemistry of gold in sea-floor hydrothermal systems of the Southwest Pacific Economic Geology 88:2182-2209 doi:10.2113/gsecongeo.88.8.2182
- Herzig PM, Hannington MD (1995) Polymetallic massive sulfides at the modern seafloor: A review Ore Geology Reviews 10:95-115
- Hoefs J (2009) Stable Isotope Geochemistry. 6th edn. Springer, Berlin, Heidelberg
- Humphris SE, Tivey MK (2000) A synthesis of geological and geochemical investigations of the TAG hydrothermal field: Insights into fluid-flow and mixing processes in a hydrothermal system. In: Dilck Y, Moores, E.M., Elthon, D., Nicolas, A. (ed) Ophiolites and oceanic crust: New insights from field studies and the Ocean Drilling Program. Geological Society of America. Special Paper 349, pp 213-235
- Huston DL (1999) Stable isotopes and their significance for understanding the genesis of volcanic-hosted massive sulfide deposits: A review. In: Barrie CT, Hannington, M.D. (ed) Volcanic-associated massive sulfide deposits: Processes and examples in modern and ancient settings, vol 8. Reviews in Economic Geology. Society of Economic Geologists, Boulder, CO, pp 157-179

- Huston DL (2000) Gold in volcanic-hosted massive sulfide deposits: Distribution, genesis, and exploration. In: Hagemann SG, Brown, P.E. (ed) Gold in 2000, vol 13. Reviews in Economic Geology. Society of Economic Geologists, Boulder, CO, pp 401-426
- Huston DL, Sie SH, Suter GF, Cooke DR, Both RA (1995) Trace elements in sulfide minerals from eastern Australian volcanic-hosted massive sulfide deposits: Part I: Proton microprobe analyses of pyrite, chalcopyrite, and sphalerite, and Part II: Selenium levels in pyrite: Comparison with  $\delta^{34}\text{S}$  values and implications for the source of sulfur in volcanogenic hydrothermal systems Economic Geology 90:1167-1196
- Huston DL, Jablonski W, Sie SH (1996) The distribution and mineral hosts of silver in eastern Australian volcanogenic massive sulfide deposits Canadian Mineralogist 34:529-546
- Huston DL, Pehrsson S, Eglington BM, Zaw K (2010) The geology and metallogeny of volcanic-hosted massive sulfide deposits: Variations through geologic time and with tectonic setting Economic Geology 105:571-591
- Kampschulte A, Strauss H (2004) The sulfur isotopic evolution of Phanerozoic seawater based on the analysis of structurally substituted sulfate in carbonates Chemical Geology 204:255-286 doi:10.1016/j.chemgeo.2003.11.013
- Kozdon R, Kita NT, Huberty JM, Fournelle JH, Johnson CA, Valley JW (2010) In situ sulfur isotope analysis of sulfide minerals by SIMS: Precision and accuracy, with application to geothermometry of ~3.5Ga Pilbara cherts Chemical Geology 243:243-253 doi:10.1016/j.chemgeo.2010.05.015
- Large RR (1992) Australian volcanic-hosted massive sulfide deposits: Features, styles, and genetic models Economic Geology 87:471-510
- Larocque ACL, Hodgson CJ, Lafleur P-J (1993) Gold distribution in the Moberly volcanic-associated massive sulfide deposit, Noranda, Quebec: A preliminary evaluation of the role of metamorphic remobilization Economic Geology 88:1443-1459
- Layton-Matthews D, Peter JM, Scott SD, Leybourne MI (2008) Distribution, mineralogy, and geochemistry of selenium in felsic volcanic-hosted massive sulfide deposits of the Finlayson Lake District, Yukon Territory, Canada Economic Geology 103:61-88 doi:10.2113/gsecongeo.103.1.61

- Lydon JW (1988) Volcanogenic massive sulphide deposits Part 2: Genetic models *Geoscience Canada* 15:43-65
- Marquis P, Hubert C, Brown AC, Rigg DM (1990) Overprinting of early, redistributed Fe and Pb-Zn mineralization by late stage Au-Ag-Cu deposition at the Dumagami mine, Bousquet district, Abitibi, Quebec *Canadian Journal of Earth Sciences* 27:1651-1671
- Maslennikov VV, Maslennikova SP, Large RR, Danyushevsky LV (2009) Study of trace element zonation in vent chimneys from the Silurian Yaman-Kasy volcanic-hosted massive sulfide deposit (southern Urals, Russia) using laser ablation-inductively coupled plasma mass spectrometry (LA-ICPMS) *Economic Geology* 104:1111-1141
- McClenaghan SH, Lentz DR, Martin J, Diegor WG (2009) Gold in the Brunswick No. 12 volcanogenic massive sulfide deposit, Bathurst Mining Camp, Canada: Evidence from bulk ore analysis and laser ablation ICP-MS data on sulfide phases *Mineralium Deposita* 44:523-557 doi:10.1007/s00126-009-0233-7
- McPhail DC (1995) Thermodynamic properties of aqueous tellurium species between 25 and 350°C *Geochimica et Cosmochimica Acta* 59:851-866
- Mercier-Langevin P, Dubé B, Lafrance B, Hannington M, Galley A, Moorhead J, Gosselin P (2007) Metallogeny of the Doyon-Bousquet-LaRonde mining camp, Abitibi greenstone belt, Quebec. In: Goodfellow WD (ed) *Mineral deposits of Canada: A synthesis of major deposit-types, district metallogeny, the evolution of geological provinces, and exploration methods*, vol Special Publication No. 5. Geological Association of Canada, Mineral Deposits Division, pp 673-701
- Mercier-Langevin P, Hannington MD, Dubé B, Bécu V (2011) The gold content of volcanogenic massive sulfide deposits *Mineralium Deposita* 46:509-539 doi:10.1007/s00126-010-0300-0
- Mercier-Langevin P, McNicoll V, Allen RL, Blight JHS, Dubé B (2013) The Boliden gold-rich volcanogenic massive sulphide deposit, Skellefte district, Sweden: new U-Pb age constraints and implications at deposit and district scale *Mineralium Deposita* 48:485-504
- Mercier-Langevin P, Hannington MD, Dubé B, Piercey SJ, Peter JM, Pehrsson SJ (2015) Precious metal enrichment processes in volcanogenic massive sulphide deposits — A summary of key features, with an emphasis on TGI-4 research contributions In: Peter JM, Mercier-Langevin P (eds)

Targeted Geoscience Initiative 4: Contributions to the Understanding of Volcanogenic Massive Sulphide Deposit Genesis and Exploration Methods Development. Geological Survey of Canada, pp 117-130

Monecke T, Petersen S, Hannington MD (2014) Constraints on water depth of massive sulfide formation: Evidence from modern seafloor hydrothermal systems in arc-related settings *Economic Geology* 109:2079-2101

Mosier DL, Berger VI, Singer DA (2009) Volcanogenic massive sulfide deposits of the world: Database and grade tonnage models.

Mottl MJ, Holland HD (1978) Chemical exchange during hydrothermal alteration of basalt by seawater – I. Experimental results for major and minor components of seawater *Geochimica et Cosmochimica Acta* 42:1103-1115

Mottl MJ, Holland HD, Corr RF (1979) Chemical exchange during hydrothermal alteration of basalt by seawater – II. Experimental results for Fe, Mn, and sulfur species *Geochimica et Cosmochimica Acta* 43:869-884

Novoselov KA, Belogub EV, Zaykov VV, Yakovleva VA (2006) Silver sulfotellurides from volcanic-hosted massive sulfide deposits in the Southern Urals *Mineralogy and Petrology* 87:327-349 doi:10.1007/s00710-006-0132-x

Ohmoto H (1996) Formation of volcanogenic massive sulfide deposits: The Kuroko perspective *Ore Geology Reviews* 10:135-177

Ohmoto H, Rye RO (1979) Isotopes of sulfur and carbon. In: Barnes HL (ed) *Geochemistry of hydrothermal ore deposits*, 2<sup>nd</sup> edn. John Wiley & Sons, New York, pp 509-567

Ohmoto H, Goldhaber MB (1997) Sulfur and carbon isotopes. In: Barnes HL (ed) *Geochemistry of hydrothermal ore deposits*, 3<sup>rd</sup> edn. John Wiley & Sons, New York, pp 517-611

Seal II RR (2006) Sulfur isotope geochemistry of sulfide minerals. In: Vaughan DJ (ed) *Sulfide mineralogy and geochemistry*, vol 61. *Reviews in Mineralogy and Geochemistry*. pp 633-677

Seward TM (1973) Thio complexes of gold and the transport of gold in hydrothermal ore solutions *Geochimica et Cosmochimica Acta* 37:379-399

- Seward TM (1976) The stability of chloride complexes of silver in hydrothermal solutions up to 350°C *Geochimica et Cosmochimica Acta* 40:1329-1341
- Seward TM, Barnes HL (1997) Metal transport by hydrothermal ore fluids. In: Barnes HL (ed) *Geochemistry of hydrothermal ore deposits*, 3<sup>rd</sup> edn. John Wiley & Sons, pp 435-486
- Shanks III WC (2001) Stable isotopes in seafloor hydrothermal systems: Vent fluids, hydrothermal deposits, hydrothermal alteration, and microbial processes. In: Valley JW, Cole, D.R. (ed) *Stable isotope geochemistry*, vol 43. *Reviews in Mineralogy and Geochemistry*. pp 469-525
- Shanks III WC, Böhlke JK, Seal II RR (1995) Stable isotopes in mid-ocean ridge hydrothermal systems: Interaction between fluids, minerals and organisms. In: Humphris SE, Zierenberg RA, Mullineaux LS, Thomson RE (eds) *Seafloor hydrothermal systems: Physical, chemical, biological, and geological interactions*, vol *Geophysical Monograph* 91. American Geophysical Union, Washington, DC, pp 194-221
- Sillitoe RH, Hannington MD, Thompson JFH (1996) High sulfidation deposits in the volcanogenic massive sulfide environment *Economic Geology* 91:204-212
- Simon G, Essene EJ (1996) Phase relations among selenides, sulfides, tellurides, and oxides; I, Thermodynamic properties and calculated equilibria *Economic Geology* 91:1183-1208 doi:10.2113/gsecongeo.91.7.1183
- Simon G, Kesler SE, Essene EJ (1997) Phase relations among selenides, tellurides, and oxides: II. Applications to selenide-bearing ore deposits *Economic Geology* 92:468-484 doi:10.2113/gsecongeo.92.4.468
- Skulski T, Castonguay S, van Staal C, Rogers N, McNicoll V, Kerr A, Escayola M (eds) (2009) Baie Verte Peninsula: An evolving geological story. Annual Field Trip, October 2-5, 2009. Geological Association of Canada, Newfoundland and Labrador Section, St. John's, NL
- Stefánsson A, Seward TM (2003) Experimental determination of the stability and stoichiometry of sulphide complexes of silver(I) in hydrothermal solutions to 400°C *Geochimica et Cosmochimica Acta* 67:1395-1413
- Stefánsson A, Seward TM (2004) Gold(I) complexing in aqueous sulphide solutions to 500°C at 500 bar *Geochimica et Cosmochimica Acta* 68:4121-4143 doi:10.1016/j.gca.2004.04.006

- Törmänen TO, Koski RA (2005) Gold enrichment and the Bi-Au association in pyrrhotite-rich massive sulfide deposits, Escanaba Trough, Southern Gorda Ridge Economic Geology 100:1135-1150 doi:10.2113/gsecongeo.100.6.1135
- Tourigny G, Brown AC, Hubert C, Crépeau R (1989) Syvolcanic and syntectonic gold mineralization at the Bousquet mine, Abitibi greenstone belt, Quebec Economic Geology 84:1875-1890
- Tourigny G, Doucet D, Bourget A (1993) Geology of the Bousquet 2 Mine: An example of a deformed, gold-bearing, polymetallic sulfide deposit Economic Geology 88:1578-1597
- Varekamp JC, Buseck PR (1984) The speciation of mercury in hydrothermal systems, with applications to ore deposition Geochimica et Cosmochimica Acta 48:177-185
- Wagner T, Boyce AJ, Jonsson E, Fallick AE (2004) Laser microprobe sulfur isotope analysis of arsenopyrite: Experimental calibration and application to the Boliden Au–Cu–As massive sulfide deposit Ore Geology Reviews 25:311-325
- Wagner T, Klemm R, Wenzel T, Mattsson B (2007) Direct evidence from laser-ablation–inductively coupled plasma–mass spectrometry analysis of invisible gold Geology 35:775-778
- Williams-Jones AE, Powell RJ, Migdisov AA (2009) Gold in solution Elements 5:281-287
- Wood SA, Crerar DA, Borcsik MA (1987) Solubility of the assemblage pyrite-pyrrhotite-magnetite-sphalerite-galena-gold-stibnite-bismuthinite-argentite-molybdenite in H<sub>2</sub>O–NaCl–CO<sub>2</sub> solutions from 200° to 350°C Economic Geology 82:1864-1887
- Wood SA, Samson IM (1998) Solubility of ore minerals and complexation of ore metals in hydrothermal solutions. In: Richards JP, Larson, P.B. (ed) Techniques in hydrothermal ore deposits geology, vol 10. Reviews in Economic Geology. Society of Economic Geologists, Boulder, CO, pp 33-80
- Zhang X, Spry PG (1994) Calculated stability of aqueous tellurium species, calaverite, and hessite at elevated temperatures Economic Geology 89:1152-1166

## CHAPTER 2

In:

Brueckner SM, Piercey SJ, Sylvester PJ, Pilgrim L, Maloney S, Hyde D, Ogilvie G  
(2011) Stratigraphy, mineralogy, geochemistry, and genesis of an Au-rich  
volcanogenic massive sulfide (VMS) system from the Baie Verte Peninsula, NW  
Newfoundland, Canada: The 1806 Zone as an example from the Ming Mine,  
Rambler Camp In: Deschênes G, Dimitrakopoulos R, Bouchard J (eds) World  
Gold 2011. Canadian Institute of Mining, Metallurgy and Petroleum, Montreal,  
QC, Canada, pp 899-911



**STRATIGRAPHY, MINERALOGY, GEOCHEMISTRY, AND GENESIS OF THE  
AU-RICH VOLCANOGENIC MASSIVE SULFIDE (VMS) SYSTEM FROM THE  
BAIE VERTE PENINSULA, NW NEWFOUNDLAND, CANADA: THE 1806  
ZONE AS AN EXAMPLE FROM THE MING MINE, RAMBLER CAMP**

SM Brueckner<sup>1</sup>, SJ Piercey<sup>1</sup>, PJ Sylvester<sup>1</sup>, L Pilgrim<sup>2</sup>, S Maloney<sup>2</sup>, D Hyde<sup>2</sup> and  
G Ogilvie<sup>2</sup>

*<sup>1</sup>Department of Earth Sciences, Memorial University of Newfoundland  
300 Prince Philip Drive, St. John's, NL, Canada, A1B 3X5*

*<sup>2</sup>Rambler Metals & Mining Canada Limited  
Route # 418, Ming's Bight Road, NL, Canada, A0K 3S0*

**ABSTRACT**

The 1806 Zone is part of a Au-rich volcanogenic massive sulfide deposit at the Rambler Camp on the Baie Verte Peninsula, northwestern Newfoundland, and is characterized by high Au grades (3.97g/t), relatively low Cu and Zn grades (0.60wt% Cu, 1.17wt% Zn), and moderate Ag grades (27.83g/t) at ca. 0.37Mt ore. Gold and Ag occur as electrum and different Ag varieties including AgHg±Au alloys, miargyrite, and pyrargyrite that occur often in close proximity to electrum. Additionally, Ag-, As-, Sb-, and Sn-bearing sulfosalts are frequently observed and usually close to electrum. These textural relations strongly favor a syngenetic/magmatic origin for the 1806 Zone, despite having a metamorphic overprint.

**Keywords** Au-rich VMS, syngenetic, magmatic volatiles, electrum, Ag-phases, sulfosalts, Rambler Camp, Newfoundland Appalachians

## **2-1 INTRODUCTION**

The 1806 Zone is one of four Cu-Au and minor Zn horizons at the formerly active Ming Mine, Rambler Camp, Newfoundland Appalachians. Measured and indicated resource for all four zones is 3.65Mt ores at 2.26wt.% Cu, 1.13g/t Au, 6.78g/t Ag, and 0.32wt.% Zn, where the 1806 Zone is most enriched in Au and Ag with 3.97g/t and 27.83g/t, respectively (Pilgrim, 2009). These data underline the status of the Rambler Camp as a world class Au-rich volcanogenic massive sulfide (VMS) deposit.

The Ming Mine, including the newly discovered Au-rich horizons, are classified as a bimodal-mafic VMS deposit affected by upper greenschist metamorphism and deformation (Tuach and Kennedy, 1978). Despite the long mining history, the genesis of this deposit and its Au-Ag--rich VMS deposits, in general, is still unresolved. Most controversial in literature are the timing of the precious metal enrichment and the influence of magmatic volatiles, and some workers favor an epigenetic origin with Au-Ag-enrichment due to later orogenic Au-Ag upgrading. This paper provides detailed stratigraphic, petrographic, mineralogical and geochemical data on the 1806 Zone and preliminary data strongly favor a syngenetic/magmatic genesis of the 1806 Zone and the Rambler Camp.

## **2-2 TECTONIC SETTING**

The Rambler Camp is located ca. 7.5km SE of the town Baie Verte on the Baie Verte Peninsula in northwestern Newfoundland. It comprises the formerly active Ming Main and Ming West Cu-Au mines and newly discovered Cu-Au and minor Zn mineralized horizons. These new horizons occur along strike and up and down plunge of Ming Main and are namely the 1806 Zone, 1807 Zone, Ming S up and down plunge of the Ming Mine (Fig. 2-1; Pilgrim, 2009). Geologically, Rambler is located in the Pacquet Harbour Group (PHG) in the Notre Dame Subzone of the Dunnage Zone in the Newfoundland Appalachians (Tuach and Kennedy, 1978; Hibbard, 1983; Castonguay et al., 2009; Skulski et al., 2009). The PHG is characterized by deformed and metamorphosed mafic to felsic volcanic and volcanoclastic rocks, and sedimentary rocks and is divided into the lower and upper portions (Castonguay et al., 2009; Skulski et al., 2009). The lower PHG contains boninite, pillowed basalt, tuff, lapilli tuff and tuff breccia, and a sequence that is commonly referred to as Rambler rhyolite. The Rambler rhyolite sequence consists of boninitic, quartz-phyric rhyodacite and felsic tuff and tuff breccia and is host to the VMS deposits of the group (Tuach and Kennedy, 1978; Hibbard, 1983; Castonguay et al., 2009; Skulski et al., 2009). Gabbroic dikes cut the lower PHG (Hibbard, 1983; Castonguay et al., 2009; Skulski et al., 2009). Uranium/Pb dating on zircons from the Rambler rhyolite revealed an early Ordovician age of 487Ma (unpublished data, V. McNicoll, 2008 in Castonguay et al., 2009; Skulski et al., 2009). The upper PHG is mainly

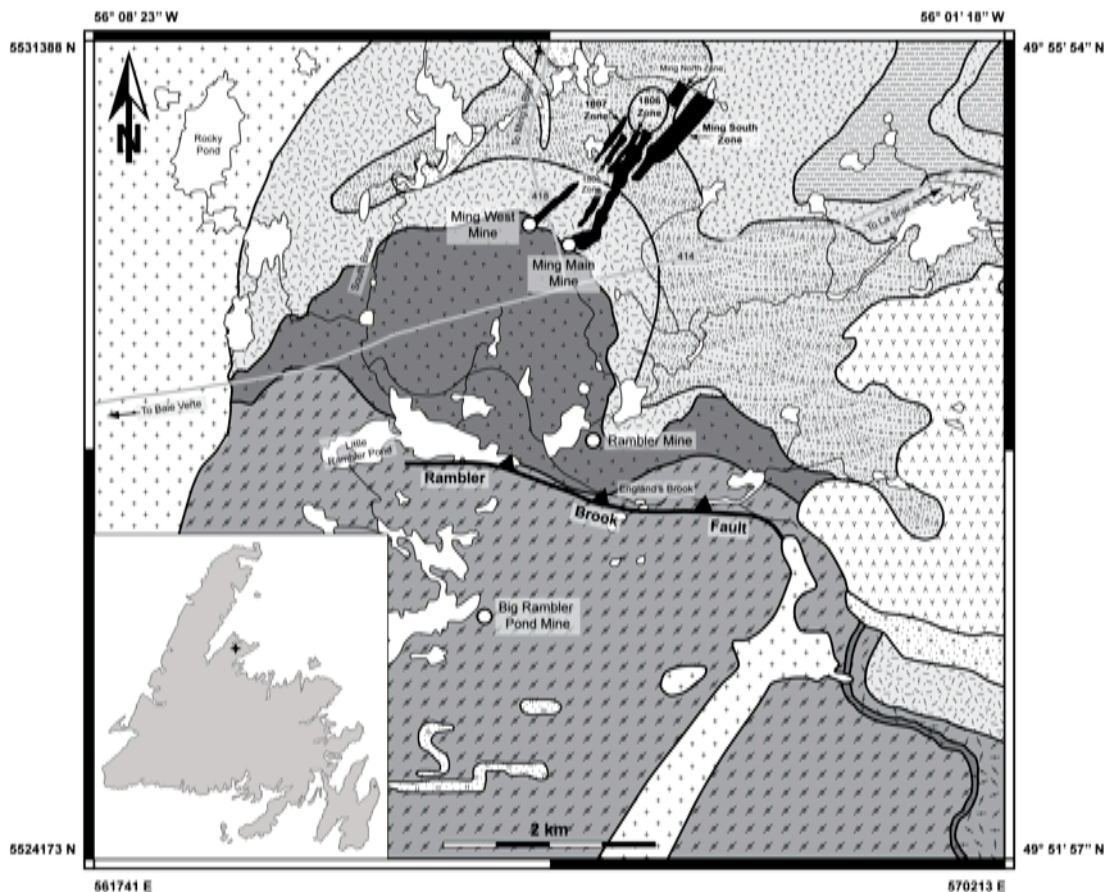
located NE of the Rambler deposit and consists of boninite, tholeiitic pillow basalt, felsic tuff, black chert and iron formation, and locally polymict conglomerate and breccia (Castonguay et al., 2009; Skulski et al., 2009). The age for the upper PHG is assumed to be younger than the lower PHG, but still of Ordovician age (Castonguay et al., 2009; Skulski et al., 2009). Several authors (Hibbard, 1983; Castonguay et al., 2009; Skulski et al., 2009) suggest a stratigraphic correlation between the rocks of the PHG and Ordovician volcanic and sedimentary rocks in the N and E of the Baie Verte Peninsula. However, sparse outcrops and Silurian intrusions make correlations between the rocks of the PHG in the center of the Baie Verte Peninsula with rocks in the N and E difficult. The Silurian intrusions occurring in the W and S of the PHG includes the Burlington Granodiorite (ca. 434-430Ma), and in the E of the PHG includes the Cape Brulé Porphyry (ca. 430Ma) and the early Silurian Cape St. John Group (Cawood et al., 1993).

The Baie Verte Peninsula is tectonically complex with four deformation events recognized (Tuach and Kennedy, 1978; Hibbard, 1983; Castonguay et al., 2009), with the most intense even being D<sub>2</sub> (Castonguay et al., 2009). This deformation event is also observed in the PHG and the Rambler rhyolite as an L>S fabric and N to NE dipping folds (Tuach and Kennedy, 1978; Hibbard, 1983; Castonguay et al., 2009). The same dipping direction is observed in the Rambler Brook Fault occurring S of the Rambler rhyolite and affecting the position of the stratigraphic units of the PHG including the sulfide mineralization horizons at the

Rambler Camp that dip ca. 32-35° to the NE (Tuach and Kennedy, 1978; Pilgrim, 2009). Deformation and metamorphism on the Baie Verte Peninsula generally increases from S to N, and the metamorphic grade changes from upper greenschist to lower amphibolite facies (Swinden and Kean, 1988; Castonguay et al., 2009).

## **2-3 METHODS**

From each drill core samples were taken usually at each meter for assay data with focus on the mineralized rhyolite. Analyses were undertaken initially at Eastern Analytical Ltd., Springdale, NL, with check and final assays undertaken at Activation Laboratories (ActLabs), Ancaster, ON. Assay data were obtained for Cu, Au, Zn, Pb, and in some cases for Ag. Gold and Ag were obtained using fire assay fusion, followed by acid digestion and finally atomic absorption spectrometry (AAS) for samples with Au contents <3g/t and Ag <0.1g/t., whereas higher grade samples had a gravimetric finish. Copper, Zn, and Pb were measured by acid digestion pre-preparation and an inductively couple plasma optical emission spectrometry (ICP-OES) finish. Data quality was checked by external reference materials and is outlined in detail in Pilgrim (2009).



#### Silurian Intrusions

- Cape Brulé Porphyry (430 Ma)**  
Porphyritic granodiorite, quartz-feldspar porphyry
- Burlington Granodiorite (434 - 430 Ma)**  
Granodiorite
- Cape St. John Group (early Silurian)**  
Rhyolitic and trachytic flows and tuffs, intrusives, locally mafic and intermediate tuffs and flows

**Highway and highway number**

**Mine location**

**Mineralization horizon**

**Underground shaft**

**Fault**

#### Ordovician rocks - Pacquet Harbour Group (PHG)

##### Upper PHG (Mid- to early Ordovician)

- Balsam Bud Cove Formation**  
Mafic epiclastic rocks, black shale
- Balsam Bud Cove Formation**  
Rhyolite (467 Ma), and felsic tuff (470 Ma)
- Venam's Bight Formation**  
Pillow basalt
- Bobby Cove Formation**  
Mafic tuff, epiclastic rocks, turbidites
- Scrape Point Formation**  
Pillow basalt, gabbro (483 Ma)

##### Lower PHG (Early Ordovician)

- Mt. Misery Formation**  
Rhyodacite, rhyolite massive flows, tuff breccia ('Rambler rhyolite'; 487 Ma)
- Mt. Misery Formation**  
Intermediate Ti-boninite, island arc tholeiitic pillow basalt, pillow breccia
- Betts Head Formation**  
Pillowed, aphyric, variolitic boninite
- Sheared gabbro**

**Figure 2-1.** (previous page) Geologic map of the studied area. Inlay in the lower right corner shows Newfoundland and the location of the map (star). The 1806 Zone of the Ming Mine is encircled. Coordinates are in WGS 84 (top and right) and UTM NAD83, Zone 21N (bottom and left); Modified after (Castonguay et al., 2009; Pilgrim, 2009) age data after (Cawood et al., 1993; Castonguay et al., 2009)

Polished thick sections (~200µm) were obtained on the ore and analyzed via scanned electron microscopy (SEM) at the INCO Innovation Center, St. John's, NL, for back scattered electron (BSE) images. Moreover, SEM was combined with semi-quantitative, energy dispersive X-ray (EDX) to detect concentration changes within ore phases. Therefore, an EDX scan was applied to a linear profile (i.e., line scan) within the thick section for 5min at 25kV detecting the intensity of the emission lines in percent for each analyzed element. Detection limits for the EDX system are nearly 1,000g/t and correlate with 4-5% intensity for the line scans.

## **2-4 STRATIGRAPHY, PETROGRAPHY, AND MINERALOGY**

### **2-4-1 STRATIGRAPHY**

The sulfide mineralization in the Rambler Camp, including the four newly discovered Cu-Au-minor Zn mineralization horizons, is associated with felsic volcanic and volcanoclastic rocks of rhyodacitic to rhyolitic composition (Fig. 2-2; Tuach and Kennedy, 1978; Castonguay et al., 2009; Skulski et al., 2010). This

felsic unit is commonly referred as Rambler rhyolite of the Mt. Misery Formation of the lower PHG. The mineralized rhyolite is often capped by a dm-thick silicified horizon, which also contains sulfide mineralization. This horizon is assumed to belong to the Mt. Misery Formation but has been affected by very strong silicification. The hanging wall is characterized by felsic and mafic tuffs and sedimentary rocks, which form together very often a turbidite sequence. These volcanic and sedimentary rocks including the turbidite are assumed to belong to the Bobby Cove Formation of the upper PHG. Pillowed basalts of the Scrape Point Formation are not observed in the drill core from the 1806 Zone and are probably diked out by fine and coarse-grained gabbroic dikes that cross-cut the stratigraphy, including the mineralized rhyolite. Moreover, thin light grey dikes of probably felsic composition occur within the rhyolite, but are not nearly as frequent as the much thicker mafic dikes.

#### *2-4-2 PETROGRAPHY*

##### *2-4-2-1 Rambler rhyolite with sulfide stringer and semi-massive to massive sulfide horizon*

Sulfide mineralization occurs as fine, mm- to several cm-thick stringers in rhyolitic volcanic and volcanoclastic rocks that range in color from bluish-grey, grey to greenish-grey. Massive flows are the dominant hosts to mineralization and are partly foliated and quartz-eye bearing and the rhyolites are variably deformed. The rhyolite flows often grade into jigsaw-fit breccias that further grade



into lapilli tuff, but these transitions are very difficult to recognize due to hydrothermal alteration; tuff breccia is present in rare cases. Where sulfide stringers are developed within clast-rich sections they occur around these clasts in an almost jigsaw-fit texture.

A 20 to 30cm thick, extremely silicified horizon very often caps the Rambler rhyolite. This unit is dominated by dirty, white to light grey quartz that contains sulfide that decreases in abundance with increasing distance from the contact with rhyolite. Often remnants of clasts can be found in this horizon, and it is assumed that this is strongly quartz altered rhyolite flow or lapilli tuff.

Sulfide phases occur most abundantly as stringers of various thickness (mm to cm) in massive rhyolitic flows or fine-grained rhyolitic tuffs to lapilli tuffs. Disseminated sulfides are rare in the sulfides but often developed within the mafic dikes. Semi-massive to massive sulfide horizons varying in thickness between a few cm and several dm are developed in the upper parts of the Rambler rhyolite and often capped by a mineralized, silicified horizon. In some cases, mafic dikes cut through the semi-massive and massive sulfide horizons. Macroscopically, pyrite, and lesser chalcopyrite and sphalerite are developed in the stringer and disseminated sulfides. The semi-massive and massive sulfide horizon is dominated by pyrite, chalcopyrite, sphalerite, pyrrhotite, galena, arsenopyrite, tetrahedrite-tennantite and in rare cases by electrum. Stringer and semi-massive to massive sulfide horizons are usually fine-grained, but pyrite porphyroblasts in pyrrhotite (i.e., buckshot texture) is present close to mafic dike

contacts within the semi-massive and massive sulfide horizons. Magnetite is the only observed oxide phase and occurs more often within the semi-massive to massive sulfide horizon in the down plunge of the 1806 Zone.

#### *2-4-2-2 Turbidite sequence*

The hanging wall turbiditic sequence in the Ming Mine is characterized by mafic and felsic tuffs to lapilli tuffs that alternate with fine, partly clast-bearing sedimentary rocks. The grain size changes gradually from coarser to fine-grained tuffs and sediments with increasing distance from the mineralized Rambler rhyolite. The coarser-grained parts are often clast-bearing with rock and mineral clasts that are often weakly elongated and mm-scale. Changes between tuffs and sedimentary rocks are transitional and not sharp. Bedding in the usually dark-colored turbiditic sequences is either weakly preserved or totally overprinted by fine foliation. Most commonly, the turbidites occur directly above the mineralized rhyolitic flows and tuffs in the hanging wall as several meter thick horizons. In more rare cases, fine-grained mafic tuff to lapilli tuff occurs in-between the rhyolite as a less than 5m thick horizon. The stratigraphic association of the tuff is not clear yet, but its correlation to the Bobby Cove Formation is strongly assumed and folding likely causes the intercalation within the Rambler rhyolite.

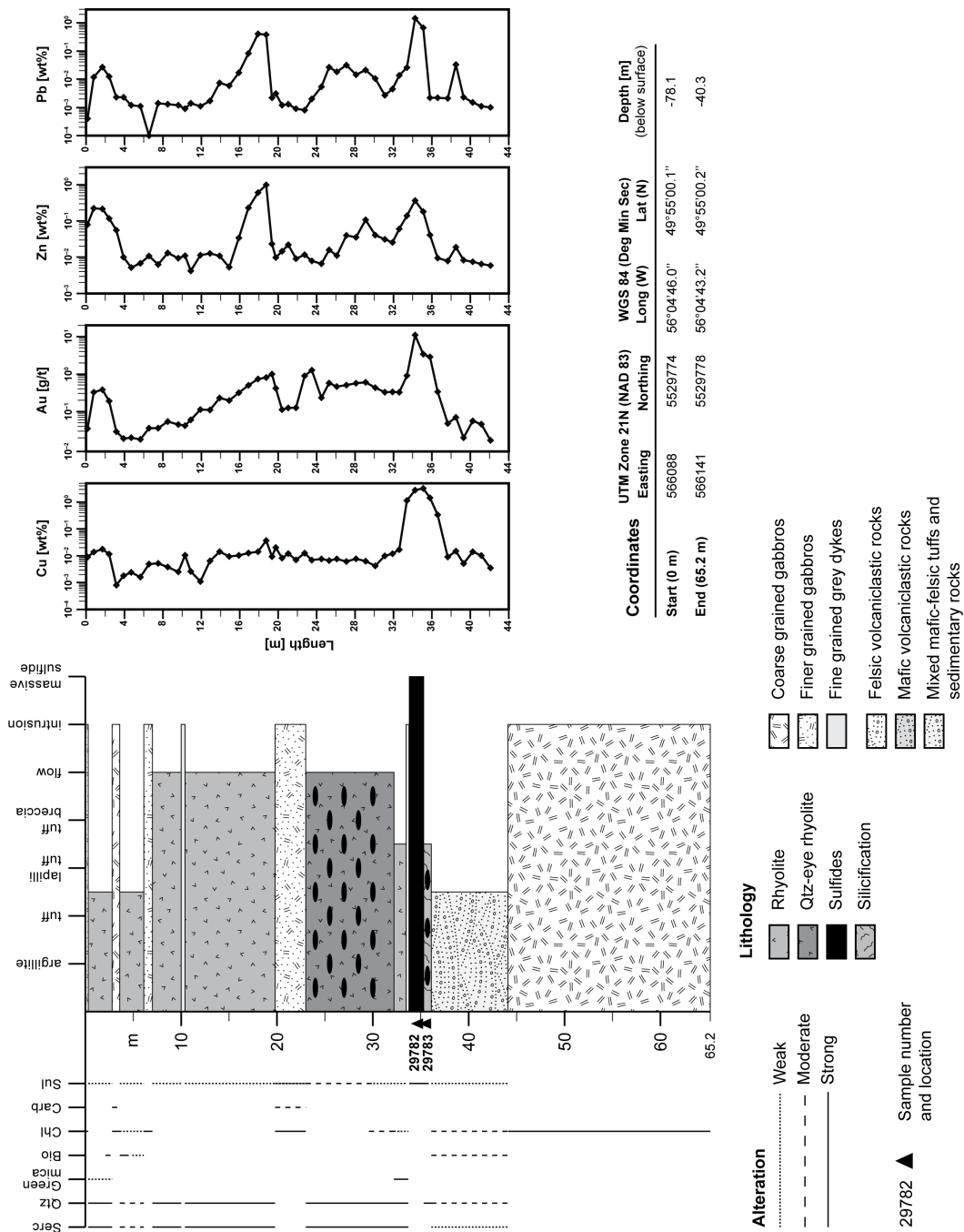
#### *2-4-2-3 Mafic dikes*

Fine- and coarse-grained mafic dikes of diabasic to gabbroic composition are very abundant and cut both the mineralized rhyolite and the hanging wall

sequence. These mafic dikes range widely in thickness from only a couple of decimeters to several decameters; thicknesses of <10m are most abundant. The dikes have sharp, variably chilled margins and show variations in grain size. Chilled margins with significant mafic mineral phases (e.g., dark mica, amphibole) and pyrite porphyroblasts are common. The mafic dikes are usually dark green in color and contain biotite, amphibole, minor feldspar, chlorite, and rare carbonate. The coarse-grained variety shows usually a porphyritic texture of mm-sized, subhedral biotite, amphibole and feldspar in a greenish, very fine-grained matrix. Fine, secondary carbonate and quartz veins often cut the dikes.

#### *2-4-2-4 Felsic dikes*

Felsic dikes are rather thin (<20cm) in comparison to their mafic counterpart, and light grey in color. They are very fine-grained and have sharp contacts to the rhyolites. They are very rare within the deposit and have limited extent.



**Figure 2-2.** Stratigraphic section of drill core RMUG08-140, 1806 Zone. Rotated core is overturned, and start and end coordinates are given both in UTM NAD83, Zone 21N and WGS 84. Assay data for Cu, Au, Zn, and Pb are from Rambler Metals & Mining Canada Ltd. Abbreviations alteration minerals: Serc – sericite, Qtz – quartz, Bio – biotite, Chl – chlorite, Carb – carbonate, Sul – sulfide

## 2-5 MINERALOGY

### 2-5-1 SULFIDE AND OXIDE MINERALOGY

Table 2-1 contains the sulfide mineralogy from the 1806 Zone from two key samples from the stratigraphic section in Figure 2-2. The following description of the observed sulfide and oxide phases is based on their abundance both in the stringer zone and semi-massive to massive horizon within the 1806 Zone.

**Table 2-1.** Sulfide and oxide mineralogy representative of the 1806 Zone on the example of two samples from drill core RMUG08-140, Section 22 (Fig. 2-2); mineral abundances: +++ major phase (>10vol.%), ++ minor phase (10-5 vol.%), + accessory phase (<5vol.%), – not observed

Sample No.	29782	29783	Sample No.	29782	29783
Depth [m]	34.49-34.64	35.43-35.48	Depth [m]	34.49-34.64	35.43-35.48
Description	Massive sulfide	Ccp and Py in massive quartz (high-grade ore)	Description	Massive sulfide	Ccp and Py in massive quartz (high-grade ore)
Py*	+++	+++	Pyr	–	–
Ccp	+++	+++	Ag-Ccp <sup>1</sup>	–	+
Sp	++	++	Ag-Tet-Ten	–	–
Po	++	+++	Stn	–	–
Asp	+	+	Boul <sup>2</sup>	–	–
Tet-Ten	–	–	Loel	–	–
Gn	+	–	N-Sb-S	–	+
El	–	+	Mag	–	–
AgHg±Au	–	–	Cass	–	–
Mia	–	+	Chr	–	–

\* **Mineral abbreviations:** Py – pyrite, Ccp – chalcopyrite, Sp – sphalerite, Po – pyrrhotite, Asp – arsenopyrite, Tet-Ten – tetrahedrite–tennantite, Gn – galena, El – electrum, AgHg±Au – AgHg ± Au alloy, Mia – miargyrite, Pyr – pyrrargyrite, Ag-Ccp – argento–chalcopyrite, Ag-Tet-Ten – argento–tetrahedrite–tennantite, Stn – stannite, Boul – boulangerite, Loel – löllingite, Ni-Sb-S –

<sup>1</sup> The mineral argento-chalcopyrite is actually silver tarnish on chalcopyrite

<sup>2</sup> The mineral boulangerite is actually meneghinite

unknown Ni-Sb sulfide, Mag – magnetite, Cass – cassiterite, Chr – chromite

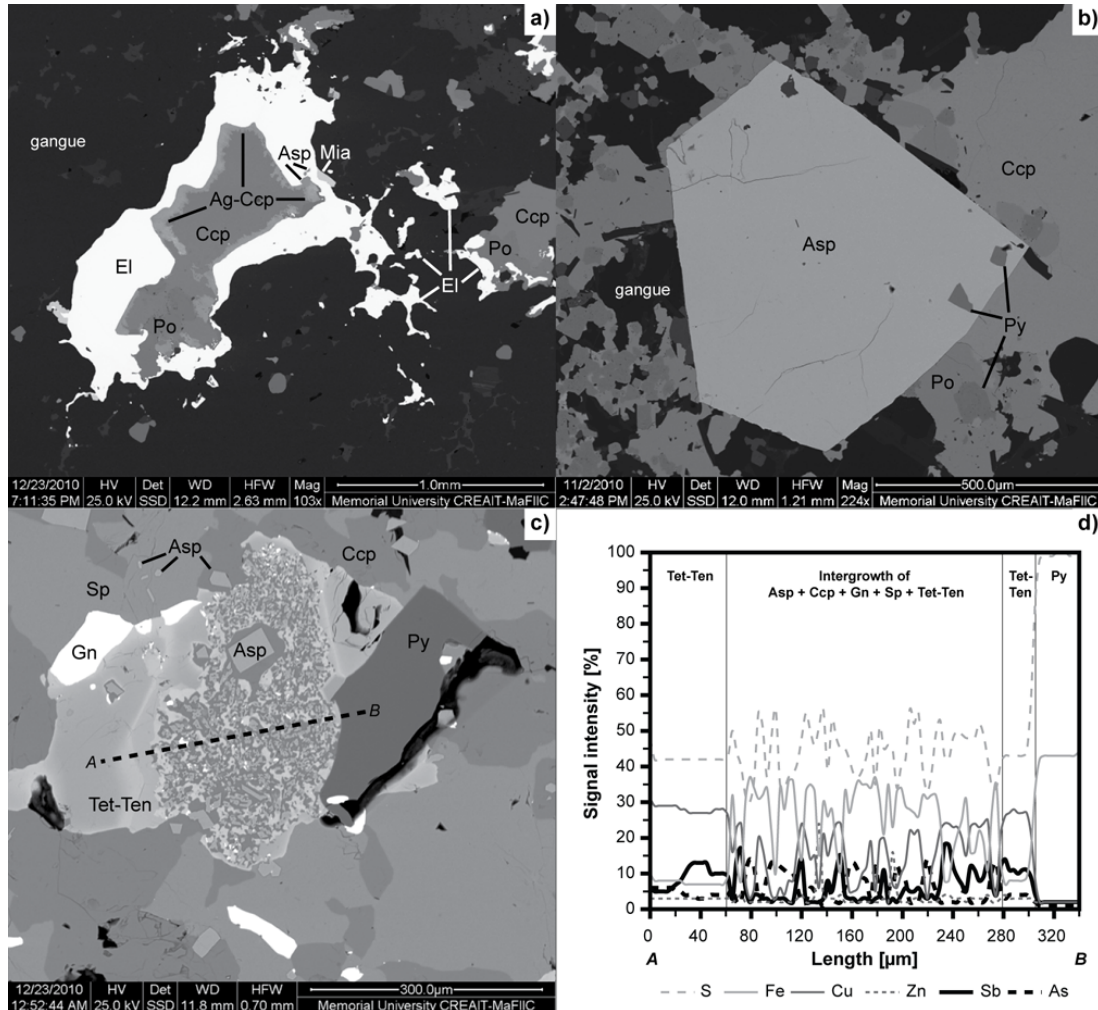
Pyrite [ $\text{FeS}_2$ ] is the most abundant sulfide phase in the 1806 Zone occurring as a major phase (>10%) in both stringer and the massive sulfide horizon. Pyrite is commonly recrystallized often with well-developed triple junctions ( $\pm 60^\circ$ ) and bulged grain boundaries. Euhedral to subhedral grains of cubic, triangular or polygonal shape pyrites are the most common form, but weakly anhedral grains or pyrite elongated parallel to foliation are also present. Grain size is highly variable with micron-scale grains in the gangue and coarser crystals, up to several mm, in the massive sulfide. Pyrite typically occurs in groups, often forming polycrystalline aggregates that are tightly packed with inter-grain voids filled with chalcopyrite, sphalerite, galena, pyrrhotite, and/or tetrahedrite-tennantite. Fine needle-like intergrowth between pyrite and arsenopyrite are rare but observed occur usually adjacent to gangue minerals. In other cases, coarse-grained crystals or even porphyroblasts, are found within sheets of chalcopyrite and/or pyrrhotite. Larger pyrite grains often contain inclusions of chalcopyrite, galena and sphalerite. Some larger grains show brittle deformation with fine cracks and veinlets partly filled with galena,  $\text{AgHg}\pm\text{Au}$  alloys, and pyrrhotite. Buckshot textures of pyrite in a pyrrhotite matrix occur only at close contact to mafic dikes.

Chalcopyrite [ $\text{CuFeS}_2$ ] is the second abundant sulfide phase and occurs as major, minor, and, in more rare cases, as an accessory (<5vol.%) phase.

While less abundant than pyrite, it is an important phase in both the stringer and semi-massive to massive sulfide, and the dominant phase within the silicified cap above the massive sulfide. Anhedral chalcopryite occurs either as small to moderate grains or as a continuous mass hosting other sulfide phases. Chalcopryite has close associations with pyrite, arsenopryite, tetrahedrite-tennantite, sphalerite, galena, pyrrhotite and electrum (Fig. 2-3a and b). Fine,  $\mu\text{m}$ -sized grains of chalcopryite are developed (1) in-between annealed pyrite aggregates, (2) as inclusions in pyrite and very rarely as inclusions in pyrrhotite and magnetite, (3) as disseminated crystals in gangue, and (4) as fine, wormy-like intergrowth with arsenopryite + tetrahedrite-tennantite  $\pm$  sphalerite  $\pm$  galena  $\pm$  electrum in tetrahedrite-tennantite (Fig. 2-3c).

Sphalerite [ $\text{ZnS}$ ] is less abundant than pyrite and chalcopryite, and occurs as a major, minor or accessory phase, but is most commonly a minor phase in the semi-massive to massive sulfide horizon. In the stringers it occurs distally from the semi-massive and massive horizon. Within semi-massive to massive sulfide horizon, sphalerite occurs as anhedral grains that have bulged or sutured grain boundaries and varies from fine grains to sheets that host pyrite, galena, and to a lesser extent chalcopryite and tetrahedrite-tennantite. Sphalerite occurs often interstitially in recrystallized pyrite, marginally in pyrrhotite, and as inclusion in pyrite. Very fine intergrowth with arsenopryite + chalcopryite + tetrahedrite-tennantite  $\pm$  galena  $\pm$  electrum are rarely observed (Fig. 2-3c). Sphalerite has weak chalcopryite disease with small rounded inclusions of chalcopryite present;

this is common in the lower parts of the semi-massive and massive sulfide horizon.



**Figure 2-3.** BSE images and line scan from samples of the 1806 Zone. **a)** Electrum in gangue (i.e. quartz) associated with other sulfides (sample 29783, RMUG08–140); **b)** Recrystallized arsenopyrite blast with marginal pyrite inclusion in chalcopyrite, pyrrhotite, pyrite (sample 29783 RMUG08–140); **c)** Myrmekitic-like intergrowth between arsenopyrite + chalcopyrite + sphalerite + tetrahedrite-tennantite + galena in tetrahedrite-tennantite (sample 29781, RMUG08–138); **d)** Line scan done with EDX-SEM from A to B of c) showing the elemental zoning especially in tetrahedrite-tennantite (e.g., inverse behavior of As and Sb); mineral



abbreviations are the same as in Table 2-2

Pyrrhotite [ $\text{Fe}_{(1-x)}\text{S}$ ] occurs close to dike contacts and is of contact metamorphic origin. The closer to the dike contacts, the more abundant pyrrhotite is and usually coarse pyrite porphyroblasts occur within pyrrhotite and pyrrhotite veins commonly cross-cut the pyrite porphyroblasts. With more distance to dike contacts pyrrhotite becomes less abundant and is only a minor or accessory phase. Sub- to anhedral grains of small to moderate size are common and occur usually with marginal sphalerite. Subhedral grains are usually prismatic. Pyrrhotite is associated with pyrite, sphalerite, chalcopyrite, arsenopyrite (Fig. 2-3b) and electrum. In the down plunge of the 1806 Zone magnetite and cassiterite occur close to pyrrhotite or on pyrrhotite margins.

Arsenopyrite [ $\text{FeAsS}$ ] occurs as a minor phase in semi-massive to massive sulfides and is euhedral to subhedral varying in size from microns to mm. Fine-grained arsenopyrite often occurs as groups of prismatic to triangular grains that are within gangue but spatially associated with pyrite or chalcopyrite. Fine, euhedral arsenopyrite cubes and prisms are found associated with electrum, pyrrhotite and sphalerite, but this is rather rare. Arsenopyrite has myrmekitic textures with small ( $<20\mu\text{m}$ ), anhedral, wormy-like arsenopyrite grains that are intergrown with chalcopyrite + tetrahedrite-tennantite  $\pm$  sphalerite  $\pm$  galena  $\pm$  electrum (Fig. 2-3c). On the margin or in the centre of this myrmekitic-like texture there is often a single, euhedral arsenopyrite grain surrounded by chalcopyrite (Fig. 2-3c) and more rarely by sphalerite. In some cases, acicular

arsenopyrite and pyrite are intergrown and occur on the margins of pyrrhotite or sphalerite. Moderately sized arsenopyrite commonly occurs as single grains with recrystallized pyrite and often contains pyrite inclusions, whereas coarser grained, euhedral porphyroblasts (up to 3mm) are often surrounded by pyrite, chalcopyrite, pyrrhotite (Fig. 2-3b), sphalerite and/or galena. Arsenopyrite commonly contains rounded inclusions of pyrite (Fig. 2-3b) or elongated inclusion of electrum that are concentrated on the rim of the arsenopyrite grains.

Tetrahedrite-tennantite  $[(\text{Cu}, \text{Fe}, \text{Ag}, \text{Zn})_{12}\text{Sb}_4\text{S}_{13}-(\text{Cu}, \text{Ag}, \text{Fe}, \text{Zn})_{12}\text{As}_4\text{S}_{13}]$  usually occurs as a minor to accessory phase in the semi-massive to massive sulfides. Tetrahedrite-tennantite occurs as subhedral to anhedral grains that are polygonal, sub-rounded or amoeboid. It occurs most commonly with chalcopyrite, sphalerite and arsenopyrite, but is also present close to galena, pyrite and rarely with electrum. Tetrahedrite-tennantite is also associated with myrmekitic textures as described above (Fig. 2-3c).

Galena  $[\text{PbS}]$  is a very common accessory phase and occurs as micron-scale, anhedral, roundish grains that occur as interstitial phases between recrystallized pyrite, along pyrite margins, as inclusions in pyrite and sphalerite, and to lesser extent with chalcopyrite, tetrahedrite-tennantite and arsenopyrite (Fig. 2-3c). Galena is more frequently present in the upper parts of the semi-massive to massive sulfide horizons and almost totally absent in the down plunge extension of the 1806 Zone.

Electrum  $[(\text{Au}, \text{Ag})]$  is an accessory within the semi-massive to massive

sulfides and also occurs in the strongly silicified cap to the Rambler rhyolite. The anhedral, partly rounded to ameboid grains range in size of 1mm to only a couple of  $\mu\text{m}$  and occur most commonly with other sulfides, especially chalcopyrite > pyrite > sphalerite >> pyrrhotite > arsenopyrite  $\approx$  tetrahedrite-tennantite > Ag-phases. Electrum occurs in quartz with and without other sulfide phases (Fig. 2-3a), when it occurs in the silicified cap horizon. It also occurs along pyrite and arsenopyrite grain boundaries, as inclusions in pyrite, arsenopyrite and pyrrhotite, within the myrmekitic-like pockets in tetrahedrite-tennantite, and with AgHg alloys as fine veinlets in pyrite.

Silver is developed in various forms within the 1806 Zone. Most commonly it occurs as AgHg $\pm$ Au alloys, which occur either as veinlets in pyrite, as inclusions in pyrite or as up to 20  $\mu\text{m}$  large, rounded grains adjacent to pyrite and chalcopyrite. Miargyrite [AgSbS<sub>2</sub>] and pyrargyrite [Ag<sub>3</sub>SbS<sub>3</sub>] are very rare and occur as  $\mu\text{m}$ -scale, anhedral, subrounded crystals. Miargyrite occurs in close proximity to electrum (Fig. 2-3a), whereas pyrargyrite occurs with electrum, sphalerite, arsenopyrite and/or pyrite. Silver-rich varieties of chalcopyrite (i.e., argento-chalcopyrite; Fig. 2-3a) and tetrahedrite-tennantite (i.e., argento-tetrahedrite-tennantite) are also present and found close proximity to AgHg $\pm$ Au alloys and/or electrum.

Stannite [Cu<sub>2</sub>(Fe, Zn)SnS<sub>4</sub>] is present in only in a few samples, mostly in the up plunge portion of the 1806 Zone. The  $\mu\text{m}$ -scale (<30 $\mu\text{m}$ ) crystals are usually anhedral, weakly elongated and occur most commonly adjacent to

sphalerite, chalcopyrite and pyrite and in close proximity to galena, pyrargyrite, and electrum. Wormy-like intergrowth between stannite and sphalerite, and stannite enclosing cassiterite occur as well, but are rare.

Boulangerite  $[\text{Pb}_5\text{Sb}_4\text{S}_{11}]$  is rare and is usually intergrown with galena in the up plunge portion of the 1806 Zone or with tetrahedrite-tennantite in the down plunge section of the 1806 Zone. The grains are anhedral and up to 50 $\mu\text{m}$  large.

Löllingite  $[\text{FeAs}_2]$  is present in only one sample of the 1806 Zone and occurs as ca. 30 $\mu\text{m}$  large, subhedral grain intergrown with triangular arsenopyrite in gangue.

An unknown Ni-Sb sulfide phase is observed in only two samples from the up plunge of the 1806 Zone. This phase occurs as ca. 10 $\mu\text{m}$  large, round grain on the margin of chalcopyrite.

Magnetite  $[\text{Fe}_3\text{O}_4]$  is the most common oxide phase in the 1806 Zone and occurs usually as accessory phase but can be a minor component in the down plunge of the 1806 Zone. Crystals range in size from a few  $\mu\text{m}$  up to 2mm and are mostly euhedral cubes. However, fragmental, rounded grains associated with pyrrhotite are present. These fragmental grains have often rounded inclusions of pyrite and chalcopyrite and are intergrown with hematite. Euhedral magnetite occurs either as groups of small to moderate-sized cubes in gangue near pyrrhotite, chalcopyrite, and cassiterite, or as coarse porphyroblasts with inclusions of various sulfide (e.g., chalcopyrite, pyrrhotite) and oxide phases (e.g., chromite). However, these magnetite porphyroblasts are rather rare.

Cassiterite [SnO<sub>2</sub>] is only a rare accessory phase in the 1806 Zone. In the down plunge of the 1806 Zone it occurs as small, rounded grains often in close proximity to magnetite, pyrrhotite, chalcopyrite, and sphalerite, and if developed stannite. In contrast, in the up plunge of the zone cassiterite is present only in two samples and always surrounded by stannite.

Chromite [FeCr<sub>2</sub>O<sub>4</sub>] is observed only in the down plunge of the 1806 Zone as cubic inclusion in magnetite.

#### *2-5-2 ALTERATION MINERALOGY*

The Rambler rhyolite is characterized by an intense sericite + quartz ± green mica ± chlorite ± biotite alteration (Figs. 2-2 and 2-3). Moreover, pyrite is the dominant sulfide alteration phase in the stringer zone accompanied sometimes by chalcopyrite and sphalerite proximal and distal, respectively, to the semi-massive and massive sulfide horizon. Strong silicification and sulfidation is often developed in the dm-strong cap horizon above the rhyolitic flow and tuff. Mafic dikes are usually strongly chloritized and show partly carbonate alteration. Single pyrite porphyroblasts can be observed randomly in the dikes as well.

### **2-6 GEOCHEMISTRY**

The assay data for Cu, Au, Zn, Pb (Fig. 2-2), and Ag show higher maximum and average values in the up plunge than in the down plunge of the

1806 Zone. In the semi-massive to massive sulfide horizon in the up plunge maximum values for Cu, Au, Zn, Pb, and Ag are 11.7wt.%, 96g/t, 34.5wt.%, 2.69wt.%, and 567g/t, respectively. In contrast, the maximum values for these elements in the semi-massive to massive sulfide horizon in the down plunge are 9.9wt.% Cu, 17.2g/t Au, 14.5wt.% Zn, and 350g/t Ag. Due to the almost absence of galena and boulangerite in the down plunge, Pb concentrations are very low. Copper, Au, Zn, Pb, and Ag data in the stringer zone in the up plunge of the 1806 Zone are usually much lower than the maximum values reported from the sulfide horizon, but can also reach elevated values with often 0.5 to > 1wt.% Cu, 1-5g/t Au, up to 1wt.% Zn, ca. 10g/t Ag, and up to 0.5wt.% Pb. However, the stringer zone in the down plunge rarely has economic concentration of base and precious metals. The assay data for the base and precious metals correlate poorly. However, Au and Ag are associated with enrichments in Cu and/or Zn (Fig. 2-2).

Metal and elemental zoning observed by EDX-SEM is preserved in tetrahedrite-tennantite (Fig. 2-3d), electrum, and Ag-Hg-Au alloys. Arsenic and Sb have inverse behavior in tetrahedrite-tennantite with increased Sb values on tetrahedrite-tennantite margins or in restricted zones within the grains (e.g., lighter grey in BSE images; Fig. 2-3c). Electrum is Ag- and Hg-bearing and have rims enriched in Ag and Hg with gold enriched in the cores of grains. The same trend is observed in Ag-Hg-Au alloys with increased Ag-Hg and decreased Au concentrations on the margin and inverse enrichments in alloy cores. Silver-rich varieties of chalcopyrite and tetrahedrite-tennantite are developed adjacent and

marginal to their Ag-free counterpart, (Fig. 2-3a) implying the preferred enrichment of Ag on phase margins.

## **2-7 DISCUSSION**

The origin of Au-Ag-rich VMS systems is still highly discussed (Hannington and Scott, 1989a; Poulsen and Hannington, 1996; Hannington et al., 1999; Huston, 2000) and often made more difficult due to the metamorphic overprint affecting many Au-Ag-rich VMS systems. Hence, a primary syngenetic origin of precious metal enrichment in VMS deposits is often questioned and a synorogenic origin is often favored in many deformed VMS districts (Wagner et al., 2007). However, evidence supporting an orogenic origin of Au and Ag including limited sulfide mineralogy (e.g., pyrite, chalcopyrite, arsenopyrite), sulfide mineralization associated with quartz veins, and narrow carbonate alteration haloes (Groves et al., 1998) are not present in the 1806 Zone at the Rambler Camp, despite the effect of deformation to the mineral texture. Textural features such as recrystallization, especially in pyrite, replacement of pyrite by metamorphic pyrrhotite and porphyroblasts of pyrite and arsenopyrite indicate that metamorphism and deformation have affected the sulfides at Ming, but it has not completely obscured the primary mineralogy and textures of the sulfides completely. The 1806 Zone consists of a complex assemblage of sulfide minerals (e.g., sulfosalts, Au-Ag-Hg-bearing phases) that cannot be explained by a hydrothermal fluid of mid-crustal, orogenic origin, but by primary hydrothermal

fluid circulating through the seafloor. Moreover, this odd sulfide mineralogy, especially the occurrence of electrum with sulfosalts containing magmatic suite elements (e.g., Ag, As, Hg, Sb, Sn) as major and minor phases, strongly suggests the potential of a contribution of magmatic volatiles to the primary, base-metal transporting hydrothermal fluid. Furthermore, the sulfosalts represent a high-sulfidation state known from many Au-rich epithermal systems (Hedenquist et al., 2000) and which was been suggested to be important for the genesis of Au-rich VMS systems (Hannington and Scott, 1989b; Sillitoe et al., 1996; Hannington et al., 1999). Additionally, electrum and Ag-phases occur predominantly with pyrite and chalcopyrite indicating a metal zoning that has been developed primarily during the waning and waxing stages of the VMS deposit (Large, 1977, 1992). The metamorphism and deformation had only the effect of zone-refinement and upgrading as seen in the occurrence of electrum and Ag-bearing phases partly along pyrite and arsenopyrite grain boundaries, brittle cracks in pyrite, and as free phase in gangue (e.g., quartz). These data favor a syngenetic origin for precious metal enrichment in the Ming VMS deposit, rather than a later orogenic overprint.

## **2-8 CONCLUSIONS**

Recent investigations on the 1806 Zone at the Ming Mine, Rambler Camp, NW Newfoundland, reveal a complex sulfide mineralogy including besides common sulfide phases such as pyrite, chalcopyrite, sphalerite and arsenopyrite,



Ag-, As-, Hg-, Sb-, and Sn-bearing sulfosalts, various Ag-phases and electrum. These minerals are mostly concentrated in semi-massive to massive sulfide horizon hosted by rhyolitic massive flows and tuff to lapilli tuff. Fine stringer beneath the semi-massive to massive sulfide horizon is most commonly pyritic and to lesser extend also chalcopyrite- and sphalerite-bearing. Often a strongly silicified and sulfide mineralized horizon caps the mineralize rhyolite. Turbidities are common in the hanging wall and mafic dikes usually cut through the footwall and hanging wall. Base and precious metals are more enriched in the up plunge than in the down plunge of the 1806 Zone indicating metal zoning. Textural and investigations by EDX-SEM on the sulfides confirm the deformation (e.g., recrystallization) done by greenschist metamorphism on the 1806 Zone. However, EDX-SEM reveals also primary sulfide associations between sulfosalts, Ag-phases, and electrum and elemental zoning in these phases. Based on (1) the observed sulfide assemblage and texture, (2) the sericite + quartz  $\pm$  green mica  $\pm$  chlorite  $\pm$  biotite alteration in the rhyolites, and (3) the metal zoning of electrum preferably occurring with pyrite  $\pm$  chalcopyrite especially in the up plunge of the 1806 Zone a syngenetic origin with magmatic contribution is strongly favored for the genesis of the studied zone. Further microscopic and geochemical work with emphasis on the sulfide and alteration assemblage in the 1806 Zone and three other newly discovered Cu-Au mineralization horizons at the Rambler Camp will be continued over the next years to confirm the here presented preliminary genetic results on Au-Ag-rich VMS deposits in the Appalachians.

## **ACKNOWLEDGEMENTS**

SMB and SJP thank Bert Fudge for assistance with the drill cores and underground, and Peter Mercer and Tim Sandford from Rambler Metals & Mining Canada Ltd. for fruitful insight discussion on the newly discovered horizons at Ming. Caroline Daoust is thanked for helpful comments to the original manuscript. S.M.B. thanks the staff of Rambler Metals & Mining Ltd. for their support during the field season of 2010. The outcome from the SEM sessions on the INCO Innovation Centre, St. John's, NL, would not be as successful as have been without the help and support of David Grant and Michael Shaffer. This research was funded by numerous grants to SJP, including an NSERC Discovery Grant, the NSERC-Altiis Industry Research Chair in the Metallogeny of Ores in Volcanic and Sedimentary Basins, and a Leverage Grant from the Industrial Research Innovation Fund from the Research and Development Corporation of Newfoundland and Labrador.

## **References**

- Castonguay S, Skulski T, van Staal C, Currie M (2009) New insights on the structural geology of the Pacquet Harbour group and Point Rousse complex, Baie Verte peninsula, Newfoundland Current Research Newfoundland and Labrador Department of Natural Resources, Geological Survey Report 09-1:147-158
- Cawood PA, van Gool JAM, Dunning GR (1993) Silurian age for movement on the Baie Verte Line: Implications for accretionary tectonics in the Northern Appalachians Geological Society of America, Abstract with Programs 25:A422

- Groves DI, Goldfarb RJ, Gebre-Mariam M, Hagemann SG, Robert F (1998) Orogenic gold deposits: A proposed classification in the context of their crustal distribution and relationship to other gold deposit types *Ore Geology Reviews* 13:7-27
- Hannington MD, Scott SD (1989a) Gold mineralization in volcanogenic massive sulfides: Implications of data from active hydrothermal vents on the modern seafloor. In: Keays RR, Ramsay, W.R.H., Groves, D.I. (ed) *The geology of gold deposits: The perspective in 1988*, vol 6. *Economic Geology Monograph*. Society of Economic Geologists, Boulder, CO, pp 491-507
- Hannington MD, Scott SD (1989b) Sulfidation equilibria as guides to gold mineralization in volcanogenic massive sulfides: Evidence from sulfide mineralogy and the composition of sphalerite *Economic Geology* 84:1978-1995
- Hannington MD, Poulsen KH, Thompson JFH, Sillitoe RH (1999) Volcanogenic gold in the massive sulfide environment. In: Barrie CT, Hannington, M.D. (ed) *Volcanic-associated massive sulfide deposits: Processes and examples in modern and ancient settings*, vol 8. *Reviews in Economic Geology*. Society of Economic Geologists, Boulder, CO, pp 325-351
- Hedenquist JW, Arribas RA, Gonzalez-Urien E (2000) Exploration for epithermal gold deposits. In: Hagemann SG, Brown, P.E. (ed) *Gold in 2000*, vol 13. *Reviews in Economic Geology*. Society of Economic Geologists, Boulder, CO, pp 245-277
- Hibbard LJ (1983) *Geology of the Baie Verte Peninsula, Newfoundland* vol 2. *Memoir*. Department of Mines and Energy, Government of Newfoundland and Labrador, Memoir 2
- Huston DL (2000) Gold in volcanic-hosted massive sulfide deposits: Distribution, genesis, and exploration. In: Hagemann SG, Brown, P.E. (ed) *Gold in 2000*, vol 13. *Reviews in Economic Geology*. Society of Economic Geologists, Boulder, CO, pp 401-426
- Large RR (1977) Chemical evolution and zonation of massive sulfide deposits in volcanic terrains *Economic Geology* 72:549-572
- Large RR (1992) Australian volcanic-hosted massive sulfide deposits: Features, styles, and genetic models *Economic Geology* 87:471-510
- Pilgrim L (2009) Mineral resource estimate for the Ming Mine, Newfoundland, Canada. Rambler Metals and Mining Canada Ltd, Baie Verte, NL

- Poulsen KH, Hannington MD (1996) Volcanic-associated massive sulphide gold. In: Eckstrand OR, Sinclair, W.D., Thorpe, R.I. (ed) *Geology of Canadian Mineral Deposit Types*. Geological Survey of Canada, *Geology of Canada Series no. 8*, Ottawa, ON, pp 183-196
- Sillitoe RH, Hannington MD, Thompson JFH (1996) High sulfidation deposits in the volcanogenic massive sulfide environment *Economic Geology* 91:204-212
- Skulski T, Castonguay, S., McNicoll, V., van Staal, C, Kidd, W, Rogers, N, Morris W, Ugalde, H, Slavinski H, Spicer W, Moussallam, Y, Kerr, I (2010) Tectonostratigraphy of the Baie Verte oceanic tract and its ophiolite cover sequence on the Baie Verte Peninsula Current Research Newfoundland and Labrador Department of Natural Resources, Geological Survey Report 10-1:315-335
- Skulski T, Castonguay S, van Staal C, Rogers N, McNicoll V, Kerr A, Escayola M (2009) Baie Verte Peninsula: An evolving geological story. Geological Association of Canada, Newfoundland and Labrador Section, St. John's, NL
- Swinden HS, Kean BF (eds) (1988) The volcanogenic sulphide districts of Central Newfoundland: A guidebook and reference manual for volcanogenic sulphide deposits in the early Paleozoic oceanic volcanic terranes of Central Newfoundland. Geological Association of Canada, Mineral Deposits Division, St. John's, NL
- Tuach J, Kennedy MJ (1978) The geologic setting of the Ming and other sulfide deposits, consolidated Rambler mines, Northeast Newfoundland *Economic Geology* 73:192-206
- Wagner T, Klemm R, Wenzel T, Mattsson B (2007) Direct evidence from laser-ablation-inductively coupled plasma-mass spectrometry analysis of invisible gold *Geology* 35:775-778

## CHAPTER 3

In:

Brueckner, SM, Piercey, SJ, Sylvester, PJ, Maloney, S, Pilgrim, L (2014).

Evidence for syngenetic precious metal enrichment in an Appalachian  
volcanogenic massive sulfide system: The 1806 Zone, Ming mine,  
Newfoundland, Canada. *Economic Geology* 109:1611-1642. doi:

10.2113/econgeo.109.6.1611

**EVIDENCE FOR SYNGENETIC PRECIOUS METAL ENRICHMENT IN AN  
APPALACHIAN VOLCANOGENIC MASSIVE SULFIDE SYSTEM: THE 1806  
ZONE, MING MINE, NEWFOUNDLAND, CANADA**

Stefanie M. Brueckner<sup>1</sup>, Stephen J. Piercey<sup>1</sup>, Paul J. Sylvester<sup>1</sup>, Stephanie  
Maloney<sup>2, 3</sup>, Larry Pilgrim<sup>2</sup>

<sup>1</sup>*Department of Earth Sciences, Memorial University of Newfoundland  
300 Prince Philip Drive, St. John's, NL, Canada, A1B 3X5*

<sup>2</sup>*Rambler Metals & Mining Canada Limited  
Route # 418, Ming's Bight Road, NL, Canada, A0K 3S0*

<sup>3</sup>*now at: Vale  
Voisey's Bay Mine Site, P.O. Box 7001, Stn. C  
Happy Valley - Goose Bay, NL, Canada, A0P 1C0*

**ABSTRACT**

The Ming deposit, Baie Verte, Newfoundland, Canada, is an early Ordovician bimodal-mafic, Cu-Au-(Zn-Ag) volcanogenic massive sulfide (VMS) deposit. The deposit consists of a number of ore lenses that are stacked in the uppermost part of the Rambler rhyolite. One of the uppermost lenses, the 1806 Zone, is enriched in Au and Ag. The deposit has been affected by Silurian-Devonian greenschist to amphibolite grade metamorphism and polyphase deformation and this has led to debates as to whether the Au-Ag-enrichment in

the deposit is syngenetic or a product of a later metamorphic and structural overprint.

The 1806 Zone consists predominantly of discordant sulfide stringer, stratabound semi-massive to massive sulfides, and a weakly mineralized silicified cap zone. The ore is largely hosted within the footwall Rambler rhyolite that is strongly altered to quartz – sericite  $\pm$  green mica with sporadic chlorite – biotite. Base and precious metal zoning is developed from the down plunge portion (Cu-Au) to the up plunge portion (Cu-Zn-Au-Ag-Pb) in the 1806 Zone. The ore mineralogy and mineral chemistry is complex and is interpreted to be of an intermediate-sulfidation-type. Pyrite and chalcopyrite are the dominant sulfide species with minor to accessory sphalerite, galena, pyrrhotite and arsenopyrite. Sulfosalts including Ag-bearing tennantite-tetrahedrite, stannite, boulangerite<sup>1</sup> and loellingite, and precious metal-rich phases are common throughout the deposit. Precious metals occur as: (1) mercurian electrum (7.93-20.57wt.% Hg); and (2) various Ag-phases (miargyrite, pyrargyrite, mercurian stephanite, unnamed AgCuFeS phase, Ag-Hg $\pm$ Au alloys) that are more abundant in the up plunge portion of the 1806 Zone. Tellurides and bismuthides are present in trace amounts. Oxides (cassiterite and magnetite) are present exclusively in the down plunge portion of the 1806 Zone.

---

<sup>1</sup> The mineral phase originally identified as boulangerite [Pb<sub>5</sub>Sb<sub>4</sub>S<sub>11</sub>] is actually of meneghinite [Pb<sub>13</sub>CuSb<sub>7</sub>S<sub>24</sub>] composition. For the remainder of this chapter the term boulangerite will be used nevertheless, because this chapter was published with the original mineral identification (i.e., boulangerite) and hence confusion is avoided between the published paper and this thesis.

The deposit geometry, metals distribution, complex ore assemblages, abundant sulfosalts, and the significant concentration of elements of the epithermal suite (e.g., Au, Ag, As, Hg, Sb, Bi) in the ore strongly contrasts with those of orogenic Au deposits and support a syngenetic or synvolcanic origin for precious metals in the Ming VMS deposit, including a possible magmatic input into the 1806 Zone ore-forming system.

Evidence for a late, syn-deformation precious metal emplacement via orogenic overprinting are lacking at the 1806 Zone and all data point to a syngenetic origin for precious metal enrichment, indicating that Ordovician Appalachian VMS deposits are favorable targets for Au. Nevertheless, Silurian-Devonian metamorphism and deformation has resulted in textural recrystallization and local remobilization of precious metals and the main fabrics largely control the current geometry of the host succession and of the Ming orebody.

### **3-1 INTRODUCTION**

Precious metal-enriched VMS deposits are of growing economic importance in a metal dependent global economy (Poulsen and Hannington, 1996; Huston, 2000; Dubé et al., 2007a; Mercier-Langevin et al., 2011). These deposits combine geological and mineralogical characteristics of typical base metal-rich VMS deposits with some specific characteristics of precious metal-rich, high-sulfidation epithermal deposits (e.g., Franklin et al., 1981, 2005; Lydon,



1984, 1988; Hannington and Scott, 1989a; Large, 1992; Franklin, 1993, 1996; Ohmoto, 1996; Poulsen and Hannington, 1996; Hannington et al., 1999; Huston, 2000; Poulsen et al., 2000; Dubé et al., 2007a; Galley et al., 2007). Contrary to base metal-only VMS deposits, Au-rich VMS deposits are commonly characterized by one or many of the following features: (1) advanced argillic style alteration; (2) complex ore mineralogy with abundant arsenopyrite and sulfosalts; (3) enrichments in elements of the epithermal suite (Ag, As, Au, Bi, Hg, Sb, Te), and 4) an association with andesite-dacite-rhyodacite-rhyolite rocks (Poulsen and Hannington, 1996; Sillitoe et al., 1996; Hannington et al., 1999; Huston, 2000; Poulsen et al., 2000; Dubé et al., 2007a; Mercier-Langevin et al., 2011). Like many ancient VMS deposits, Au-rich VMS deposits are commonly metamorphosed and deformed and often in close proximity to major deformation zones and orogenic Au deposits. This metamorphic overprint and close spatial relationship to orogenic Au deposits often lead to arguments about the origin of precious metal enrichment in these deposits. In the literature, both syngenetic (e.g., Tourigny et al., 1993; Dubé et al., 2007b; Mercier-Langevin et al., 2013) and synorogenic (e.g., Marquis et al., 1990) origins were proposed to explain the precious metal enrichment in VMS deposits. The former, syngenetic concept often involves the contribution of magmatic fluids similar to high-sulfidation epithermal Au deposits (Sillitoe et al., 1996), mostly based on the presence of elements of the epithermal suite such as Au, Ag, As, Sb ± Bi, Hg, and Te that are commonly enriched in such VMS systems. In contrast, the deformed nature of the deposits has led other authors to suggest that precious metals are added

subsequent to VMS formation and represent an orogenic precious metal upgrading to mineralization (e.g., Marquis et al., 1990).

The Newfoundland Appalachians are a Paleozoic orogenic belt with a diachronous history of magmatism, deformation, and metamorphism, and hosts both orogenic Au and precious metal-rich VMS deposits. The deposits formed during the various stages of the Appalachian orogenesis during the closure of the Iapetus and Rheic oceans (van Staal, 2007; van Staal and Barr, 2012). The Baie Verte Peninsula, NW Newfoundland, hosts both precious metal-rich VMS deposits and orogenic Au deposits. Orogenic Au deposits within the peninsula are structurally controlled, hosted in vein systems within ophiolitic and associated rocks, and are related to Siluro-Devonian orogenesis (Salinic and Acadian orogenies; Stog'er Tight, Deer Cove, Pine Cove; Patey and Wilton, 1993; Ramezani et al., 2000). The Au-Ag-bearing VMS deposits of the consolidated Rambler and Ming Camp (e.g., Ming (Main), Ming West, Rambler Main, East Rambler, Big Rambler Pond) are hosted within bimodal to ophiolitic sequences, are associated with massive sulfide, and have been moderately metamorphosed and poly-phase deformed during the Salinic and Acadian orogenies (Tuach and Kennedy, 1978; Tuach, 1988; van Staal, 2007; Castonguay et al., 2009; van Staal and Barr, 2012). Thus, The Baie Verte Peninsula, and the actively mined Au-Ag-bearing Ming VMS deposit provides an important location to address relevant genetic questions regarding to the precious metal emplacement in metamorphosed and deformed Au-Ag-bearing VMS deposits.

The Ming VMS deposit is a bimodal-mafic, Cu-Au-(Zn-Ag) VMS deposit hosted within early Ordovician rocks of the Baie Verte oceanic tract. The deposit was mined for Cu and Au during the late 1970s to early 1980s (Ming Main), and again briefly in the mid-1990s (Ming West). Total production at Ming Main was 4.7 million short tons averaging 2.17% Cu, with some Zn, Au and Ag. The Ming West deposit was brought into production in October 1995. The deposit was mined in 1995-96, producing 142,173 short tons at 3.98% Cu, 0.17oz/ton Au, and 0.44oz/ton Ag from the upper part of the deposit (Pilgrim, 2009). Since late 2011, Rambler Metals and Mining, Canada Ltd is mining the Ming VMS deposit. Exploration in the early 2000s led to the discovery of new ore zones parallel to and along strike to the previously mined area from the Ming Mine main shaft. Four of these zones (1806, 1807, Ming South and Ming North) have National Instrument 43-101 compliant resources; this highest grades of Cu, Au and Ag are in the 1806 and 1807 zones. All newly discovered zones have elevated Au grades (measured resources of 1.15Mt @ 2.14wt.% Cu, 2.40ppm Au, 14.11ppm Ag, and 0.78wt.% Zn; Pilgrim, 2009), which makes it one of the most Au-Ag-rich VMS deposits of the Appalachians in terms of Au grades. Amongst these four zones, the 1806 Zone has the highest Au contents (measured resources of 267,000 tonnes @ 0.56wt.% Cu, 4.31ppm Au, 32.15pm Ag, and 1.31wt.% Zn), which puts this zone into the small sub-class of auriferous or precious metal-rich VMS deposits (Poulsen and Hannington, 1996; Poulsen et al., 2000; Mercier-Langevin et al., 2011). The 1806 Zone is also less structurally complex than the other zones and provides an ideal opportunity to evaluate the potential for

syngenetic versus an orogenic origin for Au-Ag-enrichment in the deposit.

In this paper a detailed documentation of the mineralogy, mineral distribution and mineral chemistry is provided for the 1806 Zone of the Ming deposit. The stratigraphic setting was established from drill core descriptions and underground mapping to document the relationships between host rock, ore, alteration, and deformation. Detailed work on ore mineralogy, petrography, and paragenesis was undertaken utilizing standard microscopy and scanning electron microscopy. Additionally, electron probe micro-analysis (EPMA) data were obtained from most documented ore minerals. The aims of this paper are to: (1) document the complex ore mineralogy, mineral chemistry and metal zonation of a precious metal-rich VMS lens; (2) discuss the genesis of a precious metal-rich VMS lens through the detailed study of the 1806 Zone of the Ming deposit in the context of syngenetic hydrothermal activity versus synorogenic deformation and metamorphism; (3) discuss the influence and role of magmatic volatiles regarding to the transport and deposition of precious metals in the VMS environment; and (4) describe the effects of later metamorphism and deformation.

## **3-2 LITHOTECTONIC SETTING**

### **3-2-1 BAIE VERTE PENINSULA**

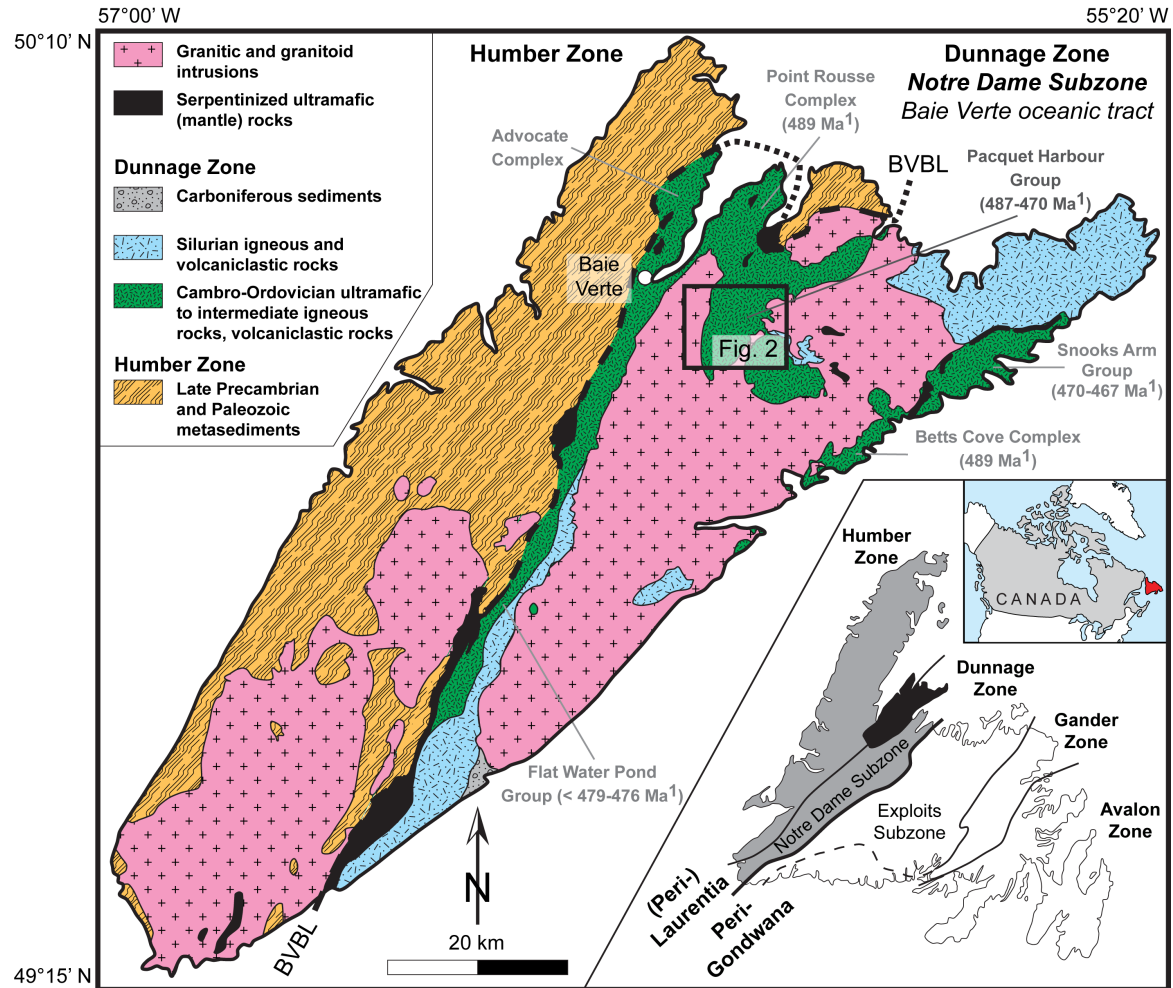
The Baie Verte Peninsula in the NW of Newfoundland is part of the Canadian Appalachians and host rocks of both the Humber Zone in the west and

the Notre Dame subzone of the Dunnage Zone in the east (Fig. 3-1). The Humber Zone represents the distal Laurentian cratonic margin, whereas the Notre Dame subzone is interpreted to represent remnant arc, back-arc, and ophiolitic rocks that were formed by supra-subduction in the Cambrian (Lushs Bight) and early Ordovician (Baie Verte oceanic tract; Hibbard, 1983; Swinden and Thorpe, 1984). The remnant arc exposed in the eastern half of the Baie Verte Peninsula is the Baie Verte oceanic tract (BVOT), which was formed in the early Ordovician in the Humber Seaway (van Staal, 2007). The basement of the BVOT consists of dominantly ultramafic to mafic (i.e., boninite, pillow basalt, gabbro) and minor felsic (i.e. rhyodacite to rhyolite) rocks and their mafic to felsic volcano-sedimentary cover sequences (Hibbard, 1983; Skulski et al., 2009, 2010). These BVOT basement rock complexes and their cover sequences are today predominantly exposed in the north-central and eastern part of the Baie Verte Peninsula and separated from each other by Silurian intrusions (Fig. 3-1). The Pacquet Harbour Group, host of the Ming deposit, is one of these complexes and divided into a lower and upper portion. The early Ordovician lower Pacquet Harbour Group (BVOT basement) consists of dominantly low-Ti boninites and basalts with minor rhyodacite to rhyolite (i.e. Rambler rhyolite). The upper Pacquet Harbour Group is the cover sequence of the lower Pacquet Harbour group and has mixed, mid-Ordovician volcano-sedimentary rocks and mafic volcanics (Hibbard, 1983; Skulski et al., 2010). Volcanogenic massive sulfide deposition was coeval with the formation of the basement rocks of the BVOT in an arc/back-arc setting (van Staal, 2007). However, the exact timing of precious

metal enrichment in the VMS deposits is partly obscured by later metamorphism and deformation. The BVOT basement rocks and their cover sequences were emplaced onto the Laurentian margin during the Taconic Orogeny during the diachronous closure of the Humber Seaway, which resulted in the collision peri-Laurentian fragments with the Laurentian margin during the mid- to late Ordovician (Hibbard, 1983; van Staal, 2007; van Staal and Barr, 2012). Subsequent orogenies in the Silurian (i.e., Salinic Orogeny) and Devonian (i.e., Acadian Orogeny) resulted in: greenschist to amphibolite facies and polyphase deformation; the formation of orogenic Au deposits; and the emplacement of granitic and granitoid bodies into the BVOT (van Staal, 2007; van Staal and Barr, 2012).

The BVOT basement rocks and their cover sequences record at least four deformation events ( $D_1$  to  $D_4$ : Table 3-1) of varying intensity (Tuach and Kennedy, 1978; Hibbard, 1983; Castonguay et al., 2009 and references therein). The  $D_2$  event, which is associated with the Silurian Salinic Orogeny, is the most prominent in the area and has strongly affected the Ming deposit resulting in prominent  $L > S$  fabrics ( $30 - 35^\circ$  dip to the NE of the strata including the sulfide-bearing horizons) and moderately metamorphism (upper greenschist to lower amphibolite facies; Tuach and Kennedy, 1978, Hibbard, 1983). The  $D_3$  deformation event (Devonian Acadian Orogeny) modified the orientation and geometry of the  $D_2$  structures (Castonguay et al., 2009). The E-W trending

Rambler Brook Fault, which is associated to D<sub>2</sub>, is located just south of the Rambler rhyolite (Fig. 3-2).

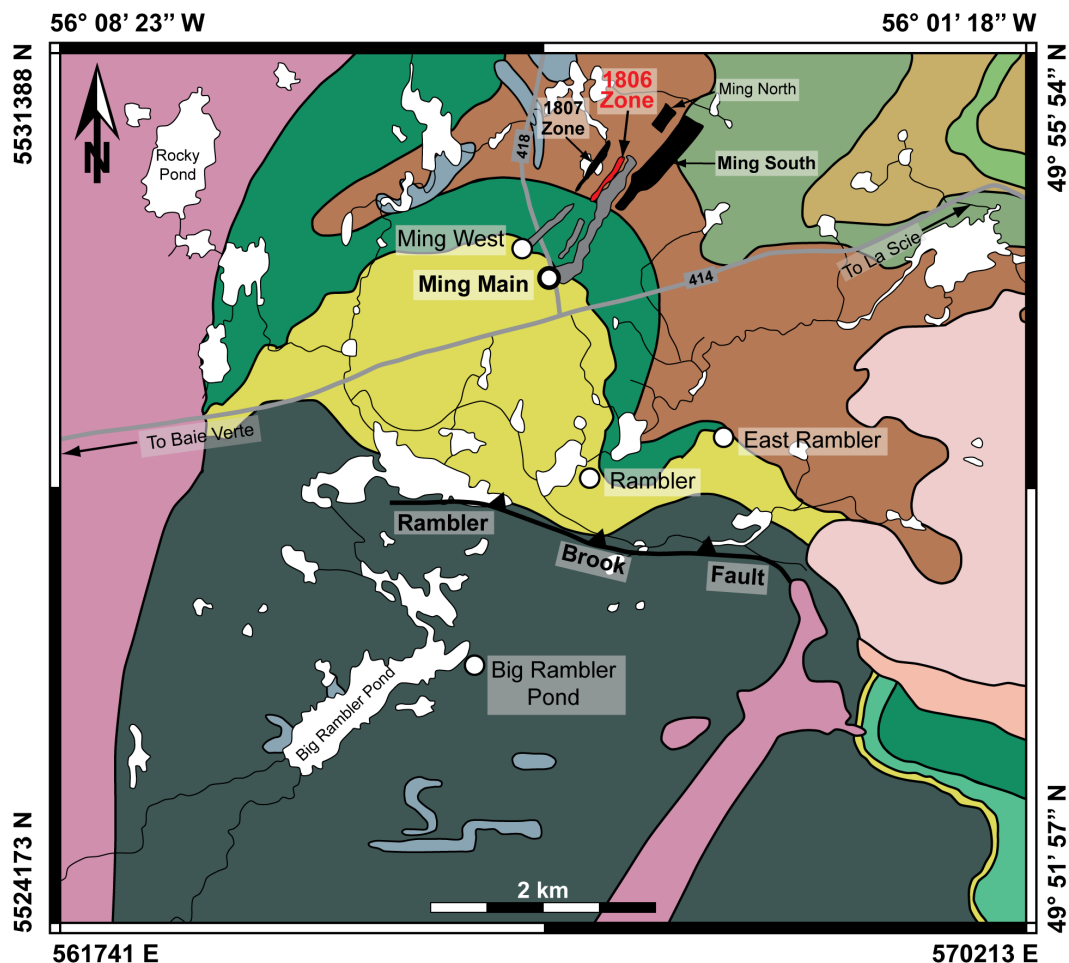


**Figure 3-1.** Simplified geologic map from the Baie Verte Peninsula after Hibbard (1983); <sup>1</sup> Age data from Castonguay et al. (2009) and Skulski et al. (2010); BVBL – Baie Verte-Brompton Line; Inlays in the lower right show the position of Newfoundland (red) within Canada and the various geologic zones of Newfoundland with the contact between (peri-)Laurentia (light grey) and (peri-)Gondwana (white; after Williams, 1979), Baie Verte Peninsula is in black

**Table 3-1.** Deformation events developed in the Pacquet Harbour Group, Baie Verte oceanic tract (BVOT; from and modified after Castonguay et al., 2009)

Deformation event	Main characteristic	Effect on Ming Mine	Related orogeny
<b>D<sub>4</sub></b>	<ul style="list-style-type: none"> <li>▪ NNE-trending, open to close upright crossfolds</li> </ul>		Alleghenian Orogeny (Permian)
<b>D<sub>3</sub></b>	<ul style="list-style-type: none"> <li>▪ Spaced (in S) to crenulation (in N) foliation shallowly SE-dipping</li> <li>▪ SE-plunging recumbent F<sub>3</sub> folds</li> </ul>	<ul style="list-style-type: none"> <li>▪ Re-folding and re-orientation down plunge</li> <li>▪ Potential structural thickening at depth</li> </ul>	Acadian Orogeny (Early to Middle Devonian)
<b>D<sub>2b</sub></b>	<ul style="list-style-type: none"> <li>▪ Steep W-dipping crenulation</li> <li>▪ S-plunging F<sub>2</sub> folds</li> <li>▪ Sinistral transpression during thrusting</li> </ul>	<ul style="list-style-type: none"> <li>▪ Modification to cigar-shape like shafts, dipping to 32-35° NE and are co-linear with the strong NE-plunging L<sub>2</sub> lineation</li> <li>▪ Dismembering and translating of the different zones by thrusting</li> </ul>	Salinic Orogeny (Silurian)
<b>D<sub>2a</sub></b>	<ul style="list-style-type: none"> <li>▪ Main fabric N to NE dipping</li> <li>▪ NE-plunging, close to isoclinal upright F<sub>2</sub> folds</li> <li>▪ S-directed faults locally string NE plunging</li> <li>▪ L<sub>2</sub> &gt; S<sub>2</sub> fabric</li> </ul>	<ul style="list-style-type: none"> <li>▪ Possible structurally thickening of sulfides in hinge zones of regional F<sub>2</sub> folds</li> </ul>	
<b>D<sub>1</sub></b>	<ul style="list-style-type: none"> <li>▪ Relic fabric</li> </ul>		Taconic Orogeny (Ordovician; Obduction of ophiolites)





#### Silurian Intrusions and effusive rocks

- Cape Brulé Porphyry (430 Ma)**  
Porphyritic granodiorite, quartz-feldspar porphyry
- Burlington Granodiorite (434 - 430 Ma)**  
Granodiorite
- Cape St. John Group (early Silurian)**  
Rhyolitic and trachytic flows and tuffs, intrusives, locally mafic and intermediate tuffs and flows

**Highway and highway number**

**Ming Main Deposit location**

**1806 Zone Mineralization horizon**

**Old, previously mined underground shaft**

**New, currently mined underground shaft**

**Fault**

**Pond**

#### Ordovician rocks - Pacquet Harbour Group (PHG)

##### Upper PHG (Mid- to Early Ordovician)

- Balsam Bud Cove Formation**  
Mafic epiclastic rocks, black shale
- Balsam Bud Cove Formation**  
Rhyolite (467 Ma), and felsic tuff (470 Ma)
- Venam's Bight Formation**  
Pillow basalt
- Bobby Cove Formation**  
Mafic tuff, epiclastic rocks, turbidites
- Scrape Point Formation**  
Pillow basalt, gabbro (483 Ma)

##### Lower PHG (Early Ordovician)

- Mt. Misery Formation**  
Rhyodacite, rhyolite massive flows, tuff breccia ('Rambler rhyolite'; 487 Ma)
- Mt. Misery Formation**  
Intermediate Ti-boninite, island arc tholeiitic pillow basalt, pillow breccia
- Betts Head Formation**  
Pillowed, aphyric, variolitic boninite
- Sheared gabbro**

**Figure 3-2.** (previous page) Detailed geologic map of the Pacquet Harbour Group (PHG) hosting the Ming (Main) Mine and previously mined volcanogenic massive sulfide deposits (modified after Castonguay et al., 2009); age data for the PHG from Castonguay et al. (2009) and Sulski et al. (2010); age data for the Silurian intrusions from Cawood et al. (1993). Datums are shown in WGS 84 (top and right) and UTM NAD83, Zone 21N (bottom and left)

### 3-2-2 CONSOLIDATED RAMBLER VMS CAMP

The Ming (or Ming Main) deposit is one of five VMS deposits (Ming, Ming West, Rambler deposit, East Rambler, Big Rambler) of the consolidated Rambler camp hosted in the lower Pacquet Harbour Group (Fig. 3-2). The Ming, Ming West, Rambler, and East Rambler deposits are stratabound, bimodal-mafic Cu-(Au) VMS deposits, which were all mined previously (Tuach and Kennedy, 1978; Pilgrim, 2009). Their ore zones are hosted within a moderately metamorphosed and poly-phase deformed felsic volcanic footwall (Rambler rhyolite), which yielded a U-Pb zircon age of 487 Ma (unpubl. data by V. McNicoll in Castonguay et al., 2009). The sulfide mineralization at Ming, Ming West and Rambler occurs as semi-massive to massive sulfide horizons and sulfide stringers. All three deposits are enriched in Cu and precious metals and dominated by pyrite–chalcopyrite assemblages with lesser pyrrhotite and sphalerite, with variable precious metal enrichment (Tuach and Kennedy, 1978). The hanging walls rocks of the Ming, Ming West, and Rambler deposits consists of mixed volcano-sedimentary and mafic igneous rocks of the ca. 470 Ma upper Pacquet Harbour

Group (Skulski et al., 2009, 2010). Rambler East is a small stratabound, low-grade Cu VMS deposit with minor Au and Ag on the edge of the Rambler rhyolite and shows only stringer and disseminated sulfide mineralization with silicic footwall (Fig. 3-2; Tuach and Kennedy, 1978; Swinden and Thorpe, 1984). The sulfide mineral assemblage is pyrite–chalcopyrite–pyrrhotite. The hanging wall consists of siliceous meta-volcanic rocks. Tuach and Kennedy (1978) interpreted Rambler East to occur in the same stratigraphic horizon than the Ming and Rambler deposits, but be formed on the fringes of the Rambler rhyolite.

The Big Rambler deposit is a small mafic Cu VMS deposit located south of the Rambler Brook fault within the boninitic Betts Head Formation of the lower Pacquet Harbour Group and occurs stratigraphically below the Rambler rhyolite (Fig. 3-2). The deposit shows disseminated and stringer sulfide mineralization of pyrrhotite, chalcopyrite and pyrite (Tuach and Kennedy, 1978).

The Ming deposit consists of a variety of zones, many discovered since the early 2000s, including: 1806 Zone, 1807 Zone, Ming S Up Plunge and Down Plunge with Lower Footwall, and Ming North (Fig. 3-3). The 1806 and 1807 zones, and Ming South with the Lower Footwall run parallel to the old mined shaft, trending NE with a plunge of 30-35°. Ming N is the extension of the old main shaft. All new discovered horizons are hosted within the Rambler rhyolite. Semi-massive to massive and stringer sulfide mineralization is common to all zones except the Lower Footwall zone and consist of pyrite and chalcopyrite with

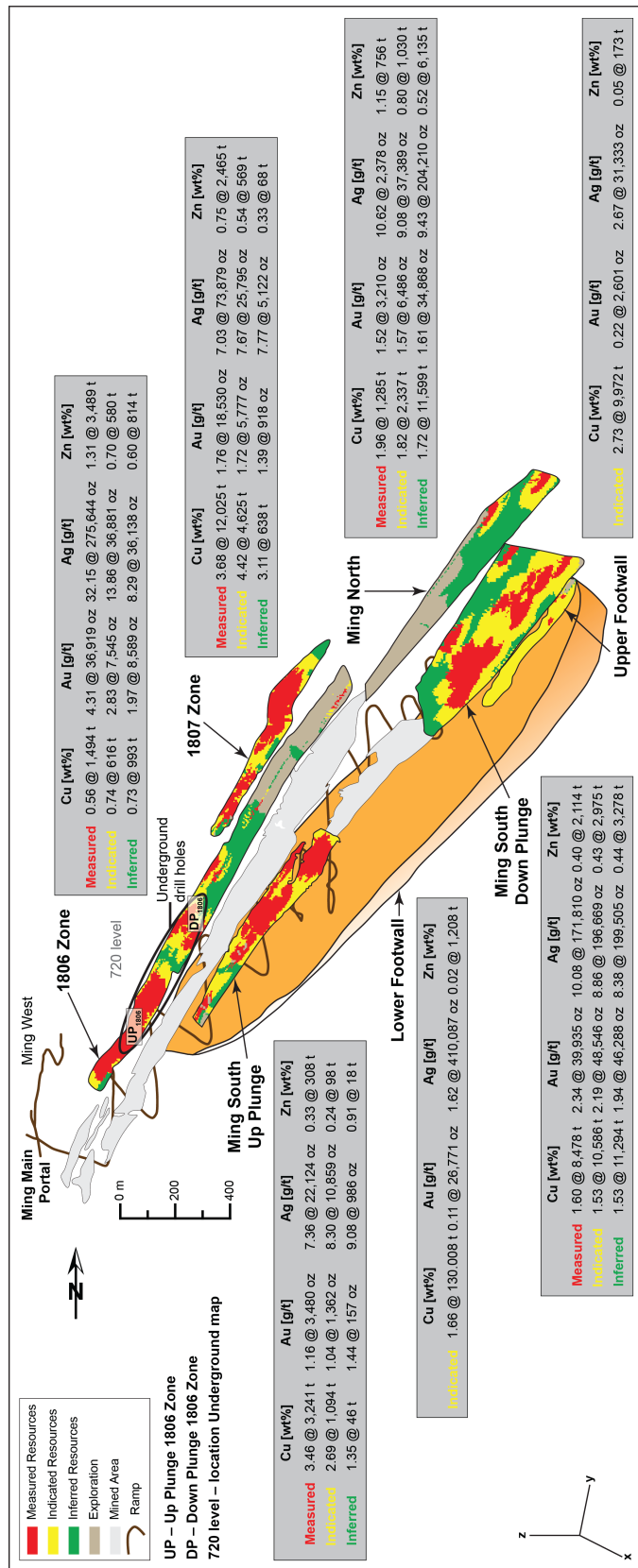
minor sphalerite–pyrrhotite ± arsenopyrite. The Lower Footwall zone contains only chalcopyrite–pyrrhotite ± pyrite stringer mineralization.

### **3-3 GEOLOGY OF THE 1806 ZONE**

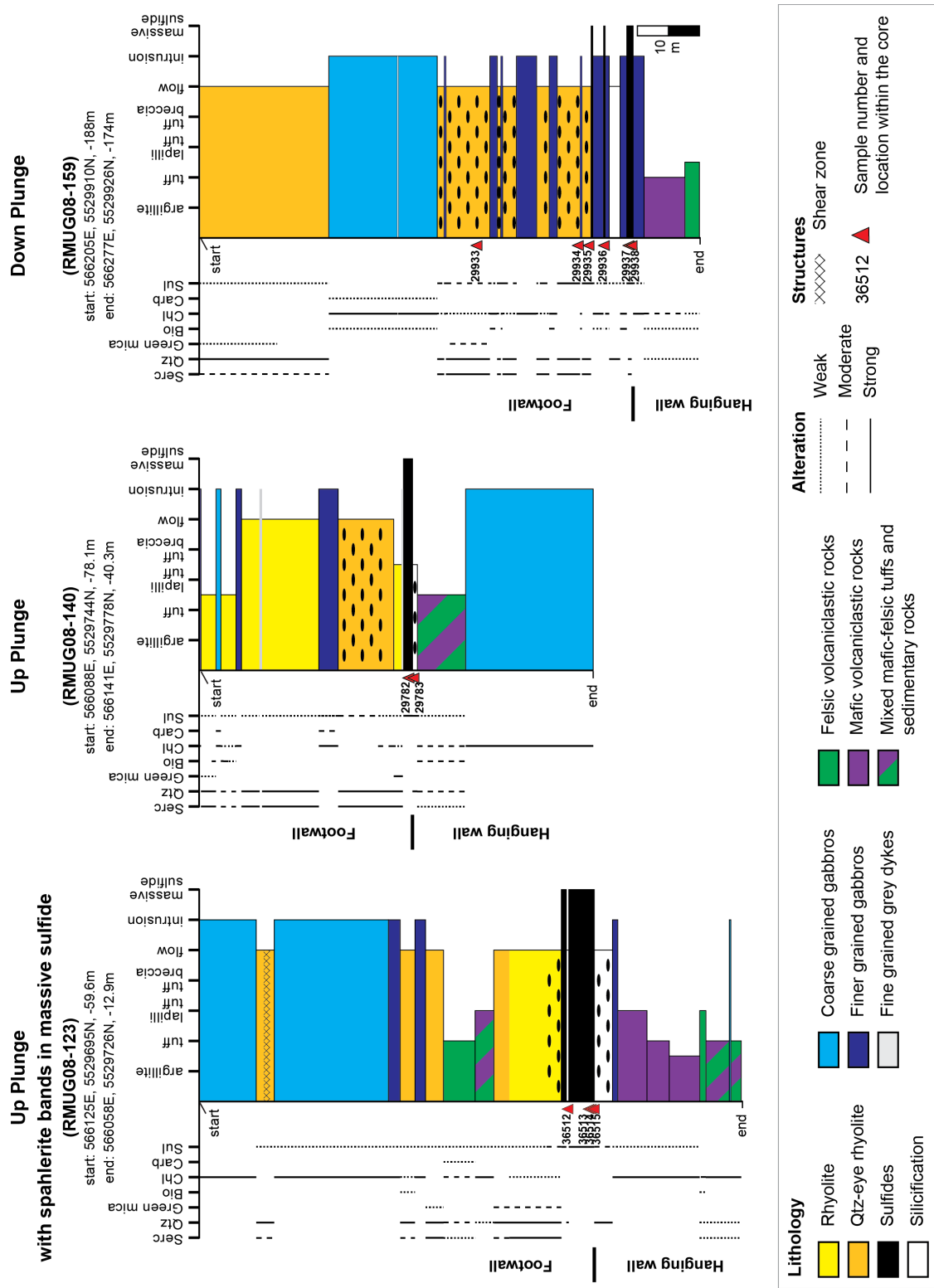
Twenty-three underground drill holes from the 1806 Zone (Fig. 3-3) were examined for stratigraphy, alteration, ore mineralogy and composition from the up plunge part and down plunge part. The terms up plunge and down plunge are used in this paper to describe two different portions of the 1806 Zone relative to the plunge of the zone (Fig. 3-3) and to highlight the variations (e.g., metal distribution, ore assemblage) between these two areas. Representative graphic drill logs from the 1806 Zone are shown in Figure 3-4. Drill core work was supplemented by underground mapping at the 720 level of the mine, in the up plunge portion of the 1806 Zone (Figs. 3-3 and 3-5). Key aspects of the mineralized succession are summarized below.

#### **3-3-1 RAMBLER RHYOLITE**

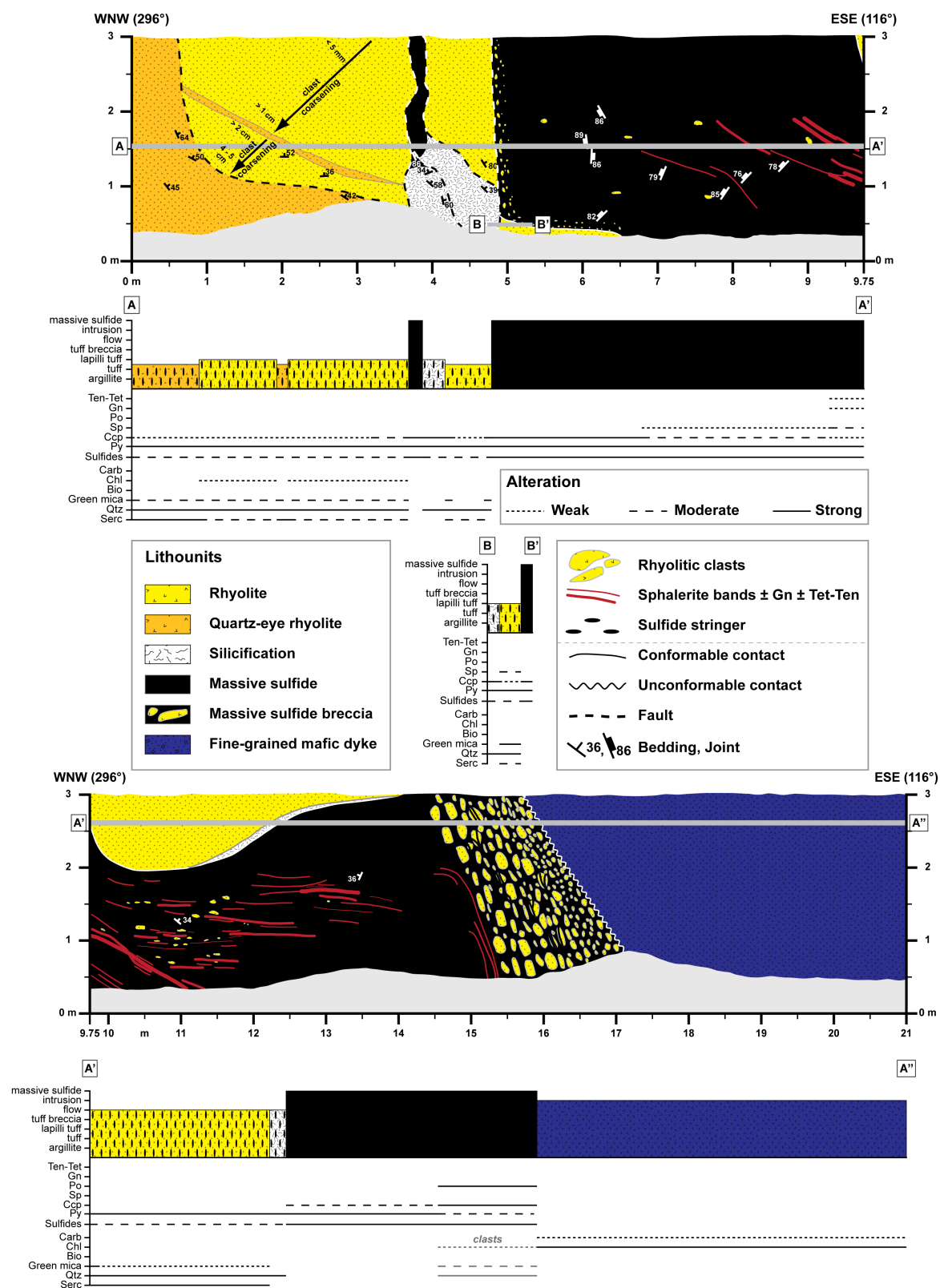
The Rambler rhyolite is a ca. 2.5 km wide sequence of felsic volcanic rocks of the lower Pacquet Harbour Group and in its upper part is the footwall to the Ming, Ming West, Rambler, and Rambler East deposits (Skulski et al., 2010). The Rambler rhyolite is dacitic to rhyolitic, grey to green with zones with purple hues, is massive to foliated, and is locally intensely altered (Fig. 3-6a).



**Figure 3-3.** Resource data for the newly explored zones at the Ming deposit from Rambler Metals and Mining Canada Ltd. ([www.ramblermines.com](http://www.ramblermines.com); Pilgrim, 2009); new zones trend NE and plunge 30-35° parallel to the previously mined area (light grey). The 1806 Zone with its up plunge (UP<sub>1806</sub>) and down plunge (DP<sub>1806</sub>) portions is focus of this paper; the 720 level marks the location of the underground map shown in Figure 3-5. Resource data are compliant with are National Instrument 43-101



**Figure 3-4.** (previous page) Stratigraphic drill core sections from the up plunge and down plunge portions of the 1806 Zone; drill holes are reversed due to underground drilling, i.e. start represents footwall and end of section is hanging wall. Coordinates for start and end of drill cores are in UTM NAD83, Zone 21N and depths are in meters below sea level. Abbreviations: Serc – sericite, Qtz – quartz, Bio – biotite, Chl –chlorite, Carb – carbonate, Sul – sulfides





**Figure 3-5.** (previous page) Underground map from the 720 level (up plunge portion) of the 1806 Zone (Fig. 3-3). Mapped wall (top: first half from 0-9.75 m, bottom: second half from 9.75-21 m) is a cross section perpendicular to the NE trending sulfide lens and shows the relationships between the massive sulfide lens (black) and the different lithologies (Rambler rhyolite, mafic dike, silicified cap horizon). Hypothetical drill profiles are shown for mapped wall (top: A-A' and B-B', bottom: A'-A'') to show variations in lithology, alteration and sulfide mineralogy; see text for details to Figure 3-5. Abbreviations: Serc – sericite, Qtz – quartz, Bio – biotite, Chl –chlorite, Carb – carbonate, Py – pyrite, Ccp – chalcopyrite, Sp – sphalerite, Po – pyrrhotite, Gn – galena, Ten-Tet – tennantite-tetrahedrite

The thickness of the Rambler rhyolite varies from a few centimeters up to 30m in drill holes (Fig. 3-4). The unit consists of various lithofacies including massive flows, rare tuff breccia and tuff to lapilli tuff (Fig. 3-4); the contacts between the various lithofacies are gradational. White and blue quartz-eyes up to 3mm commonly occur in all lithofacies. In the down plunge part of the 1806 Zone quartz eye bearing rhyolite flows predominate, whereas in the up plunge portion flows alternate with tuffs to lapilli tuffs (Fig. 3-4). Rhyolitic lapilli tuff, tuff breccias and flows are often clast-bearing or show remnants of clasts (i.e., ghost clasts). Clasts are usually silicified, sub-angular to sub-rounded and up to 3 cm in size (Fig. 3-6b, c). Rhyolitic units with coarse clasts and ghost clasts are found proximal to the semi-massive to massive sulfide horizon (Figs. 3-4, 3-5, and 3-6b).

### 3-3-2 MINERALIZED ZONES

The 1806 Zone mineralization consists of: (1) discordant sulfide stringers in footwall rocks; (2) concordant to stratabound semi-massive to massive sulfides; and (3) sulfide veinlets and disseminations in a silicified cap horizon. Stringers (30-50 % sulfide in host rock) in footwall rhyolite vary in intensity, but the thickness and abundance of the sulfide veins increase towards semi-massive to massive sulfides. Sulfide stringer zones are usually up to 10 m thick but can locally be up to 20m thick (Fig. 3-4). The contact with the overlying semi-massive and/or massive sulfides is sharp (Fig. 3-6b). The sulfide veins are composed of pyrite, chalcopyrite, and sphalerite (Fig. 3-6c). Sulfide stringers are often transposed into the main foliation or have a random orientation around clasts and ghost clasts (Fig. 3-6c).

#### 3-3-2-1 *Semi-massive to massive sulfides*

The semi-massive to massive sulfides consist of more than 50 % sulfides with minor, small to coarse, rounded to sub-angular and altered (quartz, sericite, green mica) rhyolite fragments, and up to 8m thick in the 1806 Zone. Alternations between semi-massive and massive sulfides are common. The semi-massive to massive sulfides contain pyrite as the main sulfide phase (Fig. 3-6d, e), which is associated with lesser amounts of chalcopyrite, sphalerite, and pyrrhotite. Electrum, arsenopyrite, galena and tetrahedrite are present in minor amounts (Fig. 3-6d). In the up plunge portion of the sulfide lens, sphalerite bands with minor galena  $\pm$  tetrahedrite commonly occur (Figs. 3-5 and 3-6g). These

sphalerite bands are 1 to 30cm thick and are parallel to the main foliation (Fig. 3-6g). Sulfides are fine-grained, but pyrite can be coarse-grained along some mafic dikes due to recrystallization, and underground near dikes the sulfides commonly occur in ~ 2m brecciated horizons with abundant coarse, sub-angular and altered rhyolite clasts in a sulfide matrix (Figs. 3-5 and 3-6h). These brecciated horizons are interpreted to be re-worked sulfide breccia due to the replacement of Rambler rhyolite by the mafic dike.

#### *3-3-2-2 Silicified horizon*

A strongly silicified horizon commonly occurs on top of the massive sulfide horizon; however, it is not present in all parts of the zone (Fig. 3-4). It is usually 30-50cm thick but is locally up to 3m. This horizon is grey-white, massive, and mineralized with remnants of former coarse rhyolite clasts (Fig. 3-6f). This ghost clast texture resembles the clast-bearing units of the Rambler rhyolite occurring usually just below the semi-massive to massive sulfide lens (Fig. 3-6b). The cap usually has a sharp contact with the massive sulfide horizon and consists of random stringers proximal to the massive sulfide horizon and becomes disseminated sulfide and electrum at distance from the massive sulfide (Fig. 3-6f). Pyrite and chalcopyrite are the main sulfide phases, but pyrrhotite, arsenopyrite, and visible electrum are also present.

### *3-3-3 HANGING WALL MAFIC, FELSIC AND MIXED VOLCANICLASTIC ROCKS*

Mafic, felsic or mixed tuffaceous rocks sit on top of the semi-massive to massive sulfide horizon or the silicified cap; they are generally 5-10 m in thickness (Fig. 3-4b, c). The volcaniclastic sequence likely correlates with the upper Pacquet Harbour Group (Skulski et al., 2010). The rocks are light to dark greenish or grayish and alternate between tuff and lapilli tuff. The contacts with the footwall strata and with mafic dikes are sharp. The hanging wall volcaniclastic rocks are generally finely laminated to thinly bedded and locally exhibit normal grading. The rocks contain a weak foliation, which often results in clast elongation, and only proximal to the mineralization does the unit contain any alteration or mineralization (i.e., fine pyrite). They are interpreted to be distal volcaniclastic turbiditic rocks.

### *3-3-4 MAFIC AND FELSIC DIKES*

#### *3-3-4-1 Mafic dikes*

Dark greenish, fine- to coarse-grained gabbro dikes cut both the footwall and hanging wall rocks and range in thickness from a few decimeters up to several tens of meters (Figs. 3-4 and 3-5). Crosscutting relationships indicate that at least two dike generations are present with fine-grained dikes cutting coarse-grained dikes. Contacts with adjacent lithologies are sharp and chilled margins are common in dikes that cut the Rambler rhyolite. The coarse-grained dikes are

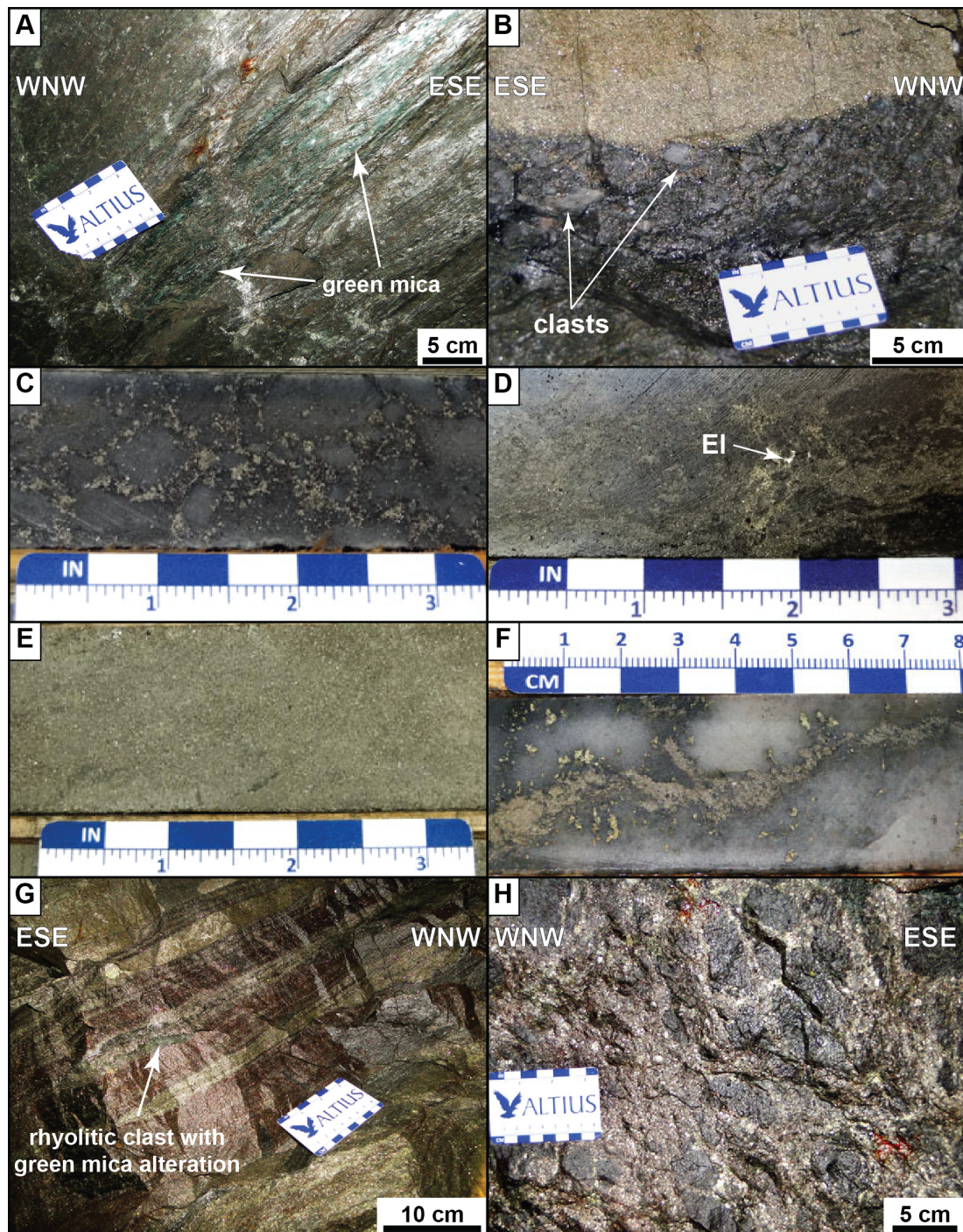
characterized by coarse biotite, amphibole, and minor feldspar set in a fine-grained greenish matrix. The fine-grained dikes have a similar mineralogy but lack feldspar and do not have any porphyroclasts. Rare pyrite cubes occur in coarse-grained and fine-grained dikes.

#### *3-3-4-2 Felsic dikes*

Very fine-grained felsic dikes are not common in the mineralized environment. They occur predominantly in the footwall, cutting the Rambler rhyolite. They are light grey, up to 20cm thick, and have sharp contacts. Alteration and sulfide mineralization are usually absent and deformation is also not observed.

#### *3-3-5 HYDROTHERMAL ALTERATION*

Quartz – sericite  $\pm$  green mica – sulfide is the dominant footwall alteration assemblage in the Rambler rhyolite (Fig. 3-6a-c); chlorite and biotite occur sporadically in the Rambler rhyolite. Green mica increases in proximity to mineralization (Figs. 3-4 and 3-5) and rhyolite clasts in the massive sulfide have green mica alteration (Fig. 3-6g). The silicified horizon has very strong quartz alteration, with lesser chlorite and sulfide (Figs. 3-4, 3-5, and 3-6f). Alteration decreases into the hanging wall and is dominated by chlorite, quartz and minor biotite  $\pm$  sericite (Fig. 3-4).



**Figure 3-6.** Rambler rhyolite and sulfide mineralization at the 1806 Zone. **(A)** Altered and deformed Rambler rhyolite with green mica (white arrows); **(B)** Sharp contact between clast-bearing rhyolitic lapilli tuff to massive sulfide lens; **(C)**

Brecciated Py-Sp stringer around sub-rounded, silicified clasts in quartz eye-bearing, rhyolitic lapilli tuff; **(D)** Stringer sulfides of Py-Ccp-Sp composition with visible El (white arrow); **(E)** Massive Py-Ccp sulfide; **(F)** Silicified horizon with ghost clasts in assumed lapilli tuff and with discordant Py-Ccp sulfide stringers; **(G)** Massive Py-Ccp sulfides with Sp bands and relictic rhyolite clasts with green mica alteration (white arrow); **(H)** Massive sulfide breccia with coarse, sub-angular rhyolite clasts in Ccp-Po-Py matrix on contact to mafic dike; see text for details to Figure 3-6. Abbreviations: Ccp – chalcopyrite, El – electrum, Py – pyrite, Sp – sphalerite

### **3-4 SULFIDE AND OXIDE MINERALOGY**

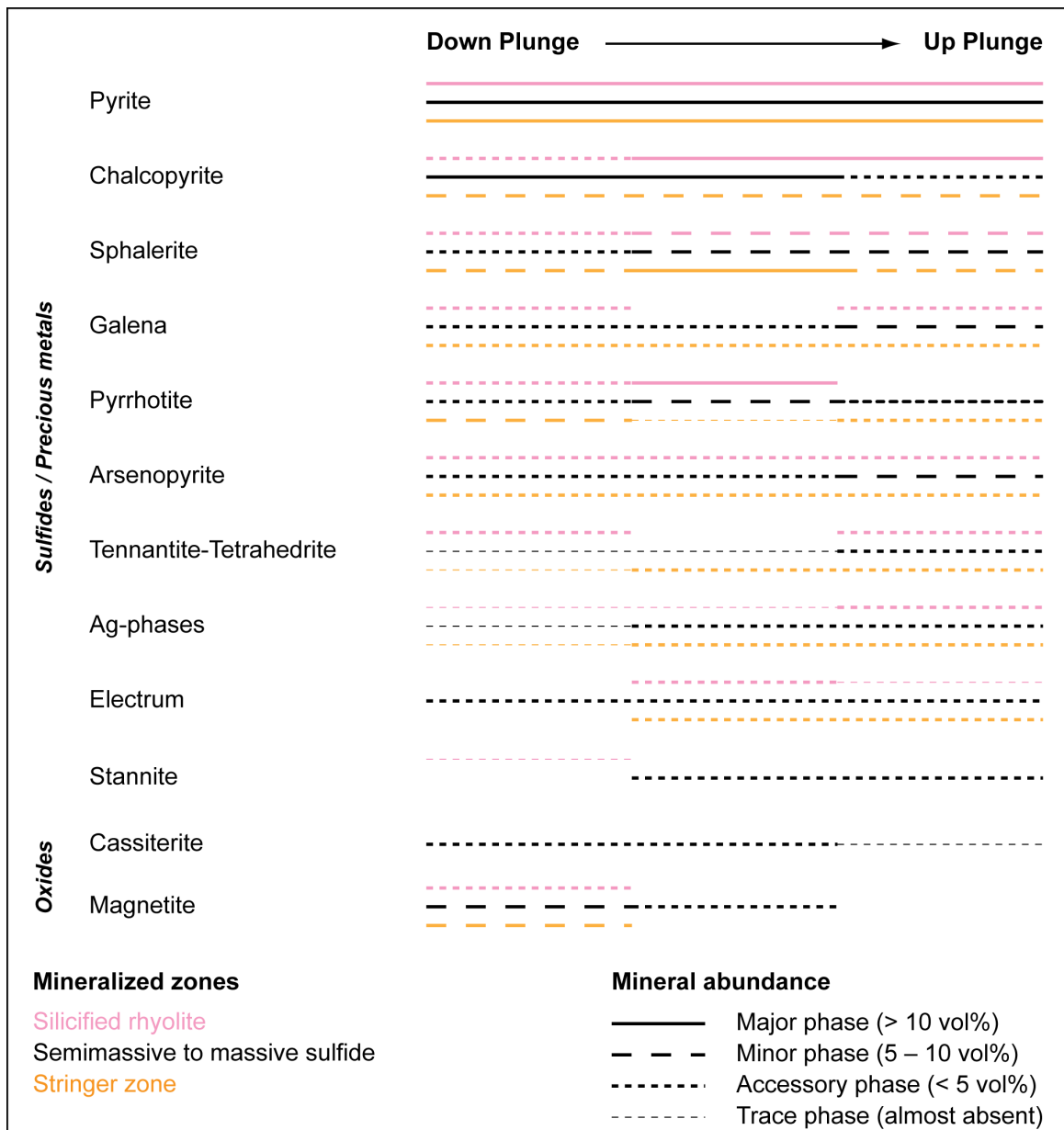
The sulfide and oxide mineralogy of the 1806 Zone was examined by optical microscopy of polished thin sections of 86 samples from 23 drill cores. Some research on the sulfide and oxide mineralogy at Ming has been previously documented in Brueckner et al. (2011); however, little work has been reported on sulfide and precious metal mineral textures, precious metal mineral associations, and the spatial variations in sulfide, sulfosalt, oxide, and precious metal minerals in the 1806 Zone.

Pyrite ( $\text{FeS}_2$ ), chalcopyrite ( $\text{CuFeS}_2$ ), sphalerite ( $\text{ZnS}$ ), pyrrhotite ( $\text{Fe}_{(1-x)}\text{S}$ ), and galena ( $\text{PbS}$ ) are the main sulfide phases in the 1806 Zone (i.e., stringer sulfides, semi-massive to massive sulfides, silicified cap horizon). Pyrite is the dominant sulfide phase. Variations in the abundances and distributions of sulfides are shown in Figure 3-7. In general, chalcopyrite and pyrrhotite are more abundant in the down plunge portion of the lens, whereas sphalerite and galena

is more abundant in the up plunge portion of the 1806 Zone (Fig. 3-7). Besides the main base metal sulfides above, there are more than 10 different sulfide, sulfosalt, precious metal, and telluride phases present in the 1806 Zone, including: arsenopyrite ( $\text{FeAsS}$ ), tennantite  $((\text{Cu}, \text{Ag})_{10}(\text{Fe}, \text{Zn})_2\text{As}_4\text{S}_{13})$  – tetrahedrite  $((\text{Cu}, \text{Ag})_{10}(\text{Fe}, \text{Zn})_2\text{Sb}_4\text{S}_{13})$ , stannite ( $\text{Cu}_2\text{FeSnS}_4$ ), Ag-phases (e.g., miargyrite ( $\text{AgSbS}_2$ ), pyrargyrite ( $\text{Ag}_3\text{SbS}_3$ ), mercurian stephanite  $((\text{Hg}, \text{Ag})_5\text{SbS}_4)$ , an unnamed  $\text{AgCuFeS}$  phase,  $\text{AgHg}$  alloys, and mercurian electrum ( $\text{AuAgHg}$  alloy) (Fig. 3-7). These phases are generally enriched in the up plunge portion of the 1806 Zone (Fig. 3-7).

Arsenopyrite is the most abundant trace to minor phase in the 1806 Zone (Fig. 3-7). Arsenopyrite occurs in three main associations: (1) with base metal sulfides, preferentially with pyrite, chalcopyrite, and pyrrhotite as euhedral to subhedral grains or as inclusions in these phases; (2) intergrown with tennantite-tetrahedrite either as small, euhedral arsenopyrite crystals (Fig. 3-8a) or as anhedral grains in a myrmekitic texture with additional chalcopyrite  $\pm$  sphalerite  $\pm$  electrum  $\pm$  galena (Fig. 3-8c to e); and (3) in close proximity to precious metal phases (Fig. 3-8c-k, m, and n). In the down plunge part, arsenopyrite also occurs with cassiterite. Arsenopyrite shows evidence for recrystallization (e.g., porphyroblast growth; Fig. 3-8i), but there are wormy-like grains with replacement-like textures containing chalcopyrite (P. Spry, pers commun, 2013) are likely original textures (Fig. 3-8c to e).





**Figure 3-7.** Sulfide mineral abundance within the 1806 Zone from down plunge portion to the up plunge portion for base metal sulfides including arsenopyrite, the most abundant sulfosalts, precious metals, and oxides

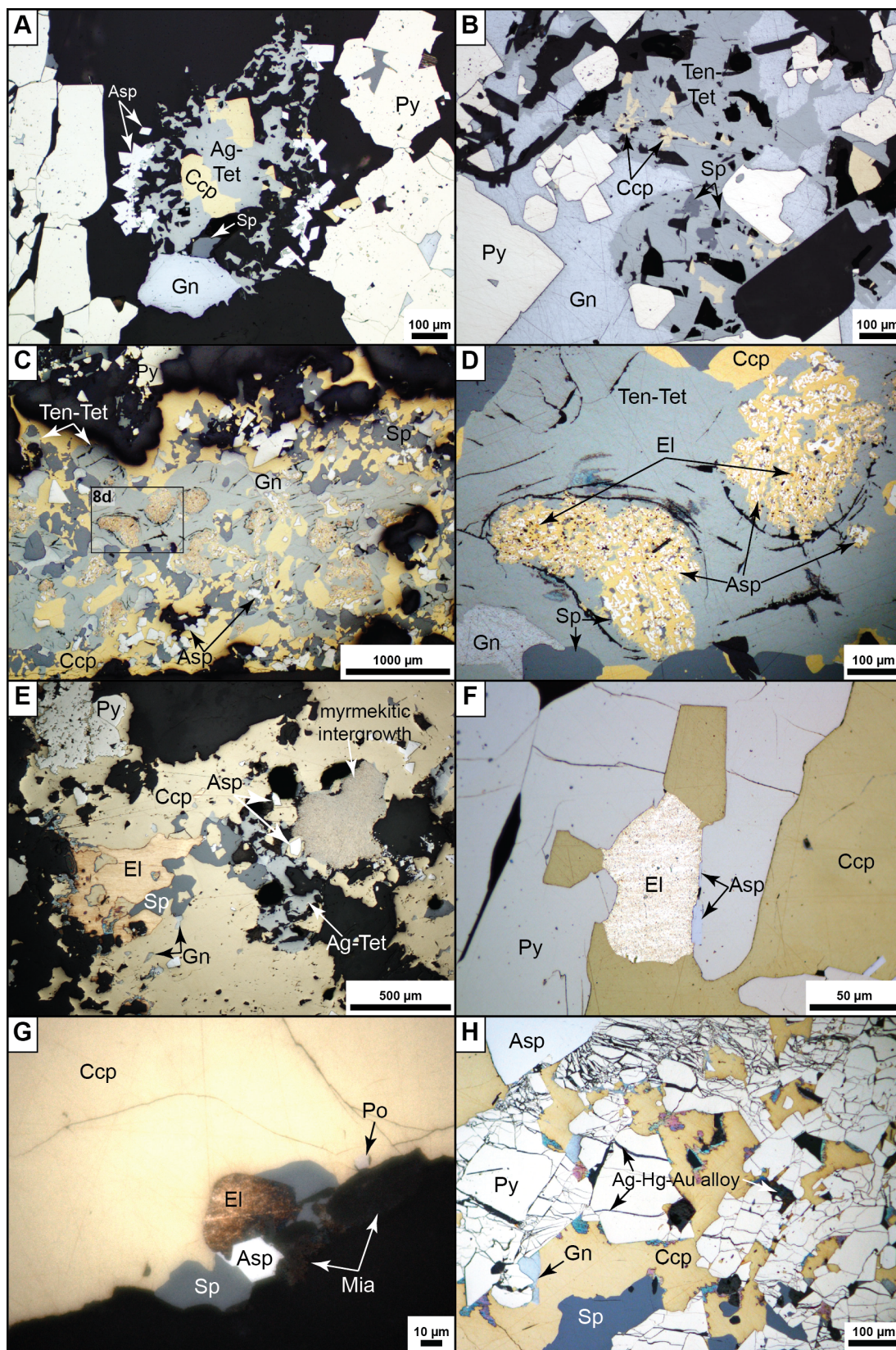
Tennantite-tetrahedrite is the most common sulfosalt and occurs throughout the 1806 Zone but is preferentially enriched in the up plunge portion of the lens (Fig. 3-7). Tennantite-tetrahedrite commonly occurs as large anhedral masses (Fig. 3-8b, c), often with myrmekitic intergrowth textures with arsenopyrite – chalcopyrite  $\pm$  sphalerite  $\pm$  electrum  $\pm$  galena (Fig. 3-8c, d). The various sulfide phases and electrum that are present in such myrmekites are most commonly anhedral (e.g., wormy-like, sub-rounded, amoeboid) with minor exceptions. Electrum is closely associated or spatially proximal to myrmekitic sulfosalts-sulfides (Fig. 3-8c-e). In the down plunge portion of the 1806 Zone tennantite-tetrahedrite occurs predominantly with chalcopyrite and/or arsenopyrite (Fig. 3-8a). In contrast, in the up plunge area tennantite-tetrahedrite is associated with arsenopyrite, sphalerite, galena, chalcopyrite, and precious metals (Fig. 3-8b, e, and l). In particular in the sphalerite bands, tennantite-tetrahedrite often replaces chalcopyrite (Fig. 3-8b).

A wide variety of Ag-phases occur predominantly in the up plunge portion of the 1806 Zone (Fig. 3-7). A Ag-Hg $\pm$ Au alloy containing less than 10wt.% Au occurs predominantly along fractures and between grain boundaries of recrystallized pyrite (Fig. 3-8h). A phase resembling chalcopyrite in composition but with up to 10wt.% Ag occurs in very close proximity to electrum and may result from a reaction between electrum and chalcopyrite (Fig. 3-8m). Miargyrite, pyrargyrite, and the other Ag-phases are usually associated with electrum (Fig. 3-8g, m), arsenopyrite (Fig. 3-8g, j, k), chalcopyrite (Fig. 3-8g, j), or with sphalerite

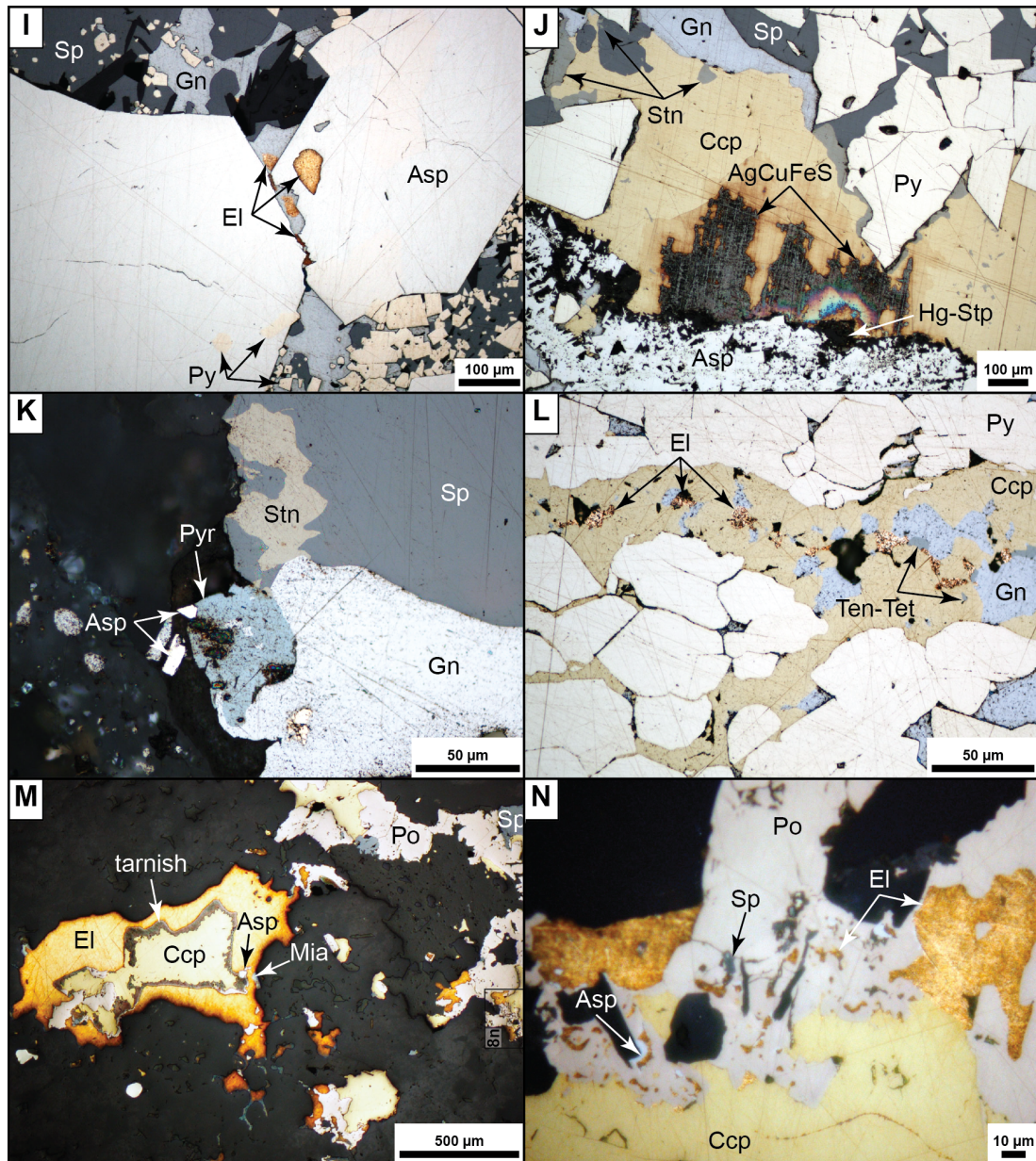
± galena (Fig. 3-8k).

Gold occurs either as electrum with elevated Hg concentration (mercurian electrum) or as a AgHgAu alloy with over 10wt.% Au; the former occurrence is by far more abundant than the latter. Associations with base metal sulfides chalcopyrite and pyrite predominate, whereas assemblages with sphalerite, galena or pyrrhotite are minor and restricted to the up plunge portion of the 1806 Zone (Fig. 3-8d to g, and 3-8l to n). Besides base metal sulfides, electrum shows a strong association with arsenopyrite, sulfosalts (e.g., tennantite-tetrahedrite, stannite), and Ag-phases and occurs always in direct vicinity to one or all of these phases. Electrum occurs in various textures as: (1) free grains with base metal sulfides, arsenopyrite, sulfosalts and/or Ag-phases; (2) as inclusions in arsenopyrite, galena, and pyrrhotite; and (3) in myrmekite texture in tennantite-tetrahedrite.

Stannite is an accessory phase and is commonly restricted to the semi-massive to massive sulfide horizon in the up plunge portion of the deposit (Fig. 3-7). It occurs with sphalerite (Fig. 3-8j, k) and/or chalcopyrite (Fig. 3-8k). Stannite (with or without cassiterite inclusions) occurs exclusively in Ag-phase- and/or electrum-bearing samples and is found proximal to precious metal phases (Fig. 3-8j, k).







**Figure 3-8.** Reflected light images of sulfide assemblages and textures from semi-massive to massive sulfides (**A, B, F-L**), sulfide stringer (**C-E**), and silicified horizon (**M, N**); (**A**) Intergrowth of AgTet with Ccp and marginal Asp (semi-massive sulfide, down plunge); (**B**) Ten-Tet replacing Ccp and partly intergrown with Sp, Gn marginal on Ten-Tet (massive sulfide, up plunge); (**C**) Ten-Tet with myrmekite textures of Asp-Ccp-Sp-Ten-Tet $\pm$ Sp $\pm$ El and marginal Ccp-Asp-Sp-Gn (sulfide stringer on contact to massive sulfide, up plunge); (**D**) Detail from 3-8c:

small, sub-roundish El in myrmekite (black arrows; sulfide stringer on contact to massive sulfide, up plunge); **(E)** El with marginal Sp in Ccp and inclose spatial relation to AgTet and very fine-grained myrmekite (sulfide stringer, up plunge); **(F)** El with marginal Asp between recrystallized Py in Ccp (semi-massive sulfide, down plunge); **(G)** Small, roundish El with Asp-Mia-Sp marginal on Ccp (semi-massive sulfides, up plunge); **(H)** Brittle deformed and recrystallized Py with Ag-Hg-Au alloy along cracks and between Py grain boundaries; Asp porphyroblast spatially close to precious metals (massive sulfide, up plunge); **(I)** El inclusions in Gn and Asp porphyroblast (massive sulfide, up plunge); **(J)** Unnamed AgCuFeS phase and Hg-Stp in Ccp on contact to intergrowth of Asp-Py and spatially close to Stn (massive sulfide, up plunge); **(K)** Pyr with Asp and Gn margin; Sp with Stn inclusion (massive sulfide, up plunge); **(L)** Small, sub-roundish El with Gn and Ten-Tet in Ccp (massive sulfide, up plunge); **(M)** Coarse El enclosing Ccp-Po-Asp and with marginal Mia in quartz; fine rim of tarnish on Ccp-El contact (silicified horizon, up plunge); **(N)** Detail of 3-8m: El as inclusions in and marginal on Po; Asp and Sp inclusions in Po, too (silicified horizon, up plunge); see text for details to Figure 8. Mineral abbreviations: AgCuFeS – unnamed AgCuFeS phase, Ag-Tet – Ag-bearing tetrahedrite, Asp – arsenopyrite, Ccp – chalcopyrite, El – electrum, Gn – galena, Hg-Stp – mercurian stephanite, Mia – miargyrite, Po – pyrrhothite, Py – pyrite, Pyr – pyrargyrite, Sp – sphalerite, Stn – stannite, Ten-Tet – tennantite-tetrahedrite

Boulangerite ( $\text{Pb}_5\text{Sb}_4\text{S}_{11}$ ), loellingite ( $\text{FeAs}_2$ ), bismuth tellurides, coloradoite ( $\text{HgTe}$ ), molybdenite ( $\text{MoS}_2$ ) and unknown sulfide phases (Ni, Sb, or In, Cd -bearing) are also present in the semi-massive to massive sulfides of the 1806 Zone. Magnetite ( $\text{Fe}_3\text{O}_4$ ) and cassiterite ( $\text{SnO}_2$ ) are more abundant in the down plunge part of the 1806 Zone and are almost entirely absent to the up plunge part (Fig. 3-7; see also Brueckner et al., 2011).

### **3-5 MINERAL CHEMISTRY**

#### *3-5-1 ANALYTICAL METHODS*

##### *3-5-1-1 Bulk metal analysis*

Copper, Zn, Pb, Ag, and Au assay data were obtained from the assay database of Rambler Metals & Mining, Canada Ltd. Samples were analyzed at Activation Laboratories, Ancaster, ON. Copper, Zn, Pb, and Ag were analyzed by applying aqua regia with an ICP finish (ActLabs Code 1E3). Activation Laboratories used a fire assay fusion followed by acid digestion and analyses by atomic absorption for Au analyses (ActLabs code 1A2). If Au assay exceeded 3,000ppb and/or Ag exceeded 100ppm the samples were treated by fire assay, nitric acid and a gravimetric finish (ActLabs code 1A3). Quality assurance at Activation Laboratories was obtained by the analysis of certified reference materials. The results were in good agreement with the certified values (Pilgrim, 2009). Moreover, blanks were analyzed for quality assurance and no contamination was reported. More detailed information about the analytical procedure and the obtained results of the reference materials are presented in Pilgrim (2009).

##### *3-5-1-2 Semi-quantitative energy-dispersive X-ray (EDX) imaging/spectroscopy*

Back scattered electron (BSE) images and elemental maps were obtained using a FEI Quanta 400 scanning electron microscope (SEM) at the Bruneau Innovation Centre at Memorial University of Newfoundland, Canada. The FEI

Quanta 400 is equipped with a Bruker silicon drift energy dispersive X-ray (EDX) detector. This system allows quick semi-quantitative detection of a variety of elements (here: Si, S, Fe, Cu, Zn, As, Ag, Au, Hg, Sb, and Sn), element maps, and EDX spectra for numerous phases and to corroborate textures documented using reflected light microscopy. The FEI Quanta 400 was run at high vacuum mode at beam energy of 20 keV and a beam current of 10nA. A scintillator detected the  $K\alpha$  emission lines of Si, S, Fe, Cu, Zn, and As, and the  $L\alpha$  emission lines of Ag, Au, Hg, Sb, and Sn. The Esprit software from Bruker (version 1.9) was used for processing for BSE and EDX data. Elemental maps done via EDX do not give specific concentrations for analyzed elements and are semi-quantitative based on raw counts per seconds. Hence, the measured intensity for each element is proportional to its concentration. Therefore, EDX scans allow detecting the occurrence of elements within minerals. In order to detect possible interferences (e.g., Zn  $K\beta$  interferes with Au  $L\alpha$ ; As  $K\alpha$  interferes with Pb  $L\alpha$ ), the mineral of interest is scanned and alternative emission lines are then used to check if elemental overlaps occur or not. If an overlap occurs, the alternative, interference-free emission line is used for semi-quantitative EDX scans.

### *3-5-1-3 Electron probe microanalysis (EPMA)*

A total of 13 samples representing all mineralized zones of the 1806 Zone were analyzed for major, minor, and trace composition in sulfides, sulfosalts, precious metal alloys, and oxides at the University of Toronto (UT) using a Cameca SX50/51 electron microprobe. A brief sample description including the



mineral assemblage and the analyzed phases in each sample is found in the Appendix (Table A3-1). A total of 17 elements (Ag, As, Au, Bi, Co, Cu, Fe, Hg, Mn, Mo, Ni, Pb, S, Sb, Sn, Te, Zn) were analyzed in each of the 17 phases (e.g., pyrite, chalcopyrite, sphalerite, galena, pyrrhotite, arsenopyrite, tennantite-tetrahedrite, miargyrite, pyrargyrite, mercurian stephanite, unnamed AgCuFeS phase, electrum, stannite, boulangerite, molybdenite, cassiterite, magnetite). The Cameca SX-50/51 is equipped with three tunable wavelength dispersive spectrometers and a Link (Oxford) Pentafet EDS detector with Be window and a pulse processor. During the measurements in April 2011 and January 2012, beam energy of 25keV and beam current of 20nA at a beam diameter of 1 $\mu$ m were applied. The takeoff angle was 40°. The measured elements were either analyzed by a LIF crystal (Fe K $\alpha$ , Cu K $\alpha$ , Zn K $\alpha$ , As K $\alpha$ , Te L $\alpha$ , Hg L $\alpha$ , Mn K $\alpha$ , Co K $\alpha$ , Ni K $\alpha$ ) or PET crystal (Sn L $\alpha$ , Pb M $\alpha$ , Bi M $\alpha$ , S K $\alpha$ , Mo L $\alpha$ , Au M $\alpha$ , Ag L $\alpha$ , Sb L $\alpha$ ). Counting times were 20 sec for Fe K $\alpha$ , S K $\alpha$ , Cu K $\alpha$ , Zn K $\alpha$ , Pb M $\alpha$ , Au M $\alpha$ , Ag L $\alpha$ , Sb L $\alpha$ , Sn L $\alpha$ , Te L $\alpha$ , Bi M $\alpha$ , Hg L $\alpha$ , Mo L $\alpha$  and 40 sec for As K $\alpha$ , Mn K $\alpha$ , Co K $\alpha$ , Ni K $\alpha$ . Off peak counting times were identical to the counting time. Detection limits for each element are found in the Appendix (Table A3-2). The detection limit for all analyzed phases is similar for measurements done in April 2011 and January 2012. Quality control was maintained by utilizing UT internal standards for each analyzed phase; calibration standards were measured at the beginning of the phase in question. Measured values on each applied internal standard are in accordance with the accepted concentrations in these standards

(Y. Liu, pers commun, 2013). Additionally, data were deemed acceptable if analytical totals fell within a range of  $100 \pm 1.5 \text{ wt.}\%$  and their stoichiometry represented the accepted mineral composition. All clean analyses of sulfide and precious metals fell within this range or were otherwise discarded. The only exception is three data points of Ag-bearing chalcopyrite-like composition with totals  $< 80 \text{ wt.}\%$ , which are discussed in detailed below. For oxides the oxygen concentration was calculated and assured via stoichiometry. Accuracy of results was monitored via UT in-house standards. The results above detection limit were within 5% of the accepted values. Moreover, wavelength scans of unknown samples were undertaken to see background conditions, potential peak overlaps and interferences, and to check the quality of minor element peaks within the unknowns. Precision of the analysis was calculated from the counting rate and is below 0.4% for all major elements; precision for minor components is between 5 and 33%. However, precision increases with increasing concentrations for minor components. Unknown and standard intensities were corrected for dead time. Standard intensities were corrected for standard drift over time by internal software corrections. Interference corrections were applied to S for interference by Co; to As for interference by Pb; to Sn for interference by Co; to Bi for interference by Au; to Mo for interference by Pb; and to Mn for interference by Hg.

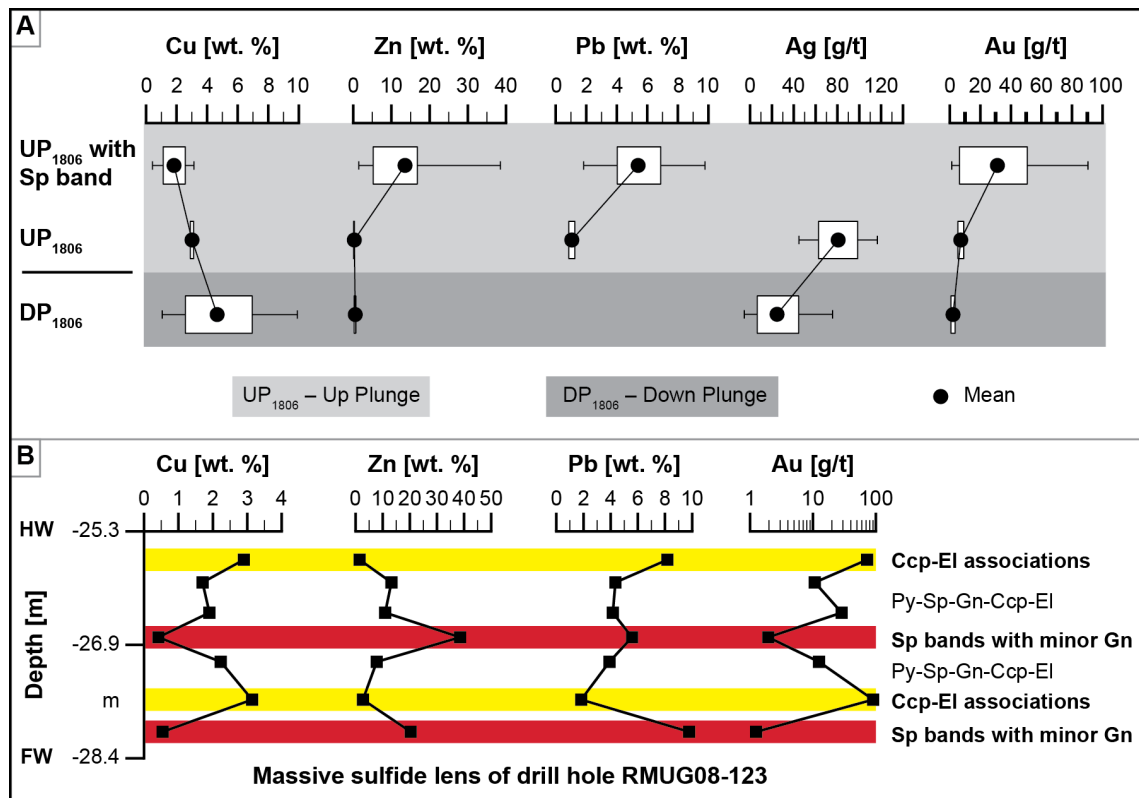
### 3-5-2 RESULTS

#### 3-5-2-1 Assay data (*Activation Laboratories*)

Assay data for Cu, Zn, Pb, Ag, and Au presented in Figure 3-9 are from the semi-massive to massive sulfide lens of three drill holes (Fig. 3-4) from the up and down plunge portion of the 1806 Zone (Table 3-2). In general, the Cu content is enriched in the down plunge area of the zone, whereas Zn, Pb, Ag, and Au are enriched in the up plunge portion of the zone (Fig. 3-9a), reflecting the dominant minerals in each portion of the zone (Fig. 3-7). In Figure 9b the metal distribution within the massive sulfide lens of drill hole RMUG08-123 (Fig. 3-4) is shown in detail and this largely reflects the varying amounts of sphalerite and galena (e.g., Zn, Pb enrichments) versus chalcopyrite (e.g., Cu enrichments). Gold is enriched in the up plunge portion of the 1806 Zone, and while this zone is enriched in Zn-Pb, Au is associated with Cu (i.e., chalcopyrite).

#### 3-5-2-2 *Semi-quantitative energy-dispersive X-ray*

Two samples from the stringer zone and the massive sulfide lens in the up plunge part are used to illustrate the close textural and chemical relationships between precious metals (e.g., electrum, Ag-phases), arsenopyrite and various sulfosalts (e.g., Ag-bearing tennantite-tetrahedrite, stannite, boulangerite).



**Figure 3-9.** Metal zoning in the semi-massive to massive sulfide lens of the 1806 Zone. **(A)** Box-Whisker plot showing variation in base and precious metal grades from down plunge (DP<sub>1806</sub>) to the up plunge (UP<sub>1806</sub>) portion; **(B)** Variations in Cu, Zn, Pb, and Au grades within the massive sulfide lens of the most upper portion of the up plunge due to the occurrence of Sp bands; depth is given in meters below sea level. See text for details; mineral abbreviations same as in Figure 3-8. Assay data from Rambler Metals and Mining Canada Ltd ([www.ramblermines.com](http://www.ramblermines.com); Pilgrim, 2009)

Energy-dispersive X-ray data for a fairly large grain of electrum (> 500 µm) from the stringer zone of the 1806 Zone associated with chalcopyrite and sphalerite (Figs. 3-8e, 3-10a, b) show the association of Au (Fig. 3-10c), Ag (Fig.

3-10d), and Hg (Fig. 3-10e) in electrum. Generally, Au occurs in the core of the grain, whereas Ag is present on the edges (Fig. 3-10c, d); electron microprobe analyses support the latter and show a weak correlation of Au with Hg (Fig. 3-10e). There is a close spatial and chemical relationship between sulfosalts and precious metals (i.e., arsenopyrite and Ag-bearing tetrahedrite in close proximity (< 500µm) to electrum; Fig. 3-10f).

In addition to electrum, Ag-phases are also associated with base metal sulfides, arsenopyrite and sulfosalts as documented in a sample from the massive sulfide lens (Fig. 3-10g to j). Moreover, EDX scans of Ag-phases also have an association with Hg (e.g., mercurian stephanite; Fig. 3-10i).

#### *3-5-2-3 Electron probe microanalysis*

Data from selected samples from the up plunge portion to the down plunge portion are compiled in Table 3-3. The complete data set can be found in the electronic Appendix (Table A3-3). Number of analyses, calculated mineral formula and detected minor elements are summarized for each analyzed phase in Table 3-4.

The major element composition of pyrite is consistent throughout the 1806 Zone with Fe and S ranging between 45.22-46.77wt.% and 52.91-53.90wt.%, respectively. All pyrite analyses have near stoichiometric compositions with some grains showing As substitution ranging from 1,065 to 9,484ppm (Fig. 3-11a). The

arsenian pyrite grains do not show any spatial association with either As-rich phases (e.g., arsenopyrite, tennantite) or electrum.

**Table 3-2.** Assay data for Cu, Zn, Pb, Ag, and Au of the semi-massive to massive sulfide lens from three representative drill holes (data from Rambler Metals & Mining Canada Ltd.)

Drill hole interval							
Sample No.	From [m]	To [m]	Ag [ppm]	Au [ppm]	Cu[wt.%]	Pb [wt.%]	Zn [wt.%]
Up Plunge with Sp bands (RMUG08-123)							
27423	58.4	59.1		1.25	0.543	9.78	20.30
27425	59.1	60.1		90.40	3.14	1.83	2.68
27426	60.1	61.1		12.50	2.23	3.91	7.78
27427	61.1	61.4		1.95	0.420	5.57	38.50
27428	61.4	62.4		28.60	1.90	4.16	10.90
27429	62.4	63.0		10.70	1.70	4.35	13.20
27431	63.0	63.6		72.80	2.90	8.18	1.47
	Average			31.17	1.83	5.40	13.55
	Std			35.97	1.06	2.72	12.73
Up Plunge (RMUG08-140)							
28104	33.8	34.7	134.20	11.00	2.79	1.45	0.364
28106	34.7	35.5	62.50	3.40	3.23	0.667	0.180
	Average		98.35	7.20	3.01	1.06	0.272
	Std		50.70	5.37	0.311	0.554	0.130
Down Plunge (RMUG08-159)							
29259	64.1	64.5	93.20	4.20	9.90		0.840
29262	64.7	65.0	74.40	0.800	8.20		0.730
29264	66.6	67.0	24.50	4.16	3.20		0.410
29271	70.6	71.0	25.30	1.01	2.37		0.410
29272	71.0	71.3	12.30	1.18	1.06		0.330
29273	71.3	71.5	24.50	1.37	3.20		0.440
	Average		42.37	2.12	4.66		0.527
	Std		33.00	1.61	3.53		0.206

**Abbreviations:** Sp - sphalerite, Std - standard deviation

Most chalcopyrite analyses are near stoichiometric with Cu, Fe, and S ranging between 32.76-35.55wt.%, 28.25-30.77wt.%, and 33.76-36.13wt.%, respectively.

Sphalerite grains from all mineralized zones within the 1806 Zone have a wide range of Fe content between 1.12-10.16wt.%, with Zn and S concentrations ranging between 54.75-65.28wt.% and 32.33-33.52wt.%, respectively. Sphalerite is near stoichiometric with Fe substituting on the Zn site (e.g., Vaughan and Craig, 1978; Di Benedetto et al., 2005; Wright, 2009). Based on the Fe content, three different populations can be distinguished (Fig. 3-11b): (1) low-Fe sphalerites have Fe contents of 1.12-2.94wt.% with Zn contents of 65.10-63.24wt.%, (2) medium-Fe sphalerites have Fe contents of 4.78-6.36wt.% at Zn values of 61.24-58.12wt.%, and (3) high-Fe sphalerites have concentrations of 8.41-10.16wt.% Fe at 57.36-54.83wt.%. Low-Fe and high-Fe sphalerites occur from the down plunge area to the up plunge area, whereas medium-Fe sphalerites are detected only in the up plunge portion of the 1806 Zone (Fig. 3-11b).

Analyzed galena grains have Pb and S content of 83.94-87.55wt.% and of 12.27-13.90wt.%, respectively, and have a minor excess of Pb in their mineral formula.

Pyrrhotite grains were measured in the semi-massive to massive sulfide horizon and in the silicified horizon in the 1806 Zone. Their major composition is homogeneous with Fe and S ranging between 59.63-60.69wt.% and 38.85-40.14wt.%, respectively.

Arsenopyrite analyses from throughout the 1806 Zone range in Fe, As, and S from 33.58-34.98wt.%, 41.69-46.68wt.%, and 19.50-23.71wt.%,

respectively. They are non-stoichiometric with deficiencies in both Fe and As (Fig. 3-11c). Furthermore, the analyzed arsenopyrite grains are more deficient in As than in Fe (Fig. 3-11c). Most arsenopyrite data show a wide abundance of minor elements including variable enrichments in transition metals (Ni, Mn) and elements of the epithermal suite (Bi, Sb, Te), including Au and Ag; however, the measured concentration of these traces cannot equalize the deficiency in either Fe or As in the arsenopyrite. The most abundant minor element in arsenopyrite is Ni; however, Ni does not show a clear correlation to any of the major phases or location within the 1806 Zone (Fig. 3-11d).

Tennantite-tetrahedrite is one of the most complex solid solution series amongst the heterogeneous sulfosalt group (Moëlo et al., 2008). Major and minor components include Cu (15.29-44.46wt.%), Ag (0.29-29.27wt.%), Fe (1.99-6.56wt.%), Zn (0.31-5.49wt.%), As (0-19.25wt.%), Sb (1.33-29.06wt.%), and S (20.99-28.52wt.%). Amongst the analyzed species, end members of tennantite ( $\text{Sb}/(\text{Sb}+\text{As}) < 0.35$ ) and tetrahedrite ( $\text{Sb}/(\text{Sb}+\text{As}) > 0.7$ ) are present, in addition to solid solutions between both end members (Fig. 3-11e). The Ag content is highly variable within tennantite-tetrahedrite, with all tennantite having Ag < 0.2 Ag apfu, and there is a general increase in Ag content with increasing Sb concentration (i.e., from tennantite-tetrahedrite to tetrahedrite; Fig. 3-11e). The highest Ag contents are found in 7 tetrahedrite analyses from the up plunge portion of the 1806 Zone (Fig. 3-11e, f). They have more than 3.5 Ag apfu and are in this paper referred to as Ag-rich tetrahedrite, also known as freibergite.

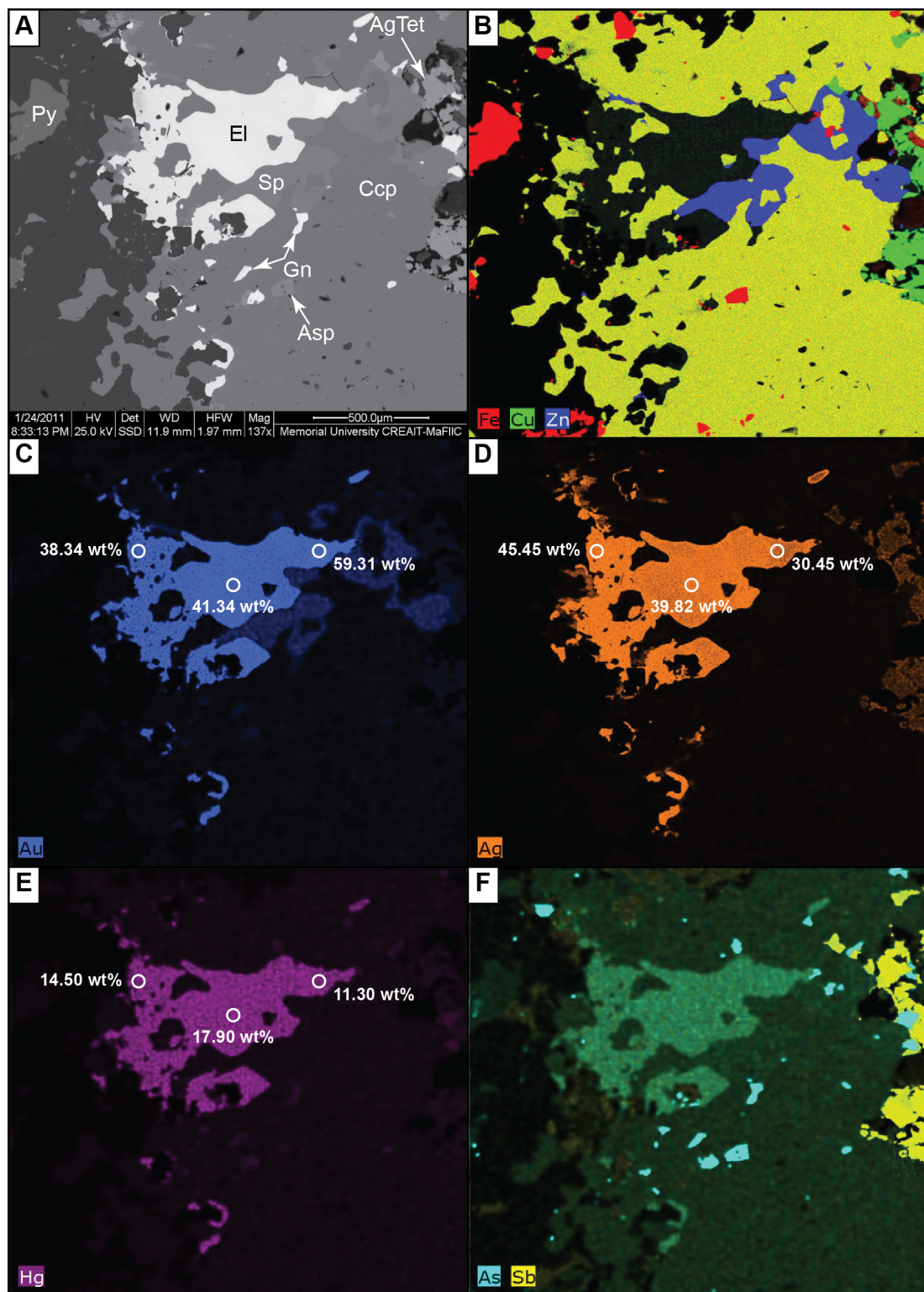


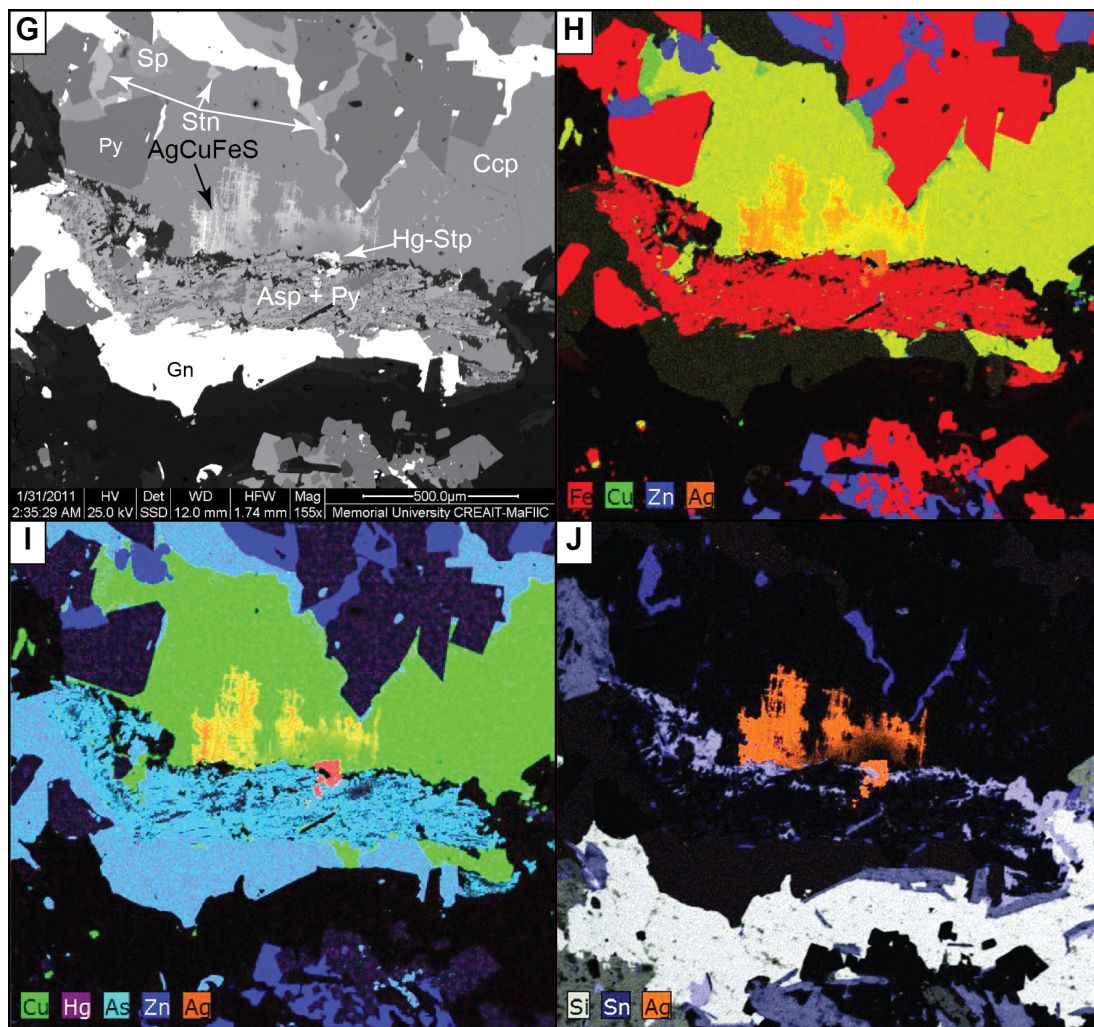
Tennantite-tetrahedrite ranges from Zn-poor to Zn-rich ( $0.2 \leq \text{Zn}/(\text{Zn}+\text{Fe}) \leq 0.7$ ) and Ag increases with increasing  $\text{Zn}/(\text{Zn}+\text{Fe})$ . In contrast, Ag-rich tetrahedrite is Zn-poor ( $\text{Zn}/(\text{Zn}+\text{Fe}) < 0.2$ ) and the Ag content decreases with increasing  $\text{Zn}/(\text{Zn}+\text{Fe})$  (Fig. 3-11e). Members of the tennantite-tetrahedrite series are both stoichiometric and non-stoichiometric.

Various Ag-phases (i.e., miargyrite, pyrargyrite, mercurian stephanite, unnamed AgCuFeS phase) from the up plunge portion of the deposit were analyzed from the 1806 Zone. They are spatially associated with, and occur in close proximity to electrum (Figs. 3-8g, j, m, and 3-10g-j), arsenopyrite (Figs. 3-8g, j, k, m, and 3-10g to j), and/or sulfosalts (Figs. 3-8g, j, k, m, and 3-10g to j). Miargyrite (Fig. 8m) has concentrations for Ag, Sb, and S between 35.90-37.52wt.%, 38.01-41.13wt.%, and 20.86-21.86wt.%, respectively; one miargyrite analysis reported elevated Zn (1.19wt.%) and Au (2.43wt.%), most likely due to contamination from adjacent sphalerite and electrum, respectively. Pyrargyrite (Fig. 3-8k) has 58.76wt.% Ag, 21.87wt.% Sb, and 17.77wt.% S. The calculated formula shows a weak deficiency on both the Ag and Sb site. Mercurian stephanite contains 57.30wt.% Ag, 11.32wt.% Sb, 15.18wt.% S, 12.74wt.% Hg, and 1.17wt.% As. An unnamed AgCuFeS phase is found next to mercurian stephanite (Figs. 3-8j, and 3-10g-j), containing Ag (27.20wt.%), Cu (22.89wt.%), Fe (22.24wt.%), and S (27.31wt.%). Mineral formula calculations based on different S apfu were unsuccessful.

The term electrum (AuAg) is used in this paper for Au-Ag alloys with > 10wt.% Au, and all analyzed electrum minerals have elevated Hg. Most of the 24 available electrum analyses are from the up plunge portion of the 1806 Zone. Gold, Ag, and Hg concentrations in electrum range between 13.87-61.99wt.%, 30.29-67.35wt.%, and 7.93-20.57wt.%, respectively (Fig. 3-12a). Most samples have > 30wt.% Au and Au/Ag ratios that range from 0.21 to 2.05 (Fig. 3-12b). All samples from the stringer zone and the silicified cap horizon, but one, show a Au/Ag ratio of about 1 ( $0.79 \leq \text{Au/Ag} \leq 1.27$ ) and the Hg concentration increases with increasing Au/Ag ratio (Fig. 3-12b). In contrast, samples from the semi-massive to massive sulfide horizon have a much wider range in Au/Ag ratio (0.21-2.05) and in general, Hg concentration decreases with increasing Au/Ag ratio (Fig. 3-12b). Some of the analyzed mercurian electrum grains were large enough to analyze the rim and core areas. Data from these grains reveal that Ag is enriched on the rim compared to the core (Fig. 3-10d), whereas Au is enriched in the core (Fig. 3-10c). Mercury does not show a uniform trend with neither Au nor Ag (Fig. 3-10c to e).

Boulangerite, stannite, cassiterite, and magnetite were also analyzed by EPMA. Both Boulangerite (falkmanite composition) and magnetite are non-stoichiometric, whereas molybdenite and cassiterite are broadly stoichiometric.

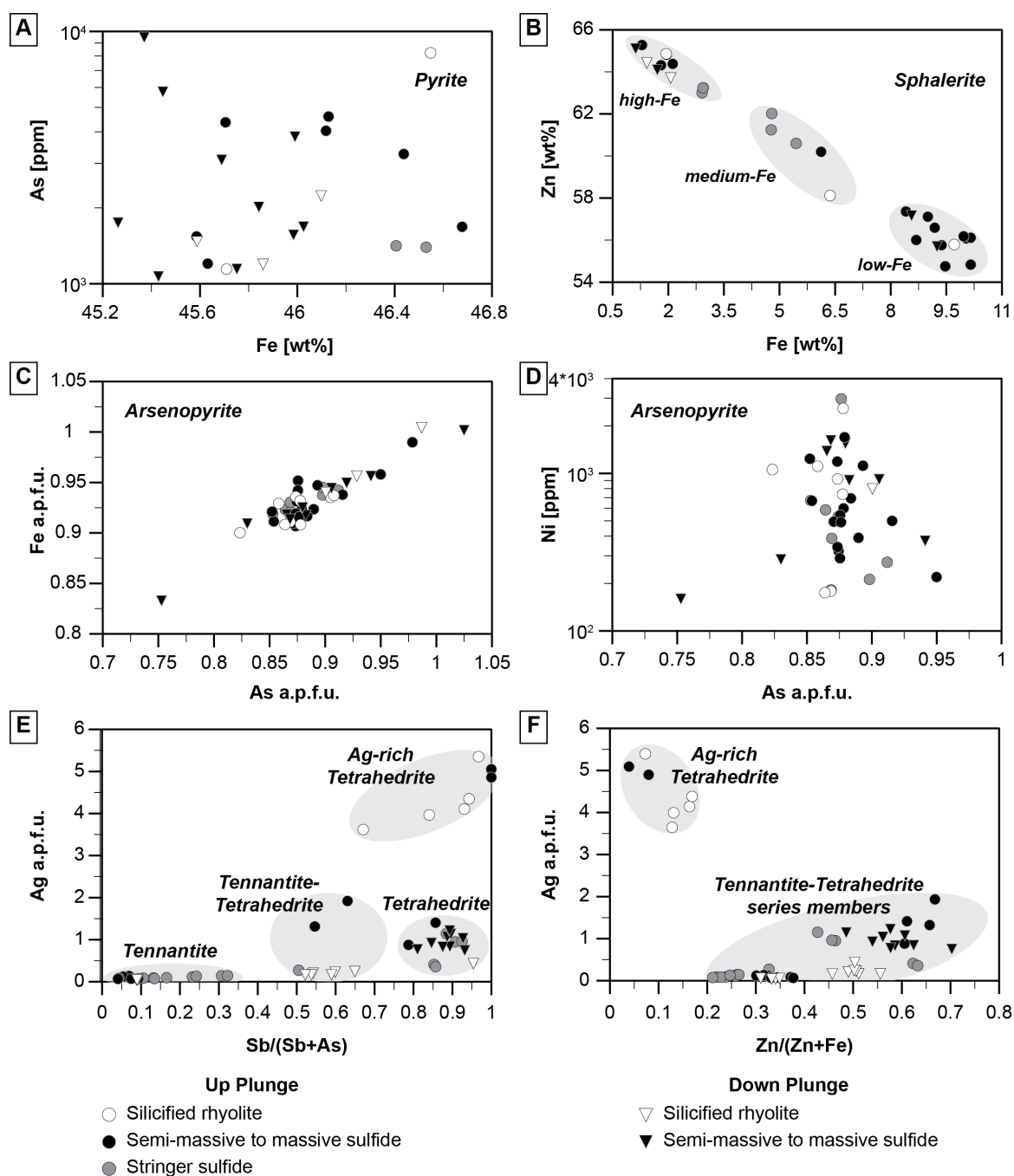




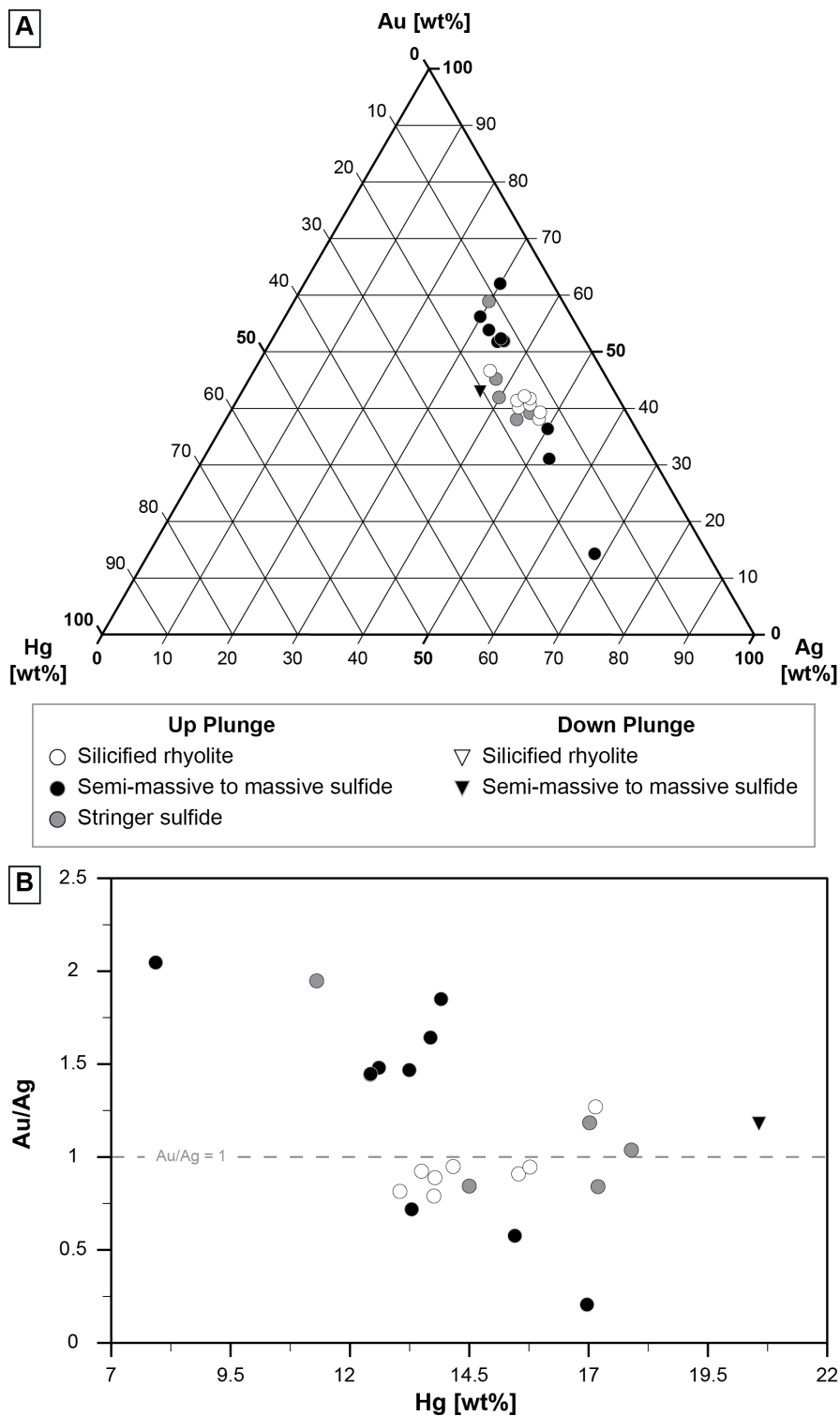
**Figure 3-10.** Back-scattered electron (BSE) images and EDX scans done by SEM on two precious metal samples from the up plunge for selected elements. Semi-quantitative EDX images give the relative occurrence of the measured elements, since only raw data are count. Interferences and/or background are recognized by running an element (i.e., Cr) that knowingly does not occur in the measured area. Mineral abbreviations as in Figure 3-8 (A) - (F) El in stringer zone (see Fig. 3-8e); (A) BSE image; (B) EDX scan of Fe, Cu, Zn highlighting Py and Asp (i.e., Fe = red), Ccp (i.e., Cu + Fe = yellow), AgTet (i.e., Cu = green), and Sp (i.e., Zn = blue); (C) EDX scan of Au highlighting the occurrence of El (dark blue); white open circles present EPMA data points and measured

concentrations, respectively; Note: Au L $\alpha$  (El) interferes with Zn K $\beta$  (Sp) causing a weak blue where Sp occurs; **(D)** EDX scan of Ag highlighting the occurrence of Ag in El (centre) and AgTet (right side); white open circles and numbers present EPMA data points and values, respectively; **(E)** EDX scan of Hg showing the occurrence of Hg in electrum; white open circles and numbers present EPMA data points and values, respectively; **(F)** EDX scans of As (turquoise) and Sb (yellow) highlighting the presence of Asp and AgTet close to El; Note: As K $\alpha$  (Asp) interferes with Pb L $\alpha$  (Gn) and Au L $\beta$  (El) resulting in a false color for El; **(G) - (J)** Ag-phases and Stn in massive sulfides (see Fig. 3-8j); **(G)** BSE image; **(H)** EDX scan of Fe, Cu, Zn, Ag highlighting Py and Asp (i.e., Fe = red), Ccp (i.e., Fe and Cu = greenish-yellow), Stn (i.e., Cu = lime green), Sp (i.e., Zn = blue), unnamed AgCuFeS phase (i.e., Fe + Cu + Ag = orange to yellow), and Hg-Stp (i.e., Ag = orange); intensity of Ag (orange) varies within the unnamed AgCuFeS phase; **(I)** EDX scan of Cu, Hg, As, Zn, Ag showing the occurrence of Hg in Stp (i.e., Ag + Hg = rose); Hg-Stp occurring marginal and within Asp-Py; Note: As K $\alpha$  (Asp) interferes with Pb L $\alpha$  (Gn) resulting in some color for both Asp and Gn; **(J)** EDX scan of Si, Sn and Ag showing the close textural and chemical relationship between both Ag-phases (i.e., Ag = orange) and Stn (i.e., Sn = dark blue in upper half of image); concentration of Ag in the unnamed AgCuFeS phase decreases proximal to Hg-Stp; Note: Sn L $\alpha$  interferes with Ca K $\alpha$  and K K $\alpha$  emission lines (i.e., light blue in lower half); see text for details to Figure 3-10





**Figure 3-11.** Compositional plots for various sulfide and sulfosalt phases based on EPMA analyses; **(A)** Fe vs As in pyrite; **(B)** Fe vs Zn in sphalerite; shaded areas highlight three distinct Fe populations within sphalerite; **(C)** - **(D)** Compositional variations in arsenopyrite; **(E)** - **(F)** Compositional variations in members of the tennantite-tetrahedrite series; see text for details to Figure 3-11



**Figure 3-12.** Compositional plots for electrum based on EPMA data; **(A)** Au-Ag-Hg ternary diagram; **(B)** Hg vs Au/Ag; see text for details to Figure 3-12

**Table 3-3.** Microprobe data for selected samples from the up plunge (UP) and down plunge (DP) of the 1806 Zone; Pyrite

Mineralized Zone	stringer	semi-massive sulfide										massive sulfide				
Plunge	UP	DP										RMUG06-145				
Drill core#	RMUG08-121	RMUG08-159										29907				
Sample No.	29902	29934														
SEM image#	P5	P2	P5a	P7	P9	P13	P2b	P8	P10	P11	P15b					
Mineral	Py	Py	Py I	Py II	Py	Py	Py	Py	Py	Py	Py					
Measuring date	Apr-11	Jan-12	Jan-12	Jan-12	Jan-12	Jan-12	Jan-12	Jan-12	Jan-12	Jan-12	Jan-12					
S [wt.%]	53.68	53.92	53.24	53.58	53.74	53.89	53.12	53.74	53.43	53.19	53.51	53.73				
Fe	46.57	45.98	45.66	45.42	45.75	45.84	45.26	45.37	45.19	45.22	45.99	45.44				
Cu [ppm]	nd	nd	nd	nd	nd	nd	550	nd	511	nd	nd	nd				
Zn	nd	nd	nd	nd	3,786	516	nd	nd	nd	nd	nd	nd				
Pb	nd	nd	nd	nd	nd	nd	2,803	nd	nd	nd	nd	nd				
As	nd	1,557	nd	1,065	1,141	2,008	1,740	9,484	nd	nd	3,830	5,770				
Sb	nd	nd	nd	nd	nd	nd	714	nd	nd	nd	nd	nd				
Sn	nd	nd	nd	nd	nd	nd	nd	nd	nd	nd	nd	nd				
Mo	nd	nd	nd	nd	nd	nd	1,327	nd	nd	nd	nd	nd				
Co	nd	nd	nd	nd	nd	nd	nd	nd	162	nd	nd	nd				
Ni	nd	nd	nd	179	nd	143	138	157	173	208	nd	234				
<b>Total</b>	<b>100.25</b>	<b>100.06</b>	<b>98.90</b>	<b>99.13</b>	<b>99.98</b>	<b>100.00</b>	<b>99.10</b>	<b>100.07</b>	<b>98.70</b>	<b>98.43</b>	<b>99.88</b>	<b>99.78</b>				



**Table 3-3. (cont.) Pyrite**

Mineralized Zone	massive sulfide										silicified horizon
Plunge	UP										
Drill core#	RMUG08-142					RMUG08-123					RMUG08-140
Sample No.	29778					36512					29783
SEM image#	P3a	P10b	P11	P16a-3	P3	P5b	P12	P7			
Mineral area	Py	Py	Py	Py N rim	Py core	Py I	Py II	Py			Py
Measuring date	Apr-11	Apr-11	Apr-11	Apr-11	Apr-11	Apr-11	Apr-11	Apr-11			Apr-11
S [wt. %]	53.63	53.66	53.77	53.41	53.23	53.47	53.18	53.62	53.34		53.90
Fe	46.76	46.44	46.65	46.19	46.12	46.68	46.68	46.11	46.77		46.55
Cu [ppm]	nd	859	545	nd	nd	nd	nd	nd	nd		nd
Zn	nd	nd	nd	nd	nd	nd	nd	nd	nd		nd
Pb	nd	nd	nd	nd	nd	nd	nd	nd	nd		nd
As	nd	3,274	nd	nd	4,607	1,678	nd	4,047	nd		8,240
Sb	nd	nd	nd	nd	nd	nd	nd	nd	nd		nd
Sn	nd	1,083	1,339	nd	nd	nd	1,032	nd	nd		nd
Mo	nd	nd	nd	nd	nd	nd	nd	nd	nd		nd
Co	nd	nd	nd	nd	nd	nd	nd	nd	nd		nd
Ni	nd	nd	nd	295	nd	475	296	741	nd		nd
<b>Total</b>	<b>100.39</b>	<b>100.63</b>	<b>100.60</b>	<b>99.63</b>	<b>99.82</b>	<b>100.36</b>	<b>99.99</b>	<b>100.21</b>	<b>100.11</b>		<b>101.27</b>

**Table 3-3. (cont.) Chalcopyrite**

Mineralized Zone	stringer				semi-massive sulfide				massive sulfide			
Plunge	UP				DP							
Drill core#	RMUG08-121				RMUG08-159				RMUG08-145			
Sample No.	29902				29934				29907			
SEM image#	P1c	P5	P14a		P2	P5a	P9	P13	P2b	P8	P10	P11
Mineral	Ccp	Ccp	Ccp I	Ccp II	Ccp	Ccp	Ccp	Ccp	Ccp	Ccp	Ccp	Ccp
Measuring date	Apr-11	Apr-11	Apr-11	Apr-11	Jan-12	Jan-12	Jan-12	Jan-12	Jan-12	Jan-12	Jan-12	Jan-12
S [wt.%]	35.35	34.83	34.92	35.02	35.01	34.98	35.45	34.94	35.12	35.27	34.92	34.84
Fe	30.49	30.38	30.48	30.48	29.86	29.93	30.21	30.05	30.27	30.10	30.20	30.09
Cu	34.93	34.72	34.94	34.57	34.24	34.26	34.28	34.44	34.36	34.24	34.39	34.23
Zn [ppm]	nd	nd	nd	699	nd	nd	nd	nd	nd	1,530	nd	nd
As	1,867	nd	nd	nd	1,200	nd	2,659	nd	nd	nd	nd	nd
Au	nd	nd	nd	nd	nd	nd	nd	nd	nd	nd	nd	nd
Ag	nd	nd	nd	nd	nd	nd	nd	nd	nd	nd	nd	nd
Sn	nd	1,212	nd	1,314	nd	nd	701	nd	nd	nd	nd	nd
Bi	nd	nd	nd	nd	nd	nd	740	nd	nd	nd	nd	nd
Mo	nd	2,099	nd	nd	nd	nd	nd	nd	nd	nd	nd	nd
Ni	nd	nd	nd	nd	nd	nd	nd	197	nd	nd	nd	nd
Total	100.96	100.26	100.33	100.27	99.23	99.16	100.34	99.45	99.75	99.76	99.51	99.16

**Table 3-3. (cont.) Chalcopyrite**

Mineralized Zone		massive sulfide						silicified horizon					
Plunge	DP	UP											
Drill core#	RMUG08-145	RMUG08-142			RMUG08-123			RMUG08-140					
Sample No.	29907	29778			36512			29783					
SEM image#	P15b	P3a	P11	P16a-3	P3	P5b	P1					P7	
Mineral area	Ccp	Ccp	Ccp	Ccp	Ccp	Ccp	Ccp	Ccp core	Ccp SW rim	Ccp	Ccp	Ccp	
Measuring date	Jan-12	Apr-11	Apr-11	Apr-11	Apr-11	Apr-11	Apr-11	Apr-11	Apr-11	Apr-11	Apr-11	Apr-11	
S [wt.%]	35.23	35.09	34.85	35.01	33.76	34.98	34.91	34.95	34.98	35.00	34.97	35.17	
Fe	29.97	30.25	30.14	30.50	28.25	30.49	30.36	30.38	30.43	30.45	30.57	30.31	
Cu	34.49	34.43	34.66	34.69	32.76	34.50	34.40	34.61	34.13	34.53	34.45	34.96	
Zn [ppm]	nd	nd	1,011	nd	nd	nd	nd	nd	nd	nd	nd	682	
As	nd	nd	nd	nd	nd	nd	nd	nd	nd	nd	nd	nd	
Au	1,074	nd	nd	nd	nd	nd	nd	nd	nd	nd	nd	nd	
Ag	nd	nd	nd	1,756	4.14	nd	1,522	3,433	4,394	nd	nd	nd	
Sn	nd	2,063	nd	960	nd	2,326	1,160	nd	nd	nd	nd	nd	
Bi	nd	nd	nd	nd	nd	nd	nd	nd	nd	nd	nd	nd	
Mo	nd	nd	nd	nd	nd	nd	nd	nd	nd	nd	nd	1,410	
Ni	nd	nd	nd	nd	nd	nd	nd	nd	nd	nd	nd	nd	
Total	99.80	99.98	99.75	100.47	98.91	100.20	99.94	100.27	99.98	99.98	100.00	100.65	

**Table 3-3. (cont.) Sphalerite**

Mineralized Zone	stringer				semi-massive sulfide				massive sulfide			
Plunge	UP				DP				UP			
Drill core#	RMUG08-121				RMUG08-159				RMUG08-123			
Sample No.	29902				29934				36512			
SEM image#	P1c	P14a			P5a	P7	P2b	P11	P3	P5b	P7b	P12
Mineral	Sp	Sp I	Sp II	Sp	Sp	Sp	Sp	Sp	Sp	Sp I	Sp II	Sp
Measuring date	Apr-11	Apr-11	Apr-11	Jan-12	Jan-12	Jan-12	Jan-12	Apr-11	Apr-11	Apr-11	Apr-11	Apr-11
S [wt. %]	33.41	33.33	33.29	33.18	33.19	33.18	33.03	32.98	33.08	33.02	33.25	32.93
Fe	5.45	4.79	4.78	1.12	1.70	1.12	8.56	1.80	9.00	9.37	8.41	9.19
Zn	60.60	62.02	61.24	65.10	64.09	65.10	57.16	64.32	57.11	55.76	57.36	56.59
Cu [ppm]	2,162	709	1,585	926	2,106	926	1,656	4,877	nd	1,802	nd	nd
As	1.14	nd	nd	nd	nd	nd	nd	nd	nd	nd	nd	nd
Bi	nd	nd	nd	1,116	nd	1,116	nd	nd	nd	nd	nd	nd
Hg	nd	2,844	2,239	nd	nd	nd	nd	nd	3,257	3,234	3,145	2,799
Mn	756	1,706	1,081	2,190	2,472	2,190	534	1,177	1,193	1,737	1,062	1,220
<b>Total</b>	<b>100.89</b>	<b>100.67</b>	<b>99.95</b>	<b>99.82</b>	<b>99.45</b>	<b>99.82</b>	<b>98.97</b>	<b>99.70</b>	<b>99.64</b>	<b>98.83</b>	<b>99.45</b>	<b>99.14</b>
												<b>99.41</b>

**Table 3-3. (cont.) Sphalerite**

Mineralized Zone	silicified horizon	
Plunge	UP	
Drill core#	RMUG08-140	
Sample No.	29783	
SEM image#	P6	P16a-3
Mineral	Sp	Sp
Measuring date	Apr-11	Apr-11
S [wt. %]	32.79	33.09
Fe	9.71	1.94
Zn	55.79	64.86
Cu [ppm]	nd	937
As	nd	nd
Bi	nd	nd
Hg	nd	nd
Mn	795	1,559
Total	98.38	100.15

**Table 3-3. (cont.) Arsenopyrite**

Mineralized Zone	stringer			semi-massive sulfide			massive sulfide		
Plunge	UP			DP					
Drill core#	RMUG08-121			RMUG08-159			RMUG08-145		
Sample No.	29902			29934			29907		
SEM image#	P1c	P5	P14a	P2	P5a	P9	P2b	P8	P11
Mineral area	Asp I	Asp II	Asp	Asp	Asp	Asp	Asp	Asp	Asp
Measuring date	Apr-11	Apr-11	Apr-11	Jan-12	Jan-12	Jan-12	Jan-12	Jan-12	Jan-12
S [wt.%]	21.30	21.46	21.86	21.61	21.45	21.73	20.91	21.69	20.52
Fe	34.55	34.76	34.98	34.65	34.87	34.71	34.38	34.49	34.17
As	43.61	43.54	43.56	43.88	43.80	44.80	44.24	43.99	45.12
Cu [ppm]	626	709	536	nd	2,024	nd	nd	nd	531
Zn	1.07	nd	nd	nd	nd	nd	nd	nd	nd
Au	nd	nd	1,485	nd	nd	nd	nd	nd	nd
Sb	nd	nd	nd	nd	nd	nd	nd	nd	2,441
Sn	nd	nd	nd	nd	nd	nd	nd	nd	nd
Te	nd	nd	nd	nd	2,543	825	nd	nd	nd
Bi	nd	nd	nd	nd	nd	nd	nd	1,296	nd
Mo	nd	nd	nd	nd	nd	nd	nd	nd	nd
Ni	2,971	182	673	387	533	904	916	1,618	372
<b>Total</b>	<b>100.89</b>	<b>99.84</b>	<b>100.66</b>	<b>100.18</b>	<b>100.62</b>	<b>101.33</b>	<b>99.63</b>	<b>100.33</b>	<b>100.04</b>
									<b>100.43</b>

**Table 3-3. (cont.) Arsenopyrite**

Mineralized Zone		massive sulfide				silicified horizon			
Plunge	DP	UP							
Drill core#	RMUG08-145	RMUG08-142				RMUG08-140			
Sample No.	29907	29778				29783			
SEM image#	P15b	P10b	P11	P5b	P1	P7			
Mineral area	Asp	Asp NE rim	Asp core	Asp SW rim	Asp	Asp NW rim	Asp core	Asp SE rim	Asp
Measuring date	Jan-12	Apr-11	Apr-11	Apr-11	Apr-11	Apr-11	Apr-11	Apr-11	Apr-11
S [wt. %]	21.68	21.10	21.79	21.17	20.83	19.81	22.00	21.44	21.37
Fe	34.66	34.79	34.94	34.74	34.52	34.15	34.48	34.78	34.82
As	43.82	44.02	43.38	43.30	42.60	45.29	42.32	43.94	43.61
Cu [ppm]	nd	nd	nd	nd	4,906	nd	1,506	nd	nd
Zn	nd	nd	nd	nd	661	nd	nd	nd	nd
Au	nd	nd	nd	nd	nd	nd	nd	nd	nd
Sb	nd	nd	nd	nd	nd	2,377	nd	nd	nd
Sn	nd	nd	nd	nd	nd	nd	nd	1,131	nd
Te	nd	nd	nd	nd	nd	nd	1,419	nd	nd
Bi	nd	nd	nd	nd	nd	nd	nd	nd	nd
Mo	nd	3,532	4,711	4,603	nd	4,123	nd	nd	nd
Ni	1,384	1,118	1,238	289	543	nd	1,057	737	921
<b>Total</b>	<b>100.29</b>	<b>100.37</b>	<b>100.71</b>	<b>99.70</b>	<b>98.56</b>	<b>99.90</b>	<b>99.20</b>	<b>100.35</b>	<b>99.89</b>
									<b>99.82</b>

**Table 3-3. (cont.) Tennantite-tetrahedrite**

Mineralized Zone	stringer	semi-massive sulfide											
Plunge	UP	DP											
Drill core#	RMUG08-121	RMUG08-159											
Sample No.	29902	29934											
SEM image#	P14a	P2				P7				P9			
Mineral area	Tet	Tet	Tet	Tet I	Tet II	Tet I	Tet II	Tet II	Tet I	Tet	Tet	Tet	Tet
Measuring Date	Apr-11	Apr-11	Apr-11	Jan-12	Jan-12	Jan-12	Jan-12	Jan-12	Jan-12	Jan-12	Jan-12	Jan-12	Jan-12
S [wt.%]	24.33	24.53	24.64	24.71	24.45	24.37	24.36	24.36	23.86	24.18	24.25	24.15	24.25
Fe	3.57	3.69	3.47	2.88	2.78	3.13	2.54	2.54	2.90	1.99	3.01	4.19	2.69
Cu	33.49	32.61	33.57	34.88	34.18	33.96	34.23	34.23	32.88	34.08	32.06	31.91	32.82
Zn	3.51	3.22	3.51	4.59	4.61	4.30	4.94	4.94	4.34	5.49	4.80	4.63	4.86
As	1.30	2.05	1.64	3.47	2.27	2.78	1.94	1.94	1.32	1.25	1.94	1.84	2.07
Sb	26.12	25.57	26.05	24.08	25.91	24.84	26.51	26.51	27.33	27.69	26.37	25.78	26.35
Ag	6.05	7.30	6.07	4.94	5.26	5.83	5.29	5.29	6.41	4.68	7.67	7.14	6.73
Pb [ppm]	nd	nd	nd	nd	1,642	nd	nd	nd	nd	nd	nd	nd	nd
Sn	nd	nd	nd	nd	nd	nd	743	743	nd	nd	nd	nd	nd
Bi	nd	nd	nd	1,700	nd	nd	nd	nd	nd	nd	nd	nd	871
Hg	1,994	nd	nd	nd	nd	nd	nd	nd	nd	nd	nd	nd	nd
Mn	nd	nd	nd	nd	nd	nd	nd	nd	nd	nd	nd	nd	nd
<b>Total</b>	<b>98.58</b>	<b>98.98</b>	<b>98.95</b>	<b>99.72</b>	<b>99.63</b>	<b>99.21</b>	<b>99.89</b>	<b>99.89</b>	<b>99.04</b>	<b>99.35</b>	<b>100.11</b>	<b>99.63</b>	<b>99.86</b>
Sb/(Sb+As)*	0.92	0.88	0.91	0.81	0.88	0.85	0.89	0.89	0.93	0.93	0.89	0.90	0.89
Zn/(Zn+Fe)*	0.46	0.43	0.46	0.58	0.59	0.54	0.62	0.62	0.56	0.70	0.58	0.49	0.61



**Table 3-3. (cont.) Tennantite-tetrahedrite and Ag-phases**

Mineralized Zone	massive sulfide				silicified horizon
Plunge	UP				
Drill core#	RMUG08-142				RMUG08-140
Sample No.	29778				29783
SEM image#	P3a				P1
Mineral area	Ten I	Ten II	Ten-Tet W part	Ten-Tet E part	Mia
Measuring date	Apr-11	Apr-11	Apr-11	Apr-11	Apr-11
S [wt.%]	28.52	28.14	25.03	25.70	21.86
Fe	4.99	5.30	2.24	2.38	35.90
Cu	42.15	41.29	30.10	32.84	0.040
Zn	2.90	3.24	5.28	5.33	0.191
As	19.05	18.14	6.28	8.08	nd
Sb	2.52	3.03	17.44	15.83	41.13
Ag	0.514	0.550	12.51	8.78	nd
Pb [ppm]	nd	nd	nd	nd	nd
Sn	nd	nd	nd	nd	nd
Bi	nd	nd	nd	nd	nd
Hg	nd	nd	nd	nd	nd
Mn	227	nd	nd	nd	nd
<b>Total</b>	<b>100.67</b>	<b>99.69</b>	<b>98.88</b>	<b>98.96</b>	<b>99.13</b>
Sb/(Sb+As)*	0.08	0.09	0.63	0.55	
Zn/(Zn+Fe)*	0.33	0.34	0.67	0.66	

Mineralized Zone	massive sulfide				silicified horizon
Plunge	UP				
Drill core#	RMUG08-123				RMUG08-140
Sample No.	36512				29783
SEM image#	P5b				P1
Mineral area	Hg-Stp	AgCuFeS	Pyr	Mia	
Measuring date	Apr-11	Apr-11	Apr-11	Apr-11	Apr-11
S [wt.%]	15.18	27.31	17.77	21.86	
Ag	57.30	27.20	58.76	35.90	
Fe	0.253	22.24	nd	0.040	
Cu	0.391	22.89	nd	0.191	
As	1.17	nd	0.104	nd	
Sb	11.32	nd	21.87	41.13	
Hg	12.74	nd	nd	nd	
Pb [ppm]	nd	nd	6,006	nd	
Au	3,502	nd	nd	nd	
Mo	2,256	nd	nd	nd	
Co	nd	nd	159	nd	
<b>Total</b>	<b>98.93</b>	<b>99.86</b>	<b>100.07</b>	<b>99.13</b>	

**Table 3-3. (cont.) Mercurian electron**

Mineralized Zone	stringer				massive sulfide				silicified horizon			
Plunge	UP				DP				UP			
Drill core#	RMUG08-21				RMUG08-159				RMUG08-140			
Sample No.	29902				29934				29778			
SEM image#	P14a				P5a				P16a-3			
Mineral area	EI	core-1	EI	E rim	EI	core-1	EI	E rim	EI	core	E rim	EI
Measuring Date	Apr-11	Apr-11	Apr-11	Apr-11	Jan-12	Apr-11	Apr-11	Apr-11	Apr-11	Apr-11	Apr-11	Apr-11
Au [wt.%]	41.34	44.96	37.43	59.31	43.48	13.87	46.61	41.18	38.30	39.18	41.73	41.73
Ag	39.82	37.96	44.52	30.45	36.88	67.35	36.70	43.53	46.97	43.09	43.97	43.97
Hg	17.90	17.02	17.20	11.30	20.57	16.97	17.15	15.77	13.05	15.53	14.16	14.16
S [ppm]	939	1,222	330	1,393	190	6,525	914	3,112	9,666	5,961	4,987	4,987
Fe	535	nd	697	366	642	4,722	526	1,637	5,423	2,752	4,745	4,745
Cu	nd	nd	nd	nd	776	1,212	nd	nd	nd	nd	nd	nd
Sb	nd	nd	693	nd	nd	nd	nd	nd	nd	nd	nd	nd
Co	nd	173	nd	nd	151	nd	157	nd	nd	nd	nd	nd
Ni	nd	nd	nd	nd	nd	210	nd	nd	nd	nd	nd	nd
<b>Total</b>	<b>99.20</b>	<b>100.09</b>	<b>99.32</b>	<b>101.24</b>	<b>101.11</b>	<b>99.45</b>	<b>100.62</b>	<b>100.98</b>	<b>99.82</b>	<b>98.67</b>	<b>100.84</b>	<b>100.84</b>
Au/Ag	1.04	1.18	0.84	1.95	1.18	0.21	1.27	0.95	0.82	0.91	0.95	0.95
Au/(Au+Ag)	0.51	0.54	0.46	0.66	0.54	0.17	0.56	0.49	0.45	0.48	0.49	0.49

**Table 3-3. (cont.) Mercurian electrum**

Mineralized Zone	silicified horizon			
Plunge	UP			
Drill core#	RMUG08-140			
Sample No.	29783			
SEM image#	P6			
Mineral area	EI I	EI II	EI III	
Measuring Date	Apr-11	Apr-11	Apr-11	Apr-11
Au [wt.%]	37.69	41.24	39.75	
Ag	47.70	44.64	44.72	
Hg	13.76	13.50	13.78	
S [ppm]	1,566	1,823	2,473	
Fe	601	1,038	1,962	
Cu	nd	nd	nd	
Sb	761	nd	961	
Co	nd	163	nd	
Ni	nd	174	nd	
<b>Total</b>	<b>99.44</b>	<b>99.70</b>	<b>98.79</b>	
Au/Ag	0.79	0.92	0.89	
Au/(Au+Ag)	0.44	0.48	0.47	

**Abbreviations:** AgCuFeS – unnamed AgCuFeS phase, Asp – arsenopyrite, Ccp – chalcopyrite, El – electrum, Hg-Stp – mercurian stephanite, Mia – miargyrite, nd – not detected, Py – pyrite, Pyr – pyargyrite, Sp – sphalerite, Ten – tennantite, Ten-Tet – tennantite-tetrahedrite, Tet – tetrahedrite

° molecular proportions

*Values in italics indicate wt.% instead of ppm*

**Table 3-4.** Summary of microprobe analyses – mineral phases, their calculated mineral formula, and detected minor elements; mineral abbreviations as in Table 3-3

Mineral	Pyrite	Chalcopyrite	Unknown Phase	Sphalerite	Galena
Number of analyses	42	58	3	30	30
Calculated mineral formula	$\text{Fe}_{0.97-1.02}\text{S}_2$	$\text{Cu}_{0.97-1.01}\text{Fe}_{0.94-1.02}\text{S}_2$	N/A	Low-Fe Sp: ( $\text{Zn}_{0.94-0.97}, \text{Fe}_{0.02-0.05}$ )S  Med-Fe Sp: ( $\text{Zn}_{0.87-0.91}, \text{Fe}_{0.08-0.11}$ )S  High-Fe Sp: ( $\text{Zn}_{0.81-0.85}, \text{Fe}_{0.15-0.18}$ )S	$\text{Pb}_{0.95-1.08}\text{S}$
Minor elements (< 1wt.%)	As, Cu, Zn, Pb, Sb, Sn, Hg, Mo, Ni	Zn, As, Au, Ag, Sn, Te, Bi, Mo, Ni	As, Hg	Cu, As, Ag, Sn, Hg, Bi, Mn, Ni	Fe, Cu, As, Zn, Ag, Sb, Te, Mn
Comments			Reaction between Ccp and El; low totals (78 - 79wt.%); only in up plunge	Low- and high-Fe sphalerites occur throughout 1806 Zone; med-Fe sphalerites are only in up plunge of 1806 Zone	

Mineral	Pyrrhotite	Arsenopyrite	Tennantite-Tetrahedrite
Number of analyses	12	48	53
Calculated mineral formula	$\text{Fe}_{1-x}\text{S}$ ( $x = 0.12-0.14$ )	$\text{Fe}_{0.83-1.00}\text{As}_{0.75-1.02}\text{S}$	Ten: ( $\text{Cu}_{9.63-10.63}, \text{Ag}_{0.04-0.14}$ ) $\Sigma=9.70-10.72$ ( $\text{Fe}_{1.23-1.60}, \text{Zn}_{0.42-0.74}$ ) $\Sigma=1.96-2.31$ ( $\text{As}_{3.02-3.90}, \text{Sb}_{0.16-0.96}$ ) $\Sigma=3.81-4.08\text{S}_{13}$  Ten-Tet: ( $\text{Cu}_{6.18-9.91}, \text{Ag}_{0.14-3.64}$ ) $\Sigma=9.62-10.08$ ( $\text{Fe}_{0.67-1.86}, \text{Zn}_{0.27-1.34}$ ) $\Sigma=1.94-2.11$ ( $\text{As}_{1.38-2.76}, \text{Sb}_{1.22-2.81}$ ) $\Sigma=3.78-4.19\text{S}_{13}$  Tet: ( $\text{Cu}_{4.60-9.64}, \text{Ag}_{0.36-5.39}$ ) $\Sigma=9.50-10.63$ ( $\text{Fe}_{0.61-2.30}, \text{Zn}_{0.09-1.45}$ ) $\Sigma=1.96-2.52$ ( $\text{As}_{0.0-0.88}, \text{Sb}_{3.26-4.37}$ ) $\Sigma=3.97-4.52\text{S}_{13}$
Minor elements (< 1wt.%)	Cu, Zn, Pb, As, Sn, Mo, Ni	Cu, Zn, Pb, Au, Ag, Sb, Sn, Te, Bi, Mo, Mn, Ni	Pb, Bi, Sn, Te, Hg, Mn
Comments	Sn-bearing Po in up plunge part and adjacent to El		Some Ag-rich tetrahedrites of freibergite composition

**Table 3-4. (cont.)**

Mineral	Ag-Phases	Mercurian electrum	Boulangerite	Stannite	Molybdenite
<b>Number of analyses</b>	5 (Mia: 2; Pyr: 1; Hg-Stp: 1; unnamed AgCuFeS phase: 1)	24	3	4	1
<b>Calculated mineral formula</b>	Mia: $\text{Ag}_{0.98-1.07}\text{Sb}_{0.96-0.99}\text{S}_2$  Pyr: $\text{Ag}_{2.95}\text{Sb}_{0.97}\text{S}_3$  Hg-Stp: $(\text{Ag}_{4.49}, \text{Hg}_{0.54})\Sigma=5.03(\text{Sb}_{0.79}, \text{As}_{0.13})\Sigma=0.92\text{S}_4$  unnamed AgCuFe S phase: N/A	N/A	$\text{Pb}_{6.65-6.27}(\text{Sb}_{3.35-3.49}, \text{Cu}_{0.49-1.06})\Sigma=3.84-4.52\text{S}_{11}$	$\text{Cu}_{1.91-1.95}(\text{Fe}_{0.92-0.96}, \text{Zn}_{0.13-0.18})\Sigma=1.07-1.12\text{Sn}_{1.00-1.01}\text{S}_4$	$(\text{Mo}_{1.02}, \text{Fe}_{0.03})\Sigma=1.05\text{S}_2$
<b>Minor elements (&lt; 1wt.%)</b>	Mia: Cu, Fe, As, Hg Pyr: As, Pb, Co Hg-Stp: Fe, Cu, Mo, Au unnamed AgCuFeS phase: N/A	S, Fe, Cu, Zn, Pb, As, Sb, Bi, Co, Ni	Fe, Zn, Ag, Sn	As, Ni, Mn	Cu, Au, Te
<b>Comments</b>		High Hg content (7.93 - 20.97wt. %)	More of falkmanite composition than boulangerite	Restricted to up plunge portion of semi-nassive to massive sulfide lense	

Mineral	Cassiterite	Magnetite
<b>Number of analyses</b>	2	9
<b>Calculated mineral formula</b>	$\text{Sn}_{0.97-0.98}\text{O}_2$	$\text{Fe}_{2.74-2.90}\text{O}_4$
<b>Minor elements (&lt; 1wt.%)</b>	Cu, As, Fe	S, Cu, Zn, Mn
<b>Comments</b>	Only in down plunge part	Only in down plunge part

### **3-6 DISCUSSION**

#### **3-6-1 *SYN-GENETIC VS. SYN-OROGENIC PRECIOUS METAL EMPLACEMENT***

The origin of precious metal enrichment in ancient VMS deposits is often contentious, particularly for deformed deposits in ancient belts where primary characteristics might have been obscured and altered by younger events. These events can be of different origin. For instance, some workers have argued that Au enrichment in some Au-rich VMS deposits were due to later orogenic overprinting and Au introduction by metamorphic fluids (e.g., Bousquet 1 and Dumagami: Tourigny et al., 1989; Marquis et al., 1990). In contrast, in other deposits, it has been argued that the enrichment in precious metals was due to epithermal (magmatic) overprinting or formation as shallow water magmatic-hydrothermal systems (e.g., Eskay Creek: Roth et al. 1999; Boliden: Bergman-Weihed et al., 1996; Wagner and Jonsson, 2001; Mercier-Langevin et al., 2013). Gold enrichment in the Rambler camp is debated as well, in large part because the deposit is poly-deformed and metamorphosed, and occurs proximal to deposits that are typical orogenic Au deposits (e.g., Deer Cove: Patey and Wilton, 1993; Stog'er Tight: Ramezani et al., 2000).

The specific characteristics of the 1806 Zone of the Ming Mine documented here illustrate that, despite significant deformation and metamorphic overprint, the precious metal mineralization is syngenetic and results from a primary or synvolcanic hydrothermal fluid. Moreover, ore mineralogy and mineral

chemistry indicate a possible magmatic input into the ore-forming hydrothermal system.

### *3-6-1-1 Architecture*

The overall architecture of the 1806 Zone is typical of most VMS deposits with a discordant (although transposed) stringer and footwall alteration zone underlying concordant or stratabound semi-massive to massive sulfides. The silicified and mineralized horizon located at the footwall – hanging wall contact (Fig. 3-4) contains remnants of the host rock (i.e., relict clasts) and strongly resembles the silica- and chlorite-altered footwall Rambler rhyolite. While there are numerous potential origins for this silicified horizon, which are not focus of this paper, its texture and aspect, and the absence of carbonates in both the horizon and its immediate wall rocks precludes the possibility that this horizon could be a late, orogenic quartz vein superimposed on the VMS system. Such orogenic quartz veins have clear, quasi-universal features that make them relatively easy to identify (e.g., Groves et al., 1998; Bierlein and Crowe, 2000), and the orogenic vein systems on the Baie Verte Peninsula are no exception (e.g., Evans and Wells, 1998; Ramezani et al., 2000). The semi-massive to massive sulfide lens of the 1806 Zone is separated from the other mineralized horizons (1807 Zone, Ming South, Ming North, Lower Footwall) and the previously mined horizon (Fig. 3-3) by mafic dikes (Pilote and Piercey, 2013). Despite the unknown age and relation of these mafic dikes relative to the massive sulfide deposition (Pilote and Piercey, 2013), an active role of these

dikes in the precious metal deposition is excluded, since sulfide mineralization is sparse in these dikes and restricted to random disseminated pyrite cubes on the sharp contacts to the mineralized lithounits (i.e., Rambler rhyolite, semi-massive and massive lens, silicified rhyolite). Furthermore, there are no enrichments in precious metals or precious metal minerals proximal to dike contacts. The contacts between mineralized footwall - sulfide lens – silicified rhyolite are sharp, but not tectonically induced. Moreover, all sulfide zones at the Ming Mine are trending NE with a plunge of 30 – 35°, which is similar to the dip of the Rambler rhyolite (Tuach and Kennedy, 1978), indicating the pre-deformational origin for the various sulfide lenses at the Ming Mine, in general, and of the 1806 Zone, specifically.

### *3-6-1-2 Alteration*

An assemblage of sericite – quartz ± green mica with sporadic biotite-chlorite dominates the alteration in the footwall Rambler rhyolite. Although advanced argillic style or aluminous alteration, characteristic of high-sulfidation epithermal deposits, is associated with a number of Au-rich VMS deposits (Sillitoe et al., 1996; Hannington et al., 1999; Huston, 2000; Dubé et al., 2007a; Mercier-Langevin et al., 2011), it is not well developed at the 1806 Zone. The sericitic alteration of the footwall of the 1806 Zone is rather common for base metal VMS deposits (e.g., Franklin et al., 1981) and in lower sulfidation epithermal Au deposits (Bierlein and Crowe, 2000; Hedenquist et al., 2000). Although the 1806 Zone does not have features characteristic of subaerial



epithermal deposits (e.g., cavity-filled veins or veinlet stockworks, bladed calcite, and native gold; Hedenquist et al., 2000), the sulfide mineral assemblage at the 1806 Zone is typical intermediate-sulfidation epithermal assemblage (Figs. 3-7, 3-8; Sillitoe and Hedenquist, 2003 and references therein).

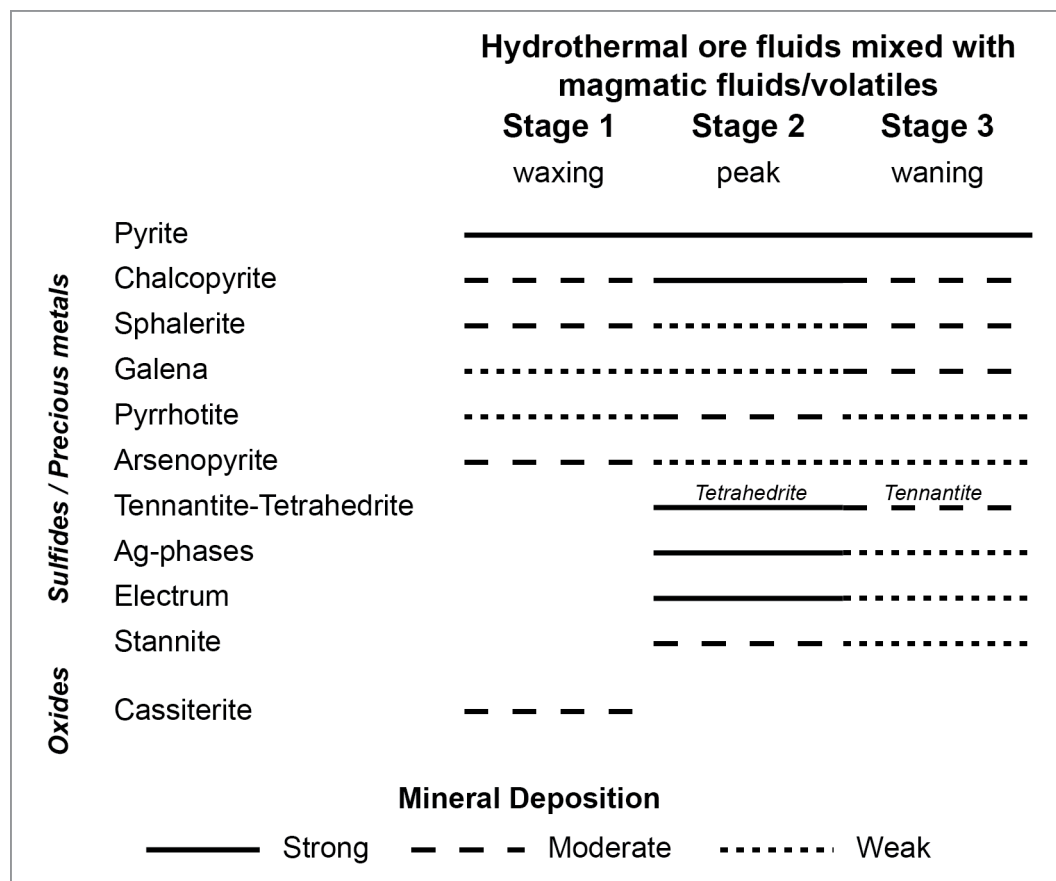
### *3-6-1-3 Metal zoning*

Metal zoning is well documented from base metal and Au- rich VMS deposits and caused by changing fluid conditions (T, pH,  $fO_2$ ) over the lifespan of the hydrothermal system (e.g., Large, 1977, 1992; Huston and Large, 1989; Ohmoto, 1996; Poulsen and Hannington, 1996; Hannington et al., 1999). Orogenic Au deposits lack this feature (Goldfarb et al., 2005). At the 1806 Zone, base metal and precious metal zoning is observed from the down plunge part (high-grade Cu zone, low-grade Zn, Au, and Ag) to the up plunge part (high-grade Zn, Pb, and precious metal contents, lower-grade Cu values; Fig. 3-9). In context of metal-associations, the 1806 Zone shows a Au-Zn-Pb-Ag association (Huston and Large, 1989; Poulsen and Hannington, 1996; Hannington et al., 1999), in which Au is predominantly concentrated in the top of the massive sulfide lens or here the up plunge portion of the 1806 Zone. However, it has to be emphasized that mineralogically Au (electrum) occurs predominantly with Cu (chalcopyrite) throughout the 1806 Zone and only with minor sphalerite predominantly in sulfide stringers and the up plunge portion of the semi-massive to massive sulfide lens. Reasons for these contradictory observations (Au-Zn-Pb-Ag association in the up plunge portion vs predominant electrum-chalcopyrite

assemblage throughout the 1806 Zone) are (1) zone refining during the lifespan of the hydrothermal system affecting both the up plunge and down plunge portions, (2) late stage, spatially limited sphalerite bands alternating with galena  $\pm$  tennantite-tetrahedrite in the upper parts of the up plunge portion (Figs. 5, and 8b), and (3) coeval transport of Cu and Au. The sphalerite bands are interpreted to be formed at declining temperatures during the waning stage of the hydrothermal system creating the Ming deposit, since they (1) run mostly parallel to the geologic contacts of the sulfide lens, (2) are weakly sheared (Fig. 3-5), (3) restricted to the upper most parts of the up plunge portion of the 1806 Zone, and (4) show microscopic replacement textures of chalcopyrite by sphalerite and tennantite-tetrahedrite (Fig. 3-8b).

#### *3-6-1-4 Ore assemblages and paragenesis*

The ore distribution and their assemblages in the 1806 Zone are complex (Fig. 3-7), with at least seventeen different sulfides, sulfosalts and precious metal phases present in various amounts in different portions of the ore lens, which has a distinct paragenesis. A pre-metamorphic paragenetic sequence is presented for the 1806 Zone in Figure 3-13 based on textural relationships between sulfides, sulfosalts, and precious metals, observed metal zoning, and ore mineral chemistry.



**Figure 3-13.** Paragenetic chart for the syn-genetic deposition of sulfides, sulfosalts, precious metals, and cassiterite at the 1806 Zone

Gold-rich VMS deposits (e.g., Boliden, Horne, Bousquet 2, LaRonde Penna, Juan de Fuca Ridge, Lau Basin; Hannington et al., 1986; Large et al., 1989; Tourigny et al., 1989; Huston et al., 1992; Herzig et al., 1993; Herzig and Hannington, 1995; Huston, 2000; Mercier-Langevin et al., 2011 and references therein) are in general characterized by relatively complex ore assemblages compared to “precious metal-poor” Cu-Zn-Pb VMS systems. In contrast, orogenic Au-deposits have a much simpler sulfide assemblage that consists of variable

amounts of one or all of the following minerals: pyrite, chalcopyrite, pyrrhotite, arsenopyrite, and in rare cases tennantite-tetrahedrite (e.g., Patey and Wilton, 1993; Groves et al., 1998; Evans and Wells, 1998; Bierlein and Crowe, 2000 and references therein; Ramezani et al., 2000).

The bulk of the Au at the 1806 Zone appears to be hosted in mercurian electrum and in minor Ag-Hg-Au alloys (Figs. 3-8d to i, 3-8l-n, 3-10a, c, d, and 3-12, Tables 3-3 and A3-3). Native Au, which is very common in orogenic Au deposits (Evans and Wells, 1998; Groves et al., 1998; Bierlein and Crowe, 2000), is not present at the 1806 Zone, and invisible Au is almost completely absent as shown by EPMA analyses of sulfides. Silver at the 1806 Zone is intimately associated with elements of the epithermal suite (i.e., As, Hg, Sb) in phases such as Ag-bearing tennantite-tetrahedrite, miargyrite, pyrargyrite, and Ag-Hg±Au alloys (Figs. 3-8a, g, h, j, k, m, 3-10g-j, 11e, f, and 3-12, Tables 3-3 and A3-3). Electrum and Ag-phases occur also in close spatial association with minerals containing elements of the epithermal suite such as arsenopyrite, Ag-bearing tennantite-tetrahedrite, stannite, and boulangerite preferably in the up plunge area of the 1806 Zone (Figs. 3-8a, d to n, and 3-10). Numerous authors (Sillitoe et al., 1996; Hannington et al., 1999; Huston, 2000; Dubé et al., 2007a) have noted that the occurrence of elements of the epithermal suite in Au-rich VMS deposits strongly suggests the potential involvement of magmatic fluids or volatiles as the source of precious metal enrichment. This is also assumed for the 1806 Zone due to the wide range and occurrence of elements of the epithermal

suite as major and minor components in almost all analyzed minerals and the spatial association between epithermal suite-enriched sulfosalts and precious metals in the up plunge portion of the 1806 Zone. Although, high-sulfidation assemblage are common to a number of VMS deposits formed in the epithermal environment (Sillitoe et al., 1996 and references therein), the ore assemblage at the 1806 Zone is of intermediate-sulfidation style explaining the absence of high aluminous, acidic alteration assemblages.

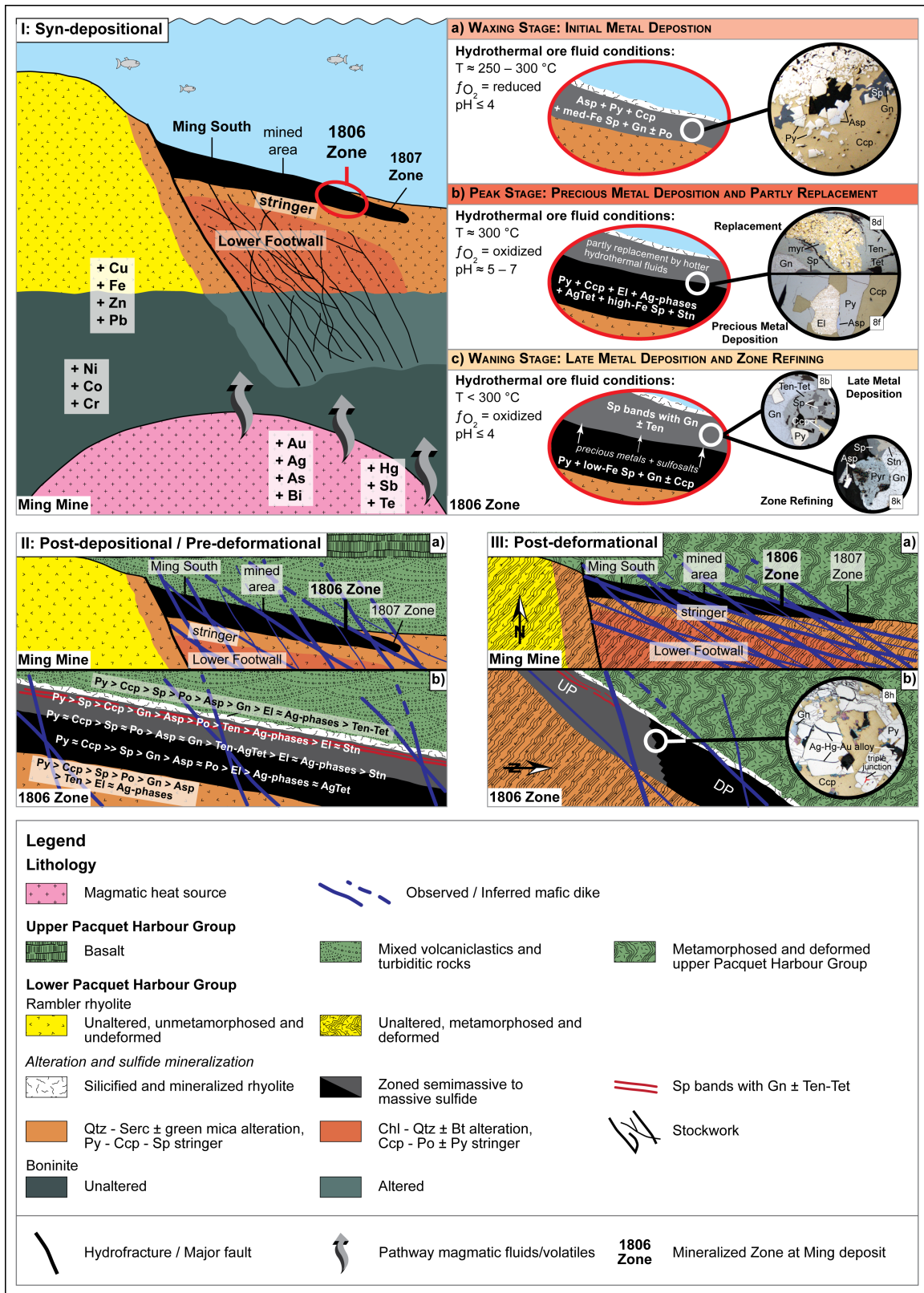
#### *3-6-1-5 Influence of deformation and metamorphism*

Despite a pre-deformation, syngenetic origin for the precious metal enrichment, mineralization and precious metals have been texturally modified during Silurian-Devonian deformation and metamorphism resulting in local remobilization of precious metals and modifications to mineral textures, especially for pyrite and arsenopyrite. Moreover, in the up plunge portion of the 1806 zone alloys of  $\text{AgHg}\pm\text{Au}$  are often found between recrystallized pyrite and along cracks in recrystallized, brittle deformed pyrite (Fig. 3-8h) indicating that the occurrence of precious metals with recrystallized and partly brittle deformed pyrite is secondary. Porphyroblasts of pyrite and arsenopyrite are common and in some cases contain inclusions of electrum, implying that gold was present prior to porphyroblast formation. Therefore, despite textural modification, the remobilization and recrystallization of gold suggests that it existed prior to metamorphism and deformation and was therefore syngenetic in origin rather than introduced during deformation and metamorphism.

### *3-6-2 DEPOSITION MODEL FOR THE 1806 ZONE AND HYDROTHERMAL ORE FLUID CONDITIONS*

A depositional model for the 1806 Zone is presented in Figure 3-14. This model combines the aforementioned evidences from: (1) the architecture of the 1806 Zone; (2) the alteration assemblage in the rhyolitic footwall; (3) the base metal and precious metal zoning from the down plunge area to the up plunge area; and (4) the complex ore assemblages for the syngenetic base and precious metal deposition via seawater and magmatic fluids. Furthermore, the metals, mineral assemblages, and paragenesis (Fig. 3-13) characterizing the 1806 Zone provide evidence to constrain the physico-chemical fluid conditions ( $T$ ,  $pH$ ,  $fO_2$ ) as the 1806 Zone was formed (Fig. 3-14).

The 1806 Zone is part of the broader Ming deposit. Although mafic dykes separate the various sulfide zones (1807 Zone, Ming South, Ming North, previously mined area) from each other, it is strongly assumed given drill core and underground field relationships that all sulfide lenses once belonged to one continuous lens. The lens has been disrupted by polyphase deformation and metamorphism resulting in existing distribution of zones. The 1806 Zone is on the edge of the Ming deposit, has highest Zn grades in the deposit, is associated with abundant minerals bearing elements of the epithermal suite, and is interpreted to represent the distal portions of a VMS mound (e.g., Lydon, 1988; Ohmoto, 1996; Figs. 3-3 and 3-14). Given that the deposit has many minerals similar to normal VMS mineralization (e.g., pyrite, sphalerite, chalcopyrite, and galena), but also



**Figure 3-14.** (previous page) Depositional model for the genesis of the 1806 Zone; **(I)** Syn-depositional processes during waxing (a), peak (b), and waning (c) stage of hydrothermal activity at the 1806 Zone; **(II)** Post-depositional / Pre-deformational state of the Ming deposit (a) and the 1806 Zone (b); **(III)** Post-deformational state of the Ming deposit (a) and the 1806 Zone (b); sketches of the 1806 Zone in II-b and III-b are perpendicular to II-a and II-b. Alphanumerical labels in I and III-b refer to Figures in this paper; see discussion for details to Figure 3-14. Mineral abbreviations same as in Figure 3-8

intermediate sulfidation mineralogy and enrichment in elements of the epithermal suite, a hybrid origin is inferred. Support for some component of leaching is consistent with the enrichments in transition metals (Cr, Mn, Ni, and Co) and Cr-bearing mica in the mineralization, are consistent with stripping via leaching as these elements are enriched in the boninitic footwall to mineralization in the Pacquet Harbour Group (Piercey et al., 1997; Skulski et al., 2010). The presence of epithermal mineralogy, however, also requires a magmatic input likely from some underlying magmatic heat source that has since been sheared off during regional deformation (Fig. 3-14-I).

During the waxing stage (Fig. 3-14-Ia) of hydrothermal activity, the up plunge portion of the 1806 Zone with the silicified horizon was formed. In this stage, arsenopyrite-pyrite-chalcopyrite-medium-Fe sphalerite and minor galena-pyrrhotite were deposited by reduced, acidic hydrothermal ore fluids at temperatures of  $\approx 250\text{-}300^{\circ}\text{C}$  (Heinrich and Eadington, 1986; Lydon, 1988; Large, 1992). Close spatial relations between (partly replaced) arsenopyrite-



pyrite-chalcopyrite suggest that the very first hydrothermal ore fluids were strongly reduced, since As is generally transported as an  $\text{H}_3\text{AsO}_3$  complex that is predominantly dependent on redox conditions (Heinrich and Eadington, 1986).

At the peak of the hydrothermal activity, the down plunge portion of the 1806 Zone was formed and the initial metal assemblage in both the up plunge portion and the silicified horizon was altered (Fig. 3-14-lb). It is suggested that weakly acidic to neutral, oxidized fluids at temperatures of  $\sim 300^\circ\text{C}$  caused the deposition of chalcopyrite, Ag-bearing tetrahedrite and precious metal phases. Evidence for this comes from: (1) the predominant occurrence of chalcopyrite with electrum and minor Ag-phases; and (2) the close chemical and spatial association between Au, Ag and sulfosalts. Moreover, these hotter, oxidized fluids partly altered the earlier deposited mineral assemblage. This is preserved in (1) myrmekites of replaced arsenopyrite-chalcopyrite-tennantite-tetrahedrite±electrum±sphalerite within tennantite-tetrahedrite (Fig. 3-8c, d); and (2) chalcopyrite disease in sphalerites. Besides pyrite, chalcopyrite, precious metals and sulfosalts, minor high-Fe sphalerites were deposited, since they are abundant throughout the 1806 Zone and in silicified footwall rhyolite. Chalcopyrite disease is present in the high-Fe sphalerites as well, but it is less abundant than in medium-Fe sphalerites. It is assumed that gold was transported as a chloro-complex during this phase given the strong association with chalcopyrite and assumed temperatures greater than  $300^\circ\text{C}$  (e.g., Seward, 1973; Hannington and

Scott, 1989b; Large et al., 1989; Huston and Large, 1989; Stefánsson and Seward, 2004; Williams-Jones et al., 2009).

The waning stage of hydrothermal activity is characterized by: (1) deposition of sphalerite-galena and minor tennantite within sphalerite bands within the up plunge portion of the 1806 Zone; and (2) zone refining affecting especially precious metals and sulfosalts (Fig. 3-14-lc). Within the sphalerite bands, chalcopyrite is often replaced by sphalerite and tennantite-tetrahedrite (Fig. 3-8b). Moreover, the elevated grades of Au and Ag (Fig. 3-9) and the higher abundance of precious metals (Fig. 3-7) in the up plunge part is a direct result of zone refining during this stage, since the vast majority of the precious metals were originally deposited at peak hydrothermal activity. Lower temperature (< 300 °C), nearly oxidized and reduced fluids transported mainly Zn and Pb (Seward, 1984; Lydon, 1988; Large, 1992; Reed and Palandri, 2006) at the waning stage of hydrothermal activity. However, the same fluids are also responsible for the remobilization of Au, Ag, and elements of the epithermal suite (As, Sb; Seward, 1976; Zotov et al., 2003; Reed and Palandri, 2006). At the waning stage, Au was finally remobilized, from the down plunge portion by lower-temperature, Zn-Pb-Ag-Sb-bearing fluids, likely as a bisulfide complex (e.g., Seward, 1973; Huston and Large, 1989; Large et al., 1989; Williams-Jones et al., 2009) with Ag and elements of the epithermal suite and deposited in the up plunge part usually with Ag-phases and sulfosalts.

The post-depositional, pre-deformational state of the 1806 Zone is illustrated in Figure 3-14-II. A vertical metal zoning within the massive sulfide horizon is clearly developed with a pyrite-chalcopyrite assemblage at the bottom (now down plunge portion) and a pyrite-chalcopyrite-sphalerite assemblage with local sphalerite bands on top (now up plunge portion). Mafic dikes intruded syn- and post-depositional and cross-cut the Ming deposit with the 1806 Zone (Pilote and Piercey, 2013).

During Silurian-Devonian metamorphism and deformation the shape of the Ming deposit in general and of the 1806 Zone in particular was deformed (Fig. 3-14-III; Table 3-1) resulting in the elongation of the sulfide lenses parallel to a regional  $F_2$  foliation (Castonguay et al., 2009). It is also strongly assumed that the sulfide horizon at the 1806 Zone was internally sheared resulting: (1) in the flattening and elongation of the sulfide lens; (2) the re-orientation of the original almost horizontal metal zoning to the recent metal zoning observed in the up plunge portion and down plunge portion; and (3) recrystallization of minerals within the ores.

The results presented herein support that the 1806 Zone of the Ming Mine formed as a result of zone refining, leaching, and magmatic-hydrothermal input into a seafloor hydrothermal system. Despite deformation and metamorphism, these processes have not introduced new gold into the deposit and only remobilized existing syngenetic precious metals.

### 3-7 CONCLUSION

The results from stratigraphy, alteration, metal distribution, ore assemblage, and mineral chemistry presented in this paper show:

1) Precious metal emplacement in the metamorphosed and (poly-phase) deformed Au-bearing Ming VMS deposit is likely syngenetic despite the lack of advanced argillic style alteration. An intermediate-sulfidation style of mineralization, and normal VMS formation, is responsible for the sericitic alteration observed in the rhyolitic footwall and rather typical of low-sulfidation epithermal deposits and base metal VMS deposits.

2) The deposition of precious metals occurred coeval with base metal sulfides, especially with chalcopyrite. However, mineral chemistry strongly supports the involvement of magmatic-hydrothermal fluids containing precious metals and elements of the epithermal suite to normal VMS hydrothermal fluids containing base and transition metals.

3) Metamorphism and poly-phase deformation changed the deposit architecture and massive sulfide geometry in the sense that the mineralized zones at the Ming deposit are now separated by mafic dikes and that the original vertical metal zoning is now sheared as seen from the different metal associations in the up plunge portion (Cu-Zn-Au-Ag) and the down plunge portion (Cu-Au). Moreover, the massive sulfide lenses are elongated parallel to foliation. Mineral textures were also altered as seen in the recrystallization of many sulfide phases and the partial syn-deformational remobilization of precious metals (occurrence along

cracks and grain boundaries of recrystallized pyrite). However, deformation and metamorphism have only modified existing precious distributions and have not resulted in syn-orogenic gold additions similar to orogenic Au deposits (Deer Cove, Stog'er Tight) found regionally on the Baie Verte Peninsula.

## **Acknowledgements**

Michael Shaffer and David Grant (Bruneau Centre, MUN) are thanked for their great support and help in the use of the SEM and its software. SMB thanks Yanan Liu (UT) for her assistance and help at the EPMA at UT. An SEG Student Research Grant to SMB was partly used for analytical work at the EPMA at UT. Discussions with Sean McClenaghan, Patrick Mercier-Langevin, and George Hudak improved the paper in the early stages of the manuscript. Special thanks goes to Scott Swinden, Patrick Mercier-Langevin and David Lentz, who improved the paper significantly with their critical and constructive reviews and comments. Staff and miners of the Ming Mine are explicitly thanked for their help, assistance and support during core logging and underground mapping. Rambler Metals and Mining Canada Ltd. provided logistical support for the project. Funding for the project was provided by grants to S. J. Piercey, including an NSERC Discovery Grant and the NSERC Altius Industrial Research Chair in Mineral Deposits supported by NSERC, Altius Minerals Ltd., and the Research and Development Corporation of Newfoundland and Labrador.

## References

- Bergman-Weiher J, Bergström U, Billström K, Weiher P (1996) Geology, tectonic setting, and origin of the Paleoproterozoic Boliden Au-Cu-As deposit, Skellefte district, northern Sweden *Economic Geology* 91:1073-1097
- Bierlein FP, Crowe DE (2000) Phanerozoic orogenic lode gold deposits. In: Hagemann SG, Brown, P.E. (ed) *Gold in 2000*, vol 13. Reviews in Economic Geology. Society of Economic Geologists, Boulder, CO, pp 103-139
- Brueckner SM, Piercey SJ, Sylvester PJ, Pilgrim L, Maloney S, Hyde D, Ogilvie G (2011) Stratigraphy, mineralogy, geochemistry, and genesis of an Au-rich volcanogenic massive sulfide (VMS) system from the Baie Verte Peninsula, NW Newfoundland, Canada: The 1806 Zone as an example from the Ming Mine, Rambler Camp. In: Deschênes G, Dimitrakopoulos R, Bouchard J (eds) *World Gold 2011*. Canadian Institute of Mining, Metallurgy and Petroleum, Montreal, QC, Canada, pp 899-911
- Castonguay S, Skulski T, van Staal C, Currie M (2009) New insights on the structural geology of the Pacquet Harbour group and Point Rousse complex, Baie Verte peninsula, Newfoundland Current Research Newfoundland and Labrador Department of Natural Resources, Geological Survey Report 09-1:147-158
- Cawood PA, van Gool JAM, Dunning GR (1993) Silurian age for movement on the Baie Verte Line: Implications for accretionary tectonics in the Northern Appalachians Geological Society of America, Abstract with Programs 25:A422
- Di Benedetto F, Bernardini GP, Costagliola P, Plant D, Vaughan DJ (2005) Compositional zoning in sphalerite crystals *American Mineralogist* 90:1384-1392
- Dubé B, Gosselin P, Mercier-Langevin P, Hannington M, Galley A (2007a) Gold-rich volcanogenic massive sulphide deposits. In: Goodfellow WD (ed) *Mineral deposits of Canada: A synthesis of major deposit-types, district metallogeny, the evolution of geological provinces, and exploration methods*, vol Special Publication No. 5. Geological Association of Canada, Mineral Deposits Division, pp 75-94
- Dubé B, Mercier-Langevin P, Hannington M, Lafrance B, Gosselin G, Gosselin P (2007b) The LaRonde Penna world-class Au-rich volcanogenic massive sulfide deposit, Abitibi, Québec: Mineralogy and geochemistry of alteration

and implications for genesis and exploration *Economic Geology* 102:633-666

Evans DTW, Wells C (1998) Epigenetic gold mineralization, Baie Verte Peninsula, Newfoundland Current Research Newfoundland Department of Mines and Energy, Geological Survey Report 98-1:39-51

Franklin JM (1993) Volcanic-associated massive sulphide deposits. In: Kirkham RV, Sinclair WD, Thorpe RI, Duke JM (eds) *Mineral Deposit Modeling*. Geological Association of Canada, Special Paper 40, pp 315-334

Franklin JM (1996) Volcanic-associated massive sulphide base metals. In: Eckstrand OR, Sinclair WD, Thorpe RI (eds) *Geology of Canadian Mineral Deposit Types*. Geological Survey of Canada, Geology of Canada Series no. 8, Ottawa, ON, pp 158-183

Franklin JM, Lydon JW, Sangster DF (1981) Volcanic-associated sulfide deposits. In: Skinner BJ (ed) *Economic Geology Seventy-Fifth Anniversary Volume*. Society of Economic Geologists, pp 485-627

Franklin JM, Gibson HL, Jonasson IR, Galley AG (2005) Volcanogenic massive sulfide deposits. In: Hedenquist JW, Thompson JFH, Goldfarb RJ, Richards JP (eds) *Economic Geology 100<sup>th</sup> Anniversary Volume, 1905-2005*. Society of Economic Geologists, pp 523-560

Galley AG, Syme R, Bailes AH (2007) Metallogeny of the Paleoproterozoic Flin Flon Belt, Manitoba and Saskatchewan. In: Goodfellow WD (ed) *Mineral deposits of Canada: A synthesis of major deposit-types, district metallogeny, the evolution of geological provinces, and exploration methods*, vol Special Publication No. 5. Geological Association of Canada, Mineral Deposits Division, pp 509-531

Goldfarb RJ, Baker T, Dubé B, Groves DI, Hart CJR, Gosselin P (2005) Distribution, character, and genesis of gold deposits in metamorphic terranes. In: Hedenquist JW, Thompson, J.F.H., Goldfarb, R.J., Richards, J.P. (ed) *Economic Geology 100<sup>th</sup> Anniversary Volume, 1905-2005*. Society of Economic Geologists, Boulder, CO, pp 407-450

Groves DI, Goldfarb RJ, Gebre-Mariam M, Hagemann SG, Robert F (1998) Orogenic gold deposits: A proposed classification in the context of their crustal distribution and relationship to other gold deposit types *Ore Geology Reviews* 13:7-27

Hannington MD, Scott SD (1989a) Gold mineralization in volcanogenic massive sulfides: Implications of data from active hydrothermal vents on the

- modern seafloor. In: Keays RR, Ramsay, W.R.H., Groves, D.I. (ed) The geology of gold deposits: The perspective in 1988, vol 6. Economic Geology Monograph. Society of Economic Geologists, Boulder, CO, pp 491-507
- Hannington MD, Scott SD (1989b) Sulfidation equilibria as guides to gold mineralization in volcanogenic massive sulfides: Evidence from sulfide mineralogy and the composition of sphalerite *Economic Geology* 84:1978-1995
- Hannington MD, Peter JM, Scott SD (1986) Gold in sea-floor polymetallic sulfide deposits *Economic Geology* 81:1867-1883
- Hannington MD, Poulsen KH, Thompson JFH, Sillitoe RH (1999) Volcanogenic gold in the massive sulfide environment. In: Barrie CT, Hannington, M.D. (ed) Volcanic-associated massive sulfide deposits: Processes and examples in modern and ancient settings, vol 8. Reviews in Economic Geology. Society of Economic Geologists, Boulder, CO, pp 325-351
- Hedenquist JW, Arribas RA, Gonzalez-Urien E (2000) Exploration for epithermal gold deposits. In: Hagemann SG, Brown, P.E. (ed) Gold in 2000, vol 13. Reviews in Economic Geology. Society of Economic Geologists, Boulder, CO, pp 245-277
- Heinrich CA, Eadington PJ (1986) Thermodynamic predictions of the hydrothermal chemistry of arsenic, and their significance for the paragenetic sequence of some cassiterite-arsenopyrite-base metal sulfide deposits *Economic Geology* 81:511-529
- Herzig PM, Hannington MD (1995) Polymetallic massive sulfides at the modern seafloor: A review *Ore Geology Reviews* 10:95-115
- Herzig PM, Hannington MD, Fouquet Y, von Stackelberg U, Petersen S (1993) Gold-rich polymetallic sulfides from the Lau back arc and implications for the geochemistry of gold in sea-floor hydrothermal systems of the Southwest Pacific *Economic Geology* 88:2182-2209  
doi:10.2113/gsecongeo.88.8.2182
- Hibbard LJ (1983) Geology of the Baie Verte Peninsula, Newfoundland vol 2. Memoir. Department of Mines and Energy, Government of Newfoundland and Labrador, Memoir 2,
- Huston DL (2000) Gold in volcanic-hosted massive sulfide deposits: Distribution, genesis, and exploration. In: Hagemann SG, Brown, P.E. (ed) Gold in



2000, vol 13. Reviews in Economic Geology. Society of Economic Geologists, Boulder, CO, pp 401-426

Huston DL, Large RR (1989) A chemical model for the concentration of gold in volcanogenic massive sulphide deposits *Ore Geology Reviews* 4:171-200

Huston DL, Bottril, RS, Creelman, RA, Zaw, K, Ramsden TR, Rand, SW, Gemmell, JB, Jablonski, W, Sie, SH, Large, RR (1992) Geologic and geochemical controls on the mineralogy and grain size of gold-bearing phases, eastern Australian volcanic-hosted massive sulfide deposits *Economic Geology* 87:542-563

Large RR (1977) Chemical evolution and zonation of massive sulfide deposits in volcanic terrains *Economic Geology* 72:549-572

Large RR (1992) Australian volcanic-hosted massive sulfide deposits: Features, styles, and genetic models *Economic Geology* 87:471-510

Large RR, Huston DL, McGoldrick PJ, Ruxton PA (1989) Gold distribution and genesis in Australian volcanogenic massive sulfide deposits and their significance for gold transport models. In: Keays RR, Ramsay, W.R.H., Groves, D.I. (ed) *The geology of gold deposits: The perspective in 1988*, vol 6. *Economic Geology Monograph*. pp 520-536

Lydon JW (1984) Volcanogenic massive sulphide deposits Part 1: A descriptive model *Geoscience Canada* 11:195-202

Lydon JW (1988) Volcanogenic massive sulphide deposits Part 2: Genetic models *Geoscience Canada* 15:43-65

Marquis P, Hubert C, Brown AC, Rigg DM (1990) Overprinting of early, redistributed Fe and Pb-Zn mineralization by late stage Au-Ag-Cu deposition at the Dumagami mine, Bousquet district, Abitibi, Quebec *Canadian Journal of Earth Sciences* 27:1651-1671

Mercier-Langevin P, Hannington MD, Dubé B, Bécu V (2011) The gold content of volcanogenic massive sulfide deposits *Mineralium Deposita* 46:509-539 doi:10.1007/s00126-010-0300-0

Mercier-Langevin P, McNicoll V, Allen RL, Blight JHS, Dubé B (2013) The Boliden gold-rich volcanogenic massive sulphide deposit, Skellefte district, Sweden: new U-Pb age constraints and implications at deposit and district scale *Mineralium Deposita* 48:485-504

- Moëlo Y et al. (2008) Sulfosalt systematics: A review. Report of the sulfosalt sub-committee of the IMA Commission on ore mineralogy *European Journal of Mineralogy* 20:7-46
- Ohmoto H (1996) Formation of volcanogenic massive sulfide deposits: The Kuroko perspective *Ore Geology Reviews* 10:135-177
- Patey KS, Wilton DHC (1993) The Deer Cove deposit, Baie Verte Peninsula, Newfoundland, a Paleozoic mesothermal lode-gold occurrence in the northern Appalachians *Canadian Journal of Earth Sciences* 30:1532-1546
- Piercey S, Jenner GA, Wilton DHC (1997) The stratigraphy and geochemistry of the southern Pacquet Harbour Group, Baie Verte Peninsula, Newfoundland: Implications for mineral exploration *Current Research Newfoundland and Labrador Department of Natural Resources, Geological Survey Report* 97-1:119-139
- Pilgrim L (2009) Mineral resource estimate for the Ming Mine, Newfoundland, Canada. Rambler Metals and Mining Canada Ltd, Baie Verte, NL
- Pilote J-L, Piercey SJ (2013) Volcano-stratigraphy of the 1807 zone of the Ming Cu-Au volcanogenic massive sulfide (VMS) deposit, Baie Verte Peninsula, northern Newfoundland *Geological Survey of Canada, Current Research* 2013-20:13 doi:10.4095/293128
- Poulsen KH, Hannington MD (1996) Volcanic-associated massive sulphide gold. In: Eckstrand OR, Sinclair, W.D., Thorpe, R.I. (ed) *Geology of Canadian Mineral Deposit Types*. Geological Survey of Canada, *Geology of Canada Series no. 8*, Ottawa, ON, pp 183-196
- Poulsen KH, Robert F, Dubé B (2000) Geological classification of Canadian gold deposits vol *Bulletin* 540. Geological Survey of Canada, Ottawa, ON
- Ramezani J, Dunning GR, Wilson MR (2000) Geologic setting, geochemistry of alteration, and U-Pb age of hydrothermal zircon from the Silurian Stog'er Tight gold prospect, Newfoundland Appalachians, Canada *Exploration and Mining Geology* 9:171-188
- Reed MH, Palandri J (2006) Sulfide mineral precipitation from hydrothermal fluids. In: Vaughan DJ (ed) *Sulfide mineralogy and geochemistry*, vol 61. *Reviews in Mineralogy and Geochemistry*. pp 609-631
- Roth T, Thompson JFH, Sillitoe RH (1999) The precious metal-rich Eskay Creek deposit, northwestern British Columbia. In: Barrie CT, Hannington, M.D. (ed) *Volcanic-associated massive sulfide deposits: Processes and*

- examples in modern and ancient settings, vol 8. Reviews in Economic Geology. Society of Economic Geologists, Boulder, CO, pp 357-373
- Seward TM (1973) Thio complexes of gold and the transport of gold in hydrothermal ore solutions *Geochimica et Cosmochimica Acta* 37:379-399
- Seward TM (1976) The stability of chloride complexes of silver in hydrothermal solutions up to 350°C *Geochimica et Cosmochimica Acta* 40:1329-1341
- Seward TM (1984) The formation of lead(II) chloride complexes to 300°C: A spectrophotometric study *Geochimica et Cosmochimica Acta* 48:121-134
- Sillitoe RH, Hedenquist JW (2003) Linkages between volcanotectonic settings, ore-fluid compositions, and epithermal precious metal deposits. In: Simmons SF, Graham I (eds) *Volcanic, geothermal, and ore-forming fluids: Rulers and witnesses of processes within the Earth*, vol Special Publication Number 10. Special Publications of the Society of Economic Geologists, Boulder, CO, pp 315-343
- Sillitoe RH, Hannington MD, Thompson JFH (1996) High sulfidation deposits in the volcanogenic massive sulfide environment *Economic Geology* 91:204-212
- Skulski T, Castonguay S, van Staal C, Rogers N, McNicoll V, Kerr A, Escayola M (2009) Baie Verte Peninsula: An evolving geological story In: Rogers N, Kerr A (eds) *Annual Field Trip, October 2-5, 2009*. Geological Association of Canada, Newfoundland and Labrador Section, St. John's, NL, pp 76
- Skulski T, Castonguay, S., McNicoll, V., van Staal, C, Kidd, W, Rogers, N, Morris W, Ugalde, H, Slavinski H, Spicer W, Moussallam, Y, Kerr, I (2010) Tectonostratigraphy of the Baie Verte oceanic tract and its ophiolite cover sequence on the Baie Verte Peninsula Current Research Newfoundland and Labrador Department of Natural Resources, Geological Survey Report 10-1:315-335
- Stefánsson A, Seward TM (2004) Gold(I) complexing in aqueous sulphide solutions to 500°C at 500 bar *Geochimica et Cosmochimica Acta* 68:4121-4143 doi:10.1016/j.gca.2004.04.006
- Swinden HS, Thorpe RI (1984) Variations in style of volcanism and massive sulfide deposition in Early to Middle Ordovician island-arc sequences of the Newfoundland Central Mobile Belt *Economic Geology* 79:1596-1619 doi:10.2113/gsecongeo.79.7.1596

- Tourigny G, Brown AC, Hubert C, Cr  peau R (1989) Syvolcanic and syntectonic gold mineralization at the Bousquet mine, Abitibi greenstone belt, Quebec Economic Geology 84:1875-1890
- Tourigny G, Doucet D, Bourget A (1993) Geology of the Bousquet 2 Mine: An example of a deformed, gold-bearing, polymetallic sulfide deposit Economic Geology 88:1578-1597
- Tuach J (1988) Geology and sulphide mineralization in the Pacquet Harbour Group. In: Swinden HS, Kean BF (eds) The volcanogenic sulphide districts of Central Newfoundland: A guidebook and reference manual for volcanogenic sulphide deposits in the early Paleozoic oceanic volcanic terranes of Central Newfoundland. Geological Association of Canada, Mineral Deposits Division, St. John's, NL, pp 49-53
- Tuach J, Kennedy MJ (1978) The geologic setting of the Ming and other sulfide deposits, consolidated Rambler mines, Northeast Newfoundland Economic Geology 73:192-206
- van Staal CR (2007) Pre-Carboniferous tectonic evolution and metallogeny of the Canadian Appalachians. In: Goodfellow WD (ed) Mineral deposits of Canada: A synthesis of major deposit-types, district metallogeny, the evolution of geological provinces, and exploration methods, vol Special Publication No. 5. Geological Association of Canada, Mineral Deposits Division, pp 793-818
- van Staal CR, Barr SM (2012) Lithospheric architecture and tectonic evolution of the Canadian Appalachians and associated Atlantic margin. In: Percival JA, Cook FA, Clowes RM (eds) Tectonic Styles in Canada: The LITHOPROBE perspective. Geological Association of Canada, Special Paper 49, St. John's, NL, pp 41-96
- Vaughan DJ, Craig JR (1978) Mineral chemistry of metal sulfides. Cambridge Earth Science Series. Cambridge University Press, Cambridge
- Wagner T, Jonsson E (2001) Mineralogy of sulfosalt-rich vein-type ores, Boliden massive sulfide deposit, Skellefte District, Northern Sweden The Canadian Mineralogist 39:855-872 doi:10.2113/gscanmin.39.3.855
- Williams H (1979) Appalachian orogen in Canada Canadian Journal of Earth Sciences 16:792-807
- Williams-Jones AE, Bowtell RJ, Migdisov AA (2009) Gold in solution Elements 5:281-287

- Wright K (2009) The incorporation of cadmium, manganese and ferrous iron in sphalerite: Insights from computer simulations *The Canadian Mineralogist* 47:615-623 doi:10.3749/canmin.47.3.615
- Zotov AV, Shikina ND, Akinfiev NN (2003) Thermodynamic properties of the Sb(III) hydroxide complex  $\text{Sb}(\text{OH})_{3(\text{aq})}$  at hydrothermal conditions *Geochimica et Cosmochimica Acta* 67:1821-1836

## APPENDIX

### APPENDIX A3-1 SAMPLE DESCRIPTION

**Table A3-1.** Analyzed samples for EPMA data, their occurrence within the 1806 zone, their mineralogy, and their analyzed phases. Mineral abbreviations as in Figure 2-8 with Boul – boulangerite, Cass – cassiterite, Mag – magnetite, Mol – molybdenite, Ten – tennantite, Tet – tetraedrite. Mineral abundances: **Major phase** (> 10vol.%), **minor phase** (5-10vol.%), accessory phase (< 5vol.%)

Sample No.	Mineralized Zone	Plunge / Section	Description	Mineralogy and abundance	Analyzed minerals (number of analyses)
29781	Stringer	Up Plunge / 22	Fine, partly sulfide stringers in rhyolite	<u>Py</u> > <u>Sp</u> > <u>Ccp</u> > Gn > Asp > Tet > Ten > El	Py (3), Ccp (5), Sp (3), Gn (3), Asp (4), Ten (6), Ten-Tet (3), Tet (3)
29902		Up Plunge / 21	Py-Ccp stringer in rhyolite flow (Au-bearing); myrmekitic like texture of Asp-Ccp-Ten-Tet ± Sp in Tet	<u>Py</u> > <u>Ccp</u> > <u>Asp</u> > <u>Sp</u> > Gn > Tet > Ten > AgTet > El	Py (1), Ccp (4), Sp (3), Gn (4), Asp (5), Tet (3), El (5)
29918	Semi-massive sulfide	Down Plunge / 2	Py-Sp stringer in semi-massive zone in rhyolite with indicated crenulation cleavage	<u>Ccp</u> > <u>Po</u> ≈ <u>Py</u> > <u>Mag</u> > <u>Sp</u> > > Cass ≈ Gn > Mol > Chr	Py (3), Ccp (5), Sp (1), Gn (1), Po (3), Asp (2), Mol (1), Cass (2), Mag (9)
29934			Py-Ccp semi-massive sulfide in rhyolite	<u>Py</u> > > <u>Ccp</u> > Sp > Gn ≈ Asp > AgTet > El	Py (6), Ccp (4), Sp (2), Gn (2), Asp (3), Tet (9)
29787		Up Plunge / 22	Semi-massive sulfide (Py+Ccp+Sp) around rhyolite	<u>Py</u> ≈ <u>Ccp</u> > > <u>Po</u> > <u>Sp</u> > > Asp ≈ Gn > AgTet > Tet > > Ten > AgHg alloy ≈ unknown AsPbFeS phase	Py (2), Ccp (5), Sp (3), Gn (3), Po (2), Asp (3), Tet (2)
29913		Up Plunge / 21	Ccp-Py stringer in rhyolite (end of semi-massive zone)	<u>Ccp</u> > <u>Py</u> > <u>Po</u> > > <u>Sp</u> > Asp > Gn > El > Mia > Boul	Py (1), Ccp (6), Sp (3), Gn (3), Po (1), Asp (2), 1 (Mia), El (6), Boul (1)
29907	Massive sulfide	Down Plunge / 2	Py in massive sulfide (dead ore?)	<u>Py</u> > > <u>Ccp</u> > Sp > Asp > > Gn ≥ Tet > AgTet > Po > Boul	Py (5), Ccp (5), Sp (1), Gn (3), Asp (5), El (1), Boul (2)
29778		Up Plunge / 22	Massive sulfide (Py)	<u>Py</u> > <u>Ccp</u> > Asp ≈ Sp > Ten ≈ Tet > Ag Tet > AgHgAu alloy > El ≈ Po	Py (5), Ccp (4), Sp (1), Gn (3), Asp (4), Ten (2), Ten-Tet (2), El (1)
36509		Up Plunge / 21	Py-Asp-Tet with black material in Py-rich sulfide	<u>Py</u> > <u>Tet</u> > <u>AgTet</u> > <u>Asp</u> > > <u>Sp</u> > Ten > Gn > Ccp > El > Ag phase	Py (2), Ccp (2), Sp (3), Gn (4), Asp (7), Ten (6), Tet (2), El (3)

**Table A3-1. (cont.)**

Sample No.	Mineralized Zone	Plunge / Section	Description	Mineralogy and abundance	Analyzed minerals (number of analyses)
36512			Sp-Gn-rich sulfide	<b>Sp</b> $\approx$ <b>Gn</b> > <b>Py</b> >> Ccp $\approx$ Asp > Stn > Ag phases > AgTet > El	Py (4), Ccp (2), Sp (5), Gn (4), Asp (1), Pyr (1), Hg-Stp (1), AgCuFeS (1), Stn (4)
29920	Silicified horizon (on contact to massive sulfide)	Down Plunge / 2	Massive Py	<b>Py</b> >> Ten/Ag-Tet > Ccp $\approx$ Sp $\approx$ Asp > Po $\approx$ Gn > Stn > Col	Py (6), Ccp (6), Sp (2), Asp (3), Ten (4), Ten-Tet (6), Tet (1)
29783	Silicified horizon	Up Plunge / 22	Ccp+Py in massive quartz [high-grade ore]	<b>Ccp</b> > <b>Py</b> > <b>Po</b> > <b>Sp</b> > Asp > El > Ag Ccp > Mia $\approx$ unknown NiSbS phase	Py (1), Ccp (5), Sp (2), Po (6), Asp (4), Mia (1), El (8)
29914		Up Plunge / 21	Fine Ccp-Py stringer in silicified horizon (massive Qtz) above stringer zone	<b>Py</b> >> <b>Ccp</b> >> Asp > Gn $\approx$ Sp > AgTet $\approx$ Ten > Tet $\approx$ Po	Py (3), Ccp (6), Sp (1), Asp (5), Ten-Tet (1), Tet (4)

## APPENDIX A3-2 DETECTION LIMITS

**Table A3-2.** Detection limits for all 17 elements analyzed in sulfides, precious metals and oxides in April 2011 and January 2012 on the microprobe at UT.

Analyzed phases	Sulfides and precious metals				Oxides	
Measurement date	April 2011		January 2012		January 2012	
Element	Mean	Std	Mean	Std	Mean	Std
S [ppm]	379	101	356	50	259	27
Fe	354	63	352	42	396	26
Cu	496	44	492	41	446	25
Zn	622	149	558	54	525	33
Pb	1,983	651	1,900	593	1,526	131
As	1,244	293	1,175	116	1,070	67
Au	1,222	293	1,160	194	1,051	90
Ag	1,269	387	1,216	355	1,053	349
Sb	586	175	552	145	574	339
Sn	925	356	834	252	598	101
Te	1,074	382	965	305	786	298
Bi	1,751	627	1,710	1,051	1,044	117
Hg	1,797	197	2,538	249	2,368	155
Mo	1,336	346	1,191	170	913	129
Mn	160	32	229	40	211	27
Co	137	19	139	19	163	10
Ni	160	24	161	21	157	11

Std – standard deviation

## APPENDIX A3-3 RESULTS EPMA ANALYSIS

**Table A3-3.** Electron microprobe data on sulfides, sulfosalts, precious metals and oxides; See electronic Appendix accompanying this thesis



## CHAPTER 4

In:

Brueckner SM, Piercey SJ, Layne GD, Piercey G (2015) Variations of sulfur isotope signatures in sulfides from the metamorphosed Ming Cu(–Au) volcanogenic massive sulfide deposit, Newfoundland Appalachians, Canada.

Mineralium Deposita. doi: 10.1007/s00126-014-0567-7

**VARIATIONS OF SULFUR ISOTOPE SIGNATURES IN SULFIDES FROM THE  
METAMORPHOSED MING CU(-AU) VOLCANOGENIC MASSIVE SULFIDE  
DEPOSIT, NEWFOUNDLAND APPALACHIANS, CANADA**

Stefanie M. Brueckner<sup>1</sup>, Stephen J. Piercey<sup>1</sup>, Graham D. Layne<sup>1</sup>, Glenn Piercey<sup>2</sup>,  
and Paul J. Sylvester<sup>1†</sup>

*<sup>1</sup>Dept. of Earth Sciences, Memorial University of Newfoundland,  
300 Prince Philip Drive, St. John's, NL, A1B 3X5, Canada*

*<sup>2</sup>Core Research Equipment and Instrument Training Network (CREAIT),  
Bruneau Centre for Research and Innovation,  
Memorial University of Newfoundland,  
P.O. Box 4200, St. John's, NL, A1C 5S7, Canada*

*<sup>†</sup> now at: Dept. of Geosciences, Texas Tech University, 125 Science Bldg.,  
Lubbock, TX 79049-1053, USA*

**ABSTRACT**

The Ming deposit is an early Ordovician, bimodal-mafic Cu-Au volcanogenic massive sulfide (VMS) deposit in the Newfoundland Appalachians that was metamorphosed to upper greenschist/lower amphibolite facies conditions and deformed in the Silurian and Devonian. The Ming deposit consists of several spatially proximal orebodies of which the 1806 Zone, 1807 Zone, Ming South Up Plunge and Down Plunge, and the Lower Footwall Zone are the focus of this paper. The orebodies have similar stratigraphic sequences. The orebodies

can be divided into (1) a silicified horizon that caps the massive sulfides, (2) semi-massive to massive sulfides, and (3) sulfide mineralization in a rhyodacitic footwall. Sulfide mineralization in a rhyodacitic footwall includes (a) sulfide stringers immediately below the semi-massive to massive sulfides and (b) chalcopyrite-pyrrhotite-pyrite stringers distally from semi-massive to massive sulfides in the Lower Footwall Zone.

Pyrite, chalcopyrite, pyrrhotite, arsenopyrite, and galena were analyzed by *in-situ* secondary ion mass spectrometry (SIMS) for sulfur isotope compositions. The isotopic signatures of pyrite, chalcopyrite, pyrrhotite, and arsenopyrite fall within a limited range of 2.8 to 12.0‰ for semi-massive to massive sulfides and sulfide mineralization in the footwall. The silicified horizon capping the semi-massive to massive sulfides has higher  $\delta^{34}\text{S}$  (5.8 – 19.6‰), especially for pyrrhotite (mean:  $17.2 \pm 2.2$ ‰, n=8). The sulfur isotope composition of galena is more heterogeneous, especially within semi-massive to massive sulfides and sulfide stringers, ranging from 0.8-17.3‰ (mean:  $6.1 \pm 4.3$ ‰, n=35) and 7.6-17.1‰ (mean:  $13.7 \pm 5.3$ ‰, n=3), respectively.

Geothermometric calculations give unreliable formation and metamorphism temperatures for neighbouring mineral pairs, because sulfides were not in isotopic equilibrium while deposited in early Ordovician or re-equilibrated during Silurian-Devonian metamorphism, respectively. Therefore, original, unequilibrated isotopic compositions of sulfides at the Ming deposit have been preserved.

Modeling of the source of sulfur shows that: (1) reduced seawater sulfate and (2) sulfur leached from igneous wall rock and/or derived from magmatic fluids are the main sources of sulfur in the Ming deposit. The influence of igneous sulfur (igneous wall rock/magmatic fluids) increases with temperature and is an important sulfur source for the semi-massive to massive sulfides and footwall mineralization, in addition to a contribution from thermochemical sulfate reduction (TSR) of seawater. It is difficult to distinguish between sulfur leached from igneous rocks and magmatic fluid-related sulfur, and it is possible that both sources contributed to the ores at the Ming deposit. In addition to igneous sulfur, the heavy isotopes of the silicified horizon are consistent with the sulfur in this horizon being derived only from thermochemical sulfate reduction of early Ordovician seawater sulfate.

**Keywords:** Sulfur isotopes, sulfides, metamorphosed VMS deposit, *in-situ* SIMS analysis, thermochemical sulfate reduction (TSR), sulfur leached from igneous wall rock and/or derived from magmatic fluids, Newfoundland Appalachians

#### **4-1 INTRODUCTION**

Volcanogenic massive sulfide (VMS) deposits form on or just below the ocean floor by the complex interaction of hydrothermal fluids with the wall rock resulting in the deposition of massive sulfides containing base and precious metals (Lydon, 1984; Franklin, 1993, 1996; Galley et al., 2007). The hydrothermal

fluids transporting metals and sulfur are predominantly modified seawater (Bischoff and Rosenbauer, 1983; Lydon, 1984; Franklin, 1996; Galley et al., 2007). However, a magmatic fluid contribution may be present in some deposits, resulting in the formation of Au-rich VMS deposits (Sillitoe et al., 1996; Hannington et al., 1999; Huston, 2000; Dubé et al., 2007; Mercier-Langevin et al., 2011). During the interaction of circulating hydrothermal ore fluids with wall rock, the physico-chemical conditions (pH, T,  $fO_2$ ,  $fS_2$ ) of the hydrothermal ore fluids change during the evolution of the hydrothermal system and result in metal zoning and complex mineral assemblages observed in VMS deposits (Large, 1992; Lydon, 1988; Franklin, 1996; Ohmoto, 1996).

The source of sulfur in these metal transporting hydrothermal fluids is variable due to the complex genesis of VMS systems: numerous studies in modern and ancient VMS deposits illustrate that the deposits have one or multiple sulfur sources (Woodruff and Shanks, 1988; Goodfellow and Peter, 1996; Gemmell et al., 2004; Bradshaw et al., 2008; Alt and Shanks, 2011). Possible sources of sulfur reported from modern hydrothermal vents, young seafloor systems and ancient VMS systems include: (1) thermochemical reduction of seawater sulfate (TSR); (2) sulfur from igneous, metamorphic and/or sedimentary wall rock; (3) magmatic fluids that have an isotopic composition towards lower  $\delta^{34}S$  due to  $SO_2$  disproportionation; and (4) bacterial sulfate reduction of seawater sulfate (BSR; Shanks et al., 1995; Ohmoto and Goldhaber, 1997; Huston, 1999; Shanks, 2001; Seal, 2006; Hoefs, 2009). Despite numerous

sulfur isotope studies on ancient VMS deposits, there are relatively few studies on ancient VMS deposits that are significantly metamorphosed to facies equal to or higher than greenschist (Bachinski, 1977, 1978; Cook and Hoefs, 1997; Bailie et al., 2010) and/or deposits enriched in precious metals (Zaw and Ross, 1992). Additionally, very few studies have focused on *in situ* analyses of VMS sulfides that are constrained by paragenesis (Bradshaw et al., 2008).

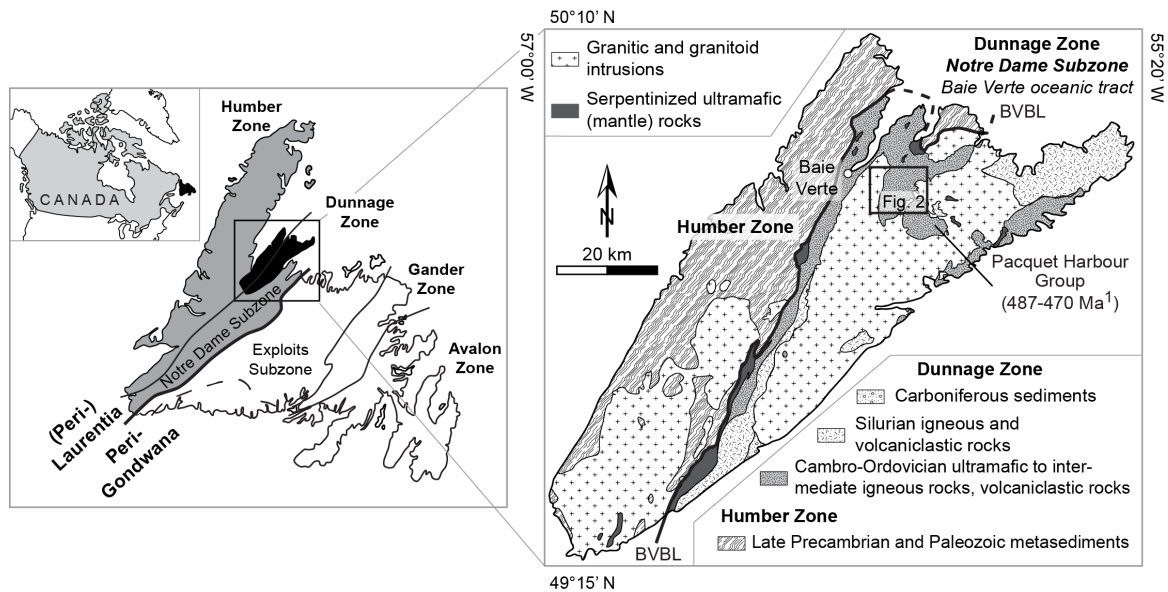
In this paper we report *in situ* secondary ion mass spectrometry (SIMS) sulfur isotope analyses of pyrite, chalcopyrite, pyrrhotite, arsenopyrite, and galena from the moderately metamorphosed and precious metal-enriched Cu-Au VMS Ming deposit, Newfoundland Appalachians (Brueckner et al., 2014). This deposit contains five different, actively mined orebodies with different styles of sulfide mineralization. These different mineralization styles are from top to bottom: (1) silicified horizon that caps massive sulfides; (2) semi-massive to massive sulfides; and (3) discordant ore mineralization in the footwall consisting of (a) the sulfide stringers immediately below massive sulfide; and (b) the Lower Footwall Zone that represents the high temperature, chlorite-rich stockwork zone that occurs distally from the massive sulfides. The mineralization styles differ in mineralogy and mineral assemblages from each other and show variations in mineral textures and compositions. Therefore, the Ming deposit provides an excellent opportunity to study the sulfur isotope variations in an ancient, metamorphosed, precious metal-bearing VMS deposit. Modelling of the sulfur isotope compositions is used to constrain the sources of sulfur in the deposit. The

results provide critical information on sulfur sources in Appalachian VMS deposits, but have implications for both base metal and precious metal-rich VMS deposits globally.

## **4-2 GEOLOGIC BACKGROUND**

### ***4-2-1 BAIE VERTE PENINSULA***

The Baie Verte Peninsula in northwest Newfoundland is part of the Canadian Appalachians and hosts both metamorphosed Precambrian rocks of Laurentia (Humber Zone) and peri-Laurentian Paleozoic rocks of the Notre Dame subzone of the Dunnage Zone (Fig. 4-1). Cambro-Ordovician ophiolitic rocks forming the basement of the Dunnage Zone are crosscut by felsic intrusions, and overlain by volcanic sequences. The ophiolitic basement rocks and their cover sequences formed in peri-Laurentian supra-subduction zones due to the closure of the Humber Seaway, and were obducted onto Laurentia during the Taconic Orogeny (Swinden and Thorpe, 1984; van Staal, 2007; van Staal and Barr, 2012). During the Salinic and Acadian orogenies in the Silurian and early Devonian, respectively, the ophiolitic basement rocks and their cover sequences were deformed and metamorphosed to upper greenschist/lower amphibolite facies. Moreover, felsic plutons intruded into the basement (Tuach and Kennedy, 1978; Hibbard, 1983; Castonguay et al., 2009).



**Figure 4-1.** Location of the study area within Newfoundland, Canada (left) and the Baie Verte Peninsula, Newfoundland (right). The geologic zones of Newfoundland are after Williams (1979) with the location of the Baie Verte Peninsula (black). The simplified geology of the Baie Verte Peninsula is after Hibbard (1983). <sup>1</sup> Age data for the Pacquet Harbour Group (PHG) from Castonguay et al. (2009) and Skulski et al. (2010)

The Pacquet Harbour Group (PHG), Baie Verte Peninsula, is a remnant ophiolitic basement assemblage that hosts the VMS deposits in the Rambler Camp (Fig. 4-2). The PHG is divided into lower and upper units. The lower PHG is early Ordovician and consists of dominantly low-Ti boninite and basalt with minor rhyodacite to rhyolite (Rambler rhyolite). The Rambler rhyolite has a U-Pb zircon age of ca. 487Ma (Castonguay et al., 2009) and is the host to VMS mineralization in the camp. The upper PHG is the cover sequence of the lower PHG, has mafic to felsic, mid-Ordovician volcano-sedimentary rocks and mafic



volcanic rocks with an age of 483 to 470Ma (Hibbard, 1983; Castonguay et al., 2009; Skulski et al., 2010). Volcanogenic massive sulfide deposition within the lower PHG was coeval with the formation of the PHG rocks in a rifted arc/back-arc setting (Piercey et al., 1997; van Staal, 2007; Skulski et al., 2010). The timing of precious metal enrichment in the VMS deposit was argued to be either of syngenetic or of metamorphic origin (Hibbard, 1983; Tuach and Kennedy, 1978). However, recent research on the Ming deposit has shown that gold and silver are of syngenetic origin and likely of magmatic-hydrothermal origin (Brueckner et al., 2014).

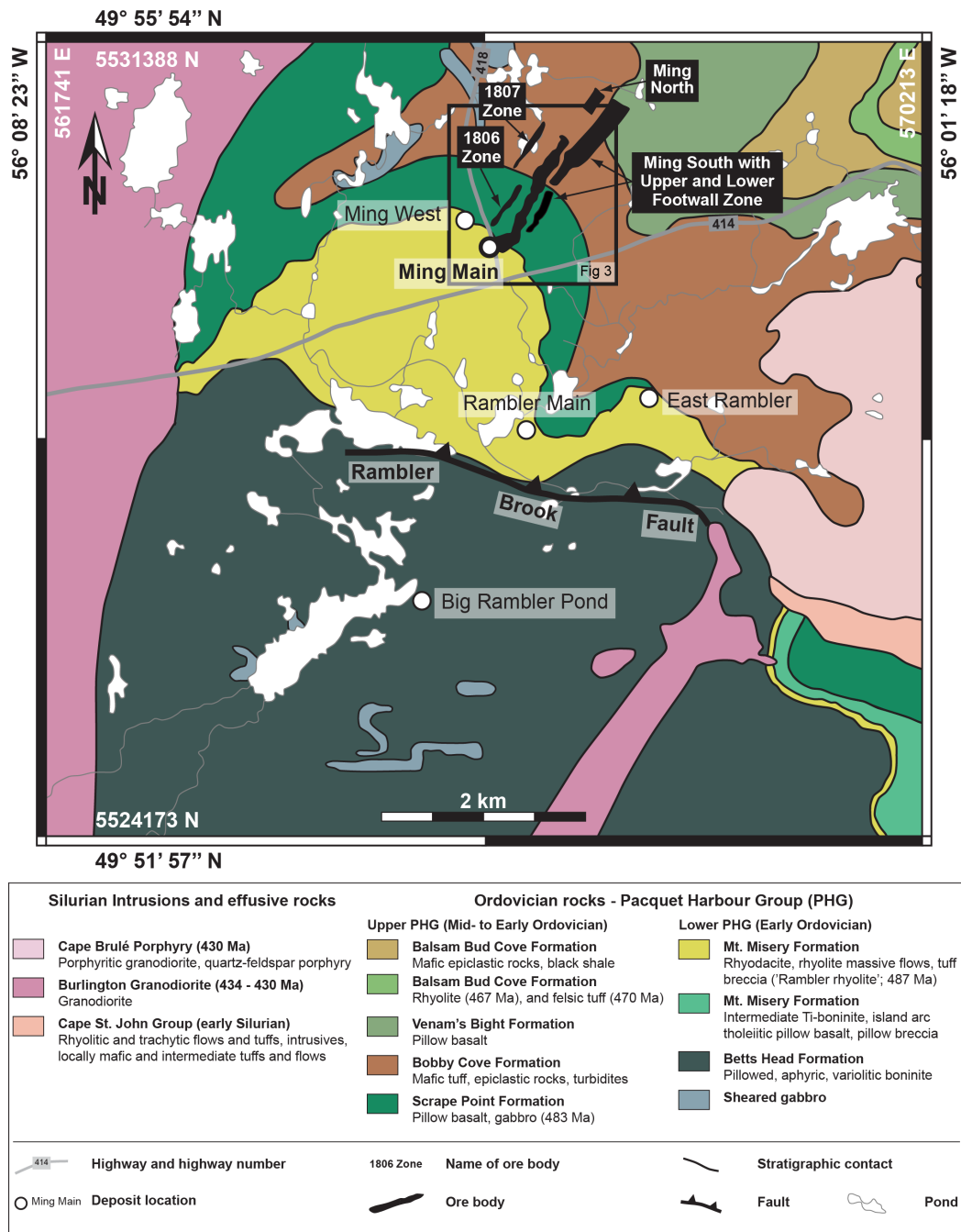
#### *4-2-2 CONSOLIDATED RAMBLER VMS CAMP*

The consolidated Rambler VMS Camp within the lower PHG consists of five VMS deposits (Ming, Ming West, Rambler Main, East Rambler, Big Rambler Pond; Fig. 4-2). The Ming deposit is the only active producer, although previous production of Cu±Au occurred at the other deposits (Tuach and Kennedy, 1978; Pilgrim, 2009). The Ming, Ming West, Rambler Main, and East Rambler deposits are stratabound, bimodal-mafic type, Cu(-Au)-bearing VMS deposits hosted in the Rambler rhyolite and dominated by pyrite–chalcopyrite assemblages with lesser pyrrhotite and sphalerite, and with variable precious metal enrichment (Tuach and Kennedy, 1978; Pilgrim 2009; Brueckner et al., 2014). In contrast, the Big Rambler Pond deposit is a small mafic Cu VMS deposit located south of the Rambler Brook fault within the boninitic Betts Head Formation of the lower PHG

and occurs stratigraphically below the Rambler rhyolite. The deposit shows disseminated and stringer sulfide mineralization of pyrrhotite, chalcopyrite and pyrite (Tuach and Kennedy, 1978).

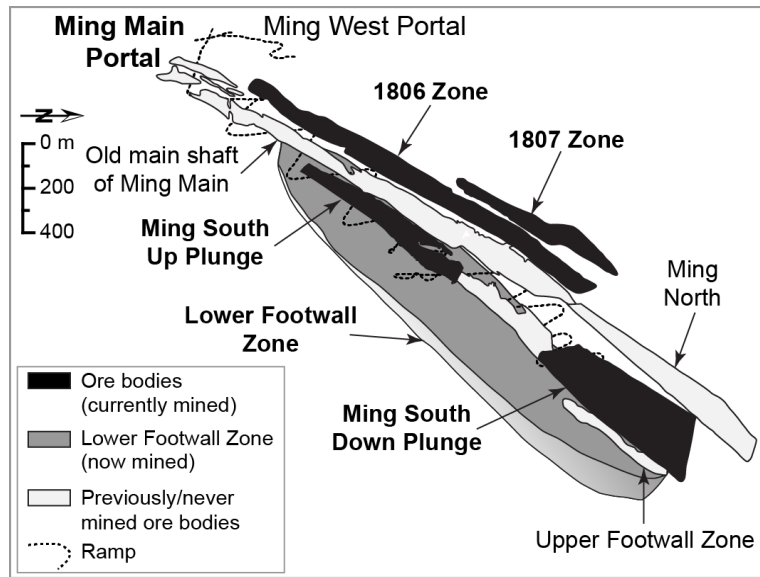
#### *4-2-3 MING MINE*

The Ming deposit is a bimodal-mafic-type Cu-Au VMS deposit and consists of several, lenticular orebodies: 1806 Zone, 1807 Zone, Ming South Up Plunge, Ming South Down Plunge, Ming North, Upper Footwall Zone, and Lower Footwall Zone (Fig. 4-3). The 1806 and 1807 zones, Ming South, and the Upper and Lower Footwall zones run parallel to an old, previously mined portion of the deposit (Ming Main), trending NE with a plunge of 30 – 35°. The Ming North orebody is the extension of the previously mined Ming main orebody (Fig. 4-3). All orebodies are hosted within the Rambler rhyolite, a ca. 2.5 km wide sequence of quartz-phyric rhyodacite, felsic tuff, and tuff breccia of the lower PHG (Skulski et al. 2010). Total (measured, indicated, and inferred) resources for the Ming deposit are 21.9 Mt with grades of 1.49 wt.% Cu, 0.61 g/t Au, 3.21 g/t Ag, and 0.19 wt.% Zn.



**Figure 4-2.** Detailed geologic map of the Pacquet Harbour Group (PHG) hosting the Ming (Main) mine and previously mined volcanogenic massive sulfide deposits (modified after Castonguay et al., 2009). Orebodies of the Ming deposit are highlighted in black. Coordinates are in UTM NAD83, Zone 21N (inside) and WGS 84 (outside)

The different orebodies have similar stratigraphic sequences that are cross-cut by mafic dikes. Styles of mineralization (Fig. 4-4, Table 4-1) are similar in the 1806 Zone, 1807 Zone, and Ming South with concordant to stratabound semi-massive to massive sulfide lenses on the footwall-hanging wall contact and narrow, discordant sulfide stringers immediately below the semi-massive and massive sulfide lenses in the rhyodacitic footwall. Specific for the 1806 Zone is a thin, strongly silicified horizon with discordant sulfide stringers on the footwall-hanging wall contact directly above semi-massive and massive sulfides. The Lower Footwall Zone that occurs beneath Ming South (Fig. 4-3) lacks both a silicified horizon and semi-massive to massive sulfides and is instead entirely made of thin, discordant sulfide stringers. In contrast to the sulfide stringers occurring in the 1806, 1807, and Ming South orebodies, alteration of the rhyodacitic footwall as well as sulfide stringer composition is different in the Lower Footwall Zone. Sulfide stringer composition is chalcopyrite–pyrrhotite±pyrite±cubanite with trace magnetite, sphalerite and Bi-tellurides. Sulfide stringers make up the entire Lower Footwall Zone, therefore the term Lower Footwall Zone is used in this paper synonymously with orebody (accumulation of low-grade to high-grade ore in a well defined shape; Fig. 4-3) and as mineralization style (sulfide mineralization that is similar in ore grade, sulfide abundance, alteration and/or host rock lithology; Fig. 4-4).



**Figure 4-3.** Simplified 3-D view of the different orebodies of the Ming deposit. Of the different orebodies, only the 1806 Zone, 1807 Zone, Ming South (Up and Down Plunge), and the Lower Footwall Zone are currently mined (in bold) and are reported in this paper

The silicified horizon, only present in the 1806 Zone, has discordant pyrite–chalcopyrite±pyrrhotite stringers with minor electrum (Figs. 4-4b, c, 4-5a). In all orebodies with the exception of the Lower Footwall Zone, semi-massive to massive sulfides commonly occur in two spatially proximal horizons, each up to 10 m thick, separated by Rambler rhyolite (Fig. 4-4a, d, e). Mineral assemblages vary between the orebodies with pyrite and chalcopyrite as the dominant sulfide phases (Fig. 4-5b to f; Table 4-1). Within the rhyodacitic footwall, sulfide mineralization occurs as discordant sulfide stringers. However, footwall mineralization is divided depending on the alteration mineralogy, sulfide content, and location (Table 4-1, Fig. 4-4a). Immediately below the massive and semi-

massive sulfides, the rhyodacitic footwall contains up to 30% discordant sulfide stringers and this area is in this paper referred to as sulfide stringer horizon (Fig. 4-4a). This horizon is up to 80m thick. Alteration of the footwall in the sulfide stringer horizon is predominantly quartz-sericite±green mica-sulfide with minor chlorite. The sulfide veinlets show a wide range of sulfide assemblages, but are predominantly of pyrite-chalcopyrite±sphalerite with minor pyrrhotite-arsenopyrite and traces of tennantite-tetrahedrite-galena-Ag-phases (Figs. 4-4f, g, 4-5g, h; Table 4-1). The second type of footwall mineralization is restricted to the Lower Footwall Zone occurring below the Ming South orebodies (Fig. 4-3). The Lower Footwall Zone hosts <20% sulfides and is up to several hundred meters thick (Fig. 4-4a, h, i). Here, discordant stringers are predominantly chalcopyrite-pyrrhotite-pyrite (Fig. 4-5i) often with minor cubanite (Fig. 4-5j) and the alteration assemblage is characterized by intense chlorite-quartz with minor magnetite-sulfide (Fig. 4-4h, i; Table 4-1). The Lower Footwall Zone is very similar to high temperature chlorite alteration in footwall stockwork VMS deposits.



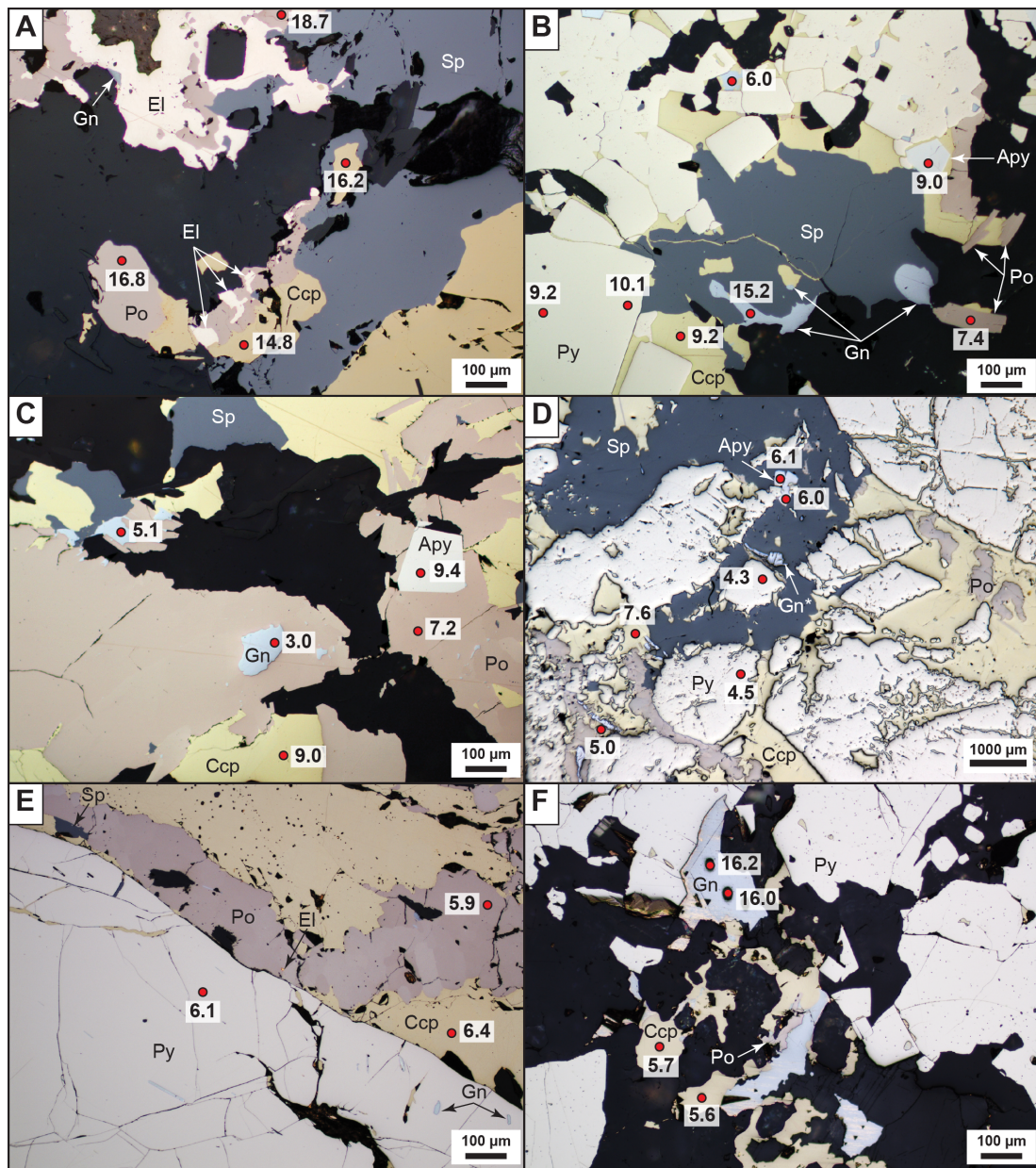
**Figure 4-4.** (previous page) Simplified stratigraphy of the Ming deposit with photographs of the different mineralization styles. **(A)** Stratigraphic section with different mineralization styles at the Ming deposit. Horizontal line on top signifies grain size of lithologies after Fisher (1961). Maximum thickness of mineralization styles is given in brackets. Sulfide mineralization in semi-massive to massive sulfides and sulfide stringer horizon occurs in 1806, 1807, and Ming South orebodies. The silicified horizon is restricted to the 1806 Zone. Sulfide stringers of the Lower Footwall Zone differ from stringers of the sulfide stringer horizon regarding location, alteration of footwall and sulfide mineralogy. However, sulfide stringers of both the sulfide stringer horizon and the Lower Footwall Zone are part of the footwall mineralization. **(B)-(I)** Representative images of the different mineralization styles. **(B)** Silicified horizon: strongly silicified rock or amorphous quartz with discordant pyrite stringers and disseminated chalcopyrite; **(C)** Silicified horizon: strongly silicified rock or amorphous quartz with brecciating pyrite stringer; **(D)** Semi-massive sulfides: remnants of altered Rambler rhyolite with homogeneous pyrite-chalcopyrite sulfides; sulfides have also thin schlieren of sphalerite with galena and tennantite-tetrahedrite; **(E)** Massive sulfide: homogeneous pyrite-chalcopyrite with thin pyrrhotite-sphalerite schlieren; **(F)** Sulfide stringer horizon: quartz eye-bearing Rambler rhyolite with sericite alteration (sericite-quartz) and thick, discordant pyrite-sphalerite stringer; **(G)** Sulfide stringer horizon: Rambler rhyolite with sericite alteration (sericite-quartz) with abundant green mica; thin sulfide stringers of pyrite-sphalerite run parallel to foliation; **(H)** Lower Footwall Zone: Rambler rhyolite with strong chlorite alteration (chlorite-minor quartz), discordant chalcopyrite-pyrrhotite stringer, and disseminated chalcopyrite; **(I)** Lower Footwall Zone: Rambler rhyolite with strong chlorite alteration (chlorite-minor quartz), secondary amphibolite, and discordant chalcopyrite-pyrrhotite; Mineral abbreviations: Amp – amphibole, Ccp – chalcopyrite, Gn – galena, Po – pyrrhotite, Py – pyrite, Sp – sphalerite, Tnt – tennantite, Ttr – tetrahedrite

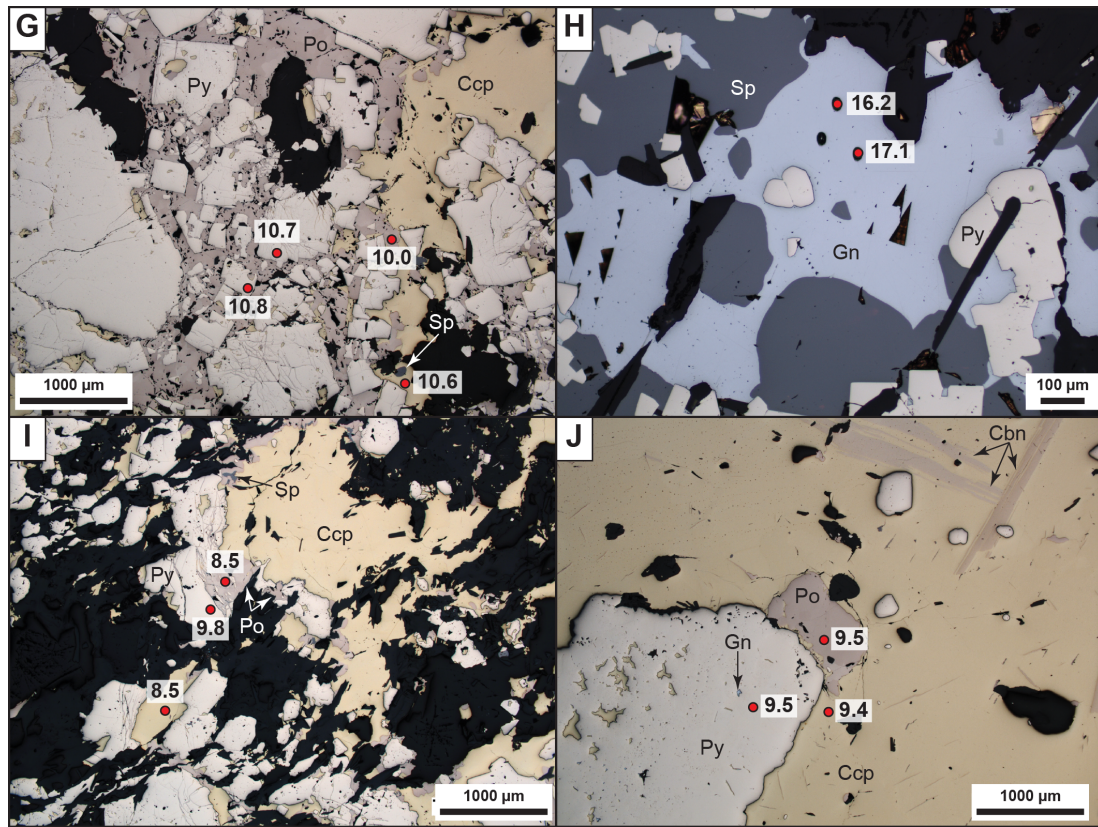


**Table 4-1.** Characteristics of the different mineralization styles at the Ming deposit

Mineralization style	Silicified horizon	Semi-massive to massive sulfides	Footwall mineralization	
			Sulfide stringer horizon	Lower Footwall Zone
<b>Orebody occurrence</b>	1806 Zone only	1806 Zone, 1807 Zone, Ming South		Lower Footwall Zone
<b>Thickness</b>	30–50 cm and locally up to 3 m	Often 2 sulfide lenses with each up to 10 m thick, locally up to 20 m	up to 80 m	Several hundred meters
<b>Alteration mineralogy of Rambler rhyolite</b>	N/A	If present then: Qz–Ser±green mica–Sul with sporadic Chl	Qz–Ser±green mica–Sul with sporadic Chl	Chl–Qz and minor Mag–Sul
<b>Type of sulfide mineralization</b>	Discordant stringers	Concordant to stratabound semi-massive and massive sulfides	Discordant stringers	Discordant stringers
<b>Sulfide mineralogy</b>	Py–Ccp with minor Po–Apy and traces of El–Tnt–Ttr	Py–Ccp±Sp with minor Apy–Po–Gn and traces of sulfosalts, tellurides and precious metals	Py–Ccp±Sp with minor Po–Apy and traces of Tnt–Ttr–Gn and Ag-phases	Ccp–Po±Py with minor Cbn

**Mineral abbreviations:** Apy – arsenopyrite, Ccp – chalcopyrite, Chl – chlorite, Cbn – cubanite, Bt – biotite, El – electrum, Gn – galena, Mag – magnetite, Po – pyrrhotite, Py – pyrite, Qz – quartz, Ser – sericite, Sp – sphalerite, Sul – sulfide(s), Tnt–Ttr – tennantite-tetrahedrite





**Figure 4-5.** Typical sulfide mineral assemblages and textures from the different mineralization styles of the Ming deposit. **(A)** Silicified horizon: pyrrhotite with electrum and marginal galena occurring adjacent to sphalerite or chalcopyrite; **(B)** Semi-massive sulfide: recrystallized pyrite with interstitial galena in chalcopyrite; pyrrhotite, arsenopyrite, and sphalerite with marginal galena also occurring in chalcopyrite; **(C)** Semi-massive sulfide: pyrrhotite with inclusions of arsenopyrite and galena, and marginal galena-sphalerite in chalcopyrite; **(D)** Massive sulfide: Coarse-grained, recrystallized pyrite in chalcopyrite with interstitial galena and surrounded by sphalerite or pyrrhotite; sphalerite with weak chalcopyrite disease and inclusions of arsenopyrite and galena with Bi-telluride lamellae; pyrrhotite surrounding recrystallized pyrite has inclusions of galena with Bi-telluride lamellae; **(E)** Massive sulfide: Coarse-grained, recrystallized pyrite in chalcopyrite and surrounded by pyrrhotite has inclusions of galena and fine fractures that are partly filled with chalcopyrite or pyrrhotite; pyrrhotite surrounding recrystallized

pyrite has small inclusion of electrum and marginal sphalerite; **(F)** Massive sulfide: Recrystallized pyrite with marginal galena in contact to gangue; disseminated chalcopyrite with pyrrhotite-galena in gangue; **(G)** Sulfide stringer horizon: Recrystallized pyrite is partly replaced by pyrrhotite; chalcopyrite with recrystallized pyrite-pyrrhotite-sphalerite; **(H)** Sulfide stringer horizon: sphalerite-galena schlieren with recrystallized pyrite; **(I)** Lower Footwall Zone: recrystallized pyrite on chalcopyrite margins is partly replaced by pyrrhotite; sphalerite occurs partly on pyrrhotite margins; **(J)** Lower Footwall Zone: chalcopyrite with cubanite exsolution lamellae, pyrite and pyrrhotite; Red circles with numbers represent data points of SIMS analysis and  $\delta^{34}\text{S}$  value, respectively; Mineral abbreviations: Apy – arsenopyrite, Cbn – cubanite, Ccp – chalcopyrite, El – electrum, Gn – galena, Gn\* – galena with Bi-telluride exsolution lamellae, Po – pyrrhotite, Py – pyrite, Sp – sphalerite

#### **4-3 SULFIDE MINERALOGY**

The sulfide mineralogy of the Ming deposit is complex and includes over 17 sulfide and precious metal phases (Brueckner et al., 2014). Pyrite and chalcopyrite are the major sulfide minerals, whereas sphalerite, pyrrhotite and galena are common minor components. Cubanite is observed as trace phase in the 1807 Zone, Ming South orebodies, and Lower Footwall Zone; however, cubanite is completely absent in the 1806 Zone. Additionally, a variety of trace minerals such as arsenopyrite, various sulfosalts (tennantite-tetrahedrite, meneghinite, stannite, loellingite), tellurides (tsumoite, hessite, altaite) and precious metal phases (electrum, miargyrite, pyrargyrite, stephanite) are present at the Ming deposit (Table 4-1).



The semi-massive to massive sulfide horizons of the various orebodies show a complex ore assemblage that varies between the different orebodies (Table 4-1). In particular, the abundance of trace sulfosalts, tellurides and precious metals varies. The 1806 Zone is the richest in gold amongst all orebodies with 2.83 g/t Au. Gold occurs predominantly as electrum and to a much lesser extent in AgHgAu alloys. Silver occurs predominantly in Ag-enriched tetrahedrite, alloys of AgHg±Au, AgSbS phases, and electrum (Brueckner et al., 2014). In the 1806 Zone, electrum occurs typically with chalcopyrite, pyrite, arsenopyrite, sulfosalts and Ag-phases. The 1807 and Ming South orebodies have higher amounts of tellurides that commonly occur texturally proximal to galena; tennantite-tetrahedrite is rare and Ag occurs predominantly as hessite (AgTe). Electrum is also less abundant in these orebodies compared to the 1806 Zone, where electrum is associated with chalcopyrite, pyrite, arsenopyrite and tellurides.

Sulfide assemblages in the silicified horizon, the sulfide stringer horizon and the Lower Footwall Zone are less complex and dominated by pyrite and chalcopyrite with minor pyrrhotite (Fig. 4-4g to j). Abundances of sphalerite, galena, arsenopyrite, cubanite, sulfosalts, tellurides and precious metals are highly variable (Brueckner et al., unpublished data). Precious metal assemblages are typically associated with chalcopyrite, arsenopyrite, and/or tellurides, but are rare compared to the semi-massive to massive sulfide lenses.

The sulfides are texturally homogenous and no distinct differences are observed between the different mineralization styles or the orebodies. Common sulfide mineral textures at the Ming deposit include replacement textures (chalcopyrite disease in sphalerite; pyrrhotite replacing pyrite; Fig. 4-4h, i) and metamorphic/deformation textures (recrystallization of pyrite, porphyroblasts of pyrite and arsenopyrite; cataclastic texture pyrite; Fig. 4-4, Table 4-2).

#### **4-4 SULFUR ISOTOPE GEOCHEMISTRY**

##### **4-4-1 METHODOLOGY**

Thirty-nine samples from the five orebodies (1806 Zone, 1807 Zone, Ming South Up Plunge and Down Plunge, Lower Footwall Zone) and representing all mineralization styles (silicified horizon, semi-massive to massive sulfides, footwall mineralization) were selected for sulfur isotope analysis. The most samples come from the 1806 Zone (n=15), because the sulfide mineralogy is the most complex of all orebodies. Seven samples each were analyzed from the 1807 Zone and Ming South Up Plunge. Four samples from Ming South Down Plunge and six samples from the Lower Footwall Zone were used for sulfur isotope analysis. Amongst the mineralization styles, the semi-massive to massive sulfides had the highest number of samples (n=23) due to the wide variations in ore mineral assemblages between the orebodies. Two to three grains of each phase were usually analyzed for  $\delta^{34}\text{S}$  in each sample to observe possible variations in the

isotope composition. The grains were chosen depending on mineral assemblage, size, and texture. In total, 338  $\delta^{34}\text{S}$  spot analyses were obtained from the 39 samples on five different minerals (pyrite: n=102; chalcopyrite: n=98; pyrrhotite: n=52; arsenopyrite: n=47, and galena: n=39). Besides samples from the different mineralization styles, one Fe oxide sample on the footwall–hanging wall contact, and a sample from a mineralized quartz vein within a mafic dyke were also analyzed to investigate possible differences in sulfur isotope signature of pyrite, chalcopyrite, and pyrrhotite in these different host lithologies.

Samples were mounted in polished epoxy sections and coated with 300Å of Au, to mitigate charging under primary ion bombardment. All analyses were performed using the Cameca IMS 4f Secondary Ion Mass Spectrometer (SIMS) at the MAF-IIC Microanalysis Facility of Memorial University and the described methodology is modified after Toman (2012) and found in Appendix A4-1. For each sample, determinations of  $\delta^{34}\text{S}$  were performed on multiple grains of pyrite, chalcopyrite, pyrrhotite, arsenopyrite and galena by bombarding the sample with a primary ion microbeam of 350–1,150pA of  $\text{Cs}^+$ , accelerated by a 10keV potential, and focused into a 5–15 $\mu\text{m}$  diameter spot. The  $\text{Cs}^+$  current depended on the analyzed sulfide phase, the size of the analyzed phase, and the matrix surrounding the analyzed grain (sulfides or non-sulfide gangue). To prevent contamination in the polished surface, each spot was first pre-sputtered for 120s with a 25 $\mu\text{m}$  square raster. Depending on the minimum diameter of the critically focused analysis, to improve the homogeneity of primary ion delivery, while

maintaining lateral resolution at better than 20 $\mu$ m. Negatively charged sputtered secondary ions were accelerated into the mass spectrometer using a potential of 4.5keV.



**Table 4-2.** Summary of abundance and textures for pyrite, chalcopyrite, pyrrhotite, arsenopyrite, and galena in the different mineralization styles of the Ming deposit

Analyzed sulfide phase	Silicified horizon	Semi-massive to massive sulfides	Sulfide stringer horizon	Footwall mineralization
<b>Pyrite</b>	<ul style="list-style-type: none"><li>Major mineral phase</li><li>Small-sized to medium-sized</li><li>Subhedral to anhedral</li><li>As single disseminated crystals in Ccp, Po, or gangue or in small groups</li><li>Recrystallized (weakly convex/concave grain boundaries, triple junctions, annealed texture when in small groups)</li><li>Inclusions rare</li></ul>	<ul style="list-style-type: none"><li>Major mineral phase</li><li>Small-sized to coarse (almost porphyroblastic)</li><li>Euhedral (cubic, polygonal) to anhedral</li><li>As single, recrystallized crystals or in groups preferably in Ccp and too lesser extent in Sp±Gn bands/schlieren</li><li>Annealed texture very common with small interstitials of Ccp, Sp, Gn, and/or Po</li><li>In annealed textures partly Apy intergrown with Py</li><li>Recrystallized (weakly convex/concave grain boundaries, triple junctions, annealed texture, brittle deformation)</li><li>Inclusions (Ccp, Po, Gn, Sp) and fine cracks common especially in coarser grains</li></ul>		<ul style="list-style-type: none"><li>Trace to minor mineral phase</li><li>Small-sized to coarse-grained</li><li>Euhedral (cubic, polygonal) to anhedral</li><li>Often as single grains in Ccp</li><li>Often replaced by Po</li><li>Inclusions in coarser grains common (gangue, Po)</li><li>Recrystallized (porphyroblasts)</li></ul>
<b>Chalcopyrite</b>	<ul style="list-style-type: none"><li>Major to minor mineral phase</li><li>Anhedral</li><li>Coarse anhedral mass or rarer as disseminated small anhedral flakes</li><li>Often 'hosting' all other sulfide phases or as small interstices between annealed Py</li><li>When in EI-bearing sample, than often adjacent to EI</li></ul>			<ul style="list-style-type: none"><li>Major mineral phase</li><li>Anhedral</li><li>Coarse anhedral mass or rarer as disseminated small anhedral flakes</li><li>Often 'hosting' all other sulfide phases or as small interstices between annealed Py</li><li>Cbn exsolution lamellae in Ccp common</li></ul>

**Table 4-2. (cont.)**

Analyzed sulfide phase	Silicified horizon	Semi-massive to massive sulfides	Sulfide stringer horizon	Footwall mineralization
<b>Pyrrhotite</b>	<ul style="list-style-type: none"> <li>Minor to trace mineral phase</li> <li>Small-sized to coarse-grained</li> <li>Anhedral</li> <li>Often on Ccp margins</li> <li>Coarser grains usually with Sp and Py inclusions</li> <li>When in EL-bearing sample, than often adjacent to EI</li> </ul>	<ul style="list-style-type: none"> <li>Minor to trace mineral phase</li> <li>Small to coarse</li> <li>Anhedral</li> <li>Often on Ccp margins or as coarse bands with Py, Sp <math>\pm</math> Gn inclusions in Ccp</li> <li>Coarser grains usually with Sp, Py and partly Gn inclusions</li> </ul>	<ul style="list-style-type: none"> <li>Trace mineral phase</li> <li>Small to medium-sized</li> <li>Euhedral (cubic, polygonal) to subhedral</li> <li>Recrystallized</li> <li>Often as single grains or twins in chalcopyrite and rarer in gangue</li> <li>Partly intergrown with Py or in myrmekite with Ccp, Tnt-Ttr, Sp <math>\pm</math> EI</li> </ul>	<ul style="list-style-type: none"> <li>Minor to major mineral phase</li> <li>Small-sized to coarse-grained</li> <li>In Ccp partly overprinting Cbn exsolution lamellae</li> <li>Often replacing Py</li> <li>Usually inclusion free</li> </ul>
<b>Arsenopyrite</b>	<ul style="list-style-type: none"> <li>Trace mineral phase</li> <li>Small-grained to medium-sized</li> <li>Euhedral (polygonal)</li> <li>Recrystallized</li> <li>Often as single grains or twins in chalcopyrite and rarer in gangue</li> </ul>	<ul style="list-style-type: none"> <li>Minor to trace mineral phase</li> <li>Small to medium-sized</li> <li>Euhedral (cubic, polygonal) to subhedral</li> <li>Recrystallized</li> <li>Often as single grains or twins in chalcopyrite and rarer in gangue</li> <li>Partly intergrown with Py or in myrmekite with Ccp, Tnt-Ttr, Sp <math>\pm</math> EI</li> </ul>	<ul style="list-style-type: none"> <li>Trace mineral phase</li> <li>Small to medium-sized</li> <li>Euhedral (cubic, polygonal)</li> <li>Recrystallized</li> <li>Often as single grains or twins in chalcopyrite and rarer in gangue</li> </ul>	<ul style="list-style-type: none"> <li>Almost completely absent</li> <li>Small-grained</li> <li>Euhedral (polygonal)</li> <li>In Ccp</li> <li>Recrystallized</li> </ul>
<b>Galena</b>	<ul style="list-style-type: none"> <li>Almost completely absent</li> <li>Very small</li> <li>Anhedral (sub-roundish)</li> <li>Interstitial between annealed Py</li> </ul>	<ul style="list-style-type: none"> <li>Trace to minor mineral phase</li> <li>Small to medium-sized</li> <li>Anhedral (amoeboid)</li> <li>Most commonly as small anhedral grains in anhedral Ccp mass, between annealed Py or with BiTe lamellae on Po</li> <li>Rarer as medium-sized grains in Sp</li> </ul>	<ul style="list-style-type: none"> <li>Trace mineral phase</li> <li>Very small</li> <li>Anhedral (sub-roundish)</li> <li>Interstitial between annealed Py</li> <li>As inclusions in Py</li> </ul>	<ul style="list-style-type: none"> <li>Almost completely absent</li> <li>Very small</li> <li>Anhedral (sub-roundish)</li> <li>Usually as inclusion in Py</li> </ul>

**Mineral abbreviations:** Apy – arsenopyrite, Cbn – cubanite, Ccp – chalcopyrite, El – electrum, Gn – galena, Po – pyrrhotite, Py – pyrite, Sp – sphalerite, Tnt-Ttr – tennantite-tetrahedrite

The instrument was operated with a medium Contrast Aperture (150 $\mu$ m), and Entrance and Exit Slits paired to give flat-topped peaks at a mass resolving power (MRP) of 2,975 (10% peak height definition) - sufficient to discriminate  $^{33}\text{SH}^-$  (and  $^{32}\text{SH}_2^-$ ) from  $^{34}\text{S}^-$ .

Overall reproducibility, based on replicate standard analyses, is typically better than  $\pm 0.5\text{‰}$  ( $1\sigma$ ). Results for the used sulfide in-house standards, their measured  $^{34}\text{S}/^{32}\text{S}$  ratio and the calculated instrument mass fractionation (IMF) factors are summarized in Appendices A4-2 and A4-3.

#### *4-4-2 RESULTS*

Results for all five analyzed mineral phases are shown in Figures 4-6 and 4-7 and are given in Appendix A4-4. For the deposit, most of the data range between +2 and +13 $\text{‰}$  with a few exceptions (Fig. 4-6). Galena has the widest range amongst all analyzed sulfide phases ( $\delta^{34}\text{S} = +0.8$  to +17.3 $\text{‰}$ ).

##### *4-4-2-1 Silicified horizon of the 1806 Zone*

Sulfides in the silicified horizon from the 1806 orebody show the widest range of sulfur isotope values amongst all mineralized zones. In general,  $\delta^{34}\text{S}$  ranges between 5.8 and 19.6 $\text{‰}$  (Fig. 4-6). Pyrrhotite displays the highest values of  $\delta^{34}\text{S}$  amongst all measured sulfides, ranging between 13.9 and 19.6 $\text{‰}$  with a mean of  $17.2 \pm 2.2\text{‰}$  ( $n=5$ ). The sulfur isotope signature for pyrite ranges between 5.8 and 17.6 $\text{‰}$  with a mean of  $11.2 \pm 4.4\text{‰}$  ( $n=8$ ). Chalcopyrite shows similar  $\delta^{34}\text{S}$

values to pyrite, ranging between 9.6-16.2‰ with a mean of  $13.1 \pm 2.9$ ‰ (n=9). Sulfur isotope data for arsenopyrite have a limited variation between 6.9 and 11.5‰ and a mean of  $9.3 \pm 1.7$ ‰ (n=5). The occurrence of galena within the silicified horizon is very limited with only one data point with  $\delta^{34}\text{S}$  of 9.4‰.

#### *4-4-2-2 Semi-massive to massive sulfides*

Most data (n=232) were obtained from this mineralized horizon. The sulfur isotope composition of semi-massive to massive sulfides is homogenous between the different orebodies despite variations in the sulfide mineral assemblages (Table 4-1). The majority of data clusters between +2 and +11‰ and the mean  $\delta^{34}\text{S}$  value for each sulfide phase is relatively lower than those in the silicified horizon and in the footwall (Figs. 4-6, 4-7). The sulfur isotope signature is uniform for pyrite (mean:  $7.4 \pm 1.5$ ‰, n=69), chalcopyrite (mean:  $7.5 \pm 1.5$ ‰, n=59), pyrrhotite (mean:  $6.3 \pm 1.6$ ‰, n=30), and arsenopyrite (mean:  $7.2 \pm 1.4$ ‰, n=39; Figs. 4-5b to f, 4-6, and 4-7). In contrast, galena has heterogeneous  $\delta^{34}\text{S}$  values ranging between 0.8 and 17.3‰ and a mean of  $6.1 \pm 4.5$ ‰ (n=35). These variations in the sulfur isotopic composition may be related to paragenetic occurrence, as galena has been deposited in different stages during syngenetic metal deposition (Brueckner et al. 2014). The analyzed galena grains are from inclusions in pyrite, in-between groups of annealed pyrite, and on margins of pyrite, arsenopyrite, or sphalerite. However, there is no relationship between textural occurrence and sulfur isotope composition (Fig. 4-5b, c, and f).

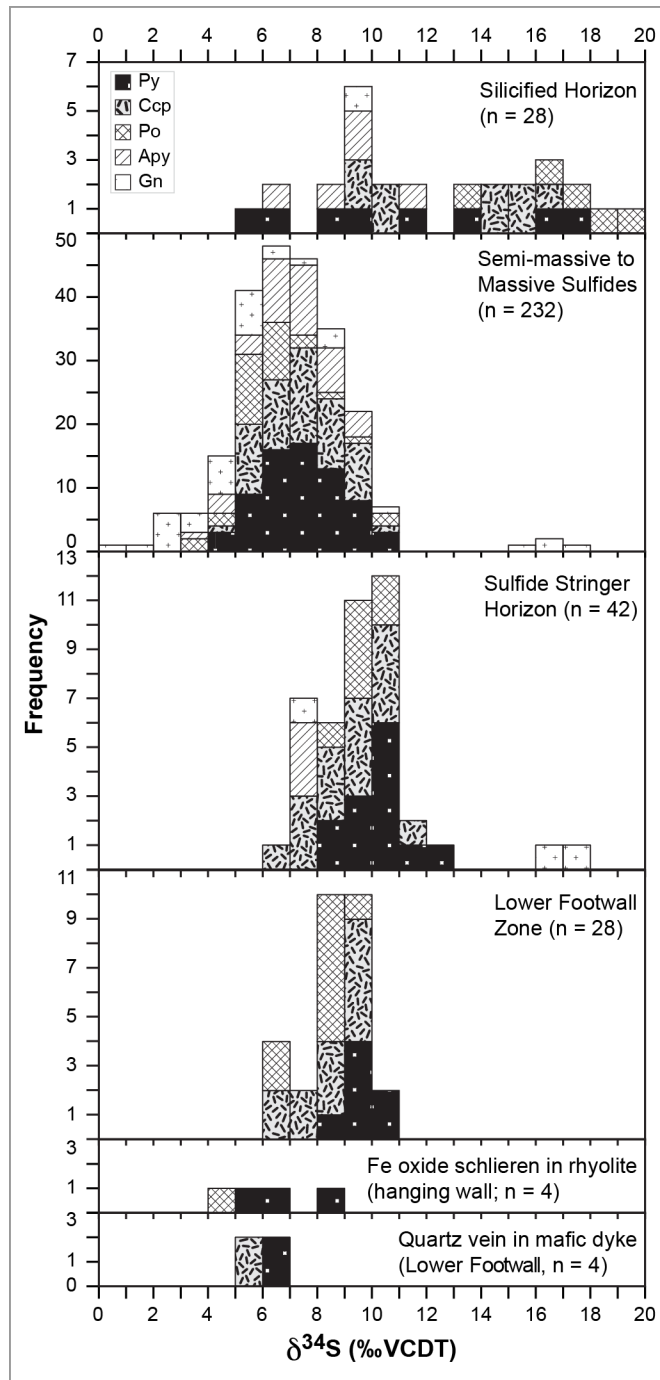
#### *4-4-2-3 Footwall Mineralization*

Forty-two sulfur isotope compositions of pyrite (n=13), chalcopyrite (n=16), and pyrrhotite (n=7) from the sulfide stringer horizon and the Lower Footwall Zone are almost identical to each other and, in general, have slightly higher values than data from the semi-massive to massive sulfides (Figs. 4-6, 4-7). All but two data points from the sulfide stringers range between 6 and 13‰. The mean  $\delta^{34}\text{S}$  value for chalcopyrite is  $9.1 \pm 1.4$ ‰ with a range of 6.4 to 11.2‰. Pyrite has a mean  $\delta^{34}\text{S}$  value of  $10.3 \pm 1.0$ ‰ with a range of 8.4 to 12.0‰ and pyrrhotite has a mean  $\delta^{34}\text{S}$  value of  $9.7 \pm 0.5$ ‰ with a range between 8.8 and 10.4‰. Arsenopyrite data were only obtained from one sample collected from the 1806 orebody. The three arsenopyrite values are homogeneous with a mean of  $7.5 \pm 0.3$ ‰, and isotopically these values are lower than those of chalcopyrite, pyrite and pyrrhotite. Galena is a trace phase within the stringer sulfides and data are from three points in two samples from the 1806 Zone and the Ming South Down Plunge orebody. Similar to the semi-massive and massive sulfides,  $\delta^{34}\text{S}$  values are heterogeneous (7.6‰, 16.2‰ and 17.1‰). In contrast to the semi-massive and massive sulfides, there is a relationship between texture and  $\delta^{34}\text{S}$ . The isotopically heavier signatures are from galena grains associated with coarse-grained sphalerite (Fig. 4-5h), whereas the low  $\delta^{34}\text{S}$  value is from a single galena grain within chalcopyrite.

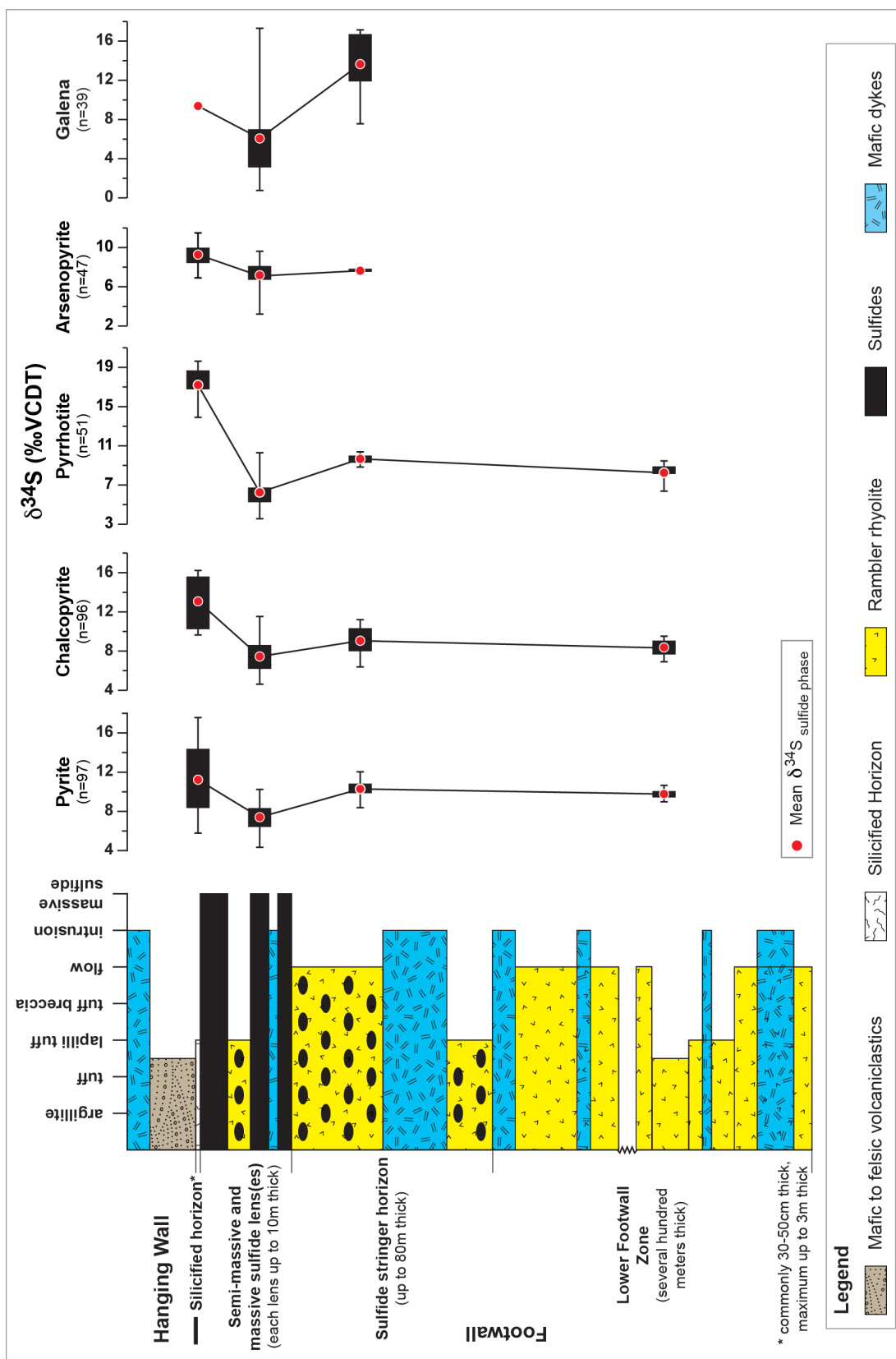
The  $\delta^{34}\text{S}$  values from the Lower Footwall Zone were obtained only from pyrite, chalcopyrite, and pyrrhotite. These  $\delta^{34}\text{S}$  values are similar to S isotope

signatures in the sulfide stringer horizon. The mean  $\delta^{34}\text{S}$  values for pyrite, chalcopyrite, and pyrrhotite are  $9.8 \pm 0.6\text{‰}$  (n=7),  $8.4 \pm 1.0\text{‰}$  (n=12), and  $8.3 \pm 1.1\text{‰}$  (n=9), respectively (Fig. 4-5i, j).

In addition to the different sulfide mineralization styles, the sulfur isotope signature of sulfides in a Fe oxide-bearing sample and a mineralized quartz vein were measured (Fig. 4-6, Appendix A4-4). The Fe oxide-bearing sample (62133) is from the Ming South Up Plunge orebody within the Rambler rhyolite with magnetite schlieren and traces of pyrite, pyrrhotite, chalcopyrite, and sphalerite. Pyrite analyses yielded three values ranging between 5.9 and 8.3‰. One pyrrhotite grain yielded a slightly lower value than pyrite with  $\delta^{34}\text{S}$  of 4.6‰. The quartz vein (36113) is within a mafic dyke in the Lower Footwall Zone and contains chalcopyrite-pyrite mineralization with traces of sphalerite. The mean  $\delta^{34}\text{S}$  values from pyrite and chalcopyrite are similar with  $6.3 \pm 0.4\text{‰}$  (pyrite, n=2) and  $5.7 \pm 0.1\text{‰}$  (chalcopyrite, n=2). The sulfur isotope data obtained from the Fe oxide-bearing sample and the quartz vein are similar to pyrite, chalcopyrite and pyrrhotite data from the semi-massive to massive sulfides (Fig. 4-6, Appendix A4-4).



**Figure 4-6.** Histogram of  $\delta^{34}\text{S}$  values of sulfides from the different mineralization styles, a sample of Fe oxide schlieren in Rambler rhyolite on top of massive sulfide, and a sample of mineralized quartz vein within a mafic dyke of the Lower Footwall Zone of the Ming deposit; n = number of analyzed data points





**Figure 4-7.** (previous page) Box-Whisker plot showing the variations in  $\delta^{34}\text{S}$  values of sulfides from the different mineralization styles of the Ming deposit. The horizontal error bars represent the total range of all spot analyses for each ore zone during the multiple analytical sessions. The horizontal dimension of the box represents the  $1\sigma$  for all spot analyses during multiple analyses; n = number of analyzed data points

## **4-5 DISCUSSION**

### **4-5-1 ISOTOPIC EQUILIBRIUM**

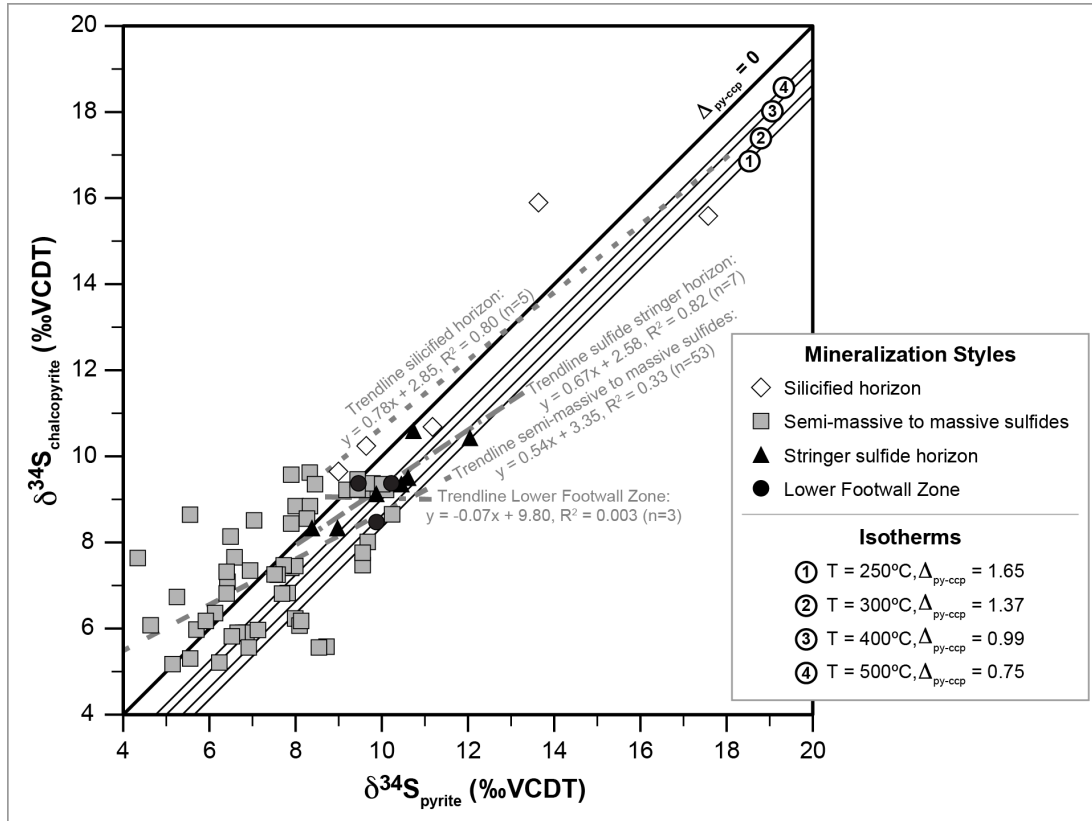
Two hundred and three mineral pairs of pyrite-chalcopyrite, pyrite-pyrrhotite, pyrrhotite-chalcopyrite, pyrite-galena, pyrrhotite-galena, and chalcopyrite-galena were tested for sulfur isotope equilibrium. Both minerals in each pair were proximal or adjacent to one another in thin section and encased by sulfide phases. The sulfur isotope fractionation factors used are those of Kajiwara and Krouse (1971). Arsenopyrite was not included because of a lack of reliable fractionation values within the temperature range of 250-500°C that affected the Ming deposit during metal deposition in the early Ordovician and during upper greenschist/lower amphibolite facies metamorphism in the Silurian-Devonian (Tuach and Kennedy, 1978; Brueckner et al., 2014).

Neighbouring mineral pairs were plotted in  $\delta$ - $\delta$  plots (Fig. 4-8; Appendix A4-5) to test if neighbouring sulfides were in isotopic equilibrium either during early Ordovician deposition or later Silurian-Devonian metamorphism. These plots are described in detail by Gregory and Criss (1986) and Gregory et al.

(1989). The purpose of these plots is to identify if neighbouring mineral pairs plot along or parallel to isotherms that would indicate isotopic equilibrium and give temperature of isotopic equilibration or if mineral pairs plot in arrays oblique to isotherms that would indicate isotopic disequilibrium. Isotherms in  $\delta$ - $\delta$  plots are a linear function of the  $\delta^{34}\text{S}$  values of the two neighbouring mineral pairs with a slope of +1 and an interception with the y-axis of  $-\delta_{1-2}$ , which is the difference in isotopic composition between mineral phases 1 and 2.

In Figure 4-8, neighbouring pyrite-chalcopyrite mineral pairs from all mineralization styles are plotted. Isotherms for temperatures of 250-500°C are given. This temperature range covers both VMS-forming temperatures of the Ming deposit ( $\approx 250$ -350°C; Brueckner et al., 2014) and upper greenschist/lower amphibolite facies conditions ( $\approx 350$ -500°C) that affected the deposit in the Silurian-Devonian (Tuach and Kennedy, 1978). Pyrite and chalcopyrite were broadly deposited at similar stages during the formation of the Ming deposit (Brueckner et al., 2014), and show arrays that plot oblique to the isotherms (Fig. 4-8). Some of the mineral pairs plot above the  $\delta_{\text{pyrite-chalcopyrite}} = 0$  line, and these mineral pairs would have reverse polarity of fractionation, which is not observed in natural sulfur isotope systems. These features argue that neighbouring pyrite-chalcopyrite mineral pairs reflect isotopic disequilibrium. The other five mineral pairs show similar results (Appendix A4-5). Therefore, isotopic equilibrium for the sulfides at the Ming deposit was not attained during metal deposition in the early

Ordovician or by isotopic re-equilibration during Silurian-Devonian metamorphism.



**Figure 4-8.**  $\delta$ - $\delta$  plot for neighbouring pyrite-chalcopyrite mineral pairs. Neighbouring pyrite-chalcopyrite mineral pairs plot in arrays oblique to isotherms of 250-500°C or above the thick black line indicating zero fractionation between pyrite and chalcopyrite ( $\delta_{py-ccp} = 0$ ). Mineral pairs above this line would have reverse polarity of fractionation, which is not observed in natural systems. Isotherms were calculated for temperatures of 250°C-500°C. Isotherms are a linear function ( $y=mx+n$ ) of the  $\delta^{34}\text{S}$  values of the two neighbouring mineral pairs; slope  $m$  is  $+1$  and intersection  $n$  with the  $y$ -axis is  $-\delta_{1-2}$ , because

$$\delta_1 - \delta_2 = \Delta_{1-2} \approx \frac{A \times 10^6}{T^2} \quad \text{and therefore} \quad \delta_2 = \delta_1 - \Delta_{1-2} \quad (\text{Ohmoto and Goldhaber, 1997}); T$$

is temperature in Kelvin;  $\delta_1$  and  $\delta_2$  is the measured  $\delta^{34}\text{S}$  value of mineral phases 1 and 2, respectively;  $\delta_{1-2}$  is the difference in isotopic sulfur composition between mineral phases 1 and 2 or the isotopic fractionation between the two minerals; and A is a constant ( $A=0.45$  for pyrite-chalcopyrite; Kajiwara and Krouse, 1971).

These results are in accordance with other studies on (metamorphosed) hydrothermal systems that showed: (1) that isotopic equilibrium between two, broadly coevally deposited phases is often prevented especially when the hydrothermal, metal-transporting and reduced sulfur bearing fluids mix with other fluids (cold seawater, magmatic fluid) of different composition (different  $m_{\text{H}_2\text{S}}/m_{\Sigma\text{Metals}}$  ratio,  $f\text{O}_2$ ,  $f\text{S}_2$ ) and/or temperature (Ohmoto and Goldhaber, 1997); and (2) that isotopic re-equilibration during metamorphism is a function of grain size, temperature, amount of fluid and if the neighbouring minerals are in direct contact to each other or not (Crowe, 1994; Ohmoto and Goldhaber, 1997). For the mineral pairs at the Ming deposit, the metamorphic temperature of upper greenschist/lower amphibolite facies was likely too low to attain isotopic re-equilibration during the Silurian-Devonian, because analyzed sulfides are relatively small and completely surrounded by other sulfide phases (Crowe, 1994).

#### 4-5-2 SULFUR SOURCES

Sulfur isotope fractionation between mineral phases, aqueous species or organisms is common and widely observed in seafloor hydrothermal systems

(Shanks et al., 1995; Ohmoto and Goldhaber, 1997; Shanks, 2001; Seal, 2006). In VMS deposits and their modern seafloor equivalents, three main sources of sulfur are common: (1) seawater sulfate with  $\delta^{34}\text{S} \approx 4\text{-}33\text{‰}$  (Claypool et al., 1980; Kampschulte and Strauss, 2004, Paytan and Grey, 2012) that is present in sulfate minerals or is reduced by thermochemical processes; (2) sulfur leached from igneous footwall rocks and/or direct contributions from magmatic fluids with  $\delta^{34}\text{S} \approx -5$  to  $+5\text{‰}$  (averaging  $0\text{‰}$ ); and (3) sulfur from microbial activity in reduced sediments via bacterial sulfate reduction (BSR), with  $\delta^{34}\text{S} \approx -50$  to  $+20\text{‰}$  (Shanks et al., 1995; Goodfellow and Peter, 1996; Ohmoto and Goldhaber, 1997; Gemmell and Sharpe, 1998; Canfield, 2001; Shanks, 2001; Seal, 2006; Hoefs, 2009).

In this section, an attempt to quantify the source(s) of sulfur at the Ming deposit by mass balance modelling is made. There are uncertainties when modelling the sulfur sources in the Ming deposit, including: (1) isotopic fractionation in a partly open vs fully open system; (2) possible evidence for bacterial activity; (3) temperature range at which seawater sulfate reduction took place; (4) range in  $\delta^{34}\text{S}$  of seawater sulfate at time of formation of the deposit; and (5) range in sulfur isotopic composition of igneous wall rock and magmatic fluid. The uncertainties and the assumptions used in the modelling are outlined below. The modelling results are compared to reported literature data to put these results for the Ming deposit in a broader context to other VMS deposits worldwide.

Evolving hydrothermal systems can be seen as fully open, because there is: (1) a constant seawater ( $\pm$ magmatic fluid/volatile) input (Herzig and Hannington, 1995; Seal, 2006); (2) the water/rock ratio changes proximal and distal to the evolving sulfide mound resulting in different alteration assemblages within the wall rock (Seyfried and Bischoff, 1981); and (3) physico-chemical parameters ( $T$ ,  $pH$ ,  $fO_2$ ,  $fS_2$ ,  $a_{S_2}$ ) of the hydrothermal fluids change based on the location within the system (proximal/distal to the heat source, the stock work zone or vents; Lydon, 1988; Ohmoto, 1996). Stratigraphy, alteration and sulfide mineral assemblage show that the criteria for a fully open system existed at the Ming deposit during its formation, because: (1) constant seawater input and the addition of magmatic volatiles/fluids to the hydrothermal fluids resulted in a complex sulfide and precious metal assemblage (Brueckner et al., 2014); (2) changes in the water/rock ratio proximal and distal to the massive sulfides due to changes in the porosity of the Rambler rhyolite resulted in different proximal and distal alteration assemblages (Fig. 4-4, Table 4-1; Pilote et al., 2014); and (3) changing physico-chemical parameters of the hydrothermal fluids due to interaction with the footwall and location relative to the hydrothermal heat source resulted in varying distributions of uncommon metal sulfides (tellurides, nisbite, breithauptite), sulfosalts (tennantite-tetrahedrite, stannite, meneghinite), and precious metals (electrum,  $AgHg\pm Au$  alloy) between the different mineralization styles and orebodies (Brueckner et al. unpubl. data). This complexity of the Ming deposit, suggests it is reasonable to assume that sulfur isotope fractionation took place in a fully open system rather than a partly open system.

The generally positive  $\delta^{34}\text{S}$  values of sulfides in the Ming deposit rule out any significant role for microbial activity in the genesis of the Ming deposit. Moreover, sediments were not directly involved in the formation of the Ming deposit and the sediments of the upper PHG are younger and deposited after the formation of the Ming deposit and therefore could not have provided biogenic sulfur to the deposit.

Sulfates do not occur in the Ming deposit illustrating that seawater sulfate in sulfate mineral form was not important in the deposit; however, the role for thermochemical sulfate reduction (TSR) of seawater sulfate was likely important in the formation of the Ming deposit, and has been shown to be important in most Phanerozoic VMS deposits (Shanks et al., 1981, 1995; Shanks and Seyfried, 1987; Ohmoto and Goldhaber, 1997; Huston, 1999; Seal, 2006). To test whether the sulfur in the Ming deposit could have been formed solely from TSR of seawater sulfate, we used the equations of Ohmoto and Rye (1979) and Ohmoto and Goldhaber (1997) and the fractionation between  $\text{H}_2\text{S}$  and sulfide of Kajiwara and Krouse (1971) (Appendix A4-6).

Minimum and maximum temperatures for TSR were assumed to be 250°C and 350°C, based on the results of Shanks et al. (1981) and the interpreted conditions of formation of the sulfide assemblages in the Ming deposit (Brueckner et al., 2014). Although Shanks et al. (1981) proposed that TSR can occur as low as 200°C, the experimental results at 200°C did not result in the formation of pyrite. Hence, Shanks et al. (1981) argued that TSR at lower temperatures is too

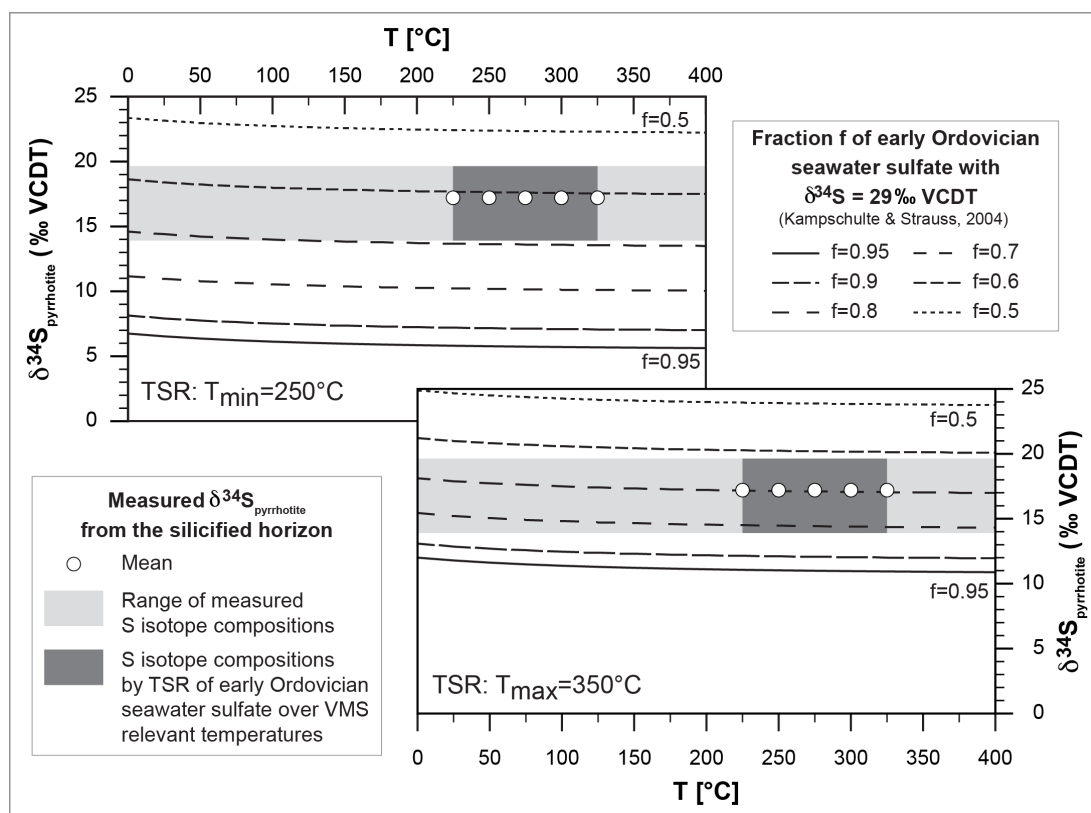
slow and high water/rock ratios are required for successful TSR reactions at temperatures as low as 200°C. These experiments and the fact that the sulfide and precious metal mineralogy at the Ming deposit indicates formation from fluids at temperatures of  $\geq 250^{\circ}\text{C}$  (Brueckner et al., 2014) are the basis for the assumed minimum and maximum temperatures of 250°C and 350°C, respectively.

For TSR modelling, the composition of early Ordovician seawater sulfate was assumed to be  $\sim 29\text{‰}$  (Claypool et al., 1980; Kampschulte and Strauss, 2004), although evaporates (Claypool et al., 1980) and carbonates associated with sulfates (CAS; Kampschulte and Strauss, 2004) show a wide range of sulfur isotopic composition for Ordovician seawater sulfate (15-30‰; Kampschulte and Strauss, 2004). Nevertheless, Kampschulte and Strauss (2004) and Paytan and Gray (2012) pointed out that the mean sulfur isotopic composition of CAS at the end of the Cambrian and beginning of the Ordovician is 30‰, a value that decreased steadily during the Ordovician. The U-Pb zircon age of the Rambler rhyolite is  $487 \pm 3 \text{ Ma}$  (Castonguay et al., 2009), which is close to, but slightly younger, than the age of the Cambro-Ordovician boundary; therefore, the  $\delta^{34}\text{S}$  composition of seawater sulfate at the time of the formation of the Ming deposit is assumed to be slightly lower (29‰) than the mean of  $\delta^{34}\text{S} = 30\text{‰}$ .

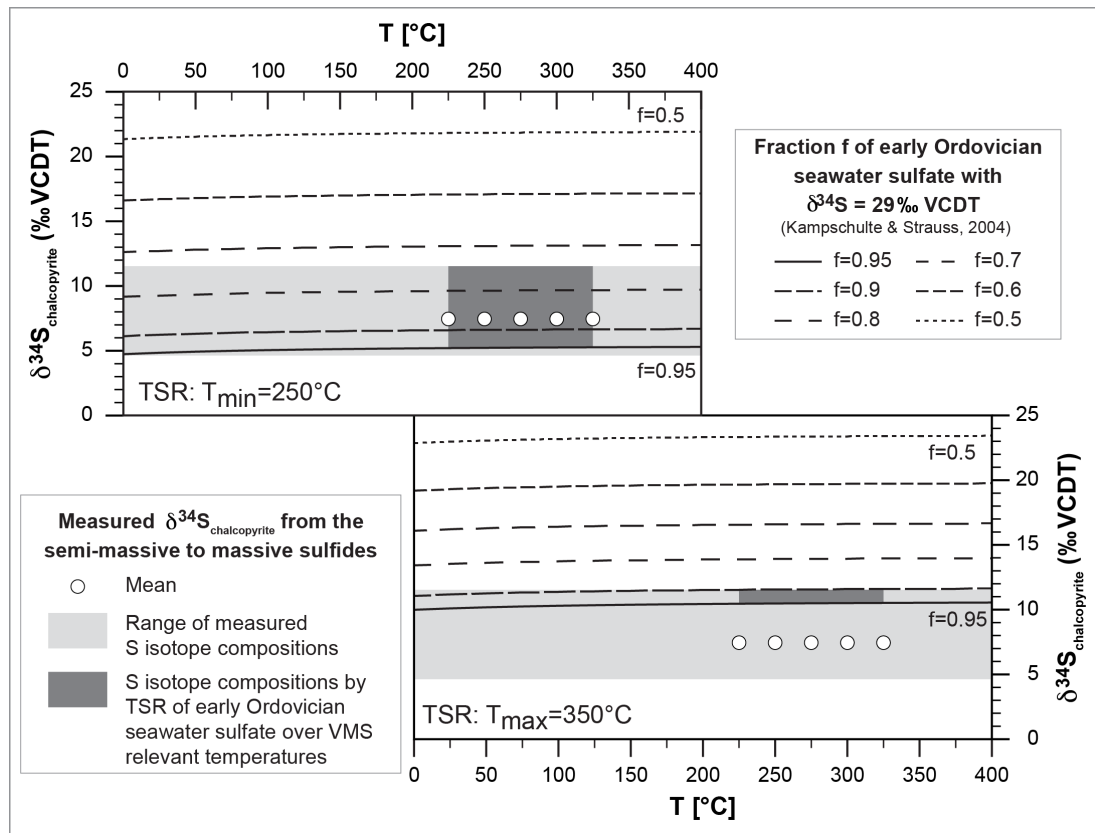
In Figures 4-9 and 4-10, results of modelled TSR  $\delta^{34}\text{S}$  values at temperatures of 250°C and 350°C are shown for pyrrhotite in the silicified horizon and chalcopryite in the semi-massive to massive sulfides, respectively. Comparison of the modelled data with the measured values show that TSR can



account for the isotopic composition of sulfides, especially of the silicified horizon, over VMS relevant temperatures (225-325°C; Fig. 4-9). Modelled pyrrhotite results for the silicified horizon show that at the assumed minimum TSR temperature of 250°C, up to 45% seawater sulfate was reduced to sulfide over VMS-relevant temperatures of 225-325°C (Fig. 4-9). However, with increasing temperatures, the magnitude of isotopic fractionation between sulfate and sulfide decreases (Fig. 4-9). Despite this weak decrease of sulfur isotopic fractionation with increasing TSR temperature, it is permissible that TSR was the dominant sulfur source for sulfides within the silicified horizon; other possible sources (sulfur leached from igneous wall rock, magmatic fluid-related sulfur or metamorphic sulfur) have lower  $\delta^{34}\text{S}$  values and most likely could not have contributed significant amounts of sulfur. Thermochemical sulfate reduction modelling for other mineralization styles show that TSR cannot be the sole source of sulfur at the Ming deposit, however. In particular, with increasing TSR temperature, the lower  $\delta^{34}\text{S}$  values in the semi-massive to massive sulfides cannot be successfully modelled using TSR as a sole source (Fig. 4-10); therefore, a second sulfur source is required. The lower  $\delta^{34}\text{S}$  values can be explained by a contribution of sulfur leached from igneous wall rock or magmatic fluid-related sulfur, likely by mixing between TSR and sulfur leached from igneous wall rock/derived from magmatic fluids.



**Figure 4-9.** Measured and calculated  $\delta^{34}\text{S}$  values of pyrrhotite in the silicified horizon of the 1806 orebody. Calculations are thermochemical sulfate reduction of reduced early Ordovician seawater using Equations (4-1) to (4-4) (Appendix A4-6) for minimum and maximum temperatures of TSR of 250°C and 350°C, respectively;  $\delta^{34}\text{S}$  of early Ordovician seawater sulfate is assumed to be  $\approx 29\text{‰}$  (Kampschulte and Strauss, 2004)

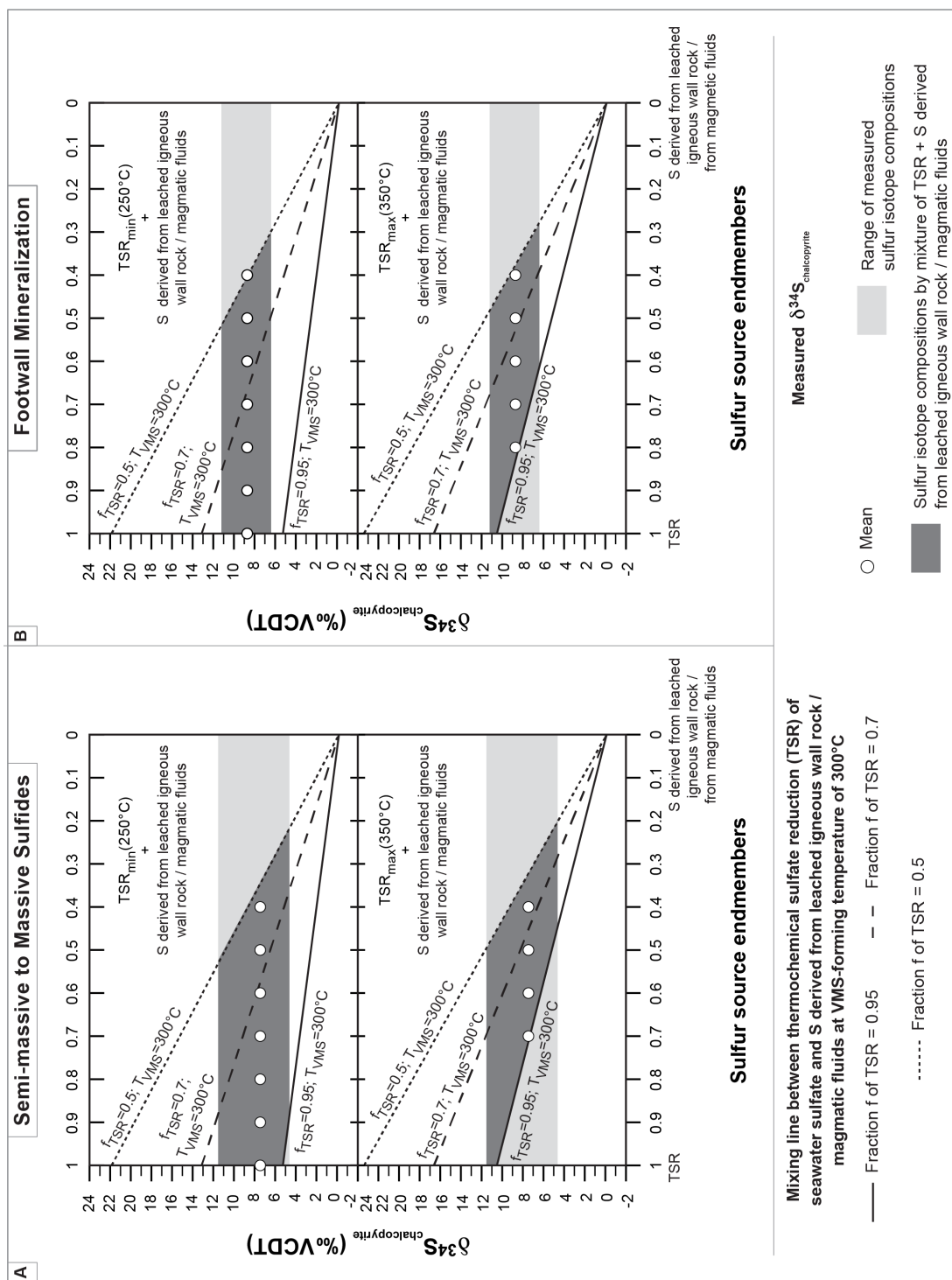


**Figure 4-10.** Measured and calculated  $\delta^{34}\text{S}$  values of chalcopyrite from the semi-massive to massive sulfides. Calculations are thermochemical sulfate reduction of reduced early Ordovician seawater by Equations (4-1) to (4-4) (Appendix A4-6) for minimum and maximum temperatures of TSR of  $250^\circ\text{C}$  and  $350^\circ\text{C}$ , respectively;  $\delta^{34}\text{S}$  of early Ordovician seawater sulfate is assumed to be  $\approx 29\text{‰}$  (Kampschulte and Strauss, 2004)

Mixing between TSR and sulfur leached from igneous wall rock/derived from magmatic fluids (igneous sulfur) was tested using equations (4-5) and (4-6) in Appendix A4-6. Calculations show that mixing between these two end members can account for the measured sulfur isotope compositions of sulfides from semi-massive to massive sulfides, the sulfide stringer horizon, and the Lower Footwall Zone at temperatures of TSR above 250°C. In Figure 4-11, the modelled mixing for chalcopyrite from the semi-massive to massive sulfides (Fig. 4-11a) and from the footwall mineralization (stringer sulfide horizon and Lower Footwall Zone; Fig. 4-11b) illustrate that with increasing temperature of TSR the input of the igneous sulfur source (wall rock/magmatic fluid) must increase as well, and that a high percentage of sulfur in the analyzed chalcopyrite can originate from sulfur leached from igneous wall rock/derived from magmatic fluids. Moreover, the average sulfur isotopic composition of chalcopyrite from the semi-massive to massive sulfides suggests that the input of igneous sulfur is higher than for chalcopyrite in footwall rocks (Fig. 4-11). For example, at a TSR temperature of 350°C and  $f=0.95$ , the input of igneous sulfur would be higher to produce average  $\delta^{34}\text{S}$  composition of chalcopyrite in semi-massive to massive sulfides (Fig. 4-11a) than to produce average  $\delta^{34}\text{S}$  for chalcopyrite in the footwall (Fig. 4-11b). Whether the origin of sulfur leached from igneous wall rock/derived from magmatic fluids is either: (1) unaltered Rambler rhyolite; (2) boninitic rocks of the PHG; or (3) magmatic fluids from a subvolcanic intrusion cannot be constrained due to the lack of sulfur isotopic composition of each possible

source. However, leached igneous (from Rambler rhyolite, boninitic basement rocks) and magmatic fluid (from subvolcanic intrusion) contributions to the sulfur budget of the deposit would be consistent with the sulfide mineral and hydrothermal alteration assemblages in the Ming deposit (Brueckner et al., 2014).

The modelling results are also consistent with the observations of Huston (1999), who compared the sulfur isotopic composition of 200 Archean to Tertiary VMS deposits and modern analogues worldwide. Huston (1999) described reduction of seawater sulfate as the dominant source of sulfur for most Paleozoic VMS deposits, especially for sulfides with  $\delta^{34}\text{S}$  values  $\geq 10\text{‰}$ . Most sulfides of the silicified horizon (Fig. 4-9) and some from the semi-massive to massive sulfides (Fig. 4-10) have sulfur isotopic compositions greater than  $10\text{‰}$ . In contrast, Huston (1999) mentioned that sulfur leached from igneous wall rock/derived from magmatic fluids could account for  $\delta^{34}\text{S}$  values between  $\approx 0\text{‰}$ - $5\text{‰}$ , but not for  $\delta^{34}\text{S}$  values above  $10\text{‰}$ . In this study, the majority of  $\delta^{34}\text{S}$  values in sulfides, especially from the semi-massive to massive sulfides and the footwall mineralization of the Ming deposit (Figs. 4-6, 4-7) are between  $+5$  and  $+10\text{‰}$ . Hence, a sole igneous sulfur source (igneous wall rock, magmatic fluids) is rather unlikely for the sulfides at the Ming deposit especially in the semi-massive to massive sulfides and footwall mineralization and mixing of the two sulfur sources reduced seawater sulfate and igneous sulfur from igneous wall rock/magmatic fluids is more reasonable for sulfides with  $\delta^{34}\text{S} \leq 10\text{‰}$  (Fig. 4-11).



**Figure 4-11.** (previous page) Measured and calculated  $\delta^{34}\text{S}$  values for chalcopyrite in **(A)** semi-massive to massive sulfides and **(B)** in the footwall; Calculations are mixing lines between both end members TSR and S derived from leached igneous wall rock/magmatic fluids using Equations (4-5) and (4-6) (Appendix A4-6). Calculations for fractionation of reduced seawater sulfate to sulfide with  $f=0.95$ ,  $0.7$ , and  $0.5$ , for VMS-forming temperature of  $300^\circ\text{C}$ , and for assumed minimum and maximum temperatures of TSR of  $250^\circ\text{C}$  and  $350^\circ\text{C}$ , respectively

#### 4-5-3 CHANGES IN SULFUR ISOTOPE COMPOSITION WITH STRATIGRAPHIC POSITION

Changes in  $\delta^{34}\text{S}$  as a function of stratigraphic position in VMS deposits are reported from various deposits (Huston, 1999). For example, sulfur isotope data from the Iron Mountain mine, California (South and Taylor, 1985), Rio Tinto, Spain (Eastoe et al., 1986), or the Madenköy VMS deposit, Turkey (Çagatay and Eastoe, 1995), show higher  $\delta^{34}\text{S}$  values in the footwall compared to the massive sulfide lens. Such an increase in  $\delta^{34}\text{S}$  from semi-massive and massive sulfides to the footwall is also observed at the Ming deposit (Figs. 4-6, 4-7). Eastoe et al. (1986) and Çagatay and Eastoe (1995) explained the higher  $\delta^{34}\text{S}$  values in the footwall as being the result of higher inputs of  $\text{H}_2\text{S}$  from reduced seawater sulfate over time, correlating with a shift of deposition from seafloor (massive sulfides) to sub-seafloor (stringer in footwall). Eastoe et al. (1986) suggested a decrease in temperature of the hydrothermal fluid or the obstruction of vents by sulfide mounds as reason for such a shift in the locus of deposition at Rio Tinto, Spain.

At the Ming deposit, alteration and sulfide mineralogy indicate similar temperatures for the semi-massive to massive sulfides and sulfide stringer horizon ( $\approx 250\text{--}300^\circ\text{C}$ ), but higher temperatures at the Lower Footwall Zone ( $>300^\circ\text{C}$ ; Pilote et al., 2014). However, the sulfur isotopic composition of sulfides from the sulfide stringer horizon below the massive sulfide and the Lower Footwall Zone are almost identical (Figs. 4-6, 4-7). The occurrence of metal sulfides is similar for all three mineralization styles, although abundances change especially to the higher temperature Lower Footwall Zone. The general metal sulfide assemblage in semi-massive to massive sulfides, sulfide stringer horizon and Lower Footwall Zone is: pyrite–chalcopyrite–pyrrhotite–sphalerite–cubanite $\pm$ arsenopyrite $\pm$ galena (Brueckner et al. unpubl. data). This rather uniform metal sulfide assemblage throughout the Ming deposit suggests that the mineralization styles were formed at the same time. Hence, a change in the locus of deposition over time (Eastoe et al., 1986) is excluded as primary source for the decrease in  $\delta^{34}\text{S}$  from the footwall to the overlying massive sulfides at the Ming deposit.

The modelling results show that the mixing of TSR with igneous sulfur (igneous wall rock/magmatic fluids) contributed the majority of sulfur to sulfides in both semi-massive to massive sulfides and footwall mineralization. Therefore, the overall change in the sulfur isotopic composition with stratigraphic position is likely related to changes in the relative contributions from these two sources. Changes in the fractionation of seawater sulfate to sulfide by TSR are directly



linked to the temperature of the hydrothermal fluid, where as the proportion of sulfide species in the hydrothermal fluid is a function of several physico-chemical parameters including temperature, pH and redox state. The hotter the hydrothermal fluid is the higher is the fractionation of seawater sulfate to sulfide and the more reduced the hydrothermal fluid becomes the higher is the amount of transported Fe- and As-species in the fluid. Indications for reduced hydrothermal fluid conditions are: (1) pyrite-pyrrhotite assemblage (Shanks et al., 1981); and (2) the occurrence of arsenopyrite and As-bearing minerals such as tennantite and löllingite (Heinrich and Eadington, 1986). Pyrite-pyrrhotite sulfide assemblage is especially common for the footwall mineralization (pyrrhotite is usually replacing pyrite; Fig. 4-5g, i). Arsenic-rich assemblages, on the other hand, such as arsenopyrite and As-bearing sulfosalts (tennantite, löllingite), are in greater abundance in the semi-massive to massive sulfides than in the footwall mineralization. Shanks et al. (1981), Lydon (1988), and Hannington et al. (1995) have illustrated that the presence of pyrrhotite in VMS mineral assemblages is consistent with high temperature reduced fluids. Similarly, Heinrich and Eadington (1986) showed that the transport of arsenic as  $(\text{As})\text{OH}_3$  also requires reduced fluids. Based on the sulfide mineral assemblage indicating reduced conditions, both stratigraphic levels (semi-massive to massive sulfides, footwall mineralization) formed under similarly reducing conditions. Hence, it is assumed that changes in TSR due to variations in redox state and temperature of the hydrothermal fluid during the formation of the Ming deposit are not the primary

cause of sulfur isotopic compositional differences between footwall and massive sulfides.

The stratigraphic variations in  $\delta^{34}\text{S}$  are more likely related to the variable contribution of sulfur leached from igneous wall rock/derived from magmatic fluids relative to TSR with a higher contribution of igneous sulfur resulting in lower  $\delta^{34}\text{S}$  values in the sulfides (Fig. 4-11; Huston, 1999). Deciphering whether this igneous sulfur is leached from the igneous footwall or a direct contribution from magmatic fluids is difficult; however, it is likely both leaching of igneous rocks and direct magmatic sources were important given the sulfide and precious metal mineral assemblages in the deposit showing both classic VMS and epithermal-like assemblages, and precious metal enrichment in the sulfides (Brueckner et al., 2014). Brueckner et al. (2014) showed there are variations in the abundance of arsenopyrite, sulfosalt and precious metal phases, and they show greater enrichments in the semi-massive to massive sulfides than in the discordant footwall stringer sulfides. Thus, changes in the footwall and semi-massive to massive sulfide horizons are due to varying contributions from TSR and especially from sulfur leached from igneous wall rock/derived from magmatic fluids; similar results were noted in many VMS deposits by Huston (1999). In contrast, the homogeneity and high  $\delta^{34}\text{S}$  values of the silicified horizon at the Ming deposit are derived solely from TSR and do not require any contribution from igneous sulfur (Fig. 4-9).

#### *4-5-4 INFLUENCE OF METAMORPHISM ON SULFUR ISOTOPE COMPOSITION AND COMPARISON TO OTHER DEPOSITS*

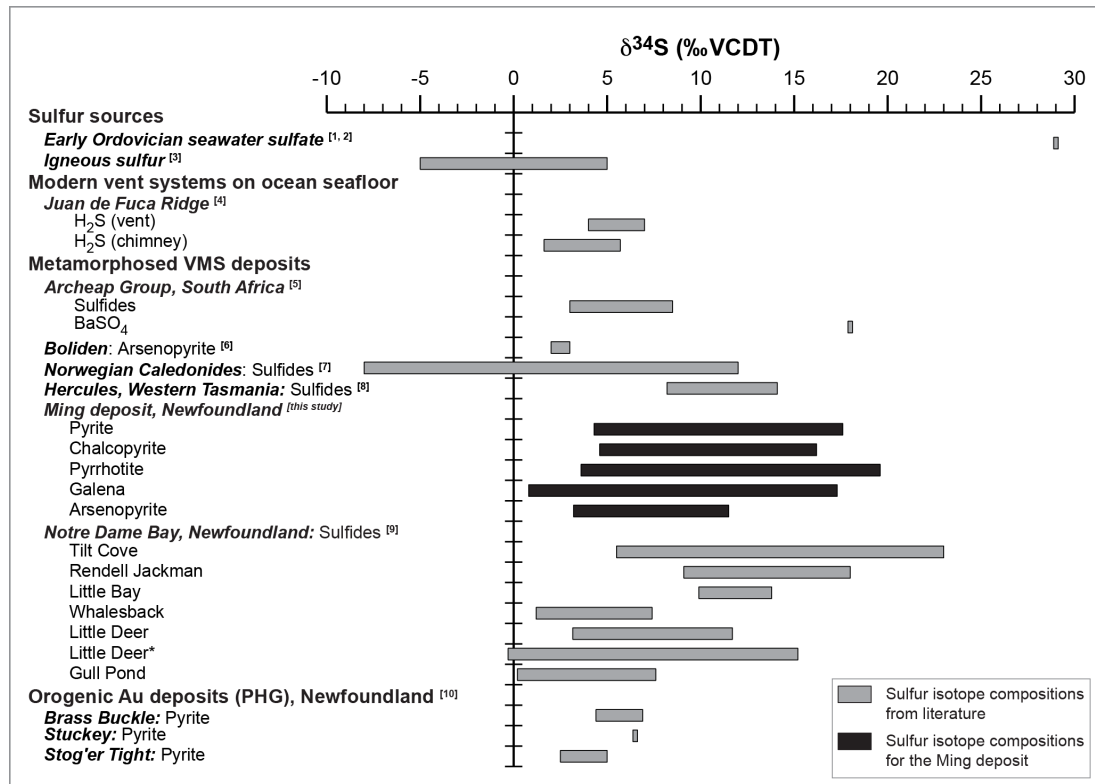
Regional metamorphism is common amongst ancient VMS deposits (Galley et al., 2007), and the effects of metamorphism on sulfur isotope composition have been extensively discussed, particularly regarding sulfur isotope fractionation on the syngenetic sulfur isotopic composition of VMS sulfides (Seal, 2006; Hoefs, 2009).

The metamorphic influence on the isotopic composition of sulfides is often difficult to distinguish from igneous wall rock/magmatic fluid signatures due to overlapping  $\delta^{34}\text{S}$  values between igneous and metamorphic rocks (Hoefs, 2009). Cook and Hoefs (1997), however, analyzed the sulfur isotopic composition of sulfides from Paleozoic metamorphosed Norwegian VMS deposits (Fig. 4-12). They concluded that sulfur isotopic equilibration caused by metamorphism is locally restricted and most sulfur isotope data represent original  $\delta^{34}\text{S}$  compositions. Seccombe et al. (1985) showed similar results for metamorphosed VMS mineralization in the Kanmantoo Group, South Australia. The sulfide pairs at the Ming deposit discussed are in isotopic disequilibrium and suggest that metamorphic homogenization of the sulfur isotopic composition of sulfides in the Ming deposit are negligible. Furthermore, despite the Ming deposit containing textures indicative of Silurian-Devonian metamorphism (annealed textures, recrystallization, porphyroblast growth, cataclastic texture; Fig. 4-5) there is no correlation between metamorphic textures and  $\delta^{34}\text{S}$  values of the sulfides (Fig. 4-

8, Appendix A4-6). These arguments alone suggest that metamorphic re-equilibration of  $\delta^{34}\text{S}$  was not a significant process in the Ming deposit for the sulfides.

In Figure 4-12, the sulfur isotopic composition of sulfides from the Ming deposit is compared to: (1) sources of reduced sulfur (Claypool et al., 1980, Kampshulte and Strauss, 2004; Hoefs, 2009); (2)  $\delta^{34}\text{S}$  values of modern vents (Shanks and Seyfried, 1987); (3) metamorphosed VMS deposits worldwide (Zaw and Ross, 1992; Cook and Hoefs, 1997; Wagner et al., 2004; Bailie et al., 2010) and of the Notre Dame Bay, Notre Dame sub-zone, Newfoundland (Bachinski, 1977, 1978; Toman, 2012); and (4) orogenic deposits of Silurian age within the PHG (Evans, 2004). Sulfur isotope data from the Ming deposit overlap with most  $\delta^{34}\text{S}$  data from other metamorphosed VMS deposits, especially with sulfides from the Archean Group, South Africa (Bailie et al., 2010), from Notre Dame Bay (Bachinski, 1977, 1978; Toman, 2012), Western Tasmania (Zaw and Ross, 1992), and partly with sulfides from the Norwegian Caledonides (Cook and Hoefs, 1997). Sulfur isotopic compositions of sulfides from these deposits are interpreted as being primary with only limited local metamorphic sulfur isotope re-equilibration (Bachinski, 1977, 1978; Zaw and Ross, 1992; Cook and Hoefs, 1997; Bailie et al., 2010; Toman, 2012). Pyrites from Silurian orogenic Au deposits (Evans, 2004) in the vicinity of the Ming deposit have similar  $\delta^{34}\text{S}$  values to some sulfides from the Ming deposit. However, the data from Evans (2004) are limited and further data for sulfides from orogenic gold deposits in the region

would be required to fully evaluate the importance of Silurian-Devonian metamorphic fluid contributions to the sulfur isotope budget of the Ming deposit. At present, the data are not supportive of a significant influence, consistent with previous arguments based on ore mineral assemblages (Brueckner et al., 2014).



**Figure 4-12.** Sulfur isotope data for different sulfur sources, metamorphosed VMS deposits including this study, and orogenic Au deposits of the Pacquet Harbour Group (PHG); Data from: **[1]** Claypool et al. (1980); **[2]** Kampschulte and Strauss (2004); **[3]** Hoefs (2009); **[4]** Shanks and Seyfried (1987); **[5]** Bailie et al. (2010); **[6]** Wagner et al. (2004); **[7]** Cook and Hoefs (1997); **[8]** Zaw and Ross (1992); and **[9]** Bachinski (1977, 1978) with new data for Little Deer\* from Toman (2012); and **[10]** Evans (2004)

## 4-6 CONCLUSIONS

The sulfur isotope results on sulfides from the base and precious metal, early Ordovician Ming Cu-Au VMS deposit lead to the following conclusions:

(1) Influence of Siluro-Devonian metamorphism/poly-phase deformation on sulfur isotope composition in the Ming deposit is negligible and did not significantly affect the overall deposit. Instead, measured  $\delta^{34}\text{S}$  values most likely reflect the original isotopic compositions of VMS mineralization; this is based on (a) isotopic disequilibrium for neighbouring mineral pairs, (b) lack of relation between metamorphic textures and  $\delta^{34}\text{S}$  composition in pyrites, and (c) the lack of evidence for metamorphic isotopic homogenization between pyrite and chalcopyrite and pyrite and pyrrhotite.

(2) Modelling of sulfur isotope compositions illustrate that sulfur was predominantly derived from mixtures of TSR of seawater sulfate combined with sulfur leached from igneous wall rock/derived from magmatic fluids (igneous sulfur). Although quantitative calculations assume many variables, the calculated contribution of sulfur leached from igneous wall rock/derived from magmatic fluids is elevated in semi-massive and massive sulfides, and stringer footwall mineralization. Moreover, with increasing temperature, the contribution of igneous sulfur in these mineralization styles is shown to increase. The source of igneous sulfur may be leaching from igneous wall rock or through direct input of magmatic fluids/volatiles, but it is not possible to decipher with sulfur isotope data alone; however, given the variations in mineral assemblages in the deposit, it is

permissive that both igneous sulfur sources were important in the Ming deposit. In contrast, the sulfur isotopic compositions in the silicified horizon that caps the 1806 Zone require only TSR of early Ordovician seawater sulfate; and

(3) Changes in  $\delta^{34}\text{S}$  between the semi-massive to massive sulfides (lower  $\delta^{34}\text{S}$  values) and the footwall mineralization (higher  $\delta^{34}\text{S}$  values) are attributed to variations in the ratio of reduced sulfur from TSR to igneous sulfur. Exclusive changes of the fractionation of seawater sulfate to sulfide or a change of the locus of deposition (seafloor to sub-seafloor) during the time of formation are unlikely; this is based on (a) sulfide mineral assemblages in the semi-massive to massive sulfides and footwall that indicate rather reduced conditions for both mineralization styles, and (b) broadly coeval deposition of sulfides in the footwall and on the seafloor at the Ming deposit.

## **Acknowledgements**

Stefanie Brueckner gives special thanks to staff and miners of the Ming Mine, who are explicitly thanked for their help, assistance and support during core logging and underground mapping. Rambler Metals and Mining Canada Ltd. provided logistical support for the project. Stefanie Brueckner also thanks especially Anthony E. Fallick, an anonymous reviewer, co-editor Karen Kelley and editor-in-chief Georges Beaudoin for their constructive, critical, and helpful comments, which improved the manuscript greatly. Funding for the project was provided by grants to Stephen Piercey, including an NSERC Discovery Grant and

the NSERC Altius Industrial Research Chair in Mineral Deposits supported by NSERC, Altius Minerals Ltd., and the Research and Development Corporation of Newfoundland and Labrador. The installation of the MAF-IIC SIMS Facility at Memorial University was catalyzed by a Leaders Opportunity Fund grant to Graham Layne from the Canada Foundation for Innovation. Ongoing support for this facility is also partially derived from an NSERC Discovery Grant to Graham Layne.

## References

- Alt JC, Shanks WC (2011) Microbial sulfate reduction and the sulfur budget for a complete section of altered oceanic basalts, IODP Hole 1256D (eastern Pacific) *Earth and Planetary Science Letters* 310:73-83 doi:10.1016/j.epsl.2011.07.027
- Bachinski DJ (1977) Sulfur isotopic composition of ophiolitic cupriferous sulfide deposits, Notre Dame Bay, Newfoundland *Economic Geology* 72:243-257
- Bachinski DJ (1978) Sulfur isotopic composition of thermally metamorphosed cupriferous iron sulfide ores associated with cordierite-antophyllite rocks, Gull Pond, Newfoundland *Economic Geology* 73:64-72
- Bailie R, Gutzmer J, Strauss H, Stüeken E, McClung C (2010) Sulfur isotope characteristics of metamorphosed Zn–Cu volcanogenic massive sulfides in the Areachap Group, Northern Cape Province, South Africa *Mineralium Deposita* 45:481-496 doi:10.1007/s00126-010-0285-8
- Bischoff JL, Rosenbauer RJ (1983) A note on the chemistry of seawater in the range 350°-500°C *Geochimica et Cosmochimica Acta* 47:139-144
- Bradshaw GD, Rowins SM, Peter JM, Taylor BE (2008) Genesis of the Wolverine volcanic sediment-hosted massive sulfide deposit, Finlayson Lake District, Yukon, Canada: Mineralogical, mineral chemical, fluid inclusion, and sulfur isotope evidence *Economic Geology* 103:35-60



- Brueckner SM, Piercey SJ, Sylvester PJ, Maloney S, Pilgrim L (2014) Evidence for syngenetic precious metal enrichment in an Appalachian volcanogenic massive sulfide system: The 1806 Zone, Ming Mine, Newfoundland, Canada *Economic Geology* 109:1611-1642  
doi:10.2113/econgeo.109.6.1611
- Çagatay MN, Eastoe CJ (1995) A sulfur isotope study of volcanogenic massive sulfide deposits of the eastern Black Sea province, Turkey *Mineralium Deposita* 30:55-66
- Canfield DE (2001) Biogeochemistry of sulfur isotopes. In: Valley JW, Cole, D.R. (ed) *Stable isotope geochemistry*, vol 43. *Reviews in Mineralogy and Geochemistry*. pp 607-636
- Castonguay S, Skulski T, van Staal C, Currie M (2009) New insights on the structural geology of the Pacquet Harbour group and Point Rousse complex, Baie Verte peninsula, Newfoundland *Current Research Newfoundland and Labrador Department of Natural Resources, Geological Survey Report 09-1*:147-158
- Claypool GE, Holser WT, Kaplan IR, Sakai H, Zak I (1980) The age curves of sulfur and oxygen isotopes in marine sulfate and their mutual interpretation *Chemical Geology* 28:199-260
- Cook NJ, Hoefs J (1997) Sulphur isotope characteristics of metamorphosed Cu-(Zn) volcanogenic massive sulphide deposits in the Norwegian Caledonides *Chemical Geology* 135:307-324
- Crowe DE (1994) Preservation of original hydrothermal  $\delta^{34}\text{S}$  values in greenschist to upper amphibolite volcanogenic massive sulfide deposits *Geology* 22
- Dubé B, Gosselin P, Mercier-Langevin P, Hannington M, Galley A (2007) Gold-rich volcanogenic massive sulphide deposits. In: Goodfellow WD (ed) *Mineral deposits of Canada: A synthesis of major deposit-types, district metallogeny, the evolution of geological provinces, and exploration methods*, vol Special Publication No. 5. Geological Association of Canada, Mineral Deposits Division, pp 75-94
- Eastoe CJ, Solomon M, Garcia Palomero F (1986) A sulfur isotope study of the massive and stockwork pyrite deposits at Rio Tinto, Spain *Transactions of the Institute of Mining and Metallurgy, Section B: Applied Earth Sciences* 95:201-207

- Evans DTW (2004) Epigenetic gold occurrences, Baie Verte Peninsula, (NTS 12H/09, 16 and 12I/01), Newfoundland vol Mineral Resource Report 11. Government of Newfoundland and Labrador, Department of Natural Resources, Geological Survey, St. John's, NL
- Fisher RV (1961) Proposed classification of volcanoclastic sediments and rocks Geological Society of America Bulletin 72:1409-1414
- Franklin JM (1993) Volcanic-associated massive sulphide deposits. In: Kirkham RV, Sinclair WD, Thorpe RI, Duke JM (eds) Mineral Deposit Modeling. Geological Association of Canada, Special Paper 40, pp 315-334
- Franklin JM (1996) Volcanic-associated massive sulphide base metals. In: Eckstrand OR, Sinclair WD, Thorpe RI (eds) Geology of Canadian Mineral Deposit Types. Geological Survey of Canada, Geology of Canada Series no. 8, Ottawa, ON, pp 158-183
- Galley A, Hannington M, Jonasson I (2007) Volcanogenic massive sulphide deposits. In: Goodfellow WD (ed) Mineral Deposits of Canada: A synthesis of major deposit-types, district metallogeny, the evolution of geological provinces, and exploration methods, vol Special Publication No. 5. Geological Association of Canada, Mineral Deposits Division, pp 141-161
- Gemmell JB, Sharpe R (1998) Detailed sulfur isotope investigation of the TAG hydrothermal mound and stockwork zone, 26°N, Mid-Atlantic Ridge. In: Herzig PM, Humphris SE, Miller DJ, Zierenberg RA (eds) Proceedings of the Ocean Drilling Program, Scientific Results, vol 158. College Station, TX, pp 71-84
- Gemmell JB, Sharpe R, Jonasson IR, Herzig PM (2004) Sulfur isotope evidence for magmatic contributions to submarine and subaerial gold mineralization: Conical seamount and the Ladolam gold deposit, Papua New Guinea Economic Geology 99:1711-1725 doi:0361-0128/01/3477/1711-15
- Goodfellow WD, Peter JM (1996) Sulphur isotope composition of the Brunswick No. 12 massive sulphide deposit, Bathurst Mining Camp, New Brunswick: Implications for ambient environment, sulphur source, and ore genesis Canadian Journal of Earth Sciences 33:231-251
- Gregory RT, Criss RE (1986) Isotopic Exchange in open and closed systems Reviews in Mineralogy and Geochemistry 16:91-127
- Gregory RT, Criss RE, Taylor Jr. HP (1989) Oxygen isotope exchange kinetics of mineral pairs in closed and open systems: Applications to problems of

hydrothermal alteration of igneous rocks and Precambrian iron formations  
Chemical Geology 75:1-42 doi:Doi 10.1016/0009-2541(89)90019-3

- Hannington MD, Jonasson IR, Herzig PM, Petersen S (1995) Physical and chemical processes of seafloor mineralization at mid-ocean ridges. In: Humphris SE, Zierenberg RA, Mullineaux LS, Thomson RE (eds) Seafloor hydrothermal systems: Physical, chemical, biological, and geological interactions, vol Geophysical Monograph 91. American Geophysical Union, Washington, DC, pp 115-157
- Hannington MD, Poulsen KH, Thompson JFH, Sillitoe RH (1999) Volcanogenic gold in the massive sulfide environment. In: Barrie CT, Hannington, M.D. (ed) Volcanic-associated massive sulfide deposits: Processes and examples in modern and ancient settings, vol 8. Reviews in Economic Geology. Society of Economic Geologists, Boulder, CO, pp 325-351
- Heinrich CA, Eadington PJ (1986) Thermodynamic predictions of the hydrothermal chemistry of arsenic, and their significance for the paragenetic sequence of some cassiterite-arsenopyrite-base metal sulfide deposits Economic Geology 81:511-529
- Herzig PM, Hannington MD (1995) Polymetallic massive sulfides at the modern seafloor: A review Ore Geology Reviews 10:95-115
- Hibbard LJ (1983) Geology of the Baie Verte Peninsula, Newfoundland vol 2. Memoir. Department of Mines and Energy, Government of Newfoundland and Labrador, Memoir 2
- Hoefs J (2009) Stable Isotope Geochemistry. 6<sup>th</sup> edn. Springer, Berlin, Heidelberg
- Huston DL (1999) Stable isotopes and their significance for understanding the genesis of volcanic-hosted massive sulfide deposits: A review. In: Barrie CT, Hannington, M.D. (ed) Volcanic-associated massive sulfide deposits: Processes and examples in modern and ancient settings, vol 8. Reviews in Economic Geology. Society of Economic Geologists, Boulder, CO, pp 157-179
- Huston DL (2000) Gold in volcanic-hosted massive sulfide deposits: Distribution, genesis, and exploration. In: Hagemann SG, Brown, P.E. (ed) Gold in 2000, vol 13. Reviews in Economic Geology. Society of Economic Geologists, Boulder, CO, pp 401-426
- Kajiwara Y, Krouse HR (1971) Sulfur isotope partitioning in metallic sulfide systems Canadian Journal of Earth Sciences 8:1397-1408

- Kampschulte A, Strauss H (2004) The sulfur isotopic evolution of Phanerozoic seawater based on the analysis of structurally substituted sulfate in carbonates *Chemical Geology* 204:255-286  
doi:10.1016/j.chemgeo.2003.11.013
- Large RR (1992) Australian volcanic-hosted massive sulfide deposits: Features, styles, and genetic models *Economic Geology* 87:471-510
- Lydon JW (1984) Volcanogenic massive sulphide deposits Part 1: A descriptive model *Geoscience Canada* 11:195-202
- Lydon JW (1988) Volcanogenic massive sulphide deposits Part 2: Genetic models *Geoscience Canada* 15:43-65
- Mercier-Langevin P, Hannington MD, Dubé B, Bécu V (2011) The gold content of volcanogenic massive sulfide deposits *Mineralium Deposita* 46:509-539  
doi:10.1007/s00126-010-0300-0
- Ohmoto H (1996) Formation of volcanogenic massive sulfide deposits: The Kuroko perspective *Ore Geology Reviews* 10:135-177
- Ohmoto H, Goldhaber MB (1997) Sulfur and carbon isotopes. In: Barnes HL (ed) *Geochemistry of hydrothermal ore deposits*, 3<sup>rd</sup> edn. John Wiley & Sons, New York, pp 517-611
- Ohmoto H, Rye RO (1979) Isotopes of sulfur and carbon. In: Barnes HL (ed) *Geochemistry of hydrothermal ore deposits*, 2<sup>nd</sup> edn. John Wiley & Sons, New York, pp 509-567
- Paytan A, Gray ET (2012) Sulfur Isotope Stratigraphy. In: Gradstein FM, Ogg JG, Schmitz M, Ogg G (eds) *The Geologic Timescale 2012*. Elsevier, Amsterdam, pp 167-180. doi:10.1016/B978-0-444-59425-9.00009-3
- Piercey S, Jenner GA, Wilton DHC (1997) The stratigraphy and geochemistry of the southern Pacquet Harbour Group, Baie Verte Peninsula, Newfoundland: Implications for mineral exploration *Current Research Newfoundland and Labrador Department of Natural Resources, Geological Survey Report* 97-1:119-139
- Pilgrim L (2009) Mineral resource estimate for the Ming Mine, Newfoundland, Canada. Rambler Metals and Mining Canada Ltd, Baie Verte, NL
- Pilote J-L, Piercey SJ, Mercier-Langevin P (2014) Stratigraphy and hydrothermal alteration of the Ming Cu-Au volcanogenic massive-sulphide deposit, Baie

Verte Peninsula, Newfoundland Geological Survey of Canada, Current Research 2014-7:18 doi:10.4095/295145

- Seal II RR (2006) Sulfur isotope geochemistry of sulfide minerals. In: Vaughan DJ (ed) Sulfide mineralogy and geochemistry, vol 61. Reviews in Mineralogy and Geochemistry. pp 633-677
- Seccombe PK, Spry PG, Both RA, Jones MT, Schiller JC (1985) Base metal mineralization in the Kanmantoo Group, South Australia: A regional sulfur isotope study *Economic Geology* 80:1824-1841
- Seyfried Jr. WE, Bischoff JL (1981) Experimental seawater-basalt interaction at 300°C, 500 bars, chemical exchange, secondary mineral formation and implications for the transport of heavy metals *Geochimica et Cosmochimica Acta* 45:135-147
- Shanks III WC (2001) Stable isotopes in seafloor hydrothermal systems: Vent fluids, hydrothermal deposits, hydrothermal alteration, and microbial processes. In: Valley JW, Cole, D.R. (ed) Stable isotope geochemistry, vol 43. Reviews in Mineralogy and Geochemistry. pp 469-525
- Shanks III WC, Böhlke JK, Seal II RR (1995) Stable isotopes in mid-ocean ridge hydrothermal systems: Interaction between fluids, minerals and organisms. In: Humphris SE, Zierenberg RA, Mullineaux LS, Thomson RE (eds) Seafloor hydrothermal systems: Physical, chemical, biological, and geological interactions, vol Geophysical Monograph 91. American Geophysical Union, Washington, DC, pp 194-221
- Shanks III WC, Seyfried Jr WE (1987) Stable isotope studies of vent fluids and chimney minerals, southern Juan de Fuca Ridge: Sodium metasomatism and seawater sulfate reduction *Journal of Geophysical Research* 92:11387-11399
- Sillitoe RH, Hannington MD, Thompson JFH (1996) High sulfidation deposits in the volcanogenic massive sulfide environment *Economic Geology* 91:204-212
- Skulski T, Castonguay, S., McNicoll, V., van Staal, C, Kidd, W, Rogers, N, Morris W, Ugalde, H, Slavinski H, Spicer W, Moussallam, Y, Kerr, I (2010) Tectonostratigraphy of the Baie Verte oceanic tract and its ophiolite cover sequence on the Baie Verte Peninsula Current Research Newfoundland and Labrador Department of Natural Resources, Geological Survey Report 10-1:315-335

- South BC, Taylor BE (1985) Stable isotope geochemistry and metal zonation at the Iron Mountain mine, West Shasta district, California *Economic Geology* 80:2177-2195
- Swinden HS, Thorpe RI (1984) Variations in style of volcanism and massive sulfide deposition in Early to Middle Ordovician island-arc sequences of the Newfoundland Central Mobile Belt *Economic Geology* 79:1596-1619 doi:10.2113/gsecongeo.79.7.1596
- Toman HC (2012) Geology and metallogeny of north-central Newfoundland and the Little Derr VMS deposit: An introduction and overview. M.Sc. thesis, Memorial University of Newfoundland, St. John's, NL [unpublished]
- Tuach J, Kennedy MJ (1978) The geologic setting of the Ming and other sulfide deposits, consolidated Rambler mines, Northeast Newfoundland *Economic Geology* 73:192-206
- van Staal CR (2007) Pre-Carboniferous tectonic evolution and metallogeny of the Canadian Appalachians. In: Goodfellow WD (ed) *Mineral deposits of Canada: A synthesis of major deposit-types, district metallogeny, the evolution of geological provinces, and exploration methods*, vol Special Publication No. 5. Geological Association of Canada, Mineral Deposits Division, pp 793-818
- van Staal CR, Barr SM (2012) Lithospheric architecture and tectonic evolution of the Canadian Appalachians and associated Atlantic margin. In: Percival JA, Cook FA, Clowes RM (eds) *Tectonic Styles in Canada: The LITHOPROBE perspective*. Geological Association of Canada, Special Paper 49, St. John's, NL, pp 41-96
- Wagner T, Boyce AJ, Jonsson E, Fallick AE (2004) Laser microprobe sulphur isotope analysis of arsenopyrite: Experimental calibration and application to the Boliden Au–Cu–As massive sulphide deposit *Ore Geology Reviews* 25:311-325
- Williams H (1979) Appalachian orogen in Canada *Canadian Journal of Earth Sciences* 16:792-807
- Woodruff LG, Shanks III WC (1988) Sulfur isotope study of chimney minerals and vent fluids from 21°N, East Pacific Rise: Hydrothermal sulfur sources and disequilibrium sulfate reduction *Journal of Geophysical Research* 93:4562-4572
- Zaw K, Large RR (1992) The precious metal-rich, South Hercules mineralization, western Tasmania: A possible subsea-floor replacement volcanic-hosted

massive sulfide deposit      Economic      Geology      87:931-952  
doi:10.2113/gsecongeo.87.3.931

## APPENDIX

### APPENDIX A4-1 METHODOLOGY

A sample-offset voltage of -60eV and Energy Window of 40eV width were deployed to purposely reduce transmission, enabling a higher primary beam current (and concomitantly faster sputter rate). This permitted faster pre-sputtering of the sample and better exclusion of exotic surface material, while maintaining count rates on  $^{32}\text{S}^-$  below  $1.3 \times 10^6$  counts per second (cps).

Signals for  $^{32}\text{S}^-$ ,  $^{34}\text{S}^-$  and a background position at 31.67Da were obtained by cyclical magnetic peak switching. Standard counting times and peak sequence used were: 0.5s at the background position, 2.0s on  $^{32}\text{S}^-$ , and 6.0s on  $^{34}\text{S}^-$ . Waiting times of 0.25s were inserted before each peak counting position to allow for magnet settling. A typical analysis consisted of accumulating 80 of these peak cycles, which takes less than 15 min (including pre-sputtering time).

Any change in overall peak intensities with time, which was typically monotonic (and quantitatively minor in its effect on measured  $^{34}\text{S}/^{32}\text{S}$ ) in a homogeneous sulfide mineral phase, was compensated for by using a standard double interpolation ratio algorithm (an approach adopted from thermal ionization mass spectrometry [TIMS]), with each  $^{34}\text{S}^-$  peak ratioed to the time-corrected interpolation of adjacent  $^{32}\text{S}^-$  peaks.

The production and detection of sputtered secondary ions produces a bias between the actual  $^{34}\text{S}/^{32}\text{S}$  of the sample and that measured by the mass spectrometer termed Instrumental Mass Fractionation (IMF). Instrumental Mass Fractionation in SIMS can generally be considered as a combination of mass discrimination effects at the site of sample sputtering with those in the ion detectors themselves. Other effects, related to the ion optics of the mass spectrometer, are reduced to comparatively insignificant levels in a properly and consistently aligned instrument.



The magnitude of IMF varies substantially among sulfide minerals. For this reason, the  $^{34}\text{S}/^{32}\text{S}$  ratio measured in samples of pyrite, chalcopyrite, pyrrhotite, arsenopyrite, and galena from the Ming Mine were corrected for IMF by comparison to replicate in run measurements of in-house reference materials during the course of each daily session. Results for the sulfide in-house standards, their measured  $^{34}\text{S}/^{32}\text{S}$  ratio and the calculated IMF factors are summarized in Appendices A4-2 and A4-3. In-house standards used were (1) UL9 ( $\delta^{34}\text{S}$ : 15.8‰) and KH87 ( $\delta^{34}\text{S}$ : 0.2‰) for pyrite; (2) USGS Norilsk ( $\delta^{34}\text{S}$ : 8.3‰) for chalcopyrite; (3) PoW1 ( $\delta^{34}\text{S}$ : 2.3‰), TL-34 ( $\delta^{34}\text{S}$ : -2.2‰), and TR1 ( $\delta^{34}\text{S}$ : -2.6‰) for pyrrhotite; (4) Arspy57 ( $\delta^{34}\text{S}$ : 2.8‰) for arsenopyrite; and (5) HT10-4A ( $\delta^{34}\text{S}$ : 14.2 ‰) for galena. In-house standards UL9 and HT10-4A are from the upper amphibolite facies Balmat deposit in the northwest Adirondack Mountains, New York. The second pyrite in-house standard KH87 is from Manitouwadge, Abitibi greenstone belt, Ontario, Canada. Chalcopyrite reference material USGS Norilsk is from the Ni-Cu deposit in Norilsk, in the northwest corner of the Siberian Shield, Russia. Its composition is 29.98% Fe, 34.63% Cu, and 34.98% S (Crowe and Vaughan, 1996). The pyrrhotite standard PoW1 is from Dalnegorsk, southeast Russia. The other two pyrrhotite in-house reference materials TL-34 and TR1 are of unknown location. In-house standard Arspy57 is a synthesized arsenopyrite with  $33.94 \pm 0.66\%$  Fe,  $46.55 \pm 1.57\%$  As, and  $19.05 \pm 0.39\%$  S (Kretschmar and Scott, 1976). G. D. Layne characterized all of these in-house materials, except USGS Norilsk, for  $\delta^{34}\text{S}$  over a period of several years. The  $\delta^{34}\text{S}$  value of each in-house standard was originally established by replicate measurements using isotope mass ratio spectrometry (IRMS), relative to the CDT (Cañon Diablo Troilite) scale. The accepted  $\delta^{34}\text{S}$  values used here have been reconciled to Vienna Cañon Diablo Troilite (and the IAEA-S-1 and IAEA-S-2 sulfur isotope reference materials) by rescaling to accommodate the relative expansion of the positive  $\delta^{34}\text{S}$  scale. This implied using more current gas-

IRMS-SF<sub>6</sub> (G-IRMS-SF<sub>6</sub>) data for the IAEA materials (Coplen et al., 2002) - i.e., the revised reference value for IAEA-S-2 from Mann et al (2009).

Analyses accumulated in 12min routinely yield internal precisions on individual  $\delta^{34}\text{S}$  determinations of better than  $\pm 0.4\text{‰}$  ( $1\sigma$ ), while producing sputter craters only a few  $\mu\text{m}$  deep. These precisions closely approach the optimum possible precision as calculated from Poisson counting statistics.

Our approach is closely comparable to the “shallow pit” approach of Kozdon et al (2010). Their study demonstrated that any effects due to grain orientation or sputtering response were subsidiary to the better than  $\pm 0.3\text{‰}$  ( $2\sigma$ ) overall reproducibility they achieved for replicate analyses of pyrite, chalcopyrite, pyrrhotite and galena using this approach - and that galena was not discernibly different in its behavior, or magnitude of variability, from these other phases under these conditions.

Results of analyzed in-house standards UL 9/9B, KH87, USGS Nor'ilsk, Po W1, TI-34, Po Tr1, Arspy 57, and HT10-4A are shown Appendices A4-2 and A4-3. The results are concise regarding to the accepted values of the used in-house standards and corrected for IMF. Appendix A4-3 also lists the daily measured  $^{34}\text{S}/^{32}\text{S}$  ratio for the used in-house standard and the calculated IMF values relative to  $\text{‰VCDT}$ .

## References

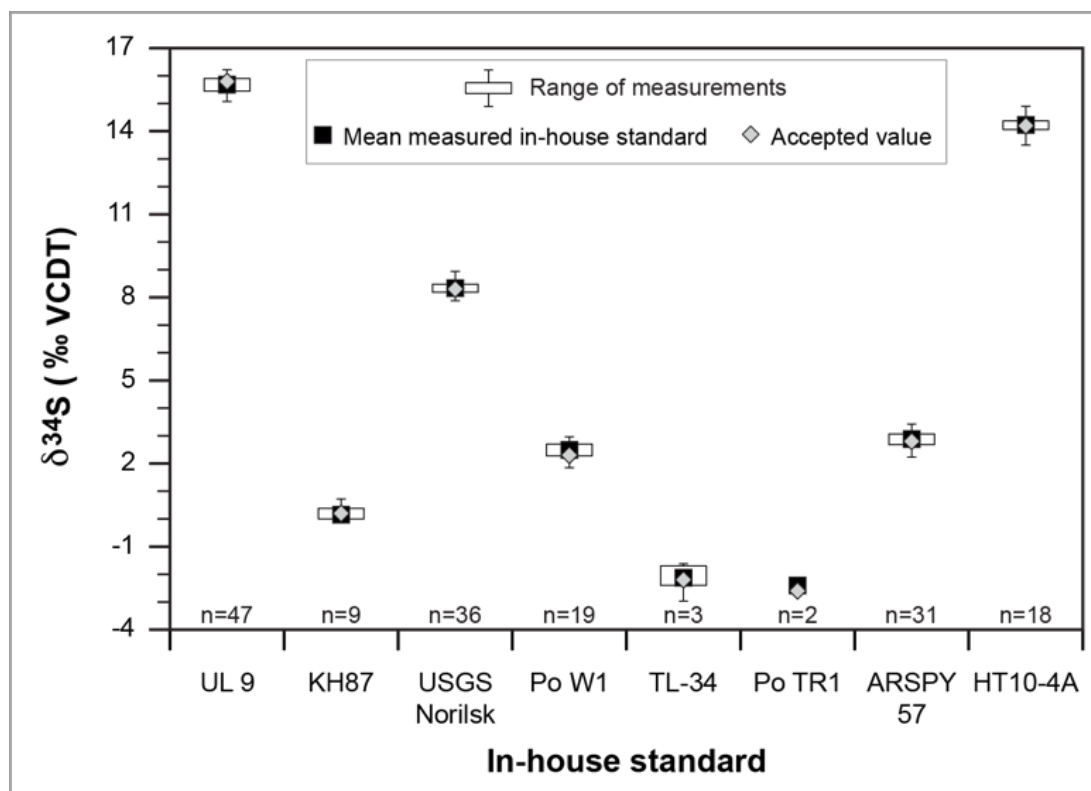
- Coplen TB, Hopple JA, Boehlke JK, Preiser HS, Rieder SE, Krouse HR, K.J.R. R, Ding T, Vocke Jr. RD, Revesz KM, Lamberty A, Taylor P, De Bievre P (2002) Compilation of minimum and maximum isotope ratios of selected elements in naturally occurring terrestrial materials and reagents Water-Resources Investigations Report 01-4222. U.S. Geological Survey, Reston, VA, pp 98
- Crowe DE, Vaughan RG (1996) Characterization and use of isotopically homogeneous standards for in situ laser microprobe analysis of  $^{34}\text{S}/^{32}\text{S}$  ratios American Mineralogist 81:187-193

Kozdon R, Kita NT, Huberty JM, Fournelle JH, Johnson CA, Valley JW (2010) In situ sulfur isotope analysis of sulfide minerals by SIMS: Precision and accuracy, with application to geothermometry of ~3.5Ga Pilbara cherts Chemical Geology 243:243-253 doi:10.1016/j.chemgeo.2010.05.015

Kretschmar U, Scott SD (1976) Phase relations involving arsenopyrite in the system Fe-As-S and their application The Canadian Mineralogist 14:364-386

Mann JL, Vocke Jr. RD, Kelly RW (2009) Revised  $\delta^{34}\text{S}$  reference values for IAEA sulfur isotope reference materials S-2 and S-3 Rapid Communications in Mass Spectrometry 23:1116-1124

#### APPENDIX A4-2 ACCURACY AND PRECISION OF ANALYZED REFERENCE MATERIALS



**Figure A4-1.** Box-Whisker plot of the results for sulfide reference materials used for IMF calibration and quality control of SIMS microanalyses. Data are the

recovered  $\delta^{34}\text{S}$  values for each individual measurement of a reference material once the IMF correction (based on the mean of replicate measurements for each day) was applied. The vertical error bars represent the total range of all spot analyses during the multiple analytical sessions. The vertical dimension of the box represents the  $1\sigma$  for all spot analyses during multiple analyses. These data demonstrate the overall reproducibility discussed for  $\delta^{34}\text{S}$  in text, and the relative homogeneity of the reference sulfide materials. All data are compiled in Appendix A4-3; n = number of analyzed data points

### APPENDIX A4-3 RESULTS OF REFERENCE MATERIAL ANALYSES

**Table A4-1.** Results of measured  $^{34}\text{S}/^{32}\text{S}$  ratio, calculated instrumental mass fractionation (IMF), and  $\delta^{34}\text{S}$  analysis corrected for IMF of the used in-house standards analyzed via SIMS; SEM – standard error mean, Stddev - standard deviation, \*accepted value, n – number of analyses

In-house standard Name	Measuring date	$^{34}\text{S}/^{32}\text{S}_{\text{measured}}$	SEM [%]	IMF <sup>calculated</sup> [‰ VCDT]	$\delta^{34}\text{S}_{\text{corrected}}$ [‰ VCDT]	SEM [1 $\sigma$ ]
<b>UL 9, UL9B (pyrite)</b>					<b>15.8*</b>	
UL 9-2	Jan 31 2012	0.044361	0.026	-11.2	15.8	0.3
UL 9-3	Jan 31 2012	0.044347	0.022	-11.5	15.5	0.2
UL 9b-1	Feb 06 2012	0.044334	0.027	-11.8	16.2	0.3
UL 9b-2	Feb 06 2012	0.044289	0.024	-12.8	15.2	0.2
UL 9b-3	Feb 06 2012	0.044310	0.024	-12.3	15.7	0.2
UL 9b-4	Feb 06 2012	0.044310	0.026	-12.3	15.7	0.3
UL 9b-1	Feb 07 2012	0.044298	0.017	-12.6	15.9	0.2
UL 9b-3	Feb 07 2012	0.044282	0.020	-13.0	15.5	0.2
UL 9b-1	Feb 08 2012	0.044234	0.019	-14.1	15.5	0.2
UL 9b-2	Feb 08 2012	0.044261	0.020	-13.5	16.2	0.2
UL 9b-3	Feb 08 2012	0.044225	0.022	-14.3	15.4	0.2
UL 9b-1	Feb 09 2012	0.044265	0.022	-13.4	15.8	0.2
UL 9b-2	Feb 09 2012	0.044247	0.017	-13.8	15.4	0.2
UL 9b-3	Feb 09 2012	0.044283	0.016	-12.9	16.2	0.2
UL 9b-4	Feb 09 2012	0.044252	0.019	-13.6	15.5	0.2
UL 9b-1	Feb 10 2012	0.044266	0.013	-13.3	15.6	0.1
UL 9b-2	Feb 10 2012	0.044276	0.018	-13.1	15.8	0.2
UL 9b-3	Feb 10 2012	0.044273	0.017	-13.2	15.7	0.2
UL 9b-1	Feb 14 2012	0.044263	0.019	-13.4	15.4	0.2
UL 9b-4	Feb 14 2012	0.044270	0.028	-13.2	15.6	0.3
UL 9b-6	Feb 14 2012	0.044285	0.027	-12.9	16.0	0.3
UL 9-1	Feb 15 2012	0.044255	0.015	-13.6	15.9	0.2
UL 9-4	Feb 15 2012	0.044234	0.023	-14.1	15.4	0.2
UL 9-5	Feb 15 2012	0.044260	0.025	-13.5	16.0	0.2
UL 9-7	Feb 15 2012	0.044233	0.017	-14.1	15.4	0.2

**Table A4-1. (cont.)**

In-house standard Name	Measuring date	$^{34}\text{S}/^{32}\text{S}_{\text{measured}}$	SEM [%]	IMF <sup>calculated</sup> [‰ VCDT]	$\delta^{34}\text{S}_{\text{corrected}}$ [‰ VCDT]	SEM [1σ]
UL 9-2	Feb 25 2012	0.044149	0.018	-16.0	15.9	0.2
UL 9-3	Feb 25 2012	0.044120	0.015	-16.6	15.2	0.2
UL 9-4	Feb 25 2012	0.044150	0.014	-16.0	15.9	0.1
UL 9-1	Feb 26 2012	0.044164	0.017	-15.6	15.8	0.2
UL 9-3	Feb 26 2012	0.044148	0.015	-16.0	15.5	0.1
UL 9-1	Mar 13 2012	0.043745	0.019	-25.2	16.0	0.2
UL 9-2	Mar 13 2012	0.043728	0.020	-25.6	15.6	0.2
UL 9-3	Mar 13 2012	0.043732	0.020	-25.5	15.7	0.2
UL 9-2	Feb 26 2013	0.044073	0.018	-17.7	15.1	0.2
UL 9-3	Feb 26 2013	0.044124	0.018	-16.6	16.2	0.2
UL 9-4	Feb 26 2013	0.044114	0.019	-16.8	16.0	0.2
UL 9-5	Feb 26 2013	0.044088	0.022	-17.4	15.4	0.2
UL 9-1	Mar 04 2013	0.044086	0.018	-17.4	15.3	0.2
UL 9-2	Mar 04 2013	0.044112	0.019	-16.8	15.9	0.2
UL 9-3	Mar 04 2013	0.044110	0.018	-16.9	15.8	0.2
UL 9-1	Mar 06 2013	0.043923	0.021	-21.1	16.2	0.2
UL 9-2	Mar 06 2013	0.043967	0.024	-20.1	15.2	0.2
UL 9-4	June 15 2013	0.044367	0.031	-11.1	15.5	0.3
UL 9-5	June 15 2013	0.044362	0.018	-11.2	15.3	0.2
UL 9-1	June 16 2013	0.044349	0.022	-11.5	15.7	0.2
UL 9-2	June 16 2013	0.044341	0.019	-11.6	15.5	0.2
UL 9-3	June 16 2013	0.044359	0.022	-11.2	15.9	0.2
<b>Mean (n=47)</b>					<b>15.7</b>	
<i>Stddev</i>					<i>0.4</i>	
<b>KH87 (pyrite)</b>					<b>0.2*</b>	
KH87-4	Jan 31 2012	0.043636	0.019	-12.2	0.1	0.2
KH87-5	Jan 31 2012	0.043627	0.022	-12.4	-0.1	0.2
KH87A-1	Feb 09 2012	0.043607	0.018	-12.9	0.3	0.2
KH87A-2	Feb 09 2012	0.043611	0.018	-12.8	0.3	0.2
KH87A-3	Feb 09 2012	0.043622	0.019	-12.5	0.6	0.2
KH87A-4	Feb 09 2012	0.043591	0.017	-13.2	-0.1	0.2
KH87-1	Feb 26 2013	0.043401	0.043	-17.6	-0.1	0.4
KH 87-1	June 15 2013	0.043700	0.020	-10.7	0.3	0.2
KH 87-2	June 16 2013	0.043644	0.018	-12.0	0.3	0.2
<b>Mean (n=9)</b>					<b>0.2</b>	
<i>Stddev</i>					<i>0.3</i>	
<b>USGS Norilsk (chalcopyrite)</b>					<b>8.3*</b>	
USGS Nor-2	Feb 27 2012	0.043724	0.017	-18.2	8.3	0.2
USGS Nor-3	Feb 27 2012	0.043728	0.021	-18.1	8.4	0.2
USGS Nor-4	Feb 27 2012	0.043723	0.019	-18.3	8.3	0.2
USGS Nor-1	Feb 28 2012	0.043748	0.019	-17.7	8.9	0.2
USGS Nor-2	Feb 28 2012	0.043711	0.020	-18.5	8.0	0.2
USGS Nor-3	Feb 28 2012	0.043717	0.016	-18.4	8.2	0.2
USGS Nor-4	Feb 28 2012	0.043720	0.017	-18.3	8.2	0.2
USGS Nor-1	Feb 29 2012	0.043679	0.020	-19.3	8.2	0.2
USGS Nor-2	Feb 29 2012	0.043692	0.015	-19.0	8.6	0.2
USGS Nor-3	Feb 29 2012	0.043675	0.019	-19.4	8.2	0.2
USGS Nor-1	Mar 01 2012	0.043684	0.017	-19.2	8.6	0.2
USGS Nor-2	Mar 01 2012	0.043677	0.020	-19.3	8.5	0.2
USGS Nor-3	Mar 01 2012	0.043650	0.019	-19.9	7.9	0.2
USGS Nor-1	Mar 02 2012	0.043645	0.019	-20.1	8.7	0.2
USGS Nor-2	Mar 02 2012	0.043629	0.019	-20.4	8.3	0.2
USGS Nor-3	Mar 02 2012	0.043612	0.018	-20.8	7.9	0.2
USGS Nor-4	Mar 02 2012	0.043636	0.020	-20.3	8.5	0.2
USGS Nor-1	Mar 16 2012	0.043273	0.023	-28.6	8.9	0.2
USGS Nor-2	Mar 16 2012	0.043238	0.021	-29.4	8.2	0.2
USGS Nor-3	Mar 16 2012	0.043247	0.021	-29.2	8.4	0.2

**Table A4-1. (cont.)**

In-house standard Name	Measuring date	$^{34}\text{S}/^{32}\text{S}_{\text{measured}}$	SEM [%]	IMF <sup>calculated</sup> [‰ VCDT]	$\delta^{34}\text{S}_{\text{corrected}}$ [‰ VCDT]	SEM [1σ]
USGS Nor-1	Feb 27 2013	0.043718	0.019	-18.4	8.1	0.2
USGS Nor-2	Feb 27 2013	0.043736	0.033	-18.0	8.6	0.3
USGS Nor-3	Feb 27 2013	0.043722	0.023	-18.3	8.3	0.2
USGS Nor-2	Mar 05 2013	0.043638	0.019	-20.2	8.3	0.2
USGS Nor-3	Mar 05 2013	0.043646	0.022	-20.0	8.5	0.2
USGS Nor-5	Mar 05 2013	0.043636	0.020	-20.3	8.2	0.2
USGS Nor-1	June 19 2013	0.043976	0.021	-12.5	8.2	0.2
USGS Nor-2	June 19 2013	0.043979	0.019	-12.4	8.3	0.2
USGS Nor-1	June 20 2013	0.043948	0.017	-13.1	8.4	0.2
USGS Nor-2	June 20 2013	0.043958	0.019	-12.9	8.2	0.2
USGS Nor-1	Sept 12 2013	0.043677	0.030	-19.3	8.9	0.3
USGS Nor-4	Sept 12 2013	0.043667	0.031	-19.6	8.7	0.3
USGS Nor-5	Sept 12 2013	0.043648	0.032	-20.0	8.3	0.3
USGS Nor-6	Sept 12 2013	0.043645	0.035	-20.0	8.2	0.3
USGS Nor-7	Sept 12 2013	0.043634	0.034	-20.3	8.0	0.3
USGS Nor-8	Sept 12 2013	0.043647	0.034	-20.0	8.3	0.3
<b>Mean (n=36)</b>					<b>8.3</b>	
<i>Stddev</i>					0.3	
<b>PO (pyrrhotite)</b>					<b>2.3*</b>	
W1-1	Mar 11 2012	0.043043	0.028	-28.0	2.3	0.3
W1-2	Mar 11 2012	0.043071	0.023	-27.3	2.9	0.2
W1-3	Mar 11 2012	0.043056	0.022	-27.7	2.6	0.2
W1-1	Feb 28 2013	0.043377	0.024	-20.2	2.5	0.2
W1-2	Feb 28 2013	0.043380	0.020	-20.2	2.5	0.2
W1-3	Feb 28 2013	0.043381	0.021	-20.2	2.5	0.2
W1-5	Feb 28 2013	0.043388	0.018	-20.0	2.7	0.2
W1-6	Feb 28 2013	0.043394	0.017	-19.9	2.8	0.2
W1-1	Mar 06 2013	0.043315	0.032	-21.7	2.5	0.3
W1-2	Mar 06 2013	0.043300	0.025	-22.0	2.2	0.3
W1-3	Mar 06 2013	0.043322	0.024	-21.5	2.7	0.2
W1-1	June 17 2013	0.043597	0.020	-15.2	2.4	0.2
W1-2	June 17 2013	0.043584	0.016	-15.5	2.2	0.2
W1-3	June 17 2013	0.043607	0.015	-15.0	2.7	0.1
W1-4	June 17 2013	0.043570	0.018	-15.8	1.9	0.2
W1-5	June 17 2013	0.043610	0.019	-14.9	2.7	0.2
W1-1	June 18 2013	0.043580	0.019	-15.6	2.2	0.2
W1-2	June 18 2013	0.043566	0.016	-15.9	1.9	0.2
W1-3	June 18 2013	0.043611	0.018	-14.9	3.0	0.2
<b>Mean (n=19)</b>					<b>2.5</b>	
<i>Stddev</i>					0.3	
<b>TL-34 (pyrrhotite)</b>					<b>-2.2*</b>	
TL-34-1	Mar 09 2012	0.042806	0.020	-29.0	-1.8	0.2
TL-34-2	Mar 09 2012	0.042813	0.020	-28.8	-1.6	0.2
TL-34-3	Mar 09 2012	0.042756	0.021	-30.2	-2.9	0.2
<b>Mean (n=3)</b>					<b>-2.1</b>	
<i>Stddev</i>					0.7	
<b>TR-W-1 (pyrrhotite)</b>					<b>-2.6*</b>	
TR-W-1	June 17 2013	0.043290	0.021	-17.4	-2.4	0.2
TR-W-1	June 18 2013				-2.4	0.2
<b>Mean (n=2)</b>					<b>-2.4</b>	
<i>Stddev</i>					0.003	
<b>ARSPY 57 (arsenopyrite)</b>					<b>2.8*</b>	
Arsby 57-1	Feb 16 2012	0.043644	0.024	-14.6	2.7	0.2
Arsby 57-2	Feb 16 2012	0.043647	0.023	-14.5	2.8	0.2
Arsby 57-3	Feb 16 2012	0.043659	0.024	-14.3	3.1	0.2
Arsby 57-1	Feb 17 2012	0.043644	0.023	-14.6	2.8	0.2

**Table A4-1. (cont.)**

In-house standard Name	Measuring date	$^{34}\text{S}/^{32}\text{S}_{\text{measured}}$	SEM [%]	IMF <sub>calculated</sub> [‰ VCDT]	$\delta^{34}\text{S}_{\text{corrected}}$ [‰ VCDT]	SEM [1σ]
Arspy 57-2	Feb 17 2012	0.043654	0.028	-14.4	3.1	0.3
Arspy 57-5	Feb 17 2012	0.043638	0.021	-14.7	2.7	0.2
Arspy 57-3	Feb 20 2012	0.043667	0.018	-14.1	2.9	0.2
Arspy 57-5	Feb 20 2012	0.043642	0.019	-14.7	2.3	0.2
Arspy 57-6	Feb 20 2012	0.043689	0.019	-13.6	3.4	0.2
Arspy 57-1N	Feb 21 2012	0.043657	0.021	-14.3	3.0	0.2
Arspy 57-2	Feb 21 2012	0.043635	0.025	-14.8	2.5	0.2
Arspy 57-3	Feb 21 2012	0.043659	0.026	-14.3	3.1	0.3
Arspy 57-3	Feb 23 2012	0.043596	0.024	-15.7	3.3	0.2
Arspy 57-4	Feb 23 2012	0.043602	0.016	-15.6	3.4	0.2
Arspy 57-5	Feb 23 2012	0.043567	0.026	-16.4	2.6	0.3
Arspy 57-6	Feb 23 2012	0.043550	0.023	-16.8	2.2	0.2
Arspy 57-1	Feb 24 2012	0.043551	0.019	-16.7	2.7	0.2
Arspy 57-2	Feb 24 2012	0.043548	0.019	-16.8	2.7	0.2
Arspy 57-3	Feb 24 2012	0.043572	0.021	-16.3	3.2	0.2
Arspy 57-4	Feb 24 2012	0.043560	0.020	-16.5	2.9	0.2
Arspy 57-2	Mar 14 2012	0.043014	0.023	-29.2	2.9	0.2
Arspy 57-3	Mar 14 2012	0.043028	0.023	-28.8	3.2	0.2
Arspy 57-4	Mar 14 2012	0.043036	0.026	-28.6	3.4	0.3
Arspy 57-3	Mar 01 2013	0.043428	0.021	-19.6	2.5	0.2
Arspy 57-4	Mar 01 2013	0.043422	0.023	-19.7	2.4	0.2
Arspy 57-2	Mar 07 2013	0.043373	0.026	-20.8	2.8	0.3
Arspy 57-4	Mar 07 2013	0.043383	0.020	-20.6	3.0	0.2
Arspy 57-5	Mar 07 2013	0.043385	0.022	-20.6	3.1	0.2
Arspy 57-3	Sept 30 2013	0.043713	0.023	-13.0	2.3	0.2
Arspy 57-4	Sept 30 2013	0.043733	0.018	-12.6	2.7	0.2
Arspy 57-5	Sept 30 2013	0.043745	0.021	-12.3	3.0	0.2
<b>Mean (n=31)</b>					<b>2.9</b>	
<i>Stddev</i>					<i>0.3</i>	
<b>HT10-4A (galena)</b>					<b>14.2*</b>	
HT10-4A-2	Mar 03 2012	0.043246	0.022	-35.1	14.1	0.2
HT10-4A-4	Mar 03 2012	0.043237	0.028	-35.3	13.9	0.3
HT10-4A-1	Mar 04 2012	0.043275	0.020	-34.4	14.8	0.2
HT10-4A-2	Mar 04 2012	0.043240	0.021	-35.2	14.0	0.2
HT10-4A-3	Mar 04 2012	0.043246	0.026	-35.1	14.1	0.3
HT10-4A-1	Mar 06 2012	0.043258	0.031	-34.8	14.2	0.3
HT10-4A-2	Mar 06 2012	0.043271	0.020	-34.5	14.5	0.2
HT10-4A-5	Mar 06 2012	0.043260	0.025	-34.7	14.2	0.3
HT10-4A-3	Mar 08 2012	0.043089	0.023	-38.7	14.1	0.2
HT10-4A-4	Mar 08 2012	0.043124	0.018	-37.9	14.9	0.2
HT10-4A-6	Mar 08 2012	0.043091	0.020	-38.7	14.2	0.2
HT10-4A-2	Mar 08 2013	0.043335	0.021	-33.0	14.6	0.2
HT10-4A-3	Mar 08 2013	0.043314	0.025	-33.5	14.1	0.2
HT10-4A-4	Mar 08 2013	0.043313	0.023	-33.5	14.1	0.2
HT10-4A-1	Sept 13 2013	0.043056	0.039	-39.5	14.2	0.4
HT10-4A-2	Sept 13 2013	0.043039	0.039	-39.9	13.9	0.4
HT10-4A-3	Sept 13 2013	0.043065	0.030	-39.3	14.5	0.3
HT10-4A-4	Sept 13 2013	0.043069	0.030	-39.2	14.5	0.3
<b>Mean (n=18)</b>					<b>14.2</b>	
<i>Stddev</i>					<i>0.3</i>	

Calculation of instrumental mass fractionation (IMF):  $IMF(\text{‰VCDT}) = 1000 \times \ln \left( \frac{^{34}\text{S}/^{32}\text{S}_{\text{measured}}}{^{34}\text{S}/^{32}\text{S}_{\text{in-house}}} \right)$

In-house standard	Formula	$^{34}\text{S}/^{32}\text{S}_{\text{in-house}}$
UL9	$1.0158 \cdot ^{34}\text{S}/^{32}\text{S}_{\text{VCDT}}$	0.044860
KH87	$1.0002 \cdot ^{34}\text{S}/^{32}\text{S}_{\text{VCDT}}$	0.044171
USGS Norilsk	$1.0083 \cdot ^{34}\text{S}/^{32}\text{S}_{\text{VCDT}}$	0.044529
Po W1	$1.0023 \cdot ^{34}\text{S}/^{32}\text{S}_{\text{VCDT}}$	0.044264
TL-34	$0.9978 \cdot ^{34}\text{S}/^{32}\text{S}_{\text{VCDT}}$	0.044065
TR-1	$0.9974 \cdot ^{34}\text{S}/^{32}\text{S}_{\text{VCDT}}$	0.044048
Arspy57	$1.0028 \cdot ^{34}\text{S}/^{32}\text{S}_{\text{VCDT}}$	0.044286
HT10-4A	$1.0142 \cdot ^{34}\text{S}/^{32}\text{S}_{\text{VCDT}}$	0.044790

---

$^{34}\text{S}/^{32}\text{S}_{\text{VCDT}} = 0.0441626$  (Ding et al., 2001)

## Reference

Ding T, Valkiers S, Kipphardt H, De Bièvre P, Taylor PDP, Gonfiantini R, Krouse R (2001) Calibrated sulfur isotope abundance ratios of three IAEA sulfur isotope reference materials and V-CDT with a reassessment of the atomic weight of sulfur. *Geochimica et Cosmochimica Acta* 65:2433-2437



## APPENDIX A4-4 RESULTS OF SULFUR ISOTOPE ANALYSES ON SULFIDES FROM THE MING DEPOSIT

**Table A4-2.** Analyzed samples from the Ming deposit, their brief description, sulfide mineralogy, and results of S isotope analysis

Sample No.	Mineral	Ore Body	Drill core#	Description	Mineralogy	Point	Area	$\delta^{34}\text{S}$ [‰ VCDT]	1 $\sigma$
<b>Silicified Horizon</b>									
29914	Pyrite	1806 Zone	RMUG08-150	Fine Ccp-Py stringer in silicified horizon (massive Qz)	<u>Py</u> >> Ccp >> Apy > Gn $\approx$ Sp > Ag Ttr $\approx$ Tnt > Ttr $\approx$ Po	Py-2		9.0	0.2
	Pyrite					Py-3		11.2	0.2
	Pyrite					Py-4		9.6	0.2
	Chalcopyrite					Ccp-2		9.6	0.2
	Chalcopyrite					Ccp-3		10.7	0.2
	Chalcopyrite					Ccp-4		10.2	0.2
	Chalcopyrite					Ccp-5		9.9	0.2
	Pyrrhotite					Po-3		13.9	0.3
	Arsenopyrite					Apy-2		8.4	0.2
	Arsenopyrite					Apy-5	rim a	10.0	0.2
	Arsenopyrite					Apy-5	rim b	9.6	0.2
	Arsenopyrite					Apy-5	core	11.5	0.2
	Galena					Gn-5		9.4	0.2
29783	Pyrite		RMUG08-140	Ccp-Py-El stringer in massive quartz [high-grade ore]	<u>Ccp</u> > <u>Py</u> > <u>Po</u> > <u>Sp</u> > Apy > El > Ag Ccp > Mia $\approx$ NiSbS phase	Py-2N		13.6	0.2
	Pyrite					Py-3N		16.6	0.2
	Pyrite					Py-3bN		17.6	0.2
	Chalcopyrite					Ccp-1a		14.8	0.2
	Chalcopyrite					Ccp-1b		16.2	0.2
	Chalcopyrite					Ccp-2		14.8	0.2
	Chalcopyrite					Ccp-3a		15.6	0.2
	Chalcopyrite					Ccp-3b		15.9	0.2
	Pyrrhotite					Po-1a		18.7	0.2
	Pyrrhotite					Po-1b		16.8	0.2
	Pyrrhotite					Po-2		17.0	0.2
	Pyrrhotite					Po-3		19.6	0.2

**Table A4-2 (cont.)**

Sample No.	Mineral	Ore Body	Drill core#	Description	Mineralogy	Point	Area	$\delta^{34}\text{S}$ [‰ VCDT]	1 $\sigma$
29920	Pyrite	1806 Zone	RMUG08-146	Py in thick sulfide stringer on contact silicified horizon—massive sulfide	<u>Py</u> >> Tnt/Ag-Ttr > Ccp $\approx$ Sp $\approx$ Apy > Po $\approx$ Gn > Stn > Col	Py-1		6.4	0.2
	Pyrite					Py-2		5.8	0.2
	Arsenopyrite					Apy-2		6.9	0.2
<b>Semi-massive to Massive Sulfides</b>									
36509	Pyrite	1806 Zone	RMUG08-120	Py-Apy-Ttr with black material in Py-rich massive sulfide	<u>Py</u> > <u>Ttr</u> > <u>AgTtr</u> > <u>Apy</u> >> <u>Sp</u> > Tnt > Gn > Ccp > El > unknown Ag phase	Py-1		7.0	0.2
	Pyrite					Py-2a		6.9	0.2
	Pyrite					Py-2b		7.5	0.2
	Pyrite					Py-3		7.7	0.2
	Chalcopyrite					Ccp-1a		8.5	0.2
	Chalcopyrite					Ccp-1b		7.3	0.2
	Chalcopyrite					Ccp-3a		7.3	0.2
	Chalcopyrite					Ccp-3b		6.8	0.2
	Arsenopyrite					Apy-1		7.9	0.2
	Arsenopyrite					Apy-2		7.5	0.2
	Arsenopyrite					Apy-3	rim a	8.3	0.2
	Arsenopyrite					Apy-3	rim b	7.3	0.2
	Arsenopyrite					Apy-3	rim b2	6.9	0.2
	Arsenopyrite					Apy-3	core	7.0	0.2
	Galena					Gn-1a		1.4	0.2
	Galena					Gn-1b		8.2	0.2
	Galena					Gn-1c		0.8	0.2
	Galena					Gn-1d		2.8	0.2
	Galena					Gn-3a		4.7	0.2
	Galena					Gn-3b1		4.6	0.2
	Galena					Gn-3b2		2.6	0.2
	Galena					Gn-3c		5.5	0.3

**Table A4-2 (cont.)**

Sample No.	Mineral	Ore Body	Drill core#	Description	Mineralogy	Point	Area	$\delta^{34}\text{S}$ [‰ VCDT]	1 $\sigma$
36512	Pyrite	1806 Zone	RMUG08-123	Sp-Gn rich massive sulfide; EI-bearing	<u>Sp <math>\approx</math> Gn &gt; Py</u> >> Ccp $\approx$ Apy > Stn > Mia > Pyr > Hg Stp > AgCuFeS > AgTtr > EI	Py-1a		6.4	0.2
	Pyrite					Py-1b		6.2	0.2
	Pyrite					Py-2		7.0	0.2
	Pyrite					Py-3a		6.0	0.3
	Pyrite					Py-3b		5.4	0.2
	Chalcopyrite					Ccp-1aN		6.8	0.2
	Chalcopyrite					Ccp-1b		6.3	0.2
	Chalcopyrite					Ccp-1a		7.3	0.4
	Galena					Gn-1b		3.3	0.2
	Galena					Gn-2		2.5	0.2
	Galena					Gn-3		4.3	0.2
	Pyrite					Py-1		7.1	0.2
36514	Pyrite	1806 Zone	RMUG08-123	Py-sTtr-Gn in massive sulfide; EI-bearing	<u>Py &gt; Gn</u> >> Ttr $\approx$ AgTtr > Sp $\approx$ Tnt $\approx$ Ccp > Apy > EI $\approx$ AgCuFeS	Py-2a		7.2	0.2
	Pyrite					Py-2b		6.5	0.2
	Chalcopyrite					Ccp-1		6.0	0.2
	Chalcopyrite					Ccp-2		5.8	0.2
	Galena					Gn-1		5.1	0.3
	Galena					Gn-2a		4.7	0.2
	Galena					Gn-2b		8.6	0.2
	Galena					Gn-2bN		8.2	0.2
	Pyrite					Py-3aN		10.0	0.1
29913	Pyrite	1806 Zone	RMUG08-124	Ccp-Py stringer in Rambler rhyolite at end of semi-massive zone; EI-bearing	<u>Ccp &gt; Py</u> > Po >> Sp > Apy > Gn > EI > Mia > Men	Py-3bN		8.4	0.1
	Pyrite					Py-4N		8.8	0.2
	Chalcopyrite					Ccp-1a		11.5	0.2
	Chalcopyrite					Ccp-1b		9.2	0.2
	Chalcopyrite					Ccp-2		8.9	0.2
	Chalcopyrite					Ccp-3		9.4	0.2
	Pyrrhotite					Po-1		9.8	0.2

Table A4-2 (cont.)

Sample No.	Mineral	Ore Body	Drill core#	Description	Mineralogy	Point	Area	$\delta^{34}\text{S} [\text{‰} \text{VCDT}]$	1 $\sigma$	
29913	Pyrrhotite	1806 Zone	RMUG08-124			Po-2		10.3	0.2	
	Pyrrhotite					Po-3		10.2	0.2	
	Galena					Gn-1		6.2	0.2	
	Galena					Gn-2		3.2	0.2	
29787	Galena		RMUG08-141	Semi-massive sulfide	Py $\approx$ Ccp >> Po > Sp >> Apy $\approx$ Gn > AgTtr >> AgHg alloy $\approx$ unknown AsPbFeS phase	Gn-3		5.2	0.2	
	Pyrite					Py-1N		9.4	0.2	
	Pyrite					Py-2N		10.2	0.2	
	Pyrite					Py-3N		9.8	0.2	
	Pyrite					Py-4N	rim a	10.1	0.1	
	Pyrite					Py-4N	rim b	9.6	0.1	
	Pyrite					Py-4N	core	9.2	0.2	
	Chalcopyrite					Ccp-1bN		9.5	0.2	
	Chalcopyrite					Ccp-1N		9.2	0.2	
Chalcopyrite	Ccp-2a		9.7	0.2						
Chalcopyrite	Ccp-2b		8.7	0.2						
Chalcopyrite	Ccp-3		9.4	0.2						
Chalcopyrite	Ccp-4		9.2	0.2						
Chalcopyrite	Ccp-5		9.0	0.2						
Pyrrhotite	Po-1		8.2	0.2						
Pyrrhotite	Po-4		7.4	0.2						
Pyrrhotite	Po-5		7.2	0.2						
Arsenopyrite	Apy-2		8.2	0.2						
Arsenopyrite	Apy-3		9.0	0.2						
Arsenopyrite	Apy-3R		9.6	0.2						
Arsenopyrite	Apy-5		9.4	0.2						
Galena	Gn-4a		15.2	0.2						
Galena	Gn-4b		6.0	0.2						
Galena	Gn-5a		3.0	0.2						
Galena	Gn-5b		5.1	0.2						

**Table A4-2 (cont.)**

Sample No.	Mineral	Ore Body	Drill core#	Description	Mineralogy	Point	Area	$\delta^{34}\text{S} [\text{‰ VCDT}]$	1 $\sigma$
29778	Pyrite	1806 Zone	RMUG08-142	Massive Py-Ccp sulfide ; El-bearing	<u>Py</u> > <u>Ccp</u> > Apy $\approx$ Sp > AgTnt-Ttr $\approx$ Gn > AgHg±Au alloy > El $\approx$ Po	Py-1c		5.2	0.2
	Pyrite					Py-2a		8.1	0.2
	Pyrite					Py-2b		5.9	0.2
	Pyrite					Py-3a		6.9	0.2
	Pyrite					Py-3b		8.5	0.2
	Pyrite					Py-4a		6.4	0.3
	Chalcopyrite					Ccp-1		6.7	0.2
	Chalcopyrite					Ccp-2		6.2	0.2
	Chalcopyrite					Ccp-3		5.6	0.2
	Chalcopyrite					Ccp-4		7.1	0.2
	Arsenopyrite					Apy-1a		6.7	0.2
	Arsenopyrite					Apy-1b		7.0	0.2
	Arsenopyrite					Apy-2		8.3	0.2
	Arsenopyrite					Apy-1bN		6.7	0.2
	Arsenopyrite					Apy-3		6.7	0.2
	Arsenopyrite					Apy-4		7.1	0.2
36520	Arsenopyrite		RMUG08-142	Grainy pyritic semi-massive sulfide; El-bearing	<u>Py</u> > <u>Sp</u> >> Ccp $\approx$ Gn > Apy > unknown Ag-phase $\approx$ AgHg > El > unknown AgSbS phase $\approx$ Stn $\approx$ Cass	Gn-4b		10.3	0.2
	Galena								
	Pyrite					Py-1a		6.9	0.2
	Pyrite								
	Pyrite					Py-2b		7.2	0.3
	Pyrite					Py-3aN		7.6	0.2
	Pyrite					Py-3b		7.5	0.2
	Pyrite					Py-4aN		8.4	0.2
	Pyrite					Py-4bN-1		7.5	0.2
	Pyrite					Py-4bN		7.7	0.2
	Pyrite					Py-4cN		9.3	0.2
	Pyrite					Py-5aN		9.3	0.2
	Pyrite					Py-5bN		8.3	0.2
	Pyrite								
	Pyrite								
	Pyrite								

**Table A4-2 (cont.)**

Sample No.	Mineral	Ore Body	Drill core#	Description	Mineralogy	Point	Area	$\delta^{34}\text{S} [\text{‰ VCDT}]$	1 $\sigma$
36505	Pyrite	1806 Zone	RMUG08-138	Sp-Py-rich massive sulfide with Gn-Apy-sulfosalts; El-bearing	<b>Sp &gt; Py</b> >> Ccp $\approx$ AgTnt-Ttr > Apy $\approx$ Gn > El > AgCuFeS $\approx$ unknown Ag-phase $\approx$ Lo	Py-1a		6.7	0.2
	Pyrite					Py-1a		6.9	0.3
	Pyrite					Py-1b		6.8	0.3
	Pyrite					Py-2		7.6	0.2
	Pyrite					Py-3		6.6	0.2
	Chalcopyrite					Ccp-1b		5.9	0.2
	Chalcopyrite					Ccp-2		7.3	0.2
	Chalcopyrite					Ccp-3		7.7	0.2
	Arsenopyrite					Apy-1a		7.0	0.3
	Arsenopyrite					Apy-1b		6.8	0.2
	Arsenopyrite					Apy-2a		8.7	0.3
	Arsenopyrite					Apy-2b		7.9	0.2
	Arsenopyrite					Apy-3		8.2	0.2
	Arsenopyrite					Gn-2		7.7	0.2
	Galena					Gn-3a		4.4	0.2
29907	Galena		RMUG08-145	Py in massive sulfide	<b>Py</b> >> <b>Ccp</b> > Sp > Apy >> Gn $\geq$ Ttr > AgTtr > Po > Men	Gn-3b		5.2	0.2
	Galena					Gn-3c		3.1	0.2
	Pyrite					Py-1		4.6	0.2
	Pyrite					Py-2		8.7	0.2
	Chalcopyrite					Ccp-1		6.1	0.2
	Chalcopyrite					Ccp-2		5.6	0.2
	Arsenopyrite					Apy-1		7.3	0.2
	Arsenopyrite					Apy-2		7.8	0.2
	Pyrite					Py-1		5.6	0.2
	Pyrite					Py-2		6.0	0.3
29918	Chalcopyrite		RMUG08-146	Thick Py-Sp stringer in semi-massive sulfide	<b>Ccp</b> > <b>Po</b> $\approx$ <b>Py</b> > <b>Mag</b> > <b>Sp</b> >> Cass $\approx$ Gn > Mol > Chr	Ccp-1		5.3	0.2
	Pyrrhotite					Po-1		4.9	0.4
	Pyrrhotite					Po-2		5.7	0.2
	Pyrrhotite					Po-3		4.4	0.2
	Pyrrhotite								

**Table A4-2 (cont.)**

Sample No.	Mineral	Ore Body	Drill core#	Description	Mineralogy	Point	Area	$\delta^{34}\text{S}$ [‰ VCDT]	1 $\sigma$
29934	Pyrite	1806 Zone	RMUG08-159	Py-Ccp semi-massive sulfide; El-bearing	<u>Py</u> >> <u>Ccp</u> > Sp > Gn $\approx$ Apy > AgTtr >> El	Py-1		8.1	0.2
	Pyrite					Py-2		7.8	0.3
	Chalcopyrite					Ccp-1		6.1	0.2
	Chalcopyrite					Ccp-2		6.8	0.2
	Arsenopyrite					Apy-1		9.3	0.2
	Arsenopyrite					Apy-2	rim	7.7	0.2
29948	Arsenopyrite	1807 Zone	RM07-19	Massive Py-Ccp sulfide	<u>Py</u> >> <u>Ccp</u> > Sp $\approx$ Po > Fe±Ti ox > Gn ss with BiTe $\approx$ Apy > Ttr > AgTtr > Gud $\approx$ Alt $\approx$ Men $\approx$ Cbn	Apy-2	core	8.4	0.3
	Pyrite					Py-1		8.3	0.2
	Pyrite					Py-2		6.5	0.1
	Chalcopyrite					Ccp-1		8.6	0.2
35552	Chalcopyrite		RM07-19c	Massive Py-Ccp sulfide; El-bearing	<u>Py</u> > <u>Ccp</u> >> Sp > Apy $\approx$ Ti ox $\approx$ FeTi ox > Gn > Po $\approx$ El	Ccp-2		8.1	0.2
	Chalcopyrite					Ccp-1		7.3	0.3
	Chalcopyrite					Ccp-2		7.4	0.2
35559	Pyrite		RM07-18a	Massive Py-Ccp sulfide; El-bearing	<u>Py</u> $\approx$ <u>Ccp</u> >> Sp > Gn ss > Apy > Tnt-Ttr > El > Mag > Lo	Py1		7.7	0.3
	Pyrite					Ccp-2		7.7	0.3
35563	Pyrite	Galena	RM07-18b	Massive Py-Ccp sulfide with Sp-Apy	<u>Py</u> > <u>Ccp</u> > Po > Sp > Gn ss with BiTe $\approx$ Apy >> Mag > Gud > NiSb phase	Py2		8.0	0.2
	Chalcopyrite					Ccp-3		7.5	0.2
	Chalcopyrite					Ccp-4		6.2	0.2
	Chalcopyrite					Ccp-5		7.5	0.2
	Arsenopyrite					Apy-1		6.8	0.2
	Arsenopyrite					Apy-2		6.0	0.2
	Arsenopyrite					Apy-3		3.2	0.2
	Arsenopyrite					Apy-4		6.8	0.2
	Galena					Gn1		17.3	0.3
	Pyrite					Py1		7.8	0.3
	Pyrite					Py2		9.6	0.2

**Table A4-2 (cont.)**

Sample No.	Mineral	Ore Body	Drill core#	Description	Mineralogy	Point	Area	$\delta^{34}\text{S} [\text{‰ VCDT}]$	1 $\sigma$
35563	Pyrite	1807 Zone	RM07-18b			Py3		9.7	0.2
	Chalcopyrite					Ccp-1		7.8	0.2
	Chalcopyrite					Ccp-2		7.5	0.2
	Chalcopyrite					Ccp-3		8.0	0.2
	Pyrrotite					Po-1		5.4	0.2
	Pyrrotite					Po-2		5.7	0.2
	Pyrrotite					Po-3		6.1	0.2
	Pyrrotite					Po-4		6.8	0.2
	Pyrrotite					Po-5		6.2	0.3
	Arsenopyrite					Apy-1		8.0	0.2
	Arsenopyrite					Apy-2		5.8	0.2
	Arsenopyrite					Apy-3		7.3	0.2
	Pyrite					Py-1		8.3	0.3
35584	Pyrite		RM07-20c	Massive Ccp-Py-Po sulfide; EI-bearing	<u>Ccp &gt; Py &gt; Po &gt; Sp &gt;&gt; Gn ss with BiTe &gt; Hess &gt; Ti ox &gt; El</u>	Py-2		8.3	0.2
	Pyrite					Py-3		8.0	0.2
	Chalcopyrite					Ccp-1		8.8	0.2
	Chalcopyrite					Ccp-2		9.6	0.2
	Pyrrotite					Po-1		5.9	0.2
	Pyrrotite					Po-2		5.4	0.3
	Pyrrotite					Po-3		5.3	0.2
	Arsenopyrite					Apy-1		7.2	0.2
	Pyrite					Py-2		7.9	0.2
	Chalcopyrite					Ccp-1		7.4	0.3
	Chalcopyrite					Ccp-2		9.6	0.2
	Chalcopyrite					Ccp-3		8.4	0.2
	Pyrrotite					Po-1		6.2	0.2
	Pyrrotite					Po-2		6.5	0.2
	Galena					Gn-1		2.2	0.3
35590			RM07-20e	Massive Py sulfide with fine Sp-Ccp bands and small Py cubes	<u>Py &gt; Ccp</u> > Sp > Po > Apy $\approx$ Mag > Gn ss with BiTe > Hess > NiSb phase $\approx$ Tnt				



**Table A4-2 (cont.)**

Sample No.	Mineral	Ore Body	Drill core#	Description	Mineralogy	Point	Area	$\delta^{34}\text{S}$ [‰ VCDT]	1 $\sigma$
36007	Pyrite	1807 Zone	RM07-20h	Massive Ccp-Py sulfide; El-bearing	<u>Ccp &gt; Py</u> > Sp > Po > Cbn > Apy > Gn ss with BiTe > Mag $\approx$ Hess $\approx$ NiSb phase $\approx$ AgTtr > Men $\approx$ El	Py-1		5.6	0.2
	Pyrite					Py-2		4.3	0.3
	Pyrite					Py-3		4.5	0.2
	Chalcopyrite					Ccp-1		8.6	0.2
	Chalcopyrite					Ccp-2		7.6	0.2
	Pyrrhotite					Po-1		5.2	0.3
	Pyrrhotite					Po-2		5.0	0.2
	Arsenopyrite					Apy-3		6.1	0.2
	Arsenopyrite					Apy-4		6.0	0.2
	Galena					Gn-1		4.5	0.2
62107	Chalcopyrite	Ming South Up Plunge	RMUG08-60	Massive Ccp-Py sulfide with Po and Mag; Po partly replacing Py; El-bearing	<u>Ccp &gt; Po</u> >> Sp >> Py $\approx$ Allo > Claus > Gn > PbTe $\approx$ Men > AgTe > BiTe $\approx$ NiSb phase > AgHg > HgTe $\approx$ El $\approx$ Mol $\approx$ Cass	Ccp1		6.9	0.4
	Chalcopyrite					Ccp2		8.5	0.3
	Pyrrhotite					Ccp3		7.6	0.3
	Pyrrhotite					Po-1		6.7	0.2
	Pyrrhotite					Po-2		6.7	0.2
62119	Pyrite		RMUG08-61	Massive Py-Ccp-Po sulfide; El-bearing	<u>Py &gt; Ccp &gt; Po</u> >> Sp > Gn > BiTe > Hess $\approx$ NiSb phase > Col $\approx$ El	Po-3		6.5	0.3
	Pyrite					Py-1		6.1	0.2
	Pyrrhotite					Po-1		5.9	0.2
29789	Pyrrhotite	Ming South Down Plunge	RM06-04e	Massive Ccp-Po-Py mineralization near Qz-vein in massive sulfide	<u>Ccp &gt; Po</u> > Py > Sp > Gn >> Hess $\approx$ NiSb phase $\approx$ NiSbS phase	Po-2		6.3	0.3
	Chalcopyrite					Ccp2		6.4	0.3
	Pyrite					Py-1		5.3	0.2
	Pyrite					Py-2		6.2	0.3
	Chalcopyrite					Ccp-1		5.2	0.2
	Chalcopyrite					Ccp-2		4.6	0.3

**Table A4-2 (cont.)**

Sample No.	Mineral	Ore Body	Drill core#	Description	Mineralogy	Point	Area	$\delta^{34}\text{S}$ [‰ VCDT]	1 $\sigma$
29789	Pyrrhotite	Ming South down Plunge	RM06-04e			Po-1		5.3	0.3
	Pyrrhotite					Po-2		3.6	0.2
36058	Pyrite		RM06-04m	Massive Py sulfide with minor Ccp	<u>Py</u> >> Gn > Ccp > Sp $\approx$ Apy > Po	Py-1		7.2	0.2
	Pyrite					Py-2		8.2	0.2
	Chalcopyrite					Ccp-1		5.6	0.3
	Chalcopyrite					Ccp-2		5.7	0.3
	Galena					Gn2		16.0	0.2
	Galena					Gn4		16.2	0.2
	Galena					Gn5		6.0	0.3
36163	Pyrite	Ming South Down Plunge	RM06-04d	Massive Ccp-Po-Py sulfide with traces of Apy	<u>Ccp</u> > <u>Po</u> > <u>Sp</u> > <u>Py</u> > Gn > Apy > Gn > AgTr $\approx$ Hess $\approx$ NiSb phase $\approx$ NiSbS phase	Py-1		5.7	0.2
	Pyrite					Py-2		5.1	0.3
	Chalcopyrite					Ccp1		6.0	0.3
	Chalcopyrite					Ccp2		5.2	0.3
	Pyrrhotite					Po-1		3.8	0.2
	Pyrrhotite					Po-2		5.1	0.3
	Arsenopyrite					Apy1		4.9	0.2
	Arsenopyrite					Apy2		4.7	0.2
	Arsenopyrite					Apy3		4.2	0.2
	Galena					Gn1		2.5	0.3
	Galena					Gn2		5.8	0.3
<b>Footwall Mineralization: Sulfide Stringer Horizon</b>									
29902	Pyrite	1806 Zone	RMUG08-121	Py-Ccp stringer in rhyolite flow; El-bearing	<u>Py</u> > <u>Ccp</u> >> <u>Apy</u> > <u>Sp</u> > Gn > Tr > Tnt > AgTr > El	Py-1a		9.0	0.3
	Pyrite					Py-1b		8.4	0.3
	Chalcopyrite					Ccp-1		8.3	0.2
	Chalcopyrite					Ccp-2		7.7	0.2
	Chalcopyrite					Ccp-3		8.9	0.2
	Chalcopyrite					Ccp-3b		7.5	0.2
	Chalcopyrite					Ccp-4		6.4	0.2
	Chalcopyrite					Ccp-5		7.1	0.2

**Table A4-2 (cont.)**

Sample No.	Mineral	Ore Body	Drill core#	Description	Mineralogy	Point	Area	$\delta^{34}\text{S}$ [‰ VCDT]	1 $\sigma$
29902	Arsenopyrite	1806 Zone	RMUG08-121			Apy-2		7.9	0.2
	Arsenopyrite					Apy-4		7.3	0.2
	Arsenopyrite					Apy-5		7.8	0.2
	Galena					Gn-4		7.6	0.2
62017	Pyrite	Ming South Up Plunge	RMUG08-104	Sp-Py stringer in green mica-enriched rhyolite on top of massive sulfide	<b>Sp &gt; Py</b> >> Gn > Ccp > Po > Apy	Py-2		9.7	0.2
	Pyrite					Py-3		10.5	0.2
	Chalcopyrite					Ccp1		9.4	0.3
	Chalcopyrite					Ccp2		8.1	0.3
62018	Galena	Ming South Up Plunge	RMUG08-64	Ccp-Py stringer in rhyolitic tuff to lapilli tuff; El-bearing	<b>Py &gt; Ccp &gt; Po</b> > Sp > Apy > Gn > El $\approx$ Mol	Gn1		16.2	0.3
	Galena					Gn2		17.1	0.3
	Pyrite					Py-2		10.7	0.2
	Pyrite					Py-3		10.8	0.2
62033	Chalcopyrite	Ming South Up Plunge	RMUG08-98	Py-Ccp stringer in rhyolitic Qz-eye lapilli tuff; El-bearing	<b>Ccp &gt; Py &gt; Po &gt; Sp</b> > Hess > Ti ox > BiTe $\approx$ Gn $\approx$ El	Ccp1		11.2	0.3
	Chalcopyrite					Ccp2		10.6	0.3
	Pyrrhotite					Po-1		9.9	0.2
	Pyrrhotite					Po-2		10.0	0.2
62044	Pyrite	Ming South Up Plunge	RMUG08-95	Ccp-Py-Po stringer in rhyolitic Qz-eye lapilli tuff; El-bearing	<b>Ccp &gt; Py <math>\approx</math> Po &gt; Sp</b> > Gn > Apy > Men > Hess $\approx$ Alt $\approx$ El	Py-1		10.6	0.2
	Pyrite					Py-2		11.0	0.2
	Chalcopyrite					Ccp1		9.6	0.3
	Chalcopyrite					Ccp2		10.3	0.3
62044	Chalcopyrite	Ming South Up Plunge	RMUG08-95	Ccp-Py-Po stringer in rhyolitic Qz-eye lapilli tuff; El-bearing	<b>Ccp &gt; Py <math>\approx</math> Po &gt; Sp</b> > Gn > Apy > Men > Hess $\approx$ Alt $\approx$ El	Ccp3		10.5	0.3
	Pyrrhotite					Po-1		9.4	0.2
	Pyrrhotite					Po-2		9.2	0.2
	Pyrite					Py-1		9.9	0.3
62044	Pyrite	Ming South Up Plunge	RMUG08-95	Ccp-Py-Po stringer in rhyolitic Qz-eye lapilli tuff; El-bearing	<b>Ccp &gt; Py <math>\approx</math> Po &gt; Sp</b> > Gn > Apy > Men > Hess $\approx$ Alt $\approx$ El	Py-2		10.1	0.2
	Chalcopyrite					Ccp2		9.1	0.3
	Pyrrhotite					Po-2		8.8	0.2

**Table A4-2 (cont.)**

Sample No.	Mineral	Ore Body	Drill core#	Description	Mineralogy	Point	Area	$\delta^{34}\text{S} [\text{‰ VCDT}]$	1 $\sigma$
36067	Pyrite	Ming South Down Plunge	RM06-04m	Ccp-Py-Po stringer in rhyolitic Qz-eye flow	<u>Py &gt; Ccp &gt; Po</u> > Sp > FeTi ox > Apy $\approx$ Gn $\approx$ BiTe $\approx$ Hess $\approx$ El	Py-1		10.0	0.2
	Pyrite					Py-2		12.0	0.3
	Pyrite					Py-3		11.2	0.2
	Chalcopyrite					Ccp-1		9.8	0.3
	Chalcopyrite					Ccp-2		10.4	0.2
	Pyrrhotite					Po-1		10.4	0.3
29797	Pyrrhotite					Po-2		10.0	0.2
<b>Footwall Mineralization: Lower Footwall Zone</b>									
29797	Pyrite	Lower Footwall Zone	RM06-04e	Ccp-Po-Py sulfide stringers; El-bearing	<u>Ccp &gt; Po <math>\approx</math> Py</u> > Cbn >> FeTi ox > Sp > Gn $\approx$ BiTe > Hess > El $\approx$ Allo	Py-1		9.5	0.2
	Pyrite					Py-2		10.2	0.2
	Pyrite					Py-3		9.4	0.2
	Chalcopyrite					Ccp-1		9.4	0.2
	Chalcopyrite					Ccp-2		9.0	0.4
	Pyrrhotite					Po-1		9.5	0.3
29800	Chalcopyrite			Ccp-Po-Py sulfide stringer	<u>Ccp &gt; Po</u> > Cbn >> FeTi ox > Sp > Py > BiTe > Hess > Gn > Alt	Ccp-1		6.9	0.3
	Chalcopyrite								
	Chalcopyrite					Ccp-2		6.9	0.4
	Chalcopyrite					Ccp-3		7.0	0.3
	Pyrrhotite					Po-1		6.6	0.3
	Pyrrhotite					Po-2		6.4	0.2
36082	Pyrite		RM06-04m	Coarse Mag with Ccp-Py-Po stringer	<u>Fe ox &gt; Ccp &gt; Po <math>\approx</math> Py</u> > Cbn > Sp > BiTe	Py-1		9.9	0.2
	Pyrite					Py-2		10.7	0.2
	Chalcopyrite					Ccp-1		8.5	0.2
	Chalcopyrite					Ccp-2		7.9	0.2
	Pyrrhotite					Po-1		8.6	0.2
	Pyrrhotite					Po-2		9.0	0.2

**Table A4-2 (cont.)**

Sample No.	Mineral	Ore Body	Drill core#	Description	Mineralogy	Point	Area	$\delta^{34}\text{S}$ [‰ VCDT]	1 $\sigma$
36091	Pyrite	Lower Footwall Zone		Ccp-Py-Po stringer with Mag; El-bearing	<u>Ccp &gt; Py <math>\approx</math> Po</u> > Fe ox > Sp > Apy > BiTe $\approx$ Hess > El	Py-1		9.0	0.3
	Pyrite					Py-2		9.8	0.2
	Chalcopyrite					Ccp1		8.7	0.3
	Chalcopyrite					Ccp2		9.0	0.3
	Chalcopyrite					Ccp3		8.5	0.3
	Pyrrhotite					Po-1		8.1	0.2
	Pyrrhotite					Po-2		8.5	0.3
36137	Chalcopyrite			Ccp-Po stringer	<u>Ccp &gt; Po &gt; Cbn</u> > Sp $\approx$ FeTi ox > BiTe $\approx$ Hess $\approx$ Claus > Scheel	Ccp2 Ccp3 Po-1 Po-2		9.5 9.2 8.8 8.9	0.3 0.4 0.2 0.3
<b>Fe oxide sample</b>									
62133	Pyrite	Ming South Up Plunge	RMUG08-91	Rambler rhyolite with fine FeOx schlieren	<u>Fe ox</u> >> Py $\approx$ Po > Ccp > Sp	Py-1		6.2	0.2
	Pyrite					Py-2		8.3	0.2
	Pyrite					Py-3		5.9	0.2
	Pyrrhotite					Po-1		4.6	0.2
<b>Quartz vein in mafic dyke</b>									
36113	Pyrite	Lower Footwall Zone		Coarse Py-Ccp mineralization in Qz vein in mafic dyke	<u>Ccp &gt; Py</u> >> Sp	Py-1		6.6	0.3
	Pyrite					Py-2		6.0	0.3
	Chalcopyrite					Ccp1		5.6	0.4
	Chalcopyrite					Ccp2		5.8	0.4

**Mineral abbreviations:** AgCcp – Ag-bearing chalcopyrite, AgCuFeS – unnamed AgCuFeS phase, AgHg±Au – Ag-Hg±Au alloy, AgSbS phase – miargyrite, pyrragrite or stephanite, AgTtr – Ag-enriched tetrahedrite, Allo – allocasite, Alt – altaite, Apy – arsenopyrite, BiTe – tsumoite or unnamed BiTe, Cass – cassiterite, Cbn – cubanite, Ccp – chalcopyrite, Chr – chromite, Claus – clausite, Col – coloradoite, El – electrum, Fe ox – Fe oxide, Gud – gudmundite, FeTi ox – FeTi oxide (ilmenite), Gn – galena, Gn ss – galena solid solution (galena with

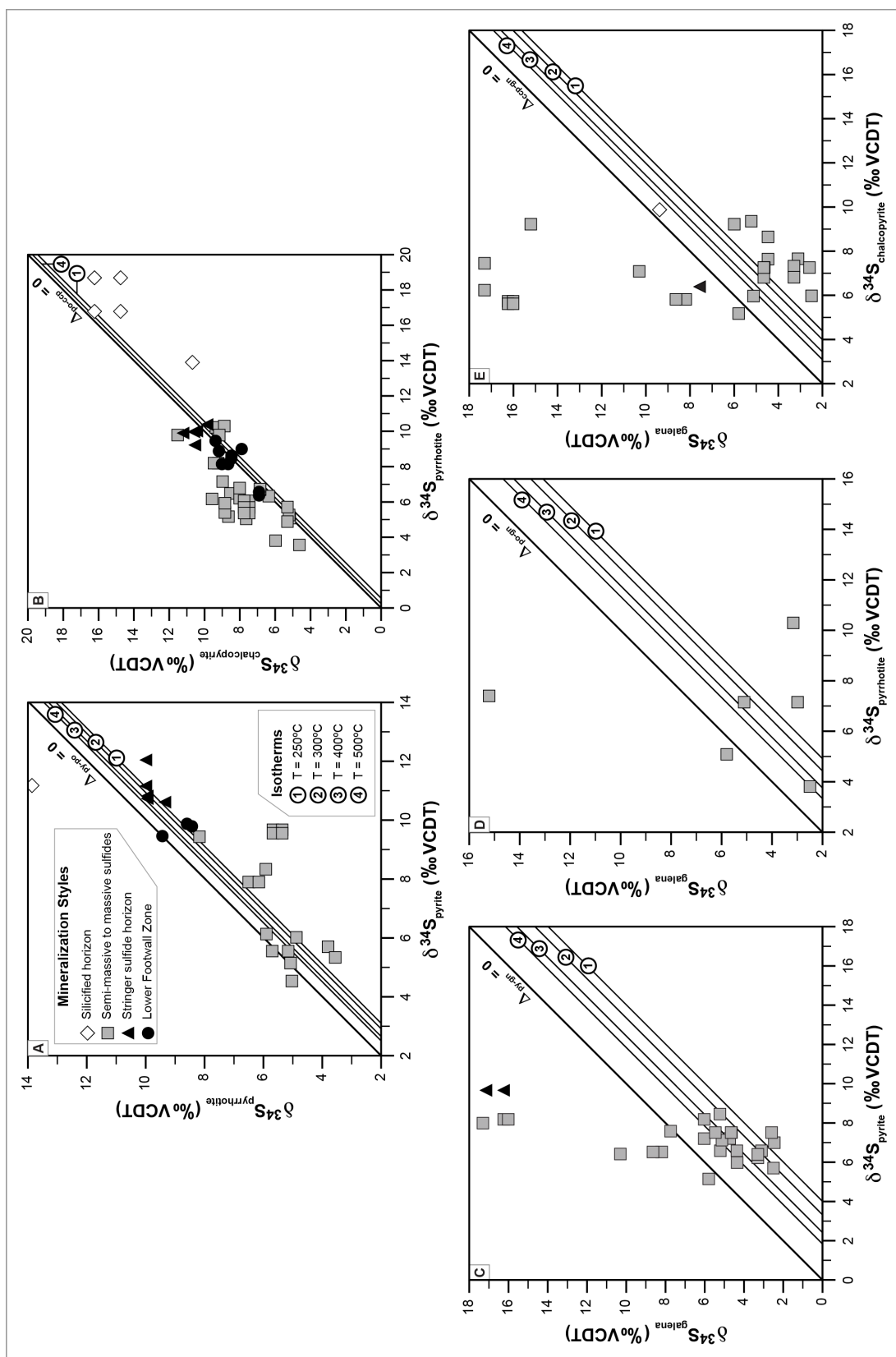
traces of AgTe, BiTe, PbTe and/or PbSe), Hg-Stp – mercurian stephanite, Hess – hessite, Lo – loellingite, Mag – magnetite, Mia – miargyrite, Men – meneghinite, Mol – molybdenite, NiSb phase – breithauptite or nisbite, NiSbS phase – ullmannite, Po – pyrrhotite, Py – pyrite, Pyr – pyargyrite, Sch – scheelite, Sp – sphalerite, Stn – stannite, Tnt – tennantite, Tnt-Ttr – tennantite-tetrahedrite, Ttr – tetrahedrite, Ti ox – Ti oxide; Mineral abundance: **Major mineral phase (> 10 vol.%)**, **Minor mineral phase (5-10 vol.%)**, Trace/accessory phase (> 5 vol.%)

## APPENDIX A4-5 ISOTOPIC EQUILIBRIUM

Neighbouring mineral pairs from the different mineralization styles are plotted in  $\delta$ - $\delta$  plots to test if isotopic equilibrium was reached during VMS formation and/or later Silurian-Devonian metamorphism. The plots are described in detail by Gregory and Criss (1984) and Gregory et al. (1989).

Isotherms were calculated for temperatures of 250°C-500°C, because this temperature range covers both VMS-forming temperatures for the Ming deposit ( $T \approx 250$ -350°C; Brueckner et al., 2014) and temperature of upper greenschist/lower amphibolite facies metamorphism ( $T \approx 350$ -500°C) that affected the Ming deposit post-genetically (Tuach and Kennedy, 1978). Isotherms are a linear function ( $y=mx+n$ ) of the  $\delta^{34}\text{S}$  values of the two neighbouring mineral pairs; slope  $m$  is +1 and intersection  $n$  with the  $y$ -axis is  $-\Delta_{1-2}$ , because  $\delta_1 - \delta_2 = \Delta_{1-2} \approx \frac{A \times 10^6}{T^2}$  and therefore  $\delta_2 = \delta_1 - \Delta_{1-2}$  (Ohmoto and Goldhaber, 1997);  $T$  is temperature in Kelvin;  $\delta_1$  and  $\delta_2$  is the measured  $\delta^{34}\text{S}$  value of mineral phases 1 and 2, respectively;  $\Delta_{1-2}$  is the difference in isotopic sulfur composition between mineral phases 1 and 2 or the isotopic fractionation between the two minerals; and  $A$  is a constant (Kajiwara and Krouse, 1971).

Neighbouring mineral pairs pyrite-pyrrhotite, pyrrhotite-chalcopryrite, pyrite-galena, pyrrhotite-galena, and chalcopryrite-galena from the different mineralization styles are plotted below (Fig. A4-2). Based on the pattern the mineral pairs show (arrays oblique to the isotherms) and/or the position relative to  $\Delta_{1-2} = 0$  (above  $\Delta_{1-2} = 0$  indicate reverse polarity of fractionation), neighbouring mineral pairs at the Ming deposit did not attain isotopic equilibrium during deposition or later metamorphism.





**Figure A4-2.** (previous page)  $\delta$ - $\delta$  plots for **(A)** neighbouring pyrite-pyrrhotite mineral pairs; **(B)** neighbouring pyrrhotite-chalcopyrite mineral pairs; **(C)** neighbouring pyrite-galena mineral pairs; **(D)** neighbouring pyrrhotite-galena mineral pairs; and **(E)** neighbouring chalcopyrite-galena mineral pairs. The isotopic fractionation between two sulfide phases is a function of temperature and given in Table A4-3 below for the plotted mineral pairs and isotherms.

**Table A4-3.** Isotopic fractionation between plotted mineral pairs for temperatures of 250-500°C. Isotherms and isotopic fractionation are not given for T=300°C and 400°C for pyrite-pyrrhotite mineral pairs, because the fractionation is very small and isotherms plot very close to each other.

Isotherm	Plot Mineral pairs	A	B	C	D	E
		$\delta^{34}\text{S}_{\text{py}} - \delta^{34}\text{S}_{\text{po}}$	$\delta^{34}\text{S}_{\text{po}} - \delta^{34}\text{S}_{\text{ccp}}$	$\delta^{34}\text{S}_{\text{py}} - \delta^{34}\text{S}_{\text{gn}}$	$\delta^{34}\text{S}_{\text{po}} - \delta^{34}\text{S}_{\text{gn}}$	$\delta^{34}\text{S}_{\text{ccp}} - \delta^{34}\text{S}_{\text{gn}}$
1	250°C	$\Delta_{\text{py-po}} = 1.10$	$\Delta_{\text{po-ccp}} = 0.55$	$\Delta_{\text{py-gn}} = 4.02$	$\Delta_{\text{po-gn}} = 2.92$	$\Delta_{\text{ccp-gn}} = 2.38$
2	300°C	$\Delta_{\text{py-po}} = 0.91$		$\Delta_{\text{py-gn}} = 3.35$	$\Delta_{\text{po-gn}} = 2.44$	$\Delta_{\text{ccp-gn}} = 1.98$
3	400°C	$\Delta_{\text{py-po}} = 0.66$		$\Delta_{\text{py-gn}} = 2.43$	$\Delta_{\text{po-gn}} = 1.77$	$\Delta_{\text{ccp-gn}} = 1.44$
4	500°C	$\Delta_{\text{py-po}} = 0.50$	$\Delta_{\text{po-ccp}} = 0.25$	$\Delta_{\text{py-gn}} = 1.84$	$\Delta_{\text{po-gn}} = 1.34$	$\Delta_{\text{ccp-gn}} = 1.09$

## References

- Brueckner SM, Piercey SJ, Sylvester PJ, Maloney S, Pilgrim L (2014) Evidence for syngenetic precious metal enrichment in an Appalachian volcanogenic massive sulfide system: The 1806 Zone, Ming Mine, Newfoundland, Canada *Economic Geology* 109:1611-1642 doi:10.2113/econgeo.109.6.1611
- Gregory RT, Criss RE (1986) Isotopic Exchange in open and closed systems *Reviews in Mineralogy and Geochemistry* 16:91-127
- Gregory RT, Criss RE, Taylor Jr. HP (1989) Oxygen isotope exchange kinetics of mineral pairs in closed and open systems: Applications to problems of hydrothermal alteration of igneous rocks and Precambrian iron formations *Chemical Geology* 75:1-42 doi:10.1016/0009-2541(89)90019-3

- Kajiwara Y, Krouse HR (1971) Sulfur isotope partitioning in metallic sulfide systems Canadian Journal of Earth Sciences 8:1397-1408
- Ohmoto H, Goldhaber MB (1997) Sulfur and carbon isotopes. In: Barnes HL (ed) Geochemistry of hydrothermal ore deposits, 3rd edn. John Wiley & Sons, New York, pp 517-611
- Tuach J, Kennedy MJ (1978) The geologic setting of the Ming and other sulfide deposits, consolidated Rambler mines, Northeast Newfoundland Economic Geology 73:192-206

#### **APPENDIX A4-6 CALCULATIONS USED FOR MODELLING S SOURCES AT THE MING DEPOSIT**

For the modelling of the most likely S source at the Ming deposit, equations from Ohmoto and Rye (1979) and Ohmoto and Goldhaber (1997) were used. The applied sulfide mineral fractionation factors with respect to H<sub>2</sub>S are from Kajiwara and Krouse (1971).

Fractionation of sulfur isotopes between seawater sulfate and H<sub>2</sub>S is a function of temperature given by:

$$1000 \ln \alpha_{H_2S-SO_4} = \frac{A \times 10^6}{T^2} + \frac{B \times 10^3}{T} + C = \delta^{34}S_{H_2S} - \delta^{34}S_{SO_4} \quad (4-1a)$$

where  $\alpha_{H_2S-SO_4}$  is the equilibrium sulfur isotopic fractionation factor between sulfide and sulfate (the ratio of <sup>34</sup>S/<sup>32</sup>S of sulfide to sulfate) during TSR, T is the temperature in Kelvin,  $\delta^{34}S_{SO_4}$  is the sulfur isotope composition of seawater sulfate, A, B, and C are constants (A = -5.26, and B = 0, and C = -6 in this particular equation), and  $\delta^{34}S_{H_2S}$  is the sulfur isotope composition of H<sub>2</sub>S generated from TSR. Minimum and maximum temperatures for TSR in VMS systems were assumed to be 250°C (523K) and 350°C (623K), respectively (Shanks et al., 1981) and applied to the Ming deposit. Moreover, sulfide mineralogy present at the Ming deposit suggests that most base and precious metals were transported in this temperature window (250°C–350°C; Seward,

1973, 1976; Lydon, 1988; Large, 1992; Ohmoto, 1996; Seward and Barnes, 1997; Huston, 2000; Brueckner et al., 2014). Using Equation (4-1a) with  $A = -5.26$  at  $T = 523K$  and  $623K$ ,  $\alpha_{H_2S-SO_4}$  is calculated by:

$$\alpha_{H_2S-SO_4} = e^{\left(\frac{5.26 \times 10^6}{T^2} - 6\right) / 1000} \quad (4-1b)$$

resulting in  $\alpha_{H_2S-SO_4} = 0.9751$  at  $250^\circ C$  and  $\alpha_{H_2S-SO_4} = 0.9806$  at  $T = 350^\circ C$ . The sulfur isotope composition of  $H_2S$  generated by TSR is calculated using Equation (4-2):

$$\delta^{34}S_{H_2S} = \delta^{34}S_{SO_4} + 1000 \times (\alpha_{H_2S-SO_4} - 1) \quad (4-2)$$

Equation (4-2) follows directly from Equation (4-1a), because  $\alpha_{H_2S-SO_4}$  is very close to 1 and hence the approximation  $1000 \ln \alpha_{H_2S-SO_4} = \delta^{34}S_{H_2S} - \delta^{34}S_{SO_4} \approx 1000 \times (\alpha_{H_2S-SO_4} - 1)$  can be made.

Since hydrothermal systems can be seen as open systems (Lydon, 1988; Herzig and Hannington, 1995; Shanks et al., 1995; Seal, 2006) Rayleigh distillation equation (4-3) is applied to calculate the sulfur isotope composition of sulfate at the time of the formation of the Ming deposit ( $\delta^{34}S_{SO_4 (parent, t)}$ ) relative to the parent composition of seawater sulfate ( $\delta^{34}S_{SO_4 (parent, t=0)}$ ) at that time, which is early Ordovician for the Ming deposit:

$$\delta^{34}S_{SO_4 (parent, t)} = (\delta^{34}S_{SO_4 (parent, t=0)} + 1000) \times f^{(\alpha_{H_2S-SO_4} - 1)} - 1000 \quad (4-3)$$

This is a function related to the amount of sulfate reduced to  $H_2S$  as measured by  $f$ , where  $f$  represents the atomic fraction of the parent  $SO_4$  ( $\delta^{34}S_{SO_4 (parent, t=0)} = \delta^{34}S_{SO_4 (parent)}$ ) reduced to  $H_2S$  ( $\delta^{34}S_{H_2S}$ ) relative to the original amount of  $SO_4$  present. For example, when  $f = 1$ , no sulfate has been reduced to sulfide; when  $f = 0.8$ , 20% of sulfate has been reduced to sulfide, and when  $f = 0$ , all sulfate has been reduced to sulfide. Equations (4-1) to (4-3) are dependent upon an assumption being made for the  $\delta^{34}S$  value of seawater sulfate ( $SO_4$ ) at time  $t$  (early Ordovician). While  $\delta^{34}S$  of seawater sulfate has varied through time,  $\delta^{34}S$

values ( $\delta^{34}\text{S}_{\text{SO}_4 \text{ (parent, } t=0\text{)}}$ ) for early Ordovician seawater is ~29‰ (Claypool et al., 1980; Kampschulte and Strauss, 2004). The sulfur isotope composition of sulfide phases pyrite, chalcopyrite, pyrrhotite, and galena formed from  $\text{H}_2\text{S}$  through TSR (Equations (4-1) to (4-3)) using early Ordovician seawater sulfate were calculated by Equation (4-4):

$$\delta^{34}\text{S}_{i(\text{TSR})} = \frac{A \times 10^6}{T^2} + \delta^{34}\text{S}_{\text{H}_2\text{S}} \quad (4-4)$$

where  $\delta^{34}\text{S}_{i(\text{TSR})}$  is the sulfur isotope composition of the sulfide phase in question formed by TSR and A is a constant. Values for constant A are used from Kajiwara and Krouse (1971) for pyrite, chalcopyrite, pyrrhotite and galena with respect to  $\text{H}_2\text{S}$ .

Igneous sulfur (sulfur leached from igneous wall rock and/or derived from magmatic fluids) as sole sulfur source was eliminated, because the measured sulfur isotope compositions were significantly higher than the average  $\delta^{34}\text{S}$  of 0‰ for igneous sulfur. However, mixing between the two possible sulfur sources TSR and igneous sulfur was calculated using equation (4-5):

$$\delta^{34}\text{S}_{i(\text{mix})} = b \times \delta^{34}\text{S}_{i(\text{TSR})} + (1 - b) \times \delta^{34}\text{S}_{i(\text{igneous})} \quad (4-5)$$

where b is the proportion of TSR derived sulfur. For example, if  $b = 1$  then all sulfur was derived from TSR, whereas if  $b = 0.6$ , 60% of all sulfur was derived from TSR and 40 % was derived from igneous sulfur. The other symbols in Equation (4-5) are  $\delta^{34}\text{S}_{i(\text{mix})}$ , which is the sulfur composition of mineral phase i formed by both TSR and igneous sulfur;  $\delta^{34}\text{S}_{i(\text{TSR})}$  is the calculated sulfur isotope composition of component i from TSR (Equation (4-4)); and  $\delta^{34}\text{S}_{i(\text{igneous})}$  is the sulfur composition of mineral phase i formed from igneous sulfur. Values for  $\delta^{34}\text{S}_{i(\text{igneous})}$  were calculated from Equation (4-6):

$$\delta^{34}\text{S}_{i(\text{igneous})} = \frac{A \times 10^6}{T^2} + 0 \quad (4-6)$$

where 0 is the  $\delta^{34}\text{S}$  value of igneous  $\text{H}_2\text{S}$  and A is a constant. Values for constant A are used from Kajiwara and Krouse (1971) for pyrite, chalcopyrite, pyrrhotite and galena with respect to  $\text{H}_2\text{S}$ .

## References

- Brueckner SM, Piercey SJ, Sylvester PJ, Maloney S, Pilgrim L (2014) Evidence for syngenetic precious metal enrichment in an Appalachian volcanogenic massive sulfide system: The 1806 Zone, Ming Mine, Newfoundland, Canada *Economic Geology* 109:1611-1642 doi:10.2113/econgeo.109.6.1611
- Claypool GE, Holser WT, Kaplan IR, Sakai H, Zak I (1980) The age curves of sulfur and oxygen isotopes in marine sulfate and their mutual interpretation *Chemical Geology* 28:199-260
- Herzig PM, Hannington MD (1995) Polymetallic massive sulfides at the modern seafloor: A review *Ore Geology Reviews* 10:95-115
- Huston DL (2000) Gold in volcanic-hosted massive sulfide deposits: Distribution, genesis, and exploration. In: Hagemann SG, Brown, P.E. (ed) *Gold in 2000*, vol 13. *Reviews in Economic Geology*. Society of Economic Geologists, Boulder, CO, pp 401-426
- Kajiwara Y, Krouse HR (1971) Sulfur isotope partitioning in metallic sulfide systems *Canadian Journal of Earth Sciences* 8:1397-1408
- Kampschulte A, Strauss H (2004) The sulfur isotopic evolution of Phanerozoic seawater based on the analysis of structurally substituted sulfate in carbonates *Chemical Geology* 204:255-286 doi:10.1016/j.chemgeo.2003.11.013
- Large RR (1992) Australian volcanic-hosted massive sulfide deposits: Features, styles, and genetic models *Economic Geology* 87:471-510
- Lydon JW (1988) Volcanogenic massive sulphide deposits Part 2: Genetic models *Geoscience Canada* 15:43-65
- Ohmoto H (1996) Formation of volcanogenic massive sulfide deposits: The Kuroko perspective *Ore Geology Reviews* 10:135-177

- Ohmoto H, Goldhaber MB (1997) Sulfur and carbon isotopes. In: Barnes HL (ed) *Geochemistry of hydrothermal ore deposits*, 3<sup>rd</sup> edn. John Wiley & Sons, New York, pp 517-611
- Ohmoto H, Rye RO (1979) Isotopes of sulfur and carbon. In: Barnes HL (ed) *Geochemistry of hydrothermal ore deposits*, 2<sup>nd</sup> edn. John Wiley & Sons, New York, pp 509-567
- Seal II RR (2006) Sulfur isotope geochemistry of sulfide minerals. In: Vaughan DJ (ed) *Sulfide mineralogy and geochemistry*, vol 61. *Reviews in Mineralogy and Geochemistry*. pp 633-677
- Seward TM (1973) Thio complexes of gold and the transport of gold in hydrothermal ore solutions. *Geochimica et Cosmochimica Acta* 37:379-399.
- Seward TM (1976) The stability of chloride complexes of silver in hydrothermal solutions up to 350°C. *Geochimica et Cosmochimica Acta* 40:1329-1341.
- Seward TM, Barnes HL (1997) Metal transport by hydrothermal ore fluids In: Barnes HL (ed) *Geochemistry of hydrothermal ore deposits*, 3<sup>rd</sup> edn. John Wiley & Sons, pp 435-486.
- Shanks III WC, Bischoff JL, Rosenbauer RJ (1981) Seawater sulfate reduction and sulfur isotope fractionation in basaltic systems: Interaction of seawater with fayalite and magnetite at 200-350°C. *Geochimica et Cosmochimica Acta* 45:1977-1995.
- Shanks III WC, Böhlke JK, Seal II RR (1995) Stable isotopes in mid-ocean ridge hydrothermal systems: Interaction between fluids, minerals and organisms. In: Humphris SE, Zierenberg RA, Mullineaux LS, Thomson RE (eds) *Seafloor hydrothermal systems: Physical, chemical, biological, and geological interactions*, vol *Geophysical Monograph* 91. American Geophysical Union, Washington, DC, pp 194-221

## CHAPTER 5

In:

Brueckner, SM, Piercey, SJ, Pilote, J-L, Layne, GD, Sylvester, PJ (2015).  
Mineralogy and mineral chemistry of the metamorphosed and precious metal-  
bearing Ming deposit, Canada. Ore Geology Reviews [submitted]

# MINERALOGY AND MINERAL CHEMISTRY OF THE METAMORPHOSED AND PRECIOUS METAL-BEARING MING DEPOSIT, CANADA

Stefanie M. Brueckner<sup>1</sup>, Stephen J. Piercey<sup>1</sup>, Jean-Luc Pilote, Graham D.  
Layne<sup>1</sup>, and Paul J. Sylvester<sup>1†</sup>

*<sup>1</sup>Dept. of Earth Sciences, Memorial University of Newfoundland,  
300 Prince Philip Drive, St. John's, NL, A1B 3X5, Canada*

*<sup>†</sup> now at: Dept. of Geosciences, Texas Tech University, 125 Science Bldg.,  
Lubbock, TX 79049-1053, USA*

## ABSTRACT

The Ming deposit in the northeastern Canadian Appalachians is a metamorphosed, bimodal-mafic, precious-metal (Au, Ag)-bearing and Cu-rich volcanogenic massive sulfide (VMS) deposit consisting of several, spatially proximal lenses in a sericite- to chlorite-altered rhyodacitic footwall. The various lenses (1807 Zone, 1806 Zone, Ming South Up Plunge, Ming South Down Plunge, and the Lower Footwall Zone) have variations in Cu, Au, Ag, and Zn grades that reflect varying physico-chemical conditions of ore formation. This study describes the complex ore mineralogy of the orebodies and constrains the genesis of the deposit using field methods, mineralogy, whole rock sulfide geochemistry, and micro-analytical methods.



The orebodies are predominantly pyrite, chalcopyrite, with lesser sphalerite, pyrrhotite, galena, and trace galena and arsenopyrite, with the exception of the Lower Footwall Zone, which consists of a high temperature (> 320°C) chalcopyrite-pyrrhotite-pyrite  $\pm$  cubanite assemblage. The other orebodies (1806, 1807, Ming South Up Plunge and Down Plunge) contain trace amounts of tellurides (hessite, altaite, tsumoite, unnamed bismuthtelluride), sulfosalts (Ag-poor and Ag-rich tennantite-tetrahedrite, meneghinite, AgSb phases, stannite), and precious metal phases (electrum, AgHg $\pm$ Au alloys). The 1807 Zone is enriched in Te, Bi, and Se, whereas the 1806 Zone is telluride-free and contains As, Sb, Hg, Au, and Ag. Mineral chemistry of sphalerite shows strong variations in Fe content (1.12-11.04wt.%). Intermediate Fe (4.33-6.33wt.% Fe) and Fe-rich (7.327-11.04wt.% Fe) sphalerite are common in all orebodies, whereas Fe-poor sphalerite (1.12-3.57wt.% Fe) occurs exclusively in the 1807 and 1806 zones. Tennantite-tetrahedrite is typically Ag-poor (0.25-2.19wt.%) in the 1807 Zone, but is significantly enriched in Ag (up to 29.3wt.%) in the 1806 Zone. Galena in the 1807 Zone and Ming South orebodies is commonly myrmekitically intergrown with tellurides and has high concentrations of Te, Bi, Se, and Ag. In contrast, galena in the 1806 Zone is less enriched in Te, Bi, and Se, but high in Ag.

Variations in mineralogy, elements of the epithermal suite (As, Bi, Hg, Sb, Se, Sn, Te) and precious metal (Ag, Au) content, and mineral chemistry between the different orebodies indicate that they were formed from predominantly reduced, acidic hydrothermal fluids with varying  $f\text{Te}_2/f\text{S}_2$ ,  $f\text{Se}_2/f\text{S}_2$ , and  $m_{\text{Bi}}/m_{\text{Sb}}$

ratios as temperatures steadily decreased from >300°C to <260°C during ore formation. In the 1807 and Ming South orebodies, late-stage deposition of Te-, Bi-, Se-, Ag-rich galena and tellurides occurred prior to precipitation of Ag-poor tennantite-tetrahedrite, whereas in the 1806 Zone hydrothermal fluids low in  $f\text{Te}_2/f\text{S}_2$ ,  $f\text{Se}_2/f\text{S}_2$ , and  $m_{\text{Bi}}/m_{\text{Sb}}$  favored the precipitation of Te-, Bi-, Se-poor galena and Ag-rich tennantite-tetrahedrite. A magmatic source for the suite of elements of the epithermal suite, and precious metals is suggested and was part of the depositional history of the Ming deposit.

**Keywords:** metamorphosed volcanogenic massive sulfide deposit, epithermal elements, precious metals, tellurides, magmatic source

## 5-1 INTRODUCTION

In recent years, the number of studies describing the detailed ore mineralogy in ancient (Cook et al., 1998; Maslennikov et al., 2009; McClenaghan et al., 2009) and modern (Törmänen and Koski, 2005) volcanogenic massive sulfide (VMS) systems using micro-analytical methods has increased. These studies commonly show complex mineral assemblages including minerals that contain elements of the epithermal suite (As, Bi, Hg, Sb, Se, Sn) and precious metals (Ag, Au), although most of these deposits do not necessarily classify as either auriferous or Au-rich (Mercier-Langevin et al., 2011). The processes suggested to explain the enrichment in elements of the epithermal suite and precious metals in these deposits vary between different studies. Nevertheless,

the application of scanning electron microscopy (SEM) and laser ablation inductively coupled plasma mass spectrometry (LA-ICP-MS) has offered new insights into the formation of these deposits. This is especially important in metamorphosed VMS deposits where detailed mineralogy and LA-ICP-MS studies can help to constrain between syngenetic and orogenic origins of metal enrichment (Wagner et al., 2004; Wohlgemuth-Ueberwasser et al., 2014). However, studies using cutting edge technologies to explain mineralogical and chemical variations between different ore lenses or chimneys in metamorphosed, precious metal-bearing VMS deposits are rare (e.g., Maslennikov et al., 2009; McClenaghan et al., 2009).

The Ming deposit in the Canadian Appalachians is a Cambro-Ordovician, bimodal-mafic, VMS deposit with elements of the epithermal suite and precious metals that was metamorphosed to upper greenschist/lower amphibolite facies conditions during the Silurian and Devonian. The several, spatially proximal orebodies of the deposit locally contain anomalous Au (up to 2.96g/t Au), enrichment in elements of the epithermal suite (magmatic-hydrothermal), and have variable precious and base metal grades. This deposit also contains lenses virtually devoid of Au, but which are enriched in base metals. Correspondingly, the Ming deposit provides a unique opportunity to study the variations in setting, style, mineralogy, and genesis of both base and precious metals in an ancient metamorphosed orebody.

In this paper, traditional reflected light microscopy and whole rock sulfide geochemistry of mineralized samples is combined with SEM, electron microprobe and LA-ICP-MS to understand the variations in elements of the epithermal suite and precious element content, mineral assemblages, mineral textures, and mineral chemistry between the different orebodies. The results are used to constrain the physio-chemical hydrothermal fluid conditions that were responsible for the variations in the orebodies of the Ming deposit. Moreover, the depositional mechanisms for semi-massive to massive sulfides and discordant sulfide stringers are explained to provide insight into the sources and deposition of base metals, elements of the epithermal suite, and precious metals. The findings of this study have implications for base and precious metal-bearing VMS deposits located in both the Appalachians and orogenic belts worldwide.

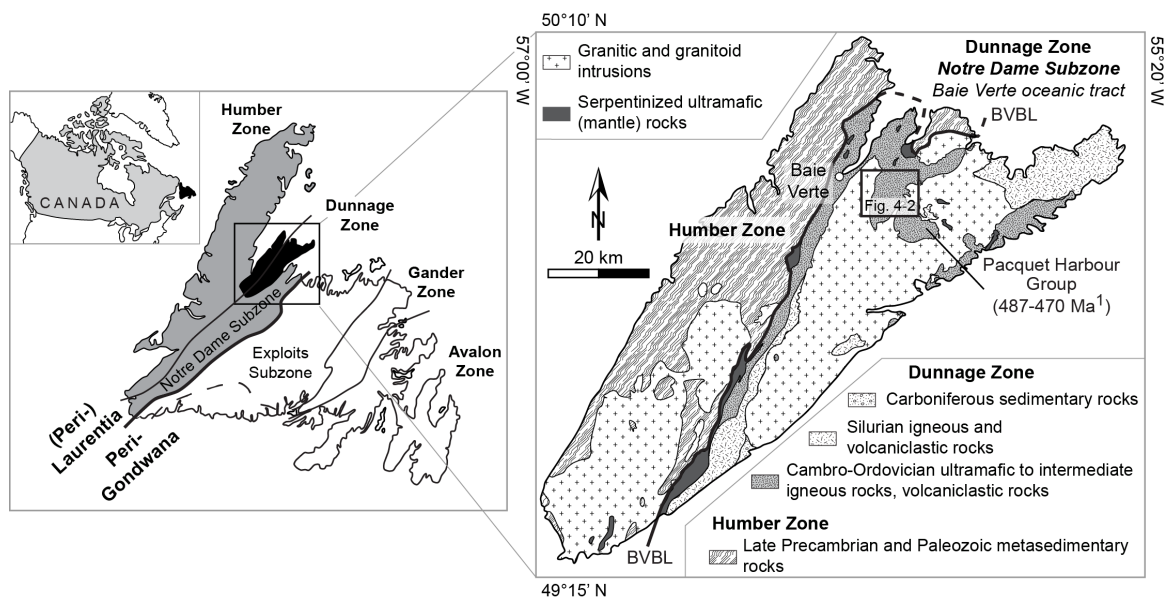
## **5-2 TECTONIC SETTING**

The Ming deposit is located on the Baie Verte Peninsula, Canadian Appalachians, which hosts both metamorphosed Precambrian rocks of Laurentia (Humber Zone) and peri-Laurentian Paleozoic rocks of the Notre Dame subzone of the Dunnage Zone. The contact between both zones is marked by the NE-SW oriented Baie Verte Brompton Line (BVBL; Fig. 5-1; Hibbard, 1983). The Ming deposit is located within the Baie Verte oceanic tract (BVOT), a Cambro-Ordovician to early Ordovician remnant arc complex in the eastern half on the peninsula. The detailed stratigraphy and tectonic environment of the BVOT are

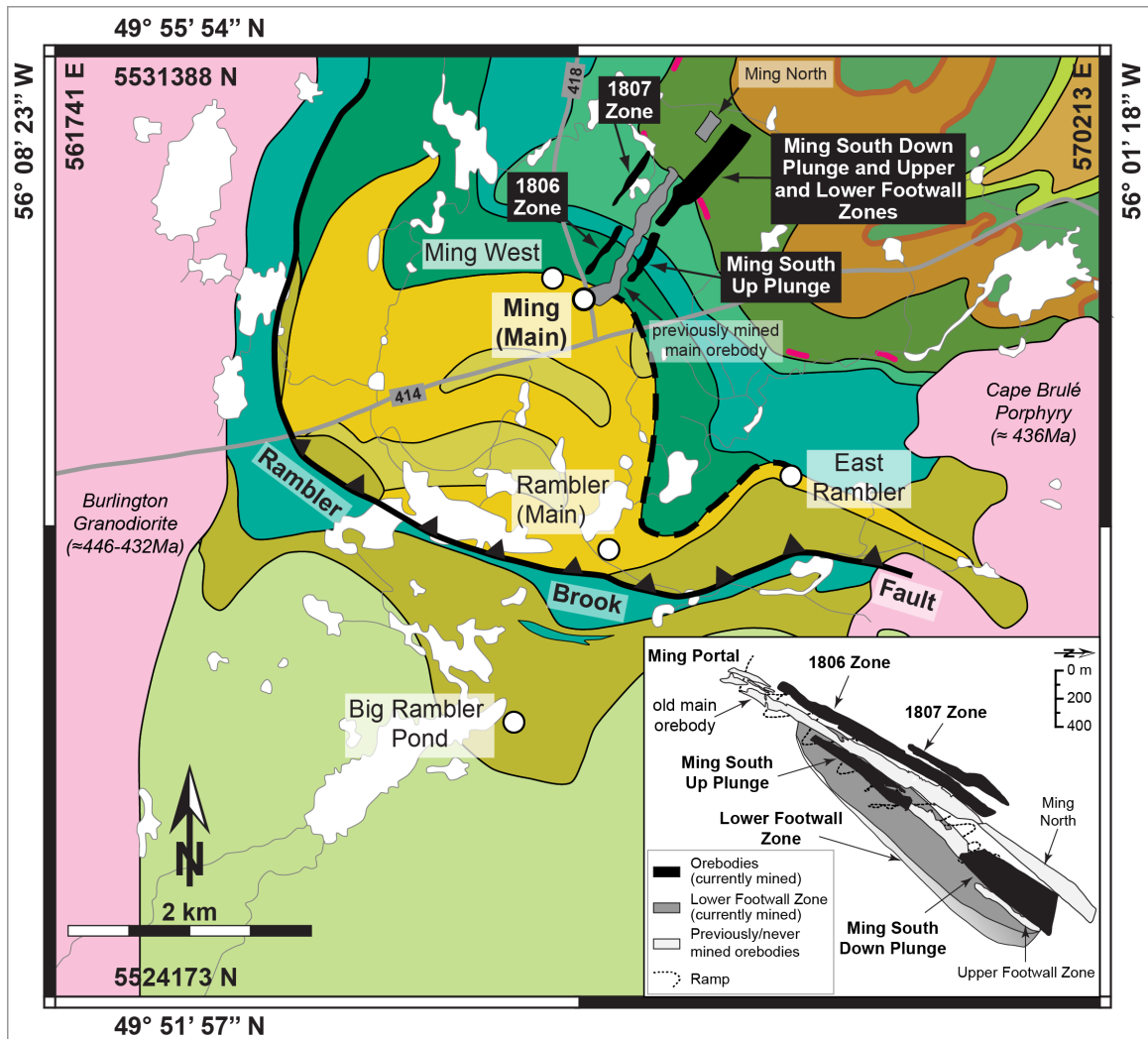
well documented (Hibbard, 1983; van Staal, 2007; Castonguay et al., 2009; Skulski et al., 2010; van Staal and Barr, 2012), and only a brief outline is provided below.

The Ming deposit is located within the Pacquet Harbour Group (PHG) in the BVOT (Fig. 5-2). The PHG is a remnant, partial ophiolitic basement assemblage consisting of low-Ti to medium-Ti boninites, tholeiitic basalts, and minor rhyodacite to rhyolite. The rhyodacitic to rhyolitic volcanic rocks form a 2.5km thick sequence of quartz-bearing, consolidated felsic tuff and tuff breccia, which is referred as Rambler rhyolite or Rambler rhyolite formation (Hibbard, 1983; Skulski et al., 2010). The Rambler rhyolite has a U-Pb zircon age of  $487 \pm 4$  Ma (unpubl. data by V. McNicoll in Castonguay et al., 2009; Skulski et al., 2010), forms the upper part of the PHG, and hosts massive sulfide mineralization (Fig. 5-2; Hibbard, 1983, Skulski et al., 2010). The formation of VMS deposits within the Rambler rhyolite was coeval with the formation of the PHG rocks in an arc setting (Swinden et al., 1984; van Staal, 2007). The ophiolitic cover sequence of the PHG is the Snooks Arm Group, which consists of early Ordovician (483-467Ma) volcano-sedimentary rocks and tholeiitic mafic volcanic rocks (Hibbard, 1983; unpubl. data by V. McNicoll in Castonguay et al., 2009; Skulski et al., 2010). The PHG with its cover sequence is interpreted to have formed in a supra-subduction setting during the closure of the Humber Seaway during the Taconic Orogeny (van Staal, 2007; van Staal and Barr, 2012).

Silurian and early Devonian intrusions (Cape Brulé Porphyry, Burlington Granodiorite, Cape St. John Group; Figs. 5-1, 5-2) formed during the Salinic and Acadian orogenies cross-cut the PHG and Snooks Arm Group and caused polyphase deformation and upper greenschist to lower amphibolite facies metamorphism (Tuach and Kennedy, 1978; Hibbard, 1983; Castonguay et al., 2009). At least four different deformation events ( $D_1$  to  $D_4$ ) are recorded in the BVOT basement rocks and their cover sequence (Tuach and Kennedy, 1978; Hibbard, 1983; Castonguay et al., 2009). Of these events,  $D_2$ , which is associated with the Silurian Salinic Orogeny, resulted in a prominent L-S fabric in the rhyodacite and the sulfide lenses (Tuach and Kennedy, 1978, Hibbard, 1983).

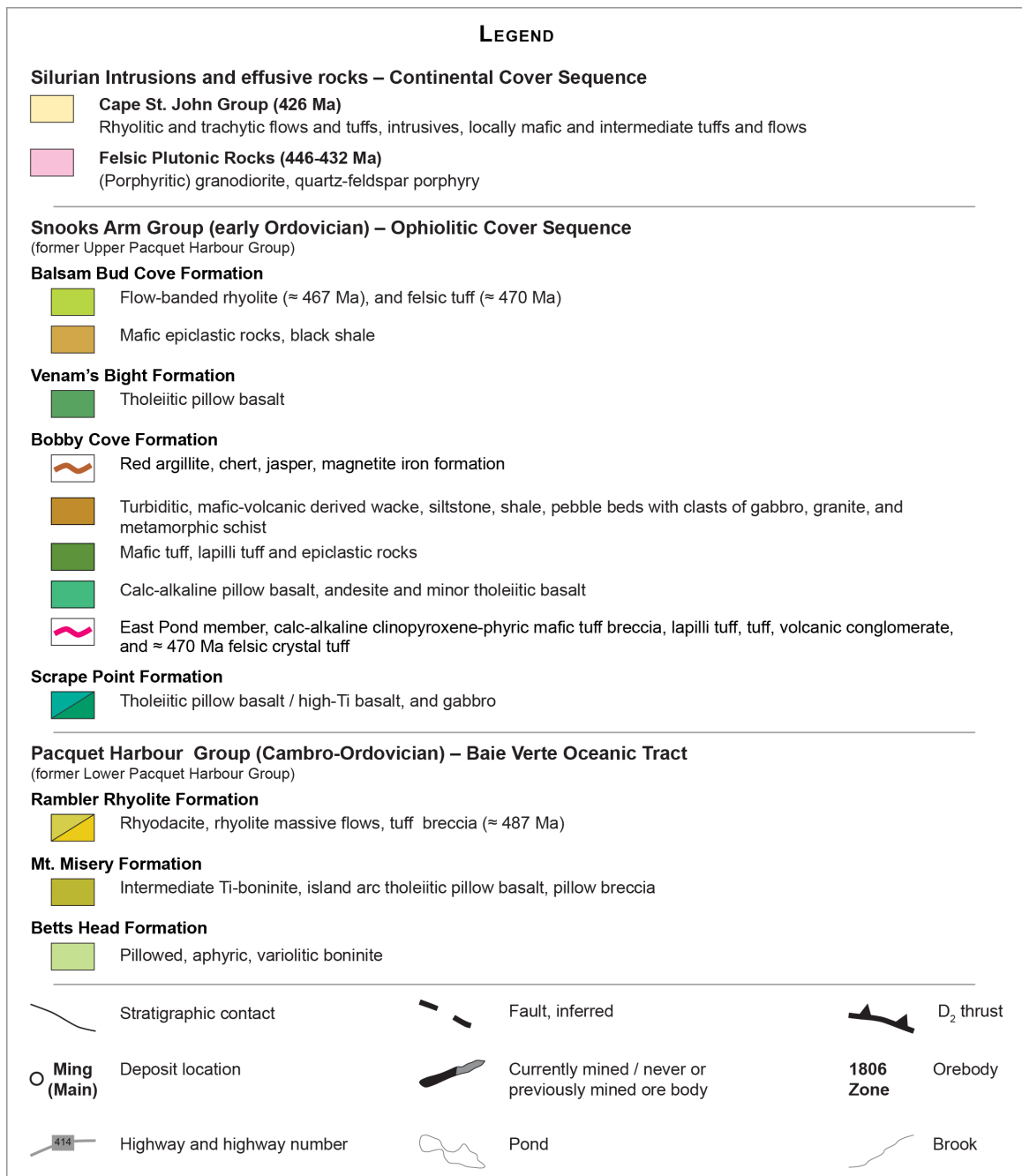


**Figure 5-1.** Geology of Newfoundland (left; after Williams, 1979) and simplified geology of the Baie Verte Peninsula (right) from Hibbard (1983). <sup>1</sup> Age data for the Pacquet Harbour Group (PHG) from Castonguay et al. (2009) and Skulski et al. (2010)



**Figure 5-2.** Detailed geological map of the Pacquet Harbour Group (PHG) with VMS deposits of the Rambler camp (modified after Skulski et al., 2010; outside coordinates are in WGS 1984 and inside coordinates are in UTM NAD83, Zone 21N). All orebodies of the Ming deposit, including mined out and present orebodies, are projected to surface and highlighted in grey and black, respectively. The inlay shows the spatial relationship between the different orebodies of the Ming deposit underground (Rambler Metals & Mining, Canada Ltd., 2011)





**Figure 5-2 (cont.).** Legend to Figure 5-2

The Ming deposit is one of five deposits that are part of the Rambler camp (Fig. 5-2). Four of these deposits (Ming, Ming West, Rambler, and East Rambler)

occur within the Rambler rhyolite formation, whereas the Big Rambler deposit occurs in the Mt. Misery formation that is stratigraphically below the Rambler rhyolite. The Ming deposit consists of several spatially proximal orebodies, that trend NE with a plunge of 30-35° and contain semi-massive to massive stratabound sulfide and discordant stringer sulfide mineralization. The different orebodies (1806 Zone, 1807 Zone, Ming South Up Plunge (MSUP), Ming South Down Plunge (MSDP), Ming North, Upper Footwall Zone and Lower Footwall Zone (LFWZ)) run parallel to and along the previously mined main orebody; the Upper and Lower Footwall zones only occur beneath the Ming South orebodies (Fig. 5-2). The total resources (measured, indicated, inferred) of the orebodies (without old main orebody) are 21.1Mt with grades of 1.49% Cu @ 328,129t, 0.61g/t Au @ 332,244oz, 3.21g/t Ag @ 2.2Moz, and 0.19% Zn @ 31,369t. The total proven and probable reserves (diluted and recovered) are 1.51Mt with grades of 1.70% Cu @ 25,727t, 2.09g/t Au @ 101,404oz, 9.48g/t Ag @ 459,788 oz, and 0.37% Zn @ 5,541t (Rambler Metals and Mining Canada Ltd, January 07, 2014). Resources for the individual orebodies and their mineral and chemical variations are shown in Table 5-1.

The focus of this paper is on the high-grade and/or high-tonnage orebodies 1806 Zone, 1807 Zone, MSUP, MSDP, and LFWZ. Upper Footwall Zone and Ming North have not been explored intensively enough by drill core to provide sufficient stratigraphic and sulfide mineralogical data for the purpose of this paper and were therefore excluded.

**Table 5-1.** Combined, measured, and indicated resource data for orebodies of the Ming deposit (Pilgrim, 2009; Rambler Metals & Mining, January 07, 2014)

Orebody	Type of sulfide mineralization	Quantity Tonnage [t]	Grades				Contained Metal			
			Cu [%]	Au [g/t]	Ag [g/t]	Zn [%]	Cu [t]	Au [oz]	Ag [oz]	Zn [oz]
1806 Zone	Semi-massive to massive sulfides, discordant sulfide stringers Ming South Up Plunge (MSUP) Ming South Down Plunge (MSDP) Lower Footwall Zone (LFWZ)	250,000	0.48	2.96	15.07	0.64	1,201	23,859	121,314	1,593
1807 Zone		268,000	5.21	2.04	15.92	0.75	13,957	17,575	137,228	2,021
Ming South Up Plunge (MSUP)		134,000	3.23	1.12	7.64	0.30	4,335	4,842	32,983	405
Ming South Down Plunge (MSDP)		1,220,000	1.56	2.26	9.39	0.42	19,047	88,481	368,479	5,089
Lower Footwall Zone (LFWZ)		17,872,000	1.40	0.09	1.32	0.01	250,520	49,237	760,538	2,409

### **5-3 STRATIGRAPHY, ALTERATION AND MINERALIZATION STYLES**

#### **5-3-1 STRATIGRAPHY AND ALTERATION OF THE RAMBLER RHYOLITE**

Stratigraphy and alteration were logged from drill core and underground mapping at the Ming deposit. Detailed underground maps and drill hole sections for the 1807, 1806, MSUP, MSDP, and LFWZ orebodies are included in Appendix A5-1.

The general stratigraphy at the Ming deposit predominantly consists of coherent, intermediate to felsic volcanic flows and volcanoclastic rocks in the footwall (i.e., Rambler rhyolite), semi-massive to massive sulfides on the footwall – hanging wall contact, and a predominantly sedimentary hanging wall (Snooks Arm Group). The volcanoclastic footwall rocks can be several hundred meters thick and typically occur as grey-bluish consolidated tuff, lapilli tuff or flows, are partly quartz-bearing, and show strong foliation (Pilote and Piercey, 2013; Brueckner et al., 2014; Pilote et al., 2014). Semi-massive to massive sulfides commonly occur as two and sometimes more lenses of variable thickness (a few centimeters up to 10m) separated from each other by Rambler rhyolite and/or mafic dikes. These mafic dikes are common at the Ming deposit and three generations of intrusive rocks cross-cut semi-massive to massive sulfides and host rocks (Pilote and Piercey, 2013; Pilote et al., 2014).

In general, alteration of the rhyodacitic footwall changes from sericite (sericite – quartz – sulfide  $\pm$  green mica  $\pm$  epidote  $\pm$  chlorite) to chlorite (chlorite –

quartz – sulfide  $\pm$  magnetite) alteration with increasing distance to the sulfide lenses. Sericite alteration is restricted to the 1807, 1806, MSUP, and MSDP orebodies. The sericite alteration is up to 100m thick. Sulfide alteration is typically weak and characterized by fine, discordant pyrite sulfide stringers with minor chalcopyrite  $\pm$  sphalerite  $\pm$  pyrrhotite or disseminated pyrite. In a narrow zone of up to 10m immediately below semi-massive to massive sulfides, sericite alteration commonly has increased amounts of green mica and sulfide stringers.

Alteration of the LFWZ consists of a pervasive chlorite – quartz assemblage with minor, discordant sulfide stringers (chalcopyrite – pyrrhotite  $\pm$  pyrite  $\pm$  cubanite), and rare magnetite. The LFWZ occurs beneath Ming South and a  $\approx$  20m thick transitional alteration zone with strong chlorite alteration and weak sericite marks the transition between the two orebodies.

The 1806 Zone contains a strong quartz alteration with weak to moderate chlorite alteration and sulfide stringers of varying composition, which occurs in a thin horizon above semi-massive and massive sulfide lenses (i.e., silicified horizon).

Pilote et al. (2014, 2015) identified other alteration assemblages in the rhyodacitic footwall; however, these are of limited spatial extent and are not considered further here.

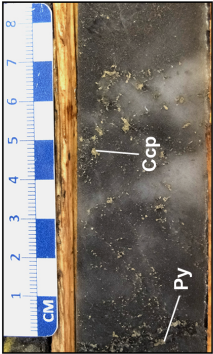
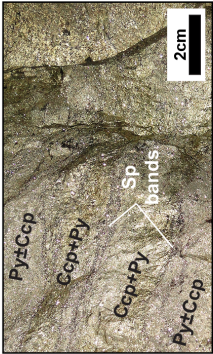
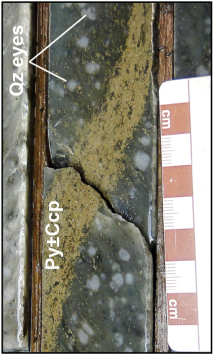
### 5-3-2 MINERALIZATION STYLES

Sulfide mineralization in the Ming deposit occurs as discordant sulfide stringers and as stratabound semi-massive to massive sulfides (Table 5-2). Sulfide stringers occur both in the footwall rhyodacitic rocks and in the hanging wall in a thin quartz altered horizon immediately above semi-massive and massive sulfides (i.e., silicified horizon) in the 1806 Zone. Sulfide stringers in the rhyodacitic footwall are composed of pyrite – chalcopyrite  $\pm$  sphalerite  $\pm$  pyrrhotite, run predominantly parallel to foliation within a sericite footwall and occur as a horizon, up to 100 m thick, immediately below the 1806 Zone and Ming South orebodies. In contrast, discordant stringers in the Lower Footwall Zone (LFWZ) consist of chalcopyrite – pyrrhotite  $\pm$  pyrite  $\pm$  cubanite in an intensely chlorite altered footwall, and are transposed into the main foliation. The several hundred meter thick LFWZ orebody is made up entirely of this sulfide mineralization style; therefore, the term LFWZ is used synonymously for both the orebody and the mineralization style herein.

Semi-massive to massive sulfides occur in the 1807, 1806, and Ming South orebodies and consist predominantly of pyrite  $\pm$  chalcopyrite with minor sphalerite  $\pm$  pyrrhotite. Sphalerite bands (0.5-30cm) and schlieren (1-5mm) of variable thickness commonly occur within a pyritic-chalcopyritic matrix in the upper parts of the 1807, 1806, and Ming South orebodies (Table 5-2). In the 1806 Zone thick sphalerite bands are common, whereas thin, mm-scale schlieren occur in other orebodies. Microscopically, recrystallized pyrite, galena, and

especially in the 1806 Zone tennantite-tetrahedrite occur as minor (5-10 vol.%) to trace (< 5 vol.%) phases within sphalerite bands.

**Table 5-2.** (next page) Different mineralization styles within the orebodies at the Ming deposit. Images on the left show typical examples for each mineralization style, whereas table on the right summarizes the main characteristics of each mineralization style. Mineral abbreviations: Ccp – chalcopyrite, Chl – chlorite, Ep – epidote, Mag – magnetite, Po – pyrrhotite, Py – pyrite, Qz – quartz, Serc – sericite Sp – sphalerite, Sul – sulfide (modified after Brueckner et al., 2015)

Mineralization Style	Orebody occurrence	Thickness	Type of alteration in Rambler rhyolite	Type and abundance of sulfide mineralization
<b>SILICIFIED HORIZON (1806 ZONE)</b> 	1806 Zone	30-50cm, but locally up to 3m	<b>Quartz alteration</b> (Qz – Chl – Sul)	Discordant sulfide stringers and disseminated sulfides (5-30%)
	<b>SEMI-MASSIVE/MASSIVE SULFIDE HORIZON</b>			
<b>SULFIDE STRINGER HORIZON</b> 	1807 Zone, 1806 Zone, MSUP, MSDP	Often 1 to 2 lenses, rarely up to 4 lenses; each lens a few cm up to several meters thick; locally lenses even up to 20m thick each; lenses separated by Rambler rhyolite or by mafic dikes	Rambler rhyolite fragments in semi-massive sulfides; <b>sericite alteration</b> (Serc – Qz – Sul ± green mica ± Ep ± Chl) with increased green mica and sulfide content	Concordant to stratabound semi-massive (50-90%) and massive sulfides (90-100%)
	<b>LOWER FOOTWALL ZONE</b>			
<b>SULFIDE STRINGER HORIZON</b> 	1807 Zone (sulfide stringer horizon only sporadically developed due to structural re-working), 1806 Zone, MSUP, MSDP	Tens of meters up to 100m	<b>Sericite alteration</b> (Serc – Qz – Sul ± green mica ± Ep ± Chl); immediately below semi-massive to massive sulfide lens(es) sericite alteration zone of increased green mica and sulfide alteration	Discordant sulfide stringers and disseminated sulfides; stringer abundance is up to 50% proximal to semi-massive to massive sulfides and up to 30% distal to semi-massive to massive sulfides
	LFWZ (below MSDP)	Up to 300m	<b>Chlorite alteration</b> (Chl – Qz – Sul ± Mag); between MSDP and LFWZ transitional alteration zone of chlorite alteration with weak sericite abundance	Discordant sulfide stringers and disseminated sulfides (5-20%)



## 5-4 SULFIDE AND PRECIOUS METAL MINERALOGY

### 5-4-1 MINERAL ABUNDANCES

The Ming deposit has a complex ore mineralogy that is shown in Table 5-3, along with mineral formulas and occurrences. The ore mineralogy consists of: (1) common metal sulfides (pyrite, chalcopyrite, sphalerite, pyrrhotite, arsenopyrite, galena, and cubanite); (2) uncommon metal sulfides including tellurides, selenides, and (sulfo-)antimonides (alloyclase, löllingite, hessite, Bi-tellurides, altaite, coloradoite, clausthalite, gudmundite, molybdenite, breithauptite, nisbite, and ullmanite-willyamite series); (3) sulfosalts (meneghinite, (Ag-bearing) tennantite-tetrahedrite, stannite, miargyrite, pyrargyrite, and mercurian stephanite); (4) precious metals (AgHg±Au alloys and electrum); and (5) oxides (cassiterite, magnetite, ilmenite, chromite, and rutile; mineral classification after Strunz and Nickel, 2001). Common metal sulfides are the dominant phases at the Ming deposit, whereas uncommon metal sulfides including tellurides, selenides, and (sulfo-)antimonides, sulfosalts, precious metals and oxides are predominantly trace phases (< 5 vol.%). However, the occurrence of tellurides, tennantite-tetrahedrite and electrum varies strongly between the different orebodies.

**Table 5-3.** Mineral abundance of metal sulfides, sulfosalts, precious metals and oxides in the orebodies of the Ming deposit. Mineral classification is after Strunz and Nickel (2001) and mineral abbreviations are after Whitney and Evans (2010). Mineral abundance: ●●● Major mineral phase (> 10 vol.%), ●● Minor mineral phase (5-10 vol.%), ● Trace mineral phase (< 5 vol.%), ○ Local trace mineral phase (observed in fewer than 3 thick sections), – not observed; n - number of investigated thick sections

Mineral phase (mineral abbreviation)	Ideal mineral formula	1807 Zone (n=53)	1806 Zone (n=71)	MSUP (n=42)	MSDP (n=43)	LFWZ (n=51)
[common] metal sulfides						
Pyrite (Py)	FeS <sub>2</sub>	●●●	●●●	●●●	●●●	●●
Chalcopyrite (Ccp)	CuFeS <sub>2</sub>	●●●	●●●	●●●	●●	●●●
Cubanite (Cbn)	CuFe <sub>2</sub> S <sub>3</sub>	●	–	○	○	●
Sphalerite (Sp)	ZnS	●●	●●	●	●	●
Pyrrhotite (Po)	Fe <sub>(1-x)</sub> S	●	●	●	●●	●●●
Arsenopyrite (Apy)	FeAsS	●	●	●	●	○
Galena (Gn)	PbS	●	●	●	●	●
[uncommon] metal sulfides including tellurides, selenides, and (sulfo-)antimonides						
Alloclasite (Allo)	Co <sub>(1-x)</sub> Fe <sub>x</sub> AsS	○	–	○	○	○
Löllingite (Loel)	FeAs <sub>2</sub>	○	○	○	–	–
Hessite (Hess)	AgTe	●	–	○	●	●
Tsumoite (Tsu)	BiTe	●	*	○	*	○
Unnamed Bi-telluride (unnamed BiTe)	Bi <sub>3</sub> Te <sub>2</sub>	●	*	○	*	*
Unidentified Bi-tellurides (BiTe)		●	○	○	●	●
Altaite (Alt)	PbTe	●	–	○	●	–
Coloradoite (Col)	HgTe	–	○	○	○	–
Clausthalite (Claus)	PbSe	○	–	○	–	○
Gudmundite (Gud)	FeSbS	●	–	–	–	–
Molybdenite (Mol)	MoS <sub>2</sub>	–	○	○	–	–
Breithauptite (Breit)	NiSb	**	–	○	**	–
Nisbite (Nis)	NiSb <sub>2</sub>	**	–	○	**	–
Unidentified NiSb phase (NiSb)		●	–	○	○	–

**Table 5-3. (cont.)**

Mineral phase (mineral abbreviation)	Ideal mineral formula	1807 Zone (n=53)	1806 Zone (n=71)	MSUP (n=42)	MSDP (n=43)	LFWZ (n=51)
<b>[uncommon] metal sulfides including tellurides, selenides, and (sulfo-)antimonides (cont.)</b>						
Ullmanite (Ull)	NiSbS	-	○	○	○	-
Willyamite (Will)	(Ni, Co)SbS	-	-	○	-	-
<b>sulfosalts</b>						
Meneghinite (Men)*	Pb <sub>13</sub> CuSb <sub>7</sub> S <sub>24</sub>	○	○	○	○	-
Tennantite-tetrahedrite (Tnt-Trt)	Cu <sub>10</sub> (Fe, Zn) <sub>2</sub> (As, Sb) <sub>4</sub> S <sub>13</sub>	●	●	○	○	-
Ag-bearing tetrahedrite (Ag-Trt)	(Ag, Cu) <sub>10</sub> (Fe, Zn) <sub>2</sub> Sb <sub>4</sub> S <sub>13</sub>	●	●	○	○	-
Stannite (Stn)	Cu <sub>2</sub> (Fe, Zn)SnS <sub>4</sub>	-	●	-	-	-
Miargyrite (Mia)	AgSbS <sub>2</sub>	-	○	-	-	-
Pyrargyrite (Pyr)	Ag <sub>3</sub> SbS <sub>3</sub>	-	○	-	-	-
Mercurian stephanite (Hg-Steph)	(Hg, Ag) <sub>5</sub> SbS <sub>4</sub>	-	○	-	-	-
<b>precious metals</b>						
Silver-mercury ± gold alloy (AgHg±Au)	(Ag, Hg, Au)	○	●	○	-	-
(Mercurian) electrum (El)	(Au, Ag)	●	●	○	○	○
<b>oxides</b>						
Cassiterite (Cst)	SnO <sub>2</sub>	-	●	○	-	-
Magnetite (Mag)	Fe <sub>3</sub> O <sub>4</sub>	●	●	●	●	●
Fe±Ti±Cr oxides (FeTi ox)	FeTiO <sub>3</sub> , TiO <sub>2</sub> , FeCrO <sub>4</sub>	●	○	○	○	●
<b>unclassified</b>						
Unnamed AgCuFeS phase	AgCuFeS	-	○	-	-	-

\* Clear identification between tsumoite and unnamed Bi-telluride was not possible due to small grain size; hence minerals with BiTe composition are labeled as unidentified Bi-tellurides

\*\* Clear identification between breithauptite and nishite was not possible due to small grain size; hence minerals with NiSb composition are labeled as unidentified NiSb phase

# Originally labeled as boulangerite in Brueckner et al. (2014); however correct mineral name is meneghinite due to elevated Cu concentration

The 1807, 1806, MSUP, and MSDP orebodies are similar in their common metal sulfide assemblage and dominated by pyrite  $\pm$  chalcopyrite with minor sphalerite  $\pm$  pyrrhotite and trace pyrrhotite – arsenopyrite – galena  $\pm$  cubanite. Cubanite is absent in the 1806 Zone, whereas in the other four orebodies it occurs as a sporadic trace phase. In contrast, the LFWZ consists of a simple sulfide assemblage dominated by chalcopyrite + pyrrhotite with minor pyrite and/or trace cubanite. Cubanite is the most common trace phase in the LFWZ, whereas sphalerite is present as small and rare, anhedral grains within chalcopyrite  $\pm$  pyrrhotite; galena and arsenopyrite are restricted to the upper part of the LFWZ.

The trace minerals in the 1807 Zone and Ming South orebodies are similar, whereas the 1806 Zone differs in its trace mineral content from these orebodies. Tellurides have the greatest variability in the 1807 Zone, where tsumoite, an unnamed bismuth telluride, hessite, and altaite are present. (Sulfo-) antimonides (nisbite, breithauptite, ullmanite-willyamite, gudmundite) are present in 1807 and Ming South orebodies; these minerals and tellurides are absent in the 1806 Zone. Tennantite-tetrahedrite and other sulfosalts are present in all orebodies, but are enriched in the 1806 Zone. Stannite and AgSbS phases (myrargyrite, pyrargyrite, mercurian stephanite) are restricted to the 1806 orebody (Brueckner et al., 2014). In the LFWZ, tellurides and selenides (Bi-tellurides, hessite and clausthalite), and electrum are rare and sulfosalts are completely absent. In the upper part of the LFWZ, electrum occurs in the

transitional sericite-chlorite alteration zone.

#### *5-4-2 MINERAL TEXTURES*

Textures in the Ming deposit are discussed in the context of: (1) replacement textures; (2) decomposition textures; (3) textures of unknown origin; (4) deformation textures; and (5) textures involving precious metals (Figs. 5-3, 5-4, and 5-5). The first four texture classes are defined by their origin, whereas the fifth texture class focuses on precious metals. This discrepancy in the classification of the observed textures is done to highlight that precious metals occur in various textures of different genetic origin at the Ming deposit. Textures in the 1807, 1806, and Ming South orebodies (Figs. 5-3, 5-5) are more complex than those in the LFWZ (Fig. 5-4).

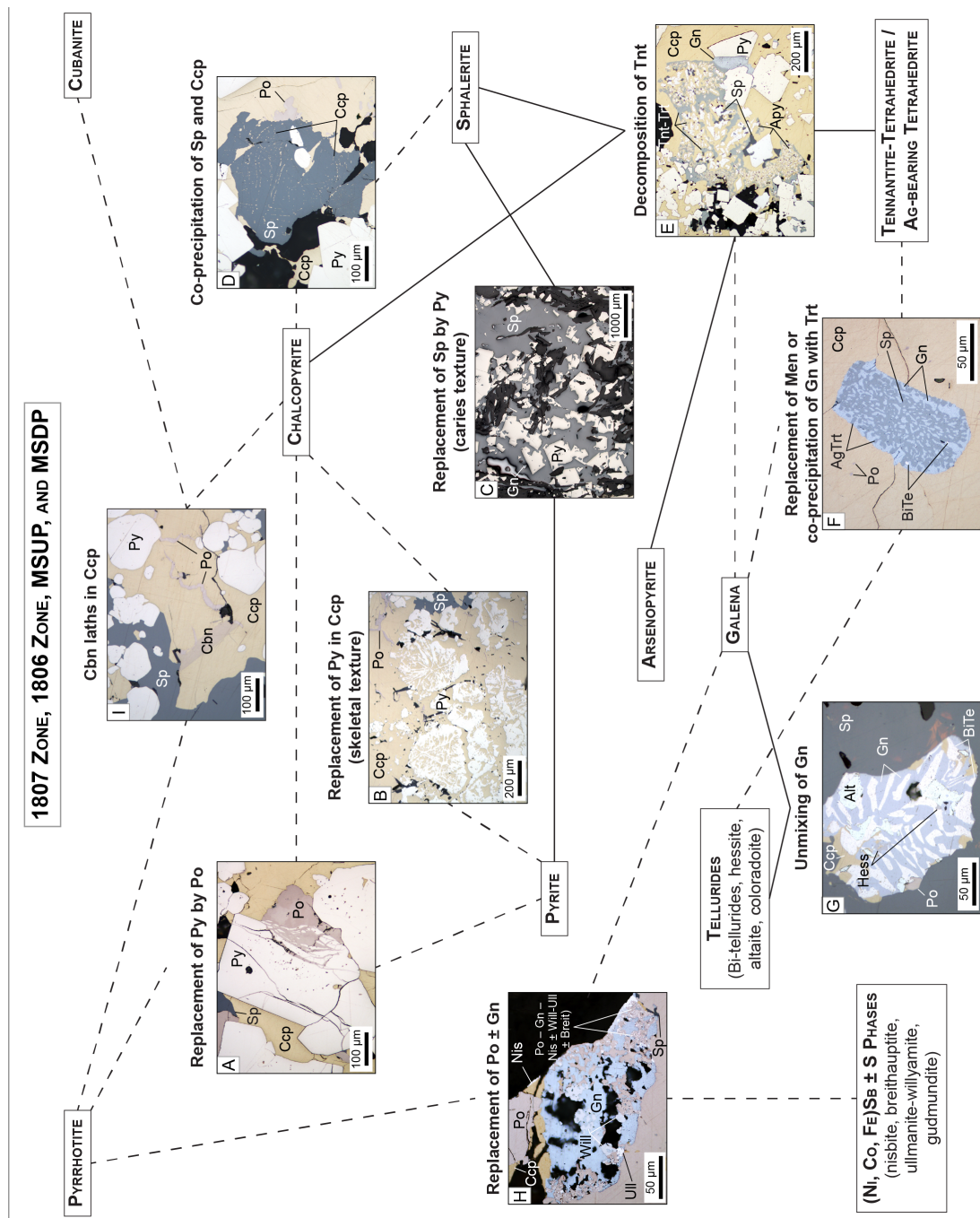
##### *5-4-2-1 Replacement textures*

Replacement textures in the 1807, 1806, and Ming South orebodies are diverse and include the replacement of pyrite by pyrrhotite (Fig. 5-3a) and chalcopyrite (skeletal texture; Fig. 5-3b), and the replacement of sphalerite by pyrite (caries texture; Fig. 5-3c) and stannite; the latter is restricted to the 1806 Zone (Brueckner et al., 2014). In contrast, in the LFWZ only the replacement of pyrite by pyrrhotite is present (Fig. 5-4a). However, this type of replacement is diagnostic in the LFWZ and less common in the other orebodies. Replacement of pyrite in the LFWZ is likely late syngenetic due to high temperature (>320°C) Cu-

Fe sulfide replacement of pyrite associated with deposit zone refining (Eldridge et al., 1983; Lydon, 1988; Craig and Vokes, 1993; Ohmoto, 1996). In the other orebodies, pyrite-pyrrhotite replacement is most likely of metamorphic origin and therefore post-syngenetic, since cubanite is rare or completely absent, and pyrrhotite is commonly proximal to cross-cutting post-ore mafic dykes, and associated with porphyroblast development.

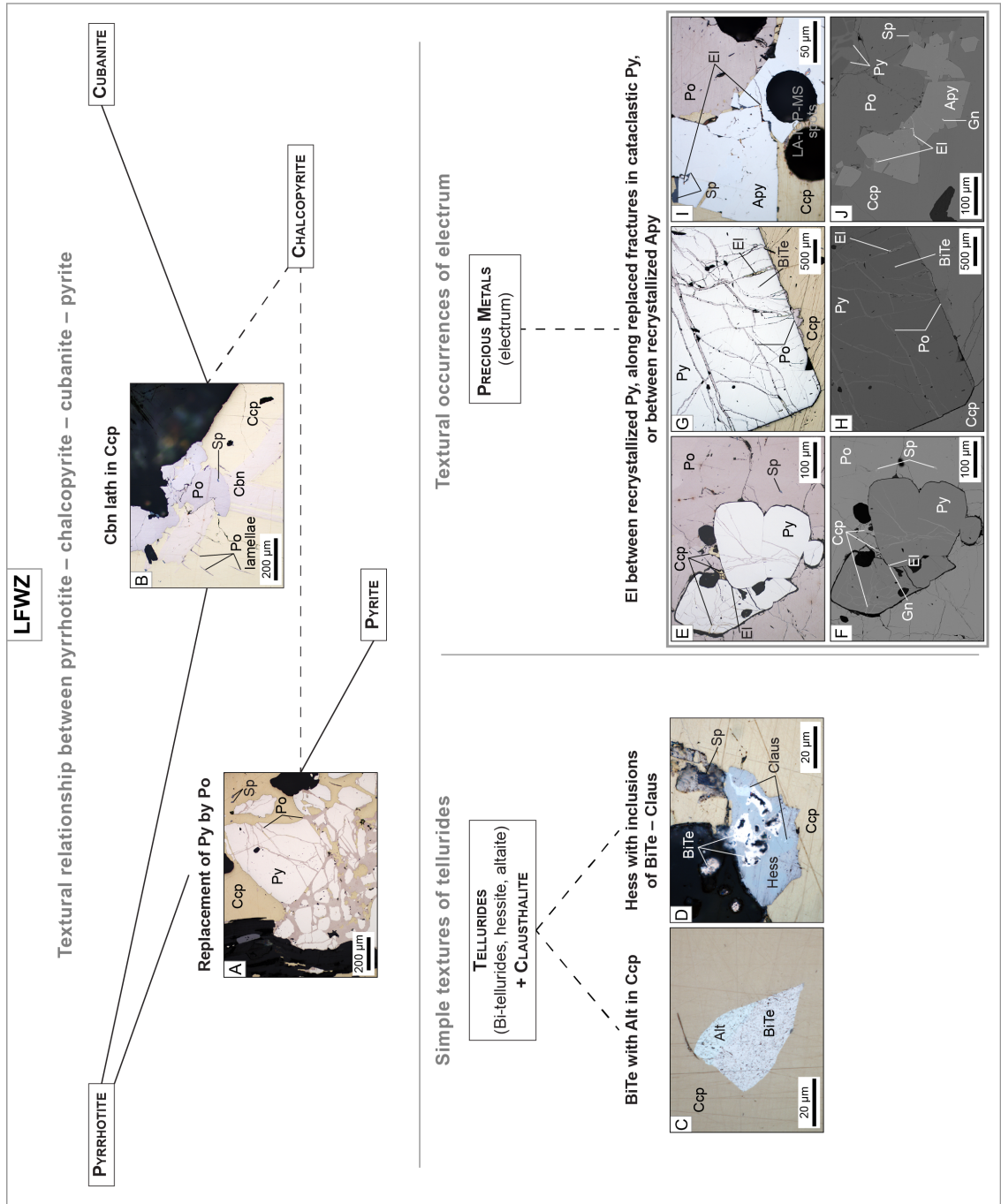
Coarse-grained pyrite in the massive and semi-massive sulfides contains cores replaced by chalcopyrite resulting in a skeletal appearance. Pyrite occurring within sphalerite bands and schlieren typically shows embayments of sphalerite (i.e., caries texture) resulting in the anhedral appearance of pyrite crystal faces.

Sphalerite in the 1807, 1806, and Ming South orebodies has blebs and lamellae of chalcopyrite that are epitaxially oriented in the host sphalerite and resembles chalcopyrite disease (Fig. 5-3d). This texture most likely represents co-precipitation of sphalerite and chalcopyrite (Nagase and Kojima, 1997) rather than replacement of sphalerite by chalcopyrite during zone refining (e.g., Barton, 1978; Barton and Bethke, 1987).



**Figure 5-3.** (previous page) Textural relationships between various sulfide minerals in the 1807, 1806, MSUP, and MSDP orebodies. Minerals forming ore textures are connected to the different textures by trajectories. Solid trajectory lines indicate that a mineral texture is abundant, whereas dashed trajectory lines indicate a rare abundance of a texture. **(A)** Replacement of pyrite by pyrrhotite (sulfide stringer horizon, MSUP). **(B)** Replacement of pyrite cores by chalcopyrite (skeletal texture; massive sulfides, 1807 Zone). **(C)** Replacement of sphalerite by euhedral to anhedral, recrystallized pyrite (carries texture). This is common in sphalerite  $\pm$  galena bands/schlieren (sulfide stringer horizon, MSUP). **(D)** Blebs and lamellae of chalcopyrite with eutaxial texture in sphalerite due to co-precipitation of both minerals (massive sulfides, MSUP). **(E)** Decomposition of tennantite into arsenopyrite + chalcopyrite + (Ag-bearing) tetrahedrite + sphalerite resulting in myrmekitic intergrowth of products that are commonly surrounded by thin rim of tennantite  $\pm$  tetrahedrite (massive sulfides, 1807 Zone). **(F)** Replacement of meneghinite or co-precipitation of galena with tetrahedrite and other phases resulting in myrmekitic intergrowth of galena + Ag-bearing tetrahedrite + Bi-telluride + sphalerite (massive sulfides, MSUP). **(G)** Unmixing of galena resulting in myrmekitic intergrowth of galena + Bi-telluride + altaite + hessite + pyrrhotite (massive sulfides, 1807 Zone). **(H)** Partial replacement of pyrrhotite in the presence of galena resulting in myrmekitic intergrowth of pyrrhotite + ullmanite-willyamite + nisbite  $\pm$  breithauptite  $\pm$  galena (massive sulfides, MSUP). **(I)** Relict of high temperature cubanite lath in chalcopyrite (massive sulfides, 1807 Zone). For mineral abbreviations see Table 5-3





**Figure 5-4.** (previous page) Textures of metal sulfides, tellurides, and electrum in the LFWZ. Minerals forming ore textures are connected to the different textures by trajectories. Solid trajectory lines indicate that a mineral texture is abundant, whereas dashed trajectory lines indicate a rare abundance of a texture. **(A)–(B)** Textural relationships between pyrrhotite – chalcopyrite – cubanite – pyrite: **(A)** Replacement of pyrite by pyrrhotite; and **(B)** high temperature cubanite laths in chalcopyrite partly overgrown by pyrrhotite. **(C)–(D)** Simple textures of tellurides: **(C)** very small crystal of Bi-telluride with altaite in chalcopyrite; and **(D)** Hesseite with inclusions of Bi-telluride and clausthalite; **(E)–(J)** occurrences of electrum in the LFWZ: **(E)** Reflected light (RL) image of submicroscopic electrum between recrystallized pyrite that are partly replaced and surrounded by pyrrhotite; **(F)** back-scattered electron (BSE) image of (E) showing submicroscopic electrum and galena between recrystallized and partly replaced pyrite; **(G)** RL image of coarse-grained, recrystallized pyrite that is partly replaced by pyrrhotite; submicroscopic electrum occurs in pyrrhotite replacing pyrite; **(H)** BSE image of (G) showing submicroscopic electrum in pyrrhotite that replaces coarse-grained, recrystallized pyrite along fractures; **(I)** RL image of recrystallized arsenopyrite on pyrrhotite; submicroscopic electrum occurs between and along fine fractures in arsenopyrite; and **(J)** BSE image of (I) showing submicroscopic electrum and galena between and along thin fractures in recrystallized arsenopyrite. For mineral abbreviations see Table 5-3.

[illegible]

**Figure 5-5.** (previous page) Textural variations of precious metals in 1807, 1806, MSUP and MSDP orebodies. Description in bold describes general textural occurrence of precious metals and text in brackets below gives mineral assemblage. Solid trajectory lines between precious metals and the different textures indicate that a mineral texture is abundant, whereas dashed trajectory lines indicate a rare abundance of a texture. **(A)** Electrum in chalcopyrite on recrystallized pyrite; interstitial between annealed pyrite is AgHg alloy (massive sulfides, 1806 Zone); **(B)** Electrum in chalcopyrite adjacent to sphalerite and pyrite, and spatially close to arsenopyrite, galena, tennantite-tetrahedrite, and stannite (massive sulfides, 1806 Zone); **(C)** Electrum marginal on chalcopyrite on contact to (silicic) gangue and adjacent to sphalerite and unknown AgCuFeS phase (silicified horizon, 1806 Zone); **(D)** Electrum with pyrrhotite, sphalerite, and miargyrite on chalcopyrite margin with contact to gangue (semi-massive sulfides, 1806 Zone); **(E)** Electrum with galena and spatially close to sphalerite in chalcopyrite with contact to gangue (stringer sulfide horizon, MSDP); **(F)** Electrum in myrmekitic intergrowth of arsenopyrite + chalcopyrite + sphalerite + tetrahedrite surrounded by relict tennantite-tetrahedrite rim (massive sulfides, 1806 Zone); **(G)** electrum as inclusions in arsenopyrite myrmekitically intergrown with chalcopyrite + sphalerite + tetrahedrite and surrounded by relict tennantite-tetrahedrite rim (massive sulfides, 1806 Zone); **(H)** electrum with galena and spatially close sphalerite + Bi-telluride between recrystallized pyrite (massive sulfides, MSDP); **(I)** Remobilized AuHgAu alloy along fractures in cataclastic pyrite (massive sulfides, 1806 Zone); **(J)** Electrum adjacent to alloclasite and along brittle fracture in alloclasite (massive sulfides, MSUP); **(K)** Electrum along cataclastic fractures in arsenopyrite and along chalcopyrite margin; electrum partly in contact with galena (massive sulfides, 1807 Zone); **(L)** Electrum occurring interstitially between recrystallized arsenopyrite and pyrite, and spatially close to unknown AgCuFeS phase (massive sulfides, 1806 Zone); **(M)** Electrum in pyrrhotite close to gudmundite  $\pm$  galena  $\pm$  sphalerite (massive sulfides, 1807 Zone); **(N)** Nisbite with breithauptite + sphalerite = chalcopyrite  $\pm$  galena  $\pm$

electrum partially replacing pyrrhotite; minute hessite marginally on galena (massive sulfides, MSDP). Inferred process of formation for each texture is given along trajectories. For mineral abbreviations see Table 5-3.

#### *5-4-2-2 Decomposition textures*

Semi-massive to massive sulfides of the 1807, 1806, and Ming South orebodies have complex myrmekitic textures composed of arsenopyrite + chalcopyrite + (Ag-bearing) tetrahedrite + sphalerite  $\pm$  galena  $\pm$  electrum that is surrounded by a fine tennantite-tetrahedrite rim (Fig. 5-3e). This myrmekite is presumably inferred due to the decomposition of As-rich tennantite resulting in Ag-bearing tetrahedrite either due to desulfidation (Miller and Craig, 1983) or an increase in Sb activity as function of pH and due to previous deposition of arsenopyrite and/or tennantite (Bortnikov et al, 1993; Cook, 1996).

#### *5-4-2-3 Textures of unknown origin*

In addition to myrmekitic intergrowth in tennantite-tetrahedrite, there are other myrmekitic textures present in the 1807 and Ming South orebodies with ambiguous origins. These textures include: (1) myrmekitic intergrowth of galena + Ag-bearing tetrahedrite + Bi-telluride  $\pm$  sphalerite  $\pm$  meneghinite (Fig. 5-3f); (2) myrmekitic texture of galena + tellurides  $\pm$  pyrrhotite (Fig. 5-3g); and (3) myrmekitic intergrowth of pyrrhotite + nisbite  $\pm$  breithauptite  $\pm$  ullmanite-willamite series  $\pm$  gudmundite  $\pm$  galena  $\pm$  electrum (Figs. 5-3h, 5-5m, n). These textures may be due to replacement (Dobbe, 1991; Wen et al., 1991; Cook et al., 1998),

co-precipitation (Gemmell et al., 1989), unmixing of the hydrothermal fluid upon deposition (Liu and Chang, 1994), or sulfide partial melting during metamorphism (Tomkins et al., 2007).

#### *5-4-2-4 Deformation textures*

Deformation textures are predominantly developed in pyrite and arsenopyrite, and include recrystallization, cataclasis, and porphyroblast growth. Pyrite recrystallization is preserved either as annealed aggregates showing triple junctions or as single cubic crystals. Arsenopyrite occurs as single recrystallized grains within annealed pyrite, adjacent to recrystallized pyrite  $\pm$  pyrrhotite, as single recrystallized crystals in chalcopyrite, or rarely in sphalerite. Porphyroblast growth is uncommon for both phases; however, where present arsenopyrite contains inclusions of pyrite, galena or electrum, whereas pyrite contains inclusions of almost all common metal sulfides with the exception of arsenopyrite.

#### *5-4-2-5 Precious metal textures*

Textures involving electrum and/or AgHg $\pm$ Au alloys are shown in Figures 5-4e to j and 5-5 for the LFWZ and other orebodies, respectively. Precious metal textures are more common in the 1807, 1806, and Ming South orebodies, and include: (1) free electrum grains in chalcopyrite on contacts with pyrite  $\pm$  sphalerite and in close spatial relationship to galena, arsenopyrite, tetrahedrite, stannite or AgHg alloy (Fig. 5-5a, b); (2) free electrum on chalcopyrite margins in contact with gangue and close spatial relationship with or adjacent to miargyrite,

unknown AgCuFeS phase, sphalerite, galena or pyrrhotite (Fig. 5-5c-e); (3) electrum as a product of tennantite decomposition either as free grains myrmekitically intergrown with arsenopyrite + chalcopyrite + sphalerite + (Ag-bearing) tetrahedrite or as inclusions in arsenopyrite (Fig. 5-5f, g); (4) electrum  $\pm$  AgHg $\pm$ Au alloy along cataclastic fractures in pyrite and arsenopyrite or between recrystallized pyrite and arsenopyrite with contact to galena, sphalerite and Bi-telluride (Figs. 5-4e, f, i, j, and 5-5h, i); (5) minute electrum grains along replacing pyrrhotite veinlets in pyrite (Fig. 5-4g, h); (6) free electrum grains with arsenopyrite or allosclerite either adjacent to or along fractures in arsenopyrite or allosclerite (Fig. 5-5i-l); and (7) electrum with nisbite  $\pm$  breithauptite or gudmundite in symplectitic intergrowth hosted in pyrrhotite – galena  $\pm$  sphalerite  $\pm$  chalcopyrite (Fig. 5-5m, n).

Of these seven different textures, textures (1) to (3) and (7) are presumably of syngenetic origin, because these textures have a close spatial relationship of precious metals with arsenopyrite  $\pm$  sulfosalts, suggesting a similar paragenesis for most of electrum and arsenopyrite  $\pm$  sulfosalts (Brueckner et al., 2014). In contrast, textures (4) and (6) are presumably the product of internal metamorphic remobilization and/or metamorphic liberation (Laroque et al., 1993; Wagner et al., 2007). The origin of the rare texture (5) is unclear, because the relative timing of pyrrhotite replacement is difficult to constrain at the Ming deposit as stated above.

### 5-4-3 PARAGENESIS

Despite strong variations in mineral assemblage and texture especially between LFWZ and the other orebodies, ore formation is interpreted to be syngenetic at the Ming deposit, whereas metamorphism and deformation resulted in minor metal remobilization and deformation textures (Fig. 5-6; Brueckner et al., 2014).

Initial metal deposition presumably began at elevated temperatures > 300°C, because: (1) Cu-Fe sulfides are dominant at the Ming deposit and chalcopyrite is preferentially deposited at temperatures >300°C (Lydon, 1988; Large, 1992; Ohmoto, 1996); (2) in the chlorite altered LFWZ high temperature (>320°C) cubanite together with other Cu-Fe sulfides dominate; (3) low temperature sulfides (sphalerite, galena), sulfosalts, and precious metals occurring predominantly in the 1807, 1806, and Ming South orebodies, are not replaced by chalcopyrite or cubanite; and (4) metal zoning is not prominent at the Ming deposit.

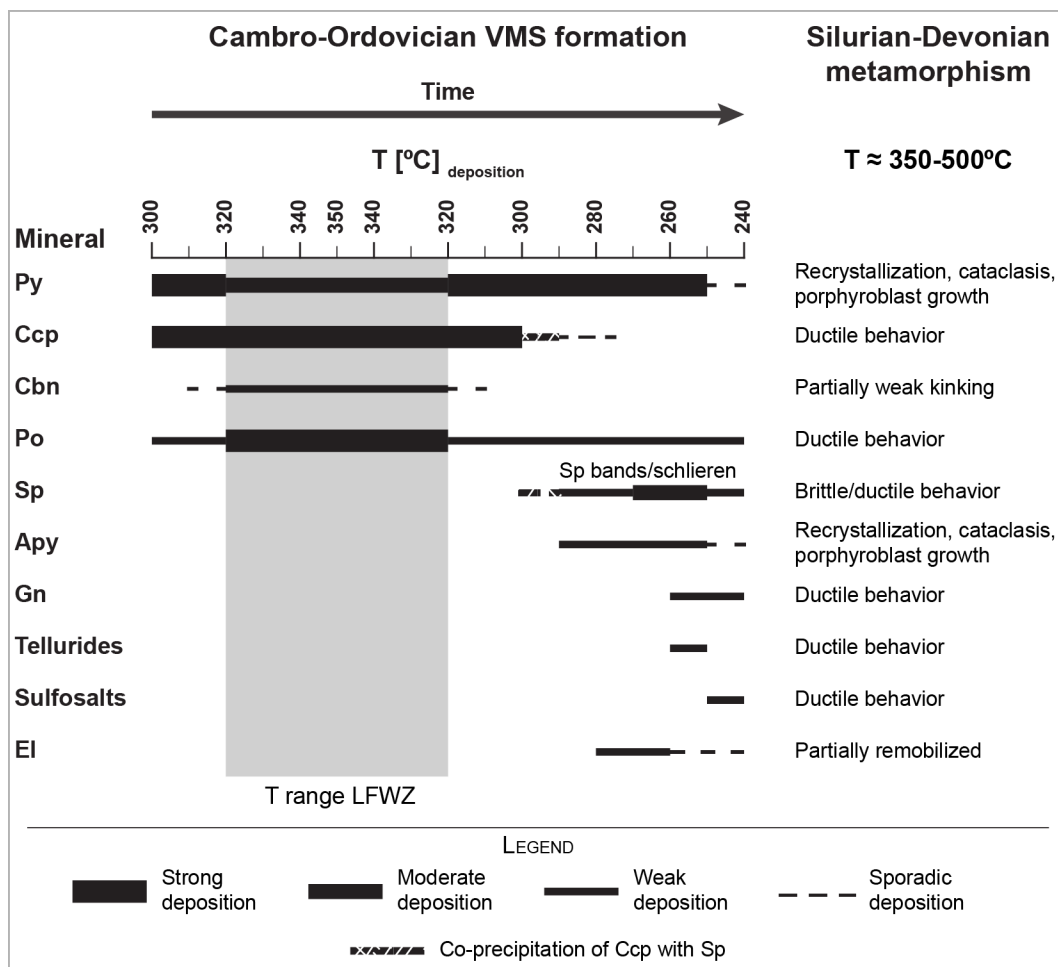
It is inferred that hydrothermal fluid temperature decreased with time resulting in the co-transport of Cu and Zn from which chalcopyrite and sphalerite eventually co-precipitated at temperatures close to 300°C. The deposition of pyrite, pyrrhotite, and sphalerite accompanied by arsenopyrite ± electrum and chalcopyrite in the absence of high temperature cubanite suggests that this mineral assemblage was deposited at temperatures below, but near 300°C (Haymon and Kastner, 1981; Haymon, 1983; Large, 1992; Ohmoto, 1996). The



deposition of sphalerite bands and schlieren in the upper part of the semi-massive to massive sulfides of the 1807, 1806, and Ming South orebodies suggests deposition at temperatures  $<300^{\circ}\text{C}$  that may have continued to lower temperatures ( $<250^{\circ}\text{C}$ ), because galena and tennantite-tetrahedrite commonly accompany sphalerite bands.

Galena, tellurides, sulfosalts, and precious metals formed during late stage at temperatures  $\leq 260^{\circ}\text{C}$  partly followed by decomposition/unmixing. Both tellurides and sulfosalts are rarely associated with pyrite and/or arsenopyrite and therefore the coeval precipitation of these phases is excluded. The deposition of (sulfo-)antimonites replacing pyrrhotite  $\pm$  galena is either late syngenetic (Dobbe, 1991) or orogenic during Silurian-Devonian metamorphism (Cook, 1996).

Despite the syngenetic deposition of most phases at the Ming deposit, including tellurides and precious metals (Brueckner et al., 2014), metamorphic remobilization played a minor role at the Ming deposit. Electrum and  $\text{AgHg}\pm\text{Au}$  alloys were partly remobilized within the orebodies and deposited along fractures in cataclastic pyrite and arsenopyrite or between recrystallized pyrite and/or arsenopyrite.



**Figure 5-6.** (previous page) Paragenetic chart of the most abundant metal sulfides, sulfosalts and precious metals occurring at the Ming deposit. Left side shows paragenesis as function of deposition temperature and time during syngenetic VMS formation, whereas right side gives textural modifications due to Silurian-Devonian metamorphism and deformation

## 5-5 WHOLE ROCK GEOCHEMISTRY AND ORE MINERAL CHEMISTRY

The analytical methods used for whole rock geochemistry, electron microprobe (EPMA) and laser inductively coupled plasma mass spectrometry (LA-ICP-MS) are given in Appendix A5-2.

### 5-5-1 WHOLE ROCK SULFIDE GEOCHEMISTRY

Plots of different elements are shown in Figures 5-7 and 5-8 and results for each orebody are compiled in Table 5-4. Correlation coefficients between the analyzed elements are given in Table 5-5. Sample description and detailed results for each sample are found in Table A5-5.

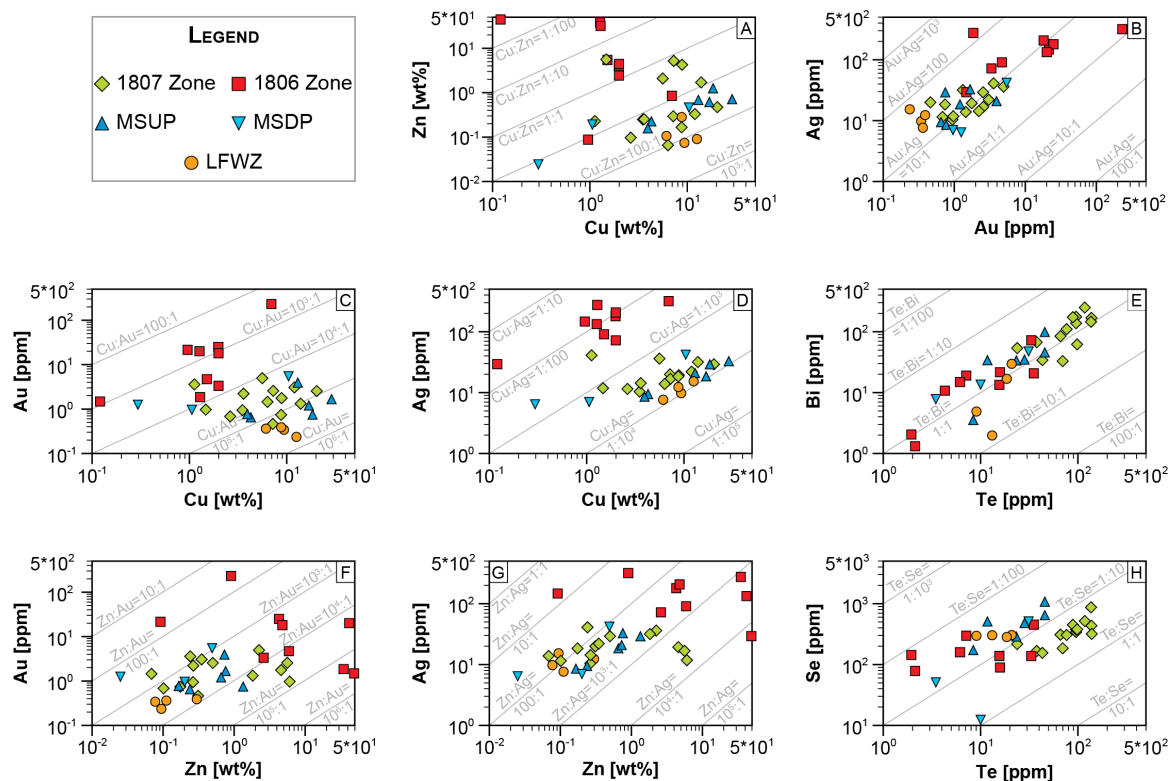
Semi-metal and metal contents from the mineralized samples of all orebodies (Tables 5-4 and A5-5) are representative of the mineralogy in the different orebodies. Copper-iron sulfide assemblages dominate over Zn-Fe sulfide assemblages at the Ming deposit resulting in elevated Cu:Zn ratios of 10:1 to 100:1, with lower Cu:Zn ratios ( $\approx 1:1$  to  $>1:100$ ) in the sphalerite-bearing 1807 and 1806 zones (Fig. 5-7a). Similar to Zn, Pb concentrations are low in the Ming deposit (7,346ppm,  $n=36$ ), and any enrichments in Pb contents are restricted to sphalerite bands.

Variations of elements of the epithermal suite and precious elements are distinctive between the orebodies (Fig. 5-8). Tellurium, Bi, and Se are especially elevated in the 1807 Zone (Te=87.6ppm, Bi=151 ppm, Se=359 ppm,  $n=14$ ), whereas the 1806 Zone has the lowest Te (13.5ppm), Bi (19.6ppm), and Se (187ppm,  $n=9$ ) concentrations (Figs. 5-7e, h, 5-8a), reflecting the different mineralogy between both orebodies (Table 5-3). Tellurium and Bi have a strong positive correlation ( $r=0.89$ , Table 5-5) in all orebodies.

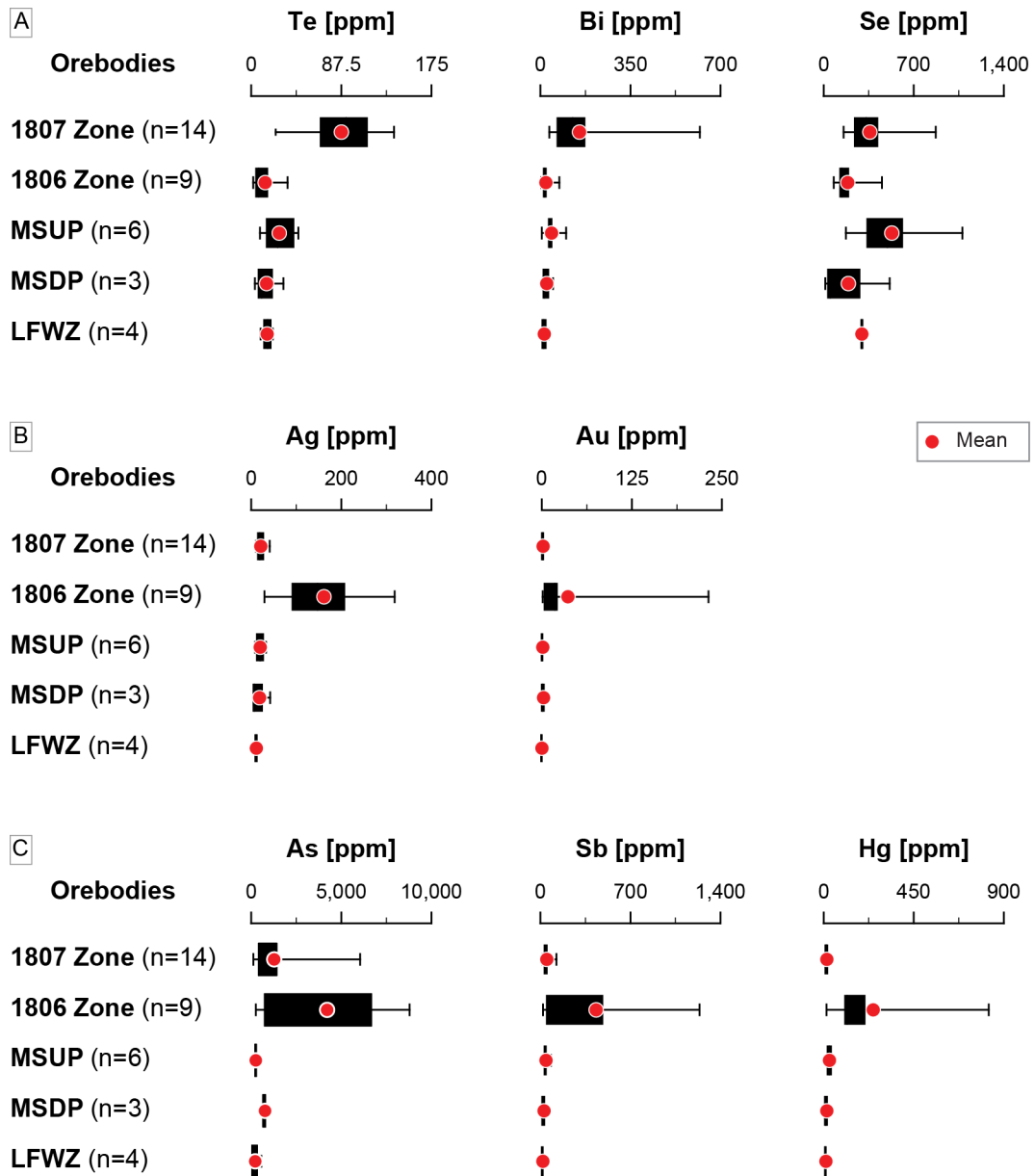
The Au:Ag ratio is fairly constant throughout the Ming deposit ranging between  $\approx 1:10$  and  $1:100$  (Fig. 5-7b) and both metals have a strong positive

correlation ( $r=0.81$ , Table 5-5). The greatest Au and Ag concentrations occur in the 1806 Zone (Fig. 5-8b) due to the greater abundance of electrum, Ag-bearing tetrahedrite, and AgSb sulfosalts. Arsenic, Sb, and Hg are also most enriched in the 1806 Zone (Fig. 5-8c); this orebody contains more tennantite-tetrahedrite, mercurian electrum, and AgHg±Au alloys than the other orebodies. Moreover, strong positive correlations exist between precious metals and As, Sb, and Hg, and between As and Sb (Table 5-5) indicating similar geochemical behavior for As, Sb, Hg, Ag, and Au. Variations of other analyzed elements are less prominent between the orebodies with the exception of transition metals V, Cr, Co, Mn, and Ni, which are enriched in the LFWZ (Table A5-5).

Metal zoning within each orebody is not very well developed, although Fe, Cu, and Zn contents vary with depth. However, the enriched Zn contents in the stratigraphic upper part of the 1807, 1806, and Ming South orebodies is due to sphalerite bands and schlieren, which occur in pyrite-chalcopyrite massive sulfide (Table 5-2) and not as a distinctive horizon or zone in the outer parts of the semi-massive to massive sulfides. Concentrations of elements of the epithermal suite and precious elements do not significantly change with depth in the different orebodies with the exception of the LFWZ, in which Ag, As, Au, Bi, and Hg decrease with increasing depth.



**Figure 5-7.** Compositional plots of selected major and trace elements from mineralized samples of the Ming deposit; data are normalized to 100wt.% sulfides: **(A)** Cu vs Zn; **(B)** Au vs Ag; **(C)** Cu vs Au; **(D)** Cu vs Ag; **(E)** Te vs Bi; **(F)** Zn vs Au; **(G)** Zn vs Ag; and **(H)** Te vs Se



**Figure 5-8.** Box-Whisker plots showing variations in **(A)** Te, Bi, and Se; **(B)** Ag and Au; and **(C)** As, Sb, and Hg in the orebodies of the Ming deposit; data are normalized to 100wt.% sulfides. The horizontal error bars represent the total range of all analyses for each orebody; n – number of analyzed samples

**Table 5-4.** Results of whole rock metal analyses for the different orebodies at the Ming deposit. Data are normalized to 100wt.% sulfides. Detailed results are found in the Table A5-5 (Appendix A5-3); n – number of analyses, Av – average, Min – minimum value, Max – maximum value, NA – no analysis

Orebody Sample No. n	1807 Zone Av $\pm 1\sigma$ 14	Min	Max	1806 Zone Av $\pm 1\sigma$ 9	Min	Max	MSUP Av $\pm 1\sigma$ 6	Min	Max
S [wt.%]	48.5 $\pm$ 3.41	39.4	52.5	45.4 $\pm$ 7.14	32.7	52.3	41.7 $\pm$ 7.71	32.0	50.6
Fe	42.2 $\pm$ 2.43	38.7	45.8	34.0 $\pm$ 13.8	14.1	45.6	43.1 $\pm$ 4.99	35.8	50.0
Cu	7.32 $\pm$ 5.30	1.1	20.3	2.01 $\pm$ 1.95	0.121	6.95	14.2 $\pm$ 9.44	3.93	28.9
Zn	1.53 $\pm$ 2.07	0.064	5.75	15.3 $\pm$ 19.0	0.085	47.0	0.609 $\pm$ 0.401	0.155	1.26
V [ppm]	50.2 $\pm$ 33.6	26.0	157.3	145 $\pm$ 114	45.0	363	89.7 $\pm$ 162	17.9	421
Cr	34.8 $\pm$ 49.3	9.1	162.3	45.4 $\pm$ 36.5	19.6	71.2	202 $\pm$ 419	6.97	952
Mn	184 $\pm$ 350	36.4	1,391	244 $\pm$ 213	39.4	710	379 $\pm$ 758	37.9	1,926
Co	330 $\pm$ 117	132	531	112 $\pm$ 108	12.1	371	273 $\pm$ 130	123	440
Ni	36.7 $\pm$ 17.4	12.5	82.6	45.4 $\pm$ 24.3	19.5	96.8	53.9 $\pm$ 44.4	20.4	141
As	1,275 $\pm$ 1,518	114	6,059	4,221 $\pm$ 3,294	251.5	8,808	251 $\pm$ 80.1	98.2	331
Se	359 $\pm$ 184	155	871	187 $\pm$ 126	78.6	453	530 $\pm$ 317	173	1,078
Ag	21.2 $\pm$ 9.70	10.4	40.9	161 $\pm$ 94.5	29.3	318	19.9 $\pm$ 9.93	8.54	32.8
Cd	102 $\pm$ 124	9.35	369	554 $\pm$ 682	6.13	1,669	32.1 $\pm$ 17.3	9.42	52.4
Sn	21.6 $\pm$ 17.9	8.22	73.0	77.2 $\pm$ 60.8	23.3	205	12.8 $\pm$ 7.66	5.98	26.6
Sb	36.3 $\pm$ 32.4	3.39	113	428 $\pm$ 485	6.59	1,248	30.0 $\pm$ 21.4	6.68	69.7
Te	87.6 $\pm$ 37.3	23.8	139	13.5 $\pm$ 12.8	1.95	35.2	27.2 $\pm$ 16.1	8.41	45.7
Ta	0.358 $\pm$ 0.184	0.099	0.749	0.290 $\pm$ 0.104	0.205	0.419	0.745 $\pm$ 0.968	0.101	2.7
Au	1.95 $\pm$ 1.29	0.461	4.95	36.4 $\pm$ 73.7	1.48	231	1.50 $\pm$ 1.26	0.651	3.94
Hg	5.91 $\pm$ 5.77	1.009	18.8	243 $\pm$ 307	4.09	833	19.3 $\pm$ 13.1	6.03	37.2
Tl	2.01 $\pm$ 0.976	0.814	4.05	8.05 $\pm$ 6.55	3.13	24.6	4.58 $\pm$ 6.51	0.996	17.8
Pb	1,814 $\pm$ 2,100	102.3	7,577	25,640 $\pm$ 50,060	1,827	158,165	962 $\pm$ 1,329	138	3,632
Bi	151 $\pm$ 149	32.9	621	19.6 $\pm$ 21.1	1.31	72.2	41.8 $\pm$ 31.3	3.54	98.9

**Table 5-4. (cont)**

Orebody Sample No. n	MSDP Av $\pm 1\sigma$ 3	Min	Max	LFWZ Av $\pm 1\sigma$ 4	Min	Max	Ming Av $\pm 1\sigma$ 36	Min	Max
S [wt. %]	46.6 $\pm$ 5.84	41.4	52.9	21.2 $\pm$ 3.72	16.3	25.2	43.4 $\pm$ 9.84	16.3	52.9
Fe	48.9 $\pm$ 3.55	46.6	53.0	68.6 $\pm$ 3.36	65.3	73.3	43.8 $\pm$ 12.2	14.1	73.3
Cu	3.93 $\pm$ 5.64	0.296	10.4	9.20 $\pm$ 2.65	6.11	12.6	7.07 $\pm$ 6.57	0.121	28.9
Zn	0.224 $\pm$ 0.220	0.023	0.460	0.135 $\pm$ 0.096	0.072	0.279	4.57 $\pm$ 11.2	0.023	47.0
V [ppm]	478 $\pm$ 437	15.8	883	912 $\pm$ 102	785	1,026	212 $\pm$ 308	15.8	1,026
Cr	154 $\pm$ 178	9.47	352	2,654 $\pm$ 1,055	1,533	4,041	543 $\pm$ 1,083	6.97	4,041
Mn	630 $\pm$ 596	33.7	1,226	3,211 $\pm$ 438	2,636	3,637	605 $\pm$ 1,032	33.7	3,637
Co	248 $\pm$ 207	9.58	386	625 $\pm$ 209	484	935	292 $\pm$ 195	9.58	935
Ni	69.9 $\pm$ 48.8	38.9	121	486 $\pm$ 153	327	681	94.4 $\pm$ 150	12.5	681
As	766 $\pm$ 111	698	894	219 $\pm$ 256	20.3	564	1,681 $\pm$ 2,395	20.3	8,808
Se	192 $\pm$ 278	12.4	513	297 $\pm$ 9.73	283	305	328 $\pm$ 222	12.4	1,078
Ag	18.5 $\pm$ 20.4	6.42	42.0	11.3 $\pm$ 3.31	7.63	15.3	54.7 $\pm$ 77.6	6.42	318
Cd	15.5 $\pm$ 17.3	3.05	35.2	9.10 $\pm$ 4.77	6.58	16.3	186 $\pm$ 400	3.05	1,669
Sn	30.4 $\pm$ 18.2	9.47	41.2	23.0 $\pm$ 4.70	17.4	27.4	35.0 $\pm$ 40.3	5.98	205
Sb	14.6 $\pm$ 14.4	5.89	31.1	5.17 $\pm$ 4.66	1.65	11.8	128 $\pm$ 292	1.65	1,248
Te	14.9 $\pm$ 14.5	3.47	31.1	15.4 $\pm$ 5.32	9.07	20.9	44.9 $\pm$ 42.6	1.95	138.8
Ta	3.22 $\pm$ 2.61	0.210	4.74	2.63 $\pm$ 0.970	1.74	3.95	1.09 $\pm$ 1.43	0.099	4.74
Au	2.56 $\pm$ 2.52	1.0	5.5	0.332 $\pm$ 0.067	0.236	0.389	10.4 $\pm$ 38.4	0.236	231
Hg	5.72 $\pm$ 9.41	0.198	16.6	1.14 $\pm$ 0.537	0.761	1.52	70.7 $\pm$ 184	0.198	833
Tl	6.62 $\pm$ 8.41	0.673	16.2	1.67 $\pm$ 0.707	0.714	2.30	4.30 $\pm$ 5.23	0.673	24.6
Pb	539 $\pm$ 208	404	779	225 $\pm$ 297	34.2	664	7,346 $\pm$ 26,263	34.2	158,165
Bi	22.9 $\pm$ 21.4	7.79	47.4	13.3 $\pm$ 12.6	1.97	29.6	74.0 $\pm$ 112	1.31	621



**Table 5-5.** Pearson's correlation coefficients of selected elements for massive sulfides and stringer sulfides from all orebodies of the Ming deposit. Data are based on sulfides normalized to 100wt. %

	S	Fe	Cu	Zn	V	Cr	Mn	Co	Ni	As	Se	Ag	Cd	Sn	Sb	Te	Ta	Au	Hg
Fe	-0.23																		
Cu	-0.31	0.44																	
Zn	0.10	-0.76	-0.25																
V	-0.67	0.34	0.07	-0.12															
Cr	-0.60	0.50	0.24	-0.50	0.55														
Mn	-0.80	0.22	0.15	-0.09	0.86	0.61													
Co	-0.20	0.62	0.58	-0.38	0.25	0.40	0.26												
Ni	-0.80	0.57	0.29	-0.44	0.75	0.67	0.81	0.32											
As	0.55	-0.37	-0.35	0.47	-0.23	-0.65	-0.36	-0.34	-0.46										
Se	-0.14	-0.05	0.25	-0.01	-0.16	0.16	0.07	0.29	0.07	-0.11									
Ag	0.17	-0.47	-0.17	0.58	0.02	-0.49	-0.12	-0.49	-0.16	0.57	-0.34								
Cd	0.12	-0.78	-0.22	0.99	-0.16	-0.51	-0.11	-0.37	-0.47	0.47	0.05	0.53							
Sn	-0.17	-0.49	-0.24	0.60	0.43	-0.22	0.36	-0.29	0.02	0.34	-0.34	0.59	0.59						
Sb	0.38	-0.42	-0.15	0.50	-0.22	-0.64	-0.30	-0.41	-0.35	0.82	0.08	0.73	0.49	0.33					
Te	0.20	0.08	0.47	-0.04	-0.30	-0.01	-0.18	0.59	-0.17	-0.07	0.51	-0.30	0.07	-0.24	-0.11				
Ta	-0.54	0.48	0.16	-0.38	0.65	0.74	0.73	0.43	0.62	-0.53	-0.01	-0.51	-0.41	-0.03	-0.63	-0.18			
Au	0.43	-0.30	-0.20	0.38	-0.12	-0.59	-0.29	-0.48	-0.30	0.59	-0.52	0.81	0.35	0.43	0.63	-0.30	-0.45		
Hg	0.26	-0.75	-0.23	0.85	-0.22	-0.57	-0.24	-0.52	-0.49	0.49	-0.12	0.71	0.82	0.52	0.61	-0.19	-0.48	0.62	
Tl	0.01	-0.33	-0.17	0.43	0.37	0.01	0.20	-0.29	-0.02	0.29	-0.20	0.58	0.38	0.50	0.36	-0.37	-0.02	0.44	0.57
Pb	0.36	-0.71	-0.47	0.70	-0.24	-0.49	-0.30	-0.51	-0.44	0.58	-0.09	0.72	0.67	0.45	0.62	-0.08	-0.61	0.52	0.68
Bi	0.39	-0.02	0.29	0.01	-0.43	-0.20	-0.38	0.42	-0.34	0.01	0.37	-0.18	0.10	-0.22	-0.06	0.89	-0.34	-0.13	-0.09
<b>Tl Pb</b>																			
Pb	0.38																		
Bi	-0.35	0.13																	

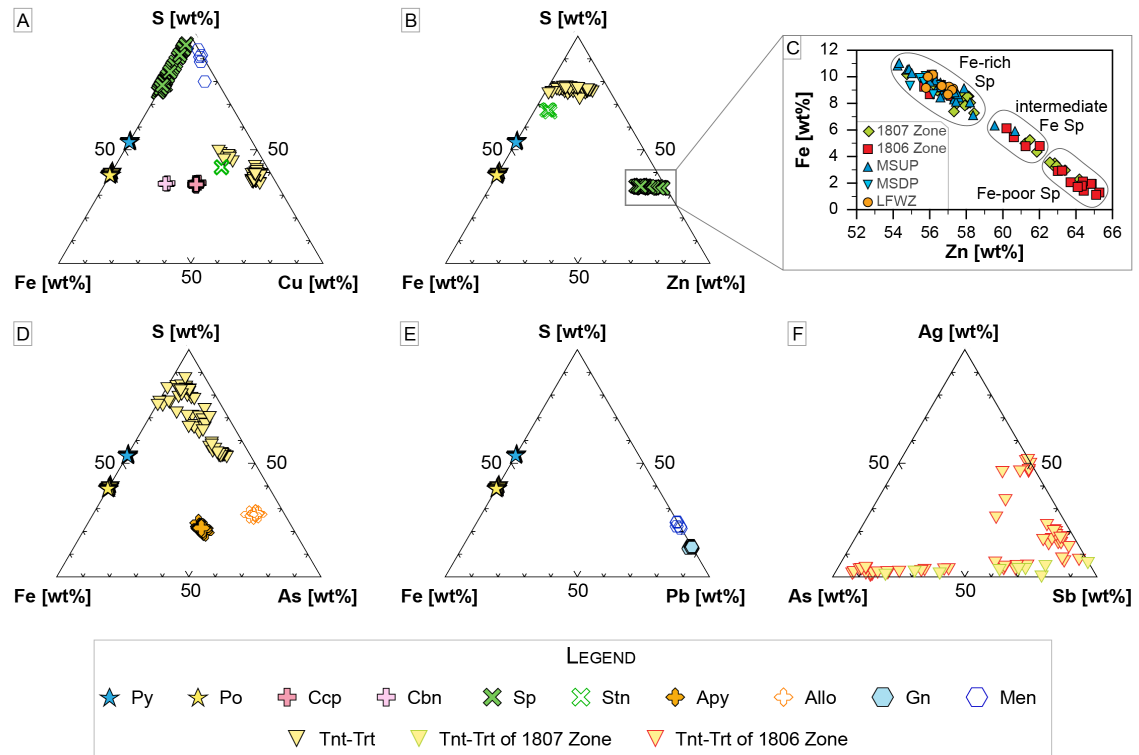
**Note:** Pearson's correlation is based on 36 samples from all orebodies; data are log normalized due to variations in the overall sulfide content of the samples; coefficients with absolute values greater than 0.33 are statistically significant at the 95% confidence level

### 5-5-2 EPMA AND LA-ICP-MS

Micro-analytical data for various mineral phases are summarized in Tables 5-6 and A5-6 (electronic Appendix eA5) and shown in Figures 5-9 to 5-11.

The analyzed minerals have generally homogeneous major and minor element compositions and are typically stoichiometric (Fig. 5-9, Table 5-6). However, Fe content in sphalerite, Ag content in tennantite-tetrahedrite, and Hg content in electrum vary. The Fe content of sphalerite is between 1.12–11.04wt.% and can be divided into three groups: (1) Fe-rich sphalerite with 7.27–11.04wt.% Fe and 54.32–58.42wt.% Zn; (2) intermediate Fe sphalerite with 4.35–6.33wt.% Fe and 59.55–61.86wt.% Zn; and (3) Fe-poor sphalerite with 1.12–3.57wt.% Fe and 65.10–62.57wt.% Zn (Fig. 9). The strongest variations in Fe among sphalerite are in the 1807 Zone (2.29–10.18wt.% Fe, n=28) and the 1806 Zone (1.12–10.16wt.% Fe, n=27; Brueckner et al., 2014). In the MSUP, MSDP, and LFWZ, sphalerite is intermediate to Fe-rich; however, Fe-rich sphalerite dominates in these three orebodies. The Ag content in tennantite-tetrahedrite of the 1807 Zone is low (0.986wt.%, n=9), whereas in the 1806 Zone tennantite-tetrahedrite shows strong variations in Ag content (0.307–29.27wt.%, n=52; Brueckner et al., 2014). Tennantite-tetrahedrite from the Ming South orebodies was not analyzed, but semi-quantitative X-ray analysis by SEM (SEM-EDX) shows low Ag concentrations in tennantite-tetrahedrite. Electrum (AuAg alloy with Au>10wt.%) in the Ming deposit has high amounts of Hg, particularly in the 1806 Zone (14.37wt.% Hg, n=22; Brueckner et al., 2014), whereas Hg in electrum of

the 1807 Zone is much lower with 3.05wt.% (n=1). Electrum from the Ming South orebodies could not be analyzed due to grain size but also showed low Hg contents using semi-quantitative SEM-EDX spectra.



**Figure 5-9.** Major compositions of sulfides and sulfosalts analyzed by EPMA: **(A)** ternary plot of Fe – S – Cu; **(B)** ternary plot of Fe – S – Zn; **(C)** binary plot of varying Fe composition in sphalerite; **(D)** ternary plot of Fe – S – As; **(E)** ternary plot of Fe – S – Pb; and **(F)** ternary plot of As – Ag – Sb showing compositional variations within tennantite-tetrahedrite of the 1806 and 1807 zones. For mineral abbreviations see Table 5-3

**Table 5-6.** Microprobe results of major and minor element concentrations for mineral phases from the Ming deposit and their calculated mineral formulae; detailed micro-analytical analyses are found in Table A5-6 (Appendix A5-3); Av – average, Min – minimum value, Max – maximum value

Mineral phase*		S [wt.%]	Fe	Cu	Zn	Pb	As	Co	Ni	Te
[common] metal sulfides										
Py (121)	Av ± 1σ	53.22 ± 0.356	45.92 ± 0.338							
	Min	52.36	45.10							
Ccp (176)	Max	53.92	46.77							
	Av ± 1σ	34.88 ± 0.309	30.52 ± 0.341	34.46 ± 0.291						
Cbn (28)	Min	33.61	29.16	33.32						
	Max	36.13	31.46	35.55						
	Av ± 1σ	35.13 ± 0.199	41.33 ± 0.294	23.40 ± 0.251						
	Min	34.80	40.92	22.83						
	Max	35.39	42.26	23.63						
	Av ± 1σ	38.93 ± 0.456	60.37 ± 0.637							
Po (83)	Min	38.20	58.11							
	Max	40.14	61.44							
Sp (97)	Av ± 1σ	33.50 ± 0.424	7.47 ± 2.78		58.44 ± 3.03					
	Min	32.33	1.12		54.24					
	Max	34.65	11.04		65.28					
	Av ± 1σ	13.19 ± 0.282				86.12 ± 0.638				
Gn (42)	Min	12.64				84.88				
	Max	13.90				87.55				
Apy (96)	Av ± 1σ	21.27 ± 0.538	34.21 ± 0.424				43.96 ± 0.686			
	Min	19.50	32.97				41.69			
	Max	23.71	34.98				46.68			
	[uncommon] metal sulfides including tellurides, selenides, and (sulfo-)antimonides									
Allo (5)	Av ± 1σ	20.04 ± 0.349	8.31 ± 1.06				44.38 ± 0.490	24.74 ± 0.614	2.15 ± 0.406	
	Min	19.61	7.15				43.55	24.01	1.79	
	Max	20.42	9.88				44.78	25.59	2.81	
	Av ± 1σ									38.52 ± 2.62
Hess (3)	Min									36.99
	Max									41.54
Tsu (9)	Av ± 1σ					5.13 ± 0.886				36.82 ± 1.80
	Min					4.30				34.78
	Max					6.96				39.34
	Av					3.42				28.35
BiTe (1)	Av					61.21				37.73
	Av ± 1σ	15.21 ± 0.085	26.73 ± 0.094							
Gud (3)	Min	15.15	26.67							
	Max	15.27	26.80							

Table 5-6. (cont.)

Mineral phase*	Ag [wt.%]	Bi	Sb	Au	Sn	Hg	Total	Mineral Formula
[common] metal sulfides								
Py (121)	Av ± 1σ Min Max						99.14 ± 0.511 98.13 100.45	Fe <sub>0.97-1.01</sub> S <sub>2</sub>
Ccp (176)	Av ± 1σ Min Max						99.85 ± 0.432 98.71 101.26	Cu <sub>0.96-1.06</sub> Fe <sub>0.94-1.05</sub> S <sub>2</sub>
Cbn (28)	Av ± 1σ Min Max						99.86 ± 0.160 99.67 100.21	Cu <sub>0.98-1.02</sub> Fe <sub>2.00-2.07</sub> S <sub>3</sub>
Po (83)	Av ± 1σ Min Max						99.30 ± 0.535 98.07 100.25	Fe <sub>0.84-0.92</sub> S
Sp (97)	Av ± 1σ Min Max						99.41 ± 0.690 97.98 100.80	(Zn <sub>0.79-0.97</sub> Fe <sub>0.02-0.19</sub> ) <sub>0.95-1.02</sub> S
Gn (42)	Av ± 1σ Min Max						99.31 ± 0.735 98.11 100.73	Pb <sub>0.95-1.06</sub> S
Apy (96)	Av ± 1σ Min Max						99.44 ± 0.678 98.07 101.24	As <sub>0.75-1.02</sub> Fe <sub>0.83-1.00</sub> S
[uncommon] metal sulfides including tellurides, selenides, and (sulfo-)antimonides								
Allo (5)	Av ± 1σ Min Max						99.61 ± 0.376 99.04 100.03	(Co <sub>0.65-0.71</sub> Ni <sub>0.05-0.08</sub> ) <sub>0.71-0.76</sub> Fe <sub>0.21-0.28</sub> As <sub>0.92-0.97</sub> S
Hess (3)	Av ± 1σ Min Max	60.64 ± 2.30 58.09 62.56					99.27 ± 1.00 98.27 100.27	Ag <sub>1.65-2.00</sub> Te
Tsu (9)	Av ± 1σ Min Max	56.89 ± 2.43 52.45 60.25	1.03 ± 0.610 0.000 1.58				99.87 ± 0.927 98.52 101.10	(Bi <sub>0.81-1.05</sub> Pb <sub>0.07-0.12</sub> Sb <sub>0.00-0.04</sub> ) <sub>0.94-1.17</sub> Te
BiTe (1) Alt (1)	Av Av	67.76	0.087				99.62 98.94	(Bi <sub>2.32</sub> Pb <sub>0.15</sub> Sb <sub>0.01</sub> ) <sub>3.07</sub> Te <sub>2</sub> Pb <sub>1.00</sub> Te
Gud (3)	Av ± 1σ Min Max		58.46 ± 0.211 58.31 58.61				100.41 ± 0.390 100.13 100.69	Fe <sub>1.01</sub> Sb <sub>1.01</sub> S

Table 5-6. (cont.)

Mineral phase*	S [wt.%]	Fe	Cu	Zn	Pb	As	Co	Ni	Te
[uncommon] metal sulfides including tellurides, selenides, and (sulfo-)antimonides (cont.)									
Breit (3)	Av $\pm 1\sigma$	0.927 $\pm$ 0.696							
	Min	0.501							
	Max	1.73							
Nis (1)	Av	0.811							
		1.09							
Men (5)	Av $\pm 1\sigma$	17.61 $\pm$ 0.966							
	Min	16.63							
	Max	18.66							
Tnt-Trt (61)	Av $\pm 1\sigma$	25.72 $\pm$ 1.93							
	Min	20.99							
	Max	28.52							
Stn (4)	Av $\pm 1\sigma$	29.48 $\pm$ 0.213							
	Min	29.19							
	Max	29.67							
El (23)	Av $\pm 1\sigma$	12.01 $\pm$ 0.168							
	Min	11.78							
	Max	12.16							
		precious metals							
		3.12 $\pm$ 1.38							
		0.314							
		5.49							
		2.33 $\pm$ 0.344							
		1.97							
		2.76							
		8.61 $\pm$ 6.84							
		0.000							
		19.25							
		59.40 $\pm$ 1.30							
		58.04							
		61.23							
		31.94 $\pm$ 0.311							
		31.65							
		32.27							
		17.25							
		sulfosalts							
		1.87 $\pm$ 0.828							
		1.12							
		3.25							
		4.50 $\pm$ 1.31							
		15.29							
		44.46							
		28.14 $\pm$ 0.156							
		27.96							
		28.28							
		66.52 $\pm$ 0.213							
		66.37							
		66.77							
		77.31							
		1.69							
		sulfosalts							
		20.06 $\pm$ 0.313							
		19.73							
		20.38							
		16.27 $\pm$ 9.78							
		1.33							
		29.56							
		5.38 $\pm$ 7.91							
		0.252							
		29.27							
		99.39 $\pm$ 0.687							
		98.82							
		100.15							
		98.16							
		(Ni <sub>0.98-1.01</sub> , Fe <sub>0.02-0.06</sub> ) <sub>1.01</sub> Sb							
		(Ni <sub>0.93</sub> , Fe <sub>0.05</sub> , Co <sub>0.06</sub> , Au <sub>0.03</sub> ) <sub>1.06</sub> Sb <sub>2</sub>							
		Pb <sub>11.56-13.67</sub> Cu <sub>0.73-2.31</sub> Sb <sub>6.68-7.62</sub> S <sub>24</sub>							
		98.17							
		99.39							
		99.33 $\pm$ 0.696							
		(Cu <sub>4.60-10.63</sub> , Ag <sub>0.04-5.39</sub> ) <sub>9.50-10.72</sub> (Fe <sub>0.61-2.30</sub> , Zn <sub>0.09-1.45</sub> ) <sub>1.94-2.52</sub> (As <sub>0.00-3.90</sub> , Sb <sub>0.16-4.37</sub> ) <sub>3.78-4.52</sub> S <sub>13</sub>							
		98.04							
		100.98							

**Table 5-6. (cont.)**

Mineral phase*	Ag [wt.%]	Bi	Sb	Au	Sn	Hg	Total	Mineral Formula
Stn (4)	Av ± 1σ Min Max			sulfosalts (cont.) 27.53 ± 0.204 27.32 27.81			99.50 ± 0.563 98.90 100.02	Cu <sub>1.91-1.95</sub> (Fe <sub>0.32-0.56</sub> , Zn <sub>0.13-0.18</sub> ) <sub>1.07-1.12</sub> Sn <sub>1.00-1.01</sub> S <sub>4</sub>
El (23)	Av ± 1σ Min Max			precious metals 45.71 ± 11.40 13.87 70.17		13.88 ± 3.52 3.05 20.57	99.70 ± 0.947 98.19 101.07	(Au, Ag, Hg) <sub>0.62-1.23</sub>

\* Mineral abbreviations as in Table 5-3 and number in brackets is number of EPMA analysis

Trace element concentrations analyzed by LA-ICP-MS of Au, Ag, As, Sb, Te, Bi, and Se in pyrite, chalcopyrite, pyrrhotite, sphalerite, arsenopyrite, galena, cubanite, and tennantite-tetrahedrite are shown in Figures 5-10 and 5-11. Gold concentrations are typically either below detection limit or below 1ppm in the analyzed sulfides. Elevated Au concentrations (>10ppm) are only present in single grains of chalcopyrite, pyrite, sphalerite, arsenopyrite, and tennantite-tetrahedrite of the 1806 Zone. All these grains occurred in close proximity to electrum and Au in these minerals did not occur as visible inclusions.

Silver is most enriched in chalcopyrite of the 1806 Zone (344ppm Ag, n=31) and in galena of the 1807, 1806, and Ming South orebodies (1,119ppm Ag, n=15). In contrast, Ag concentrations in the other minerals are low and typically less than 50ppm (Table A5-6).

Arsenic concentrations are greatest in pyrite (1,694ppm, n=45), pyrrhotite (1,025ppm, n=34), and chalcopyrite (909ppm, n= 61). Arsenic varies strongly within these minerals in all orebodies and shows no particular preference in any orebody (Fig. 5-10). Galena, sphalerite, and cubanite contain much less As (Table A5-6). Antimony shows similar trends to As, but concentrations in the analyzed phases are much lower and rarely exceed 25ppm (Figs. 5-10, 5-11). The exception is galena, where Sb has a similar pattern to Ag, and is strongly enriched (1,128ppm, n=15).

Tellurium concentrations are generally low (<50ppm), but show a strong spatial preference for minerals of the MSUP and 1807 Zone, and to a lesser

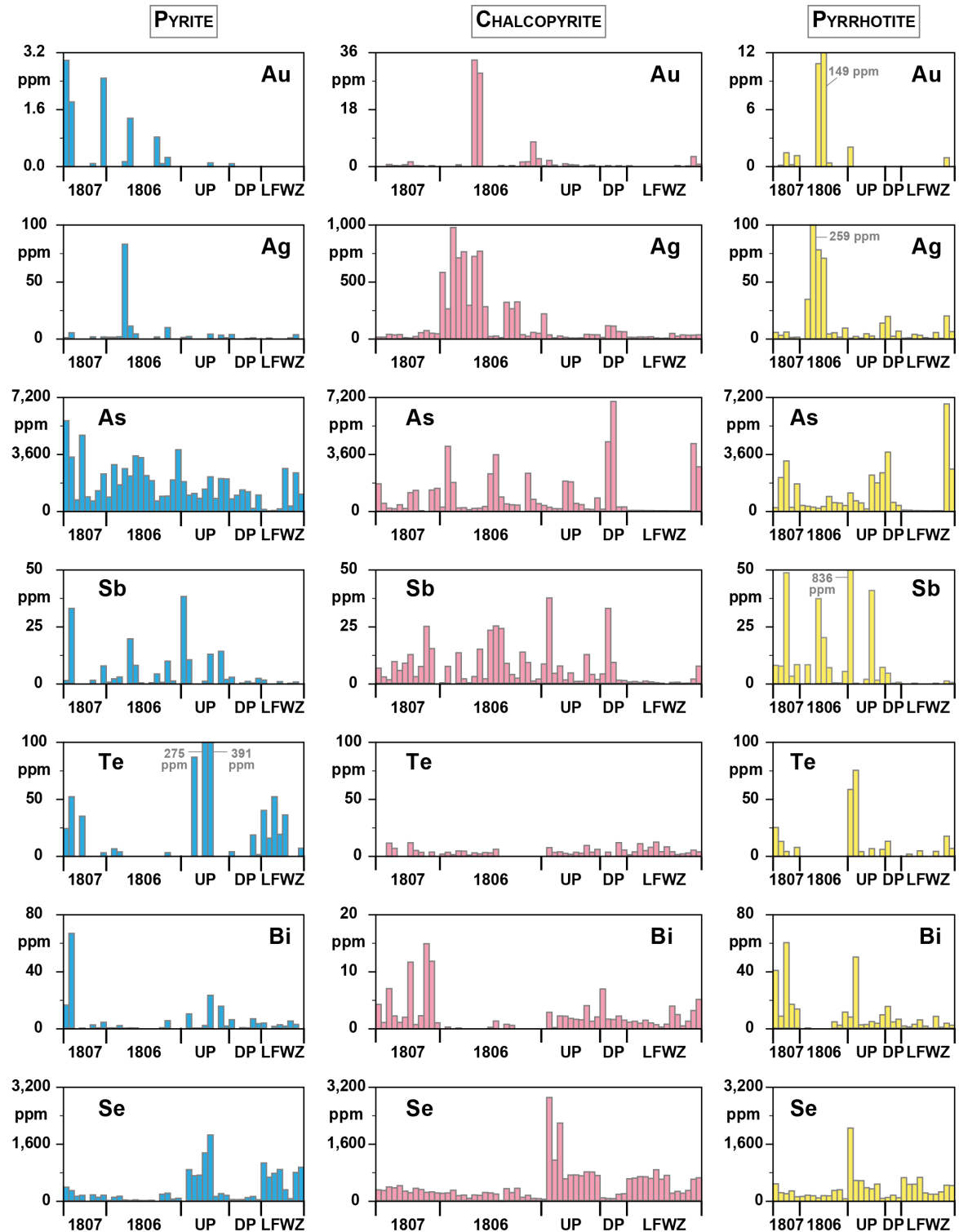


extent in the MSDP and 1806 Zone (Figs. 5-10, 5-11). Arsenopyrite and galena have the greatest Te contents with 646ppm (n=96) and 540ppm (n=42), respectively. Tellurium is especially enriched in galena that is low in Sb (Fig. 5-11). Bismuth shows very similar trends to Te and is greatest in galena of the 1807 Zone and Ming South orebodies (2,466ppm, n=3). Enriched Bi concentrations (228ppm) also occur in two Ag-rich tetrahedrites of the 1806 Zone. Selenium concentrations vary between minerals and among orebodies. Pyrite, chalcopyrite, and pyrrhotite in the Ming deposit have, in general, Se above 300ppm; however, Se in these minerals is higher in the MSUP and LFWZ than in 1807, 1806 and MSDP (Fig. 5-10, Table A5-6). Selenium is highly variable in sphalerite and arsenopyrite, and is lower in these minerals in the 1806 Zone and MSDP relative to sphalerite and arsenopyrite in the other orebodies. High Se contents in galena of the 1807 Zone and MSUP, and high Se in Ag-rich tetrahedrite of the 1806 Zone are correlated with enriched Te and Bi concentrations in the same grains.

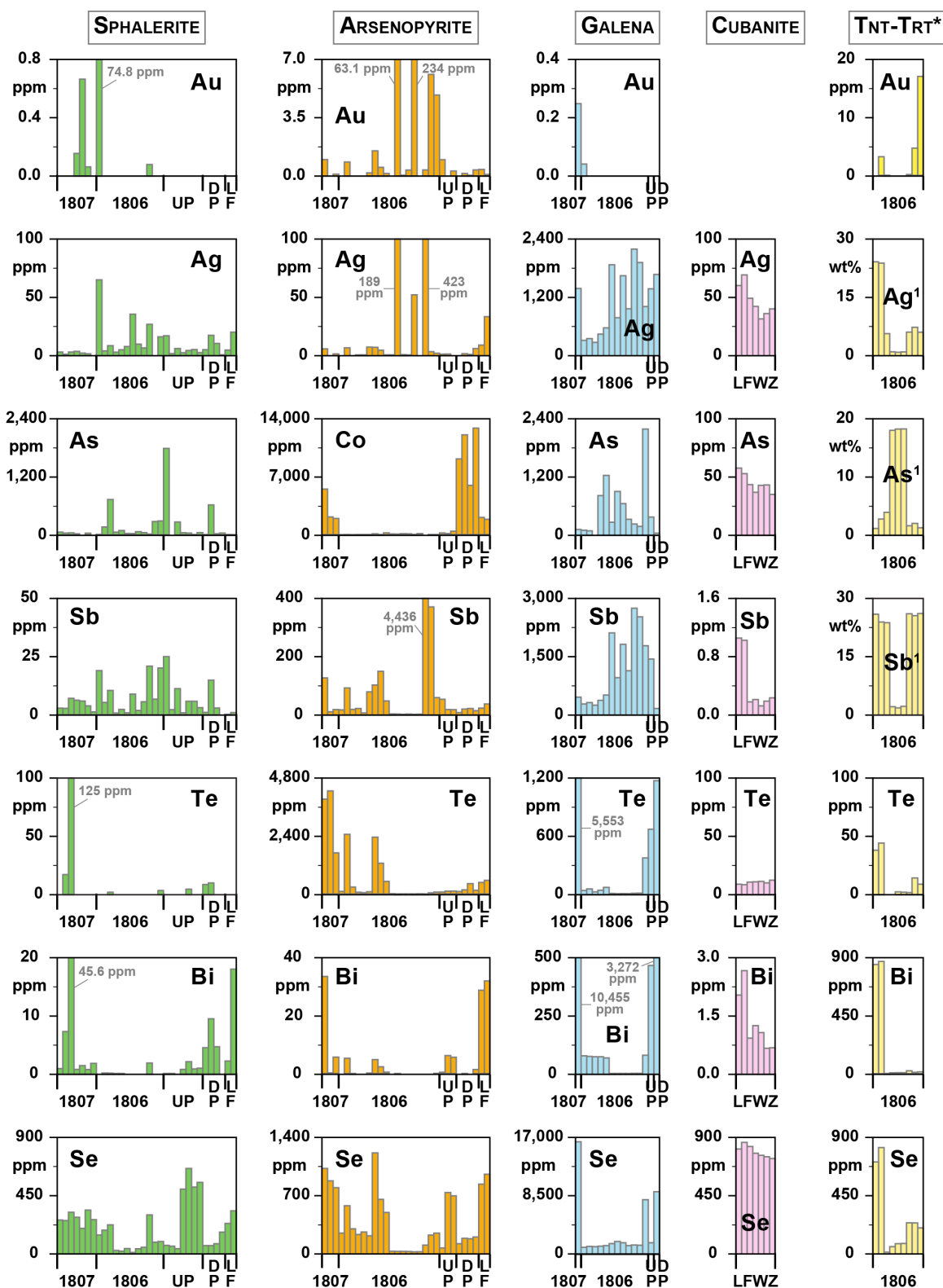
In the analyzed minerals, transition metals (Co, Cr, Mn, Ni, Ti, V) are either depleted or have concentrations below the detection limit. The exceptions are Co and Ni, which are preferably enriched in high temperature phases, but also are enriched in sphalerite and arsenopyrite of the Ming South and LFWZ orebodies (Table A5-6).

Sphalerite in all orebodies has enriched Cd and Mn concentrations (Table A5-6) due to the preferred substitution of both elements in sphalerite (Di

Benedetto et al., 2005; Cook et al., 2009).



**Figure 5-10.** (previous page) Histograms of LA-ICP-MS data for selected trace elements for pyrite, chalcopyrite, and pyrrhotite; UP = MSUP, DP = MSDP



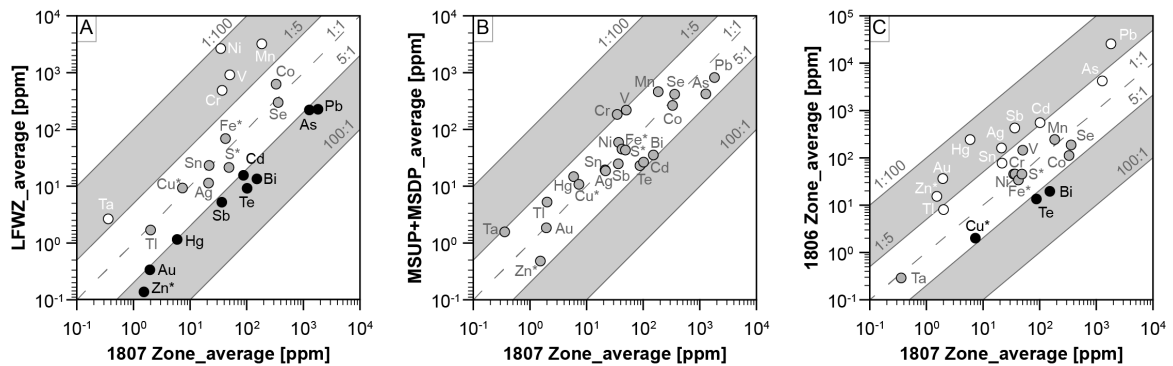
**Figure 5-11.** (previous page) Histograms of LA-ICP-MS data of selected trace elements for sphalerite, arsenopyrite, galena, cubanite, and tetrahedrite-tennantite; UP or U = MSUP, DP or D = MSDP, LF = LFWZ, \*tennantite-tetrahedrite, <sup>1</sup> Ag, As and Sb for tennantite-tetrahedrite are from EPMA analysis and given in wt.%; no analyses of Au in cubanite are above detection limits

## 5-6 DISCUSSION

### 5-6-1 HYDROTHERMAL FLUID CONDITIONS

The transport of elements in hydrothermal fluids is controlled by various physico-chemical parameters, with temperature, pH, redox state, and  $fS_2$  being most critical and changes in these parameters affecting metal transport and precipitation (Barton and Skinner, 1979; Butterfield et al., 1990; Seward and Barnes, 1997; Sack and Ebel, 2006). Pressure is typically neglected, since it has no significant effect on the transport and deposition of elements in ascending hydrothermal fluids within VMS forming deposits as long as the fluids have not boiled (Barton and Skinner, 1979; Simon and Essene, 1996; Monecke et al., 2014).

At the Ming deposit, differing element composition of the different orebodies (Fig. 5-12) indicates that different hydrothermal fluid conditions were responsible for the formation of the (1) LFWZ, (2) the 1807 Zone, MSUP, and MSDP, and (3) the 1806 Zone. The fluid conditions are constrained by using common metal sulfides, and elements of the epithermal suite and precious elements.



**Figure 5-12.** Comparison of the average metal concentration in **(A)** 1807 Zone vs LFWZ; **(B)** 1807 Zone vs Ming South orebodies; and **(C)** 1807 vs 1806 Zone. Elements enriched in the LFWZ or 1806 Zone have white circles; elements with no significant enrichment or depletion in the comparing orebodies have grey circles; and metals and semi-metals enriched in the 1807 Zone have black circles; data are normalized to 100wt.% sulfides; \* S, Fe, Cu, and Zn are in wt.%, whereas the other metals and semi-metals are in ppm

#### 5-6-1-1 Common metal sulfides

The role of temperature in the metal budgets in VMS deposits is well established (e.g., Lydon, 1988; Large, 1992; Ohmoto, 1996). However, providing quantitative estimates of temperatures in both modern and ancient VMS deposits often is difficult due to the lack of mineral phases in equilibrium, which itself arises from the dynamic nature of VMS deposit formation (e.g., zone refining; Lydon, 1988; Large, 1992; Ohmoto, 1996). This lack of equilibrium is clearly documented at the Ming deposit by this and previous work (Brueckner et al., 2014, 2015). Nevertheless, temperature assumptions can be made from mineral textures, assemblages, and paragenetic relationships (Figs. 5-3 to 5-6). The

LFWZ with its dominant Cu-Fe sulfide assemblage and chlorite alteration presumably formed at temperatures hotter than 300°C, and this area also represents the stockwork zone. In contrast, ore mineral assemblages (pyrite – chalcopyrite with minor pyrrhotite – sphalerite and trace arsenopyrite – galena – tellurides – sulfosalts – precious metals) of the other orebodies strongly indicate formation temperatures of 300°C and below.

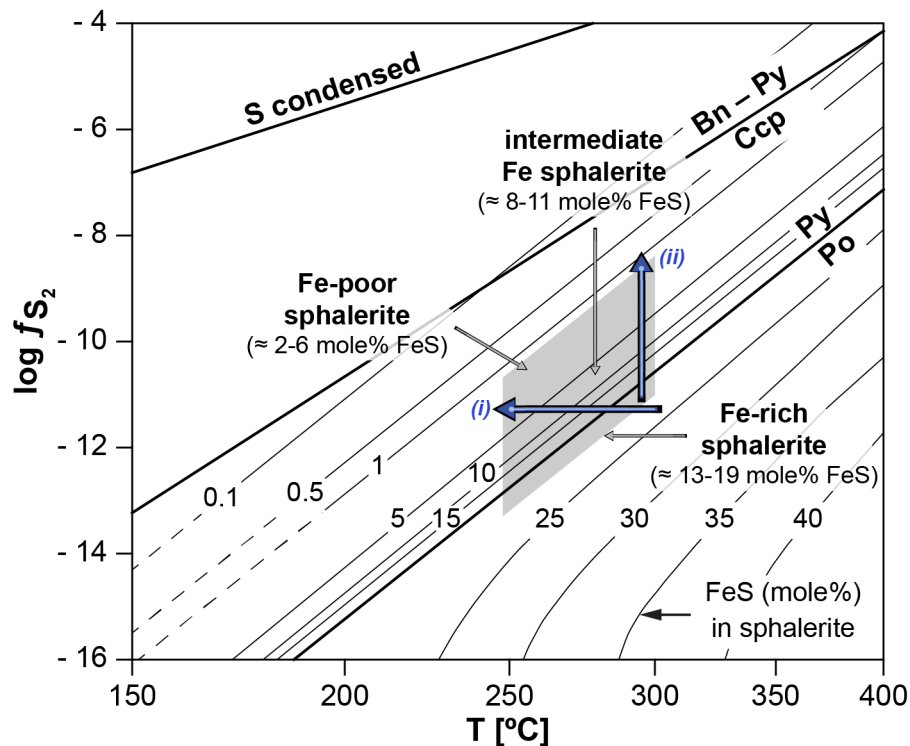
Sulfidation state and fluid redox conditions have also an effect on the mineral assemblages and compositions at the Ming deposit and this is well recorded in the highly variable Fe contents in sphalerite (Table 5-6; Fig. 5-9b, c). Iron-poor sphalerite is restricted to the 1807 and 1806 zones, whereas Fe-rich and intermediate-Fe sphalerite are found in all orebodies (Fig. 5-9c). The substitution of  $\text{Fe}^{2+}$  for  $\text{Zn}^{2+}$  in sphalerite is very common (Barton and Toulmin, 1966; Di Benedetto et al., 2005; Cook et al., 2009) and a function of the redox state of the co-existing hydrothermal fluid (Barton and Toulmin, 1966; Hannington and Scott, 1989): the greater the amount of  $\text{Fe}^{2+}$  in sphalerite, the more reduced the coexisting hydrothermal fluid. Mineral assemblages indicating higher oxidation state (hematite-magnetite) or higher sulfidation state (chalcopyrite-bornite-pyrite) are not present. Therefore, the hydrothermal fluids depositing sphalerite were rather reduced. Barton and Toulmin (1966) showed that the Fe content in sphalerite is also a function of the sulfidation state of the co-existing hydrothermal fluid. In Figure 5-13, the Fe content in sphalerite is shown as function of  $f\text{S}_2$  at different temperatures. At the Ming deposit, sphalerite co-exists

with pyrite  $\pm$  pyrrhotite or galena  $\pm$  sulfosalts  $\pm$  tellurides. The varying Fe contents in sphalerite at the Ming deposit can be explained by variations in both  $fS_2$  and temperature. In Figure 5-13, the range of FeS (mole%) in sphalerite is shown. In scenario (i) temperature decreases and  $fS_2$  remains constant, resulting in decreasing FeS in sphalerite. In scenario (ii)  $fS_2$  increases and temperature remains constant. Both scenarios are seen as extreme end members, since sphalerite deposition occurs over a temperature range in VMS deposits and at various  $fS_2$  (Haymon and Kastner, 1981; Scott, 1983; Lydon, 1988; Large, 1992; Ohmoto, 1996). Moreover, the occurrence of sphalerite with different minerals (pyrite, pyrrhotite, galena, tellurides, sulfosalts) at the Ming deposit also indicates variations in both  $fS_2$  and temperature of the hydrothermal fluids depositing sphalerite.

The pH of hydrothermal fluids forming the Ming VMS deposit can be inferred from mineral assemblages in the different orebodies and comparisons to modern hydrothermal vent sites. Of the common metals, Pb and Zn are transported as chloride complexes and are most sensitive to changes in pH (Lydon, 1988). Relatively acid conditions ( $pH \approx 2-4$ ) are needed to account for an increased solubility of both Zn and Pb in the hydrothermal fluid and changes to higher pH due to, for instance, the interaction with cold, neutral seawater, results in the deposition of Zn and Pb sulfides (Large 1977, 1992; Ohmoto, 1996). Therefore, the hydrothermal fluid transporting Zn and Pb was acidic. Acidic hydrothermal fluids are also inferred for the transport of Fe sulfides (pyrite,



pyrrhotite) and Cu-Fe sulfides (chalcopyrite, cubanite) at hotter temperatures, because: (1) Fe and Cu complexes are stable at acidic conditions (Yund and Kullerud, 1966; Barton and Skinner, 1979); and (2) hydrothermal vent fluids especially from black smokers on sediment free vent sites have acidic pH values (German and von Damm, 2003).



**Figure 5-13.** Temperature vs  $\log fS_2$  diagram showing varying Fe contents in sphalerite co-existing with pyrite (py) – pyrrhotite (po). Contours of mole percent FeS in sphalerite coexisting with Fe sulfides and the sulfidation boundaries for pyrite-pyrrhotite and bornite (bn) + pyrite (py) – chalcopyrite (ccp) are from Scott and Barnes (1971) and Czamanske (1974). Grey area represents range of Fe content in sphalerite. Blue arrows labeled (i) and (ii) indicate extreme end scenarios that can cause changes of Fe content in sphalerite; see text for details.

#### *5-6-1-2 Role of elements of the epithermal suite and precious metals*

There is a spatial and mineralogical preferences of: (1) Te, Bi, and Se for the 1807 Zone and MSUP and to lesser extent for MSDP and LFWZ; (2) Ag and Au between the different orebodies; and (3) As, Sb, and Hg for the 1806 Zone (Figs. 8, 12). Even though these elements only occur in trace minerals at the Ming deposit, they indicate that different fluid conditions were responsible for the formation of the different orebodies, because in addition to T, pH,  $fO_2$ , and  $fS_2$ , chemical parameters such as  $fTe_2$ ,  $fSe_2$ ,  $m_{Bi}$ , and  $m_{Sb}$  control the transport and deposition of these metals (Table 5-7).

##### *5-6-1-2-1 Te, Bi, and Se*

Telluride minerals are not common in VMS deposits and are only known from a few VMS deposits worldwide (Ural Mountains: Vikentyev, 2006; Novoselov et al., 2006; Maslennikov et al., 2009; Abitibi greenstone belt: Thorpe and Harris, 1973; Tourigny et al., 1993). At the Ming deposit hessite ( $Ag_2Te$ ), altaite ( $PbTe$ ), tsumoite ( $BiTe$ ), unnamed bismuth-telluride ( $Bi_3Te_2$ ), and coloradoite ( $HgTe$ ) occur specifically in the 1807 Zone and to lesser extent in the other orebodies with the exception of the 1806 Zone in which tellurides are practically absent (Table 5-3).

Afifi et al. (1988a) showed that Te is preferentially transported as vapor phase ( $Te_{2(g)}$ ) in hydrothermal fluids, although studies from Zhang and Spry (1994) and McPhail (1995) described the possible occurrence of aqueous Te

species in hydrothermal fluids. The formation of tellurides mainly depends on a high  $f\text{Te}_2/f\text{S}_2$  ratio and to lesser extent on the redox state of the hydrothermal fluid (Afifi et al., 1988a). A high  $f\text{Te}_2/f\text{S}_2$  ratio promotes telluride deposition over the substitution of  $\text{Te}^{2-}$  for  $\text{S}^{2-}$  in sulfides (Afifi et al., 1988a, b; Zhang and Spry, 1994). Tellurides are common in epithermal deposits and are typically found in low-sulfidation epithermal systems (Acupan, Philippines: Cooke and McPhail, 2001; Emperor gold deposit, Fiji: Pals et al., 2003). Moreover, tellurides (e.g., frobergite) that indicate oxidized hydrothermal fluid conditions are extremely rare even in epithermal deposits (Afifi et al., 1988a, b). Therefore, the deposition of tellurides in the 1807, Ming South, and LFWZ orebodies suggests reduced hydrothermal fluid conditions at a relatively high  $f\text{Te}_2/f\text{S}_2$  ratio.

Galena-telluride symplectites are common in the 1807 Zone and MSUP (Fig. 5-3g) and are related to the miscibility gap between  $\text{PbS}$  –  $\text{PbTe}$  below  $800^\circ\text{C}$  (Liu and Chang, 1994) and the oversaturation of the hydrothermal fluid in Ag, Te, Bi, and Se relative to Pb. In the LFWZ, tellurides also occur, but are not associated with galena (Fig. 5-4c, d). The lack of galena in the LFWZ is explained due to changes in pH (Lydon, 1988), whereas telluride deposition was much more controlled by the  $f\text{Te}_2/f\text{S}_2$  ratio (Afifi et al., 1988a). During late stage ore formation, the cooler, reduced, and acidic hydrothermal fluids transporting Pb, Zn, Ag, Te, and Bi among other metals ascended through the stockwork zone. The absence of galena in this assemblage was likely due to a lack of a pH increase (e.g. Lydon, 1988), and/or low  $f\text{S}_2$  that would have otherwise

encouraged galena deposition. The deposition of tellurides in the LFWZ stockwork was likely due to either: (1) boiling; (2) conductive cooling; (3) mixing; and/or (4) gas condensation of vapor phase transporting  $\text{Te}_{2(g)}$  into hydrothermal fluid (Cooke and McPhail, 2001). Deciphering the key processes above in the LFWZ is difficult given the state of deformation in the deposit; however, Cooke and McPhail (2001) stated that if Te is transported as aqueous species, its transport is highly temperature dependent. Temperature change is likely the best explanation for the occurrence of tellurides in the LFWZ because Te is transported as both an aqueous species and a vapor phase, and small changes in temperature of the hydrothermal fluid resulted in the deposition of tellurides and clausthalite in the absence of galena. This deposition also decreased the  $f\text{Te}_2/f\text{S}_2$  and  $f\text{Se}_2/f\text{S}_2$  ratios in the coexisting hydrothermal fluid, which discouraged telluride and selenide deposition in the overlying MSDP (Table 5-3). Nevertheless, the hydrothermal fluid depositing galena in the MSDP was still sufficiently enriched in Te, Bi, Se, and Ag to account for enriched Te, Bi, Se, and Ag in galena in the MSDP (Fig. 5-11, Table A5-6). In the 1806 Zone, Te-, Bi-, and Se-poor galena, and the absence of tellurides, indicate that the  $f\text{Te}_2/f\text{S}_2$  ratio in the hydrothermal fluids was much lower than in the other orebodies.

At the Ming deposit, Bi occurs either as major element in tellurides (tsumoite, unnamed Bi-telluride) or as an enriched trace element in galena of the 1807 and Ming South orebodies, and Ag-rich tetrahedrite of the 1806 Zone (Fig. 5-11). The strong association of Bi with galena can be explained by the solid

solution between  $\text{AgBiS}_2$  and  $\text{PbS}$  (Van Hook, 1960). Amcoff (1984) and Huston et al. (1996) showed that the coupled substitution of AgBi for Pb, especially at temperatures below  $390^\circ\text{C}$ , controls the overall distribution of Ag. However, for the Ming deposit this coupled substitution also controls the overall Bi content due to the predominant association of Bi with galena. The deposition of Bi, which is primarily transported as a neutral hydroxide complex (Wood et al., 1987), is largely dependent on a temperature decrease or an increase in  $\text{H}_2\text{S}$  concentration (Huston et al., 1996). The  $\text{H}_2\text{S}$  concentration is typically fairly constant throughout the formation of VMS deposits (Huston et al., 1996), and is ruled out as a precipitation mechanism. However, decrease in temperature is very likely the cause of Bi precipitation with hessite, altaite and galena in semi-massive to massive sulfides or with hessite and clausthalite in the LFWZ due to interaction with ambient seawater and cooler wallrock.

Selenium rarely occurs as selenide minerals in VMS deposits (Hannington et al., 1999a, b; Layton-Matthews et al., 2008; Maslennikov et al., 2009). However, enriched selenium contents are reported from several ancient (Wolverine and Kudzu Ze Kaya: Layton-Matthews et al., 2008; Yaman-Kaya: Maslennikov et al., 2009) and modern VMS ( $13^\circ\text{N}$  East Pacific Rise: Auclair et al., 1987) deposits. At the Ming deposit, selenides are rare, and only clausthalite ( $\text{PbSe}$ ) irregularly occurs with tellurides. There are two major reasons that commonly prohibit selenide deposition in VMS systems, even if the hydrothermal fluid has relatively high Se contents and a high  $f\text{Se}_2/f\text{S}_2$  ratio: (1) the highly

chalcophile character of Se and the similar atomic radius between  $S^{2-}$  and  $Se^{2-}$  result in the preferred substitution of  $Se^{2-}$  for  $S^{2-}$ , which decreases the  $fSe_2/fS_2$  ratio of the hydrothermal fluid; and (2) most VMS systems are formed by reduced fluids that hinder the oxidation of  $S^{2-}$  to  $SO_4^{2-}$ , which would change the valence and radius of S making it less attractive for substitution by  $Se^{2-}$  (Simon and Essene, 1996). Therefore, selenide deposition is not only controlled by  $fSe_2$ , but also by the redox state of the hydrothermal fluid.

The highly variable Se contents between minerals and orebodies at the Ming deposit are attributed to the preferred transport of Se at elevated temperatures together with Cu, the solid solution between PbSe – PbS that occurs over a wide temperature range, and the common substitution of  $Se^{2-}$  for  $S^{2-}$  (Simon and Essene, 1996; Simon et al., 1997). Therefore, the main factors controlling precipitation of Se from reduced, acidic hydrothermal fluids at Ming were: (1) decrease in temperature of hot hydrothermal fluids resulting in enriched Se contents in high temperature minerals (e.g., chalcopyrite, pyrite, pyrrhotite, and cubanite observed in the MSUP and LFWZ); (2) increase in pH and decrease in temperature of the hydrothermal fluid resulting in the precipitation of galena with enriched Se due to the solid solution between PbSe and PbS (e.g., 1807 and Ming South orebodies); and (3) decrease in the  $fSe_2/fS_2$  ratio due to preferred substitution of  $Se^{2-}$  for  $S^{2-}$  in sulfides precipitating from reduced hydrothermal fluids.

**Table 5-7.** Summary of occurrence, preferred host minerals, mineral associations, and inferred transport and precipitation conditions for elements of the epithermal suite and precious metal bearing elements at the Ming deposit. Mineral abbreviations as in Table 5-3

Element	Preferred orebody occurrence	Host mineral phases	Associated minerals	Dominant species during transport	Favored transport conditions	Predominant precipitation conditions	Reference
As major/minor component <sup>1</sup>			As elevated trace component <sup>2</sup>				
Te	1807 Zone	alt, hess, tsu, unnamed BiTe	Ag-, Bi-, Se-rich gn, Fe-rich sp, po, claus	Te <sub>2(g)</sub> , aqueous Te species	wide range in T; reduced fluids with low <i>f</i> S <sub>2</sub> and elevated <i>f</i> Te <sub>2</sub>	decrease in <i>f</i> Te <sub>2</sub> , decrease in T if Te is transported as aqueous species	Affi et al. (1988a; b); McPhail (1995); Zhang and Spry (1994)
Bi	1807 Zone	tsu, unnamed BiTe	Ag-, Te-, Se-rich gn, hess, alt, claus, Fe-rich sp, po	Bi(OH) <sub>3</sub>	wide range in T; reduced fluid; elevated <i>m</i> <sub>H<sub>2</sub>O</sub> in hydrothermal fluid	decrease in T	Wood et al. (1987); Huston et al. (1996)
Se	1807 Zone, MSUP, LFWZ	claus	tellurides, Ag-, Bi-, Te-rich gn	Se <sub>2(g)</sub> , aqueous Se species	elevated and lower T favoring the transport of Cu and Pb, respectively; reduced, acidic fluids; high <i>f</i> Se <sub>2</sub> / <i>f</i> S <sub>2</sub> ratio	decrease in <i>f</i> Se <sub>2</sub> , decrease in T causing ccp precipitation, increase in pH causing gn precipitation	Auclair et al. (1987); Simon and Essene (1996); Simon et al. (1997)
Ag	1807 + 1806 zones	AgHg±Au alloys, el, hess, pyr, mia, Hg-steph, Ag-rich trt	as hess, alt, tsu, unnamed BiTe, Bi, Te-, Se-rich gn, po, claus as Ag-rich trt, tnt, apy, sp ± el ± gn as AgSb phases: sp, ccp, gn, apy, ccp, el, po	AgCl <sub>2</sub> , AgCl <sup>o</sup>	wide range of T, reduced, acidic fluids	increase in pH, decrease in T	Seward (1976), Amcoff (1984), Huston et al (1996)

**Table 5-7 (cont.)**

Element	Preferred orebody occurrence	Host mineral phases	As major/minor component <sup>1</sup>	As elevated trace component <sup>2</sup>	Associated minerals	Dominant species during transport	Favored transport conditions	Predominant precipitation conditions	Reference
Au	1806 Zone	el, AgHgAu alloys	el, AgHgAu alloys	ccp, po, apy (1806 Zone)	apy, tent-trt, ccp, sp, py	Au(HS) <sub>2</sub> <sup>-</sup> , Au(HS) <sup>0</sup>	lower temperature (< 350°C), reduced fluids	decrease in T, oxidation	Seward (1973), Williams-Jones et al. (2009)
As	1806 Zone	allo, apy, loel, tnt	py, po, ccp (all orebodies); gn (1806 Zone)	<u>as single crystals:</u> py ± po <u>in myrmekite:</u> tnt-trt, ccp, sp ± el ± gn	As(OH) <sub>3</sub>		lower temperature, reduced fluids	increase in fO <sub>2</sub>	Heinrich and Eadington (1986)
Sb	1806 Zone	mia, pyr, trt	apy (1806 Zone); gn (1806 > MSUP > 1807 ≈ MSDP); el (1806 Zone); tsu and unnamed BiTe (1807 Zone)	<u>as trt:</u> tnt, apy, sp, ccp ± el ± gn <u>as AgSb phases:</u> sp, ccp, gn, apy, ccp, el, po	at T>275°C: Sb(OH) <sub>3</sub> at T<275°C: Sb <sub>2</sub> S <sub>3</sub> (OH) <sub>2</sub>		wide range in T; elevated m <sub>sb</sub> in hydrothermal fluid; reduced fluid	decrease in T, increase in fO <sub>2</sub>	Wood et al. (1987); Krupp (1989); Huston et al. (1996)
Hg	1806 Zone	AgHg±Au alloys, el, Hg-steph	N/A*		apy, tnt-trt, ccp, sp, py, pyr	Hg <sub>0</sub> and/or aqueous Hg (chloro?)species	T>200°C; relatively reduced fluids	increase in pH and/or fO <sub>2</sub>	Varekamp and Buseck (1984); Kim et al. (2000)

<sup>1</sup> based on EPMA analysis (Tables 5-6, A5-6); <sup>2</sup> based on LA-ICP-MS analysis (Table A5-6); \* Hg was not analyzed by LA-ICP-MS and hence trace element concentrations are not available



#### 5-6-1-2-2 Ag and Au

The mineralogical distribution of Ag varies between the 1807 Zone with Ming South orebodies (hessite > Ag-poor tennantite-tetrahedrite > electrum) and the 1806 Zone (Ag-bearing to Ag-rich tennantite-tetrahedrite > electrum > AgSb sulfosalts). The concentration of Ag in sulfides is typically depleted with the exception of galena and chalcopyrite (Figs. 5-10, 5-11). Variations in mineralogy, distribution and Ag concentration are mainly controlled by temperature, redox state, pH, and the concentration of Bi, Sb and H<sub>2</sub>S in the hydrothermal fluid (Huston et al., 1996).

Amcoff (1984) showed that the coupled substitution of AgBi and AgSb for Pb accounts for enriched Ag contents in galena. The higher the Bi and/or Sb concentration is in the hydrothermal fluid, the higher the probability of Ag incorporation into galena due to coupled substitution. Galena in the 1807 and Ming South orebodies is enriched in Bi (Fig. 5-11, Table A5-6) and commonly associated with tellurides indicating that AgBi substitution dominated over AgSb for Pb in these orebodies. Moreover, the deposition of Ag-, Bi-, Te-, and Se-rich galena coevally with tellurides including hessite resulted in the depletion of Ag in the coexisting hydrothermal fluid, and the  $f\text{Te}_2/f\text{S}_2$  and  $m_{\text{Bi}}/m_{\text{Sb}}$  ratios decreased. From this co-existing fluid, Ag-poor tennantite-tetrahedrite deposited. In the 1806 Zone galena is Ag- and Sb-rich, but Bi-, Te-, and Se-poor indicating that AgSb substitution for PbS dominated due to cooler fluid temperatures and lower Bi contents in the hydrothermal fluid (Amcoff, 1984; Huston et al., 1996).

Chalcopyrite in the 1806 Zone has greater Ag contents than in the other orebodies, indicating that Ag substitution for Cu occurred from reduced and Bi-poor, hot hydrothermal fluids (Huston et al., 1996). The enriched Ag concentrations especially in tetrahedrite of the 1806 Zone (Brueckner et al., 2014) are either caused by fractional crystallization of tennantite-tetrahedrite from a hydrothermal fluid due to decrease in temperature (Hackbarth and Petersen, 1984), the substitution of Sb-Ag for As-Cu (Miller and Craig, 1983), or the decomposition of As-rich tennantite into Ag-rich tetrahedrite due to increase in Sb activity (Bortnikov et al., 1993, Cook, 1996). All three processes are very likely for Ag-rich tetrahedrite in the 1806 Zone, because a wide compositional range in tennantite-tetrahedrite (Table 6) and decomposition of tennantite (Figs. 5-3e, 5-5f, g) is observed.

The main Au-bearing mineral in all orebodies is electrum;  $\text{AgHg}\pm\text{Au}$  alloys are very rare throughout the deposit and Au concentrations in sulfides are typically very low with the exception of the 1806 Zone (Figs. 5-10, 5-11). Enriched Au contents in chalcopyrite, pyrrhotite, sphalerite, or arsenopyrite occur in grains adjacent to electrum suggest that either electrum deposited simultaneously with these phases from reduced, acidic hydrothermal fluids of varying temperature, or Au diffusion between electrum and these minerals occurred (Birchenall, 1974; Pals et al., 2003).

The mineralogical association of electrum with arsenopyrite, sulfosalts and/or Ag-bearing phases (Fig. 5-5) indicates Au transport by thio-complexes at

temperatures < 300°C together with As and Ag ± Sb (Table 5-7; Seward, 1973). The deposition of Au with Ag as electrum was controlled by temperature, redox state, and pH of the hydrothermal fluid (Williams-Jones et al., 2009) and occurred prior to telluride deposition (Fig. 5-6).

#### *5-6-1-2-3 As, Sb, and Hg*

Arsenopyrite occurs with either pyrite ± pyrrhotite or as myrmekitic intergrowths with tennantite-tetrahedrite – chalcopyrite – sphalerite ± galena ± electrum. These two different assemblages formed under different hydrothermal fluid conditions. The presence of arsenopyrite with pyrite ± pyrrhotite suggests formation from reduced hydrothermal fluids, because As is predominantly transported as a hydroxide complex and is very sensitive to changes in redox state (Table 5-7; Heinrich and Eadington, 1986). In contrast, tennantite-tetrahedrite precipitates from more oxidized hydrothermal fluids (Huston et al., 1996). Smith and Huston (1992) showed that under more oxidized hydrothermal fluid conditions, As cannot precipitate as arsenopyrite but can instead be incorporated into tennantite. Texturally, tennantite is not associated with pyrrhotite at the Ming deposit. Therefore, it can be assumed that arsenopyrite occurring with pyrite ± pyrrhotite precipitated from reduced, acidic hydrothermal fluids prior to tennantite deposition, which precipitated from more oxidized, acidic hydrothermal fluids. Some tennantite grains in the 1807 and 1806 zones are decomposed to Ag-bearing tetrahedrite – arsenopyrite – chalcopyrite – sphalerite ± electrum ± galena (Figs. 5-3e, 5-5f, g). This decomposition of As-rich tennantite

was presumably caused by changes in Sb activity and/or pH of the co-existing hydrothermal fluid (Bortnikov et al., 1993; Cook, 1996).

Antimony-bearing minerals commonly have Ag (Ag-bearing to Ag-rich tetrahedrite, myargyrite, pyrargyrite, mercurian stephanite) and preferentially occur in the 1806 Zone. Transport and precipitation conditions for Sb complexes are not well constrained, although cooler ( $T < 275^{\circ}\text{C}$ ), more oxidized fluid conditions with enriched  $m_{\text{Sb}}$  are favored for Sb transport (Wood et al., 1987; Huston et al. 1996).

Mercury is enriched in the 1806 Zone compared to the other orebodies (Figs. 5-8, 5-12) and occurs predominantly in electrum and to lesser extent as  $\text{AgHg}\pm\text{Au}$  alloys and mercurian stephanite. Transport conditions for Hg are not well constrained and different opinions exist as to whether Hg is either transported as a vapor phase (Varekamp and Buseck, 1984; Smith and Huston, 1992) or as an aqueous species (Kim et al. 2000). However, the close mineralogical, chemical, and textural association with both Ag and Au indicates similar transport and deposition conditions for Hg, which are temperatures  $< 300^{\circ}\text{C}$ , transport as chloro-complex in reduced, acidic hydrothermal fluids.

## ***5-6-2 GENESIS OF THE OREBODIES AT THE MING DEPOSIT***

### ***5-6-2-1 Source of metals***

The complexity of ore mineral assemblages indicates a complex origin of

metals for the Ming deposit and potentially diverse sources. As illustrated in many studies, the base metals Cu, Zn, and Pb can reasonably be attributed to leaching from the wall rock (Large 1977, 1992; Franklin, 1993, 1996; Ohmoto, 1996). In contrast, the enrichments in elements of the epithermal suite (As, Bi, Hg, Sb, Se, Sn, Te) and precious metals (Ag, Au) are much more difficult to explain by wall rock leaching alone. Sillitoe et al. (1996) argued that elements of the epithermal suite and precious metals in VMS deposits are of magmatic-hydrothermal origin. Similarly, Brueckner et al. (2014) showed that sulfosalts and precious metals in the 1806 Zone were syngenetic and likely of magmatic origin. Since precious metals and sulfosalts also occur in the other orebodies of the Ming deposit, a magmatic origin is assumed for Ag, As, Au, Hg, Sb, and Sn occurring in the 1807 Zone, MSUP, MSDP, and LFWZ.

The presence of Te and Bi is also consistent with a magmatic origin (Afifi et al., 1988a, b). Tellurium rarely is present as an aqueous species in hydrothermal fluids and is most commonly transported in the vapor phase (Afifi et al., 1988a; Zhang and Spry, 1994; McPhail, 1995). The abundance of Te-phases, in particular in the 1807 Zone, Ming South orebodies, and LFWZ (Table 5-3), suggests a high  $f\text{Te}_2/f\text{S}_2$  ratio and that the tellurides in the deposit formed via vapor transport and subsequent condensation of those vapors. Bismuth correlates well with Te (Fig. 5-7e), but is most likely transported as neutral hydroxide complex over a wide range of temperature (Wood et al., 1987). However, both Te and Bi concentrations are low in rhyolitic rocks and boninites

(e.g.,  $\text{Te} < 12 \text{ ppm}$ ,  $\text{Bi} < 3 \text{ ppm}$ ; GEOROC database, Lehnert et al., 2000), therefore, it seems unlikely that leaching could account for these phases in the Ming deposit and instead a magmatic origin for these two elements and associated minerals is favored.

The presence of Se and selenides in the Ming deposit also indicates the potential influence of magmatic volatiles to the metal budget at the Ming deposit. In their study, Layton-Matthews et al. (2008) explained the differing Se contents in VMS deposits of the Finlayson Lake District, Yukon Territory, by different Se sources: seawater; sedimentary wall rock; felsic volcanic, volcanoclastic and intrusive rocks; and magmatic source from volatile degassing. Hannington et al. (1999b) used the  $\text{Se}/\text{S} \times 10^6$  ratio and the strong affinity of Se with other magmatically derived elements (e.g., Te, Bi, In) as indications that Se was of magmatic origin in the Kidd Creek deposit. At the Ming deposit, the  $\text{Se}/\text{S} \times 10^6$  ratio varies between the different orebodies (1807 Zone:  $\text{Se}/\text{S} \times 10^6 = 753$ ; 1806 Zone:  $\text{Se}/\text{S} \times 10^6 = 455$ ; MSUP:  $\text{Se}/\text{S} \times 10^6 = 1,267$ ; MSDP:  $\text{Se}/\text{S} \times 10^6 = 453$ ; LFWZ:  $\text{Se}/\text{S} \times 10^6 = 1,436$ ) due to variations in the overall Se content of each orebody (Table 5-4). Huston et al. (1995) and Hannington et al. (1999b) assumed that a high  $\text{Se}/\text{S} \times 10^6$  ratio ( $> 500$ ) indicate a magmatic origin, and  $\text{Se}/\text{S} \times 10^6 < 500$  is indicative of seawater or sedimentary Se. The orebodies at the Ming deposit have both higher ( $> 500$ : 1807 Zone, MSUP, LFWZ) and lower ( $< 500$ : 1806 Zone, MSDP)  $\text{Se}/\text{S} \times 10^6$  ratios implying different Se sources for the different orebodies. Sedimentary wall rock is excluded as a possible Se source for the Ming deposit.

due its absence in the regional footwall stratigraphic package of the PHG (Hibbard, 1983; Castonguay et al., 2009; Skulski, 2010). Felsic volcanic, volcanoclastic, and intrusive rocks are also an unlikely Se source, because Se concentration in these rocks is extremely low ( $\text{Se} < 16$  ppm; GEOROC database, Lehnert et al., 2000) and, as shown by Layton-Matthews et al. (2008), unrealistically large hydrothermal circulation cells would be needed to account for enriched Se concentrations in the Ming deposit. Therefore, seawater and magmatic (i.e., subvolcanic) sources are the most likely sources for Se at the Ming deposit, although discerning between these two sources is difficult.

#### *5-6-2-2 Genetic model*

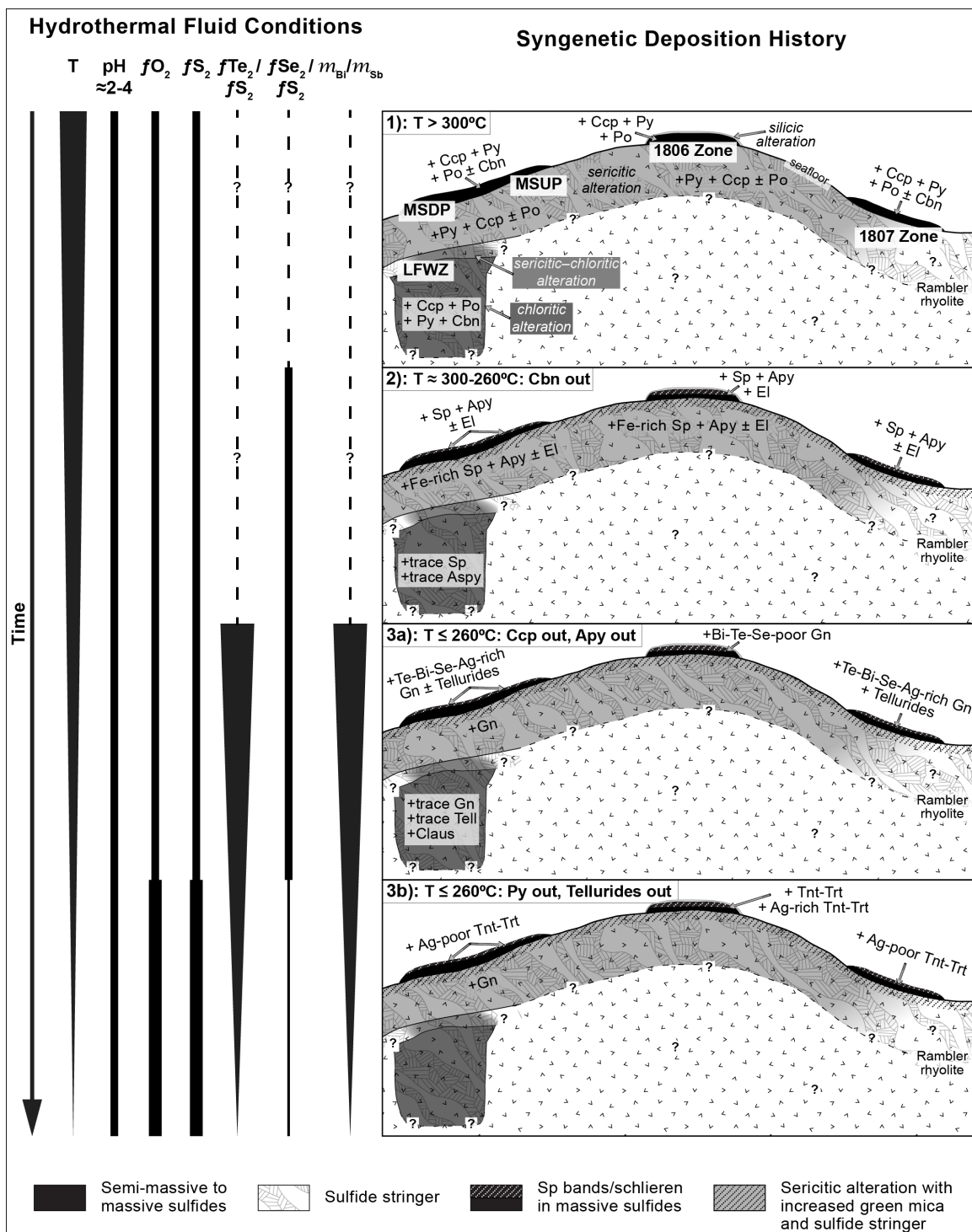
The formation of the Ming deposit (Fig. 5-14) can be attributed to three main stages of ore deposition based on the physio-chemical controls described above, including: (1) hot ( $>300^{\circ}\text{C}$ ), reduced, acidic hydrothermal fluids; (2) lower temperature ( $300\text{-}260^{\circ}\text{C}$ ), reduced, acidic hydrothermal fluids; and (3) low temperature ( $<260^{\circ}\text{C}$ ), acidic, reduced to slightly oxidized hydrothermal fluids with varying  $f\text{Te}_2/f\text{S}_2$ ,  $f\text{Se}_2/f\text{S}_2$ , and  $m_{\text{Bi}}/m_{\text{Sb}}$  ratios.

During the first stage, primarily Cu and Fe were transported and deposited as pyrite, pyrrhotite, chalcopyrite and/or cubanite due to decrease in temperature caused by the interaction of hot hydrothermal fluids with colder seawater. These fluids also carried Bi and Se, since Bi and Se concentrations in chalcopyrite of the 1807 Zone and the silicified horizon of the 1806 Zone are enriched.

During the second deposition stage, sphalerite, arsenopyrite, and electrum were deposited coincidently with ongoing precipitation of chalcopyrite, pyrite, and pyrrhotite. Chalcopyrite and sphalerite partly co-precipitated at temperatures close to 300°C, since both minerals are locally eutaxially intergrown (Fig. 5-3d). However, chalcopyrite precipitation decreased with decreasing temperature.

The third deposition stage is the most complex and responsible for the different mineral assemblages between 1807, MSUP, and MSDP orebodies and the 1806 Zone. In all orebodies precipitation of sphalerite, pyrite, and pyrrhotite continued. However, in the 1807 and Ming South orebodies, deposition of Te-, Bi-, Se-, and Ag-rich galena accompanied by tellurides occurred as well due to high ratios in  $f\text{Te}_2/f\text{S}_2$  and  $f\text{Se}_2/f\text{S}_2$ , and enriched  $m_{\text{Bi}}/m_{\text{Sb}}$  in the hydrothermal fluid. Galena and telluride deposition was followed by Ag-poor tennantite-tetrahedrite deposition, as the co-existing hydrothermal fluid became relatively enriched in  $f\text{S}_2$  and  $m_{\text{Sb}}$  after the precipitation of galena and tellurides. In contrast, Te-, Bi-, Se-poor galena, tennantite, Ag-bearing to Ag-rich tetrahedrite, and other sulfosalts were deposited in the 1806 Zone from slightly cooler, more oxidized, acidic, Bi-poor hydrothermal fluids with low  $f\text{Te}_2/f\text{S}_2$ ,  $f\text{Se}_2/f\text{S}_2$ , and  $m_{\text{Bi}}/m_{\text{Sb}}$  ratios. However, the reasons why hydrothermal fluid conditions of the latest deposition stage differed between the different orebodies remain uncertain and may be attributed to different hydrothermal reservoirs.





**Figure 5-14.** (previous page) Genetic model for the syngenetic formation of the Ming VMS deposit. Changes in physico-chemical hydrothermal fluid conditions as function of time are given on left side; mineral assemblages in each sketch indicate first precipitation of these minerals; mineral abbreviations as in Table 5-3 and Tell - tellurides; see text for details

The decomposition textures observed in tennantite-tetrahedrite (Fig. 5-3e) and galena (Fig. 5-3g) are the product of disequilibrium between these mineral phases and the coexisting fluid at late stage syngenetic deposition. Lower temperature hydrothermal fluids of the second and third stage minimally affected the LFWZ, because tellurides, sulfosalts, and precious metals are either scarce or completely absent in the LFWZ. However, indications that these cooler fluids circulated through the LFWZ are seen from the sporadic occurrence of electrum, arsenopyrite, galena, and tellurides in the LFWZ.

The occurrence of tellurides and/or precious metals in both epithermal (Cooke and McPhail, 2001; Pals et al., 2003) and VMS (Hannington et al., 1999c; Huston, 2000; Gill et al., 2015) deposits is commonly explained by boiling of the ascending hydrothermal fluids. However, at the Ming deposit, it is difficult to determine if boiling of the hydrothermal fluids or mixing of hydrothermal fluids with ambient seawater was the predominant metal deposition mechanism resulting in the formation of the different mineral assemblages. This is because the tectonic setting and therefore the paleo water depth at which the Ming deposit formed is not well constrained (Castonguay et al., 2009; Skulski et al., 2010; van

Staal and Barr, 2012). Moreover, the ductile and brittle behavior of sulfides at the Ming deposit caused by deformation and metamorphism makes it difficult to clearly identify primary depositional features. Boiling, however, remains a possible mechanism for precious metal deposition but requires further evidence and testing to see if it was the main mechanism of precious metal deposition.

Syngenetic zone refining at the Ming deposit played only a subordinate role or was not significant, although it is a common process in VMS formation worldwide (Eldridge et al., 1983; Large, 1992; Ohmoto, 1996). There is no distinctive metal zoning at the Ming deposit, although sphalerite bands and schlieren are common in the semi-massive to massive sulfides of the 1807, 1806, and Ming South orebodies. However, these bands and schlieren occur in a predominantly pyrite-chalcopyrite matrix and are interpreted to be a product of late stage hydrothermal fluids (stages 2 and 3). The occurrence of Au and Ag also shows no spatial preference to the outer parts (now up plunge parts) of the massive and semi-massive sulfide lenses in the different orebodies, indicative of zone refining. Remobilization of precious metals, which is documented by the presence of  $\text{AgHg} \pm \text{Au}$  alloys  $\pm$  electrum along fractures in cataclastic and recrystallized pyrite and interstitially between recrystallized pyrite  $\pm$  arsenopyrite, is interpreted to be the product of Silurian-Devonian metamorphism and deformation of pre-existing precious metals during a later event, rather than due to syngenetic zone refining (Brueckner et al., 2014).

The enrichment of elements of the epithermal suite (As, Bi, Hg, Sb, Te, Tl) and precious metals (Ag, Au) was observed in ancient and modern VMS systems (Sillitoe et al., 1996; Monecke et al., 2009; Kiliyas et al., 2013). Modern examples including shallow sub-marine seamounts Kolombo, Greece, and Palinuro, Italy, showed that vent fluids have enriched concentrations of elements of the epithermal suite As, Bi, Hg, Sb, Tl, and precious elements Ag and Au (Monecke et al. 2009; Kiliyas et al., 2013). The intermediate sulfidation mineral assemblage at the Ming deposit is characterized by its enrichment in elements of the epithermal suite and precious metals. Similarly to the modern examples, the Ming deposit shows an overlap of VMS and epithermal mineralization. The significance of this overlap presumably suggests that Au-rich epithermal deposits and VMS deposits enriched in elements of the epithermal suite and precious metals: (1) could both form in a similar tectonic setting; (2) have both a direct magmatic contribution that upgrades the polymetallic and precious metal content of particularly VMS deposits; and (3) could both form via sub-seafloor boiling at shallow water depth (<1,500m) (Sillitoe et al., 1996; Sillitoe and Hedenquist, 2003; Monecke et al. 2009, 2014; Kiliyas et al., 2013). Although, tectonic setting, paleo water depth, and metal deposition processes are ambiguous at the Ming deposit as discussed above, the occurrence of syngenetic epithermal mineralization provides tectonic and genetic constraints that require further investigation.

## 5-7 CONCLUSIONS

The precious metal bearing, bimodal Cu(-Au) Ming VMS deposit has a complex genesis. This study illustrates that the existing variations in mineralogy and ore grade between the proximal 1807 Zone, 1806 Zone, MSUP, MSDP, and LFWZ orebodies can be explained by variations in hydrothermal fluid conditions during the lifespan of Cambro-Ordovician VMS formation. The following conclusions are inferred from this study:

1) The LFWZ with its chlorite alteration and chalcopyrite-pyrrhotite  $\pm$  pyrite  $\pm$  cubanite assemblage represents the high temperature stockwork zone, whereas the other orebodies have sericite alteration and both high and low temperature mineral assemblages that were formed as individual sulfide lenses.

2) Variations in elements of the epithermal suite (As, Bi, Hg, Sb, Se, Te) and precious metals (Ag, Au) between the different orebodies are a direct result of the variations in mineral assemblages and mineral chemistry due to changes in temperature, pH,  $fO_2$ ,  $fTe_2/fS_2$ ,  $fSe_2/fS_2$ , and  $m_{Bi}/m_{Sb}$  of the hydrothermal fluids forming the Ming deposit.

3) Ore formation at the Ming deposit was greatly influenced by elements of the epithermal suite and precious metals, which have at least partly a magmatic origin.

4) The Ming deposit was most likely formed over a short time span, because syngenetic zone refining is not prominent in the orebodies of the Ming deposit.

### **Acknowledgements**

Stefanie M Brueckner thanks geologists, engineers, miners, and staff from Rambler Metals & Mining, Canada Ltd for their continuous logistic support. Special thanks go to Paul Legrow, Larry Pilgrim, Peter Mercer, Tim Sanford, Hubert Jenkins, and Norman Williams. Microprobe and LA-ICP-MS analyses would not have been successful without the great assistance of Yanan Liu (University of Toronto) and Joe Petrus (Laurentian University), respectively. Dave Grant and Michael Shaffer (MUN) are thanked for their help at the SEM. Special thanks goes to reviewers James Saunders, Sean McClenaghan and co-editor Jeffrey Mauk for their constructive comments that improved this paper. This research has been funded by Rambler Metals and Mining Canada Ltd., and other grants to Stephen J. Piercey, including an NSERC Discovery Grant, and the NSERC-Altius Industrial Research Chair funded by NSERC, Altius Resources Inc., and the Research and Development Corporation of Newfoundland and Labrador.

## References

- Afifi AM, Kelly WC, Essene EJ (1988a) Phase relations among tellurides, sulfides, and oxides: I. Thermochemical data and calculated equilibria. *Economic Geology* 83: 377-394
- Afifi AM, Kelly WC, Essene EJ (1988b) Phase relations among tellurides, sulfides, and oxides: II. Applications to telluride-bearing ore deposits. *Economic Geology* 83: 395-404
- Amcoff Ö (1984) Distribution of silver in massive sulfide ores. *Mineralium Deposita* 19: 63-69
- Auclair G, Fouquet Y, Bohn M (1987) Distribution of selenium in high-temperature hydrothermal sulfide deposits at 13° North, East Pacific Rise. *Canadian Mineralogist* 25: 577-587
- Barton PB, Toulmin P (1966) Phase relations involving sphalerite in the Fe-Zn-S system. *Economic Geology* 61: 815-849
- Barton JR, PB (1978) Some ore textures involving sphalerite from the Furutobe mine, Akita prefecture, Japan. *Mining Geology* 28:293-300
- Barton PB, Skinner BJ (1979) Sulfide mineral stabilities. *In* Barnes HL (ed): *Geochemistry of hydrothermal ore deposits*. 2<sup>nd</sup> edition, John Wiley & Sons, New York: 278-403
- Barton JR., PB, Bethke, PM (1987) Chalcopyrite disease in sphalerite: Pathology and epidemiology. *American Mineralogist* 72 (5-6): 451-467
- Birchenall CE (1974) Diffusion in sulfides *In*: Hofmann AW, Giletti BJ, Yoder Jr. HS, Yund RA (eds) *Geochemical transport and kinetics*. Carnegie Institution of Washington, Publication 634, pp 53-68.
- Bortnikov NS, Genkin AD, Troneva NV (1993) Tennantite decomposition: Evidence from the Kedabek copper deposit, Azerbaijan. *Mineralogy and Petrology* 47 (2-4):171-181. doi:10.1007/BF01161565
- Brueckner SM, Piercey SJ, Sylvester PJ, Maloney S, Pilgrim L (2014) Evidence for syngenetic precious metal enrichment in an Appalachian volcanogenic massive sulfide system: The 1806 Zone, Ming Mine, Newfoundland, Canada. *Economic Geology* 109 (6): 1611-1642. doi:10.2113/econgeo.109.6.1611
- Brueckner SM, Piercey SJ, Layne, GD, Piercey G, Sylvester, PJ (2015) Variations of sulphur isotope signatures in sulphides from the

metamorphosed Ming Cu-(Au) volcanogenic massive sulphide deposit, Newfoundland Appalachians. *Mineralium Deposita* 50 (5):619-640. doi:10.1007/s00126-014-0567-7

Butterfield DA, Massoth GJ, McDuff RE, Lupton JE, Lilley MD (1990) Geochemistry of hydrothermal fluids from axial seamount hydrothermal emissions study vent field, Juan de Fuca ridge: Subseafloor boiling and subsequent fluid-rock interaction: *Journal of Geophysical Research* 95, B8: 12895-12921

Castonguay S, Skulski T, van Staal C, Currie M (2009) New insights on the structural geology of the Pacquet Harbour group and Point Rousse complex, Baie Verte peninsula, Newfoundland. Current Research Newfoundland and Labrador Department of Natural Resources, Geological Survey Report 09-1:147-158

Cook NJ (1996) Mineralogy of the sulphide deposits at Sulitjelma, northern Norway. *Ore Geology Reviews* 11 (5):303-338. doi:10.1016/S0169-1368(96)00009-1

Cook NJ, Spry PG, Vokes FM (1998) Mineralogy and textural relationships among sulphosalts and related minerals in the Bleikvassli Zn-Pb-(Cu) deposit, Nordland, Norway *Mineralium Deposita* 34:35-56

Cook NJ, Ciobanu CL, Pring A, Skinner W, Shimizu M, Danyushevski L, Saini-Eidukat B, Melcher F (2009) Trace and minor elements in sphalerite: A LA-ICPMS study. *Geochimica et Cosmochimica Acta* 73: 4761-4791. doi:10.1016/j.gca.2009.05.045

Cooke DR, McPhail DC (2001) Epithermal Au-Ag-Te mineralization, Acupan, Baguio District, Philippines: Numerical simulations of mineral deposition. *Economic Geology* 96: 109-131

Craig JR, Vokes FM (1993) The metamorphism of pyrite and pyritic ores: An overview *Mineralogical Magazine* 57:3-18

Czamanske GK (1974) The FeS content of sphalerite along the chalcopyrite-pyrite-bornite sulfur fugacity buffer. *Economic Geology* 69: 1328-1334

Di Benedetto F, Bernardini GP, Costagliola P, Plant D, Vaughan DJ (2005) Compositional zoning in sphalerite crystals *American Mineralogist* 90:1384-1392



- Dobbe RTM (1991) Ullmannite, cobaltian ullmannite and willyamite from Tunaberg, Bergslagen, central Sweden. *Canadian Mineralogist* 29 (2):199-205
- Eldridge CS, Barton Jr, PB, Ohmoto H (1983) Mineral textures and their bearing on formation of the Kuroko ore bodies. In Ohmoto H (ed.) *The Kuroko and related massive sulfide deposits*. Society of Economic Geologists, Boulder, CO, 5:241-281
- Franklin JM (1993) Volcanic-associated massive sulphide deposits. In Kirkham RV, Sinclair WD, Thorpe RI, Duke JM (eds.) *Mineral Deposit Modeling*, Geological Association of Canada, Special Paper 40: 315-334
- Franklin JM (1996) Volcanic-associated massive sulphide base metals. In Eckstrand OR, Sinclair WD, Thorpe RI (eds.). *Geology of Canadian Mineral Deposit Types*: Ottawa, ON, Geological Survey of Canada, *Geology of Canada Series no. 8*: 158-183
- Gemmell B, Zantop H, Birnie RW (1989) Silver sulfosalts of the Santo Niño vein, Fresnillo district, Zacatacas, Mexico. *Canadian Mineralogist* 27: 401-418
- German CR, von Damm KL (2003) Hydrothermal processes. In Holland HD, Turekian KH (eds) *The Oceans and Marine Geochemistry*. *Treatise on Geochemistry*, Vol. 6, Elsevier: 181-222
- Gill SB, Piercey SJ, Layton-Matthews D, Layne GD, Piercey G Mineralogical, sulfur, and lead isotopic study of the Lemarchant Zn-Pb-Cu-Ag-Au-VMS deposit: Implications for precious-metal enrichment processes in the VMS environment. In: Peter JM, Mercier-Langevin P (eds) *Targeted Geoscience Initiative 4: Contributions to the understanding of volcanogenic massive sulfide deposit genesis and exploration methods development*. Geological Survey of Canada, Open File 7853: 183-195
- Hackbarth CJ, Petersen U (1984) A fractional crystallization model for the deposition of argentian tetrahedrite. *Economic Geology* 79: 448-460
- Hannington MD, Scott SD (1989) Gold mineralization in volcanogenic massive sulfides: Implications of data from active hydrothermal vents on the modern seafloor, in Keays RR, Ramsay WRH, Groves DI (ed) *The geology of gold deposits: The perspective in 1988*. Boulder, CO, Society of Economic Geologists Volume 6: 491-507
- Hannington MD, Bleeker W, Kjarsgaard I (1999a) Sulfide mineralogy, geochemistry, and ore genesis of the Kidd Creek deposit: Part I. North, central and south orebodies. In Hannington MD, Barrie CT (eds) *The giant*

- Kidd Creek volcanogenic massive sulfide deposit, western Abitibi Subprovince, Canada. Volume 10: Boulder, CO, Society of Economic Geologists: 163-224
- Hannington MD, Bleeker W, Kjarsgaard I (1999b) Sulfide mineralogy, geochemistry, and ore genesis of the Kidd Creek deposit: Part II. The bornite zone. The giant Kidd Creek volcanogenic massive sulfide deposit, western Abitibi Subprovince, Canada. Volume 10: Boulder, CO, Society of Economic Geologists: 225-266
- Hannington MD Poulsen KH, Thompson JFH, Sillitoe RH (1999c) Volcanogenic gold in the massive sulfide environment. *In* Barrie CT, Hannington MD (eds) Volcanic-associated massive sulfide deposits: Processes and examples in modern and ancient settings, Volume 8: Boulder, CO, Society of Economic Geologists: 325-351
- Haymon RM (1983) Growth history of hydrothermal black smoker chimneys. *Nature* 301:695-698. doi:10.1038/301695a0
- Haymon RM, Kastner M (1981) Hot spring deposits on the East Pacific Rise at 21°N: Preliminary description of mineralogy and genesis. *Earth and Planetary Science Letters* 53:363-381
- Hibbard LJ (1983) Geology of the Baie Verte Peninsula, Newfoundland, vol 2. Memoir. Department of Mines and Energy, Government of Newfoundland and Labrador, Memoir 2
- Heinrich CA, Eadington PJ (1986) Thermodynamic predictions of the hydrothermal chemistry of arsenic, and their significance for the paragenetic sequence of some cassiterite-arsenopyrite-base metal sulfide deposits. *Economic Geology* 81: 511-529
- Huston DL (2000) Gold in volcanic-hosted massive sulfide deposits: Distribution, genesis, and exploration *In*: Hagemann SG, Brown, P.E. (ed) *Gold in 2000*. Society of Economic Geologists, Boulder, CO, pp 401-426
- Huston DL, Sie SH, Suter GF, Cooke DR, Both RA (1995) Trace elements in sulfide minerals from eastern Australian volcanic-hosted massive sulfide deposits: Part I: Proton microprobe analyses of pyrite, chalcopyrite, and sphalerite, and Part II: Selenium levels in pyrite: Comparison with  $\delta^{34}\text{S}$  values and implications for the source of sulfur in volcanogenic hydrothermal systems. *Economic Geology* 90: 1167-1196
- Huston DL, Jablonski W, Sie SH (1996) The distribution and mineral hosts of

silver in Eastern Australian volcaogenic massive sulfide deposits. *Canadian Mineralogist* 34: 529-546

Kilias SP, Nomikou P, Papanikolaou D, Polymenakou PN, Godelitsas A, Argyraki A, Carey S, Gameletsos P, Mertzimekis TJ, Stathopoulou E, Goettlicher J, Steininger J, Betzelou K, Loivanos I, Christakis C, Croff Bell K, Scoullou M (2013) New insights into hydrothermal vent processes in the unique shallow-submarine arc-volcano, Kolumbo (Santorini), Greece. *Scientific Reports* 3:13. doi: 10.1038/srep02421

Kim CS, Brown Jr GE, Rytuba JJ (2000) Characterization and speciation of mercury-bearing mine wastes using X-ray absorption spectroscopy. *The Science of the Total Environment* 261: 157-168

Layton-Matthews D, Peter JM, Scott SD, Leybourne MI (2008) Distribution, mineralogy, and geochemistry of selenium in felsic volcanic-hosted massive sulfide deposits of the Finlayson Lake District, Yukon Territory, Canada. *Economic Geology* 103: 61-88

Large RR (1977) Chemical evolution and zonation of massive sulfide deposits in volcanic terrains. *Economic Geology* 72:549-572

Large RR (1992) Australian volcanic-hosted massive sulfide deposits: Features, styles, and genetic models. *Economic Geology* 87 (3):471-510. doi:10.2113/gsecongeo.87.3.471

Larocque ACL, Hodgson CJ, Lafleur P-J (1993) Gold distribution in the Moberly volcanic-associated massive sulfide deposit, Noranda, Quebec: A preliminary evaluation of the role of metamorphic remobilization. *Economic Geology* 88:1443-1459

Lehnert K, Su Y, Langmuir CH, Sarbas B, Nohl U (2000) A global geochemical database structure for rocks. *G<sup>3</sup> – Geochemistry, Geophysics, Geosystems* 1. doi: 0.1029/1999GC000026View/save citation

Liu H, Chang LLY (1994) Phase relations in the system PbS–PbSe–PbTe. *Mineralogical Magazine* 58:567-578

Lydon JW (1988) Volcanogenic massive sulphide deposits Part 2: Genetic models: *Geoscience Canada* 15:43-65

Maslennikov VV, Maslennikova SP, Large RR, and Danyushevsky LV (2009) Study of trace element zonation in vent chimneys from the Silurian Yaman-Kasy volcanic-hosted massive sulfide deposit (southern Urals, Russia)

using laser ablation-inductively coupled plasma mass spectrometry (LA-ICPMS). *Economic Geology*: 1111-1141

McClenaghan SH, Lentz DR, Martin J, Diegor WG (2009) Gold in the Brunswick No. 12 volcanogenic massive sulfide deposit, Bathurst Mining Camp, Canada: Evidence from bulk ore analysis and laser ablation ICP-MS data on sulfide phases. *Mineralium Deposita* 44:523-557. doi: 10.1007/s00126-009-0233-7

McPhail DC (1995) Thermodynamic properties of aqueous tellurium species between 25 and 350°C. *Geochimica et Cosmochimica Acta* 59: 851-866

Mercier-Langevin P, Hannington MD, Dubé B, Bécu V (2011) The gold content of volcanogenic massive sulfide deposits. *Mineralium Deposita* 46 (5-6):509-539. doi:10.1007/s00126-010-0300-0

Miller JW, Craig JR (1983) Tetrahedrite-tennantite series compositional variations in the Cofer deposit, Mineral district, Virginia. *American Mineralogist* 68 (1-2):227-234.

Ohmoto H (1996) Formation of volcanogenic massive sulfide deposits: The Kuroko perspective. *Ore Geology Reviews* 10 (3-6):135-177. doi:10.1016/0169-1368(95)00021-6

Monecke T, Petersen S, Lackschewitz K, Hügler M, Hannington MD, Gemmell JB (2009) Shallow submarine hydrothermal systems in the Aeolian Volcanic Arc, Italy. *EOS* 90:110-111

Monecke T, Petersen S, Hannington MD (2014) Constraints on water depth of massive sulfide formation: Evidence from modern seafloor hydrothermal Systems in arc-related settings. *Economic Geology* 109: 2079-2101

Nagase T, Kojima S (1997) An SEM examination of the chalcopyrite disease texture and its genetic implications. *Mineralogical Magazine* 61: 89-97

Novoselov KA, Belogub EV, Zaykov VV, Yakovleva VA (2006) Silver sulfotellurides from volcanic-hosted massive sulfide deposits in the Southern Urals. *Mineralogy and Petrology* 87: 327-349

Pals DW, Spry PG, Chrysosoulis S (2003) Invisible gold and tellurium in arsenic-rich pyrite from the Emperor Gold Deposit, Fiji: Implications for gold distribution and deposition. *Economic Geology* 98: 479-493

Pilgrim L (2009) Mineral resource estimate for the Ming Mine, Newfoundland, Canada. Rambler Metals and Mining Canada Ltd, Baie Verte, NL

- Pilote J-L, Piercey SJ (2013) Volcano-stratigraphy of the 1807 zone of the Ming Cu-Au volcanogenic massive sulfide (VMS) deposit, Baie Verte Peninsula, northern Newfoundland. Geological Survey of Canada, Current Research v. 2013-20: 13 p. doi:10.4095/293128
- Pilote J-L, Piercey SJ, Mercier-Langevin, P (2014) Stratigraphy and hydrothermal alteration of the Ming Cu-Au volcanogenic massive sulphide deposit, Baie Verte Peninsula, Newfoundland. Geological Survey of Canada, Current Research 2014-17: 18p. doi:10.4095/295145
- Pilote J-L, Piercey SJ, Mercier-Langevin P (2015) Volcanic architecture and alteration assemblages of the Ming Cu-Au-(Zn-Ag) VMS deposit, Baie Verte, Newfoundland and Labrador: Implications for Au-enrichment processes and exploration methods development In: Peter JM, Mercier-Langevin P (eds) Targeted Geoscience Initiative 4: Contributions to the understanding of volcanogenic massive sulfide deposit genesis and exploration. Geological Survey of Canada, Open File 7853: 1897-210
- Rambler Metals and Mining Canada Ltd (2011). Ming mine project: 3D model of the Ming mine looking West. Retrieved from: <http://www.ramblermines.com/3d-model.php>
- Rambler Metals and Mining Canada Ltd (January 27, 2014). Rambler updates the reserve and resource estimates at its Ming copper-gold mine. Press release. Retrieved from: [http://ramblermines.com/files/2014-01-27-\\_-\\_Rambler-MM\\_Reserve-and-Resource-Update.pdf](http://ramblermines.com/files/2014-01-27-_-_Rambler-MM_Reserve-and-Resource-Update.pdf)
- Sack RO, Ebel DS (2006) Thermochemistry of sulfide mineral solutions. In Vaughan DJ (ed) Sulfide mineralogy and geochemistry. Reviews in Mineralogy and Geochemistry 71: 265-364
- Scott SD, Barnes HL (1971) Sphalerite geothermometry and geobarometry Economic Geology 66: 653-669
- Scott SD (1983) Chemical behaviour of sphalerite and arsenopyrite in hydrothermal and metamorphic environments. Mineralogical Magazine 47: 427-435
- Seward TM (1973) Thio complexes of gold and the transport of gold in hydrothermal ore solutions. Geochimica et Cosmochimica Acta 37: 379-399
- Seward TM (1976) The stability of chloride complexes of silver in hydrothermal solutions up to 350°C. Geochimica et Cosmochimica Acta 40: 1329-1341

- Seward TM, Barnes HL (1997). Metal transport by hydrothermal ore fluids, *In* Barnes HL (ed) *Geochemistry of hydrothermal ore deposits*. 3<sup>rd</sup> edition, John Wiley & Sons, New York: 435-486
- Sillitoe RH, Hannington MD, Thompson JFH (1996) High sulfidation deposits in the volcanogenic massive sulfide environment. *Economic Geology* 91: 204-212
- Sillitoe RH, Hedenquist JW (2003) Linkages between volcanotectonic settings, ore-fluid compositions, and epithermal precious metal deposits *In*: Simmons SF, Graham I (eds) *Volcanic, geothermal, and ore-forming fluids: Rulers and witnesses of processes within the Earth*. Special Publications of the Society of Economic Geologists, Boulder, CO, pp 315-343
- Simon G, Essene EJ (1996) Phase relations among selenides, sulfides, tellurides, and oxides: Part I. Thermodynamic properties and calculated equilibria. *Economic Geology* 91: 1183-1208
- Simon G, Kesler SE, Essene EJ (1997) Phase relations among selenides, sulfides, tellurides, and oxides: Part II. Applications to selenide-bearing ore deposits. *Economic Geology* 92: 468-484
- Skulski T, Castonguay S, McNicoll V, van Staal C, Kidd W, Rogers N, Morris W, Ugalde H, Slavinski H, Spicer W, Moussallam Y, Kerr I (2010) Tectonostratigraphy of the Baie Verte oceanic tract and its ophiolite cover sequence on the Baie Verte Peninsula. *Current Research Newfoundland and Labrador Department of Natural Resources, Geological Survey Report* 10-1:315-335
- Smith RN, Huston DL (1992) Distribution and association of selected trace elements at the Rosebery deposit, Tasmania. *Economic Geology* 87: 706-719
- Strunz H, Nickel EH (2001) *Strunz Mineralogical Tables* (9<sup>th</sup> edition). E. Schweizerbart'sche Verlagsbuchhandlung, Berlin and Stuttgart: 870 pp
- Swinden HS, Thorpe RI (1984) Variations in style of volcanism and massive sulfide deposition in Early to Middle Ordovician island-arc sequences of the Newfoundland Central Mobile Belt *Economic Geology* 79:1596-1619. doi:10.2113/gsecongeo.79.7.1596
- Thorpe RI, Harris DC (1973) Mattagamite and telluroantimony, two new telluride minerals from Mattagami Lake Mine, Matagami area, Quebec. *Canadian Mineralogist* 12: 55-60
- Törmänen TO, Koski RA (2005) Gold enrichment and the Bi-Au association in

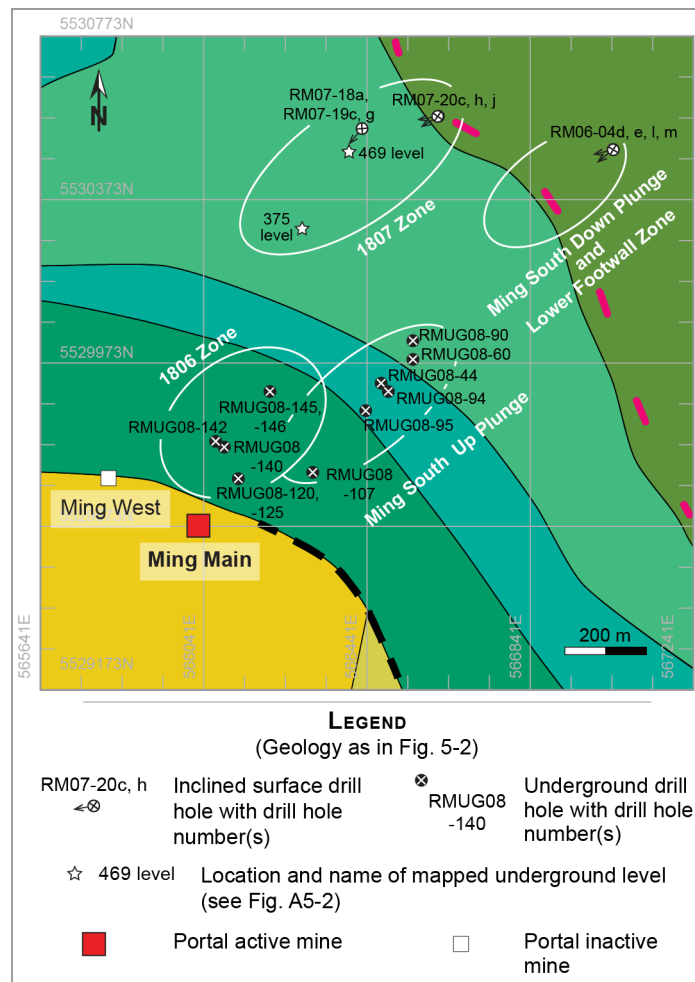
- pyrrhotite-rich massive sulfide deposits, Escanaba Trough, Southern Gorda Ridge. *Economic Geology* 100: 1135-1150
- Tomkins AG, Pattison DRM, Frost BR (2007) On the initiation of metamorphic sulfide anatexis. *Journal of Petrology* 48 (3):511-535. doi:10.1093/petrology/egl070
- Tourigny G, Doucet D, Bourget A (1993) Geology of the Bousquet 2: An example of a deformed, gold-bearing, polymetallic sulfide deposit. *Economic Geology* 88: 1578-1597
- Tuach J, Kennedy MJ (1978) The geologic setting of the Ming and other sulfide deposits, consolidated Rambler mines, Northeast Newfoundland. *Economic Geology* 73:192-206
- van Hook HJ (1960) The ternary system  $\text{Ag}_2\text{S}$ – $\text{Bi}_2\text{S}_3$ – $\text{PbS}$ . *Economic Geology* 55: 759-788
- van Staal CR (2007) Pre-Carboniferous tectonic evolution and metallogeny of the Canadian Appalachians. In: Goodfellow WD (ed) *Mineral deposits of Canada: A synthesis of major deposit-types, district metallogeny, the evolution of geological provinces, and exploration methods*, vol Special Publication No. 5. Geological Association of Canada, Mineral Deposits Division, pp 793-818
- van Staal CR, Barr SM (2012) Lithospheric architecture and tectonic evolution of the Canadian Appalachians and associated Atlantic margin. In: Percival JA, Cook FA, Clowes RM (eds) *Tectonic Styles in Canada: The LITHOPROBE perspective*. Geological Association of Canada, Special Paper 49, St. John's, NL, pp 41-96
- Varekamp JC, Buseck PR (1984) The speciation of mercury in hydrothermal systems, with applications to ore deposition. *Geochimica et Cosmochimica Acta* 48: 177-185
- Vikentyev IV (2006) Precious metal and telluride mineralogy of large volcanic-hosted massive sulfide deposits in the Urals. *Mineralogy and Petrology* 87: 305-326
- Wagner T, Boyce AJ, Jonsson E, and Fallick AE (2004) Laser microprobe sulphur isotope analysis of arsenopyrite: Experimental calibration and application to the Boliden Au–Cu–As massive sulphide deposit. *Ore Geology Reviews* 25: 311-325

- Wagner T, Klemm R, Wenzel T, Mattsson B (2007) Direct evidence from laser-ablation–inductively coupled plasma–mass spectrometry analysis of invisible gold. *Geology* 35:775-778
- Wen N, Ashworth JR, Ixer RA (1991) Evidence for the mechanism of the reaction producing a bournonite-galena symplectite from meneghinite. *Mineralogical Magazine* 55 (379):153-158
- Whitney DL, Evans BW (2010) Abbreviations for names of rock-forming minerals. *American Mineralogist* 95:185-187. doi: 10.2138/Am.2010.3371
- Williams H (1979) Appalachian orogen in Canada. *Canadian Journal of Earth Sciences* 16:792-807
- Williams-Jones AE, Powell RJ, Migdisov AA (2009) Gold in solution. *Elements* 5:281-287
- Wohlgemuth-Ueberwasser CC, Viljoen F, and McClung CR (2014) Metamorphic alteration of the massive sulfide horizon from the Salt River VMS deposit (South Africa). *Ore Geology Reviews* 56: 45-52
- Wood SA, Crerar DA, Borcsik MP (1987) Solubility of the assemblage pyrite-pyrrhotite-magnetite-sphalerite-galena-gold-stibnite-bismuthinite-argentite-molybdenite in H<sub>2</sub>O-NaCl-CO<sub>2</sub> solutions from 200° to 350°C. *Economic Geology* 82:1864-1887
- Yund RA, Kullerød G (1966) Thermal stability of assemblages in the Cu-Fe-S system. *Journal of Petrology* 7 (3):454-488. doi:10.1093/petrology/7.3.454
- Zhang X, Spry PG (1994) Calculated stability of aqueous tellurium species, calaverite, and hessite at elevated temperatures. *Economic Geology* 89: 1152-1166

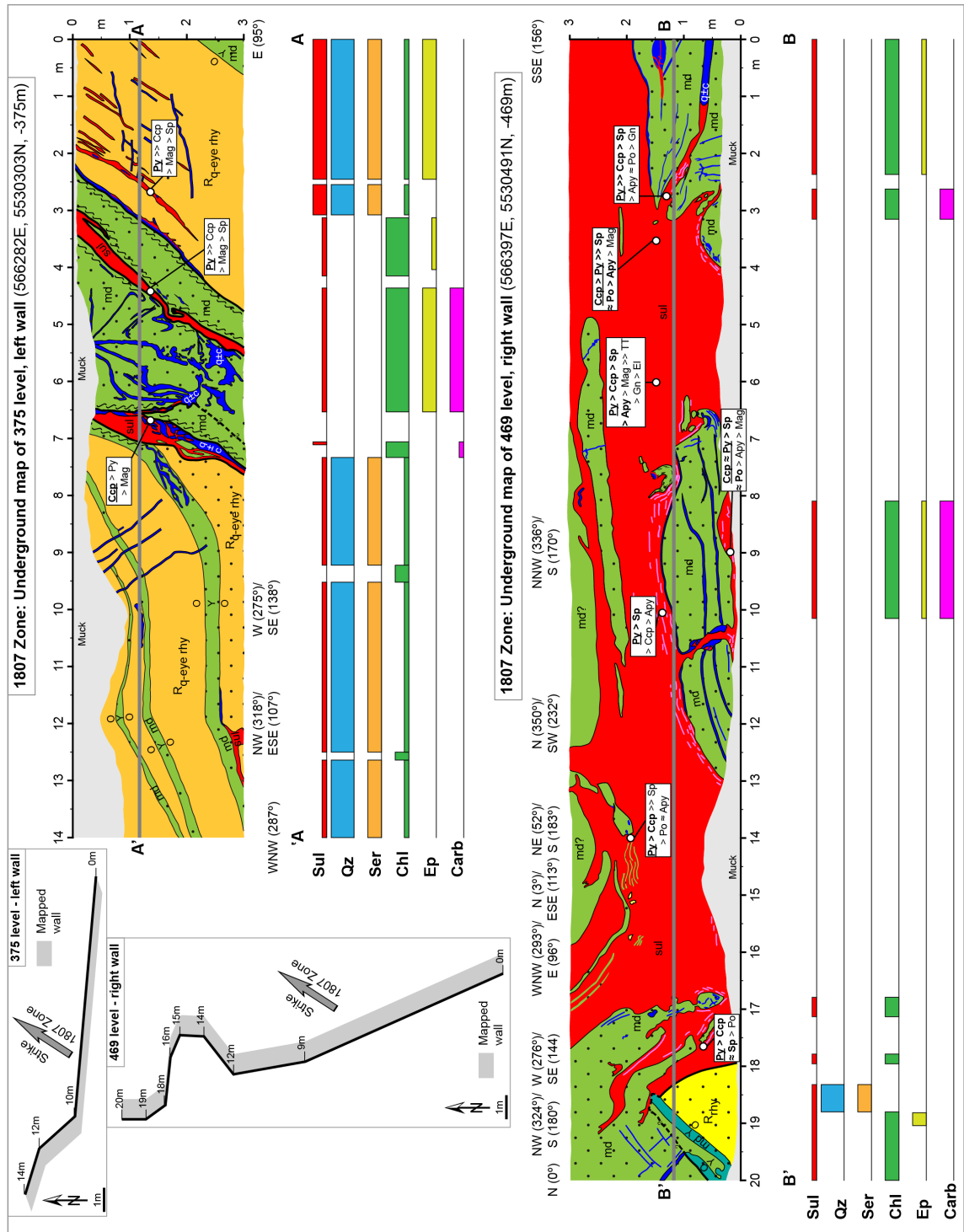








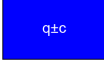

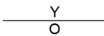




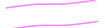

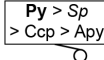



## APPENDIX

### APPENDIX A5-1 STRATIGRAPHY

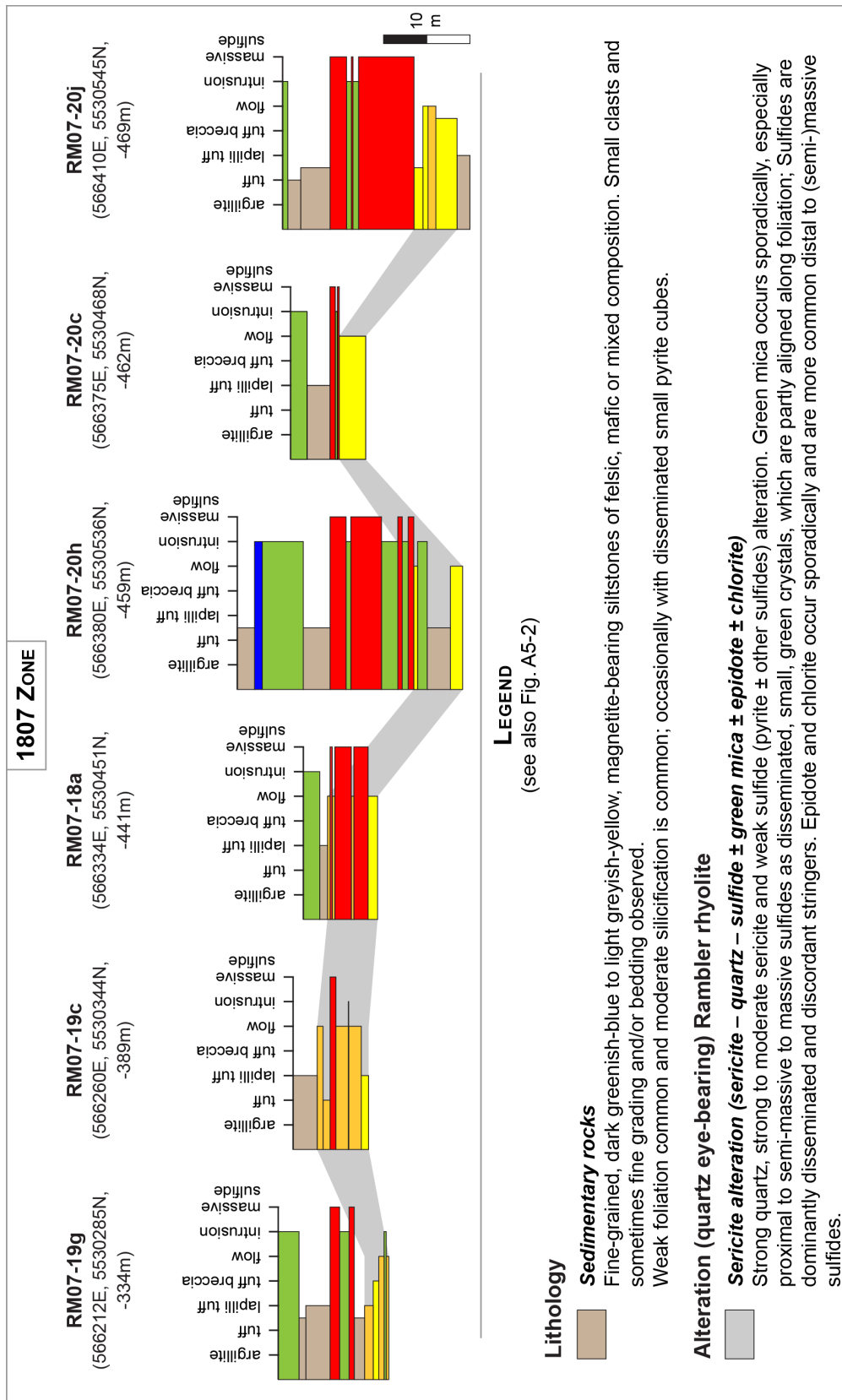


**Figure A5-1.** Location of orebodies (white ovals) relative to surface geology (modified after Skulski et al., 2010) with selected surface and underground drill holes (white and black circles) and mapped underground levels (stars). The detailed stratigraphy of the shown drill holes and underground levels are presented in Figures A5-2 to A5-6; coordinates are in UTM NAD83, Zone 21N

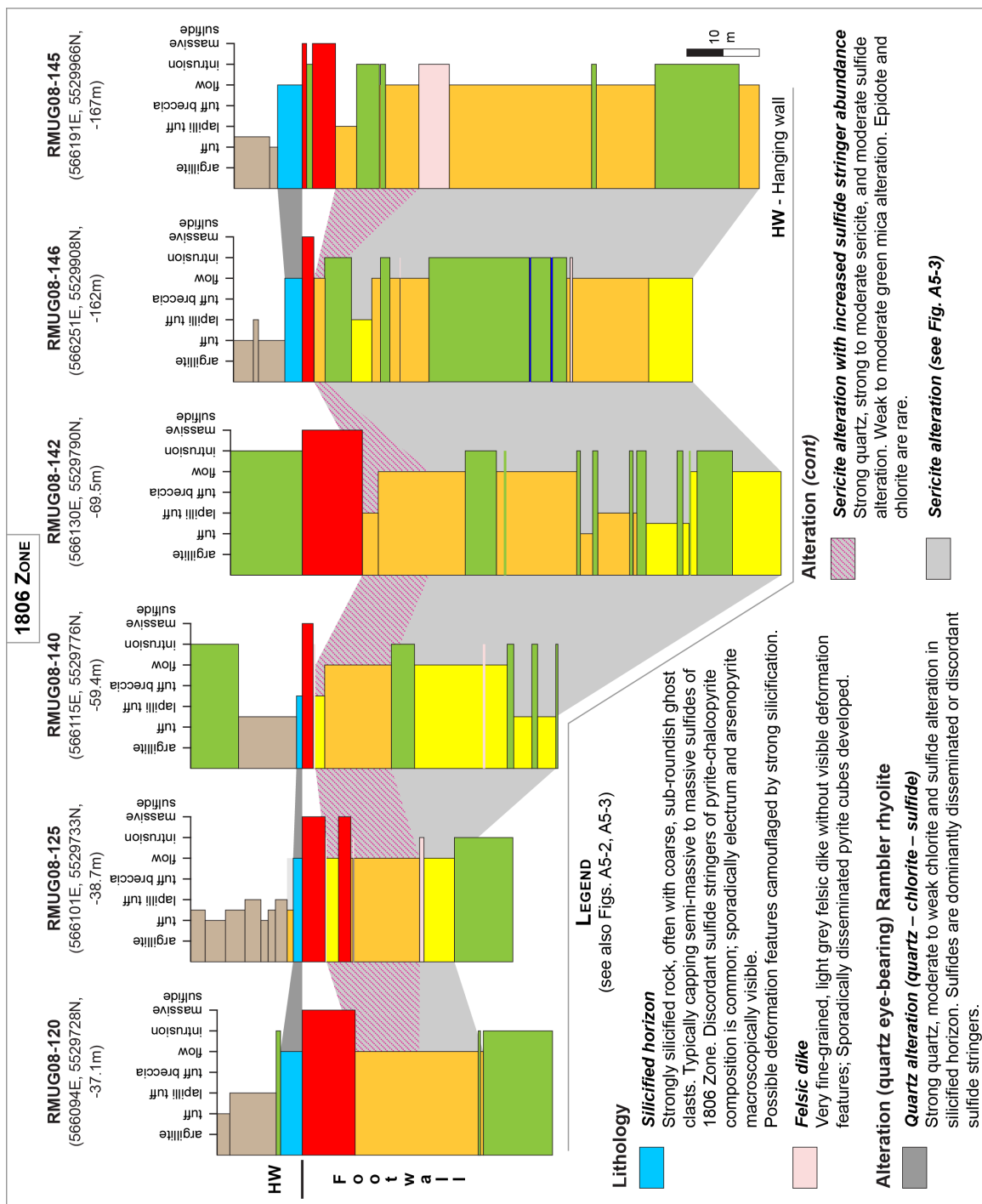


Lithology			LEGEND		
	<b>Rambler rhyolite / Quartz-bearing Rambler rhyolite</b>				
					
	Dominantly grey to bluish-grey, felsic volcanoclastic rock (consolidated tuff, lapilli tuff, tuff breccia or flow) of rhyodacitic to rhyolitic composition; silicified clasts in fine-grained matrix common especially proximal to massive sulfides; quartz-bearing variety has small, sub-roundish, bluish to white quartz eyes in varying abundance.				
	Often with fine sulfide stringers, especially proximal to massive sulfide. Strongly foliated.				
	<b>Mafic dike / Assumed mafic dike</b>				
					
	Green, fine-grained to medium-grained, gabbroic to dioritic mafic dike often with aligned and disseminated biotite and amphibole in fine-grained matrix. Feldspar blasts are rare.				
	Strongly foliated and with strong secondary silicification.				
	<b>Mafic dike</b>				
	Bluish, fine-grained mafic dike of unknown composition with disseminated and aligned biotite in fine-grained matrix.				
	Moderate foliation and with strong secondary silicification.				
	<b>(Semi-)Massive sulfide</b>				
	Homogeneous (semi-)massive sulfide has dominantly pyritic composition with chalcopyrite, occasional sphalerite bands and trace magnetite $\pm$ pyrrhotite amongst other trace sulfide/precious metal phases; chalcopyrite is dominant sulfide phase on direct contact to quartz $\pm$ carbonate veins.				
	<b>Quartz <math>\pm</math> carbonate veins</b>				
	White to orange, blocky quartz $\pm$ carbonate veins often with predominantly chalcopyrite mineralization when in direct contact with massive sulfide. Veins occur predominantly in (sheared) gabbroic to dioritic mafic dikes and on contacts between massive sulfide and gabbroic to dioritic dikes.				
	Deformation (boudinage, folding) is common.				
Contacts					
	<b>Geologic boundary</b>		<b>Geologic boundary between (intrusive) rocks showing relative age: younger, older</b>		
	<b>Fault</b>		<b>Fault, inferred</b>		<b>Shear zone</b>
Mineralogy					
	<b>Disseminated pyrite</b>			<b>Sphalerite bands</b>	
	Small, often cubic flakes of pyrite disseminated in Rambler rhyolite and mafic dikes.			Up to 5 cm thick sphalerite bands, sometimes with microscopic pyrrhotite in massive sulfide and preferably on the contact to gabbroic to dioritic mafic dikes.	
	<b>Strongly aligned biotite in mafic dike</b>			<b>Sulfide mineralogy and location of massive sulfide sample</b>	
Mineral abundance and abbreviations					
Major component (> 10 vol.%)		Minor component (5-10 vol.%)	Trace component (< 5 vol.%)		
Apy – arsenopyrite		Ccp – chalcopyrite	El – electrum		
Gn – galena		Mag – magnetite	Po – pyrrhotite		
Py – pyrite		Sp – sphalerite	TT – tennantite-tetrahedrite		
Alteration					
	Strong alteration		Moderate alteration		Weak alteration
Sul – sulfides		Qz – quartz		Ser – sericite	
Chl – chlorite		Ep – epidote		Carb – carbonate	

**Figure A5-2.** (previous pages) Underground maps of the 375 level (top) and 469 level (bottom) of the 1807 Zone. The trend of both mapped walls relative to magnetic north is shown in the upper right corner. The mapped walls run oblique to the NE striking 1807 Zone (grey arrow). Maps on top and bottom show the relationship between the different stratigraphic units at the 375 level and the 469 level, respectively. A simplified alteration of the main stratigraphic units Rambler rhyolite and mafic dike(s) is given below each map along a hypothetical profile (i.e., 375 level: A–A', 469 level: B–B'). Mineral assemblages of the massive sulfide lens(es) is shown along the mapped walls; coordinates are in UTM NAD83, Zone 21N and depth is given in meters below sea level

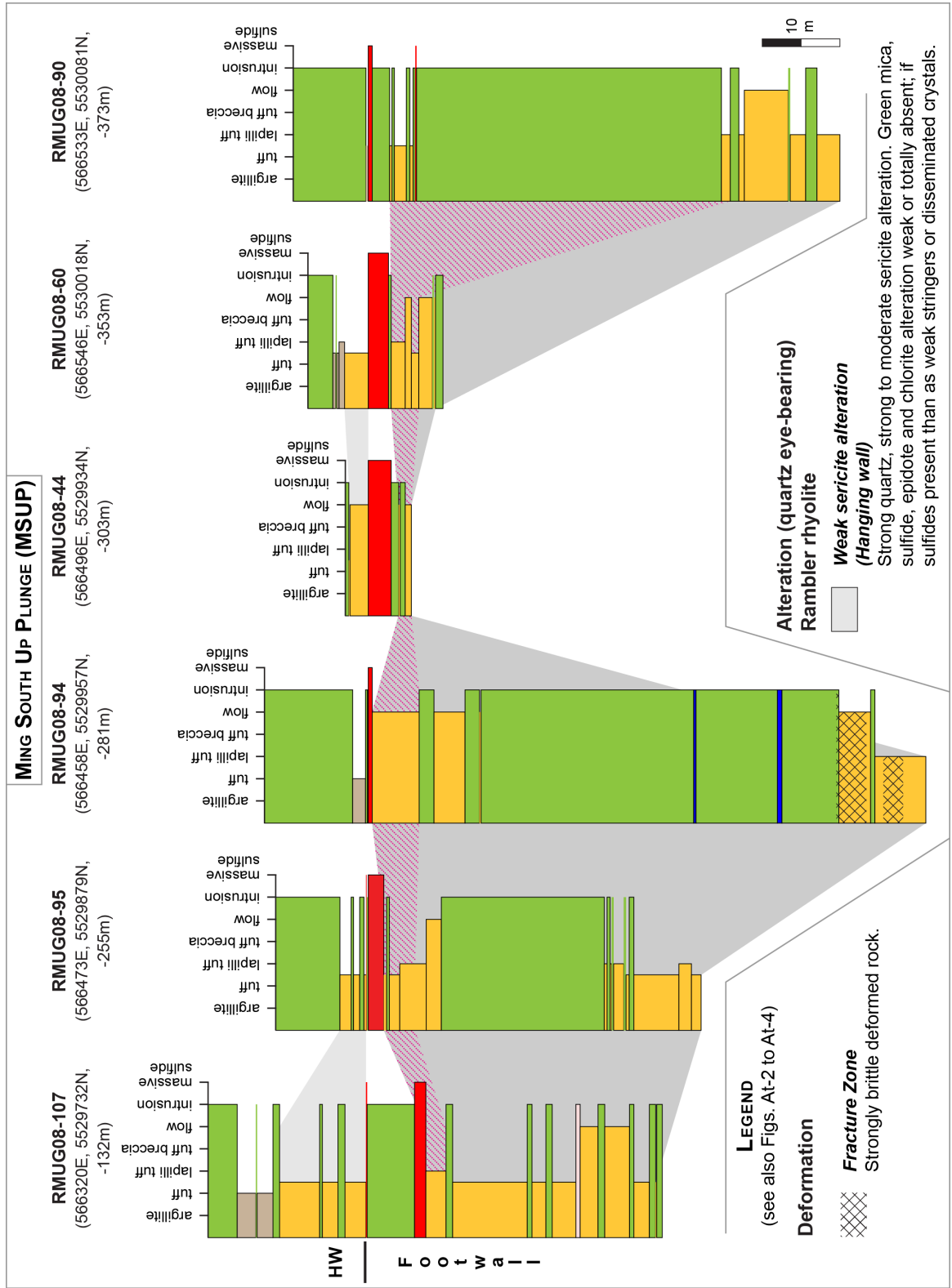


**Figure A5-3.** (previous page) Stratigraphy and simplified alteration for selected surface drill hole sections from the 1807 Zone orebody. Due to the structural complexity of the 1807 Zone, the hanging wall – footwall contact cannot be given; coordinates below drill hole name are for the upper most semi-massive to massive sulfide lens and given in UTM NAD83, Zone 21N, depth is given in meters below sea level

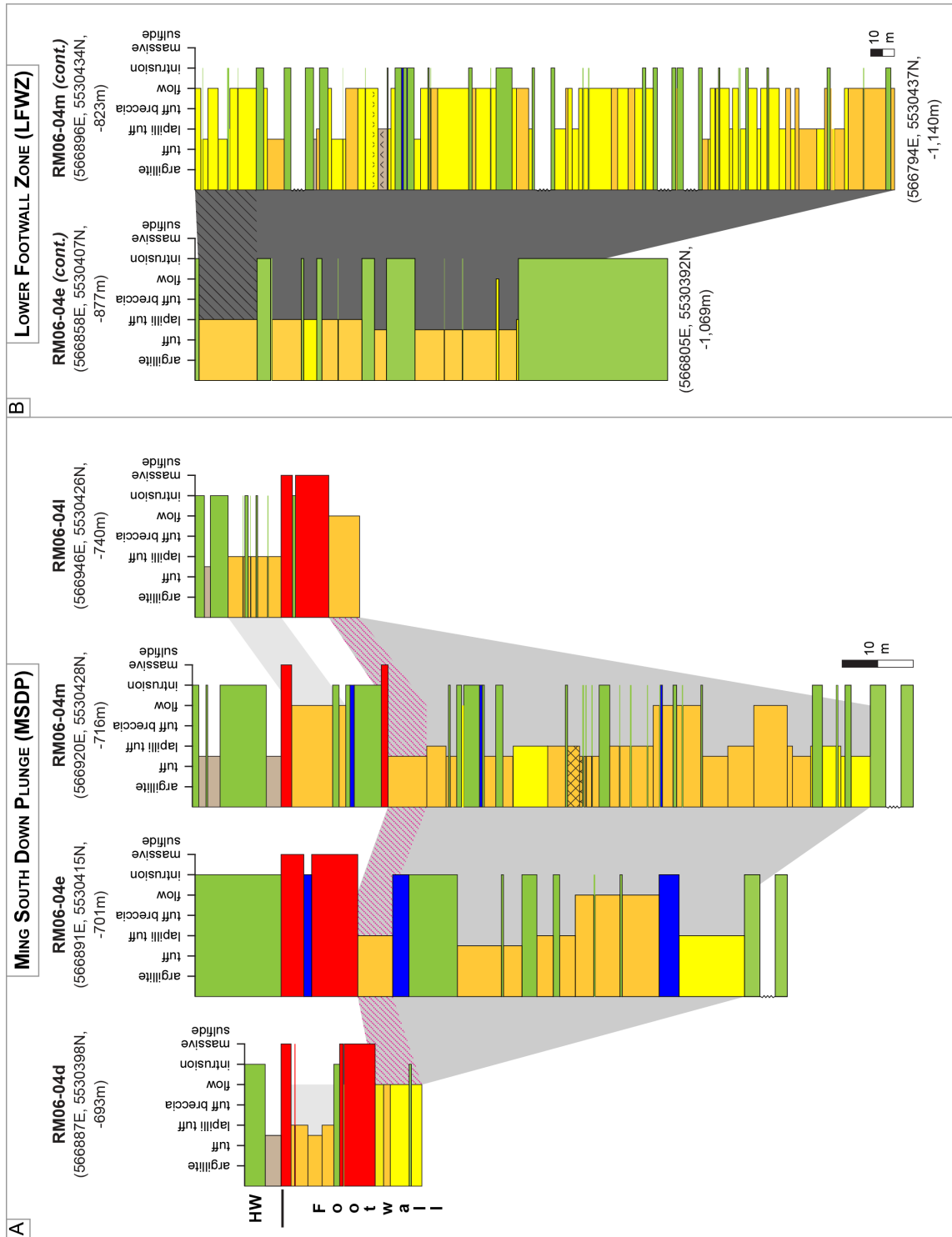




**Figure A5-4.** (previous page) Stratigraphy and simplified alteration for selected underground drill holes from the 1806 Zone orebody. Hanging wall – footwall contact is marked on top of the semi-massive to massive sulfide lens; coordinates below drill hole name are for the upper most semi-massive to massive sulfide lens and given in UTM NAD83, Zone 21N, depth is given in meters below sea level





**Figure A5-5.** Stratigraphy and simplified alteration for selected underground drill holes from the Ming South Up Plunge (MSUP) orebody. Hanging wall – footwall contact is marked on top of the semi-massive to massive sulfide lens; coordinates below drill hole name are for the upper most semi-massive to massive sulfide lens and given in UTM NAD83, Zone 21N, depth is given in meters below sea level



LEGEND	
(see also Figs. A5-2 to A5-5)	
<b>Alteration (quartz eye-bearing) Rambler rhyolite</b>	
	<b>Transition sericite (sericite – quartz – sulfide – chlorite ± epidote) to chlorite(chlorite – quartz – sulfide ± magnetite) alteration</b> Strong quartz, moderate chlorite alteration, and weak sulfide and sericite alteration. Sericite is fainting in and out. Sericite is in transition to completely disappear in alteration assemblage of the Lower Footwall Zone and be fully replaced by chlorite. Sulfides occur as discordant stringers.
	<b>Chlorite alteration (chlorite – quartz – sulfide ± magnetite)</b> Strong to moderate chlorite and quartz alteration, weak sulfide alteration. Sulfides occur as discordant stringers.

**Figure A5-6.** (previous page) Stratigraphy and simplified alteration for selected surface drill holes (RM06-04e, -04m) and drill hole sections (RM06-04d, -04l) from **(A)** the Ming South Down Plunge (MSDP) and **(B)** the Lower Footwall Zone (LFWZ). **(A)** Hanging wall – footwall contact is marked on top of the semi-massive to massive sulfide lens; coordinates below drill hole name are for the upper most semi-massive to massive sulfide lens and given in UTM NAD83, Zone 21N, depth is given in meters below sea level; **(B)** Drill holes RM06-04e and RM06-04m continue uninterrupted from their shown sections in (A); coordinates and depth below drill hole name are for the upper most shown unit (RM06-04e; mafic dike, RM06-04m: Rambler rhyolite flow); coordinates and depth below drill holes are for the end of drill holes

## Reference

Skulski T, Castonguay S, McNicoll V, van Staal C, Kidd W, Rogers N, Morris W, Ugalde H, Slavinski H, Spicer W, Moussallam Y, Kerr I (2010) Tectonostratigraphy of the Baie Verte oceanic tract and its ophiolite cover sequence on the Baie Verte Peninsula. Current Research Newfoundland and Labrador Department of Natural Resources, Geological Survey Report 10-1:315-335

## **APPENDIX A5-2 ANALYTICAL METHODS**

### **A5-2-1 WHOLE ROCK SULFIDE GEOCHEMISTRY**

Mineralized whole rock samples (n=36) were analyzed at Activation Laboratories (ActLabs), Ancaster, ON, Canada. The samples were from the semi-massive to massive sulfide horizon and from the footwall mineralization (sulfide stringer zone and Lower Footwall Zone). Additionally, three pulp samples of known composition were analyzed for quality control and assurance. All rock samples were crushed to a grain size of 1.7mm, mechanically split by riffing to obtain a representative sample and then pulverized to at least 95wt.% at a grain size of 106 µm by a mild steel mill. The mill is free of Ni or Cr, but the pulverized sample can be contaminated with up to 0.2wt.% Fe depending on the hardness of the sample (Actlabs Groups of Companies, 2007).

The following elements were analyzed at Actlabs: Ag, As, Au, Bi, Cd, Co, Cr, Cu, Fe, Hg, Mn, Ni, Pb, S, Sb, Se, Sn, Ta, Te, Tl, V, and Zn. Sulfur was analyzed via infrared digestion (IR, code 4F-S). Copper, Zn, and Pb were analyzed via inductively coupled plasma-optical emission spectrometry (ICP-OES, code 8-assay products), when the concentrations exceeded 10,000 ppm, 1000,000 ppm, and 5,000 ppm, respectively. For Cu, Zn, and Pb concentrations below the upper detection limit, ActLabs used total digestion – inductively coupled plasma mass spectrometry (TD-ICP-MS: Cu and Zn) and total digestion – inductively coupled plasma optical emission spectrometry TD-ICP-OES (Pb: code ultratrace-3). Gold was measured via instrumental neutron activation analysis (INAA: code ultratrace-3) when the concentration was below 300,000 ppb and via fire assay with a gravimetric finish (FA-GRA: code 1A3) when Au concentrations exceeded of 300,000ppb. Mercury was analyzed via aqua regia-Hg cold vapor flow injection mercury system (CV-FIMS: code 1G) for concentrations <100,000ppb and via INAA for concentrations > 100,000ppb. Analyses of Bi, Co, Se, Sn, Ta, Te, and Tl were done via TD-ICP-MS. Silver, Cd, Mn, Mo, Ni and V were analyzed via TD-ICP-OES. Arsenic, Cr, Fe, and Sb were

analyzed via INAA. Further details on the methodology can be obtained from Activation Laboratories (2012).

Quality control and quality assurance were monitored using certified reference materials, in-house standards, duplicates, and blanks during sample analysis. Reference materials used by ActLabs had similar matrices than the unknown samples and were run after every 20 samples (IR, TD-ICP-MS, Hg-(CV) FIMS) or every 40 samples (ICP-OES, INAA, TD-ICP-OES, FA-Gra). Additionally, the reference materials CDN-HLHZ, CDN-HLLC, and CDN-HLHC were shipped in as pulp samples and were analyzed as unknowns after every 20 samples to provide a check on laboratory performance. Precision and accuracy of analyzed reference materials and duplicates are summarized for the elements of interest in Table A5-1. Precision for reference materials is given as percent relative standard deviation ( $RSD_i(\%)$ , Jenner, 1996):

$$RSD_i(\%) = 100 * \frac{s_i}{\mu_i} \quad (5-1)$$

where  $s_i$  is the standard deviation of the mean from the series of analytical runs for element  $i$ , and  $\mu_i$  is the mean value of element  $i$  over the series of analytical runs for element  $i$ . Table A5-1 shows that precision for most elements is below 10wt.% showing that the analyses are sufficiently precise. Precision of duplicate analysis is reported as percent average coefficient of variation ( $CV_{av}(\%)$ ; Abzalov, 2008):

$$CV_{av}(\%) = 100 \times \sqrt{\frac{2}{N} \sum_{i=1}^N \left( \frac{(a_i - b_i)^2}{(a_i + b_i)^2} \right)} \quad (5-2)$$

where  $N$  is the number of duplicate pairs, and  $a_i$  and  $b_i$  are the original and duplicate analyses of the  $i^{th}$  sample pair. In general, precision for field (62002, 62008, 62014, 62158, 62200, 62172, 36256) and pulp (A2 = CDN-HLHZ, B1 = CDN-HLLC) duplicates is <10%. Precision >10% occurs for elements Cd, Mn, Ge, Ta, Te, Tl, and V, since concentrations of these elements are generally low and irregular within in the samples.

**Table A5-1.** Summary of precision and accuracy for RMs and duplicates used in this study

Unit symbol	LOD <sup>1</sup>	LOQ <sup>1</sup>	RM <sup>1</sup> Method <sup>1</sup>	GXR-1		GXR-4		GXR-6		MP-1b	
				RSD (%) <sup>1</sup>	RD (%) <sup>1</sup>	RSD (%) <sup>1</sup>	RD (%) <sup>1</sup>	RSD (%) <sup>1</sup>	RD (%) <sup>1</sup>	RSD (%) <sup>1</sup>	RD (%) <sup>1</sup>
S	wt.%	0.010	0.033	IR	—	—	—	—	—	—	—
Fe	wt.%	0.01	0.033	INAA	—	5.93	—	—	—	—	-1.22
Cu	ppm	0.200	0.660	TD-ICP-MS	2.48	2.70	1.77	-7.90	0.583	10.3	—
Cu	wt.%	0.001	0.003	ICP-OES	—	—	—	—	—	—	—
Zn	ppm	0.500	1.65	TD-ICP-MS	1.80	3.16	1.93	0.411	1.02	16.9	—
Zn	wt.%	0.001	0.003	ICP-OES	—	—	—	—	—	—	-1.62
V	ppm	2.00	6.60	TD-ICP-OES	—	7.50	—	6.90	—	-12.9	—
Cr	ppm	2.00	6.60	INAA	—	25.0	—	—	—	—	—
Mn	ppm	1.00	3.30	TD-ICP-OES	—	1.29	—	8.39	—	13.9	—
Co	ppm	0.100	0.330	TD-ICP-MS	0.912	-5.49	1.06	-8.22	0.000	-0.725	—
Ni	ppm	1.00	3.30	TD-ICP-OES	—	2.44	—	9.52	—	3.70	—
As	ppm	0.500	1.65	INAA	—	2.58	—	—	—	—	-1.30
Se	ppm	0.100	0.330	TD-ICP-MS	2.85	-10.2	1.27	-0.893	8.32	-9.57	—
Ag	ppm	0.300	0.990	TD-ICP-OES	—	2.26	—	-10.0	—	-69.2	—
Cd	ppm	0.300	0.990	TD-ICP-OES	—	-18.2	—	-53.5	—	—	—
Sn	ppm	1.00	3.30	TD-ICP-MS	0.000	-59.3	0.000	25.0	0.000	-41.2	—
Sb	ppm	0.100	0.330	INAA	—	-0.820	—	—	—	—	11.3
Te	ppm	0.100	0.330	TD-ICP-MS	0.790	-31.2	8.32	-12.4	—	—	—
Ta	ppm	0.100	0.330	TD-ICP-MS	—	—	9.43	-5.06	—	—	—
Au	ppb	2.00	6.60	INAA	—	4.24	—	—	—	—	—
Au	g/tonne	0.030	0.099	FA-Gra	—	—	—	—	—	—	—
Hg	ppb	5.00	16.5	Hg-(CV) FIMS	4.59	2.31	4.24	1.82	8.92	3.43	—
Hg	ppm	1.00	3.30	INAA	—	-23.1	—	—	—	—	—
Tl	ppm	0.050	0.165	TD-ICP-MS	0.000	-5.13	1.42	-6.56	1.95	-0.909	—
Pb	ppm	3.00	9.90	TD-ICP-OES	—	-2.74	—	-19.2	—	-4.95	—
Pb	wt.%	0.003	0.001	ICP-OES	—	—	—	—	—	0.909	—
Bi	ppm	0.020	0.066	TD-ICP-MS	1.10	-7.25	1.96	-5.00	0.000	-34.5	—

**Table A5-1 (cont.)**

Unit symbol	LOD <sup>1</sup>	LOQ <sup>1</sup>	RM <sup>1</sup> Method <sup>1</sup>	SDC-1		SAR-M		DNC-1a		SBC-1	
				RSD (%) <sup>1</sup>	RD (%) <sup>1</sup>	RSD (%) <sup>1</sup>	RD (%) <sup>1</sup>	RSD (%) <sup>1</sup>	RD (%) <sup>1</sup>	RSD (%) <sup>1</sup>	RD (%) <sup>1</sup>
S	wt.%	0.010	0.033	IR	—	—	—	—	—	—	—
Fe	wt.%	0.01	0.033	INAA	—	—	—	—	—	—	—
Cu	ppm	0.200	0.660	TD-ICP-MS	3.46	22.7	1.68	10.7	2.01	0.83	9.68
Cu	wt.%	0.001	0.003	ICP-OES	—	—	—	—	—	—	—
Zn	ppm	0.500	1.65	TD-ICP-MS	3.23	6.31	2.12	10.3	1.89	2.49	6.72
Zn	wt.%	0.001	0.003	ICP-OES	—	—	—	—	—	—	—
V	ppm	2.00	6.60	TD-ICP-OES	—	48.0	—	11.6	—	—	5.00
Cr	ppm	2.00	6.60	INAA	—	—	—	—	—	—	—
Mn	ppm	1.00	3.30	TD-ICP-OES	—	7.39	—	4.41	—	—	—
Co	ppm	0.100	0.330	TD-ICP-MS	3.95	-0.556	3.14	-15.9	2.91	2.27	-3.74
Ni	ppm	1.00	3.30	TD-ICP-OES	—	-5.26	—	13.3	—	—	8.70
As	ppm	0.500	1.65	INAA	—	—	—	—	—	—	—
Se	ppm	0.100	0.330	TD-ICP-MS	—	—	15.7	131	—	—	—
Ag	ppm	0.300	0.990	TD-ICP-OES	—	—	—	15.4	—	—	—
Cd	ppm	0.300	0.990	TD-ICP-OES	—	—	—	-1.33	—	—	0.000
Sn	ppm	1.00	3.30	TD-ICP-MS	0.000	-66.7	0.000	8.70	—	0.000	21.2
Sb	ppm	0.100	0.330	INAA	—	—	—	—	—	—	—
Te	ppm	0.100	0.330	TD-ICP-MS	—	—	35.4	-58.3	—	—	—
Ta	ppm	0.100	0.330	TD-ICP-MS	—	—	—	—	—	0.000	0.000
Au	ppb	2.00	6.60	INAA	—	—	—	—	—	—	—
Au	g/tonne	0.030	0.099	FA-Gra	—	—	—	—	—	—	—
Hg	ppb	5.00	16.5	Hg-(CV) FIMS	—	—	—	—	—	—	—
Hg	ppm	1.00	3.30	INAA	—	—	—	—	—	—	—
Tl	ppm	0.050	0.165	TD-ICP-MS	5.66	-10.7	3.74	-21.2	—	3.25	-2.25
Pb	ppm	3.00	9.90	TD-ICP-OES	—	-12.0	—	3.87	—	—	-17.1
Pb	wt.%	0.003	0.01	ICP-OES	—	—	—	—	—	—	—
Bi	ppm	0.020	0.066	TD-ICP-MS	0.000	-90.4	4.10	-28.9	—	5.66	-10.7



**Table A5-1 (cont.)**

Unit symbol	LOD <sup>1</sup>	LOQ <sup>1</sup>	RM <sup>1</sup> Method <sup>1</sup>	LKSD-4		BaSO <sub>4</sub>		DMMAS 115		PTC-1a	OREAS 14P		OREAS 13b	
				RSD (%) <sup>1</sup>	RD (%) <sup>1</sup>	RSD (%) <sup>1</sup>	RD (%) <sup>1</sup>	RD (%) <sup>1</sup>	RD (%) <sup>1</sup>	RD (%) <sup>1</sup>	RD (%) <sup>1</sup>	RD (%) <sup>1</sup>	RD (%) <sup>1</sup>	RD (%) <sup>1</sup>
S wt. %	0.010	0.033	IR	7.07	14.9	1.62	0.571	—	—	—	—	—	—	—
Fe wt. %	0.01	0.033	INAA	—	—	—	—	0.758	—	—	—	—	—	—
Cu ppm	0.200	0.660	TD-ICP-MS	—	—	—	—	—	—	—	—	—	—	—
Cu wt. %	0.001	0.003	ICP-OES	—	—	—	—	—	—	-2.29	2.31	—	2.28	—
Zn ppm	0.500	1.65	TD-ICP-MS	—	—	—	—	—	—	—	—	—	—	—
Zn wt. %	0.001	0.003	ICP-OES	—	—	—	—	—	—	—	—	—	65.4	—
V ppm	2.00	6.60	TD-ICP-OES	—	—	—	—	—	—	—	—	—	—	—
Cr ppm	2.00	6.60	INAA	—	—	—	—	-4.00	—	—	—	—	—	—
Mn ppm	1.00	3.30	TD-ICP-OES	—	—	—	—	—	—	—	—	—	—	—
Co ppm	0.100	0.330	TD-ICP-MS	—	—	—	—	—	—	—	—	—	—	—
Ni ppm	1.00	3.30	TD-ICP-OES	—	—	—	—	—	—	—	—	—	—	—
As ppm	0.500	1.65	INAA	—	—	—	—	7.02	—	—	—	—	—	—
Se ppm	0.100	0.330	TD-ICP-MS	—	—	—	—	—	—	—	—	—	—	—
Ag ppm	0.300	0.990	TD-ICP-OES	—	—	—	—	—	—	—	—	—	—	—
Cd ppm	0.300	0.990	TD-ICP-OES	—	—	—	—	—	—	—	—	—	—	—
Sn ppm	1.00	3.30	TD-ICP-MS	—	—	—	—	—	—	—	—	—	—	—
Sb ppm	0.100	0.330	INAA	—	—	—	—	-30.9	—	—	—	—	—	—
Te ppm	0.100	0.330	TD-ICP-MS	—	—	—	—	—	—	—	—	—	—	—
Ta ppm	0.100	0.330	TD-ICP-MS	—	—	—	—	—	—	—	—	—	—	—
Au ppb	2.00	6.60	INAA	—	—	—	—	-12.8	—	—	—	—	—	—
Au g/tonne	0.030	0.099	FA-Gra	—	—	—	—	—	—	—	—	—	—	—
Hg ppb	5.00	16.5	Hg-(CV) FIMS	—	—	—	—	—	—	—	—	—	—	—
Hg ppm	1.00	3.30	INAA	—	—	—	—	—	—	—	—	—	—	—
Tl ppm	0.050	0.165	TD-ICP-MS	—	—	—	—	—	—	—	—	—	—	—
Pb ppm	3.00	9.90	TD-ICP-OES	—	—	—	—	—	—	—	—	—	—	—
Pb wt. %	0.003	0.01	ICP-OES	—	—	—	—	—	—	-2.00	—	—	—	—
Bi ppm	0.020	0.066	TD-ICP-MS	—	—	—	—	—	—	—	—	—	—	—

**Table A5-1 (cont.)**

Unit symbol	LOD <sup>1</sup>	LOQ <sup>1</sup>	RM <sup>1</sup> Method <sup>1</sup>	Ccu-1d RD (%) <sup>1</sup>	CPB-2 RD (%) <sup>1</sup>	CZN-4 RD (%) <sup>1</sup>	CDN-GS- 6A RD (%) <sup>1</sup>	CDN-HLHZ RSD (%) <sup>1</sup>	CDN-HLHZ RD (%) <sup>1</sup>	CDN-HLLC RSD (%) <sup>1</sup>	CDN-HLLC RD (%) <sup>1</sup>
S	wt.%	0.010	0.033	IR	—	—	—	1.60	—	0.215	—
Fe	wt.%	0.01	0.033	INAA	—	—	—	2.22	—	1.08	—
Cu	ppm	0.200	0.660	TD-ICP-MS	—	—	—	1.52	-2.24	—	—
Cu	wt.%	0.001	0.003	ICP-OES	-0.54	1.74	—	—	—	3.98	-4.70
Zn	ppm	0.500	1.65	TD-ICP-MS	—	—	—	2.69	2.87	0.46	2.66
Zn	wt.%	0.001	0.003	ICP-OES	0.000	-0.072	—	5.40	4.24	2.44	-3.65
V	ppm	2.00	6.60	TD-ICP-OES	—	—	—	0.000	—	4.56	—
Cr	ppm	2.00	6.60	INAA	—	—	—	14.3	—	12.6	—
Mn	ppm	1.00	3.30	TD-ICP-OES	—	—	—	2.00	—	5.50	—
Co	ppm	0.100	0.330	TD-ICP-MS	—	—	—	2.50	—	0.43	—
Ni	ppm	1.00	3.30	TD-ICP-OES	—	—	—	2.06	—	13.66	—
As	ppm	0.500	1.65	INAA	—	—	—	2.41	—	0.75	—
Se	ppm	0.100	0.330	TD-ICP-MS	—	—	—	—	—	3.18	—
Ag	ppm	0.300	0.990	TD-ICP-OES	—	—	—	4.78	-0.593	4.58	-0.307
Cd	ppm	0.300	0.990	TD-ICP-OES	—	—	—	0.000	—	2.91	—
Sn	ppm	1.00	3.30	TD-ICP-MS	—	—	—	17.0	—	7.44	—
Sb	ppm	0.100	0.330	INAA	—	—	—	1.94	—	1.27	—
Te	ppm	0.100	0.330	TD-ICP-MS	—	—	—	84.9	—	28.3	—
Ta	ppm	0.100	0.330	TD-ICP-MS	—	—	—	101.0	—	70.7	—
Au	ppb	2.00	6.60	INAA	—	—	—	7.06	-25.8	6.43	-15.2
Au	g/tonne	0.030	0.099	FA-Gra	—	—	6.04	—	—	—	—
Hg	ppb	5.00	16.5	Hg-(CV) FIMS	—	—	—	10.2	—	7.77	—
Hg	ppm	1.00	3.30	INAA	—	—	—	—	—	—	—
Tl	ppm	0.050	0.165	TD-ICP-MS	—	—	—	4.66	—	3.32	—
Pb	ppm	3.00	9.90	TD-ICP-OES	—	—	—	—	—	2.56	-14.3
Pb	wt.%	0.003	0.01	ICP-OES	-1.91	1.02	—	3.85	1.29	—	—
Bi	ppm	0.020	0.066	TD-ICP-MS	—	—	—	20.8	—	1.54	—

**Table A5-1 (cont.)**

Unit symbol	LOD <sup>1</sup>	LOQ <sup>1</sup>	RM <sup>1</sup> /Duplicate Method <sup>1</sup>	CDN-HLHC RSD (%) <sup>1</sup>	RD (%) <sup>1</sup>	62002 CV <sub>av</sub> (%) <sup>1</sup>	62008 CV <sub>av</sub> (%) <sup>1</sup>	62014 CV <sub>av</sub> (%) <sup>1</sup>	62158 CV <sub>av</sub> (%) <sup>1</sup>	B1 CV <sub>av</sub> (%) <sup>1</sup>	62200 CV <sub>av</sub> (%) <sup>1</sup>
S wt. %	0.010	0.033	IR	1.66	—	0.164	—	—	0.140	—	—
Fe wt. %	0.01	0.033	INAA	0.000	—	—	—	—	—	—	—
Cu ppm	0.200	0.660	TD-ICP-MS	—	—	—	—	—	—	—	0.912
Cu wt. %	0.001	0.0033	ICP-OES	2.20	7.79	—	—	6.95	—	—	—
Zn ppm	0.500	1.65	TD-ICP-MS	0.868	4.04	—	0.176	—	—	—	2.49
Zn wt. %	0.001	0.0033	ICP-OES	4.11	-4.89	—	—	0.000	—	—	—
V ppm	2.00	6.60	TD-ICP-OES	2.89	—	—	8.16	—	—	—	14.6
Cr ppm	2.00	6.60	INAA	0.000	—	—	—	—	—	—	—
Mn ppm	1.00	3.30	TD-ICP-OES	4.30	—	—	12.6	—	—	—	17.7
Co ppm	0.100	0.330	TD-ICP-MS	1.20	—	—	2.53	—	—	—	1.55
Ni ppm	1.00	3.30	TD-ICP-OES	9.91	—	—	8.32	—	—	—	0.000
As ppm	0.500	1.65	INAA	1.07	—	—	—	—	—	—	—
Se ppm	0.100	0.330	TD-ICP-MS	1.21	—	—	3.01	—	—	—	9.47
Ag ppm	0.300	0.990	TD-ICP-OES	5.14	-0.901	—	3.76	—	—	—	1.37
Cd ppm	0.300	0.990	TD-ICP-OES	2.53	—	—	3.13	—	—	—	16.3
Sn ppm	1.00	3.30	TD-ICP-MS	5.24	—	—	6.43	—	—	—	7.44
Sb ppm	0.100	0.330	INAA	0.989	—	—	—	—	—	—	—
Te ppm	0.100	0.330	TD-ICP-MS	20.2	—	—	1.06	—	—	—	10.6
Ta ppm	0.100	0.330	TD-ICP-MS	0.000	—	—	—	—	—	—	70.7
Au ppb	2.00	6.60	INAA	12.9	-7.87	—	—	—	—	—	—
Au g/tonne	0.030	0.099	FA-Gra	—	—	—	—	—	—	—	—
Hg ppb	5.00	16.5	Hg-(CV) FIMS	6.12	—	—	—	—	—	9.67	—
Hg ppm	1.00	3.30	INAA	—	—	—	—	—	—	—	—
Tl ppm	0.050	0.165	TD-ICP-MS	1.14	—	—	0.623	—	—	—	13.3
Pb ppm	3.00	9.90	TD-ICP-OES	0.989	-15.9	—	1.65	—	—	—	0.922
Pb wt. %	0.003	0.0099	ICP-OES	—	—	—	—	3.31	—	—	—
Bi ppm	0.020	0.066	TD-ICP-MS	0.592	—	—	2.99	—	—	—	4.22

**Table A5-1 (cont.)**

Unit symbol	LOD <sup>1</sup>	LOQ <sup>1</sup>	Duplicate Method <sup>1</sup>	62172 CV <sub>av</sub> (%) <sup>1</sup>	36256 CV <sub>av</sub> (%) <sup>1</sup>	A2 CV <sub>av</sub> (%) <sup>1</sup>
S wt. %	0.010	0.033	IR	0.285	—	0.995
Fe wt. %	0.01	0.033	INAA	1.07	—	—
Cu ppm	0.200	0.660	TD-ICP-MS	—	—	—
Cu wt. %	0.001	0.003	ICP-OES	0.714	—	—
Zn ppm	0.500	1.65	TD-ICP-MS	1.93	—	—
Zn wt. %	0.001	0.003	ICP-OES	0.140	—	—
V ppm	2.00	6.60	TD-ICP-OES	4.04	—	—
Cr ppm	2.00	6.60	INAA	—	—	—
Mn ppm	1.00	3.30	TD-ICP-OES	1.84	—	—
Co ppm	0.100	0.330	TD-ICP-MS	3.34	—	—
Ni ppm	1.00	3.30	TD-ICP-OES	10.3	—	—
As ppm	0.500	1.65	INAA	0.759	—	—
Se ppm	0.100	0.330	TD-ICP-MS	3.62	—	—
Ag ppm	0.300	0.990	TD-ICP-OES	2.42	—	—
Cd ppm	0.300	0.990	TD-ICP-OES	1.79	—	—
Sn ppm	1.00	3.30	TD-ICP-MS	0.000	—	—
Sb ppm	0.100	0.330	INAA	3.24	—	—
Te ppm	0.100	0.330	TD-ICP-MS	13.1	—	—
Ta ppm	0.100	0.330	TD-ICP-MS	106	—	—
Au ppb	2.00	6.60	INAA	9.35	—	—
Au g/tonne	0.030	0.099	FA-Gra	—	—	—
Hg ppb	5.00	16.5	Hg-(CV) FIMS	3.84	4.90	—
Hg ppm	1.00	3.30	INAA	0.000	—	—
Tl ppm	0.050	0.165	TD-ICP-MS	6.88	—	—
Pb ppm	3.00	9.90	TD-ICP-OES	1.26	—	—
Pb wt. %	0.003	0.01	ICP-OES	0.000	—	—
Bi ppm	0.020	0.066	TD-ICP-MS	3.43	—	—

<sup>1</sup> RM - Reference material; LOD - Limit of detection; LOQ - Limit of quantification (LOQ=3.3\*LOD); Method abbreviations see text; RSD (%) - Percent relative standard deviation (precision for RMs, Eq. (5-1)); RD (%) - Percent relative difference (accuracy, Eq. (5-3)); CV<sub>av</sub>(%) - Percent average coefficient of variation (precision for duplicate analysis, Eq. (5-2)).

— No value calculated, because element was not measured or measured concentration was below/above detection limit

Accuracy was checked via RMs and is reported as percent relative difference:

$$RD_i(\%) = 100 * \left( \frac{\mu_i - c_i}{c_i} \right) \quad (5-3)$$

where  $RD_i(\%)$  is the percent relative difference,  $\mu_i$  is the mean value of element  $i$  over the series of analytical runs for element  $i$ , and  $c_i$  is the “known” or “certified” value of element  $i$  for the RM. Accuracy could only be checked for elements analyzed via IR, TD-ICP-MS, and Hg-(CV) FIMS, because RMs were analyzed every 20 samples. Moreover, accuracy for RMs CDN-HLHZ, CDN-HLLC, and CDN-HLHC is only reported for Au, Ag, Cu, Zn, and Pb, because only these elements are certified. Overall accuracy is  $-10\% \leq RD \leq +10\%$  and hence sufficient for work herein. However, accuracy for some elements is above  $\pm 10\%$ , because concentrations of some elements are close to the detection limit (Sn, Te, Ta, Hg, Cd, Ag, Bi, Pb) or can have a nugget effect (Au). Nevertheless, accuracy for the analyzed elements in the used RMs is in general good.

#### A5-2-2 *ELECTRON PROBE MICRO-ANALYSIS (EPMA)*

Electron microprobe micro-analysis was conducted on a wavelength dispersive Cameca SX50/51 electron microprobe at the Department of Geology, University of Toronto (UT) between April 2011 and May 2013. In total, 17 elements (Ag, As, Au, Bi, Co, Cu, Fe, Hg, Mn, Mo, Ni, Pb, S, Sb, Sn, Te, Zn) on 36 samples from all orebodies of the Ming deposit were analyzed. Analyzed minerals include pyrite, chalcopyrite, cubanite, sphalerite, pyrrhotite, arsenopyrite, alloclasite, galena, meneghinite, loellingite, tsumoite, unnamed Bi-telluride, hessite, altaite, breithauptite, nisbite, gudmundite, tennantite-tetrahedrite, AgHg alloy, and electrum. Detailed information regarding instrumentation and analysis are found in Brueckner et al. (2014).

Quality control was maintained by utilizing UT internal standards for each

analyzed phase; calibration standards were measured at the beginning of the phase in question. Measured values on each applied internal standard are in accordance with the accepted concentrations in these standards (pers commun Y. Liu, 2013). Additionally, data were deemed acceptable if analytical totals fell within a range of  $100 \pm 1.5 \text{ wt.}\%$  and their stoichiometry represented the accepted mineral composition. All clean analyses of sulfide and precious metals fell within this range or were otherwise discarded. Accuracy of results was monitored via UT in-house standards. The results above detection limit were within 5% of the accepted values. Precision of the analysis was calculated from the counting rate and is presented together with the detection limits in Tables A5-2 and A5-3. In this paper, major elements have usually a precision between 0.2-0.5 %, but this precision can be up to 2wt.% if there are solid solution series within minerals (e.g., Fe and Zn in sphalerite, As and Sb in tennantite-tetrahedrite). Minor elements (0.5-2.0vol.%) have precisions between 1-10% in the analyzed minerals, since precision increases with increasing concentrations for minor components. Unknown and standard intensities were corrected for dead time. Standard intensities were corrected for standard drift over time by internal software corrections. Interference corrections were applied to S for interference by Co; to As for interference by Pb; to Sn for interference by Co; to Bi for interference by Au; to Mo for interference by Pb; and to Mn for interference by Hg.

**Table 5-2.** Precision data for major element components of analyzed minerals; n - number of analysis

Element	Mineral	n	Mean [%]	1 $\sigma$ [%]	Element	Mineral	n	Mean [%]	1 $\sigma$ [%]
Fe	Py	139	0.364	0.013	Te	BiTe	14	0.987	0.088
S	Py	139	0.333	0.040	Bi	BiTe	14	0.834	0.051
Fe	Ccp	181	0.436	0.015	Pb	BiTe	14	3.86	1.58
S	Ccp	181	0.438	0.048	Sb	BiTe	14	9.98	7.84
Cu	Ccp	181	0.481	0.016	Pb	Alt	2	0.858	0.008
Fe	Cbn	9	0.395	0.001	Te	Alt	2	0.955	0.010
S	Cbn	9	0.484	0.002	Fe	Gud	2	0.503	0.001
Cu	Cbn	9	0.612	0.002	S	Gud	2	0.725	0.002
Fe	Sp	109	1.11	0.225	Sb	Gud	2	0.334	0.001
S	Sp	109	0.471	0.051	Sb	Nis	5	0.308	0.019
Zn	Sp	109	0.382	0.021	Sn	Nis	5	8.53	0.755
Fe	Po	86	0.319	0.013	Ni	Nis	5	0.214	0.031
S	Po	86	0.397	0.047	S	Men	11	0.566	0.064
Fe	Asp	107	0.402	0.017	Cu	Men	11	2.58	0.469
S	Asp	107	0.608	0.072	Pb	Men	11	0.746	0.106
As	Asp	107	0.454	0.018	Sb	Men	11	0.669	0.013
S	Gn	87	0.646	0.084	Fe	Tnt-Trt	68	1.21	0.066
Pb	Gn	87	0.606	0.070	S	Tnt-Trt	68	0.522	0.057
Fe	Allo	5	1.06	0.268	Cu	Tnt-Trt	68	0.455	0.017
S	Allo	5	0.713	0.009	Zn	Tnt-Trt	68	2.12	0.240
As	Allo	5	0.469	0.004	As	Tnt-Trt	68	2.06	0.746
Co	Allo	5	0.219	0.044	Ag	Tnt-Trt	68	6.97	2.48
Fe	Loel	1	0.467		Sb	Tnt-Trt	68	0.893	0.138
S	Loel	1	2.77		Fe	AgHg	2	2.34	0.35
As	Loel	1	0.371		Ag	AgHg	2	0.64	0.01
Fe	Hess	6	6.83	4.91	Hg	AgHg	2	0.64	0.00
Ag	Hess	6	0.533	0.022	Au	El	25	0.917	0.093
Te	Hess	6	0.963	0.038	Ag	El	25	0.846	0.189
					Hg	El	25	2.19	1.67

**Mineral abbreviations:** AgHg – AgHg alloy, Allo – alloclasite, Alt – altaite, Apy – arsenopyrite, BiTe – Bi–tellurides, Cbn – cubanite, Ccp – chalcopyrite, Col – coloradoite, El – electrum, Gn – galena, Gud – gudmundite, Hess – hessite, Loel – löllingite, Mia – miargyrite, Men – meneghinite, Nis – nisbite, Po – pyrrhotite, Py – pyrite, Sp – sphalerite, Stn – stannite, Tnt-Trt – tennantite–tetrahedrite

**Table 5-3.** Limit of detection (LOD) for major and minor elements analyzed by EPMA

Element	n	LOD [ppm]	1 $\sigma$ [ppm]	Element	n	LOD [ppm]	1 $\sigma$ [ppm]
Fe	927	372	23	Sb	927	559	19
S	927	371	47	Sn	927	783	160
Cu	927	482	36	Te	927	904	199
Zn	927	573	45	Bi	927	1,630	412
Pb	927	1,937	290	Hg	927	2,097	341
As	927	1,179	105	Mn	927	140	4
Au	927	1,668	618	Co	927	155	11
Ag	927	1,217	193	Ni	927	388	144

*A5-2-3 LASER ABLATION INDUCTIVELY COUPLED PLASMA MASS SPECTROMETRY (LA-ICP-MS)*

In situ LA-ICP-MS analysis was conducted on 22 thick sections ( $\approx 200\mu\text{m}$ ) from all orebodies of the Ming deposits to detect the trace element composition in 15 mineral phases (pyrite, chalcopyrite, cubanite, sphalerite, pyrrhotite, arsenopyrite, galena, alloclasite, tsumoite, tetrahedrite-tennantite, stannite, pyrargyrite, miargyrite, AgHg alloy, electrum). For this study 20 elements ( $^{56}\text{Fe}$ ,  $^{33}\text{S}$ ,  $^{47}\text{Ti}$ ,  $^{51}\text{V}$ ,  $^{53}\text{Cr}$ ,  $^{55}\text{Mn}$ ,  $^{59}\text{Co}$ ,  $^{61}\text{Ni}$ ,  $^{63}\text{Cu}$ ,  $^{66}\text{Zn}$ ,  $^{75}\text{As}$ ,  $^{82}\text{Se}$ ,  $^{109}\text{Ag}$ ,  $^{111}\text{Cd}$ ,  $^{118}\text{Sn}$ ,  $^{121}\text{Sb}$ ,  $^{125}\text{Te}$ ,  $^{197}\text{Au}$ ,  $^{208}\text{Pb}$ ,  $^{209}\text{Bi}$ ) were of interest for the purpose of this paper. Analyses were undertaken at Laurentian University on a Thermo X-Series II quadrupole ICP-MS coupled to a Resonetics RESolution M-50 213nm ArF excimer laser with a 20ns pulse length. The LA-ICP-MS was operated with a forward power of 1,440W. For analysis, a spot size of  $34\mu\text{m}$  beam diameter with a repetition rate of 5Hz and an energy density of  $7\text{J}/\text{cm}^2$  was used to analyze sample spots that were analyzed prior by EPMA. The ablation cell was a Laurin Technic two-volume sample cell. Ablation was performed in an atmosphere of pure He (0.65L/min). Immediately after the ablated material left the ablation cell, a mix of Ar (0.75L/min) and  $\text{N}_2$  (0.006L/min) carried the ablated material directly into the torch. Each spot had a total acquisition time of 60s consisting of 30s ablation time and 30s washout time.

The LA-ICP-MS was calibrated daily and the production of molecular



species was monitored by  $^{232}\text{Th}^{16}\text{O}/^{232}\text{Th}$ , which was  $< 0.2\%$ . Due to the low level of molecular oxide production no correction was applied to the analyte signal intensities for such interfering species. Dwell times for the analyzed elements were 10ms, except for S, Ti, V, Cr, Mn, Fe, Co, Ni, Cu, and Zn, which had a dwell time of 5ms. Data reduction was done by Lolite v.2.5.

The synthetic glass reference material NIST 610 was used as calibration standard. Reference materials MASS-1 and Po725 were used as external standards to monitor instrumental drift and data quality. Concentrations for the used reference materials were the recommended values (1) from the GeoReM database v.16 for NIST 610 (Jochum et al., 2005), (2) from Wilson et al. (2002) for MASS-1, and (3) from Sylvester (2008) for Po725. Reference materials NIST 610 and Po725 were analyzed at the beginning, the end, and if applicable after 10 spots each. MASS-1 was analyzed three times each at the beginning and the end of each sample analysis. The used internal standards were  $^{56}\text{Fe}$  (pyrite, chalcopyrite, cubanite, sphalerite, pyrrhotite, arsenopyrite, alloclasite, tetrahedrite-tennantite, stannite),  $^{109}\text{Ag}$  (pyrargyrite, miargyrite, AgHg alloy, electrum),  $^{125}\text{Te}$  (tsumoite), and  $^{208}\text{Pb}$  (galena). Although  $^{40}\text{Ar}^{16}\text{O}$  interferes with  $^{56}\text{Fe}$ , this interference was assumed to be negligible due to the low oxygen production rate. Sulfur as internal standard was neglected due to several reasons outlined by Danyushevsky et al. (2011) including large memory effect of S during LA-ICP-MS analysis or the high level of various interferences on S. Danyushevsky et al. (2011) showed that Pb as internal standard for galena analysis is also suitable.

In Table A5-4, results for NIST 610, MASS-1, and S and Au in Po725 are presented for calibration with NIST 610 and various internal standards. Precision and accuracy for NIST 610 independently on the internal standard are usually within 5% of the recommended values for NIST 610 (GeoReM, Jochum et al., 2005). Exceptions are S and Se, which exceed both in precision and accuracy. These elevated values for both elements are attributed to instrument or sampling

effect for S and the volatility of Se.

The measured data especially for MASS-1 calibrated with NIST 610 and  $^{56}\text{Fe}$  are imprecise ( $\text{RSD}\approx 31\text{-}109\%$ ). This imprecision is presumably caused by: (1) inhomogeneity of MASS-1; (2) sampling problem especially in elements enriched in MASS-1 (S, Fe, Cu, Zn) compared to silicate RM NIST 610 that has fairly low concentrations in these elements; (3) partial fractionation of S during ablation (Danyushevsky et al., 2011), and (4) instrumental problems. The measured values for MASS-1 were compared to the recommended data of Wilson (2002), Danyushevsky et al. (2011) and Yuan et al. (2012). Danyushevsky et al. (2011) used a 193 nm excimer laser for analysis and  $^{57}\text{Fe}$  as internal standard. Yuan et al. (2012) used NIST 610 as calibration standard and Fe as internal standard. Accuracy for MASS-1 is  $<20\%$  for most measured elements except Mn, Ag, and Cd when measured data compared to Yuan et al. (2012). This is most likely due to the same calibration approach. Accuracy of the measured data of MASS-1 when compared to both Wilson et al. (2001) and Danyushevsky et al. (2011) varies strongly. Obtained data for MASS-1 when calibrated with  $^{109}\text{Ag}$  show good precision ( $<20\%$ ) with the exception of As and Au (i.e., nugget effect of Au) and good accuracy ( $<20\%$ ) against the recommended data of Wilson et al. (2002) for most elements.

Measured S and Au data for Po725 when calibrated with NIST 610 and  $^{56}\text{Fe}$  show good precision and accuracy for Au ( $\text{RSD}\approx 7\%$ ,  $\text{RD}\approx 15\%$ ), whereas S is rather imprecise (29%) and inaccurate (-93%) due to sampling effects (i.e., largely differing S composition between NIST 610 and Po 725).

For quality assurance purposes Po725 was used as calibration standard with  $^{56}\text{Fe}$  as internal standard on NIST 610 and Po725. Precision and accuracy for Au in both NIST 610 and Po725 are good, whereas S is highly imprecise and inaccurate in NIST 610 due to sampling effects.

Possible micro-inclusions within the analyzed minerals were identified in Iolite v.2.5 through time-resolved signals. In these signals, counting rates of trace

elements were compared to counting rates of major elements (e.g., Cu vs Zn in sphalerite) and abnormal patterns (e.g., peaks in trace element of interest) indicated possible micro-inclusion. These micro-inclusions were usually cut out from the signal and not used for data reduction; however, some of these micro-inclusion signals could not be cut due to their frequency or relatively low signal count.

**Table A5-4.** Precision and accuracy for reference materials NIST 610, MASS-1, and Po 725 calibrated against NIST 610, themselves and with various internal standards; RM – reference material, Av – average, Precision: RSD [%] – relative standard deviation (see equation (1)); Accuracy: RD [%] – relative difference (see equation (2)), Uncert – uncertainty

RM	Calibration of NIST 610 by NIST 610 and <sup>56</sup> Fe					Calibration of NIST 610 by NIST 610 and <sup>109</sup> Ag					Calibration of NIST 610 by NIST 610 and <sup>125</sup> Te				
	NIST 610 Av [ppm] (n=61)	NIST 610 1σ [ppm]	NIST 610 RSD [%]	NIST 610 RD [%]		NIST 610 Av [ppm] (n=17)	NIST 610 1σ [ppm]	NIST 610 RSD [%]	NIST 610 RD [%]		NIST 610 Av [ppm] (n=3)	NIST 610 1σ [ppm]	NIST 610 RSD [%]	NIST 610 RD [%]	
S	606	1.48	0.243	5.46		576	12.5	2.17	0.138		671	20.6	3.06	16.8	
Ti	447	0.781	0.175	-1.01		452	0.126	0.028	-0.036		432	3.14	0.727	-4.34	
V	448	1.01	0.226	-0.496		450	0.407	0.090	0.008		442	1.51	0.342	-1.67	
Cr	407	0.844	0.207	-0.199		408	0.355	0.087	-0.015		406	1.74	0.430	-0.567	
Mn	454	0.709	0.156	2.32		444	0.330	0.074	0.037		485	1.51	0.312	9.17	
Fe						466	9.42	2.022	1.754		458	2.62	0.572	-0.103	
Co	409	0.669	0.164	-0.311		410	0.054	0.013	-0.034		406	1.74	0.430	-1.05	
Ni	458	0.951	0.208	-0.196		461	2.61	0.565	0.556		446	25.7	5.76	-2.78	
Cu	438	0.544	0.124	-0.587		441	0.200	0.045	0.041		429	0.872	0.203	-2.64	
Zn	459	0.805	0.175	-0.186		461	0.014	0.003	0.129		459	10.9	2.37	-0.209	
As	323	0.473	0.146	-0.622		325	0.663	0.204	0.082		318	1.74	0.548	-2.12	
Se	131	0.340	0.260	-5.31		138	0.339	0.245	0.226		109	0.231	0.211	-21.0	
Ag	248	0.422	0.170	-1.22							239	0.349	0.146	-4.87	
Cd	267	0.712	0.267	-1.12		270	0.277	0.103	0.176		262	4.910	1.87	-2.95	
Sn	421	0.724	0.172	-1.98		430	0.166	0.039	-0.010		397	1.744	0.440	-7.76	
Sb	389	0.659	0.169	-1.69		396	0.281	0.071	0.062		368	0.087	0.024	-6.97	
Te	302	0.640	0.212	-0.081		302	0.182	0.060	-0.066						
Au	23.4	0.061	0.260	-0.713		24	0.042	0.179	0.115		23.0	0.063	0.273	-2.40	
Pb	426	0.872	0.205	-0.046		427	0.247	0.058	0.124		424	2.615	0.616	-0.397	
Bi	377	0.469	0.124	-1.77		384	0.221	0.058	0.081		359	0.959	0.267	-6.56	

**Table A5-4 (cont.)**

RM	Calibration of NIST 610 by NIST 610 and <sup>208</sup> Pb					Calibration of NIST 610 by Po 725 and <sup>56</sup> Fe					Recommended values (GeoReM)		
	NIST 610 Av [ppm] (n=17)	NIST 610 1σ [ppm]	NIST 610 RSD [%]	NIST 610 RD [%]	NIST 610 RD [%]	NIST 610 Av [ppm] (n=51)	NIST 610 1σ [ppm]	NIST 610 RSD [%]	NIST 610 RD [%]	NIST 610 RD [%]	NIST 610 Av [ppm]	NIST 610 Uncert [ppm]	
S	608	56.9	9.35	5.79	-0.480	10,125	2,434	24.04	1660.8		575	138	
Ti	450	11.2	2.50	0.031	0.031						452	30	
V	450	6.79	1.51	0.317	2.74						450	86	
Cr	409	4.68	1.14	1.15	0.156						408	64	
Mn	456	19.7	4.31	0.892	-0.180						444	10	
Fe	463	6.77	1.46	0.379	-0.100						458	9	
Co	411	5.24	1.28	-4.78	-0.748						410	46	
Ni	463	3.62	0.782	0.506	-0.227						458.7	4	
Cu	440	8.11	1.84	0.379	-0.180						441	48	
Zn	462	6.02	1.30	0.379	-0.100						460	38	
As	325	5.99	1.84	0.379	-0.100						325	24	
Se	131	15.0	11.5	0.379	-0.100						138	4	
Ag	249	7.13	2.86	0.379	-0.100						251	38	
Cd	269	6.71	2.50	0.379	-0.100						270	10	
Sn	424	18.6	4.40	0.379	-0.100						430	36	
Sb	391	15.3	3.90	0.379	-0.100						396	56	
Te	304	2.41	0.795	0.379	-0.100						302		
Au	23.5	0.411	1.74	0.379	-0.100	21.2	0.725	3.43	-10.4		23.6	8	
Pb											426	1	
Bi	379	14.5	3.81	-1.24							384	98	

**Table A5-4 (cont.)**

RM	Calibration of MASS-1 by NIST 610 and <sup>56</sup> Fe						Calibration of MASS-1 by NIST 610 and <sup>109</sup> Ag					[1]	[2]	[3]
	MASS-1 Av [ppm] (n=75)						MASS-1 Av [ppm] (n=9)							
Av [ppm] (n=75)	1σ [ppm]	RSD [%]	RD <sup>1</sup> [%]	RD <sup>2</sup> [%]	RD <sup>3</sup> [%]	Av [ppm] (n=9)	1σ [ppm]	RSD [%]	RD <sup>1</sup> [%]					
S	15,199	16,509	109	-94.5		-171	19,583	3,573	18.2	-92.9	276,000		163,600	
V	66.4	21.7	32.7	5.47			58.5	3.56	6.08	-7.07	63			
Cr	67.2	46.5	69.2	81.7	-11.5		64.5	2.19	3.39	74.3	37	76.0		
Mn	250	81.8	32.8	-3.95		-34.1	222	8.67	3.91	-14.6	260		305	
Fe							121,992	17,905	14.7	-21.8	156,000	145,500	156,000	
Co	73.6	24.6	33.4	9.84	49.3	6.86	65.4	1.77	2.71	-2.36	67	49.3	71	
Cu	136,085	41,911	30.8	1.56	11.5	11.1	123,578	14,252	11.5	-7.78	134,000	121,997	128,500	
Zn	222,587	183,629	82.5	5.99	14.1	-16.9	194,672	21,809	11.2	-7.30	210,000	195,011	244,600	
As	84.1	77.0	91.6	29.4	22.3	14.7	77.3	22.0	28.5	18.9	65	68.8	78	
Se	78.4	34.2	43.6	47.9	40.5		66.2	9.41	14.2	24.9	53	55.8		
Ag	75.8	28.3	37.3	13.1	12.3	61.9					67	67.5	57	
Cd	111.6	55.2	49.4	59.5	22.3	-72.7	93.8	7.10	7.57	34.0	70	91.3	182	
Sn	69.4	26.1	37.6	26.3	22.0	19.2	62.3	0.556	0.89	13.2	55	56.9	63	
Sb	75.2	29.0	38.6	36.7	1.04	19.8	62.7	1.36	2.17	14.0	55	74.4	68	
Au	59.3	24.9	41.9	26.2	-4.04	-2.19	58.8	15.9	27.0	25.2	47	61.8	60	
Bi	84.1	30.9	36.7	1102	20.7	37.9	74.8	1.38	1.84	968	7	69.7	70	

**[1]** Wilson et al. (2002); **RD<sup>1</sup> [%]** – relative difference of measured values to values from Wilson et al. (2002)

**[2]** Danyushevsky et al. (2011): LA-ICP-MS values measured with 193nm excimer laser, <sup>57</sup>Fe used as internal standard; **RD<sup>2</sup> [%]** – relative difference of measured values to values from Danyushevsky et al. (2011)

**[3]** Yuan et al. (2012): LA-ICP-MS values calibrated with NIST 610 as calibration standard and Fe as internal standard; **RD<sup>3</sup> [%]** – relative difference of measured values to values from Yuan et al. (2012)

**Table A5-4 (cont.)**

RM	Calibration of Po725 by NIST 610 and <sup>56</sup> Fe					Calibration of Po725 by Po725 and <sup>56</sup> Fe					Recommended values (Sylvester, 2008)		
	Po725 Av [ppm]	Po725 1σ [ppm]	Po725 RSD [%]	Po725 RD [%]		Po725 Av [ppm] (n=60)	Po725 1σ [ppm]	Po725 RSD [%]	Po725 RD [%]		Po725 Av [ppm]	Po725 Uncert [ppm]	
S	28,700	8,176	28.5	-92.7		390,893	41.2	0.011	-0.053		391,100	1,700	
Au	51.2	3.45	6.73	15.2		44.5	0.002	0.005	0.040		44.5	2.5	

## References

- Abzalov M (2008) Quality control of assay data: A review of procedures for measuring and monitoring precision and accuracy. *Exploration and Mining Geology* 17 (3-4):131-144. doi:10.2113/gsemg.17.3-4.131
- Actlabs (2012) Methods. Retrieved from: <http://www.actlabs.com/list.aspx?menu=64&app=226&cat1=549&tp=12&lk=no>
- Actlabs Groups of Companies (2007) 2007 international schedule of services and fees. Retrieved from: [http://www.actlabs.com/pricelist/serviceguide07\\_international.pdf](http://www.actlabs.com/pricelist/serviceguide07_international.pdf)
- Brueckner SM, Piercey SJ, Sylvester PJ, Maloney S, Pilgrim L (2014) Evidence for syngenetic precious metal enrichment in an Appalachian volcanogenic massive sulfide system: The 1806 Zone, Ming Mine, Newfoundland, Canada. *Economic Geology* 109 (6): 1611-1642. doi:10.2113/econgeo.109.6.1611
- Danyushevsky L, Robinson P, Gilbert S, Norman M, Large R, McGodrick P, Shelley M (2011) Routine quantitative multi-element analysis of sulphide minerals by laser ablation ICP-MS: Standard development and consideration of matrix effects. *Geochemistry: Exploration, Environment, Analysis* 11:51-60. doi:10.1144/1467-7873/09-244
- Jenner GA (1996) Trace element geochemistry of igneous rocks: Geochemical nomenclature and analytical geochemistry. In Wyman DA (ed.) *Trace element geochemistry of volcanic Rocks: Applications for massive sulfide exploration*. Geological Association of Canada, Short Course Notes 12:51-77
- Jochum KP, Nohl U, Herwig K, Lammel E, Stoll B, Hoffmann AW (2005) GeoReM: a new geochemical database for reference materials and isotopic standards. *Geostandards and Geoanalytical Research* 29 (3):333-338. doi:10.1111/j.1751-908X.2005.tb00904.x
- Wilson SA, Ridley WI, Koenig AE (2002) Development of sulfide calibration standards for the laser ablation inductively-coupled mass spectrometry technique. *Journal of Analytical Atomic Spectrometry* 17 (4):406-409. doi:10.1039/b108787h
- Yuan J-H, Zhan X-C, Fan C-Z, Zhao L-H, Sun D-Y, Jia Z-R, Hu M-Y, Kuai L-J (2012) Quantitative analysis of sulfide minerals by laser ablation-inductively coupled plasma-mass spectrometry using glass reference materials with



matrix normalization plus sulfur internal standardization calibration.  
Chinese Journal of Analytical Chemistry 40 (2):201-207.  
doi:10.1016/S1872-2040(11)60528-z

# APPENDIX A5-3 RESULTS OF WHOLE ROCK GEOCHEMISTRY, EPMA, AND LA-ICP-MS

**Table A5-5.** Detailed results of whole rock geochemistry for 36 mineralized samples from the Ming deposit

Orebody	1807 Zone	1807 Zone	1807 Zone	1807 Zone	1807 Zone	1807 Zone	1807 Zone	1807 Zone	1807 Zone	1807 Zone	1807 Zone	1807 Zone
Sample No.	62002_UG	62004_UG	62006_UG	62008_UG	62010_UG	62014_UG	62153_UG	62154_UG	62156_UG	62157_UG	62157_UG	62157_UG
Depth below sea level [m]	-375	-375	-375	-375	-375	-375	-375	-375	-469	-469	-469	-469
Description	massive sulfide	contact sheared mafic dyke - massive sulfide - lense - rhyolite	contact Quartz vein - massive sulfide - lense - mafic dyke	massive sulfide near sheared mafic dyke	massive Py-Ccp sulfide with fragments close to mafic dyke	massive Py-Ccp sulfide	massive Py-Ccp sulfide with schlieren	massive Py-Ccp sulfide with Po or Sp	massive Py-Ccp sulfide with schlieren	massive Py-Ccp sulfide with Po or Sp	massive Py-Ccp sulfide with Po or Sp	massive Py-Ccp sulfide with Po or Sp
S [wt.%]	52.5	51.3	39.4	46.9	48.1	50.5	51.6	45.1	49.3	47.8	47.8	47.8
Fe	45.6	45.8	39.4	40.5	42.7	42.8	44.0	38.7	41.4	39.2	39.2	39.2
Cu	1.12	2.63	20.32	11.99	8.75	6.34	3.60	13.90	5.60	7.26	7.26	7.26
Zn	0.225	0.094	0.469	0.326	0.163	0.064	0.249	1.72	2.12	5.32	5.32	5.32
V [ppm]	29.2	30.8	157	53.3	56.7	45.1	31.1	29.4	26.0	60.8	60.8	60.8
Cr	48.7	11.7	162	10.2		21.5	19.7					
Mn	82.9	72.3	1,391	57.4	145	49.4	180	99.4	62.9	159	159	159
Co	132	258	150	461	305	431	531	282	219	401	401	401
Ni	44.0	39.5	82.6	38.9	39.8	34.6	33.5	34.3	52.7	18.4	18.4	18.4
As	317	287	114	564	1,146	879	1,089	2,455	6,059	1,524	1,524	1,524
Se	217	155	377	871	306	309	449	518	318	377	377	377
Ag	40.9	11.5	29.2	22.0	18.4	13.9	14.3	31.8	36.1	16.8	16.8	16.8
Cd	11.8	9.67	40.9	32.4	16.5	9.347	23.8	149	165	369	369	369
Sn	8.53	10.6	25.0	22.5	9.6	9.670	19.7	73.0	16.0	40.2	40.2	40.2
Sb	14.1	13.7	12.5	23.4	31.2	25.9	30.7	113	99.4	40.5	40.5	40.5
Te	23.8	43.2	98.1	136	76.5	66.2	88.8	118	139	95.7	95.7	95.7
Ta	0.366	0.425	0.749	0.307			0.415	0.101		0.412	0.412	0.412
Au	3.58	0.682	2.55	3.06	0.741	1.45	2.22	1.32	4.95	2.56	2.56	2.56
Hg	3.00	1.39	4.52	2.40	2.11	1.01	1.74	10.3	9.00	18.8	18.8	18.8
Tl	2.95	1.17	3.17	2.33	2.97	4.05	1.32	1.12	1.36	0.814	0.814	0.814
Pb	4,581	326	362	350	749	1,364	2,551	1,562	7,577	707	707	707
Bi	53.7	34.1	61.9	145	110	84.6	173	250	621	138	138	138

**Table A5-5. (cont.)**

Orebody	1807 Zone	1807 Zone	1807 Zone	1807 Zone	1807 Zone	1806 Zone	1806 Zone	1806 Zone	1806 Zone	1806 Zone	1806 Zone	1806 Zone
Sample No.	62158_UG	62159_UG	62162_UG	62186_UG	62186_UG	36303_UG	36306_UG	36308_UG	36204_UG	36206_UG	36208_UG	1806 Zone
Depth below sea level [m]	-469	-469	-469	-389	-389	-70	-70	-71	-71	-71	-71	36208_UG
Description	massive Py-Ccp sulfide with Po or Sp	massive Py-Ccp sulfide with Po or Sp	massive Py-Ccp sulfide with Po or Sp	massive Py-Ccp sulfide with rhyolitic fragments	massive Py-Ccp sulfide with rhyolitic fragments	Sp bands with alternating Ccp in massive sulfides	massive Py-Ccp sulfides with fine Sp bands	massive Py-Ccp sulfides with Sp bands	massive Py-Ccp sulfides with Sp bands	thick Sp bands in massive Py-Ccp sulfides	massive Py-Ccp sulfides with fine Sp bands	1806 Zone
S [wt.%]	50.8	48.7	46.4	51.0	51.0	32.7	38.5	49.9	50.9	37.4	50.0	50.0
Fe	41.4	43.6	40.0	45.1	45.1	15.9	17.5	41.8	43.7	14.1	42.0	42.0
Cu	1.47	7.18	8.85	3.51	3.51	1.29	1.27	1.99	1.99	0.1	1.98	1.98
Zn	5.75	0.3	4.35	0.2	0.2	33.4	40.2	4.54	2.46	47.0	4.06	4.06
V [ppm]	40.3	63.8	52.5	26.7	26.7	113.4	57.4	74.8	109.0	104.3	45.0	45.0
Cr	9.08	14.2		15.4	15.4	19.6						
Mn	93.8	36.4	71.3	79.2	79.2	710	202	39.4	263	426	84.6	84.6
Co	408	293	399	353	353	62.9	12.1	36.1	371	34	115	115
Ni	22.2	19.2	12.5	42.1	42.1	43.8	22.7	24.8	65.3	19.5	48.0	48.0
As	918	528	1,625	351	351	4,669	5,173	8,808	2,756	251	8,218	8,218
Se	342	167	434	185	185	453	143	78.6	138	159	89.5	89.5
Ag	11.8	19.9	19.3	10.4	10.4	274.9	133.2	207	72.0	29.3	180.0	180.0
Cd	314	22.9	234	24.3	24.3	1,254	1,424	142	91.9	1,669	161	161
Sn	11.1	13.2	35.7	8.22	8.22	205	72.7	23.3	33.5	110	24.6	24.6
Sb	26.7	17.9	56.1	3.39	3.39	383	479	1,203	120.5	6.59	358.9	358.9
Te	95.8	37.7	137.7	69.7	69.7	35.2	1.95	2.12	15.6	6.15	15.9	15.9
Ta	0.403	0.304	0.099				0.205		0.419	0.329		
Au	0.969	0.461	1.76	0.944	0.944	1.85	20.08	18.10	3.33	1.48	24.96	24.96
Hg	14.0	1.44	11.5	1.39	1.39	200.7	707.8	110.2	4.09	833.4	118.9	118.9
Tl	1,906	1,579	2,279	1,079	1,079	8,203	8,952	8,161	3,238	6,248	3,128	3,128
Pb	3,319	1,032	810	102	102	158,165	16,900	7,655	4,800	10,025	9,643	9,643
Bi	176	67.2	168	32.9	32.9	20.7	2.05	1.31	13.4	14.9	21.6	21.6

Table A5-5. (cont.)

Orebody	1806 Zone	1806 Zone	1806 Zone	MSUP	MSUP	MSUP	MSUP	MSUP	MSUP	MSUP	MSUP	MSDP
Sample No.	36211_UG	36213_UG	36225_UG	62169_DH	62170_DH	62171_DH	62172_DH	62173_DH	62174_DH	62200_DH		
Depth below sea level [m]	-70	-70	-70	-362	-361	-360	-301	-300	-352	-717		
Description	contact clast-bearing rhy flow - massive Ccp-Py sulfides	massive Py-Ccp sulfides with Po and coarse Py	massive Py-Ccp sulfides	massive Py-Ccp-Po sulfide	massive Py-Ccp sulfide with Sp bands	rhyolitic lap tuff with Ccp-Py stringer	massive Ccp-Py sulfide with Po schlieren	massive Ccp-Py-Po sulfide	massive Ccp-Py sulfide with Po-Mag	massive Py-Ccp sulfide		
S [wt. %]	49.1	47.4	52.3	43.6	50.6	32.0	49.5	40.5	34.1	52.9		
Fe	41.6	44.3	45.6	42.4	45.1	50.0	45.8	39.6	35.8	46.6		
Cu	1.51	6.95	0.957	13.0	3.93	16.9	4.28	18.4	28.9	0.296		
Zn	5.61	0.850	0.085	0.686	0.155	0.615	0.222	1.26	0.713	0.023		
V [ppm]	363	122	315	26.2	22.5	421	17.9	20.9	30.2	15.8		
Cr	71.2				29	952	15.0	6.97	7.04	9.47		
Mn	105	91.1	276	67.5	111	1,926	37.9	58.7	71.4	33.7		
Co	150	110	116	218	429	221	440	209	123	9.58		
Ni	49.4	37.9	96.8	44.3	29.3	141	20.4	34.0	54.1	38.9		
As	731	691	6,696	243	262	331	277	295	98.2	698		
Se	138		297	1,078	480	173	510	289	647	50.9		
Ag	90.5	318	147	20.9	8.54	18.5	9.45	29.2	32.8	6.42		
Cd	201	37.5	6.13	38.2	9.42	41.2	12.0	52.4	39.3	3.05		
Sn	62.5	128	35.7	16.1	9.22	26.6	5.98	11.9	7.04	9.47		
Sb	33.6	16.6	1,248	69.7	22.3	20.4	6.68	27.7	33.1	6.63		
Te	33.1	4.30	7.13	45.7	28.3	8.41	11.8	23.3	45.7	3.47		
Ta		0.205		0.202	0.615	2.66	0.698	0.199	0.101	0.210		
Au	4.69	231	21.5	3.94	0.769	1.20	0.651	0.748	1.670	1.25		
Hg	105	97.5	8.234	30.6	6.033	12.2	6.430	37.2	23.0	0.198		
Tl	24.6	5.53	4.47	1.60	1.73	17.8	1.75	3.66	0.996	0.673		
Pb	19,475	2,273	1,827	391	803	138	554	253	3,632	404		
Bi	72.2	10.8	19.1	45.6	34.9	3,542	34.1	33.7	98.9	7.79		

Table A5-5. (cont.)

Orebody	MSDP	MSDP	MSDP	FWZ	FWZ	FWZ	FWZ
Sample No.	36228_DH	36235_DH	36251_DH	36256_DH	36260_DH	36280_DH	FWZ
Depth below sea level [m]	-732	-732	-783	-898	-930	-947	-1,075
Description	rhyolite with sulfide stringer	rhyolite with sulfide stringer	Ccp-Py-Po sulfide stringer in rhyolitic lapilli tuff	rhyolitic flow with sulfide stringer	Amph-rich part of rhyolitic flow with sulfide stringer and weak Bt-Mag	lapilli tuff with disseminated Ccp	
S [wt. %]	41.4	45.4	22.3	25.2	21.1	16.3	
Fe	47.1	53.0	67.9	67.8	65.3	73.3	
Cu	10.4	1.06	8.77	6.11	12.6	9.35	
Zn	0.460	0.188	0.279	0.103	0.088	0.072	
V [ppm]	535	883	888	947	785	1,026	
Cr	352	100	1,533	2,276	2,767	4,041	
Mn	1,226	630	2,636	3,125	3,447	3,637	
Co	386	348	935	523	560	484	
Ni	121	49.5	327	410	681	525	
As	894	707	265	564	20.3	27.9	
Se	513	12.4	283	303	305	297	
Ag	42.0	7.01	12.3	7.63	15.3	9.77	
Cd	35.2	8.25	16.3	6.58	6.59	6.98	
Sn	40.6	41.2	17.4	26.3	27.4	20.9	
Sb	31.1	5,890	2,323	11.8	1.647	4.886	
Te	31.1	10.0	18.6	13.2	20.9	9.07	
Ta	4.74	4.71	1.74	3.95	2.74	2.09	
Au	5.46	0.960	0.389	0.362	0.236	0.342	
Hg	16.6	0.383	0.761	1.52			
Tl	16.2	2.94	2.09	1.58	0.714	2.303	
Pb	779	435	152	51.3	664	34.2	
Bi	47.4	13.5	16.8	1.97	29.6	4.89	

**Table A5-6.** Results of EPMA (major and minor elements in wt.%) and LA-ICP-MS (trace elements in ppm) analysis for analyzed mineral phases. See electronic Appendix A5 accompanying this thesis

## CHAPTER 6

## 6-1 CONCLUSIONS

The goal of this thesis was to constrain the genesis of a metamorphosed, precious metal-bearing VMS deposit. In this study, field and detailed microscopic observations were combined with micro-analytical techniques to constrain: (1) syngenetic vs. synorogenic timing of precious metal emplacement; (2) origin of sulfur; (3) hydrothermal fluid conditions; (4) deposition mechanism resulting in the formation of semi-massive, massive and stringer sulfides; and (5) the origin of elements of the epithermal suite and precious metals.

The relative timing of precious metal emplacement was investigated using the precious metal-rich 1806 Zone. The findings from this study showed that electrum (AuAg alloy with >10wt.% Ag) is the primary Au phase in the 1806 Zone and has variable Hg contents ranging from 7.9-20.6wt.%. Electrum occurs in various textures (i.e., free grains, inclusions, myrmekitic intergrowth); however, Au incorporated within mineral structure of other sulfides (pyrite, arsenopyrite) was not detected, suggesting that “invisible Au” is not developed in the 1806 Zone. Alloys of AgHgAu are less common and occur with recrystallized pyrite either along cataclastic fractures or between grain boundaries. The mineral assemblage in the 1806 Zone accompanying Au and Ag is complex and consists of intermediate sulfidation state (i.e., tetrahedrite-tennantite, AgSb phases).

Precious metals and elements of the elements of the epithermal suite had at least in part a magmatic origin, although advanced argillic style



alteration is absent from the felsic footwall. Evidence for a magmatic origin is the close spatial relationship between precious metals and minerals bearing elements of the epithermal suite (arsenopyrite, sulfosalts), and the chemical affinity of precious metals with elements of the epithermal suite (e.g., Ag with Sb, Au and Ag with Hg). Magmatic fluids/volatiles most likely originated from a subvolcanic intrusion or magma chamber.

Textural and chemical results on the various ore minerals of the 1806 Zone strongly suggest that syngenetic precious metal emplacement took place coevally with base metal (Cu, Zn, Pb) deposition during the Cambro-Ordovician. However, Silurian-Devonian metamorphism internally remobilized Au and Ag, redistributing it between recrystallized and/or within cataclastic pyrite. Therefore, metamorphism and deformation affected the precious metal-bearing Ming deposit in the sense of post-genetic, internal zone refining but had less of an effect on the overall metal budget.

The second focus of this study was on sulfur and its origin. The sulfur isotopic composition of sulfides from the Ming deposit was investigated in Chapter 4. *In situ* SIMS analyses of pyrite, chalcopyrite, pyrrhotite, arsenopyrite, and galena from all orebodies of the Ming deposit showed little variations between the orebodies. Subtle variations illustrate that the majority of sulfur was derived from (1) Cambro-Ordovician seawater by thermochemical sulfate reduction (TSR), and (2) igneous sources. Igneous sulfur was leached from the igneous wall rock, carried by magmatic fluids or volatiles from subvolcanic magma chambers, or a combination of both. The results are in

agreement with mineralogical and chemical observations from the first study and imply that the Ming VMS system contained a magmatic fluid component, consistent with igneous sulfur isotope values of the sulfides. Subsequent Silurian-Devonian metamorphism apparently had minimal impact on the isotopic composition of sulfides at the Ming deposit. The results of the sulfur isotope study are in good agreement with other isotopic studies of metamorphosed VMS deposits that showed: (1) the involvement of both TSR and igneous sulfur (wall rock  $\pm$  magmatic sulfur) in sediment-free VMS deposits; and (2) the lack of isotopic equilibration during deposition and later metamorphism between neighboring sulfide phases.

The last paper in the thesis focused on mineralogy, geochemistry, and hydrothermal fluid conditions of the different orebodies of the Ming deposit, possible sources for precious metals and elements of the epithermal suite, and genesis of the Ming deposit. The different ore bodies in the deposit are remarkably variable in geochemistry and mineralogy and reflect a complex genesis but with similar depositional mechanisms for all orebodies. There are strong mineralogical and chemical variations between the precious metal-bearing 1806 Zone, other massive sulfide lenses that contain precious metals and elements of the epithermal suite (1807 Zone, Ming South orebodies), and the high temperature stockwork zone (LFWZ).

Variations between various orebodies reflect differences in physico-chemical fluid conditions, in particular temperature, oxidation state, sulfidation state,  $f\text{Te}_2/f\text{S}_2$ ,  $f\text{Se}_2/f\text{S}_2$ , and  $m_{\text{Bi}}/m_{\text{Sb}}$  ratios, whereas pH was fairly constant

throughout the formation of the Ming deposit. In particular, higher fluid temperatures were responsible for the formation of the LFWZ, whereas lower fluid temperatures were responsible for the formation of the other orebodies. Metals were deposited in the various orebodies predominantly due to mixing of hydrothermal fluids with ambient seawater, whereas conductive cooling played only a subordinate role and was restricted to direct contact of wall rock and hydrothermal fluid. Boiling may have played an important role in particular in the deposition of precious metals. However, metamorphism and deformation make it difficult deciphering the role boiling played at the Ming deposit.

Precious metals and elements of the epithermal suite were largely derived from magmatic fluids, likely expelled from a subvolcanic magma chamber. The results of the third study support the findings made in the first paper and illustrate the important role of magmatic fluids/volatiles in producing the complex ore mineralogy of arsenides, tellurides, sulfosalts and precious metal minerals in precious metal-bearing VMS deposits.

## **6-2 SUGGESTIONS FOR FURTHER RESEARCH**

This thesis has contributed greatly to our understanding of precious metal-bearing VMS deposits and their genesis. However, while every research project answers questions, they also raise numerous questions that remain unanswered. Future research in this area should focus on the Ming deposit itself, the adjacent VMS deposits of the Rambler VMS camp, and the younger orogenic Au deposits in close vicinity to the Ming deposit.

At the Ming deposit, a detailed stratigraphy of the deposit and its structure would help to understand the influence of metamorphism and deformation on the architecture of the deposit. Moreover, detailed stratigraphic observations and geochemistry would help to constrain the tectonic setting in which the Ming deposit was formed. So far, the tectonic setting is only loosely constrained to the extent that it was formed in a supra-subduction zone (van Staal, 2007; van Staal and Barr, 2012). However, it is not yet clear at what water depth the Ming deposit was formed. Such data would provide crucial information regarding the general tectonic environment of the Notre Dame subzone during the Cambro-Ordovician.

A detailed study of the alteration mineralogy, chemistry, and its distribution in the deposit would be useful for understanding the genesis of the deposit, and lithogeochemical vectoring during exploration. This would also enhance and test the findings of this study regarding the physico-chemical hydrothermal fluid conditions during deposit formation.

Investigations on the sulfide minerals at the Ming deposit itself were the primary focus of this study to provide genetic implications for the formation of precious metal-bearing VMS deposits. Nevertheless, further investigations focusing on different isotope systems including Pb, Cu, Fe, Se, and/or Hg are recommended to provide further insight into the origin of these metals and semi-metals and to constrain possible fractionation processes during hydrothermal activity (e.g., Zhu et al., 2000; Sharma et al., 2001; Coplen et al., 2002; Rouxel et al., 2002; Larson et al., 2003; Kosler et al., 2005; Smith et al.,

2008; Sherman et al., 2009). For instance, Pb isotopes in galena and Cu isotopes in chalcopyrite and/or cubanite can be helpful to constrain sources of Pb and Cu, respectively. The origin of Cu in hydrothermal systems from wallrock and magmatic sources has been discussed in literature (e.g., Stanton, 1978, 1982a, b; Heinrich, 2007; Zajacz et al., 2012). Selenium isotopes may also provide a critical tool for identifying a magmatic and seawater sources of Se for the sulfides at the Ming deposit. However, the  $\text{Se}/\text{S} \times 10^6$  ratio is not a very distinctive in this regard (Layton-Matthew et al., 2008) and, hence, Se isotopes would be complementary to the results of the S isotope investigations in this study due to the strong geochemical affinity between S and Se.

In this study, many parameters of the hydrothermal fluid conditions were constrained; however, salinity was not. Salinity can be a critical parameter in VMS deposits, because many metals are transported as chloride complexes in hydrothermal fluids; increasing salinity also affects the boiling curve of hydrothermal fluids (Monecke et al., 2014). In order to determine the salinity of the hydrothermal fluids that were involved in the formation of the Ming deposit and to test if boiling took place, fluid inclusions could be analyzed, although metamorphism and deformation could have altered the original fluid composition and pressure of the inclusions (Ramboz et al., 1982; Giles and Marshall, 1994).

The absolute age of sulfide mineralization at the Ming deposit is so far only indirectly constrained by limited U-Pb age determinations from zircon of the Rambler rhyolite. Using other isotopic systems to determine in particular

the age of metal deposition would be helpful. Geochronological systems for sulfide minerals are limited, but Re/Os isotopes in pyrite (Mathur et al., 1999) and arsenopyrite (Morelli et al., 2005, 2007) have been used to determine mineralization ages. LA-ICP-MS analyses for Re and Os in pyrite and arsenopyrite from the Ming deposit, however, showed that concentrations for both elements are below detection limits. Hence, substantial chemical concentration of Re and Os would be necessary to use Re/Os geochronology for pyrite and arsenopyrite at the Ming deposit to determine the mineralization age, and indirect age data from other hydrothermal minerals within the Rambler rhyolite might more usefully constrain the mineralization age.

The Ming deposit is part of the consolidated Rambler VMS camp, which consists in total of five VMS deposits located in the Pacquet Harbour Group. All five VMS deposits are spatially associated with one another. Four deposits are located within the same stratigraphic level, whereas the Big Rambler deposit occurs stratigraphically below the other deposits within the Betts Head Formation. All five deposits are primarily Cu-bearing with varying Au contents. A comparative study focused on the stratigraphy, structure, alteration assemblage, and sulfide mineralogy of the remaining four deposits of the Rambler VMS camp is suggested, because similarities and differences between the deposits could be established. These similarities and differences would be helpful to provide insights into the genesis of the deposits of the consolidated Rambler VMS camp. Moreover, the tectonic setting of the Pacquet Harbour Group in detail and the Baie Verte oceanic tract, in general,

could be further reconstructed from such a comparative approach. The comparison between the different deposits would also be helpful regarding the hydrothermal fluid conditions. Similarities and/or differences in ore mineral assemblage and chemistry for the different deposit could give further implications about the involvement of one or more magmatic sources.

The relative timing of precious metal emplacement at the Ming deposit was an essential objective of this study and results indicate a syngenetic origin. Moreover, Silurian-Devonian metamorphism apparently did not affect the metal budget significantly, although Silurian-Devonian orogenic Au deposits occur in close vicinity to the Ming deposit. Hence, investigations on these orogenic Au deposits would be helpful to determine differences in alteration and sulfide mineral assemblage and what fluid conditions were responsible for the formation of the orogenic Au deposits. Moreover, it should be determined why orogenic Au deposition played no role at the Ming deposit, whereas it was significant in the formation of spatially associated orogenic Au deposits such as Pine Cove or Stog'er Tight (Evans and Wells, 1998; Evans, 1999, 2004; Ramezani et al., 2000).

The suggestions above would complement the present study and would provide further implications for the formation of precious metal-bearing VMS deposits in orogenic belts globally.

## References

- Coplen TB, Hopple JA, Boehlke JK, Preiser HS, Rieder SE, Krouse HR, K.J.R. R, Ding T, Vocke Jr. RD, Revesz KM, Lamberty A, Taylor P, De Bièvre P (2002) Compilation of minimum and maximum isotope ratios of selected elements in naturally occurring terrestrial materials and reagents Water-Resources Investigations Report 01-4222. U.S. Geological Survey, Reston, VA, pp 98
- Evans DTW (1999) Epigenetic gold mineralization, Baie Verte Peninsula, Newfoundland. Current Research, Newfoundland Department of Mines and Energy, Geological Survey Report 99-1:163-182
- Evans DTW (2004) Epigenetic gold occurrences, Baie Verte Peninsula, (NTS 12H/09, 16 and 12I/01), Newfoundland In: Pereira CPG (ed). Government of Newfoundland and Labrador, Department of Natural Resources, Geological Survey, St. John's, NL
- Evans DTW, Wells C (1998) Epigenetic gold mineralization, Baie Verte Peninsula, Newfoundland. Current Research Newfoundland Department of Mines and Energy, Geological Survey Report 98-1:39-51
- Giles AD, Marshall, B (1994) Fluid inclusion studies on a multiply deformed, metamorphosed volcanic-associated massive sulfide deposit, Joma Mine, Norway. *Economic Geology* 89:803-819. doi: 10.2113/gsecongeo.89.4.803
- Heinrich CA (2007) Fluid-fluid interactions in magmatic-hydrothermal ore formation. In: Liebscher A, Heinrich, C.A. (ed) *Fluid-fluid interactions*, vol 65. *Reviews in Mineralogy and Geochemistry*. pp 363-387
- Larson PB, Maher K, Ramos FC, Chang Z, Gaspar M, Meinert LD (2003) Copper isotope ratios in magmatic and hydrothermal ore-forming environments. *Chemical Geology* 201:337-350 doi:10.1016/j.chemgeo.2003.08.006
- Layton-Matthews D, Peter JM, Scott SD, Leybourne MI (2008) Distribution, mineralogy, and geochemistry of selenium in felsic volcanic-hosted massive sulfide deposits of the Finlayson Lake District, Yukon Territory, Canada. *Economic Geology* 103:61-88. doi: 10.2113/gsecongeo.103.1.61
- Mathur R, Ruiz J, Tornos F (1999) Age and sources of the ore at Tharsis and Rio Tinto, Iberian Pyrite belt, from Re-Os isotopes. *Mineralium Deposita* 34:790-793



- Monecke T, Petersen S, Hannington MD (2014) Constraints on water depth of massive sulfide formation: Evidence from modern seafloor hydrothermal systems in arc-related settings. *Economic Geology* 109:2079-2101
- Morelli R, Creaser RA, Seltnann R, Stuart FM, Selby D, Graupner T (2007) Age and source constraints for the giant Muruntau gold deposit, Uzbekistan, from coupled Re-Os-He isotopes in arsenopyrite. *Geology* 35:795-798 doi:10.1130/G23521A.1
- Morelli RM, Creaser RA, Selby D, Kontak DJ, Horne RJ (2005) Rhenium-osmium geochronology of arsenopyrite in Meguma Group gold deposits, Meguma Terrane, Nova Scotia, Canada: Evidence for multiple gold-mineralizing events. *Economic Geology* 100:1229-1442 doi:10.2113/gsecongeo.100.6.1229
- Ramboz C, Pichavant M, Weisbrod A (1982) Fluid immiscibility in natural processes: Use and misuse of fluid inclusion data. II. Interpretation of fluid inclusion data in terms of immiscibility. *Chemical Geology* 37:29-48
- Ramezani J, Dunning GR, Wilson MR (2000) Geologic setting, geochemistry of alteration, and U-Pb age of hydrothermal zircon from the Silurian Stog'er Tight gold prospect, Newfoundland Appalachians, Canada. *Exploration and Mining Geology* 9:171-188
- Rouxel O, Ludden J, Carignan J, Marin L, Fouquet Y (2002) Natural variations of Se isotopic composition determined by hydride generation multiple collector inductively coupled plasma mass spectrometry. *Geochimica et Cosmochimica Acta* 66:3191-3199 doi:Pii S0016-7037(02)00918-3 doi:10.1016/S0016-7037(02)00918-3
- Sharma M, Polizzotto M, Anbar AD (2001) Iron isotopes in hot springs along the Juan de Fuca Ridge. *Earth and Planetary Science Letters* 194:39-51
- Sherman LS, Blum JD, Nordstrom DK, McCleskey RB, Barkey T, Vetriani C (2009) Mercury isotopic composition of hydrothermal systems in the Yellowstone Plateau volcanic field and Guaymas Basin sea-floor rift. *Earth and Planetary Science Letters* 279:86-96
- Smith CN, Kesler SE, Blum JD, Rytuba JJ (2008) Isotope geochemistry of mercury in source rocks, mineral deposits and spring deposits of the California Coast Ranges, USA. *Earth and Planetary Science Letters* 269:399-407 doi:10.1016/J.Epsl.2008.02.029
- Stanton RL (1978) Mineralization in island arcs with particular reference to the South-west Pacific region. *Proceedings - Australasian Institute of Mining and Metallurgy* 268:9-19

- Stanton RL (1982a) Metamorphism of a stratiform sulfide orebody at Mount Misery, Einasleigh, Queensland, Australia: I. Observations. Transactions - Institution of Mining and Metallurgy Section B: Applied Earth Science 91:47-71
- Stanton RL (1982b) Metamorphism of a stratiform sulfide orebody at Mount Misery, Einasleigh, Queensland, Australia: II. Implications. Transactions - Institution of Mining and Metallurgy Section B: Applied Earth Science 91:72-80
- Zajacz Z, Candela PA, Piccoli PM, Wälle M, Sanchez-Valle C (2012) Gold and copper in volatile saturated mafic to intermediate magmas: Solubilities, partitioning, and implications for ore deposit formation. *Geochimica et Cosmochimica Acta* 91:140-159
- van Staal CR (2007) Pre-Carboniferous tectonic evolution and metallogeny of the Canadian Appalachians In: Goodfellow WD (ed) Mineral deposits of Canada: A synthesis of major deposit-types, district metallogeny, the evolution of geological provinces, and exploration methods. Geological Association of Canada, Mineral Deposits Division, pp 793-818
- van Staal CR, Barr SM (2012) Lithospheric architecture and tectonic evolution of the Canadian Appalachians and associated Atlantic margin In: Percival JA, Cook FA, Clowes RM (eds) Tectonic Styles in Canada: The LITHOPROBE perspective. Geological Association of Canada, Special Paper 49, St. John's, NL, pp 41-96
- Zhu XK, O'Nions RK, Guo Y, Belshaw NS, Rickard D (2000) Determination of natural Cu-isotope variation by plasma-source mass spectrometry: Implications for use as geochemical tracers. *Chemical Geology* 163:139-149 doi:10.1016/S0009-2541(99)00076-5

## **ELECTRONIC APPENDIX**

<b>Table A3-3</b>	Electron microprobe data on sulfides, sulfosalts, precious metals and oxides
<b>Table A5-6</b>	Results of EPMA (major and minor elements in wt.%) and LA-ICP-MS (trace elements in ppm) analysis for analyzed mineral phases
<b>Electronic Appendix eA1</b>	Detailed coordinates of logged drill hole sections from the Ming deposit
<b>Electronic Appendix eA2</b>	Stratigraphic sections of logged drill holes from the Ming deposit
<b>Electronic Appendix eA3</b>	Detailed mineralogy of sulfide samples from the Ming deposit based on RL and partly SEM observations
<b>Electronic Appendix eA4</b>	Compilation of methods applied to sulfide samples from all orebodies of the Ming deposit
<b>Electronic Appendix eA5</b>	Detailed results of EPMA (major and minor elements in wt.%) and LA-ICP-MS (trace elements in ppm) analysis for analyzed mineral phases of sulfides from the Ming deposit.

**Table A3-3.** Electron microprobe data on sulfides, sulfosalts, precious metals and oxides for the 1806 Zone presented in chapter 2

nd – not detected

*Trace data in Italics are in wt. % and not in ppm***Pyrite (FeS<sub>2</sub>)**

Zone		stringer up plunge				down plunge				semi-mass	
Mineralized Zone Plunge	Section	22		21		RMUG08-146 29918		RMUG08-121 29902		RMUG 299	
Drill core#	Sample No.	RMUG08-138 29781		P20 Py		P2 Py		P5 Py		P5a Py I	
SEM image#	Mineral	P12a Py	P19a-1 Py	P14 Py		P9 Py		P14 Py		P2 Py	
area	Measuring date	Apr-11	Apr-11	Apr-11	Jan-12	Jan-12	Jan-12	Jan-12	Jan-12	Jan-12	Jan-12
S [wt%]		53.51	53.48	53.68	53.31	53.26	53.92	53.82	53.24	53.92	53.56
Fe		46.41	46.64	46.57	46.02	45.68	45.98	45.93	45.66	45.98	45.42
Cu [ppm]		nd	nd	nd	525	2,314	nd	525	nd	nd	nd
Zn		2,086	nd	nd	nd	1,157	nd	nd	nd	nd	nd
Pb		nd	nd	nd	nd	nd	nd	1,618	nd	nd	nd
As		1,411	nd	nd	1,678	3,099	1,557	nd	nd	1,065	nd
Au		nd	nd	nd	nd	nd	nd	nd	nd	nd	nd
Ag		nd	nd	nd	nd	nd	nd	nd	nd	nd	nd
Sb		nd	nd	nd	nd	nd	nd	nd	nd	nd	nd
Sn		nd	nd	nd	nd	nd	nd	nd	nd	nd	nd
Te		nd	nd	nd	nd	nd	nd	nd	nd	nd	nd
Bi		nd	nd	nd	nd	nd	nd	nd	nd	nd	nd
Hg		nd	nd	nd	nd	nd	nd	nd	nd	nd	nd
Mo		nd	nd	nd	389	1,522	nd	96	nd	nd	nd
Mn		nd	nd	nd	nd	nd	nd	nd	nd	nd	nd
Co		nd	nd	nd	nd	nd	nd	nd	nd	nd	nd
Ni		369	nd	nd	185	151	nd	nd	nd	nd	179
<b>Total</b>		<b>100.31</b>	<b>100.13</b>	<b>100.25</b>	<b>99.61</b>	<b>99.77</b>	<b>100.06</b>	<b>99.98</b>	<b>98.90</b>	<b>100.06</b>	<b>99.13</b>

**Mineral Formula Calculation based on 2 S atoms (AB<sub>2</sub>: FeS<sub>2</sub>)**

A – Fe (Total)	1.00	1.00	1.00	1.00	0.99	0.99	0.98	0.98	0.99	0.97
B - S (Total)	2	2	2	2	2	2	2	2	2	2
<b>Total</b>	<b>3.00</b>	<b>3.00</b>	<b>3.00</b>	<b>3.00</b>	<b>2.99</b>	<b>2.99</b>	<b>2.98</b>	<b>2.98</b>	<b>2.99</b>	<b>2.98</b>

**Chalcopyrite (CuFeS<sub>2</sub>)**

Zone	Mineralized Zone Plunge	stringer up plunge

ive sulfide		1806											
08-159 334	P7 Py	up plunge				21				down plunge			
		22				RMUG08-124				2			
		RMUG08-141				29913				RMUG06-145			
		P12	P13	P9		P17-2	P8	P2b	P8	P10	P11	P15b	
		Py	Py	Py		Py	Py	Py	Py	Py	Py	Py	
Jan-12	Jan-12	Jan-12	Jan-12	Jan-12	Jan-12	Jan-12	Apr-11	Jan-12	Jan-12	Jan-12	Jan-12	Jan-12	Jan-12
53.74	53.89	53.12	53.12	53.89	52.94	53.47	53.47	53.74	53.43	53.19	53.51	53.73	
45.75	45.84	45.26	45.26	45.84	45.73	46.62	46.62	45.37	45.19	45.22	45.99	45.44	
nd	nd	550	550	nd	751	nd	nd	nd	511	nd	nd	nd	
3,786	516	nd	nd	nd	nd	nd	nd	nd	nd	nd	nd	nd	
nd	nd	2,803	2,803	nd	nd	nd	nd	nd	nd	nd	nd	nd	
1,141	2,008	1,740	1,740	2,008	1,536	nd	nd	9,484	nd	nd	3,830	5,770	
nd	nd	nd	nd	nd	nd	nd	nd	nd	nd	nd	nd	nd	
nd	nd	714	714	nd	nd	nd	nd	nd	nd	nd	nd	nd	
nd	nd	nd	nd	nd	nd	nd	nd	nd	nd	nd	nd	nd	
nd	nd	nd	nd	nd	nd	nd	nd	nd	nd	nd	nd	nd	
nd	nd	nd	nd	nd	nd	nd	nd	nd	nd	nd	nd	nd	
nd	nd	1,327	1,327	nd	1,154	nd	nd	nd	nd	nd	nd	nd	
nd	nd	nd	nd	nd	nd	nd	nd	nd	nd	nd	nd	nd	
nd	nd	nd	nd	nd	nd	nd	nd	nd	162	nd	nd	nd	
nd	143	138	138	143	142	nd	nd	157	173	208	nd	234	
99.98	100.00	99.10	99.10	100.00	99.49	98.77	100.09	100.07	98.70	98.43	99.88	99.78	
		down plunge				semi-massive sulfide							
0.98	0.98	0.98	0.98	0.98	0.98	0.99	1.00	0.97	0.97	0.98	0.99	0.97	
2	2	2	2	2	2	2	2	2	2	2	2	2	
2.98	2.98	2.98	2.98	2.98	2.98	2.99	3.00	2.98	2.97	2.98	2.99	2.98	

[illegible]

silicified horizon/rhyolite (contact to massive sulfide)									
down plunge					up plunge				
RMUG08-146 29920					RMUG08-140 29783				
P1 Py	P5 Py	P6 Py	P8 Py	P10d Py	P14 Py	P7 Py	P8 Py	P13 Py	P15 Py
Jan-12	Jan-12	Jan-12	Jan-12	Jan-12	Jan-12	Apr-11	Jan-12	Jan-12	Jan-12
53.63	53.74	53.86	53.55	53.50	53.44	53.90	53.49	53.81	53.57
45.93	45.70	46.09	45.85	45.58	45.33	46.55	45.86	45.70	45.87
nd	nd	nd	nd	1,605	nd	nd	nd	nd	1,453
nd	nd	nd	nd	1,013	nd	nd	nd	nd	nd
nd	nd	nd	nd	nd	nd	nd	nd	nd	nd
nd	nd	2,224	1,191	1,466	nd	8,240	nd	1,141	nd
nd	nd	nd	nd	nd	nd	nd	nd	nd	nd
nd	nd	nd	nd	nd	nd	nd	nd	nd	nd
nd	nd	nd	nd	nd	nd	nd	nd	nd	nd
nd	nd	nd	nd	nd	nd	nd	nd	nd	nd
nd	nd	nd	nd	nd	nd	nd	nd	nd	nd
nd	nd	nd	nd	nd	nd	nd	nd	nd	nd
nd	nd	nd	2,685	nd	nd	nd	nd	nd	nd
nd	nd	nd	nd	nd	nd	nd	1,431	1,321	nd
nd	nd	nd	nd	nd	nd	nd	nd	nd	nd
nd	nd	nd	nd	nd	nd	nd	nd	nd	nd
nd	nd	150	nd	nd	nd	nd	339	218	339
99.56	99.44	100.19	99.79	99.49	98.77	101.27	99.52	99.78	99.61
0.98	0.98	0.98	0.98	0.98	0.97	0.99	0.98	0.98	0.98
2	2	2	2	2	2	2	2	2	2
2.98	2.98	2.99	2.99	2.98	2.97	3.01	2.98	2.98	2.98
massive sulfide					up plunge				
					silicified h				

silicified horizon/silicified rhyolite up plunge	orizon/rhyolite (contact to massive sulfide) down plunge
---	---



Section Drill core# Sample No. SEM image# Mineral area	22 RMUG08-138 29781				21 RMUG08-121 29902			
	P12a Ccp	P18-1 Ccp	P19a-1 Ccp I	P20 Ccp	P1c Ccp	P5 Ccp	P14a Ccp I	P2 Ccp
Measuring date	Apr-11	Apr-11	Apr-11	Apr-11	Apr-11	Apr-11	Apr-11	Jan-12
S [wt%]	34.59	34.87	35.16	35.07	35.35	34.83	34.92	36.13
Fe	30.11	30.11	30.35	30.37	30.49	30.38	30.48	29.67
Cu	34.53	34.49	34.80	34.72	34.93	34.72	34.94	35.46
Zn [ppm]	nd	nd	nd	1,053	nd	nd	nd	nd
Pb	nd	nd	nd	nd	nd	nd	nd	nd
As	1,436	nd	nd	nd	1,867	nd	nd	nd
Au	nd	nd	nd	nd	nd	nd	nd	nd
Ag	nd	nd	nd	nd	nd	nd	nd	nd
Sb	nd	nd	nd	nd	nd	nd	nd	1,755
Sn	2,089	nd	1,907	1,912	nd	nd	nd	nd
Te	nd	nd	nd	nd	nd	1,212	nd	nd
Bi	nd	nd	nd	nd	nd	nd	nd	nd
Hg	nd	nd	nd	nd	nd	nd	nd	nd
Mo	nd	1,628	2,186	nd	nd	2,099	nd	nd
Mn	nd	nd	nd	nd	nd	nd	nd	nd
Co	nd	nd	nd	nd	nd	nd	nd	nd
Ni	nd	nd	nd	nd	nd	nd	nd	nd
Total	99.57	99.64	100.72	100.10	100.96	100.26	100.33	101.44

#### Mineral Formula Calculation based on 2 S atoms (ADX<sub>2</sub>: CuFeS<sub>2</sub>)

A1 – Cu	1.01	1.00	1.00	1.00	1.00	1.01	1.01	0.99
A2 – Ag								
A-Total	1.01	1.00	1.00	1.00	1.00	1.01	1.01	0.99
D1 – Fe	1.00	0.99	0.99	0.99	0.99	1.00	1.00	0.94
D2 – Zn								
D-Total	1.00	0.99	0.99	0.99	0.99	1.00	1.00	0.94
Z - S (Total)	2	2	2	2	2	2	2	2
Total	4.01	3.99	3.99	3.99	3.99	4.01	4.00	3.93

#### Sphalerite (ZnS)

Zone		22 RMUG08-138 29781		21 RMUG08-121 29902		21 RMUG08-146 29918		21 RMUG08-159 29934	
Mineralized Zone		P12a	P19a-1	P20	P1c	down plunge	P7	P5a	P7
Plunge									
Section									
Drill core#									
Sample No.									
SEM image#									

7

8

22				21			
RMUG08-142 29778		RMUG08-120 36509		RMUG08-123 36512			
P3a Ccp	P11 Ccp	P16a-3 Ccp	P11 Ccp	P17 Ccp	P3 Ccp	P5b Ccp	P5 Ccp
Apr-11	Apr-11	Apr-11	Jan-12	Jan-12	Apr-11	Jan-12	Jan-12
35.09	34.85	35.01	35.19	34.96	34.98	34.91	35.32
30.25	30.14	30.50	30.01	30.05	30.49	30.36	30.44
34.43	34.66	34.69	34.19	34.49	34.50	34.40	34.35
nd	1,011	nd	5,367	nd	nd	nd	nd
nd	nd	nd	nd	nd	nd	nd	nd
nd	nd	nd	nd	nd	nd	nd	nd
nd	nd	nd	nd	nd	nd	nd	nd
nd	nd	1,756	nd	927	nd	1,286	nd
2,063	nd	960	1,126	5,388	2,326	1,160	2,221
nd	nd	nd	nd	nd	nd	nd	nd
nd	nd	nd	740	nd	nd	nd	nd
nd	nd	nd	nd	nd	nd	nd	nd
nd	nd	nd	nd	nd	nd	nd	nd
nd	nd	nd	nd	nd	nd	nd	nd
nd	nd	nd	nd	nd	nd	nd	nd
nd	nd	nd	nd	nd	nd	nd	nd
99.80	99.98	100.47	100.12	100.14	100.20	99.94	100.13
							100.12
0.99	0.99	1.00	0.98	1.00	1.00	0.99	0.99
0.99	0.99	1.00	0.07	1.00	1.00	0.99	0.99
0.98	0.99	1.00	1.05	0.99	1.00	1.00	0.97
0.98	0.99	1.00	0.96	0.99	1.00	1.00	0.97
2	2	2	2	2	2	2	2
3.97	3.98	4.00	4.01	3.98	4.00	3.99	3.96
							3.98

2 RMUG08-146 29920				22 RMUG08-140 29783						
P6 Ccp	P8 Ccp	P10d Ccp	P14 Ccp	P1 Ccp core	Ccp SW rim	P5 Ccp	P6 Ccp	P7 Ccp	P6a Ccp	P7 Ccp
Jan-12	Jan-12	Jan-12	Jan-12	Apr-11	Apr-11	Apr-11	Apr-11	Apr-11	Jan-12	Jan-12
35.11	35.16	34.99	35.55	34.95	34.98	35.00	34.97	35.17	34.90	34.86
30.50	29.98	29.69	29.80	30.43	30.31	30.45	30.57	30.31	29.93	30.39
33.86	34.45	34.42	34.36	34.61	34.13	34.53	34.45	34.96	34.08	34.20
nd	nd	5,638	nd	nd	nd	nd	nd	682	nd	nd
nd	nd	nd	nd	nd	nd	nd	nd	nd	nd	nd
nd	nd	nd	nd	nd	nd	nd	nd	nd	nd	2,392
nd	nd	nd	nd	3,433	4,394	nd	nd	nd	nd	nd
1,386	nd	nd	nd	nd	nd	nd	nd	nd	nd	nd
nd	nd	nd	nd	nd	nd	nd	nd	nd	nd	nd
nd	nd	nd	nd	nd	nd	nd	nd	nd	nd	nd
nd	nd	nd	nd	nd	nd	nd	nd	nd	nd	nd
nd	nd	nd	nd	nd	nd	nd	nd	1,410	nd	nd
nd	nd	nd	nd	nd	nd	nd	nd	nd	nd	nd
nd	nd	nd	nd	nd	nd	nd	nd	nd	nd	nd
nd	nd	nd	nd	nd	nd	nd	nd	nd	nd	nd
99.61	99.59	99.67	99.71	100.27	99.98	99.98	100.00	100.65	98.91	99.69
0.97	0.99	0.99	0.98	1.00	0.98	1.00	0.99	1.00	0.99	0.99
0.97	0.99	0.99	0.98	1.00	0.98	1.00	0.99	1.00	0.99	0.99
1.00	0.98	0.97	0.96	1.00	1.00	1.00	1.00	0.99	0.99	1.00
1.00	0.98	0.97	0.96	1.00	1.00	1.00	1.00	0.99	0.99	1.00
2	2	2	2	2	2	2	2	2	2	2
3.97	3.97	3.97	3.94	4.00	3.98	4.00	4.00	3.99	3.97	3.99

21 RMUG08-150 29914					
P8 Ccp		P10 Ccp	P13 Ccp	P15 Ccp	
Jan-12	Jan-12	Jan-12	Jan-12	Jan-12	
35.21	34.74	35.16	35.09	35.09	
30.50	30.51	30.72	30.35	30.35	
34.21	34.43	34.42	34.29	34.29	
nd	nd	nd	775	775	
nd	nd	nd	nd	nd	
nd	nd	md	nd	nd	
nd	nd	nd	nd	nd	
nd	1,132	nd	881	881	
nd	nd	nd	nd	nd	
879	nd	nd	nd	nd	
nd	nd	nd	nd	nd	
nd	nd	nd	nd	nd	
nd	nd	nd	nd	nd	
nd	nd	nd	nd	nd	
nd	nd	nd	nd	nd	
nd	nd	nd	nd	nd	
100.00	99.80	100.30	99.90	99.90	
0.98	1.00	0.99	0.99	0.99	
0.98	1.00	0.99	0.99	0.99	
1.00	1.01	1.00	0.99	0.99	
1.00	1.01	1.00	0.99	0.99	
2	2	2	2	2	
3.98	4.01	3.99	3.98	3.98	

Mineral Formula Calculation based on 1 S atom (AX: ZnS)	
A1 – Zn	0.94
A2– Fe	0.05
A3 – As	
A-Total	0.99
X – S (Total)	1
	1

## Galena (PbS)

Zone									
Mineralized Zone			Mineralized Zone			Zone			
Plunge			Plunge			Plunge			
Section			Section			Section			
Drill core#			Drill core#			Drill core#			
Sample No.			Sample No.			Sample No.			
Mineral			Mineral			Mineral			
area			area			area			
P12a			P12a			P12a			
Gn			Gn			Gn			
P19a-1			P19a-1			P19a-1			
Gn			Gn			Gn			
RMUG08-138			RMUG08-138			RMUG08-138			
29781			29781			29781			
22			22			22			
stringer			stringer			stringer			
up plunge			up plunge			up plunge			
21			21			21			
RMUG08-121			RMUG08-121			RMUG08-121			
29902			29902			29902			
P5			P5			P5			
Gn			Gn			Gn			
P14a			P14a			P14a			
Gn I			Gn I			Gn I			
Gn II			Gn II			Gn II			
RMUG08-146			RMUG08-146			RMUG08-146			
29918			29918			29918			
P7			P7			P7			
Gn			Gn			Gn			
P5a			P5a			P5a			
Gn			Gn			Gn			
down plunge			down plunge			down plunge			
2			2			2			
RMUG08-159			RMUG08-159			RMUG08-159			
29934			29934			29934			
P2			P2			P2			
Gn			Gn			Gn			
Jan-12			Jan-12			Jan-12			
12.64			12.64			12.64			
85.59			85.59			85.59			
3,593			3,593			3,593			
5,200			5,200			5,200			
nd			nd			nd			
452			452			452			
nd			nd			nd			

Sp	Sp		Sp		Sp		Sp		Sp		Sp
	Jan-12	Jan-12	Apr-11	Apr-11	Jan-12	Jan-12	Apr-11	Apr-11	Jan-12	Jan-12	
33.18	33.29	33.52	33.37	33.31	33.03	32.98	33.36	33.05	32.88	33.08	
9.47	8.69	9.97	10.16	10.04	8.56	1.80	2.12	1.95	1.29	9.00	
54.75	56.01	56.18	56.11	56.08	57.16	64.32	64.38	64.81	65.28	57.11	
1,573	6,285	1,037	913	1,921	1,656	4,877	nd	489	1,715	nd	
nd	nd	nd	nd	nd	nd	nd	nd	nd	nd	nd	
nd	nd	1,491	nd	nd	nd	nd	nd	1,010	nd	nd	
nd	nd	nd	nd	nd	nd	nd	nd	nd	nd	nd	
nd	nd	nd	nd	nd	nd	nd	nd	nd	nd	nd	
nd	nd	nd	nd	nd	nd	nd	nd	nd	nd	nd	
nd	nd	nd	nd	nd	nd	nd	nd	nd	nd	nd	
nd	nd	nd	nd	nd	nd	nd	nd	nd	nd	nd	
5,683	2,858	1,880	2,630	nd	nd	nd	nd	nd	nd	3,257	
nd	nd	nd	nd	nd	nd	nd	nd	nd	nd	nd	
3,279	3,234	1,082	1,064	941	534	1,177	984	747	715	1,193	
nd	nd	nd	nd	nd	nd	nd	nd	nd	nd	nd	
nd	nd	nd	nd	nd	nd	nd	nd	nd	nd	nd	
98.46	99.22	100.21	100.10	99.71	98.97	99.70	99.96	100.04	99.69	99.64	

	0.81	0.83	0.82	0.83	0.85	0.96	0.95	0.96	0.97	0.85
	0.16	0.15	0.17	0.17	0.15	0.03	0.04	0.03	0.02	0.16
0.97	0.97	0.97	0.99	1.00	1.00	0.99	0.98	1.00	1.00	1.00
1	1	1	1	1	1	1	1	1	1	1
1.97	1.97	1.99	2.00	2.00	2.00	1.99	1.98	2.00	2.00	2.00

[illegible]



Sp I Apr-11	Sp II Apr-11	Sp Apr-11	Sp Apr-11	Sp Jan-12	Sp Apr-11	Sp Apr-11	Sp Jan-12	Sp Apr-11	Sp Jan-12
33.02	33.25	32.93	32.69	32.33	32.91	32.79	32.91	33.09	32.94
9.37	8.41	9.19	6.12	2.06	1.42	9.71	1.42	1.94	6.36
55.76	57.36	56.59	60.20	63.70	64.42	55.79	64.42	64.86	58.12
1,802	nd	nd	nd	7,221	5,337	nd	5,337	937	2,041
nd	nd	nd	nd	nd	nd	nd	nd	nd	nd
nd	nd	nd	nd	nd	nd	nd	nd	nd	1.40
nd	nd	nd	nd	nd	nd	nd	nd	nd	nd
nd	nd	nd	nd	nd	nd	nd	nd	nd	nd
nd	nd	nd	nd	nd	nd	nd	nd	nd	nd
nd	nd	nd	nd	nd	nd	nd	nd	nd	nd
nd	nd	nd	nd	nd	nd	nd	nd	nd	nd
nd	nd	nd	nd	nd	nd	nd	nd	nd	nd
3,234	3,145	3,145	2,799	nd	nd	nd	nd	nd	nd
nd	nd	nd	nd	nd	nd	nd	nd	nd	nd
1,737	1,062	1,162	1,220	3,226	3,020	795	3,020	1,559	320
nd	nd	nd	nd	nd	nd	nd	nd	nd	nd
nd	nd	nd	nd	nd	nd	nd	nd	nd	nd
<b>98.83</b>	<b>99.45</b>	<b>99.14</b>	<b>99.41</b>	<b>99.14</b>	<b>99.74</b>	<b>98.38</b>	<b>99.74</b>	<b>100.15</b>	<b>99.06</b>
0.83	0.85	0.84	0.90	0.97	0.96	0.83	0.96	0.96	0.87
0.16	0.15	0.16	0.11	0.04	0.02	0.17	0.02	0.03	0.11
0.99	0.99	1.00	1.01	1.00	0.98	1.00	0.98	0.99	0.99
1	1	1	1	1	1	1	1	1	1
<b>1.99</b>	<b>1.99</b>	<b>2.00</b>	<b>2.01</b>	<b>2.00</b>	<b>1.98</b>	<b>2.00</b>	<b>1.98</b>	<b>1.99</b>	<b>1.99</b>

massive sulfide									
up plunge					21				
P16a-3 Gn	P6b Gn I	RMUG08-120 36509 Gn II	P17 Gn I	Gn II	P3 Gn	P5b Gn I	Gn II	P12 Gn	
Apr-11	Jan-12	Jan-12	Jan-12	Jan-12	Apr-11	Apr-11	Apr-11	Apr-11	Apr-11
13.24	13.31	13.26	13.20	13.36	13.33	13.26	13.43	13.22	
86.28	87.26	86.85	86.23	86.39	85.27	85.79	86.68	85.91	
1,751	nd	nd	nd	nd	502	nd	nd	nd	
1,039	nd	nd	1,278	3,920	nd	nd	nd	nd	
nd	1,347	1,383	679	nd	nd	nd	nd	nd	

[illegible]

## Mineral Formula Calculation based on 1 S atom (BX: PbS)

	2.00	2.01	2.01	2.05	2.03	2.02	2.00	2.09	1.95	2.08
B1 – Pb	1.00	1.01	1.01	1.00	1.02	1.01	1.00	1.08	0.95	1.05
B2 – Cu	1.00	1.01	1.01	1.00	1.02	1.01	1.00	1.08	0.95	1.05
<i>B-Total</i>	1	1	1	1	1	1	1	1	1	1
X – S (Total)	2.00	2.01	2.01	2.05	2.03	2.02	2.00	2.09	1.95	2.08

Pyrrhotite ( $\text{Fe}_{(1-x)}\text{S}$  with  $x = 0 - 0.17$ )

Zone							
Mineralized Zone		1806 Zone					
Plunge		semi-massive sulfide			silicified horizon/rhyolite up plunge		
Section	down plunge			up plunge			
Drill core#	2 RMUG08-146 29918	P2 Po	P7 Po	22 RMUG08-141 29787	21 RMUG-124 29913		
Sample No.							
SEM image#							
Mineral	Po	Po	Po	P15 Po	P6 Po	P1 Po	P5 Po
area							
Measuring date	Jan-12	Jan-12	Jan-12	Jan-12	Apr-11	Apr-11	Apr-11
S [wt%]	40.14	39.68	40.02	39.31	39.01	39.36	39.61
Fe	60.02	59.76	60.23	60.54	59.68	60.29	60.22
Cu [ppm]	nd	1,320	nd	449	nd	777	856
Zn	nd	nd	nd	nd	nd	nd	nd
Pb	nd	1,685	nd	nd	nd	nd	nd
As	nd	nd	nd	nd	nd	nd	nd
Au	nd	nd	nd	nd	nd	nd	nd
Ag	nd	nd	nd	nd	nd	nd	nd
Sb	nd	nd	nd	nd	nd	nd	nd
Sn	nd	nd	nd	nd	nd	nd	nd
Te	nd	nd	nd	nd	1,447	1,353	1,079
Bi	nd	nd	nd	nd	nd	nd	nd
Hg	nd	nd	nd	nd	nd	nd	nd

[illegible]

6	Po II		Apr-11		P7 Po
	Apr-11		Apr-11		
	39.61		39.07		
	60.24		60.20		
			nd		
			663		619
			nd		nd
			nd		2,176
			nd		nd
			nd		nd
			nd		nd
			1,130		nd
			nd		nd
			nd		nd
			nd		nd

17

18

[illegible]

1806 Zone											
down plunge				massive sulfide				up plunge			
2 RMUG08-145 29907				22 RMUG08-142 29778				P6b Asp II core			
P11				P10b				Asp I			
Asp left				Asp NE rim				rim			
Jan-12				Apr-11				Jan-12			
20.52	19.50	21.68	21.10	21.79	21.17	20.83	20.75	20.33	21.24	21.13	21.13
34.17	34.01	34.66	34.79	34.94	34.74	34.52	33.89	33.92	33.87	33.73	33.73
45.12	46.68	43.82	44.02	43.38	43.30	42.60	44.39	45.12	43.49	43.64	43.64
531	nd	nd	nd	nd	nd	4,906	nd	nd	nd	nd	nd
nd	nd	nd	nd	nd	nd	661	nd	nd	nd	nd	nd
nd	nd	nd	nd	nd	nd	nd	nd	nd	nd	nd	nd
nd	nd	nd	nd	nd	nd	nd	nd	nd	nd	nd	nd
nd	nd	nd	nd	nd	nd	nd	nd	nd	nd	nd	nd
nd	2,441	nd	nd	nd	nd	nd	nd	nd	nd	nd	nd
nd	nd	nd	nd	nd	nd	nd	nd	nd	nd	nd	nd
nd	nd	nd	nd	nd	nd	nd	nd	nd	nd	nd	nd
1,296	nd	nd	nd	nd	nd	nd	nd	nd	nd	nd	nd
nd	nd	nd	nd	nd	nd	nd	nd	716	nd	nd	nd
nd	nd	nd	3,532	4,711	4,603	nd	nd	nd	nd	nd	nd
nd	nd	nd	nd	nd	nd	nd	nd	nd	nd	nd	nd
nd	nd	nd	nd	nd	nd	nd	nd	nd	nd	nd	nd
372	nd	1,384	1,118	1,238	289	543	499	220	490	694	694
100.04	100.43	100.29	100.37	100.71	99.70	98.56	99.09	99.46	98.65	98.57	98.57

1	silicified horizon/rhyolite (contact to massive sulfide) down plunge										silicifi			
	Asp III Jan-12	P11 Asp rim-a Jan-12	core Jan-12	RMUG08-123 P5b Asp Apr-11	P6 Asp Jan-12	P8 Asp Jan-12	P14 Asp Jan-12	P7 Asp Apr-11	Asp NW rim Apr-11	Asp core Apr-11	Asp SE rim Apr-11			
	21.02	21.35	21.27	19.81	20.71	21.09	19.62	22.00	21.44	21.37	21.57			
	33.81	33.82	33.58	34.15	34.48	34.52	34.30	34.48	34.78	34.82	34.90			
	43.70	43.43	43.40	45.29	44.92	44.37	45.22	42.32	43.94	43.61	43.24			
	nd	nd	nd	nd	504	2,051	1,229	1,506	nd	nd	nd			
	nd	nd	nd	nd	nd	nd	nd	nd	nd	nd	nd			
	nd	nd	nd	nd	nd	nd	nd	nd	nd	nd	nd			
	nd	nd	nd	nd	nd	1,412	nd	nd	nd	nd	nd			
	nd	nd	nd	nd	nd	nd	nd	nd	nd	nd	nd			
	nd	nd	nd	2,377	nd	nd	nd	nd	nd	nd	nd			
	nd	nd	nd	nd	nd	nd	nd	nd	1,131	nd	nd			
	nd	nd	nd	nd	nd	nd	1,087	1,419	nd	nd	nd			
	1,248	nd	nd	nd	885	nd	nd	nd	nd	nd	nd			
	nd	nd	nd	nd	nd	nd	nd	nd	nd	nd	nd			
	nd	nd	nd	4,123	nd	nd	nd	nd	nd	nd	nd			
	34.7	nd	nd	nd	nd	nd	218	nd	nd	nd	nd			
	nd	nd	nd	nd	nd	nd	nd	nd	nd	nd	nd			
	390	494	1,189	nd	nd	797	nd	1,057	737	921	1,110			
	98.73	98.66	98.37	99.90	100.24	100.41	99.40	99.20	100.35	99.89	99.82			



ed horizon/sil rhyolite up plunge	21 RMUG08-150 29914					
	P6a		P8		P13	
	Asp	Jan-12	Asp	Jan-12	Asp rim-a	Jan-12
	20.61	21.38	21.38	21.56	21.56	20.83
	33.63	33.82	33.82	34.10	34.10	33.92
	43.71	43.85	43.85	43.51	43.51	44.04
	1,392	nd	nd	746	746	nd
	3,160	nd	nd	nd	nd	nd
	nd	nd	nd	1,654	1,654	nd
	nd	1,012	1,012	nd	nd	nd
	nd	947	947	nd	nd	nd
	nd	nd	nd	nd	553	nd
	nd	nd	nd	nd	nd	nd
	nd	nd	nd	nd	nd	nd
	nd	nd	nd	nd	nd	nd
	nd	nd	nd	nd	nd	nd
	nd	nd	nd	nd	nd	nd
	nd	193	193	nd	nd	nd
	nd	nd	nd	nd	nd	nd
	nd	2,585	2,585	175	175	179
	98.41	99.53	99.53	99.43	98.85	99.06

A1 – Fe	0.95	0.94	0.92	0.94	0.93	0.93	0.92	0.92	0.93	0.83
A2 – Zn					0.02					
A-Total	0.95	0.94	0.92	0.94	0.96	0.93	0.92	0.92	0.93	0.83
B – As	0.90	0.90	0.86	0.91	0.88	0.87	0.85	0.87	0.87	0.75
X – S (Total)	1	1	1	1	1	1	1	1	1	1
Total	2.84	2.84	2.79	2.85	2.83	2.80	2.77	2.79	2.81	2.59

0.91	0.95	0.93	0.92	0.92	0.93	0.91	0.92	0.91	0.94	0.91
0.91	0.95	0.93	0.92	0.92	0.93	0.91	0.92	0.91	0.94	0.91
0.83	0.92	0.88	0.88	0.87	0.87	0.88	0.88	0.85	0.91	0.87
1	1	1	1	1	1	1	1	1	1	1
2.74	2.87	2.80	2.80	2.79	2.81	2.79	2.80	2.77	2.85	2.78

0.96	1.00	0.92	0.95	0.92	0.94	0.95	0.94	0.96	0.92	0.92
0.96	1.00	0.92	0.95	0.92	0.94	0.95	0.94	0.96	0.92	0.92
0.94	1.02	0.87	0.89	0.85	0.88	0.88	0.92	0.95	0.88	0.88
1	1	1	1	1	1	1	1	1	1	1
2.90	3.03	2.78	2.84	2.77	2.82	2.83	2.85	2.91	2.79	2.80

0.92	0.91	0.91	0.91	0.99	0.96	0.94	1.00	0.90	0.93	0.94	0.93
0.92	0.91	0.91	0.91	0.99	0.96	0.94	1.00	0.90	0.93	0.94	0.93
0.89	0.87	0.87	0.87	0.98	0.93	0.90	0.99	0.82	0.88	0.87	0.86
1	1	1	1	1	1	1	1	1	1	1	1
<b>2.81</b>	<b>2.78</b>	<b>2.78</b>	<b>2.78</b>	<b>2.97</b>	<b>2.88</b>	<b>2.84</b>	<b>2.99</b>	<b>2.72</b>	<b>2.81</b>	<b>2.81</b>	<b>2.79</b>

0.94	0.91	0.91	0.91	0.94	0.91
0.94	0.91	0.91	0.91	0.94	0.91
0.91	0.88	0.86	0.86	0.91	0.87
1	1	1	1	1	1
2.84	2.79	2.77	2.77	2.84	2.78

nd – not detected

28

				semi-massive sulfide									
				down plunge									
				2									
				RMUG08-159									
				29934									



[illegible]

21 RMUG08-120 36509		silicified horizon/rhyolite (contact 1 down plunge 2 RMUG08-146 29920									
P17		P1									
Tet II	Ten	Ten rim-a	Ten core	Ten rim-b	Ten I	Ten-Tet I	Tet I	Ten II	Ten III core	Ten III rim-b	
Jan-12	Jan-12	Jan-12	Jan-12	Jan-12	Jan-12	Jan-12	Jan-12	Jan-12	Jan-12	Jan-12	Jan-12
24.17	28.09	27.86	28.29	28.12	27.47	26.09	24.43	27.78	27.35	27.43	
2.58	5.26	5.21	5.13	5.19	5.34	3.20	3.54	5.00	5.08	5.86	
31.69	41.80	41.40	41.75	41.57	41.89	38.53	35.89	42.05	41.87	41.13	
4.74	2.66	2.82	2.88	2.92	3.12	4.69	4.20	3.13	3.07	3.08	
2.66	18.54	18.24	18.23	18.00	17.35	7.70	0.861	17.49	17.49	17.49	
25.92	1.73	2.22	1.85	2.14	2.79	17.98	29.06	2.92	2.78	2.77	
8.83	0.869	0.963	0.885	1.01	0.307	1.10	2.72	0.374	0.290	0.422	
nd	1,829	nd	nd	nd	nd	nd	1,635	nd	2,845	nd	
nd	nd	nd	nd	nd	nd	nd	nd	nd	nd	nd	
nd	nd	nd	nd	nd	nd	nd	1,419	nd	nd	nd	
nd	nd	nd	nd	nd	nd	nd	nd	nd	nd	nd	
nd	nd	nd	nd	nd	666	4,011	1,714	729	2,538	1,014	
nd	nd	nd	nd	nd	nd	nd	nd	nd	nd	nd	
nd	nd	nd	nd	nd	nd	nd	nd	nd	nd	nd	
nd	nd	315	nd	nd	501	458	nd	527	463	528	
nd	nd	nd	nd	nd	nd	nd	nd	nd	nd	nd	
nd	nd	nd	nd	nd	nd	nd	nd	nd	nd	nd	
100.60	99.13	98.74	99.00	98.94	98.37	99.74	101.19	98.87	98.51	98.35	
0.86	0.05	0.07	0.06	0.07	0.09	0.59	0.95	0.09	0.09	0.09	
0.61	0.30	0.32	0.32	0.32	0.33	0.56	0.50	0.35	0.34	0.31	
8.60	9.76	9.75	9.68	9.70	10.01	9.69	9.64	9.93	10.04	9.84	
1.41	0.12	0.13	0.12	0.14	0.04	0.16	0.43	0.05	0.04	0.06	
10.02	9.88	9.88	9.80	9.84	10.05	9.85	10.07	9.98	10.08	9.89	
0.80	1.40	1.40	1.36	1.38	1.45	0.92	1.08	1.34	1.39	1.60	
1.25	0.60	0.65	0.65	0.66	0.72	1.15	1.10	0.72	0.72	0.72	
2.05	2.00	2.04	2.00	2.00	2.18	2.06	2.18	2.06	2.10	2.31	
12.06	11.89	11.92	11.81	11.88	12.22	11.92	12.25	12.05	12.19	12.21	
0.61	3.67	3.64	3.59	3.56	3.51	1.64	0.20	3.50	3.56	3.55	
3.67	0.21	0.27	0.22	0.26	0.35	2.36	4.07	0.36	0.35	0.35	

o massive sulfide)		silicified horizon/rhyolite up plunge											
		21						29914					
		P8		P10d		P14		P7		P15		P15	
		Ten-Tet I	Ten-Tet II	Ten-Tet I	Ten-Tet II	Ten-Tet	(Ag)Tet I	(Ag)Tet rim-a	(Ag)Tet core-a	(Ag)Tet core-b	(Ag)Tet rim-b	(Ag)Tet rim-b	
Jan-12	Jan-12	Jan-12	Jan-12	Jan-12	Jan-12	Jan-12	Jan-12	Jan-12	Jan-12	Jan-12	Jan-12		
25.34	25.69	25.82	26.02	26.01	20.99	22.57	22.07	23.34	23.07				
3.71	3.54	4.19	3.60	3.74	6.00	5.39	5.28	5.81	5.70				
38.00	38.51	39.00	38.62	38.92	15.54	19.16	18.22	21.99	20.08				
4.39	4.25	4.13	4.41	4.21	0.550	1.23	1.26	0.999	1.01				
6.47	7.45	8.82	8.56	8.54	0.561	1.19	0.981	5.78	2.79				
19.49	18.09	15.67	16.17	16.50	26.79	25.94	26.26	19.14	23.92				
1.58	1.52	1.07	1.10	1.39	29.27	24.15	25.00	22.00	23.83				
nd	nd	nd	nd	nd	nd	nd	nd	nd	nd				
nd	nd	nd	nd	nd	nd	nd	nd	nd	nd				
626	588	nd	nd	nd	nd	nd	nd	nd	nd				
nd	nd	nd	nd	nd	nd	nd	1,010	nd	nd				
1,801	2,711	5,649	7,427	1,393	nd	nd	nd	nd	nd				
nd	nd	nd	nd	nd	nd	nd	nd	nd	nd				
nd	nd	nd	nd	nd	nd	nd	nd	nd	nd				
232	196	231	nd	449	nd	nd	nd	nd	nd				
nd	nd	nd	nd	nd	nd	nd	nd	nd	nd				
nd	nd	nd	nd	nd	nd	nd	nd	nd	nd				
99.26	99.41	99.29	99.22	99.49	99.69	99.62	99.16	99.07	100.39				
0.65	0.60	0.52	0.54	0.54	0.97	0.93	0.94	0.67	0.84				
0.50	0.51	0.46	0.51	0.49	0.07	0.16	0.17	0.13	0.13				
9.84	9.84	9.91	9.74	9.81	4.86	5.57	5.42	6.18	5.71				
0.24	0.23	0.16	0.16	0.21	5.39	4.14	4.38	3.64	3.99				
10.08	10.06	10.07	9.90	10.02	10.25	9.71	9.79	9.82	9.70				
1.09	1.03	1.21	1.03	1.07	2.13	1.78	1.79	1.86	1.85				
1.10	1.06	1.02	1.08	1.03	0.17	0.35	0.36	0.27	0.28				
2.20	2.08	2.23	2.11	2.10	2.30	2.13	2.15	2.13	2.12				
12.28	12.15	12.30	12.02	12.12	12.55	11.84	11.95	11.95	11.83				
1.42	1.61	1.90	1.83	1.83	0.15	0.29	0.25	1.38	0.67				
2.63	2.41	2.08	2.13	2.17	4.37	3.94	4.07	2.81	3.55				

B-Total	3.98	3.94	3.98	4.07	4.06	3.98	3.98	3.97	3.92
X – S (Total)	13	13	13	13	13	13	13	13	13
Total	28.96	28.57	28.67	28.86	28.92	28.82	28.80	28.68	28.59

### Ag-phases (Miargyrite – AgSbS<sub>2</sub>; Pyragyrite – Ag<sub>3</sub>SbS<sub>3</sub>; Stephanite – Ag<sub>5</sub>SbS<sub>4</sub>; unnamed AgCuFeS phase)

Zone									
1806 Zone									
Mineralized Zone	semi-massive sulfide	massive sulfide		silicified horizon/rhyolite					
Plunge	up plunge	up plunge	up plunge	up plunge	up plunge				
Section	21	21	21	22	22				
Drill core#	RMUG08-124	RMUG08-123	RMUG08-140	RMUG08-140	RMUG08-141				
Sample No.	29913	36512	29783	29783	29787				
SEM image#	P3b	P5b	P7b	P1	P12				
Mineral	Mia	Hg-Stp	AgCuFeS	Mia	Paraschernerite				
Measuring date	Apr-11	Apr-11	Apr-11	Apr-11	Jan-12				
S [wt%]	20.86	15.18	27.31	21.86	3.51				
Ag	37.52	57.30	27.20	35.90	57.64				
Fe	0.066	0.253	22.24	0.040	1.53				
Cu	0.328	0.391	22.89	0.191	2.67				
As	0.172	1.17	nd	nd	0.489				
Sb	38.01	11.32	nd	41.13	5.41				
Hg	0.755	12.74	nd	nd	26.05				
Zn [ppm]	1.19	nd	nd	nd	1,066				
Pb	nd	nd	6,006	nd	nd				
Au	2.43	3,502	nd	nd	3,074				
Sn	nd	nd	nd	nd	nd				
Te	nd	nd	nd	nd	nd				
Bi	nd	nd	nd	nd	nd				
Mo	nd	2,256	nd	nd	3,269				
Mn	nd	nd	nd	nd	nd				
Co	nd	nd	159	nd	nd				
Ni	nd	nd	nd	nd	nd				
Total	101.34	98.93	99.86	99.13	98.04				

### Unsuccessfully detected Ag-phases (Tot

Zone									
Mineralized Zor									
Plunge	semi-massive sulfi								
Section	up plunge								
Drill core#	22								
Sample No.	RMUG08-141								
SEM image#	P12								
Mineral	Paraschernerite								
Measuring date	Jan-12								
S [wt%]	0.491								
Ag	47.83								
Fe	2.05								
Cu	0.499								
As	nd								
Sb	0.445								
Hg	52.04								
Zn [ppm]	nd								
Pb	nd								
Au	nd								
Sn	nd								
Te	nd								
Bi	nd								
Mo	1,45								
Mn	nd								
Co	260								
Ni	nd								
Total	104.84								

### Mineral Formula Calculation based on 2 S at

Ag <sub>3</sub> Hg <sub>2</sub>	
Ag	3
Hg	1.76
Au	
A-Total	
Sb	
As	
D-Total	
Cu	

### Mineral Formula Calculation based on 2 S atoms (ADX<sub>2</sub>; AgSbS<sub>2</sub>), 3 S atoms (A<sub>3</sub>DX<sub>3</sub>; Ag<sub>3</sub>SbS<sub>3</sub>), and 4 S atoms (A<sub>3</sub>DX<sub>4</sub>; Ag<sub>5</sub>SbS<sub>4</sub>)

Ag <sub>3</sub> SbS <sub>3</sub>	
A1 – Ag	1.07
A2 – Hg	4.49
A3 – Au	0.54
A-Total	6.10
D1 – Sb	0.04
D2 – As	1.11
D-Total	1.15
Cu	0.96

3.98 13	3.97 13	4.03 13	3.99 13	4.12 13	4.14 13	4.12 13	4.17 13	4.23 13	4.21 13	4.17 13
28.86	28.98	28.87	28.84	29.20	29.20	29.28	29.30	29.37	29.26	29.25

als too low/high)

1806 Zone										
de	massive sulfide up plunge 21			silicified horizon/rhyolite up plunge 21						
RMUG08-124 29913 P8 Mia	21 29913 P8 Mia	RMUG08-120 36509 P16	RMUG08-123 36512 P5b	RMUG08-120 36512 P5b	RMUG08-150 29914 P7	P15				
		AgCuAsS	AgHgSbS phase	AgSbS phase	Pyr (?)					
Apr-11	Jan-12	Apr-11	Jan-12	Jan-12	Jan-12					
21.54	15.78	13.05	20.07	16.41						
35.20	58.00	52.50	45.09	50.61						
0.372	0.048	0.360	5.21	0.101						
0.157	10.08	0.493	2.99	0.297						
nd	6.43	1.39	2.19	0.150						
40.59	1.81	10.59	21.82	23.10						
nd	nd	15.94	nd	nd						
nd	1,739	726	7,357	nd						
nd	nd	nd	nd	1,126						
nd	nd	4,482	nd	nd						
nd	nd	nd	nd	nd						
nd	nd	nd	nd	nd						
nd	nd	nd	nd	nd						
nd	nd	nd	nd	nd						
nd	nd	nd	nd	nd						
nd	nd	nd	nd	nd						
nd	nd	nd	nd	nd						
97.85	92.32	94.85	98.10	90.77						

atoms (ADX<sub>2</sub>: AgSbS<sub>2</sub>), 3 S atoms (A<sub>3</sub>DX<sub>3</sub>: Ag<sub>3</sub>SbS<sub>3</sub>), and 3 Ag atoms (A<sub>3</sub>B<sub>2</sub>:

0.97 2.75

0.97 2.75  
0.99 1.11

0.99 1.11

4.08 13	4.20 13	4.24 13	4.12 13	4.02 13	3.96 13	3.78 13	3.86 13	4.02 13	4.08 13	4.14 13
29.41	29.26	29.05	30.15	28.74	28.80	28.62	28.57	29.56	29.77	29.28

4.29	3.88	3.92	3.81	3.82	3.86	4.00	4.27	3.86	3.91	3.89
13	13	13	13	13	13	13	13	13	13	13
29.35	28.77	28.84	28.62	28.70	29.09	28.92	29.51	28.91	29.09	29.10

4.05	4.03	3.98	3.96	4.00	4.52	4.23	4.32	4.19	4.22
13	13	13	13	13	13	13	13	13	13
29.33	29.18	29.28	28.97	29.12	30.07	29.07	29.27	29.14	29.05







	P 6		
	EI I	EI II	EI III
	Apr-11	Apr-11	Apr-11
	37.69	41.24	39.75
	47.70	44.64	44.72
	13.76	13.50	13.78
	1,566	1,823	2,473
	601	1,038	1,962
	nd	nd	nd
	nd	nd	nd
	nd	nd	nd
	nd	nd	nd
	761	nd	961
	nd	nd	nd
	nd	nd	nd
	nd	nd	nd
	nd	nd	nd
	nd	nd	nd
	nd	163	nd
	nd	174	nd
	99.44	99.70	98.79
	0.79	0.92	0.89
	0.44	0.48	0.47
	37.90	41.37	40.23
	47.97	44.77	45.27
	13.84	13.54	13.95

Mineralized Zone	semi-mass up plunge	massive sulfide down plunge
Plunge	21	2
Section	RMUG08-124	RMUG08-145
Drill core#	29913	29907
Sample No.	P12	P10
SEM image#	Boul	Boul
Mineral	Apr-11	Jan-12
Measuring date	Jan-12	Jan-12
S [wt%]	17.08	17.05
Pb	60.25	58.61
Sb	19.76	20.38
Cu	1.51	3.25
Fe [ppm]	638	1.01
Zn	1,130	nd
As	nd	nd
Au	nd	nd
Ag	nd	2,703
Sn	nd	1,147
Te	nd	nd
Bi	nd	nd
Hg	nd	nd
Mo	nd	nd
Mn	nd	nd
Co	nd	nd
Ni	nd	nd
<b>Total</b>	<b>98.79</b>	<b>100.68</b>

#### Mineral Formula Calculation based on 11 S atoms ( $B_3D_4X_{11}$ ( $Pb_5Sb_4S_{11}$ ))

B – Pb (Total)	6.01	5.85	6.27
D1 – Sb	3.35	3.46	3.49
D2 – Cu	0.49	1.06	0.49
D3 – Fe		0.37	
<i>D-Total</i>	3.84	4.89	3.99
X – S (Total)	11	11	11
<b>Total</b>	<b>20.87</b>	<b>21.75</b>	<b>21.33</b>

#### Stannite ( $Cu_2FeSnS_4$ )

Zone	1806 Zone
Mineralized Zone	massive sulfide
Section	21
Plunge	upper up plunge
Drill core#	RMUG08-123
Sample No.	36512
SEM image#	P3
Mineral	P5b
Measuring date	Apr-11
	Stn I
	Stn II
	Stn
	Apr-11
	P7b

S [wt%]	29.59	29.19	29.67	29.47
Fe	12.10	12.16	12.01	11.78
Sn	27.50	27.32	27.81	27.49
Cu	28.06	28.26	28.28	27.96
Zn	2.76	1.97	2.16	2.43
Pb [ppm]	nd	nd	nd	nd
As	1,364	nd	nd	1,942
Au	nd	nd	nd	nd
Ag	nd	nd	nd	nd
Sb	nd	nd	nd	nd
Te	nd	nd	nd	nd
Bi	nd	nd	nd	nd
Hg	nd	nd	nd	nd
Mo	nd	nd	nd	nd
Mn	nd	nd	nd	178
Co	nd	nd	nd	nd
Ni	nd	189	nd	nd
Total	100.15	98.92	99.94	99.35

Mineral Formula Calculation based on 4 S atoms (A <sub>2</sub> DEX <sub>4</sub> ; Cu <sub>2</sub> (Fe, Zn)SnS <sub>4</sub> )				
A – Cu (Total)	1.91	1.95	1.92	1.92
D1 – Fe	0.94	0.96	0.93	0.92
D2 – Zn	0.18	0.13	0.14	0.16
D-Total	1.12	1.09	1.07	1.08
E – Sn	1.00	1.01	1.01	1.01
X – S (Total)	4	4	4	4
Total	8.04	8.06	8.01	8.00

Molybdenite (MoS<sub>2</sub>)

Zone	1806 Zone
Mineralized Zone	semi-massive sulfide
Plunge	down plunge
Section	2
Drill core#	RMUG08-146
Sample No.	29918
SEM image#	P9
Mineral	Mol
Measuring date	Jan-12
S [wt%]	38.68
Fe	1.08
Pb	nd
As	nd
Mo	58.78
Cu [ppm]	1,904

Zn	nd
Au	4,147
Ag	nd
Sb	nd
Sn	nd
Te	782
Bi	nd
Hg	nd
Mn	nd
Co	nd
Ni	nd
Total	99.22

Mineral Formula Calculation based on 2 S atoms (AX <sub>2</sub> : MoS <sub>2</sub> )	
A1 – Mo	1.02
A2 – Fe	0.03
A-Total	1.05
B – S (Total)	2
Total	3.05

Table A3-3. (cont.)

nd – not detected  
Trace data in *italics* are in wt. % and not in ppm

Cassiterite (SnO2)

Zone	1806 Zone
Mineralized Zone	semi-massive sulfide
Plunge	down plunge
Section	2
Drill core#	RMUG08-146
Sample No.	29918
SEM image#	P2
Mineral	Cass
Measuring date	Jan-12
Sn [wt%]	78.52
S [ppm]	nd
Fe	3,800
Cu	1,571
Zn	nd
Pb	nd
As	2,438
Au	nd
Ag	nd
Sb	nd
Te	nd
Bi	nd
Hg	nd
Mo	nd
Mn	nd
Co	nd
Ni	nd
Total	79.30
Calculated O	21.48

Mineral Formula Calculation based on 2 O

atoms (AX <sub>2</sub> : SnO <sub>2</sub> )	
A – Sn (Total)	0.98
X – O (Total)	2
Total	2.98

Magnetite (Fe<sub>3</sub>O<sub>4</sub>)

Zone	1806 Zone
------	-----------

Mineralized zone		semi-massive sulfide									
Plunge	Section	down plunge									
Drill core#	Section	2									
Sample No.	Section	RMUG08-146									
SEM image#	Section	29918									
Mineral	Mineral										
area	area										
Measuring date	Measuring date										
		P2		P4c		P14		Mag I		Mag II	
		Mag	Mag	Mag	Mag	Mag	Mag	Mag	Mag	Mag	Mag
		core	rim-a	rim-b	rim-a	rim-b	rim-a	rim-a	rim-a	core	rim-b
		Jan-12	Jan-12	Jan-12	Jan-12	Jan-12	Jan-12	Jan-12	Jan-12	Jan-12	Jan-12
Fe [wt%]		71.34	71.56	71.44	70.42	71.14	71.39	71.21	71.57	71.11	71.11
S [ppm]		nd	231	nd	nd	nd	nd	242	nd	297	297
Cu		nd	nd	nd	nd	nd	484	nd	nd	nd	nd
Zn		nd	nd	648	621	nd	nd	nd	614	nd	nd
Pb		nd	nd	nd	nd	nd	nd	nd	nd	nd	nd
As		nd	nd	nd	nd	nd	nd	nd	nd	nd	nd
Au		nd	nd	nd	nd	nd	nd	nd	nd	nd	nd
Ag		nd	nd	nd	nd	nd	nd	nd	nd	nd	nd
Sb		nd	nd	nd	nd	nd	nd	nd	nd	nd	nd
Sn		nd	nd	nd	nd	nd	nd	nd	nd	nd	nd
Bi		nd	nd	nd	nd	nd	nd	nd	nd	nd	nd
Hg		nd	nd	nd	nd	nd	nd	nd	nd	nd	nd
Mo		nd	nd	nd	nd	nd	nd	nd	nd	nd	nd
Mn		446	657	528	857	771	713	575	599	421	421
Co		nd	nd	nd	nd	nd	nd	nd	nd	nd	nd
Ni		nd	nd	nd	nd	nd	nd	nd	nd	nd	nd
Total		71.38	71.65	71.56	70.57	71.22	71.51	71.29	71.69	71.18	71.18
Calculated O		28.62	28.35	28.44	29.43	28.78	28.49	28.71	28.31	28.82	28.82
Mineral Formula Calculation based on 4 O atoms (AB <sub>2</sub> X <sub>4</sub> : Fe <sub>3</sub> O <sub>4</sub> )											
A+B - Fe (Total)		2.86	2.89	2.88	2.74	2.83	2.87	2.84	2.90	2.83	2.83
X - O (Total)		4	4	4	4	4	4	4	4	4	4
Total		6.86	6.89	6.88	6.74	6.83	6.87	6.84	6.90	6.83	6.83



Table A5-6. Results EPMA

Mineral phase*	S [wt %]	Fe	Cu	Zn	Pb	As	Co	Ni	Te	Ag
<b>Common Metal Sulfides</b>										
<b>Py (121)</b>	Av $\pm$ stdev	53.22 $\pm$ 0.356	45.92 $\pm$ 0.338							
	Min	52.36	45.10							
	Max	53.92	46.77							
<b>Ccp (176)</b>	Av $\pm$ stdev	34.88 $\pm$ 0.309	30.52 $\pm$ 0.341	34.46 $\pm$ 0.291						
	Min	33.61	29.16	33.32						
	Max	36.13	31.46	35.55						
<b>Cbn (28)</b>	Av $\pm$ stdev	35.13 $\pm$ 0.199	41.33 $\pm$ 0.294	23.40 $\pm$ 0.251						
	Min	34.80	40.92	22.83						
	Max	35.39	42.26	23.63						
<b>Po (83)</b>	Av $\pm$ stdev	38.93 $\pm$ 0.456	60.37 $\pm$ 0.637							
	Min	38.20	58.11							
	Max	40.14	61.44							
<b>Sp (97)</b>	Av $\pm$ stdev	33.50 $\pm$ 0.424	7.47 $\pm$ 2.78	58.44 $\pm$ 3.03						
	Min	32.33	1.12	54.24						
	Max	34.65	11.04	65.28						
<b>Gn (42)</b>	Av $\pm$ stdev	13.19 $\pm$ 0.282		86.12 $\pm$ 0.638						
	Min	12.64		84.88						
	Max	13.90		87.55						
<b>Asp (96)</b>	Av $\pm$ stdev	21.27 $\pm$ 0.538	34.21 $\pm$ 0.424		43.96 $\pm$ 0.686					
	Min	19.50	32.97		41.69					
	Max	23.71	34.98		46.68					
<b>Uncommon Metal Sulfides</b>										
<b>Allo (5)</b>	Av $\pm$ stdev	20.04 $\pm$ 0.349	8.31 $\pm$ 1.06		44.38 $\pm$ 0.490	24.74 $\pm$ 0.614	2.15 $\pm$ 0.406			
	Min	19.61	7.15		43.55	24.01	1.79			
	Max	20.42	9.88		44.78	25.59	2.81			
<b>Hess (3)</b>	Av $\pm$ stdev							38.52 $\pm$ 2.62	60.64 $\pm$ 2.30	
	Min							36.99	58.09	
	Max							41.54	62.56	
<b>Tsu (9)</b>	Av $\pm$ stdev									
	Min									
	Max									
<b>BiTe (1)</b>	Av $\pm$ stdev									
<b>Alt (1)</b>	Av $\pm$ stdev									
<b>Gud (3)</b>	Av $\pm$ stdev	15.21 $\pm$ 0.085	26.73 $\pm$ 0.094							
	Min	15.15	26.67							
	Max	15.27	26.80							
<b>Breit (3)</b>	Av $\pm$ stdev		0.927 $\pm$ 0.696					31.94 $\pm$ 0.311		
	Min		0.501					31.65		
	Max		1.73					32.27		
<b>Nis (1)</b>	Av $\pm$ stdev		0.811				1.09	17.25		

Mineral phase*	Bi	Sb	Au	Sn	Hg	Total	Mineral Formula
<b>Common Metal Sulfides</b>							
Py (121)						99.14 ± 0.511	Fe <sub>0.97-1.01</sub> S <sub>2</sub>
						98.13	
						100.45	
Ccp (176)						99.85 ± 0.432	Cu <sub>0.96-1.06</sub> Fe <sub>0.94-1.05</sub> S <sub>2</sub>
						98.71	
						101.26	
Cbn (28)						99.86 ± 0.160	Cu <sub>0.96-1.02</sub> Fe <sub>2.00-2.07</sub> S <sub>3</sub>
						99.67	
						100.21	
Po (83)						99.30 ± 0.535	Fe <sub>0.84-0.92</sub> S
						98.07	
						100.25	
Sp (97)						99.41 ± 0.690	(Zn <sub>0.79-0.97</sub> Fe <sub>0.02-0.19</sub> ) <sub>0.95-1.02</sub> S
						97.98	
						100.80	
Gn (42)						99.31 ± 0.735	Pb <sub>0.95-1.06</sub> S
						98.11	
						100.73	
Asp (96)						99.44 ± 0.678	As <sub>0.75-1.02</sub> Fe <sub>0.83-1.00</sub> S
						98.07	
						101.24	
<b>Uncommon Metal Sulfides</b>							
Allo (5)						99.61 ± 0.376	(Co <sub>0.65-0.71</sub> Ni <sub>0.05-0.08</sub> ) <sub>0.71-0.78</sub> Fe <sub>0.21-0.28</sub> As <sub>0.92-0.97</sub> S
						99.04	
						100.03	
Hess (3)						99.27 ± 1.00	Ag <sub>1.65-2.00</sub> Te
						98.27	
						100.27	
Tsu (9)	56.89 ± 2.43	1.03 ± 0.610				99.87 ± 0.927	(Bi <sub>0.81-1.05</sub> Pb <sub>0.07-0.12</sub> Sb <sub>0.00-0.04</sub> ) <sub>0.94-1.17</sub> Te
	52.45	0.000				98.52	
	60.25	1.58				101.10	
BiTe (1)						99.62	(Bi <sub>2.92</sub> Pb <sub>0.15</sub> Sb <sub>0.01</sub> ) <sub>3.07</sub> Te <sub>2</sub>
Alt (1)						98.94	Pb <sub>1.00</sub> Te
Gud (3)						100.41 ± 0.390	Fe <sub>1.07</sub> Sb <sub>1.01</sub> S
	58.46 ± 0.211					100.13	
	58.31	58.61				100.69	
Breit (3)	66.52 ± 0.213					99.39 ± 0.687	(Ni <sub>0.98-1.01</sub> Fe <sub>0.02-0.06</sub> ) <sub>1.01-1.04</sub> Sb
	66.37	66.77				98.82	
	66.77	77.31				100.15	
Nis (1)			1.69			98.16	(Ni <sub>0.93</sub> Fe <sub>0.05</sub> Co <sub>0.06</sub> Au <sub>0.03</sub> ) <sub>1.06</sub> Sb <sub>2</sub>

Table A5-6. Results EPMA

Mineral phase*	S [wt %]	Fe	Cu	Zn	Pb	As	Co	Ni	Te	Ag
<b>Sulfosalts</b>										
Men (5)	Av ± stdev Min Max	17.61 ± 0.966 16.63 18.66	1.87 ± 0.828 1.12 3.25	59.40 ± 1.30 58.04 61.23						
Tnt-Trt (61)	Av ± stdev Min Max	25.72 ± 1.93 20.99 28.52	35.73 ± 7.25 15.29 44.46	3.12 ± 1.38 0.314 5.49	8.61 ± 6.84 0.000 19.25					5.38 ± 7.91 0.252 29.27
Stn (4)	Av ± stdev Min Max	12.01 ± 0.213 29.19 29.67	28.14 ± 0.156 27.96 28.28	2.33 ± 0.344 1.97 2.76						
<b>Precious Metals and Alloys</b>										
EI (23)	Av ± stdev Min Max									40.11 ± 8.79 26.02 67.35

Mineral phase*	Bi	Sb	Au	Sn	Hg	Total	Mineral Formula
<b>Sulfosalts</b>							
Men (5)							<b>Pb<sub>11.56-13.67</sub>Cu<sub>0.73-2.31</sub>Sb<sub>6.68-7.62</sub>S<sub>24</sub></b>
Av ± stdev	20.06 ± 0.313				98.94 ± 0.530	98.17	
Min	19.73					99.39	
Max	20.38						
Tnt-Trt (61)							<b>(Cu<sub>4.60-10.63</sub>Ag<sub>0.04-5.39</sub>)<sub>9.50-10.72</sub>(Fe<sub>0.61-2.30</sub>Zn<sub>0.09-1.45</sub>)<sub>1.94-2.52</sub>(As<sub>0.00-3.90</sub>Sb<sub>0.16-4.37</sub>)<sub>3.78-4.52</sub>S<sub>13</sub></b>
Av ± stdev	16.27 ± 9.78				99.33 ± 0.696	98.04	
Min	1.33					100.98	
Max	29.56						
Stn (4)							<b>Cu<sub>1.91-1.95</sub>(Fe<sub>0.92-0.96</sub>Zn<sub>0.13-0.18</sub>)<sub>1.07-1.12</sub>Sn<sub>1.00-1.01</sub>S<sub>4</sub></b>
Av ± stdev			27.53 ± 0.204	27.32	99.50 ± 0.563	98.90	
Min				27.81		100.02	
Max							
<b>Precious Metals and Alloys</b>							
El (23)							<b>(Au, Ag, Hg)<sub>0.62-1.23</sub></b>
Av ± stdev		45.71 ± 11.40			13.88 ± 3.52 ± 0.947	3.05	
Min		13.87				98.19	
Max		70.17				20.57	
						101.07	

Table A5-6. Results LA-ICP-MS

Mineral phase*	S [ppm]	Ti	V	Cr	Mn	Fe	Co	Ni	Cu	Zn
<b>Common</b>										
<b>Metal</b>										
<b>Sulfides</b>										
<b>Py (45)</b>										
Av $\pm 1\sigma$		12.0 $\pm 5.46$	5.77 $\pm 7.59$	3.11 $\pm 1.62$	24.5 $\pm 22.9$		276 $\pm 298$	184 $\pm 270$	533 $\pm 1,140$	302 $\pm 805$
Min		4.39	0.14	1.83	2.67		0.458	19.379	0.669	2.95
Max		31.7	20.4	5.93	56.9		1.363	1,578	5,378	3,628
<b>Ccp (61)</b>										
Av $\pm 1\sigma$		8.39 $\pm 3.95$	23.8 $\pm 41.3$	12.3 $\pm 11.2$	10.6 $\pm 15.9$		34.4 $\pm 87.8$	94.6 $\pm 117$		652 $\pm 121$
Min		2.38	0.163	5.76	1.07		0.262	23.6		165
Max		19.9	107	25.2	56.4		390	230		1,431
<b>Cbn (14)</b>										
Av $\pm 1\sigma$		5.24 $\pm 1.24$	—	—	—		12.3 $\pm 20.3$	24.2 $\pm 12.6$		635 $\pm 368$
Min		3.60	—	—	—		0.507	15.3		287
Max		6.73	—	—	—		57.4	33.1		1,259
<b>Sp (32)</b>										
Av $\pm 1\sigma$		7.80 $\pm 3.73$	5.27 $\pm 7.70$	12.0	902 $\pm 622$		57.2 $\pm 74.5$	30.1 $\pm 10.1$	647 $\pm 1,044$	
Min		3.68	0.416	12.0	68.5		0.22	18.0	10.8	
Max		20.5	18.8	12.0	2,146		239	41.5	5,189	
<b>Po (34)</b>										
Av $\pm 1\sigma$		8.88 $\pm 5.87$	29.4 $\pm 46.5$	6.58 $\pm 4.02$	27.6 $\pm 33.9$		111 $\pm 156$	151 $\pm 133$	712 $\pm 1,787$	396 $\pm 669$
Min		2.63	1.02	1.45	3.67		1.14	13.2	0.729	3.04
Max		26.1	116	12.6	102		671	529	8,043	2,678
<b>Asp (30)</b>										
Av $\pm 1\sigma$		6.55 $\pm 2.88$	8.13 $\pm 19.9$	1.16 $\pm 0.674$	20.4 $\pm 31.3$		1,887 $\pm 3,620$	672 $\pm 567$	263 $\pm 706$	36.9 $\pm 86.9$
Min		3.25	0.143	0.678	1.91		0.102	75.0	0.708	0.743
Max		18.2	53.3	1.63	82.6		12,783	1,893	3,039	321
<b>Gn (15)</b>										
Av $\pm 1\sigma$		3.15 $\pm 1.26$	2.65 $\pm 3.36$	—	3.55 $\pm 3.48$	1,656 $\pm 2,289$	0.320 $\pm 0.149$	—	167 $\pm 252$	299 $\pm 241$
Min		1.46	0.236	—	1.21	46.0	0.215	—	0.504	18.9
Max		5.44	6.83	—	7.55	5,670	0.426	—	755	562
<b>Uncommon Metal Sulfides</b>										
<b>Allo (4)</b>										
Av $\pm 1\sigma$		13.3 $\pm 7.25$	—	—	2.87			1,527 $\pm 1,813$	751 $\pm 641$	
Min		7.29	—	—	2.87			240	22.62	
Max		23.2	—	—	2.87			3,600	1,229	
<b>Hess (3)<sup>#</sup></b>										
Av $\pm 1\sigma$		NA	NA	NA	206	2,438 $\pm 867$	—	171	1,927 $\pm 1,891$	—
Min		NA	NA	NA	206	1,441		171	590	
Max		NA	NA	NA	206	3,020		171	3,264	
<b>Tsu (9)<sup>#</sup></b>										
Av $\pm 1\sigma$		NA	NA	NA	143	5,780 $\pm 2,930$	—	—	3,973 $\pm 2,769$	2,927 $\pm 907$
Min		NA	NA	NA	143	3,416	—	—	874	1,957
Max		NA	NA	NA	143	9,871	—	—	6,204	3,914
<b>BiTe (1)<sup>#</sup></b>										
Av		NA	NA	NA	—	6,101	—	—	—	—
<b>Alt (1)<sup>#</sup></b>										
Av		NA	NA	NA	—	1,060	—	—	—	8,639
<b>Gud (3)<sup>#</sup></b>										
Av $\pm 1\sigma$		NA	NA	NA	—	—	—	202	614	—
Min		NA	NA	NA	—	—	—	202	614	—
Max		NA	NA	NA	—	—	—	202	614	—
<b>Breit (3)<sup>#</sup></b>										
Av $\pm 1\sigma$		NA	NA	NA	—	—	785 $\pm 577$	—	1,400 $\pm 652$	—
Min		NA	NA	NA	—	—	141	—	821	—
Max		NA	NA	NA	—	—	1,254	—	2,107	—
<b>Nis (1)<sup>#</sup></b>										
Av		NA	NA	NA	—	—	—	—	1,531	—

Mineral phase*	As	Se	Mo	Ag	Cd	Sn	Sb	Te	Au	Hg
<b>Py (45)</b>	Av ± 1σ Min Max	335 ± 426 8.17 1,847	52.2 ± 130 0.298 473	6.07 ± 16.9 0.110 82.7	8.15 ± 12.1 1.02 37.2	35.6 ± 123 0.212 496	6.06 ± 9.45 0.170 38.2	56.8 ± 102 1.66 391	0.931 ± 1.07 0.083 2.98	NA NA NA
<b>Ccp (61)</b>	Av ± 1σ Min Max	909 ± 1,379 22.9 4,30	19.9 ± 19.6 2.34 49.7	133 ± 227 7.27 979	14.0 ± 10.8 0.751 73.9	131 ± 165 8.45 982	6.93 ± 8.54 0.049 37.5	5.03 ± 3.13 1.08 12.5	2.74 ± 7.68 0.062 33.5	NA NA NA
<b>Cbn (14)</b>	Av ± 1σ Min Max	44.6 ± 8.11 35.2 57.7	790 ± 45.60 737 861	47.0 ± 13.6 31.5 69.3	19.1 ± 6.64 13.0 32.8	23.2 ± 19.5 8.37 54.6	0.432 ± 0.417 0.125 1.06	10.5 ± 1.34 8.61 12.4	— — —	NA NA NA
<b>Sp (32)</b>	Av ± 1σ Min Max	167 ± 356 5.20 1,778	204 ± 172 12.2 660	10.1 ± 13.2 0.845 65.1	8.010 ± 5.942 3.095 37,554	13.1 ± 43.7 0.117 216	6.97 ± 6.69 0.261 25.0	24.5 ± 44.6 2.14 125	15.2 ± 33.3 0.063 74.8	NA NA NA
<b>Po (34)</b>	Av ± 1σ Min Max	1,025 ± 1,435 34.1 6,774	349 ± 349 69.9 2,054	18.2 ± 47.6 0.502 259	8.84 ± 8.75 1.14 25.5	2.38 ± 6.64 0.079 27.1	42.1 ± 166 0.058 836	16.8 ± 21.6 2.00 75.5	18.5 ± 49.1 0.152 149	NA NA NA
<b>Asp (30)</b>	Av ± 1σ Min Max	390 ± 354 25.8 1,214	6.04 ± 7.27 0.321 27.3	31.7 ± 92.1 0.251 423	9.91 ± 18.9 0.136 38.2	193 ± 721 0.069 2,698	193 ± 805 2.26 4,436	646 ± 1,142 3.11 4,240	15.0 ± 51.2 0.041 230	NA NA NA
<b>Gn (15)</b>	Av ± 1σ Min Max	540 ± 594 44.7 2,187	3,286 ± 4,409 963 16,343	1,119 ± 651 274 2,195	30.6 ± 46.1 7.24 192	159 ± 189 3.85 480	1,128 ± 887 169 2,749	540 ± 1,425 10.8 5,553	0.145 ± 0.147 0.041 0.249	NA NA NA
<b>Allo (4)</b>	Av ± 1σ Min Max	1,465 ± 833 362 2,318	— — —	40.7 ± 44.0 4.29 94.0	13.3 ± 7.25 7.29 23.2	0.867 ± 0.396 0.542 1.31	88.4 ± 124 6.05 270	179 ± 99.2 76.5 309	13.2 ± 2.54 10.2 16.3	NA NA NA
<b>Hess (3)<sup>#</sup></b>	Av ± 1σ Min Max	1,684 ± 604 1,257 2,111	NA NA NA	NA NA NA	NA NA NA	— — —	872 872 872	NA NA NA	— — —	3,716 ± 2,279 2,105 5,327
<b>Tsu (9)<sup>#</sup></b>	Av ± 1σ Min Max	2,497 ± 1,539 1,387 5,437	NA NA NA	2,422 ± 2,173 990 4,922	NA NA NA	— — —	— — —	— — —	— — —	— — —
<b>BiTe (1)<sup>#</sup></b>	Av Min	2,528 1,228	NA NA	— —	NA NA	799 1,026	2,274	NA NA	— —	— —
<b>Alt (1)<sup>#</sup></b>	Av Min	3,461 1,228	NA NA	— —	NA NA	2,522 ± 86.7 3,460	— —	2,560 2,560	— —	— —
<b>Gud (3)<sup>#</sup></b>	Av Min	1,228 1,228	NA NA	— —	NA NA	3,583	— —	2,560	— —	— —
<b>Breit (3)<sup>#</sup></b>	Av ± 1σ Min Max	NA NA NA	NA NA NA	— — —	NA NA NA	4,203 ± 213 3,958	— — —	— — —	— — —	2,147 2,147 2,147
<b>Nis (1)<sup>#</sup></b>	Av	2,349	NA	—	NA	4,761	—	6,750	—	—

Mineral phase*	Ti		Pb	Bi
<b>Py (45)</b>	Av $\pm 1\sigma$	1.30 $\pm 1.94$	84.0 $\pm 177$	5.68 $\pm 12.3$
	Min	0.058	0.069	0.023
	Max	6.57	709	66.5
<b>Ccp (61)</b>	Av $\pm 1\sigma$	0.571 $\pm 0.743$	59.6 $\pm 194$	2.60 $\pm 3.13$
	Min	0.018	0.100	0.116
	Max	3.75	1,366	14.9
<b>Cbn (14)</b>	Av $\pm 1\sigma$	0.056	29.7 $\pm 9.72$	1.33 $\pm 0.750$
	Min	0.056	18.3	0.671
	Max	0.056	44.2	2.67
<b>Sp (32)</b>	Av $\pm 1\sigma$	0.380 $\pm 0.489$	126 $\pm 455$	4.60 $\pm 9.84$
	Min	0.038	0.134	0.030
	Max	1.97	2,479	45.6
<b>Po (34)</b>	Av $\pm 1\sigma$	0.851 $\pm 0.816$	585 $\pm 1,298$	10.0 $\pm 14.8$
	Min	0.024	0.302	0.098
	Max	3.55	6,168	60.0
<b>Asp (30)</b>	Av $\pm 1\sigma$	1.74 $\pm 5.44$	72.6 $\pm 156$	7.04 $\pm 11.4$
	Min	0.046	0.421	0.024
	Max	23.4	666	33.3
<b>Gn (15)</b>	Av $\pm 1\sigma$	53.8 $\pm 72.2$		978 $\pm 2,751$
	Min	16.7		3.03
	Max	271		10,455
<b>Allo (4)</b>	Av $\pm 1\sigma$	0.768 $\pm 0.774$	551 $\pm 254$	47.9 $\pm 27.2$
	Min	0.271	229	11.8
	Max	1.66	869	70.2
<b>Hess (3)<sup>#</sup></b>	Av $\pm 1\sigma$	NA	—	—
	Min	NA		
	Max	NA		
<b>Tsu (9)<sup>#</sup></b>	Av $\pm 1\sigma$	NA		
	Min	NA		
	Max	NA		
<b>BiTe (1)<sup>#</sup></b>	Av	NA		—
<b>Alt (1)<sup>#</sup></b>	Av	NA		1,422
<b>Gud (3)<sup>#</sup></b>	Av $\pm 1\sigma$	NA	1,054	1,422
	Min	NA	1,054	1,422
	Max	NA	1,054	1,422
<b>Breit (3)<sup>#</sup></b>	Av $\pm 1\sigma$	NA	504	—
	Min	NA	504	—
	Max	NA	504	—
<b>Nis (1)<sup>#</sup></b>	Av	NA	—	1,240

Table A5-6. Results LA-ICP-MS

Mineral phase*	S [ppm]	Ti	V	Cr	Mn	Fe	Co	Ni	Cu	Zn
<b>Uncommon</b>										
<b>Metal</b>										
<b>Sulfides</b>										
<b>(continued)</b>										
<b>Men (5)<sup>#</sup></b>	<b>Av ± 1σ</b>	<b>NA</b>	<b>NA</b>	<b>NA</b>	<b>-</b>	<b>3,416 ± 3,962</b>	<b>156</b>	<b>-</b>	<b>4,237 ± 4,395</b>	
	<i>Min</i>	NA	NA	NA	-	445	156	-	1,130	
	<i>Max</i>	NA	NA	NA	-	10,051	156	-	7,345	
<b>Sulfosalts</b>										
<b>Tnt-Trt (9)</b>	<b>Av ± 1σ</b>	<b>5.06 ± 1.89</b>	<b>0.740 ± 0.899</b>	<b>1.41 ± 1.39</b>	<b>61.7 ± 31.5</b>		<b>0.944 ± 1.14</b>	<b>-</b>		
	<i>Min</i>	3.08	0.087	0.424	24.4		0.137	-		
	<i>Max</i>	8.00	2.49	2.39	102		1.75	-		
<b>Stn (3)</b>	<b>Av ± 1σ</b>	<b>5.48 ± 3.08</b>	<b>0.315</b>	<b>-</b>	<b>274 ± 57.9</b>		<b>1.14 ± 0.178</b>	<b>22.8</b>		
	<i>Min</i>	2.80	0.315	-	212		1.03	22.8		
	<i>Max</i>	8.17	0.315	-	326		1.35	22.8		
<b>Precious Metal and Alloys</b>										
<b>El (8)</b>	<b>Av ± 1σ</b>	<b>191 ± 116</b>	<b>-</b>	<b>-</b>	<b>5.53</b>	<b>301 ± 314</b>	<b>-</b>	<b>-</b>	<b>228 ± 172</b>	<b>134 ± 193</b>
	<i>Min</i>	97.4	-	-	5.53	29.1	-	-	122	1.48
	<i>Max</i>	453	-	-	5.53	906	-	-	427	418



Mineral phase*	As	Se	Mo	Ag	Cd	Sn	Sb	Te	Au	Hg
<i>Men (5)<sup>#</sup></i>	<i>Av ± 1σ</i>	NA	—	2,703	NA	1,380 ± 239		1,139	—	—
	<i>Min</i>	NA	—	2,703	NA	1,147		1,139	—	—
	<i>Max</i>	NA	—	2,703	NA	1,645		1,139	—	—
<i>Tnt-Trt (9)</i>	<i>Av ± 1σ</i>	272 ± 293	—		623 ± 251	20.1 ± 28.5		16.0 ± 17.9	5.00 ± 6.98	NA
	<i>Min</i>	14.10	—		404	0.799		1.77	0.021	NA
	<i>Max</i>	821	—		1,029	71.6		44.3	17.0	NA
<i>Stn (3)</i>	<i>Av ± 1σ</i>	66.5 ± 25.2	—	341 ± 179	1,072 ± 233		30.2 ± 5.64	—	0.817	NA
	<i>Min</i>	37.5	—	219	897		25.2	—	0.817	NA
	<i>Max</i>	82.9	—	546	1,337		36.3	—	0.817	NA
<i>EI (8)</i>	<i>Av ± 1σ</i>	1.64 ± 0.748	—		3.40 ± 1.23	0.259 ± 0.065	635 ± 325	4.85 ± 3.18		NA
	<i>Min</i>	1.09	—		2.53	0.213	248	1.20		NA
	<i>Max</i>	2.74	—		4.27	0.305	1,126	7.01		NA

Mineral phase*	Tl		Pb		Bi
<i>Men (5)<sup>#</sup></i>	<i>Av ± 1σ</i>	<i>NA</i>			—
	<i>Min</i>	<i>NA</i>			—
	<i>Max</i>	<i>NA</i>			—
<b>Tnt-Trt (9)</b>	<b>Av ± 1σ</b>	<b>6.89 ± 10.1</b>	<b>784 ± 1,203</b>	<b>52.7 ± 99.3</b>	
	<i>Min</i>	0.088	3.59	0.294	
	<i>Max</i>	24.9	2,966	231	
<b>Stn (3)</b>	<b>Av ± 1σ</b>	<b>0.585 ± 0.577</b>	<b>79.2 ± 1.89</b>		—
	<i>Min</i>	0.188	77.8		—
	<i>Max</i>	1.25	80.5		—
<b>EI (8)</b>	<b>Av ± 1σ</b>	<b>0.063 ± 0.019</b>	<b>0.228 ± 0.134</b>		—
	<i>Min</i>	0.045	0.045		—
	<i>Max</i>	0.089	0.334		—

Table A5-6. Results of EPMA analysis (major elements in wt%) and LA-ICP-MS analysis (trace elements in ppm) for pyrite; – not detected or below detection limit

Ore body	Mineralization style	Mineral phase*	S [wt %]	Fe	Total	Mineral Formula	Ti [ppm]	V	Cr	Mn
1807	semi-massive to massive sulfides**	Py (31, 8)	Av ± stdev Min Max	53.01 ± 0.299 52.41 53.56	45.93 ± 0.236 45.31 46.37	98.94 ± 0.388 98.13 99.74	Fe <sub>0.97-1.01</sub> S <sub>2</sub> 11.7 ± 2.22 8.78	2.20 ± 2.74 0.264 4.14	5.93 5.93 5.93	– – –
1806	silicified horizon	Py (4, 2)	Av ± stdev Min Max	53.69 ± 0.194 53.49 53.90	45.99 ± 0.379 45.70 46.55	99.68 ± 0.514 99.34 100.45	Fe <sub>0.98-0.99</sub> S <sub>2</sub> 8.72 ± 1.95 7.34 10.1	– – –	– – –	– – –
1806	semi-massive to massive sulfides	Py (34, 10)	Av ± stdev Min Max	53.50 ± 0.261 52.91 53.92	45.91 ± 0.469 45.19 46.77	99.41 ± 0.563 98.38 100.41	Fe <sub>0.97-1.01</sub> S <sub>2</sub> 11.8 ± 7.60 4.39 31.7	8.28 ± 8.61 0.141 20.4	2.74 2.74 2.74	31.8 ± 21.7 19.2 56.9
1806	sulfide stringer horizon	Py (4, 2)	Av ± stdev Min Max	53.56 ± 0.088 53.48 53.68	46.54 ± 0.097 46.41 46.64	100.10 ± 0.138 99.92 100.25	Fe <sub>1.00</sub> S <sub>2</sub> 8.84 ± 2.25 7.25 10.4	– – –	– – –	– – –
1806	All	Py (42, 14)	Av ± stdev Min Max	53.52 ± 0.248 52.91 53.92	45.98 ± 0.472 45.19 46.77	99.50 ± 0.567 98.38 100.45	Fe <sub>0.97-1.01</sub> S <sub>2</sub> 10.9 ± 6.53 4.39 31.7	8.28 ± 8.61 0.141 20.4	2.74 2.74 2.74	31.8 ± 21.7 19.2 56.9
MSUP	sulfide stringer (hanging wall)	Py (4, 1)	Av ± stdev Min Max	53.27 ± 0.138 53.12 53.40	46.01 ± 0.151 45.90 46.22	99.28 ± 0.225 99.09 99.59	Fe <sub>0.99-1.00</sub> S <sub>2</sub> 17.0 – –	– – –	– – –	– – –
MSUP	semi-massive to massive sulfides	Py (7, 5)	Av ± stdev Min Max	52.88 ± 0.214 52.55 53.18	46.00 ± 0.098 45.80 46.08	98.87 ± 0.198 98.62 99.20	Fe <sub>0.99-1.01</sub> S <sub>2</sub> 20.7 ± 6.41 13.8 28.1	– – –	– – –	– – –
MSUP	sulfide stringer horizon	Py (11, 3)	Av ± stdev Min Max	53.19 ± 0.314 52.73 53.74	45.87 ± 0.239 45.45 46.27	99.06 ± 0.472 98.18 99.91	Fe <sub>0.98-1.00</sub> S <sub>2</sub> 11.0 ± 2.58 8.64 13.7	– – –	– – –	– – –
MSUP	All	Py (22, 9)	Av ± stdev Min Max	53.10 ± 0.298 52.55 53.74	45.94 ± 0.194 45.45 46.27	99.04 ± 0.381 98.18 99.91	Fe <sub>0.98-1.01</sub> S <sub>2</sub> 17.1 ± 6.67 8.64 28.1	– – –	2.30 2.30 2.30	– – –
MSDP	semi-massive to massive sulfides	Py (7, 4)	Av ± stdev Min Max	53.08 ± 0.244 52.58 53.33	45.87 ± 0.210 45.51 46.14	99.10 ± 0.312 98.78 99.55	Fe <sub>0.98-1.01</sub> S <sub>2</sub> 12.6 ± 1.12 11.0 13.4	0.509 0.509 0.509	1.83 1.83 1.83	– – –
MSDP	sulfide stringer horizon	Py (3, 2)	Av ± stdev Min Max	52.98 ± 0.198 52.77 53.17	45.80 ± 0.214 45.61 46.03	98.91 ± 0.102 98.81 99.01	Fe <sub>0.99-1.00</sub> S <sub>2</sub> 7.25 ± 1.20 6.41 8.10	– – –	– – –	2.67 2.67 2.67
MSDP	All	Py (10, 6)	Av ± stdev Min Max	53.05 ± 0.225 52.58 53.33	45.85 ± 0.202 45.51 46.14	99.04 ± 0.273 98.78 99.55	Fe <sub>0.98-1.01</sub> S <sub>2</sub> 10.8 ± 2.96 6.41 13.4	0.509 0.509 0.509	1.83 1.83 1.83	2.67 2.67 2.67
LFWZ	LFWZ	Py (16, 8)	Av ± stdev Min Max	53.14 ± 0.338 52.36 53.59	45.74 ± 0.264 45.10 46.14	99.09 ± 0.367 98.41 99.64	Fe <sub>0.97-1.01</sub> S <sub>2</sub> 9.56 ± 1.78 6.89 12.4	0.595 0.595 0.595	2.76 2.76 2.76	– – –
MING	All	Py (121, 45)	Av ± stdev Min Max	53.22 ± 0.356 52.36 53.92	45.92 ± 0.338 45.10 46.77	99.14 ± 0.511 98.13 100.45	Fe <sub>0.97-1.01</sub> S <sub>2</sub> 12.0 ± 5.46 4.39 31.7	5.77 ± 7.59 0.14 20.4	3.11 ± 1.62 1.83 5.93	24.5 ± 22.9 2.67 56.9

Table A5-6. (cont.)

Ore body	Mineralization style	Mineral phase*	Co	Ni	Cu	Zn	As	Se	Mo	Ag
1807	semi-massive to massive sulfides**	Py (33, 8)	266 ± 185	64.0 ± 21.0	1,660 ± 2,151	190 ± 200	2,499 ± 1,967	198 ± 101	105	2.16 ± 1.95
		Min	13.4	49.2	45.9	57.4	667	101	105	0.78
		Max	530	78.8	5,378	489	5,732	384	105	5.06
1806	silicified horizon	Py (4, 2)	11.7 ± 10.9	158 ± 89.4	142	—	1,933 ± 1,449	56.5 ± 63.0	0.425	1.13 ± 0.019
		Min	3.99	94.6	142	—	908	11.9	0.425	1.12
		Max	19.5	221	142	—	2,957	101	0.425	1.15
1806	semi-massive to massive sulfides	Py (34, 8)	244 ± 207	186 ± 138	367 ± 667	608 ± 1,243	2,037 ± 996	69.4 ± 83.5	88.9 ± 189	18.4 ± 31.9
		Min	0.458	50.97	1.79	8.23	664	8.17	1.34	1.35
		Max	583	523	1,837	3,628	3,518	215	473	82.7
1806	sulfide stringer horizon	Py (4, 4)	20.0 ± 1.41	121 ± 14.6	130	41.4	2,944 ± 1,349	60.7 ± 15.5	—	—
		Min	19.0	111	130	41.37	1,990	49.7	—	—
		Max	21.0	132	130	41.37	3,898	71.7	—	—
1806	All	Py (42, 14)	168 ± 199	173 ± 120	316 ± 586	545 ± 1,178	2,151 ± 1,050	66.1 ± 70.9	76.3 ± 175	14.1 ± 28.0
		Min	0.46	50.97	1.79	8.23	664	8.17	0.425	1.12
		Max	583	523	1,837	3,628	3,898	215	473	82.7
MSUP	sulfide stringer (hanging wall)	Py (4, 1)	92.5	180	39.1	23.0	1,887	—	28.1	0.921
		Min	—	—	—	—	—	—	—	—
		Max	—	—	—	—	—	—	—	—
MSUP	semi-massive to massive sulfides	Py (7, 5)	348 ± 383	120 ± 80.2	141 ± 130	8.73	1,322 ± 529	1,099 ± 492	—	2.78 ± 1.46
		Min	112	38.2	49.6	8.73	835	705	—	1.75
		Max	1,028	240	290	8.73	2,192	1,847	—	3.81
MSUP	sulfide stringer horizon	Py (13, 3)	134 ± 35.0	69.5	—	—	1,652 ± 718	160 ± 39.4	0.916	1.80 ± 1.59
		Min	98.9	69.5	—	—	823	123	0.916	0.678
		Max	169	69.5	—	—	2,077	202	0.916	2.92
MSUP	All	Py (24, 9)	248 ± 296	121 ± 72.8	115 ± 118	15.9 ± 10.1	1,495 ± 562	747 ± 612	14.5 ± 19.2	2.02 ± 1.33
		Min	92.5	38.2	39.1	8.73	823	123	0.916	0.678
		Max	1,028	240	290	23.0	2,192	1,847	28.1	3.81
MSDP	semi-massive to massive sulfides	Py (7, 4)	362 ± 358	47.4 ± 41.8	1.66 ± 1.41	26.0 ± 21.8	1,107 ± 249	49.9 ± 27.6	3.73 ± 3.90	1.80 ± 2.39
		Min	12.8	19.4	0.669	10.6	798	34.1	0.298	0.110
		Max	792	95.4	2.66	41.4	1,361	91.3	7.96	3.49
MSDP	sulfide stringer horizon	Py (3, 2)	176 ± 51.2	28.5	149 ± 35.1	148 ± 205	619 ± 596	76.7 ± 66.9	—	0.568
		Min	140	28.5	124	2.95	198	29.5	—	0.568
		Max	212	28.5	174	293	1,040	124	—	0.568
MSDP	All	Py (10, 6)	300 ± 294	34.1 ± 36.1	75.4 ± 87.5	87.0 ± 138	944 ± 414	58.9 ± 39.3	3.73 ± 3.90	1.39 ± 1.83
		Min	12.78	0.00	0.67	2.95	198	29.5	0.298	0.110
		Max	792	95.4	174	293	1,361	124	7.96	3.49
LFWZ	LFWZ	Py (16, 8)	460 ± 463	416 ± 575	439 ± 488	2.98	875 ± 1,107	686 ± 338	—	1.41 ± 1.70
		Min	60.4	94.5	93.5	2.98	43.1	59.2	—	0.31
		Max	1,363	1,578	784	2.98	2,716	1,063	—	3.37
MING	All	Py (125, 45)	276 ± 298	184 ± 270	533 ± 1,140	302 ± 805	1,694 ± 1,267	335 ± 426	52.2 ± 130	6.07 ± 16.9
		Min	0.458	19.379	0.669	2.95	43.08	8.17	0.298	0.110
		Max	1,363	1,578	5,378	3,628	5,732	1,847	473	82.7

Table A5-6. (cont.)

Ore body	Mineralization style	Mineral phase*	Cd	Sn	Sb	Te	Au	Ti	Pb	Bi
1807	semi-massive to massive sulfides**	Py (33, 8)	5.29 ± 6.04	3.88 ± 3.23	10.9 ± 15.0	28.8 ± 20.6	1.84 ± 1.26	6.57	135 ± 257	14.9 ± 26.0
		Av ± stdev								
		Min	1.02	0.897	1.34	3.17	0.088	6.57	0.096	0.023
		Max	9.56	7.49	33.0	52.4	2.98	6.57	709	66.5
1806	silicified horizon	Py (4, 2)			1.35 ± 1.07	6.72			3.67 ± 2.15	0.217 ± 0.016
		Av ± stdev								
		Min		0.427	0.596	6.72			2.15	0.206
		Max		0.427	2.10	6.72			5.18	0.229
1806	semi-massive to massive sulfides	Py (34, 8)	11.3 ± 17.3	78.9 ± 184	5.73 ± 6.66	3.68 ± 0.521	0.536 ± 0.548	1.06 ± 0.561	193 ± 248	1.29 ± 0.202
		Av ± stdev								
		Min	1.31	0.582	0.303	3.31	0.087	0.191	4.95	0.041
		Max	37.2	496	19.6	4.04	1.36	1.75	625	5.19
1806	sulfide stringer horizon	Py (4, 4)			1.16				1.86	
		Av ± stdev								
		Min		0.558	1.16				1.86	
		Max		0.558	1.16				1.86	
1806	All	Py (42, 14)	11.3 ± 17.3	51.5 ± 163	4.52 ± 5.95	4.69 ± 1.80	0.536 ± 0.548	1.06 ± 0.561	142 ± 225	1.02 ± 1.77
		Av ± stdev								
		Min	1.31	0.427	0.303	3.31	0.087	0.191	1.86	0.041
		Max	37.2	496	19.6	6.72	1.36	1.75	625	5.19
MSUP	sulfide stringer (hanging wall)	Py (4, 1)			38.2			0.686	32.2	
		Av ± stdev								
		Min								
		Max								
MSUP	semi-massive to massive sulfides	Py (7, 5)			8.13 ± 6.24	251 ± 153	0.106	0.163 ± 0.148	24.1 ± 38.1	6.98 ± 9.83
		Av ± stdev								
		Min			1.06	87.1	0.106	0.058	0.069	0.052
		Max			12.9	391	0.106	0.267	89.6	23.0
MSUP	sulfide stringer horizon	Py (13, 3)			8.01 ± 8.74				18.0 ± 14.8	8.46 ± 9.85
		Av ± stdev								
		Min			1.83				7.51	1.50
		Max			14.2				28.4	15.4
MSUP	All	Py (24, 9)			13.1 ± 13.5	251 ± 153	0.106	0.337 ± 0.320	23.6 ± 29.7	7.40 ± 9.01
		Av ± stdev								
		Min			1.06	87.1	0.106	0.058	0.069	0.052
		Max			38.2	391	0.106	0.686	89.6	23.0
MSDP	semi-massive to massive sulfides	Py (7, 4)	3.19	0.473 ± 0.369	1.34 ± 1.31	4.08	0.830	0.890	106 ± 192	2.18 ± 3.27
		Av ± stdev								
		Min	3.19	0.212	0.264	4.08	0.083	0.089	0.544	0.243
		Max	3.19	0.734	2.80	4.08	0.083	0.089	394	5.96
MSDP	sulfide stringer horizon	Py (3, 2)	6.41		1.29 ± 1.43	10.2 ± 12.1			21.8 ± 29.7	4.84 ± 2.41
		Av ± stdev								
		Min	6.41		0.284	1.66			0.741	3.13
		Max	6.41		2.30	18.8			42.8	6.54
MSDP	All	Py (10, 6)	4.80 ± 2.28	0.473 ± 0.369	1.32 ± 1.17	8.17 ± 9.26	0.083	0.089	78.0 ± 156	3.24 ± 2.99
		Av ± stdev								
		Min	3.19	0.212	0.264	1.66	0.083	0.089	0.544	0.243
		Max	6.41	0.734	2.80	18.8	0.083	0.089	394	6.54
LFWZ	LFWZ	Py (16, 8)			0.818 ± 0.570	28.6 ± 17.1			5.31 ± 2.98	2.70 ± 1.40
		Av ± stdev								
		Min		0.217	0.170	7.14			1.08	1.21
		Max		0.217	1.55	52.4			9.92	4.96
MING	All	Py (125, 45)	8.15 ± 12.1	35.6 ± 123	6.06 ± 9.45	56.8 ± 102	0.931 ± 1.07	1.30 ± 1.94	84.0 ± 177	5.68 ± 12.3
		Av ± stdev								
		Min	1.02	0.212	0.170	1.66	0.083	0.058	0.069	0.023
		Max	37.2	496	38.2	391	2.98	6.57	709	66.5

\* Numbers in brackets are number of EPMA analysis, number of LA-ICP-MS analysis

\*\* Samples from 1807 Zone are exclusively from semi-massive to massive sulfides

Table A5-6. Results of EPMA analysis (major elements in wt%) and LA-ICP-MS analysis (trace elements in ppm) for chalcopyrite; – not detected or below detection limit

Ore body	Mineralization style	Mineral phase*	S [wt %]	Cu	Fe	Total	Mineral Formula	Ti [ppm]	V	Cr
1807	semi-massive to massive sulfides**	Ccp (35, 12)	Av ± stdev Min Max	34.75 ± 0.307 34.03 35.28	30.63 ± 0.251 30.10 31.20	99.80 ± 0.467 98.77 100.79	$\text{Cu}_{0.98-1.02}\text{Fe}_{0.99-1.04}\text{S}_2$	12.4 ± 4.03 5.58 19.9	35.5 ± 49.6 0.392 70.5	6.01 6.01 6.01
1806	silicified horizon	Ccp (17, 9)	Av ± stdev Min Max	35.08 ± 0.190 34.74 35.55	30.28 ± 0.309 29.69 30.72	99.74 ± 0.385 98.91 100.44	$\text{Cu}_{0.97-1.00}\text{Fe}_{0.96-1.01}\text{S}_2$	5.80 ± 1.97 4.05 9.22	5.96 5.96 5.96	– – –
1806	semi-massive to massive sulfides	Ccp (31, 6)	Av ± stdev Min Max	35.13 ± 0.298 34.78 36.13	30.17 ± 0.404 29.16 30.77	99.74 ± 0.487 98.71 101.26	$\text{Cu}_{0.96-1.02}\text{Fe}_{0.94-1.02}\text{S}_2$	6.64 ± 1.94 4.51 9.50	37.5 ± 60.1 0.357 107	25.2 25.2 25.2
1806	sulfide stringer horizon	Ccp (9, 4)	Av ± stdev Min Max	34.98 ± 0.216 34.59 35.35	30.34 ± 0.146 30.11 30.49	100.00 ± 0.473 99.22 100.77	$\text{Cu}_{0.99-1.01}\text{Fe}_{0.99-1.00}\text{S}_2$	5.20 ± 2.17 2.38 7.59	– – –	– – –
1806	All	Ccp (57, 19)	Av ± stdev Min Max	35.09 ± 0.259 34.59 36.13	30.23 ± 0.351 29.16 30.77	99.78 ± 0.459 98.71 101.26	$\text{Cu}_{0.96-1.02}\text{Fe}_{0.94-1.02}\text{S}_2$	5.96 ± 1.96 2.38 9.50	29.6 ± 51.5 0.357 107	25.2 25.2 25.2
MSUP	sulfide stringer (hanging wall)	Ccp (4, 1)	Av ± stdev Min Max	34.66 ± 0.127 34.47 34.75	30.99 ± 0.364 30.57 31.46	99.95 ± 0.641 99.03 100.49	$\text{Cu}_{0.99-1.00}\text{Fe}_{1.02-1.04}\text{S}_2$	7.11 – –	– – –	– – –
MSUP	semi-massive to massive sulfides	Ccp (17, 7)	Av ± stdev Min Max	34.69 ± 0.393 33.61 35.50	30.75 ± 0.223 30.44 31.27	99.94 ± 0.424 99.03 100.85	$\text{Cu}_{0.98-1.04}\text{Fe}_{1.00-1.05}\text{S}_2$	11.6 ± 4.22 6.85 17.5	0.16 0.163 0.163	– – –
MSUP	sulfide stringer horizon	Ccp (19, 3)	Av ± stdev Min Max	34.82 ± 0.208 34.42 35.21	30.67 ± 0.175 30.28 30.93	99.92 ± 0.393 99.15 100.57	$\text{Cu}_{0.99-1.01}\text{Fe}_{1.00-1.02}\text{S}_2$	9.70 ± 3.22 7.42 12.0	– – –	– – –
MSUP	All	Ccp (40, 11)	Av ± stdev Min Max	34.75 ± 0.299 33.61 35.50	30.74 ± 0.231 30.28 31.46	99.93 ± 0.420 99.03 100.85	$\text{Cu}_{0.98-1.04}\text{Fe}_{1.00-1.05}\text{S}_2$	10.8 ± 3.92 6.85 17.5	0.163 0.163 0.163	– – –
MSDP	semi-massive to massive sulfides	Ccp (12, 3)	Av ± stdev Min Max	34.80 ± 0.272 34.06 35.13	30.45 ± 0.228 30.13 30.74	99.58 ± 0.426 98.94 100.25	$\text{Cu}_{0.98-1.02}\text{Fe}_{0.99-1.02}\text{S}_2$	9.51 9.51 9.51	– – –	5.76 5.76 5.76
MSDP	sulfide stringer horizon	Ccp (4, 2)	Av ± stdev Min Max	34.77 ± 0.135 34.65 34.95	30.72 ± 0.242 30.37 30.93	99.94 ± 0.251 99.75 100.31	$\text{Cu}_{0.99-1.01}\text{Fe}_{1.00-1.02}\text{S}_2$	4.28 4.28 4.28	– – –	– – –
MSDP	All	Ccp (16, 5)	Av ± stdev Min Max	34.79 ± 0.241 34.06 35.13	30.52 ± 0.253 30.13 30.93	99.67 ± 0.414 98.94 100.31	$\text{Cu}_{0.98-1.02}\text{Fe}_{0.99-1.02}\text{S}_2$	6.90 ± 3.70 4.28 9.51	– – –	5.76 5.76 5.76
LFWZ	LFWZ	Ccp (28, 14)	Av ± stdev Min Max	34.83 ± 0.230 34.37 35.19	30.64 ± 0.173 30.14 30.87	100.04 ± 0.257 99.46 100.53	$\text{Cu}_{0.98-1.02}\text{Fe}_{0.99-1.03}\text{S}_2$	6.38 ± 1.69 4.07 9.79	0.770 0.770 0.770	– – –
MING	All	Ccp (176, 61)	Av ± stdev Min Max	34.88 ± 0.309 33.61 36.13	30.52 ± 0.341 29.16 31.46	99.85 ± 0.432 98.71 101.26	$\text{Cu}_{0.96-1.06}\text{Fe}_{0.94-1.05}\text{S}_2$	8.39 ± 3.95 2.38 19.9	23.8 ± 41.3 0.163 107	12.3 ± 11.2 5.76 25.2

Table C2-2. (cont.)

Ore body	Mineralization style	Mineral phase*	Min	Co	Ni	Zn	As	Se	Mo	Ag
1807	semi-massive to massive sulfides**	Ccp (35, 12)	Av $\pm$ stdev	34.9 $\pm$ 67.4	23.6	705 $\pm$ 322	768 $\pm$ 631	301 $\pm$ 66.4	7.64 $\pm$ 8.01	35.7 $\pm$ 20.1
			Min	1.13	23.6	364	33.09	218	2.34	9.59
			Max	198	23.6	1,431	1,731	420	16.9	74.3
1806	silicified horizon	Ccp (17, 9)	Av $\pm$ stdev	—	—	732 $\pm$ 205	817 $\pm$ 1,343	181 $\pm$ 64.5	—	598 $\pm$ 256
			Min	—	—	302	101	68.5	—	265
			Max	—	—	1,017	4,101	293	—	979
1806	semi-massive to massive sulfides	Ccp (31, 6)	Av $\pm$ stdev	59.9	—	487 $\pm$ 207	1,345 $\pm$ 1,324	220 $\pm$ 125	38.0	163 $\pm$ 157
			Min	59.9	—	165	382	4.30	38.0	13.3
			Max	59.9	—	781	3,567	347	38.0	326
1806	sulfide stringer horizon	Ccp (9, 4)	Av $\pm$ stdev	—	—	495 $\pm$ 68.7	1,208 $\pm$ 1,038	93.2 $\pm$ 41.5	8.54	43.1 $\pm$ 14.5
			Min	—	—	406	480	59.1	8.54	25.3
			Max	—	—	568	2,397	150	8.54	58.5
1806	All	Ccp (57, 19)	Av $\pm$ stdev	59.9	—	604 $\pm$ 216	1,058 $\pm$ 1,247	175 $\pm$ 92.9	23.2 $\pm$ 20.8	344 $\pm$ 316
			Min	59.9	—	165	101	4.30	8.54	13.3
			Max	59.9	—	1,017	4,101	347	37.95	979
MSUP	sulfide stringer (hanging wall)	Ccp (4, 1)	Av $\pm$ stdev	—	—	705	365	39.9	—	221
			Min	—	—	—	—	—	—	—
			Max	—	—	—	—	—	—	—
MSUP	semi-massive to massive sulfides	Ccp (17, 7)	Av $\pm$ stdev	168 $\pm$ 190	130 $\pm$ 141	778 $\pm$ 205	745 $\pm$ 781	1,281 $\pm$ 899	—	17.5 $\pm$ 10.4
			Min	1.44	30.4	421	156	616	—	9.35
			Max	390	230	1,044	1,899	2,896	—	36.5
MSUP	sulfide stringer horizon	Ccp (19, 3)	Av $\pm$ stdev	2.36 $\pm$ 2.83	—	482 $\pm$ 108	358 $\pm$ 411	774 $\pm$ 57.3	—	39.5 $\pm$ 2.23
			Min	0.356	—	375	110	708	—	37.9
			Max	4.36	—	591	832	808	—	42.1
MSUP	All	Ccp (40, 11)	Av $\pm$ stdev	113 $\pm$ 171	130 $\pm$ 141	691 $\pm$ 215	605 $\pm$ 662	1,030 $\pm$ 804	—	42.0 $\pm$ 60.9
			Min	0.356	30.4	375	110	39.9	—	9.35
			Max	390	230	1,044	1,899	2,896	—	221
MSDP	semi-massive to massive sulfides	Ccp (12, 3)	Av $\pm$ stdev	—	—	457 $\pm$ 101	3,816 $\pm$ 3,441	66.5 $\pm$ 11.7	49.7	82.5 $\pm$ 58.3
			Min	—	—	341	125	58.3	49.7	15.2
			Max	—	—	527	6,936	80.0	49.7	118
MSDP	sulfide stringer horizon	Ccp (4, 2)	Av $\pm$ stdev	0.394 $\pm$ 0.187	—	659 $\pm$ 83.3	268 $\pm$ 4.07	187 $\pm$ 12.1	—	65.9 $\pm$ 1.23
			Min	0.262	—	600	265	179	—	65.1
			Max	0.526	—	718	271	196	—	66.8
MSDP	All	Ccp (16, 5)	Av $\pm$ stdev	0.394 $\pm$ 0.187	—	538 $\pm$ 138	2,397 $\pm$ 3,114	115 $\pm$ 67.0	49.7	75.9 $\pm$ 42.2
			Min	0.262	—	341	125	58.3	49.7	15.2
			Max	0.526	—	718	6,936	196	49.7	118
LFWZ	LFWZ	Ccp (28, 14)	Av $\pm$ stdev	3.28 $\pm$ 2.34	—	679 $\pm$ 288	535 $\pm$ 1,304	544 $\pm$ 210	—	24.0 $\pm$ 12.8
			Min	0.414	—	270	22.9	211	—	7.27
			Max	26.1	—	1,311	4,270	869	—	50.2
MING	All	Ccp (176, 61)	Av $\pm$ stdev	10.6 $\pm$ 15.9	94.6 $\pm$ 117	652 $\pm$ 121	909 $\pm$ 1,379	434 $\pm$ 472	19.9 $\pm$ 19.6	133 $\pm$ 227
			Min	1.07	23.6	165	22.9	4.30	2.34	7.27
			Max	56.4	230	1,431	6,936	2,896	49.7	979

Table C2-2. (cont.)

Ore body	Mineralization style	Mineral phase*	Cd	Sn	Sb	Te	Au	Ti	Pb	Bi
1807	semi-massive to massive sulfides**	Ccp (35, 12)	16.6 ± 7.43	69.1 ± 43.7	8.93 ± 6.75	7.22 ± 3.76	0.379 ± 0.424	0.738 ± 0.656	79.9 ± 105	5.03 ± 5.07
		Av ± stdev								
		Min	5.02	14.6	1.59	3.65	0.086	0.083	8.37	0.735
		Max	31.7	141	25.0	12.0	1.35	1.95	369	14.9
1806	silicified horizon	Ccp (17, 9)	9.47 ± 4.07	203 ± 101	5.41 ± 5.88	2.92 ± 1.31	21.1 ± 18.0	0.189 ± 0.211	4.76 ± 7.96	0.207 ± 0.129
		Av ± stdev								
		Min	4.79	102	0.258	1.08	0.405	0.037	0.100	0.116
		Max	16.86	375	15.0	4.84	33.5	0.602	24.6	0.298
1806	semi-massive to massive sulfides	Ccp (31, 6)	5.19 ± 2.56	452 ± 277	14.6 ± 10.7	4.69 ± 2.27	0.166 ± 0.026	0.748 ± 0.461	110 ± 233	0.746 ± 0.455
		Av ± stdev								
		Min	0.751	251	2.31	3.09	0.147	0.112	1.33	0.260
		Max	7.92	982	25.2	6.29	0.185	1.26	584	1.35
1806	sulfide stringer horizon	Ccp (9, 4)	4.65 ± 1.16	209 ± 76.4	6.44 ± 6.06	—	3.16 ± 3.01	0.175 ± 0.079	5.63 ± 8.07	—
		Av ± stdev								
		Min	3.05	142	1.03	—	1.29	0.119	0.561	—
		Max	5.68	288	13.7	—	7.62	0.231	17.7	—
1806	All	Ccp (57, 19)	7.10 ± 3.84	283 ± 202	8.69 ± 8.55	3.24 ± 1.55	8.47 ± 13.3	0.427 ± 0.427	38.1 ± 133	0.566 ± 0.453
		Av ± stdev								
		Min	0.751	102	0.258	1.08	0.147	0.037	0.100	0.116
		Max	16.9	982	25.2	6.29	33.5	1.26	584	1.35
MSUP	sulfide stringer (hanging wall)	Ccp (4, 1)	6.28	95.9	8.47	—	0.145	0.201	4.45	—
		Av ± stdev								
		Min	—	—	—	—	—	—	—	—
		Max	—	—	—	—	—	—	—	—
MSUP	semi-massive to massive sulfides	Ccp (17, 7)	12.5 ± 4.53	52.2 ± 49.9	8.18 ± 13.1	3.74 ± 1.89	0.725 ± 0.634	0.965 ± 1.57	20.4 ± 30.7	1.80 ± 0.835
		Av ± stdev								
		Min	7.38	8.45	0.828	1.78	0.292	0.051	2.12	0.200
		Max	19.7	120	37.5	7.68	1.81	3.75	89.1	2.89
MSUP	sulfide stringer horizon	Ccp (19, 3)	7.83 ± 1.24	23.4 ± 4.29	6.07 ± 5.76	6.47 ± 2.91	0.208 ± 0.155	0.248 ± 0.142	14.0 ± 13.1	2.38 ± 1.42
		Av ± stdev								
		Min	6.90	19.3	1.70	3.73	0.098	0.153	4.14	1.31
		Max	9.24	27.9	12.6	9.52	0.318	0.411	28.9	4.05
MSUP	All	Ccp (40, 11)	10.7 ± 4.40	48.3 ± 43.8	7.63 ± 10.6	4.56 ± 2.45	0.523 ± 0.558	0.641 ± 1.18	17.2 ± 25.0	2.00 ± 1.01
		Av ± stdev								
		Min	6.28	8.45	0.828	1.78	0.098	0.051	2.12	0.200
		Max	19.7	120	37.5	9.52	1.81	3.75	89.1	4.05
MSDP	semi-massive to massive sulfides	Ccp (12, 3)	45.9 ± 39.6	213 ± 262	15.4 ± 15.3	3.68	0.144	0.816 ± 0.755	532 ± 730	3.43 ± 3.07
		Av ± stdev								
		Min	18.0	48.5	4.12	3.68	0.144	0.282	6.45	1.63
		Max	73.9	515	32.9	3.68	0.144	1.35	1,366	6.97
MSDP	sulfide stringer horizon	Ccp (4, 2)	19.0 ± 0.925	13.0 ± 1.04	1.33 ± 0.091	8.85 ± 4.54	0.121	0.224 ± 0.002	6.19 ± 2.61	1.87 ± 0.509
		Av ± stdev								
		Min	18.4	12.2	1.26	5.64	0.121	0.223	4.34	1.51
		Max	19.7	13.7	1.39	12.1	0.121	0.225	8.04	2.23
MSDP	All	Ccp (16, 5)	32.5 ± 27.6	133 ± 215	9.77 ± 13.3	7.13 ± 4.39	0.132 ± 0.017	0.520 ± 0.554	322 ± 591	2.80 ± 2.34
		Av ± stdev								
		Min	18.0	12.2	1.26	3.68	0.121	0.223	4.34	1.51
		Max	73.9	515	32.9	12.1	0.144	1.35	1,366	6.97
LFWZ	LFWZ	Ccp (28, 14)	18.4 ± 7.87	43.7 ± 19.5	1.10 ± 1.99	5.37 ± 3.43	0.793 ± 1.26	0.554 ± 0.974	10.9 ± 10.5	1.75 ± 1.43
		Av ± stdev								
		Min	8.47	17.1	0.049	1.44	0.062	0.018	2.36	0.302
		Max	38.4	76.7	7.53	12.5	3.01	2.29	43.3	5.15
MING	All	Ccp (176, 61)	14.0 ± 10.8	131 ± 165	6.93 ± 8.54	5.03 ± 3.13	2.74 ± 7.68	0.571 ± 0.743	59.6 ± 194	2.60 ± 3.13
		Av ± stdev								
		Min	0.751	8.45	0.049	1.08	0.062	0.018	0.100	0.116
		Max	73.9	982	37.5	12.5	33.5	3.75	1,366	14.9

\* Numbers in brackets are number of EPMA analysis, number of LA-ICP-MS analysis

\*\* Samples from 1807 Zone are exclusively from semi-massive to massive sulfides



Table A5-6. Results of EPMA analysis (major elements in wt%) and LA-ICP-MS analysis (trace elements in in ppm) for cubanite from the LFWZ; – not detected or below detection limit

Ore body <sup>s</sup>	Mineralization style	Mineral phase*	S [wt %]	Cu	Fe	Total	Mineral Formula	Ti [ppm]	V	Cr
LFWZ	LFWZ	Cbn (28, 14)	Av ± stdev	23.40 ± 0.199	41.33 ± 0.294	99.86 ± 0.160	Cu <sub>0.98-1.02</sub> Fe <sub>2.00-2.07</sub> S <sub>3</sub>	5.24 ± 1.24	–	–
		Min	34.80	22.83	40.92	99.67		3.60	–	–
		Max	35.39	23.63	42.26	100.21		6.73	–	–

Table A5-6... (cont.)

Ore body <sup>s</sup>	Mineralization style	Mineral phase*	Av ± stdev	Min	Co	Ni	Zn	As	Se	Mo	Ag
LFWZ	LFWZ	Ccp (28, 14)	Av ± stdev	–	12.3 ± 20.3	24.2 ± 12.6	635 ± 368	44.6 ± 8.11	790 ± 45.6	–	47.0 ± 13.6
			Min	–	0.507	15.3	287	35.2	737	–	31.5
			Max	–	57.4	33.1	1,259	57.7	861	–	69.3

Table A5-6... (cont.)

Ore body <sup>§</sup>	Mineralization style	Mineral phase*	Cd	Sn	Sb	Te	Au	Tl	Pb	Bi
LFWZ	LFWZ	Ccp (28, 14)	Av ± stdev	23.2 ± 19.5	0.432 ± 0.417	10.5 ± 1.34	–	0.056	29.7 ± 9.72	1.33 ± 0.750
			Min	8.37	0.125	8.61	–	0.056	18.3	0.671
			Max	54.6	1.06	12.4	–	0.056	44.2	2.67

<sup>§</sup> Cubanite was only analyzed by both EPMA and LA-ICP-MS for the LFWZ

\* Numbers in brackets are number of EPMA analysis, number of LA-ICP-MS analysis

\*\* Samples from 1807 Zone are exclusively from semi-massive to massive sulfides

Table A5-6. Results of EPMA analysis (major elements in wt%) and LA-ICP-MS analysis (trace elements in ppm) for pyrrhotite; – not detected or below detection limit, NA – nc

Ore body <sup>s</sup>	Mineralization style	Mineral phase*	S [wt %]	Fe	Total	Mineral Formula	Ti [ppm]	V	Cr	Mn
1807	semi-massive to massive sulfides**	Po (10, 5)	Av ± stdev Min Max	38.93 ± 0.268 38.20 59.81	60.57 ± 0.368 99.50 ± 0.381	Fe <sub>0.88±0.92</sub> S	8.25 ± 2.89 5.44 105	105	12.6 12.6 12.6	12.0 12.0 12.0
1806	sulfidized horizon	Po (6, 6)	Av ± stdev Min Max	39.32 ± 0.304 38.85 59.63	60.11 ± 0.245 99.43 ± 0.514	Fe <sub>0.87±0.88</sub> S	5.54 ± 2.19 3.07 102	1.41 ± 0.427 1.02 1.87	2.53 ± 1.53 1.45 3.61	12.9 ± 8.99 3.67 21.64
1806	semi-massive to massive sulfides	Po (6, 3)	Av ± stdev Min Max	39.60 ± 0.432 39.01 40.14	60.15 ± 0.411 99.75 ± 0.599	Fe <sub>0.86±0.88</sub> S	9.66 ± 9.05 2.63 19.9	64.6 ± 73.0 13.0 116	7.37 ± 0.571 6.96 7.77	42.4 ± 50.7 6.54 78.3
1806	All	Po (12, 9)	Av ± stdev Min Max	39.46 ± 0.385 38.85 59.63	60.13 ± 0.323 99.59 ± 0.558	Fe <sub>0.86±0.88</sub> S	7.60 ± 6.31 2.63 102	26.7 ± 50.3 1.02 116	4.95 ± 2.95 1.45 7.77	24.7 ± 30.8 3.67 78.3
MSUP	sulfide stringer (hanging wall)	Po (3, 0)	Av ± stdev Min Max	39.82 ± 0.178 39.62 58.11	58.32 ± 0.187 98.14 ± 0.096	Fe <sub>0.84±0.85</sub> S	NA NA NA	NA NA NA	NA NA NA	NA NA NA
MSUP	semi-massive to massive sulfides	Po (16, 3)	Av ± stdev Min Max	38.56 ± 0.215 38.29 59.26	60.64 ± 0.633 99.19 ± 0.599	Fe <sub>0.87±0.92</sub> S	12.0 ± 12.3 3.12 26.1	– – –	– – –	10.9 10.9 10.9
MSUP	sulfide stringer horizon	Po (9, 3)	Av ± stdev Min Max	39.24 ± 0.245 38.99 61.13	60.21 ± 0.494 99.44 ± 0.478	Fe <sub>0.87±0.90</sub> S	8.05 ± 0.300 7.84 100.21	– – –	– – –	– – –
MSUP	All	Po (28, 6)	Av ± stdev Min Max	38.91 ± 0.496 38.29 59.81	60.25 ± 0.896 99.16 ± 0.642	Fe <sub>0.84±0.92</sub> S	10.4 ± 8.98 3.12 26.1	– – –	– – –	10.9 10.9 10.9
MSDP	semi-massive to massive sulfides	Po (8, 2)	Av ± stdev Min Max	39.13 ± 0.255 38.70 59.52	59.86 ± 0.306 98.98 ± 0.240	Fe <sub>0.87±0.90</sub> S	10.6 ± 7.24 5.44 15.7	11.9 11.9 11.9	3.40 3.40 3.40	102 102 102
MSDP	sulfide stringer horizon	Po (3, 2)	Av ± stdev Min Max	38.91 ± 0.296 38.57 60.32	60.49 ± 0.237 99.39 ± 0.452	Fe <sub>0.88±0.90</sub> S	7.29 7.29 98.89	– – –	– – –	– – –
MSDP	All	Po (11, 4)	Av ± stdev Min Max	39.07 ± 0.271 38.57 59.52	60.03 ± 0.404 99.10 ± 0.343	Fe <sub>0.87±0.90</sub> S	9.47 ± 5.46 5.44 15.7	11.9 11.9 11.9	3.4 3.40 3.40	102 102 102
LFWZ	LFWZ	Po (22, 10)	Av ± stdev Min Max	38.61 ± 0.219 38.20 59.63	60.73 ± 0.306 99.34 ± 0.433	Fe <sub>0.88±0.92</sub> S	9.03 ± 5.75 4.78 20.0	6.98 ± 8.32 1.10 12.9	10.3 10.3 10.3	13.8 ± 4.93 10.3 17.3
MING	All	Po (83, 34)	Av ± stdev Min Max	38.93 ± 0.456 38.20 40.14	60.37 ± 0.637 99.30 ± 0.535	Fe <sub>0.84±0.92</sub> S	8.88 ± 5.87 2.63 26.1	29.4 ± 46.5 1.02 116	6.58 ± 4.02 1.45 12.6	27.6 ± 33.9 3.67 102

Table A5-6. (cont.)

Ore body <sup>s</sup>	Mineralization style	Mineral phase*	Co	Ni	Cu	Zn	As	Se	Mo	Ag
1807	semi-massive to massive sulfides**	Po (10, 5)	63.8 ± 78.1	—	416 ± 400	292 ± 393	1,503 ± 1,272	272 ± 136	306 ± 484	3.70 ± 2.21
		Min	1.14	—	3.57	13.5	227	125	3.39	1.51
		Max	176	—	837	570	3,183	490	865	6.12
1806	sulfidized horizon	Po (6, 6)	—	45.0 ± 21.9	14.2 ± 11.4	7.77 ± 3.50	397 ± 269	155 ± 27.3	0.964	89.5 ± 99.2
		Min	—	13.2	3.28	5.29	193	93.4	0.964	4.51
		Max	—	67.4	31.4	10.2	933	169	0.964	259
1806	semi-massive to massive sulfides	Po (6, 3)	2.10 ± 1.35	180 ± 32.3	542	40.4	477 ± 102	232 ± 141	723	5.57 ± 4.02
		Min	1.14	143	542	40.4	360	69.9	723	1.66
		Max	3.05	201	542	40.4	547	323	723	9.70
1806	All	Po (12, 9)	2.10 ± 1.35	95.6 ± 73.8	102 ± 216	18.6 ± 19.0	424 ± 222	173 ± 86.0	362 ± 510	58.1 ± 86.7
		Min	1.14	13.2	3.28	5.29	193	69.9	0.964	1.66
		Max	3.05	201	542	40.4	933	323	723	259
MSUP	sulfide stringer (hanging wall)	Po (3, 0)	NA	NA	NA	NA	NA	NA	NA	NA
		Min	NA	NA	NA	NA	NA	NA	NA	NA
		Max	NA	NA	NA	NA	NA	NA	NA	NA
MSUP	semi-massive to massive sulfides	Po (16, 3)	77.7 ± 32.5	176.0	20.20	1,370 ± 1,851	784 ± 331	1,072 ± 850	—	1.33 ± 0.803
		Min	55.8	176	20.2	60.9	528	578	—	0.848
		Max	115	176	20.2	2,678	1,157	2,054	—	2.25
MSUP	sulfide stringer horizon	Po (9, 3)	34.3 ± 40.5	48.6	8.043	239 ± 39.0	1,410 ± 1,119	404 ± 69.9	—	3.67 ± 1.40
		Min	3.99	48.6	8.043	211	149	348	—	2.68
		Max	80.3	48.6	8.043	266	2,285	482	—	4.66
MSUP	All	Po (28, 6)	56.0 ± 40.6	112 ± 89.9	4,032 ± 5,673	804 ± 1,253	1,097 ± 814	738 ± 652	—	2.26 ± 1.57
		Min	3.99	48.6	20.2	60.9	149	348	—	0.85
		Max	115	176	8.043	2,678	2,285	2,054	—	4.66
MSDP	semi-massive to massive sulfides	Po (8, 2)	122 ± 83.2	55.0	369 ± 23.7	27.5	3,082 ± 920	94.9 ± 17.6	—	16.9 ± 4.19
		Min	63.3	55.0	352	27.5	2,431	82.4	—	14.0
		Max	181	55.0	386	27.5	3,733	107	—	19.9
MSDP	sulfide stringer horizon	Po (3, 2)	16.0 ± 2.98	111	876 ± 1,238	338 ± 461	466 ± 137	135 ± 52.0	—	4.73 ± 3.22
		Min	14.1	111	0.729	12.2	370	98.4	—	2.45
		Max	17.9	111	1,751	664	563	172	—	7.00
MSDP	All	Po (11, 4)	69.1 ± 77.8	82.8 ± 39.3	623 ± 772	235 ± 372	1,774 ± 1,603	115 ± 39.3	—	10.8 ± 7.68
		Min	14.1	55.0	0.729	12.2	370	82.4	—	2.45
		Max	181	111	1,751	664	3,733	172	—	19.9
LFWZ	LFWZ	Po (22, 10)	202 ± 217	224 ± 167	329 ± 561	446 ± 352	983 ± 2,195	407 ± 178	—	4.45 ± 6.01
		Min	52.1	64.8	3.53	3.04	34.1	198	—	0.502
		Max	671	529	976	864	6,774	670	—	20.3
MING	All	Po (83, 34)	111 ± 156	151 ± 133	712 ± 1,787	396 ± 669	1,025 ± 1,435	349 ± 349	329 ± 428	18.2 ± 47.6
		Min	1.14	13.2	0.729	3.04	34.1	69.9	0.964	0.502
		Max	671	529	8,043	2,678	6,774	2,054	865	259

Table A5-6. (cont.)

Ore body <sup>§</sup>	Mineralization style	Mineral phase*	Cd	Sn	Sb	Te	Au	Ti	Pb	Bi
1807	semi-massive to massive sulfides**	Po (10, 5)	6.43	1.11 ± 1.40	15.3 ± 18.8	12.7 ± 9.22	0.743 ± 0.662	1.18 ± 0.551	2,655 ± 2,246	27.8 ± 21.8
		Min	6.43	0.346	3.33	4.30	0.152	0.585	145	8.43
		Max	6.43	3.21	48.7	25.4	1.45	2.01	6,168	60.0
1806	sulfidized horizon	Po (6, 6)	—	0.373 ± 0.103	18.3 ± 14.1	—	53.4 ± 83.0	0.558 ± 0.239	13.1 ± 9.14	0.174
		Min	—	0.301	7.04	—	0.391	0.388	2.35	0.174
		Max	—	0.446	37.3	—	149	0.974	25.28	0.174
1806	semi-massive to massive sulfides	Po (6, 3)	1.14	14.3 ± 18.1	2.02 ± 2.95	—	—	1.52 ± 1.83	139 ± 133	5.97 ± 4.80
		Min	1.14	1.58	0.209	—	—	0.024	34.7	2.07
		Max	1.14	27.1	5.42	—	—	3.55	289	11.3
1806	All	Po (12, 9)	1.14	7.36 ± 13.2	11.3 ± 13.3	—	53.4 ± 83.0	0.918 ± 1.11	60.4 ± 96.8	4.52 ± 4.87
		Min	1.14	0.301	0.209	—	0.391	0.024	2.35	0.174
		Max	1.14	27.1	37.3	—	149	3.55	289	11.3
MSUP	sulfide stringer (hanging wall)	Po (3, 0)	NA	NA	NA	NA	NA	NA	NA	NA
		Min	NA	NA	NA	NA	NA	NA	NA	NA
		Max	NA	NA	NA	NA	NA	NA	NA	NA
MSUP	semi-massive to massive sulfides	Po (16, 3)	13.6 ± 16.8	1.6	418 ± 591	46.1 ± 37.3	2.06	0.296 ± 0.362	460 ± 300	20.0 ± 26.0
		Min	1.70	1.58	0.140	4.16	2.06	0.040	207	2.36
		Max	25.5	1.58	836	75.5	2.06	0.55	791	49.9
MSUP	sulfide stringer horizon	Po (9, 3)	—	0.47	14.9 ± 22.6	6.74	—	0.782 ± 0.940	39.5 ± 32.0	3.55 ± 1.02
		Min	—	0.470	1.69	6.74	—	0.117	17.5	2.60
		Max	—	0.470	41.0	6.74	—	1.45	76.2	4.63
MSUP	All	Po (28, 6)	13.6 ± 16.8	1.02 ± 0.782	176 ± 369	36.3 ± 36.3	2.06	0.539 ± 0.646	250 ± 299	11.8 ± 18.8
		Min	1.70	0.470	0.140	4.16	2.06	0.040	17.5	2.36
		Max	25.5	1.58	836	75.5	2.06	1.45	791	49.9
MSDP	semi-massive to massive sulfides	Po (8, 2)	—	0.862	6.00 ± 1.83	9.71 ± 5.03	—	1.05 ± 0.536	1,812 ± 1,489	12.3 ± 4.16
		Min	—	0.862	4.70	6.15	—	0.675	759	9.38
		Max	—	0.862	7.29	13.3	—	1.43	2,865	15.3
MSDP	sulfide stringer horizon	Po (3, 2)	1.21	—	0.394 ± 0.475	—	—	—	6.03 ± 0.070	5.36 ± 1.39
		Min	1.21	—	0.058	—	—	—	5.98	4.37
		Max	1.21	—	0.731	—	—	—	6.08	6.34
MSDP	All	Po (11, 4)	1.21	0.862	3.20 ± 3.41	9.71 ± 5.03	—	1.05 ± 0.536	909 ± 1,351	8.84 ± 4.75
		Min	1.21	0.862	0.058	6.15	—	0.675	5.98	4.37
		Max	1.21	0.862	7.29	13.27	—	1.43	2,865	15.3
LFWZ	LFWZ	Po (22, 10)	11.6 ± 5.60	0.248 ± 0.139	0.569 ± 0.574	7.19 ± 6.14	0.934	0.189 ± 0.104	41.1 ± 81.3	2.71 ± 2.55
		Min	6.39	0.079	0.133	2.00	0.934	0.116	0.302	0.098
		Max	17.5	0.399	1.34	17.7	0.934	0.262	269	8.28
MING	All	Po (83, 34)	8.84 ± 8.75	2.38 ± 6.64	42.1 ± 166	16.8 ± 21.6	18.5 ± 49.1	0.851 ± 0.816	585 ± 1,298	10.0 ± 14.8
		Min	1.14	0.079	0.058	2.00	0.152	0.024	0.302	0.098
		Max	25.5	27.1	836	75.5	149	3.55	6,168	60.0

<sup>§</sup> Pyrrhotite was not analyzed by both EPMA and LA-ICP-MS for the silicified horizon of the 1806 Zone

\* Numbers in brackets are number of EPMA analysis, number of LA-ICP-MS analysis

\*\* Samples from 1807 Zone are exclusively from semi-massive to massive sulfides

Table A5-6. Results of EPMA analysis (major elements in wt%) and LA-ICP-MS analysis (trace elements in ppm) for sphalerite; – not detected or below detection limit

Ore body	Mineralization style	Mineral phase*	S [wt %]			Zn	Fe	Total	Mineral Formula	Ti [ppm]	V
1807	semi-massive to massive sulfides**	Sp (28, 7)	Av ± stdev	33.67 ± 0.251	59.12 ± 2.60	6.90 ± 2.37	99.70 ± 0.634	(Zn <sub>0.80-0.94</sub> ,Fe <sub>0.04-0.18</sub> ) <sub>0.96-0.99</sub> S	7.47 ± 2.49	1.53	
			Min	33.27	54.75	2.29	98.22		3.68	1.53	
			Max	34.07	64.19	10.18	100.70		11.0	1.53	
1806	silicified horizon	Sp (6, 1)	Av ± stdev	33.08 ± 0.306	62.22 ± 1.13	3.97 ± 1.16	99.27 ± 0.502	(Zn <sub>0.89-0.95</sub> ,Fe <sub>0.05-0.09</sub> ) <sub>0.98-1.00</sub> S	—	—	
			Min	32.67	60.60	2.91	98.77		—	—	
			Max	33.41	63.24	5.45	100.14		—	—	
1806	semi-massive to massive sulfides	Sp (17, 9)	Av ± stdev	33.14 ± 0.209	59.54 ± 4.04	6.40 ± 3.72	99.08 ± 0.576	(Zn <sub>0.82-0.97</sub> ,Fe <sub>0.02-0.17</sub> ) <sub>0.97-1.01</sub> S	6.98 ± 3.57	6.94 ± 10.3	
			Min	32.69	55.70	1.12	97.99		3.94	0.416	
			Max	33.52	65.28	10.16	99.86		13.9	18.8	
1806	sulfide stringer horizon	Sp (4, 2)	Av ± stdev	32.78 ± 0.325	62.19 ± 4.29	3.79 ± 3.96	98.76 ± 0.805	(Zn <sub>0.83-0.97</sub> ,Fe <sub>0.02-0.17</sub> ) <sub>0.98-1.00</sub> S	3.92	—	
			Min	32.33	55.79	1.42	98.10		3.92	—	
			Max	33.09	64.86	9.71	99.90		3.92	—	
1806	All	Sp (27, 12)	Av ± stdev	33.07 ± 0.270	60.53 ± 3.76	5.47 ± 3.48	99.07 ± 0.592	(Zn <sub>0.82-0.97</sub> ,Fe <sub>0.02-0.17</sub> ) <sub>0.97-1.01</sub> S	6.60 ± 3.48	6.94 ± 10.3	
			Min	32.33	55.70	1.12	97.99		3.92	0.416	
			Max	33.52	65.28	10.16	100.14		13.9	18.8	
MSUP	sulfide stringer (hanging wall)	Sp (7, 3)	Av ± stdev	33.64 ± 0.231	58.51 ± 1.19	7.72 ± 1.28	99.87 ± 0.583	(Zn <sub>0.83-0.89</sub> ,Fe <sub>0.10-0.16</sub> ) <sub>0.97-1.00</sub> S	8.14 ± 1.27	—	
			Min	33.31	57.35	5.91	98.79		6.88	—	
			Max	33.92	60.66	9.13	100.69		9.43	—	
MSUP	semi-massive to massive sulfides	Sp (5, 2)	Av ± stdev	33.54 ± 0.095	54.84 ± 0.709	10.53 ± 0.537	98.91 ± 0.207	(Zn <sub>0.79-0.82</sub> ,Fe <sub>0.17-0.19</sub> ) <sub>0.98-0.99</sub> S	8.59 ± 0.654	—	
			Min	33.46	54.24	9.64	98.56		8.13	—	
			Max	33.67	56.01	11.04	99.11		9.06	—	
MSUP	sulfide stringer horizon	Sp (13, 2)	Av ± stdev	33.55 ± 0.638	56.77 ± 0.676	8.97 ± 0.629	99.30 ± 0.753	(Zn <sub>0.81-0.86</sub> ,Fe <sub>0.14-0.18</sub> ) <sub>0.95-1.02</sub> S	15.0 ± 7.71	4.00	
			Min	32.56	55.02	8.13	98.40		9.56	4.00	
			Max	34.65	57.60	10.27	100.80		20.5	4.00	
MSUP	All	Sp (25, 7)	Av ± stdev	33.57 ± 0.469	56.87 ± 1.52	8.93 ± 1.27	99.38 ± 0.703	(Zn <sub>0.79-0.89</sub> ,Fe <sub>0.10-0.19</sub> ) <sub>0.95-1.02</sub> S	10.2 ± 4.81	4.00	
			Min	32.56	54.24	5.91	98.40		6.88	4.00	
			Max	34.65	60.66	11.0	100.80		20.5	4.00	
MSDP	semi-massive to massive sulfides	Sp (5, 2)	Av ± stdev	33.74 ± 0.238	55.67 ± 0.517	9.50 ± 0.521	98.91 ± 0.786	(Zn <sub>0.80-0.83</sub> ,Fe <sub>0.15-0.17</sub> ) <sub>0.96-0.98</sub> S	4.01	—	
			Min	33.34	54.92	8.68	97.98		4.01	—	
			Max	33.95	56.19	9.95	99.85		4.01	—	
MSDP	sulfide stringer horizon	Sp (3, 2)	Av ± stdev	33.99 ± 0.389	56.52 ± 0.689	9.45 ± 0.587	99.96 ± 0.467	(Zn <sub>0.81-0.82</sub> ,Fe <sub>0.15-0.17</sub> ) <sub>0.96-0.98</sub> S	10.0	—	
			Min	33.60	55.79	8.90	99.45		10.0	—	
			Max	34.37	57.16	10.07	100.37		10.0	—	
MSDP	All	Sp (8, 4)	Av ± stdev	33.83 ± 0.304	55.99 ± 0.695	9.48 ± 0.504	99.30 ± 0.844	(Zn <sub>0.80-0.83</sub> ,Fe <sub>0.15-0.17</sub> ) <sub>0.96-0.98</sub> S	7.03 ± 4.26	—	
			Min	33.34	54.92	8.68	97.98		4.01	—	
			Max	34.37	57.16	10.07	100.37		10.0	—	
LFWZ	LFWZ	Sp (9, 2)	Av ± stdev	33.72 ± 0.251	56.63 ± 0.572	9.32 ± 0.447	99.68 ± 0.584	(Zn <sub>0.81-0.84</sub> ,Fe <sub>0.15-0.17</sub> ) <sub>0.97-0.98</sub> S	4.32	—	
			Min	33.28	55.79	8.67	98.23		4.32	—	
			Max	34.04	57.28	10.06	100.18		4.32	—	
MING	All	Sp (97, 32)	Av ± stdev	33.50 ± 0.424	58.44 ± 3.03	7.47 ± 2.78	99.41 ± 0.690	(Zn <sub>0.79-0.97</sub> ,Fe <sub>0.02-0.19</sub> ) <sub>0.95-1.02</sub> S	7.80 ± 3.73	5.27 ± 7.70	
			Min	32.33	54.24	1.12	97.98		3.68	0.416	
			Max	34.65	65.28	11.04	100.80		20.5	18.8	

Table A5-6. (cont.)

Ore body	Mineralization style	Mineral phase*	Cr	Mn	Co	Ni	Cu	As	Se	Mo
1807	semi-massive to massive sulfides**	Sp (28, 7)	Av $\pm$ stdev	403 $\pm$ 211	64.2 $\pm$ 60.1	-	183 $\pm$ 231	37.4 $\pm$ 12.7	275 $\pm$ 46.4	17.7
		Min		205	0.682	-	24.0	21.6	198	17.7
		Max		849	126	-	591	56.3	339	17.7
1806	silicified horizon	Sp (6, 1)	Av $\pm$ stdev	2,146	-	-	437	9.13	147	-
		Min		-	-	-	-	-	-	-
		Max		-	-	-	-	-	-	-
1806	semi-massive to massive sulfides	Sp (17, 9)	Av $\pm$ stdev	1,095 $\pm$ 448	0.634 $\pm$ 0.387	18.0	1,047 $\pm$ 1,676	136 $\pm$ 226	101 $\pm$ 107	-
		Min	12.0	634	0.361	18.0	101	17.6	12.2	-
		Max	12.0	1,731	0.908	18.0	5,189	728	302	-
1806	sulfide stringer horizon	Sp (4, 2)	Av $\pm$ stdev	1,933 $\pm$ 166	-	-	447 $\pm$ 213	280 $\pm$ 9.50	94.0 $\pm$ 4.18	-
		Min	-	1,816	-	-	296	273	91.0	-
		Max	-	2,051	-	-	597	287	96.9	-
1806	All	Sp (27, 12)	Av $\pm$ stdev	1,322 $\pm$ 566	0.634 $\pm$ 0.387	18.0	896 $\pm$ 1,457	149 $\pm$ 206	104 $\pm$ 92.3	-
		Min	12.0	634	0.361	18.0	101	9.13	12.2	-
		Max	12.0	2,146	0.908	18.0	5,189	728	302	-
MSUP	sulfide stringer (hanging wall)	Sp (7, 3)	Av $\pm$ stdev	1,393 $\pm$ 359	4.90 $\pm$ 2.55	41.5	56.0 $\pm$ 73.8	1,021 $\pm$ 1,070	56.3 $\pm$ 13.2	-
		Min	-	980	3.10	41.5	10.8	265	41.6	-
		Max	-	1,619	6.71	41.5	141	1,778	67.1	-
MSUP	semi-massive to massive sulfides	Sp (5, 2)	Av $\pm$ stdev	1,538 $\pm$ 141	182 $\pm$ 8.11	-	696 $\pm$ 207	38.7 $\pm$ 4.79	581 $\pm$ 112	-
		Min	-	1,439	177	-	550	35.3	501	-
		Max	-	1,638	188	-	842	42.1	660	-
MSUP	sulfide stringer horizon	Sp (13, 2)	Av $\pm$ stdev	498 $\pm$ 69.7	13.3 $\pm$ 2.98	-	420 $\pm$ 217	26.4 $\pm$ 28.8	534 $\pm$ 25.8	-
		Min	-	449	11.2	-	267	6.12	516	-
		Max	-	548	15.4	-	573	46.8	553	-
MSUP	All	Sp (25, 7)	Av $\pm$ stdev	1,179 $\pm$ 517	66.9 $\pm$ 89.7	41.5	343 $\pm$ 319	362 $\pm$ 700	343 $\pm$ 273	-
		Min	-	449	3.10	41.5	10.8	6.12	41.6	-
		Max	-	1,638	188	41.5	842	1,778	660	-
MSDP	semi-massive to massive sulfides	Sp (5, 2)	Av $\pm$ stdev	460 $\pm$ 176	28.9 $\pm$ 40.5	26.8	556 $\pm$ 140	311 $\pm$ 429	64.9 $\pm$ 0.604	-
		Min	-	334	0.224	26.8	457	7.74	64.5	-
		Max	-	586	57.5	26.8	654	615	65.3	-
MSDP	sulfide stringer horizon	Sp (3, 2)	Av $\pm$ stdev	278 $\pm$ 296	5.14 $\pm$ 2.70	34.2	634 $\pm$ 499	28.7 $\pm$ 10.7	124 $\pm$ 63.2	-
		Min	-	68.5	3.23	34.2	282	21.1	79.5	-
		Max	-	487	7.05	34.2	987	36.2	169	-
MSDP	All	Sp (8, 4)	Av $\pm$ stdev	369 $\pm$ 226	17.0 $\pm$ 27.2	30.5 $\pm$ 5.27	595 $\pm$ 302	170 $\pm$ 297	94.6 $\pm$ 50.1	-
		Min	-	68.45	0.224	26.8	282	7.74	64.5	-
		Max	-	586	57.5	34.2	987	615	169	-
LFWZ	LFWZ	Sp (9, 2)	Av $\pm$ stdev	91.9 $\pm$ 232	140 $\pm$ 139	-	1,945 $\pm$ 1,722	5.67 $\pm$ 0.665	285 $\pm$ 68.8	-
		Min	-	167	42.1	-	727	5.20	236	-
		Max	-	297	239	-	3,163	6.13	334	-
MING	All	Sp (97, 32)	Av $\pm$ stdev	902 $\pm$ 622	57.2 $\pm$ 74.5	30.1 $\pm$ 10.1	647 $\pm$ 1,044	167 $\pm$ 356	204 $\pm$ 172	17.7
		Min	12.0	68.5	0.22	18.0	10.8	5.20	12.2	17.7
		Max	12.0	2,146	239	41.5	5,189	1,778	660	17.7



Table A5-6. (cont.)

Ore body	Mineralization style	Mineral phase*	Ag	Cd	Sn	Sb	Te	Au	Tl	Pb
1807	semi-massive to massive sulfides**	Sp (28, 7)	2.51 ± 0.973	7,628 ± 1,303	0.390 ± 0.342	4.29 ± 2.16	71.1 ± 76.2	0.294 ± 0.324	0.077 ± 0.056	22.8 ± 35.1
		Av ± stdev								
		Min	1.22	6,369	0.117	1.26	17.2	0.063	0.038	3.48
		Max	3.72	10,000	0.835	7.06	125	0.665	0.117	101
1806	silicified horizon	Sp (6, 1)	65.1	7,907	1.93	18.9	—	74.8	0.498	3.41
		Av ± stdev								
		Min	—	—	—	—	—	—	—	—
		Max	—	—	—	—	—	—	—	—
1806	semi-massive to massive sulfides	Sp (17, 9)	12.0 ± 11.3	5,409 ± 1,450	31.5 ± 69.5	6.33 ± 6.47	2.14	0.080	0.474 ± 0.740	15.7 ± 9.83
		Av ± stdev								
		Min	3.07	3,095	0.959	0.761	2.14	0.080	0.056	3.81
		Max	35.6	7,359	216	20.9	2.14	0.080	1.97	33.3
1806	sulfide stringer horizon	Sp (4, 2)	16.2	6,172 ± 1,004	0.646 ± 0.141	13.4 ± 9.44	3.58	—	—	2.23 ± 1.93
		Av ± stdev								
		Min	16.2	5,462	0.546	6.71	3.58	—	—	0.86
		Max	16.2	6,882	0.745	20.1	3.58	—	—	3.59
1806	All	Sp (27, 12)	17.2 ± 18.9	5,744 ± 1,481	23.9 ± 60.9	8.56 ± 7.52	2.86 ± 1.02	37.4 ± 52.8	0.477 ± 0.676	12.1 ± 10.3
		Av ± stdev								
		Min	3.07	3,095	0.546	0.761	2.14	0.080	0.056	0.864
		Max	65.1	7,907	216	20.9	3.58	74.8	1.97	33.3
MSUP	sulfide stringer (hanging wall)	Sp (7, 3)	8.37 ± 7.91	6,179 ± 1,009	0.344	12.8 ± 11.5	—	—	—	86.0 ± 130
		Av ± stdev								
		Min	1.78	5,049	0.344	2.21	—	—	—	9.71
		Max	17.1	6,992	0.344	25.0	—	—	—	236
MSUP	semi-massive to massive sulfides	Sp (5, 2)	3.48 ± 1.41	5,846 ± 460	0.358	3.36 ± 3.51	4.77	—	0.040	52.8 ± 67.9
		Av ± stdev								
		Min	2.49	5,539	0.358	0.874	4.77	—	0.040	4.84
		Max	4.48	6,190	0.358	5.84	4.77	—	0.040	101
MSUP	sulfide stringer horizon	Sp (13, 2)	3.96 ± 1.81	6,459 ± 458	1.30 ± 1.05	4.46 ± 1.93	—	—	0.178 ± 0.114	12.9 ± 9.51
		Av ± stdev								
		Min	2.68	6,135	0.555	3.10	—	—	0.097	6.14
		Max	5.25	6,782	2.04	5.83	—	—	0.258	19.6
MSUP	All	Sp (25, 7)	5.71 ± 5.29	6,169 ± 685	0.826 ± 0.819	7.72 ± 8.33	4.77	—	0.132 ± 0.113	55.6 ± 86.7
		Av ± stdev								
		Min	1.78	5,049	0.344	0.874	4.77	—	0.040	4.84
		Max	17.15	6,992	2.04	25.0	4.77	—	0.258	236
MSDP	semi-massive to massive sulfides	Sp (5, 2)	11.3 ± 8.71	23,150 ± 20,370	9.97 ± 11.8	7.95 ± 9.74	9.44 ± 0.951	—	0.718 ± 0.079	1,580 ± 1,271
		Av ± stdev								
		Min	5.13	8,746	1.60	1.06	8.77	—	0.662	681
		Max	17.5	37,554	18.3	14.8	10.1	—	0.773	2,479
MSDP	sulfide stringer horizon	Sp (3, 2)	5.71 ± 6.88	8,455 ± 5,123	—	2.95	—	—	0.107	7.47 ± 10.4
		Av ± stdev								
		Min	0.845	4,832	—	2.95	—	—	0.107	0.134
		Max	10.6	12,077	—	2.95	—	—	0.107	14.8
MSDP	All	Sp (8, 4)	8.50 ± 7.17	15,802 ± 14,800	9.97 ± 11.8	6.29 ± 7.47	9.44 ± 0.951	—	0.514 ± 0.357	794 ± 1,168
		Av ± stdev								
		Min	0.845	4,832	1.60	1.06	8.77	—	0.107	0.134
		Max	17.5	37,554	18.3	14.8	10.1	—	0.773	2,479
LFWZ	LFWZ	Sp (9, 2)	12.5 ± 10.9	13,808 ± 1,933	1.06 ± 0.054	0.609 ± 0.492	—	—	0.647	27.9 ± 25.9
		Av ± stdev								
		Min	4.84	12,441	1.03	0.261	—	—	0.647	9.55
		Max	20.2	15,175	1.10	0.957	—	—	0.647	46.2
MING	All	Sp (97, 32)	10.1 ± 13.2	8,010 ± 5,942	13.1 ± 43.7	6.97 ± 6.69	24.5 ± 44.6	15.2 ± 33.3	0.380 ± 0.489	126 ± 455
		Av ± stdev								
		Min	0.845	3,095	0.117	0.261	125	0.063	0.038	0.134
		Max	65.1	37,554	216	25.0	125	74.8	1.97	2,479

\* Numbers in brackets are number of EPMA analysis, number of LA-ICP-MS analysis

\*\* Samples from 1807 Zone are exclusively from semi-massive to massive sulfides

Table A5-6. (cont.)

Ore body	Mineralization style	Mineral phase*	Bi	
1807	semi-massive to massive sulfides**	Sp (28, 7)	Av ± stdev	8.43 ± 16.6
			Min	0.823
			Max	45.6
1806	silicified horizon	Sp (6, 1)	Av ± stdev	bdl
			Min	—
			Max	—
1806	semi-massive to massive sulfides	Sp (17, 9)	Av ± stdev	0.493 ± 0.814
			Min	0.030
			Max	1.94
1806	sulfide stringer horizon	Sp (4, 2)	Av ± stdev	—
			Min	—
			Max	—
1806	All	Sp (27, 12)	Av ± stdev	0.493 ± 0.814
			Min	0.030
			Max	1.94
MSUP	sulfide stringer_hanging wall	Sp (7, 3)	Av ± stdev	0.126 ± 0.032
			Min	0.103
			Max	0.148
MSUP	semi-massive to massive sulfides	Sp (5, 2)	Av ± stdev	1.51 ± 0.930
			Min	0.853
			Max	2.17
MSUP	sulfide stringer horizon	Sp (13, 2)	Av ± stdev	0.994 ± 0.082
			Min	0.936
			Max	1.05
MSUP	All	Sp (25, 7)	Av ± stdev	0.877 ± 0.753
			Min	0.103
			Max	2.17
MSDP	semi-massive to massive sulfides	Sp (5, 2)	Av ± stdev	7.05 ± 3.50
			Min	4.57
			Max	9.52
MSDP	sulfide stringer horizon	Sp (3, 2)	Av ± stdev	4.73
			Min	4.73
			Max	4.73
MSDP	All	Sp (8, 4)	Av ± stdev	6.27 ± 2.81
			Min	4.57
			Max	9.52
LFWZ	LFWZ	Sp (9, 2)	Av ± stdev	10.2 ± 11.1
			Min	2.28
			Max	18.0
MING	All	Sp (97, 32)	Av ± stdev	4.60 ± 9.84
			Min	0.030
			Max	45.6

Table A5-6. Results of EPMA analysis (major elements in wt%) and LA-ICP-MS analysis (trace elements in ppm) for arsenopyrite; – not detected or below detection limit, NA - n

Ore body	Mineralization style	Mineral phase*	S [wt %]		As	Fe	Total	Mineral Formula	Ti [ppm]	V	Cr
1807	semi-massive to massive sulfides**	Asp (30, 3)	Av ± stdev	21.26 ± 0.365	43.95 ± 0.480	34.11 ± 0.374	99.31 ± 0.675	As <sub>0.83±0.02</sub> Fe <sub>0.89±0.05</sub> S	6.84 ± 0.883	–	–
		Min		20.77	43.17	33.17	98.16		5.83	–	–
		Max		22.19	44.97	34.64	100.51		7.46	–	–
1806	silicified horizon	Asp (9, 6)	Av ± stdev	21.29 ± 0.394	43.71 ± 0.251	34.53 ± 0.360	99.53 ± 0.686	As <sub>0.85±0.01</sub> Fe <sub>0.92±0.06</sub> S	4.87 ± 1.17	1.91	–
		Min		20.75	43.44	33.88	98.15		3.25	1.91	–
		Max		21.86	44.23	34.98	100.39		6.37	1.91	–
1806	semi-massive to massive sulfides	Asp (25, 10)	Av ± stdev	21.23 ± 0.783	43.97 ± 1.01	34.28 ± 0.400	99.48 ± 0.775	As <sub>0.75±1.02</sub> Fe <sub>0.83±1.00</sub> S	6.13 ± 1.35	13.6 ± 26.5	0.678
		Min		19.50	41.69	33.58	98.26		3.73	0.183	0.678
		Max		23.71	46.68	34.94	101.24		8.23	53.27	0.678
1806	sulfide stringer horizon	Asp (11, 2)	Av ± stdev	21.18 ± 0.631	43.78 ± 0.795	34.38 ± 0.373	99.43 ± 0.525	As <sub>0.82±0.09</sub> Fe <sub>0.90±1.00</sub> S	9.43 ± 2.69	0.581	–
		Min		19.62	42.32	33.82	98.80		7.52	0.581	–
		Max		22.00	45.22	34.90	100.16		11.3	0.581	–
1806	All	Asp (45, 18)	Av ± stdev	21.23 ± 0.674	43.89 ± 0.847	34.35 ± 0.390	99.48 ± 0.690	As <sub>0.75±1.02</sub> Fe <sub>0.83±1.00</sub> S	6.07 ± 1.91	9.46 ± 21.5	0.678
		Min		19.50	41.69	33.58	98.15		3.25	0.183	0.678
		Max		23.71	46.68	34.98	101.24		11.3	53.3	0.678
MSUP	sulfide stringer (hanging wall)	Asp (3, 1)	Av ± stdev	21.52 ± 0.073	43.63 ± 0.181	34.19 ± 0.209	99.35 ± 0.428	As <sub>0.87</sub> Fe <sub>0.91±0.02</sub> S	9.18	0.143	1.63
		Min		21.45	43.43	34.00	98.88				
		Max		21.60	43.78	34.41	99.72				
MSUP	sulfide stringer horizon	Asp (7, 2)	Av ± stdev	21.65 ± 0.361	44.12 ± 0.468	34.35 ± 0.152	100.12 ± 0.306	As <sub>0.85±0.02</sub> Fe <sub>0.89±0.04</sub> S	18.2	–	–
		Min		20.91	43.66	34.10	99.76		18.2	–	–
		Max		21.97	44.75	34.48	100.58		18.2	–	–
MSUP	All	Asp (10, 3)	Av ± stdev	21.61 ± 0.303	43.97 ± 0.456	34.30 ± 0.175	99.89 ± 0.491	As <sub>0.85±0.02</sub> Fe <sub>0.89±0.04</sub> S	13.7 ± 6.39	0.143	1.63
		Min		20.91	43.43	34.00	98.88		9.18	0.143	1.63
		Max		21.97	44.75	34.48	100.58		18.2	0.143	1.63
MSDP	semi-massive to massive sulfides	Asp (7, 4)	Av ± stdev	21.13 ± 0.372	44.14 ± 0.570	33.61 ± 0.519	98.89 ± 0.444	As <sub>0.87±0.01</sub> Fe <sub>0.89±0.06</sub> S	5.74 ± 0.753	–	–
		Min		20.42	43.35	32.97	98.07		5.19	–	–
		Max		21.55	44.79	34.22	99.36		6.59	–	–
LFWZ	LFWZ	Asp (4, 2)	Av ± stdev	21.22 ± 0.428	44.45 ± 0.638	34.12 ± 0.453	99.78 ± 0.586	As <sub>0.87±0.03</sub> Fe <sub>0.89±0.05</sub> S	4.41 ± 0.603	–	–
		Min		20.79	43.80	33.51	98.91		3.99	–	–
		Max		21.60	45.01	34.56	100.14		4.84	–	–
MING	All	Asp (96, 30)	Av ± stdev	21.27 ± 0.538	43.96 ± 0.686	34.21 ± 0.424	99.44 ± 0.678	As <sub>0.75±1.02</sub> Fe <sub>0.83±1.00</sub> S	6.55 ± 2.88	8.13 ± 19.9	1.16 ± 0.674
		Min		19.50	41.69	32.97	98.07		3.25	0.143	0.678
		Max		23.71	46.68	34.98	101.24		18.2	53.3	1.63

Table A5-6. (cont.)

Ore body <sup>s</sup>	Mineralization style	Mineral phase*	Mn	Co	Ni	Cu	Zn	Se	Mo	Ag
1807	semi-massive to massive sulfides**	Asp (30, 3)	Av ± stdev Min	3,173 ± 1,989 1,935	980 ± 318 641	197 ± 244 24.4	23.8 ± 23.3 7.34	900 ± 117 796	2.57 2.57	3.67 ± 3.10 1.48
1806	silicified horizon	Asp (9, 6)	Max Av ± stdev Min	5,468 3.50 ± 3.00 0.102	1,272 315 ± 299 75.0	370 74.6 ± 16.6 56.8	40.3 3.84 ± 3.73 1.43	1,027 309 ± 136 219	2.57 4.99 4.99	5.87 3.73 ± 3.84 0.251
1806	semi-massive to massive sulfides	Asp (25, 10)	Max Av ± stdev Min	7.94 87.7 ± 59.1 11.11	832 407 ± 263 82.6	94.2 382 ± 1,074 0.708	8.14 161 ± 226 0.743	580 266 ± 403 25.8	4.99 2.62 ± 2.06 0.321	7.34 75.4 ± 144 0.357
1806	sulfide stringer horizon	Asp (11, 2)	Max Av ± stdev Min	211 15.0 ± 0.518 14.6	942 420 ± 171 299	3,039 3.65 ± 1.01 2.94	321 6.24 6.24	1,214 239 ± 16.1 228	5.46 15.1 ± 17.2 2.91	423 2.74 ± 0.925 2.09
1806	All	Asp (45, 18)	Max Av ± stdev Min	15.3 49.4 ± 59.3 0.102	541 378 ± 258 75.0	4.37 240 ± 806 0.708	6.24 56.6 ± 130 0.743	250 277 ± 304 25.83	27.3 5.35 ± 7.92 0.321	3.40 46.6 ± 115 0.251
MSUP	sulfide stringer (hanging wall)	Asp (3, 1)	Max Av ± stdev Min	211 189	942 1,108	3,039 119	321	1,214 72.1	27.28 11.2	423 1.36
MSUP	sulfide stringer horizon	Asp (7, 2)	Max Av ± stdev Min	264 ± 204 120	143 ± 50.8 107	— —	37.9 37.9	718 ± 28.4 698	5.50 5.50	1.41 1.41
MSUP	All	Asp (10, 3)	Max Av ± stdev Min	408 239 ± 150 120	179 465 ± 559 107	— 119 119	37.9 37.9 37.9	738 503 ± 373 72.1	5.50 8.36 ± 4.04 5.50	1.41 1.39 ± 0.038 1.36
MSDP	semi-massive to massive sulfides	Asp (7, 4)	Max Av ± stdev Min	408 9,935 ± 3,120 5,908	1,108 1,373 ± 583 744	119 83.8 ± 143 0.849	37.9 2.29 ± 0.621 1.85	738 175 ± 35.3 123	11.2 8.92 ± 10.7 1.35	1.41 2.97 ± 2.77 1.09
LFWZ	LFWZ	Asp (4, 2)	Max Av ± stdev Min	12,783 1,948 ± 160 1,835	1,893 1,768 ± 125 1,680	249 1,393 1,393	2.72 25.3 ± 26.3 6.71	204 898 ± 84.4 838	16.48 — —	6.16 21.3 ± 17.3 9.06
MING	All	Asp (96, 30)	Max Av ± stdev Min	2,061 1,887 ± 3,620 0.102	1,856 672 ± 567 75.0	1,393 263 ± 706 0.708	43.9 36.9 ± 86.9 0.743	957 390 ± 354 25.8	— 6.04 ± 7.27 0.321	33.5 31.7 ± 92.1 0.251
			Max	12,783	1,893	3,039	321	1,214	27.3	423

Table A5-6. (cont.)

Ore body <sup>s</sup>	Mineralization style	Mineral phase*	Cd	Sn	Sb	Te	Au	Tl	Pb	Bi
1807	semi-massive to massive sulfides**	Asp (30, 3)	Av ± stdev Min Max	1.63 1.63 1.63	52.4 ± 65.0 11.0 127	3,278 ± 1,382 1,694 4,240	0.742 ± 0.908 0.099 1.38	0.248 ± 0.026 0.230 0.267	95.9 ± 92.8 1.26 187	13.1 ± 17.7 0.251 33.3
1806	silicified horizon	Asp (9, 6)	Av ± stdev Min Max	0.136 0.136 0.136	0.282 ± 0.378 0.080 0.849	39.8 ± 36.6 7.07 2,453	0.567 ± 0.532 0.191 0.943	0.348 ± 0.375 0.046 0.858	21.6 ± 45.7 0.421 115	1.83 ± 2.97 0.034 5.26
1806	semi-massive to massive sulfides	Asp (25, 10)	Av ± stdev Min Max	38.2 38.2 38.2	1,349 ± 1,908 0.085 2,698	416 ± 789 3.11 2,338	37.1 ± 81.2 0.047 230	4.08 ± 9.48 0.062 23.4	115 ± 245 3.47 666	1.93 ± 2.16 0.028 4.81
1806	sulfide stringer horizon	Asp (11, 2)	Av ± stdev Min Max	— — —	0.122 ± 0.075 0.069 59.8	61.7 ± 20.1 47.5 75.9	6.47 ± 1.04 5.74 7.21	0.579 ± 0.166 0.462 0.696	26.7 ± 2.90 24.7 28.8	0.085 0.085 0.085
1806	All	Asp (45, 18)	Av ± stdev Min Max	19.2 ± 26.9 0.136 38.2	337 ± 954 0.069 2,698	408 ± 785 3.11 2,453	25.9 ± 66.9 0.047 230	2.25 ± 6.67 0.046 23.4	65.6 ± 169 0.421 666	1.66 ± 2.22 0.028 5.26
MSUP	sulfide stringer (hanging wall)	Asp (3, 1)	Av ± stdev Min Max	— — —	— — 54.1	79.9	1.73	2.27	29.9	0.469
MSUP	sulfide stringer horizon	Asp (7, 2)	Av ± stdev Min Max	— — —	0.400 0.400 0.400	116 ± 1.69 115 118	0.340 0.340 0.340	— — —	242 ± 336 4.30 479	5.89 ± 0.402 5.60 6.17
MSUP	All	Asp (10, 3)	Av ± stdev Min Max	— — —	0.400 0.400 0.400	104 ± 21.1 79.9 118	1.04 ± 0.985 0.340 1.73	2.27 2.27 2.27	171 ± 267 4.30 479	4.08 ± 3.14 0.469 6.17
MSDP	semi-massive to massive sulfides	Asp (7, 4)	Av ± stdev Min Max	— — —	0.475 ± 0.042 0.445 0.505	212 ± 147 98.10 428	0.187 ± 0.163 0.041 0.363	0.269 ± 0.161 0.155 0.383	21.8 ± 32.7 1.80 59.5	0.719 ± 0.982 0.024 1.41
LFWZ	LFWZ	Asp (4, 2)	Av ± stdev Min Max	— — —	1.08 ± 0.773 0.531 1.624	519 ± 63.0 474 563	0.296 ± 0.252 0.118 0.474	0.971 0.971 0.971	17.6 ± 2.27 16.0 19.2	30.2 ± 2.25 28.6 31.8
MING	All	Asp (96, 30)	Av ± stdev Min Max	9.91 ± 18.9 0.136 38.2	193 ± 721 0.069 2,698	646 ± 1,142 3.11 4,240	15.0 ± 51.2 0.041 230	1.74 ± 5.44 0.046 23.4	72.6 ± 156 0.421 666	7.04 ± 11.4 0.024 33.3

\* Arsenopyrite was not analyzed by both EPMA and LA-ICP-MS for the semi-massive to massive sulfides from the MSUP ore body and the sulfide stringer horizon from the MSDP ore

body  
\* Numbers in brackets are number of EPMA analysis, number of LA-ICP-MS analysis  
\*\* Samples from 1807 Zone are exclusively from semi-massive to massive sulfides

Table A5-6. Results of EPMA analysis (major elements in wt%) and LA-ICP-MS analysis (trace elements in ppm) for galena; – not detected or below detection limit, NA - no ana

Ore body <sup>s</sup>	Mineralization style	Mineral phase*	S [wt %]		Pb		Total	Mineral Formula	Ti [ppm]	V	Cr	Mn
1807	semi-massive to massive sulfides**	Gn (4, 1)	Av ± stdev	12.90 ± 0.266	85.87 ± 0.579	98.77 ± 0.542	98.11	Pb <sub>1.00-1.06</sub> S	–	–	–	–
			Min	12.64	85.37	98.11						
			Max	13.23	86.39	99.36						
1806	semi-massive to massive sulfides	Gn (20, 11)	Av ± stdev	13.32 ± 0.266	86.10 ± 0.733	99.42 ± 0.758	99.42 ± 0.758	Pb <sub>0.95-1.05</sub> S	3.07 ± 1.25	2.65 ± 3.63	–	1.54 ± 0.468
			Min	12.64	84.88	98.22			1.46	0.236	–	1.21
			Max	13.90	87.55	100.73			5.44	6.83	–	1.88
1806	sulfide stringer horizon	Gn (7, 1)	Av ± stdev	13.26 ± 0.164	86.36 ± 0.567	99.61 ± 0.698	98.70	Pb <sub>1.00-1.02</sub> S	3.00	–	–	7.55
			Min	12.95	85.75	98.70						
			Max	13.41	87.14	100.52						
1806	All	Gn (27, 12)	Av ± stdev	13.30 ± 0.242	86.17 ± 0.693	99.47 ± 0.735	98.22	Pb <sub>1.00-1.02</sub> S	3.07 ± 1.18	2.65 ± 3.63	–	3.55 ± 3.48
			Min	12.64	84.88	98.22			1.46	0.236	–	1.21
			Max	13.90	87.55	100.73			5.44	6.83	–	7.55
MSUP	sulfide stringer (hanging wall)	Gn (2, 1)	Av ± stdev	13.23 ± 0.138	86.54 ± 0.337	99.76 ± 0.198	99.62	Pb <sub>1.00-1.02</sub> S	2.07	–	–	–
			Min	13.13	86.30	99.62						
			Max	13.33	86.77	99.91						
MSDP	semi-massive to massive sulfides	Gn (8, 1)	Av ± stdev	12.96 ± 0.233	86.07 ± 0.526	99.03 ± 0.714	98.11	Pb <sub>1.01-1.05</sub> S	5.07	–	–	–
			Min	12.66	85.36	98.11						
			Max	13.28	86.95	100.22						
MSDP	sulfide stringer horizon	Gn (1, 0)	Av ± stdev	13.00	85.44	98.44	98.44	Pb <sub>1.02</sub> S	NA	NA	NA	NA
			Min	–	–	–	–					
			Max	–	–	–	–					
MSDP	All	Gn (9, 1)	Av ± stdev	12.96 ± 0.218	86.00 ± 0.535	98.96 ± 0.696	98.11	Pb <sub>1.01-1.05</sub> S	5.07	–	–	–
			Min	12.66	85.36	98.11						
			Max	13.28	86.95	100.22						
MING	All	Gn (42, 15)	Av ± stdev	13.19 ± 0.282	86.12 ± 0.638	99.31 ± 0.735	98.11	Pb <sub>0.95-1.06</sub> S	3.15 ± 1.26	2.65 ± 3.36	–	3.55 ± 3.48
			Min	12.64	84.88	98.11			1.46	0.236	–	1.21
			Max	13.90	87.55	100.73			5.44	6.83	–	7.55

Table A5-6. (cont.)

Ore body <sup>s</sup>	Mineralization style	Mineral phase*	Fe	Co	Ni	Cu	Zn	As	Se	Mo
1807	semi-massive to massive sulfides**	Gn (4, 1)	Av ± stdev Min Max	-	-	-	163	122	16,343	-
1806	semi-massive to massive sulfides	Gn (20, 11)	Av ± stdev Min Max	0.215 0.215 0.215	-	82.7 ± 89.4 0.504 217	319 ± 254 18.9 562	483 ± 294 92.4 1,233	1,302 ± 262 963 1,834	-
1806	sulfide stringer horizon	Gn (7, 1)	Av ± stdev Min Max	0.426 5,145	-	755	-	2,187	7,906	-
1806	All	Gn (27, 12)	Av ± stdev Min Max	0.320 ± 0.149 46.0 5,670	-	167 ± 252 0.504 755	319 ± 254 18.9 562	638 ± 635 92.4 2,187	1,852 ± 1,932 963 7,906	-
MSUP	sulfide stringer (hanging wall)	Gn (2, 1)	Av ± stdev Min Max	-	-	-	-	377	1,641	-
MSDP	semi-massive to massive sulfides	Gn (8, 1)	Av ± stdev Min Max	-	-	-	-	44.7	9,083	-
MSDP	sulfide stringer horizon	Gn (1, 0)	Av ± stdev Min Max	NA	NA	NA	NA	NA	NA	NA
MSDP	All	Gn (9, 1)	Av ± stdev Min Max	-	-	-	-	44.7	9,083	-
MING	All	Gn (42, 15)	Av ± stdev Min Max	0.320 ± 0.149 46.0 5,670	-	167 ± 252 0.504 755	299 ± 241 18.9 562	540 ± 594 44.7 2,187	3,286 ± 4,409 963 16,343	-



Table A5-6. (cont.)

Ore body <sup>s</sup>	Mineralization style	Mineral phase*	Ag	Cd	Sn	Sb	Te	Au	Tl	Bi
1807	semi-massive to massive sulfides**	Gn (4, 1)	Av ± stdev Min Max	26.2	21.2	458	5,553	0.249	271	10,455
1806	semi-massive to massive sulfides	Gn (20, 11)	1,031 ± 734 274 2,195 Max	15.0 ± 4.92 7.24 24.2 Max	211 ± 198 16.4 480 Max	1,188 ± 953 255 2,749 Max	29.8 ± 22.7 10.8 75.0 Max	0.041 0.041 0.041 Max	28.8 ± 7.64 21.9 42.7 Max	36.2 ± 37.6 3.03 79.4 Max
1806	sulfide stringer horizon	Gn (7, 1)	Av ± stdev Min Max	192	17.8	1,784	378	–	21.9	81.8
1806	All	Gn (27, 12)	1,029 ± 700 274 2,195 Max	29.8 ± 51.3 7.24 192 Max	195 ± 197 16.4 480 Max	1,237 ± 925 255 2,749 Max	58.8 ± 103 10.8 378 Max	0.041 0.041 0.041 Max	28.2 ± 7.55 21.9 42.7 Max	40.0 ± 38.2 3.03 81.8 Max
MSUP	sulfide stringer (hanging wall)	Gn (2, 1)	Av ± stdev Min Max	20.3	3.85	1,439	673	–	16.7	467
MSDP	semi-massive to massive sulfides	Gn (8, 1)	Av ± stdev Min Max	54.8	28.3	169	1,173	–	181	3,272
MSDP	sulfide stringer horizon	Gn (1, 0)	Av ± stdev Min Max	NA	NA	NA	NA	NA	NA	NA
MSDP	All	Gn (9, 1)	Av ± stdev Min Max	54.8	28.3	169	1,173	–	181	3,272
MING	All	Gn (42, 15)	1,119 ± 651 274 2,195 Max	30.6 ± 46.1 7.24 192 Max	159 ± 189 3.85 480 Max	1,128 ± 887 169 2,749 Max	540 ± 1,425 10.8 5,553 Max	0.145 ± 0.147 0.041 0.249 Max	53.8 ± 72.2 16.7 271 Max	978 ± 2,751 3.03 10,455 Max

<sup>s</sup> Galena was not analyzed by both EPMA and LA-ICP-MS for the silicified horizon of the 1806 Zone, the semi-massive to massive sulfides and the sulfide stringer horizon from the MSUP ore body, and the LFWZ

\* Numbers in brackets are number of EPMA analysis, number of LA-ICP-MS analysis

\*\* Samples from 1807 Zone are exclusively from semi-massive to massive sulfides

Table A5-6. Results of EPMA analysis (major elements in wt%) and LA-ICP-MS analysis (trace elements in ppm) for alloclastite; – not detected or below detection limit

Ore body <sup>s</sup>	Mineralization style	Mineral phase*	S [wt %]		Co	Ni	Fe	As	Total	Mineral Formula
1807	semi-massive to massive sulfides**	Allo (1, 1)	Av ± stdev	20.42	25.11	1.83	7.97	44.70	100.03	(Co <sub>0.67</sub> Ni <sub>0.03</sub> ) <sub>0.71±0.76</sub> Fe <sub>0.22</sub> As <sub>0.94</sub> S
			Min	–	–	–	–	–	–	–
MSUP	semi-massive to massive sulfides	Allo (4, 3)	Av ± stdev	19.94 ± 0.318	24.65 ± 0.667	2.23 ± 0.422	8.39 ± 1.20	44.30 ± 0.526	99.51 ± 0.338	(Co <sub>0.65±0.71</sub> Ni <sub>0.05±0.08</sub> ) <sub>0.71±0.76</sub> Fe <sub>0.21±0.28</sub> As <sub>0.92±0.97</sub> S
			Min	19.61	24.01	1.79	7.15	43.55	99.04	–
MING	All	Allo (5, 4)	Av ± stdev	20.04 ± 0.349	24.74 ± 0.614	2.15 ± 0.406	8.31 ± 1.06	44.38 ± 0.490	99.61 ± 0.376	(Co <sub>0.65±0.71</sub> Ni <sub>0.05±0.08</sub> ) <sub>0.71±0.76</sub> Fe <sub>0.21±0.28</sub> As <sub>0.92±0.97</sub> S
			Min	19.61	24.01	1.79	7.15	43.55	99.04	–
			Max	20.42	25.59	2.81	9.88	44.78	100.03	–

Table A5-6. (cont.)

Ore body <sup>s</sup>	Mineralization style	Mineral phase*	Ti [ppm]	V	Cr	Mn	Cu	Zn	Se	Mo	Ag
1807	semi-massive to massive sulfides**	Allo (1, 1)	Av $\pm$ stdev	—	—	—	741	22.6	362	—	4.78
		Min	—	—	—	—	—	—	—	—	—
		Max	—	—	—	—	—	—	—	—	—
MSUP	semi-massive to massive sulfides	Allo (4, 3)	Av $\pm$ stdev	—	—	2.87	1,920 $\pm$ 2,376	1,15 $\pm$ 162	1,833 $\pm$ 480	—	52.6 $\pm$ 45.2
		Min	7.29	—	—	2.87	240	1,000	1,359	—	4.29
		Max	23.2	—	—	2.87	3,600	1,229	2,318	—	94.0
MING	All	Allo (5, 4)	Av $\pm$ stdev	—	—	2.87	1,527 $\pm$ 1,813	751 $\pm$ 641	1,465 $\pm$ 833	—	40.7 $\pm$ 44.0
		Min	7.29	—	—	2.87	240	22.62	362	—	4.29
		Max	23.2	—	—	2.87	3,600	1,229	2,318	—	94.0

Table A5-6. (cont.)

Ore body <sup>s</sup>	Mineralization style	Mineral phase*	Cd	Sn	Sb	Te	Au	Tl	Pb	Bi
1807	semi-massive to massive sulfides**	Allo (1, 1)	Av $\pm$ stdev Min Max	0.542 — —	6.05 — —	193 — —	12.8 — —	— — —	260 — —	42.2 — —
MSUP	semi-massive to massive sulfides	Allo (4, 3)	Av $\pm$ stdev Min Max	1.03 $\pm$ 0.394 0.752 1.31	116 $\pm$ 136 16.80 270	174 $\pm$ 121 76.51 309	13.4 $\pm$ 3.10 10.2 16.3	0.768 $\pm$ 0.774 0.271 1.66	648 $\pm$ 363 229 869	49.8 $\pm$ 33.0 11.8 70.2
MING	All	Allo (5, 4)	Av $\pm$ stdev Min Max	0.867 $\pm$ 0.396 0.542 1.31	88.4 $\pm$ 124 6.05 270	179 $\pm$ 99.2 76.5 309	13.2 $\pm$ 2.54 10.2 16.3	0.768 $\pm$ 0.774 0.271 1.66	551 $\pm$ 254 229 869	47.9 $\pm$ 27.2 11.8 70.2

<sup>s</sup> Allocated was not analyzed by both EPMA and LA-ICP-MS for 1806 Zone, the hanging wall and the sulfide stringer horizon from the MSUP ore body, and the MSDP ore body and the LFWZ

\* Numbers in brackets are number of EPMA analysis, number of LA-ICP-MS analysis

\*\* Samples from 1807 Zone are exclusively from semi-massive to massive sulfides

Table A5-6. Results of EPMA analysis for hessite; – not detected or below detection limit

Ore body <sup>s</sup>	Mineralization style	Mineral phase*	Te [wt%]	Ag	Total	Mineral Formula	S [ppm]	Mn	Fe	Co
MSUP	semi-massive to massive sulfides	Hess (1)	Av ± stdev Min Max	61.26	98.27	Ag <sub>1.96</sub> Te	1,023	–	3,020	–
MSDP	semi-massive to massive sulfides	Hess (1)	Av ± stdev Min Max	62.56	98.27	Ag <sub>2.00</sub> Te	550	–	1,441	–
LFWZ	LFWZ	Hess (1)	Av ± stdev Min Max	58.09	98.27	Ag <sub>1.65</sub> Te	945	206	2,853	–
MING	All	Hess (3)	Av ± stdev Min Max	60.64 ± 2.30 38.52 ± 2.62 36.99 41.54	99.27 ± 1.00 98.27 100.27	Ag <sub>1.65-2.00</sub> Te	839 ± 254 550 1,023	206 206 206	2,438 ± 867 1,441 3,020	–

Table A5-6. Results of EPMA analysis for altaite; – not detected or below detection limit

Ore body <sup>s</sup>	Mineralization style	Mineral phase*	Te [wt%]	Pb	Total	Mineral Formula	S [ppm]	Mn	Fe	Co
MSUP	sulfide stringer horizon	Alt (1)	Av ± stdev Min Max	61.21	98.94	Pb <sub>1.00</sub> Te	1,087	–	1,060	–
MING	All	Alt (1)	Av ± stdev Min Max	61.21	98.94	Pb <sub>1.00</sub> Te	1,087	–	1,060	–

Table A5-6. (cont.)

Ore body <sup>s</sup>	Mineralization style	Mineral phase*	Av ± stddev	Ni	Cu	Zn	As	Mo	Sn	Sb	Au
MSUP	semi-massive to massive sulfides	Hess (1)	Av ± stddev Min Max	171	590	–	2,111	–	–	872	–
MSDP	semi-massive to massive sulfides	Hess (1)	Av ± stddev Min Max	–	–	–	1,257	–	–	–	–
LFWZ	LFWZ	Hess (1)	Av ± stddev Min Max	–	3,264	–	–	–	–	–	–
MING	All	Hess (3)	Av ± stddev Min Max	171 171 171	1,927 ± 1,891 590 3,264	–	1,684 ± 604 1,257 2,111	–	–	872 872 872	–

Table A5-6. (cont.)

Ore body <sup>s</sup>	Mineralization style	Mineral phase*	Av ± stddev	Ni	Cu	Zn	As	Mo	Ag	Sn	Sb
MSUP	sulfide stringer horizon	Alt (1)	Av ± stddev Min Max	–	–	8,639	3,461	–	–	1,026	2,274
MING	All	Alt (1)	Av ± stddev Min Max	–	–	8,639	3,461	–	–	1,026	2,274

Table A5-6. (cont.)

Ore body <sup>§</sup>	Mineralization style	Mineral phase*	Hg	Pb	Bi
MSUP	semi-massive to massive sulfides	Hess (1)	Av ± stdev Min Max	5,327	–
MSDP	semi-massive to massive sulfides	Hess (1)	Av ± stdev Min Max	2,105	–
LFWZ	LFWZ	Hess (1)	Av ± stdev Min Max	–	–
MING	All	Hess (3)	Av ± stdev Min Max	3,716 ± 2,279 2,105 5,327	–

<sup>§</sup> Hessite was not analyzed by EPMA for the 1807 and 1806 ore bodies

\* Numbers in brackets are number of EPMA analysis

Table A5-6. (cont.)

Ore body <sup>§</sup>	Mineralization style	Mineral phase*	Au	Hg	Bi
MSUP	sulfide stringer horizon	Alt (1)	Av ± stdev Min Max	–	–
MING	All	Alt (1)	Av ± stdev Min Max	–	–

<sup>§</sup> Altite was not analyzed by EPMA for the 1807, 1806, MSDP, and LFWZ ore bodies

\* Numbers in brackets are number of EPMA analysis

Table A5-6. Results of EPMA analysis for tsumoite; – not detected or below detection limit

Ore body <sup>s</sup>	Mineralization style	Mineral phase*	Te [wt%]		Bi	Pb	Sb	Total	Mineral Formula	S [ppm]
1807	semi-massive to massive sulfides**	Tsu (7)	Av ± stdev	36.70 ± 1.86	56.75 ± 2.79	5.13 ± 0.924	1.29 ± 0.373	99.88 ± 1.01	(Bi <sub>0.81-1.05</sub> , Pb <sub>0.07-0.12</sub> , Sb <sub>0.02-0.04</sub> ) <sub>0.94-1.17</sub> Te	567 ± 148
			Min	34.78	52.45	4.30	0.561	98.52		412
			Max	39.34	60.25	6.96	1.58	101.10		814
LFWZ	LFWZ	Tsu (2)	Av ± stdev	37.23 ± 2.17	57.39 ± 0.015	5.10 ± 1.08	0.128 ± 0.192	98.21 ± 0.902	(Bi <sub>0.90-0.98</sub> , Pb <sub>0.07-0.10</sub> , Sb <sub>0.00-0.01</sub> ) <sub>0.94-1.09</sub> Te	796 ± 169
			Min	35.69	57.38	4.34	0.000	99.21		677
			Max	38.77	57.40	5.87	0.255	100.49		915
MING	All	Tsu (9)	Av ± stdev	36.82 ± 1.80	56.89 ± 2.43	5.13 ± 0.886	1.03 ± 0.610	99.87 ± 0.927	(Bi <sub>0.81-1.05</sub> , Pb <sub>0.07-0.12</sub> , Sb <sub>0.00-0.04</sub> ) <sub>0.94-1.17</sub> Te	624 ± 176
			Min	34.78	52.45	4.30	0.000	98.52		412
			Max	39.34	60.25	6.96	1.58	101.10		915

Table A5-6. Results of EPMA analysis for unnamed bismuth-telluride; – not detected or below detection limit

Ore body <sup>s</sup>	Mineralization style	Mineral phase*	Te [wt%]		Bi	Pb	Sb	Total	Mineral Formula	S [ppm]
MSUP	semi-massive to massive sulfides	BiTe (1)	Av ± stdev	28.35	67.76	3.42	0.087	99.62	(Bi <sub>2.92</sub> , Pb <sub>0.15</sub> , Sb <sub>0.01</sub> ) <sub>3.07</sub> Te <sub>2</sub>	975
			Min							
			Max							
MING	All	BiTe (1)	Av ± stdev	28.35	67.76	3.42	0.087	99.62	(Bi <sub>2.92</sub> , Pb <sub>0.15</sub> , Sb <sub>0.01</sub> ) <sub>3.07</sub> Te <sub>2</sub>	975
			Min							
			Max							



Table A5-6. (cont.)

Ore body <sup>s</sup>	Mineralization style	Mineral phase*	Min	Fe	Co	Ni	Cu	Zn	As	Mo
1807	semi-massive to massive sulfides**	Tsu (7)	Av ± stdev Min Max	4,659 ± 1,758 3,416 5,902	-	-	874	2,927 ± 907 1,957 3,914	2,715 ± 1,614 1,387 5,437	-
LFWZ	LFWZ	Tsu (2)	Av ± stdev Min Max	6,900 ± 4,201 3,930 9,871	-	-	5,523 ± 964 4,841 6,204	-	1,408 1,408 1,408	-
MING	All	Tsu (9)	Av ± stdev Min Max	5,780 ± 2,930 3,416 9,871	-	-	3,973 ± 2,769 874 6,204	2,927 ± 907 1,957 3,914	2,497 ± 1,539 1,387 5,437	-

Table A5-6. (cont.)

Ore body <sup>s</sup>	Mineralization style	Mineral phase*	Min	Fe	Co	Ni	Cu	Zn	As	Mo
MSUP	semi-massive to massive sulfides	BiTe (1)	Av ± stdev Min Max	6,101	-	-	-	-	2,528	-
MING	All	BiTe (1)	Av ± stdev Min Max	6,101	-	-	-	-	2,528	-

Table A5-6. (cont.)

Ore body <sup>§</sup>	Mineralization style	Mineral phase*	Ag	Sn	Au	Hg
1807	semi-massive to massive sulfides**	Tsu (7)	Av ± stdev Min Max	-	-	-
LFWZ	LFWZ	Tsu (2)	Av ± stdev Min Max	-	-	-
			3,138 ± 2,524 1,353 4,922	-	-	-
MING	All	Tsu (9)	Av ± stdev Min Max	-	-	-
			2,422 ± 2,173 990 4,922	-	-	-

<sup>§</sup> Tsuolite was not analyzed by EPMA for the 1806 Zone, MSUP and MSDP ore bodies

\* Numbers in brackets are number of EPMA analysis

\*\* Samples from 1807 Zone are exclusively from semi-massive to massive sulfides

Table A5-6. (cont.)

Ore body <sup>§</sup>	Mineralization style	Mineral phase*	Ag	Sn	Au	Hg
MSUP	semi-massive to massive sulfides	BiTe (1)	Av ± stdev Min Max	799	-	-
MING	All	BiTe (1)	Av ± stdev Min Max	799	-	-

<sup>§</sup> Unnamed bismuth-telluride was not analyzed by EPMA for the 1807, 1806, MSDP, and LFWZ ore bodies

\* Numbers in brackets are number of EPMA analysis

Table A5-6. Results of EPMA analysis for gudmundite; – not detected or below detection limit

Ore body <sup>s</sup>	Mineralization style	Mineral phase*	S [wt%]	Fe	Sb	Total	Mineral Formula	Mn [ppm]	Co	Ni
1807	semi-massive to massive sulfides**	Gud (3)	Av ± stdev	26.73 ± 0.094	58.46 ± 0.211	100.41 ± 0.390	Fe <sub>1.01</sub> Sb <sub>1.01</sub> S	–	–	202
			Min	15.15	58.31	100.13				
			Max	26.80	58.61	100.69				
MING	All	Gud (3)	Av ± stdev	26.73 ± 0.094	58.46 ± 0.211	100.41 ± 0.390	Fe <sub>1.01</sub> Sb <sub>1.01</sub> S	–	–	202
			Min	15.15	58.31	100.13				
			Max	26.80	58.61	100.69				

Table A5-6. (cont.)

Ore body <sup>s</sup>	Mineralization style	Mineral phase*	Cu	Zn	As	Mo	Ag	Sn	Te	Au
1807	semi-massive to massive sulfides**	Gud (3)	Av ± stdev	-	1,228	-	-	2,522 ± 86.7	2,560	-
			Min	-	1,228	-	-	3,460	2,560	-
			Max	-	1,228	-	-	3,583	2,560	-
MING	All	Gud (3)	Av ± stdev	-	1,228	-	-	2,522 ± 86.7	2,560	-
			Min	-	1,228	-	-	3,460	2,560	-
			Max	-	1,228	-	-	3,583	2,560	-

Table A5-6. (cont.)

Ore body <sup>s</sup>	Mineralization style	Mineral phase*	Hg	Pb	Bi
1807	semi-massive to massive sulfides**	Gud (3)	Av ± stdev	1,054	1,422
			Min	1,054	1,422
			Max	1,054	1,422
MING	All	Gud (3)	Av ± stdev	1,054	1,422
			Min	1,054	1,422
			Max	1,054	1,422

<sup>s</sup> Gudmundite was not analyzed by EPMA for 1806 Zone, MSUP, MSDP, and LFWZ ore bodies

\* Numbers in brackets are number of EPMA analysis

\*\* Samples from 1807 Zone are exclusively from semi-massive to massive sulfides

Table A5-6. Results of EPMA analysis for breithauptite; – not detected or below detection limit

Ore body <sup>s</sup>	Mineralization style	Mineral phase*	Sb [wt%]		Ni	Fe	Total	Mineral Formula	S [ppm]	Mn
MSUP	semi-massive to massive sulfides	Breit (3)	Av ± stdev	66.52 ± 0.213	31.94 ± 0.311	0.927 ± 0.696	99.39 ± 0.687	(Ni <sub>0.98-1.01</sub> Fe <sub>0.02-0.06</sub> ) <sub>1.01-1.04</sub> Sb	1,013 ± 576	–
			Min	66.37	31.65	0.501	98.82		606	–
			Max	66.77	32.27	1.73	100.15		1,421	–
MING	All	Breit (3)	Av ± stdev	66.52 ± 0.213	31.94 ± 0.311	0.927 ± 0.696	99.39 ± 0.687	(Ni <sub>0.98-1.01</sub> Fe <sub>0.02-0.06</sub> ) <sub>1.01-1.04</sub> Sb	1,013 ± 576	–
			Min	66.37	31.65	0.501	98.82		606	–
			Max	66.77	32.27	1.73	100.15		1,421	–

Table A5-6. (cont.)

Ore body <sup>s</sup>	Mineralization style	Mineral phase*	Co	Cu	Zn	As	Mo	Ag	Sn	Te
MSUP	semi-massive to massive sulfides	Breit (3)	Av ± stdev	1,400 ± 652	—	—	—	—	4,203 ± 213	—
			Min	821	—	—	—	—	3,958	—
			Max	2,107	—	—	—	—	4,339	—
MING	All	Breit (3)	Av ± stdev	1,400 ± 652	—	—	—	—	4,203 ± 213	—
			Min	821	—	—	—	—	3,958	—
			Max	2,107	—	—	—	—	4,339	—

Table A5-6. (cont.)

Ore body <sup>§</sup>	Mineralization style	Mineral phase*	Au	Hg	Pb	Bi
MSUP	semi-massive to massive sulfides	Breit (3)	Av ± stdev	2,147	504	-
			Min	2,147	504	-
			Max	2,147	504	-
MING	All	Breit (3)	Av ± stdev	2,147	504	-
			Min	2,147	504	-
			Max	2,147	504	-

<sup>§</sup> Breithauptite was not analyzed by EPMA for the 1807, 1806, MSDP and LFWZ ore bodies

\* Numbers in brackets are number of EPMA analysis



Table A5-6. Results of EPMA analysis for nisbite; – not detected or below detection limit

Ore body <sup>s</sup>	Mineralization style	Mineral phase*	Sb [wt%]	Ni	Fe	Co	Au	Total	Mineral Formula
MSUP	semi-massive to massive sulfides	Nis (1)	Av ± stdev	17.25	0.811	1.09	1.69	98.16	(Ni <sub>0.33</sub> Fe <sub>0.05</sub> Co <sub>0.06</sub> Au <sub>0.03</sub> ) <sub>1.06</sub> Sb <sub>2</sub>
			Min Max						
MING	All	Nis (1)	Av ± stdev	17.25	0.811	1.09	1.69	98.16	(Ni <sub>0.33</sub> Fe <sub>0.05</sub> Co <sub>0.06</sub> Au <sub>0.03</sub> ) <sub>1.06</sub> Sb <sub>2</sub>
			Min Max						

Table A5-6. (cont.)

Ore body <sup>s</sup>	Mineralization style	Mineral phase*	S [ppm]	Mn	Cu	Zn	As	Mo	Ag	Sn
MSUP	semi-massive to massive sulfides	Nis (1)	Av ± stdev	-	1,531	-	2,349	-	-	4,761
			Min							
			Max							
MING	All	Nis (1)	Av ± stdev	-	1,531	-	2,349	-	-	4,761
			Min							
			Max							

Table A5-6. (cont.)

Ore body <sup>§</sup>	Mineralization style	Mineral phase*	Te	Hg	Pb	Bi
MSUP	semi-massive to massive sulfides	Nis (1)	Av ± stdev	–	–	1,240
			Min			
			Max			
MING	All	Nis (1)	Av ± stdev	–	–	1,240
			Min			
			Max			

<sup>§</sup> Nisbite was not analyzed by EPMA for the 1807, 1806, MSDP and LFWZ ore bodies

\* Numbers in brackets are number of EPMA analysis

Table A5-6. Results of EPMA analysis for meneghinite; – not detected or below detection limit

Ore body <sup>s</sup>	Mineralization style	Mineral phase*	S [wt %]		Pb	Cu	Sb	Total	Mineral Formula
1806	semi-massive to massive sulfides	Men (3)	Av ± stdev	16.92 ± 0.250	60.03 ± 1.32	2.08 ± 1.01	20.06 ± 0.309	99.09 ± 0.430	Pb <sub>12.77-13.64</sub> Cu <sub>1.07-2.31</sub> Sb <sub>7.31-7.62</sub> S <sub>24</sub>
			Min	16.63	58.61	1.48	19.76	98.60	
			Max	17.08	61.23	3.25	20.38	99.39	
MSUP	sulfide stringer horizon	Men (2)	Av ± stdev	18.65 ± 0.008	58.46 ± 0.594	1.55 ± 0.608	20.04 ± 0.449	98.71 ± 0.761	Pb <sub>11.56-11.72</sub> Cu <sub>0.73-1.29</sub> Sb <sub>6.68-6.90</sub> S <sub>24</sub>
			Min	18.65	58.04	1.12	19.73	98.17	
			Max	18.66	58.88	1.98	20.36	99.25	
MING	All	Men (5)	Av ± stdev	17.61 ± 0.966	59.40 ± 1.30	1.87 ± 0.828	20.06 ± 0.313	98.94 ± 0.530	Pb <sub>11.56-13.67</sub> Cu <sub>0.73-2.31</sub> Sb <sub>6.68-7.62</sub> S <sub>24</sub>
			Min	16.63	58.04	1.12	19.73	98.17	
			Max	18.66	61.23	3.25	20.38	99.39	

Table A5-6. (cont.)

Ore body <sup>s</sup>	Mineralization style	Mineral phase*	Mn [ppm]	Fe	Co	Ni	Zn	As	Mo	Ag
1806	semi-massive to massive sulfides	Men (3)	Av ± stdev	4,235 ± 5,083	-	-	1,130	-	-	2,703
			Min	638	-	-	1,130	-	-	2,703
			Max	10,051	-	-	1,130	-	-	2,703
MSUP	sulfide stringer horizon	Men (2)	Av ± stdev	2,186 ± 2,463	156	-	7,345	1,629	-	-
			Min	445	156	-	7,345	1,629	-	-
			Max	3,927	156	-	7,345	1,629	-	-
MING	All	Men (5)	Av ± stdev	3,416 ± 3,962	156	-	4,237 ± 4,395	1,629	-	2,703
			Min	445	156	-	1,130	1,629	-	2,703
			Max	10,051	156	-	7,345	1,629	-	2,703

Table A5-6. (cont.)

Ore body <sup>s</sup>	Mineralization style	Mineral phase*	Sn	Te	Au	Hg	Bi
1806	semi-massive to massive sulfides	Men (3)	Av ± stdev	1,180 ± 46.2	-	-	-
			Min	1,147	-	-	-
			Max	1,212	-	-	-
MSUP	sulfide stringer horizon	Men (2)	Av ± stdev	1,581 ± 90.8	1,139	-	-
			Min	1,516	1,139	-	-
			Max	1,645	1,139	-	-
MING	All	Men (5)	Av ± stdev	1,380 ± 239	1,139	-	-
			Min	1,147	1,139	-	-
			Max	1,645	1,139	-	-

\* Meneghnite was not analyzed by EPMA for the 1807 Zone, the silified horizon and sulfide stringer zone of the 1806 Zone, the semi-massive to massive sulfides of the MSUP ore body, the MSDP ore body, and the LFWZ

\* Numbers in brackets are number of EPMA analysis

Table A5-6. Results of EPMA analysis (major elements in wt%) and LA-ICP-MS analysis (trace elements in ppm) for tennantite-tetrahedrite; – not detected or below detection limit, NA - no analysis

Ore body <sup>s</sup>	Mineralization style	Mineral phase*	S [wt %]	Cu	Ag	Fe	Zn	As	Sb	Total
1807	semi-massive to massive	Tnt-Trt (9, 0)	Av ± stdev	39.05 ± 1.72	0.986 ± 0.622	5.60 ± 0.605	2.11 ± 0.563	8.75 ± 5.43	16.21 ± 8.26	99.08 ± 0.591
		Min	24.61	36.43	0.252	4.57	1.38	0.000	4.07	98.04
		Max	28.50	41.59	2.19	6.33	3.37	16.86	29.56	99.86
1806	sulfidized horizon	Tnt-Trt (14, 2)	Av ± stdev	38.39 ± 3.36	2.32 ± 2.36	4.68 ± 1.26	2.82 ± 1.04	10.42 ± 6.85	14.01 ± 9.47	99.19 ± 0.563
		Min	24.33	32.61	0.538	2.44	1.84	1.30	3.51	98.32
		Max	28.10	41.86	7.30	5.86	4.93	18.26	26.12	100.17
1806	semi-massive to massive sulfides	Tnt-Trt (23, 4)	Av ± stdev	34.91 ± 7.35	6.58 ± 7.49	3.87 ± 1.40	3.80 ± 1.40	8.19 ± 7.95	16.81 ± 11.38	99.62 ± 0.735
		Min	21.32	15.29	0.471	1.99	0.314	0.000	1.33	98.48
		Max	28.52	44.46	28.07	6.56	5.49	19.25	27.69	100.98
1806	sulfide stringer horizon	Tnt-Trt (15, 3)	Av ± stdev	32.50 ± 10.08	9.06 ± 11.66	4.66 ± 1.03	2.98 ± 1.53	7.47 ± 5.98	17.57 ± 8.74	99.17 ± 0.714
		Min	20.99	15.54	0.307	3.20	0.550	0.561	2.77	98.19
		Max	27.78	42.05	29.27	6.00	4.69	17.49	29.06	100.72
1806	All	Tnt-Trt (52, 9)	Av ± stdev	35.15 ± 7.69	6.15 ± 8.34	4.31 ± 1.31	3.30 ± 1.40	8.58 ± 7.10	16.27 ± 10.09	99.38 ± 0.708
		Min	20.99	15.29	0.307	1.99	0.314	0.000	1.33	98.19
		Max	28.52	44.46	29.27	6.56	5.49	19.25	29.06	100.98
MING	All	Tnt-Trt (61, 9)	Av ± stdev	35.73 ± 7.25	5.38 ± 7.91	4.50 ± 1.31	3.12 ± 1.38	8.61 ± 6.84	16.27 ± 9.78	99.33 ± 0.696
		Min	20.99	15.29	0.252	1.99	0.314	0.000	1.33	98.04
		Max	28.52	44.46	29.27	6.56	5.49	19.25	29.56	100.98

Table A5-6. (cont.)

Ore body <sup>§</sup>	Mineralization style	Mineral phase*	Mineral Formula	Ti [ppm]	V	Cr
1807	semi-massive to massive sulfides**	Tnt-Trt (9, 0)	Av ± stdev Min Max	NA	NA	NA
1806	silicified horizon	Tnt-Trt (14, 2)	Av ± stdev Min Max	5.73 ± 2.78 3.77 7.70	0.633 0.633 0.633	NA
1806	semi-massive to massive sulfides	Tnt-Trt (23, 4)	Av ± stdev Min Max	4.14 ± 1.47 3.08 6.28	0.893 ± 1.39 0.087 2.49	0.424 0.424 0.424
1806	sulfide stringer horizon	Tnt-Trt (15, 3)	Av ± stdev Min Max	5.85 ± 2.02 4.00 8.00	0.565 ± 0.242 0.394 0.736	2.39 2.39 2.39
1806	All	Tnt-Trt (52, 9)	Av ± stdev Min Max	5.06 ± 1.89 3.08 8.00	0.740 ± 0.899 0.087 2.49	1.41 ± 1.39 0.424 2.39
MING	All	Tnt-Trt (61, 9)	Av ± stdev Min Max	5.06 ± 1.89 3.08 8.00	0.740 ± 0.899 0.087 2.49	1.41 ± 1.39 0.424 2.39



Table A5-6. (cont.)

Ore body <sup>s</sup>	Mineralization style	Mineral phase*	Mn	Co	Ni	Se	Mo	Cd	Sn	Te
1807	semi-massive to massive sulfides**	Tnt-Trt (9, 0)	NA	NA	NA	NA	NA	NA	NA	NA
		Av ± stdev								
		Min								
1806	silicified horizon	Tnt-Trt (14, 2)	33.8 ± 6.95	0.137	NA	766 ± 78.1	NA	723 ± 338	35.4 ± 45.0	41.2 ± 4.39
		Av ± stdev								
		Min	28.9	0.137	—	711	—	484	3.61	38.1
		Max	38.7	0.137	—	821	—	961	67.3	44.3
1806	semi-massive to massive sulfides	Tnt-Trt (23, 4)	92.1 ± 14.0	—	—	57.8 ± 31.1	—	567 ± 308	19.0 ± 35.0	2.22 ± 0.198
		Av ± stdev								
		Min	71.3	—	—	14.1	—	404	0.799	2.08
		Max	102	—	—	81.2	—	1,029	71.6	2.36
1806	sulfide stringer horizon	Tnt-Trt (15, 3)	39.7 ± 17.2	1.75	—	227 ± 22.4	—	630 ± 192	11.3 ± 6.57	8.36 ± 6.32
		Av ± stdev								
		Min	24.4	1.75	—	201	—	500	5.32	1.77
		Max	58.3	1.75	—	240	—	851	18.3	14.4
1806	All	Tnt-Trt (52, 9)	61.7 ± 31.5	0.944 ± 1.14	—	272 ± 293	—	623 ± 251	20.1 ± 28.5	16.0 ± 17.9
		Av ± stdev								
		Min	24.4	0.137	—	14.1	—	404	0.799	1.77
		Max	102	1.75	—	821	—	1,029	71.6	44.3
MING	All	Tnt-Trt (61, 9)	61.7 ± 31.5	0.944 ± 1.14	—	272 ± 293	—	623 ± 251	20.1 ± 28.5	16.0 ± 17.9
		Av ± stdev								
		Min	24.4	0.137	—	14.10	—	404	0.799	1.77
		Max	102	1.75	—	821	—	1,029	71.6	44.3

Table A5-6. (cont.)

Ore body <sup>s</sup>	Mineralization style	Mineral phase*	Au	Tl	Pb	Bi
1807	semi-massive to massive sulfides**	Tnt-Trt (9, 0)	NA	NA	NA	NA
		Av ± stdev				
		Min	NA	NA	NA	NA
		Max	NA	NA	NA	NA
1806	silicified horizon	Tnt-Trt (14, 2)	3.19	13.1 ± 16.8	250 ± 316	228 ± 4.42
		Av ± stdev	3.19	1.21	25.9	225
		Min	3.19	24.9	473	231
		Max	0.021	0.448 ± 0.518	6.34 ± 3.89	1.55 ± 0.848
1806	semi-massive to massive sulfides	Tnt-Trt (23, 4)	0.021	0.088	3.59	0.294
		Av ± stdev	0.021	1.04	9.09	2.08
		Min	0.021	9.22 ± 10.2	1,658 ± 1,503	4.18 ± 1.55
		Max	7.27 ± 8.70	2.43	16.8	2.84
1806	sulfide stringer horizon	Tnt-Trt (15, 3)	0.153	21.0	2,966	5.87
		Av ± stdev	5.00 ± 6.98	6.89 ± 10.1	784 ± 1,203	52.7 ± 99.3
		Min	0.021	0.088	3.59	0.294
		Max	17.0	24.9	2,966	231
MING	All	Tnt-Trt (61, 9)	5.00 ± 6.98	6.89 ± 10.1	784 ± 1,203	52.7 ± 99.3
		Av ± stdev	0.021	0.088	3.59	0.294
		Min	17.0	24.9	2,966	231
		Max				

<sup>s</sup> Tennantite-tetrahedrite was not analyzed by both EPMA and LA-ICP-MS for the MSUP, MSDP, and the LFVZ ore bodies

\* Numbers in brackets are number of EPMA analysis, number of LA-ICP-MS analysis

\*\* Samples from 1807 Zone are exclusively from semi-massive to massive sulfides

Table A5-6. Results of EPMA analysis (major elements in wt%) and LA-ICP-MS analysis (trace elements in in ppm) for stannite; – not detected or below detection limit

Ore body <sup>s</sup>	Mineralization style	Mineral phase*	S [wt%]			Cu	Fe	Zn	Sn	Total
1806	semi-massive to massive sulfides	Stn (4, 3)	Av ± stdev	29.48 ± 0.213	28.14 ± 0.156	12.01 ± 0.168	2.33 ± 0.168	27.53 ± 0.344	99.50 ± 0.204	99.50 ± 0.563
			Min	29.19	27.96	11.78	11.78	1.97	27.32	98.90
			Max	29.67	28.28	12.16	12.16	2.76	27.81	100.02
MING	All	Stn (4, 3)	Av ± stdev	29.48 ± 0.213	28.14 ± 0.156	12.01 ± 0.168	2.33 ± 0.168	27.53 ± 0.344	99.50 ± 0.204	99.50 ± 0.563
			Min	29.19	27.96	11.78	11.78	1.97	27.32	98.90
			Max	29.67	28.28	12.16	12.16	2.76	27.81	100.02

Table A5-6. (cont.)

Ore body <sup>s</sup>	Mineralization style	Mineral phase*	Mineral Formula	Ti [ppm]	V	Cr	Mn	Co
1806	semi-massive to massive sulfides	Stn (4, 3)	Av ± stdev					
			Min	5.48 ± 3.08	0.315	—	274 ± 57.9	1.14 ± 0.178
			Max	2.80	0.315	—	212	1.03
MING	All	Stn (4, 3)	Min	8.17	0.315	—	326	1.35
			Av ± stdev	5.48 ± 3.08	0.315	—	274 ± 57.9	1.14 ± 0.178
			Max	2.80	0.315	—	212	1.03
				8.17	0.315	—	326	1.35

Table A5-6. (cont.)

Ore body <sup>s</sup>	Mineralization style	Mineral phase*	Ni	As	Se	Mo	Ag	Cd	Sb	Te
1806	semi-massive to massive sulfides	Stn (4, 3)	Av $\pm$ stdev	584 $\pm$ 177	66.5 $\pm$ 25.2	-	341 $\pm$ 179	1,072 $\pm$ 233	30.2 $\pm$ 5.64	-
			Min	458	37.5	-	219	897	25.2	-
			Max	787	82.9	-	546	1,337	36.3	-
MING	All	Stn (4, 3)	Av $\pm$ stdev	584 $\pm$ 177	66.5 $\pm$ 25.2	-	341 $\pm$ 179	1,072 $\pm$ 233	30.2 $\pm$ 5.64	-
			Min	458	37.5	-	219	897	25.2	-
			Max	787	82.9	-	546	1,337	36.3	-

Table A5-6. (cont.)

Ore body <sup>s</sup>	Mineralization style	Mineral phase*	Au	Tl	Pb	Bi
1806	semi-massive to massive sulfides	Stn (4, 3)	Av $\pm$ stddev	0.817	0.585 $\pm$ 0.577	79.2 $\pm$ 1.89
			Min	0.817	0.188	77.8
			Max	0.817	1.25	80.5
MING	All	Stn (4, 3)	Av $\pm$ stddev	0.817	0.585 $\pm$ 0.577	79.2 $\pm$ 1.89
			Min	0.817	0.188	77.8
			Max	0.817	1.25	80.5

<sup>s</sup> Stannite was not analyzed by both EPMA and LA-ICP-MS for the 1807, MSUP, MSDP and LFWZ ore bodies

\* Numbers in brackets are number of EPMA analysis, LA-ICP-MS analysis

Ore body <sup>s</sup>	Mineralization style	Mineral phase*	Au [wt%]	Ag	Hg	Total	Mineral Formula	S [ppm]	Ti	V
1807	semi-massive to massive sulfides**	El (1, 0)	Av ± stdev Min	70.17	26.02	3.05	99.24	(Au, Ag, Hg) <sub>1.27</sub>	NA	NA
			Max						NA	NA
1806	silicified horizon	El (7, 5)	Av ± stdev Min	40.93 ± 2.94 37.69	44.03 ± 3.58 36.70	14.45 ± 1.47 13.05	99.41 ± 0.921 98.25	(Au, Ag, Hg) <sub>0.79-0.97</sub>	234 ± 131 105	– –
			Max	46.61	47.70	17.15	100.48		453	–
1806	semi-massive to massive sulfides	El (10, 0)	Av ± stdev Min	47.34 ± 13.72 13.87	39.01 ± 11.34 30.29	13.71 ± 3.27 7.93	100.05 ± 0.942 98.19	(Au, Ag, Hg) <sub>0.62-1.13</sub>	NA NA	NA NA
			Max	61.99	67.35	20.57	101.04		NA	NA
1806	sulfide stringer horizon	El (5, 3)	Av ± stdev Min	44.28 ± 8.91 37.43	39.64 ± 6.02 30.45	15.58 ± 2.72 11.30	99.50 ± 1.05 98.29	(Au, Ag, Hg) <sub>0.82-1.13</sub>	120 ± 28.3 97.4	– –
			Max	59.31	45.45	17.90	101.07		152	–
1806	All	El (22, 8)	Av ± stdev Min	44.60 ± 10.32 13.87	40.75 ± 8.43 30.29	14.37 ± 2.67 7.93	99.72 ± 0.964 98.19	(Au, Ag, Hg) <sub>0.62-1.13</sub>	191 ± 116 97.4	– –
			Max	61.99	67.35	20.57	101.07		453	–
MING	All	El (23, 8)	Av ± stdev Min	45.71 ± 11.40 13.87	40.11 ± 8.79 26.02	13.88 ± 3.52 3.05	99.70 ± 0.947 98.19	(Au, Ag, Hg) <sub>0.62-1.23</sub>	191 ± 116 97.4	– –
			Max	70.17	67.35	20.57	101.07		453	–

Table A5-6. (cont.)

Ore body <sup>s</sup>	Mineralization style	Mineral phase*	Cr	Mn	Fe	Co	Ni	Cu	Zn	As
1807	semi-massive to massive sulfides**	El (1, 0)	NA	NA	NA	NA	NA	NA	NA	NA
		Av ± stdev								
		Min								
		Max								
1806	silicified horizon	El (7, 5)	—	5.53	277 ± 370	—	—	281 ± 206	116 ± 197	85.4 ± 34.6
		Av ± stdev		5.53	29.1			136	1.48	51.8
		Min		5.53	906			427	343	135
		Max								
1806	semi-massive to massive sulfides	El (10, 0)	NA	NA	NA	NA	NA	NA	NA	NA
		Av ± stdev								
		Min								
		Max								
1806	sulfide stringer horizon	El (5, 3)	—	—	341 ± 260	—	—	122	153 ± 230	125 ± 13.8
		Av ± stdev			57.4			122	14.0	112
		Min			569			122	418	140
		Max								
1806	All	El (22, 8)	—	5.53	301 ± 314	—	—	228 ± 172	134 ± 193	100 ± 34.1
		Av ± stdev		5.53	29.1			122	1.48	51.8
		Min		5.53	906			427	418	140
		Max								
MING	All	El (23, 8)	—	5.53	301 ± 314	—	—	228 ± 172	134 ± 193	100 ± 34.1
		Av ± stdev		5.53	29.1			122	1.48	51.8
		Min		5.53	906			427	418	140
		Max								



Table A5-6. (cont.)

Ore body <sup>s</sup>	Mineralization style	Mineral phase*	Se	Mo	Cd	Sn	Sb	Te	Tl	Pb
1807	semi-massive to massive sulfides**	El (1, 0)	NA	NA	NA	NA	NA	NA	NA	NA
		Av ± stdev								
		Min	NA	NA	NA	NA	NA	NA	NA	NA
		Max	NA	NA	NA	NA	NA	NA	NA	NA
1806	silicified horizon	El (7, 5)	1.64 ± 0.748	—	2.53	0.305	688 ± 221	6.68 ± 0.475	0.054 ± 0.010	0.273 ± 0.087
		Av ± stdev								
		Min	1.09	—	2.53	0.305	456	6.34	0.045	0.211
		Max	2.74	—	2.53	0.305	983	7.01	0.064	0.334
1806	semi-massive to massive sulfides	El (10, 0)	NA	NA	NA	NA	NA	NA	NA	NA
		Av ± stdev								
		Min	NA	NA	NA	NA	NA	NA	NA	NA
		Max	NA	NA	NA	NA	NA	NA	NA	NA
1806	sulfide stringer horizon	El (5, 3)	—	—	4.27	0.213	546 ± 503	1.20	0.089	0.183 ± 0.195
		Av ± stdev								
		Min	—	—	4.27	0.213	248	1.20	0.089	0.045
		Max	—	—	4.27	0.213	1,126	1.20	0.089	0.321
1806	All	El (22, 8)	1.64 ± 0.748	—	3.40 ± 1.23	0.259 ± 0.065	635 ± 325	4.85 ± 3.18	0.063 ± 0.019	0.228 ± 0.134
		Av ± stdev								
		Min	1.09	—	2.53	0.213	248	1.20	0.045	0.045
		Max	2.74	—	4.27	0.305	1,126	7.01	0.089	0.334
MING	All	El (23, 8)	1.64 ± 0.748	—	3.40 ± 1.23	0.259 ± 0.065	635 ± 325	4.85 ± 3.18	0.063 ± 0.019	0.228 ± 0.134
		Av ± stdev								
		Min	1.09	—	2.53	0.213	248	1.20	0.045	0.045
		Max	2.74	—	4.27	0.305	1,126	7.01	0.089	0.334

Table A5-6. (cont.)

Ore body <sup>s</sup>	Mineralization style	Mineral phase*	Bi
1807	semi-massive to massive sulfides**	El (1, 0)	NA
		Av ± stdev	NA
		Min	NA
		Max	NA
1806	silicified horizon	El (7, 5)	-
		Av ± stdev	-
		Min	-
		Max	-
1806	semi-massive to massive sulfides	El (10, 0)	NA
		Av ± stdev	NA
		Min	NA
		Max	NA
1806	sulfide stringer horizon	El (5, 3)	-
		Av ± stdev	-
		Min	-
		Max	-
1806	All	El (22, 8)	-
		Av ± stdev	-
		Min	-
		Max	-
MING	All	El (23, 8)	-
		Av ± stdev	-
		Min	-
		Max	-

<sup>s</sup>Electrum was not analyzed by both EPMA and LA-ICP-MS for the MSUP, MSDP, and the LFWZ ore bodies

\* Numbers in brackets are number of EPMA analysis, number of LA-ICP-MS analysis

\*\* Samples from 1807 Zone are exclusively from semi-massive to massive sulfides

**Table eA1.** Detailed coordinates of logged drill hole sections from the 1807 Zone; coordinates in UTM 21N NAD83 (data from Rambler Metals & Mining Canada Ltd)

Drill hole #	Drill hole intervall			Coordinates		Depth below	Coordinates		Depth below
	From [m]	To [m]	Length [m]	X_start (E)	Y_start (N)	sea level Z_start [m]	X_end (E)	Y_end (N)	sea level Z_end [m]
<b>RM07-19</b>									
RM07-19	585.1	586.6	1.50	566243	5530360	-382	566243	5530360	-384
RM07-19	586.6	588.1	1.50	566243	5530360	-384	566242	5530359	-385
RM07-19	588.1	589.6	1.50	566242	5530359	-385	566241	5530359	-386
RM07-19	589.6	591.1	1.50	566241	5530359	-386	566241	5530358	-387
RM07-19	591.1	592.6	1.50	566241	5530358	-387	566240	5530358	-389
RM07-19	592.6	594.1	1.50	566240	5530358	-389	566240	5530357	-390
RM07-19	594.1	595.6	1.50	566240	5530357	-390	566239	5530357	-391
RM07-19	595.6	597.1	1.50	566239	5530357	-391	566239	5530356	-393
RM07-19	597.1	598.6	1.50	566239	5530356	-393	566238	5530356	-394
RM07-19	598.6	600.1	1.50	566238	5530356	-394	566238	5530355	-395
<b>RM07-19a</b>									
RM07-19a	595.0	596.5	1.50	566219	5530309	-356	566218	5530309	-357
RM07-19a	596.5	598.0	1.50	566218	5530309	-357	566218	5530308	-358
RM07-19a	598.0	599.5	1.50	566218	5530308	-358	566217	5530307	-359
RM07-19a	599.5	601.0	1.50	566217	5530307	-359	566216	5530306	-361
<b>RM07-19c</b>									
RM07-19c	586.2	587.7	1.50	566262	5530346	-384	566262	5530345	-385
RM07-19c	587.7	589.2	1.50	566262	5530345	-385	566261	5530345	-387
RM07-19c	589.2	590.7	1.50	566261	5530345	-387	566261	5530344	-388
RM07-19c	590.7	592.2	1.50	566261	5530344	-388	566261	5530344	-389
RM07-19c	592.2	593.7	1.50	566261	5530344	-389	566260	5530343	-391
RM07-19c	593.7	595.2	1.50	566260	5530343	-391	566260	5530342	-392
RM07-19c	595.2	596.7	1.50	566260	5530342	-392	566259	5530342	-393
<b>RM07-19e</b>									
RM07-19e	588.7	590.2	1.50	566239	5530304	-353	566238	5530303	-354
RM07-19e	590.2	591.7	1.50	566238	5530303	-354	566238	5530302	-355
RM07-19e	591.7	593.2	1.50	566238	5530302	-355	566237	5530301	-356
RM07-19e	593.2	594.7	1.50	566237	5530301	-356	566237	5530300	-357
RM07-19e	594.7	596.2	1.50	566237	5530300	-357	566236	5530299	-359
RM07-19e	596.2	597.7	1.50	566236	5530299	-359	566236	5530298	-360
<b>RM07-19g</b>									
RM07-19g	589.6	591.1	1.50	566215	5530290	-329	566215	5530289	-330
RM07-19g	591.1	592.6	1.50	566215	5530289	-330	566214	5530288	-331
RM07-19g	592.6	594.1	1.50	566214	5530288	-331	566213	5530287	-332
RM07-19g	594.1	595.6	1.50	566213	5530287	-332	566212	5530286	-333
RM07-19g	595.6	597.1	1.50	566212	5530286	-333	566212	5530285	-334
RM07-19g	597.1	598.6	1.50	566212	5530285	-334	566211	5530284	-335
RM07-19g	598.6	600.1	1.50	566211	5530284	-335	566210	5530283	-336
RM07-19g	600.1	601.6	1.50	566210	5530283	-336	566210	5530282	-337
RM07-19g	601.6	603.1	1.50	566210	5530282	-337	566209	5530281	-338
<b>RM07-18</b>									
RM07-18a	593.5	594.5	1.00	566338	5530451	-438	566338	5530451	-439
RM07-18a	594.5	595.5	1.00	566338	5530451	-439	566338	5530451	-440
RM07-18a	595.5	596.5	1.00	566338	5530451	-440	566337	5530451	-440
RM07-18a	596.5	597.5	1.00	566337	5530451	-440	566337	5530451	-441
RM07-18a	597.5	598.5	1.00	566337	5530451	-441	566337	5530450	-442
RM07-18a	598.5	599.5	1.00	566337	5530450	-442	566337	5530450	-443
RM07-18a	599.5	600.5	1.00	566337	5530450	-443	566337	5530450	-444
RM07-18a	600.5	601.5	1.00	566337	5530450	-444	566336	5530450	-445
RM07-18a	601.5	602.5	1.00	566336	5530450	-445	566336	5530450	-446
RM07-18a	602.5	603.5	1.00	566336	5530450	-446	566336	5530450	-447
RM07-18a	603.5	604.5	1.00	566336	5530450	-447	566336	5530450	-448
<b>RM07-18b</b>									
RM07-18b	599.5	601.0	1.50	566323	5530474	-442	566323	5530474	-444
RM07-18b	601.0	602.5	1.50	566323	5530474	-444	566323	5530474	-445
RM07-18b	602.5	604.0	1.50	566323	5530474	-445	566322	5530474	-446
RM07-18b	604.0	605.5	1.50	566322	5530474	-446	566322	5530474	-448
RM07-18b	605.5	607.0	1.50	566322	5530474	-448	566321	5530474	-449
RM07-18b	607.0	608.5	1.50	566321	5530474	-449	566321	5530474	-451
RM07-18b	608.5	610.0	1.50	566321	5530474	-451	566321	5530473	-452
RM07-18b	610.0	611.5	1.50	566321	5530473	-452	566320	5530473	-454
RM07-18b	611.5	613.0	1.50	566320	5530473	-454	566320	5530473	-455

RM07-18d	598.6	600.1	1.50	566285	5530445	-424	566284	5530445	-425
RM07-18d	600.1	601.6	1.50	566284	5530445	-425	566284	5530445	-426
RM07-18d	601.6	603.1	1.50	566284	5530445	-426	566283	5530445	-428
RM07-18e	598.0	599.5	1.50	566351	5530433	-442	566350	5530432	-443
RM07-18e	599.5	601.0	1.50	566350	5530432	-443	566350	5530432	-445
RM07-18e	601.0	602.5	1.50	566350	5530432	-445	566350	5530432	-446
RM07-18e	602.5	604.0	1.50	566350	5530432	-446	566350	5530432	-447
<b>RM07-20</b>									
RM07-20	654.2	657.2	2.99	566403	5530507	-469	566402	5530507	-472
RM07-20	657.2	660.2	2.99	566402	5530507	-472	566401	5530507	-474
RM07-20a	638.1	641.1	3.00	566424	5530496	-460	566423	5530496	-462
RM07-20a	641.1	644.1	3.00	566423	5530496	-462	566422	5530495	-465
RM07-20a	644.1	647.1	3.00	566422	5530495	-465	566420	5530495	-468
RM07-20a	647.1	650.1	3.00	566420	5530495	-468	566419	5530495	-470
RM07-20b	664.1	667.1	2.99	566363	5530489	-456	566361	5530489	-458
RM07-20b	667.1	670.1	2.99	566361	5530489	-458	566359	5530489	-461
RM07-20b	670.1	673.1	2.99	566359	5530489	-461	566358	5530488	-463
RM07-20c	660.2	663.2	2.99	566378	5530469	-457	566376	5530469	-460
RM07-20c	663.2	666.2	2.99	566376	5530469	-460	566375	5530468	-462
RM07-20c	666.2	669.2	2.99	566375	5530468	-462	566373	5530468	-465
RM07-20e	657.7	660.7	2.99	566357	5530504	-445	566355	5530504	-447
RM07-20e	660.7	663.7	2.99	566355	5530504	-447	566353	5530504	-450
RM07-20e	663.7	666.7	2.99	566353	5530504	-450	566352	5530504	-452
RM07-20g	650.1	653.1	3.00	566393	5530527	-460	566391	5530527	-462
RM07-20g	653.1	656.1	3.00	566391	5530527	-462	566390	5530527	-465
RM07-20g	656.1	659.1	3.00	566390	5530527	-465	566388	5530527	-468
RM07-20g	659.1	662.0	3.00	566388	5530527	-468	566387	5530527	-470
RM07-20g	662.0	665.0	3.00	566387	5530527	-470	566385	5530527	-473
RM07-20h	644.1	647.1	3.00	566386	5530535	-449	566385	5530535	-451
RM07-20h	647.1	650.1	3.00	566385	5530535	-451	566383	5530536	-454
RM07-20h	650.1	653.1	3.00	566383	5530536	-454	566381	5530536	-456
RM07-20h	653.1	656.1	3.00	566381	5530536	-456	566380	5530536	-459
RM07-20h	656.1	659.0	3.00	566380	5530536	-459	566378	5530536	-461
RM07-20h	659.0	662.0	3.00	566378	5530536	-461	566376	5530536	-464
RM07-20h	662.0	665.0	3.00	566376	5530536	-464	566375	5530537	-466
RM07-20h	665.0	668.0	3.00	566375	5530537	-466	566373	5530537	-469
RM07-20h	668.0	671.0	3.00	566373	5530537	-469	566371	5530537	-471
RM07-20i	650.7	653.7	3.00	566372	5530549	-445	566370	5530549	-447
RM07-20i	653.7	656.7	3.00	566370	5530549	-447	566368	5530549	-450
RM07-20i	656.7	659.7	3.00	566368	5530549	-450	566366	5530550	-452
RM07-20j	646.6	648.6	2.00	566412	5530544	-464	566411	5530545	-466
RM07-20j	648.6	650.6	2.00	566411	5530545	-466	566410	5530545	-468
RM07-20j	650.6	652.6	2.00	566410	5530545	-468	566410	5530545	-469
RM07-20j	652.6	654.6	2.00	566410	5530545	-469	566409	5530546	-471
RM07-20j	654.6	656.6	2.00	566409	5530546	-471	566408	5530546	-473
RM07-20j	656.6	658.6	2.00	566408	5530546	-473	566407	5530546	-475
RM07-20j	658.6	660.6	2.00	566407	5530546	-475	566406	5530547	-477
RM07-20j	660.6	662.6	2.00	566406	5530547	-477	566405	5530547	-478
RM07-20j	662.6	664.6	2.00	566405	5530547	-478	566405	5530547	-480
RM07-20j	664.6	666.6	2.00	566405	5530547	-480	566404	5530548	-482
RM07-20j	666.6	668.6	2.00	566404	5530548	-482	566403	5530548	-484
RM07-20j	668.6	670.6	2.00	566403	5530548	-484	566402	5530548	-485
RM07-20k	647.1	649.1	2.00	566421	5530540	-469	566421	5530540	-471
RM07-20k	649.1	651.1	2.00	566421	5530540	-471	566420	5530540	-473
RM07-20k	651.1	653.1	2.00	566420	5530540	-473	566419	5530540	-475
RM07-20k	653.1	655.1	2.00	566419	5530540	-475	566418	5530540	-477
RM07-20k	655.1	657.1	2.00	566418	5530540	-477	566418	5530540	-478
RM07-20k	657.1	659.1	2.00	566418	5530540	-478	566417	5530540	-480

RM07-20k	659.1	661.1	2.00	566417	5530540	-480	566416	5530541	-482
RM07-20k	661.1	663.1	2.00	566416	5530541	-482	566415	5530541	-484
RM07-20k	663.1	665.1	2.00	566415	5530541	-484	566415	5530541	-486
RM07-20k	665.1	667.1	2.00	566415	5530541	-486	566414	5530541	-488
RM07-20l	652.6	654.1	1.50	566401	5530566	-461	566400	5530566	-462
RM07-20l	654.1	655.6	1.50	566400	5530566	-462	566400	5530567	-464
RM07-20l	655.6	657.1	1.50	566400	5530567	-464	566399	5530567	-465
RM07-20l	657.1	658.6	1.50	566399	5530567	-465	566398	5530567	-466
RM08-20m	657.0	659.0	2.00	566424	5530571	-475	566424	5530571	-476
RM08-20m	659.0	661.0	2.00	566424	5530571	-476	566423	5530572	-478
RM08-20m	661.0	663.0	2.00	566423	5530572	-478	566422	5530572	-480
RM08-20m	663.0	665.0	2.00	566422	5530572	-480	566422	5530573	-482
RM08-20m	665.0	667.0	2.00	566422	5530573	-482	566421	5530573	-484
RM08-20m	667.0	669.0	2.00	566421	5530573	-484	566420	5530574	-486
RM08-20m	669.0	671.0	2.00	566420	5530574	-486	566420	5530574	-487
RM08-20m	671.0	673.0	2.00	566420	5530574	-487	566419	5530575	-489
RM08-20m	673.0	675.0	2.00	566419	5530575	-489	566419	5530576	-491
RM08-20m	675.0	677.0	2.00	566419	5530576	-491	566418	5530576	-493
RM08-20na	657.5	659.0	1.50	566434	5530556	-485	566433	5530556	-486
RM08-20na	659.0	660.5	1.50	566433	5530556	-486	566433	5530556	-487
RM08-20na	660.5	662.0	1.50	566433	5530556	-487	566432	5530557	-489
RM08-20o	653.1	654.1	1.00	566404	5530577	-465	566403	5530577	-466
RM08-20o	654.1	655.1	1.00	566403	5530577	-466	566403	5530577	-467
RM08-20o	655.1	656.1	1.00	566403	5530577	-467	566402	5530577	-467
RM08-20o	656.1	657.1	1.00	566402	5530577	-467	566402	5530577	-468
RM08-20o	657.1	658.1	1.00	566402	5530577	-468	566402	5530578	-469
RM08-20o	658.1	659.1	1.00	566402	5530578	-469	566401	5530578	-470
RM08-20o	659.1	660.1	1.00	566401	5530578	-470	566401	5530578	-471
RM08-20o	660.1	661.1	1.00	566401	5530578	-471	566400	5530578	-472
RM08-20o	661.1	662.1	1.00	566400	5530578	-472	566400	5530579	-473

**Table eA1.** Detailed coordinates of logged drill hole sections from the 1806 Zone; coordinates in UTM 21N NAD83 (data from Rambler Metals & Mining Canada Ltd)

Drill hole #	Drill hole intervall			Coordinates		Depth below sea level	Coordinates		Depth below sea level
	From [m]	To [m]	Length [m]	X_start (E)	Y_start (N)	Z_start [m]	X_end (E)	Y_end (N)	Z_end [m]
Section 21									
RMUG08-120	0.0	2.9	2.88	566128	5529696	-60.2	566126	5529698	-58.9
RMUG08-120	2.9	5.8	2.88	566126	5529698	-58.9	566124	5529700	-57.7
RMUG08-120	5.8	8.6	2.88	566124	5529700	-57.7	566122	5529701	-56.4
RMUG08-120	8.6	11.5	2.88	566122	5529701	-56.4	566120	5529703	-55.1
RMUG08-120	11.5	14.4	2.88	566120	5529703	-55.1	566118	5529705	-53.8
RMUG08-120	14.4	17.3	2.88	566118	5529705	-53.8	566116	5529707	-52.5
RMUG08-120	17.3	20.2	2.88	566116	5529707	-52.5	566115	5529709	-51.2
RMUG08-120	20.2	23.0	2.88	566115	5529709	-51.2	566113	5529710	-49.9
RMUG08-120	23.0	25.9	2.88	566113	5529710	-49.9	566111	5529712	-48.6
RMUG08-120	25.9	28.8	2.88	566111	5529712	-48.6	566109	5529714	-47.4
RMUG08-120	28.8	31.7	2.88	566109	5529714	-47.4	566107	5529716	-46.1
RMUG08-120	31.7	34.6	2.88	566107	5529716	-46.1	566105	5529717	-44.8
RMUG08-120	34.6	37.4	2.88	566105	5529717	-44.8	566103	5529719	-43.5
RMUG08-120	37.4	40.3	2.88	566103	5529719	-43.5	566102	5529721	-42.2
RMUG08-120	40.3	43.2	2.88	566102	5529721	-42.2	566100	5529723	-40.9
RMUG08-120	43.2	46.1	2.88	566100	5529723	-40.9	566098	5529725	-39.7
RMUG08-120	46.1	49.0	2.88	566098	5529725	-39.7	566096	5529726	-38.4
RMUG08-120	49.0	51.8	2.88	566096	5529726	-38.4	566094	5529728	-37.1
RMUG08-120	51.8	54.7	2.88	566094	5529728	-37.1	566092	5529730	-35.8
RMUG08-120	54.7	57.6	2.88	566092	5529730	-35.8	566091	5529732	-34.6
RMUG08-120	57.6	60.5	2.88	566091	5529732	-34.6	566089	5529734	-33.3
RMUG08-120	60.5	63.4	2.88	566089	5529734	-33.3	566087	5529736	-32.0
RMUG08-120	63.4	66.2	2.88	566087	5529736	-32.0	566085	5529737	-30.7
RMUG08-120	66.2	69.1	2.88	566085	5529737	-30.7	566083	5529739	-29.5
RMUG08-120	69.1	72.0	2.88	566083	5529739	-29.5	566081	5529741	-28.2
RMUG08-121	0.0	3.0	2.95	566128	5529696	-60.6	566127	5529699	-59.9
RMUG08-121	3.0	5.9	2.95	566127	5529699	-59.9	566125	5529702	-59.2
RMUG08-121	5.9	8.9	2.95	566125	5529702	-59.2	566124	5529704	-58.6
RMUG08-121	8.9	11.8	2.95	566124	5529704	-58.6	566123	5529707	-57.9
RMUG08-121	11.8	14.8	2.95	566123	5529707	-57.9	566121	5529709	-57.2
RMUG08-121	14.8	17.7	2.95	566121	5529709	-57.2	566120	5529712	-56.5
RMUG08-121	17.7	20.7	2.95	566120	5529712	-56.5	566119	5529714	-55.8
RMUG08-121	20.7	23.6	2.95	566119	5529714	-55.8	566117	5529717	-55.1
RMUG08-121	23.6	26.6	2.95	566117	5529717	-55.1	566116	5529719	-54.4
RMUG08-121	26.6	29.5	2.95	566116	5529719	-54.4	566115	5529722	-53.7
RMUG08-121	29.5	32.5	2.95	566115	5529722	-53.7	566114	5529724	-53.0
RMUG08-121	32.5	35.4	2.95	566114	5529724	-53.0	566112	5529727	-52.3
RMUG08-121	35.4	38.4	2.95	566112	5529727	-52.3	566111	5529730	-51.6
RMUG08-121	38.4	41.3	2.95	566111	5529730	-51.6	566110	5529732	-50.9
RMUG08-121	41.3	44.3	2.95	566110	5529732	-50.9	566108	5529735	-50.2
RMUG08-121	44.3	47.2	2.95	566108	5529735	-50.2	566107	5529737	-49.6
RMUG08-121	47.2	50.2	2.95	566107	5529737	-49.6	566106	5529740	-48.9
RMUG08-121	50.2	53.1	2.95	566106	5529740	-48.9	566104	5529742	-48.2
RMUG08-121	53.1	56.1	2.95	566104	5529742	-48.2	566103	5529745	-47.5
RMUG08-121	56.1	59.0	2.95	566103	5529745	-47.5	566102	5529748	-46.8
RMUG08-121	59.0	62.0	2.95	566102	5529748	-46.8	566101	5529750	-46.1
RMUG08-121	62.0	64.9	2.95	566101	5529750	-46.1	566099	5529753	-45.4
RMUG08-121	64.9	67.9	2.95	566099	5529753	-45.4	566098	5529755	-44.7
RMUG08-121	67.9	70.8	2.95	566098	5529755	-44.7	566097	5529758	-43.9
RMUG08-121	70.8	73.8	2.95	566097	5529758	-43.9	566096	5529760	-43.2
RMUG08-121	73.8	76.7	2.95	566096	5529760	-43.2	566094	5529763	-42.5
RMUG08-121	76.7	79.7	2.95	566094	5529763	-42.5	566093	5529765	-41.8
RMUG08-121	79.7	82.6	2.95	566093	5529765	-41.8	566092	5529768	-41.1
RMUG08-123	0.0	2.9	2.91	566125	5529695	-59.7	566123	5529696	-58.1
RMUG08-123	2.9	5.8	2.91	566123	5529696	-58.1	566121	5529697	-56.5
RMUG08-123	5.8	8.7	2.91	566121	5529697	-56.5	566118	5529698	-55.0
RMUG08-123	8.7	11.7	2.91	566118	5529698	-55.0	566116	5529699	-53.4
RMUG08-123	11.7	14.6	2.91	566116	5529699	-53.4	566114	5529700	-51.9
RMUG08-123	14.6	17.5	2.91	566114	5529700	-51.9	566112	5529701	-50.3
RMUG08-123	17.5	20.4	2.91	566112	5529701	-50.3	566109	5529702	-48.7

RMUG08-123	20.4	23.3	2.91	566109	5529702	-48.7	566107	5529703	-47.1
RMUG08-123	23.3	26.2	2.91	566107	5529703	-47.1	566105	5529704	-45.6
RMUG08-123	26.2	29.1	2.91	566105	5529704	-45.6	566103	5529705	-44.0
RMUG08-123	29.1	32.0	2.91	566103	5529705	-44.0	566100	5529706	-42.4
RMUG08-123	32.0	35.0	2.91	566100	5529706	-42.4	566098	5529707	-40.9
RMUG08-123	35.0	37.9	2.91	566098	5529707	-40.9	566096	5529708	-39.3
RMUG08-123	37.9	40.8	2.91	566096	5529708	-39.3	566094	5529709	-37.8
RMUG08-123	40.8	43.7	2.91	566094	5529709	-37.8	566092	5529710	-36.2
RMUG08-123	43.7	46.6	2.91	566092	5529710	-36.2	566089	5529711	-34.6
RMUG08-123	46.6	49.5	2.91	566089	5529711	-34.6	566087	5529712	-33.1
RMUG08-123	49.5	52.4	2.91	566087	5529712	-33.1	566085	5529713	-31.5
RMUG08-123	52.4	55.4	2.91	566085	5529713	-31.5	566083	5529714	-30.0
RMUG08-123	55.4	58.3	2.91	566083	5529714	-30.0	566080	5529715	-28.4
RMUG08-123	58.3	61.2	2.91	566080	5529715	-28.4	566078	5529716	-26.9
RMUG08-123	61.2	64.1	2.91	566078	5529716	-26.9	566076	5529717	-25.3
RMUG08-123	64.1	67.0	2.91	566076	5529717	-25.3	566074	5529719	-23.8
RMUG08-123	67.0	69.9	2.91	566074	5529719	-23.8	566072	5529720	-22.2
RMUG08-123	69.9	72.8	2.91	566072	5529720	-22.2	566069	5529721	-20.7
RMUG08-123	72.8	75.7	2.91	566069	5529721	-20.7	566067	5529722	-19.1
RMUG08-123	75.7	78.7	2.91	566067	5529722	-19.1	566065	5529723	-17.6
RMUG08-123	78.7	81.6	2.91	566065	5529723	-17.6	566063	5529724	-16.0
RMUG08-123	81.6	84.5	2.91	566063	5529724	-16.0	566060	5529725	-14.5
RMUG08-123	84.5	87.4	2.91	566060	5529725	-14.5	566058	5529726	-12.9
RMUG08-124	0.0	3.0	2.97	566127	5529696	-60.7	566125	5529698	-59.8
RMUG08-124	3.0	5.9	2.97	566125	5529698	-59.8	566123	5529700	-58.9
RMUG08-124	5.9	8.9	2.97	566123	5529700	-58.9	566121	5529702	-57.9
RMUG08-124	8.9	11.9	2.97	566121	5529702	-57.9	566119	5529704	-57.0
RMUG08-124	11.9	14.9	2.97	566119	5529704	-57.0	566116	5529705	-56.1
RMUG08-124	14.9	17.8	2.97	566116	5529705	-56.1	566114	5529707	-55.1
RMUG08-124	17.8	20.8	2.97	566114	5529707	-55.1	566112	5529709	-54.2
RMUG08-124	20.8	23.8	2.97	566112	5529709	-54.2	566110	5529711	-53.2
RMUG08-124	23.8	26.8	2.97	566110	5529711	-53.2	566108	5529713	-52.3
RMUG08-124	26.8	29.7	2.97	566108	5529713	-52.3	566106	5529715	-51.4
RMUG08-124	29.7	32.7	2.97	566106	5529715	-51.4	566104	5529717	-50.5
RMUG08-124	32.7	35.7	2.97	566104	5529717	-50.5	566102	5529719	-49.5
RMUG08-124	35.7	38.7	2.97	566102	5529719	-49.5	566100	5529721	-48.6
RMUG08-124	38.7	41.6	2.97	566100	5529721	-48.6	566098	5529723	-47.7
RMUG08-124	41.6	44.6	2.97	566098	5529723	-47.7	566095	5529724	-46.8
RMUG08-124	44.6	47.6	2.97	566095	5529724	-46.8	566093	5529726	-45.9
RMUG08-124	47.6	50.6	2.97	566093	5529726	-45.9	566091	5529728	-44.9
RMUG08-124	50.6	53.5	2.97	566091	5529728	-44.9	566089	5529730	-44.0
RMUG08-124	53.5	56.5	2.97	566089	5529730	-44.0	566087	5529732	-43.1
RMUG08-124	56.5	59.5	2.97	566087	5529732	-43.1	566085	5529734	-42.2
RMUG08-124	59.5	62.4	2.97	566085	5529734	-42.2	566083	5529736	-41.3
RMUG08-124	62.4	65.4	2.97	566083	5529736	-41.3	566081	5529738	-40.4
RMUG08-124	65.4	68.4	2.97	566081	5529738	-40.4	566079	5529740	-39.5
RMUG08-124	68.4	71.4	2.97	566079	5529740	-39.5	566077	5529742	-38.6
RMUG08-124	71.4	74.3	2.97	566077	5529742	-38.6	566075	5529743	-37.7
RMUG08-124	74.3	77.3	2.97	566075	5529743	-37.7	566072	5529745	-36.8
RMUG08-124	77.3	80.3	2.97	566072	5529745	-36.8	566070	5529747	-35.9
RMUG08-124	80.3	83.3	2.97	566070	5529747	-35.9	566068	5529749	-34.9
RMUG08-124	83.3	86.2	2.97	566068	5529749	-34.9	566066	5529751	-34.0
RMUG08-124	86.2	89.2	2.97	566066	5529751	-34.0	566064	5529753	-33.2
RMUG08-124	89.2	92.2	2.97	566064	5529753	-33.1	566062	5529755	-32.3
RMUG08-124	92.2	95.2	2.97	566062	5529755	-32.3	566060	5529757	-31.4
RMUG08-124	95.2	98.1	2.97	566060	5529757	-31.4	566058	5529759	-30.5
RMUG08-124	98.1	101.1	2.97	566058	5529759	-30.5	566056	5529761	-29.6
RMUG08-125	0.0	3.0	2.97	566128	5529696	-60.6	566126	5529698	-59.3
RMUG08-125	3.0	5.9	2.97	566126	5529698	-59.3	566124	5529700	-58.0
RMUG08-125	5.9	8.9	2.97	566124	5529700	-58.0	566123	5529703	-56.7
RMUG08-125	8.9	11.9	2.97	566123	5529703	-56.7	566121	5529705	-55.4
RMUG08-125	11.9	14.8	2.97	566121	5529705	-55.4	566120	5529707	-54.2
RMUG08-125	14.8	17.8	2.97	566120	5529707	-54.2	566118	5529709	-52.9
RMUG08-125	17.8	20.8	2.97	566118	5529709	-52.9	566117	5529711	-51.6
RMUG08-125	20.8	23.7	2.97	566117	5529711	-51.6	566115	5529713	-50.3
RMUG08-125	23.7	26.7	2.97	566115	5529713	-50.3	566113	5529716	-49.0
RMUG08-125	26.7	29.7	2.97	566113	5529716	-49.0	566112	5529718	-47.7
RMUG08-125	29.7	32.6	2.97	566112	5529718	-47.7	566110	5529720	-46.4

RMUG08-125	32.6	35.6	2.97	566110	5529720	-46.4	566109	5529722	-45.1
RMUG08-125	35.6	38.6	2.97	566109	5529722	-45.1	566107	5529724	-43.9
RMUG08-125	38.6	41.5	2.97	566107	5529724	-43.9	566106	5529726	-42.6
RMUG08-125	41.5	44.5	2.97	566106	5529726	-42.6	566104	5529729	-41.3
RMUG08-125	44.5	47.5	2.97	566104	5529729	-41.3	566103	5529731	-40.0
RMUG08-125	47.5	50.4	2.97	566103	5529731	-40.0	566101	5529733	-38.7
RMUG08-125	50.4	53.4	2.97	566101	5529733	-38.7	566099	5529735	-37.4
RMUG08-125	53.4	56.4	2.97	566099	5529735	-37.4	566098	5529737	-36.2
RMUG08-125	56.4	59.3	2.97	566098	5529737	-36.2	566096	5529740	-34.9
RMUG08-125	59.3	62.3	2.97	566096	5529740	-34.9	566095	5529742	-33.6
RMUG08-125	62.3	65.3	2.97	566095	5529742	-33.6	566093	5529744	-32.3
RMUG08-125	65.3	68.2	2.97	566093	5529744	-32.3	566092	5529746	-31.1
RMUG08-125	68.2	71.2	2.97	566092	5529746	-31.1	566090	5529748	-29.8
RMUG08-150	0.0	3.0	2.96	566124	5529693	-59.1	566122	5529693	-57.3
RMUG08-150	3.0	5.9	2.96	566122	5529693	-57.3	566119	5529693	-55.6
RMUG08-150	5.9	8.9	2.96	566119	5529693	-55.6	566117	5529693	-53.8
RMUG08-150	8.9	11.8	2.96	566117	5529693	-53.8	566115	5529693	-52.0
RMUG08-150	11.8	14.8	2.96	566115	5529693	-52.0	566112	5529693	-50.2
RMUG08-150	14.8	17.7	2.96	566112	5529693	-50.2	566110	5529694	-48.5
RMUG08-150	17.7	20.7	2.96	566110	5529694	-48.5	566108	5529694	-46.7
RMUG08-150	20.7	23.6	2.96	566108	5529694	-46.7	566105	5529694	-44.9
RMUG08-150	23.6	26.6	2.96	566105	5529694	-44.9	566103	5529694	-43.1
RMUG08-150	26.6	29.6	2.96	566103	5529694	-43.1	566101	5529694	-41.3
RMUG08-150	29.6	32.5	2.96	566101	5529694	-41.3	566098	5529694	-39.5
RMUG08-150	32.5	35.5	2.96	566098	5529694	-39.5	566096	5529694	-37.7
RMUG08-150	35.5	38.4	2.96	566096	5529694	-37.7	566094	5529694	-35.9
RMUG08-150	38.4	41.4	2.96	566094	5529694	-35.9	566091	5529695	-34.1
RMUG08-150	41.4	44.3	2.96	566091	5529695	-34.1	566089	5529695	-32.3
RMUG08-150	44.3	47.3	2.96	566089	5529695	-32.3	566087	5529695	-30.5
RMUG08-150	47.3	50.3	2.96	566087	5529695	-30.5	566084	5529695	-28.7
RMUG08-150	50.3	53.2	2.96	566084	5529695	-28.7	566082	5529696	-26.9
RMUG08-150	53.2	56.2	2.96	566082	5529696	-26.9	566080	5529696	-25.0
RMUG08-150	56.2	59.1	2.96	566080	5529696	-25.0	566077	5529696	-23.2
RMUG08-150	59.1	62.1	2.96	566077	5529696	-23.2	566075	5529697	-21.4
RMUG08-150	62.1	65.0	2.96	566075	5529697	-21.4	566073	5529697	-19.5
RMUG08-150	65.0	68.0	2.96	566073	5529697	-19.5	566070	5529697	-17.7
RMUG08-150	68.0	70.9	2.96	566070	5529697	-17.7	566068	5529698	-15.9
RMUG08-150	70.9	73.9	2.96	566068	5529698	-15.9	566066	5529698	-14.0
RMUG08-150	73.9	76.9	2.96	566066	5529698	-14.0	566064	5529699	-12.2
RMUG08-150	76.9	79.8	2.96	566064	5529699	-12.2	566061	5529699	-10.4
RMUG08-150	79.8	82.8	2.96	566061	5529699	-10.4	566059	5529700	-8.5
RMUG08-150	82.8	85.7	2.96	566059	5529700	-8.5	566057	5529700	-6.7
RMUG08-150	85.7	88.7	2.96	566057	5529700	-6.7	566055	5529700	-4.9
RMUG08-150	88.7	91.6	2.96	566055	5529700	-4.9	566052	5529701	-3.0
RMUG08-150	91.6	94.6	2.96	566052	5529701	-3.0	566050	5529701	-1.2
RMUG08-150	94.6	97.6	2.96	566050	5529701	-1.2	566048	5529702	0.7
RMUG08-151	0.0	3.0	2.96	566124	5529693	-59.0	566122	5529692	-57.2
RMUG08-151	3.0	5.9	2.96	566122	5529692	-57.2	566120	5529692	-55.4
RMUG08-151	5.9	8.9	2.96	566120	5529692	-55.4	566117	5529691	-53.6
RMUG08-151	8.9	11.9	2.96	566117	5529691	-53.6	566115	5529690	-51.8
RMUG08-151	11.9	14.8	2.96	566115	5529690	-51.8	566113	5529690	-50.0
RMUG08-151	14.8	17.8	2.96	566113	5529690	-50.0	566111	5529689	-48.2
RMUG08-151	17.8	20.7	2.96	566111	5529689	-48.2	566108	5529689	-46.4
RMUG08-151	20.7	23.7	2.96	566108	5529689	-46.4	566106	5529688	-44.5
RMUG08-151	23.7	26.7	2.96	566106	5529688	-44.5	566104	5529687	-42.7
RMUG08-151	26.7	29.6	2.96	566104	5529687	-42.7	566102	5529687	-40.9
RMUG08-151	29.6	32.6	2.96	566102	5529687	-40.9	566099	5529686	-39.0
RMUG08-151	32.6	35.6	2.96	566099	5529686	-39.0	566097	5529686	-37.2
RMUG08-151	35.6	38.5	2.96	566097	5529686	-37.2	566095	5529685	-35.4
RMUG08-151	38.5	41.5	2.96	566095	5529685	-35.4	566093	5529685	-33.5
RMUG08-151	41.5	44.4	2.96	566093	5529685	-33.5	566090	5529684	-31.7
RMUG08-151	44.4	47.4	2.96	566090	5529684	-31.7	566088	5529683	-29.8
RMUG08-151	47.4	50.4	2.96	566088	5529683	-29.8	566086	5529683	-28.0
RMUG08-151	50.4	53.3	2.96	566086	5529683	-28.0	566084	5529682	-26.1
RMUG08-151	53.3	56.3	2.96	566084	5529682	-26.1	566081	5529682	-24.3
RMUG08-151	56.3	59.3	2.96	566081	5529682	-24.3	566079	5529681	-22.5
RMUG08-151	59.3	62.2	2.96	566079	5529681	-22.5	566077	5529681	-20.6
RMUG08-151	62.2	65.2	2.96	566077	5529681	-20.6	566074	5529681	-18.8



RMUG08-151	65.2	68.1	2.96	566074	5529681	-18.8	566072	5529680	-16.9
RMUG08-151	68.1	71.1	2.96	566072	5529680	-16.9	566070	5529680	-15.1
RMUG08-151	71.1	74.1	2.96	566070	5529680	-15.1	566068	5529679	-13.2
RMUG08-151	74.1	77.0	2.96	566068	5529679	-13.2	566065	5529679	-11.4
RMUG08-151	77.0	80.0	2.96	566065	5529679	-11.4	566063	5529678	-9.5
RMUG08-151	80.0	83.0	2.96	566063	5529678	-9.5	566061	5529678	-7.7
RMUG08-151	83.0	85.9	2.96	566061	5529678	-7.7	566059	5529678	-5.8
RMUG08-151	85.9	88.9	2.96	566059	5529678	-5.8	566056	5529677	-3.9
RMUG08-151	88.9	91.8	2.96	566056	5529677	-3.9	566054	5529677	-2.1
RMUG08-151	91.8	94.8	2.96	566054	5529677	-2.1	566052	5529676	-0.2
RMUG08-151	94.8	97.8	2.96	566052	5529676	-0.2	566049	5529676	1.7
RMUG08-151	97.8	100.7	2.96	566049	5529676	1.7	566047	5529676	3.5
RMUG08-151	100.7	103.7	2.96	566047	5529676	3.5	566045	5529675	5.4
RMUG08-151	103.7	106.7	2.96	566045	5529675	5.4	566043	5529675	7.3

## Section 22

RMUG08-136	0.0	2.9	2.87	566072	5529788	-79.2	566075	5529788	-78.0
RMUG08-136	2.9	5.7	2.87	566075	5529788	-78.0	566077	5529788	-76.8
RMUG08-136	5.7	8.6	2.87	566077	5529788	-76.8	566080	5529789	-75.6
RMUG08-136	8.6	11.5	2.87	566080	5529789	-75.6	566082	5529789	-74.3
RMUG08-136	11.5	14.3	2.87	566082	5529789	-74.3	566085	5529789	-73.1
RMUG08-136	14.3	17.2	2.87	566085	5529789	-73.1	566087	5529789	-71.9
RMUG08-136	17.2	20.1	2.87	566087	5529789	-71.9	566090	5529790	-70.6
RMUG08-136	20.1	22.9	2.87	566090	5529790	-70.6	566093	5529790	-69.3
RMUG08-136	22.9	25.8	2.87	566093	5529790	-69.3	566095	5529790	-68.1
RMUG08-136	25.8	28.7	2.87	566095	5529790	-68.1	566098	5529790	-66.8
RMUG08-136	28.7	31.6	2.87	566098	5529790	-66.8	566100	5529790	-65.5
RMUG08-136	31.6	34.4	2.87	566100	5529790	-65.5	566103	5529791	-64.2
RMUG08-136	34.4	37.3	2.87	566103	5529791	-64.2	566105	5529791	-62.9
RMUG08-136	37.3	40.2	2.87	566105	5529791	-62.9	566108	5529791	-61.7
RMUG08-136	40.2	43.0	2.87	566108	5529791	-61.7	566111	5529791	-60.4
RMUG08-136	43.0	45.9	2.87	566111	5529791	-60.4	566113	5529792	-59.1
RMUG08-136	45.9	48.8	2.87	566113	5529792	-59.1	566116	5529792	-57.9
RMUG08-136	48.8	51.6	2.87	566116	5529792	-57.9	566118	5529792	-56.6
RMUG08-136	51.6	54.5	2.87	566118	5529792	-56.6	566121	5529792	-55.3
RMUG08-136	54.5	57.4	2.87	566121	5529792	-55.3	566123	5529792	-54.1
RMUG08-136	57.4	60.2	2.87	566123	5529792	-54.1	566126	5529792	-52.8
RMUG08-136	60.2	63.1	2.87	566126	5529792	-52.8	566128	5529793	-51.5
RMUG08-137A	0.0	2.9	2.92	566072	5529788	-79.5	566075	5529788	-78.7
RMUG08-137A	2.9	5.8	2.92	566075	5529788	-78.7	566078	5529789	-77.9
RMUG08-137A	5.8	8.8	2.92	566078	5529789	-77.9	566081	5529789	-77.1
RMUG08-137A	8.8	11.7	2.92	566081	5529789	-77.1	566083	5529789	-76.3
RMUG08-137A	11.7	14.6	2.92	566083	5529789	-76.3	566086	5529790	-75.5
RMUG08-137A	14.6	17.5	2.92	566086	5529790	-75.5	566089	5529790	-74.7
RMUG08-137A	17.5	20.4	2.92	566089	5529790	-74.7	566092	5529790	-73.9
RMUG08-137A	20.4	23.4	2.92	566092	5529790	-73.9	566094	5529791	-73.0
RMUG08-137A	23.4	26.3	2.92	566094	5529791	-73.0	566097	5529791	-72.2
RMUG08-137A	26.3	29.2	2.92	566097	5529791	-72.2	566100	5529791	-71.3
RMUG08-137A	29.2	32.1	2.92	566100	5529791	-71.3	566103	5529791	-70.4
RMUG08-137A	32.1	35.1	2.92	566103	5529791	-70.4	566106	5529791	-69.5
RMUG08-137A	35.1	38.0	2.92	566106	5529791	-69.5	566108	5529792	-68.5
RMUG08-137A	38.0	40.9	2.92	566108	5529792	-68.5	566111	5529792	-67.6
RMUG08-137A	40.9	43.8	2.92	566111	5529792	-67.6	566114	5529792	-66.6
RMUG08-137A	43.8	46.7	2.92	566114	5529792	-66.6	566117	5529792	-65.6
RMUG08-137A	46.7	49.7	2.92	566117	5529792	-65.6	566119	5529792	-64.6
RMUG08-137A	49.7	52.6	2.92	566119	5529792	-64.6	566122	5529793	-63.6
RMUG08-137A	52.6	55.5	2.92	566122	5529793	-63.6	566125	5529793	-62.6
RMUG08-137A	55.5	58.4	2.92	566125	5529793	-62.6	566127	5529793	-61.5
RMUG08-137A	58.4	61.3	2.92	566127	5529793	-61.5	566130	5529793	-60.5
RMUG08-137A	61.3	64.3	2.92	566130	5529793	-60.5	566133	5529794	-59.4
RMUG08-137A	64.3	67.2	2.92	566133	5529794	-59.4	566136	5529794	-58.4
RMUG08-137A	67.2	70.1	2.92	566136	5529794	-58.4	566138	5529794	-57.3
RMUG08-138	0.0	3.0	2.95	566087	5529773	-78.3	566089	5529772	-76.6
RMUG08-138	3.0	5.9	2.95	566089	5529772	-76.6	566092	5529771	-74.9
RMUG08-138	5.9	8.9	2.95	566092	5529771	-74.9	566094	5529770	-73.3
RMUG08-138	8.9	11.8	2.95	566094	5529770	-73.3	566096	5529769	-71.6
RMUG08-138	11.8	14.8	2.95	566096	5529769	-71.6	566098	5529768	-69.9
RMUG08-138	14.8	17.7	2.95	566098	5529768	-69.9	566101	5529767	-68.2

RMUG08-138	17.7	20.7	2.95	566101	5529767	-68.2	566103	5529766	-66.5
RMUG08-138	20.7	23.6	2.95	566103	5529766	-66.5	566105	5529766	-64.8
RMUG08-138	23.6	26.6	2.95	566105	5529766	-64.8	566107	5529765	-63.0
RMUG08-138	26.6	29.5	2.95	566107	5529765	-63.1	566109	5529764	-61.3
RMUG08-138	29.5	32.5	2.95	566109	5529764	-61.3	566112	5529763	-59.6
RMUG08-138	32.5	35.4	2.95	566112	5529763	-59.6	566114	5529762	-57.9
RMUG08-138	35.4	38.4	2.95	566114	5529762	-57.9	566116	5529761	-56.2
RMUG08-138	38.4	41.3	2.95	566116	5529761	-56.2	566118	5529760	-54.5
RMUG08-138	41.3	44.3	2.95	566118	5529760	-54.5	566121	5529759	-52.8
RMUG08-138	44.3	47.2	2.95	566121	5529759	-52.8	566123	5529758	-51.1
RMUG08-138	47.2	50.2	2.95	566123	5529758	-51.1	566125	5529757	-49.4
RMUG08-138	50.2	53.1	2.95	566125	5529757	-49.4	566127	5529756	-47.7
RMUG08-138	53.1	56.1	2.95	566127	5529756	-47.7	566129	5529755	-46.0
RMUG08-138	56.1	59.0	2.95	566129	5529755	-46.0	566132	5529754	-44.3
RMUG08-138	59.0	62.0	2.95	566132	5529754	-44.3	566134	5529753	-42.6
RMUG08-138	62.0	64.9	2.95	566134	5529753	-42.6	566136	5529752	-40.9
RMUG08-138	64.9	67.9	2.95	566136	5529752	-40.9	566138	5529751	-39.2
RMUG08-139	0.0	3.0	2.96	566088	5529774	-78.7	566091	5529774	-77.5
RMUG08-139	3.0	5.9	2.96	566091	5529774	-77.5	566093	5529774	-76.3
RMUG08-139	5.9	8.9	2.96	566093	5529774	-76.3	566096	5529775	-75.1
RMUG08-139	8.9	11.8	2.96	566096	5529775	-75.1	566099	5529775	-73.9
RMUG08-139	11.8	14.8	2.96	566099	5529775	-73.9	566101	5529775	-72.7
RMUG08-139	14.8	17.8	2.96	566101	5529775	-72.7	566104	5529775	-71.5
RMUG08-139	17.8	20.7	2.96	566104	5529775	-71.5	566107	5529775	-70.3
RMUG08-139	20.7	23.7	2.96	566107	5529775	-70.3	566110	5529775	-69.0
RMUG08-139	23.7	26.7	2.96	566110	5529775	-69.0	566112	5529775	-67.8
RMUG08-139	26.7	29.6	2.96	566112	5529775	-67.8	566115	5529775	-66.6
RMUG08-139	29.6	32.6	2.96	566115	5529775	-66.6	566118	5529776	-65.4
RMUG08-139	32.6	35.5	2.96	566118	5529776	-65.4	566120	5529776	-64.2
RMUG08-139	35.5	38.5	2.96	566120	5529776	-64.2	566123	5529776	-63.0
RMUG08-139	38.5	41.5	2.96	566123	5529776	-63.0	566126	5529776	-61.8
RMUG08-139	41.5	44.4	2.96	566126	5529776	-61.8	566128	5529776	-60.6
RMUG08-139	44.4	47.4	2.96	566128	5529776	-60.6	566131	5529776	-59.4
RMUG08-139	47.4	50.4	2.96	566131	5529776	-59.4	566134	5529776	-58.2
RMUG08-139	50.4	53.3	2.96	566134	5529776	-58.2	566137	5529776	-57.0
RMUG08-139	53.3	56.3	2.96	566137	5529776	-57.0	566139	5529776	-55.8
RMUG08-139	56.3	59.2	2.96	566139	5529776	-55.8	566142	5529777	-54.6
RMUG08-139	59.2	62.2	2.96	566142	5529777	-54.6	566145	5529777	-53.4
RMUG08-140	0.0	3.0	2.96	566088	5529774	-78.1	566090	5529774	-76.5
RMUG08-140	3.0	5.9	2.96	566090	5529774	-76.5	566093	5529774	-74.9
RMUG08-140	5.9	8.9	2.96	566093	5529774	-74.9	566095	5529774	-73.3
RMUG08-140	8.9	11.9	2.96	566095	5529774	-73.3	566098	5529775	-71.6
RMUG08-140	11.9	14.8	2.96	566098	5529775	-71.6	566100	5529775	-69.9
RMUG08-140	14.8	17.8	2.96	566100	5529775	-69.9	566103	5529775	-68.2
RMUG08-140	17.8	20.7	2.96	566103	5529775	-68.2	566105	5529775	-66.4
RMUG08-140	20.7	23.7	2.96	566105	5529775	-66.4	566107	5529776	-64.7
RMUG08-140	23.7	26.7	2.96	566107	5529776	-64.7	566110	5529776	-62.9
RMUG08-140	26.7	29.6	2.96	566110	5529776	-62.9	566112	5529776	-61.2
RMUG08-140	29.6	32.6	2.96	566112	5529776	-61.2	566114	5529776	-59.4
RMUG08-140	32.6	35.6	2.96	566114	5529776	-59.4	566117	5529776	-57.7
RMUG08-140	35.6	38.5	2.96	566117	5529776	-57.7	566119	5529776	-55.9
RMUG08-140	38.5	41.5	2.96	566119	5529776	-55.9	566122	5529777	-54.2
RMUG08-140	41.5	44.5	2.96	566122	5529777	-54.2	566124	5529777	-52.5
RMUG08-140	44.5	47.4	2.96	566124	5529777	-52.5	566126	5529777	-50.7
RMUG08-140	47.4	50.4	2.96	566126	5529777	-50.7	566129	5529777	-49.0
RMUG08-140	50.4	53.3	2.96	566129	5529777	-49.0	566131	5529777	-47.2
RMUG08-140	53.3	56.3	2.96	566131	5529777	-47.2	566134	5529777	-45.5
RMUG08-140	56.3	59.3	2.96	566134	5529777	-45.5	566136	5529778	-43.8
RMUG08-140	59.3	62.2	2.96	566136	5529778	-43.8	566138	5529778	-42.0
RMUG08-140	62.2	65.2	2.96	566138	5529778	-42.0	566141	5529778	-40.3
RMUG08-141	0.0	3.0	2.96	566088	5529774	-78.9	566090	5529773	-78.0
RMUG08-141	3.0	5.9	2.96	566090	5529773	-78.0	566093	5529773	-77.0
RMUG08-141	5.9	8.9	2.96	566093	5529773	-77.0	566096	5529772	-76.0
RMUG08-141	8.9	11.9	2.96	566096	5529772	-76.0	566099	5529772	-75.1
RMUG08-141	11.9	14.8	2.96	566099	5529772	-75.1	566102	5529772	-74.1
RMUG08-141	14.8	17.8	2.96	566102	5529772	-74.1	566104	5529771	-73.1
RMUG08-141	17.8	20.7	2.96	566104	5529771	-73.1	566107	5529771	-72.2

RMUG08-141	20.7	23.7	2.96	566107	5529771	-72.2	566110	5529770	-71.2
RMUG08-141	23.7	26.7	2.96	566110	5529770	-71.2	566113	5529770	-70.3
RMUG08-141	26.7	29.6	2.96	566113	5529770	-70.3	566115	5529769	-69.3
RMUG08-141	29.6	32.6	2.96	566115	5529769	-69.3	566118	5529769	-68.4
RMUG08-141	32.6	35.6	2.96	566118	5529769	-68.4	566121	5529768	-67.5
RMUG08-141	35.6	38.5	2.96	566121	5529768	-67.5	566124	5529768	-66.5
RMUG08-141	38.5	41.5	2.96	566124	5529768	-66.5	566126	5529768	-65.6
RMUG08-141	41.5	44.5	2.96	566126	5529768	-65.6	566129	5529767	-64.7
RMUG08-141	44.5	47.4	2.96	566129	5529767	-64.7	566132	5529767	-63.7
RMUG08-141	47.4	50.4	2.96	566132	5529767	-63.7	566135	5529766	-62.8
RMUG08-141	50.4	53.3	2.96	566135	5529766	-62.8	566138	5529766	-61.9
RMUG08-141	53.3	56.3	2.96	566138	5529766	-61.9	566140	5529765	-61.0
RMUG08-141	56.3	59.3	2.96	566140	5529765	-61.0	566143	5529765	-60.1
RMUG08-141	59.3	62.2	2.96	566143	5529765	-60.1	566146	5529764	-59.2
RMUG08-141	62.2	65.2	2.96	566146	5529764	-59.2	566149	5529764	-58.3
RMUG08-141	65.2	68.2	2.96	566149	5529764	-58.3	566151	5529763	-57.3
RMUG08-141	68.2	71.1	2.96	566151	5529763	-57.3	566154	5529763	-56.4
RMUG08-141	71.1	74.1	2.96	566154	5529763	-56.4	566157	5529762	-55.5
RMUG08-141	74.1	77.0	2.96	566157	5529762	-55.5	566160	5529762	-54.6
RMUG08-141	77.0	80.0	2.96	566160	5529762	-54.6	566163	5529761	-53.7
RMUG08-141	80.0	83.0	2.96	566163	5529761	-53.7	566165	5529761	-52.7
RMUG08-141	83.0	85.9	2.96	566165	5529761	-52.7	566168	5529760	-51.8
RMUG08-141	85.9	88.9	2.96	566168	5529760	-51.8	566171	5529760	-50.9

RMUG08-142	0.0	2.9	2.92	566073	5529788	-79.7	566075	5529788	-79.2
RMUG08-142	2.9	5.8	2.92	566075	5529788	-79.2	566078	5529788	-78.7
RMUG08-142	5.8	8.8	2.92	566078	5529788	-78.7	566081	5529788	-78.2
RMUG08-142	8.8	11.7	2.92	566081	5529788	-78.2	566084	5529789	-77.7
RMUG08-142	11.7	14.6	2.92	566084	5529789	-77.7	566087	5529789	-77.2
RMUG08-142	14.6	17.5	2.92	566087	5529789	-77.2	566090	5529789	-76.7
RMUG08-142	17.5	20.5	2.92	566090	5529789	-76.7	566093	5529789	-76.2
RMUG08-142	20.5	23.4	2.92	566093	5529789	-76.2	566096	5529789	-75.7
RMUG08-142	23.4	26.3	2.92	566096	5529789	-75.7	566098	5529789	-75.2
RMUG08-142	26.3	29.2	2.92	566098	5529789	-75.2	566101	5529790	-74.7
RMUG08-142	29.2	32.1	2.92	566101	5529790	-74.7	566104	5529790	-74.2
RMUG08-142	32.1	35.1	2.92	566104	5529790	-74.2	566107	5529790	-73.6
RMUG08-142	35.1	38.0	2.92	566107	5529790	-73.6	566110	5529790	-73.1
RMUG08-142	38.0	40.9	2.92	566110	5529790	-73.1	566113	5529790	-72.6
RMUG08-142	40.9	43.8	2.92	566113	5529790	-72.6	566116	5529790	-72.1
RMUG08-142	43.8	46.8	2.92	566116	5529790	-72.1	566119	5529790	-71.6
RMUG08-142	46.8	49.7	2.92	566119	5529790	-71.6	566121	5529790	-71.0
RMUG08-142	49.7	52.6	2.92	566121	5529790	-71.0	566124	5529790	-70.5
RMUG08-142	52.6	55.5	2.92	566124	5529790	-70.5	566127	5529790	-70.0
RMUG08-142	55.5	58.5	2.92	566127	5529790	-70.0	566130	5529790	-69.5
RMUG08-142	58.5	61.4	2.92	566130	5529790	-69.5	566133	5529790	-68.9
RMUG08-142	61.4	64.3	2.92	566133	5529790	-68.9	566136	5529790	-68.4
RMUG08-142	64.3	67.2	2.92	566136	5529790	-68.4	566139	5529790	-67.9
RMUG08-142	67.2	70.1	2.92	566139	5529790	-67.9	566142	5529790	-67.3
RMUG08-142	70.1	73.1	2.92	566142	5529790	-67.3	566144	5529790	-66.8
RMUG08-142	73.1	76.0	2.92	566144	5529790	-66.8	566147	5529790	-66.3
RMUG08-142	76.0	78.9	2.92	566147	5529790	-66.3	566150	5529790	-65.8
RMUG08-142	78.9	81.8	2.92	566150	5529790	-65.8	566153	5529790	-65.2
RMUG08-142	81.8	84.8	2.92	566153	5529790	-65.2	566156	5529790	-64.7
RMUG08-142	84.8	87.7	2.92	566156	5529790	-64.7	566159	5529790	-64.2
RMUG08-142	87.7	90.6	2.92	566159	5529790	-64.2	566162	5529790	-63.6

## Section 2

RMUG08-143	0.0	2.9	2.92	566203	5529911	-187	566204	5529912	-185
RMUG08-143	2.9	5.8	2.92	566204	5529912	-185	566205	5529913	-182
RMUG08-143	5.8	8.8	2.92	566205	5529913	-182	566206	5529913	-180
RMUG08-143	8.8	11.7	2.92	566206	5529913	-180	566208	5529914	-177
RMUG08-143	11.7	14.6	2.92	566208	5529914	-177	566209	5529915	-175
RMUG08-143	14.6	17.5	2.92	566209	5529915	-175	566210	5529915	-172
RMUG08-143	17.5	20.4	2.92	566210	5529915	-172	566211	5529916	-170
RMUG08-143	20.4	23.4	2.92	566211	5529916	-170	566213	5529917	-167
RMUG08-143	23.4	26.3	2.92	566213	5529917	-167	566214	5529918	-165
RMUG08-143	26.3	29.2	2.92	566214	5529918	-165	566215	5529918	-162
RMUG08-143	29.2	32.1	2.92	566215	5529918	-162	566217	5529919	-160
RMUG08-143	32.1	35.0	2.92	566217	5529919	-160	566218	5529920	-157
RMUG08-143	35.0	37.9	2.92	566218	5529920	-157	566219	5529921	-155

RMUG08-143	37.9	40.9	2.92	566219	5529921	-155	566220	5529921	-152
RMUG08-143	40.9	43.8	2.92	566220	5529921	-152	566222	5529922	-150
RMUG08-143	43.8	46.7	2.92	566222	5529922	-150	566223	5529923	-147
RMUG08-143	46.7	49.6	2.92	566223	5529923	-147	566224	5529923	-144
RMUG08-143	49.6	52.5	2.92	566224	5529923	-144	566225	5529924	-142
RMUG08-143	52.5	55.5	2.92	566225	5529924	-142	566227	5529925	-139
RMUG08-143	55.5	58.4	2.92	566227	5529925	-139	566228	5529926	-137
RMUG08-143	58.4	61.3	2.92	566228	5529926	-137	566229	5529926	-134
RMUG08-144	0.0	3.0	2.95	566202	5529912	-188	566202	5529915	-187
RMUG08-144	3.0	5.9	2.95	566202	5529915	-187	566203	5529917	-186
RMUG08-144	5.9	8.9	2.95	566203	5529917	-186	566204	5529920	-185
RMUG08-144	8.9	11.8	2.95	566204	5529920	-185	566205	5529922	-184
RMUG08-144	11.8	14.8	2.95	566205	5529922	-184	566206	5529925	-183
RMUG08-144	14.8	17.7	2.95	566206	5529925	-183	566207	5529928	-182
RMUG08-144	17.7	20.7	2.95	566207	5529928	-182	566208	5529930	-181
RMUG08-144	20.7	23.6	2.95	566208	5529930	-181	566209	5529933	-180
RMUG08-144	23.6	26.6	2.95	566209	5529933	-180	566210	5529935	-179
RMUG08-144	26.6	29.5	2.95	566210	5529935	-179	566211	5529938	-178
RMUG08-144	29.5	32.5	2.95	566211	5529938	-178	566212	5529941	-176
RMUG08-144	32.5	35.4	2.95	566212	5529941	-176	566213	5529943	-175
RMUG08-144	35.4	38.4	2.95	566213	5529943	-175	566213	5529946	-174
RMUG08-144	38.4	41.3	2.95	566213	5529946	-174	566214	5529948	-173
RMUG08-144	41.3	44.3	2.95	566214	5529948	-173	566215	5529951	-172
RMUG08-144	44.3	47.2	2.95	566215	5529951	-172	566216	5529953	-171
RMUG08-144	47.2	50.2	2.95	566216	5529953	-171	566217	5529956	-170
RMUG08-145	0.0	2.9	2.90	566201	5529913	-188	566200	5529915	-187
RMUG08-145	2.9	5.8	2.90	566200	5529915	-187	566200	5529918	-186
RMUG08-145	5.8	8.7	2.90	566200	5529918	-186	566199	5529921	-184
RMUG08-145	8.7	11.6	2.90	566199	5529921	-184	566199	5529923	-183
RMUG08-145	11.6	14.5	2.90	566199	5529923	-183	566198	5529926	-182
RMUG08-145	14.5	17.4	2.90	566198	5529926	-182	566198	5529929	-181
RMUG08-145	17.4	20.3	2.90	566198	5529929	-181	566197	5529931	-180
RMUG08-145	20.3	23.2	2.90	566197	5529931	-180	566197	5529934	-179
RMUG08-145	23.2	26.1	2.90	566197	5529934	-179	566196	5529937	-178
RMUG08-145	26.1	29.0	2.90	566196	5529937	-178	566196	5529939	-177
RMUG08-145	29.0	31.9	2.90	566196	5529939	-177	566196	5529942	-176
RMUG08-145	31.9	34.8	2.90	566196	5529942	-176	566195	5529945	-175
RMUG08-145	34.8	37.7	2.90	566195	5529945	-175	566195	5529947	-174
RMUG08-145	37.7	40.6	2.90	566195	5529947	-174	566194	5529950	-173
RMUG08-145	40.6	43.5	2.90	566194	5529950	-173	566194	5529953	-172
RMUG08-145	43.5	46.4	2.90	566194	5529953	-172	566193	5529955	-171
RMUG08-145	46.4	49.3	2.90	566193	5529955	-171	566193	5529958	-170
RMUG08-145	49.3	52.2	2.90	566193	5529958	-170	566192	5529961	-169
RMUG08-145	52.2	55.1	2.90	566192	5529961	-169	566192	5529963	-168
RMUG08-145	55.1	58.0	2.90	566192	5529963	-168	566191	5529966	-167
RMUG08-145	58.0	60.9	2.90	566191	5529966	-167	566190	5529969	-166
RMUG08-145	60.9	63.8	2.90	566190	5529969	-166	566190	5529971	-165
RMUG08-145	63.8	66.7	2.90	566190	5529971	-165	566189	5529974	-164
RMUG08-145	66.7	69.6	2.90	566189	5529974	-164	566188	5529976	-163
RMUG08-145	69.6	72.5	2.90	566188	5529976	-163	566187	5529979	-161
RMUG08-146	0.0	0.3	0.26	566205	5529910	-187	566205	5529910	-187
RMUG08-146	0.3	0.5	0.26	566205	5529910	-187	566205	5529910	-187
RMUG08-146	0.5	0.8	0.26	566205	5529910	-187	566205	5529910	-187
RMUG08-146	0.8	1.0	0.26	566205	5529910	-187	566206	5529910	-186
RMUG08-146	1.0	1.3	0.26	566206	5529910	-186	566206	5529910	-186
RMUG08-146	1.3	1.6	0.26	566206	5529910	-186	566206	5529910	-186
RMUG08-146	1.6	1.8	0.26	566206	5529910	-186	566206	5529910	-186
RMUG08-146	1.8	2.1	0.26	566206	5529910	-186	566207	5529910	-186
RMUG08-146	2.1	2.3	0.26	566207	5529910	-186	566207	5529910	-186
RMUG08-146	2.3	2.6	0.26	566207	5529910	-186	566207	5529910	-186
RMUG08-146	2.6	2.9	0.26	566207	5529910	-186	566207	5529910	-186
RMUG08-146	2.9	3.1	0.26	566207	5529910	-186	566207	5529910	-185
RMUG08-146	3.1	3.4	0.26	566207	5529910	-185	566208	5529910	-185
RMUG08-146	3.4	3.7	0.26	566208	5529910	-185	566208	5529910	-185
RMUG08-146	3.7	3.9	0.26	566208	5529910	-185	566208	5529910	-185
RMUG08-146	3.9	4.2	0.26	566208	5529910	-185	566208	5529910	-185
RMUG08-146	4.2	4.4	0.26	566208	5529910	-185	566209	5529910	-185

RMUG08-146	4.4	4.7	0.26	566209	5529910	-185	566209	5529910	-185
RMUG08-146	4.7	5.0	0.26	566209	5529910	-185	566209	5529910	-185
RMUG08-146	5.0	5.2	0.26	566209	5529910	-185	566209	5529910	-184
RMUG08-146	5.2	5.5	0.26	566209	5529910	-184	566210	5529910	-184
RMUG08-146	5.5	5.7	0.26	566210	5529910	-184	566210	5529910	-184
RMUG08-146	5.7	6.0	0.26	566210	5529910	-184	566210	5529910	-184
RMUG08-146	6.0	6.3	0.26	566210	5529910	-184	566210	5529910	-184
RMUG08-146	6.3	6.5	0.26	566210	5529910	-184	566210	5529910	-184
RMUG08-146	6.5	6.8	0.26	566210	5529910	-184	566211	5529910	-184
RMUG08-146	6.8	7.0	0.26	566211	5529910	-184	566211	5529910	-184
RMUG08-146	7.0	7.3	0.26	566211	5529910	-184	566211	5529910	-183
RMUG08-146	7.3	7.6	0.26	566211	5529910	-183	566211	5529910	-183
RMUG08-146	7.6	7.8	0.26	566211	5529910	-183	566212	5529910	-183
RMUG08-146	7.8	8.1	0.26	566212	5529910	-183	566212	5529910	-183
RMUG08-146	8.1	8.3	0.26	566212	5529910	-183	566212	5529910	-183
RMUG08-146	8.3	8.6	0.26	566212	5529910	-183	566212	5529910	-183
RMUG08-146	8.6	8.9	0.26	566212	5529910	-183	566213	5529910	-183
RMUG08-146	8.9	9.1	0.26	566213	5529910	-183	566213	5529910	-183
RMUG08-146	9.1	9.4	0.26	566213	5529910	-183	566213	5529910	-183
RMUG08-146	9.4	9.7	0.26	566213	5529910	-183	566213	5529910	-182
RMUG08-146	9.7	9.9	0.26	566213	5529910	-182	566213	5529910	-182
RMUG08-146	9.9	10.2	0.26	566213	5529910	-182	566214	5529910	-182
RMUG08-146	10.2	10.4	0.26	566214	5529910	-182	566214	5529910	-182
RMUG08-146	10.4	10.7	0.26	566214	5529910	-182	566214	5529910	-182
RMUG08-146	10.7	11.0	0.26	566214	5529910	-182	566214	5529910	-182
RMUG08-146	11.0	11.2	0.26	566214	5529910	-182	566215	5529910	-182
RMUG08-146	11.2	11.5	0.26	566215	5529910	-182	566215	5529910	-182
RMUG08-146	11.5	11.7	0.26	566215	5529910	-182	566215	5529910	-181
RMUG08-146	11.7	12.0	0.26	566215	5529910	-181	566215	5529910	-181
RMUG08-146	12.0	12.3	0.26	566215	5529910	-181	566216	5529910	-181
RMUG08-146	12.3	12.5	0.26	566216	5529910	-181	566216	5529910	-181
RMUG08-146	12.5	12.8	0.26	566216	5529910	-181	566216	5529910	-181
RMUG08-146	12.8	13.0	0.26	566216	5529910	-181	566216	5529910	-181
RMUG08-146	13.0	13.3	0.26	566216	5529910	-181	566216	5529910	-181
RMUG08-146	13.3	13.6	0.26	566216	5529910	-181	566217	5529910	-181
RMUG08-146	13.6	13.8	0.26	566217	5529910	-181	566217	5529910	-180
RMUG08-146	13.8	14.1	0.26	566217	5529910	-180	566217	5529910	-180
RMUG08-146	14.1	14.3	0.26	566217	5529910	-180	566217	5529910	-180
RMUG08-146	14.3	14.6	0.26	566217	5529910	-180	566218	5529910	-180
RMUG08-146	14.6	14.9	0.26	566218	5529910	-180	566218	5529910	-180
RMUG08-146	14.9	15.1	0.26	566218	5529910	-180	566218	5529910	-180
RMUG08-146	15.1	15.4	0.26	566218	5529910	-180	566218	5529910	-180
RMUG08-146	15.4	15.7	0.26	566218	5529910	-180	566219	5529910	-180
RMUG08-146	15.7	15.9	0.26	566219	5529910	-180	566219	5529910	-179
RMUG08-146	15.9	16.2	0.26	566219	5529910	-179	566219	5529910	-179
RMUG08-146	16.2	16.4	0.26	566219	5529910	-179	566219	5529910	-179
RMUG08-146	16.4	16.7	0.26	566219	5529910	-179	566219	5529910	-179
RMUG08-146	16.7	17.0	0.26	566219	5529910	-179	566220	5529910	-179
RMUG08-146	17.0	17.2	0.26	566220	5529910	-179	566220	5529910	-179
RMUG08-146	17.2	17.5	0.26	566220	5529910	-179	566220	5529910	-179
RMUG08-146	17.5	17.7	0.26	566220	5529910	-179	566220	5529910	-179
RMUG08-146	17.7	18.0	0.26	566220	5529910	-179	566221	5529910	-178
RMUG08-146	18.0	18.3	0.26	566221	5529910	-178	566221	5529910	-178
RMUG08-146	18.3	18.5	0.26	566221	5529910	-178	566221	5529910	-178
RMUG08-146	18.5	18.8	0.26	566221	5529910	-178	566221	5529910	-178
RMUG08-146	18.8	19.0	0.26	566221	5529910	-178	566222	5529910	-178
RMUG08-146	19.0	19.3	0.26	566222	5529910	-178	566222	5529910	-178
RMUG08-146	19.3	19.6	0.26	566222	5529910	-178	566222	5529910	-178
RMUG08-146	19.6	19.8	0.26	566222	5529910	-178	566222	5529910	-178
RMUG08-146	19.8	20.1	0.26	566222	5529910	-178	566222	5529909	-177
RMUG08-146	20.1	20.4	0.26	566222	5529909	-177	566223	5529909	-177
RMUG08-146	20.4	20.6	0.26	566223	5529909	-177	566223	5529909	-177
RMUG08-146	20.6	20.9	0.26	566223	5529909	-177	566223	5529909	-177
RMUG08-146	20.9	21.1	0.26	566223	5529909	-177	566223	5529909	-177
RMUG08-146	21.1	21.4	0.26	566223	5529909	-177	566224	5529909	-177
RMUG08-146	21.4	21.7	0.26	566224	5529909	-177	566224	5529909	-177
RMUG08-146	21.7	21.9	0.26	566224	5529909	-177	566224	5529909	-177
RMUG08-146	21.9	22.2	0.26	566224	5529909	-177	566224	5529909	-177
RMUG08-146	22.2	22.4	0.26	566224	5529909	-177	566225	5529909	-176
RMUG08-146	22.4	22.7	0.26	566225	5529909	-176	566225	5529909	-176

RMUG08-146	22.7	23.0	0.26	566225	5529909	-176	566225	5529909	-176
RMUG08-146	23.0	23.2	0.26	566225	5529909	-176	566225	5529909	-176
RMUG08-146	23.2	23.5	0.26	566225	5529909	-176	566225	5529909	-176
RMUG08-146	23.5	23.7	0.26	566225	5529909	-176	566226	5529909	-176
RMUG08-146	23.7	24.0	0.26	566226	5529909	-176	566226	5529909	-176
RMUG08-146	24.0	24.3	0.26	566226	5529909	-176	566226	5529909	-176
RMUG08-146	24.3	24.5	0.26	566226	5529909	-176	566226	5529909	-175
RMUG08-146	24.5	24.8	0.26	566226	5529909	-175	566227	5529909	-175
RMUG08-146	24.8	25.0	0.26	566227	5529909	-175	566227	5529909	-175
RMUG08-146	25.0	25.3	0.26	566227	5529909	-175	566227	5529909	-175
RMUG08-146	25.3	25.6	0.26	566227	5529909	-175	566227	5529909	-175
RMUG08-146	25.6	25.8	0.26	566227	5529909	-175	566227	5529909	-175
RMUG08-146	25.8	26.1	0.26	566227	5529909	-175	566228	5529909	-175
RMUG08-146	26.1	26.4	0.26	566228	5529909	-175	566228	5529909	-175
RMUG08-146	26.4	26.6	0.26	566228	5529909	-175	566228	5529909	-174
RMUG08-146	26.6	26.9	0.26	566228	5529909	-174	566228	5529909	-174
RMUG08-146	26.9	27.1	0.26	566228	5529909	-174	566229	5529909	-174
RMUG08-146	27.1	27.4	0.26	566229	5529909	-174	566229	5529909	-174
RMUG08-146	27.4	27.7	0.26	566229	5529909	-174	566229	5529909	-174
RMUG08-146	27.7	27.9	0.26	566229	5529909	-174	566229	5529909	-174
RMUG08-146	27.9	28.2	0.26	566229	5529909	-174	566230	5529909	-174
RMUG08-146	28.2	28.4	0.26	566230	5529909	-174	566230	5529909	-174
RMUG08-146	28.4	28.7	0.26	566230	5529909	-174	566230	5529909	-173
RMUG08-146	28.7	29.0	0.26	566230	5529909	-173	566230	5529909	-173
RMUG08-146	29.0	29.2	0.26	566230	5529909	-173	566230	5529909	-173
RMUG08-146	29.2	29.5	0.26	566230	5529909	-173	566231	5529909	-173
RMUG08-146	29.5	29.7	0.26	566231	5529909	-173	566231	5529909	-173
RMUG08-146	29.7	30.0	0.26	566231	5529909	-173	566231	5529909	-173
RMUG08-146	30.0	30.3	0.26	566231	5529909	-173	566231	5529909	-173
RMUG08-146	30.3	30.5	0.26	566231	5529909	-173	566232	5529909	-173
RMUG08-146	30.5	30.8	0.26	566232	5529909	-173	566232	5529909	-172
RMUG08-146	30.8	31.0	0.26	566232	5529909	-172	566232	5529909	-172
RMUG08-146	31.0	31.3	0.26	566232	5529909	-172	566232	5529909	-172
RMUG08-146	31.3	31.6	0.26	566232	5529909	-172	566233	5529909	-172
RMUG08-146	31.6	31.8	0.26	566233	5529909	-172	566233	5529909	-172
RMUG08-146	31.8	32.1	0.26	566233	5529909	-172	566233	5529909	-172
RMUG08-146	32.1	32.4	0.26	566233	5529909	-172	566233	5529909	-172
RMUG08-146	32.4	32.6	0.26	566233	5529909	-172	566233	5529909	-172
RMUG08-146	32.6	32.9	0.26	566233	5529909	-172	566234	5529909	-171
RMUG08-146	32.9	33.1	0.26	566234	5529909	-171	566234	5529909	-171
RMUG08-146	33.1	33.4	0.26	566234	5529909	-171	566234	5529909	-171
RMUG08-146	33.4	33.7	0.26	566234	5529909	-171	566234	5529909	-171
RMUG08-146	33.7	33.9	0.26	566234	5529909	-171	566235	5529909	-171
RMUG08-146	33.9	34.2	0.26	566235	5529909	-171	566235	5529909	-171
RMUG08-146	34.2	34.4	0.26	566235	5529909	-171	566235	5529909	-171
RMUG08-146	34.4	34.7	0.26	566235	5529909	-171	566235	5529909	-171
RMUG08-146	34.7	35.0	0.26	566235	5529909	-171	566236	5529909	-170
RMUG08-146	35.0	35.2	0.26	566236	5529909	-170	566236	5529909	-170
RMUG08-146	35.2	35.5	0.26	566236	5529909	-170	566236	5529909	-170
RMUG08-146	35.5	35.7	0.26	566236	5529909	-170	566236	5529909	-170
RMUG08-146	35.7	36.0	0.26	566236	5529909	-170	566236	5529909	-170
RMUG08-146	36.0	36.3	0.26	566236	5529909	-170	566237	5529909	-170
RMUG08-146	36.3	36.5	0.26	566237	5529909	-170	566237	5529909	-170
RMUG08-146	36.5	36.8	0.26	566237	5529909	-170	566237	5529909	-170
RMUG08-146	36.8	37.0	0.26	566237	5529909	-170	566237	5529909	-169
RMUG08-146	37.0	37.3	0.26	566237	5529909	-169	566238	5529909	-169
RMUG08-146	37.3	37.6	0.26	566238	5529909	-169	566238	5529909	-169
RMUG08-146	37.6	37.8	0.26	566238	5529909	-169	566238	5529909	-169
RMUG08-146	37.8	38.1	0.26	566238	5529909	-169	566238	5529909	-169
RMUG08-146	38.1	38.4	0.26	566238	5529909	-169	566238	5529909	-169
RMUG08-146	38.4	38.6	0.26	566238	5529909	-169	566239	5529909	-169
RMUG08-146	38.6	38.9	0.26	566239	5529909	-169	566239	5529909	-169
RMUG08-146	38.9	39.1	0.26	566239	5529909	-169	566239	5529909	-168
RMUG08-146	39.1	39.4	0.26	566239	5529909	-168	566239	5529909	-168
RMUG08-146	39.4	39.7	0.26	566239	5529909	-168	566240	5529909	-168
RMUG08-146	39.7	39.9	0.26	566240	5529909	-168	566240	5529909	-168
RMUG08-146	39.9	40.2	0.26	566240	5529909	-168	566240	5529909	-168
RMUG08-146	40.2	40.4	0.26	566240	5529909	-168	566240	5529909	-168
RMUG08-146	40.4	40.7	0.26	566240	5529909	-168	566241	5529909	-168
RMUG08-146	40.7	41.0	0.26	566241	5529909	-168	566241	5529909	-168

RMUG08-146	41.0	41.2	0.26	566241	5529909	-168	566241	5529909	-167
RMUG08-146	41.2	41.5	0.26	566241	5529909	-167	566241	5529909	-167
RMUG08-146	41.5	41.7	0.26	566241	5529909	-167	566241	5529909	-167
RMUG08-146	41.7	42.0	0.26	566241	5529909	-167	566242	5529909	-167
RMUG08-146	42.0	42.3	0.26	566242	5529909	-167	566242	5529909	-167
RMUG08-146	42.3	42.5	0.26	566242	5529909	-167	566242	5529908	-167
RMUG08-146	42.5	42.8	0.26	566242	5529908	-167	566242	5529908	-167
RMUG08-146	42.8	43.0	0.26	566242	5529908	-167	566243	5529908	-167
RMUG08-146	43.0	43.3	0.26	566243	5529908	-167	566243	5529908	-166
RMUG08-146	43.3	43.6	0.26	566243	5529908	-166	566243	5529908	-166
RMUG08-146	43.6	43.8	0.26	566243	5529908	-166	566243	5529908	-166
RMUG08-146	43.8	44.1	0.26	566243	5529908	-166	566244	5529908	-166
RMUG08-146	44.1	44.4	0.26	566244	5529908	-166	566244	5529908	-166
RMUG08-146	44.4	44.6	0.26	566244	5529908	-166	566244	5529908	-166
RMUG08-146	44.6	44.9	0.26	566244	5529908	-166	566244	5529908	-166
RMUG08-146	44.9	45.1	0.26	566244	5529908	-166	566244	5529908	-166
RMUG08-146	45.1	45.4	0.26	566244	5529908	-166	566245	5529908	-165
RMUG08-146	45.4	45.7	0.26	566245	5529908	-165	566245	5529908	-165
RMUG08-146	45.7	45.9	0.26	566245	5529908	-165	566245	5529908	-165
RMUG08-146	45.9	46.2	0.26	566245	5529908	-165	566245	5529908	-165
RMUG08-146	46.2	46.4	0.26	566245	5529908	-165	566246	5529908	-165
RMUG08-146	46.4	46.7	0.26	566246	5529908	-165	566246	5529908	-165
RMUG08-146	46.7	47.0	0.26	566246	5529908	-165	566246	5529908	-165
RMUG08-146	47.0	47.2	0.26	566246	5529908	-165	566246	5529908	-165
RMUG08-146	47.2	47.5	0.26	566246	5529908	-165	566246	5529908	-164
RMUG08-146	47.5	47.7	0.26	566246	5529908	-164	566247	5529908	-164
RMUG08-146	47.7	48.0	0.26	566247	5529908	-164	566247	5529908	-164
RMUG08-146	48.0	48.3	0.26	566247	5529908	-164	566247	5529908	-164
RMUG08-146	48.3	48.5	0.26	566247	5529908	-164	566247	5529908	-164
RMUG08-146	48.5	48.8	0.26	566247	5529908	-164	566248	5529908	-164
RMUG08-146	48.8	49.1	0.26	566248	5529908	-164	566248	5529908	-164
RMUG08-146	49.1	49.3	0.26	566248	5529908	-164	566248	5529908	-164
RMUG08-146	49.3	49.6	0.26	566248	5529908	-164	566248	5529908	-163
RMUG08-146	49.6	49.8	0.26	566248	5529908	-163	566249	5529908	-163
RMUG08-146	49.8	50.1	0.26	566249	5529908	-163	566249	5529908	-163
RMUG08-146	50.1	50.4	0.26	566249	5529908	-163	566249	5529908	-163
RMUG08-146	50.4	50.6	0.26	566249	5529908	-163	566249	5529908	-163
RMUG08-146	50.6	50.9	0.26	566249	5529908	-163	566249	5529908	-163
RMUG08-146	50.9	51.1	0.26	566249	5529908	-163	566250	5529908	-163
RMUG08-146	51.1	51.4	0.26	566250	5529908	-163	566250	5529908	-163
RMUG08-146	51.4	51.7	0.26	566250	5529908	-163	566250	5529908	-162
RMUG08-146	51.7	51.9	0.26	566250	5529908	-162	566250	5529908	-162
RMUG08-146	51.9	52.2	0.26	566250	5529908	-162	566251	5529908	-162
RMUG08-146	52.2	52.4	0.26	566251	5529908	-162	566251	5529908	-162
RMUG08-146	52.4	52.7	0.26	566251	5529908	-162	566251	5529908	-162
RMUG08-146	52.7	53.0	0.26	566251	5529908	-162	566251	5529908	-162
RMUG08-146	53.0	53.2	0.26	566251	5529908	-162	566251	5529908	-162
RMUG08-146	53.2	53.5	0.26	566251	5529908	-162	566252	5529908	-162
RMUG08-146	53.5	53.7	0.26	566252	5529908	-162	566252	5529908	-161
RMUG08-146	53.7	54.0	0.26	566252	5529908	-161	566252	5529908	-161
RMUG08-146	54.0	54.3	0.26	566252	5529908	-161	566252	5529908	-161
RMUG08-146	54.3	54.5	0.26	566252	5529908	-161	566253	5529908	-161
RMUG08-146	54.5	54.8	0.26	566253	5529908	-161	566253	5529908	-161
RMUG08-146	54.8	55.1	0.26	566253	5529908	-161	566253	5529908	-161
RMUG08-146	55.1	55.3	0.26	566253	5529908	-161	566253	5529908	-161
RMUG08-146	55.3	55.6	0.26	566253	5529908	-161	566254	5529908	-161
RMUG08-146	55.6	55.8	0.26	566254	5529908	-161	566254	5529908	-160
RMUG08-146	55.8	56.1	0.26	566254	5529908	-160	566254	5529908	-160
RMUG08-146	56.1	56.4	0.26	566254	5529908	-160	566254	5529908	-160
RMUG08-146	56.4	56.6	0.26	566254	5529908	-160	566254	5529908	-160
RMUG08-146	56.6	56.9	0.26	566254	5529908	-160	566255	5529908	-160
RMUG08-146	56.9	57.1	0.26	566255	5529908	-160	566255	5529908	-160
RMUG08-146	57.1	57.4	0.26	566255	5529908	-160	566255	5529908	-160
RMUG08-146	57.4	57.7	0.26	566255	5529908	-160	566255	5529908	-159
RMUG08-146	57.7	57.9	0.26	566255	5529908	-159	566256	5529908	-159
RMUG08-146	57.9	58.2	0.26	566256	5529908	-159	566256	5529908	-159
RMUG08-146	58.2	58.4	0.26	566256	5529908	-159	566256	5529908	-159
RMUG08-146	58.4	58.7	0.26	566256	5529908	-159	566256	5529908	-159
RMUG08-146	58.7	59.0	0.26	566256	5529908	-159	566256	5529908	-159
RMUG08-146	59.0	59.2	0.26	566256	5529908	-159	566257	5529908	-159

RMUG08-146	59.2	59.5	0.26	566257	5529908	-159	566257	5529908	-159
RMUG08-146	59.5	59.7	0.26	566257	5529908	-159	566257	5529908	-158
RMUG08-146	59.7	60.0	0.26	566257	5529908	-158	566257	5529908	-158
RMUG08-146	60.0	60.3	0.26	566257	5529908	-158	566258	5529908	-158
RMUG08-146	60.3	60.5	0.26	566258	5529908	-158	566258	5529908	-158
RMUG08-146	60.5	60.8	0.26	566258	5529908	-158	566258	5529908	-158
RMUG08-146	60.8	61.1	0.26	566258	5529908	-158	566258	5529908	-158
RMUG08-146	61.1	61.3	0.26	566258	5529908	-158	566259	5529908	-158
RMUG08-146	61.3	61.6	0.26	566259	5529908	-158	566259	5529908	-158
RMUG08-146	61.6	61.8	0.26	566259	5529908	-158	566259	5529908	-157
RMUG08-146	61.8	62.1	0.26	566259	5529908	-157	566259	5529908	-157
RMUG08-146	62.1	62.4	0.26	566259	5529908	-157	566259	5529908	-157
RMUG08-146	62.4	62.6	0.26	566259	5529908	-157	566260	5529908	-157
RMUG08-146	62.6	62.9	0.26	566260	5529908	-157	566260	5529908	-157
RMUG08-146	62.9	63.1	0.26	566260	5529908	-157	566260	5529908	-157
RMUG08-146	63.1	63.4	0.26	566260	5529908	-157	566260	5529908	-157
RMUG08-147	0.0	2.9	2.88	566199	5529912	-188	566197	5529914	-186
RMUG08-147	2.9	5.8	2.88	566197	5529914	-186	566196	5529916	-185
RMUG08-147	5.8	8.6	2.88	566196	5529916	-185	566194	5529918	-184
RMUG08-147	8.6	11.5	2.88	566194	5529918	-184	566193	5529920	-182
RMUG08-147	11.5	14.4	2.88	566193	5529920	-182	566191	5529923	-181
RMUG08-147	14.4	17.3	2.88	566191	5529923	-181	566190	5529925	-180
RMUG08-147	17.3	20.2	2.88	566190	5529925	-180	566188	5529927	-179
RMUG08-147	20.2	23.0	2.88	566188	5529927	-179	566186	5529929	-177
RMUG08-147	23.0	25.9	2.88	566186	5529929	-177	566185	5529931	-176
RMUG08-147	25.9	28.8	2.88	566185	5529931	-176	566183	5529933	-175
RMUG08-147	28.8	31.7	2.88	566183	5529933	-175	566182	5529935	-173
RMUG08-147	31.7	34.6	2.88	566182	5529935	-173	566181	5529937	-172
RMUG08-147	34.6	37.4	2.88	566181	5529937	-172	566179	5529939	-171
RMUG08-147	37.4	40.3	2.88	566179	5529939	-171	566178	5529941	-169
RMUG08-147	40.3	43.2	2.88	566178	5529941	-169	566176	5529943	-168
RMUG08-147	43.2	46.1	2.88	566176	5529943	-168	566175	5529945	-167
RMUG08-147	46.1	49.0	2.88	566175	5529945	-167	566173	5529948	-165
RMUG08-147	49.0	51.8	2.88	566173	5529948	-165	566172	5529950	-164
RMUG08-147	51.8	54.7	2.88	566172	5529950	-164	566170	5529952	-163
RMUG08-147	54.7	57.6	2.88	566170	5529952	-163	566169	5529954	-161
RMUG08-147	57.6	60.5	2.88	566169	5529954	-161	566167	5529956	-160
RMUG08-147	60.5	63.4	2.88	566167	5529956	-160	566166	5529958	-159
RMUG08-147	63.4	66.2	2.88	566166	5529958	-159	566165	5529960	-157
RMUG08-147	66.2	69.1	2.88	566165	5529960	-157	566163	5529962	-156
RMUG08-147	69.1	72.0	2.88	566163	5529962	-156	566162	5529965	-155
RMUG08-148	0.0	94.2	94.20	566199	5529913	-189	566199	5530007	-184
RMUG08-149	0.0	101.8	101.80	566199	5529913	-188	566208	5530013	-201



**Table eA1.** Detailed coordinates of logged drill hole sections from the MSUP orebody; coordinates in UTM 21N NAD83 (data from Rambler Metals & Mining Canada Ltd)

Drill hole intervall				Coordinates		Depth below sea level	Coordinates		Depth below sea level
Drill hole #	From [m]	To [m]	Length [m]	X_start (E)	Y_start (N)	Z_start [m]	X_end (E)	Y_end (N)	Z_end [m]
<b>Section 24</b>									
RMUG08-107	0.0	2.9	2.88	566307	5529708	-147	566308	5529710	-146
RMUG08-107	2.9	5.8	2.88	566308	5529710	-146	566309	5529712	-144
RMUG08-107	5.8	8.6	2.88	566309	5529712	-144	566311	5529714	-143
RMUG08-107	8.6	11.5	2.88	566311	5529714	-143	566312	5529717	-142
RMUG08-107	11.5	14.4	2.88	566312	5529717	-142	566313	5529719	-140
RMUG08-107	14.4	17.3	2.88	566313	5529719	-140	566314	5529721	-139
RMUG08-107	17.3	20.1	2.88	566314	5529721	-139	566315	5529723	-137
RMUG08-107	20.1	23.0	2.88	566315	5529723	-137	566316	5529726	-136
RMUG08-107	23.0	25.9	2.88	566316	5529726	-136	566317	5529728	-134
RMUG08-107	25.9	28.8	2.88	566317	5529728	-134	566318	5529730	-133
RMUG08-107	28.8	31.6	2.88	566318	5529730	-133	566320	5529732	-132
RMUG08-107	31.6	34.5	2.88	566320	5529732	-132	566321	5529735	-130
RMUG08-107	34.5	37.4	2.88	566321	5529735	-130	566322	5529737	-129
RMUG08-107	37.4	40.3	2.88	566322	5529737	-129	566323	5529739	-127
RMUG08-107	40.3	43.1	2.88	566323	5529739	-127	566324	5529741	-126
RMUG08-107	43.1	46.0	2.88	566324	5529741	-126	566325	5529744	-124
RMUG08-107	46.0	48.9	2.88	566325	5529744	-124	566326	5529746	-123
RMUG08-107	48.9	51.8	2.88	566326	5529746	-123	566327	5529748	-121
RMUG08-107	51.8	54.6	2.88	566327	5529748	-121	566328	5529750	-120
RMUG08-107	54.6	57.5	2.88	566328	5529750	-120	566329	5529752	-118
RMUG08-107	57.5	60.4	2.88	566329	5529752	-118	566330	5529755	-117
RMUG08-109	0.0	2.9	2.91	566307	5529707	-147	566310	5529709	-146
RMUG08-109	2.9	5.8	2.91	566310	5529709	-146	566312	5529710	-144
RMUG08-109	5.8	8.7	2.91	566312	5529710	-144	566314	5529711	-143
RMUG08-109	8.7	11.6	2.91	566314	5529711	-143	566316	5529713	-142
RMUG08-109	11.6	14.5	2.91	566316	5529713	-142	566318	5529714	-140
RMUG08-109	14.5	17.5	2.91	566318	5529714	-140	566320	5529715	-139
RMUG08-109	17.5	20.4	2.91	566320	5529715	-139	566323	5529717	-137
RMUG08-109	20.4	23.3	2.91	566323	5529717	-137	566325	5529718	-136
RMUG08-109	23.3	26.2	2.91	566325	5529718	-136	566327	5529719	-135
RMUG08-109	26.2	29.1	2.91	566327	5529719	-135	566329	5529720	-133
RMUG08-109	29.1	32.0	2.91	566329	5529720	-133	566331	5529722	-131
RMUG08-109	32.0	34.9	2.91	566331	5529722	-131	566334	5529723	-130
RMUG08-109	34.9	37.8	2.91	566334	5529723	-130	566336	5529724	-128
RMUG08-109	37.8	40.7	2.91	566336	5529724	-128	566338	5529725	-127
RMUG08-109	40.7	43.6	2.91	566338	5529725	-127	566340	5529726	-125
RMUG08-109	43.6	46.5	2.91	566340	5529726	-125	566342	5529727	-123
RMUG08-109	46.5	49.5	2.91	566342	5529727	-123	566344	5529728	-122
RMUG08-109	49.5	52.4	2.91	566344	5529728	-122	566346	5529729	-120
RMUG08-109	52.4	55.3	2.91	566346	5529729	-120	566348	5529730	-118
RMUG08-109	55.3	58.2	2.91	566348	5529730	-118	566350	5529731	-116
RMUG08-109	58.2	61.1	2.91	566350	5529731	-116	566353	5529732	-115
RMUG08-109	61.1	64.0	2.91	566353	5529732	-115	566355	5529733	-113
<b>Section 4</b>									
RMUG08-104	0.0	2.9	2.95	566382	5529820	-224	566384	5529820	-223
RMUG08-104	2.9	5.9	2.95	566384	5529820	-223	566387	5529821	-221
RMUG08-104	5.9	8.8	2.95	566387	5529821	-221	566389	5529822	-220
RMUG08-104	8.8	11.8	2.95	566389	5529822	-220	566391	5529823	-219
RMUG08-104	11.8	14.7	2.95	566391	5529823	-219	566394	5529825	-217
RMUG08-104	14.7	17.7	2.95	566394	5529825	-217	566396	5529826	-216
RMUG08-104	17.7	20.6	2.95	566396	5529826	-216	566399	5529827	-215
RMUG08-104	20.6	23.6	2.95	566399	5529827	-215	566401	5529828	-213
RMUG08-104	23.6	26.5	2.95	566401	5529828	-213	566404	5529829	-212
RMUG08-104	26.5	29.5	2.95	566404	5529829	-212	566406	5529830	-211
RMUG08-104	29.5	32.4	2.95	566406	5529830	-211	566408	5529831	-209
RMUG08-104	32.4	35.4	2.95	566408	5529831	-209	566411	5529832	-208
RMUG08-104	35.4	38.3	2.95	566411	5529832	-208	566413	5529833	-207
RMUG08-104	38.3	41.3	2.95	566413	5529833	-207	566416	5529834	-205
RMUG08-104	41.3	44.2	2.95	566416	5529834	-205	566418	5529835	-204
RMUG08-104	44.2	47.2	2.95	566418	5529835	-204	566420	5529835	-202

RMUG08-104	47.2	50.1	2.95	566420	5529835	-202	566423	5529836	-201
RMUG08-104	50.1	53.1	2.95	566423	5529836	-201	566425	5529837	-200
RMUG08-104	53.1	56.0	2.95	566425	5529837	-200	566428	5529838	-198
RMUG08-106	0.0	2.9	2.87	566381	5529819	-223	566383	5529819	-221
RMUG08-106	2.9	5.7	2.87	566383	5529819	-221	566385	5529818	-219
RMUG08-106	5.7	8.6	2.87	566385	5529818	-219	566387	5529818	-217
RMUG08-106	8.6	11.5	2.87	566387	5529818	-217	566388	5529818	-214
RMUG08-106	11.5	14.4	2.87	566388	5529818	-214	566390	5529818	-212
RMUG08-106	14.4	17.2	2.87	566390	5529818	-212	566392	5529818	-210
RMUG08-106	17.2	20.1	2.87	566392	5529818	-210	566394	5529818	-208
RMUG08-106	20.1	23.0	2.87	566394	5529818	-208	566395	5529817	-205
RMUG08-106	23.0	25.9	2.87	566395	5529817	-205	566397	5529817	-203
RMUG08-106	25.9	28.7	2.87	566397	5529817	-203	566399	5529817	-201
RMUG08-106	28.7	31.6	2.87	566399	5529817	-201	566401	5529817	-198
RMUG08-106	31.6	34.5	2.87	566401	5529817	-198	566402	5529817	-196
RMUG08-106	34.5	37.4	2.87	566402	5529817	-196	566404	5529817	-194
RMUG08-106	37.4	40.2	2.87	566404	5529817	-194	566406	5529816	-192
RMUG08-106	40.2	43.1	2.87	566406	5529816	-192	566408	5529816	-189
RMUG08-106	43.1	46.0	2.87	566408	5529816	-189	566409	5529816	-187
RMUG08-106	46.0	48.9	2.87	566409	5529816	-187	566411	5529816	-185
RMUG08-106	48.9	51.7	2.87	566411	5529816	-185	566413	5529816	-183
RMUG08-106	51.7	54.6	2.87	566413	5529816	-183	566415	5529816	-180

## Section 5

RMUG08-95	0.0	2.9	2.89	566437	5529861	-258	566440	5529862	-258
RMUG08-95	2.9	5.8	2.89	566440	5529862	-258	566442	5529863	-257
RMUG08-95	5.8	8.7	2.89	566442	5529863	-257	566445	5529864	-257
RMUG08-95	8.7	11.6	2.89	566445	5529864	-257	566448	5529866	-257
RMUG08-95	11.6	14.4	2.89	566448	5529866	-257	566450	5529867	-257
RMUG08-95	14.4	17.3	2.89	566450	5529867	-257	566453	5529868	-257
RMUG08-95	17.3	20.2	2.89	566453	5529868	-257	566455	5529870	-256
RMUG08-95	20.2	23.1	2.89	566455	5529870	-256	566458	5529871	-256
RMUG08-95	23.1	26.0	2.89	566458	5529871	-256	566460	5529872	-256
RMUG08-95	26.0	28.9	2.89	566460	5529872	-256	566463	5529874	-256
RMUG08-95	28.9	31.8	2.89	566463	5529874	-256	566466	5529875	-256
RMUG08-95	31.8	34.7	2.89	566466	5529875	-256	566468	5529876	-256
RMUG08-95	34.7	37.6	2.89	566468	5529876	-256	566471	5529877	-255
RMUG08-95	37.6	40.5	2.89	566471	5529877	-255	566473	5529879	-255
RMUG08-95	40.5	43.3	2.89	566473	5529879	-255	566476	5529880	-255
RMUG08-95	43.3	46.2	2.89	566476	5529880	-255	566479	5529881	-255
RMUG08-95	46.2	49.1	2.89	566479	5529881	-255	566481	5529882	-254
RMUG08-95	49.1	52.0	2.89	566481	5529882	-254	566484	5529883	-254
RMUG08-95	52.0	54.9	2.89	566484	5529883	-254	566486	5529885	-254
RMUG08-97	0.0	2.8	2.85	566437	5529860	-257	566439	5529862	-255
RMUG08-97	2.8	5.7	2.85	566439	5529862	-255	566440	5529864	-254
RMUG08-97	5.7	8.5	2.85	566440	5529864	-254	566442	5529866	-252
RMUG08-97	8.5	11.4	2.85	566442	5529866	-252	566443	5529868	-251
RMUG08-97	11.4	14.2	2.85	566443	5529868	-251	566445	5529870	-249
RMUG08-97	14.2	17.1	2.85	566445	5529870	-249	566446	5529872	-248
RMUG08-97	17.1	19.9	2.85	566446	5529872	-248	566448	5529874	-246
RMUG08-97	19.9	22.8	2.85	566448	5529874	-246	566449	5529875	-245
RMUG08-97	22.8	25.6	2.85	566449	5529875	-245	566451	5529877	-244
RMUG08-97	25.6	28.5	2.85	566451	5529877	-244	566452	5529879	-242
RMUG08-97	28.5	31.3	2.85	566452	5529879	-242	566454	5529881	-241
RMUG08-97	31.3	34.2	2.85	566454	5529881	-241	566455	5529883	-239
RMUG08-97	34.2	37.0	2.85	566455	5529883	-239	566457	5529885	-238
RMUG08-97	37.0	39.9	2.85	566457	5529885	-238	566458	5529887	-236
RMUG08-97	39.9	42.7	2.85	566458	5529887	-236	566460	5529889	-235
RMUG08-97	42.7	45.6	2.85	566460	5529889	-235	566461	5529891	-233
RMUG08-97	45.6	48.4	2.85	566461	5529891	-233	566463	5529893	-232
RMUG08-98	0.0	2.9	2.90	566433	5529869	-258	566433	5529871	-258
RMUG08-98	2.9	5.8	2.90	566433	5529871	-258	566434	5529874	-257
RMUG08-98	5.8	8.7	2.90	566434	5529874	-257	566434	5529877	-257
RMUG08-98	8.7	11.6	2.90	566434	5529877	-257	566434	5529880	-257
RMUG08-98	11.6	14.5	2.90	566434	5529880	-257	566435	5529883	-256
RMUG08-98	14.5	17.4	2.90	566435	5529883	-256	566435	5529886	-256
RMUG08-98	17.4	20.3	2.90	566435	5529886	-256	566436	5529888	-255

RMUG08-98	20.3	23.2	2.90	566436	5529888	-255	566436	5529891	-255
RMUG08-98	23.2	26.1	2.90	566436	5529891	-255	566436	5529894	-255
RMUG08-98	26.1	29.0	2.90	566436	5529894	-255	566436	5529897	-254
RMUG08-98	29.0	31.9	2.90	566436	5529897	-254	566437	5529900	-254
RMUG08-98	31.9	34.9	2.90	566437	5529900	-254	566437	5529903	-253
RMUG08-98	34.9	37.8	2.90	566437	5529903	-253	566437	5529906	-253
RMUG08-98	37.8	40.7	2.90	566437	5529906	-253	566438	5529908	-252
RMUG08-98	40.7	43.6	2.90	566438	5529908	-252	566438	5529911	-252
RMUG08-98	43.6	46.5	2.90	566438	5529911	-252	566438	5529914	-251
RMUG08-98	46.5	49.4	2.90	566438	5529914	-251	566439	5529917	-251
RMUG08-98	49.4	52.3	2.90	566439	5529917	-251	566439	5529920	-250
RMUG08-98	52.3	55.2	2.90	566439	5529920	-250	566440	5529923	-250
RMUG08-98	55.2	58.1	2.90	566440	5529923	-250	566440	5529925	-249
RMUG08-98	58.1	61.0	2.90	566440	5529925	-249	566440	5529928	-249
RMUG08-98	61.0	63.9	2.90	566440	5529928	-249	566441	5529931	-248
RMUG08-98	63.9	66.8	2.90	566441	5529931	-248	566441	5529934	-248
RMUG08-98	66.8	69.7	2.90	566441	5529934	-248	566442	5529937	-247

## Section 9

RMUG08-93	0.0	2.9	2.91	566495	5529909	-318	566494	5529910	-315
RMUG08-93	2.9	5.8	2.91	566494	5529910	-315	566493	5529912	-313
RMUG08-93	5.8	8.7	2.91	566493	5529912	-313	566492	5529914	-311
RMUG08-93	8.7	11.6	2.91	566492	5529914	-311	566490	5529915	-309
RMUG08-93	11.6	14.5	2.91	566490	5529915	-309	566489	5529917	-307
RMUG08-93	14.5	17.5	2.91	566489	5529917	-307	566488	5529918	-305
RMUG08-93	17.5	20.4	2.91	566488	5529918	-305	566487	5529920	-303
RMUG08-93	20.4	23.3	2.91	566487	5529920	-303	566486	5529922	-300
RMUG08-93	23.3	26.2	2.91	566486	5529922	-300	566485	5529923	-298
RMUG08-93	26.2	29.1	2.91	566485	5529923	-298	566484	5529925	-296
RMUG08-93	29.1	32.0	2.91	566484	5529925	-296	566483	5529927	-294
RMUG08-93	32.0	34.9	2.91	566483	5529927	-294	566482	5529928	-292
RMUG08-93	34.9	37.8	2.91	566482	5529928	-292	566481	5529930	-289
RMUG08-93	37.8	40.7	2.91	566481	5529930	-289	566480	5529931	-287
RMUG08-93	40.7	43.6	2.91	566480	5529931	-287	566479	5529933	-285
RMUG08-93	43.6	46.5	2.91	566479	5529933	-285	566478	5529935	-283
RMUG08-93	46.5	49.5	2.91	566478	5529935	-283	566477	5529936	-281
RMUG08-93	49.5	52.4	2.91	566477	5529936	-281	566476	5529938	-278
RMUG08-93	52.4	55.3	2.91	566476	5529938	-278	566475	5529939	-276
RMUG08-93	55.3	58.2	2.91	566475	5529939	-276	566474	5529941	-274
RMUG08-93	58.2	61.1	2.91	566474	5529941	-274	566473	5529943	-272
RMUG08-93	61.1	64.0	2.91	566473	5529943	-272	566472	5529944	-269

RMUG08-94	0.0	2.9	2.94	566494	5529909	-318	566493	5529911	-317
RMUG08-94	2.9	5.9	2.94	566493	5529911	-317	566491	5529913	-315
RMUG08-94	5.9	8.8	2.94	566491	5529913	-315	566489	5529915	-313
RMUG08-94	8.8	11.7	2.94	566489	5529915	-313	566488	5529917	-312
RMUG08-94	11.7	14.7	2.94	566488	5529917	-312	566486	5529919	-310
RMUG08-94	14.7	17.6	2.94	566486	5529919	-310	566485	5529921	-309
RMUG08-94	17.6	20.5	2.94	566485	5529921	-309	566483	5529923	-307
RMUG08-94	20.5	23.5	2.94	566483	5529923	-307	566482	5529925	-306
RMUG08-94	23.5	26.4	2.94	566482	5529925	-306	566480	5529927	-304
RMUG08-94	26.4	29.4	2.94	566480	5529927	-304	566479	5529929	-303
RMUG08-94	29.4	32.3	2.94	566479	5529929	-303	566477	5529931	-301
RMUG08-94	32.3	35.2	2.94	566477	5529931	-301	566476	5529933	-300
RMUG08-94	35.2	38.2	2.94	566476	5529933	-300	566474	5529935	-298
RMUG08-94	38.2	41.1	2.94	566474	5529935	-298	566473	5529937	-297
RMUG08-94	41.1	44.0	2.94	566473	5529937	-297	566471	5529939	-295
RMUG08-94	44.0	47.0	2.94	566471	5529939	-295	566470	5529941	-293
RMUG08-94	47.0	49.9	2.94	566470	5529941	-293	566468	5529943	-292
RMUG08-94	49.9	52.8	2.94	566468	5529943	-292	566467	5529945	-290
RMUG08-94	52.8	55.8	2.94	566467	5529945	-290	566465	5529947	-289
RMUG08-94	55.8	58.7	2.94	566465	5529947	-289	566464	5529949	-287
RMUG08-94	58.7	61.6	2.94	566464	5529949	-287	566462	5529951	-286
RMUG08-94	61.6	64.6	2.94	566462	5529951	-286	566461	5529953	-284
RMUG08-94	64.6	67.5	2.94	566461	5529953	-284	566460	5529955	-283
RMUG08-94	67.5	70.4	2.94	566460	5529955	-283	566458	5529957	-281
RMUG08-94	70.4	73.4	2.94	566458	5529957	-281	566457	5529959	-280
RMUG08-94	73.4	76.3	2.94	566457	5529959	-280	566455	5529961	-278
RMUG08-94	76.3	79.2	2.94	566455	5529961	-278	566454	5529963	-276
RMUG08-94	79.2	82.2	2.94	566454	5529963	-276	566452	5529965	-275

RMUG08-94	82.2	85.1	2.94	566452	5529965	-275	566451	5529967	-273
RMUG08-96	0.0	3.0	2.95	566493	5529908	-318	566491	5529908	-315
RMUG08-96	3.0	5.9	2.95	566491	5529908	-315	566489	5529908	-313
RMUG08-96	5.9	8.9	2.95	566489	5529908	-313	566487	5529909	-311
RMUG08-96	8.9	11.8	2.95	566487	5529909	-311	566485	5529909	-309
RMUG08-96	11.8	14.8	2.95	566485	5529909	-309	566484	5529909	-307
RMUG08-96	14.8	17.7	2.95	566484	5529909	-307	566482	5529909	-304
RMUG08-96	17.7	20.7	2.95	566482	5529909	-304	566480	5529910	-302
RMUG08-96	20.7	23.6	2.95	566480	5529910	-302	566478	5529910	-300
RMUG08-96	23.6	26.6	2.95	566478	5529910	-300	566476	5529911	-298
RMUG08-96	26.6	29.5	2.95	566476	5529911	-298	566474	5529911	-296
RMUG08-96	29.5	32.5	2.95	566474	5529911	-296	566472	5529911	-293
RMUG08-96	32.5	35.4	2.95	566472	5529911	-293	566470	5529912	-291
RMUG08-96	35.4	38.4	2.95	566470	5529912	-291	566468	5529912	-289
RMUG08-96	38.4	41.3	2.95	566468	5529912	-289	566466	5529913	-287
RMUG08-96	41.3	44.3	2.95	566466	5529913	-287	566464	5529913	-285
RMUG08-96	44.3	47.3	2.95	566464	5529913	-285	566462	5529914	-282
RMUG08-96	47.3	50.2	2.95	566462	5529914	-282	566461	5529914	-280
RMUG08-96	50.2	53.2	2.95	566461	5529914	-280	566459	5529915	-278
RMUG08-96	53.2	56.1	2.95	566459	5529915	-278	566457	5529915	-276
RMUG08-96	56.1	59.1	2.95	566457	5529915	-276	566455	5529916	-273
RMUG08-96	59.1	62.0	2.95	566455	5529916	-273	566453	5529916	-271
RMUG08-96	62.0	65.0	2.95	566453	5529916	-271	566451	5529917	-269
RMUG08-96	65.0	67.9	2.95	566451	5529917	-269	566449	5529918	-267
RMUG08-96	67.9	70.9	2.95	566449	5529918	-267	566448	5529918	-265
RMUG08-96	70.9	73.8	2.95	566448	5529918	-265	566446	5529919	-262
RMUG08-96	73.8	76.8	2.95	566446	5529919	-262	566444	5529919	-260
RMUG08-96	76.8	79.7	2.95	566444	5529919	-260	566442	5529920	-258
RMUG08-96	79.7	82.7	2.95	566442	5529920	-258	566440	5529921	-256
RMUG08-96	82.7	85.6	2.95	566440	5529921	-256	566439	5529921	-253
RMUG08-96	85.6	88.6	2.95	566439	5529921	-253	566437	5529922	-251
RMUG08-96	88.6	91.5	2.95	566437	5529922	-251	566435	5529923	-249
RMUG08-96	91.5	94.5	2.95	566435	5529923	-249	566433	5529923	-247
RMUG08-99	0.0	2.9	2.91	566495	5529907	-317	566494	5529907	-314
RMUG08-99	2.9	5.8	2.91	566494	5529907	-314	566493	5529907	-311
RMUG08-99	5.8	8.7	2.91	566493	5529907	-311	566491	5529908	-309
RMUG08-99	8.7	11.7	2.91	566491	5529908	-309	566490	5529908	-306
RMUG08-99	11.7	14.6	2.91	566490	5529908	-306	566489	5529908	-304
RMUG08-99	14.6	17.5	2.91	566489	5529908	-304	566487	5529909	-301
RMUG08-99	17.5	20.4	2.91	566487	5529909	-301	566486	5529909	-299
RMUG08-99	20.4	23.3	2.91	566486	5529909	-299	566485	5529910	-296
RMUG08-99	23.3	26.2	2.91	566485	5529910	-296	566483	5529910	-294
RMUG08-99	26.2	29.1	2.91	566483	5529910	-294	566482	5529911	-291
RMUG08-99	29.1	32.1	2.91	566482	5529911	-291	566481	5529911	-288
RMUG08-99	32.1	35.0	2.91	566481	5529911	-288	566479	5529911	-286
RMUG08-99	35.0	37.9	2.91	566479	5529911	-286	566478	5529912	-283
RMUG08-99	37.9	40.8	2.91	566478	5529912	-283	566477	5529912	-281
RMUG08-99	40.8	43.7	2.91	566477	5529912	-281	566475	5529913	-278
RMUG08-99	43.7	46.6	2.91	566475	5529913	-278	566474	5529913	-276
RMUG08-99	46.6	49.5	2.91	566474	5529913	-276	566473	5529914	-273
RMUG08-99	49.5	52.5	2.91	566473	5529914	-273	566471	5529914	-271
RMUG08-99	52.5	55.4	2.91	566471	5529914	-271	566470	5529915	-268
RMUG08-99	55.4	58.3	2.91	566470	5529915	-268	566469	5529915	-265
RMUG08-99	58.3	61.2	2.91	566469	5529915	-265	566468	5529916	-263
RMUG08-99	61.2	64.1	2.91	566468	5529916	-263	566466	5529917	-260
RMUG08-99	64.1	67.0	2.91	566466	5529917	-260	566465	5529917	-258
RMUG08-99	67.0	69.9	2.91	566465	5529917	-258	566464	5529918	-255
RMUG08-99	69.9	72.9	2.91	566464	5529918	-255	566463	5529918	-252
RMUG08-99	72.9	75.8	2.91	566463	5529918	-252	566462	5529919	-250
RMUG08-99	75.8	78.7	2.91	566462	5529919	-250	566460	5529919	-247
RMUG08-99	78.7	81.6	2.91	566460	5529919	-247	566459	5529920	-245
Section 8									
RMUG08-44	24.0	28.8	4.80	566496	5529930	-305	566496	5529934	-303
RMUG08-44	28.8	33.6	4.80	566496	5529934	-303	566496	5529938	-300
RMUG08-44	33.6	38.4	4.80	566496	5529938	-300	566496	5529942	-298

## Section 14

RMUG08-60	52.1	55.0	2.89	566546	5530013	-361	566546	5530015	-358
RMUG08-60	55.0	57.9	2.89	566546	5530015	-358	566546	5530016	-356
RMUG08-60	57.9	60.8	2.89	566546	5530016	-356	566546	5530018	-353
RMUG08-60	60.8	63.6	2.89	566546	5530018	-353	566545	5530019	-351
RMUG08-60	63.6	66.5	2.89	566545	5530019	-351	566545	5530020	-348
RMUG08-60	66.5	69.4	2.89	566545	5530020	-348	566545	5530022	-346
RMUG08-60	69.4	72.3	2.89	566545	5530022	-346	566545	5530023	-343
RMUG08-61	44.9	47.9	2.99	566559	5530014	-369	566559	5530015	-367
RMUG08-61	47.9	50.9	2.99	566559	5530015	-367	566560	5530017	-364
RMUG08-61	50.9	53.8	2.99	566560	5530017	-364	566560	5530019	-362
RMUG08-61	53.8	56.8	2.99	566560	5530019	-362	566560	5530021	-359
RMUG08-61	56.8	59.8	2.99	566560	5530021	-359	566561	5530022	-357
RMUG08-63	0.0	3.0	2.99	566551	5529984	-405	566549	5529985	-403
RMUG08-63	3.0	6.0	2.99	566549	5529985	-403	566547	5529985	-400
RMUG08-63	6.0	9.0	2.99	566547	5529985	-400	566545	5529986	-398
RMUG08-63	9.0	12.0	2.99	566545	5529986	-398	566543	5529987	-396
RMUG08-63	12.0	15.0	2.99	566543	5529987	-396	566542	5529987	-394
RMUG08-63	15.0	18.0	2.99	566542	5529987	-394	566540	5529988	-391
RMUG08-63	18.0	21.0	2.99	566540	5529988	-391	566538	5529989	-389
RMUG08-63	21.0	24.0	2.99	566538	5529989	-389	566536	5529990	-387
RMUG08-63	24.0	27.0	2.99	566536	5529990	-387	566535	5529990	-384
RMUG08-63	27.0	29.9	2.99	566535	5529990	-384	566533	5529991	-382
RMUG08-63	29.9	32.9	2.99	566533	5529991	-382	566531	5529992	-380
RMUG08-63	32.9	35.9	2.99	566531	5529992	-380	566529	5529993	-377
RMUG08-63	35.9	38.9	2.99	566529	5529993	-377	566528	5529993	-375
RMUG08-63	38.9	41.9	2.99	566528	5529993	-375	566526	5529994	-373
RMUG08-63	41.9	44.9	2.99	566526	5529994	-373	566524	5529995	-371
RMUG08-63	44.9	47.9	2.99	566524	5529995	-371	566522	5529996	-368
RMUG08-63	47.9	50.9	2.99	566522	5529996	-368	566521	5529997	-366
RMUG08-63	50.9	53.9	2.99	566521	5529997	-366	566519	5529997	-364
RMUG08-63	53.9	56.9	2.99	566519	5529997	-364	566517	5529998	-361
RMUG08-63	56.9	59.9	2.99	566517	5529998	-361	566516	5529999	-359
RMUG08-63	59.9	62.9	2.99	566516	5529999	-359	566514	5530000	-357
RMUG08-63	62.9	65.9	2.99	566514	5530000	-357	566512	5530001	-354
RMUG08-63	65.9	68.9	2.99	566512	5530001	-354	566511	5530002	-352
RMUG08-63	68.9	71.9	2.99	566511	5530002	-352	566509	5530003	-350
RMUG08-63	71.9	74.9	2.99	566509	5530003	-350	566507	5530004	-347
RMUG08-63	74.9	77.9	2.99	566507	5530004	-347	566506	5530005	-345
RMUG08-63	77.9	80.9	2.99	566506	5530005	-345	566504	5530006	-343
RMUG08-63	80.9	83.8	2.99	566504	5530006	-343	566503	5530007	-340
RMUG08-63	83.8	86.8	2.99	566503	5530007	-340	566501	5530008	-338
RMUG08-63	86.8	89.8	2.99	566501	5530008	-338	566499	5530009	-336
RMUG08-63	89.8	92.8	2.99	566499	5530008	-336	566498	5530010	-333
RMUG08-63	92.8	95.8	2.99	566498	5530010	-333	566496	5530011	-331
RMUG08-63	95.8	98.8	2.99	566496	5530011	-331	566495	5530012	-329
RMUG08-63	98.8	101.8	2.99	566495	5530012	-329	566493	5530013	-326
RMUG08-63	101.8	104.8	2.99	566493	5530013	-326	566492	5530014	-324
RMUG08-63	104.8	107.8	2.99	566492	5530014	-324	566490	5530015	-322
RMUG08-64	0.0	3.0	2.99	566552	5529982	-405	566551	5529982	-402
RMUG08-64	3.0	6.0	2.99	566551	5529982	-402	566550	5529982	-399
RMUG08-64	6.0	9.0	2.99	566550	5529982	-399	566549	5529981	-397
RMUG08-64	9.0	12.0	2.99	566549	5529981	-397	566547	5529981	-394
RMUG08-64	12.0	15.0	2.99	566547	5529981	-394	566546	5529981	-391
RMUG08-64	15.0	17.9	2.99	566546	5529981	-391	566545	5529981	-388
RMUG08-64	17.9	20.9	2.99	566545	5529981	-388	566544	5529980	-386
RMUG08-64	20.9	23.9	2.99	566544	5529980	-386	566543	5529980	-383
RMUG08-64	23.9	26.9	2.99	566543	5529980	-383	566542	5529980	-380
RMUG08-64	26.9	29.9	2.99	566542	5529980	-380	566540	5529980	-377
RMUG08-64	29.9	32.9	2.99	566540	5529980	-377	566539	5529980	-375
RMUG08-64	32.9	35.9	2.99	566539	5529980	-375	566538	5529979	-372
RMUG08-64	35.9	38.9	2.99	566538	5529980	-372	566537	5529979	-369
RMUG08-64	38.9	41.9	2.99	566537	5529979	-369	566536	5529979	-366
RMUG08-64	41.9	44.9	2.99	566536	5529979	-366	566535	5529979	-363
RMUG08-64	44.9	47.9	2.99	566535	5529979	-363	566534	5529979	-361
RMUG08-64	47.9	50.8	2.99	566534	5529979	-361	566533	5529979	-358
RMUG08-64	50.8	53.8	2.99	566533	5529979	-358	566532	5529979	-355
RMUG08-64	53.8	56.8	2.99	566532	5529979	-355	566531	5529979	-352

RMUG08-64	56.8	59.8	2.99	566531	5529979	-352	566530	5529979	-349
RMUG08-64	59.8	62.8	2.99	566530	5529979	-349	566529	5529979	-347
RMUG08-64	62.8	65.8	2.99	566529	5529979	-347	566528	5529979	-344
RMUG08-64	65.8	68.8	2.99	566528	5529979	-344	566527	5529979	-341
RMUG08-64	68.8	71.8	2.99	566527	5529979	-341	566526	5529978	-338
RMUG08-64	71.8	74.8	2.99	566526	5529978	-338	566525	5529979	-335
RMUG08-64	74.8	77.8	2.99	566525	5529979	-335	566524	5529979	-332
RMUG08-64	77.8	80.8	2.99	566524	5529979	-332	566523	5529979	-330
RMUG08-64	80.8	83.7	2.99	566523	5529979	-330	566522	5529979	-327
RMUG08-64	83.7	86.7	2.99	566522	5529979	-327	566521	5529979	-324
RMUG08-64	86.7	89.7	2.99	566521	5529979	-324	566520	5529979	-321
RMUG08-64	89.7	92.7	2.99	566520	5529979	-321	566520	5529979	-318
RMUG08-64	92.7	95.7	2.99	566520	5529979	-318	566519	5529979	-315
RMUG08-64	95.7	98.7	2.99	566519	5529979	-315	566518	5529979	-312

## Section 13

RMUG08-90	0.0	2.9	2.92	566553	5530034	-406	566552	5530036	-405
RMUG08-90	2.9	5.8	2.92	566552	5530036	-405	566551	5530038	-403
RMUG08-90	5.8	8.8	2.92	566551	5530038	-403	566550	5530041	-401
RMUG08-90	8.8	11.7	2.92	566550	5530041	-401	566549	5530043	-400
RMUG08-90	11.7	14.6	2.92	566549	5530043	-400	566548	5530045	-398
RMUG08-90	14.6	17.5	2.92	566548	5530045	-398	566547	5530047	-397
RMUG08-90	17.5	20.5	2.92	566547	5530047	-397	566546	5530050	-395
RMUG08-90	20.5	23.4	2.92	566546	5530050	-395	566545	5530052	-393
RMUG08-90	23.4	26.3	2.92	566545	5530052	-393	566544	5530054	-392
RMUG08-90	26.3	29.2	2.92	566544	5530054	-392	566543	5530056	-390
RMUG08-90	29.2	32.2	2.92	566543	5530056	-390	566542	5530059	-389
RMUG08-90	32.2	35.1	2.92	566542	5530059	-389	566541	5530061	-387
RMUG08-90	35.1	38.0	2.92	566541	5530061	-387	566540	5530063	-386
RMUG08-90	38.0	40.9	2.92	566540	5530063	-386	566539	5530066	-384
RMUG08-90	40.9	43.9	2.92	566539	5530066	-384	566538	5530068	-382
RMUG08-90	43.9	46.8	2.92	566538	5530068	-382	566537	5530070	-381
RMUG08-90	46.8	49.7	2.92	566537	5530070	-381	566536	5530072	-379
RMUG08-90	49.7	52.6	2.92	566536	5530072	-379	566536	5530075	-378
RMUG08-90	52.6	55.6	2.92	566536	5530075	-378	566535	5530077	-376
RMUG08-90	55.6	58.5	2.92	566535	5530077	-376	566534	5530079	-374
RMUG08-90	58.5	61.4	2.92	566534	5530079	-374	566533	5530081	-373
RMUG08-90	61.4	64.3	2.92	566533	5530081	-373	566532	5530084	-371
RMUG08-90	64.3	67.3	2.92	566532	5530084	-371	566531	5530086	-370
RMUG08-90	67.3	70.2	2.92	566531	5530086	-370	566530	5530088	-368
RMUG08-90	70.2	73.1	2.92	566530	5530088	-368	566529	5530091	-366
RMUG08-91	0.0	2.9	2.92	566556	5530031	-407	566559	5530030	-405
RMUG08-91	2.9	5.8	2.92	566559	5530030	-405	566561	5530030	-404
RMUG08-91	5.8	8.8	2.92	566561	5530030	-404	566564	5530030	-403
RMUG08-91	8.8	11.7	2.92	566564	5530030	-403	566566	5530029	-402
RMUG08-91	11.7	14.6	2.92	566566	5530029	-402	566569	5530029	-400
RMUG08-91	14.6	17.5	2.92	566569	5530029	-400	566572	5530028	-399
RMUG08-91	17.5	20.4	2.92	566572	5530028	-399	566574	5530028	-398
RMUG08-91	20.4	23.4	2.92	566574	5530028	-398	566577	5530028	-397
RMUG08-91	23.4	26.3	2.92	566577	5530028	-397	566580	5530027	-395
RMUG08-91	26.3	29.2	2.92	566580	5530027	-395	566582	5530027	-394
RMUG08-91	29.2	32.1	2.92	566582	5530027	-394	566585	5530026	-393
RMUG08-91	32.1	35.1	2.92	566585	5530026	-393	566587	5530026	-391
RMUG08-91	35.1	38.0	2.92	566587	5530026	-391	566590	5530026	-390
RMUG08-91	38.0	40.9	2.92	566590	5530026	-390	566592	5530025	-389
RMUG08-91	40.9	43.8	2.92	566592	5530025	-389	566595	5530025	-388
RMUG08-91	43.8	46.7	2.92	566595	5530025	-388	566598	5530025	-386
RMUG08-91	46.7	49.7	2.92	566598	5530025	-386	566600	5530024	-385
RMUG08-91	49.7	52.6	2.92	566600	5530024	-385	566603	5530024	-384
RMUG08-91	52.6	55.5	2.92	566603	5530024	-384	566605	5530023	-382
RMUG08-91	55.5	58.4	2.92	566605	5530023	-382	566608	5530023	-381
RMUG08-91	58.4	61.3	2.92	566608	5530023	-381	566611	5530022	-380
RMUG08-91	61.3	64.3	2.92	566611	5530022	-380	566613	5530022	-379
RMUG08-91	64.3	67.2	2.92	566613	5530022	-379	566616	5530021	-377
RMUG08-91	67.2	70.1	2.92	566616	5530021	-377	566618	5530021	-376

**Table eA1.** Detailed coordinates of logged drill hole sections from the MSDP and LFWZ orebodies; coordinates in UTM 21N NAD83 (data from Rambler Metals & Mining Canada Ltd)

Drill hole #	Drill hole intervall			Coordinates		Depth below sea level	Coordinates		Depth below sea level
	From [m]	To [m]	Length [m]	X_start (E)	Y_start (N)	Z_start [m]	X_end (E)	Y_end (N)	Z_end [m]
<b>RM06-04d</b>									
RM06-04d	875.3	878.3	3.00	566888	5530400	-687	566888	5530399	-690
RM06-04d	878.3	881.3	3.00	566888	5530399	-690	566887	5530398	-693
RM06-04d	881.3	884.3	3.00	566887	5530398	-693	566887	5530398	-696
RM06-04d	884.3	887.3	3.00	566887	5530398	-696	566886	5530397	-698
RM06-04d	887.3	890.3	3.00	566886	5530397	-698	566886	5530396	-701
RM06-04d	890.3	893.3	3.00	566886	5530396	-701	566885	5530395	-704
RM06-04d	893.3	896.3	3.00	566885	5530395	-704	566884	5530395	-707
RM06-04d	896.3	899.3	3.00	566884	5530395	-707	566884	5530394	-710
RM06-04d	899.3	902.2	3.00	566884	5530394	-710	566883	5530393	-713
<b>RM06-04e</b>									
RM06-04e	879.3	881.3	2.00	566892	5530416	-694	566892	5530416	-696
RM06-04e	881.3	883.3	2.00	566892	5530416	-696	566891	5530416	-698
RM06-04e	883.3	885.3	2.00	566891	5530416	-698	566891	5530415	-700
RM06-04e	885.3	887.3	2.00	566891	5530415	-700	566891	5530415	-702
RM06-04e	887.3	889.3	2.00	566891	5530415	-702	566890	5530415	-704
RM06-04e	889.3	891.3	2.00	566890	5530415	-704	566890	5530415	-706
RM06-04e	891.3	893.3	2.00	566890	5530415	-706	566889	5530415	-708
RM06-04e	893.3	895.3	2.00	566889	5530415	-708	566889	5530415	-710
RM06-04e	895.3	897.3	2.00	566889	5530415	-710	566889	5530415	-712
RM06-04e	897.3	899.3	2.00	566889	5530415	-712	566888	5530415	-714
RM06-04e	899.3	901.3	2.00	566888	5530415	-714	566888	5530415	-716
RM06-04e	901.3	903.3	2.00	566888	5530415	-716	566888	5530414	-718
RM06-04e	903.3	905.3	2.00	566888	5530414	-718	566887	5530414	-720
RM06-04e	905.3	907.3	2.00	566887	5530414	-720	566887	5530414	-722
RM06-04e	907.3	909.3	2.00	566887	5530414	-722	566886	5530414	-724
RM06-04e	909.3	911.3	2.00	566886	5530414	-724	566886	5530414	-726
RM06-04e	911.3	913.3	2.00	566886	5530414	-726	566886	5530414	-728
RM06-04e	913.3	915.3	2.00	566886	5530414	-728	566885	5530414	-729
RM06-04e	915.3	917.3	2.00	566885	5530414	-729	566885	5530414	-731
RM06-04e	917.3	919.3	2.00	566885	5530414	-731	566885	5530414	-733
RM06-04e	919.3	921.3	2.00	566885	5530414	-733	566884	5530414	-735
RM06-04e	921.3	923.3	2.00	566884	5530414	-735	566884	5530414	-737
RM06-04e	923.3	925.3	2.00	566884	5530414	-737	566884	5530414	-739
RM06-04e	925.3	927.3	2.00	566884	5530414	-739	566883	5530413	-741
RM06-04e	927.3	929.3	2.00	566883	5530413	-741	566883	5530413	-743
RM06-04e	929.3	931.3	2.00	566883	5530413	-743	566883	5530413	-745
RM06-04e	931.3	933.3	2.00	566883	5530413	-745	566882	5530413	-747
RM06-04e	933.3	935.3	2.00	566882	5530413	-747	566882	5530413	-749
RM06-04e	935.3	937.3	2.00	566882	5530413	-749	566882	5530413	-751
RM06-04e	937.3	939.3	2.00	566882	5530413	-751	566881	5530413	-753
RM06-04e	939.3	941.3	2.00	566881	5530413	-753	566881	5530413	-755
RM06-04e	941.3	943.3	2.00	566881	5530413	-755	566881	5530413	-757
RM06-04e	943.3	945.3	2.00	566881	5530413	-757	566881	5530413	-759
RM06-04e	945.3	947.3	2.00	566881	5530413	-759	566880	5530413	-761
RM06-04e	947.3	949.2	2.00	566880	5530413	-761	566880	5530413	-763
RM06-04e	949.2	951.2	2.00	566880	5530413	-763	566880	5530413	-765
RM06-04e	951.2	953.2	2.00	566880	5530413	-765	566879	5530413	-767
RM06-04e	953.2	955.2	2.00	566879	5530413	-767	566879	5530412	-769
RM06-04e	955.2	957.2	2.00	566879	5530412	-769	566879	5530412	-771
RM06-04e	957.2	959.2	2.00	566879	5530412	-771	566878	5530412	-773
RM06-04e	959.2	961.2	2.00	566878	5530412	-773	566878	5530412	-775
RM06-04e	961.2	963.2	2.00	566878	5530412	-775	566878	5530412	-777
RM06-04e	963.2	965.2	2.00	566878	5530412	-777	566877	5530412	-779
RM06-04e	965.2	967.2	2.00	566877	5530412	-779	566877	5530412	-781
RM06-04e	967.2	969.2	2.00	566877	5530412	-781	566876	5530412	-783
RM06-04e	969.2	971.2	2.00	566876	5530412	-783	566876	5530412	-785
RM06-04e	971.2	973.2	2.00	566876	5530412	-785	566876	5530412	-787
RM06-04e	973.2	975.2	2.00	566876	5530412	-787	566875	5530412	-789
RM06-04e	975.2	977.2	2.00	566875	5530412	-789	566875	5530412	-791
RM06-04e	977.2	979.2	2.00	566875	5530412	-791	566875	5530411	-793
RM06-04e	979.2	981.2	2.00	566875	5530411	-793	566874	5530411	-794

RM06-04e	981.2	983.2	2.00	566874	5530411	-794	566874	5530411	-796
RM06-04e	983.2	985.2	2.00	566874	5530411	-796	566874	5530411	-798
RM06-04e	985.2	987.2	2.00	566874	5530411	-798	566873	5530411	-800
RM06-04e	987.2	989.2	2.00	566873	5530411	-800	566873	5530411	-802
RM06-04e	989.2	991.2	2.00	566873	5530411	-802	566873	5530411	-804
RM06-04e	991.2	993.2	2.00	566873	5530411	-804	566872	5530411	-806
RM06-04e	993.2	995.2	2.00	566872	5530411	-806	566872	5530411	-808
RM06-04e	995.2	997.2	2.00	566872	5530411	-808	566872	5530411	-810
RM06-04e	997.2	999.2	2.00	566872	5530411	-810	566871	5530410	-812
RM06-04e	999.2	1001.2	2.00	566871	5530410	-812	566871	5530410	-814
RM06-04e	1001.2	1003.2	2.00	566871	5530410	-814	566871	5530410	-816
RM06-04e	1003.2	1005.2	2.00	566871	5530410	-816	566870	5530410	-818
RM06-04e	1005.2	1007.2	2.00	566870	5530410	-818	566870	5530410	-820
RM06-04e	1007.2	1009.2	2.00	566870	5530410	-820	566869	5530410	-822
RM06-04e	1009.2	1011.2	2.00	566869	5530410	-822	566869	5530410	-824
RM06-04e	1011.2	1013.2	2.00	566869	5530410	-824	566869	5530410	-826
RM06-04e	1013.2	1015.2	2.00	566869	5530410	-826	566868	5530410	-828
RM06-04e	1015.2	1017.2	2.00	566868	5530410	-828	566868	5530410	-830
RM06-04e	1017.2	1019.2	2.00	566868	5530410	-830	566868	5530409	-832
RM06-04e	1019.2	1021.2	2.00	566868	5530409	-832	566867	5530409	-834
RM06-04e	1021.2	1023.2	2.00	566867	5530409	-834	566867	5530409	-836
RM06-04e	1023.2	1025.2	2.00	566867	5530409	-836	566866	5530409	-838
RM06-04e	1025.2	1027.2	2.00	566866	5530409	-838	566866	5530409	-840
RM06-04e	1027.2	1029.2	2.00	566866	5530409	-840	566866	5530409	-842
RM06-04e	1029.2	1031.2	2.00	566866	5530409	-842	566865	5530409	-843
RM06-04e	1031.2	1033.2	2.00	566865	5530409	-843	566865	5530409	-845
RM06-04e	1033.2	1035.2	2.00	566865	5530409	-845	566864	5530409	-847
RM06-04e	1035.2	1037.2	2.00	566864	5530409	-847	566864	5530409	-849
RM06-04e	1037.2	1039.2	2.00	566864	5530409	-849	566863	5530408	-851
RM06-04e	1039.2	1041.2	2.00	566863	5530408	-851	566863	5530408	-853
RM06-04e	1041.2	1043.2	2.00	566863	5530408	-853	566863	5530408	-855
RM06-04e	1043.2	1045.2	2.00	566863	5530408	-855	566862	5530408	-857
RM06-04e	1045.2	1047.2	2.00	566862	5530408	-857	566862	5530408	-859
RM06-04e	1047.2	1049.2	2.00	566862	5530408	-859	566861	5530408	-861
RM06-04e	1049.2	1051.2	2.00	566861	5530408	-861	566861	5530408	-863
RM06-04e	1051.2	1053.2	2.00	566861	5530408	-863	566861	5530408	-865
RM06-04e	1053.2	1055.2	2.00	566861	5530408	-865	566860	5530408	-867
RM06-04e	1055.2	1057.2	2.00	566860	5530408	-867	566860	5530407	-869
RM06-04e	1057.2	1059.2	2.00	566860	5530407	-869	566859	5530407	-871
RM06-04e	1059.2	1061.2	2.00	566859	5530407	-871	566859	5530407	-873
RM06-04e	1061.2	1063.2	2.00	566859	5530407	-873	566858	5530407	-875
RM06-04e	1063.2	1065.2	2.00	566858	5530407	-875	566858	5530407	-877
RM06-04e	1065.2	1067.2	2.00	566858	5530407	-877	566858	5530407	-879
RM06-04e	1067.2	1069.2	2.00	566858	5530407	-879	566857	5530407	-881
RM06-04e	1069.2	1071.2	2.00	566857	5530407	-881	566857	5530407	-883
RM06-04e	1071.2	1073.2	2.00	566857	5530407	-883	566856	5530406	-884
RM06-04e	1073.2	1075.2	2.00	566856	5530406	-884	566856	5530406	-886
RM06-04e	1075.2	1077.1	2.00	566856	5530406	-886	566855	5530406	-888
RM06-04e	1077.1	1079.1	2.00	566855	5530406	-888	566855	5530406	-890
RM06-04e	1079.1	1081.1	2.00	566855	5530406	-890	566855	5530406	-892
RM06-04e	1081.1	1083.1	2.00	566855	5530406	-892	566854	5530406	-894
RM06-04e	1083.1	1085.1	2.00	566854	5530406	-894	566854	5530406	-896
RM06-04e	1085.1	1087.1	2.00	566854	5530406	-896	566853	5530406	-898
RM06-04e	1087.1	1089.1	2.00	566853	5530406	-898	566853	5530405	-900
RM06-04e	1089.1	1091.1	2.00	566853	5530405	-900	566852	5530405	-902
RM06-04e	1091.1	1093.1	2.00	566852	5530405	-902	566852	5530405	-904
RM06-04e	1093.1	1095.1	2.00	566852	5530405	-904	566851	5530405	-906
RM06-04e	1095.1	1097.1	2.00	566851	5530405	-906	566851	5530405	-908
RM06-04e	1097.1	1099.1	2.00	566851	5530405	-908	566850	5530405	-910
RM06-04e	1099.1	1101.1	2.00	566850	5530405	-910	566850	5530404	-912
RM06-04e	1101.1	1103.1	2.00	566850	5530404	-912	566849	5530404	-914
RM06-04e	1103.1	1105.1	2.00	566849	5530404	-914	566849	5530404	-915
RM06-04e	1105.1	1107.1	2.00	566849	5530404	-915	566848	5530404	-917
RM06-04e	1107.1	1109.1	2.00	566848	5530404	-917	566848	5530404	-919
RM06-04e	1109.1	1111.1	2.00	566848	5530404	-919	566848	5530404	-921
RM06-04e	1111.1	1113.1	2.00	566848	5530404	-921	566847	5530404	-923
RM06-04e	1113.1	1115.1	2.00	566847	5530404	-923	566847	5530403	-925
RM06-04e	1115.1	1117.1	2.00	566847	5530403	-925	566846	5530403	-927
RM06-04e	1117.1	1119.1	2.00	566846	5530403	-927	566846	5530403	-929
RM06-04e	1119.1	1121.1	2.00	566846	5530403	-929	566845	5530403	-931



RM06-04e	1121.1	1123.1	2.00	566845	5530403	-931	566845	5530403	-933
RM06-04e	1123.1	1125.1	2.00	566845	5530403	-933	566844	5530403	-935
RM06-04e	1125.1	1127.1	2.00	566844	5530403	-935	566844	5530403	-937
RM06-04e	1127.1	1129.1	2.00	566844	5530403	-937	566843	5530402	-939
RM06-04e	1129.1	1131.1	2.00	566843	5530402	-939	566843	5530402	-941
RM06-04e	1131.1	1133.1	2.00	566843	5530402	-941	566842	5530402	-943
RM06-04e	1133.1	1135.1	2.00	566842	5530402	-943	566842	5530402	-944
RM06-04e	1135.1	1137.1	2.00	566842	5530402	-944	566841	5530402	-946
RM06-04e	1137.1	1139.1	2.00	566841	5530402	-946	566841	5530402	-948
RM06-04e	1139.1	1141.1	2.00	566841	5530402	-948	566840	5530401	-950
RM06-04e	1141.1	1143.1	2.00	566840	5530401	-950	566840	5530401	-952
RM06-04e	1143.1	1145.1	2.00	566840	5530401	-952	566839	5530401	-954
RM06-04e	1145.1	1147.1	2.00	566839	5530401	-954	566839	5530401	-956
RM06-04e	1147.1	1149.1	2.00	566839	5530401	-956	566838	5530401	-958
RM06-04e	1149.1	1151.1	2.00	566838	5530401	-958	566838	5530401	-960
RM06-04e	1151.1	1153.1	2.00	566838	5530401	-960	566837	5530401	-962
RM06-04e	1153.1	1155.1	2.00	566837	5530401	-962	566837	5530400	-964
RM06-04e	1155.1	1157.1	2.00	566837	5530400	-964	566836	5530400	-966
RM06-04e	1157.1	1159.1	2.00	566836	5530400	-966	566835	5530400	-968
RM06-04e	1159.1	1161.1	2.00	566835	5530400	-968	566835	5530400	-969
RM06-04e	1161.1	1163.1	2.00	566835	5530400	-969	566834	5530400	-971
RM06-04e	1163.1	1165.1	2.00	566834	5530400	-971	566834	5530400	-973
RM06-04e	1165.1	1167.1	2.00	566834	5530400	-973	566833	5530399	-975
RM06-04e	1167.1	1169.1	2.00	566833	5530399	-975	566833	5530399	-977
RM06-04e	1169.1	1171.1	2.00	566833	5530399	-977	566832	5530399	-979
RM06-04e	1171.1	1173.1	2.00	566832	5530399	-979	566832	5530399	-981
RM06-04e	1173.1	1175.1	2.00	566832	5530399	-981	566831	5530399	-983
RM06-04e	1175.1	1177.1	2.00	566831	5530399	-983	566831	5530399	-985
RM06-04e	1177.1	1179.1	2.00	566831	5530399	-985	566830	5530399	-987
RM06-04e	1179.1	1181.1	2.00	566830	5530399	-987	566829	5530398	-989
RM06-04e	1181.1	1183.1	2.00	566829	5530398	-989	566829	5530398	-991
RM06-04e	1183.1	1185.1	2.00	566829	5530398	-991	566828	5530398	-992
RM06-04e	1185.1	1187.1	2.00	566828	5530398	-992	566828	5530398	-994
RM06-04e	1187.1	1189.1	2.00	566828	5530398	-994	566827	5530398	-996
RM06-04e	1189.1	1191.1	2.00	566827	5530398	-996	566827	5530398	-998
RM06-04e	1191.1	1193.1	2.00	566827	5530398	-998	566826	5530397	-1000
RM06-04e	1193.1	1195.1	2.00	566826	5530397	-1000	566826	5530397	-1002
RM06-04e	1195.1	1197.1	2.00	566826	5530397	-1002	566825	5530397	-1004
RM06-04e	1197.1	1199.1	2.00	566825	5530397	-1004	566824	5530397	-1006
RM06-04e	1199.1	1201.1	2.00	566824	5530397	-1006	566824	5530397	-1008
RM06-04e	1201.1	1203.0	2.00	566824	5530397	-1008	566823	5530397	-1010
RM06-04e	1203.0	1205.0	2.00	566823	5530397	-1010	566823	5530397	-1012
RM06-04e	1205.0	1207.0	2.00	566823	5530397	-1012	566822	5530396	-1013
RM06-04e	1207.0	1209.0	2.00	566822	5530396	-1013	566821	5530396	-1015
RM06-04e	1209.0	1211.0	2.00	566821	5530396	-1015	566821	5530396	-1017
RM06-04e	1211.0	1213.0	2.00	566821	5530396	-1017	566820	5530396	-1019
RM06-04e	1213.0	1215.0	2.00	566820	5530396	-1019	566820	5530396	-1021
RM06-04e	1215.0	1217.0	2.00	566820	5530396	-1021	566819	5530396	-1023
RM06-04e	1217.0	1219.0	2.00	566819	5530396	-1023	566819	5530396	-1025
RM06-04e	1219.0	1221.0	2.00	566819	5530396	-1025	566818	5530395	-1027
RM06-04e	1221.0	1223.0	2.00	566818	5530395	-1027	566817	5530395	-1029
RM06-04e	1223.0	1225.0	2.00	566817	5530395	-1029	566817	5530395	-1031
RM06-04e	1225.0	1227.0	2.00	566817	5530395	-1031	566816	5530395	-1033
RM06-04e	1227.0	1229.0	2.00	566816	5530395	-1033	566816	5530395	-1034
RM06-04e	1229.0	1231.0	2.00	566816	5530395	-1034	566815	5530395	-1036
RM06-04e	1231.0	1233.0	2.00	566815	5530395	-1036	566814	5530395	-1038
RM06-04e	1233.0	1235.0	2.00	566814	5530395	-1038	566814	5530394	-1040
RM06-04e	1235.0	1237.0	2.00	566814	5530394	-1040	566813	5530394	-1042
RM06-04e	1237.0	1239.0	2.00	566813	5530394	-1042	566813	5530394	-1044
RM06-04e	1239.0	1241.0	2.00	566813	5530394	-1044	566812	5530394	-1046
RM06-04e	1241.0	1243.0	2.00	566812	5530394	-1046	566811	5530394	-1048
RM06-04e	1243.0	1245.0	2.00	566811	5530394	-1048	566811	5530394	-1050
RM06-04e	1245.0	1247.0	2.00	566811	5530394	-1050	566810	5530394	-1052
RM06-04e	1247.0	1249.0	2.00	566810	5530394	-1052	566810	5530393	-1053
RM06-04e	1249.0	1251.0	2.00	566810	5530393	-1053	566809	5530393	-1055
RM06-04e	1251.0	1253.0	2.00	566809	5530393	-1055	566808	5530393	-1057
RM06-04e	1253.0	1255.0	2.00	566808	5530393	-1057	566808	5530393	-1059
RM06-04e	1255.0	1257.0	2.00	566808	5530393	-1059	566807	5530393	-1061
RM06-04e	1257.0	1259.0	2.00	566807	5530393	-1061	566807	5530393	-1063
RM06-04e	1259.0	1261.0	2.00	566807	5530393	-1063	566806	5530393	-1065

RM06-04e	1261.0	1263.0	2.00	566806	5530393	-1065	566805	5530392	-1067
RM06-04e	1263.0	1265.0	2.00	566805	5530392	-1067	566805	5530392	-1069
<b>RM06-04I</b>									
RM06-04I	902.6	904.1	1.50	566947	5530426	-728	566947	5530426	-729
RM06-04I	904.1	905.6	1.50	566947	5530426	-729	566947	5530426	-731
RM06-04I	905.6	907.1	1.50	566947	5530426	-731	566947	5530426	-732
RM06-04I	907.1	908.6	1.50	566947	5530426	-732	566947	5530426	-734
RM06-04I	908.6	910.1	1.50	566947	5530426	-734	566946	5530426	-735
RM06-04I	910.1	911.6	1.50	566946	5530426	-735	566946	5530426	-737
RM06-04I	911.6	913.1	1.50	566946	5530426	-737	566946	5530426	-738
RM06-04I	913.1	914.6	1.50	566946	5530426	-738	566946	5530426	-740
RM06-04I	914.6	916.1	1.50	566946	5530426	-740	566946	5530426	-741
RM06-04I	916.1	917.6	1.50	566946	5530426	-741	566946	5530426	-743
RM06-04I	917.6	919.1	1.50	566946	5530426	-743	566946	5530426	-744
RM06-04I	919.1	920.6	1.50	566946	5530426	-744	566946	5530426	-746
RM06-04I	920.6	922.1	1.50	566946	5530426	-746	566946	5530426	-747
RM06-04I	922.1	923.6	1.50	566946	5530426	-747	566946	5530425	-749
RM06-04I	923.6	925.1	1.50	566946	5530425	-749	566946	5530425	-750
RM06-04I	925.1	926.6	1.50	566946	5530425	-750	566946	5530425	-752
<b>RM06-04m</b>									
RM06-04m	883.2	884.7	1.50	566923	5530427	-705	566923	5530427	-706
RM06-04m	884.7	886.2	1.50	566923	5530427	-706	566922	5530427	-708
RM06-04m	886.2	887.7	1.50	566922	5530427	-708	566922	5530428	-709
RM06-04m	887.7	889.2	1.50	566922	5530428	-709	566922	5530428	-711
RM06-04m	889.2	890.7	1.50	566922	5530428	-711	566922	5530428	-712
RM06-04m	890.7	892.2	1.50	566922	5530428	-712	566921	5530428	-714
RM06-04m	892.2	893.7	1.50	566921	5530428	-714	566921	5530428	-715
RM06-04m	893.7	895.2	1.50	566921	5530428	-715	566921	5530428	-717
RM06-04m	895.2	896.7	1.50	566921	5530428	-717	566920	5530428	-718
RM06-04m	896.7	898.2	1.50	566920	5530428	-718	566920	5530428	-720
RM06-04m	898.2	899.7	1.50	566920	5530428	-720	566920	5530429	-721
RM06-04m	899.7	901.2	1.50	566920	5530429	-721	566920	5530429	-723
RM06-04m	901.2	902.7	1.50	566920	5530429	-723	566919	5530429	-724
RM06-04m	902.7	904.2	1.50	566919	5530429	-724	566919	5530429	-725
RM06-04m	904.2	905.7	1.50	566919	5530429	-725	566919	5530429	-727
RM06-04m	905.7	907.2	1.50	566919	5530429	-727	566918	5530429	-728
RM06-04m	907.2	908.7	1.50	566918	5530429	-728	566918	5530429	-730
RM06-04m	908.7	910.2	1.50	566918	5530429	-730	566918	5530429	-731
RM06-04m	910.2	911.7	1.50	566918	5530429	-731	566918	5530429	-733
RM06-04m	911.7	913.2	1.50	566918	5530429	-733	566917	5530429	-734
RM06-04m	913.2	914.7	1.50	566917	5530429	-734	566917	5530430	-736
RM06-04m	914.7	916.2	1.50	566917	5530430	-736	566917	5530430	-737
RM06-04m	916.2	917.7	1.50	566917	5530430	-737	566917	5530430	-739
RM06-04m	917.7	919.2	1.50	566917	5530430	-739	566916	5530430	-740
RM06-04m	919.2	920.7	1.50	566916	5530430	-740	566916	5530430	-742
RM06-04m	920.7	922.2	1.50	566916	5530430	-742	566916	5530430	-743
RM06-04m	922.2	923.7	1.50	566916	5530430	-743	566915	5530430	-745
RM06-04m	923.7	925.2	1.50	566915	5530430	-745	566915	5530430	-746
RM06-04m	925.2	926.7	1.50	566915	5530430	-746	566915	5530430	-748
RM06-04m	926.7	928.2	1.50	566915	5530430	-748	566914	5530431	-749
RM06-04m	928.2	929.7	1.50	566914	5530431	-749	566914	5530431	-750
RM06-04m	929.7	931.2	1.50	566914	5530431	-750	566914	5530431	-752
RM06-04m	931.2	932.7	1.50	566914	5530431	-752	566914	5530431	-753
RM06-04m	932.7	934.2	1.50	566914	5530431	-753	566913	5530431	-755
RM06-04m	934.2	935.7	1.50	566913	5530431	-755	566913	5530431	-756
RM06-04m	935.7	937.1	1.50	566913	5530431	-756	566913	5530431	-758
RM06-04m	937.1	938.6	1.50	566913	5530431	-758	566912	5530431	-759
RM06-04m	938.6	940.1	1.50	566912	5530431	-759	566912	5530431	-761
RM06-04m	940.1	941.6	1.50	566912	5530431	-761	566912	5530431	-762
RM06-04m	941.6	943.1	1.50	566912	5530431	-762	566911	5530431	-764
RM06-04m	943.1	944.6	1.50	566911	5530431	-764	566911	5530431	-765
RM06-04m	944.6	946.1	1.50	566911	5530431	-765	566911	5530431	-767
RM06-04m	946.1	947.6	1.50	566911	5530431	-767	566910	5530432	-768
RM06-04m	947.6	949.1	1.50	566910	5530432	-768	566910	5530432	-769
RM06-04m	949.1	950.6	1.50	566910	5530432	-769	566910	5530432	-771
RM06-04m	950.6	952.1	1.50	566910	5530432	-771	566909	5530432	-772
RM06-04m	952.1	953.6	1.50	566909	5530432	-772	566909	5530432	-774
RM06-04m	953.6	955.1	1.50	566909	5530432	-774	566908	5530432	-775

RM06-04m	955.1	956.6	1.50	566908	5530432	-775	566908	5530432	-777
RM06-04m	956.6	958.1	1.50	566908	5530432	-777	566908	5530432	-778
RM06-04m	958.1	959.6	1.50	566908	5530432	-778	566907	5530432	-780
RM06-04m	959.6	961.1	1.50	566907	5530432	-780	566907	5530432	-781
RM06-04m	961.1	962.6	1.50	566907	5530432	-781	566907	5530432	-783
RM06-04m	962.6	964.1	1.50	566907	5530432	-783	566906	5530432	-784
RM06-04m	964.1	965.6	1.50	566906	5530432	-784	566906	5530432	-785
RM06-04m	965.6	967.1	1.50	566906	5530432	-785	566906	5530432	-787
RM06-04m	967.1	968.6	1.50	566906	5530432	-787	566905	5530432	-788
RM06-04m	968.6	970.1	1.50	566905	5530432	-788	566905	5530432	-790
RM06-04m	970.1	971.6	1.50	566905	5530432	-790	566905	5530432	-791
RM06-04m	971.6	973.1	1.50	566905	5530432	-791	566904	5530433	-793
RM06-04m	973.1	974.6	1.50	566904	5530433	-793	566904	5530433	-794
RM06-04m	974.6	976.1	1.50	566904	5530433	-794	566903	5530433	-796
RM06-04m	976.1	977.6	1.50	566903	5530433	-796	566903	5530433	-797
RM06-04m	977.6	979.1	1.50	566903	5530433	-797	566903	5530433	-799
RM06-04m	979.1	980.6	1.50	566903	5530433	-799	566902	5530433	-800
RM06-04m	980.6	982.1	1.50	566902	5530433	-800	566902	5530433	-801
RM06-04m	982.1	983.6	1.50	566902	5530433	-801	566902	5530433	-803
RM06-04m	983.6	985.1	1.50	566902	5530433	-803	566901	5530433	-804
RM06-04m	985.1	986.6	1.50	566901	5530433	-804	566901	5530433	-806
RM06-04m	986.6	988.1	1.50	566901	5530433	-806	566900	5530433	-807
RM06-04m	988.1	989.6	1.50	566900	5530433	-807	566900	5530433	-809
RM06-04m	989.6	991.1	1.50	566900	5530433	-809	566900	5530433	-810
RM06-04m	991.1	992.6	1.50	566900	5530433	-810	566899	5530433	-812
RM06-04m	992.6	994.1	1.50	566899	5530433	-812	566899	5530433	-813
RM06-04m	994.1	995.6	1.50	566899	5530433	-813	566899	5530433	-814
RM06-04m	995.6	997.1	1.50	566899	5530433	-814	566898	5530433	-816
RM06-04m	997.1	998.6	1.50	566898	5530433	-816	566898	5530433	-817
RM06-04m	998.6	1000.1	1.50	566898	5530433	-817	566897	5530433	-819
RM06-04m	1000.1	1001.6	1.50	566897	5530433	-819	566897	5530433	-820
RM06-04m	1001.6	1003.1	1.50	566897	5530433	-820	566897	5530434	-822
RM06-04m	1003.1	1004.6	1.50	566897	5530434	-822	566896	5530434	-823
RM06-04m	1004.6	1006.1	1.50	566896	5530434	-823	566896	5530434	-825
RM06-04m	1006.1	1007.6	1.50	566896	5530434	-825	566896	5530434	-826
RM06-04m	1007.6	1009.1	1.50	566896	5530434	-826	566895	5530434	-828
RM06-04m	1009.1	1010.6	1.50	566895	5530434	-828	566895	5530434	-829
RM06-04m	1010.6	1012.1	1.50	566895	5530434	-829	566894	5530434	-830
RM06-04m	1012.1	1013.6	1.50	566894	5530434	-830	566894	5530434	-832
RM06-04m	1013.6	1015.1	1.50	566894	5530434	-832	566894	5530434	-833
RM06-04m	1015.1	1016.6	1.50	566894	5530434	-833	566893	5530434	-835
RM06-04m	1016.6	1018.1	1.50	566893	5530434	-835	566893	5530434	-836
RM06-04m	1018.1	1019.6	1.50	566893	5530434	-836	566893	5530434	-838
RM06-04m	1019.6	1021.1	1.50	566893	5530434	-838	566892	5530434	-839
RM06-04m	1021.1	1022.6	1.50	566892	5530434	-839	566892	5530434	-841
RM06-04m	1022.6	1024.1	1.50	566892	5530434	-841	566891	5530434	-842
RM06-04m	1024.1	1025.6	1.50	566891	5530434	-842	566891	5530434	-843
RM06-04m	1025.6	1027.1	1.50	566891	5530434	-843	566891	5530434	-845
RM06-04m	1027.1	1028.6	1.50	566891	5530434	-845	566890	5530434	-846
RM06-04m	1028.6	1030.1	1.50	566890	5530434	-846	566890	5530434	-848
RM06-04m	1030.1	1031.6	1.50	566890	5530434	-848	566889	5530434	-849
RM06-04m	1031.6	1033.1	1.50	566889	5530434	-849	566889	5530434	-851
RM06-04m	1033.1	1034.6	1.50	566889	5530434	-851	566889	5530434	-852
RM06-04m	1034.6	1036.1	1.50	566889	5530434	-852	566888	5530435	-854
RM06-04m	1036.1	1037.6	1.50	566888	5530435	-854	566888	5530435	-855
RM06-04m	1037.6	1039.1	1.50	566888	5530435	-855	566887	5530435	-857
RM06-04m	1039.1	1040.6	1.50	566887	5530435	-857	566887	5530435	-858
RM06-04m	1040.6	1042.1	1.50	566887	5530435	-858	566887	5530435	-859
RM06-04m	1042.1	1043.6	1.50	566887	5530435	-859	566886	5530435	-861
RM06-04m	1043.6	1045.1	1.50	566886	5530435	-861	566886	5530435	-862
RM06-04m	1045.1	1046.6	1.50	566886	5530435	-862	566885	5530435	-864
RM06-04m	1046.6	1048.1	1.50	566885	5530435	-864	566885	5530435	-865
RM06-04m	1048.1	1049.6	1.50	566885	5530435	-865	566885	5530435	-867
RM06-04m	1049.6	1051.1	1.50	566885	5530435	-867	566884	5530435	-868
RM06-04m	1051.1	1052.6	1.50	566884	5530435	-868	566884	5530435	-869
RM06-04m	1052.6	1054.1	1.50	566884	5530435	-869	566883	5530435	-871
RM06-04m	1054.1	1055.6	1.50	566883	5530435	-871	566883	5530435	-872
RM06-04m	1055.6	1057.1	1.50	566883	5530435	-872	566883	5530435	-874
RM06-04m	1057.1	1058.6	1.50	566883	5530435	-874	566882	5530435	-875
RM06-04m	1058.6	1060.1	1.50	566882	5530435	-875	566882	5530435	-877

RM06-04m	1060.1	1061.6	1.50	566882	5530435	-877	566881	5530435	-878
RM06-04m	1061.6	1063.1	1.50	566881	5530435	-878	566881	5530435	-880
RM06-04m	1063.1	1064.6	1.50	566881	5530435	-880	566880	5530435	-881
RM06-04m	1064.6	1066.1	1.50	566880	5530435	-881	566880	5530435	-882
RM06-04m	1066.1	1067.6	1.50	566880	5530435	-882	566880	5530435	-884
RM06-04m	1067.6	1069.1	1.50	566880	5530435	-884	566879	5530435	-885
RM06-04m	1069.1	1070.6	1.50	566879	5530435	-885	566879	5530435	-887
RM06-04m	1070.6	1072.1	1.50	566879	5530435	-887	566878	5530435	-888
RM06-04m	1072.1	1073.6	1.50	566878	5530435	-888	566878	5530435	-890
RM06-04m	1073.6	1075.1	1.50	566878	5530435	-890	566878	5530435	-891
RM06-04m	1075.1	1076.6	1.50	566878	5530435	-891	566877	5530435	-893
RM06-04m	1076.6	1078.1	1.50	566877	5530435	-893	566877	5530436	-894
RM06-04m	1078.1	1079.6	1.50	566877	5530436	-894	566876	5530436	-895
RM06-04m	1079.6	1081.1	1.50	566876	5530436	-895	566876	5530436	-897
RM06-04m	1081.1	1082.6	1.50	566876	5530436	-897	566876	5530436	-898
RM06-04m	1082.6	1084.1	1.50	566876	5530436	-898	566875	5530436	-900
RM06-04m	1084.1	1085.6	1.50	566875	5530436	-900	566875	5530436	-901
RM06-04m	1085.6	1087.1	1.50	566875	5530436	-901	566874	5530436	-903
RM06-04m	1087.1	1088.6	1.50	566874	5530436	-903	566874	5530436	-904
RM06-04m	1088.6	1090.1	1.50	566874	5530436	-904	566873	5530436	-905
RM06-04m	1090.1	1091.6	1.50	566873	5530436	-905	566873	5530436	-907
RM06-04m	1091.6	1093.1	1.50	566873	5530436	-907	566873	5530436	-908
RM06-04m	1093.1	1094.6	1.50	566873	5530436	-908	566872	5530436	-910
RM06-04m	1094.6	1096.1	1.50	566872	5530436	-910	566872	5530436	-911
RM06-04m	1096.1	1097.6	1.50	566872	5530436	-911	566871	5530436	-913
RM06-04m	1097.6	1099.1	1.50	566871	5530436	-913	566871	5530436	-914
RM06-04m	1099.1	1100.6	1.50	566871	5530436	-914	566870	5530436	-916
RM06-04m	1100.6	1102.1	1.50	566870	5530436	-916	566870	5530436	-917
RM06-04m	1102.1	1103.6	1.50	566870	5530436	-917	566870	5530436	-918
RM06-04m	1103.6	1105.1	1.50	566870	5530436	-918	566869	5530436	-920
RM06-04m	1105.1	1106.6	1.50	566869	5530436	-920	566869	5530436	-921
RM06-04m	1106.6	1108.1	1.50	566869	5530436	-921	566868	5530436	-923
RM06-04m	1108.1	1109.6	1.50	566868	5530436	-923	566868	5530436	-924
RM06-04m	1109.6	1111.1	1.50	566868	5530436	-924	566868	5530436	-926
RM06-04m	1111.1	1112.6	1.50	566868	5530436	-926	566867	5530436	-927
RM06-04m	1112.6	1114.1	1.50	566867	5530436	-927	566867	5530436	-928
RM06-04m	1114.1	1115.6	1.50	566867	5530436	-928	566866	5530436	-930
RM06-04m	1115.6	1117.1	1.50	566866	5530436	-930	566866	5530436	-931
RM06-04m	1117.1	1118.6	1.50	566866	5530436	-931	566865	5530436	-933
RM06-04m	1118.6	1120.1	1.50	566865	5530436	-933	566865	5530437	-934
RM06-04m	1120.1	1121.6	1.50	566865	5530437	-934	566864	5530437	-936
RM06-04m	1121.6	1123.1	1.50	566864	5530437	-936	566864	5530437	-937
RM06-04m	1123.1	1124.6	1.50	566864	5530437	-937	566864	5530437	-939
RM06-04m	1124.6	1126.1	1.50	566864	5530437	-939	566863	5530437	-940
RM06-04m	1126.1	1127.6	1.50	566863	5530437	-940	566863	5530437	-941
RM06-04m	1127.6	1129.1	1.50	566863	5530437	-941	566862	5530437	-943
RM06-04m	1129.1	1130.6	1.50	566862	5530437	-943	566862	5530437	-944
RM06-04m	1130.6	1132.1	1.50	566862	5530437	-944	566861	5530437	-946
RM06-04m	1132.1	1133.6	1.50	566861	5530437	-946	566861	5530437	-947
RM06-04m	1133.6	1135.1	1.50	566861	5530437	-947	566861	5530437	-949
RM06-04m	1135.1	1136.6	1.50	566861	5530437	-949	566860	5530437	-950
RM06-04m	1136.6	1138.1	1.50	566860	5530437	-950	566860	5530437	-951
RM06-04m	1138.1	1139.6	1.50	566860	5530437	-951	566859	5530437	-953
RM06-04m	1139.6	1141.1	1.50	566859	5530437	-953	566859	5530437	-954
RM06-04m	1141.1	1142.6	1.50	566859	5530437	-954	566858	5530437	-956
RM06-04m	1142.6	1144.1	1.50	566858	5530437	-956	566858	5530437	-957
RM06-04m	1144.1	1145.6	1.50	566858	5530437	-957	566857	5530437	-959
RM06-04m	1145.6	1147.1	1.50	566857	5530437	-959	566857	5530437	-960
RM06-04m	1147.1	1148.6	1.50	566857	5530437	-960	566857	5530437	-961
RM06-04m	1148.6	1150.1	1.50	566857	5530437	-961	566856	5530437	-963
RM06-04m	1150.1	1151.6	1.50	566856	5530437	-963	566856	5530437	-964
RM06-04m	1151.6	1153.1	1.50	566856	5530437	-964	566855	5530437	-966
RM06-04m	1153.1	1154.6	1.50	566855	5530437	-966	566855	5530437	-967
RM06-04m	1154.6	1156.1	1.50	566855	5530437	-967	566854	5530437	-969
RM06-04m	1156.1	1157.6	1.50	566854	5530437	-969	566854	5530437	-970
RM06-04m	1157.6	1159.1	1.50	566854	5530437	-970	566853	5530437	-971
RM06-04m	1159.1	1160.6	1.50	566853	5530437	-971	566853	5530437	-973
RM06-04m	1160.6	1162.1	1.50	566853	5530437	-973	566853	5530437	-974
RM06-04m	1162.1	1163.6	1.50	566853	5530437	-974	566852	5530437	-976
RM06-04m	1163.6	1165.1	1.50	566852	5530437	-976	566852	5530438	-977

RM06-04m	1165.1	1166.6	1.50	566852	5530438	-977	566851	5530438	-979
RM06-04m	1166.6	1168.1	1.50	566851	5530438	-979	566851	5530438	-980
RM06-04m	1168.1	1169.6	1.50	566851	5530438	-980	566850	5530438	-982
RM06-04m	1169.6	1171.1	1.50	566850	5530438	-982	566850	5530438	-983
RM06-04m	1171.1	1172.6	1.50	566850	5530438	-983	566849	5530438	-984
RM06-04m	1172.6	1174.1	1.50	566849	5530438	-984	566849	5530438	-986
RM06-04m	1174.1	1175.6	1.50	566849	5530438	-986	566849	5530438	-987
RM06-04m	1175.6	1177.1	1.50	566849	5530438	-987	566848	5530438	-989
RM06-04m	1177.1	1178.6	1.50	566848	5530438	-989	566848	5530438	-990
RM06-04m	1178.6	1180.1	1.50	566848	5530438	-990	566847	5530438	-992
RM06-04m	1180.1	1181.6	1.50	566847	5530438	-992	566847	5530438	-993
RM06-04m	1181.6	1183.1	1.50	566847	5530438	-993	566846	5530438	-994
RM06-04m	1183.1	1184.6	1.50	566846	5530438	-994	566846	5530438	-996
RM06-04m	1184.6	1186.1	1.50	566846	5530438	-996	566845	5530438	-997
RM06-04m	1186.1	1187.6	1.50	566845	5530438	-997	566845	5530438	-999
RM06-04m	1187.6	1189.1	1.50	566845	5530438	-999	566844	5530438	-1000
RM06-04m	1189.1	1190.6	1.50	566844	5530438	-1000	566844	5530438	-1002
RM06-04m	1190.6	1192.1	1.50	566844	5530438	-1002	566844	5530438	-1003
RM06-04m	1192.1	1193.6	1.50	566844	5530438	-1003	566843	5530438	-1004
RM06-04m	1193.6	1195.1	1.50	566843	5530438	-1004	566843	5530438	-1006
RM06-04m	1195.1	1196.6	1.50	566843	5530438	-1006	566842	5530438	-1007
RM06-04m	1196.6	1198.1	1.50	566842	5530438	-1007	566842	5530438	-1009
RM06-04m	1198.1	1199.6	1.50	566842	5530438	-1009	566841	5530438	-1010
RM06-04m	1199.6	1201.1	1.50	566841	5530438	-1010	566841	5530438	-1012
RM06-04m	1201.1	1202.6	1.50	566841	5530438	-1012	566840	5530438	-1013
RM06-04m	1202.6	1204.0	1.50	566840	5530438	-1013	566840	5530438	-1014
RM06-04m	1204.0	1205.5	1.50	566840	5530438	-1014	566839	5530438	-1016
RM06-04m	1205.5	1207.0	1.50	566839	5530438	-1016	566839	5530438	-1017
RM06-04m	1207.0	1208.5	1.50	566839	5530438	-1017	566838	5530438	-1019
RM06-04m	1208.5	1210.0	1.50	566838	5530438	-1019	566838	5530438	-1020
RM06-04m	1210.0	1211.5	1.50	566838	5530438	-1020	566838	5530438	-1021
RM06-04m	1211.5	1213.0	1.50	566838	5530438	-1021	566837	5530438	-1023
RM06-04m	1213.0	1214.5	1.50	566837	5530438	-1023	566837	5530438	-1024
RM06-04m	1214.5	1216.0	1.50	566837	5530438	-1024	566836	5530438	-1026
RM06-04m	1216.0	1217.5	1.50	566836	5530438	-1026	566836	5530438	-1027
RM06-04m	1217.5	1219.0	1.50	566836	5530438	-1027	566835	5530438	-1029
RM06-04m	1219.0	1220.5	1.50	566835	5530438	-1029	566835	5530438	-1030
RM06-04m	1220.5	1222.0	1.50	566835	5530438	-1030	566834	5530438	-1031
RM06-04m	1222.0	1223.5	1.50	566834	5530438	-1031	566834	5530438	-1033
RM06-04m	1223.5	1225.0	1.50	566834	5530438	-1033	566833	5530438	-1034
RM06-04m	1225.0	1226.5	1.50	566833	5530438	-1034	566833	5530438	-1036
RM06-04m	1226.5	1228.0	1.50	566833	5530438	-1036	566832	5530438	-1037
RM06-04m	1228.0	1229.5	1.50	566832	5530438	-1037	566832	5530438	-1038
RM06-04m	1229.5	1231.0	1.50	566832	5530438	-1038	566831	5530438	-1040
RM06-04m	1231.0	1232.5	1.50	566831	5530438	-1040	566831	5530438	-1041
RM06-04m	1232.5	1234.0	1.50	566831	5530438	-1041	566830	5530438	-1043
RM06-04m	1234.0	1235.5	1.50	566830	5530438	-1043	566830	5530438	-1044
RM06-04m	1235.5	1237.0	1.50	566830	5530438	-1044	566829	5530438	-1046
RM06-04m	1237.0	1238.5	1.50	566829	5530438	-1046	566829	5530438	-1047
RM06-04m	1238.5	1240.0	1.50	566829	5530438	-1047	566828	5530438	-1048
RM06-04m	1240.0	1241.5	1.50	566828	5530438	-1048	566828	5530438	-1050
RM06-04m	1241.5	1243.0	1.50	566828	5530438	-1050	566827	5530438	-1051
RM06-04m	1243.0	1244.5	1.50	566827	5530438	-1051	566827	5530438	-1053
RM06-04m	1244.5	1246.0	1.50	566827	5530438	-1053	566826	5530438	-1054
RM06-04m	1246.0	1247.5	1.50	566826	5530438	-1054	566826	5530438	-1055
RM06-04m	1247.5	1249.0	1.50	566826	5530438	-1055	566825	5530438	-1057
RM06-04m	1249.0	1250.5	1.50	566825	5530438	-1057	566825	5530438	-1058
RM06-04m	1250.5	1252.0	1.50	566825	5530438	-1058	566824	5530438	-1060
RM06-04m	1252.0	1253.5	1.50	566824	5530438	-1060	566824	5530438	-1061
RM06-04m	1253.5	1255.0	1.50	566824	5530438	-1061	566823	5530438	-1063
RM06-04m	1255.0	1256.5	1.50	566823	5530438	-1063	566823	5530438	-1064
RM06-04m	1256.5	1258.0	1.50	566823	5530438	-1064	566822	5530438	-1065
RM06-04m	1258.0	1259.5	1.50	566822	5530438	-1065	566822	5530438	-1067
RM06-04m	1259.5	1261.0	1.50	566822	5530438	-1067	566821	5530438	-1068
RM06-04m	1261.0	1262.5	1.50	566821	5530438	-1068	566821	5530438	-1070
RM06-04m	1262.5	1264.0	1.50	566821	5530438	-1070	566820	5530438	-1071
RM06-04m	1264.0	1265.5	1.50	566820	5530438	-1071	566820	5530438	-1072
RM06-04m	1265.5	1267.0	1.50	566820	5530438	-1072	566819	5530438	-1074
RM06-04m	1267.0	1268.5	1.50	566819	5530438	-1074	566819	5530438	-1075
RM06-04m	1268.5	1270.0	1.50	566819	5530438	-1075	566818	5530438	-1077

RM06-04m	1270.0	1271.5	1.50	566818	5530438	-1077	566818	5530438	-1078
RM06-04m	1271.5	1273.0	1.50	566818	5530438	-1078	566817	5530438	-1079
RM06-04m	1273.0	1274.5	1.50	566817	5530438	-1079	566817	5530438	-1081
RM06-04m	1274.5	1276.0	1.50	566817	5530438	-1081	566816	5530438	-1082
RM06-04m	1276.0	1277.5	1.50	566816	5530438	-1082	566816	5530438	-1084
RM06-04m	1277.5	1279.0	1.50	566816	5530438	-1084	566815	5530438	-1085
RM06-04m	1279.0	1280.5	1.50	566815	5530438	-1085	566815	5530438	-1087
RM06-04m	1280.5	1282.0	1.50	566815	5530438	-1087	566814	5530438	-1088
RM06-04m	1282.0	1283.5	1.50	566814	5530438	-1088	566814	5530438	-1089
RM06-04m	1283.5	1285.0	1.50	566814	5530438	-1089	566813	5530438	-1091
RM06-04m	1285.0	1286.5	1.50	566813	5530438	-1091	566813	5530438	-1092
RM06-04m	1286.5	1288.0	1.50	566813	5530438	-1092	566812	5530438	-1094
RM06-04m	1288.0	1289.5	1.50	566812	5530438	-1094	566811	5530438	-1095
RM06-04m	1289.5	1291.0	1.50	566811	5530438	-1095	566811	5530438	-1096
RM06-04m	1291.0	1292.5	1.50	566811	5530438	-1096	566810	5530438	-1098
RM06-04m	1292.5	1294.0	1.50	566810	5530438	-1098	566810	5530438	-1099
RM06-04m	1294.0	1295.5	1.50	566810	5530438	-1099	566809	5530438	-1101
RM06-04m	1295.5	1297.0	1.50	566809	5530438	-1101	566809	5530438	-1102
RM06-04m	1297.0	1298.5	1.50	566809	5530438	-1102	566808	5530438	-1103
RM06-04m	1298.5	1300.0	1.50	566808	5530438	-1103	566808	5530438	-1105
RM06-04m	1300.0	1301.5	1.50	566808	5530438	-1105	566807	5530438	-1106
RM06-04m	1301.5	1303.0	1.50	566807	5530438	-1106	566807	5530438	-1108
RM06-04m	1303.0	1304.5	1.50	566807	5530438	-1108	566806	5530438	-1109
RM06-04m	1304.5	1306.0	1.50	566806	5530438	-1109	566806	5530438	-1110
RM06-04m	1306.0	1307.5	1.50	566806	5530438	-1110	566805	5530437	-1112
RM06-04m	1307.5	1309.0	1.50	566805	5530437	-1112	566805	5530437	-1113
RM06-04m	1309.0	1310.5	1.50	566805	5530437	-1113	566804	5530437	-1115
RM06-04m	1310.5	1312.0	1.50	566804	5530437	-1115	566803	5530437	-1116
RM06-04m	1312.0	1313.5	1.50	566803	5530437	-1116	566803	5530437	-1117
RM06-04m	1313.5	1315.0	1.50	566803	5530437	-1117	566802	5530437	-1119
RM06-04m	1315.0	1316.5	1.50	566802	5530437	-1119	566802	5530437	-1120
RM06-04m	1316.5	1318.0	1.50	566802	5530437	-1120	566801	5530437	-1122
RM06-04m	1318.0	1319.5	1.50	566801	5530437	-1122	566801	5530437	-1123
RM06-04m	1319.5	1321.0	1.50	566801	5530437	-1123	566800	5530437	-1124
RM06-04m	1321.0	1322.5	1.50	566800	5530437	-1124	566800	5530437	-1126
RM06-04m	1322.5	1324.0	1.50	566800	5530437	-1126	566799	5530437	-1127
RM06-04m	1324.0	1325.5	1.50	566799	5530437	-1127	566798	5530437	-1129
RM06-04m	1325.5	1327.0	1.50	566798	5530437	-1129	566798	5530437	-1130
RM06-04m	1327.0	1328.5	1.50	566798	5530437	-1130	566797	5530437	-1131
RM06-04m	1328.5	1330.0	1.50	566797	5530437	-1131	566797	5530437	-1133
RM06-04m	1330.0	1331.5	1.50	566797	5530437	-1133	566796	5530437	-1134
RM06-04m	1331.5	1333.0	1.50	566796	5530437	-1134	566796	5530437	-1135
RM06-04m	1333.0	1334.5	1.50	566796	5530437	-1135	566795	5530437	-1137
RM06-04m	1334.5	1336.0	1.50	566795	5530437	-1137	566795	5530437	-1138
RM06-04m	1336.0	1337.5	1.50	566795	5530437	-1138	566794	5530437	-1140

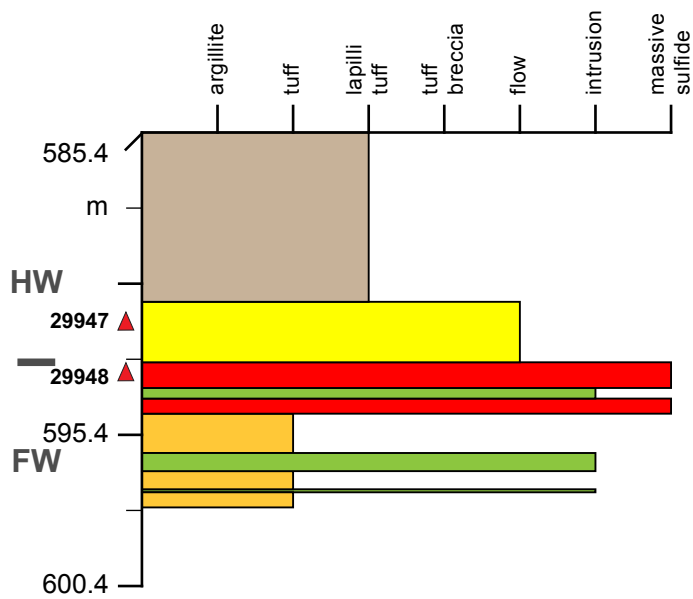
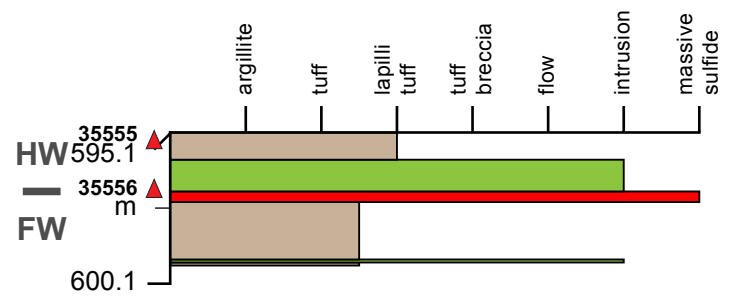
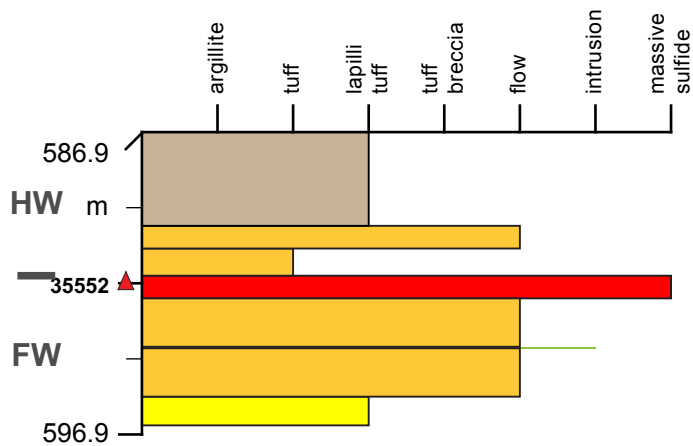
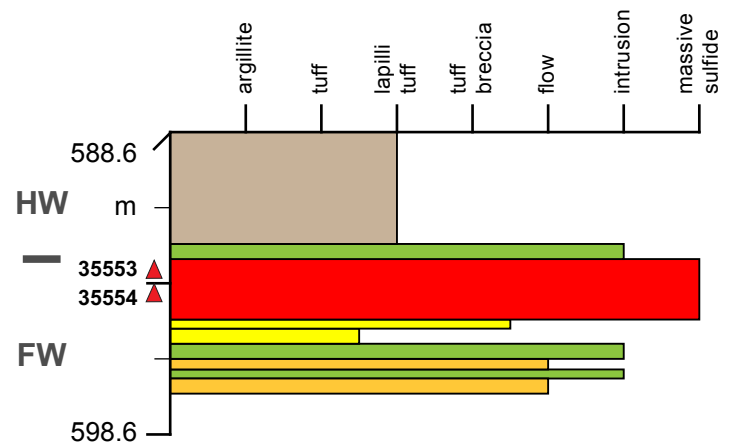
## ELECTRONIC APPENDIX 2

### STRATIGRAPHIC SECTION OF LOGGED DRILLHOLES



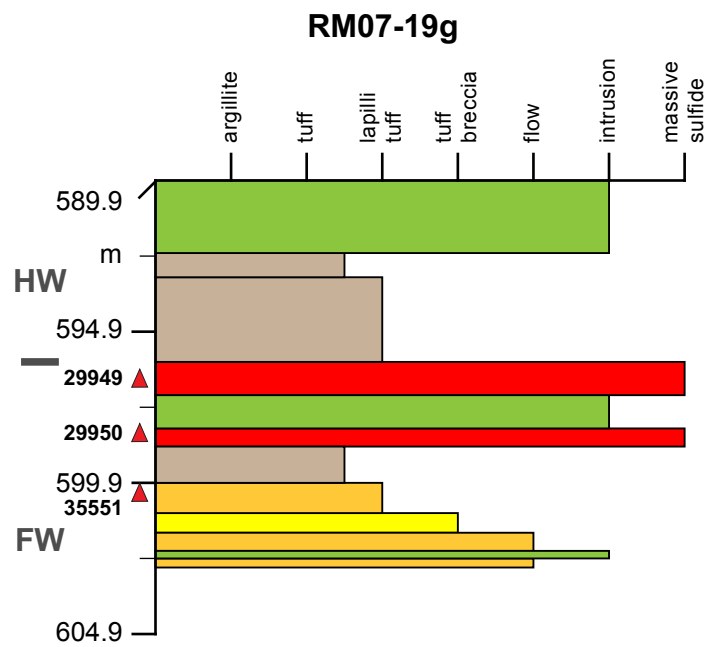
**Figure eA2.** Stratigraphic sections of logged drillholes from the orebodies of the Ming deposit; coordinates for each drill holes are found in Table eA1; mineralogy of samples are found in Table eA3

**1807 Zone: RM07-19**

**RM07-19****RM07-19a****RM07-19c****RM07-19e**

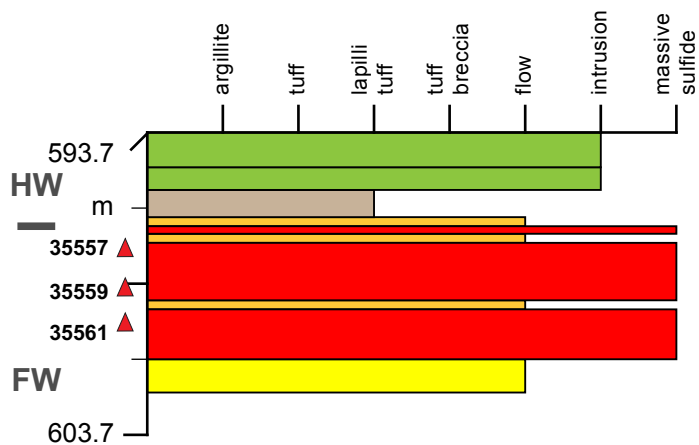


**1807 Zone: RM07-19**

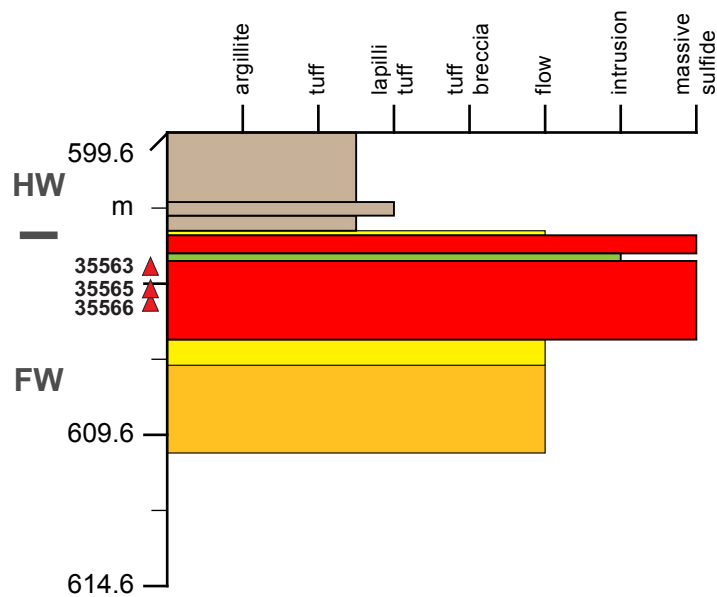


**1807 Zone: RM07-18**

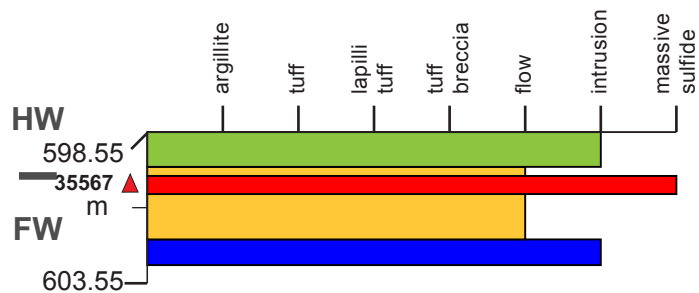
**RM07-18a**



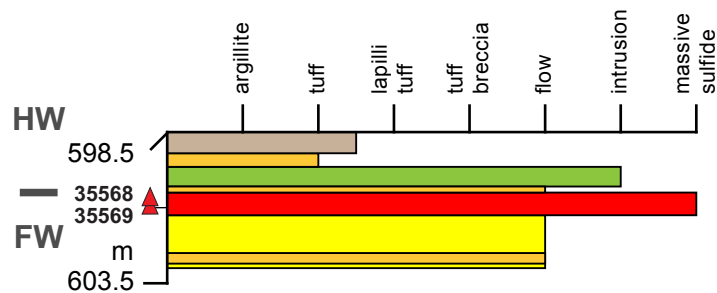
**RM07-18b**



**RM07-18d**

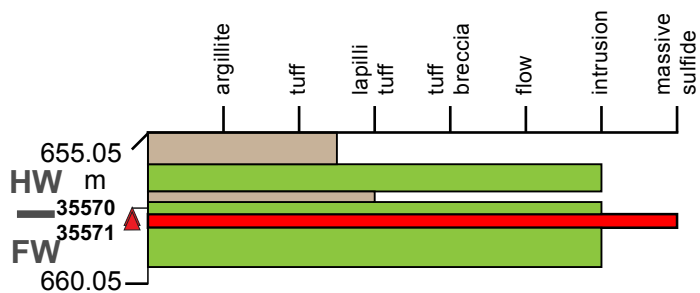


**RM07-18e**

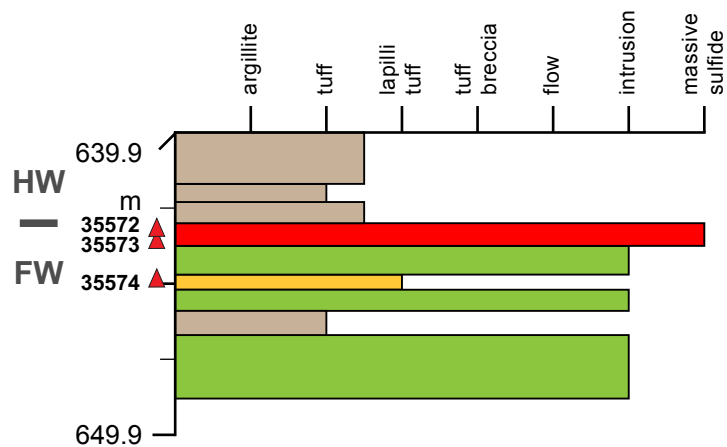


**1807 Zone: RM07-20**

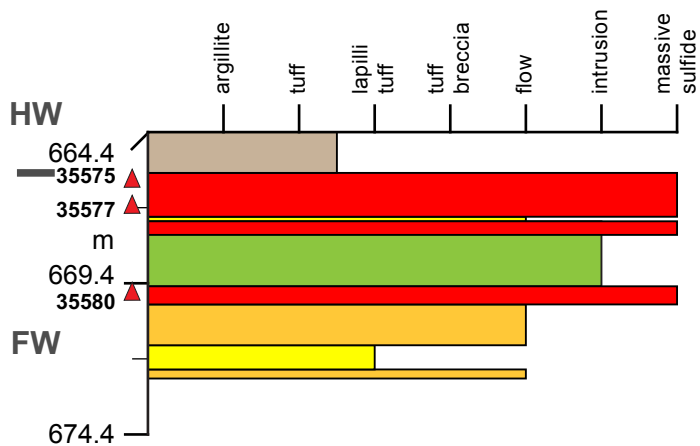
**RM07-20**



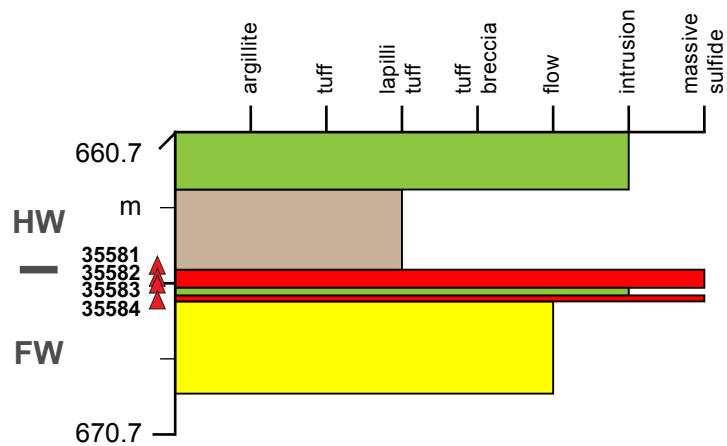
**RM07-20a**



**RM07-20b**

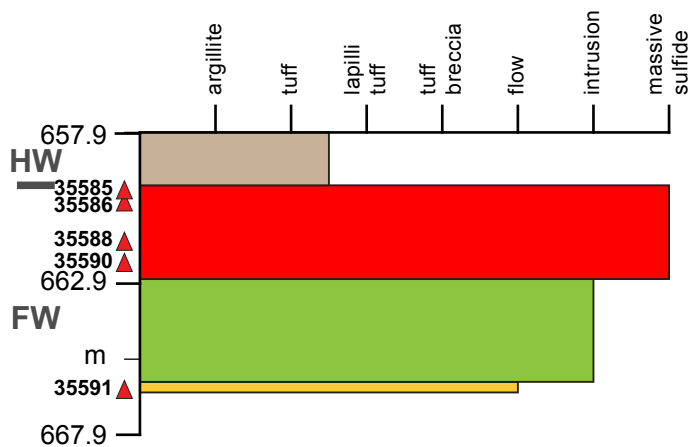


**RM07-20c**

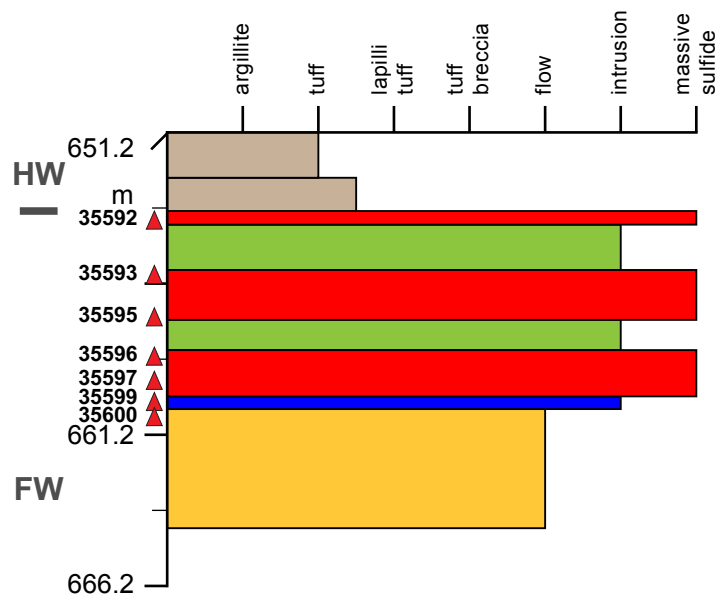


## 1807 Zone: RM07-20

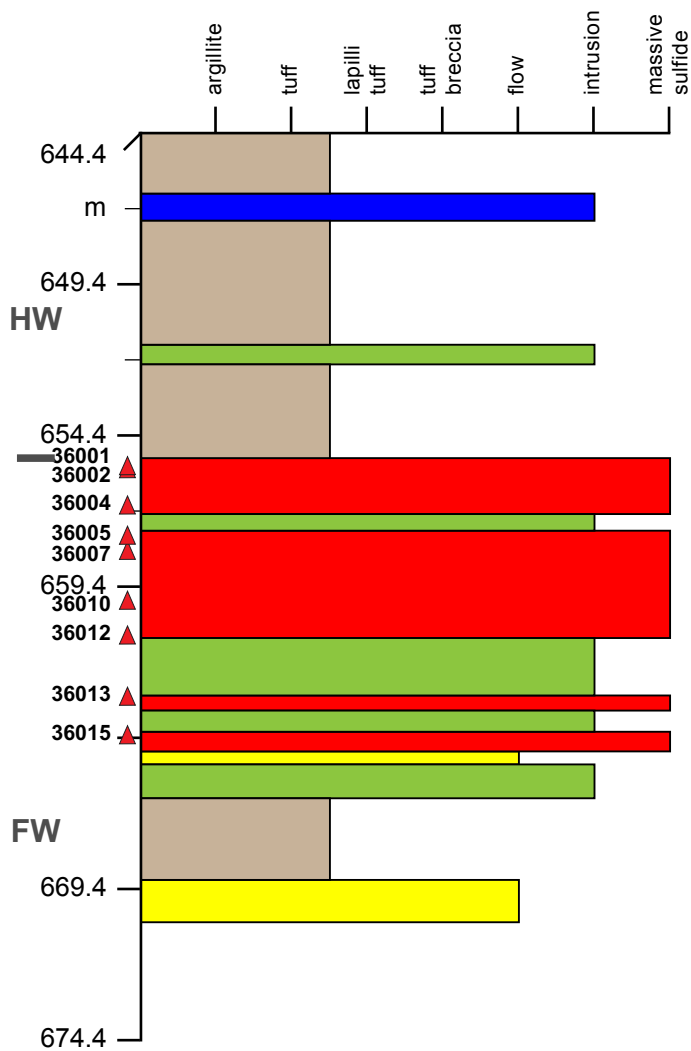
RM07-20e



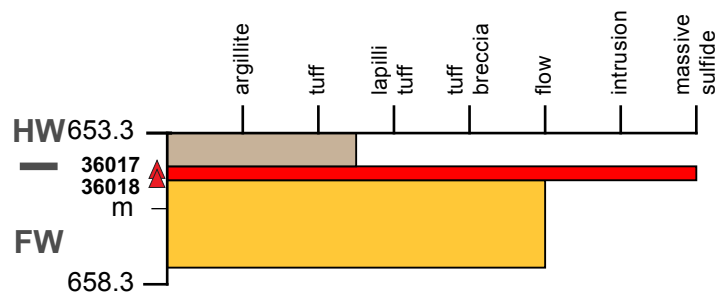
RM07-20g



RM07-20h

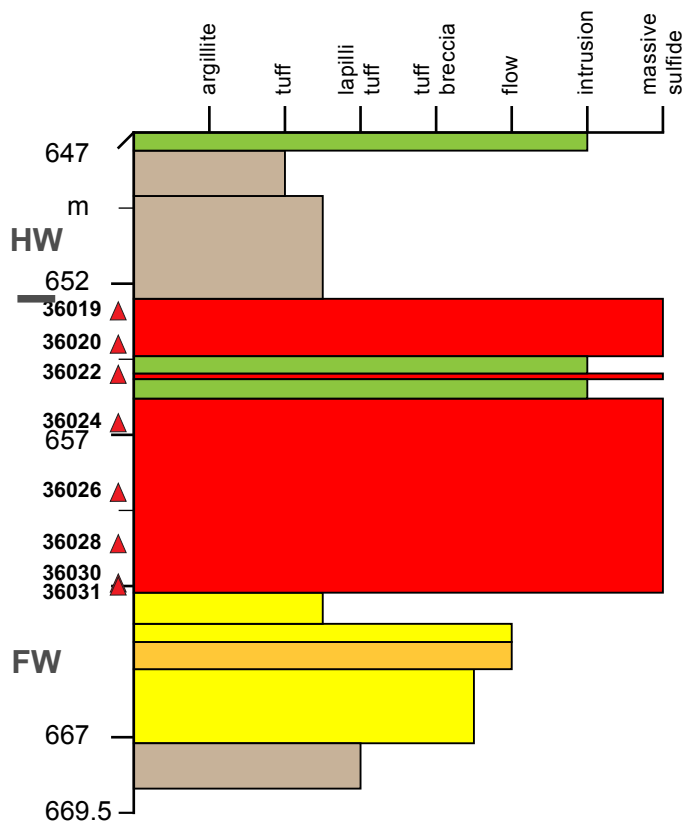


RM07-20i

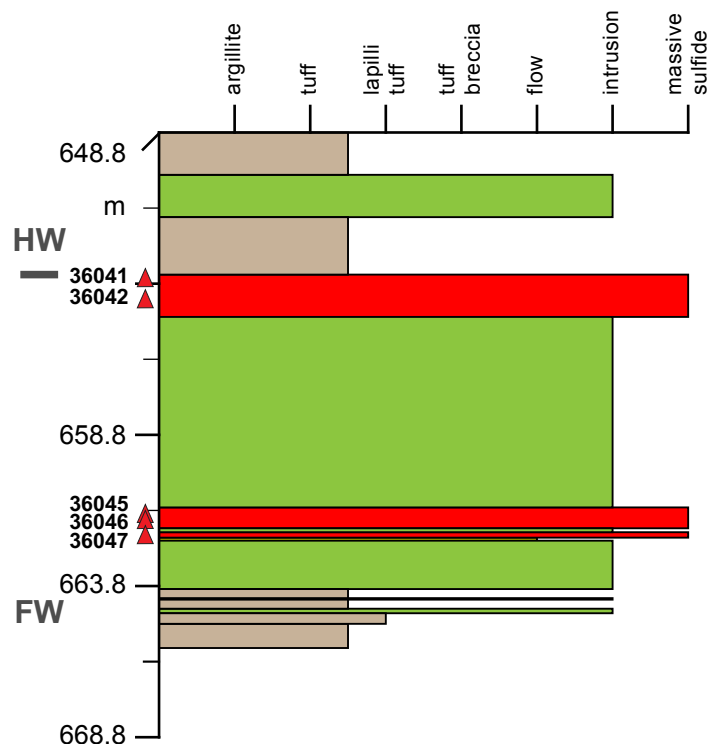


## 1807 Zone: RM07-20

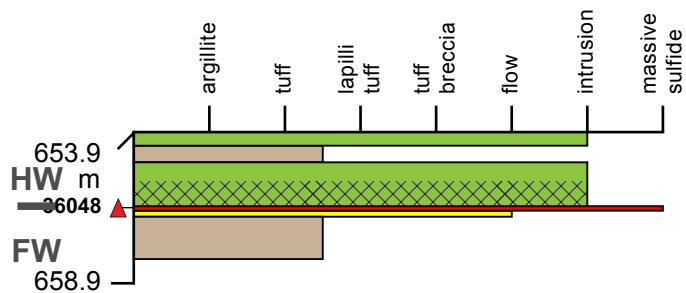
RM07-20j



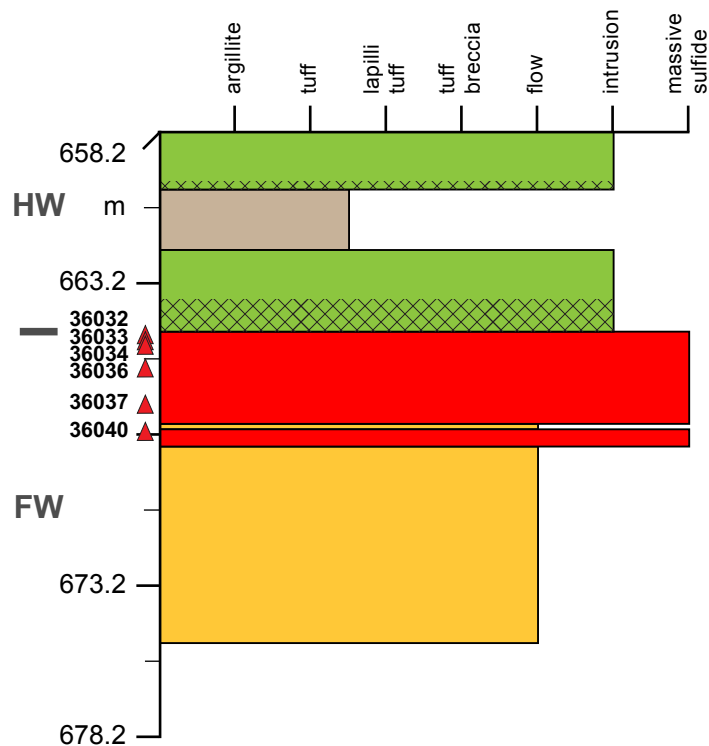
RM07-20k



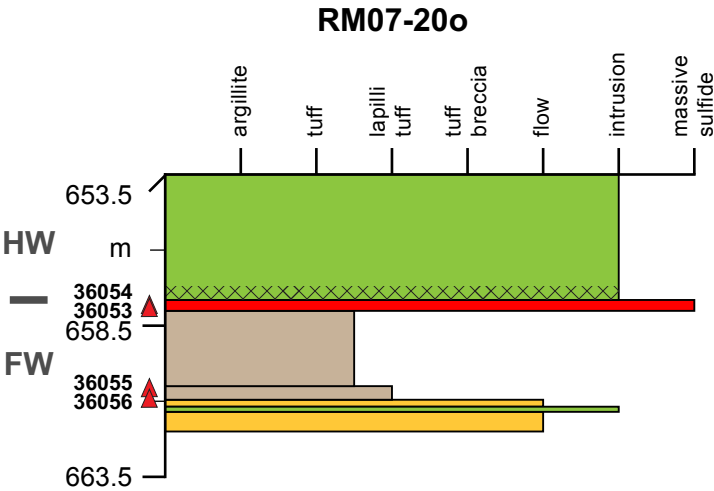
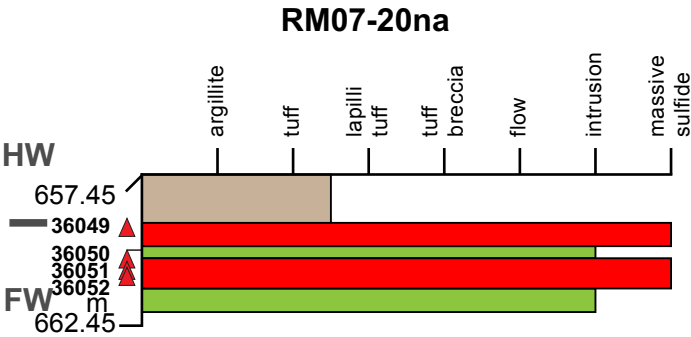
RM07-20i



RM07-20m

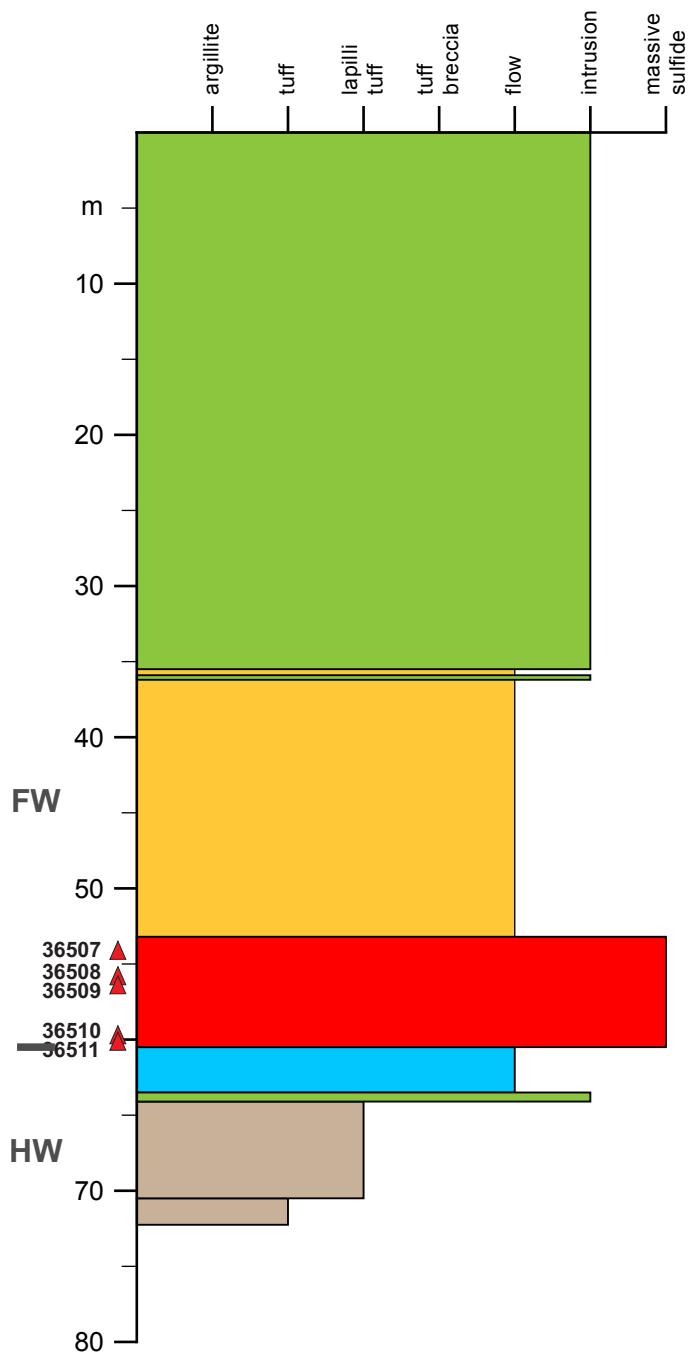


1807 Zone: RM07-20

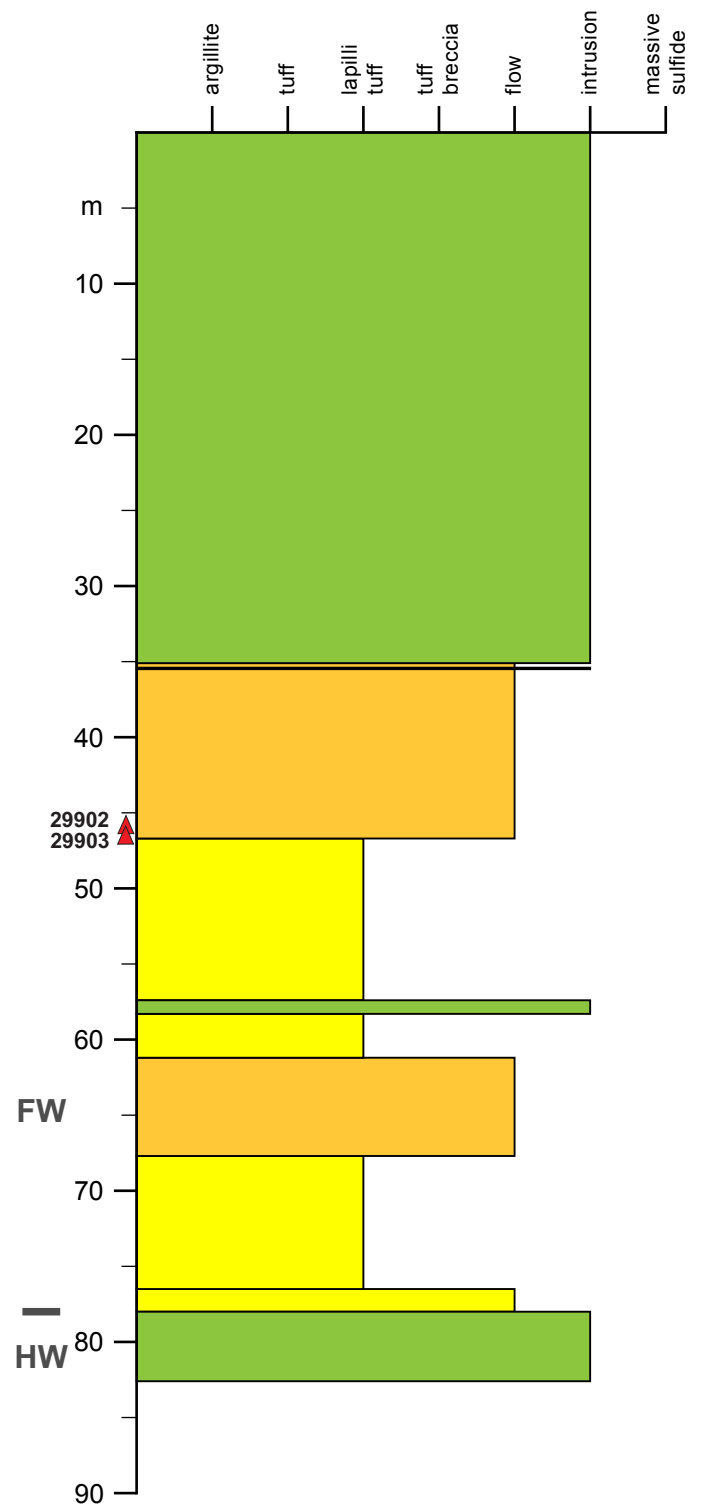


**1806 Zone: Section 21**

**RMUG08-120**

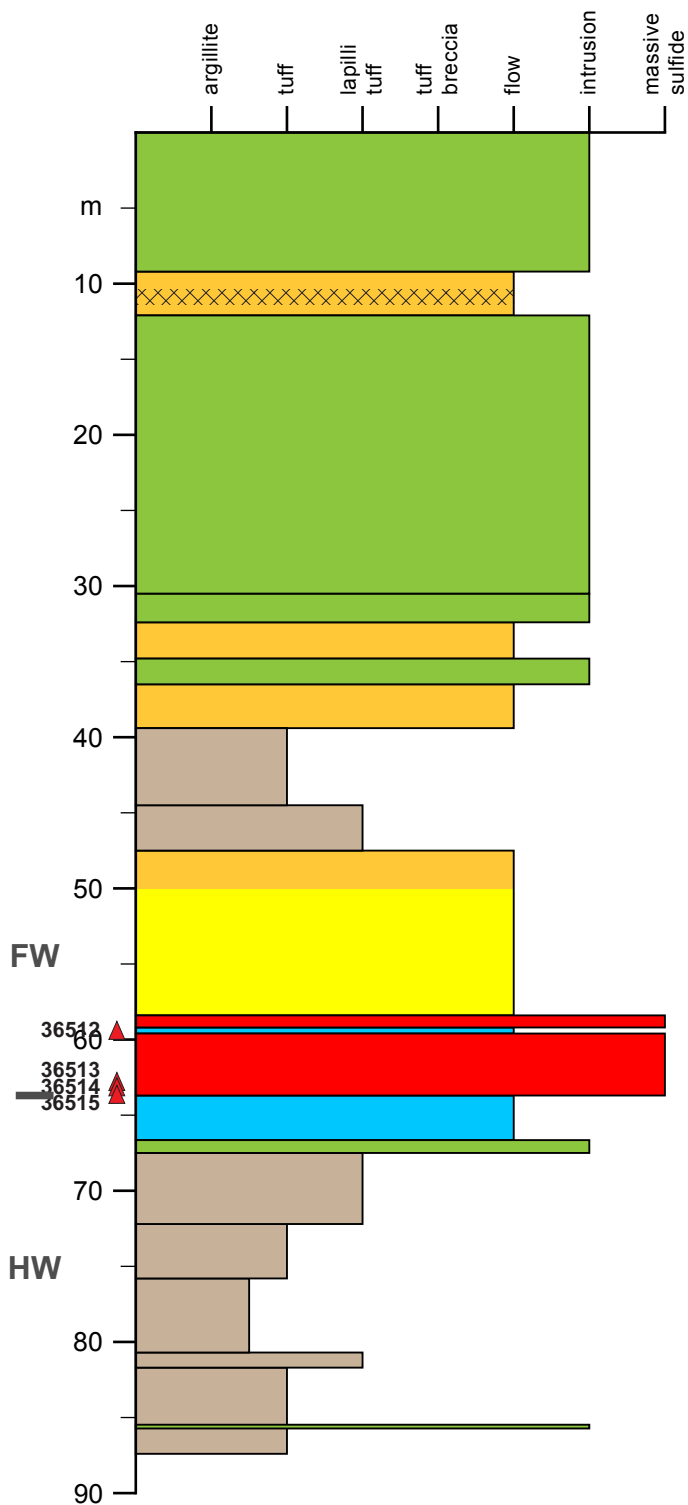


**RMUG08-121**

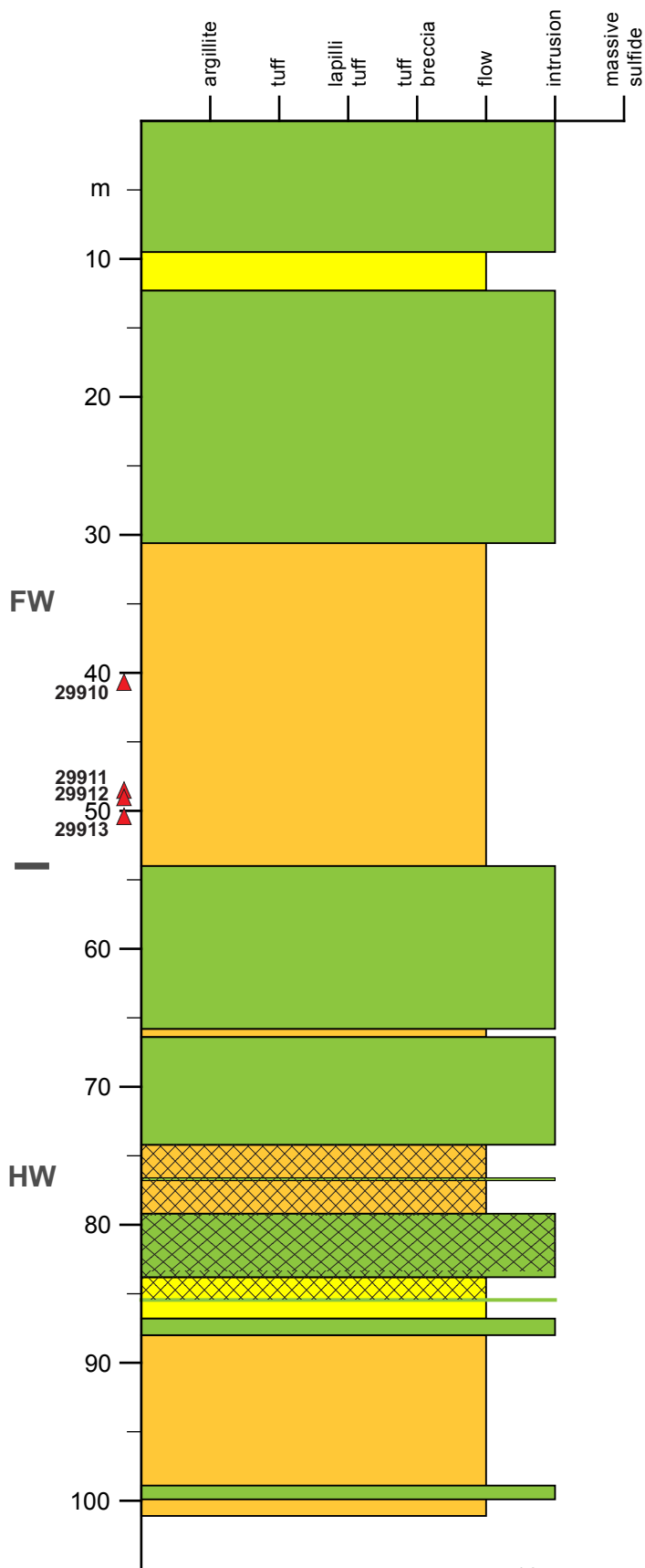


**1806 Zone: Section 21**

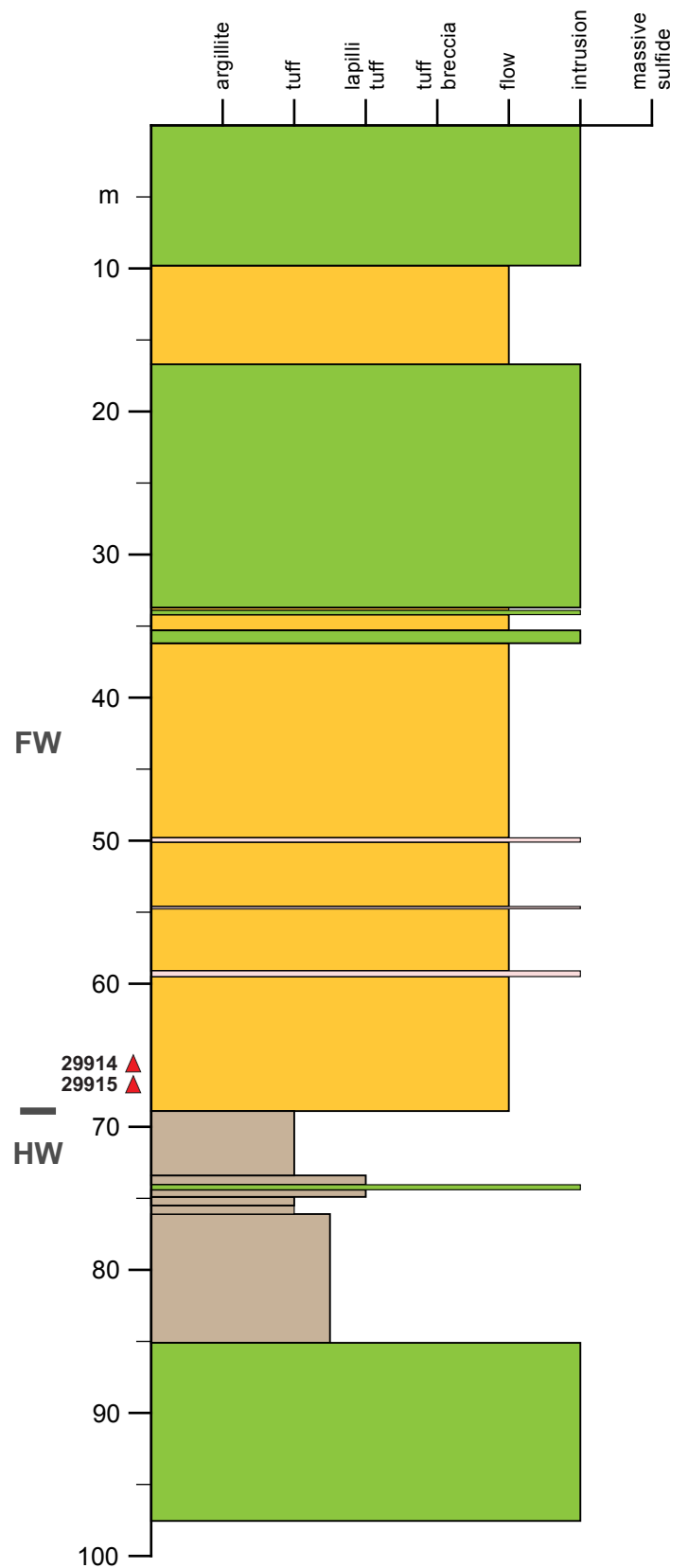
**RMUG08-123**



**RMUG08-124**

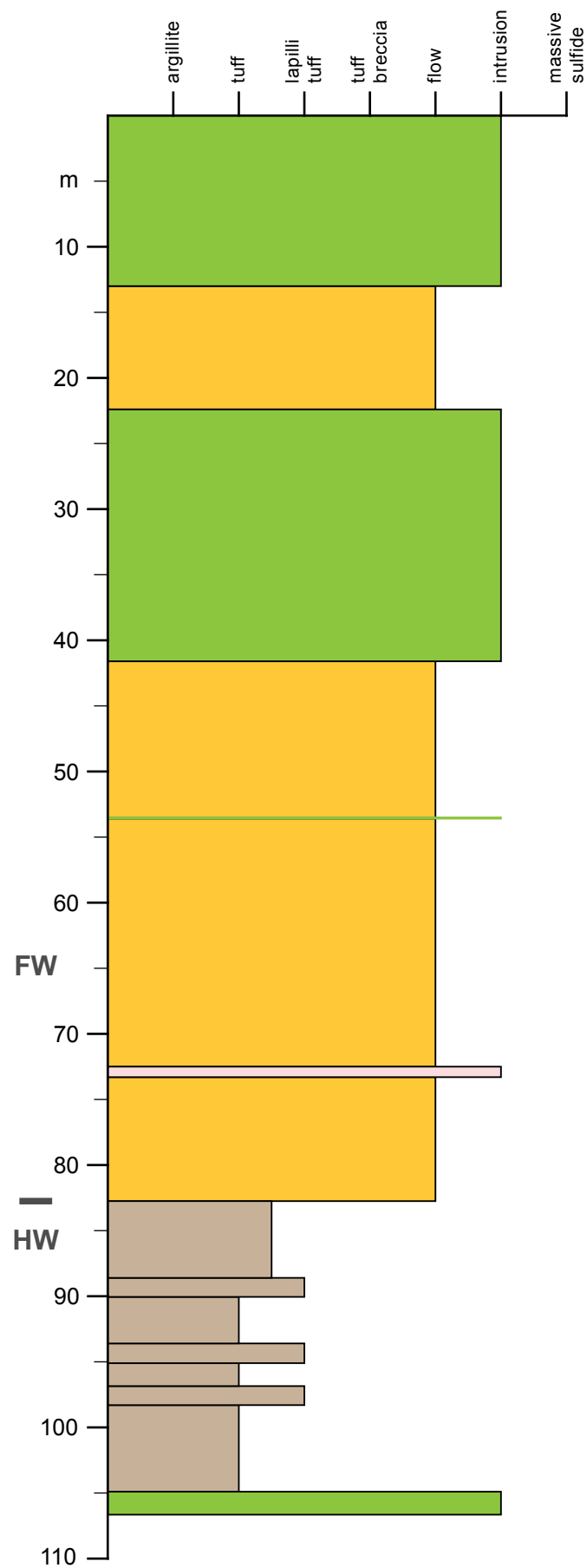




**RMUG08-150**

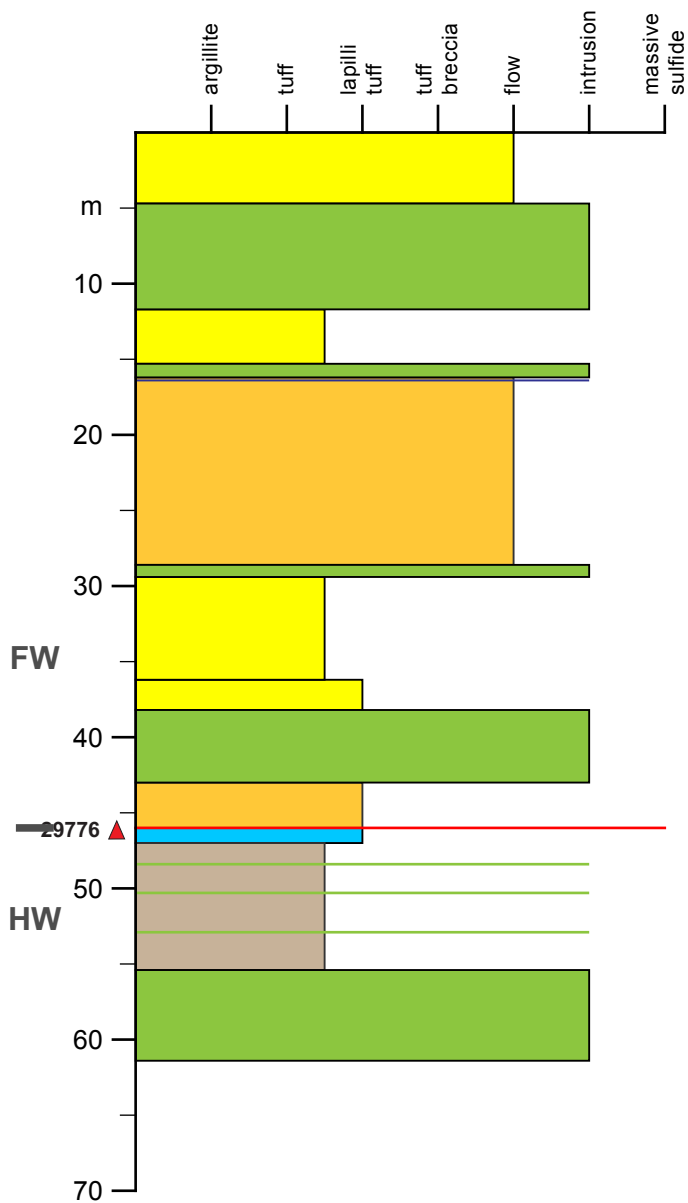
**1806 Zone: Section 21**

**RMUG08-151**

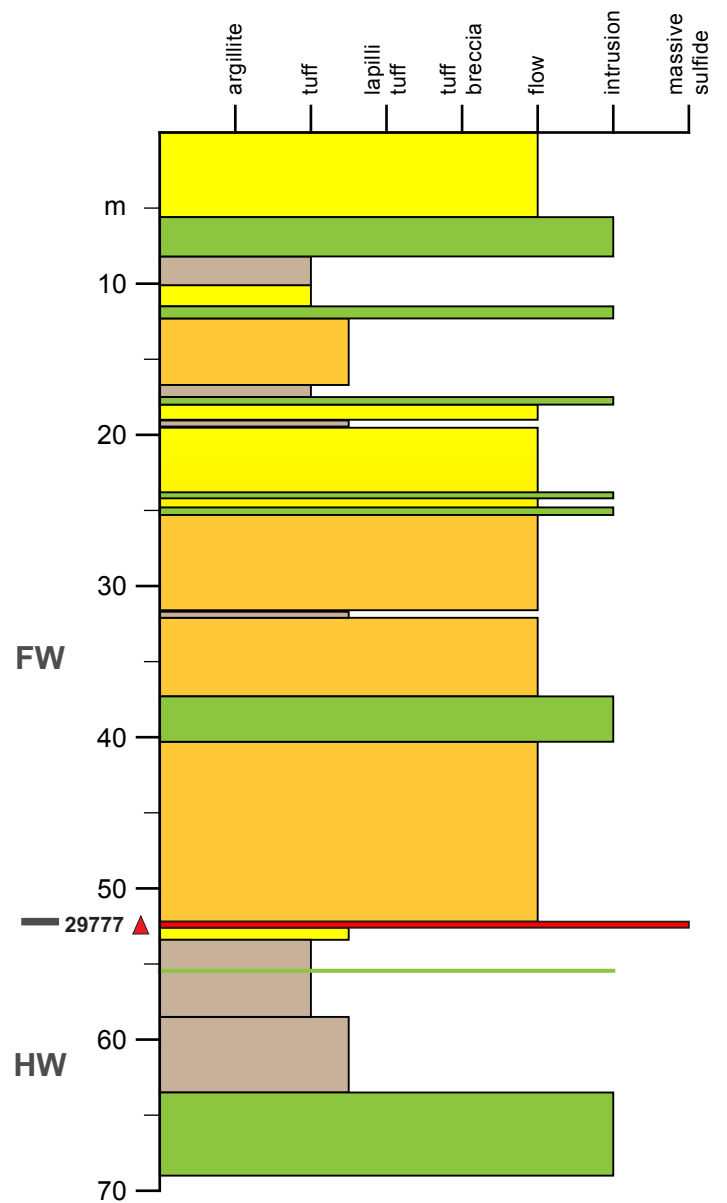


**1806 Zone: Section 22**

**RMUG08-136**

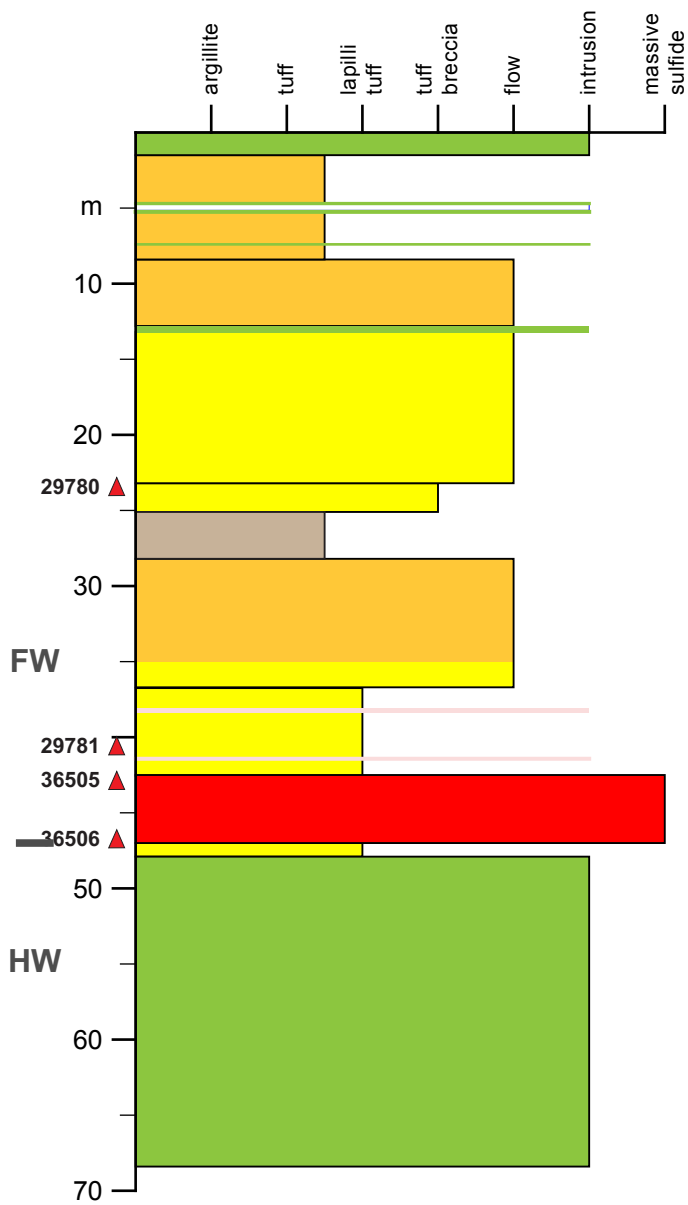


**RMUG08-137A**

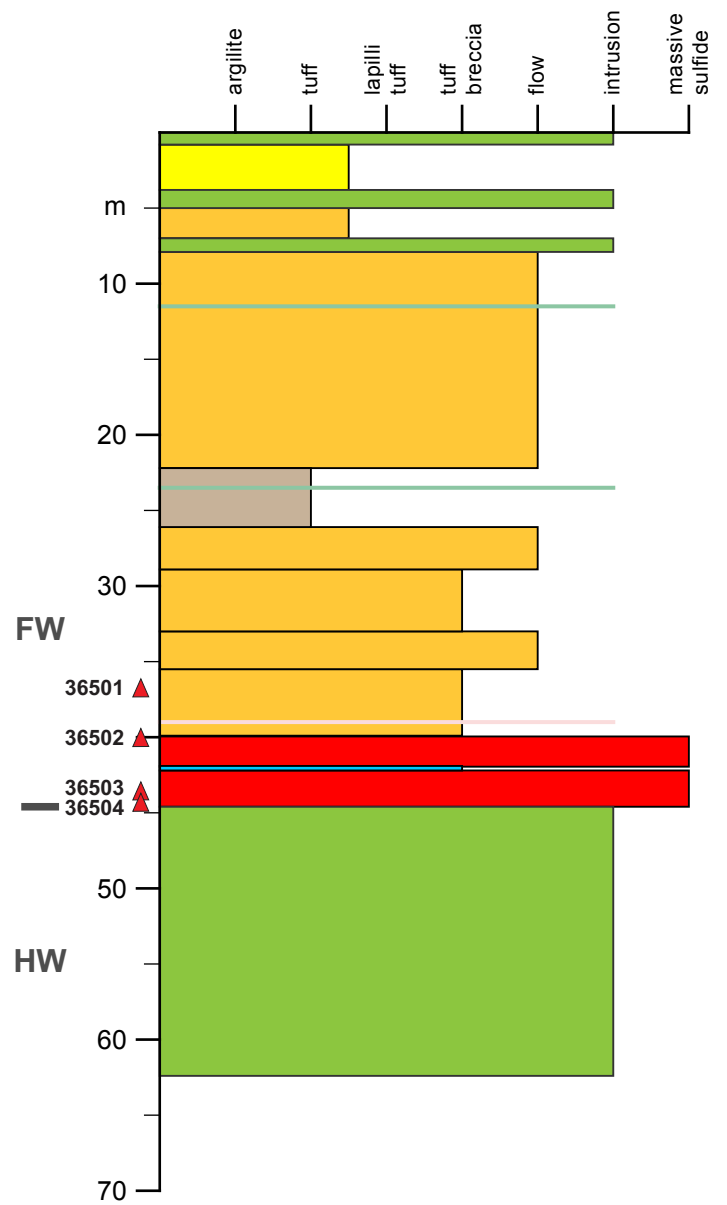


**1806 Zone: Section 22**

**RMUG08-138**

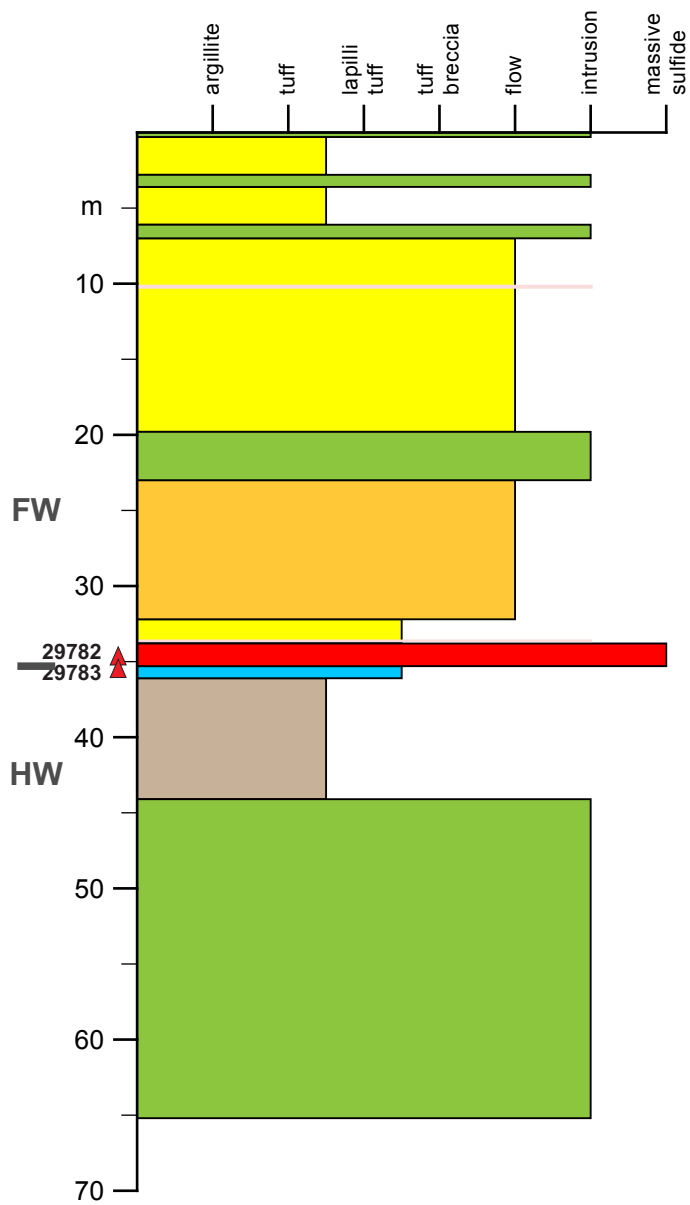


**RMUG08-139**

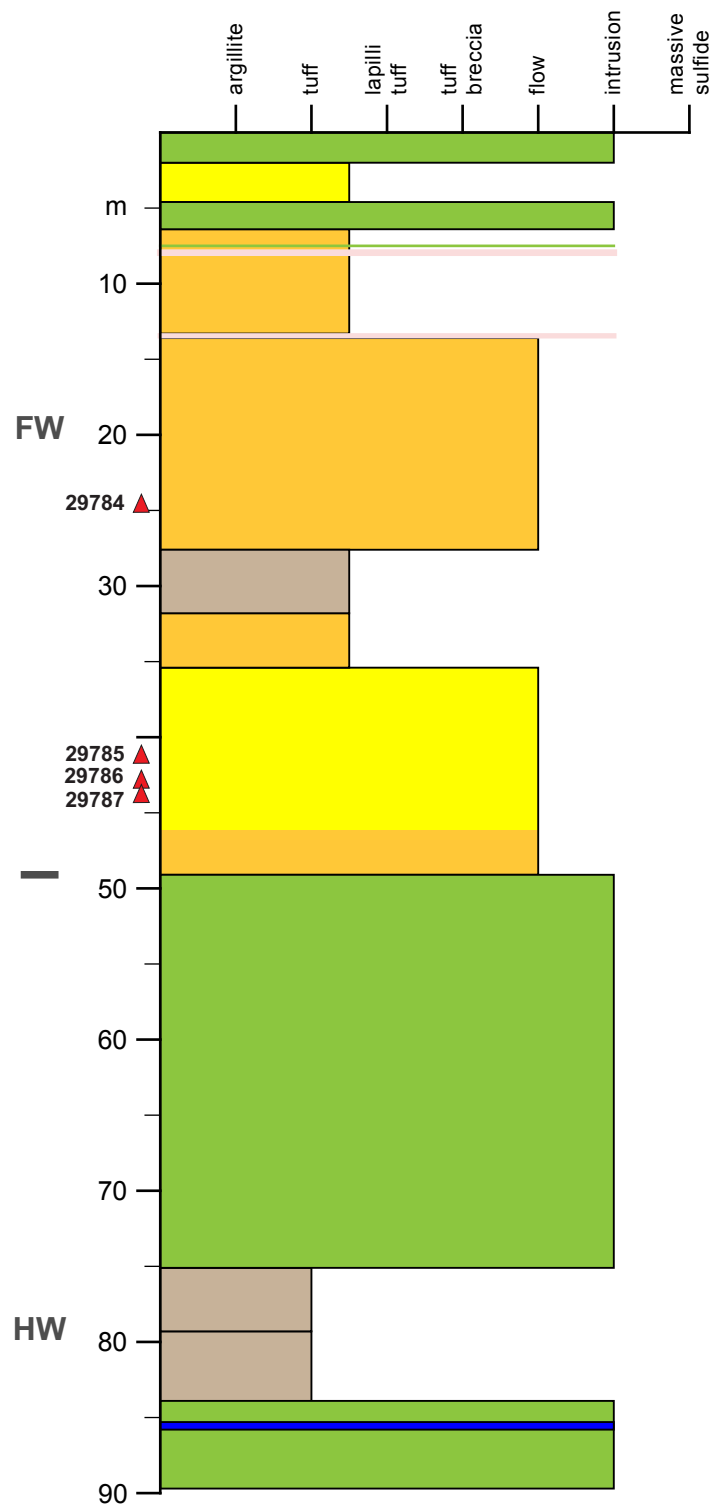


**1806 Zone: Section 22**

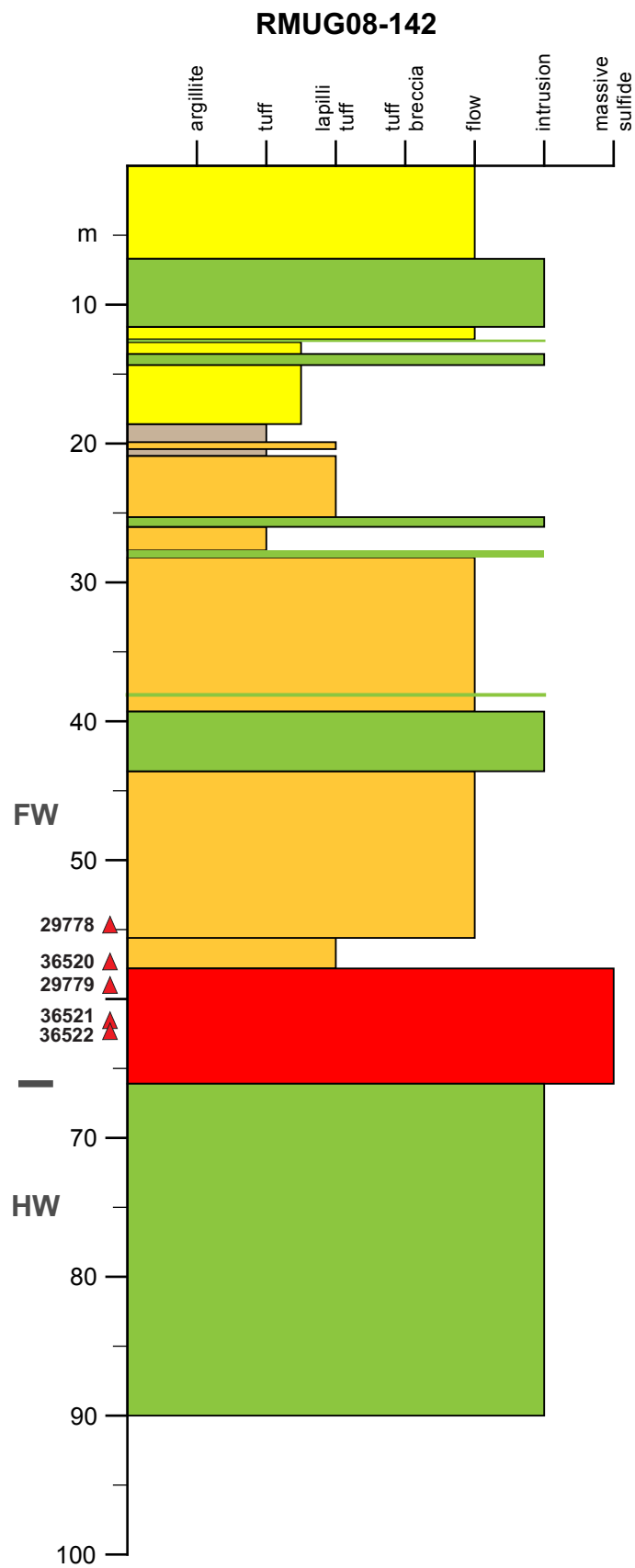
**RMUG08-140**



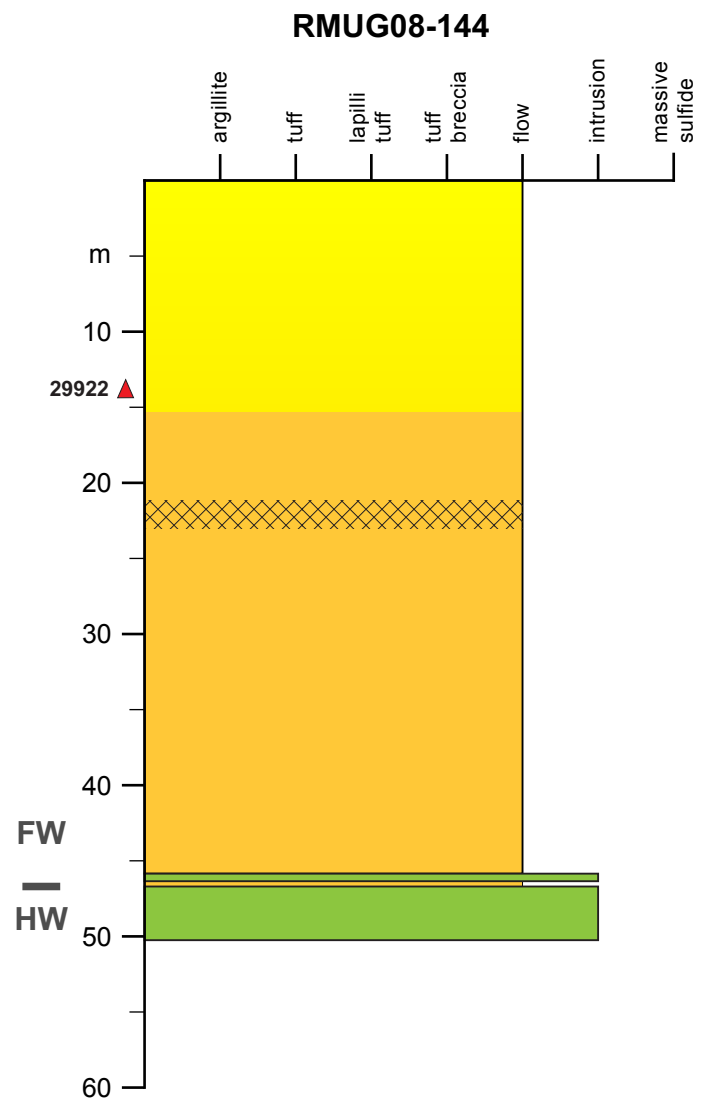
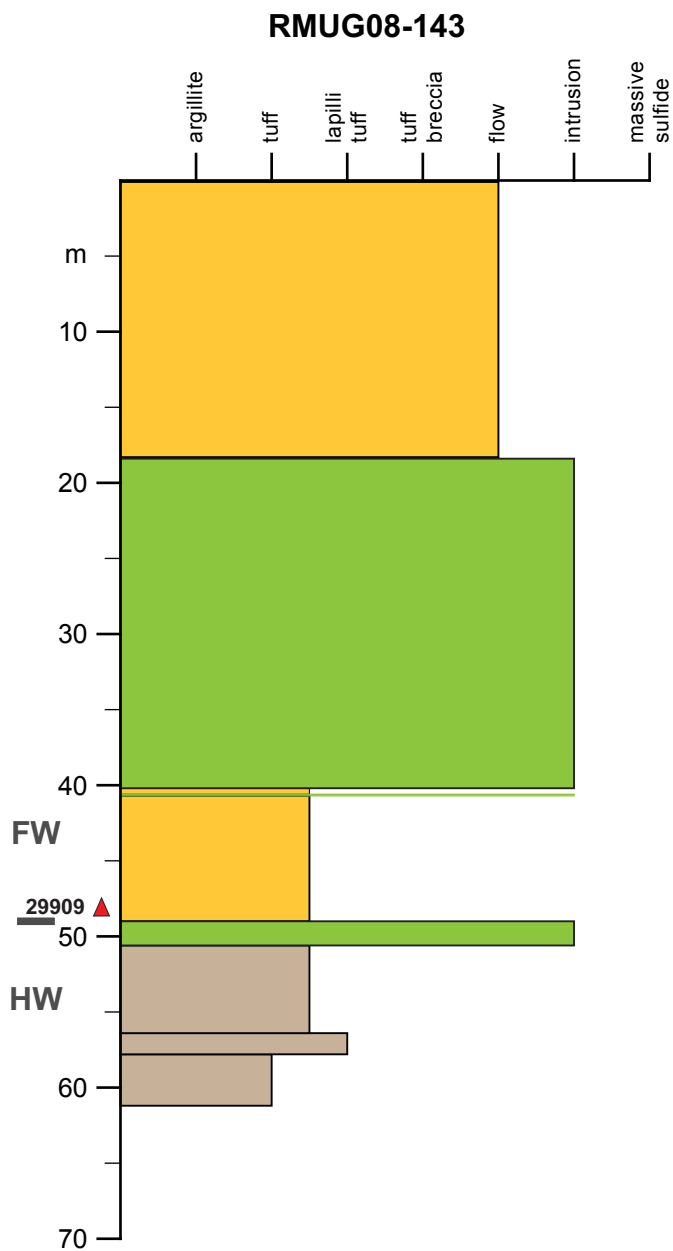
**RMUG08-141**



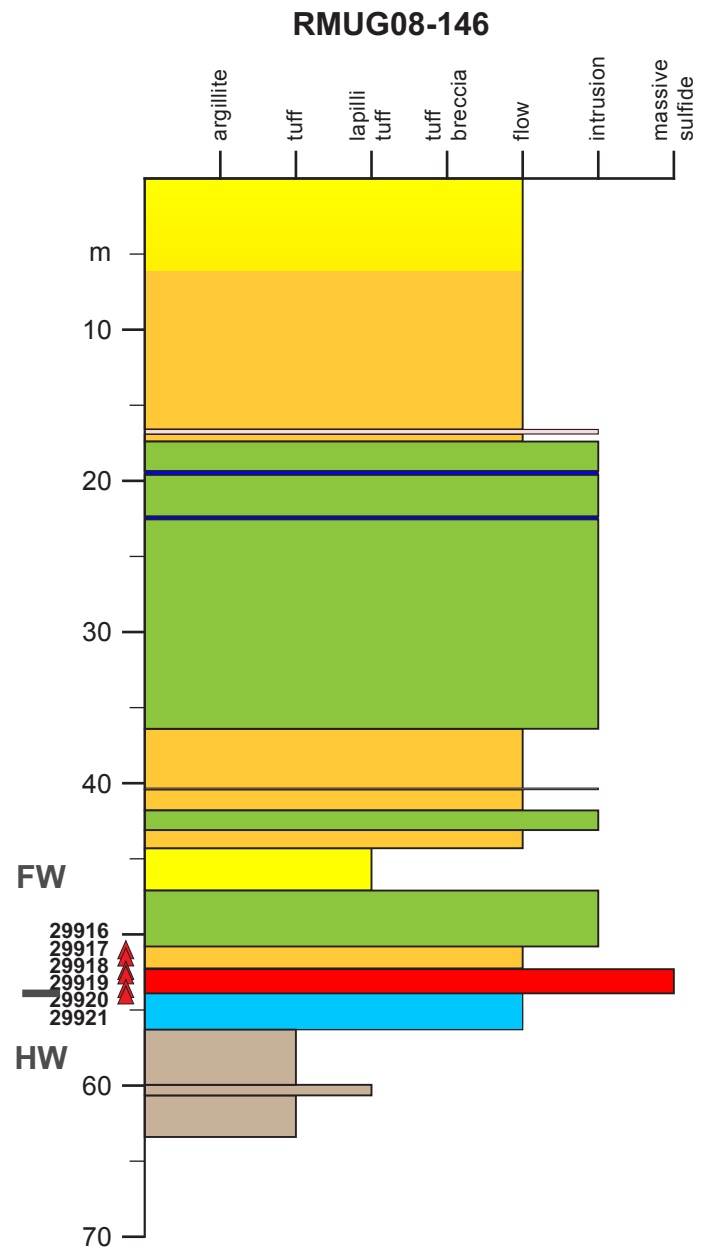
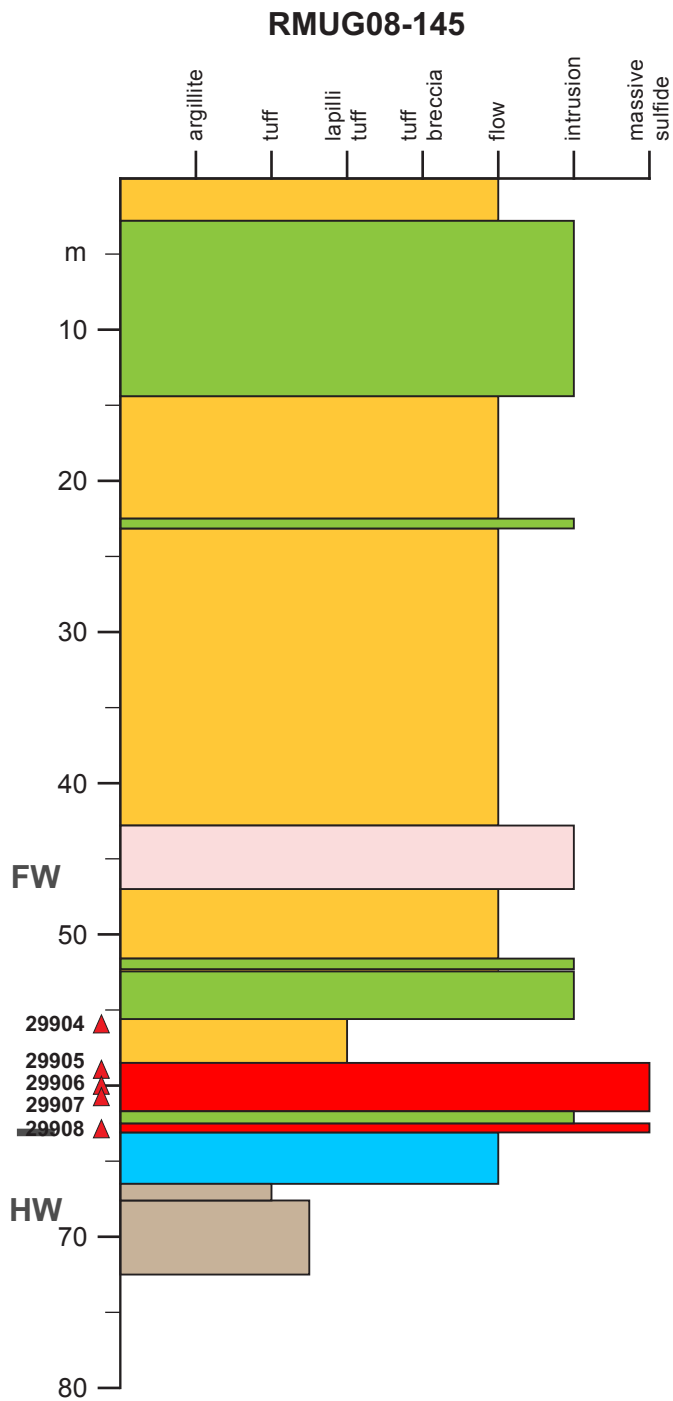
**1806 Zone: Section 22**



**1806 Zone: Section 2**



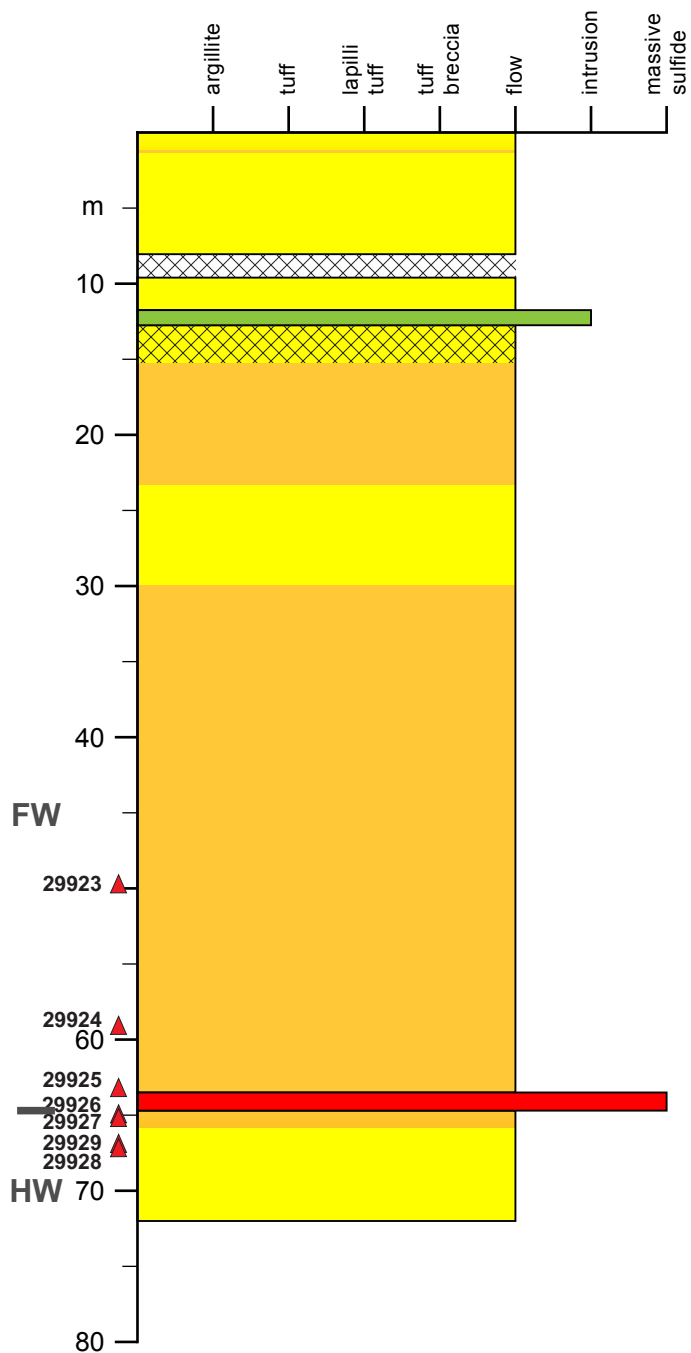
**1806 Zone: Section 2**



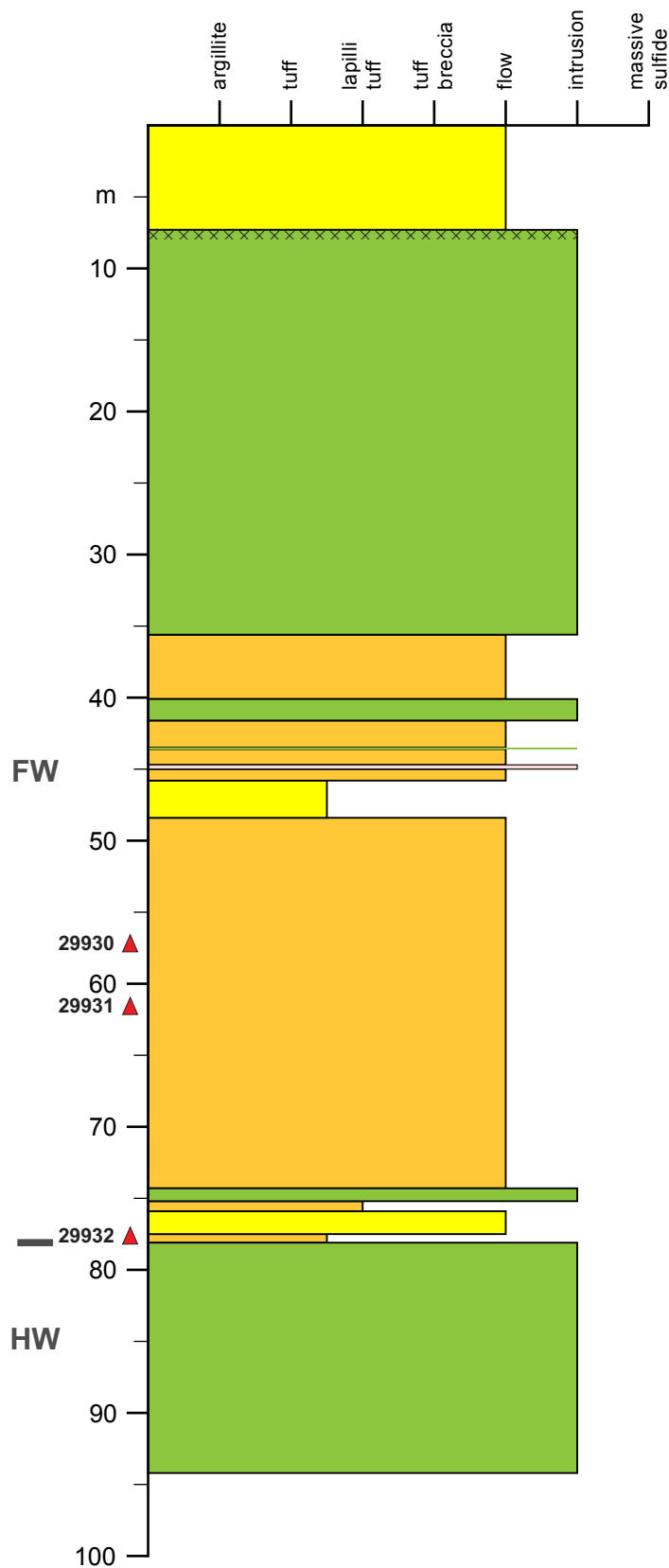


**1806 Zone: Section 2**

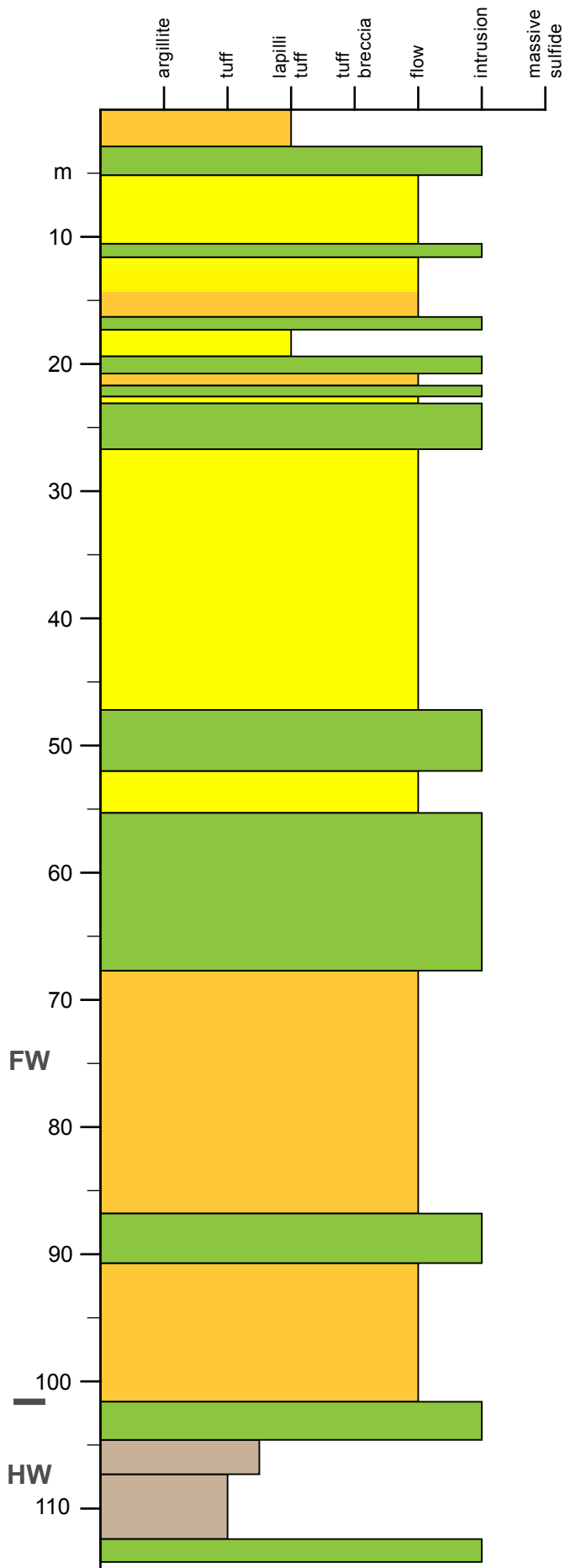
**RMUG08-147**



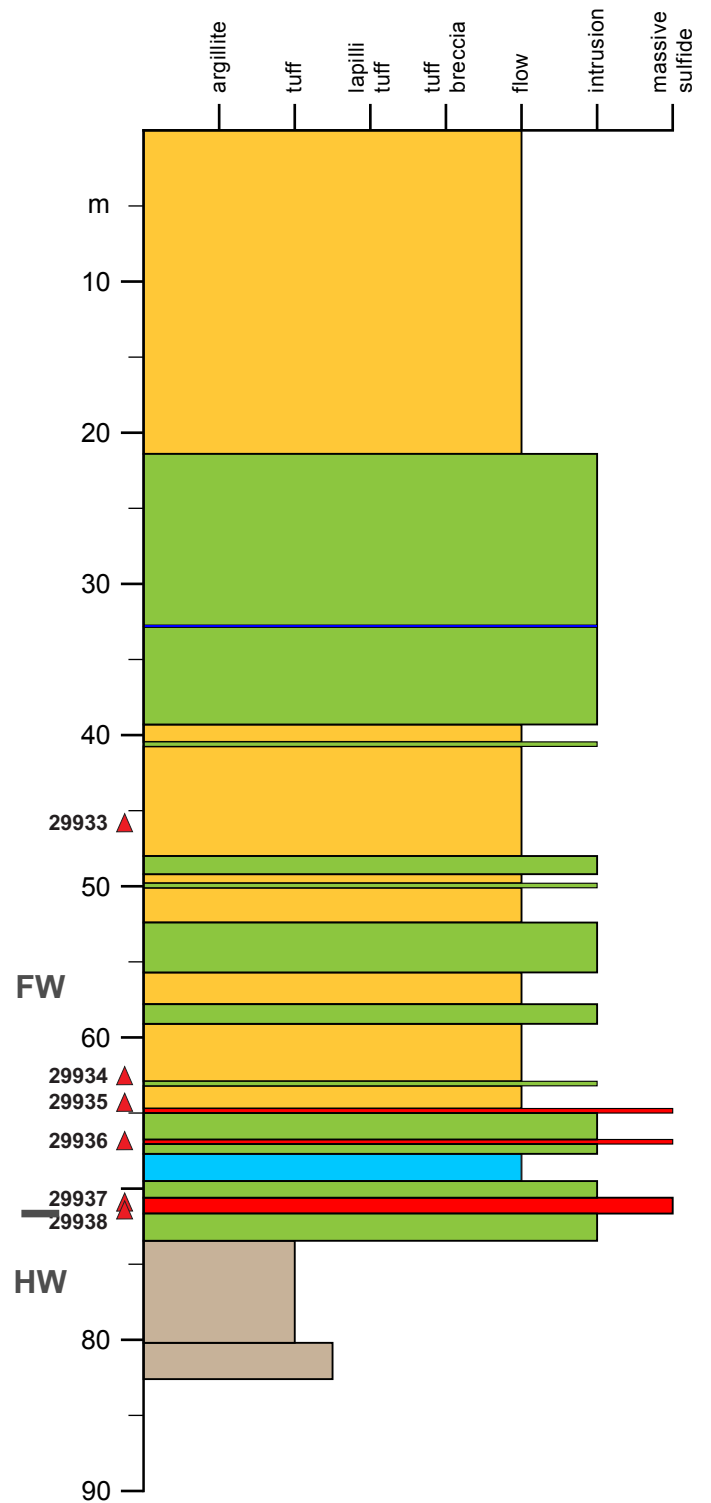
**RMUG08-148**



**RMUG08-149**

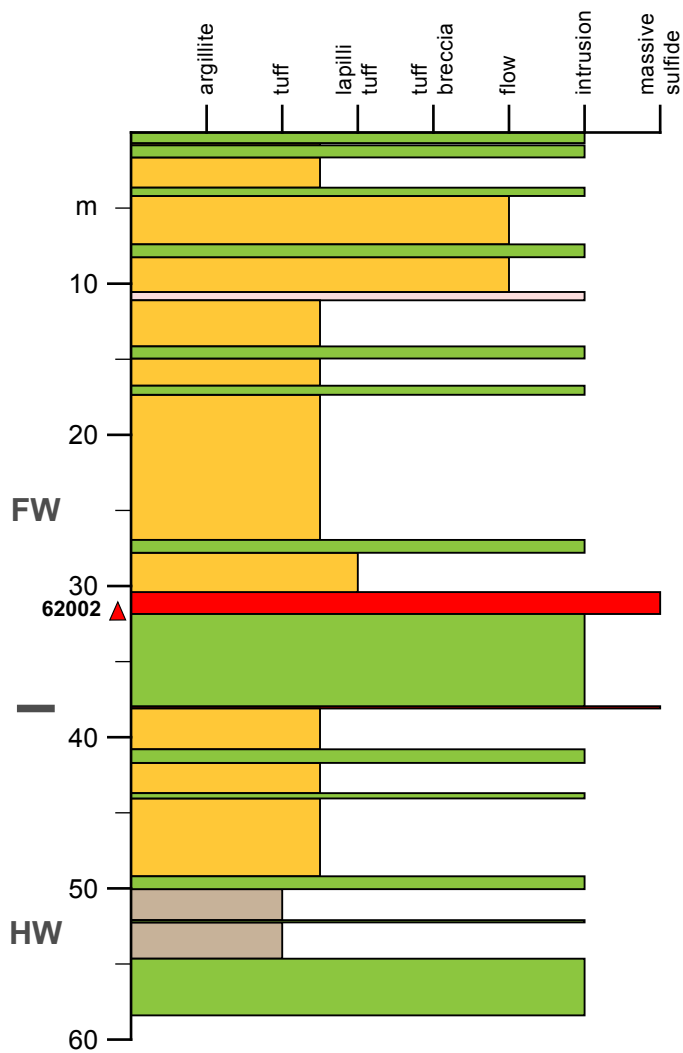


**RMUG08-159**

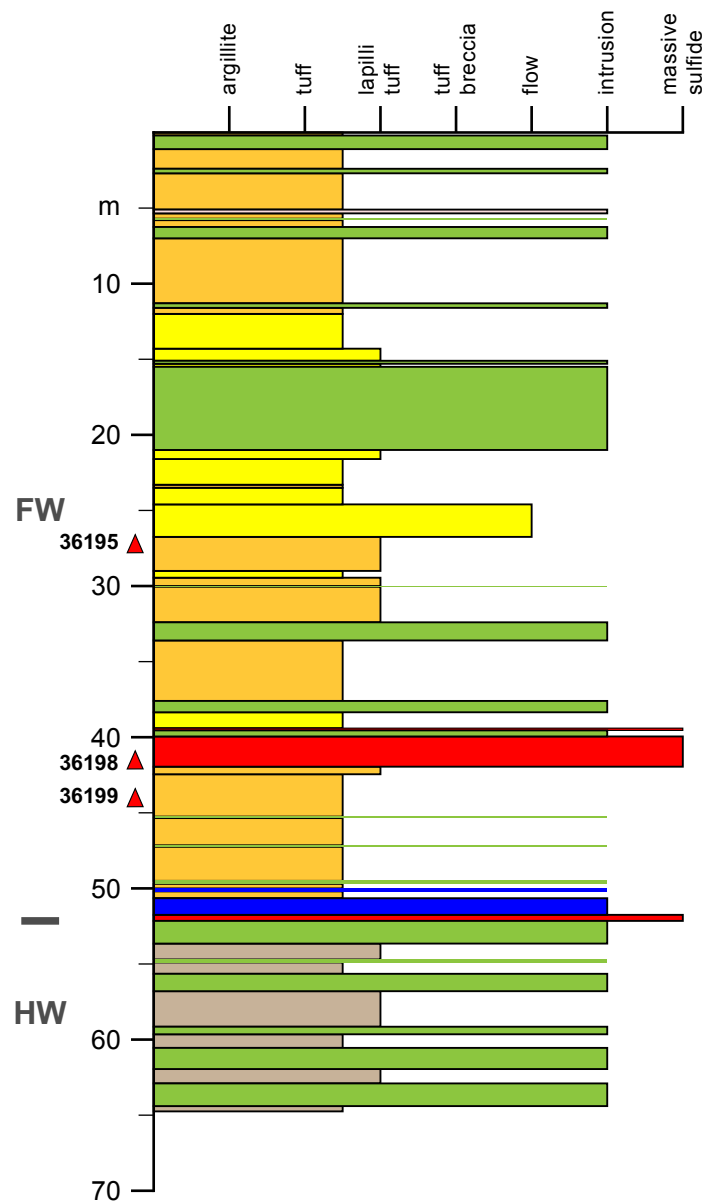


# Ming South Up Plunge: Section 24

RMUG08-107

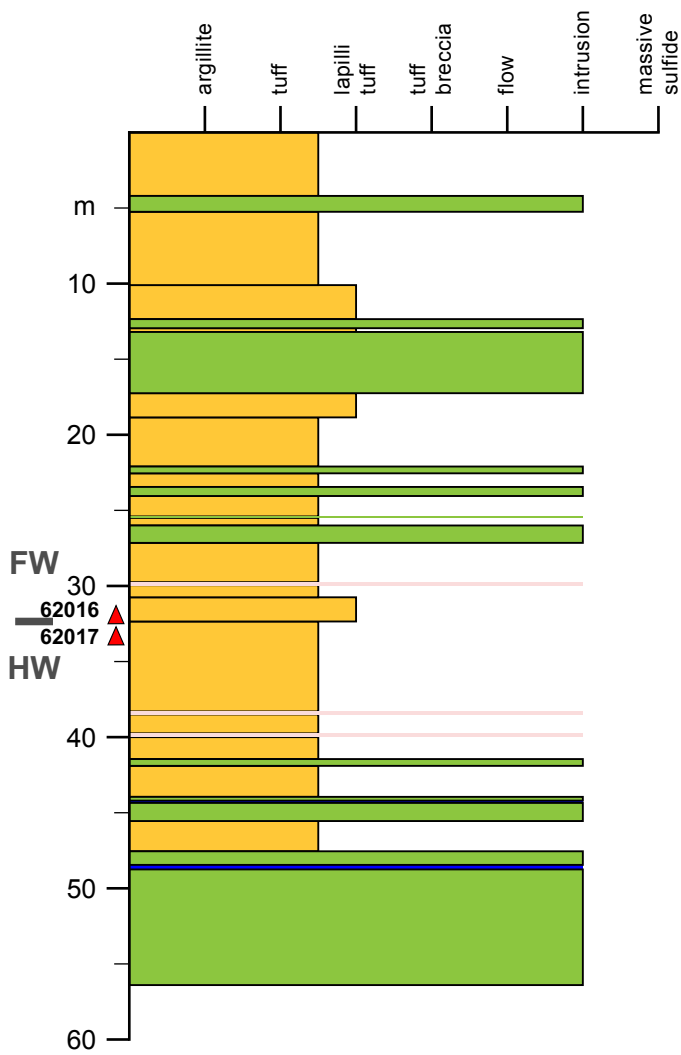


RMUG08-109

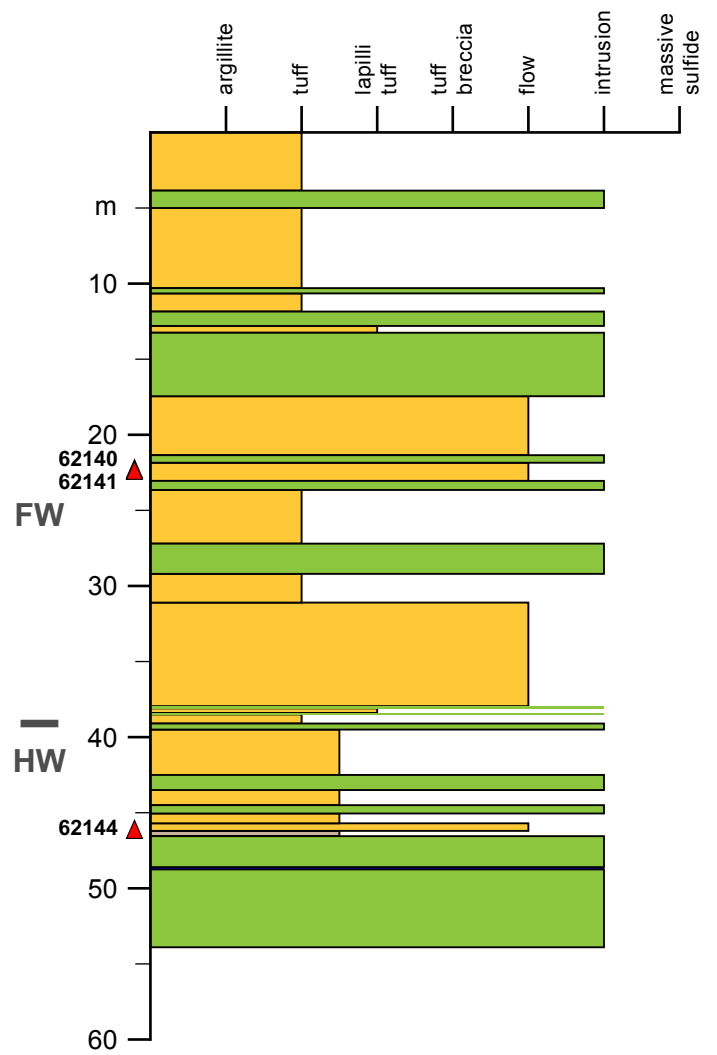


# Ming South Up Plunge: Section 4

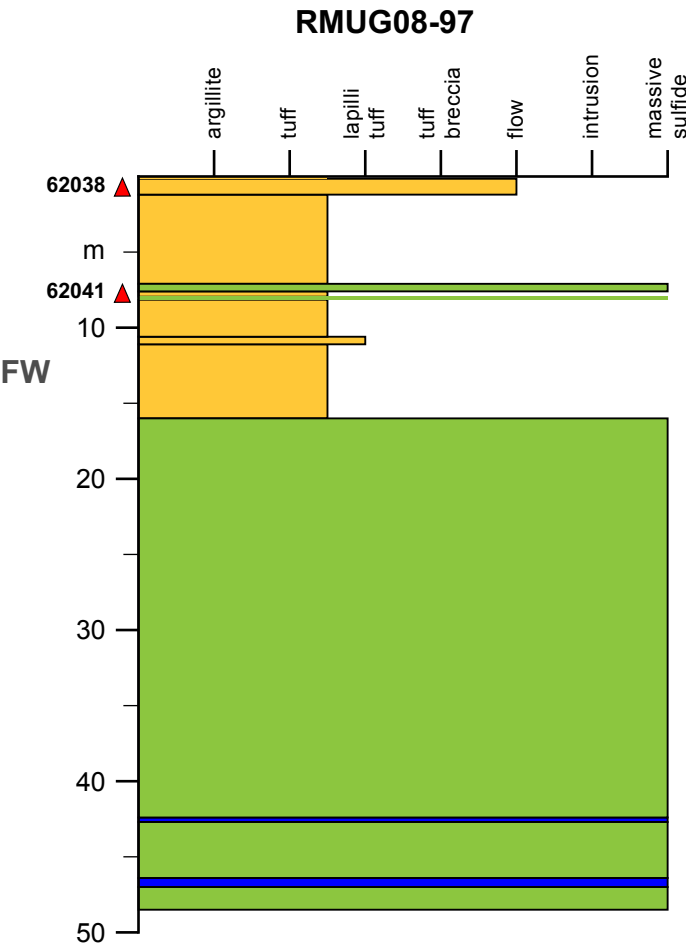
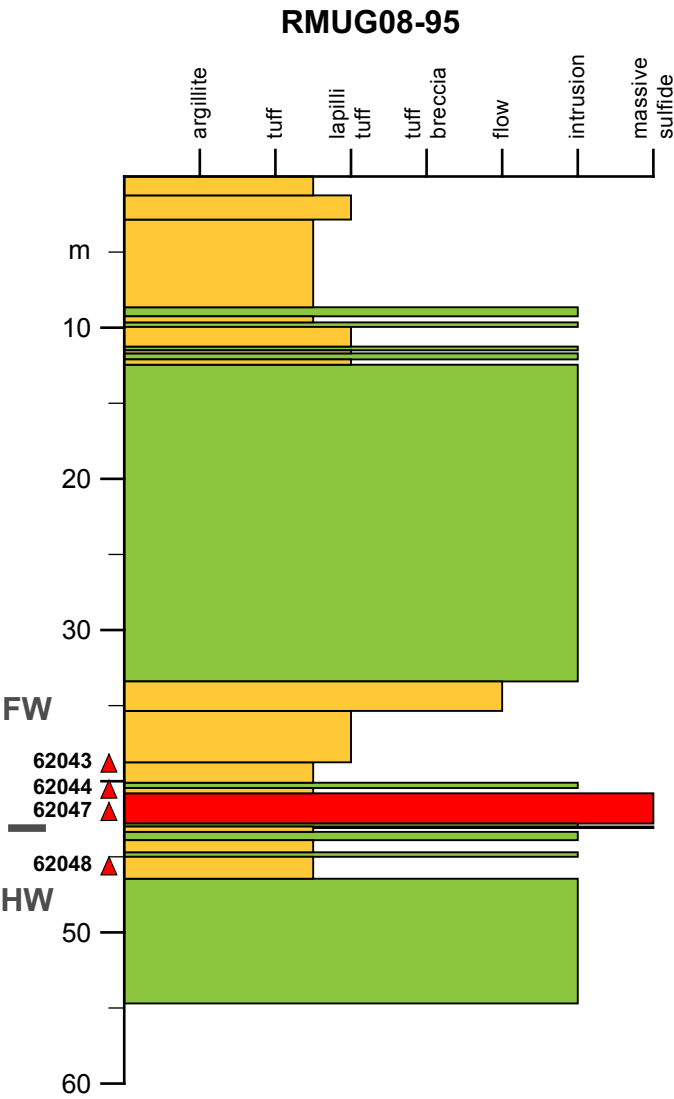
RMUG08-104



RMUG08-106

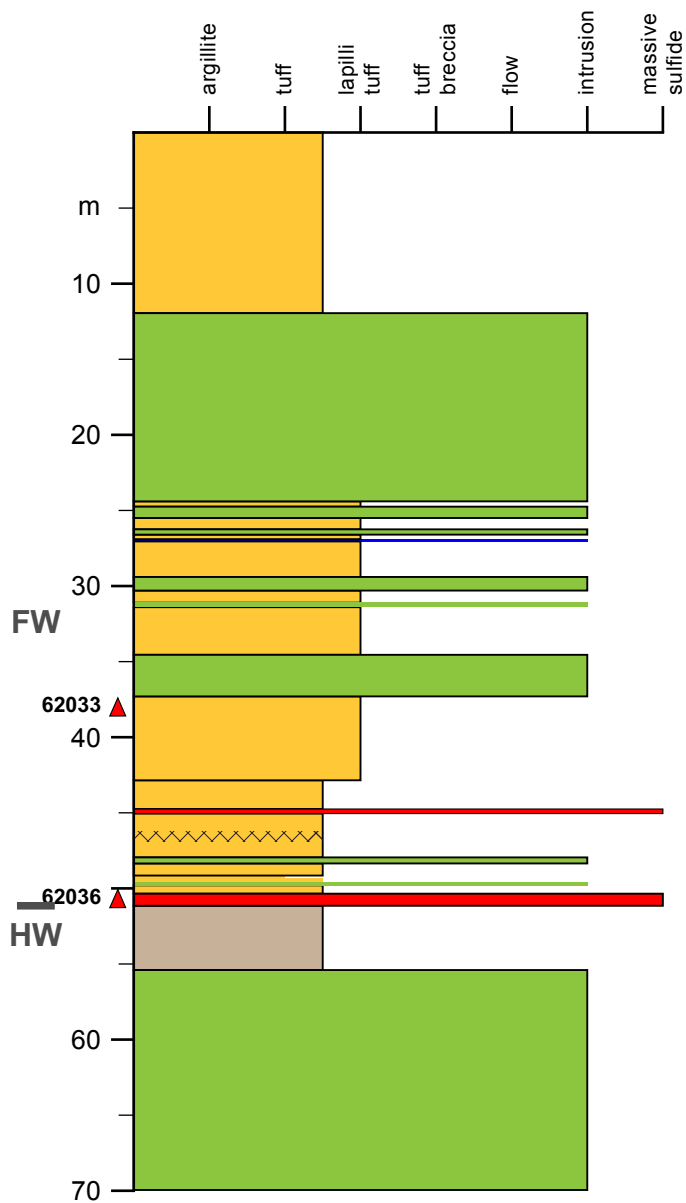


Ming South Up Plunge: Section 5

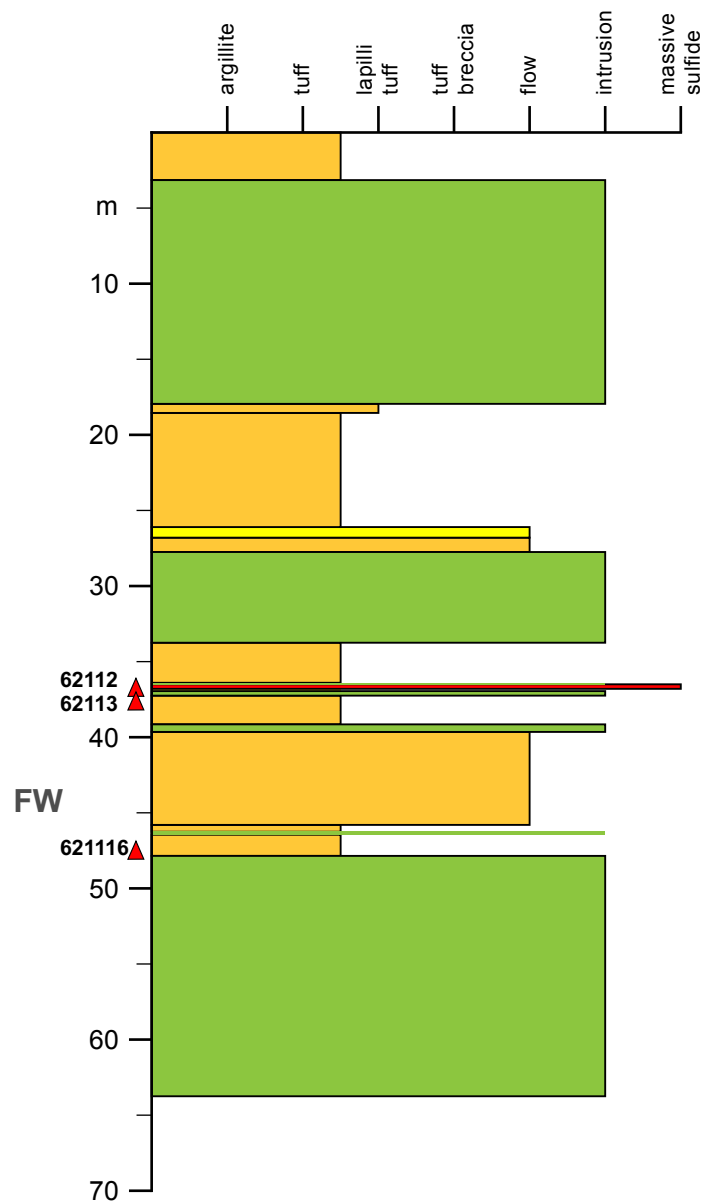


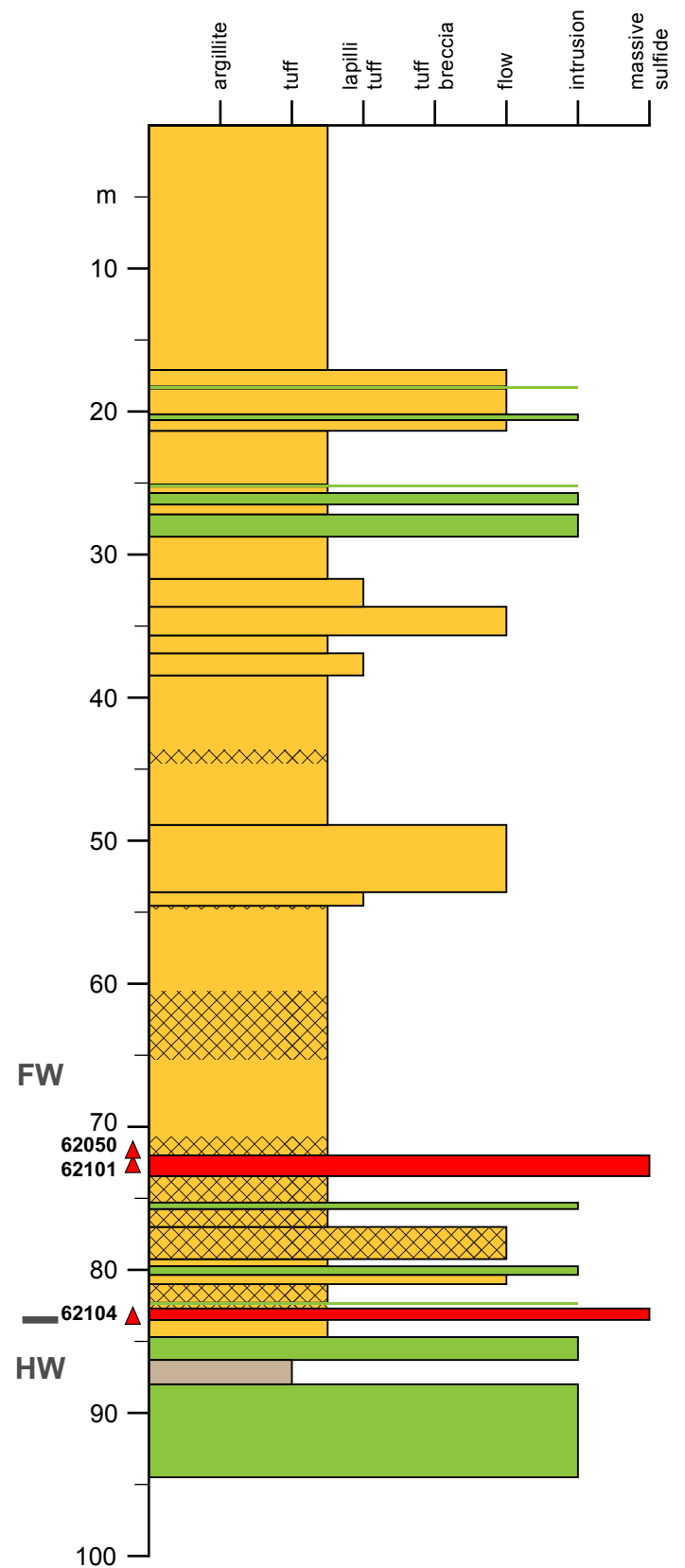
# Ming South Up Plunge: Section 5 and Section 9

RMUG08-98

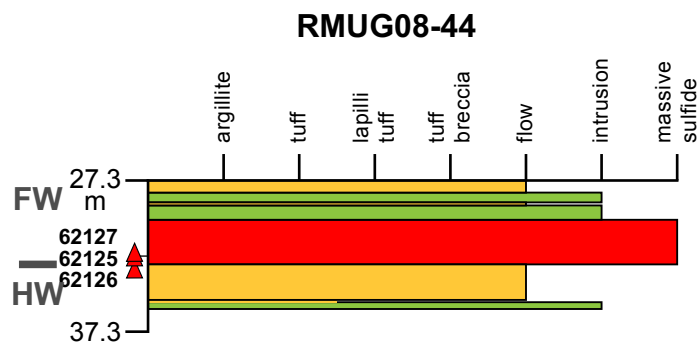
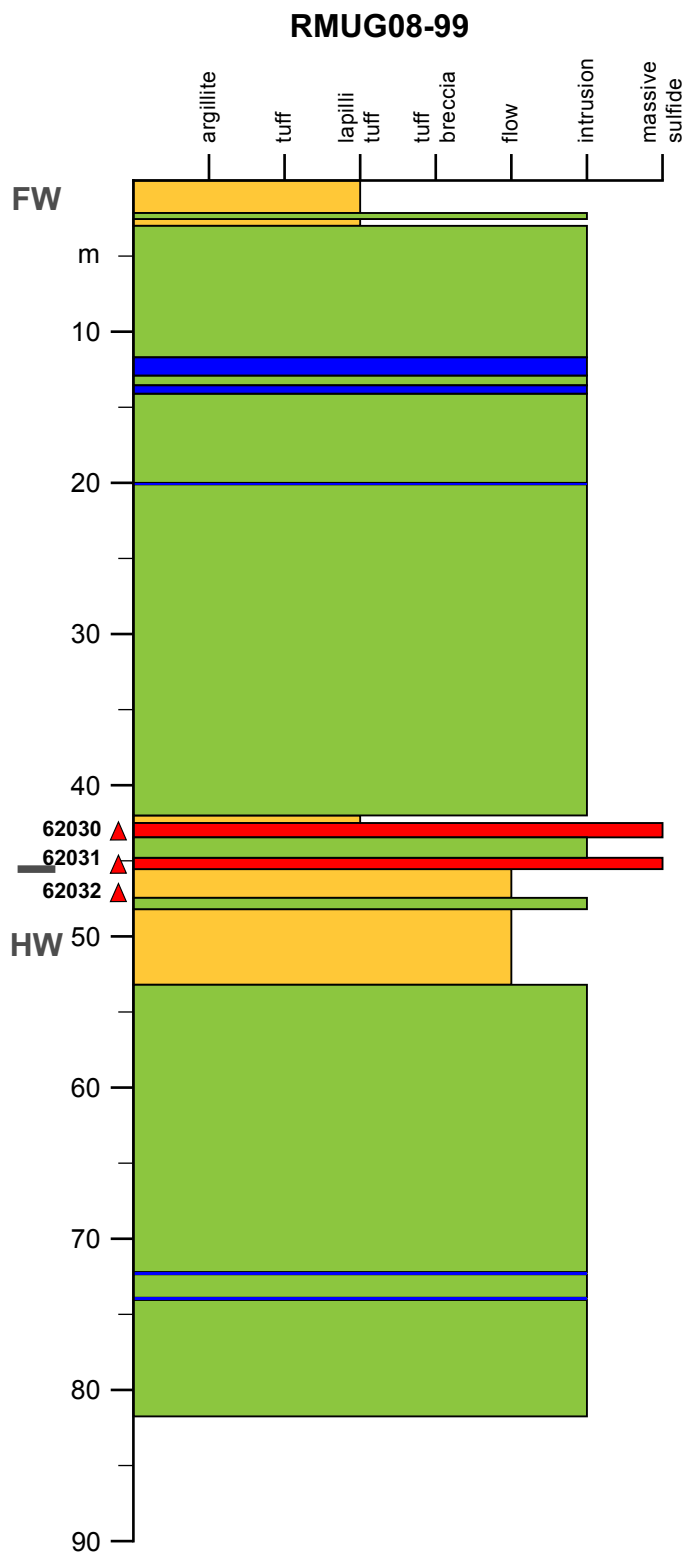


RMUG08-93



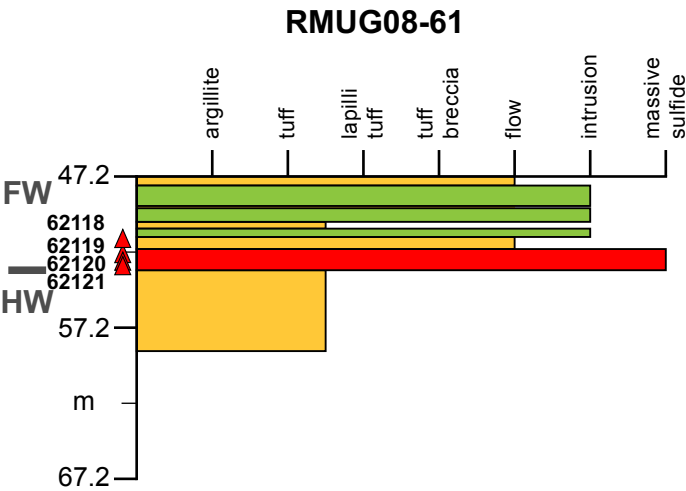
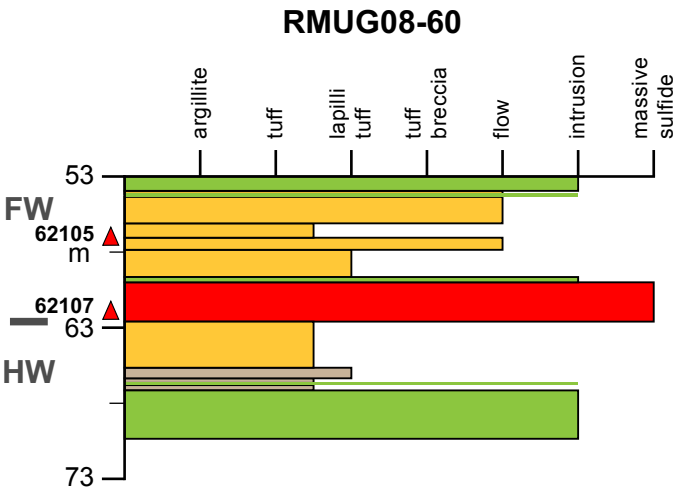
**RMUG08-96**

# Ming South Up Plunge: Section 9 and Section 8

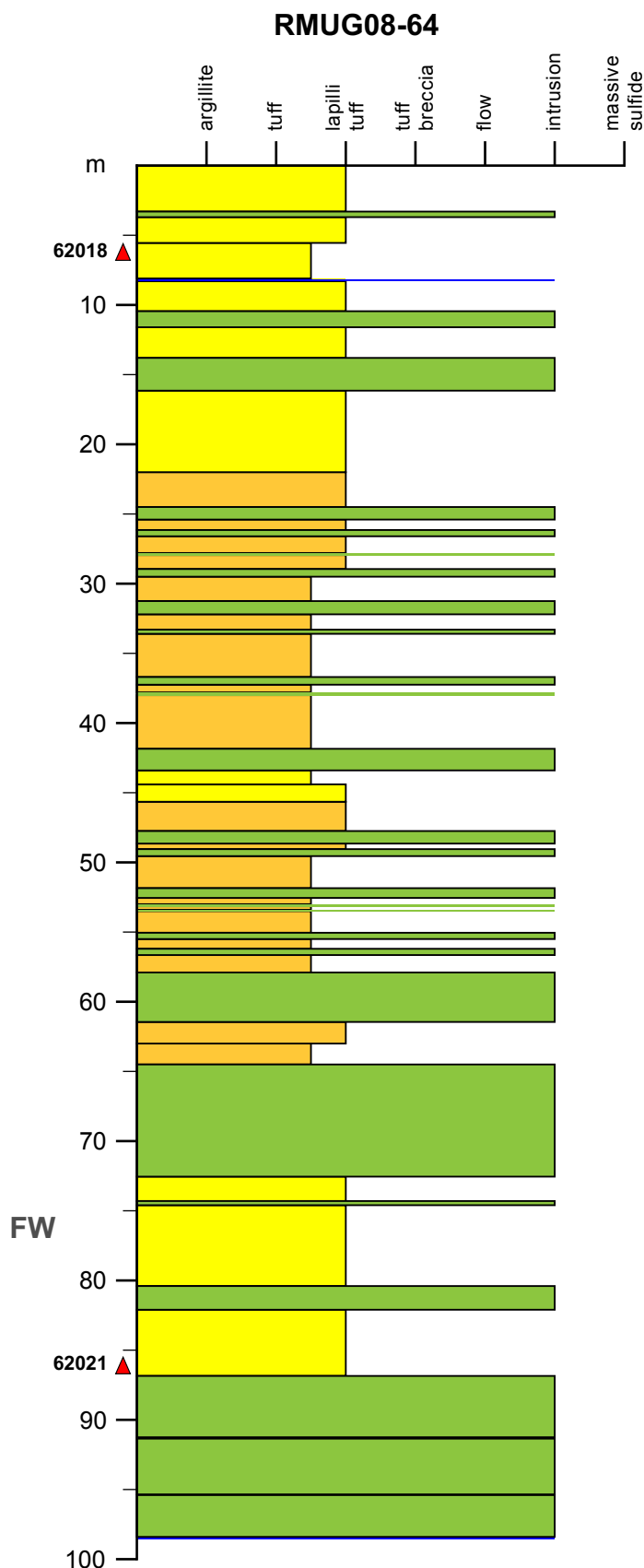
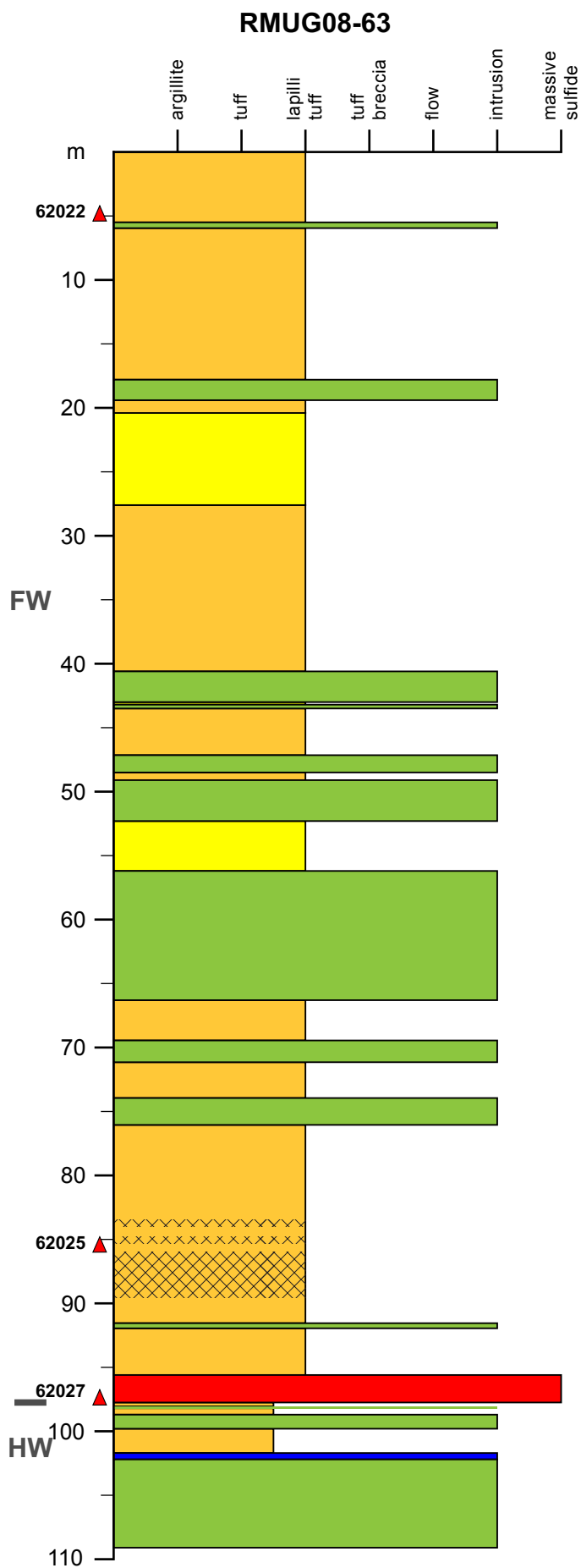




Ming South Up Plunge: Section 14

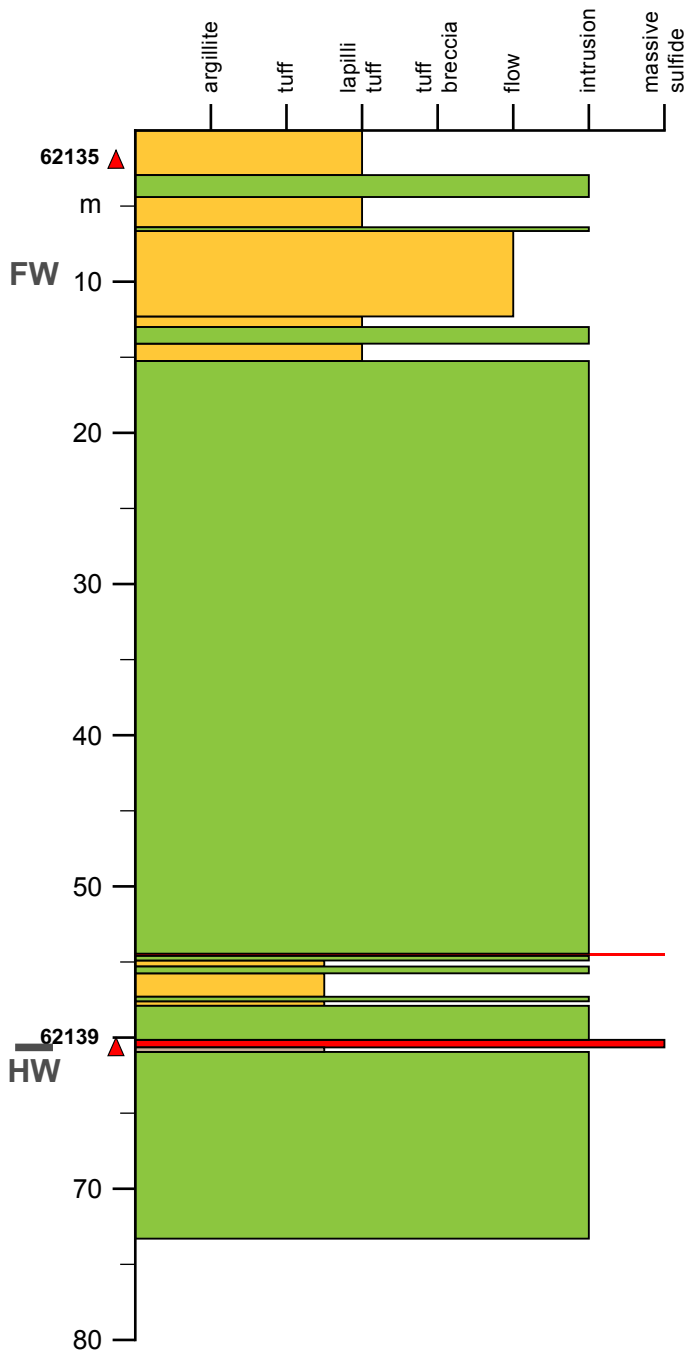


**Ming South Up Plunge: Section 14**

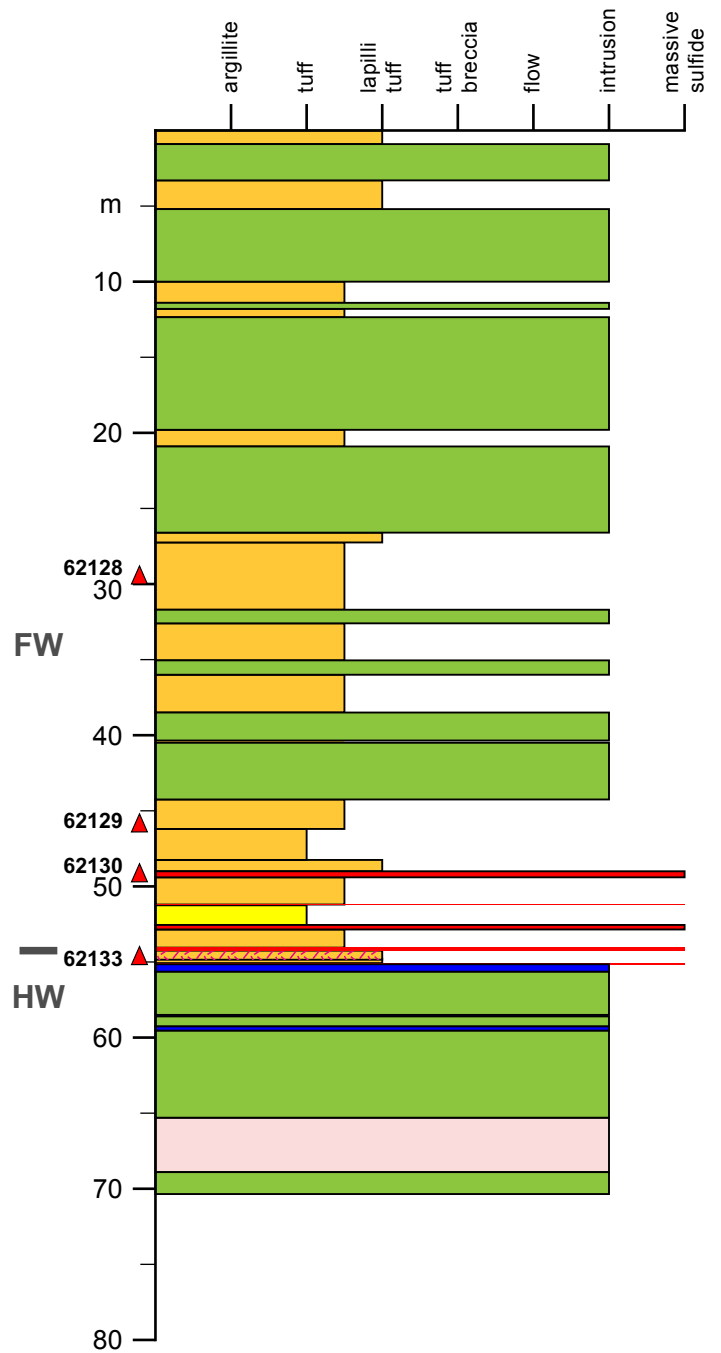


# Ming South Up Plunge: Section 13

RMUG08-90



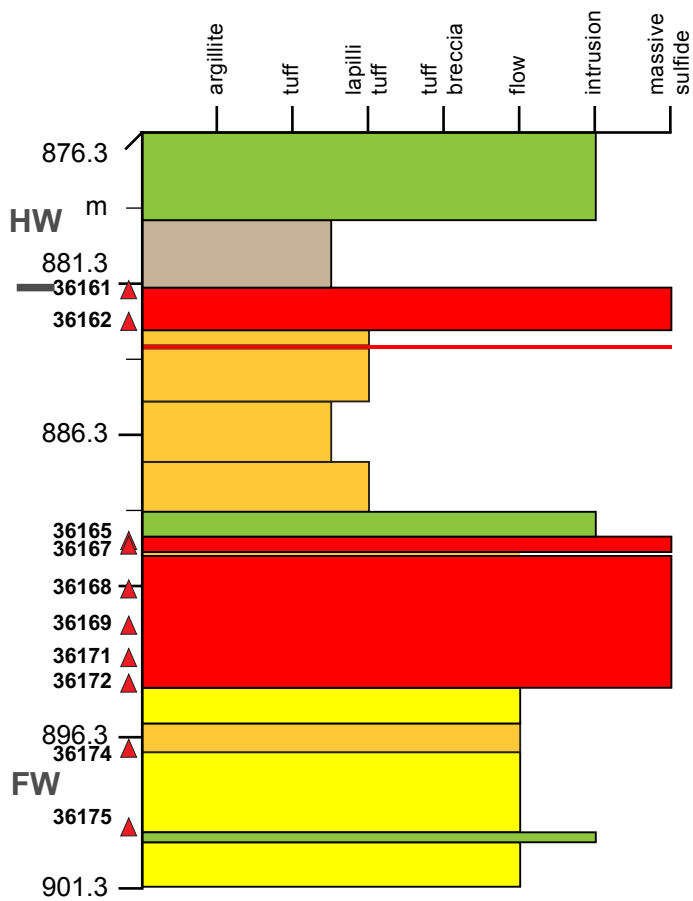
RMUG08-91



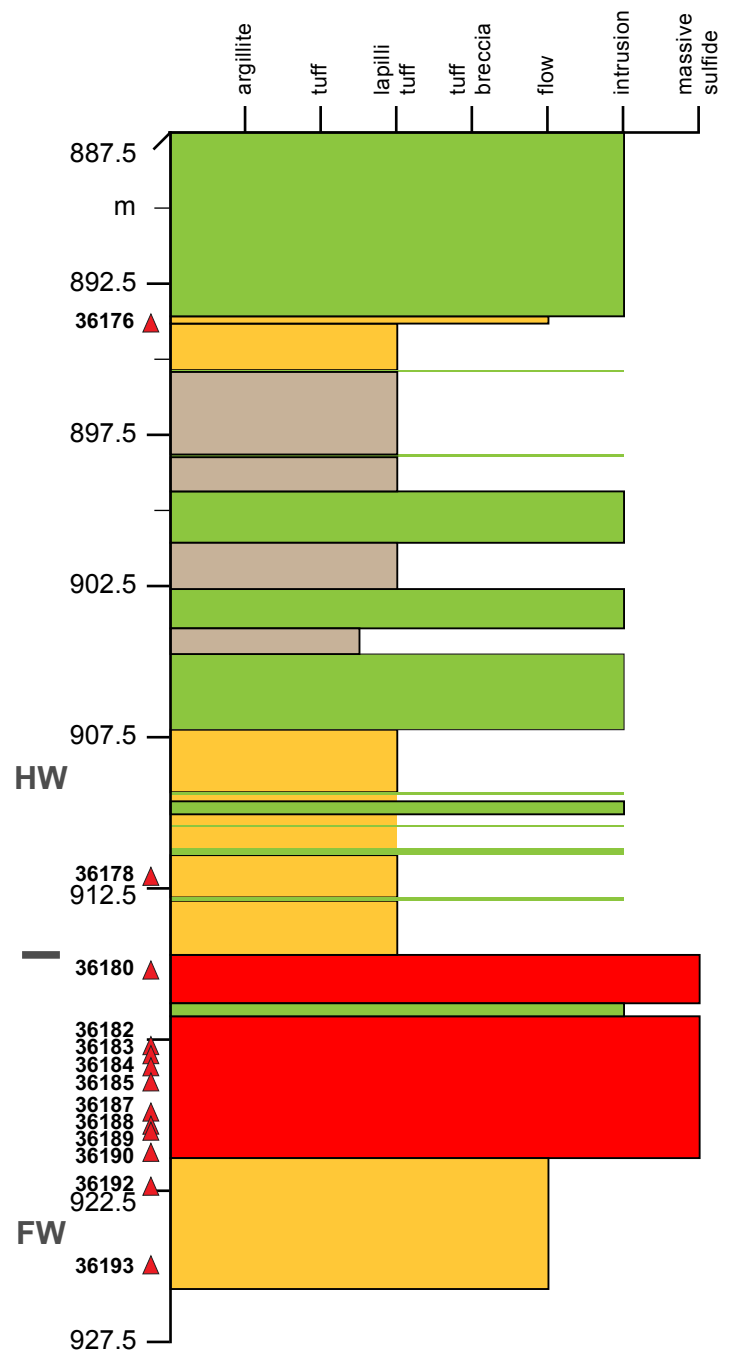
Fe oxide schlieren in quartz eye-bearing Rambler rhyolite (hanging wall). Schlieren are up to 5cm thick and run parallel to foliation

# Ming South Down Plunge

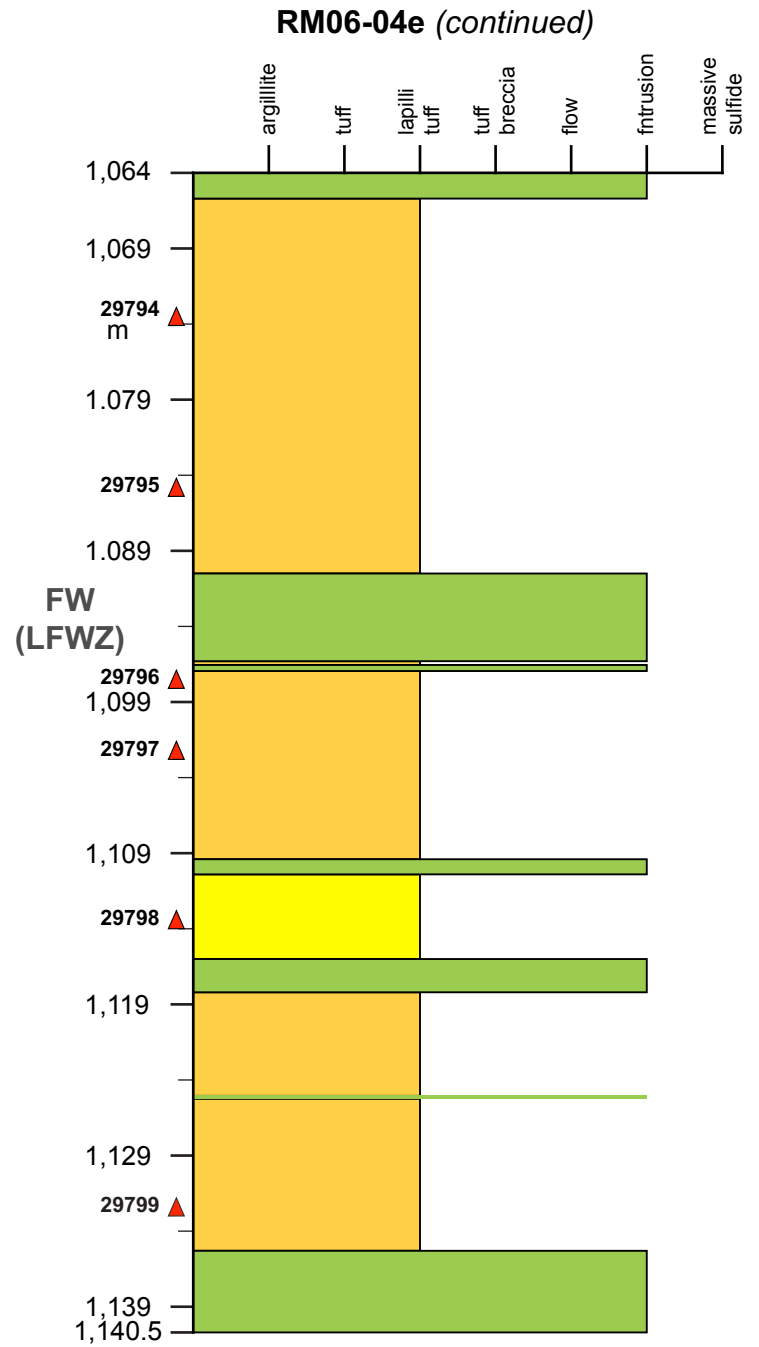
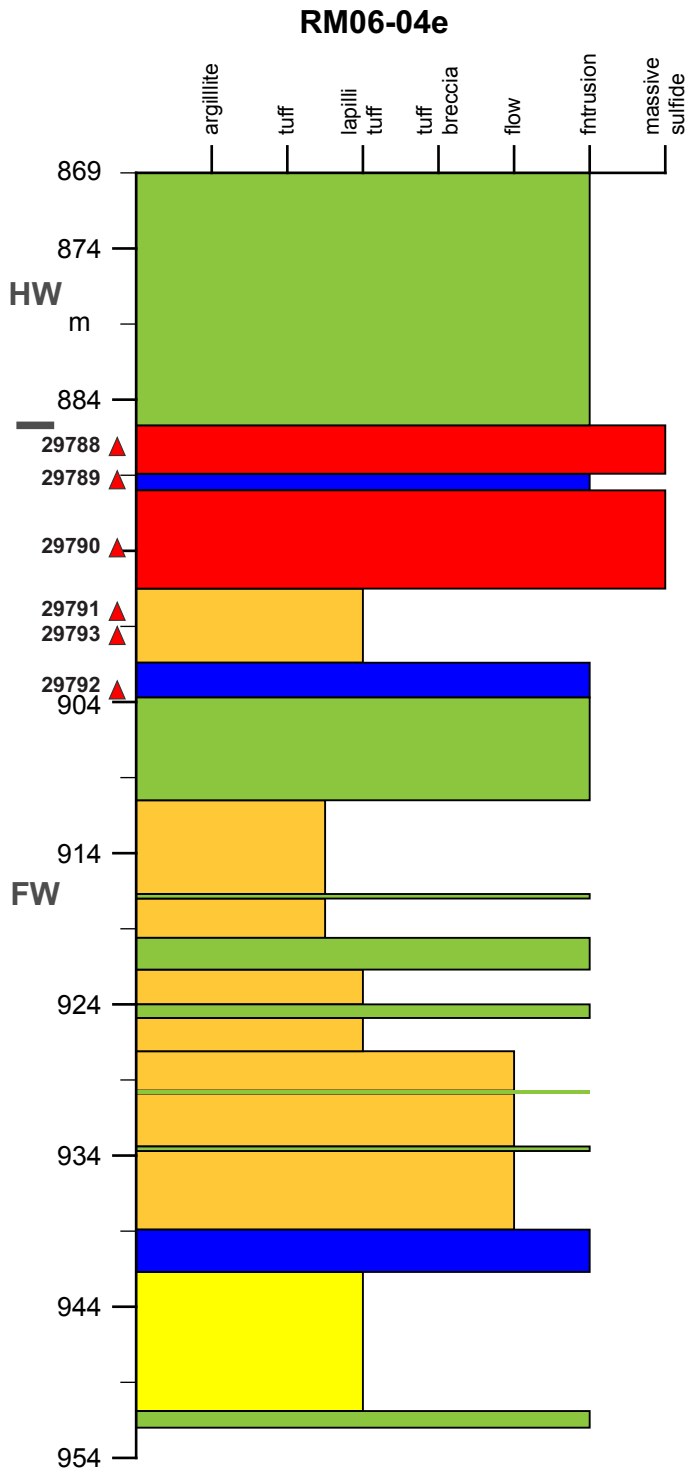
RM06-04d



RM06-04I

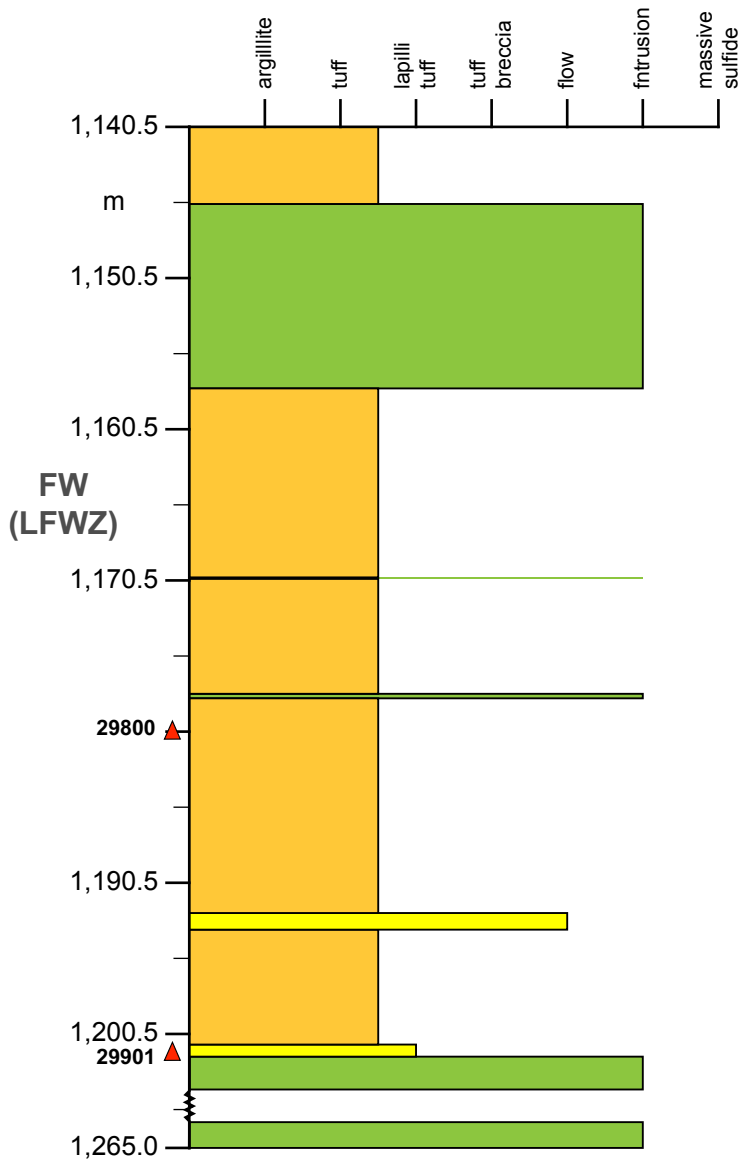


# Ming South Down Plunge and Lower Footwall Zone

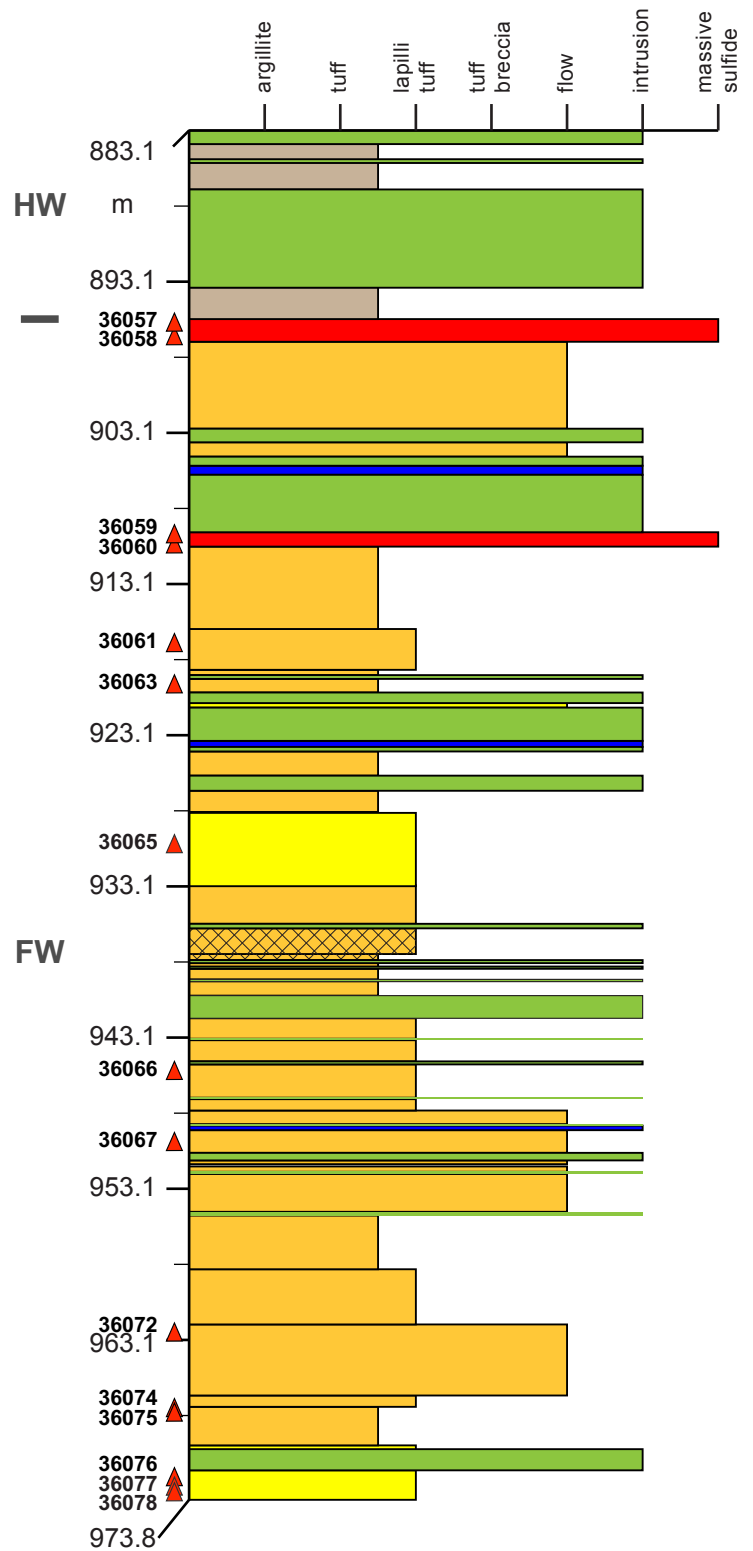


# Ming South Down Plunge and Lower Footwall Zone

**RM06-04e (continued)**

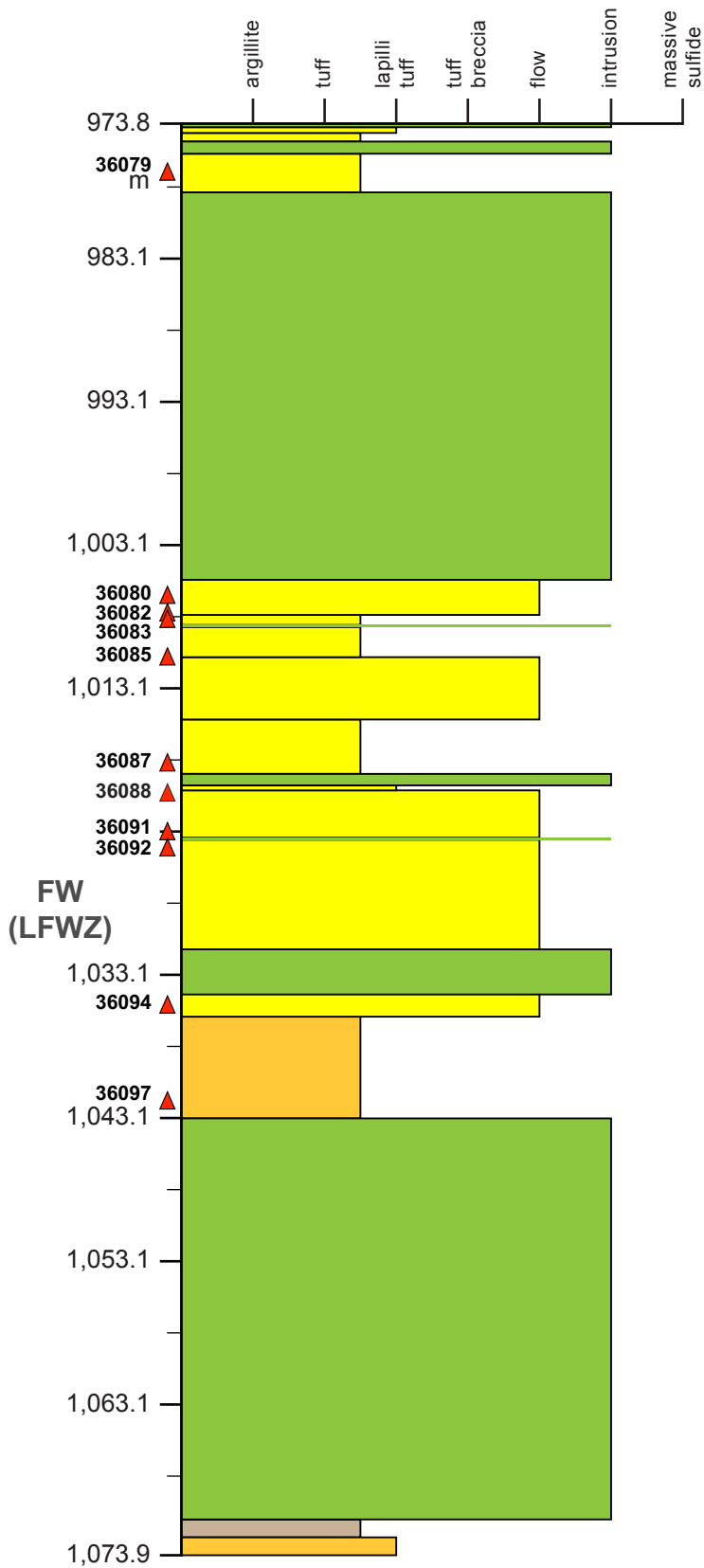


**RM06-04m**

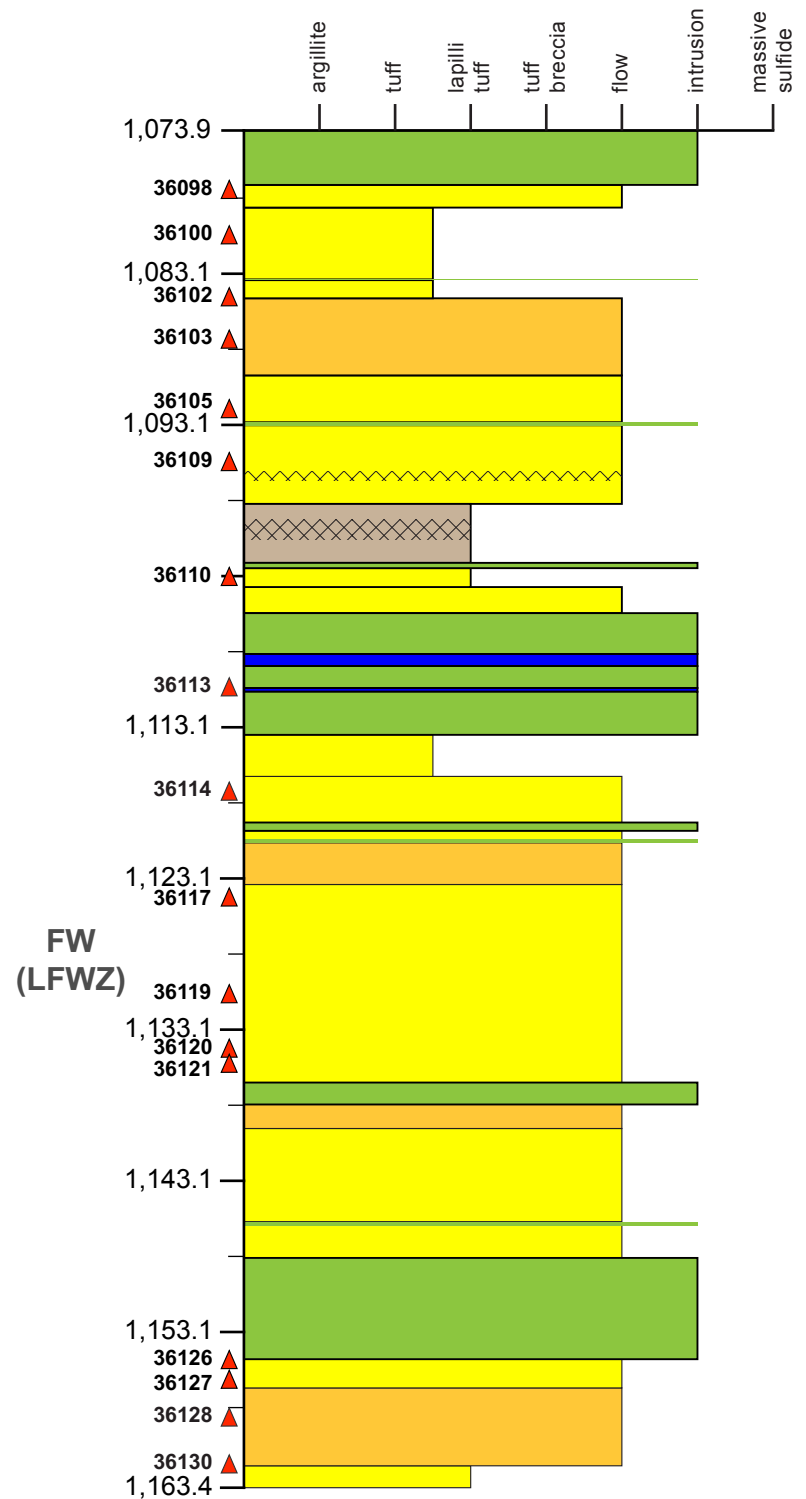


# Lower Footwall Zone

RM06-04m (continued)

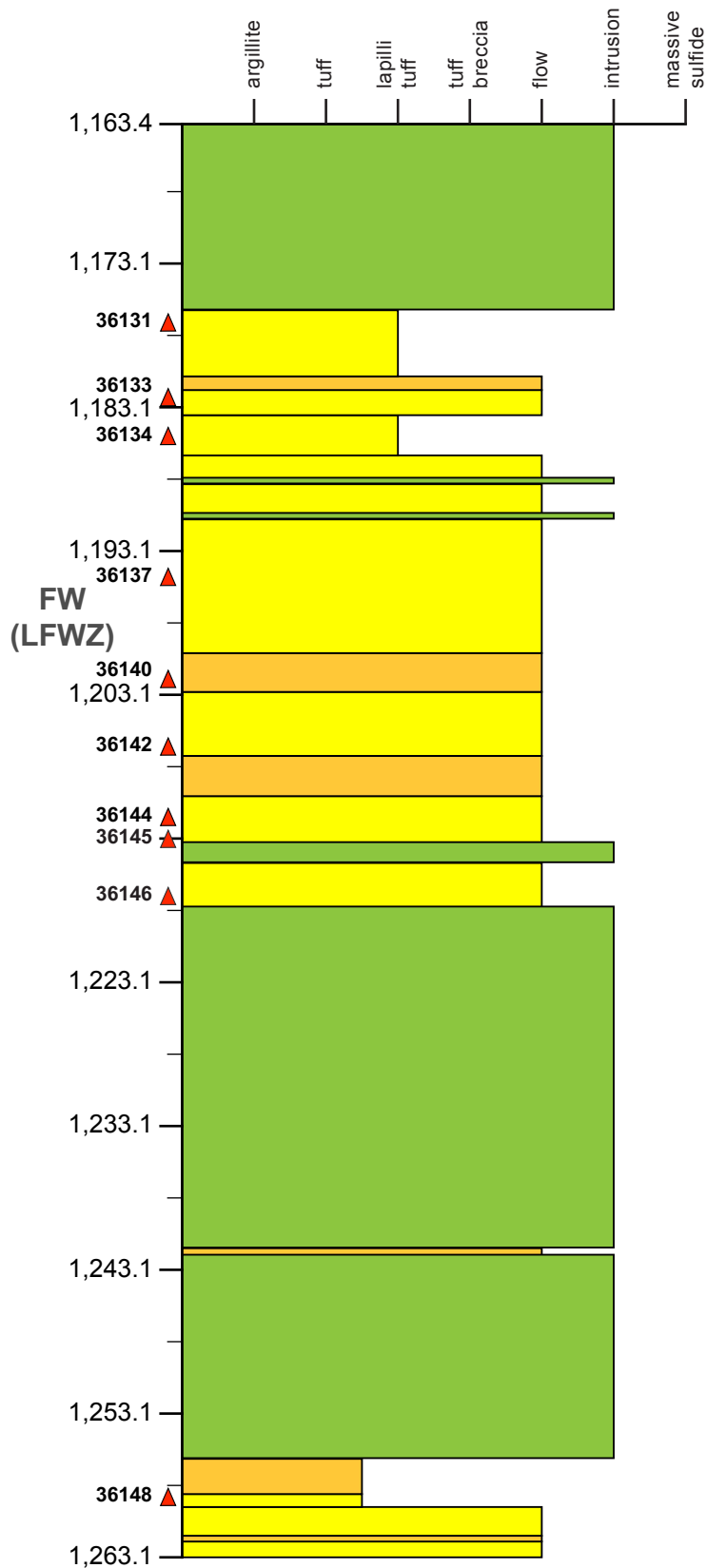


RM06-04m (continued)

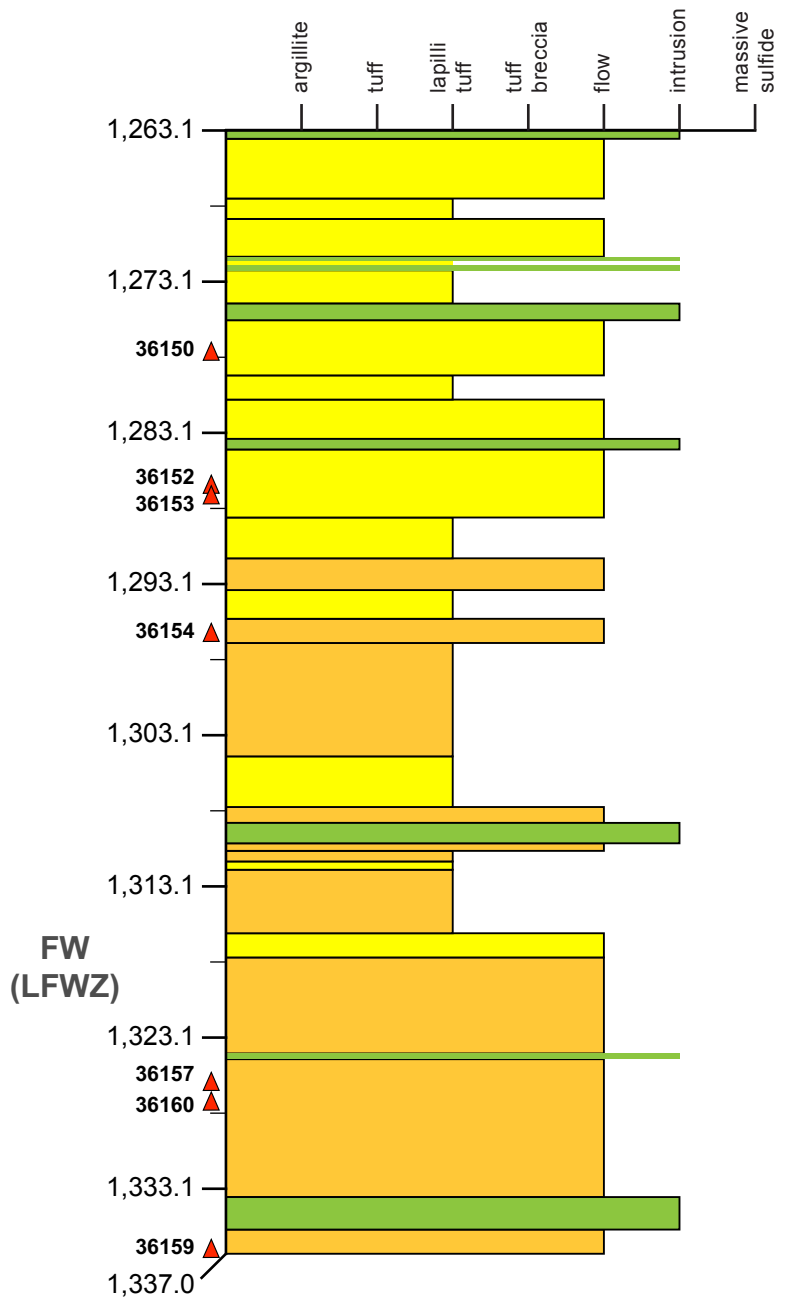


# Lower Footwall Zone

RM06-04m (continued)



RM06-04m (continued)





**Table eA3-1.** Detailed mineralogy of sulfide samples from the Ming deposit based on RL and partly SEM observations

<b>Abbreviation</b>	<b>Mineral</b>	<b>Chemical formula* **</b>	<b>common impurities*</b>
AgHg±Au	Ag-Hg±Au alloy	NA	
Ag-Tet	Ag-Tetrahedrite	(Cu, Ag, Fe, Zn) <sub>12</sub> Sb <sub>4</sub> S <sub>15</sub>	Pb, Zn, Fe, As
Allo	Alloclasite	(Co, Fe)AsS	
Alt	Altaite	PbTe	Ag, Au, Cu, Fe, S, Se
Asp	Arsenopyrite	FeAsS	Ag, Au, Co, Sn, Ni, Sb, Bi, Cu, Pb
BiTe	Tsumoite or unnamed Bi-telluride	BiTe or Bi <sub>3</sub> Te <sub>2</sub>	S, Se
Breit	Breithauptite	NiSb	
Cass	Cassiterite	SnO <sub>2</sub>	Fe, Ta, Nb, Zn, W, Mn, Sc, Ge, In, Sc, Ga
Cbn	Cubanite		
Ccp	Chalcopyrite	CuFeS <sub>2</sub>	Ag, Au, In, Ti, Sn, Te
Claus	Clausthalite	PbSe	
Col	Coloradoite	HgTe	Pb
El	Electrum	(Au, Ag)	
FeTiCrV ox	Fe±Ti±Cr±V oxides (magnetite,	Fe <sub>3</sub> O <sub>4</sub> , FeTiO <sub>3</sub> , TiO <sub>2</sub> , FeCr <sub>2</sub> O <sub>4</sub> ,	Mg, Zn, Mn, Ni, Cr, Ti, V, Al
Gn	Galena	PbS	Ag, Cu, Fe, Bi
Gud	Gudmundite	FeSbS or FeSb <sub>2</sub> S <sub>4</sub>	Ni or Mn, Cu, Pb, Ag
Hess	Hessite	Ag <sub>2</sub> Te	Pb, Cu, Fe, S, Au
Mag	Magnetite	Fe <sub>3</sub> O <sub>4</sub> , [Fe <sup>2+</sup> Fe <sup>3+</sup> O <sub>4</sub> ]	As, Fe
Men	Meneghinite	Pb <sub>13</sub> CuSb <sub>7</sub> S <sub>24</sub>	
Mia	Miargyrite	AgSbS <sub>2</sub>	
Mol	Molybdenite	MoS <sub>2</sub>	
NiSb	Breithauptite or Nisbite	NiSb or NiSb <sub>2</sub>	
Nis	Nisbite	NiSb <sub>2</sub>	Ni, Co, Cu
Po	Pyrrhotite	Fe <sub>(1-x)</sub> S	Ni, Co, As, Cu, Zn, Ag, Au, Ti, Se, V
Py	Pyrite	FeS <sub>2</sub>	As
Pyr	Pyargyrite	Ag <sub>3</sub> SbS <sub>3</sub>	
Sch	Scheelite	Ca(WO <sub>4</sub> ) <sub>4</sub>	
Sp	Sphalerite	ZnS	Mn, Cd, Hg, In, Ti, Ga, Ge, Sb, Sn, Pb, Ag
Stn	Stannite	Cu <sub>2</sub> (Fe, Zn)SnS <sub>4</sub>	Ag, Zn, Cd, In
Stp	Stephanite	Ag <sub>5</sub> SbS <sub>4</sub>	As, Cu, Fe

Ten	Tennantite	(Cu, Ag, Fe, Zn) <sub>12</sub> <b>As<sub>4</sub>S<sub>13</sub></b>	Sb, Bi, Pb
Tet	Tetrahedrite	(Cu, Ag, Fe, Zn) <sub>12</sub> <b>Sb<sub>4</sub>S<sub>14</sub></b>	Ag, Pb, Zn, Fe, As
Tsu	Tsumoite	<b>BiTe</b>	
Ulm	Ullmanite	<b>NiSbS</b>	Fe, Co, As, Bi
unknown phase		NA	
unnamed BiTe	unnamed Bi-telluride	<b>Bi<sub>3</sub>Te<sub>2</sub></b>	
Will	Willyamite	<b>(Ni, Co)SbS</b>	

\* Data from [www.mindat.org](http://www.mindat.org)

\*\* essential elements in **bold**

Color code	Mineral abundance	Abbreviation
stringer (hanging wall)	Major phase (> 10 vol%)	+++
silicified horizon	Minor phase (5-10 vol%)	++
semi-massive sulfide	Trace/accessory (> 5 vol%)	+
massive sulfide	Not observed	-
stringer (footwall)	questionable	?
LFWZ		
Qtz-vein		
FeOx rhy in hanging wall		

Table eA3-1. 1807 Zone (up plunge portion)

Drill hole	Sample No.	Mineralization style	Description	Comment	Depth_min [m]
RM07-19g	35551	stringer (footwall)	fine, ± brecciated Py-Ccp stringer in Qtz-eye flow or tuff to lap tuff	no SEM	600.40
RM07-19g	29949	semi-massive sulfide	semi-mass Py-Ccp sul in rhy flow	no SEM	596.45
RM07-19g	29950	semi-massive sulfide	semi-mass Ccp-Py-Po sul in rhy flow	SEM: myrmekitic intergrowth of Gn with BiTe	598.28
RM07-19e	35554	semi-massive sulfide	semi-mass Py-Ccp-Sp/Asp (?) sul in rhy, close to upper dyke contact	no SEM	594.09
RM07-19	29948	massive sulfide	massive Py-Ccp sulfide	myrmekite with Asp- Ccp-Sp-Tet/AgTet as inclusion in Py; myrmekitic intergrowth between Gn and BiTe	593.51
RM07-19c	35552	massive sulfide	massive Py-Ccp sulfide	El-bearing	592.07
RM07-19e	35553	massive sulfide	massive Py-Ccp sul with small silicic rhy fragments	no SEM	593.19
RM07-19a	35556	massive sulfide	massive Py sulfide	myrmekite of Asp-Ccp-El in Py and of Asp-Tet-Ccp in Py; El-bearing	597.19
RM07-19a	35555	stringer (hanging wall)	Ccp-Py stringer in felsic tuff	no SEM	595.42
RM07-19	29947	stringer (hanging wall)	Py-Ccp stringer in clast-bearing rhy flow	no SEM	591.70

<sup>1</sup> Gn commonly enriched with Se ± Te ± Bi

Depth_ max [m]	Mineral abundance	Py	Ccp	Cbn	Sp	Po	Asp	Gn1	Allo	Loel	Hess
600.44	<u>Ccp</u> >> Fe±Ti ox ≈ Py > Sp	+	+++	-	+	-	-	-	-	-	-
596.49	Py > Ccp >>> Sp > Fe±Ti ox	+++	+++	-	+	-	-	-	-	-	-
598.32	Py >>> Ccp > Po >>> Sp > TiO > Gn with BiTe > Asp	+++	+++	-	+	+	+	+	-	-	-
594.13	<u>Ccp</u> > Py >>> Sp > Fe±Ti ox ≈ Gn	+++	+++	-	+	-	-	+	-	-	-
593.54	Py >>> Ccp > Sp ≈ Po > Fe±Ti ox > Gn with BiTe ≈ Asp > Tet > AgTet > Gud ≈ Alt ≈ Men ≈ Cbn	+++	++	+	+	+	+	+	-	-	-
592.11	Py > Ccp >>> Sp > Asp ≈ TiO ≈ FeTiO > Gn > El > Po ≈ Cbn	+++	+++	+	+	-	+	+	-	-	-
593.23	<u>Ccp</u> >>> Py >>> Sp >>> Fe±Ti ox > Gn	++	+++	-	+	-	-	+	-	-	-
597.23	Py >>> Ccp >>> Sp > Asp > Mag ≈ Tet > Gn BiTe >>> Po ≈ El	+++	++	-	+	+	+	+	-	-	-
595.46	<u>Ccp</u> > Py >> Fe±Ti ox >>> Sp	+++	+++	-	+	-	-	-	-	-	-
591.74	Py > <u>Ccp</u> >>> Fe±Ti ox ≈ Po	+++	+++	-	-	+	-	-	-	-	-

BiTe	Alt	Col	Claus	Gud	Mol	NiSb	UII	Will	Men	Ten	Tet	Ag-Tet	Stn
-	-	-	-	-	-	-	-	-	-	-	-	-	-
-	-	-	-	-	-	-	-	-	-	-	-	-	-
+	-	-	-	-	-	-	-	-	-	-	-	-	-
-	-	-	-	-	-	-	-	-	-	-	-	-	-
+	+	-	-	+	-	-	-	-	+	-	+	+	-
-	-	-	-	-	-	-	-	-	-	-	-	-	-
-	-	-	-	-	-	-	-	-	-	-	-	-	-
+	-	-	-	-	-	-	-	-	-	-	+	-	-
-	-	-	-	-	-	-	-	-	-	-	-	-	-
-	-	-	-	-	-	-	-	-	-	-	-	-	-
-	-	-	-	-	-	-	-	-	-	-	-	-	-

Mia	Pyr	Stp	Ag-Hg±Au	Elec	Cass	FeTiCrV ox	Scheel	unknown phase
-	-	-	-	-	-	+(FeTi ox)	-	-
-	-	-	-	-	-	+(FeTi ox)	-	-
-	-	-	-	-	-	+(Ti ox)	-	-
-	-	-	-	-	-	-	-	-
-	-	-	-	-	-	+(Fe±Ti ox)	-	-
-	-	-	-	-	-	+(Ilm, TiO2)	-	-
-	-	-	-	-	-	+(Fe±Ti ox)	-	-
-	-	-	-	+	-	+(Mag)	-	-
-	-	-	-	-	-	+(Fe±Ti ox)	-	-
-	-	-	-	-	-	+(Fe±Ti ox)	-	-

Table eA3-1. 1807 Zone (mid plunge portion)

Drill hole	Sample No.	Mineralization style	Description	Comment	Depth_min [m]
RM07-18e	35568	semi-massive sulfide	thick Py-Ccp band with Py XX in semi-mass sul	no SEM	600.69
RM07-18e	35569	semi-massive sulfide	fine Ccp-Py-silvery phase stringer in Qtz-eye rhy flow of semi-mass sul	no SEM	601.09
RM07-18a	35557	massive sulfide	coarse mass Py-Ccp-Po sul, near upper contact	fine myrmekite with Ccp-Asp-Sp±Ten; El- and telluride-bearing	597.55
RM07-18a	35559	massive sulfide	mass Ccp-Py sul, Ccp around Py 'clasts' (replacement of former rhy clasts?)	fine myrmekite with Ccp-Asp-Sp-Gn-Ten-TellPy; El-bearing	598.85
RM07-18a	35561	massive sulfide	mass Py sul with Ccp schlieren/stringer, close to lower contact	no SEM	600.01
RM07-18b	35563	massive sulfide	mass Py-Ccp sul with Sp-Asp? Band with Py blasts between Py 'clasts' surrounded by Ccp	SEM; Telluride-bearing; myrmekitic intergrowth between Gn and	603.94
RM07-18b	35565	massive sulfide	mass Py-Ccp sul with Sp-Asp?-Ccp around Py 'clasts', similar texture as in 35563	no SEM	604.61
RM07-18b	35566	massive sulfide	mass Py-Ccp-Sp sul, Ccp-Sp around Py 'clasts'	SEM; Telluride-bearing; myrmekitic intergrowth between Gn and	605.46
RM07-18d	35567	massive sulfide	mass Py sul with Ccp schlieren/stringer and small Py XX	SEM; Telluride-bearing; myrmekitic intergrowth between Gn and	600.29

<sup>1</sup> Gn commonly enriched with Se ± Te ± Bi



Depth_ max [m]	Mineral abundance	Py	Ccp	Cbn	Sp	Po	Asp	Gn1	Allo	Loel	Hess
600.73	<b>Py &gt;&gt;&gt; Ccp &gt; Po &gt; Sp &gt;&gt;&gt; Gn ≈ Mag</b>	+++	++	—	+	+	—	+	—	—	—
601.13	<b>Py ≈ Ccp &gt;&gt;&gt; Po ≈ Sp &gt;&gt;&gt; Mag &gt; Gn</b>	+++	+++	—	+	+	—	+	—	—	—
597.59	<b>Ccp &gt; Py &gt;&gt;&gt; Sp ≈ Po &gt; Gn with BiTe &gt; Mag</b> > Asp > Ten-Tet > Alt ≈ El > Loel	+++	+++	—	+	+	+	+	—	+	—
598.89	<b>Py ≈ Ccp &gt;&gt;&gt; Sp &gt; Gn &gt; Asp &gt; Ten-Tet &gt; El &gt; Mag</b> Mag > Loel	+++	+++	—	+	—	+	+	—	+	—
600.05	<b>Py &gt;&gt;&gt; Ccp &gt; Po &gt; Sp &gt; Gn ≈ Mag</b>	+++	++	—	+	+	—	+	—	—	—
603.98	<b>Py &gt; Ccp &gt; Po &gt; Sp &gt; Cbn &gt; Gn with BiTe ≈</b> Asp >> Mag > Gud > NiSb	+++	+++	+	+	+	+	+	—	—	—
604.65	<b>Py &gt; Ccp &gt;&gt;&gt; Sp &gt; Asp &gt; Po &gt; Cbn ≈ Mag</b>	+++	+++	+	++	+	+	—	—	—	—
605.50	<b>Ccp &gt; Py &gt; Sp &gt; Po &gt; Cbn &gt;&gt;&gt; Asp &gt; Gn</b> with BiTe > Ten-Tet > AgTet > Hess ≈ NiSb ≈ Men > Scheel	+++	+++	+	++	++	+	+	—	—	+
600.34	<b>Py &gt;&gt;&gt; Ccp &gt; Sp &gt;&gt;&gt; Po &gt; Asp &gt; Gn with BiTe</b> > Tet > AgTet > Alt ≈ Gud > NiSb	+++	++	—	+	+	+	+	—	—	—

BiTe	Alt	Col	Claus	Gud	Mol	NiSb	Ull	Will	Men	Ten	Tet	Ag-Tet	Stn
-	-	-	-	-	-	-	-	-	-	-	-	-	-
-	-	-	-	-	-	-	-	-	-	-	-	-	-
+	+	-	-	-	-	-	-	-	-	+	+	-	-
-	-	-	-	-	-	-	-	-	-	+	+	-	-
+	-	-	-	-	-	-	-	-	-	-	-	-	-
+	-	-	-	+	-	+	-	-	-	-	-	-	-
-	-	-	-	-	-	-	-	-	-	-	-	-	-
+	-	-	-	-	-	+	-	-	+	+	+	+	-
+	+	-	-	+	-	+	-	-	-	-	+	+	-

Mia	Pyr	Stp	AgHg±Au	El	Cass	FeTiCrV ox	Scheel	unknown phase
-	-	-	-	-	-	+(Mag)	-	-
-	-	-	-	-	-	+(Mag)	-	-
-	-	-	-	+	-	+(Mag)	-	-
-	-	-	-	+	-	+(Mag)	-	-
-	-	-	-	-	-	+(Mag)	-	-
-	-	-	-	-	-	+(Mag)	-	-
-	-	-	-	-	-	+(Mag)	-	-
-	-	-	-	-	-	-	+	-
-	-	-	-	-	-	-	-	-

Table eA3-1. 1807 Zone (down plunge portion)

Drill hole	Sample No.	Mineralization style	Description	Comment	Depth_min [m]
RM07-20a	35574	stringer (footwall)	Py-Ccp stringer in rhy lap tuff	SEM	644.92
RM07-20e	35591	stringer (footwall)	mass Py sul with Ccp and mm-large cubic Py XX in Qtz-eye rhy flow on lower contact	no SEM	666.40
RM07-20g	35600	stringer (footwall)	fine Py-Ccp stringer in mas Qtz-eye rhy flow	no SEM	660.63
RM07-20	35570	semi-massive sulfide	Ccp stringer and diss Ccp in mass rhy of semi-mass sul	no SEM	657.84
RM07-20a	35572	semi-massive sulfide	Ccp-Py stringer and diss Py-Ccp in semi-mass sul	no SEM	643.06
RM07-20a	35573	semi-massive sulfide	mass Py-Ccp sul in semi-mass sul, on lower contact	no SEM	643.53
RM07-20c	35582	semi-massive sulfide	Py-Ccp stringer in Qtz-eye lap tuff of semi-mass sul	no SEM; Telluride-bearing; myrmekitic intergrowth between Gn and BiTe	665.54
RM07-20i	36017	semi-massive sulfide	diss Ccp-py in semi-mass ul, near upper contact	no SEM; weak Py replacement by Po	654.47
RM07-20i	36018	semi-massive sulfide	mass Ccp stringer with Py-Po in semi-mass sul	no SEM	654.76
RM07-20	35571	massive sulfide	coarse, mass Ccp-Py-Po sul	no SEM	657.98
RM07-20b	35575	massive sulfide	mass Py-Ccp sul with coarse Py and rhy clasts	SEM	665.93
RM07-20b	35577	massive sulfide	mass Py-Ccp sul with coarser Py XX	SEM	667.17
RM07-20b	35580	massive sulfide	mass Py sul with Ccp schlieren/stringer	no SEM	670.28
RM07-20c	35583	massive sulfide	mass Py-Ccp sul	no SEM	665.77
RM07-20c	35584	massive sulfide	mass Ccp-Py-Po sul on lower contact and affected by intercalated md above	SEM; El-bearing; Telluride-bearing; myrmekitic intergrowth between Gn and BiTe-Hess	666.30
RM07-20e	35585	massive sulfide	mass Py-Ccp sul with Po and silicic rhy fragments, close to upper contact	no SEM	659.80
RM07-20e	35586	massive sulfide	mass Py sul with small Py XX and minor Ccp	SEM; Telluride-bearing; myrmekitic intergrowth between Gn and BiTe-Hess	660.17
RM07-20e	35588	massive sulfide	mass Py-Ccp-Sp sul(Ccp-Sp $\pm$ brecciated around Py)	no SEM	661.48
RM07-20e	35590	massive sulfide	mass Py sul with fine Sp-Ccp bands and small Py XX	SEM; Telluride-bearing; myrmekitic intergrowth between Gn and BiTe-Hess	662.18
RM07-20g	35592	massive sulfide	mass Py-Ccp-Sp sul, near lower contact to intercalated md	no SEM; Telluride-bearing; myrmekitic intergrowth between Gn and BiTe-Alt	654.12
RM07-20g	35593	massive sulfide	mass Py sul with coarse Py XX and fine sp	no SEM	655.93
RM07-20g	35595	massive sulfide	mass Ccp-Sp-Py sul, on lower contact to intercalated md	no SEM	657.32
RM07-20g	35596	massive sulfide	mass Py-Ccp sul with Sp-Asp/Tet (?) stringer/band	SEM; Telluride-bearing; myrmekitic intergrowth between Gn and BiTe-Hess	658.64
RM07-20g	35597	massive sulfide	mass Py sul with weak Ccp-Sp stringer	SEM; myrmekite of Asp-Ccp-Sp on Po; El- and AgHgAu alloy-bearing; Telluride-bearing; myrmekitic intergrowth between Gn and BiTe-Hess	659.38
RM07-20h	36001	massive sulfide	mass Py sul with Po band and minor Ccp, close to upper contact	no SEM; Telluride-bearing; myrmekitic intergrowth between Gn and BiTe	655.35
RM07-20h	36002	massive sulfide	mass Py-Ccp-Po sul with rhy fragments	no SEM; Telluride-bearing; myrmekitic intergrowth between Gn and BiTe	655.60
RM07-20h	36004	massive sulfide	mass Py sul with Ccp stringer and Po band	no SEM	656.68
RM07-20h	36005	massive sulfide	mass Ccp sul with Py-Sp and rhy fragments	SEM; myrmekite of Asp-AgTet-Ccp in Ccp; Telluride-bearing; myrmekitic intergrowth between Gn and BiTe-Alt	657.72

Depth_ max [m]	Mineral abundance	Py	Ccp	Cbn	Sp	Po	Asp	Gn1	Allo	Loel	Hess
644.96	<u>Py &gt; Mag &gt; Po &gt; Ccp &gt;&gt; Asp ≈ Sp &gt; Gn</u>	+++	+	-	+	++	+	+	-	-	-
666.44	<u>Py &gt; Sp &gt; Ccp &gt; Po &gt;&gt; Mag &gt; Asp</u>	+++	++	-	+++	+	+	-	-	-	-
660.67	<u>Ccp &gt; Py &gt;&gt; Sp &gt; Asp</u>	+++	+++	-	+	-	+	-	-	-	-
657.88	<u>Ccp &gt;&gt; Py &gt; Po &gt; Sp</u>	+	+++	-	+	+	-	-	-	-	-
643.10	<u>Py &gt;&gt; Ccp &gt;&gt; Po &gt; Fe±Ti ox ≈ Sp</u>	+++	+++	-	+	+	-	-	-	-	-
643.57	<u>Py &gt;&gt; Ccp &gt;&gt; Sp &gt; Po</u>	+++	+	-	+	+	-	-	-	-	-
665.58	<u>Py &gt;&gt; Ccp &gt; Sp ≈ Mag &gt; Po &gt; Gn with BiTe</u>	+++	++	-	+	+	-	+	-	-	-
654.51	<u>Py &gt; Ccp &gt;&gt; Po &gt; Sp &gt; Gn</u>	+++	+++	-	+	++	-	+	-	-	-
654.80	<u>Ccp &gt;&gt; Po &gt; Py &gt; Sp ≈ Asp</u>	+	+++	-	+	++	+	-	-	-	-
658.02	<u>Ccp &gt;&gt; Py &gt; Po &gt;&gt; Fe±Ti ox &gt; Sp &gt; Cbn</u>	++	+++	+	+	+	-	-	-	-	-
665.97	<u>Py &gt;&gt; Ccp ≈ Sp &gt; Po &gt; Asp &gt; Gn with BiTe &gt; Mag</u>	+++	+	-	+	+	+	+	-	-	-
667.21	<u>Py &gt;&gt; Sp &gt; Ccp &gt; Gn &gt; Po</u>	+++	+	-	+	+	-	+	-	-	-
670.32	<u>Py &gt; Ccp &gt;&gt; Sp &gt; Po &gt;&gt; Gn ≈ Asp</u>	+++	+++	-	+	+	+	+	-	-	-
665.81	<u>Py &gt;&gt; Ccp &gt; Sp &gt; Mag ≈ Po &gt; Gn</u>	+++	+	-	+	+	-	+	-	-	-
666.34	<u>Ccp &gt; Py &gt; Po &gt; Sp &gt;&gt; Gn with BiTe &gt; Hess &gt; Ti ox &gt; El</u>	+++	+++	-	+	++	-	+	-	-	+
659.84	<u>Py &gt;&gt; Ccp &gt; Po &gt; Sp &gt; Asp &gt; Gn</u>	+++	++	-	+	+	+	+	-	-	-
660.21	<u>Py &gt; Ccp &gt;&gt; Sp &gt; Mag &gt; Gn with BiTe &gt; Asp &gt; Po &gt; Hess &gt; Scheel</u>	+++	+++	-	+	+	+	+	-	-	+
661.52	<u>Py &gt; Ccp &gt; Po &gt; Sp &gt; Asp</u>	+++	+++	-	+	++	+	-	-	-	-
662.22	<u>Py &gt; Ccp &gt; Sp &gt; Po &gt; Asp ≈ Mag &gt; Gn with BiTe &gt; Hess &gt; NiSb ≈ Ten</u>	+++	+++	-	+	+	+	+	-	-	+
654.16	<u>Py &gt; Sp &gt;&gt; Ccp &gt; Po ≈ Gn with BiTe &gt; Alt</u>	+++	++	-	+++	+	-	+	-	-	-
655.97	<u>Py &gt;&gt; Ccp &gt;&gt; Sp &gt; Asp &gt; Gn</u>	+++	++	-	+	-	+	+	-	-	-
657.36	<u>Py &gt; Ccp &gt; Sp &gt; Asp &gt; Po &gt; Mag &gt; Gn</u>	+++	+++	-	++	+	+	+	-	-	-
658.68	<u>Py &gt; Ccp ≈ Sp &gt; Po &gt; Asp ≈ Gn with BiTe &gt; Hess ≈ Gud ≈ NiSb</u>	+++	+++	-	+++	+	+	+	-	-	+
659.42	<u>Py &gt; Ccp &gt; Sp &gt; Po &gt; Asp &gt; Mag &gt; Gn with BiTe &gt; Gud &gt; Hess ≈ El ≈ AgHg±Au</u>	+++	+++	-	+++	+	+	+	-	-	+
655.39	<u>Py &gt; Ccp &gt; Po ≈ Sp &gt; Asp &gt; Gn with BiTe</u>	+++	+++	-	++	++	+	+	-	-	-
655.64	<u>Ccp &gt; Py &gt; Po &gt; Sp &gt; Asp &gt; Gn &gt; BiTe</u>	+++	+++	-	++	++	+	+	-	-	-
656.72	<u>Py &gt; Ccp &gt; Po &gt; Sp &gt; Asp &gt; Mag</u>	+++	+++	-	++	++	+	-	-	-	-
657.76	<u>Ccp &gt; Sp &gt;&gt; Py &gt; Asp &gt; Po ≈ Gn with BiTe &gt; Alt ≈ AgTet &gt; NiSb</u>	++	+++	-	+++	+	+	+	-	-	-

[illegible]

[illegible]

RM07-20h	36007	massive sulfide	mass sul with Py 'clasts' with Ccp around, El ?	SEM: El with NiSb phase; Telluride-bearing; myrmekitic intergrowth between Gn and BiTe-Hess	658.16
RM07-20h	36010	massive sulfide	mass Py sul with Ccp stringer + Sp around Py 'clasts'	SEM: Telluride-bearing; myrmekitic intergrowth between Gn and BiTe-Hess-Alt-Claus SEM	659.91
RM07-20h	36012	massive sulfide	mass Py sul with Ccp-Sp stringer, close to lower contact to intercalated md	no SEM	660.95
RM07-20h	36013	massive sulfide	mass Ccp sul with Py, on upper conatct and small dyke	no SEM	663.04
RM07-20h	36015	massive sulfide	mass Py-Ccp sul with Sp-Po, close to upper contact of intercalated md	SEM: Telluride-bearing; myrmekitic intergrowth between Gn and BiTe-Hess	664.32
RM07-20j	36019	massive sulfide	mass Py sul with small Py XX, minor Ccp ?, near upper contact	SEM: Telluride-bearing; myrmekitic intergrowth between Gn and tellurides	652.89
RM07-20j	36020	massive sulfide	mass Py sul with Ccp stringer, Po and rhy fragments	SEM: myrmekite of Asp-Ccp-Tet±Sp±Gn in Sp or Ccp; Telluride-bearing; myrmekitic intergrowth between Gn and BiTe	653.95
RM07-20j	36022	massive sulfide	mass Py sul, near upper contact to intercalated md	no SEM	655.03
RM07-20g	35599	Qtz-vein directly below mass sul	coarse Ccp in Qtz vein	no SEM	660.08
RM07-20c	35581	stringer (hanging wall)	Py stringer in felsic lap tuff	no SEM	665.08

<sup>1</sup> Gn commonly enriched with Se ± Te ± Bi



658.20	<u>Ccp &gt; Py &gt; Sp &gt; Po &gt; Asp &gt; Gn with BiTe &gt; Cbn &gt; Mag ≈ Hess ≈ NiSb ≈ Ull ≈ Will ≈ AgTet &gt; Men ≈ El</u>	+++	+++	+	++	++	++	+	+	+	+	-	-	+
659.95	<u>Ccp &gt; Py &gt; Sp &gt; Po &gt; Gn with BiTe &gt; Asp ≈ Mag &gt; Allo ≈ Hess &gt; Alt ≈ Claus</u>	+++	+++	-	++	++	++	+	+	+	+	+	-	+
660.99	<u>Py &gt; Ccp &gt; Sp &gt;&gt; Po ≈ Mag &gt; Cbn &gt; Asp ≈ Gn</u>	+++	+++	+	++	++	++	+	+	+	+	-	-	-
663.08	<u>Py &gt; Ccp &gt; Sp &gt; Po &gt; Cbn &gt;&gt; Mag &gt; Gn &gt; NiSb</u>	+++	+++	+	+++	+++	+++	+	-	+	+	-	-	-
664.36	<u>Py &gt; Ccp &gt; Sp &gt; Po &gt; Gn with BiTe &gt; Mag &gt; Hess</u>	+++	+++	-	+++	+++	+++	+	-	+	+	-	-	+
652.93	<u>Py &gt; Ccp &gt;&gt; Sp &gt; Gn ≈ Po ≈ Asp &gt; BiTe &gt; Hess</u>	+++	++	-	+	+	+	+	+	+	+	-	-	+
653.99	<u>Py &gt;&gt; Ccp &gt; Sp &gt; Asp &gt; Gn with BiTe &gt; Tet</u>	+++	+++	-	+	+	+	+	+	+	+	-	-	-
655.07	<u>Py &gt; Ccp &gt;&gt; Sp &gt; Asp &gt; Mag ≈ Po &gt; Gn</u>	+++	+++	-	+	+	+	+	+	+	+	-	-	-
660.12	<u>Ccp &gt; Sp ≈ Po &gt; Asp</u>	-	+++	-	++	++	++	+	+	-	-	-	-	-
665.12	<u>Py &gt;&gt; Ccp &gt; Po &gt; Sp ≈ Fe±Ti ox &gt; Asp &gt; Gn</u>	+++	+	-	+	+	+	+	+	+	+	-	-	-

+										
						+				
+										
+										
+										
+			+							
	+									
	+									
+	+			+	+	+				

[illegible]

Table eA3-1. 1807 Zone (underground sulfide samples)

Level feet - metres below sealevel	wall	Sample No.	Mineralization style	Description	Comment
1600 - 375	left wall	62006	Quartz vein	contact Quartz vein – massive sulfide lense - mafic dyke	no SEM; mafic dike has strong chlorite alteration and modest calcite and epidote alteration
1600 - 375	left wall	62002	massive sulfide	massive sulfide on eastern contact to sheared mafic dyke	no SEM
1600 - 375	left wall	62004	massive sulfide	contact sheared mafic dyke - western sulfide lense - rhyolite	no SEM
1600 - 375	left wall	62008	massive sulfide	massive sulfide near sheared mafic dyke, NE dipping and ± horizontal running	no SEM; telluride bearing; myrmekitic intergrowth between Gn and BiTe
1600 - 375	right wall	62010	massive sulfide	massive Py-Ccp sulfide with rhy fragments close to mafic dyke; 62010 + 62011 one sample for WR metal	no SEM
1600 - 375	right wall	62014	massive sulfide	mid-part of massive Py-Ccp sulfide limited by sheared mafic dyke	no SEM
2000 - 469	right wall	62153	massive sulfide	massive Py-Ccp sulfide with Po or Sp schlieren, on contact to md or rhy?	no SEM; Sp bands
2000 - 469	right wall	62154	massive sulfide	massive Py-Ccp sulfide with Po or Sp	no SEM; Sp and Po schlieren
2000 - 469	right wall	62156	massive sulfide	massive Py-Ccp sulfide with Sp schlieren	no SEM; EI bearing; weak myrmekite in Tnt-Trt of Asp-Cop-TT-Sp-EI
2000 - 469	right wall	62157	massive sulfide	massive Py-Ccp sulfide with Po or Sp	no SEM; Sp bands and Po schlieren
2000 - 469	right wall	62158	massive sulfide	massive Py-Ccp sulfide with Po or Sp	no SEM; patches of Sp between recrystallized Py
2000 - 469	right wall	62159	massive sulfide	massive Py-Ccp sulfide with Po or Sp, near rhy fragment and dyke of unknown composition	no SEM
2000 - 469	right wall	62162	massive sulfide	massive Py-Ccp sulfide with Po or Sp on mafic dyke clast	no SEM; Sp bands

<sup>1</sup> Gn commonly enriched with Se ± Te ± Bi

<sup>2</sup> Gn not visible at RL\_ but likely sub-microscopically visible as tiny roundish crystals marginal on Pv at SEM

Distance from start [m]	Height from ground [m]	Mineral abundance	Py	Ccp	Cbn	Sp	Po	Asp	Gn <sup>1</sup>	Allo
6.6	1.5	Ccp > Py > Mag	+	+++	—	—	—	—	2	—
2.5	1.5	Py >>> Ccp > Mag > Sp	+++	+	—	+	—	—	+	—
4.1	1.5	Py >>> Ccp > Mag > Gn ≈ Sp	+++	+	—	+	—	—	2	—
> 24	≈ 1.8	Py > Ccp >>> Sp > Mag > Ten-Tet > Gn with BiTe	+++	++	—	+	—	—	+	—
≈ 17	0.5	Py > Ccp > Sp ≈ Mag	+++	++	—	+	—	—	2	—
> 19	N/A	Py > Ccp > Sp ≈ Asp	+++	++	—	+	—	+	2	—
2.7	1.1	Py > Ccp > Sp > Asp ≈ Po > Gn	+++	++	—	++	+	+	+	—
3.6	1.4	Ccp > Py >>> Sp ≈ Po > Asp > Mag	+++	+++	—	++	++	++	2	—
6.0	1.4	Py > Ccp > Sp > Asp > Mag >> Ten-Tet > Gn > El	+++	++	—	++	—	++	+	—
9.0	0.1	Ccp ≈ Py > Sp > Po > Asp > Mag	+++	+++	—	++	++	+	2	—
10.0	1.3	Py > Sp > Ccp > Asp	+++	+	—	++	—	+	2	—
14.5	2.0	Py > Ccp >>> Sp > Po ≈ Asp	+++	++	—	+	+	+	2	—
17.6	0.8	Py > Ccp ≈ Sp > Po	+++	++	—	++	+	—	2	—

22

Ag-Tet	Stn	Mia	Pyr	Stp	AgHg±Au	El	Cass	FeTiCrV ox	Scheel	unknown phse
-	-	-	-	-	-	-	-	+ (Mag)	-	-
-	-	-	-	-	-	-	-	+ (Mag)	-	-
-	-	-	-	-	-	-	-	+ (Mag)	-	-
+ (?)	-	-	-	-	-	-	-	+ (Mag)	-	-
-	-	-	-	-	-	-	-	+ (Mag)	-	-
-	-	-	-	-	-	-	-	-	-	-
-	-	-	-	-	-	-	-	-	-	-
-	-	-	-	-	-	-	-	-	-	-
-	-	-	-	-	-	-	-	+ (Mag)	-	-
+ (?)	-	-	-	-	-	+	-	+ (Mag) + (Mag)	-	-
-	-	-	-	-	-	-	-	+ (Mag)	-	-
-	-	-	-	-	-	-	-	-	-	-
-	-	-	-	-	-	-	-	-	-	-
-	-	-	-	-	-	-	-	-	-	-
-	-	-	-	-	-	-	-	-	-	-

Table eA3-1.1806 Zone section 21 (up plunge portion)

Drill Hole	Sample No	Mineralization style	Description	Comment	Depth_ min [m]	Depth_ max [m]
RMUG08-121	29902	stringer	Py-Ccp stringer in rhyolite flow (Au-bearing)	myrmekitic like tex of Asp-Ccp-Tet/ten ±Sp in Tet; El-bearing	46.39	46.44
RMUG08-121	29903	stringer	Ccp-Py stringer in rhyolite flow		46.51	46.56
RMUG08-124	29910	stringer	sulfide stringer (Py+Sp) in rhyolite		40.78	40.83
RMUG08-124	29911	semi-massive sulfide	sulfide stringer (Py+Sp; semi-massive) in rhyolite		48.60	48.65
RMUG08-124	29912	semi-massive sulfide	sulfide stringer (Py+Sp+Ccp; semi-massive) in rhyolite		49.13	49.18
RMUG08-124	29913	semi-massive sulfide	Ccp-Py stringer in rhyolite (end of semi-massive zone)	El-bearing	50.50	50.55
RMUG08-125	36517	semi-massive sulfide	Py-sph-cpy-asy sulfide		52.09	52.13
RMUG08-125	36516	massive sulfide	Ga-sph-cpy-rich sulfide with sulfosalts		49.56	49.61
RMUG08-125	36518	massive sulfide	Py-sph-asy-cpy sulfide	myrmekitic like tex of Asp-Ccp-Tet/ten ±Sp in Tet	54.26	54.29
RMUG08-125	36519	massive sulfide	Py-asy-py-tetra sulfide	El-bearing	55.28	55.33
RMUG08-120	36507	massive sulfide	Sph-py-sulfosalt sulfides		54.20	54.24
RMUG08-120	36508	massive sulfide	Py-rich sulfide with aspy-tetra-cpy; Au-rich zone	El-bearing	55.88	55.93
RMUG08-120	36509	massive sulfide	Py-asy-py-tetra with black material in py-rich sulfide.	El-bearing	56.48	56.52
RMUG08-120	36510	massive sulfide	Py-asy-cpy sulfide; py>>asy-cpy		59.61	59.65
RMUG08-120	36511	massive sulfide	Ga-sph-chl-rich sulfide	El-bearing	60.22	60.25
RMUG08-123	36512	massive sulfide	Sph-ga-rich sulfide	El-bearing	59.48	59.53
RMUG08-123	36513	massive sulfide	Py-cpy-rich sulfide; Au-rich zone	El-bearing	63.09	63.14
RMUG08-123	36514	massive sulfide	Py-sulfosalt-ga sulfides	El-bearing	63.54	63.59
RMUG08-123	36515	contact massive sulfide- silicified horizon	Cpy-py-asy sulfide	El-bearing	63.63	63.67
RMUG08-150	29914	stringer	fine Ccp-Py stringer in silicified horizon (massive Qtz) above stringer zone		65.67	65.72
RMUG08-150	29915	stringer	stringer (Py+minor Ccp) in silicified horizon (massive Qtz)		67.13	67.18



Mineral abundance	Py	Ccp	Cbn	Sp	Po	Asp	Gn	Allo	Loel	Hess
<u>Py &gt; Ccp &gt;&gt; Asp &gt; Sp &gt; Gn &gt; Tet &gt; Ten &gt; AgTet &gt; El</u>	+++	+++	-	++	-	++	+	-	-	-
<u>Py &gt; Ccp &gt;&gt; Asp &gt; Sp &gt;&gt; Gn &gt; Tet &gt; Ten</u>	+++	++	-	+	-	+	+	-	-	-
<u>Py &gt;&gt; Sp &gt;&gt; Gn &gt; Ccp &gt; Asp &gt; AgTet ≈ Men &gt; Tet</u>	+++	+	-	++	-	+	+	-	-	-
<u>Py &gt;&gt; Sp &gt;&gt; Ccp ≈ Asp &gt; Gn &gt; Tet &gt;&gt; Po</u>	+++	++	-	++	+	++	+	-	-	-
<u>Py &gt; Sp &gt; Ccp &gt;&gt; Asp &gt; Gn &gt; Tet ≈ Ten &gt; AgTet &gt; Po</u>	+++	+++	-	+++	+	+	+	-	-	-
<u>Ccp &gt; Py &gt; Po &gt;&gt; Sp &gt; Asp &gt; Gn &gt; El &gt; Mia &gt; Men</u>	+++	+++	-	++	++	+	+	-	-	-
<u>Sp &gt; Py &gt;&gt; Ccp &gt; Gn &gt; Asp</u>	+++	+	-	+++	-	+	+	-	-	-
<u>Sp &gt; Py ≈ Gn &gt;&gt; Ccp &gt;&gt; Asp</u>	+++	++	-	+++	-	+	+++	-	-	-
<u>Py &gt; Sp &gt; Ten &gt; Gn &gt; Asp &gt; Ccp ≈ Tet &gt; AgTet ≈ AgHg alloy</u>	+++	+	-	+++	-	+	+	-	-	-
<u>Py &gt;&gt; Ccp &gt; Tet ≈ Gn &gt; Sp ≈ Ten &gt; Asp &gt; AgTet &gt; Stn &gt; El &gt; Cass ≈ unnamed</u>	+++	+	-	+	-	+	+	-	-	-
<u>Py &gt; Sp &gt;&gt; Ccp &gt; Gn &gt; Asp &gt; Stn</u>	+++	+	-	+++	-	+	+	-	-	-
<u>Py &gt;&gt; Asp &gt; Ccp ≈ Sp &gt; Gn &gt; Tet &gt; El ≈ AgTet ≈ Ten ≈ AgCuFeS ≈ AgHg±Au</u>	+++	+	-	+	-	++	+	-	-	-
<u>Py &gt; Tet &gt; AgTet &gt; Asp &gt;&gt; Sp &gt; Ten &gt; Gn &gt; Ccp &gt; El &gt; unknown Ag phase</u>	+++	+	-	++	-	+++	+	-	-	-
<u>Py &gt; Gn &gt;&gt; Ccp &gt; Asp &gt; Tet &gt; Sp &gt; AgTet</u>	+++	+	-	+	-	+	+++	-	-	-
<u>Py &gt; Gn &gt;&gt; Ccp &gt; Sp ≈ Tet ≈ Ten &gt; AgTet &gt; Asp &gt; El</u>	+++	+	-	+	-	+	+++	-	-	-
<u>Sp ≈ Gn &gt; Py &gt;&gt; Ccp ≈ Asp &gt; Stn &gt; Pyr &gt; Stp &gt; AgCuFeS &gt; AgTet &gt; El</u>	+++	+	-	+++	-	+	+++	-	-	-
<u>Py &gt;&gt; Ccp &gt; Asp ≈ Gn &gt; Tet &gt; Sp &gt;&gt; El ≈ AgTet ≈ AgCuFeS phase</u>	+++	++	-	+	-	+	+	-	-	-
<u>Py &gt; Gn &gt;&gt; Tet ≈ AgTet &gt; Sp ≈ Ten ≈ Ccp &gt; Asp &gt; El ≈ AgCuFeS phase</u>	+++	+	-	+	-	+	+++	-	-	-
<u>Ccp &gt; Py &gt; Sp &gt; Gn ≈ Asp &gt; El &gt; AgCuFeS phase &gt; Tet ≈ AgTet</u>	+++	+++	-	++	-	+	+	-	-	-
<u>Py &gt;&gt; Ccp &gt;&gt; Asp &gt; Gn ≈ Sp &gt; AgTet ≈ Ten &gt; Tet ≈ Po</u>	+++	++	-	+	+	+	+	-	-	-
<u>Py &gt;&gt; Gn ≈ Ccp</u>	+++	+	-	-	-	-	+	-	-	-

26

27

Table eA3-1.1806 Zone section 22 (up plunge portion)

Drill Hole	Sample No	Mineralization style	Description	Depth_ min [m]	Depth_ max [m]	Comment
RMUG08-138	29780	stringer	Py+Ccp stringers in rhyolite	23.40	23.45	
RMUG08-138	29781	stringer	fine, partly sulfide stringers in rhyolite	40.55	40.60	Myrmekite of Asp+Ccp+Tet±Sp in Tet; El-bearing
RMUG08-141	29784	stringer	sulfide stringers (Py+Sp) in rhyolite	24.50	24.55	
RMUG08-139	36501	stringer	Stringer py-ga-sph-asp in felsic lapillistone	36.70	36.77	
RMUG08-139	36502	stringer on contact to massive sulfide	Cpy-py-sulfosalt ores with gangue, aspy.	40.00	40.04	Myrmekite of Asp+Ccp+Tet±Sp±El in Ten-Tett; El-bearing
RMUG08-141	29785	semi-massive sulfide	semi-massive sulfide (Py+Sp) around clast	41.10	41.15	
RMUG08-141	29786	semi-massive sulfide	semi-massive sulfide (Py+Ccp) in rhyolite	42.75	42.80	Exsolution or Atoll-tex in Tet of Asp+Ccp+Tet±Sp
RMUG08-141	29787	semi-massive sulfide	semi-massive sulfide (Py+Ccp+Sp) around rhyolite	43.70	43.75	Exsolution or Atoll-tex in Tet of Asp+Ccp+Tet±Sp
RMUG08-142	29778	massive sulfide on contact to lower stringer	massive sulfide (Py)	57.85	57.90	precious metals and sulfosalts preferably near/at brittle deformed Py; El-bearing
RMUG08-138	36505	massive sulfide	Sph-rich sulfide with ga-asp-sulfosalts	42.84	42.88	Exsolution or Atoll-tex in Tet of Asp+Ccp+Tet±Sp±El; El-bearing
RMUG08-138	36506	massive sulfide	Buckshot sulfides with py-po-sph	46.71	46.74	Partly coarse Py-blasts
RMUG08-139	36503	massive sulfide	Cpy-sph-ga sulfides	43.53	43.57	
RMUG08-139	36504	massive sulfide	Buckshot sulfides with Po-Py-Ccp	44.28	44.32	Coarse Py-blasts of different growth generation (at least 2) = buckshot texture
RMUG08-142	29779	massive sulfide	sul stringers in massive sulfide near rhyolite clast	62.20	62.25	
RMUG08-142	36520	massive sulfide	Grainy pyritic sulfide	60.51	60.55	El-bearing
RMUG08-142	36521	massive sulfide	Cu-rich sulfide with sph, po, sulfosalts	64.74	64.78	
RMUG08-142	36522	massive sulfide on contact to mafic dyke	Buckshot sulfides with py-po-sph	65.53	65.57	
RMUG08-136	29776	massive sulfide	Py-Ccp bearing massive sulfide	46.10	46.17	
RMUG08-137A	29777	massive sulfide	massive sulfide, Py + minor Ccp [dead sulfide]	52.39	52.45	
RMUG08-140	29782	massive sulfide	massive sulfide (Py)	34.59	34.64	
RMUG08-140	29783	silicified horizon	Ccp+Py in massive quartz [high-grade ore]	35.43	35.48	El-bearing

Mineral abundance	Py	Ccp	Cbn	Sp	Po	Asp	Gn	Allo	Loel	Hess
<u>Py &gt; Sp</u> >> Ccp > Asp ≈ AgTen-Tet ≈ Gn	+++	+	-	+++	-	+	+	-	-	-
<u>Py &gt; Sp &gt; Ccp</u> > Gn > Asp > AgTen-Tet > El	+++	+++	-	+++	+	+	+	-	-	-
<u>Py &gt; Sp</u> >> Asp > Ccp > AgTen-Tet > Gn	+++	+	-	+++	-	+	+	-	-	-
<u>Py &gt; Asp &gt; Sp &gt; Gn</u> > Ccp > AgTen-Tet	+++	+	-	++	-	+++	++	-	-	-
<u>Py &gt; Ccp &gt; Sp &gt; AgTen-Tet</u> > Asp > Gn > El	+++	+++	-	++	-	+	+	-	-	-
<u>Py &gt; Sp</u> >> Ccp > Gn > Asp	+++	+	-	+++	-	+	+	-	-	-
<u>Py &gt; Ccp</u> > Asp > AgTen-Tet > Sp > Gn	+++	++	-	+	-	+	+	-	-	-
<u>Py ≈ Ccp</u> >> <u>Po &gt; Sp</u> >> Asp ≈ Gn > AgTet >> AgHg±Au alloy	+++	+++	-	++	++	+	+	-	-	-
<u>Py &gt; Ccp</u> > Asp ≈ Sp > AgTen-Tet ≈ Gn > AgHg±Au > El ≈ Po	+++	+++	-	+	+	+	+	-	-	-
<u>Sp &gt; Py</u> >> Ccp ≈ AgTen-Tet > Asp ≈ Gn > El > unnamed AgCuFeS phase ≈ unknown Ag-phase ≈ Loel	+++	+	-	+++	-	+	+	-	+	-
<u>Sp &gt; Po &gt; Py</u> >> Gn ≈ Ccp	++	+	-	+++	+++	-	+	-	-	-
<u>Sp &gt; Ccp ≈ Po &gt; Py</u> >> Gn ≈ Asp ≈ AgCuFeS > unknown Ag-phase ≈ Stn > Ull	+++	+++	-	+++	+++	+	+	-	-	-
<u>Po &gt; Py</u> >> Ccp > Sp > Gn	+++	+	-	+	+++	-	+	-	-	-
<u>Py &gt; Sp &gt; Ccp</u> > Gn > Po ≈ Asp > Stn > Cass	+++	++	-	+++	+	+	+	-	-	-
<u>Py &gt; Sp</u> >> Ccp ≈ Gn > Asp > unknown Ag-phase ≈ AgHg±Au > El > Mia ≈ Stn ≈ Cass	+++	+	-	++	-	+	+	-	-	-
<u>Py &gt; Ccp</u> > <u>Po &gt; Sp</u> >> Gn > Mag >> AgCuFeS > AgHg±Au	+++	+++	-	+	++	-	+	-	-	-
<u>Po ≈ Py &gt; Ccp</u> >> Sp > Gn ≈ Mag > AgHg±Au ≈ Asp	+++	++	-	+	+++	+	+	-	-	-
<u>Py</u> >> Ccp ≈ Po > Sp > Gn ≈ Asp	+++	+	-	+	+	+	+	-	-	-
<u>Py</u> >> <u>Ccp ≈ Po &gt; Sp</u> > Gn ≈ Asp	+++	++	-	+	+	+	+	-	-	-
<u>Py &gt; Ccp</u> > <u>Po &gt; Sp</u> > Asp > Gn	+++	+++	-	++	++	+	+	-	-	-
<u>Ccp &gt; Py &gt; Po &gt; Sp</u> > Asp > El > Ag Ccp > Mia ≈ Ull	+++	+++	-	++	+++	+	-	-	-	-

30

Pyr	Stp	AgHg±Au	El	Cass	FeTiCrV ox	Sch	unknown phase
-	-	-	-	-	-	-	-
-	-	-	+	-	-	-	-
-	-	-	-	-	-	-	-
-	-	-	-	-	-	-	-
-	-	-	+	-	-	-	-
-	-	-	-	-	-	-	-
-	-	-	-	-	-	-	-
-	-	+	-	-	-	-	-
-	-	+	+	-	-	-	-
-	-	-	+	-	-	-	+ (AgCuFeS, unknown Ag phase)
-	-	-	-	-	-	-	-
-	-	-	-	-	-	-	+ (AgCuFeS, unknown Ag phase)
-	-	-	-	-	-	-	-
-	-	-	-	+	-	-	-
-	-	+	+	+	-	-	-
-	-	+	-	-	+ (Mag)	-	+ (AgCuFeS)
-	-	+	-	-	+ (Mag)	-	-
-	-	-	-	-	-	-	-
-	-	-	-	-	-	-	-
-	-	-	-	-	-	-	-
-	-	-	+	-	-	-	-

Table eA3-1.1806 Zone section 2 (down plunge portion)

Drill Hole	Sample No	Mineralization style	Description	Comment	Depth_min [m]
RMUG08-147	29923	weak stringer (Footwall)	sulfide stringer (Py+Ccp) in massive rhyolite		49.80
RMUG08-144	29922	weak stringer (Footwall)	Sp-Py stringer with accessory Tet/Asp in massive rhyolite [only observed polyminerale stringer in core]		13.88
RMUG08-148	29930	weak stringer (Footwall)	Py-Ccp stringer in rhyolite		57.28
RMUG08-146	29916	stringer	Py stringer in massive rhyolite		51.12
RMUG08-146	29917	stringer	Py-Ccp-Sp stringer in massive rhyolite		51.60
RMUG08-143	29909	stringer	polyminerale stringer (Po+Ccp+Sp) in tuffaceous rhyolite		48.16
RMUG08-159	29933	stringer	Py-Sp stringer in rhyolite		45.90
RMUG08-147	29924	stringer	Py stringer in Fuchsite-bearing, massive rhyolite		59.16
RMUG08-145	29904	stringer	massive $\pm$ brecciated sulfide stringer (Sp+Py+Ccp) in rhyolite		56.02
RMUG08-148	29931	stringer	cm-wide Py stringer in rhyolite	recrys Py with Asp-Tet zoning	61.66
RMUG08-148	29932	stringer	Ccp-Py stringer in felsic (lapilli) tuff		77.71
RMUG08-146	29918	semi-massive sulfide	Py-Sp stringer in semi-massive zone at beginning of massive sulfide; in rhyolite with indicated crenulation cleavage		52.48
RMUG08-159	29934	semi-massive sulfide	Py-Ccp semi-mass sul in rhyolite	El-bearing	62.63
RMUG08-159	29935	semi-massive sulfide	Py-Ccp semi-mass sul in rhyolite		64.39
RMUG08-147	29925	semi-massive sulfide	Ccp stringer of semi-mass sul in rhyolite near contact to massive sulfide		63.28
RMUG08-147	29927	semi-massive sulfide	Ccp stringer in semi-massive sulfide close to contact with silicified horizon	myrmekite of Ccp-Asp-Tet-Ten - Sp $\pm$ Gn in Tet-Ten	65.26
RMUG08-159	29937	semi-massive sulfide	Py+minor Ccp in semi-massive part of 2 <sup>nd</sup> massive sulfide horizon		70.99
RMUG08-146	29919	massive sulfide	Py porphyroblasts in Py-Po-Ccp matrix (buckshot texture) in massive sulfide		52.75
RMUG08-159	29936	massive sulfide	Py-Ccp in massive sulfide horizon, close to contact with mafic dyke	El-bearing	66.93
RMUG08-159	29938	massive sulfide	Py-Ccp in massive sulfide horizon, close to contact with mafic dyke	Telluride-bearing	71.51
RMUG08-147	29926	massive sulfide	Py and minor phases (Ccp+Asp) in massive sulfide		65.02
RMUG08-145	29905	massive sulfide	Ccp+Py in massive sulfide	myrmekite of Ccp-Asp-Tet-Ten $\pm$ Sp $\pm$ Gn in Tet-Ten	58.98
RMUG08-145	29906	massive sulfide	Sp+Py in massive sulfide	simple myrmekitic intergrowth of Asp $\pm$ Ccp in Tet-Ten	60.08
RMUG08-145	29907	massive sulfide	Py in massive sulfide (dead ore?)	Tet-Ten intergrowth with Men	60.84
RMUG08-145	29908	massive sulfide	Py in massive sulfide close to lower contact with silicified horizon		62.96



Depth_ max [m]	Mineral abundance	Py	Ccp	Cbn	Sp	Po	Asp	Gn	Allo	Loel	Hess
49.85	<u>Py ≈ Asp</u> >> Sp > Gn > Ccp ≈ Tet	+++	+	-	+	-	+++	+	-	-	-
13.92	<u>Sp ≈ Py</u> > Gn >> Tet/Ten >> Ccp > Asp	+++	+	-	+++	-	+	++	-	-	-
57.33	<u>Py</u> >>> Sp ≈ Gn ≈ Tet/Ten > Ccp > Asp	+++	+	-	+	-	+	+	-	-	-
51.16	<u>Py</u> >>> Po > Ccp > Mag > Sp ≈ Gn	+++	+	-	+	++	-	+	-	-	-
51.64	<u>Po &gt; Py</u> > Ccp >>> Gn > Sp > Mag ≈ Asp	+++	++	-	+	+++	+	+	-	-	-
48.20	<u>Po &gt; Ccp</u> > Mag >>> Sp > Py ≈ Gn > AgCuFeS	+	+++	-	+	+++	-	+	-	-	-
45.95	<u>Py</u> > Sp > Ccp > Gn > Po	+++	+	-	++	+	-	+	-	-	-
59.21	<u>Py</u> >>> Sp ≈ Gn >>> Ccp ≈ AgTet ≈ Asp	+++	+	-	+	-	+	+	-	-	-
56.07	<u>Py</u> >>> Sp ≈ Ccp >>> Gn	+++	++	-	++	-	-	+	-	-	-
61.70	<u>Py</u> >>> Asp ≈ Ten > Sp > Gn ≈ Ccp > Tet ≈ Mag	+++	+	-	+	-	+	+	-	-	-
77.75	<u>Ccp &gt; Py</u> ≈ Sp > Gn	+++	+++	-	+++	-	-	++	-	-	-
52.53	<u>Ccp &gt; Po</u> ≈ <u>Py</u> > Mag > Sp >>> Cass ≈ Gn > Mol > Chr	+++	+++	-	++	+++	-	+	-	-	-
62.68	<u>Py</u> >>> Ccp > Sp > Gn ≈ Asp > AgTet >> El	+++	++	-	+	-	+	+	-	-	-
64.43	<u>Py</u> >>> Ccp > Po > Sp > Gn > Asp	+++	++	-	+	+	+	+	-	-	-
63.32	<u>Ccp ≥ Py</u> > Po > Sp > Asp > AgTet ≈ Gn ≈ Rt	+++	+++	-	+	++	+	+	-	-	-
65.30	<u>Ccp ≈ Py</u> >>> Asp >>> Sp > Po ≈ AgTet	+++	+++	-	+	+	++	-	-	-	-
71.04	<u>Py</u> >>> Ccp >>> Sp > Gn > Po > Asp > Sch	+++	++	-	+	+	+	+	-	-	-
52.80	<u>Py</u> > Ccp > Po > Mag >>> Sp ≈ Cass > Ilm > unknown Cd-bearing phase	+++	+++	-	+	++	-	-	-	-	-
66.98	<u>Py</u> > Ccp >>> Po > Sp >>> Asp > Sch > AgHg±Au ≈ El	+++	+++	-	+	++	+	+	-	-	-
71.56	<u>Py</u> > Ccp > Sp >>> Gn > Po > Mia ≈ BiTe	+++	+++	-	++	+	-	+	-	-	-
65.06	<u>Py</u> >>> Ccp > Asp > Sp ≈ Gn ≈ Rt	+++	+	-	+	-	+	+	-	-	-
59.03	<u>Py</u> > Ccp > Sp > Asp > Gn > Ten > Tet	+++	++	-	++	-	+	+	-	-	-
60.13	<u>Py</u> > Sp >>> Gn > Ccp > Asp > Tet >>> unknown Ag phase	+++	+	-	+++	-	+	+	-	-	-
60.88	<u>Py</u> >>> Ccp > Sp > Asp >>> Gn ≥ Tet > AgTet > Po > Men	+++	++	-	+	+	+	+	-	-	-
63.01	<u>Py</u> >>> Ccp > Sp ≈ Mag > Gn > Asp > Po	+++	+	-	+	+	+	+	-	-	-

34

35

<b>RMUG08-146</b>	29920	contact massive sulfide- massive Py in massive sulfide (dead ore?) silicified horizon	Telluride-bearing	53.68
<b>RMUG08-146</b>	29921	silicified horizon	massive Py stringer in massive Qtz (silicified horizon)	54.11
<b>RMUG08-147</b>	29928	silicic horizon/semi- massive sulfide	massive sulfide stringer (Py+ minor phases) in silicified horizon	67.25
<b>RMUG08-147</b>	29929	silicic horizon/semi- massive sulfide	brecciated sulfide stringer (Py+Ccp+Sp) in silicified horizon	66.97

Scheelite - to test if contamination

53.73	$\underline{\text{Py}} \gg \text{Tet/Ag-Tet} > \text{Ccp} \approx \text{Sp} \approx \text{Asp} > \text{Po} \approx \text{Gn} > \text{Stn} > \text{Col}$	+++	+	-	+	+	+	+	+	-	-	-	-
54.15	$\underline{\text{Py}} \gg \text{Ccp} > \text{Sp} \gg \text{Asp} \approx \text{Po} \approx \text{Gn} > \text{Tet/Ten}$	+++	+	-	+	+	+	+	+	-	-	-	-
67.30	$\underline{\text{Py}} \gg \text{Mag} > \text{Ccp} \approx \text{Sp} > \text{Gn}$	+++	+	-	+	+	+	+	+	-	-	-	-
67.02	$\underline{\text{Py}} \gg \text{Mag} > \text{Ccp} \approx \text{Sp} > \text{Gn} > \text{Mol}$	+++	+	-	+	+	+	+	+	-	-	-	-

+			
+			
+	+		
+	+		
			+
+			

		+ (Mag)	+ (Mag)

Table eA3-1. Ming South Up Plunge

Drill Hole	Section	Sample No	Mineralization style	Description	Comment
RMUG08-109	24	36195	stringer (footwall)	Py±Ccp stringer in quartz eye lap tuff with weak Bt	no SEM
RMUG08-106	4	62140	stringer (footwall)	thick Py-Ccp±Sp stringer in quartz eye flow (sul mod)	no SEM
RMUG08-106	4	62141	stringer (footwall)	Py-Sp±Ccp stringer in quartz eye flow (sul mod)	no SEM; fine Sp bands
RMUG08-95	5	62043	stringer (footwall)	thick Py-Ccp-Po stringer in rhy flow (or lap tuff)	no SEM
RMUG08-95	5	62044	stringer (footwall)	Ccp-Py(-Po) stringer in quartz eye tuff to lap uff between mafic dyke and massive sulfide	SEM + EPMA + SIMS; E/- and Telluride-bearing
RMUG08-97	5	62038	stringer (footwall)	Ccp-Po stringer with Py cubes (weak buckshot tex) in quartz eye flow (or tuff to lap tuff?)	no SEM; Py partly replaced by Po
RMUG08-97	5	62041	stringer (footwall)	fine Py±Ccp±Sp stringer on mafic dyke contact (representative of complex unit)	no SEM: Ccp disease common in Sp
RMUG08-98	5	62033	stringer (footwall)	Py-Ccp stringer in quart eye lap tuff	SEM + EPMA + SIMS; E/- and Telluride-bearing
RMUG08-93	9	62113	stringer (footwall)	Py-Sp-Ccp stringer in quartz eye tuff to lap tuff	no SEM
RMUG08-94	9	62108	stringer (footwall)	Py-Sp-Ccp stringer in quartz eye flow (sul mod)	no SEM; fine Sp bands
RMUG08-96	9	62050	stringer (footwall)	Py-Sp-Ccp stringer in Fuchs-bearing quartz eye tuff to lap tuff	no SEM
RMUG08-60	14	62105	stringer (footwall)	Ccp-Po stringer with Mag in quartz eye tuff to lap tuff	no SEM
RMUG08-61	14	62118	stringer (footwall)	Ccp-Py stringer in quartz eye flow	no SEM; Po sporadically and weakly replacing Py
RMUG08-63	14	62022	stringer (footwall)	Ccp-Py-Po stringer in quartz eye lap tuff	no SEM; rare and weak Py replacement by Po
RMUG08-63	14	62025	stringer (footwall)	Py-Ccp-Sp stringer in quartz eye lap tuff (between fracture zones)	no SEM
RMUG08-64	14	62018	stringer (footwall)	Ccp-Py stringer in rhy tuff to lap tuff	SEM + EPMA + SIMS; E/-bearing; Po partly replacing Py
RMUG08-64	14	62021	stringer (footwall)	Ccp-Py(-Po?) stringer in rhy lap tuff (sul mod)	no SEM; Po almost completely replacing Py
RMUG08-90	13	62135	stringer (footwall)	Py-Ccp-Po (or Sp) stringer in quartz eye lap tuff	no SEM
RMUG08-91	13	62128	stringer (footwall)	brecciated Py-Po-Ccp stringer around coarse silic clasts in quartz eye tuff to lap tuff (sul mod)	no SEM
RMUG08-91	13	62129	stringer (footwall)	fine Py-Sp±Ccp stringer in quartz eye tuff to lap tuff with mod Fuchs	no SEM
RMUG08-93	9	62116	semi-massive sulfide	semi-massive Py-Ccp-Po sul in quartz eye tuff to lap tuff	no SEM
RMUG08-99	9	62031	semi-massive sulfide	semi-massive Py-Ccp-Sp sul in quartz eye lap tuff, sulfides around ghost clasts, Py cubes and Sp bands	SEM
RMUG08-91	13	62132	semi-massive sulfide	(semi-)mass Py-Ccp sul with po and rhy fragments	no SEM
RMUG08-107	24	62002	massive sulfide	massive Py-Ccp sul	no SEM
RMUG08-109	24	36198	massive sulfide	massive Py-Ccp sul with very fine Sp bands	no SEM
RMUG08-104	4	62016	massive sulfide	massive Py-Ccp stringer in ±semi-massive quartz eye lap tuff	no SEM
RMUG08-95	5	62047	massive sulfide	massive Py-Ccp sul after mafic dyke on lower contact	no SEM; sporadically Po replacing Py; common Ccp disease in Sp
RMUG08-98	5	62036	massive sulfide	massive Py-Ccp sul with fine Sp bands	no SEM
RMUG08-93	9	62112	massive sulfide	massive Py-Ccp sul with Po	no SEM
RMUG08-94	9	62110	massive sulfide	massive Ccp-Py sul with Po (Mag?)	SEM; myrmekite in Gn with AgTet-Hess-Breit-BiTe
RMUG08-96	9	62101	massive sulfide	massive Py-Ccp±Sp sul	no SEM
RMUG08-96	9	62104	massive sulfide	massive Py-Ccp sul	no SEM
RMUG08-99	9	62030	massive sulfide	massive Py-Ccp sul with fine Sp bands	no SEM; Sp in Sp bands often with Ccp disease



Depth_m in [m]	Depth_m ax [m]	Mineral Abundance	Py	Ccp	Cbn	Sp	Po	Asp	Gn	Allo	Loel
27.14	27.18	<u>Py</u> >>> Sp > Fe±Ti Ox > Gn ≈ Ccp	+++	+	-	+	-	-	+	-	-
21.76	21.80	<u>Py</u> >>> Ccp > Sp > Asp > Gn > Po	+++	+	-	+	+	+	+	-	-
21.83	21.87	<u>Sp</u> ≈ <u>Py</u> > Gn > Ccp > Asp > Po	+++	+	-	+++	+	+	++	-	-
38.83	38.87	<u>Py</u> >>> Ccp > Po ≈ Sp > Gn > Cbn	+++	+	+	+	+	-	+	-	-
40.64	40.68	<u>Ccp</u> > <u>Py</u> ≈ <u>Po</u> > <u>Sp</u> > Gn > Asp > Men > Hess ≈ Alt ≈ El	+++	+++	-	++	+++	+	+	-	-
0.70	0.74	<u>Po</u> > <u>Py</u> > <u>Ccp</u> >>> Sp > Gn > Boul ≈ NiSbS	+++	+++	-	+	+++	-	+	-	-
7.90	7.94	<u>Py</u> >>> Sp > Ccp >>> Po	+++	+	-	+	+	-	-	-	-
38.03	38.07	<u>Ccp</u> > <u>Py</u> > <u>Po</u> > <u>Sp</u> > Hess > Ti ox > BiTe ≈ Gn ≈ El	+++	+++	-	+	+++	-	+	-	-
37.56	37.60	<u>Py</u> >>> <u>Ccp</u> > Sp ≈ Po > Gn > Te-phase (Col?)	+++	++	-	+	+	-	+	-	-
67.07	67.11	<u>Sp</u> > <u>Py</u> >>> Gn > Ccp	+++	+	-	+++	-	-	+	-	-
71.63	71.67	<u>Py</u> > <u>Sp</u> > Gn > Asp ≈ Ccp	+++	+	-	+++	-	+	++	-	-
56.92	56.96	<u>Ccp</u> >>> <u>Po</u> > Sp > Py	+	+++	-	+	++	-	-	-	-
51.30	51.34	<u>Ccp</u> >>> <u>Py</u> > Sp ≈ Po	+++	+++	-	+	++	-	-	-	-
4.78	4.82	<u>Py</u> >>> <u>Ccp</u> >>> <u>Po</u> > Sp > Asp	+++	+++	-	+	++	+	-	-	-
85.39	85.43	<u>Py</u> >>> Ccp > Sp > Po > Gn	+++	+	-	+	+	-	+	-	-
6.23	6.27	<u>Py</u> > <u>Ccp</u> > <u>Po</u> > Sp > Asp > Gn > Cbn > El ≈ Mol	+++	+++	+	+	++	+	+	-	-
86.06	86.10	<u>Ccp</u> > <u>Po</u> >>> <u>Py</u> > Sp	+	+++	-	+	+++	-	-	-	-
1.90	1.94	<u>Ccp</u> > Gn ≈ <u>Sp</u> > <u>Py</u> > Po	++	+++	-	+++	+	-	+++	-	-
29.43	29.47	<u>Sp</u> ≈ <u>Ccp</u> >>> Gn > Py ≈ Po > Asp > NiSb	+	+++	-	+++	+	+	++	-	-
45.73	45.77	<u>Py</u> > <u>Sp</u> > Gn >>> Ccp > Asp > Ten-Tet ≈ Cbn	+++	+	+	++	-	+	+	-	-
48.00	48.04	<u>Py</u> > <u>Po</u> >>> Ccp > Sp > Fe ox	+++	+	-	+	+++	-	-	-	-
45.37	45.41	<u>Py</u> >>> <u>Sp</u> > <u>Ccp</u> >>> Gn > Po	+++	++	-	+++	+	-	+	-	-
54.12	54.16	<u>Py</u> >>> <u>Ccp</u> > Po > Sp > Gn	+++	++	-	+	+	-	+	-	-
32.01	32.05	<u>Py</u> >>> <u>Sp</u> > Ccp > Gn ≈ Fe ox	+++	+	-	++	-	-	+	-	-
41.50	41.54	<u>Py</u> >>> <u>Sp</u> >>> Asp > Ccp > Gn > Mag > Po	+++	+	-	++	-	+	+	-	-
31.89	31.93	<u>Py</u> >>> Ccp Sp > Gn > Fe±Ti ox	+++	+	-	+	-	-	+	-	-
43.04	43.08	<u>Py</u> > <u>Ccp</u> >>> Sp ≈ Po	+++	+++	-	+	+	-	-	-	-
50.50	50.54	<u>Py</u> >>> Ccp > Po > Gn > Sp	+++	+	-	+	+	-	+	-	-
36.68	36.72	<u>Ccp</u> > <u>Py</u> > <u>Po</u> >>> Sp > Asp	+++	+++	-	+	+++	+	-	-	-
71.54	71.58	<u>Ccp</u> > <u>Po</u> > <u>Sp</u> > Py > Asp > Gn > AgTet > Nis > Ull > Breit ≈ Will ≈ Hess > BiTe	+	+++	-	++	+++	+	+	-	-
72.60	72.64	<u>Py</u> >>> Sp > Ccp > Asp > Gn ≈ Po	+++	+	-	+	+	+	+	-	-
83.14	83.18	<u>Py</u> >>> <u>Ccp</u> > Po > Sp	++	++	-	+	+	-	-	-	-
43.14	43.18	<u>Py</u> >>> <u>Sp</u> > Ccp > Po	+++	+	-	++	+	-	-	-	-

[illegible]

43

RMUG08-44	8 62125	massive sulfide	massive Ccp-Po-Py sul with thick Po schlieren	no SEM; weak Py replacement by Po
RMUG08-44	8 62127	massive sulfide	massive Py-Ccp sul with Ccp around Py clasts and fine Po schlieren (replacement tex?)	no SEM
RMUG08-60	14 62107	massive sulfide	massive Ccp-Py sul with Po and Mag	SEM + EPMA + SIMS; El-, AgHg- and Telluride-bearing; Po partly replacing Py
RMUG08-61	14 62119	massive sulfide	massive Py-Ccp-Po sul	SEM + EPMA + SIMS; Telluride- and NiSb-bearing; Po partly replacing Py
RMUG08-61	14 62120	massive sulfide	massive Py sul with rhy clasts ('transition' subseafloor to seafloor deposition?)	no SEM; weak Py replacement by Po
RMUG08-61	14 62121	massive sulfide	massive Py-Ccp-Sp sul	no SEM; weak Py replacement by Po
RMUG08-63	14 62027	massive sulfide	massive Py-Ccp sul, near upper and lower contact	no SEM
RMUG08-90	13 62139	massive sulfide	massive Py-Ccp sul with very fine Sp bands (?)	no SEM
RMUG08-91	13 62130	massive sulfide	massive Py-Ccp sul with Po schlieren	no SEM; myrmekite of Asp-Ccp±Po-Sp+Ten-Tet often as incl in Py
RMUG08-109	24 36199	stringer (hanging wall)	fine Py±Ccp stringer around quartz eyes in quartz eye tuff to lap tuff (Fsp/Ep alt parallel fol?)	no SEM
RMUG08-104	4 62017	stringer (hanging wall)	Sp-Py stringer in Fuch-enriched quartz eye tuff to lap tuff, Sp out @ 33.33; Sp bands	SEM + EPMA + SIMS
RMUG08-106	4 62144	stringer (hanging wall)	Py(-Ccp-Po?) stringer in quartz eye, Chl + sil flow (white Quartz eyes)	no SEM
RMUG08-95	5 62048	stringer (hanging wall)	Py-Ccp-Po stringer in quartz eye tuff to lap tuff (hanging wall representative)	no SEM
RMUG08-99	9 62032	stringer (hanging wall)	Py-Ccp stringer in quartz eye lap tuff after Fuchs is out (representative also of mod sul zone @ 45.55-46.6)	SEM
RMUG08-44	8 62126	stringer (hanging wall)	Ccp-Po±Py stringer in quartz eye flow	no SEM; Po replacing Py
RMUG08-91	13 62133	FeOx rhy in hanging wall	rhyolite with fine FeOx schlieren	SEM + EPMA + SIMS; Fe ox sample!

45

46

47

Table eA3-1. Ming South Down Plunge

Drill Hole	Sample No	Mineralization style	Description	Comment	Depth_m in [m]
RM06-04e	29791	stringer (footwall)	sulfide stringers in felsic volcanics	no SEM	898.00
RM06-04e	29792	stringer (footwall)	Ccp in massive Qtz	no SEM	903.15
RM06-04e	29793	stringer (footwall)	Ccp stringer in felsic volcanic (tuffaceous rhyolite?)	no SEM; Py often partly replaced by Po; Telluride-bearing	899.55
RM06-04d	36174	stringer (footwall)	fine Py±Ccp stringer in mass rhy flow	no SEM; Telluride-bearing	896.85
RM06-04d	36175	stringer (footwall)	fine Py±Ccp stringer in mass rhy flow, near lower contact to md	no SEM	899.11
RM06-04l	36187	stringer in semi-massive sulfide	Ccp-Py stringer in Qtz-eye lap tuff of semi-mass sul	no SEM	919.25
RM06-04l	36192	stringer (footwall)	fine Py stringer in Qtz-eye flow	no SEM	922.46
RM06-04l	36193	stringer (footwall)	fine Py-Sp? stringer in Qtz-eye flow	no SEM	924.55
RM06-04m	36061	stringer (footwall)	Py-Ccp stringer in Qtz-eye lap tuff	no SEM	916.95
RM06-04m	36063	stringer (footwall)	Py-Ccp stringer in Qtz-eye tuff to lap tuff	no SEM; sporadic and weak replacement of Py by Po	919.09
RM06-04m	36065	stringer (footwall)	Ccp-Py stringer in rhy tuff to lap tuff	no SEM; sporadic and weak replacement of Py by Po	930.25
RM06-04m	36066	stringer (footwall)	Py-Ccp-Sp stringer in F-bearing, Qtz-eye lap tuff	no SEM	945.29
RM06-04m	36067	stringer (footwall)	Ccp-Py-Po stringer in Qtz-eye rhy flow	SEM + EPMA + SIMS; El- and Telluride-bearing	949.98
RM06-04m	36072	stringer (footwall)	Ccp-Po-Py stringer in Qtz-eye rhy flow	no SEM; El- and telluride-bearing	962.57
RM06-04m	36075	stringer (footwall)	Py-Ccp stringer in Qtz-eye tuff to lap tuff	no SEM	967.89
RM06-04m	36076	stringer (footwall)	Py-Ccp stringer in rhy lap tuff	no SEM; Telluride-bearing	972.06
RM06-04m	36077	stringer (footwall)	Py-Ccp stringer in rhy lap tuff	no SEM	972.87
RM06-04m	36078	stringer (footwall)	Py-Ccp stringer in rhy lap tuff	no SEM	973.07
RM06-04m	36079	stringer (footwall)	Ccp-Po stringer in rhy tuff to lap tuff	no SEM	977.29
RM06-04d	36167	stringer in massive sulfide	Py-Sp stringer in intercalated rhy flow in mass sul	no SEM	890.24
RM06-04m	36074	semi-massive sulfide	semi-mass Ccp-Po stringer in Qtz-eye tuff to lap tuff	no SEM	967.62
RM06-04d	36171	semi-massive sulfide	semi-mass Py-Ccp-Sp sul in rhy flow	SEM; Telluride-bearing	893.73
RM06-04d	36172	semi-massive sulfide	semi-mass Py-Ccp sul in Fuchs-bearing rhy flow	SEM; Telluride-bearing	894.51
RM06-04e	29788	massive sulfide	massive sulfide (Py+Po)	no SEM	887.10
RM06-04e	29789	massive sulfide	massive Ccp-Po-Py mineralization near Qtz-vein in massive sulfide	SEM + EPMA + SIMS	889.25
RM06-04e	29790	massive sulfide	massive sulfide (Py+Po)	no SEM	893.75
RM06-04m	36057	massive sulfide	mass Py sul with minor Ccp and small rhy fragments, near upper contact	no SEM	895.75
RM06-04m	36058	massive sulfide	mass Py sul with minor Ccp, smal Py XX and rhy fragments, near lower contact	SEM + EPMA + SIMS	896.71
RM06-04m	36059	massive sulfide	mass Py sul with Ccp-Po	no SEM	909.36
RM06-04m	36060	massive sulfide	Py-Ccp stringer around rhy fragments in mass sul, on lower contact	SEM; Telluride-bearing	910.57



Depth_m ax [m]	Mineral Abundance	Py	Ccp	Cbn	Sp	Po	Asp	Gn	Allo	Loel	Hess
898.05	<u>Py</u> >>> Sp > Ccp > Po ≈ Gn	+++	++	-	++	+	-	+	-	-	-
903.20	Ccp > Po > <u>Py</u> > Sp > NiSb	++	+++	-	++	+++	-	-	-	-	-
899.60	Ccp > <u>Py</u> ≈ Po >>> Sp ≈ Mag > Gn > BiTe	+++	+++	-	+	+++	-	+	-	-	-
896.89	<u>Py</u> >>> Sp > Ccp > Po > Gn > Asp > BiTe	+++	+	-	+	+	+	+	-	-	-
899.15	<u>Py</u> > Ccp >>> Sp ≈ Asp	+++	+++	-	++	-	++	-	-	-	-
919.35	<u>Py</u> > Ccp > Po > Sp > Asp	+++	+++	-	+	++	+	+	-	-	-
922.50	<u>Py</u> >>> Gn > Sp ≈ Ccp > Ten-Tet	+++	+	-	+	-	-	+	-	-	-
924.59	<u>Py</u> >>> Sp > Ccp > Asp > Po > Gn	+++	+	-	+	+	+	+	-	-	-
916.99	<u>Py</u> >>> Ccp > Sp > Po > Asp ≈ Gn	+++	+	-	+	+	+	+	-	-	-
919.13	Ccp > <u>Po</u> >>> <u>Py</u> >>> Sp > FeTi ox ≈ Gn	++	+++	-	+	+++	-	+	-	-	-
930.29	Ccp > <u>Py</u> > Po > Sp > Asp	+++	+++	-	++	++	+	-	-	-	-
945.33	<u>Py</u> >>> Sp ≈ Ccp ≈ Gn > Po > Cbn	+++	+	+	++	+	-	+	-	-	-
950.02	<u>Py</u> > Ccp > Po > Sp > FeTi ox > Asp ≈ Gn ≈ BiTe ≈ Hess ≈ El	+++	+++	-	+	++	+	+	-	-	+
962.61	Ccp > <u>Po</u> > Mag > <u>Py</u> > Sp > Gn > Cbn > BiTe > El	++	+++	+	+	+++	-	+	-	-	-
967.93	Ccp > <u>Py</u> > Po > Mag > Sp	+++	+++	-	+	++	-	-	-	-	-
972.10	<u>Py</u> >>> Mag > Ccp ≈ Sp > Po ≈ BiTe ≈ Gn	+++	+	-	+	+	-	+	-	-	-
972.91	<u>Py</u> > <u>Po</u> >>> Ccp > Mag > Sp	+++	+	-	+	++	-	-	-	-	-
973.11	<u>Py</u> >>> Ccp > Sp > FeTi ox > Po > Gn	+++	+	-	+	+	-	+	-	-	-
977.33	Ccp > <u>Po</u> >>> <u>Py</u> ≈ Sp	+	+++	-	+	+++	-	-	-	-	-
890.28	<u>Py</u> >>> Mag > Sp > Ccp > Gn	+++	+	-	+	-	-	+	-	-	-
967.66	Ccp > <u>Po</u> > <u>Py</u> > Sp > Asp ≈ FeTi ox	++	+++	-	+	+++	+	-	-	-	-
893.77	<u>Py</u> >>> Sp > Ccp > Po > Asp > Gn ≈ Mag > AgTet > Alt ≈ Men ≈ Stn	+++	+	-	+	+	+	+	-	-	-
894.55	<u>Py</u> >>> Ccp > Sp > Mag >>> Gn > Asp > Alt	+++	+	-	+	-	-	+	-	-	-
887.15	<u>Py</u> >>> Gn > Ccp > Sp > Po > Asp	+++	+	-	+	+	+	+	-	-	-
889.30	Ccp > <u>Po</u> > <u>Py</u> > Sp > Cbn > Gn >>> Hess ≈ NiSb ≈ Ull	++	+++	+	+	+++	-	+	-	-	+
893.80	<u>Py</u> >>> Sp ≈ Ccp > Po	+++	+	-	+	+	-	-	-	-	-
895.79	<u>Py</u> >>> Ccp > Po > Sp > Gn	+++	+	-	+	+	-	+	-	-	-
896.75	<u>Py</u> >>> Gn > Ccp > Sp ≈ Asp > Po	+++	+	-	+	+	+	+	-	-	-
909.40	<u>Py</u> >>> Ccp > Sp ≈ Po > Gn ≈ Asp	+++	+	-	+	+	+	+	-	-	-
910.61	<u>Py</u> >>> Ccp > Sp > Po > Asp ≥ Gn > Alt ≈ Hess	+++	++	-	+	+	+	+	-	-	+

50

51

RM06-04d	36161 massive sulfide	mass Py-Ccp sul with upper silicic part and Py stringers, on upper contact	no SEM	881.48
RM06-04d	36163 massive sulfide	mass Ccp-Po-Py sul with Tet or Asp, on contact to intercalated Qtz-eye lap tuff	SEM + EPMA + SIMS; Telluride-bearing	882.81
RM06-04d	36165 massive sulfide	mass Py-Ccp sul with Po and silicic clasts, near upper contact	no SEM	889.78
RM06-04d	36168 massive sulfide	mass Py-Ccp sul with Ccp-Po-coarse Py schlieren	no SEM	891.40
RM06-04d	36169 massive sulfide	mass Py-Ccp sul	no SEM	892.56
RM06-04i	36180 massive sulfide	mass Py-Ccp sul with Po-coarser Py	no SEM	914.98
RM06-04i	36182 massive sulfide	mass Ccp-Py sul with Ccp-Po 'schlieren'	no SEM; El- and Telluride-bearing	917.45
RM06-04i	36183 massive sulfide	mass Py sul with Sp bands	no SEM; Telluride-bearing	917.93
RM06-04i	36184 massive sulfide	mass Ccp-Py sul with silicic clasts	no SEM; Telluride-bearing	918.22
RM06-04i	36185 massive sulfide	mass Py-Ccp sul with coarser Py + Po (?)	no SEM; Telluride-bearing	918.66
RM06-04i	36188 massive sulfide	Ccp-Py sul around coarse silicic ±Fuchs-bearing clasts	no SEM; Telluride-bearing	920.05
RM06-04i	36189 massive sulfide	mass Py-Ccp sul with partly coarse Py XX	no SEM	920.29
RM06-04i	36190 massive sulfide	mass Py-Ccp sul with Sp or Po and coarser Py and silicic clasts, near lower contact	no SEM; Telluride-bearing	921.03
RM06-04i	36176 stringer (hanging wall)	thick Py stringer with minor Ccp and silicic rhy clasts in mass rhy flow, on lower contact	no SEM	883.60
RM06-04i	36178 stringer (hanging wall)	Py-Ccp stringer in Qtz-eye lap tuff	no SEM	911.94

53

	+														
													+		
													+		
						+									
	+														
	+														
	+														
		+				+	+	-	+	+	-	+			
						+	+	-	+	+	-	+			

55

Table eA3-1. Lower Footwall Zone

Drill Hole	Sample No	Mineralization style	Description	Comment	Depth_m in [m]
RM06-04e	29794	LFWZ	Ccp stringers	no SEM; Py often partly replaced by Po	1,073.32
RM06-04e	29795	LFWZ	Ccp stringer in tuff	no SEM	1,084.60
RM06-04e	29796	LFWZ	sulfide stringers (Ccp) in tuff	no SEM; Py partly replaced by Po	1,097.34
RM06-04e	29797	LFWZ	sulfide stringers (Ccp+Po+Py) in tuff	SEM + EPMA + SIMS: El- and telluride-bearing; Py partly replaced by Po	1,102.00
RM06-04e	29798	LFWZ	sulfide stringers (Ccp+Po) slightly brecciated around tuffaceous matrix	no SEM; Py partly replaced by Po	1,113.23
RM06-04e	29799	LFWZ	massive sulfide stringer (Ccp+Po) in tuff	no SEM	1,132.15
RM06-04e	29800	LFWZ	sulfide stringer (Ccp+Po+Py) in tuff around Qtz	SEM + EPMA + SIMS: Telluride-bearing	1,180.38
RM06-04e	29901	LFWZ	massive sulfide stringer (Ccp+Po) in dyke or tuff at contact to secondary Qtz	SEM: El- and Telluride-bearing; Py partly replaced by Po	1,205.00
RM06-04m	36080	LFWZ	Ccp-Py stringer in rhy flow	no SEM	1,006.69
RM06-04m	36082	LFWZ	coarse Mag, Ccp-Py-Po stringer in Qtz-eye tuff to lap tuff	SEM + EPMA + SIMS; Mag-blasts; Po partly replacing Py	1,008.07
RM06-04m	36083	LFWZ	Ccp-Po-Py stringer in Qtz-eye tuff to lap tuff	no SEM; very weak Py replacement by Po	1,008.16
RM06-04m	36085	LFWZ	Ccp-Po-Py stringer in rhy flow	no SEM; very weak Py replacement by Po	1,010.96
RM06-04m	36087	LFWZ	Ccp-Py-Po stringer in rhy lap tuff	no SEM; very weak Py replacement by Po	1,018.35
RM06-04m	36088	LFWZ	Ccp-Py stringer in rhy flow	no SEM; very weak Py replacement by Po	1,020.46
RM06-04m	36091	LFWZ	Ccp-Py-Po stringer with Mag in rhy flow	SEM + EPMA + SIMS; El- and Telluride-bearing; Po often replacing Py	1,023.24
RM06-04m	36092	LFWZ	coarse Ccp-Po-Py stringer with finer Py in rhy flow	no SEM	1,023.82
RM06-04m	36094	LFWZ	Py-Ccp stringer in rhy flow	no SEM	1,035.31
RM06-04m	36097	LFWZ	Ccp-Po and Ccp-Py stringer in Qtz-eye tuff to lap tuff with Chl-Mag-rich interlayer between both stringer	no SEM	1,042.00
RM06-04m	36098	LFWZ	Ccp-Po stringer in rhy flow	no SEM	1,077.76
RM06-04m	36100	LFWZ	Ccp-Po stringer in rhy flow	no SEM; Py partly replaced by Po	1,078.81
RM06-04m	36102	LFWZ	Ccp-Po stringer in rhy tuff to lap tuff (or flow?), on lower contact	no SEM; Po partly replacing Py	1,084.93
RM06-04m	36103	LFWZ	Ccp-Py stringer in Qtz-eye rhy flow	no SEM; Po partly replacing Py	1,087.68
RM06-04m	36105	LFWZ	Ccp-Po-Py stringer and Mag in rhy flow	no SEM; Py partly replaced by Po	1,092.26



Depth_m ax [m]	Mineral Abundance	Py	Ccp	Cbn	Sp	Po	Asp	Gn	Allo	Loel	Hess
1,073.37	<u>Ccp &gt;&gt; Po &gt; Py &gt; Sp &gt; Cbn &gt;&gt; FeTi ox &gt; unknown phase</u>	++	+++	+	+	++	-	1	-	-	-
1,084.65	<u>Ccp &gt;&gt; Cbn &gt; Po &gt; Sp &gt; Py &gt; unknown phase</u>	+	+++	+	+	+	-	1	-	-	-
1,097.39	<u>Ccp &gt;&gt; Po &gt; Mag &gt; Py &gt; FeTi ox &gt; Sp</u>	+	+++	-	+	++	-	1	-	-	-
1,102.05	<u>Ccp &gt; Po ≈ Py &gt; Cbn &gt;&gt; FeTi ox &gt; Sp &gt; Gn ≈ Tsu &gt; Hess ≈ BiTe &gt; El ≈ Allo</u>	+++	+++	++	+	+++	-	+	+	-	+
1,113.28	<u>Ccp ≈ Po &gt;&gt; Py &gt;&gt; Sp</u>	++	+++	-	+	+++	-	1	-	-	-
1,132.20	<u>Ccp &gt;&gt; Po &gt; Cbn &gt;&gt; Mag &gt;&gt; Py ≈ Sp</u>	+	+++	++	+	+++	-	1	-	-	-
1,180.43	<u>Ccp &gt; Po &gt; Cbn &gt;&gt; Mag &gt; Sp &gt; Py &gt; BiTe &gt; Hess &gt; Gn &gt; Alt</u>	+	+++	++	+	+++	-	+	-	-	+
1,205.05	<u>Ccp &gt; Py ≈ Po &gt;&gt; Mag ≈ Sp &gt; FeTi ox (Ilm) &gt; BiTe &gt; El ≈ Hess</u>	+++	+++	-	+	+++	-	1	-	-	+
1,006.73	<u>Py &gt; Po &gt; Ccp &gt; Sp</u>	+++	++	-	+	+++	-	1	-	-	-
1,008.11	<u>Mag &gt; Ccp &gt; Po ≈ Py &gt; Cbn &gt; Sp &gt; BiTe</u>	++	+++	+	+	++	-	-	-	-	-
1,008.20	<u>Ccp &gt; Po &gt;&gt; Py &gt; Mag &gt; Sp</u>	++	+++	-	+	+++	-	1	-	-	-
1,011.00	<u>Py &gt; Po ≈ Ccp &gt; Mag &gt; Sp &gt; unknown phase</u>	+++	+++	-	+	+++	-	1	-	-	-
1,018.39	<u>Py &gt; Ccp &gt; Po &gt; Mag &gt;&gt; Sp</u>	+++	+++	-	+	++	-	1	-	-	-
1,020.50	<u>Py &gt; Ccp &gt; Po &gt; Mag &gt; FeTi ox &gt; Sp</u>	+++	++	-	+	++	-	1	-	-	-
1,023.28	<u>Ccp &gt; Py ≈ Po &gt; Fe ox &gt; Sp &gt; Asp &gt; BiTe ≈ Hess &gt; El</u>	+++	+++	-	+	+++	+	-	-	-	+
1,023.86	<u>Ccp &gt; Po &gt; Py &gt; Mag &gt; Sp</u>	++	+++	-	+	+++	-	1	-	-	-
1,035.35	<u>Py &gt; Po &gt; Ccp &gt; Sp</u>	+++	+	-	+	+	-	1	-	-	-
1,042.04	<u>Py &gt;&gt; Ccp &gt; Po &gt; Sp</u>	+++	++	-	+	++	-	1	-	-	-
1,077.80	<u>Ccp &gt; Po &gt; Sp ≈ Mag &gt; Py &gt; BiTe &gt; Hess &gt; unknown phase</u>	+	+++	-	+	+++	-	1	-	-	+
1,078.85	<u>Ccp &gt; Po &gt; Py &gt; Sp &gt; Mag &gt; Cbn &gt; BiTe ≈ Gn</u>	+	+++	+	+	+++	-	+	-	-	-
1,084.97	<u>Ccp &gt;&gt; Po &gt; Fe ox &gt; Py &gt;&gt; Sp</u>	++	+++	-	+	++	-	1	-	-	-
1,087.72	<u>Ccp &gt; Py &gt; Po &gt; Mag ≈ FeTi ox &gt; Cbn ≈ Sp</u>	+++	+++	+	+	++	-	1	-	-	-
1,092.30	<u>Ccp &gt; Po &gt; Py &gt; Mag &gt; FeTi ox &gt; Sp ≈ Cbn</u>	+++	+++	+	+	+++	-	1	-	-	-

[illegible]

[illegible]

RM06-04m	36109	LFWZ	Ccp-Po stringer with coarse Py, Mag and mafic clast in rhy flow	no SEM; coarse Py partly replaced by Po	1,095.83
RM06-04m	36110	LFWZ	Ccp-Po-Py stringer with partly coarse Py and Mag in rhy lap tuff	no SEM; coarse Py partly replaced by Po	1,103.38
RM06-04m	36114	LFWZ	thick Ccp-Po stringer in rhy flow	no SEM; very weak Py replacement by Po	1,117.61
RM06-04m	36117	LFWZ	Ccp-Po stringer with Mag/Bt in rhy flow	no SEM; Py often partly replaced by Po	1,124.61
RM06-04m	36119	LFWZ	Ccp-Po stringer with Mag/Bt in rhy flow	no SEM; Py often partly replaced by Po	1,131.04
RM06-04m	36120	LFWZ	mass Ccp-Po stringer in Amph-rich part of rhy flow	no SEM; Po partly replacing Py	1,134.55
RM06-04m	36121	LFWZ	Ccp-Po stringer with mafic parts in Amph-rich part of rhy flow	no SEM; Py almost absent	1,135.54
RM06-04m	36126	LFWZ	Ccp-Py-Po stringer with Amph-bearing mafic parts in rhy flow	no SEM; Py often partly replaced by Po	1,155.16
RM06-04m	36127	LFWZ	±brecciated Ccp-Po-Py stringer in rhy flow	no SEM; no Py	1,156.53
RM06-04m	36128	LFWZ	Ccp-Po-Py stringer with silicic clasts and mafic parts in Qtz-eye rhy flow	no SEM; no Py	1,158.97
RM06-04m	36130	LFWZ	Ccp stringer folded with silicic clasts in rhy lap tuff	no SEM; no Py	1,162.09
RM06-04m	36131	LFWZ	Ccp-Po stringer with Amph-bearing mafic parts in rhy lap tuff	no SEM; no Py; telluride-bearing	1,177.19
RM06-04m	36133	LFWZ	±brecciated Ccp-Po stringer around Amph-bearing mafic clasts in rhy flow	no SEM; Py almost absent	1,182.86
RM06-04m	36134	LFWZ	Ccp-Po stringer with mafic parts in rhy lap tuff (or flow?)	no SEM; Py almost completely replaced by Po	1,185.13
RM06-04m	36137	LFWZ	Ccp-Po stringer with mafic parts in rhy flow	SEM + EPMA + SIMS; Telluride-bearing	1,194.85
RM06-04m	36140	LFWZ	brecciated Ccp-Po stringer around Amph-bearing mafic clasts in rhy flow, close to upper contact	no SEM; no Py + oxides	1,202.03
RM06-04m	36142	LFWZ	Ccp-Po-Py stringer with very coarse Amph (Bt?) in Chl-rich part of rhy flow	no SEM; Py almost absent	1,206.68
RM06-04m	36144	LFWZ	thick Ccp-Po-Py stringer with mafics and mafic parts in rhy flow (or lap tuff?)	no SEM; no Py + oxides	1,211.55
RM06-04m	36145	LFWZ	folded Ccp stringer with weak cren cleavage in rhy flow (or lap tuff?), near lower contact	no SEM; no Py	1,213.24
RM06-04m	36146	LFWZ	fine Ccp-Py-Po stringer in rhy flow	no SEM; Py almost absent	1,217.09

1,095.88	<u>Ccp &gt; Py &gt; Po &gt; Mag</u> $\approx$ FeTi ox > Sp	+++	+++	-	+	+++	1	-	-	-	-
1,103.42	<u>Ccp &gt; Py &gt; Po &gt; Sp</u> > unknown phase	+++	+++	-	+	+++	1	-	-	-	-
1,117.65	<u>Ccp &gt; Po &gt; Py &gt; Mag</u> > FeTi ox > Sp > unknown phase	+	+++	-	+	+++	1	-	-	-	-
1,124.65	<u>Ccp &gt; Po &gt;&gt;&gt; Py &gt; Cub</u> $\approx$ Sp > unknown phase	+	+++	-	+	+++	1	-	-	-	-
1,131.08	<u>Ccp &gt; Po <math>\approx</math> Py &gt;&gt;&gt; Sp</u> > unknown phase	+++	+++	-	+	+++	1	-	-	-	-
1,134.59	<u>Ccp &gt; Po &gt; Mag &gt; Cub &gt; Py &gt; Sp</u> $\approx$ unknown phase	+	+++	+	+	+++	1	-	-	-	-
1,135.58	<u>Ccp &gt; Po &gt; Cub &gt; FeTi ox &gt; Sp</u> $\approx$ unknown phase $\approx$ Py	+	+++	++	+	+++	-	-	-	-	-
1,155.20	<u>Ccp &gt; Py &gt; Po &gt;&gt;&gt; FeTi ox &gt; Sp</u>	+++	+++	-	+	+++	1	-	-	-	-
1,156.57	<u>Ccp &gt; Po &gt; Cub &gt; FeTi ox &gt; Mag</u> > unknown phase $\approx$ Sp	-	+++	++	+	+++	-	-	-	-	-
1,159.01	<u>Ccp &gt; Po &gt; Cbn &gt;&gt;&gt; FeTi ox &gt; unknown phase</u> $\approx$ Mag > Sp	-	+++	++	+	+++	-	-	-	-	-
1,162.13	<u>Ccp &gt; Po &gt;&gt;&gt; Mag</u> > FeTi ox $\approx$ unknown phase > Sp	-	+++	-	+	+++	-	-	-	-	-
1,177.23	<u>Ccp &gt; Po &gt; Cub &gt; FeTi ox &gt; BiTe</u> > Mag > unknown phase $\approx$ Sp > Hess	-	+++	++	+	+++	-	-	-	-	+
1,182.90	<u>Ccp &gt; Po &gt;&gt;&gt; FeTi ox &gt; Mag &gt; Sp</u> $\approx$ unknown phase $\approx$ Py	+	+++	-	+	+++	-	-	-	-	-
1,185.17	<u>Ccp &gt; Po &gt;&gt;&gt; Py</u> $\approx$ FeTi ox > Mag > Sp $\approx$ unknown phase	+	+++	-	+	+++	-	-	-	-	-
1,194.89	<u>Ccp &gt; Po &gt; Cbn &gt; Sp</u> $\approx$ FeTi ox > BiTe $\approx$ Hess $\approx$ Claus > Scheel	-	+++	++	+	+++	-	-	-	-	+
1,203.07	<u>Ccp &gt; Po &gt; Cbn &gt;&gt;&gt; Sp &gt; Gn</u> > unknown phase	-	+++	++	+	+++	+	-	-	-	-
1,206.72	<u>Ccp &gt; Po &gt; Cub &gt; Sp</u> > unknown phase > Mag $\approx$ FeTi ox > Py $\approx$ Gn > BiTe	+	+++	++	+	+++	+	-	-	-	-
1,211.59	<u>Ccp &gt; Po &gt; Cub &gt; Sp</u> > unknown phase > Gn > BiTe	-	+++	++	+	+++	+	-	-	-	-
1,213.28	<u>Ccp &gt; Po &gt;&gt;&gt; Sp</u> > Mag > unknown phase $\approx$ FeTi ox	-	+++	-	+	+++	-	-	-	-	-
1,217.13	<u>Ccp &gt; Po &gt;&gt;&gt; Sp</u> > Mag $\approx$ Py > unknown phase	+	+++	-	+	+++	-	-	-	-	-

62



RM06-04m	36148	LFWZ	Ccp-Po stringer on mafic clast in rhy flow	no SEM; coarse Py often replaced by Ccp-Po	1,262.40
RM06-04m	36150	LFWZ	Ccp-Po stringer around mafic clasts in rhy flow	SEM; Telluride-bearing; coarse Py often replaced by Po	1,277.79
RM06-04m	36152	LFWZ	Ccp-Po stringer with coarse Py in Chl-mafics rich part of rhy flow	no SEM; Py partly replaced by Po	1,286.55
RM06-04m	36153	LFWZ	fine Ccp-Po stringer on mafic part in Qtz-enriched rhy flow	no SEM; no Py	1,287.30
RM06-04m	36154	LFWZ	fine Ccp-Po-Py stringer on Chl in Qtz-eye lap tuff	no SEM; Py rare, not replaced; no oxides	1,296.40
RM06-04m	36157	LFWZ	fine Ccp-Po-Py stringer on mafic clast, mafics in Qtz-eye rhy flow	no SEM; no replacement of Py by Po observed	1,326.10
RM06-04m	36159	LFWZ	Ccp-Po stringer in Qtz-eye flow	no SEM; no replacement of Py	1,337.16
RM06-04m	36160	LFWZ	Ccp-Po-Py stringer, mafics in Qtz-eye flow	no SEM; Py partly replaced by Po	1,327.44
RM06-04m	36113	Qtz-vein in md	coarse Py-Ccp min in Qtz vein in md	SEM + SIMS	1,110.67

<sup>1</sup> Gn not visible at RL, but likely sub-microscopically visible as tiny roundish crystals marginal on Pv at SEM

<sup>2</sup> small unknown anhedral brownish XX in Cco maybe Po



65

[illegible]

67

**Table eA4-1.** Compilation of methods applied to sulfides from the 1807 Zone. Abbreviations: EPMA - electron probe micro-analysis, LA-ICP-MS - laser ablation in electron microscopy, SIMS - secondary ion mass spectrometry, x - applied, – not applied, NA - not available

Drill hole	Sample No.	Alternative Sample No. <sup>1</sup>	Mineralization style	Comment	Depth_m in [m]	Depth_m ax [m]	Photo	Thick section [200 µm]
RM07-19	29947	Z-121T	stringer (hanging wall)	Py-Ccp stringer in clast-bearing rhy flow	591.70	591.74	x (2pics)	x
RM07-19	29948	Z-122T	massive sulfide	massive Py-Ccp sulfide	593.51	593.54	x	x
RM07-19g	29949	Z-123T	semi-massive sulfide	semi-mass Py-Ccp sul in rhy flow	596.45	596.49	x	x
RM07-19g	29950	Z-124T	semi-massive sulfide	semi-mass Ccp-Py-Po sul in rhy flow	598.28	598.32	x	x
RM07-19g	35551	Z-125T	stringer (footwall)	fine, ± brecciated Py-Ccp stringer in Qtz-eye flow or tuff to lap tuff	600.40	600.44	x	x
RM07-19c	35552	Z-126T	massive sulfide	massive Py-Ccp sulfide	592.07	592.11	x	x
RM07-19e	35553	Z-127T	massive sulfide	massive Py-Ccp sul with small silicic rhy fragments	593.19	593.23	x	x
RM07-19e	35554	Z-128T	semi-massive sulfide	semi-mass Py-Ccp-Sp/Asp (?) sul in rhy, close to upper dyke contact	594.09	594.13	x	x
RM07-19a	35555	Z-129T	stringer (hanging wall)	Ccp-Py stringer in Qtz-eye rhy lap tuff	595.42	595.46	x (2pics)	x
RM07-19a	35556	Z-130T	massive sulfide	massive Py sulfide	597.19	597.23	x (2pics)	x
RM07-18a	35557	Z-131T	massive sulfide	coarse mass Py-Ccp-Po sul, near upper contact	597.55	597.59	x	x
RM07-18a	35559	Z-132T	massive sulfide	mass Ccp-Py sul, Ccp around Py 'clasts' (replacement of former rhy clasts?)	598.85	598.89	x	x
RM07-18a	35561	Z-133T	massive sulfide	mass Py sul with Ccp schlieren/stringer, close to lower contact	600.01	600.05	x	x
RM07-18b	35563	Z-134T	massive sulfide	mass Py-Ccp sul with Sp-Asp? Band with Py blasts between Py 'clasts' surrounded by Ccp	603.94	603.98	x	x
RM07-18b	35565	Z-135T	massive sulfide	mass Py-Ccp sul with Sp-Asp? Ccp around Py 'clasts', similar texture as in 35563	604.61	604.65	x	x
RM07-18b	35566	Z-136T	massive sulfide	mass Py-Ccp-Sp sul, Ccp-Sp around Py 'clasts'	605.46	605.50	x	x
RM07-18d	35567	Z-137T	massive sulfide	mass Py sul with Ccp schlieren/stringer and small Py XX	600.29	600.34	x	x
RM07-18e	35568	Z-138T	semi-massive sulfide	thick Py-Ccp band with Py XX in semi-mass sul	600.69	600.73	x	x
RM07-18e	35569	Z-139T	semi-massive sulfide	fine Ccp-Py-silvery phase stringer in Qtz-eye rhy flow of semi-mass sul	601.09	601.13	x	x
RM07-20	35570	Z-140T	semi-massive sulfide	Ccp stringer and diss Ccp in mass rhy of semi-mass sul	657.84	657.88	x	x
RM07-20	35571	Z-141T	massive sulfide	coarse, mass Ccp-Py-Po sul	657.98	658.02	x	x
RM07-20a	35572	Z-142T	semi-massive sulfide	Ccp-Py stringer and diss Py-Ccp in semi-mass sul	643.06	643.10	x	x
RM07-20a	35573	Z-143T	semi-massive sulfide	mass Py-Ccp sul in semi-mass sul, on lower contact	643.53	643.57	x	x
RM07-20a	35574	Z-144T	stringer (footwall)	Py-Ccp stringer in rhy lap tuff	644.92	644.96	x	x
RM07-20b	35575	Z-145T	massive sulfide	mass Py-Ccp sul with coarse Py and rhy clasts	665.93	665.97	x	x
RM07-20b	35577	Z-146T	massive sulfide	mass Py-Ccp sul with coarse Py XX	667.17	667.21	x	x
RM07-20b	35580	Z-147T	massive sulfide	mass Py sul with Ccp schlieren/stringer	670.28	670.32	x	x
RM07-20c	35581	Z-148T	stringer (hanging wall)	Py stringer in Qtz-eye lap tuff	665.08	665.12	x	x
RM07-20c	35582	Z-149T	semi-massive sulfide	Py-Ccp stringer in Qtz-eye lap tuff of semi-mass sul	665.54	665.58	x	x
RM07-20c	35583	Z-150T	massive sulfide	mass Py-Ccp sul	665.77	665.81	x	x
RM07-20c	35584	Z-151T	massive sulfide	mass Ccp-Py-Po sul on lower contact and affected by intercalated md above	666.30	666.34	x	x
RM07-20e	35585	Z-152T	massive sulfide	mass Py-Ccp sul with Po and silicic rhy fragments, close to upper contact	659.80	659.84	x	x

[illegible]

RM07-20e	35586	Z-153T	massive sulfide	mass Py sul with small Py XX and minor Ccp	660.17	660.21	x	x
RM07-20e	35588	Z-154T	massive sulfide	mass Py-Ccp-Sp sul (Ccp-Sp ± brecciated around Py)	661.48	661.52	x	x
RM07-20e	35590	Z-155T	massive sulfide	mass Py sul with fine Sp-Ccp bands and small Py XX	662.18	662.22	x	x
RM07-20e	35591	Z-156T	stringer (footwall)	mass Py sul with Ccp and mm-large cubic Py XX in Qtz-eye rhy flow on lower contact	666.40	666.44	x	x
RM07-20g	35592	Z-157T	massive sulfide	mass Py-Ccp-Sp sul, near lower contact to intercalated md	654.12	654.16	x	x
RM07-20g	35593	Z-158T	massive sulfide	mass Py sul with coarse Py XX and fine sp	655.93	655.97	x	x
RM07-20g	35595	Z-159T	massive sulfide	mass Ccp-Sp-Py sul, on lower contact to intercalated md	657.32	657.36	x	x
RM07-20g	35596	Z-160T	massive sulfide	mass Py-Ccp sul with Sp-Asp/Tet (?) stringer/band	658.64	658.68	x	x
RM07-20g	35597	Z-161T	massive sulfide	mass Py sul with weak Ccp-Sp stringer	659.38	659.42	x	x
RM07-20g	35599	Z-162T	Qtz-vein directly below mass sul	coarse Ccp in Qtz vein	660.08	660.12	x	x
RM07-20g	35600	Z-163T	stringer (footwall)	fine Py-Ccp stringer in mas Qtz-eye rhy flow	660.63	660.67	x	x
RM07-20h	36001	Z-164T	massive sulfide	mass Py sul with Po band and minor Ccp, close to upper contact	655.35	655.39	x	x
RM07-20h	36002	Z-165T	massive sulfide	mass Py-Ccp-Po sul with rhy fragments	655.60	655.64	x	x
RM07-20h	36004	Z-166T	massive sulfide	mass Py sul with Ccp stringer and Po band	656.68	656.72	x	x
RM07-20h	36005	Z-167T	massive sulfide	mass Ccp sul with Py-Sp and rhy fragments	657.72	657.76	x	x
RM07-20h	36007	Z-168T	massive sulfide	mass sul with Py 'clasts' with Ccp around, El ?	658.16	658.20	x	x
RM07-20h	36010	Z-169T	massive sulfide	mass Py sul with Ccp stringer + Sp around Py 'clasts'	659.91	659.95	x	x
RM07-20h	36012	Z-170T	massive sulfide	mass Py sul with Ccp-Sp stringer, close to lower contact to intercalated md	660.95	660.99	x	x
RM07-20h	36013	Z-171T	massive sulfide	mass Ccp sul with Py, on upper contact and small dyke	663.04	663.08	x	x
RM07-20h	36015	Z-172T	massive sulfide	mass Py-Ccp sul with Sp-Po, close to upper contact of intercalated md	664.32	664.36	x	x
RM07-20i	36017	Z-173T	semi-massive sulfide	diss Ccp-py in semi-mass ul, near upper contact	654.47	654.51	x	x
RM07-20i	36018	Z-174T	semi-massive sulfide	mass Ccp stringer with Py-Po in semi-mass sul	654.76	654.80	x	x
RM07-20j	36019	Z-175T	massive sulfide	mass Py sul with small Py XX, minor Ccp ?, near upper contact	652.89	652.93	x	x
RM07-20j	36020	Z-176T	massive sulfide	mass Py sul with Ccp stringer, Po and rhy fragments	653.99	653.99	x	x
RM07-20j	36022	Z-177T	massive sulfide	mass Py sul, near upper contact to intercalated md	655.03	655.07	x	x
RM07-20j	36024	Z-178T	massive sulfide	mass Py-Ccp sul with Sp	656.62	656.66	x	x
RM07-20j	36026	Z-179T	massive sulfide	mass Ccp-Py sul with Sp	658.93	658.97	x	x
RM07-20j	36028	Z-180T	massive sulfide	mass Ccp sul with Py-Sp	660.55	660.59	x	x
RM07-20j	36030	Z-181T	massive sulfide	mass Ccp-Py sul, Py 'clasts' surrounded by Ccp-Po stringer	661.89	661.93	x	x
RM07-20j	36031	Z-182T	massive sulfide	mass Ccp sul with Po (+silver phase?), near lower contact	662.03	662.07	x	x
RM07-20m	36032	Z-183T	massive sulfide	mass Ccp sul with Py-Po, on upper contact	664.85	664.89	x	x
RM07-20m	36033	Z-184T	massive sulfide	mass Py sul with minor Ccp-Sp	665.14	665.18	x	x
RM07-20m	36034	Z-185T	massive sulfide	mass Py-Ccp sul with Ccp stringer + coarse Py	665.24	665.28	x	x
RM07-20m	36036	Z-186T	massive sulfide	mass Py sul with Ccp-Sp	666.64	666.68	x	x
RM07-20m	36037	Z-187T	massive sulfide	mass Py sul with coarse Py XX, Ccp-Sp	667.22	667.26	x	x
RM07-20m	36040	Z-188T	massive sulfide	mass Py sul with Sp band and coarser Py XX	668.08	668.12	x	x
RM07-20k	36041	Z-189T	massive sulfide	mass Py-Ccp sul with partly coarse Py XX, near upper contact	653.62	653.66	x	x
RM07-20k	36042	Z-190T	massive sulfide	mass Ccp-Py sul with Py XX (+ silvery phase?)	654.25	654.29	x	x
RM07-20k	36045	Z-191T	massive sulfide	mass Py-Ccp sul with Ccp stringer around Py 'clasts'	661.41	661.45	x	x
RM07-20k	36046	Z-192T	massive sulfide	mass Ccp-Py sul with Sp-silvery phase (Gn?) -Po	661.61	661.65	x	x
RM07-20k	36047	Z-192AT	massive sulfide	mass Py-Ccp sul with Ccp stringer in Py, silvery phase and rhy fragments, near lower contact	662.10	662.14	x	x
RM07-20l	36048	Z-193T	massive sulfide	mass Ccp-Py sul, transition Ccp- to Py-rich, coarse Py XX	656.40	656.44	x	x



RM07-20na	36049	Z-194T	massive sulfide	mass Py-Ccp sul with coarse Py XX, near upper contact	659.18	659.22	x	x
RM07-20na	36050	Z-195T	massive sulfide	mass Py-Ccp sul with coarse Py XX, near upper contact	660.24	660.28	x	x
RM07-20na	36051	Z-196T	massive sulfide	mass Py-Ccp sul with fine Sp band	660.54	660.58	x	x
RM07-20na	36052	Z-197T	massive sulfide	mass Py-Ccp sul with buckshot Py in Sp (or Po?), near lower contact	660.79	660.83	x	x
RM07-20o	36053	Z-198T	massive sulfide	mass Py sul with Ccp-Po and small Py XX, near upper contact	657.77	657.81	x	x
RM07-20o	36054	Z-199T	massive sulfide	mass Py-Ccp sul with coarse Py XX, near lower contact	657.90	657.94	x	x
RM07-20o	36055	Z-200T	stringer (footwall)	coarse Py-Ccp in sul stringer in mixed lap tuff, on upper contact	660.54	660.58	x	x
RM07-20o	36056	Z-201T	stringer (footwall)	coarse Ccp-Po-Py stringer in mixed lap tuff, on lower contact	660.86	660.90	x	x
RM07-18a	35558	NA	massive sulfide	mass Py-Ccp-Po sul	598.70	598.74	x	-
RM07-18a	35560	NA	massive sulfide	mass Py-Ccp sul with tiny Py XX	599.84	599.88	x	-
RM07-18b	35562	NA	massive sulfide	mass Py-Ccp sul on contact to strongly silicified mass rhy flow	603.05	603.09	x	-
RM07-18b	35564	NA	massive sulfide	mass Py-Ccp sul with Ccp schlieren/stringer around Py 'clasts'	604.43	604.47	x	-
RM07-20b	35576	NA	massive sulfide	mass Py-Ccp sul with small Py XX	666.38	666.42	x	-
RM07-20b	35578	NA	massive sulfide	mass Py-Ccp sul with coarser Py XX, on upper contact to intercalated Qtz-eye rhy flow	667.36	667.40	x	-
RM07-20b	35579	NA	massive sulfide	fine mass Py-Ccp sul with fine Sp bands (?)	670.15	670.29	x	-
RM07-20e	35587	NA	massive sulfide	mass Py-Ccp sul with fine Sp band (start of Sp band)	660.95	660.99	x	-
RM07-20e	35589	NA	massive sulfide	mass Py sul with prominent Ccp-Sp banding	661.68	661.72	x	-
RM07-20g	35594	NA	massive sulfide	mass Ccp-Py-Sp sul	656.78	656.82	x	-
RM07-20g	35598	NA	massive sulfide	mass Ccp-Py sul with fine Sp	659.78	659.82	x	-
RM07-20h	36003	NA	massive sulfide	mass Py-Ccp sul with coarser Py XX, Sp ?	656.01	656.05	x	-
RM07-20h	36006	NA	massive sulfide	mass Py-Ccp sul with Po	657.94	657.98	x	-
RM07-20h	36008	NA	massive sulfide	mass Py-Ccp sul	658.76	658.80	x	-
RM07-20h	36009	NA	massive sulfide	mass Py-Ccp sul with coarser Py XX	659.14	659.18	x	-
RM07-20h	36011	NA	massive sulfide	mass Py sul with Ccp stringer, Sp + coarse Py XX	660.50	666.54	x	-
RM07-20h	36014	NA	massive sulfide	mass Py sul with Ccp-Po bands	663.34	663.38	x	-
RM07-20h	36016	NA	massive sulfide	mass Py sul with Ccp-Po stringer around Py 'clasts'	664.45	664.49	x	-
RM07-20j	36021	NA	massive sulfide	mass Py sul, near lower contact to intercalated md	654.25	654.29	x	-
RM07-20j	36023	NA	massive sulfide	mass Py sul with Ccp, near upper contact to intercalated md	656.08	656.12	x	-
RM07-20j	36025	NA	massive sulfide	mass Py-Ccp sul	657.96	658.00	x	-
RM07-20j	36027	NA	massive sulfide	mass Py sul with Ccp-Sp stringer around Py 'clasts'	659.95	659.99	x	-
RM07-20j	36029	NA	massive sulfide	mass Py sul with Sp-Ccp stringer	661.18	661.22	x	-
RM07-20m	36035	NA	massive sulfide	mass Py-Ccp sul with Ccp stringer + coarse Py + Po	665.56	665.60	x	-
RM07-20m	36038	NA	massive sulfide	mass Py sul with Ccp-Sp, near intercalated rhy flow	667.70	667.74	x	-
RM07-20m	36039	NA	massive sulfide	mass Py sul with Ccp-Sp, near lower contact	668.42	668.46	x	-
RM07-20k	36043	NA	massive sulfide	mass Py-Ccp sul with coarser Py + Po, near lower contact	654.73	654.77	x	-
RM07-20k	36044	NA	massive sulfide	mass Ccp sul with Py-Sp, on upper contact	661.25	661.29	x	-

analyzed @ INCO (SEM, SIMS), UT (EPMA), and Laurentian University (LA-ICP-MS)

1 Alternative Sample No is engraved on back of thin-section slides



[illegible]

**Table eA4-1. (continued)** Compilation of methods applied to sulfide samples from the 1806 Zone. Abbreviations: EPMA - electron probe micro-analysis, LA-ICP electron microscopy, SIMS - secondary ion mass spectrometry, x - applied, - not applied, SJP - Stephen J Piercey

Drill hole	Section	Sample No.	Alternative Sample No <sup>1</sup>	Mineralization style	Comment	Depth_m in [m]	Depth_m ax [m]	Photo
RMUG08-143	2	29909	A-34	stringer	polymineralic stringer (Py+Sp+Ccp) in tuffaceous rhyolite	48.16	48.20	x
RMUG08-144	2	29922	A-47	stringer	Sp-Py stringer with accessory Asp/Tet in massive rhyolite [only observed polymineralic stringer in core]	13.88	13.92	x
RMUG08-145	2	29904	A-29	stringer	massive ± brecciated sulfide stringer (Sp+Py+Ccp) in rhyolite	55.02	55.07	x
RMUG08-145	2	29905	A-30	massive sulfide	Ccp+Py in massive sulfide	58.98	59.03	x
RMUG08-145	2	29906	A-31	massive sulfide	Sp+Py in massive sulfide	60.08	60.13	x
RMUG08-145	2	29907	A-32	massive sulfide	Py in massive sulfide (dead ore?)	60.84	60.88	x
RMUG08-145	2	29908	A-33	massive sulfide	Py in massive sulfide close to lower contact with silicified horizon	62.96	63.01	x
RMUG08-146	2	29916	A-41	stringer	Py stringer in massive rhyolite	51.12	51.16	x
RMUG08-146	2	29917	A-42	stringer	Py-Ccp-Sp stringer in massive rhyolite	51.60	51.64	x
RMUG08-146	2	29918	A-43	semi-massive sulfide	Py-Sp stringer in semi-massive zone at beginning of massive sulfide; in rhyolite with indicated crenulation cleavage	42.48	52.53	x
RMUG08-146	2	29919	A-44	massive sulfide	Py porphyroblast in Py-Po-Ccp matrix (buckshot texture) in massive sulfide	52.75	52.80	x
RMUG08-146	2	29920	A-45	massive sulfide	massive Py in massive sulfide (dead ore?)	53.68	53.73	x
RMUG08-146	2	29921	A-46	silicic horizon	massive Py stringer in massive Qtz (silicified horizon)	54.11	54.15	x
RMUG08-147	2	29923	A-48	stringer	sulfide stringer (Py+Ccp) in massive rhyolite	49.80	49.85	x
RMUG08-147	2	29924	A-49	stringer	Py stringer in Fuchsite-bearing, massive rhyolite	59.16	59.21	x
RMUG08-147	2	29925	A-50	stringer	Ccp stringer in rhyolite near contact to massive sulfide	63.28	63.32	x
RMUG08-147	2	29926	A-51	massive sulfide	Py and minor phases (Ccp+Asp/Tet+Au?) in massive sulfide	65.02	65.06	x
RMUG08-147	2	29927	A-52	massive sulfide	Ccp stringer (Au-bearing) in massive sulfide close to contact with silicified horizon	65.26	65.30	x
RMUG08-147	2	29928	A-53	silicic horizon	massive sulfide stringer (Py+ minor phases) in silicified horizon	67.25	67.30	x
RMUG08-147	2	29929	A-54	silicic horizon	brecciated sulfide stringer (Py+Ccp+Sp?) in silicified horizon	66.97	67.02	x
RMUG08-148	2	29930	A-55	stringer	Py-Ccp stringer in rhyolite	57.28	57.33	x
RMUG08-148	2	29931	A-56	stringer	cm-wide Py stringer in rhyolite	61.66	61.70	x
RMUG08-148	2	29932	A-57	stringer	Ccp-Py stringer in felsic (lapilli) tuff	77.71	77.75	x
RMUG08-148	2	29933	A-58	stringer	Py-Ccp stringer in rhyolite	45.90	45.95	x
RMUG08-148	2	29934	A-59	stringer	Py-Ccp stringer in rhyolite, Au-bearing	62.63	62.68	x
RMUG08-148	2	29935	A-60	stringer	Ccp-Py stringer in rhyolite	64.39	64.43	x
RMUG08-148	2	29936	A-61	massive sulfide	Ccp-Py in massive sulfide horizon, close to contact with mafic dyke	66.93	66.98	x
RMUG08-148	2	29937	A-62	semi-massive sulfide	Py+minor Ccp in semi-massive part of 2 <sup>nd</sup> massive sulfide horizon	70.99	71.04	x
RMUG08-148	2	29938	A-63	massive sulfide	Ccp-Py in massive sulfide horizon, close to contact with mafic dyke	71.51	71.56	x
RMUG08-120	21	36507			Sph-py-sulfosalt sulfides	54.20	54.24	SJP
RMUG08-120	21	36508			Py-rich sulfide with aspy-tetra-cpy; Au-rich zone	55.88	55.93	SJP
RMUG08-120	21	36509			Py-aspy-tetra with black material in py-rich sulfide.	56.48	56.52	SJP
RMUG08-120	21	36510			Py-aspy-cpy sulfide; py>>aspy,cpy	59.61	59.65	SJP

p-MS - laser ablation inductively coupled plasma mass spectrometry, SEM - scanning

[illegible]

RMUG08-120	21	36511	A-27	stringer	Ga-sph-chl-rich sulfide	60.22	60.25	SJP
RMUG08-121	21	29902	A-28	stringer	Py-Ccp stringer in rhyolite flow (Au-bearing)	46.39	46.44	x
RMUG08-121	21	29903		stringer	Ccp-Py stringer in rhyolite flow	46.51	46.56	x
RMUG08-123	21	36512			Sph-ga-rich sulfide	59.48	59.53	SJP
RMUG08-123	21	36513			Py-cpy-rich sulfide; Au-rich zone	63.09	63.14	SJP
RMUG08-123	21	36514			Py-sulfosalt-ga sulfides	63.54	63.59	SJP
RMUG08-123	21	36515			Cpy-py-assy sulfide	63.63	63.67	SJP
RMUG08-124	21	29910	A-35	stringer	sulfide stringer (Py+Sp) in rhyolite	40.78	40.83	x
RMUG08-124	21	29911	A-36	stringer	sulfide stringer (Py+Sp; semi-massive) in rhyolite	48.60	48.65	x
RMUG08-124	21	29912	A-37	stringer	sulfide stringer (Py+Sp+Ccp; semi-massive) in rhyolite	49.13	49.18	x
RMUG08-124	21	29913	A-38	stringer	Ccp-Py stringer in rhyolite (end of semi-massive zone)	50.50	50.55	x
RMUG08-125	21	36516			Ga-sph-cpy-rich sulfide with sulfosalts	49.56	49.61	SJP
RMUG08-125	21	36517			Py-sph-cpy-assy sulfide	52.09	52.13	SJP
RMUG08-125	21	36518			Py-sph-assy-cpy sulfide	54.26	54.29	SJP
RMUG08-125	21	36519			Py-assy-tetra sulfide	55.28	55.33	SJP
RMUG08-150	21	29914	A-39	stringer	fine Ccp-Py stringer in silicified horizon (massive Qtz) above stringer zone	65.67	65.72	x
RMUG08-150	21	29915	A-40	stringer	stringer (Py+minor Ccp) in silicified horizon (massive Qtz) above stringer zone	67.13	67.18	x
RMUG08-136	22	29776	A-1	massive sulfide	Py-Ccp bearing massive sulfide	46.10	46.17	x
RMUG08-137A	22	29777	A-2	massive sulfide	massive sulfide, Py + minor Ccp [dead sulfide]	52.39	52.45	x
RMUG08-138	22	29780	A-5	stringer	Py+Ccp stringers in rhyolite	23.40	23.45	x
RMUG08-138	22	29781	A-6	stringer	fine, partly sulfide stringers in rhyolite	40.55	40.60	x
RMUG08-138	22	36505			Sph-rich sulfide with ga-assy-sulfosalts	42.84	42.88	SJP
RMUG08-138	22	36506			Buckshot sulfides with py-po-sph	46.71	46.74	SJP
RMUG08-139	22	36501			Stringer py-ga-sph-assy in felsic lapillistone	36.70	36.77	SJP
RMUG08-139	22	36502			Cpy-py-sulfosalt ores with gangue, aspy.	40.00	40.04	SJP
RMUG08-139	22	36503			Cpy-sph-ga sulfides	43.53	43.57	SJP
RMUG08-139	22	36504			Buckshot sulfides with Po-sph-py-assy-cpy	44.28	44.32	SJP
RMUG08-140	22	29782	A-7	massive sulfide	massive sulfide (Py)	34.59	34.64	x
RMUG08-140	22	29783	A-8	silicic horizon	Ccp+Py in massive quartz [high-grade ore]	35.43	35.48	x
RMUG08-141	22	29784	A-9	stringer	sulfide stringers (Py+Sp) in rhyolite	24.50	24.55	x
RMUG08-141	22	29785	A-10	semi-massive sulfide	semi-massive sulfide (Py+Sp) around clast	41.10	41.15	x
RMUG08-141	22	29786	A-11	semi-massive sulfide	semi-massive sulfide (Py+Ccp) in rhyolite	42.75	42.80	x
RMUG08-141	22	29787	A-12	semi-massive sulfide	semi-massive sulfide (Py+Ccp+Sp) around rhyolite	43.70	43.75	x
RMUG08-142	22	29778	A-3	massive sulfide	massive sulfide (Py)	57.85	57.90	x
RMUG08-142	22	29779	A-4	massive sulfide	sul stringers in massive sulfide near rhyolite clast	62.20	62.50	x
RMUG08-142	22	36520			Grainy pyritic sulfide	60.51	60.55	SJP
RMUG08-142	22	36521			Cu-rich sulfide with sph, po, sulfosalts	64.74	64.78	SJP
RMUG08-142	22	36522			Buckshot sulfides with py-po-sph	65.53	65.57	SJP

analyzed @ INCO (SEM, SIMS), UT (EPMA), and Laurentian University (LA-ICP-MS)

1 Alteration Sampla Mo is analyzed on back of thick-section slides

2 Basite of Ph identified as Mn Cn and/or tetrahedrite, jennanite at Q ID

\* Polishing problems with 29781, sample 36505 as substitute for isotope studies



**Table eA4-1. (continued)** Compilation of methods applied to sulfide samples from the Ming South Up Plunge orebody. Abbreviations: EPMA - electron probe microspectrometry, SEM - scanning electron microscopy, SIMS - secondary ion mass spectrometry, x - applied, – not applied, NA - not available

Drill hole	Section	Sample No.	Alternative Sample No <sup>1</sup>	Mineralization style	Comment	Depth_m in [m]	Depth_m ax [m]	Photo
RMUG08-109	24	36195	H-11T	stringer (footwall)	Py±Ccp stringer in quartz eye lap tuff with weak Bt	27.14	27.18	x
RMUG08-109	24	36198	H-12T	massive sulfide	massive Py-Ccp sul with very fine Sp bands	41.50	41.54	x
RMUG08-109	24	36199	H-13T	stringer (hanging wall)	fine Py±Ccp stringer around quartz eyes in quartz eye tuff to lap tuff (Fsp/Ep alt parallel fol?)	44.94	44.98	x
RMUG08-107	24	62002	H-14T	massive sulfide	massive Py-Ccp sul	32.01	32.05	x
RMUG08-104	4	62016	H-15T	massive sulfide	massive Py-Ccp stringer in ±semi-massive quartz eye lap tuff	31.89	31.93	x
RMUG08-104	4	62017	H-16T	stringer (hanging wall)	Sp-Py stringer in Fuch-enriched quartz eye tuff to lap tuff, Sp out at 33.33m	33.25	33.29	x
RMUG08-64	14	62018	H-17T	stringer (footwall)	Ccp-Py stringer in rhy tuff to lap tuff	6.23	6.27	x
RMUG08-64	14	62021	H-18T	stringer (footwall)	Ccp-Py(-Po?) stringer in rhy lap tuff (sul mod)	86.06	86.10	x
RMUG08-63	14	62022	H-19T	stringer (footwall)	Ccp-Py-Po stringer in quartz eye lap tuff	4.78	4.82	x
RMUG08-63	14	62025	H-20T	stringer (footwall)	Py-Ccp-Sp stringer in quartz eye lap tuff (between fracture zones)	85.39	85.43	x
RMUG08-63	14	62027	H-21T	massive sulfide	massive Py-Ccp sul, near upper and lower contact	97.60	97.64	x
RMUG08-99	9	62030	H-22T	massive sulfide	massive Py-Ccp sul with fine Sp bands	43.14	43.18	x
RMUG08-99	9	62031	H-23T	semi-massive sulfide	semi-massive Py-Ccp-Sp sul in quartz eye lap tuff, sulfides around ghost clasts, Py cubes and Sp bands	45.37	45.41	x
RMUG08-99	9	62032	H-24T	stringer (hanging wall)	Py-Ccp stringer in quartz eye lap tuff after Fuchs is out (representative also of mod sul zone at 45.55-46.6m)	47.11	47.15	x
RMUG08-98	5	62033	H-25T	stringer (footwall)	Py-Ccp stringer in quartz eye lap tuff	38.03	38.07	x
RMUG08-98	5	62036	H-26T	massive sulfide	massive Py-Ccp sul with fine Sp bands	50.50	50.54	x
RMUG08-97	5	62038	H-27T	stringer (footwall)	Ccp-Po stringer with Py cubes (weak buckshot tex) in quartz eye flow (or tuff to lap tuff?)	0.70	0.74	x
RMUG08-97	5	62041	H-28T	stringer (footwall)	fine Py±Ccp±Sp stringer on mafic dyke contact (representative of complex unit)	7.90	7.94	x
RMUG08-95	5	62043	H-29T	stringer (footwall)	thick Py-Ccp-Po stringer in rhy flow (or lap tuff)	38.83	38.87	x
RMUG08-95	5	62044	H-30T	stringer (footwall)	Ccp-Py(-Po) stringer in quartz eye tuff to lap uff between mafic dyke and massive sulfide	40.64	40.68	x
RMUG08-95	5	62047	H-31T	massive sulfide	massive Py-Ccp sul after mafic dyke on lower contact	43.04	43.08	x
RMUG08-95	5	62048	H-32T	stringer (hanging wall)	Py-Ccp-Po stringer in quartz eye tuff to lap tuff (hanging wall representative)	45.62	45.66	x
RMUG08-96	9	62050	H-33T	stringer (footwall)	Py-Sp-Ccp stringer in Fuchs-bearing quartz eye tuff to lap tuff	71.63	71.67	x
RMUG08-96	9	62101	H-34T	massive sulfide	massive Py-Ccp±Sp sul	72.60	72.64	x
RMUG08-96	9	62104	H-35T	massive sulfide	massive Py-Ccp sul	83.14	83.18	x
RMUG08-60	14	62105	H-36T	stringer (footwall)	Ccp-Po stringer with Mag in quartz eye tuff to lap tuff	56.92	56.96	x
RMUG08-60	14	62107	H-37T	massive sulfide	massive Ccp-Py sul with Po and Mag	61.77	61.81	x
RMUG08-94	9	62108	H-38T_no block left	stringer (footwall)	Py-Sp-Ccp stringer in quartz eye flow (sul mod)	67.07	67.11	x
RMUG08-94	9	62110	H-39T	massive sulfide	massive Ccp-Py sul with Po (Mag?)	71.54	71.58	x
RMUG08-93	9	62112	H-40T	massive sulfide	massive Py-Ccp sul with Po	36.68	36.72	x
RMUG08-93	9	62113	H-41T	stringer (footwall)	Py-Sp-Ccp stringer in quartz eye tuff to lap tuff	37.56	37.60	x
RMUG08-93	9	62116	H-42T	semi-massive sulfide	semi-massive Py-Ccp-Po sul in quartz eye tuff to lap tuff	48.00	48.04	x

[illegible]

RMUG08-61	14	62118	H-43T	stringer (footwall)	Ccp-Py stringer in quartz eye flow	51.30	51.34	x
RMUG08-61	14	62119	H-44T	massive sulfide	massive Py-Ccp-Po sul	52.32	52.36	x
RMUG08-61	14	62120	H-45T	massive sulfide	massive Py sul with rhy clasts ('transition' subseafloor to seafloor deposition?)	52.82	52.86	x
RMUG08-61	14	62121	H-46T	massive sulfide	massive Py-Ccp-Sp sul	53.07	53.11	x
RMUG08-44	8	62125	H-47T_no block left	massive sulfide	massive Ccp-Po-Py sul with thick Po schlieren	32.31	32.35	x
RMUG08-44	8	62126	H-48T	stringer (hanging wall)	Ccp-Po±Py stringer in quartz eye flow	33.06	33.10	x
RMUG08-44	8	62127	H-49T	massive sulfide	massive Py-Ccp sul with Ccp around Py clasts and fine Po schlieren (replacement tex?)	32.00	32.04	x
RMUG08-91	13	62128	H-50T	stringer (footwall)	brecciated Py-Po-Ccp stringer around coarse silic clasts in quartz eye tuff to lap tuff (sul mod)	29.43	29.47	x
RMUG08-91	13	62129	H-51T	stringer (footwall)	fine Py-Sp±Ccp stringer in quartz eye tuff to lap tuff with mod Fuchs	45.73	45.77	x
RMUG08-91	13	62130	H-52T	massive sulfide	massive Py-Ccp sul with Po schlieren	49.07	49.11	x
RMUG08-91	13	62132	H-53T	semi-massive sulfide	(semi-)mass Py-Ccp sul with po and rhy fragments	54.12	54.16	x
RMUG08-91	13	62133	H-54T	FeOx rhy in hanging wall	rhyolite with fine FeOx schlieren	54.43	54.47	x
RMUG08-90	13	62135	H-55T	stringer (footwall)	Py-Ccp-Po (or Sp) stringer in quartz eye lap tuff	1.90	1.94	x
RMUG08-90	13	62139	H-56T	massive sulfide	massive Py-Ccp sul with very fine Sp bands (?)	60.53	60.57	x
RMUG08-106	4	62140	H-57T	stringer (footwall)	thick Py-Ccp±Sp stringer in quartz eye flow (sul mod)	21.76	21.80	x
RMUG08-106	4	62141	H-58T_no block left	stringer (footwall)	Py-Sp±Ccp stringer in quartz eye flow (sul mod)	21.83	21.87	x
RMUG08-106	4	62144	H-59T	stringer (hanging wall)	Py(-Ccp-Po?) stringer in quartz eye, Chl + sil flow (white Quartz eyes)	46.61	46.65	x
RMUG08-109	24	36196	NA	massive sulfide	massive Py-Ccp sul with silvery phase (Asp/Tet?) and rhy fragments on upper contact	39.48	39.52	x
RMUG08-109	24	36197	NA	massive sulfide	massive Py-Ccp sul with Po schlieren near rhy fragment	40.07	40.11	x
RMUG08-107	24	36200	NA	massive sulfide	massive Py-Ccp sul with fine Sp bands	31.85	31.89	x
RMUG08-64	14	62019	NA	stringer (footwall)	Py-Sp stringer in rhy lap tuff with weak Fuchs	13.51	13.55	x
RMUG08-64	14	62020	NA	stringer (footwall)	Py-Ccp stringer + Mag in quartz eye lap tuff	62.83	62.87	x
RMUG08-63	14	62023	NA	stringer (footwall)	Ccp-Py(-Po?) stringer in quartz eye lap tuff	39.71	39.75	x
RMUG08-63	14	62024	NA	stringer (footwall)	Py stringer in lap tuff	54.94	54.98	x
RMUG08-63	14	62026	NA	semi-massive sulfide	semi-massive Py-Ccp±Sp sul in (quartz eye?) lap tuff	96.89	96.93	x
RMUG08-63	14	62028	NA					x
RMUG08-99	9	62029	NA	massive sulfide	massive Ccp-Po-Py sul with weak Py buckshot tex	42.73	42.77	x
RMUG08-98	5	62034	NA	stringer (footwall)	Sp-Py(±Ccp) stringer in quartz eye tuff to lap tuff	44.47	44.51	x
RMUG08-98	5	62035	NA	massive sulfide	massive Py-Ccp sul with fine Sp bands (on upper contact)	44.79	44.83	x
RMUG08-98	5	62037	NA	massive sulfide	massive Py-Ccp sul with rhy fragments	50.75	50.79	x
RMUG08-97	5	62039	NA	stringer (footwall)	fine Py-Sp-Ccp stringer in quartz eye tuff to lap tuff	3.43	3.47	x
RMUG08-97	5	62040	NA	stringer (footwall)	thick Py-Sp-Ccp stringer in quartz eye tuff to lap tuff (sul mod)	4.24	4.28	x
RMUG08-95	5	62042	NA	stringer (footwall)		35.26	35.30	x
RMUG08-95	5	62045	NA	massive sulfide	massive Py-Ccp sul with fine Sp band	40.99	41.03	x
RMUG08-95	5	62046	NA	massive sulfide	massive Ccp-Py (-Po?) sul near mafic dyke contact	42.65	42.69	x
RMUG08-96	9	62049	NA	stringer (footwall)	Py-Ccp-Po stringer in sericitized in quartz eye flow (or lap tuff?)	52.46	52.50	x
RMUG08-96	9	62102	NA	massive sulfide	massive Py-Ccp sul	73.19	73.23	x
RMUG08-96	9	62103	NA	stringer (in between massive sulfide horizons)	Py-Ccp±Sp stringer in deformed quartz eye tuff to lap tuff on mafic dyke contact	82.14	82.18	x
RMUG08-60	14	62106	NA	stringer (footwall)	fine Py stringer in quartz eye lap tuff	59.06	59.10	x



14

RMUG08-94	9	62109	NA	stringer (footwall)	Py-Sp-Ccp stringer in quartz eye flow (sul mod, near semi-mass sul)	71.09	71.13	x
RMUG08-93	9	62111	NA	stringer (footwall)	Py-Po-Ccp stringer in quartz eye tuff to lap tuff	35.81	35.85	x
RMUG08-93	9	62114	NA	stringer (footwall)	Py-Ccp stringer in quartz eye flow (close to sul decrease)	40.83	40.87	x
RMUG08-93	9	62115	NA	stringer (hanging wall?)	Py-Sp-Ccp stringer in quartz eye tuff to lap tuff with white quartz eyes	46.56	46.60	x
RMUG08-61	14	62117	NA	stringer (footwall)	Py-Ccp stringer in quartz eye tuff to lap tuff (or lap tuff?)	50.52	50.57	x
RMUG08-61	14	62122	NA	stringer (hanging wall)	Ccp-Py stringer in quartz eye tuff to lap tuff	53.66	53.70	x
RMUG08-44	8	62123	NA	stringer (footwall)	Py-Ccp stringer in quartz eye flow	27.59	27.63	x
RMUG08-44	8	62124	NA	massive sulfide	massive Py-Ccp sul with fine Po schlieren with Ccp halo and fine Py cubes	30.88	30.92	x
RMUG08-91	13	62131	NA	massive sulfide	massive Py-Ccp sul with fine Po	52.78	52.82	x
RMUG08-91	13	62134	NA	semi-massive sulfide	(semi-)mass Py-Ccp sul on contact to quartz vein in mafic dyke	54.96	55.00	x
RMUG08-90	13	62136	NA	stringer (footwall)	Py-Ccp stringer in quartz eye lap tuff	14.30	14.34	x
RMUG08-90	13	62137	NA	stringer (footwall)	Py-Ccp-Po stringer in quartz eye lap tuff	56.74	56.78	x
RMUG08-90	13	62138	NA	massive sulfide	massive Py-Ccp sul with end of buckshot texture	60.25	60.29	x
RMUG08-106	4	62142	NA	stringer (footwall)	Py-Sp-Ccp stringer in quartz eye flow (white Quartz eyes)	31.34	31.38	x
RMUG08-106	4	62143	NA	stringer (footwall)	Py-Ccp stringer in quartz eye flow (white Quartz eyes)	35.93	35.97	x

analyzed @ INCO (SEM, SIMS), UT (EPMA), and Laurentian University (LA-ICP-MS)

1 Alternative Sample No. is engraved on back of thin-section slides

2 no reflected light images taken but full descriptions available

| | | | | | | | | | | | | | | | | |

| | | | | | | | | | | | | | | | | |

| | | | | | | | | | | | | | | | | |

| | | | | | | | | | | | | | | | | |

| | | | | | | | | | | | | | | | | |

| | | | | | | | | | | | | | | | | |

**Table eA4-1. (continued)** Compilation of methods applied to sulfide samples from the Ming South Down Plunge and Lower Footwall Zone (LFWZ) orebodies. Abt laser ablation inductively coupled plasma mass spectrometry, SEM - scanning electron microscopy, SIMS - secondary ion mass spectrometry, x - applied, - not applied

Drill hole	Sample No.	Alternative Sample No1	Mineralization style	Comment	Depth_m in [m]	Depth_m ax [m]	Photo	Thick section [200 µm]
RM06-04e	29788	A-13	massive sulfide	massive sulfide (Py+Po)	887.10	887.15	x	x
RM06-04e	29789	A-14	massive sulfide	massive Ccp-Po-Py mineralization near Qtz-vein in massive sulfide	889.25	889.30	x	x
RM06-04e	29790	A-15	massive sulfide	massive sulfide (Py+Po)	893.75	893.80	x	x
RM06-04e	29791	A-16	stringer (footwall)	sulfide stringers in felsic volcanics	898.00	898.05	x	x
RM06-04e	29792	A-17	stringer (footwall)	Ccp in massive Qtz	903.15	903.20	x	x
RM06-04e	29793	A-18	stringer (footwall)	Ccp stringer in felsic volcanic (tuffaceous rhyolite?)	899.55	899.60	x	x
RM06-04e	29794	A-19	LFWZ	Ccp stringers	1,073.32	1,073.37	x	x
RM06-04e	29795	A-20	LFWZ	Ccp stringer in tuff	1,084.60	1,084.65	x	x
RM06-04e	29796	A-21	LFWZ	sulfide stringers (Ccp) in tuff	1,097.34	1,097.39	x	x
RM06-04e	29797	A-22	LFWZ	sulfide stringers (Ccp+Po+Py) in tuff	1,102.00	1,102.05	x	x
RM06-04e	29798	A-23	LFWZ	sulfide stringers (Ccp+Po) slightly brecciated around tuffaceous matrix	1,113.23	1,113.28	x	x
RM06-04e	29799	A-24	LFWZ	massive sulfide stringer (Ccp+Po) in tuff	1,132.15	1,132.20	x	x
RM06-04e	29800	A-25	LFWZ	sulfide stringer (Ccp+Po+Py) in tuff around Qtz	1,180.38	1,180.43	x	x
RM06-04e	29901	A-26	massive sulfide	massive sulfide stringer (Ccp+Po) in dyke or tuff at contact to secondary Qtz	1,205.00	1,205.05	x	x
RM06-04m	36057	Z-37T	massive sulfide	mass Py sul with minor Ccp and small rhy fragments, near upper contact	895.75	895.79	x	x
RM06-04m	36058	Z-38T	massive sulfide	mass Py sul with minor Ccp, smal Py XX and rhy fragments, near lower contact	896.71	896.75	x	x
RM06-04m	36059	Z-39T	massive sulfide	mass Py sul with Ccp-Po	909.36	909.40	x	x
RM06-04m	36060	Z-40T	massive sulfide	Py-Ccp stringer around rhy fragments in mass sul, on lower contact	910.57	910.61	x	x
RM06-04m	36061	Z-41T	stringer (footwall)	Py-Ccp stringer in Qtz-eye lap tuff	916.95	916.99	x	x
RM06-04m	36063	Z-42T	stringer (footwall)	Py-Ccp stringer in Qtz-eye tuff to lap tuff	919.09	919.13	x	x
RM06-04m	36065	Z-43T	stringer (footwall)	Ccp-Py stringer in rhy tuff to lap tuff	930.25	930.29	x	x
RM06-04m	36066	Z-44T	stringer (footwall)	Py-Ccp-Sp stringer in F-bearing, Qtz-eye lap tuff	945.29	945.33	x	x
RM06-04m	36067	Z-45T	stringer (footwall)	Ccp-Py-Po stringer in Qtz-eye rhy flow	949.98	950.02	x	x
RM06-04m	36072	Z-46T	stringer (footwall)	Ccp-Po-Py stringer in Qtz-eye rhy flow	962.57	962.61	x	x
RM06-04m	36074	Z-47T	semi-massive sulfide	semi-mass Ccp-Po stringer in Qtz-eye tuff to lap tuff	967.62	967.66	x	x
RM06-04m	36075	Z-48T	stringer (footwall)	Py-Ccp stringer in Qtz-eye tuff to lap tuff	967.89	967.93	x	x
RM06-04m	36076	Z-49T	stringer (footwall)	Py-Ccp stringer in rhy lap tuff	972.06	972.10	x	x
RM06-04m	36077	Z-50T	stringer (footwall)	Py-Ccp stringer in rhy lap tuff	972.87	972.91	x	x
RM06-04m	36078	Z-51T	stringer (footwall)	Py-Ccp stringer in rhy lap tuff	973.07	973.11	x	x
RM06-04m	36079	Z-52T	stringer (footwall)	Ccp-Po stringer in rhy tuff to lap tuff	977.29	977.33	x	x
RM06-04m	36080	Z-53T	LFWZ	Ccp-Py stringer in rhy flow	1,006.69	1,006.73	x	x
RM06-04m	36082	Z-54T	LFWZ	coarse Mag, Ccp-Py-Po stringer in Qtz-eye tuff to lap tuff	1,008.07	1,008.11	x	x
RM06-04m	36083	Z-55T	LFWZ	Ccp-Po-Py stringer in Qtz-eye tuff to lap tuff	1,008.16	1,008.20	x	x
RM06-04m	36085	Z-56T	LFWZ	Ccp-Po-Py stringer in rhy flow	1,010.96	1,011.00	x	x
RM06-04m	36087	Z-57T	LFWZ	Ccp-Py-Po stringer in rhy lap tuff	1,018.35	1,018.39	x	x
RM06-04m	36088	Z-58T	LFWZ	Ccp-Py stringer in rhy flow	1,020.46	1,020.50	x	x

Abbreviations: EPMA - electron probe micro-analysis, LA-ICP-MS -  
laser ablation inductively coupled plasma mass spectrometry, NA - not available

Ore microscopy	METHODS			
	SEM	EPMA	LA-ICP-MS	SIMS
X	-	-	-	-
X	X	X	-	X
X	-	-	-	-
X	-	-	-	-
X	-	-	-	-
X	-	-	-	-
X	-	-	-	-
X	-	-	-	-
X	X	X	X	X
X	-	-	-	-
X	-	-	-	-
X	X	X	X	X
X	X	-	-	-
X	X	-	-	-
X	X	-	-	-
X	X	X	X	X
X	-	-	-	-
X	X	-	-	-
X	-	-	-	-
X	-	-	-	-
X	-	-	-	-
X	X	X	X	X
√2,3	-	-	-	-
√2,3	-	-	-	-
√2,3	-	-	-	-
√2,3	-	-	-	-
√2,3	-	-	-	-
√2,3	-	-	-	-
√2,3	-	-	-	-
√2,3	X	X	X	X
√2,3	-	-	-	-
√2,3	-	-	-	-
√2,3	-	-	-	-
√2,3	-	-	-	-

RM06-04m	36091	Z-59T	LFWZ	Ccp-Py-Po stringer with Mag in rhy flow	1,023.24	1,023.28	x	x
RM06-04m	36092	Z-60T	LFWZ	coarse Ccp-Po-Py stringer with finer Py in rhy flow	1,023.82	1,023.86	x	x
RM06-04m	36094	Z-61T	LFWZ	Py-Ccp stringer in rhy flow	1,035.31	1,035.35	x	x
RM06-04m	36097	Z-62T	LFWZ	Ccp-Po and Ccp-Py stringer in Qtz-eye tuff to lap tuff with Chl-Mag-rich interlayer between both stringer	1,042.00	1,042.04	x	x
RM06-04m	36098	Z-63T	LFWZ	Ccp-Po stringer in rhy flow	1,077.76	1,077.80	x	x
RM06-04m	36100	Z-64T	LFWZ	Ccp-Po stringer in rhy flow	1,078.81	1,078.85	x	x
RM06-04m	36102	Z-65T	LFWZ	Ccp-Po stringer in rhy tuff to lap tuff (or flow?), on lower contact	1,084.93	1,084.97	x	x
RM06-04m	36103	Z-66T	LFWZ	Ccp-Py stringer in Qtz-eye rhy flow	1,087.68	1,087.72	x	x
RM06-04m	36105	Z-67T	LFWZ	Ccp-Po-Py stringer and Mag in rhy flow	1,092.26	1,092.30	x	x
RM06-04m	36109	Z-68T	LFWZ	Ccp-Po stringer with coarse Py, Mag and mafic clast in rhy flow	1,095.83	1,095.88	x	x
RM06-04m	36110	Z-69T	LFWZ	Ccp-Po-Py stringer with partly coarse Py and Mag in rhy lap tuff	1,103.38	1,103.42	x	x
RM06-04m	36113	Z-70T	Qtz-vein in md	coarse Py-Ccp min in Qtz vein in md	1,110.67	1,110.71	x	x
RM06-04m	36114	Z-71T	LFWZ	thick Ccp-Po stringer in rhy flow	1,117.61	1,117.65	x	x
RM06-04m	36117	Z-72T	LFWZ	Ccp-Po stringer with Mag/Bt in rhy flow	1,124.61	1,124.65	x	x
RM06-04m	36119	Z-73T	LFWZ	Ccp-Po stringer with Mag/Bt in rhy flow	1,131.04	1,131.08	x	x
RM06-04m	36120	Z-74T	LFWZ	mass Ccp-Po stringer in Amph-rich part of rhy flow	1,134.55	1,134.59	x	x
RM06-04m	36121	Z-75T	LFWZ	Ccp-Po stringer with mafic parts in Amph-rich part of rhy flow	1,135.54	1,135.58	x	x
RM06-04m	36126	Z-76T	LFWZ	Ccp-Py-Po stringer with Amph-bearing mafic parts in rhy flow	1,155.16	1,155.20	x	x
RM06-04m	36127	Z-77T	LFWZ	#brecciated Ccp-Po-Py stringer in rhy flow	1,156.53	1,156.57	x	x
RM06-04m	36128	Z-78T	LFWZ	Ccp-Po-Py stringer with silicic clasts and mafic parts in Qtz-eye rhy flow	1,158.97	1,159.01	x	x
RM06-04m	36130	Z-79T	LFWZ	Ccp stringer folded with silicic clasts in rhy lap tuff	1,162.09	1,162.13	x	x
RM06-04m	36131	Z-80T	LFWZ	Ccp-Po stringer with Amph-bearing mafic parts in rhy lap tuff	1,177.19	1,177.23	x	x
RM06-04m	36133	Z-81T	LFWZ	#brecciated Ccp-Po stringer around Amph-bearing mafic clasts in rhy flow	1,182.86	1,182.90	x	x
RM06-04m	36134	Z-82T	LFWZ	Ccp-Po stringer with mafic parts in rhy lap tuff (or flow?)	1,185.13	1,185.17	x	x
RM06-04m	36137	Z-83T	LFWZ	Ccp-Po stringer with mafic parts in rhy flow	1,194.85	1,194.89	x	x
RM06-04m	36140	Z-84T	LFWZ	brecciated Ccp-Po stringer around Amph-bearing mafic clasts in rhy flow, close to upper contact	1,202.03	1,203.07	x	x
RM06-04m	36142	Z-85T	LFWZ	Ccp-Po-Py stringer with very coarse Amph (Bt?) in Chl-rich part of rhy flow	1,206.68	1,206.72	x	x
RM06-04m	36144	Z-86T	LFWZ	thick Ccp-Po-Py stringer with mafics and mafic parts in rhy flow (or lap tuff?)	1,211.55	1,211.59	x	x
RM06-04m	36145	Z-87T	LFWZ	folded Ccp stringer with weak cren cleavage in rhy flow (or lap tuff?), near lower contact	1,213.24	1,213.28	x	x
RM06-04m	36146	Z-88T	LFWZ	fine Ccp-Py-Po stringer in rhy flow	1,217.09	1,217.13	x	x
RM06-04m	36148	Z-89T	LFWZ	Ccp-Po stringer on mafic clast in rhy flow	1,262.40	1,262.44	x	x
RM06-04m	36150	Z-90T	LFWZ	Ccp-Po stringer around mafic clasts in rhy flow	1,277.79	1,277.83	x	x
RM06-04m	36152	Z-91T	LFWZ	Ccp-Po stringer with coarse Py in Chl-mafics rich part of rhy flow	1,286.55	1,286.59	x	x
RM06-04m	36153	Z-92T	LFWZ	fine Ccp-Po stringer on mafic part in Qtz-enriched rhy flow	1,287.30	1,287.34	x	x
RM06-04m	36154	Z-93T	LFWZ	fine Ccp-Po-Py stringer on Chl in Qtz-eye lap tuff	1,296.40	1,296.44	x	x
RM06-04m	36155	Z-94T	LFWZ	fine Ccp-Po-Py stringer in rhy lap tuff with mafics	1,305.23	1,305.27	x	x
RM06-04m	36157	Z-95T	LFWZ	fine Ccp-Po-Py stringer on mafic clast, mafics in Qtz-eye rhy flow	1,326.10	1,326.14	x	x
RM06-04m	36159	Z-96T	LFWZ	Ccp-Po stringer in Qtz-eye flow	1,337.16	1,337.20	x	x
RM06-04m	36160	Z-97T	LFWZ	Ccp-Po-Py stringer, mafics in Qtz-eye flow	1,327.44	1,327.48	x	x
RM06-04d	36161	Z-98T	massive sulfide	mass Py-Ccp sul with upper silicic part and Py stringers, on upper contact	881.48	881.52	x	x

20

RM06-04d	36163	Z-99T	massive sulfide	mass Ccp-Po-Py sul with Tet or Asp, on contact to intercalated Qtz-eye lap tuff	882.81	882.85	x	x
RM06-04d	36165	Z-100T	massive sulfide	mass Py-Ccp sul with Po and silicic clasts, near upper contact	889.78	889.82	x	x
RM06-04d	36167	Z-101T	stringer in massive sulfide	Py-Sp stringer in intercalated rhy flow in mass sul	890.24	890.28	x	x
RM06-04d	36168	Z-102T	massive sulfide	mass Py-Ccp sul with Ccp-Po-coarse Py schlieren	891.40	891.44	x	x
RM06-04d	36169	Z-103T	massive sulfide	mass Py-Ccp sul	892.56	892.60	x	x
RM06-04d	36171	Z-104T	semi-massive sulfide	semi-mass Py-Ccp-Sp sul in rhy flow	893.73	893.77	x	x
RM06-04d	36172	Z-105T	semi-massive sulfide	semi-mass Py-Ccp sul in Fuchs-bearing rhy flow	894.51	894.55	x	x
RM06-04d	36174	Z-106T	stringer (footwall)	fine Py±Ccp stringer in mass rhy flow	896.85	896.89	x	x
RM06-04d	36175	Z-107T	stringer (footwall)	fine Py±Ccp stringer in mass rhy flow, near lower contact to md	899.11	899.15	x	x
RM06-04i	36176	Z-108T	stringer (hanging wall)	thick Py stringer with minor Ccp and silicic rhy clasts in mass rhy flow, on lower contact	883.60	883.64	x	x
RM06-04i	36178	Z-109T	stringer (hanging wall)	Py-Ccp stringer in Qtz-eye lap tuff	911.94	911.98	x	x
RM06-04i	36180	Z-110T	massive sulfide	mass Py-Ccp sul with Po-coarser Py	914.98	915.02	x	x
RM06-04i	36182	Z-111T	massive sulfide	mas Ccp-Py sul with Ccp-Po 'schlieren'	917.45	917.49	x	x
RM06-04i	36183	Z-112T	massive sulfide	mass Py sul with Sp bands	917.93	917.97	x	x
RM06-04i	36184	Z-113T	massive sulfide	mass Ccp-Py sul with silicic clasts	918.22	918.26	x	x
RM06-04i	36185	Z-114T	massive sulfide	mass Py-Ccp sul with coarser Py + Po (?)	918.66	918.70	x	x
RM06-04i	36187	Z-115T	semi-massive sulfide	Ccp-Py stringer in Qtz-eye lap tuff of semi-mass sul	919.25	919.35	x	x
RM06-04i	36188	Z-116T	massive sulfide	Ccp-Py sul around coarse silicic ±Fuchs-bearing clasts	920.05	920.06	x	x
RM06-04i	36189	Z-117T	massive sulfide	mass Py-Ccp sul with partly coarse Py XX	920.29	920.33	x	x
RM06-04i	36190	Z-118T	massive sulfide	mass Py-Ccp sul with Sp or Po and coarser Py and silicic clasts, near lower contact	921.03	921.07	x	x
RM06-04i	36192	Z-119T	stringer (footwall)	fine Py stringer in Qtz-eye flow	922.46	922.50	x	x
RM06-04i	36193	Z-120T	stringer (footwall)	fine Py-Sp? stringer in Qtz-eye flow	924.55	924.59	x	x
RM06-04m	36062	NA	stringer (footwall)	Py-Ccp stringer in Qtz-eye lap tuff	917.87	917.91	x	-
RM06-04m	36064	NA	stringer (footwall)	Py-Ccp stringer in Qtz-eye tuff to lap tuff	927.85	927.89	x	-
RM06-04m	36068	NA	stringer (footwall)	Ccp-Py-Po stringer in Qtz-eye rhy flow	954.21	954.25	x	-
RM06-04m	36069	NA	stringer (footwall)	coarse Py-Ccp stringer in Qtz-eye tuff to lap tuff	955.08	955.12	x	-
RM06-04m	36070	NA	stringer (footwall)	folded Py-Ccp stringer in Qtz-eye tuff to lap tuff	956.87	956.91	x	-
RM06-04m	36071	NA	stringer (footwall)	Ccp-Po-Py stringer in Qtz-eye lap tuff	958.56	958.60	x	-
RM06-04m	36073	NA	stringer (footwall)	Ccp-Po-Py stringer in Qtz-eye rhy flow	964.94	964.98	x	-
RM06-04m	36081	NA	stringer (footwall)	Ccp-Py-Po stringer in rhy flow	1,006.86	1,006.90	x	-
RM06-04m	36084	NA	stringer (footwall)	Ccp-Po-Py stringer in Qtz-eye tuff to lap tuff	1,010.05	1,010.09	x	-
RM06-04m	36086	NA	stringer (footwall)	Ccp-Py-Po stringer in rhy flow	1,014.02	1,014.06	x	-
RM06-04m	36089	NA	stringer (footwall)	Ccp-Po-Py stringer in rhy flow	1,021.50	1,021.54	x	-
RM06-04m	36090	NA	stringer (footwall)	Ccp-Py-Po stringer with silicic clasts in rhy flow	1,022.34	1,022.38	x	-
RM06-04m	36093	NA	stringer (footwall)	Ccp-Po-Py stringer near mafic clast in rhy flow	1,025.85	1,025.89	x	-
RM06-04m	36095	NA	stringer (footwall)	fine Py-Ccp stringer in Qtz-eye tuff to lap tuff	1,039.10	1,039.14	x	-
RM06-04m	36096	NA	stringer (footwall)	fine Py-Ccp stringer in Qtz-eye tuff to lap tuff	1,041.18	1,041.22	x	-
RM06-04m	36099	NA	stringer (footwall)	fine Ccp-Py-Po stringer in rhy flow	1,078.19	1,078.23	x	-
RM06-04m	36101	NA	stringer (footwall)	Ccp-Po stringer with Mag (?) in rhy tuff to lap tuff (or flow?)	1,081.21	1,081.25	x	-
RM06-04m	36104	NA	stringer (footwall)	Ccp stringer with coarse Py, Mag in rhy tuff to lap tuff (or flow?)	1,084.64	1,084.68	x	-
RM06-04m	36106	NA	stringer (footwall)	Ccp-Po-Py stringer and Mag in rhy flow	1,093.81	1,093.85	x	-
RM06-04m	36107	NA	stringer (footwall)	Ccp-Po stringer with fine Py and Amph-bearing mafic clast in rhy flow	1,094.27	1,094.31	x	-
RM06-04m	36108	NA	stringer (footwall)	Ccp-Py-Po stringer with mafic clast in rhy flow	1,094.99	1,095.03	x	-
RM06-04m	36111	NA	stringer (footwall)	Ccp-Po-Py stringer with partly coarse Py, Mag and mafic clast in rhy lap tuff	1,103.92	1,103.96	x	-
RM06-04m	36112	NA	stringer (footwall)	Ccp-Py-Po stringer with (silicic) clast in rhy flow	1,105.40	1,105.44	x	-



[illegible]

RM06-04m	36115	NA	stringer (footwall)	Ccp-Po-Py stringer with Amph-bearing mafic clasts in rhy flow in between md's	1,120.31	1,120.35	x	-
RM06-04m	36116	NA	stringer (footwall)	Ccp-Po stringer with Mag/Bt in Qtz-eye rhy flow	1,123.05	1,123.09	x	-
RM06-04m	36118	NA	stringer (footwall)	Ccp-Po stringer with Mag/Bt in rhy flow	1,128.32	1,128.36	x	-
RM06-04m	36122	NA	stringer (footwall)	Ccp-Po stringer in Qtz-eye rhy flow	1,139.35	1,139.39	x	-
RM06-04m	36123	NA	stringer (footwall)	Ccp-Po stringer with mafic, Amph-bearing clasts in rhy flow	1,142.29	1,142.33	x	-
RM06-04m	36124	NA	stringer (footwall)	Ccp-Po stringer with mafic, Amph-bearing clasts, Mag/Bt in rhy flow	1,142.94	1,142.98	x	-
RM06-04m	36125	NA	stringer (footwall)	Ccp-Po stringer with Mag/Bt and mafic clasts in rhy flow	1,145.27	1,145.32	x	-
RM06-04m	36129	NA	stringer (footwall)	#brecciated Ccp-Po-Py stringer around Amph-bearing mafic parts in Qtz-eye rhy flow	1,159.47	1,159.51	x	-
RM06-04m	36132	NA	stringer (footwall)	Ccp stringer with minor Po around mafic clasts in in rhy lap tuff	1,178.69	1,178.73	x	-
RM06-04m	36135	NA	stringer (footwall)	Ccp-Po stringer with mafic parts in rhy lap tuff (or flow?)	1,186.22	1,186.26	x	-
RM06-04m	36136	NA	stringer (footwall)	finely folded Ccp-Po stringer in rhy flow	1,191.58	1,191.62	x	-
RM06-04m	36138	NA	stringer (footwall)	Ccp-Po stringer around mafic clasts with mafics (Bt, Amph) in rhy flow	1,198.77	1,198.81	x	-
RM06-04m	36139	NA	stringer (footwall)	fine Ccp-Po stringer with mafics and mafic parts/clasts in Qtz-eye rhy flow	1,202.15	1,202.19	x	-
RM06-04m	36141	NA	stringer (footwall)	Po-Ccp stringer with mafics and mafic parts in rhy flow	1,205.80	1,205.84	x	-
RM06-04m	36143	NA	stringer (footwall)	#brecciated Ccp-Po stringer in fol Qtz-eye rhy flow	1,208.40	1,208.44	x	-
RM06-04m	36147	NA	stringer (footwall)	Ccp-Po stringer on mafic clast in rhy flow	1,260.69	1,260.73	x	-
RM06-04m	36149	NA	stringer (footwall)	#brecciated Ccp-Po stringer + diss Ccp in rhy lap tuff	1,268.02	1,268.06	x	-
RM06-04m	36151	NA	stringer (footwall)	Ccp-Po stringer on mafic clasts in rhy flow	1,278.78	1,278.82	x	-
RM06-04m	36156	NA	stringer (footwall)	Ccp-Po stringer around mafic clast, mafics in Qtz-eye rhy flow	1,321.55	1,321.59	x	-
RM06-04m	36158	NA	stringer (footwall)	fine Ccp-Po+Py stringer with weak mafics in Qtz-eye rhy flow	1,333.08	1,333.12	x	-
RM06-04d	36162	NA	massive sulfide	mass Py-Ccp sul with fine Po schlieren and coarse Py, on contact to intercalated Fuchs-bearing Qtz-eye lap tuff	882.12	882.16	x	-
RM06-04d	36164	NA	massive sulfide	mass Py-Ccp sul, on lower contact	883.35	883.39	x	-
RM06-04d	36166	NA	massive sulfide	mass Py-Ccp sul with silicic clasts, on contact to intercalated rhy flow in mas sul	890.13	890.17	x	-
RM06-04d	36170	NA	semi-massive sulfide	semi-mass Py-Ccp sul with silvery phase (Asp/Tet?)	893.53	893.57	x	-
RM06-04d	36173	NA	stringer (footwall)	fine Py+Ccp stringer in mass rhy flow	895.77	895.81	x	-
RM06-04l	36177	NA	stringer (hanging wall)	Py-Ccp stringer in Qtz-eye lap tuff	911.38	911.42	x	-
RM06-04l	36179	NA	stringer (hanging wall)	Py-Ccp stringer in Qtz-eye lap tuff	913.24	913.28	x	-
RM06-04l	36181	NA	massive sulfide	mass Ccp-Py-Po sul, on upper contact to intercalated Qtz-eye rhy flow	915.63	915.67	x	-
RM06-04l	36186	NA	massive sulfide	mass Py-Ccp sul on contact to semi-mass sul	919.15	919.19	x	-
RM06-04l	36191	NA	stringer (footwall)	fine Py stringer in Qtz-eye flow	921.74	921.78	x	-
RM06-04l	36194	NA	stringer (footwall)	fine Py-Ccp stringer in Qtz-eye flow	924.85	924.89	x	-

analyzed @ INCO (SEM, SIMS), UT (EPMA), and Laurentian University (LA-ICP-MS)

<sup>1</sup> Alternative Sampla Nn is engraved on back of thick-section slides

<sup>3</sup> only general description available

<sup>2</sup> no reflected light images taken

[illegible]

**Table eA5-1.** Results of EPMA (major and minor elements in wt%) and LA-ICP-MS (trace elements in ppm) analysis for analyzed mineral phases of sulfides from the Ming deposit. Detailed mineralogical description of analyzed samples can be found in eA4.

<b>Abbreviation</b>	<b>Mineral</b>
Ag-Tet	Ag-bearing Tetrahedrite
Allo	Alloclasite
Alt	Altaite
Apy	Arsenopyrite
Breit	Breithauptite
Cbn	Cubanite
Ccp	Chalcopyrite
Claus	Clausthalite
Col	Coloradoite
El	Electrum
Gn	Galena
Gud	Gudmundite
Hess	Hessite
Men	Meneghinite
Mia	Miargyrite
Mol	Molybdenite
Nis	Nisbite
Po	Pyrrhotite
Py	Pyrite
Pyr	Pyargyrite
Sp	Sphalerite
Stn	Stannite
Hg-Stp	Mercurian stephanite
Ten	Tennantite
Ten-Tet	Tennantite-tetrahedrite
Tet	Tetrahedrite
Tsu	Tsumoite
unnamed BiTe	unnamed Bi-telluride

**Table eA5-1.** Results of EPMA (major and minor elements in wt%) and LA-ICP-MS (trace elements in ppm) analysis for analyzed mineral phases of sulfides from the 18

Drill Hole	Sample No.	Mineralization style	Mineral	SEM image No	S [wt%]_EPMA	Fe [wt%]_EPMA	Fe [ppm]_EPMA	Fe [ppm]_LA	Ti [ppm]_LA
RM07-19	29948	semi-massive to massive sulfides	Ccp	P3	34.03	30.91			
RM07-19	29948	semi-massive to massive sulfides	Ccp	P4	34.48	31.20			
RM07-19	29948	semi-massive to massive sulfides	Ccp	P5	34.28	30.72			
RM07-19	29948	semi-massive to massive sulfides	Ccp	P12	34.53	30.73			
RM07-19	29948	semi-massive to massive sulfides	Ccp	P16	34.49	30.96			
RM07-19	29948	semi-massive to massive sulfides	Py	P3	53.41	45.94			
RM07-19	29948	semi-massive to massive sulfides	Py	P4	53.03	46.13			
RM07-19	29948	semi-massive to massive sulfides	Py	P5	53.56	45.87			
RM07-19	29948	semi-massive to massive sulfides	Py	P12	52.94	46.03			
RM07-19	29948	semi-massive to massive sulfides	Py	P16	52.96	45.82			
RM07-19	29948	semi-massive to massive sulfides	Py	P17	53.04	46.03			
RM07-19	29948	semi-massive to massive sulfides	Apy	P3	21.26	34.37			
RM07-19	29948	semi-massive to massive sulfides	Apy	P17	21.07	34.21			
RM07-19	29948	semi-massive to massive sulfides	Po	P12	39.25	60.37			
RM07-19	29948	semi-massive to massive sulfides	Sp	P4	33.42	10.18			
RM07-19	29948	semi-massive to massive sulfides	Sp	P12	33.31	9.40			
RM07-19	29948	semi-massive to massive sulfides	Sp	P16	33.56	9.38			
RM07-19	29948	semi-massive to massive sulfides	Tnt-Trt	P4	25.49	4.57			
RM07-19c	35552	semi-massive to massive sulfides	Ccp	P1	34.79	30.64		19.9	
RM07-19c	35552	semi-massive to massive sulfides	Ccp	P2	34.96	30.44		10	
RM07-19c	35552	semi-massive to massive sulfides	Ccp	P5b	34.56	30.12			
RM07-19c	35552	semi-massive to massive sulfides	Ccp	P7	34.90	30.70			
RM07-19c	35552	semi-massive to massive sulfides	Ccp	P10	34.58	30.85			
RM07-19c	35552	semi-massive to massive sulfides	Py	P1	53.22	45.9		11.1	
RM07-19c	35552	semi-massive to massive sulfides	Py	P2	53.22	46.29		13.3	
RM07-19c	35552	semi-massive to massive sulfides	Py	P5b	52.81	45.58		12.4	
RM07-19c	35552	semi-massive to massive sulfides	Py	P7	53.15	46.37		14.8	
RM07-19c	35552	semi-massive to massive sulfides	Py	P10	52.71	46.00		12.5	
RM07-19c	35552	semi-massive to massive sulfides	Apy I_rim a	P2	21.55	34.19		10	
RM07-19c	35552	semi-massive to massive sulfides	Apy I_core	P2	21.07	34.18			
RM07-19c	35552	semi-massive to massive sulfides	Apy I_rim b	P2	21.23	34.17			
RM07-19c	35552	semi-massive to massive sulfides	Apy II_core	P2	22.19	34.64			
RM07-19c	35552	semi-massive to massive sulfides	Apy	P5b	21.32	33.81			
RM07-19c	35552	semi-massive to massive sulfides	Apy	P10	20.84	34.49			
RM07-19c	35552	semi-massive to massive sulfides	Sp	P1	33.62	5.25		11.0	
RM07-19c	35552	semi-massive to massive sulfides	Sp	P5b	33.49	5.00			
RM07-19c	35552	semi-massive to massive sulfides	El	P5b	0.000		3,150		
RM07-18a	35559	semi-massive to massive sulfides	Ccp	P2	34.72	30.66			
RM07-18a	35559	semi-massive to massive sulfides	Ccp	P6	34.71	30.75			
RM07-18a	35559	semi-massive to massive sulfides	Ccp	P9	34.96	30.48			
RM07-18a	35559	semi-massive to massive sulfides	Ccp	P14a	34.96	30.27			
RM07-18a	35559	semi-massive to massive sulfides	Ccp	P26	34.78	30.1			
RM07-18a	35559	semi-massive to massive sulfides	Ccp	P24	34.82	30.92			
RM07-18a	35559	semi-massive to massive sulfides	Py	P1	52.69	46.15			
RM07-18a	35559	semi-massive to massive sulfides	Py	P6	53.18	45.71			

07 Zone. Detailed mineralogical description of analyzed samples can be found in eA4. Abbreviation: LA – LA-ICP-MS, SEM - scanning elctron microscope

V [ppm]_LA	Cr [ppm]_LA	Mn [ppm]_LA	Co [ppm]_LA	Co [wt%]_EPMA	Ni [ppm]_LA	Ni [wt%]_EPMA	Cu [ppm]_LA	Cu [wt%]_EPMA	Zn [ppm]_LA	Zn [wt%]_EPMA
								34.36		
								34		
								34.12		
								34.36		
								34.48		
0	0	0	0	0	0	0	0	38.44	665	54.75
0	0	0	0	7	0	0	0	34.7	1,431	56.22
								34.52		56.49
0	0	0	0	17.8	0	0	0	34.57	614	3.37
0.392	0	0	0	0	0	0	0	34.68	632	
0	0	0	13.4	0	0	0	0	34.77	0	
0.264	0	0	86.1	0	0	0	45.9		57.4	
							796			
0	0	0	259	0	49	0	0		0	
0	0	0	209	0	0	511	511		117	
0	0	0	205	1.02	0	0	24			61.48
										61.23
								34.54		
								34.33		
								34.51		
								34.81		
								34.34		
								34.55		

4

Te [ppm]_LA	Te [wt%]_EPMA	Au [ppm]_LA	Au [wt%]_EPMA	Hg [wt%]_EPMA	Tl [ppm]_LA	Pb [ppm]_LA	Pb [wt%]_EPMA	Bi [ppm]_LA	Bi [wt%]_EPMA
									A
3.65		0.086			0.49	21.4		2.3	
0		0			1.95	52.7		14.9	
3.78		0.144			1.84	178		11.8	
0		0			0.083	17		1.03	
0		0			0	0.096		0	
0		0.088			0	25.4		2.29	
0		0			0	2.5		0.25	
3.17		2.48			0	98.4		4.14	
0		0			0	5.77		1.89	
			70.17	3.05					



RM07-18a	35559	semi-massive to massive sulfides	Py	P9	53.38	46.01	
RM07-18a	35559	semi-massive to massive sulfides	Py	P14a	53.12	46.13	
RM07-18a	35559	semi-massive to massive sulfides	Py	P26	53.13	45.84	
RM07-18a	35559	semi-massive to massive sulfides	Apy	P2	20.77	34.09	
RM07-18a	35559	semi-massive to massive sulfides	Apy	P6	20.79	34.26	
RM07-18a	35559	semi-massive to massive sulfides	Apy	P9	21.82	34.35	
RM07-18a	35559	semi-massive to massive sulfides	Apy I	P14a	21.07	33.98	
RM07-18a	35559	semi-massive to massive sulfides	Apy II	P14a	21.06	34.33	
RM07-18a	35559	semi-massive to massive sulfides	Apy_rim a	P24	21.36	34.39	
RM07-18a	35559	semi-massive to massive sulfides	Apy_core	P24	21.76	34.59	
RM07-18a	35559	semi-massive to massive sulfides	Apy_rim b	P24	21.76	34.48	
RM07-18a	35559	semi-massive to massive sulfides	Apy I	P26	21.36	33.98	
RM07-18a	35559	semi-massive to massive sulfides	Apy II	P26	21.15	34.64	
RM07-18a	35559	semi-massive to massive sulfides	Sp	P2	33.35	3.31	
RM07-18a	35559	semi-massive to massive sulfides	Sp	P6	33.92	4.35	
RM07-18a	35559	semi-massive to massive sulfides	Sp	P9	33.62	3.57	
RM07-18a	35559	semi-massive to massive sulfides	Sp I	P14a	33.53	3.36	
RM07-18a	35559	semi-massive to massive sulfides	Sp II	P14a	33.85	3.5	
RM07-18a	35559	semi-massive to massive sulfides	Sp	P24	33.8	2.96	
RM07-18a	35559	semi-massive to massive sulfides	Sp	P26	33.37	2.29	
RM07-18a	35559	semi-massive to massive sulfides	Gn	P9	12.74	0.477	4,772
RM07-18a	35559	semi-massive to massive sulfides	Gn	P14a	12.81	1.33	13,322
RM07-18a	35559	semi-massive to massive sulfides	Gn	P26	13.23	0.053	533
RM07-18a	35559	semi-massive to massive sulfides	Tnt-Trt	P9	26.97	6.14	
RM07-18a	35559	semi-massive to massive sulfides	Tnt-Trt	P9	26.29	5.82	
RM07-18a	35559	semi-massive to massive sulfides	Tnt-Trt	P2	25.52	5.28	
RM07-18a	35559	semi-massive to massive sulfides	Tnt-Trt	P6	26.3	5.73	
RM07-18a	35559	semi-massive to massive sulfides	Tnt-Trt I	P14a	26.22	5.82	
RM07-18a	35559	semi-massive to massive sulfides	Tnt-Trt II	P14a	27.3	6.33	
RM07-18a	35559	semi-massive to massive sulfides	Tnt-Trt I	P26	28.5	5.96	
RM07-18a	35559	semi-massive to massive sulfides	Tnt-Trt II	P26	24.61	4.76	13.8
RM07-18b	35563	semi-massive to massive sulfides	Ccp	P3	34.41	30.64	8.61
RM07-18b	35563	semi-massive to massive sulfides	Ccp	P5	34.85	30.73	
RM07-18b	35563	semi-massive to massive sulfides	Ccp	P7	34.78	30.46	11.6
RM07-18b	35563	semi-massive to massive sulfides	Ccp	P10	34.7	30.64	
RM07-18b	35563	semi-massive to massive sulfides	Ccp	P14	34.89	30.68	14.4
RM07-18b	35563	semi-massive to massive sulfides	Py	P3	52.66	46.15	11.5
RM07-18b	35563	semi-massive to massive sulfides	Py	P5	52.71	45.81	
RM07-18b	35563	semi-massive to massive sulfides	Py	P7	52.48	46	
RM07-18b	35563	semi-massive to massive sulfides	Py	P10	52.47	45.66	
RM07-18b	35563	semi-massive to massive sulfides	Py	P14	52.38	45.22	7.46
RM07-18b	35563	semi-massive to massive sulfides	Apy_core	P5	21.23	33.92	
RM07-18b	35563	semi-massive to massive sulfides	Apy_rim	P5	21.32	34.43	5.83
RM07-18b	35563	semi-massive to massive sulfides	Apy	P10	21.07	34.3	11.2
RM07-18b	35563	semi-massive to massive sulfides	Po	P3	38.85	60.69	5.91
RM07-18b	35563	semi-massive to massive sulfides	Po	P5	38.2	60.92	
RM07-18b	35563	semi-massive to massive sulfides	Po	P7	38.84	61.08	
RM07-18b	35563	semi-massive to massive sulfides	Po	P14	39.14	60.95	
RM07-18b	35563	semi-massive to massive sulfides	Sp	P3	33.97	8.52	8.44
RM07-18b	35563	semi-massive to massive sulfides	Sp	P7	33.39	7.84	5.88
RM07-18b	35563	semi-massive to massive sulfides	Gn	P3	12.21	0.18	0
					1,796		

[illegible]

[illegible]

85.37  
84.63  
85.37

0	0.447	0.273	8.37	2.02
12	1.35	0.596	369	11.7
5.21	0.144	0.159	126	0.735
0	0	0	0	0
35.3	0	0	0.279	0.023
4.240	0	0	1.26	0.251
1.694	0.099	0.23	100	5.66
0	0.206	1.41	2,901	16.8
7.92	1.16	0.585	2,620	13.5
0	0.665	0.117	101	1.5
0	0.063	0.038	11.5	0.823
5,553	0.249	271		10,455

85.7

RM07-18b	35563	semi-massive to massive sulfides	Gud	P14	15.27	26.80	
RM07-18b	35563	semi-massive to massive sulfides	Gud	P14	15.15	26.67	
RM07-20c	35584	semi-massive to massive sulfides	Ccp	P7	35.19	30.59	
RM07-20c	35584	semi-massive to massive sulfides	Ccp	P9	35.08	30.12	
RM07-20c	35584	semi-massive to massive sulfides	Ccp	P10	34.31	30.74	
RM07-20c	35584	semi-massive to massive sulfides	Ccp	P15	34.65	30.59	
RM07-20c	35584	semi-massive to massive sulfides	Py	P10	52.95	45.61	
RM07-20c	35584	semi-massive to massive sulfides	Py	P15	52.98	45.83	
RM07-20c	35584	semi-massive to massive sulfides	Apy	P15	21.07	34.07	
RM07-20c	35584	semi-massive to massive sulfides	Po	P10	39.23	60.39	
RM07-20c	35584	semi-massive to massive sulfides	Po	P15	39.35	60.44	
RM07-20c	35584	semi-massive to massive sulfides	Sp	P7	34.06	7.27	
RM07-20c	35584	semi-massive to massive sulfides	Sp	P9	33.51	7.38	
RM07-20c	35584	semi-massive to massive sulfides	Sp	P15	33.99	7.97	
RM07-20c	35584	semi-massive to massive sulfides	Gn I	P9	13	0.246	2,462
RM07-20c	35584	semi-massive to massive sulfides	Gn II	P9	12.64	0.076	762
RM07-20e	35590	semi-massive to massive sulfides	Ccp	P4	34.97	30.28	
RM07-20e	35590	semi-massive to massive sulfides	Ccp	P6	34.99	30.38	
RM07-20e	35590	semi-massive to massive sulfides	Ccp	P8	35.19	30.68	
RM07-20e	35590	semi-massive to massive sulfides	Py	P4	53.03	45.79	
RM07-20e	35590	semi-massive to massive sulfides	Py	P6	53.05	45.81	
RM07-20e	35590	semi-massive to massive sulfides	Py	P8	53.14	46.35	
RM07-20e	35590	semi-massive to massive sulfides	Apy_rim a	P8	21.1	33.59	
RM07-20e	35590	semi-massive to massive sulfides	Apy_rim b	P8	20.78	34.21	
RM07-20e	35590	semi-massive to massive sulfides	Apy_rim a	P8	21.86	33.78	
RM07-20e	35590	semi-massive to massive sulfides	Apy_rim b	P8	21.22	32.74	
RM07-20e	35590	semi-massive to massive sulfides	Sp	P4	33.74	8.34	
RM07-20e	35590	semi-massive to massive sulfides	Sp	P6	34.07	8.41	18.1
RM07-20e	35590	semi-massive to massive sulfides	Sp	P8	34.04	8.53	12
RM07-20h	36007	semi-massive to massive sulfides	Ccp	P4	35.08	30.6	
RM07-20h	36007	semi-massive to massive sulfides	Ccp	P7	34.66	30.8	
RM07-20h	36007	semi-massive to massive sulfides	Ccp	P11	34.4	30.76	
RM07-20h	36007	semi-massive to massive sulfides	Ccp	P18	34.18	30.67	
RM07-20h	36007	semi-massive to massive sulfides	Py	P4	53.45	45.31	
RM07-20h	36007	semi-massive to massive sulfides	Py	P7	52.41	45.93	
RM07-20h	36007	semi-massive to massive sulfides	Py	P11	53.15	45.82	
RM07-20h	36007	semi-massive to massive sulfides	Py	P16	52.93	45.78	
RM07-20h	36007	semi-massive to massive sulfides	Py	P18	52.8	45.97	8.78
RM07-20h	36007	semi-massive to massive sulfides	Apy_rim a	P11	20.98	33.43	
RM07-20h	36007	semi-massive to massive sulfides	Apy_core	P11	21.35	33.34	
RM07-20h	36007	semi-massive to massive sulfides	Apy_rim b	P11	20.86	33.82	7.23
RM07-20h	36007	semi-massive to massive sulfides	Apy I	P18	20.94	33.17	
RM07-20h	36007	semi-massive to massive sulfides	Apy II	P18	21.73	34.07	
RM07-20h	36007	semi-massive to massive sulfides	Apy_rim a	P11	20.98	33.43	
RM07-20h	36007	semi-massive to massive sulfides	Apy_core	P11	21.35	33.34	
RM07-20h	36007	semi-massive to massive sulfides	Apy_rim b	P11	20.86	33.82	
RM07-20h	36007	semi-massive to massive sulfides	Apy I	P18	20.94	33.17	
RM07-20h	36007	semi-massive to massive sulfides	Apy II	P18	21.73	34.07	
RM07-20h	36007	semi-massive to massive sulfides	Po	P4	38.9	60.48	5.44
RM07-20h	36007	semi-massive to massive sulfides	Po	P11	38.46	60.62	10.1
RM07-20h	36007	semi-massive to massive sulfides	Sp	P4	33.27	8.96	

[illegible]

58.61  
58.31

43.88

43.67  
44.38  
43.26  
43.56

189  
152  
408

386  
360  
420

0  
2.34  
0

42.0  
36.7  
39.9

24.8  
17.7  
21.6

129  
102  
82.5

1.59  
9.5  
5.64

5,732

44.1  
43.74  
43.58  
44.05  
43.82  
44.1  
43.74  
43.58  
44.05  
43.82

384  
1,027

0  
2.57

0.781  
5.87

1.02  
0

0.897  
1.63

1.34  
127

227  
2,128

490  
239

865  
0

5.87  
3.27

0  
6.43

0.435  
0.346

8.1  
7.76

86.36  
86.39

11.6	0.523	0	55.1	7.04
7.05	0.206	0.403	77	2.25
0	0.132	0.859	13.8	1.12
24.5	2.98	0	111	16.2
3.901	1.38	0.267	187	33.3
25.4	0	2.01	6,168	40.5
13.2	0.152	0.909	145	8.43



RM07-20h	36007	semi-massive to massive sulfides	Sp	P11	33.98	9.35			
RM07-20h	36007	semi-massive to massive sulfides	Sp	P16	33.84	8.05			
RM07-20h	36007	semi-massive to massive sulfides	Sp	P18	33.59	8.62			8.37
RM07-20h	36007	semi-massive to massive sulfides	Tsu	P4	0.057	0.342	3.416		
RM07-20h	36007	semi-massive to massive sulfides	Tsu	P7	0.065	0.590	5.902		
RM07-20h	36007	semi-massive to massive sulfides	Po	P18 (with Fe from P11)	38.46	60.62			0
RM07-20h	36010	semi-massive to massive sulfides	Ccp	P6	34.95	30.57			5.58
RM07-20h	36010	semi-massive to massive sulfides	Ccp	P4	35.28	31.05			9.58
RM07-20h	36010	semi-massive to massive sulfides	Ccp	P12	35.22	30.57			
RM07-20h	36010	semi-massive to massive sulfides	Py	P4	52.31	45.37			
RM07-20h	36010	semi-massive to massive sulfides	Py	P6	53.51	46.23			9.51
RM07-20h	36010	semi-massive to massive sulfides	Po	P4	39.11	59.81			
RM07-20h	36010	semi-massive to massive sulfides	Sp	P6	33.43	7.99			
RM07-20h	36010	semi-massive to massive sulfides	Sp	P11	33.82	8.04			
RM07-20h	36010	semi-massive to massive sulfides	Sp	P12	33.64	8.17			
RM07-20h	36010	semi-massive to massive sulfides	Sp	P13	33.57	7.35			
RM07-20h	36010	semi-massive to massive sulfides	Allo I	P4	20.42	7.97			8.52
RM07-20h	36010	semi-massive to massive sulfides	Tsu	P6	0.000	0.000	0		
RM07-20h	36010	semi-massive to massive sulfides	Tsu I	P11	0.045	0.000	0		
RM07-20h	36010	semi-massive to massive sulfides	Tsu	P12	0.051	0.000	0		
RM07-20h	36010	semi-massive to massive sulfides	Tsu	P12	0.081	0.000	0		
RM07-20h	36010	semi-massive to massive sulfides	Tsu	P13	0.041	0.000	0		

1.53	0	849	78.6	0	44.5	56.76 57.77 57.84
105	12.6	12	21.5	0	837	0
0	0	3.78	1.13	0	34.65	364
0	0	0	198	23.6	34.21	513
					34.28	
4.14	5.93	0	530	0	5,378	489
						57.48 58.22 57.89 58.52
0	0	0		25.11	1.83	741
						22.6

---

16

0	0.155	0	5.17	0.854	59.43
					60.25
4.3	1.45	0.964	1,443	60	
0	0	0.724	29.1	1.09	
0	0	0	11.6	4.28	
52.4	1.82	6.57	709	66.5	
193	12.8	0	260	42.2	57.32
					57.66
					54.09
					56.06
					52.45

**Table eA5-1. (continued)** Results of EPMA (major and minor elements in wt%) and LA-ICP-MS (trace elements in ppm) analysis for analyzed mineral phases of sulfides

Drill Hole	Section	Sample No.	Mineralization style	Mineral	SEM image No	S [wt%]_EPMA	Fe [wt%]_EPMA	Fe [ppm]_EPMA	Fe [ppm]_LA
RMUG08-121	21	29902	sulfide stringer horizon	Ccp	P1c	35.35	30.49		
RMUG08-121	21	29902	sulfide stringer horizon	Ccp	P5	34.83	30.38		
RMUG08-121	21	29902	sulfide stringer horizon	Ccp I	P14a	34.92	30.48		
RMUG08-121	21	29902	sulfide stringer horizon	Ccp II	P14a	35.02	30.48		
RMUG08-121	21	29902	sulfide stringer horizon	Py	P5	53.68	46.57		
RMUG08-121	21	29902	sulfide stringer horizon	Apy I	P1c	21.3	34.55		
RMUG08-121	21	29902	sulfide stringer horizon	Apy II	P1c	21.46	34.76		
RMUG08-121	21	29902	sulfide stringer horizon	Apy I	P5	21.86	34.98		
RMUG08-121	21	29902	sulfide stringer horizon	Apy II	P5	21.61	34.65		
RMUG08-121	21	29902	sulfide stringer horizon	Apy	P14a	21.45	34.87		
RMUG08-121	21	29902	sulfide stringer horizon	Sp	P1c	33.41	5.45		
RMUG08-121	21	29902	sulfide stringer horizon	Sp I	P14a	33.33	4.79		
RMUG08-121	21	29902	sulfide stringer horizon	Sp II	P14a	33.29	4.78		
RMUG08-121	21	29902	sulfide stringer horizon	Gn	P1c	13.26	0.564	5,638	
RMUG08-121	21	29902	sulfide stringer horizon	Gn	P5	12.95			5,145
RMUG08-121	21	29902	sulfide stringer horizon	Gn I	P14a	13.12			
RMUG08-121	21	29902	sulfide stringer horizon	Gn II	P14a	13.31			
RMUG08-121	21	29902	sulfide stringer horizon	Tet_N rim	P14a	24.33	3.57		
RMUG08-121	21	29902	sulfide stringer horizon	Tet_core	P14a	24.53	3.69		
RMUG08-121	21	29902	sulfide stringer horizon	Tet_S rim	P14a	24.64	3.47		
RMUG08-121	21	29902	sulfide stringer horizon	EL_core-1	P14a	0.094		535	569
RMUG08-121	21	29902	sulfide stringer horizon	EL_E rim	P14a	0.122			
RMUG08-121	21	29902	sulfide stringer horizon	EL_W rim I	P14a	0.139		366	396
RMUG08-121	21	29902	sulfide stringer horizon	EL_W rim II	P14a	0.033		697	57
RMUG08-121	21	29902	sulfide stringer horizon	EL_W rim II	P14a	0.102		304	
RMUG08-124	21	29913	semi-massive to massive sulfides	Ccp	P3b	35.04	30.38		
RMUG08-124	21	29913	semi-massive to massive sulfides	Ccp I	P6	34.78	30.77		
RMUG08-124	21	29913	semi-massive to massive sulfides	Ccp II	P6	35.01	30.19		
RMUG08-124	21	29913	semi-massive to massive sulfides	Ccp	P12	34.86	30.51		
RMUG08-124	21	29913	semi-massive to massive sulfides	Ccp	P13	34.92	30.38		
RMUG08-124	21	29913	semi-massive to massive sulfides	Py	P8	53.47	46.62		
RMUG08-124	21	29913	semi-massive to massive sulfides	Apy	P3b	21.01	33.78		
RMUG08-124	21	29913	semi-massive to massive sulfides	Apy	P13	21.8	34.59		
RMUG08-124	21	29913	semi-massive to massive sulfides	Po	P6	39.01	59.68		
RMUG08-124	21	29913	semi-massive to massive sulfides	Sp	P3b	33.52	9.97		
RMUG08-124	21	29913	semi-massive to massive sulfides	Sp	P6	33.37	10.16		
RMUG08-124	21	29913	semi-massive to massive sulfides	Sp	P12	33.31	10.04		
RMUG08-124	21	29913	semi-massive to massive sulfides	Gn II	P6	13.65	0.144	1,437	
RMUG08-124	21	29913	semi-massive to massive sulfides	Gn	P12	13.33	0	0	
RMUG08-124	21	29913	semi-massive to massive sulfides	Gn	P13	13.36	0	0	
RMUG08-124	21	29913	semi-massive to massive sulfides	Men	P12	17.08		638	
RMUG08-124	21	29913	semi-massive to massive sulfides	El	P3b	0.144		712	
RMUG08-124	21	29913	semi-massive to massive sulfides	El I	P6	0.110		0	
RMUG08-124	21	29913	semi-massive to massive sulfides	El II_NW rim	P6	0.142		453	
RMUG08-124	21	29913	semi-massive to massive sulfides	El II_core	P6	0.098		834	

[illegible]

scope

[illegible]

[illegible]



[illegible]

6.88	5.96	0	0	0	0	0	34.08	566
							34.2	
9.22	0	0	0	0	0	0	34.21	
4.46	0	0	0	0	0	0	34.43	814
							34.42	1,017
10.1	0	0	0	19.5	95	0		0
7.34	0	0	0	3.99	221	142		0
3.96	0	0	0	0.102	75	0		0
5.8	0	0	1.93	4.95	104	81.4		8.14
6.37	0	0	0	0.18	129	0		0
3.77	0	0	38.7	0	0		15.54	
							19.16	
							18.22	
							21.99	
7.7	0.633	0	28.9	0.137	0		20.08	
							34.19	
4.51	0	0	0	0	0		34.49	165
10.1	11.9	0	0	430	119	38.8		8.23
16	20.4	2.74	19.2	137	81.2	415		725
8.94	0.141	0	0	386	287	4.11		95.8
6.78	0	0	0	18.4	230	1.69		0
5.91	0	0	0	117	358	5.06		0.743
6.65	0.522	0.678	0	100	400	5.09		0
3.73	0	0	0	102	308	1.42		0
8.23	0.273	0	0	59	533	0.708		0
5.68	0.183	0	0	81.8	317	1.42		0
0	1.57	0	789	0	0	101		
5.68	0	0	729	0	0	284		
3.14	0.236	0	0	0	0	26.2		558
3.13	0	0	0	0	0	0		0
4.34	0	0	0	0	0	0.504		0
0	0	0	0	0	0	0		0
5.44	6.83	0	0	0	0	82.1		562
3.08	2.49	0.424	71.3	0	0		44.25	
							44.46	
							35.23	
							31.69	
3.9	0	0	97.1	0	0		41.8	
							41.4	

1,814	293	0	979	32.65 35.34	4.79	375	0
4,101 252	217 209	0 0	265 585		7.83 6.5	373 186	7.43 0.258
2,957 908	101 11.9	0.425 0	1.12 1.15		0 0	0 0.427	2.1 0.596
	43.71 43.85 43.51 44.04 43.54	0 4.99 0	0 6.75 0		0 0.136 0	0 0.119 0	17.5 93 19.2
58.12 0.55 1.23 1.26 0.999	0.561 1.19 0.981 5.78	0		29.27 24.15 25 22	484	3.61	
1.01	2.79	0		23.83	961	67.3	
896 2,710 2,240 3,518	4.3 24.7 12.8 26 25.8 27 29.8 32.2 32 33.1	0 13.3 3.92 0 0 5.46 0 1.96 1.56	13.3 82.7 10.9 4.06 52.2 0 0.75 0.881 189 0.439		0.751 0 4.29 0 0 0 0 0 0 0	982 0.686 1.41 0 0.085 0 0 0 0 0	24 0 19.6 8.03 2.26 2.89 3.6 2.68 3.61 4.06
64.38 64.81 65.28		0	3.07		4,334	3.71	0.761
	22.1	0	5.03		3,667	21.3	2.32
90.3 105 92.4 0		0 0 0 0	316 353 274	0.032 0.035 0.027	14.1 13.9 7.99	29.1 30.1 16.4	285 320 255
1,233 818		0 0	574 444	0.057 0.044 0.471	7.24 11.4	37.7 19.4	515 379
3.22 3.16 4.77 4.74 2.66 2.82	19.15 19.25 3.95 2.66 18.54 18.24	0		5.69 8.83 0.869 0.963	1,029	71.6	
	81.2	0			419	1.26	

	1.56	0	53.63 52.32	13.69 12.61	0.099	0.189	0
	3.59 2	0 0			0.215 0	24.6 0.216	0.298 0
	6.72 0	0 0			0 0	2.15 5.18	0.229 0.206
	104 2,453 285	0 0.943 0			0.088 0.858 0	3.65 115 0.715	0 5.26 0.034
26.79 25.94 26.26 19.14	38.1	0			1.21	25.9	225
23.92	44.3	3.19			24.9	473	231
	0	0.147			0.112	1.33	0
	0	0.142			1.19	18	0.041
	0	1.36			1.75	625	0.224
	0	0			0	0	0.164
	3.76	230			0	11.5	0
	5.94	0			0	0	0
	5.49	0.356			0.129	18	0
	4.95	0.047			0	0	0
	4.15	63.4			0	8.47	0.028
	10.6	0			0.062	0	0
	0	0			0.14	4.18	0.072
	0	0			0	3.81	0.03
	43.2	0.041			22.9	87.26	79.4
	59	0			23.8	86.85	77
	28.7	0			25.2	86.85	75.2
	75	0			25.6	86.23	70.3
	46.4	0			21.9	86.39	75.2
1.33 1.4 23.74 25.92 1.73 2.22	0	0.021			1.04	9.09	0.294
	2.08	0			0.088	0	2.04

RMUG08-120	21	36509	semi-massive to massive sulfides	Ten_core	P17	28.29	5.13	
RMUG08-120	21	36509	semi-massive to massive sulfides	Ten_rim b	P17	28.12	5.19	
RMUG08-120	21	36509	semi-massive to massive sulfides	El I	P6b	0.145		0
RMUG08-120	21	36509	semi-massive to massive sulfides	El III	P6b	0.178		1,947
RMUG08-123	21	36512	semi-massive to massive sulfides	Ccp	P3	34.98	30.49	
RMUG08-123	21	36512	semi-massive to massive sulfides	Ccp	P5b	34.91	30.36	
RMUG08-123	21	36512	semi-massive to massive sulfides	Py	P3	53.47	46.68	
RMUG08-123	21	36512	semi-massive to massive sulfides	Py I	P5b	53.18	46.68	
RMUG08-123	21	36512	semi-massive to massive sulfides	Py II	P5b	53.62	46.11	
RMUG08-123	21	36512	semi-massive to massive sulfides	Py	P12	53.34	46.77	
RMUG08-123	21	36512	semi-massive to massive sulfides	Apy	P5b	19.81	34.15	
RMUG08-123	21	36512	semi-massive to massive sulfides	Sp	P3	33.08	9	
RMUG08-123	21	36512	semi-massive to massive sulfides	Sp I	P5b	33.02	9.37	
RMUG08-123	21	36512	semi-massive to massive sulfides	Sp II	P5b	33.25	8.41	
RMUG08-123	21	36512	semi-massive to massive sulfides	Sp	P7b	32.93	9.19	
RMUG08-123	21	36512	semi-massive to massive sulfides	Sp	P12	32.69	6.12	
RMUG08-123	21	36512	semi-massive to massive sulfides	Gn	P3	13.33	0.05	502
RMUG08-123	21	36512	semi-massive to massive sulfides	Gn I	P5b	13.26	0	2,729
RMUG08-123	21	36512	semi-massive to massive sulfides	Gn II	P5b	13.43	0	438
RMUG08-123	21	36512	semi-massive to massive sulfides	Gn	P7b	13.12	0.037	503
RMUG08-123	21	36512	semi-massive to massive sulfides	Gn I	P12	13.22	0	0
RMUG08-123	21	36512	semi-massive to massive sulfides	Gn II	P12	13.22	0	5,670
RMUG08-123	21	36512	semi-massive to massive sulfides	Stn	P3	29.59	12.1	0
RMUG08-123	21	36512	semi-massive to massive sulfides	Stn I	P5b	29.19	12.16	
RMUG08-123	21	36512	semi-massive to massive sulfides	Stn II	P5b	29.67	12.01	
RMUG08-123	21	36512	semi-massive to massive sulfides	Stn	P7b	29.47	11.78	
RMUG08-142	22	29778	semi-massive to massive sulfides	Ccp	P3a	35.09	30.25	
RMUG08-142	22	29778	semi-massive to massive sulfides	Ccp	P11	34.85	30.14	
RMUG08-142	22	29778	semi-massive to massive sulfides	Ccp	P16a-3	35.01	30.5	
RMUG08-142	22	29778	semi-massive to massive sulfides	Ccp	P16a-3	33.76	28.25	
RMUG08-142	22	29778	semi-massive to massive sulfides	Py	P3a	53.63	46.76	
RMUG08-142	22	29778	semi-massive to massive sulfides	Py	P10b	53.66	46.44	
RMUG08-142	22	29778	semi-massive to massive sulfides	Py	P11	53.77	46.65	
RMUG08-142	22	29778	semi-massive to massive sulfides	Py	P16a-3	53.41	46.19	
RMUG08-142	22	29778	semi-massive to massive sulfides	Py	P16a-3	53.23	46.12	
RMUG08-142	22	29778	semi-massive to massive sulfides	Apy_NE rim	P10b	21.1	34.79	
RMUG08-142	22	29778	semi-massive to massive sulfides	Apy_core	P10b	21.79	34.94	
RMUG08-142	22	29778	semi-massive to massive sulfides	Apy_SW rim	P10b	21.17	34.74	
RMUG08-142	22	29778	semi-massive to massive sulfides	Apy	P11	20.83	34.52	
RMUG08-142	22	29778	semi-massive to massive sulfides	Sp	P11	32.98	1.8	
RMUG08-142	22	29778	semi-massive to massive sulfides	Gn	P3a	13.16	0.634	6,336
RMUG08-142	22	29778	semi-massive to massive sulfides	Gn-1	P11	13.08	0.689	6,888
RMUG08-142	22	29778	semi-massive to massive sulfides	Gn	P16a-3	13.24	0.175	1,751
RMUG08-142	22	29778	semi-massive to massive sulfides	Ten I	P3a	28.52	4.99	
RMUG08-142	22	29778	semi-massive to massive sulfides	Ten II	P3a	28.14	5.3	
RMUG08-142	22	29778	semi-massive to massive sulfides	Ten-Tet_W part	P11	25.03	2.24	
RMUG08-142	22	29778	semi-massive to massive sulfides	Ten-Tet_E part	P11	25.7	2.38	
RMUG08-142	22	29778	semi-massive to massive sulfides	El	P16a-3	0.653		4,722
RMUG08-138	22	29781	sulfide stringer horizon	Ccp	P12a	34.59	30.11	
RMUG08-138	22	29781	sulfide stringer horizon	Ccp	P18-1	34.87	30.11	
RMUG08-138	22	29781	sulfide stringer horizon	Ccp I	P19a-1	35.16	30.35	

[illegible]

[illegible]

1.85	2.36	0	0	61.99	7.93	0	3.59	2.08
2.14	0	0	0	35.72	13.29	0.213	0	1.79
	0	0	0			0	4.95	0
	0	0	0			0	0	0
	0	0	0			0	8.39	0
	0	0.832	0.832			1.16	379	0
	3.11	0.437	0.437			23.4	666	0
	0	0	0			0	33.3	0
	0	0	0			0.311	22	0
	0	0	0			0	0	0
	0	0	0			0.083	17.6	0
	12.6	0	0			42.7		3.36
	10.8	0	0			39.2		3.64
	11.7	0	0			36		3.28
	11.2	0	0			34.1		3.03
	14.3	0	0			23.4		3.87
	15.1	0	0			22.3		4.03
	0	0	0			1.25	0	0
	0	0	0			0.188	77.8	0
	0	0.817	0.817			0.32	80.5	0

86  
85.14  
86.28

2.52  
3.03  
17.44  
15.83

13.87 16.97



RMUG08-138	22 29781	sulfide stringer horizon	Ccp II	P19a-1	35.02	30.32
RMUG08-138	22 29781	sulfide stringer horizon	Ccp	P20	35.07	30.37
RMUG08-138	22 29781	sulfide stringer horizon	Py	P12a	53.51	46.41
RMUG08-138	22 29781	sulfide stringer horizon	Py	P19a-1	53.48	46.64
RMUG08-138	22 29781	sulfide stringer horizon	Py	P20	53.58	46.53
RMUG08-138	22 29781	sulfide stringer horizon	Apy	P12a	20.9	34.4
RMUG08-138	22 29781	sulfide stringer horizon	Apy	P18-1	20.75	33.88
RMUG08-138	22 29781	sulfide stringer horizon	Apy	P19a-1	21.51	34.57
RMUG08-138	22 29781	sulfide stringer horizon	Apy	P20	20.76	34.07
RMUG08-138	22 29781	sulfide stringer horizon	Sp	P12a	32.9	2.94
RMUG08-138	22 29781	sulfide stringer horizon	Sp	P19a-1	32.85	2.91
RMUG08-138	22 29781	sulfide stringer horizon	Sp	P20	32.67	2.94
RMUG08-138	22 29781	sulfide stringer horizon	Gn	P12a	13.41	0.035
RMUG08-138	22 29781	sulfide stringer horizon	Gn	P19a-1	13.35	
RMUG08-138	22 29781	sulfide stringer horizon	Gn	P20	13.39	
RMUG08-138	22 29781	sulfide stringer horizon	Ten_N rim	P12a	27.28	5.65
RMUG08-138	22 29781	sulfide stringer horizon	Ten_Tet_S rim	P12a	27.41	5.22
RMUG08-138	22 29781	sulfide stringer horizon	Ten_E rim	P12a	28.1	5.86
RMUG08-138	22 29781	sulfide stringer horizon	Tet I	P18-1	25.23	2.44
RMUG08-138	22 29781	sulfide stringer horizon	Ten	P18-1	27.96	5.72
RMUG08-138	22 29781	sulfide stringer horizon	Tet III	P18-1	24.99	2.5
RMUG08-138	22 29781	sulfide stringer horizon	Ten_W rim	P19a-1	27.63	5.54
RMUG08-138	22 29781	sulfide stringer horizon	Ten_core	P19a-1	28.1	5.64
RMUG08-138	22 29781	sulfide stringer horizon	Ten_I_W part	P20	27.93	5.79
RMUG08-138	22 29781	sulfide stringer horizon	Ten-Tet I_E	P20	26.49	4.89
RMUG08-138	22 29781	sulfide stringer horizon	Ten-Tet II	P20	27.2	5.48
RMUG08-140	22 29783	silicified horizon	Ccp	P1	34.95	30.38
RMUG08-140	22 29783	silicified horizon	Ccp	P1	34.98	30.43
RMUG08-140	22 29783	silicified horizon	Ccp	P5	35	30.45
RMUG08-140	22 29783	silicified horizon	Ccp	P6	34.97	30.57
RMUG08-140	22 29783	silicified horizon	Ccp	P7	35.17	30.31
RMUG08-140	22 29783	silicified horizon	Py	P7	53.9	46.55
RMUG08-140	22 29783	silicified horizon	Apy	P1	22	34.48
RMUG08-140	22 29783	silicified horizon	Apy_NW rim	P7	21.44	34.78
RMUG08-140	22 29783	silicified horizon	Apy_core	P7	21.37	34.82
RMUG08-140	22 29783	silicified horizon	Apy_SE rim	P7	21.57	34.9
RMUG08-140	22 29783	silicified horizon	Po	P1	39.36	60.29
RMUG08-140	22 29783	silicified horizon	Po_Sw rim	P5	39.4	60.1
RMUG08-140	22 29783	silicified horizon	Po_N rim	P5	39.61	60.22
RMUG08-140	22 29783	silicified horizon	Po I	P6	38.85	59.63
RMUG08-140	22 29783	silicified horizon	Po II	P6	39.61	60.24
RMUG08-140	22 29783	silicified horizon	Po	P7	39.07	60.2
RMUG08-140	22 29783	silicified horizon	Sp	P6	32.79	9.71
RMUG08-140	22 29783	silicified horizon	Sp	P16a-3	33.09	1.94
RMUG08-140	22 29783	silicified horizon	ElI_core	P1	0.091	526
RMUG08-140	22 29783	silicified horizon	El I_E rim a	P1	0.311	1,637
RMUG08-140	22 29783	silicified horizon	P1-El rim b (Ag from E rim)	P1		91.8
RMUG08-140	22 29783	silicified horizon	El II	P1		313
RMUG08-140	22 29783	silicified horizon	El II	P5		43.5
RMUG08-140	22 29783	silicified horizon				29.1
RMUG08-140	22 29783	silicified horizon				5.423
RMUG08-140	22 29783	silicified horizon				4,745

[illegible]

[illegible]

[illegible]

RMUG08-140	22 29783	silicified horizon	El I	P6	0.157	601	906
RMUG08-140	22 29783	silicified horizon	El II	P6	0.182	1,038	
RMUG08-140	22 29783	silicified horizon	El III	P6	0.247	1,962	
RMUG08-141	22 29787	semi-massive to massive sulfides	Ccp	P12	35.17		
RMUG08-141	22 29787	semi-massive to massive sulfides	Ccp	P15	35.01	30.66	
RMUG08-141	22 29787	semi-massive to massive sulfides	Ccp	P17-2	34.82	30.58	
RMUG08-141	22 29787	semi-massive to massive sulfides	Ccp	P17-2	35.1	30.52	
RMUG08-141	22 29787	semi-massive to massive sulfides	Ccp	P18	35.2	30.3	
RMUG08-141	22 29787	semi-massive to massive sulfides	Py	P12	53.63	30.41	
RMUG08-141	22 29787	semi-massive to massive sulfides	Py	P17-2	52.94	45.58	
RMUG08-141	22 29787	semi-massive to massive sulfides	Apy_rim-a	P15	21.3	45.73	
RMUG08-141	22 29787	semi-massive to massive sulfides	Apy_core	P15	21.26	34.09	
RMUG08-141	22 29787	semi-massive to massive sulfides	Apy_rim-b	P15	21.28	34.47	
RMUG08-141	22 29787	semi-massive to massive sulfides	Po	P15	39.31	33.88	
RMUG08-141	22 29787	semi-massive to massive sulfides	Po	P15	39.43	60.54	
RMUG08-141	22 29787	semi-massive to massive sulfides	Sp	P18	32.65	60.69	
RMUG08-141	22 29787	semi-massive to massive sulfides	Sp	P15	33.18	10.16	
RMUG08-141	22 29787	semi-massive to massive sulfides	Sp	P18	33.29	9.47	
RMUG08-141	22 29787	semi-massive to massive sulfides	Gn_rim a	P18	13.26	8.69	
RMUG08-141	22 29787	semi-massive to massive sulfides	Gn_core	P18	13.19	0.043	433
RMUG08-141	22 29787	semi-massive to massive sulfides	Gn_rim b	P18	13.32	0	0
RMUG08-141	22 29787	semi-massive to massive sulfides	(Ag)Tet	P12	21.78	6.2	
RMUG08-141	22 29787	semi-massive to massive sulfides	(Ag)Tet I	P17-2	21.32	6.56	
RMUG08-145	2 29907	semi-massive to massive sulfides	Ccp	P2b	35.12	30.27	
RMUG08-145	2 29907	semi-massive to massive sulfides	Ccp	P8	35.27	30.1	
RMUG08-145	2 29907	semi-massive to massive sulfides	Ccp	P10	34.92	30.2	
RMUG08-145	2 29907	semi-massive to massive sulfides	Ccp	P11	34.84	30.09	
RMUG08-145	2 29907	semi-massive to massive sulfides	Ccp	P15b	35.23	29.97	
RMUG08-145	2 29907	semi-massive to massive sulfides	Py	P2b	53.74	45.37	
RMUG08-145	2 29907	semi-massive to massive sulfides	Py	P8	53.43	45.19	
RMUG08-145	2 29907	semi-massive to massive sulfides	Py	P10	53.19	45.22	
RMUG08-145	2 29907	semi-massive to massive sulfides	Py	P11	53.51	45.99	
RMUG08-145	2 29907	semi-massive to massive sulfides	Py	P15b	53.73	45.44	
RMUG08-145	2 29907	semi-massive to massive sulfides	Apy	P2b	20.91	34.38	
RMUG08-145	2 29907	semi-massive to massive sulfides	Apy	P8	21.69	34.49	
RMUG08-145	2 29907	semi-massive to massive sulfides	Apy_left	P11	20.52	34.17	
RMUG08-145	2 29907	semi-massive to massive sulfides	Apy_right	P11	19.5	34.01	
RMUG08-145	2 29907	semi-massive to massive sulfides	Apy	P15b	21.68	34.66	
RMUG08-145	2 29907	semi-massive to massive sulfides	Sp	P2b	33.03	8.56	
RMUG08-145	2 29907	semi-massive to massive sulfides	Sp	P15(Fe from P	33.03	8.56	5,991
RMUG08-145	2 29907	semi-massive to massive sulfides	Gn	P2b	12.47	0.599	8,356
RMUG08-145	2 29907	semi-massive to massive sulfides	Gn	P8	12.47	0.836	4,349
RMUG08-145	2 29907	semi-massive to massive sulfides	Gn	P15b	13.9	0.435	
RMUG08-145	2 29907	semi-massive to massive sulfides	Men	P2b	17.05	1.01	
RMUG08-145	2 29907	semi-massive to massive sulfides	Men	P10	16.63		2,018
RMUG08-146	2 29918	semi-massive to massive sulfides	Ccp	P2	36.13	29.67	
RMUG08-146	2 29918	semi-massive to massive sulfides	Ccp	P4c	35.43	30.68	
RMUG08-146	2 29918	semi-massive to massive sulfides	Ccp	P7	35.31	29.31	
RMUG08-146	2 29918	semi-massive to massive sulfides	Ccp	P9	35.72	29.16	
RMUG08-146	2 29918	semi-massive to massive sulfides	Ccp	P14	35.67	29.2	
RMUG08-146	2 29918	semi-massive to massive sulfides	Py	P2	53.31	46.02	

[illegible]

[illegible]

7.01	37.69 41.24 39.75	13.76 13.50 13.78	0.064	0.334	0.000
27 25.66					
					85.59 87.55 87.17
3.09	0		0.908	26.6	0.26
6.29 4.04	0 0		1.26 0.191	13.3 56.8	1.35 1.77
2.338	1.55		0.516	82.5	4.81
1.264	0.526		0.26	11.8	2.36
520 0 2.14	0.156 0 0		0.063 0.056 1.97	3.47 12 12.3	0.537 0.214 0.206
20.38 20.06					
	0		1.01	28.8	0.777
0	0.185		0.24	5.16	0.598
0	0		0.963	584	0



RMUG08-146	2	29918	semi-massive to massive sulfides	Py	P9	53.26	45.68
RMUG08-146	2	29918	semi-massive to massive sulfides	Py	P14	53.82	45.93
RMUG08-146	2	29918	semi-massive to massive sulfides	Apy	P2	23.71	34.37
RMUG08-146	2	29918	semi-massive to massive sulfides	Apy	P14	21.87	34.62
RMUG08-146	2	29918	semi-massive to massive sulfides	Po	P2	40.14	60.02
RMUG08-146	2	29918	semi-massive to massive sulfides	Po	P7	39.68	59.76
RMUG08-146	2	29918	semi-massive to massive sulfides	Po	P14	40.02	60.23
RMUG08-146	2	29918	semi-massive to massive sulfides	Sp	P7	33.23	9.25
RMUG08-146	2	29918	semi-massive to massive sulfides	Gn	P7	12.27	0.121
RMUG08-146	2	29920	semi-massive to massive sulfides	Ccp	P1	35.32	29.82
RMUG08-146	2	29920	silicified horizon	Ccp	P5	35.19	30.44
RMUG08-146	2	29920	silicified horizon	Ccp	P6	35.11	30.5
RMUG08-146	2	29920	silicified horizon	Ccp	P8	35.16	29.98
RMUG08-146	2	29920	silicified horizon	Ccp	P10d	34.99	29.69
RMUG08-146	2	29920	silicified horizon	Ccp	P14	35.55	29.8
RMUG08-146	2	29920	silicified horizon	Py	P1	53.63	45.93
RMUG08-146	2	29920	silicified horizon	Py	P5	53.74	45.7
RMUG08-146	2	29920	silicified horizon	Py	P6	53.86	46.09
RMUG08-146	2	29920	silicified horizon	Py	P8	53.55	45.85
RMUG08-146	2	29920	silicified horizon	Py	P10d	53.5	45.58
RMUG08-146	2	29920	silicified horizon	Py	P14	53.44	45.33
RMUG08-146	2	29920	silicified horizon	Apy	P6	20.71	34.48
RMUG08-146	2	29920	silicified horizon	Apy	P8	21.09	34.52
RMUG08-146	2	29920	silicified horizon	Apy	P14	19.62	34.3
RMUG08-146	2	29920	silicified horizon	Sp	P5	32.33	2.06
RMUG08-146	2	29920	silicified horizon	Sp	P10d	32.91	1.42
RMUG08-146	2	29920	silicified horizon	Ten I	P1	27.47	5.34
RMUG08-146	2	29920	silicified horizon	Ten-Tet I	P1	26.09	3.2
RMUG08-146	2	29920	silicified horizon	Tet I	P1	24.43	3.54
RMUG08-146	2	29920	silicified horizon	Ten II	P1	27.78	5
RMUG08-146	2	29920	silicified horizon	Ten III_core	P1	27.35	5.08
RMUG08-146	2	29920	silicified horizon	Ten III_rim b	P1	27.43	5.86
RMUG08-146	2	29920	silicified horizon	Ten-Tet I	P8	25.34	3.71
RMUG08-146	2	29920	silicified horizon	Ten-Tet II	P8	25.69	3.54
RMUG08-146	2	29920	silicified horizon	Ten-Tet I	P10d	25.82	4.19
RMUG08-146	2	29920	silicified horizon	Ten-Tet II	P10d	26.02	3.6
RMUG08-146	2	29920	silicified horizon	Ten-Tet	P14	26.01	3.74
RMUG08-159	2	29934	semi-massive to massive sulfides	Ccp	P2	35.01	29.86
RMUG08-159	2	29934	semi-massive to massive sulfides	Ccp	P5a	34.98	29.93
RMUG08-159	2	29934	semi-massive to massive sulfides	Ccp	P9	35.45	30.21
RMUG08-159	2	29934	semi-massive to massive sulfides	Ccp	P13	34.94	30.05
RMUG08-159	2	29934	semi-massive to massive sulfides	Py	P2	53.92	45.98
RMUG08-159	2	29934	semi-massive to massive sulfides	Py I	P5a	53.24	45.66
RMUG08-159	2	29934	semi-massive to massive sulfides	Py II	P5a	53.58	45.42
RMUG08-159	2	29934	semi-massive to massive sulfides	Py	P7	53.74	45.75
RMUG08-159	2	29934	semi-massive to massive sulfides	Py	P9	53.89	45.84
RMUG08-159	2	29934	semi-massive to massive sulfides	Py	P13	53.12	45.26
RMUG08-159	2	29934	semi-massive to massive sulfides	Apy	P2	20.97	34.67
RMUG08-159	2	29934	semi-massive to massive sulfides	Apy	P5a	21.54	34.69
RMUG08-159	2	29934	semi-massive to massive sulfides	Apy	P9	21.73	34.71
RMUG08-159	2	29934	semi-massive to massive sulfides	Sp	P5a	33.19	1.7

1,205

[illegible]

[illegible]

0	0	0.978	93.6	4.51
0	0	0.024	34.7	2.07
0	0	3.55	289	11.3
0	0.08	0.283	20.6	1.94
				85.38

2.79
17.98
29.06
2.92
2.78
2.77
19.49
18.09
15.67
16.17
16.5

RMUG08-159	2	29934	semi-massive to massive sulfides	Sp	P7	33.18	1.12	0
RMUG08-159	2	29934	semi-massive to massive sulfides	Gn	P2	13.86	0	3,593
RMUG08-159	2	29934	semi-massive to massive sulfides	Gn	P5a	12.64	0.359	
RMUG08-159	2	29934	semi-massive to massive sulfides	Tet I	P2	24.71	2.88	
RMUG08-159	2	29934	semi-massive to massive sulfides	Tet II_core	P2	24.45	2.78	
RMUG08-159	2	29934	semi-massive to massive sulfides	Tet II_rim a	P2	24.37	3.13	
RMUG08-159	2	29934	semi-massive to massive sulfides	Tet II_rim b	P2	24.36	2.54	
RMUG08-159	2	29934	semi-massive to massive sulfides	Tet I	P7	23.86	2.9	
RMUG08-159	2	29934	semi-massive to massive sulfides	Tet	P9	24.18	1.99	
RMUG08-159	2	29934	semi-massive to massive sulfides	Tet_rim a	P13	24.25	3.01	
RMUG08-159	2	29934	semi-massive to massive sulfides	Tet_rim b	P13	24.15	4.19	
RMUG08-159	2	29934	semi-massive to massive sulfides	Tet_core	P13	24.25	2.69	
RMUG08-159	2	29934	semi-massive to massive sulfides	El	P5a	0.019		642

34.88  
34.18  
33.96  
34.23  
32.88  
34.08  
32.06  
31.91  
32.82

---

65.1			
4.59	3.47	4.94	
4.61	2.27	5.26	
4.3	2.78	5.83	
4.94	1.94	5.29	
4.34	1.32	6.41	
5.49	1.25	4.68	
4.8	1.94	7.67	
4.63	1.84	7.14	
4.86	2.07	6.73	
		36.88	

24.08	84.88
25.91	85.59
24.84	
26.51	
27.33	
27.69	
26.37	
25.78	
26.35	
	43.48
	20.57



**Table eA5-1. (continued)** Results of EPMA (major and minor elements in wt%) and LA-ICP-MS (trace elements in ppm) analysis for analyzed mineral phases of sulfide:

Drill Hole	Section	Sample No.	Mineralization style	Mineral	SEM image#	S [wt%]_EPMA	Fe [wt%]_EPMA	Fe [ppm]_EPMA	Fe [ppm]_LA
RMUG08-104	4	62017	sulfide stringer in Rambler rhyolite hanging wall	Ccp	P10	34.68	30.93		
RMUG08-104	4	62017	sulfide stringer in Rambler rhyolite hanging wall	Ccp	P6	34.75	30.99		
RMUG08-104	4	62017	sulfide stringer in Rambler rhyolite hanging wall	Py	P2	53.37	46.22		
RMUG08-104	4	62017	sulfide stringer in Rambler rhyolite hanging wall	Py	P4	53.12	46.03		
RMUG08-104	4	62017	sulfide stringer in Rambler rhyolite hanging wall	Py	P6	53.4	45.9		
RMUG08-104	4	62017	sulfide stringer in Rambler rhyolite hanging wall	Py	P10	53.19	45.91		
RMUG08-104	4	62017	sulfide stringer in Rambler rhyolite hanging wall	Apy I	P2	21.45	34		
RMUG08-104	4	62017	sulfide stringer in Rambler rhyolite hanging wall	Apy II	P2	21.6	34.17		
RMUG08-104	4	62017	sulfide stringer in Rambler rhyolite hanging wall	Apy III	P2	21.52	34.41		
RMUG08-104	4	62017	sulfide stringer in Rambler rhyolite hanging wall	Sp	P10	33.85	8.83		
RMUG08-104	4	62017	sulfide stringer in Rambler rhyolite hanging wall	Sp	P6	33.92	8.69		
RMUG08-104	4	62017	sulfide stringer in Rambler rhyolite hanging wall	Sp	P4	33.49	5.91		
RMUG08-104	4	62017	sulfide stringer in Rambler rhyolite hanging wall	Sp	P2	33.79	6.33		
RMUG08-104	4	62017	sulfide stringer in Rambler rhyolite hanging wall	Gn	P4	13.33			0
RMUG08-104	4	62017	sulfide stringer in Rambler rhyolite hanging wall	Gn	P6	13.11	0.356	3,561	
RMUG08-104	4	62017	sulfide stringer in Rambler rhyolite hanging wall	Gn	P10	13.13	0	0	
RMUG08-95	5	62044	sulfide stringer horizon	Ccp	P3	34.5	30.75		
RMUG08-95	5	62044	sulfide stringer horizon	Ccp	P5	34.72	30.66		
RMUG08-95	5	62044	sulfide stringer horizon	Ccp	P7	34.62	30.59		
RMUG08-95	5	62044	sulfide stringer horizon	Ccp	P9	35.16	30.61		
RMUG08-95	5	62044	sulfide stringer horizon	Ccp	P10	34.69	30.28		
RMUG08-95	5	62044	sulfide stringer horizon	Ccp	P11	34.63	30.82		
RMUG08-95	5	62044	sulfide stringer horizon	Ccp	P12	35.21	30.54		
RMUG08-95	5	62044	sulfide stringer horizon	Py	P3	53.21	45.89		
RMUG08-95	5	62044	sulfide stringer horizon	Py	P5	52.96	45.61		
RMUG08-95	5	62044	sulfide stringer horizon	Py	P12	53.15	45.79		
RMUG08-95	5	62044	sulfide stringer horizon	Apy_rim a	P5	21.71	34.44		
RMUG08-95	5	62044	sulfide stringer horizon	Apy_core	P5	21.63	34.42		
RMUG08-95	5	62044	sulfide stringer horizon	Apy_rim b	P5	21.97	34.16		
RMUG08-95	5	62044	sulfide stringer horizon	Apy	P12	20.91	34.1		
RMUG08-95	5	62044	sulfide stringer horizon	Po	P5	39.28	59.67		
RMUG08-95	5	62044	sulfide stringer horizon	Po	P11	39.48	59.99		
RMUG08-95	5	62044	sulfide stringer horizon	Sp	P9	33.72	8.45		
RMUG08-95	5	62044	sulfide stringer horizon	Sp II	P9	32.56	8.81		
RMUG08-95	5	62044	sulfide stringer horizon	Sp	P10	33.65	9.23		
RMUG08-95	5	62044	sulfide stringer horizon	Sp	P11	34.49	8.66		
RMUG08-95	5	62044	sulfide stringer horizon	Gn	P3	12.19	1.74		17,441
RMUG08-95	5	62044	sulfide stringer horizon	Men_core	P10	18.65			445
RMUG08-98	5	62033	sulfide stringer horizon	Ccp I	P1	35.04	30.49		
RMUG08-98	5	62033	sulfide stringer horizon	Ccp II	P1	34.8	30.93		
RMUG08-98	5	62033	sulfide stringer horizon	Ccp	P2	34.84	30.74		
RMUG08-98	5	62033	sulfide stringer horizon	Ccp	P5	34.78	30.36		
RMUG08-98	5	62033	sulfide stringer horizon	Ccp	P6b	34.82	30.82		
RMUG08-98	5	62033	sulfide stringer horizon	Ccp	P10	35.04	30.8		
RMUG08-98	5	62033	sulfide stringer horizon	Py	P1	53.64	46.27		

s from the Ming South Up Plunge orebody. Detailed mineralogical description of analyzed samples can be found in eA4. Abbreviation: LA – LA-ICP-MS, SEM - s

Ti [ppm]_LA	V [ppm]_LA	Cr [ppm]_LA	Mn [ppm]_LA	Co [ppm]_LA	Co [wt%]_EPMA	Ni [ppm]_LA	Ni [wt%]_EPMA	Cu [ppm]_LA	Cu [wt%]_EPMA	Zn [ppm]_LA
7.11	0	0	0	0	0	0	0	34.47	34.47	705
								34.48		
17		0	2.3	0	92.5	180		39.1		23
9.18		0.143	1.63	0	189	1,108		119		0
6.88		0	0	980	6.71	41.5		141		
8.1		0	0	1,581	0	0		10.8		
9.43		0	0	1,619	3.1	0		16.1		
2.07		0	0	0	0	0		0		0
									34.2	
									34.79	
									34.38	
									34.46	
									34.31	
									34.42	
									34.49	
										1.12
										34.19
										34.03
										34.29
										34.55
										34.53
										34.73

scanning elctron microscope

Zn	As	As	Se	Mo	Ag	Ag	Cd	Sn	Sn	Sb
[wt%]_EPMA	As [ppm]_LA	[wt%]_EPMA	Se [ppm]_LA	Mo [ppm]_LA	[ppm]_ppm	[wt%]_EPMA	[ppm]_LA	[ppm]_LA	[wt%]_EPMA	[ppm]_LA
	365		39.9	0	221		6.28	95.9		8.47
	1,887		0	28.1	0.921		0	0		38.2
		43.43	72.1	11.2	1.36		0	0		54.1
		43.69								
		43.78								
57.35	265		41.6	0	6.18		5,049	0.344		11.2
57.53										
60.66	0		60.3	0	1.78		6,495	0		2.21
59.55	1,778		67.1	0	17.1		6,992	0		25
	377			0	1,376		20.3	3.85		1,439
		44.02								
		44.53								
		43.66								
		44.75								
56.58										
57.13										
56.56										
56.79										

[illegible]

RMUG08-98	5	62033	sulfide stringer horizon	Py	P2	53.21	45.91
RMUG08-98	5	62033	sulfide stringer horizon	Py	P5	53.74	45.83
RMUG08-98	5	62033	sulfide stringer horizon	Py	P6b	52.31	44.91
RMUG08-98	5	62033	sulfide stringer horizon	Py	P10	53.09	46.19
RMUG08-98	5	62033	sulfide stringer horizon	Po	P5	39.25	59.72
RMUG08-98	5	62033	sulfide stringer horizon	Po	P6b	39.24	59.82
RMUG08-98	5	62033	sulfide stringer horizon	Po	P10	38.99	60.06
RMUG08-98	5	62033	sulfide stringer horizon	Sp	P2	32.83	8.13
RMUG08-98	5	62033	sulfide stringer horizon	Sp	P5	32.89	8.45
RMUG08-98	5	62033	sulfide stringer horizon	Sp I	P6b	33.25	8.3
RMUG08-98	5	62033	sulfide stringer horizon	Sp II	P6b	33.24	9.01
RMUG08-98	5	62033	sulfide stringer horizon	Sp	P10	33.13	10.27
RMUG08-98	5	62033	sulfide stringer horizon	Men	P12	18.66	3,927
RMUG08-60	14	62107	semi-massive to massive sulfides	Ccp	P1	34.88	
RMUG08-60	14	62107	semi-massive to massive sulfides	Ccp	P2	34.82	30.58
RMUG08-60	14	62107	semi-massive to massive sulfides	Ccp	P8	34.58	31.23
RMUG08-60	14	62107	semi-massive to massive sulfides	Ccp	P10	34.52	30.62
RMUG08-60	14	62107	semi-massive to massive sulfides	Ccp	P12	34.98	30.73
RMUG08-60	14	62107	semi-massive to massive sulfides	Ccp I	P13	34.7	30.54
RMUG08-60	14	62107	semi-massive to massive sulfides	Ccp II	P13	35.5	30.73
RMUG08-60	14	62107	semi-massive to massive sulfides	Ccp III	P13	34.61	30.88
RMUG08-60	14	62107	semi-massive to massive sulfides	Ccp	P14	34.32	31.27
RMUG08-60	14	62107	semi-massive to massive sulfides	Ccp	P15	34.54	30.71
RMUG08-60	14	62107	semi-massive to massive sulfides	Ccp	P16	34.71	30.71
RMUG08-60	14	62107	semi-massive to massive sulfides	Ccp	P21	34.95	30.54
RMUG08-60	14	62107	semi-massive to massive sulfides	Ccp	P24	33.61	30.96
RMUG08-60	14	62107	semi-massive to massive sulfides	Py	P8	52.81	30.69
RMUG08-60	14	62107	semi-massive to massive sulfides	Py	P10	53.1	46.06
RMUG08-60	14	62107	semi-massive to massive sulfides	Po	P1	38.3	45.96
RMUG08-60	14	62107	semi-massive to massive sulfides	Po	P7	38.97	60.67
RMUG08-60	14	62107	semi-massive to massive sulfides	Po	P8	38.68	59.26
RMUG08-60	14	62107	semi-massive to massive sulfides	Po	P10	38.91	61.44
RMUG08-60	14	62107	semi-massive to massive sulfides	Po	P12	38.68	60.84
RMUG08-60	14	62107	semi-massive to massive sulfides	Po	P13	38.38	60.89
RMUG08-60	14	62107	semi-massive to massive sulfides	Po	P13	38.71	59.23
RMUG08-60	14	62107	semi-massive to massive sulfides	Po	P14	38.48	61.18
RMUG08-60	14	62107	semi-massive to massive sulfides	Po	P16	38.79	61.04
RMUG08-60	14	62107	semi-massive to massive sulfides	Po	P16	38.29	59.32
RMUG08-60	14	62107	semi-massive to massive sulfides	Po	P21	38.62	60.88
RMUG08-60	14	62107	semi-massive to massive sulfides	Po I	P24	38.37	61.15
RMUG08-60	14	62107	semi-massive to massive sulfides	Po II	P24	38.33	61.15
RMUG08-60	14	62107	semi-massive to massive sulfides	Sp	P12	33.49	60.94
RMUG08-60	14	62107	semi-massive to massive sulfides	Sp	P15	33.61	10.59
RMUG08-60	14	62107	semi-massive to massive sulfides	Sp	P16	33.67	11.04
RMUG08-60	14	62107	semi-massive to massive sulfides	Sp	P24	33.48	10.53
RMUG08-60	14	62107	semi-massive to massive sulfides	Allo	P8	19.61	10.84
RMUG08-60	14	62107	semi-massive to massive sulfides	Allo_rim a	P10	20.22	8.78
RMUG08-60	14	62107	semi-massive to massive sulfides	Allo_core	P10	19.73	7.75
RMUG08-60	14	62107	semi-massive to massive sulfides	Allo_rim b	P10	20.21	7.15
RMUG08-60	14	62107	semi-massive to massive sulfides	Hess	P24	0.102	9.88
RMUG08-60	14	62107	semi-massive to massive sulfides	Alt	P9	0.109	0.302
							0.106

[illegible]

[illegible]

[illegible]



RMUG08-60	14 62107	semi-massive to massive sulfides	Unknown	P24	0.098	0.610	6,101
RMUG08-60	14 62107	semi-massive to massive sulfides	BlTe				
RMUG08-60	14 62107	semi-massive to massive sulfides	Breit	P14	0.000		
RMUG08-61	14 62119	semi-massive to massive sulfides	Breit	P24	0.061		5,502
RMUG08-61	14 62119	semi-massive to massive sulfides	Ccp	P7	34.61	30.71	5,011
RMUG08-61	14 62119	semi-massive to massive sulfides	Ccp	P8	34.46	30.7	
RMUG08-61	14 62119	semi-massive to massive sulfides	Ccp	P11	34.89	30.78	
RMUG08-61	14 62119	semi-massive to massive sulfides	Ccp	P17	35.06	30.44	
RMUG08-61	14 62119	semi-massive to massive sulfides	Py	P7	52.78	46.08	
RMUG08-61	14 62119	semi-massive to massive sulfides	Py I	P8	52.55	46.08	
RMUG08-61	14 62119	semi-massive to massive sulfides	Py II	P8	53.18	46.03	
RMUG08-61	14 62119	semi-massive to massive sulfides	Py	P17	52.79	45.96	
RMUG08-61	14 62119	semi-massive to massive sulfides	Py	P18	52.94	45.8	
RMUG08-61	14 62119	semi-massive to massive sulfides	Po	P7	38.5	60.6	
RMUG08-61	14 62119	semi-massive to massive sulfides	Po	P11	38.37	60.06	
RMUG08-61	14 62119	semi-massive to massive sulfides	Po	P15	38.55	60.46	
RMUG08-61	14 62119	semi-massive to massive sulfides	Po	P18	38.39	60.3	
RMUG08-61	14 62119	semi-massive to massive sulfides	Sp	P7	33.46	9.64	
RMUG08-61	14 62119	semi-massive to massive sulfides	Breit	P11	0.142	1.73	
RMUG08-61	14 62119	semi-massive to massive sulfides	Nis	P7	0.138		8,114
RMUG08-64	14 62018	sulfide stringer horizon	Ccp I	P1	34.72	30.65	
RMUG08-64	14 62018	sulfide stringer horizon	Ccp II	P1	34.96	30.72	
RMUG08-64	14 62018	sulfide stringer horizon	Ccp	P2	34.95	30.72	
RMUG08-64	14 62018	sulfide stringer horizon	Ccp	P6	34.42	30.55	
RMUG08-64	14 62018	sulfide stringer horizon	Ccp	P9	34.73	30.92	
RMUG08-64	14 62018	sulfide stringer horizon	Ccp	P11	34.87	30.81	
RMUG08-64	14 62018	sulfide stringer horizon	Py	P1	52.96	46.06	
RMUG08-64	14 62018	sulfide stringer horizon	Py	P2	52.73	45.45	
RMUG08-64	14 62018	sulfide stringer horizon	Py	P6	52.34	45.64	
RMUG08-64	14 62018	sulfide stringer horizon	Py	P9	52.91	45.8	
RMUG08-64	14 62018	sulfide stringer horizon	Py	P11	53.46	45.79	
RMUG08-64	14 62018	sulfide stringer horizon	Apy	P1	21.89	34.44	
RMUG08-64	14 62018	sulfide stringer horizon	Apy	P6	21.91	34.48	
RMUG08-64	14 62018	sulfide stringer horizon	Apy	P9	21.54	34.37	
RMUG08-64	14 62018	sulfide stringer horizon	Po	P1	39.07	60.72	
RMUG08-64	14 62018	sulfide stringer horizon	Po	P2	39.01	60.47	
RMUG08-64	14 62018	sulfide stringer horizon	Po	P9	39.74	60.28	
RMUG08-64	14 62018	sulfide stringer horizon	Po	P11	39.07	61.13	
RMUG08-64	14 62018	sulfide stringer horizon	Sp	P2	33.94	9.56	
RMUG08-64	14 62018	sulfide stringer horizon	Sp	P6	33.74	9.74	
RMUG08-64	14 62018	sulfide stringer horizon	Sp	P9	34.65	8.73	
RMUG08-64	14 62018	sulfide stringer horizon	Sp	P11	34.08	9.35	
RMUG08-64	14 62018	sulfide stringer horizon	Po (overlap with Asp?)	P6	37.44	58.59	
RMUG08-91	13 62133	Fe oxide schlieren in Rambler rhyolite (hanging wall)	Ccp	P6	34.73	31.46	
RMUG08-91	13 62133	Fe oxide schlieren in Rambler rhyolite (hanging wall)	Ccp	P15	34.47	30.57	
RMUG08-91	13 62133	Fe oxide schlieren in Rambler rhyolite (hanging wall)	Po	P1	39.96	58.11	
RMUG08-91	13 62133	Fe oxide schlieren in Rambler rhyolite (hanging wall)	Po	P6	39.88	58.37	
RMUG08-91	13 62133	Fe oxide schlieren in Rambler rhyolite (hanging wall)	Po	P15	39.62	58.47	
RMUG08-91	13 62133	Fe oxide schlieren in Rambler rhyolite (hanging wall)	Sp	P7	33.42	8.08	
RMUG08-91	13 62133	Fe oxide schlieren in Rambler rhyolite (hanging wall)	Sp	P9	33.68	9.13	

[illegible]

0.000	247	2,896	0	36.5	19.7	97.6	37.5
	162	1,139	0	11.2	16.9	96.7	4.39
	156	2,179	0	27.2	10.8	120	7.61
	1,032	876	0	1.75	0	0	10.5
	1,138	705	0	0	0	0	0
	835	722	0	0	0	0	0
	1,157	2,054	0	0.848	25.5	1.58	836

56.01

132	808	0	42.1	7.34	19.3	12.6
110	806	0	38.6	6.9	23	3.91
832	708	0	37.9	9.24	27.9	1.7
823	123	0	0	0	0	0
2,077	202	0	2.92	0	0	14.2
2,056	156	0.916	0.678	0	0	1.83
	43.67	0	1.41	0	0.4	19
	43.71	5.5	0	0	0	18.2
	44.51					
149	381	0	4.66	0	0	2.06
1,796	482	0	0	0	0.47	1.69
6.12	516	0	5.25	6,135	2.04	5.83
46.8	553	0	2.68	6,782	0.555	3.1
2,285	348	0	2.68	0	0	41

56.58  
56.32  
57.41  
56.47

58.2  
57.87

0.338	28.35			3.42	67.76
66.37		7.68	1.81		
66.43		3.53	0.292		
				3.75	2.89
				0.12	0.2
		4.02	0		
		0	0	0.32	2.25
		87.1	0	0.267	9.95
			0	0	0.062
			0		
			0	0	0.075
		58.8	2.06	0.551	7.82
66.77	1.69				
77.31					
		9.52	0.098		4.05
		3.73	0.318	0.181	1.31
		6.15	0	0.153	2.07
				0.411	
		0	0	0	0
		0	0	0	15.4
		0	0	0	1.5
		115	0	0	6.17
		118	0.34	0	5.6
		0	0	0	2.6
		0	0	1.45	3.44
		0	0	0.258	0.936
		0	0	0.097	1.05
		6.74	0	0.117	4.63

RMUG08-91	13 62133	Fe oxide schlieren in Rambler rhyolite (hanging wall)	Sp	P15	33.31	7.11
-----------	----------	---	----	-----	-------	------



58.37





**Table eA5-1. (continued)** Results of EPMA (major and minor elements in wt%) and LA-ICP-MS (trace elements in ppm) analysis for analyzed mineral phases of sulfide

Orebody	Drill Hole	Sample No.	Mineralization style	Mineral	SEM image#	S [wt%]_EPMA	Fe [wt%]_EPMA	Fe [ppm]_EPMA	Fe [ppm]_LA
MSDP	RM06-04e	29789	semi-massive to massive sulfides	Ccp	P2	34.79	30.74		
MSDP	RM06-04e	29789	semi-massive to massive sulfides	Ccp	P5	34.92	30.64		
MSDP	RM06-04e	29789	semi-massive to massive sulfides	Ccp	P9	34.75	30.24		
MSDP	RM06-04e	29789	semi-massive to massive sulfides	Py I	P9	53.12	45.99		
MSDP	RM06-04e	29789	semi-massive to massive sulfides	Py II	P9	53.12	46.04		
MSDP	RM06-04e	29789	semi-massive to massive sulfides	Po	P2	38.7	60.33		
MSDP	RM06-04e	29789	semi-massive to massive sulfides	Po	P5	39.19	59.61		
MSDP	RM06-04e	29789	semi-massive to massive sulfides	Po	P9	39.27	59.88		
MSDP	RM06-04e	29789	semi-massive to massive sulfides	Sp	P2	33.79	9.95		
MSDP	RM06-04m	36058	semi-massive to massive sulfides	Ccp	P2	34.88	30.39		
MSDP	RM06-04m	36058	semi-massive to massive sulfides	Ccp	P12	34.06	30.29		
MSDP	RM06-04m	36058	semi-massive to massive sulfides	Ccp	P13	34.79	30.65		
MSDP	RM06-04m	36058	semi-massive to massive sulfides	Py	P2	53.17	45.72		
MSDP	RM06-04m	36058	semi-massive to massive sulfides	Py	P10	53.33	45.86		
MSDP	RM06-04m	36058	semi-massive to massive sulfides	Py	P12	52.58	46.14		
MSDP	RM06-04m	36058	semi-massive to massive sulfides	Py	P13	53.25	45.51		
MSDP	RM06-04m	36058	semi-massive to massive sulfides	Apy	P2	21.42	34.22		
MSDP	RM06-04m	36058	semi-massive to massive sulfides	Po	P13	38.92	59.78		
MSDP	RM06-04m	36058	semi-massive to massive sulfides	Sp	P13	33.73	9.33		
MSDP	RM06-04m	36058	semi-massive to massive sulfides	Gn	P2	13.13	0.593	5.928	
MSDP	RM06-04m	36058	semi-massive to massive sulfides	Gn	P12	13.28	0.43	4.296	
MSDP	RM06-04m	36058	semi-massive to massive sulfides	Gn	P13	13.1	0.508	5.076	
MSDP	RM06-04m	36067	sulfide stringer horizon	Ccp	P4	34.65	30.76		
MSDP	RM06-04m	36067	sulfide stringer horizon	Ccp	P7	34.69	30.93		
MSDP	RM06-04m	36067	sulfide stringer horizon	Ccp	P9	34.95	30.37		
MSDP	RM06-04m	36067	sulfide stringer horizon	Ccp	P14	34.79	30.81		
MSDP	RM06-04m	36067	sulfide stringer horizon	Py	P7	53.17	45.77		
MSDP	RM06-04m	36067	sulfide stringer horizon	Py	P9	53	45.61		
MSDP	RM06-04m	36067	sulfide stringer horizon	Py	P14	52.77	46.03		
MSDP	RM06-04m	36067	sulfide stringer horizon	Po	P7	39.02	60.76		
MSDP	RM06-04m	36067	sulfide stringer horizon	Po	P9	38.57	60.32		
MSDP	RM06-04m	36067	sulfide stringer horizon	Po	P14	39.13	60.38		
MSDP	RM06-04m	36067	sulfide stringer horizon	Sp	P7	33.6	10.07		
MSDP	RM06-04m	36067	sulfide stringer horizon	Sp	P9	34	8.9		
MSDP	RM06-04m	36067	sulfide stringer horizon	Sp	P14	34.37	9.38		
MSDP	RM06-04m	36067	sulfide stringer horizon	Gn	P4	13	0.081	813	
MSDP	RM06-04d	36163	semi-massive to massive sulfides	Ccp I	P2	34.6	30.21		
MSDP	RM06-04d	36163	semi-massive to massive sulfides	Ccp II	P2	34.79	30.13		
MSDP	RM06-04d	36163	semi-massive to massive sulfides	Ccp	P5	35.09	30.68		
MSDP	RM06-04d	36163	semi-massive to massive sulfides	Ccp	P7	34.89	30.57		
MSDP	RM06-04d	36163	semi-massive to massive sulfides	Ccp	P11	34.86	30.22		
MSDP	RM06-04d	36163	semi-massive to massive sulfides	Ccp	P16	35.13	30.69		
MSDP	RM06-04d	36163	semi-massive to massive sulfides	Py	P16	52.98	45.87		
MSDP	RM06-04d	36163	semi-massive to massive sulfides	Apy_rim a	P5	20.96	33.14		

as from the Ming South Down Plunge (MSDP) and Lower Footwall Zone (LFWZ) orebodies. Detailed mineralogical description of analyzed samples can be found

[illegible]

d in eA4. Abbreviation: LA – LA-ICP-MS, SEM - scanning elctron microscope

Zn [wt%]_EPMA	As [ppm]_LA	As [wt%]_EPMA	Se [ppm]_LA	Mo [ppm]_LA	Ag [ppm]_ppm	Ag [wt%]_EPMA	Cd [ppm]_LA	Sn [ppm]_LA	Sn [wt%]_EPMA	Sb [ppm]_LA
56.11	125		80	0	15.2		73.9	515		4.12
	798		36.2	0.298	3.49		0	0		2.8
	1,024		34.1	0	0		0	0.212		0
	1,361		38.1	7.96	0		3.19	0		0.264
			43.35 43.48							
54.92	7.74		65.3	0	5.13		37,554	1.6		1.06
55.79 57.16 56.61	265		179	0	66.8		19.7	13.7		1.39
	271		196	0	65.1		18.37	12.2		1.26
	198		124	0	0.568		6.41	0		0.284
	1,040		29.5	0	0		0	0		2.3
	563		172	0	2.45		0	0		0.058
	370		98.4	0	7		1.21	0		0.731
	21.1		79.5	0	10.6		4,832	0		2.95
	36.2		169	0	0.845		12,077	0		0
	4,387		61.4	49.7	118		18	76.1		32.9
	6,936 1,245		58.3 91.3 123	0 2.94 0	114 0.11 0		0 0 0	48.5 0.734 0		9.21 0.963 8.29
			44.52							

Sb	Te	Te	Au	Au	Hg	Tl	Pb	Pb	Bi	Bi
[wt%]_EPMA	[ppm]_LA	[wt%]_EPMA	[ppm]_LA	[wt%]_EPMA	[wt%]_EPMA	[ppm]_LA	[ppm]_LA	[wt%]_EPMA	[ppm]_LA	[wt%]_EPMA

0		0	0	0.282	1,366	6.97				
4.08		0.083	0.089	0.089	394	5.96				
0		0	0	0	0.544	0				
0		0	0	0	21.4	0.337				
8.77		0	0.662	0.662	681	4.57				
						86.25				
						86.95				
						86.05				
12.1		0.121	0.223	0.223	8.04	2.23				
5.64		0	0.225	0.225	4.34	1.51				
18.8		0	0	0	0.741	6.54				
1.66		0	0	0	42.8	3.13				
0		0	0	0	6.08	4.37				
0		0	0	0	5.98	6.34				
0		0	0.107	0.107	14.8	4.73				
0		0	0	0	0.134	0				
						85.44				
3.68		0.144	1.35	1.35	224	1.69				
0		0	0	0	6.45	1.63				
0		0	0	0	8.26	0.243				
98.1		0	0	0	0	0				

MSDP	RM06-04d	36163	semi-massive to massive sulfides	Apv_core	P5	21.18	32.97	
MSDP	RM06-04d	36163	semi-massive to massive sulfides	Apv_rim b	P5	21.09	33.95	
MSDP	RM06-04d	36163	semi-massive to massive sulfides	Apv	P7	21.3	33.19	
MSDP	RM06-04d	36163	semi-massive to massive sulfides	Apv	P16	21.55	33.64	
MSDP	RM06-04d	36163	semi-massive to massive sulfides	Po	P16	39.02	60.31	
MSDP	RM06-04d	36163	semi-massive to massive sulfides	Po	P11	39.3	59.52	
MSDP	RM06-04d	36163	semi-massive to massive sulfides	Po	P7	39.09	59.68	
MSDP	RM06-04d	36163	semi-massive to massive sulfides	Po	P5	39.53	59.73	
MSDP	RM06-04d	36163	semi-massive to massive sulfides	Sp	P5	33.95	9.62	
MSDP	RM06-04d	36163	semi-massive to massive sulfides	Sp	P7	33.34	8.68	
MSDP	RM06-04d	36163	semi-massive to massive sulfides	Sp	P16	33.87	9.92	
MSDP	RM06-04d	36163	semi-massive to massive sulfides	Gn	P1	12.76	0.098	981
MSDP	RM06-04d	36163	semi-massive to massive sulfides	Gn	P2	13.08	0	0
MSDP	RM06-04d	36163	semi-massive to massive sulfides	Gn	P7	12.67	0.415	4,154
MSDP	RM06-04d	36163	semi-massive to massive sulfides	Gn	P11	12.66	0.617	6,169
MSDP	RM06-04d	36163	semi-massive to massive sulfides	Hess	P1	0.055	0.144	1,441
MSDP	RM06-04d	36163	semi-massive to massive sulfides	Ccp I	P5	34.69	30.61	
FWZ	RM06-04e	29797	Lower Footwall Zone	Ccp II	P5	34.97	30.73	
FWZ	RM06-04e	29797	Lower Footwall Zone	Ccp	P13	34.95	30.82	
FWZ	RM06-04e	29797	Lower Footwall Zone	Ccp	P15a	34.95	30.56	
FWZ	RM06-04e	29797	Lower Footwall Zone	Ccp	P17	34.76	30.68	
FWZ	RM06-04e	29797	Lower Footwall Zone	Ccp	P19	35.07	30.45	
FWZ	RM06-04e	29797	Lower Footwall Zone	Ccp	P21	34.81	30.62	
FWZ	RM06-04e	29797	Lower Footwall Zone	Ccp	P23	35.19	30.53	
FWZ	RM06-04e	29797	Lower Footwall Zone	Py I	P5	53.09	45.64	
FWZ	RM06-04e	29797	Lower Footwall Zone	Py II	P5	53.4	45.83	
FWZ	RM06-04e	29797	Lower Footwall Zone	Py	P12	53.35	45.59	
FWZ	RM06-04e	29797	Lower Footwall Zone	Py	P12	53.15	45.75	
FWZ	RM06-04e	29797	Lower Footwall Zone	Py	P12	53.59	45.76	
FWZ	RM06-04e	29797	Lower Footwall Zone	Py	P13	53.56	45.58	
FWZ	RM06-04e	29797	Lower Footwall Zone	Py	P15b	53.4	45.57	
FWZ	RM06-04e	29797	Lower Footwall Zone	Py	P17	53.49	45.1	
FWZ	RM06-04e	29797	Lower Footwall Zone	Cbn I	P21	35.24	40.92	
FWZ	RM06-04e	29797	Lower Footwall Zone	Cbn II	P21	35.23	41.02	
FWZ	RM06-04e	29797	Lower Footwall Zone	Po II	P5	38.62	60.8	
FWZ	RM06-04e	29797	Lower Footwall Zone	Po	P12	38.6	60.94	
FWZ	RM06-04e	29797	Lower Footwall Zone	Po	P15b	38.4	60.55	
FWZ	RM06-04e	29797	Lower Footwall Zone	Po	P17	38.67	60.86	
FWZ	RM06-04e	29797	Lower Footwall Zone	Po	P21	38.7	60.77	
FWZ	RM06-04e	29797	Lower Footwall Zone	Sp	P17	34.01	8.67	
FWZ	RM06-04e	29797	Lower Footwall Zone	Sp	P23	33.53	9.01	
FWZ	RM06-04e	29797	Lower Footwall Zone	Sp	P21	33.97	9.31	
FWZ	RM06-04e	29800	Lower Footwall Zone	Ccp	P6	34.37	30.83	
FWZ	RM06-04e	29800	Lower Footwall Zone	Ccp	P8	35.02	30.74	
FWZ	RM06-04e	29800	Lower Footwall Zone	Ccp	P11	34.8	30.28	
FWZ	RM06-04e	29800	Lower Footwall Zone	Ccp	P16	34.99	30.69	
FWZ	RM06-04e	29800	Lower Footwall Zone	Ccp	P20	34.97	30.81	
FWZ	RM06-04e	29800	Lower Footwall Zone	Ccp	P21	35.11	30.42	
FWZ	RM06-04e	29800	Lower Footwall Zone	Ccp	P22	34.96	30.14	
FWZ	RM06-04e	29800	Lower Footwall Zone	Cbn I core	P22	34.8	41.62	
FWZ	RM06-04e	29800	Lower Footwall Zone	Cbn I rim	P22	34.9	41.43	

6.59	0	0	1.91	11,970	1,893	1.58	1.85
5.19	0	0	0	5,908	744	0.849	0
5.42	0	0	0	12,783	1,843	249	2.72
15.7	0	0	0	181	0	386	0
5.44	11.9	3.4	102	63.3	55	352	27.5
0	0	0	586	57.5	26.8	654	
5.07	0	0	0	0	0	0	0
4.9	0	0	0	3.06	0		465
6.15	0	0	0	1.11	0		593
5.56	0	0	0	1.77	0		996
6.93	0	0	1.63	0.414	0		555
6.46	0	0	0	0.625	0		490
9.63	0	0	0	69.8	94.5	0	0
7.79	0	0	0	110	179	0	2.98
10.5	0	0	0	113	333	0	0
9.02	0.595	0	0	600	1,578	0	0
0	0	0	0	0.507	0		559
0	0	0	0	57.4	0		1,259
0	0	0	0	671	480	0	0
6.18	0	0	0	190	64.8	0	0
6.21	0	0	0	90.1	88.9	3.53	3.04
8.32	0	0	0	2.19	0		1,134
5.24	0.77	0	4.93	2.62	0		270
4.73	0	0	0	1.96	0		603
5.16	0	0	0	0.616	0		445
							23.33

55.67 56.19 55.46	44.62	188	1.35	1.68	62.56	0	0.445	20.4
	44.32	183	0	1.09		0	0	22.4
	44.79	204	16.5	6.16		0	0.505	14.8
	43.92	107	0	19.9		0	0.862	4.7
3.733								
55.67 56.19 55.46	2.431	82.4	0	14	62.56	0	0	7.29
	615	64.5	0	17.5		8,746	18.3	14.8
	44.7		0	1,672		54.8	28.3	169
56.99 57.22 56.65	49.9	615	0	15.7	62.56	17.1	42	0.612
	47.3	633	0	15		17.7	40	0.793
	45.5	675	0	19.3		23.3	34.8	0.419
	39.9	672	0	18.2		17.3	25.6	0.970
56.99 57.22 56.65	40.1	625	0	21.4	62.56	10.8	36.8	0.640
	127	1,063	0	0		0	0	1.55
	43.1	664	0	0.312		0	0	0
56.99 57.22 56.65	67.9	772	0	0	62.56	0	0	0
	167	879	0	0		0	0	0.857
	57.7	810	0	60.2		19.5	47.7	1.06
	52.9	861	0	69.3		32.8	54.6	1.03
56.99 57.22 56.65	77.2	663	0	0.803	62.56	0	0	0
	68.1	475	0	1.06		0	0.079	0
	47.5	479	0	4.2		0	0.189	0.134
56.99 57.22 56.65	35.7	869	0	10.5	62.56	28.4	24.7	0.296
	30.2	601	0	7.27		8.47	20.5	0.062
	30.1	711	0	9.52		15.6	17.1	0
56.99 57.22 56.65	42.9	762	0	31.5	62.56	13.3	8.37	0.125

167	0.158	0.383	4.06	0.024
428	0.041	0	1.8	0
155	0.363	0.155	59.5	1.41
13.3	0	0.675	2,865	15.3
6.15	0	1.43	759	9.38
10.1	0	0.773	2,479	9.52
1,173	0	181		3,272
			85.36	
			85.86	
			85.53	
			85.98	
			0.000	0
0.000	36.99	0	11.7	1.16
1.44	0.141	0.042	13	1.32
3.96	0			
11.2	0	0	6.05	0.978
5.06	0	0	5.92	1.49
7.96	0	0	8.18	1.02
40.4	0	0	5.84	3.56
16	0	0	0	0
52.4	0	0	1.08	1.21
19.4	0	0	9.92	2.39
9	0	0	18.3	2.04
8.61	0	0	29.1	2.67
0	0	0	9.24	1.52
2	0	0	48.4	0.926
0	0	0	7.67	2.76
12.5	0	0	5.8	0.712
4.1	0	0.018	2.52	0.302
8.38	0	0	9.1	0.802
11.4	0	0.056	38.2	1.07



LFWZ	RM06-04e	29800	Lower Footwall Zone	Cbn II	P22	35.28	41.39	
LFWZ	RM06-04e	29800	Lower Footwall Zone	Cbn III	P22	34.93	41.39	
LFWZ	RM06-04e	29800	Lower Footwall Zone	Cbn	P8	35.09	41.15	
LFWZ	RM06-04e	29800	Lower Footwall Zone	Cbn I	P6	35.35	41.08	
LFWZ	RM06-04e	29800	Lower Footwall Zone	Cbn II	P6	35.39	41.04	
LFWZ	RM06-04e	29800	Lower Footwall Zone	Po	P11	38.32	60.22	
LFWZ	RM06-04e	29800	Lower Footwall Zone	Po	P16	38.46	60.47	
LFWZ	RM06-04e	29800	Lower Footwall Zone	Po	P20	38.94	60.82	
LFWZ	RM06-04e	29800	Lower Footwall Zone	Tsu	P11	0.068	0.987	9.871
LFWZ	RM06-04e	29800	Lower Footwall Zone	Tsu	P21	0.092	0.393	3.930
LFWZ	RM06-04m	36082	Lower Footwall Zone	Ccp	P3	34.57	30.59	
LFWZ	RM06-04m	36082	Lower Footwall Zone	Ccp	P4a	35.06	30.83	
LFWZ	RM06-04m	36082	Lower Footwall Zone	Ccp	P7	35.08	30.65	
LFWZ	RM06-04m	36082	Lower Footwall Zone	Ccp	P8	34.43	30.8	
LFWZ	RM06-04m	36082	Lower Footwall Zone	Ccp	P9	34.63	30.82	
LFWZ	RM06-04m	36082	Lower Footwall Zone	Py	P3	52.83	46.04	
LFWZ	RM06-04m	36082	Lower Footwall Zone	Py	P8	53.22	45.92	
LFWZ	RM06-04m	36082	Lower Footwall Zone	Py	P9	53.2	46.14	
LFWZ	RM06-04m	36082	Lower Footwall Zone	Cbn	P9	35.12	42.26	
LFWZ	RM06-04m	36082	Lower Footwall Zone	Po	P3	38.48	61.2	
LFWZ	RM06-04m	36082	Lower Footwall Zone	Po	P4b	38.45	60.42	
LFWZ	RM06-04m	36082	Lower Footwall Zone	Po	P7	38.76	60.49	
LFWZ	RM06-04m	36082	Lower Footwall Zone	Po	P8	38.41	60.46	
LFWZ	RM06-04m	36082	Lower Footwall Zone	Po	P9	38.94	61.25	
LFWZ	RM06-04m	36082	Lower Footwall Zone	Sp	P3	33.59	10.01	
LFWZ	RM06-04m	36082	Lower Footwall Zone	Sp	P3	34.04	10.06	
LFWZ	RM06-04m	36082	Lower Footwall Zone	Sp	P7	33.66	9.26	
LFWZ	RM06-04m	36082	Lower Footwall Zone	Sp	P9	33.7	9.11	
LFWZ	RM06-04m	36091	Lower Footwall Zone	Ccp	P4a	34.95	30.71	
LFWZ	RM06-04m	36091	Lower Footwall Zone	Ccp	P6b	35.15	30.72	
LFWZ	RM06-04m	36091	Lower Footwall Zone	Ccp	P9	34.62	30.74	
LFWZ	RM06-04m	36091	Lower Footwall Zone	Ccp	P10	34.47	30.49	
LFWZ	RM06-04m	36091	Lower Footwall Zone	Ccp I	P12	34.55	30.63	
LFWZ	RM06-04m	36091	Lower Footwall Zone	Py	P6b	52.97	46.12	
LFWZ	RM06-04m	36091	Lower Footwall Zone	Py	P4a	52.71	45.61	
LFWZ	RM06-04m	36091	Lower Footwall Zone	Py	P9	53.02	45.54	
LFWZ	RM06-04m	36091	Lower Footwall Zone	Py	P10	52.83	45.77	
LFWZ	RM06-04m	36091	Lower Footwall Zone	Py	P12	52.36	45.96	
LFWZ	RM06-04m	36091	Lower Footwall Zone	Apy I_rim a	P6b	21.6	33.51	
LFWZ	RM06-04m	36091	Lower Footwall Zone	Apy I_rim b	P6b	20.79	34.32	
LFWZ	RM06-04m	36091	Lower Footwall Zone	Apy II	P6b	20.9	34.07	
LFWZ	RM06-04m	36091	Lower Footwall Zone	Apy	P10	21.56	34.56	
LFWZ	RM06-04m	36091	Lower Footwall Zone	Po I	P4a	38.57	60.7	
LFWZ	RM06-04m	36091	Lower Footwall Zone	Po II	P4a	38.7	60.94	
LFWZ	RM06-04m	36091	Lower Footwall Zone	Po I	P6b	38.95	61.03	
LFWZ	RM06-04m	36091	Lower Footwall Zone	Po II	P6b	38.74	60.56	
LFWZ	RM06-04m	36091	Lower Footwall Zone	Po	P9	38.48	60.32	
LFWZ	RM06-04m	36091	Lower Footwall Zone	Po	P10	39.01	60.49	
LFWZ	RM06-04m	36091	Lower Footwall Zone	Po	P12	38.58	60.97	
LFWZ	RM06-04m	36091	Lower Footwall Zone	Sp	P4a	33.73	9.33	
LFWZ	RM06-04m	36091	Lower Footwall Zone	Sp	P6b	33.28	9.16	

6.13	0	0	0	0	12.3	33.1	23.14	1,047
3.6	0	0	0	0	5.09	15.3	23.4	447
4.56	0	0	0	0	6.98	0	23.6	398
6.73	0	0	0	0	3.37	0	23.44	287
							23.62	
7.06	0	0	0	0	531	529	0	480
9.79	0	0	0	0	3.61	0	34.47	554
8.02	0	0	0	0	0.524	0	34.22	666
4.37	0	0	0	0	0.456	0	34.27	424
4.07	0	0	0	0	1.57	0	34.55	795
12.43	0	2.76	0	0	1.363	129	34.44	0
6.89	0	0	0	0	592	0		0
6.37	0	0	0	0	69	197	22.83	0
16.3	12.9	10.3	17.3	0	52.1	111	0	864
5.38	0	0	0	0	56.8	175	0	0
4.78	0	0	0	0	102	178	5.57	0
4.32	0	0	297	0	42.1	0	727	
0	0	0	167	0	239	0	3,163	
7.22	0	0	0	0	26.1	0	34.23	654
7.62	0	0	0	0	1.13	0	34.23	
11.1	0	0	0	0	60.4	0	34.85	1,311
							34.86	0
							34.28	
9.15	0	0	0	0	769	183	784	0
							0	0
3.99	0	0	0	0	2,061	1,680		439
4.84	0	0	10	0	1,835	1,856	1,393	6.71
							0	
0	1.10	0	10.3	0	105	189	976	0
20.0	0	0	0	0	152	0	0	436

55.9 56.09 57.06 57.28	43.2	750	0	36.1	19.9	9.35	0.19
	35.2	737	0	40.1	17.8	11.7	0.236
	43.5	830	0	49.3	17.5	18.9	0.181
	36.9	777	0	42.3	13	11.9	0.213
	45.4	670	0	3.33	6.39	0.189	0
	25.1	211	0	50.2	12.1	75.6	0.373
	24.2	211	0	36.4	13.7	59	0.049
	28.8	261	0	25.9	16	63.2	0.496
	22.9	286	0	34.1	14.6	76.7	0.12
	2,716	309	0	0	0	0	0
348	59.2	0	0.551	0	0	0.17	
55.9 56.09 57.06 57.28	40.5	233	0	1.35	0	0	0
	39.9	198	0	5.8	18	0.387	0.133
	34.1	198	0	0.502	0	0	0
	37.3	264	0	0.508	0	0	0
	6.13	236	0	4.84	12,441	1.03	0.261
	5.2	334	0	20.2	15,175	1.1	0.957
	4,270	602	0	34.7	24.1	55	1.9
	2,802	643	0	37.5	38.4	40.5	7.53
	2,444	798	0	3.37	0	0.217	0.692
	1,089	943	0	0	0	0	0
43.8 44.98 45.01 44.01							
		838	0	9.06	0.92	0.531	23.7
		957	0	33.5	0.318	1.62	38
6,774	452	0	20.3	0	0	1.34	
2,668	442	0	6.59	10.9	0.399	0.665	

10.1	0	0	0	44.2	0	0.671
12.4	0	0	0	33.4	0	0.683
10.8	0	0	0	18.5	0	0.933
11	0	0	0	26.3	0	1.25
4.87	0	0	0.116	269	5.84	57.38
0.273	38.77				4.34	57.40
0.255	35.69				5.87	
4.13	0	0	0.156	20.2	3.98	
2.19	0	0	0	2.36	0.509	
1.66	0.157	0.268	0.268	7.21	2.49	
3.05	0.062	0	0	4.35	1.34	
36.4	0	0	0	4.19	1.44	
0	0	0	0	6.8	4.96	
0	0	0	0	5.69	1.47	
4.41	0	0	0	24.8	8.28	
0	0	0	0	0.302	0.098	
0	0	0	0	1.4	0.674	
0	0	0	0	9.55	2.28	
0	0	0.647	0.647	46.2	18	
5.53	3.01	0	0	12.5	3.2	
3.99	0.595	2.29	2.29	43.3	5.15	
0	0	0	0	4.06	2.63	
7.14	0	0	0	0	0	
474	0.474	0	0	16	28.6	
563	0.118	0.971	0.971	19.2	31.8	
17.7	0.934	0.262	0.262	20.8	3.42	
6.96	0	0	0	23.6	2.12	

LFWZ	RM06-04m	36137	Lower Footwall Zone	Cop	P3	34.84	30.65
LFWZ	RM06-04m	36137	Lower Footwall Zone	Cop	P5	34.69	30.87
LFWZ	RM06-04m	36137	Lower Footwall Zone	Cop	P9	34.7	30.55
LFWZ	RM06-04m	36137	Lower Footwall Zone	Po	P5	38.44	61.3
LFWZ	RM06-04m	36137	Lower Footwall Zone	Po	P9	38.2	60.52
LFWZ	RM06-04m	36137	Lower Footwall Zone	Hess	P3	0.095	2.853

34.72  
34.55  
34.61



58.09

